GEOLOGICAL SURVEY OF WESTERN AUSTRALIA

BULLETIN 137

GEOLOGICAL EVOLUTION AND MINERALIZATION OF THE MURCHISON PROVINCE WESTERN AUSTRALIA

BY
KEITH P. WATKINS AND ARTHUR H. HICKMAN

DEPARTMENT OF MINES
WESTERN AUSTRALIA

GEOLOGICAL EVOLUTION AND MINERALIZATION OF THE MURCHISON PROVINCE WESTERN AUSTRALIA



FRONTISPIECE

Aerial view, looking southeast, of the Star Pit (foreground) and St George Pit (background, right) at Mount Magnet. The Star Pit, including separate mining operations by Hill 50 Gold Mine NL and Metana Minerals NL, was developed during the 1980s to extract large tonnages of low-grade, near-surface ore above the underground mines of Morning Star, North Morning Star, and Evening Star. The town of Mount Magnet (background, left) services mining operations, mineral exploration projects, and the pastoral industry throughout the central part of the Murchison Province.
Photography reproduced by courtesy of Metana Minerals NL.



GEOLOGICAL SURVEY OF WESTERN AUSTRALIA

BULLETIN 137

GEOLOGICAL EVOLUTION AND MINERALIZATION OF THE MURCHISON PROVINCE WESTERN AUSTRALIA

BY
KEITH P. WATKINS AND ARTHUR H. HICKMAN

with contributions from
Anthony L. Ahmat, Richard Davy, and Ian R. Fletcher

Perth 1990

MINISTER FOR MINES
THE HONOURABLE JEFF CARR M.L.A.

DIRECTOR GENERAL OF MINES
D.R. KELLY

DIRECTOR, GEOLOGICAL SURVEY OF WESTERN AUSTRALIA
PHILLIP E. PLAYFORD

National Library of Australia
Cataloguing-in-publication entry

Watkins, Keith P., 1954 –
Geological evolution and mineralization of the Murchison Province, Western Australia.

Bibliography
ISBN 0 7309 1003 2

1. Geology, Stratigraphic — Western Australia — Murchison Region. 2. Mineralogy — Western Australia — Murchison Region. 3. Murchison Region (W.A.). I. Hickman, A.H. (Arthur Hugh), 1947 – . II. Geological Survey of Western Australia. III. Title. (Series: Bulletin (Geological Survey of Western Australia); 137).

559.413

ISSN 0085 8137

Copies available from:
The Director
Geological Survey of Western Australia
100 Plain Street
East Perth, Western Australia 6004
Ph. (09) 222 3168

Contents

Page

Summary xiv

Chapter 1 Introduction

Location and geography of the study area 1
Previous investigations 2
Objectives and methods of investigation 2
Nomenclature 3
Supracrustal rocks 3
Dyke rocks and subvolcanic intrusions 3
Plutonic rocks 4
Geological framework 4
Boundaries of the Murchison Province 4
Weathering and alteration 4
Bulletin authorship 6

Chapter 2 Supracrustal rocks

Previous stratigraphic schemes 7
Method of stratigraphic subdivision and correlation 7
Murchison Supergroup 7
Distribution of rocks 8
Luke Creek Group 10
Murrouli Basalt 10
Definition and distribution 10
Lithostratigraphy 10
Geochemistry 14
Golconda Formation 21
Definition and distribution 21
Lithostratigraphy 22
Geochemistry 22
Gabanintha Formation 26
Definition and distribution 26
Lithostratigraphy 26
Geochemistry 28
Geochronology 45
Windaning Formation 49
Definition and distribution 49
Lithostratigraphy 50
Geochemistry 52
Mount Farmer Group 54
Porlell Subgroup 55
Definition and distribution of formations 55
Lordy Basalt 55
Stockyard Basalt 58
Woolgra Formation 58
Lithostratigraphy 58
Lordy Basalt 58
Stockyard Basalt 60
Woolgra Formation 61
Geochemistry 62
Sm–Nd geochronology 65
Yalgoo Subgroup 65
Definition and distribution of formations.. 65
Wadgingarra Basalt 65
Camberathunun Formation 67
Lithostratigraphy 67
Geochemistry 67
Quinns Basalt 69
Definition and distribution 69
Lithostratigraphy 70
Geochemistry 70
Mindoola Formation 74
Definition and distribution 74
Lithostratigraphy 74
Geochemistry 74

Page

Dalgaranga Formation 76
Definition and distribution 76
Lithostratigraphy 77
Geochemistry 78
Wattle Creek Basalt 79
Definition and distribution 79
Lithostratigraphy 79
Geochemistry 79
Billabalong Basalt 81
Definition and distribution 81
Lithostratigraphy 81
Coocoowilya Formation 81
Definition and distribution 81
Lithostratigraphy 81
Singleton Basalt 83
Definition and distribution 83
Lithostratigraphy 85
Geochemistry 85
Mougooderra Formation 88
Definition and distribution 88
Lithostratigraphy 91
Geochemistry 93
Wongan Hills greenstone belt 95
Styles of volcanism 96
Synthesis 96
Greenstone stratigraphy 96
Geochemistry 97
Origin and crystallization of mafic magmas 97
Origin and crystallization of felsic magmas 98
Bimodal volcanism 99
Chemostratigraphic variation 99
Geochronology 100

Chapter 3 Gneiss and granitoids

Pegmatite-banded gneiss 101
Field relations 101
Petrography 106
Geochemistry and petrogenesis 106
Geochronology and isotope geochemistry 109
Recrystallized monzogranite 111
Field relations 111
Petrography 118
Geochemistry and petrogenesis 119
Geochronology and isotope geochemistry 123
Post-folding granitoids 123
Field relations 123
Petrography 124
Geochemistry and petrogenesis 127
Geochronology and isotope geochemistry 130
Synthesis 136

Chapter 4 Mafic and ultramafic intrusive rocks

Gabbroid complex near Dalgaranga 137
Concordant sills 137
Cross-cutting intrusions 138

Chapter 5 Structure

Deformation scheme 141
D_1: horizontal structures 141
Pegmatite-banded gneiss 141
Luke Creek Group 141
D_2: east–west folding 143
D_2 structures in greenstones 143
D_2 structures in pegmatite-banded gneiss and recrystallized monzogranite 143
F_2–F_1 fold patterns 143
D_3: north–south folds 144
Major D_3 structures 144
Minor D_3 structures in greenstones 144
Minor D_3 structures in recrystallized monzogranite 144
Minor D_3 structures in pegmatite-banded gneiss 145
Fold patterns 145
F_3–F_1 fold patterns 145

Page

Dome-and-basin patterns 145
Large-scale heterogeneous D_3 strain 146
D_4: shear zones and faults 146
D_5: Mingah Range fault and shear-zone system 150
Fabric development. 151
Structural control of granitoid emplacement 151
Pegmatite-banded gneiss 151
Recrystallized monzogranite 152
Post-folding granitoids 152
Diapirism 152
Synthesis 153

Chapter 6 Metamorphism

Previous work 155
Compilation of Plate 3 155
Distribution of metamorphic facies 155
M_1: contact metamorphism of greenstones by mafic intrusions 156
Distribution of M_1 metamorphism 156
Mineral assemblages and textures 156
P–T conditions of M_1 metamorphism 156
M_2: contact metamorphism of greenstones by pegmatite-banded gneiss and recrystallized monzogranite protoliths 157
Distribution of M_2 metamorphism 157
Mineral assemblages and textures 158
P–T conditions of M_2 metamorphism 159
M_3: regional metamorphism of greenstones, pegmatite-banded gneiss, and recrystallized monzogranite 159
Distribution of M_3 metamorphism 159
Mineral assemblages and textures 159
P–T conditions of M_3 metamorphism 161
Timing of M_3 metamorphism 161
Big Bell metamorphism 162
Thermal model of metamorphism 162

Chapter 7 Economic geology

Gold 165
Description of gold deposits 165
Abbotts 165
Big Bell 168
Burnakura 169
Chesterfield 169
Cuddingwarra 169
Cue 170
Day Dawn 172
Fields Find 174
Gabanintha 175
Garden Gully (Kyarra) 175
Goodingnow (Paynes Find) 176
Gullewa 176
Lake Austin 177
Lennonville 178
Mainland 181
Meekatharra 181
Messenger Patch 186
Moyagee 187
Mount Gibson 187
Mount Magnet 187
Munarra Gully 192
Nannine 192
Noongal (Melville) 193
Pinnacles (Jasper Hill) 195
Quinns 196
Reedy 198
Rothsay 200
Stake Well 200
Star of the East 200
Tuckabianna 200
Tuckanarra 201
Warda Warra 201
Yalgoo 203
Yaloginda 203
Yuin 205
Minor gold mining centres and localities 205

Page

Additional gold occurrences 207
Discussion and interpretation 207
Regional distribution of gold deposits 207
Lithological associations of gold deposits 208
Structural controls 209
Association with post-folding granitoids and minor intrusions 212
Stratigraphic controls 214
Gold deposit types and associated alteration 214
Epigenetic 214
Syngenetic 216
Regional productivity variation 217
Relations to crustal evolution 218
Future exploration 220
Gold-related metals 221
Silver 221
Antimony 221
Arsenic 221
Copper–zinc 221
Golden Grove 224
Mount Mulcahy 224
Gabanintha 225
Iron ore 225
Koolanooka. 225
Mungada 225
Mount Gibson 225
Weld Range 226
Tallering Range 226
Lead 226
Tungsten–molybdenum–bismuth 226
Mount Mulgine 226
Callie Soak 227
Noongal 227
Bonnie Venture 227
Other minor occurrences 227
Vanadium–titanium 228
Gabanintha 228
Buddadoo 228
Nickel–chromium 228
Pegmatite metals 228
Beryllium 228
Lithium 229
Tin–tantalum 229
Other metals 229
Uranium 229
Platinum-group elements 230
Non-metallic and industrial minerals 230
Asbestos (chrysotile) 230
Barite 230
Construction material 230
Emerald 230
Feldspar 231
Gypsum 231
Kaolin 231
Magnesite 231
Ochre 231
Talc. 231

Chapter 8 Crustal evolution

Previous models of granite–greenstone evolution 233
Nature of the basement 233
Lithological evidence 233
Geophysical evidence 233
Geochemical and isotopic evidence 234
Evidence for ancient crustal rocks in adjacent terranes 234
Tectonic considerations 234
Conclusion 234
Model of crustal evolution for the Murchison Province 234
Constraints 234
Tectonic setting 235
Stages of crustal development 235

References. **241**

Appendices

Page

Appendix I. Localities referred to in the text 253

Appendix II. Geochemical analyses 257
Sample preparation and analyses 257
Computing methods 257
Variation in sample composition at a single locality 260

Appendix III. Geochronology 263
Sample preparation and analysis 263
Sm–Nd geochronology 263
Supracrustal rocks 263
Granitoid rocks 264
Rb–Sr geochronology 265

Plates

(in separate wallet)

1. Murchison Province: Precambrian geology and mineral deposits
2. Murchison Province: Stratigraphy, structure, and mineralization
3. Murchison Province: Metamorphic facies

Figures

Page

1. The three granite–greenstone provinces of the Yilgarn Craton 1
2. Distribution of major crustal components in the Murchison Province 5
3. The Murchison Supergroup: groups, subgroups, formations, and rock types 9
4. Sample traverses and outcrop geology of the Murrouli Basalt 11
5. Murrouli Basalt analyses plotted on AFM and Jensen diagrams 15
6. Chemostratigraphic variation in two of the Murrouli Basalt traverses 16
7. Y–Zr and Ti–Zr diagrams for Murrouli Basalt samples 18
8. Zr/Y–Zr diagram for Murrouli Basalt samples.. 19
9. Ni–MgO and Cr–MgO diagrams for the Murrouli Basalt 20
10. Y–Cr diagram for Murrouli Basalt samples 20
11. REE patterns for basalts from the Murrouli Range traverse 21
12. Geology of the type area for the Golconda Formation 22
13. Golconda Formation basalts plotted on an AFM diagram and a Jensen diagram 23
14. Zr–Al_2O_3 plot for banded iron-formation drill-core samples from The Island on CUE 24
15. High field strength element interrelationships for Golconda Formation basalts 25
16. REE patterns for Golconda Formation basalt from Swan Bore 26
17. Photograph of graded bedding in Gabanintha Formation epiclastic sandstone, 3 km west-northwest of Trenton Hill 28
18. Locations of sample traverses in the Gabanintha Formation. 29
19. Geological maps and stratigraphic columns of areas traversed for geochemical samples in the Gabanintha Formation 30
20. Gabanintha Formation volcanic rocks plotted on AFM and Jensen diagrams 36
21. Bimodal compositions of Gabanintha Formation volcanic rocks 38
22. Y–Zr diagrams for Gabanintha Formation basalt 44
23. Zr/Y–Zr diagrams for Gabanintha Formation tholeiitic basalt 45
24. Ni–MgO and Cr–MgO diagrams for Gabanintha Formation basalt 46
25. Cr–Y diagrams for Gabanintha Formation basalt 47
26. REE patterns for Gabanintha Formation basalts 48
27. Examples of stratigraphic variation in Gabanintha Formation basalt chemistry in individual sample traverses 48
28. Y–Zr diagram for Gabanintha Formation felsic volcanic rocks 50
29. Harker variation diagrams for Gabanintha Formation felsic volcanic rocks 51
30. REE patterns for Gabanintha Formation felsic volcanic rocks 52
31. Outcrop geology of the type area for the Windaning Formation 54
32. Photographs of Windaning Formation jaspilitic banded iron-formation, and Windaning Formation grey-white chert 54
33. Harker variation diagrams for Windaning Formation felsic volcanic rocks 56
34. Y–Zr and Ti–Zr diagrams for Windaning Formation volcanic rocks 57
35. REE patterns for Windaning Formation felsic volcanic rocks 57
36. Zr–Al_2O_3 plot for unweathered Windaning Formation jaspilitic banded iron-formation 57
37. Zr/Y–Zr and Cr–Y diagrams for Windaning Formation tholeiitic basalt from Noongal 58
38. Geological outcrop map of the Porlell Subgroup, showing sample locations and stratigraphic relations 59
39. Photograph of pyroclastic flow deposit in the Lordy Basalt 60
40. Photomicrograph of well-preserved pyroxene needle-spinifex texture 60
41. Photomicrograph of well-preserved basaltic texture in Stockyard Basalt tholeiite 61
42. Photograph of volcanogenic sedimentary rock from the Woolgra Formation, showing microfaulting and graded-bedding 61
43. Schematic stratigraphy of the Woolgra Formation 61
44. Bimodal composition of the Porlell Subgroup; A — SiO_2-frequency histogram, B — Jensen diagram 62
45. Y–Zr and Ti–Zr diagrams for Porlell Subgroup rocks 63
46. Zr/Y–Zr diagram for Porlell Subgroup tholeiitic basalt and Cr–Y diagram for Porlell Subgroup basalt 64
47. REE patterns for Porlell Subgroup basalt 65
48. Harker variation diagrams for Woolgra Formation felsic volcanic rocks 66
49. REE patterns for Woolgra Formation felsic volcanic rocks 67
50. Chemostratigraphic variation in the Woolgra Formation 67
51. Sm–Nd isochron plot for Woolgra Formation sample 81492 whole-rock, and mineral and material separates 68
52. Outcrop geology and schematic stratigraphy of the Yalgoo Subgroup, and locations of sample raverses in the Wadgingarra Basalt 69
53. Geochemistry of the Wadgingarra Basalt 71
54. Outcrop geology of the Quinns Basalt and location of geochemistry samples 72
55. Geochemistry of the Quinns Basalt 73
56. Outcrop geology of the Mindoola Formation showing locations of geochemistry samples in traverses 17 and 38 74
57. Photographs of Mindoola Formation high-Mg basalt pillow lava with interpillow breccia, and variolitic texture in Mindoola Formation high-Mg basalt 75
58. Y–Zr and Ti–Zr diagrams for the Mindoola Formation 76
59. Outcrop geology of the Dalgaranga Formation showing locations of geochemistry samples 77
60. Photograph of compositional banding in Dalgaranga Formation dacite tuff 78

Page

61. Photograph of volcanogenic sandstone and conglomerate in the Dalgaranga Formation 78
62. Y–Zr diagram for Dalgaranga Formation felsic volcanic rocks 79
63. Harker variation diagrams for Dalgaranga Formation felsic volcanic rocks 80
64. REE patterns for Dalgaranga Formation felsic volcanic rocks 81
65. Outcrop geology of the Wattle Creek Basalt 82
66. Stratigraphy of the Wattle Creek Basalt in the type area 83
67. Outcrop geology of the Billabalong Basalt 83
68. Schematic stratigraphy of the Billabalong Basalt 84
69. Photograph of fine layering in tholeiitic tuff in the Billabalong Basalt 84
70. Outcrop geology of the Coocoowilya Formation 84
71. Outcrop geology, sample locations, and schematic stratigraphy of the Singleton Basalt 86
72. Photographs of pyroclastic basalt breccia with tuffaceous matrix; and fine-grained basalt tuff 88
73. Geochemistry of the Singleton Basalt 89
74. Distribution, outcrop geology, and geochemistry sample localities of the Mougooderra Formation in the southern Murchison Province 90
75. Photograph of conglomerate at the base of the Mougooderra Formation 92
76. Geochemistry of Mougooderra Formation basalt 94
77. Regional setting and geology of the Wongan Hills greenstone belt 95
78. Schematic disposition of stratigraphic formations in the Murchison Supergroup 97
79. Compositional fields of Murchison Supergroup high-Mg basalt and tholeiitic basalt on a Cr–Y diagram 98
80. Compositional fields of the two types of Murchison Supergroup basalt plotted on Y–Zr and Ti–Zr diagrams 98
81. Compositional fields and REE pattern characteristics of the two types of Murchison Supergroup felsic volcanic rocks 99
82. Compositional fields of mafic and felsic volcanic rocks from bimodal sequences in the Murchison Supergroup plotted on an Y–Zr diagram 99
83. Photograph of monzogranite–granodiorite component of pegmatite-banded gneiss 101
84. Photograph of interlayered monzogranite–granodiorite gneiss and pegmatite bands forming typical pegmatite-banded gneiss 102
85. Photograph of raft of pegmatite-banded gneiss in recrystallized monzogranite from the western part of the Murchison Province 102
86. Photograph of two phases of monzogranite–granodiorite gneiss, showing a dyke of monzogranite gneiss truncating banding in the surrounding gneiss 103
87. Photograph of pegmatite-banded gneiss interlayered with amphibolite, at the margin of a large amphibolite-BIF raft in the gneiss 103
88. Photograph of recrystallized monzogranite dyke and veins intruding pegmatite-banded gneiss 104
89. Photograph of intrusive contact between porphyritic recrystallized monzogranite and the margin of a large coherent raft of pegmatite-banded gneiss 104
90. Photograph of partly assimilated xenolith of pegmatite-banded gneiss in equigranular recrystallized monzogranite 104
91. Photographs of examples of nebulitic banding in recrystallized monzogranite 105
92. Photographs of injection migmatites formed by lit-par-lit intrusion of a fractionated phase of recrystallized monzogranite into pegmatite-banded gneiss 105
93. Complexly folded and interlayered BIF, amphibolite, and pegmatite-banded gneiss, south of Yalgoo 106
94. Photomicrograph of pegmatite-banded gneiss showing granoblastic texture 107
95. Photomicrograph of pegmatite-banded gneiss showing mortar texture 107
96. Granitoid geochemistry sample localities 108
97. Log(CaO/(Na_2O + K_2O))–SiO_2 diagram for pegmatite-banded gneiss samples compared with other Archaean granitoids and gneisses 109
98. Pegmatite-banded gneiss compositions plotted on a Na_2O–K_2O–CaO ternary diagram 109
99. Major oxide Harker variation diagrams for pegmatite-banded gneiss samples 110
100. Pegmatite-banded gneiss compositions on a Rb–Sr plot 111
101. REE patterns for Badja pegmatite-banded gneiss 112
102. Pegmatite-banded gneiss compositions plotted on CIPW norm diagrams 112
103. Distribution of map figures which show locations of granitoid geochronology samples 113
104. Locations of pegmatite-banded gneiss geochronology samples 114
105. Rb–Sr isochron plots for pegmatite-banded gneiss 115
106. Photographs of textures of recrystallized monzogranite 115
107. Photographs of cognate inclusions in recrystallized monzogranite 116
108. Photographs of accidental xenoliths in recrystallized monzogranite 116
109. Photographs of features of recrystallized monzogranite–greenstone belt contact zones 117
110. Photograph of pegmatites intruding recrystallized monzogranite 118
111. Photomicrographs of foliated recrystallized monzogranite 118
112. Photomicrographs of unfoliated recrystallized monzogranite 119
113. Log(CaO/(Na_2O + K_2O))–SiO_2 diagram for recrystallized monzogranite compared with pegmatite-banded gneiss and other Archaean granitoids and gneisses 120
114. Recrystallized monzogranite compositions plotted on a Na_2O–K_2O–CaO ternary diagram 120
115. Major oxide Harker variation diagrams for recrystallized monzogranite 121
116. REE patterns for recrystallized monzogranite samples 122
117. Recrystallized monzogranite compositions plotted on CIPW norm diagrams 123
118. Locations of recrystallized monzogranite geochronology samples 124

Page

119. Rb–Sr isochron plots for recrystallized monzogranite 125
120. Photographs of xenoliths in post-folding granitoids 126
121. Photomicrograph of post-folding granitoid with igneous hypidiomorphic granular texture 127
122. Photomicrograph of post-folding monzogranite of the Damperwah pluton showing two-phase textural development of quartz 127
123. Photomicrograph of post-folding syenogranite of the Koolanooka pluton showing bimodal grain-size distribution 127
124. Log(CaO/(Na_2O + K_2O))–SiO_2 diagram for post-folding granitoids compared with recrystallized monzogranite, pegmatite-banded gneiss, and other Archaean granitoids 129
125. Post-folding granitoid compositions plotted on a Na_2O–K_2O–CaO ternary diagram 130
126. Major oxide Harker variation diagrams for post-folding granitoids 131
127. REE patterns for post-folding granitoid samples 132
128. Post-folding granitoid compositions plotted on CIPW norm diagrams 133
129. Locations of post-folding granitoid geochronology samples 134
130. Rb–Sr isochron plots for post-folding granitoids 135
131. Geology of the gabbroid complex near Dalgaranga 138
132. Azimuths of late cross-cutting mafic dykes in the Murchison Province 139
133. Photograph of dome-and-basin fold pattern in pegmatite-banded gneiss 141
134. Fold patterns in greenstone belts 142
135. Photograph of minor F_1 rootless isocline in banded iron-formation, north of Mount Yagahong 143
136. Photograph of anastamosing shear surfaces in high-Mg basalt 144
137. Photographs of minor F_3 folds in banded iron-formation, east of Poona and near Gnows Nest 145
138. Photograph of xenoliths of felsic volcanic rocks in the marginal zone of a recrystallized monzogranite southeast of Pindathuna Homestead 145
139. Photographs of S_3 foliation in recrystallized equigranular monzogranite and porphyritic monzogranite 146
140. Minor F_3–F_1 interference fold in banded iron-formation from the Island on CUE 147
141. Minor dome-and-basin fold patterns in pegmatite-banded gneiss and in sedimentary rocks of the Mougooderra Formation 148
142. Simplified geology of the Yalgoo region showing large-scale fold patterns 149
143. D_4 fault and shear-zone azimuths 150
144. Photographs of recrystallized, silicified, quartz–andalusite mylonite, and cataclastic mylonite, in shear zones 150
145. D_5 Mingah Range fault and shear-zone azimuths 150
146. Photomicrograph of recrystallized penetrative foliation in amphibolite 151
147. Photomicrograph of recrystallized mylonite 151
148. Photograph of boudinaged amphibolite unit in pegmatite-banded gneiss, 5 m from a major contact with greenstones 152
149. Photomicrograph of granoblastic texture in mafic granulite from the M_1 contact aureole surrounding the layered mafic intrusion southwest of Gabanintha 157
150. Photomicrograph of granoblastic texture in an amphibolite raft in monzogranite 159
151. Photomicrographs of partial retrogression due to overprinting of M_2 assemblages by M_3 metamorphism 161
152. Metamorphic models for eastern Yilgarn greenstone belts 162
153. Qualitative thermal model for Murchison Province metamorphism 163
154. Distribution and relative productivity of the principal gold-producing centres in the Murchison Province 166
155. Geological setting of the principal mines at Cue and Day Dawn 171
156. Geological setting of the principal mines at Mount Magnet and Lennonville 179
157. Geological setting of the principal mines at Meekatharra 182
158. Geological map of Paddys Flat, Meekatharra 183
159. Vertical aerial photograph of the area between Mount Magnet and Star Pit 191
160. Geological map of Noongal 194
161. Geological map of Quinns 197
162 Geological map of Reedy 199
163. Geological map of Tuckanarra 202
164. Geological map of Yaloginda 204
165. Lithological associations of Murchison Province gold deposits 209
166. Metallogenetic domains (gold) of the Murchison Province 210
167. Host lithologies of the four metallogenetic domains of the Murchison Province 211
168. Major shear zones and faults of the Murchison Province 213
169. Principal types of Murchison Province gold deposits 215
170. Differences in gold mineralization, northeastern and southwestern parts of the Murchison Province 218
171. Crustal evolution in the Murchison Province 136

Tables

		Page
1.	Precambrian geological history of the Murchison Province	6
2.	Comparison of Hallberg's (1976) and Baxter's (1982) regional stratigraphic compilations of Murchison Province greenstone belts	8
3.	Mean compositions of Murrouli Basalt tholeiite units	14
4.	Mean compositions of Golconda Formation banded iron-formations	23
5.	Mean compositions of Golconda Formation basalts	24
6.	Central felsic volcanic centres in the Gabanintha Formation	27
7.	Sample traverses on the Gabanintha Formation	35
8.	Mean compositions of Gabinantha Formation Type-I and Type-II basalts	39
9.	Mean compositions of Gabanintha Formation Type-I tholeiitic basalt	40
10.	Mean compositions of Gabanintha Formation Type-I high-Mg basalt	41
11.	Mean compositions of Gabanintha Formation Type-II tholeiitic basalt	42
12.	Mean compositions of Gabanintha Formation Type-II high-Mg basalt	43
13.	Mean compositions of Gabanintha Formation felsic volcanic rocks	49
14.	Published geochronology of the Gabanintha Formation	53
15.	Mean compositions of Windaning Formation banded iron-formation	55
16.	Mean compositions of Windaning Formation felsic volcanic rocks	55
17.	Mean compositions of four Windaning Formation tholeiitic basalts from Noongal	55
18.	Mean compositions of Lordy Basalt	63
19.	Mean compositions of Stockyard Basalt	64
20.	Mean compositions of dacite and andesite lava from the Woolgra Formation	65
21.	Mean compositions of Wadgingarra Basalt	70
22.	Mean compositions of Quinns Basalt	72
23.	Mean compositions of Mindoola Formation Basalts	76
24.	Mean compositions of Dalgaranga Formation felsic volcanic rocks	78
25.	Mean compositions of Singleton Basalt	88
26.	Mean compositions of Mougooderra Formation sedimentary rocks	93
27.	Mean compositions of Mougooderra Formation basalts	93
28.	Mean compositions of pegmatite-banded gneiss	109
29.	Mean compositions of recrystallized monzogranite	120
30.	Published Rb–Sr isochrons of Murchison Province granitoids	126
31.	Mean compositions of post-folding granitoids	128
32.	Chemistry of mineral phases and geothermometry of M_1 granulite facies rocks	158
33.	Compositions of garnet and biotite, and geothermometry of M_2 mineral assemblages	160
34.	Total production of gold from the Murchison Province prior to 31 December 1987	167
35.	Total gold production from the principal mines at the Cue mining centre to 31 December 1987	172
36.	Total gold production from the principal mines at the Day Dawn mining centre to 31 December 1987	173
37.	Total gold production from the principal mines at the Lennonville mining centre to 31 December 1987	180
38.	Total gold production from the principal mines at the Mount Magnet mining centre to 31 December 1987	188
39.	Minor gold-mining centres and localities	206
40.	New gold occurrences identified in the Murchison province	208
41.	Historical gold production (to 31 December 1987) of deposits associated with the major faults and shear zones of the Murchison Province	212
42.	Gold mineralization during the Archaean crustal evolution of the Murchison Province	219

Summary

Chapter 1: Introduction

The Murchison Province is the westernmost of three granite–greenstone provinces which, with the Western Gneiss Terrane, comprise the Archaean Yilgarn Craton. The province is about 100 000 km^2 in area, less than 5% of which is exposed rock. Many outcrops were affected by deep weathering in the Cainozoic. The landscape is generally flat and monotonous and the climate is semi-arid. The first economic discovery of gold was made in 1890 at Yuin; gold mining has since developed into the main industry of the region. Most previous geoscientific investigations were related to the Geological Survey of Western Australia 1:250 000 mapping program in the region, between 1966 and 1983, although much unpublished work has been done by mineral exploration companies.

The principal aim of this bulletin is to describe and relate the geological evolution of the province and its mineral deposits (principally gold). Between 1982 and 1986 the CUE 1:250 000 sheet was remapped and reconnaissance mapping of the rest of the province was undertaken. Detailed mapping was carried out around major mining centres; 1382 rock samples were analysed for major oxides and/or trace elements, and 2500 thin sections of rocks collected during this study, and by previous workers, were examined. Three 1:500 000 scale geological maps covering 95 000 km^2 of the Murchison Province were compiled from this work:

Plate 1: Precambrian geology and mineral deposits
Plate 2: Stratigraphy, structure, and mineralization
Plate 3: Metamorphic facies.

Chapter 2: Supracrustal rocks

The supracrustal rocks of the greenstone belts comprise the Murchison Supergroup, which is divided into two groups, the Luke Creek Group, and the overlying Mount Farmer Group. The four component formations of the Luke Creek Group are continuous throughout most greenstone belts in the province, forming a layered stratigraphy about 10 km thick. In contrast, the Mount Farmer Group comprises the remnants of nine broadly contemporaneous volcanic centres and one epiclastic sedimentary basin, each of limited lateral extent, developed on an infrastructure of Luke Creek Group rocks. This group has a maximum preserved thickness of 5 km. The supergroup consists of about 70% mafic rocks and 20% felsic volcanic and associated volcaniclastic rocks. Of the remainder, in the Luke Creek Group about 5% are banded iron-formation, and 5% are ultramafic rocks; in the Mount Farmer Group about 4% are ultramafic rocks, and 6% are epiclastic sedimentary rocks.

Tholeiitic basalt was derived by varying degrees of partial melting (5–30%) of upper mantle plagioclase lherzolite, followed by crystal fractionation of olivine, pyroxenes and, for fractionated rocks, plagioclase and magnetite. High-Mg basalt may have been generated by further partial melting of olivine-rich residues. There were fundamental differences in the chemistry of the upper mantle beneath the southern and northern parts of the Murchison Province during development of the Luke Creek Group; these are reflected in the compositions of basaltic rocks. However, there is no evidence for regional variation in the chemistry of Mount Farmer Group basaltic rocks, most of which have been contaminated by assimilation of felsic crustal material. Felsic volcanic rocks were derived by partial melting of both mafic and felsic crustal source rocks.

There may be an appreciable time gap between formation of the two stratigraphic groups. U–Pb zircon data from rocks of the upper part of the Luke Creek Group give ages of around 3000 Ma. A Sm–Nd isochron age of 2818 ± 57 Ma was determined on mineral separates from the Woolgra Formation of the Mount Farmer Group in the northern Murchison Province.

Chapter 3: Gneiss and granitoids

Four suites of siliceous plutonic rocks have intruded the Murchison Supergroup. Two have been folded and metamorphosed and are now pegmatite-banded gneiss and recrystallized monzogranite. The other two, post-folding granitoids suite I and suite II, retain igneous mineralogy and texture.

Pegmatite-banded gneiss protoliths comprising granodiorite, monzogranite, and pegmatite intruded the base of the Luke Creek Group as subhorizontal sheets at about 2920 Ma. These rocks are preserved in a belt in the west of the province and elsewhere as rafts and enclaves in recrystallized monzogranite. Their abundance decreases towards the east.

Voluminous intrusions of monzogranite intruded the base of the Murchison Supergroup as thick subhorizontal sheets. Two of these intrusions gave U–Pb zircon ages of 2690 Ma and 2681 Ma. They now occupy much of the regions between greenstone belts. This suite was recrystallized during regional metamorphism.

Post-folding granitoid plutons have subcircular and oval-shaped outcrops, and truncate stratigraphic units and tectonic features associated with folding. They intrude only greenstone belts, and have not been found wholly within older granitoid bodies. Suite I comprises tonalite, trondhjemite, granodiorite, and monzogranite plutons, confined mainly to the northern Murchison Province; suite II plutons comprise quartz-rich monzogranite and syenogranite plutons, confined mainly to the southern part of the province. Two suite II plutons gave U–Pb zircon ages of 2641 Ma and 2617 Ma.

Pegmatite-banded gneiss, recrystallized monzogranite, and suite I post-folding granitoids were derived by partial melting of mafic crustal rocks. Most suite II post-folding granitoids were derived by partial melting of siliceous granulite which was older than the other source rocks and at least as old as basal greenstones.

Chapter 4: Mafic and ultramafic intrusive rocks

Two types of mafic and ultramafic intrusions are abundant: concordant sills in greenstone belts, and cross-cutting dykes, sills, and plugs in both granitoids and greenstones. Subvolcanic concordant sills occur in all basalt sequences. Many are composite bodies, exceeding 1 km in thickness, comprising numerous thin sills and screens of country rock. Cross-cutting intrusions of dolerite and gabbro, most of which are dykes, represent the last phase of igneous activity in the Murchison Province, about 2400 Ma.

A major layered ultramafic–mafic body intrudes the Dalgaranga greenstone belt. It consists of a stack of seven broadly conformable sills, six of them at least 1 km thick. The sills become more differentiated upwards in the stack, from an olivine-norite sill at the base to the two uppermost sills, each consisting of layers of peridotite, pyroxenite, gabbro, and quartz leucogabbro.

Chapter 5: Structure

Five regional phases of deformation affected Murchison Province granitoids and greenstones. The first phase involved recumbent folding and thrusting of Luke Creek Group rocks, and development of banding in pegmatite-banded gneiss. Upright, easterly trending, tight folds developed during the second phase of deformation which affected pegmatite-banded gneiss, recrystallized monzogranite, and the whole of the Murchison Supergroup. Much more intense, north-northeasterly to north-northwesterly trending, upright, tight and isoclinal folds and associated penetrative fabrics formed during the third phase of deformation which established the dominant tectonic grain of the province. Large-scale shear zones formed during the fourth phase of deformation. Many are over 100 km long, up to 1 km wide, and probably extend at least to the lower crust. Movements appear to be mainly dextral with offsets of several kilometres, although some record vertical movements. These shear zones probably controlled emplacement of post-folding granitoids. There was much overlap between the third and fourth phases of deformation which were generated during the same compression event. Dome-and-basin fold patterns, formed by refolding of second phase folds by third phase folds, and by generation of large-scale sheath folds in fourth phase shear zones, largely control the present distribution of granites and greenstones. The last phase

of deformation is confined to the northwestern Murchison Province. A system of easterly to southeasterly trending shear zones and faults imbricated the Mingah Range greenstone belt and surrounding granitoids. These structures are probably related to the Proterozoic Capricorn Orogeny to the northwest of the Yilgarn Craton.

Chapter 6: Metamorphism

Three types of metamorphism have been recognized in the Murchison Province. The first is amphibolite and granulite facies contact metamorphism of greenstones by large mafic intrusions. This is of local importance and only one contact aureole, near Gabanintha, is well preserved. The second type is low- to mid-amphibolite facies contact metamorphism of basal greenstones by pegmatite-banded gneiss and recrystallized monzogranite protoliths. Contact aureoles vary from a few hundred metres to a few kilometres wide and were superimposed on a pre-existing regional thermal gradient. The third type is regional metamorphism of the Murchison Supergroup, pegmatite-banded gneiss, and recrystallized monzogranite. This metamorphism was in greenschist facies for most of the province, but was in amphibolite facies in the southwest, and prehnite–pumpellyite facies in the cores of two greenstone belts in the north. Regional metamorphism followed dome-and-basin folding. It was caused by thermal relaxation towards steady-state conditions of folded isotherms which resulted in heating in synclines and cooling in anticlines. Synclinal greenstone belts record prograde metamorphism in greenschist and amphibolite facies which overprinted earlier contact metamorphic aureoles. Anticlinal granitoids record retrograde metamorphism from igneous mineral assemblages to greenschist and amphibolite facies assemblages. Thermal relaxation was terminated by uplift and erosion before steady-state conditions were achieved, resulting in lower metamorphic grade in the cores of some greenstone belts. Greater uplift exposed higher grade rocks in the southwest of the province. Post-folding granitoids intruded greenstone belts during the uplift stage and were probably generated by metamorphic processes deep in the crust.

Chapter 7: Mineralization

In terms of past production, the Murchison Province is Western Australia's second most important gold-mining region after the Eastern Goldfields. Major opportunities still exist for further exploration and important new discoveries.

Gold mineralization is almost entirely epigenetic and is intimately associated with major faults and shear zones through the greenstone belts of the area. It is preferentially hosted by banded iron-formation, and ultramafic and mafic rocks, and is largely restricted to the lower part of the stratigraphic succession. Many deposits occur within about 3 km of post-folding granitoid contacts, suggesting either a genetic relationship to granitic intrusion (perhaps through greenstone dehydration along paths of magma ascent) or common source regions and structural controls.

There is a major difference between the historical productivities of the northeastern and southwestern halves of the province, the northeast averaging 31 kg Au/km^2 from greenstone belts, and the southwest 1.7 kg/km^2. Moreover, three distinct metallogenic domains can be recognized in the northeast, each dominated by a particular style of gold mineralization. Gold-bearing hydrothermal fluids were generated in the lower crust, and possibly upper mantle, in response to elevated P–T conditions in areas of large-scale downward crustal movements. Productivity differences between the northeast and southwest, and variations between the northeastern domains, are consistent with differences in source composition, regional structure, and available host lithologies.

Archaean gold mineralization was not a single event but spanned a period of some 400 million years. Although most gold deposits formed shortly after the peak of regional metamorphism, and are therefore about 2650–2600 million years old, older episodes of mineralization are represented by a 3000 Ma syngenetic base-metal–gold deposit, 2800 Ma conglomerate-hosted gold deposits, and epigenetic deposits associated with earlier deformation events.

Mineral commodities other than gold have been of little economic significance.

Chapter 8: Crustal evolution

Models for the evolution of granite–greenstone terranes depend critically on the nature of the basement and the type of tectonic regime that existed. Both of these factors are poorly understood for the Archaean. Several lines of evidence suggest that the basement to the Murchison Supergroup consisted of siliceous granulite overlying mafic granulite. These layers were heterogeneous and contained units of garnet amphibolite and tonalite. The tectonic setting for initial development of greenstones was probably a large extensional ensialic basin.

Extensive basalt lava plains formed in deep water on the basin floor, generated by partial melting of uppermost mantle rocks beneath the subsiding basin. Elevation of isotherms, due to mafic magmatic activity and subsidence, induced partial melting in the crust which generated felsic-volcanic complexes, locally containing base-metal mineralization. Banded iron-formations were deposited during quiescent periods in the waning stages of two major volcanic episodes.

Following deposition of the Luke Creek Group, horizontal tectonic compression associated with closure of the basin formed recumbent folds and thrusts. Some epigenetic gold mineralization is associated with these thrusts. During this deformation, at about 2920 Ma, pegmatite-banded gneiss protoliths intruded the base of the Luke Creek Group as thick sheets.

Mount Farmer Group shield volcanoes and stratovolcanoes developed in shallow-water to subaerial environments on an infrastructure of Luke Creek Group rocks. An epiclastic sedimentary basin also developed about this time in the southern part of the province. Conglomerate-hosted gold deposits indicate erosion of earlier syngenetic and epigenetic gold deposits in the Luke Creek Group.

Thick subhorizontal sheets of monzogranite intruded the base of the Murchison Supergroup; two of these have been dated at 2690 Ma and 2680 Ma. This was followed, within 40 million years, by large-scale dome-and-basin folding and regional metamorphism. The folding resulted from lateral compression and was largely responsible for the granite–greenstone pattern. Major shear zones developed as a result of continuing regional compression, from late in the last phase of folding to some time after intrusion of post-folding granitoids, later than 2617 Ma. Post-folding granitoid magmas may have used the shear zones as pathways for ascent to the upper crust.

Most epigenetic gold mineralization occurs in or adjacent to the shear zones or associated fracture systems. The deposits are concentrated within banded iron-formation, chert, basalt, and ultramafic rocks of the upper three formations of the Luke Creek Group. They formed after the peak of regional metamorphism, at temperatures in the range 250–350°C and pressures of 100–250 MPa.

Swarms of dolerite and gabbro dykes, with less abundant plugs and sills, intruded the crust about 2400 Ma. The northwest of the province was imbricated by shear zones and faults associated with the Capricorn Orogeny on the northwest margin of the Yilgarn Craton.

Chapter 1

Introduction

Location and geography of the study area

The Murchison Province is the westernmost of three granite–greenstone provinces in the Yilgarn Craton, an Archaean craton in the southern part of Western Australia (Gee et al., 1981). For this study the geology of a 95 000 km^2 region was investigated, comprising the main greenstone belts and associated granitoids of the province (Fig. 1).

The towns of Meekatharra (1018), Cue (399), Mount Magnet (1000), Perenjori (241), Morawa (595), Yalgoo, Paynes Find, and Pindar lie within the area studied (1986 population census figures given for towns with a population of more than 200). There are numerous sheep stations in the region, and in the southwest of the area much land has been cleared for arable farming of wheat and other crops. Outside the wheat-farming areas, gold mining is the main industry.

The climate is semi-arid for most of the area; average annual rainfall is about 200 mm in the northern and central regions, increasing rapidly towards the southwest to about 350 mm. In the low rainfall region the flora is dominated by mulga (*Acacia*) bush and annual grasses. In the higher rainfall region, in the southwest, gum (*Eucalyptus*) trees are abundant in some areas, particularly over greenstone rocks. Saltbush is abundant near salt lakes, and river gums proliferate on the banks of major creeks throughout the region (Beard, 1976; Groves, 1981).

Most of the land is flat and monotonous; its elevation varies gradually between about 280 m and 680 m above sea level. The southeastern two-thirds of the region forms part of Jutson's (1950) 'Salinaland' and the northwestern part is in Jutson's (1950) 'Murchisonia'. Salinaland is characterized by many salt lakes, some forming chains, which constitute the main drainages. Intermittent creeks drain internally into these lake systems. Watercourses in 'Murchisonia' are the larger intermittent creeks, such as the Murchison and Sanford Rivers, which drain westwards, ultimately into the Indian Ocean. A broad, low, northeasterly trending watershed separates these divisions.

During the Oligocene and Miocene, when the Yilgarn region had a humid tropical climate, a deeply weathered layer consisting mainly of laterite duricrust overlying saprolite developed over most of the craton (Butt, 1981). It formed a gently undulating surface overlain by sand derived from the laterite; isolated ranges of hills rose above this surface. The surface was extensively dissected and is now preserved as mesas and tablelands of duricrust, most of them overlain by sandplain and bounded by breakaways. Rock is exposed in areas of active sheetwash between the duricrust plateau and watercourses, where erosion has cut

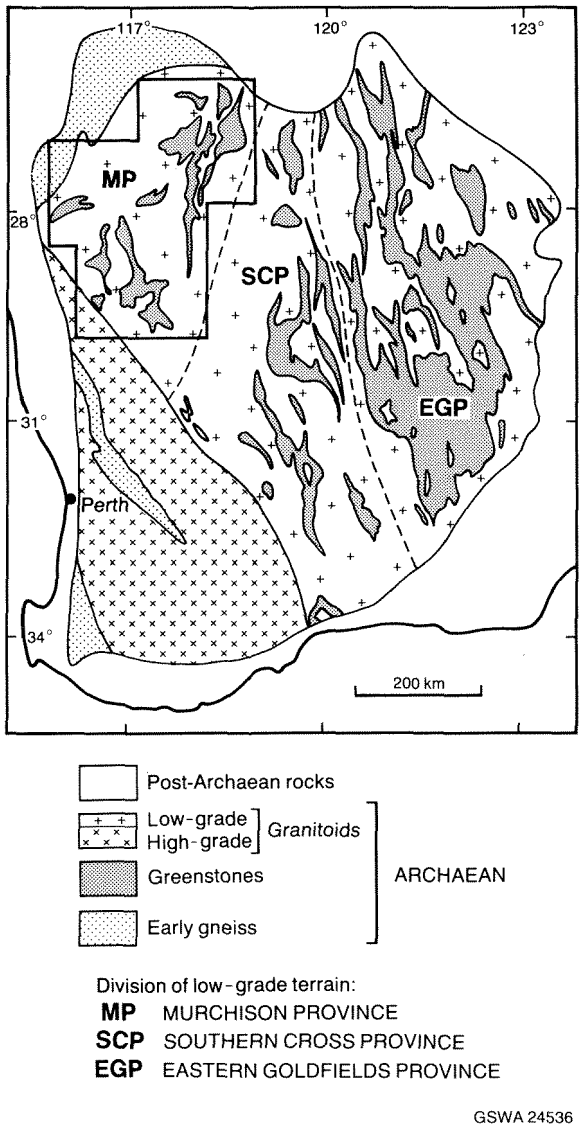


Figure 1. The three granite–greenstone provinces of the Yilgarn Craton. The area studied is indicated.

below the saprolite zone or where outcrops were originally higher than the duricrust plateau. The major drainages (i.e. major creeks and salt lake systems) are probably remnants of an ancient river system which has been successively superimposed on the Tertiary plateau and on the present erosion surface (Johnstone et al., 1973; van de Graaff et al., 1977; Butt, 1981). Large calcrete deposits occur in and around these drainage systems. Supracrustal rocks generally form subdued, elongate hills, and many prominent ridges and ranges contain layers of banded iron-formation, or gabbroid intrusions. Granitoid rocks are exposed as prominent monoliths or 'whalebacks' and as flat pavements. Less than five percent of the region is exposed rock.

Previous investigations

Exploration

The first European explorers in the region were A. C. and F. T. Gregory, who traversed the region in 1846 (Gregory and Gregory, 1884), and R. C. Austin, the Government Assistant Surveyor (Austin, 1855). The exploration journals of Forrest (1875) and Giles (1889) also contain references to the region.

The first economic gold discovery was made at Yuin in 1890 (Maitland, 1919). A gold rush followed discovery of gold at Nannine in 1891, and most gold-producing centres had been discovered by the end of 1892.

Geoscientific studies

Most published work on the Murchison Province has been written by staff of the Geological Survey of Western Australia (GSWA). Earlier accounts focused on the geology of gold-mining centres, but later work was concerned mainly with regional geology, particularly the production of 1:250 000 scale geological maps. Between 1973 and 1985 the GSWA published first edition 1:250 000 scale geological maps of CUE* (de la Hunty, 1973), MURGOO (Baxter, 1974), YALGOO (Muhling and Low, 1977), BELELE (Elias, 1982), GLENGARRY (Elias et al., 1982), KIRKALOCKA (Baxter et al., 1983), NINGHAN (Lipple et al., 1983), PERENJORI (Baxter and Lipple, 1985), and SANDSTONE (in collaboration with the Bureau of Mineral Resources (BMR), Tingey, 1985). Subsequently, a second edition 1:250 000 scale geological map of CUE was published (Watkins et al., 1987). In addition, Watkins (1990) has compiled a summary of the geology of the Murchison Province.

The BMR has published 1:250 000 and 1:1 000 000 scale aeromagnetic, radiometric, and Bouguer anomaly gravity maps covering the Murchison Province. Some of these aeromagnetic and radiometric data have been interpreted by Waller and Beattie (1971).

All earlier work in the Murchison Province, by GSWA staff and others, is cited in the explanatory notes which accompany GSWA 1:250 000 scale geological maps. Subsequent published work is cited in appropriate sections of this bulletin. Much work has been done by mineral exploration company geologists, but little has been published.

Objectives and methods of investigation

The main objectives of this bulletin are to describe the geological evolution of Murchison Province greenstone belts and associated granitoids, and to document the main occurrences and styles of mineralization and to relate these to the regional geology.

One hundred and sixteen man-weeks of fieldwork were completed during 1982–1986. During this period the CUE 1:250 000 sheet was remapped (Watkins et al., 1987) and reconnaissance mapping of the remaining area was carried out. Detailed mapping was undertaken in regions of structural and/or stratigraphic interest, around principal mining centres, and where previous mapping was in error. Approximately 2500 thin sections of rocks collected in the region were examined. These included some samples from earlier studies by the Geological Survey. Three 1:500 000 scale maps (in separate wallet) were compiled from this work:

Plate 1: Precambrian geology and mineral deposits
Plate 2: Stratigraphy, structure and mineralization
Plate 3: Metamorphic facies

A total of 1382 rock samples were analysed for major oxides and/or trace elements (Appendix II). Samples were assigned to one of four groups:

(a) Volcanic rocks — 742 samples were collected, mainly from traverses across stratigraphic formations. These samples were collected for studies of chemostratigraphy and petrogenesis; a few clastic sedimentary rock samples were included in this group. The sampling interval varied between a few tens of metres and a few hundred metres, depending on availability of fresh outcrop. At each sampling locality, 1–2 kg of fresh, representative material was collected. Rocks containing veins, varioles, amygdules, or other heterogeneities were avoided.

(b) Granitoids — 191 samples were collected for classification and petrogenetic studies. At each sampling locality, 2–4 kg of fresh, representative material was collected. In most cases splits of these samples were made for isotopic analysis.

(c) Banded iron-formation (BIF) — 208 samples were collected from traverses across stratigraphic formations and from drill core. These samples were collected

* Map sheet names are printed in capitals to avoid confusion with identical place names.

for chemostratigraphic and mineralization studies. At each surface sample locality, 1–3 kg of representative material was collected. Samples were obtained from drill core at two sites, to compare fresh material with the oxidized surface samples; each sample consisted of up to 30 cm of half or quarter core.

(d) A total of 241 miscellaneous samples were collected from mineral deposits or prospects for mineralization studies.

Forty samples, included in groups (a) and (b), were collected for an investigation of compositional variation at single-sample localities. Eight samples were collected from each of five sites, which were generally < 9 m^2 in area. Lithologies sampled in this way were high-Mg basalt, tholeiitic basalt, dacite, recrystallized monzogranite, and a post-folding granitoid. An analysis of the variations in composition of each group of these samples is given in Appendix II. Also given there are descriptions of sampling, analytical and computation procedures, and listings of analyses for each of the four sample groups (on microfiche in pocket at back).

One hundred and fifteen samples were collected for Rb–Sr, Sm–Nd, and U–Pb isotopic analyses to provide radiometric ages and petrogenetic information. Sampling and analytical procedures are described in Appendix III. Tables of isotopic results are also given in this appendix.

Nomenclature

Supracrustal rocks

All supracrustal rocks in the Murchison Province were metamorphosed under conditions ranging from prehnite–pumpellyite to granulite facies. In addition, most rocks have been deformed, and many are now schistose or strongly foliated and/or lineated. Igneous or sedimentary nomenclature is used where the protolith has been clearly identified, otherwise metamorphic terms are used.

Ultramafic rocks

Most ultramafic rocks are schistose, and igneous features are poorly preserved; hence, metamorphic names are generally used here. Following Arndt and Nisbet (1982, p. 23) ultramafic volcanic rocks are termed komatiites. Most have olivine bladed-spinifex texture with MgO > 18% (anhydrous). Ultramafic cumulates formed by settling of mafic minerals within basaltic flows are not included in this definition (Arndt and Nisbet, 1982, p. 23).

Mafic rocks

The composition of basalt in the Murchison Province forms a continuous spectrum between tholeiite with high Fe and V, and basalt with high Mg, Ni, and Cr. Different terms have been used to describe high Mg–Ni–Cr basalt, including high-Mg basalt, magnesian basalt, komatiitic basalt, and mafic komatiite (Arndt and Nisbet, 1982; Hallberg, 1983). There is little agreement on criteria for distinguishing between these rocks and tholeiitic basalt (see references cited in Arndt and Nisbet, 1982). These authors propose that high Mg–Ni–Cr basalt which is spatially associated with komatiite, and which has spinifex texture, should be called komatiitic basalt. However, komatiite is very rare in the Murchison Province, and although most high Mg–Ni–Cr basalt contains spinifex texture, much does not. Furthermore, some basalts with tholeiitic chemistry contain needle-spinifex texture. Following Hallberg (1983), the non-genetic term 'high-Mg basalt' is used for these rocks. For the purposes of classification in the computer file (Appendix II, microfiche in back pocket), high-Mg basalt is distinguished from tholeiitic basalt if two of the three following criteria are satisfied: MgO > 9%, Cr > 600 ppm, Ni > 175 ppm. If only two criteria are met the third should be close to the boundary value. These values were selected after completing an extensive search of literature on Archaean basalts. However, it is stressed that Murchison Province basalts form a compositional spectrum from high-Fe tholeiite to high-Mg basalt; the values are thus somewhat arbitrary. Nomenclature for mafic pyroclastic rocks follows IUGS recommendations (Schmid, 1981).

Felsic rocks

Use of the terms rhyolite, dacite, and andesite follows IUGS recommendations (Le Bas et al., 1986); where chemical analyses or petrographic observations are not available the term 'felsic' is used. The term rhyodacite is not used (Le Maitre, 1976). Nomenclature for felsic volcaniclastic rocks follows that of Lajoie (1984). However, Lajoie's (1984) use of the term 'epiclastic' — referring to fragments eroded from volcanic rocks, whether consolidated or not, and included in the term 'volcaniclastic' — is not followed here. These types of deposits are termed 'volcanogenic sediments'.

Sedimentary rocks

Nomenclature for sedimentary rocks follows that of Pettijohn (1975). Sedimentary rocks are termed 'epiclastic' where they have been eroded from older, consolidated rocks.

Dyke rocks and subvolcanic intrusions

Nomenclature for ultramafic cumulate and gabbroic rocks, which occur mainly in sills, follows that of Streckeisen (1974). However, many of these rocks are metamorphosed and deformed, and metamorphic names are therefore used. Dolerite is distinguished from gabbro by grain size (fine to

medium grained), by the presence of subophitic to ophitic texture, and euhedral, often skeletal, opaque phases. The term 'porphyry' is used to describe subordinate porphyritic sheet intrusions of rhyolite, dacite or andesite.

Plutonic rocks

Nomenclature for plutonic rocks follows IUGS recommendations (Streckeisen, 1976). The term 'granite', therefore, refers to Streckeisen's (1976) entire field 3, which includes syenogranite (field 3a) and monzogranite (field 3b). Monzogranite is equivalent to adamellite (compare Hallberg, 1983, figure 4, with Libby, 1978, figure 3). Following Streckeisen (1976), the term granitoid refers collectively to all plutonic rocks that have between 20% and 60% quartz.

The two earliest granitoid suites in the Murchison Province are deformed and metamorphosed; the first is now a gneiss, and the second is strongly foliated in part; thus, metamorphic names are used to describe them. Later granitoid phases are not generally deformed or metamorphosed and igneous terminology is used for them.

Geological framework

The Murchison Province occupies the northwestern part of the granite–greenstone terrane of the Yilgarn Craton (Fig. 1). It contains six major crustal components: two greenstone sequences and four suites of granitoids (Fig. 2). The two greenstone sequences, the Luke Creek Group and the overlying Mount Farmer Group, together form the Murchison Supergroup. The Luke Creek Group consists of laterally extensive (province-wide) lava plains (cf. Dimroth et al., 1982) and banded iron-formations (BIF), and associated rocks. The Mount Farmer Group consists of nine distinct volcanic centres and one sedimentary basin, each of limited lateral extent. The four suites of granitoids are a granodiorite–monzogranite suite (now pegmatite-banded gneiss), a voluminous monzogranite suite (now folded, foliated, and metamorphosed), and two compositionally diverse suites of post-folding granitoids. The first of these suites intruded only the Luke Creek Group, while the latter three intruded both greenstone groups. No basement has been recognized to the Murchison Supergroup.

Five major phases of deformation have been recognized. An early phase of recumbent folding and thrusting was followed by two phases of upright, tight and isoclinal folding. Finally, two extensive systems of shear zones and faults were developed. All rocks in the Province are metamorphosed except post-folding granitoids and late cross-cutting dykes. Grades range from prehnite–pumpellyite to granulite facies; however, most rocks are in greenschist or lower-amphibolite facies. The Precambrian geological history of the province is summarized in Table 1.

Boundaries of the Murchison Province

Only some of the boundaries of the Murchison Province (Gee et al., 1981) are included in the study area (Fig. 1) and these were not specifically investigated. To the north, northwest, and west the Murchison Province is in tectonic contact with the older Narryer Gneiss Complex (Myers, 1988; referred to informally as the early gneiss complex in the Plates). To the northeast the granite–greenstone rocks are unconformably overlain by rocks of the Proterozoic Nabberu Basin (Elias et al., 1982). The boundaries to the east and south are imprecisely known.

Gee et al. (1981) distinguished the Murchison Province from the adjacent Southern Cross Province (Griffin, 1990) in the east and southeast. The main criterion for distinguishing these provinces is that they have slightly different tectonic trends — north to north-northeast in the Murchison Province, and north-northwest in the Southern Cross Province. Gee et al. (1981) also thought that high-Mg basalt was scarce in the Murchison Province and abundant in the Southern Cross Province. However, tectonic trends in much of the southern portion of the Murchison Province are north to north-northwest, and high-Mg basalt is almost as abundant as tholeiitic basalt. Further work is needed to establish whether there are grounds for invoking a major geological boundary between these provinces. To the southwest, the Murchison Province is in contact with the southern part of the Western Gneiss Terrane (Gee et al., 1981). The nature of this contact is unknown.

Weathering and alteration

Nearly all rocks in the Murchison Province are weathered or altered to some extent so that original mineralogies, and the textures of many, are not preserved. The only rocks that contain original mineral assemblages are unaltered post-folding granitoids and cross-cutting mafic dykes.

In some areas, Tertiary deep-weathering has bleached the rocks (Butt, 1981) so much that they may be identified only from texture. Hallberg (1984) has advocated the use of Zr–TiO_2 plots to identify weathered rocks; however, this approach was not necessary because, for most, enough fresh rock is exposed to allow mapping of major units. Many rocks have undergone recent weathering, particularly medium- to coarse-grained and porphyritic granitoids; this has involved oxidation of iron and leaching of iron and potassium. Banded iron-formations are almost completely oxidized at the surface.

Distinguishing between original, and altered, rock compositions is a major problem in geochemical interpretation of metamorphic rocks. In the Murchison Province modification of primary compositions may have been affected by a number of processes, including:

(a) synformational alteration, e.g. rock–seawater

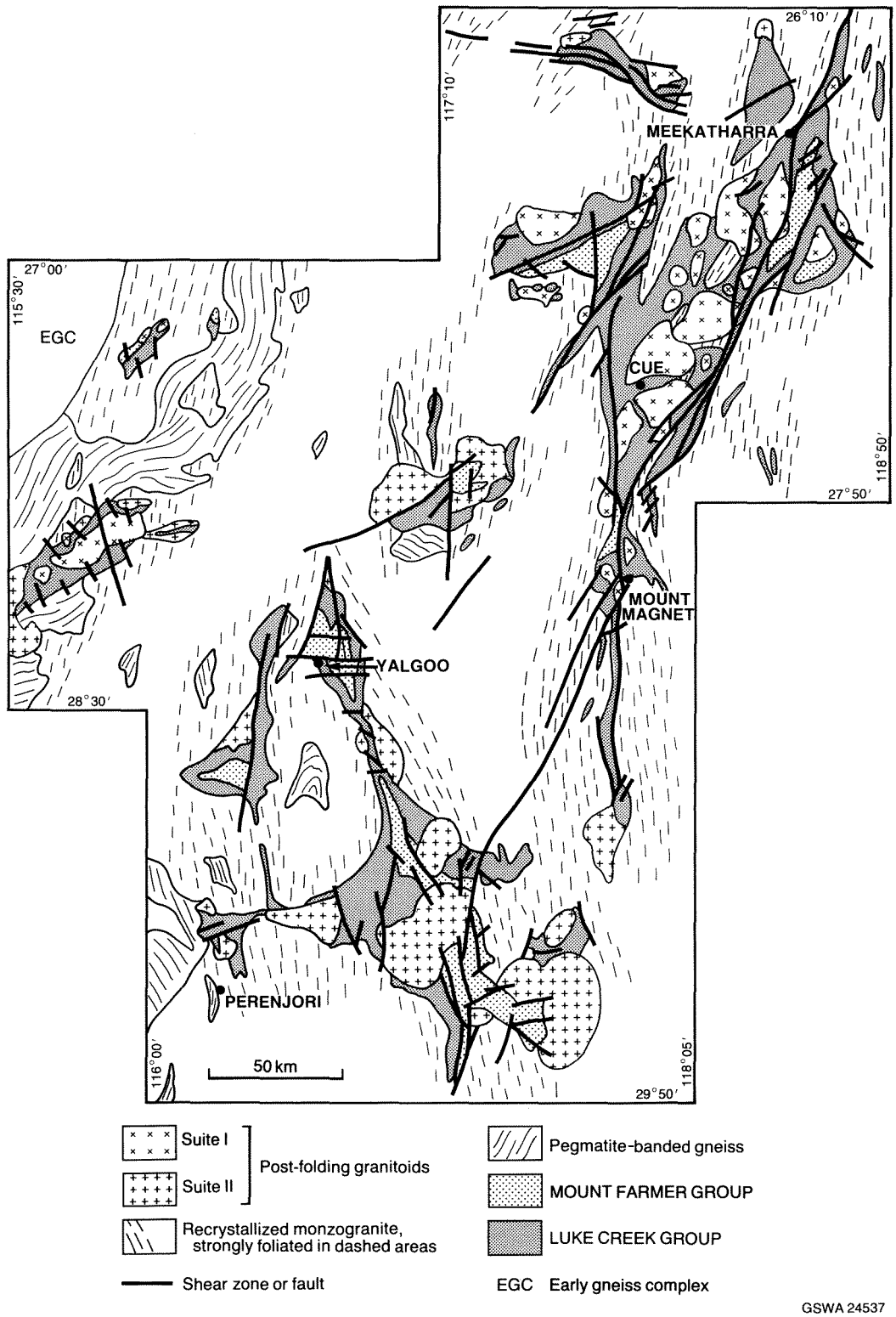


Figure 2. Distribution of major crustal components in the Murchison Province.

TABLE 1. PRECAMBRIAN GEOLOGICAL HISTORY OF THE MURCHISON PROVINCE

(1)	Deposition of Luke Creek Group greenstones on inferred basement at c. 3000 Ma
(2)	Intrusion of monzogranite and granodiorite sheets at c. 2920 Ma
(3)	D_1: development of major recumbent folds, and thrusts, in the Luke Creek Group; development of pegmatite-banded gneiss by deformation of granitoid sheets; (2) and (3) could have been contemporaneous
(4)	Deposition of Mount Farmer Group greenstones unconformably on the Luke Creek Group and pegmatite-banded gneiss at c.2800 Ma
(5)	Intrusion of voluminous monzogranite, as thick sheets, into the base of the Murchison Supergroup at c. 2690–2680 Ma; development of amphibolite facies contact metamorphic aureoles
(6)	D_2: tight east-west trending, upright folding of granitoids and greenstones
(7)	D_3: tight and isoclinal, north-northwest to north-northeasterly trending, upright folding of granitoids and greenstones; D_3 much more intensely developed than D_2
(8)	Regional metamorphism of granitoids and greenstones, mainly in greenschist facies, at c. 2680–2640 Ma
(9)	Intrusion of post-folding granitoid plutons into greenstone belts and contacts between greenstone belts and earlier granitoids at c.2640–2620 Ma
(10)	D_4: development of northwesterly to northeasterly trending, steeply inclined shear zones and faults; shear zones initiated during late D_3
(11)	Intrusion of westerly to west-southwesterly trending mafic dyke suite at c. 2420 Ma
(12)	D_5: development of easterly to southeasterly trending shear zones and faults in the northwestern part of the province

interaction in submarine lavas and deuteric alteration in granitoids;
(b) burial, regional, and contact metamorphism;
(c) epigenetic mineralization;
(d) surface or near-surface weathering, particularly in the Cainozoic.

These alteration processes have been reviewed recently by Hallberg (1983). It is very difficult to recognize pre-metamorphic alteration petrographically, because alteration textures were modified during recrystallization. Thus, it is usually necessary to rely on geochemical data to recognize early alteration, as in category (a) above. The main types of syn- or post-metamorphic alteration observed are silicification, epidotization, chloritization, serpentinization, and carbonatization; these are typical of Archaean granite–greenstone terranes (Condie, 1981).

For geochemical interpretation, analysed rocks were grouped into three alteration categories based on their petrography and geochemistry (Appendix II):

(a) no visible alteration in thin section; geochemical analysis is typical of rock type (category 1 in Appendix II);
(b) evidence of some alteration in thin section; geochemical analysis is typical of rock type (category 2 in Appendix II);
(c) clear evidence in thin section of alteration; and/or anomalous geochemistry (category 3 in Appendix II).

If a metamorphosed rock has anomalous geochemistry, but no visible alteration, it is assumed that the anomaly is due to pre-metamorphic alteration which has been obscured during recrystallization; the rock is thus classified in category 3. In general, only categories 1 and 2 analyses are used in petrogenetic and chemostratigraphic interpretation in this bulletin. However, in some traverses, where nearly all rocks have been classified in category 3, 'least-mobile' elements, such as Ti, Zr, Y, Nb, P (Pearce and Cann, 1973; Floyd and Winchester, 1975), may be used in interpretation of geochemistry.

Bulletin authorship

Chapters 1–6 and 8 were written by K.P. Watkins and Chapter 7 by A.H. Hickman. Maps showing sample traverses 41–52 in Chapter 2 were compiled by A.H. Hickman. Much of the data in the geochemistry data files in Appendix II (microfiche in back pocket) were compiled by R. Davy, who also prepared some of the geochemistry figures in Chapters 2 and 3. A.L. Ahmat carried out microprobe work for geothermometry in Chapter 6 and some petrographic work for compilation of Plate 3. I. R. Fletcher carried out the Sm–Nd analyses and contributed to the sections on Sm–Nd isotope geochemistry.

Chapter 2

Supracrustal rocks

Supracrustal rocks occur in arcuate 'greenstone' belts lying between large regions of granitoids (Plates 1 and 2). Mafic volcanic and intrusive rocks are the main lithologies in these belts; in contrast with the Eastern Goldfields Province, ultramafic rocks are only a small component. Most clastic sedimentary rocks are derived from adjacent felsic volcanic centres (Ayres, 1983), although one major epiclastic basin was developed in the upper part of the greenstone succession. BIF is abundant in two laterally extensive stratigraphic marker units. Granitoids intrude the lower portion of the greenstone succession; its original base and the rocks on which it was deposited are not preserved.

Previous stratigraphic schemes

Following the first systematic regional mapping in the Murchison Province, de la Hunty (1973) and Baxter (1974) defined stratigraphic formations on CUE and MURGOO. A four-part stratigraphy was subsequently proposed for most of the province, based on the concept of 'lithological associations' (Hallberg, 1976; Muhling and Low, 1977; Elias et al., 1982; Baxter et al., 1983; Lipple et al., 1983; Baxter and Lipple, 1985). Muhling and Low (1977, p. 17) stated that lithological associations 'constitute entities of lithological similarity and lithogenic significance, in which the individual lithologies of the association commonly occur together'. The four lithological associations of this stratigraphic scheme are:

(a) upper felsic-sedimentary association;
(b) upper mafic association;
(c) lower felsic-sedimentary association;
(d) lower mafic association.

Baxter (1982) reviewed this scheme for the southern Murchison Province and added a fifth, uppermost association, of only local importance, comprising shale and BIF. There is agreement between the authors cited above that the lowest unit consists dominantly of mafic rocks and BIF. However, Baxter and Lipple (1985) did not recognize BIF in the Koolanooka greenstone belt in this association. There is less agreement about the composition of the lower felsic-sedimentary association, particularly regarding the occurrence of BIF and the proportions of felsic volcanic to sedimentary rocks. For the upper mafic association, there is disagreement about the proportions of high-Mg and tholeiitic basalt, and the occurrence of BIF. There is wide variation in the types of felsic volcanic and sedimentary rocks reported by different authors for the upper felsic-sedimentary association. On YALGOO, the upper mafic association overlies the upper felsic-sedimentary association (Muhling and Low, 1977). The two regional compilations of Hallberg (1976) and Baxter (1982) are compared in Table 2. Archibald (1982) and Baxter (1982) mapped the Mount Magnet region and part of the Yalgoo–Singleton greenstone belt, respectively. They proposed more detailed stratigraphic schemes for these areas which differ, at least in part, from the regional scheme.

Method of stratigraphic subdivision and correlation

The supracrustal stratigraphy of Murchison Province greenstone belts is subdivided in this bulletin according to the Field Geologists Guide to Lithostratigraphic Nomenclature in Australia (Staines, 1985). Greenstone belt rocks are divided into 17 formations on the basis of their lithology and relative superposition; these formations are combined into a system of two subgroups, two groups, and one supergroup (Fig. 3). The formations are mappable units, consisting of one dominant lithology or an assemblage of associated lithologies. Because of poor exposure, type areas have been defined for these formations rather than type sections.

The stratigraphic subdivision was proposed informally by Watkins et al. (1987), following remapping of the CUE 1:250 000 sheet. That subdivision is expanded in this chapter; lithostratigraphic formations, subgroups, groups, and a supergroup are formally defined. Regional stratigraphic correlations are based on superposition of lithologies relative to distinctive marker units, particularly the Golconda and Windaning Formations. Outcrops were not assigned to a lithostratigraphic formation if their stratigraphic positions relative to a marker horizon could not be determined (Plate 2).

Murchison Supergroup

The supracrustal sequence in Murchison Province greenstone belts is defined here as the Murchison Supergroup

TABLE 2. COMPARISON OF HALLBERG'S (1976) AND BAXTER'S (1982) REGIONAL STRATIGRAPHIC COMPILATIONS OF MURCHISON PROVINCE GREENSTONE BELTS

Lithological association	*Hallberg (1976) Murchison Province and north Southern Cross Province*	*Baxter (1982) Southern Murchison Province*
Upper felsic-sedimentary association	Volcaniclastic sedimentary rocks and calc-alkaline volcanic rocks in the north; conglomerate, sandstone, and shale in the south	Conglomerate, siltstone and shale; BIF near base
Upper mafic association	High-Mg and tholeiitic basalt with well-developed pillows; minor felsic volcanic rocks; BIF absent	Mainly tholeiitic basalt and high-Mg basalt; greater proportion of high-Mg basalt and pyroclastic rocks, and lower proportion of BIF, than in the lower mafic association
Lower felsic-sedimentary association	Fine-grained sedimentary rocks (black shale, siltstone), felsic tuff, abundant BIF	Pelitic and volcaniclastic sedimentary rocks, felsic volcanic rocks; BIF absent
Lower mafic association	Unpillowed basalt,ultramafic schist, gabbro, BIF; felsic volcanic rocks absent; high-Mg basalt rare	Tholeiitic basalt and dolerite interlayered with BIF

(Fig. 3). The name 'Murchison Supergroup' replaces Johnson's (1950a) 'Murchison System', although the former does not include the Jack Hills greenstone belt. The term 'system' is not permissible under the Field Geologist's Guide to Lithostratigraphic Nomenclature in Australia (Staines, 1985). 'Murchison Supergroup' is distinct from the Cretaceous 'Murchison House Group' defined by Clarke and Teichert (1948) which is regarded as obsolete (Johnstone et al., 1958, p. 14).

The Murchison Supergroup consists of two groups, the Luke Creek Group and the Mount Farmer Group, which include two subgroups — the Porlell and Yalgoo Subgroups — and seventeen formations (Fig. 3, Plate 2). There are three fundamental differences between the Luke Creek Group and the Mount Farmer Group:

(a) The stratigraphy of the two groups is markedly different. In the Luke Creek Group the four component formations form a superposed sequence which is continuous throughout most Murchison Province greenstone belts. They form a 'layer-cake' type of stratigraphic sequence. In contrast, subgroups and formations in the Mount Farmer Group are broadly contemporaneous. They are of limited lateral extent, each being restricted to a part of one greenstone belt, except for one formation (the Mougooderra Formation), which forms parts of two adjacent greenstone belts. They are thought to represent individual volcanic centres and one epiclastic sedimentary basin (the Mougooderra Formation), deposited on an infrastructure of Luke Creek Group rocks. This style of stratigraphic development was recognized by Gee et al. (1981) and Baxter (1982) who noted stratigraphic continuity at lower levels, and diversity of rock types between regions at upper levels.

(b) Structures associated with the first major deformation event are seen only in the Luke Creek Group.

(c) The earliest granitoid phase, the pegmatite-banded gneiss, intrudes only Luke Creek Group rocks.

These differences suggest that the boundary between the two groups is an unconformity. Layering in the Mount Farmer Group appears to be broadly parallel to that in the Luke Creek Group. The boundary between the two groups has been observed only at the base of the Mougooderra Formation, where an angular unconformity separates it from the underlying Windaning Formation. However, there is some evidence to suggest that the Mougooderra Formation may also overlie the Singleton Basalt (Lipple, 1982a). Thus, the base of the Mount Farmer Group in this region may be atypical. The thickness of the supergroup varies considerably. The mean cumulative thickness of Luke Creek Group formations is about 10 km. Mount Farmer subgroups and formations vary in thickness from 1 km to 5 km (Fig. 3). However, the combined mean thicknesses of all four Luke Creek Group formations, and one of the thickest Mount Farmer Group formations, is approached only in the northern part of the Meekatharra–Wydgee greenstone belt (Plate 2). Elsewhere, the stratigraphic thicknesses of greenstone belts are less than the cumulative mean of formation thicknesses, although the latter are difficult to estimate because of structural complexity and intrusion by granitoids.

Distribution of rocks

Mafic volcanic and intrusive rocks dominate the Murchison Supergroup (Fig. 3); they comprise approximately 70% of both its groups. Felsic volcanic and associated volcaniclastic rocks account for a further 20% of each

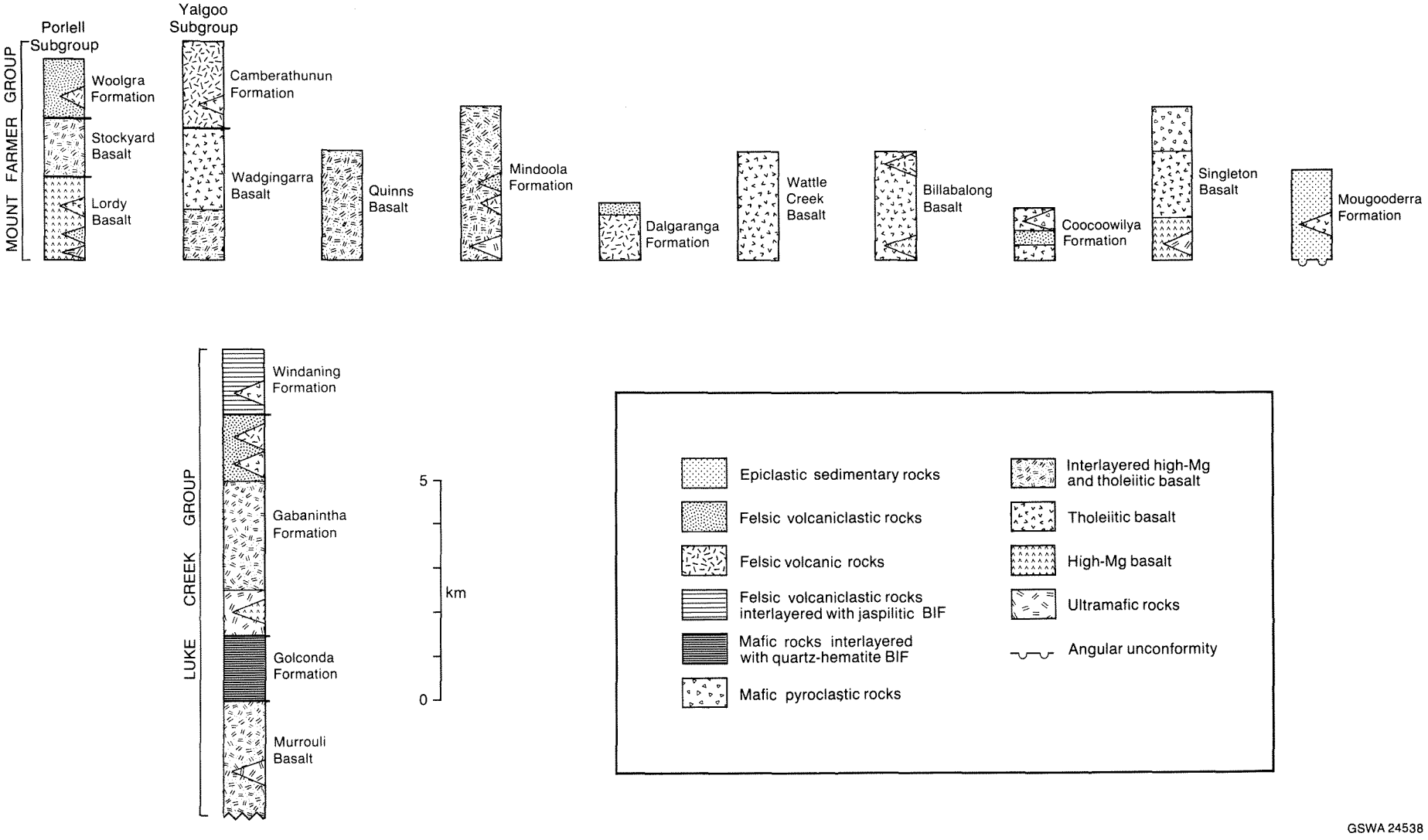


Figure 3. The Murchison Supergroup: groups, subgroups, formations, and rock types. Stratigraphic thicknesses are approximate and may be extensively modified by deformation and intrusion of sills. Thicknesses of Luke Creek Group formations vary along strike, and are averaged in the column.

group. The remaining rocks of the Luke Creek Group comprise about 5% ultramafic rocks, and 5% BIF; those of the Mount Farmer Group comprise about 4% ultramafic rocks, and 6% epiclastic sedimentary rocks.

Most of the ultramafic rocks are chlorite–tremolite(–talc) schists, serpentinites, and, less commonly, talc–carbonate schists. Only a few occurrences of bladed spinifex-textured komatiite have been found. With the exceptions of these komatiites, and serpentinite with relic cumulate texture, it is generally difficult to determine whether ultramafic rocks had an extrusive or intrusive origin. Most ultramafic rocks of the Murchison Supergroup occur in the lower parts of the Gabanintha Formation, and in the Lordy Basalt and Mindoola Formation (Fig. 3). However, thin ultramafic units are abundant in sequences of high-Mg basalts throughout the greenstone sequence, and the bases of most layered intrusions are also ultramafic. In some areas ultramafic rocks are strongly silicified, forming a light brown siliceous cap rock, e.g. at Yaloginda, Cuddingwarra, and Lennonville.

Mafic rocks occur as basalt lava flows, pyroclastic rocks, and gabbro and dolerite sills. Approximately 70% of basalt is tholeiitic; the remainder is fine-grained or needle spinifex-textured high-Mg basalt. Tholeiitic and high-Mg basalts are interlayered in many formations (Fig. 3). In the Luke Creek Group, most basalt occurs in thick monotonous sequences and shows few distinctive morphological features, although some pillow lavas are present. In the Mount Farmer Group, pillow lavas and pyroclastic rocks are relatively abundant. Gabbro and dolerite sills are common in most basalt sequences, and form much of the mafic stratigraphy; most are thought to be synvolcanic intrusions (cf. Hallberg and Wilson, 1983).

Felsic lava and tuff generally occur in laterally restricted volcanic complexes within the greenstone sequence. In the Luke Creek Group these complexes are associated with locally thick sequences of felsic volcaniclastic rocks in the upper part of the Gabanintha Formation, and in the Windaning Formation. It is likely that the volcaniclastic rocks were derived by erosion of felsic volcanic complexes (Ayres, 1983). In the Mount Farmer Group the same association exists between felsic volcanic and volcaniclastic rocks, although both rock types are confined to relatively small regions. Rhyolite and dacite are the dominant felsic volcanic rocks in the Luke Creek Group, but dacite and andesite dominate those in the Mount Farmer Group. Volcaniclastic rocks range from breccia and conglomerate through poorly sorted, coarse-grained sandstone to fine-grained, laminated siliceous rocks. Sedimentary structures such as graded bedding and cross-bedding are abundant in these rocks.

Epiclastic sedimentary rocks are rare in the Luke Creek Group, where most sedimentary rocks derive from felsic volcanism. In the Mount Farmer Group, the Mougooderra Formation is the only significant occurrence of epiclastic sedimentary rocks.

Luke Creek Group

The Luke Creek Group comprises four laterally extensive lithostratigraphic formations — the Murrouli Basalt and the Golconda, Gabanintha, and Windaning Formations (Fig. 3) — which can be recognized throughout most of the province. The four formations can be divided informally into two sequences. In the lower sequence a thick pile of mafic rocks, the Murrouli Basalt, is capped by BIF interlayered with mafic rocks, the Golconda Formation. The upper sequence appears to be a typical Archaean bimodal sequence (e.g. Thurston and Fryer, 1983; Thurston et al., 1985; Jensen, 1985). The Gabanintha Formation forms the major part of this sequence. It comprises ultramafic rocks, and high-Mg and tholeiitic basalt, overlain by interlayered felsic volcanic and volcaniclastic rocks, sedimentary rocks, and basalt. This formation is capped by the Windaning Formation, which consists of abundant BIF interlayered with felsic volcanic and volcaniclastic rocks, sedimentary rocks, and rare basalt. The abundant BIF in the Golconda and Windaning Formations, at the top of the two sequences, are important marker horizons for determining the greenstone stratigraphy of the province.

The Luke Creek Group derives its name from Luke Creek which flows from Meekatharra, west-northwest over the four component formations of the group, and into the Yalgar River drainage system (see BELELE 1:250 000 geological sheet).

Murrouli Basalt

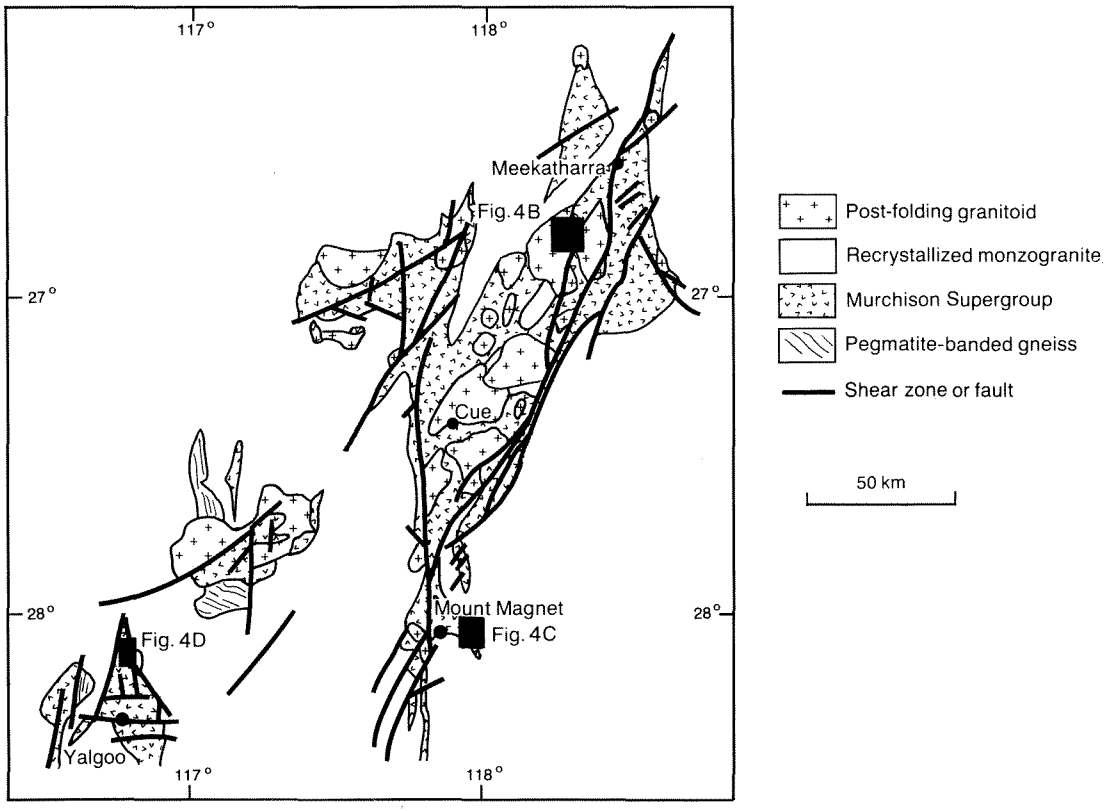
Definition and distribution

The Murrouli Basalt is defined here as a succession of tholeiitic and high-Mg basalts and some ultramafic rocks, and associated gabbro and dolerite sills, which lies at the base of the Murchison Supergroup. It occurs in the Murrouli Range, in the vicinity of Cullculli Homestead, around Mount Magnet, near Kirkalocka Homestead in the Meekatharra–Wydgee greenstone belt, to the west of Noongal Homestead in the Yalgoo–Singleton greenstone belt, and northwest of Bunnawarra Homestead in the Gullewa greenstone belt (Plate 2). Elsewhere, the formation either was not developed, or was excised from the greenstone belts by granitoid intrusions. The type area of the Murrouli Basalt is in the Murrouli Range between Murrouli Bore in the west, and Little Gap Well in the east (Figs 4A and B). In this area the Murrouli Basalt consists mainly of tholeiitic basalt, gabbro, and dolerite, interlayered with minor units of high-Mg basalt. The base of the formation is an intrusive contact with a post-folding tonalite. Its top is marked by a 450 m-thick gabbro sill immediately below BIF of the overlying Golconda Formation. The Murrouli Basalt is 4400 m thick in this area. The base of the Murrouli Basalt is always in intrusive or tectonic contact with granitoids. No basement to the formation has been recognized.

Lithostratigraphy

Tholeiitic basalt, high-Mg basalt, and gabbro and doler-

A. Locations of sampled areas



References for Figures 4B, C, D.

Cainozoic deposits

MURROULI BASALT

Tholeiitic basalt

High-Mg basalt

Interlayered high-Mg and tholeiitic basalt

Gabbro and dolerite

Pyroxenite

Ultramafic rock

Mafic pyroclastics

BIF

GOLCONDA FORMATION

BIF and mafic rocks

GRANITOIDS

Post-folding granitoid

Recrystallized granitoid

Shear zone or fault

Homestead

Bore or well

Mine (abandoned)

Prospect (abandoned)

Road

Track

In stratigraphic columns :

Sheared granitoid contact

Intrusive granitoid contact

UT — Upper tholeiite

MT — Middle tholeiite

LT — Lower tholeiite

HM — High-Mg basalt

Note: Codes in brackets following sample numbers refer to 'rock type' and 'degree of alteration' as defined in Appendix II.

GSWA 24539 A

Figure 4A. Locations of Murrouli Basalt sample traverses in a regional context, and legend for Figures 4B, C, D. Note that map scales are not uniform.

B. Traverse 1: Murrouli Range

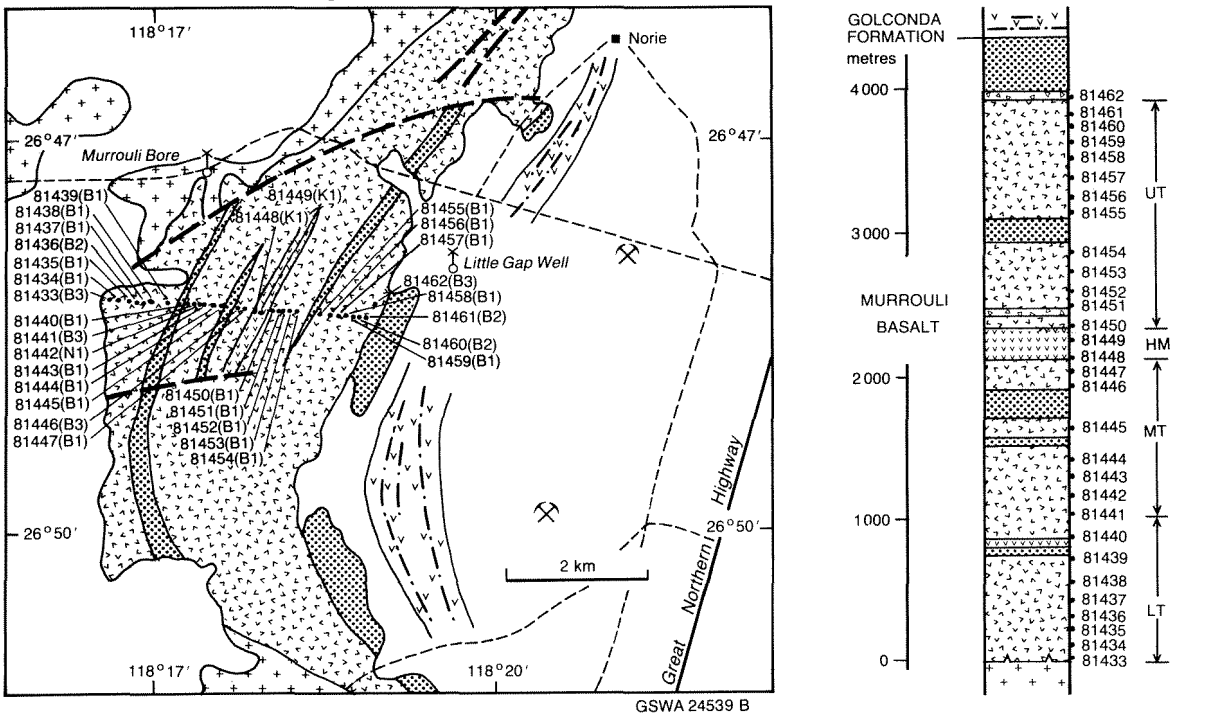


Figure 4B.

C. Traverse 41: Mount Magnet

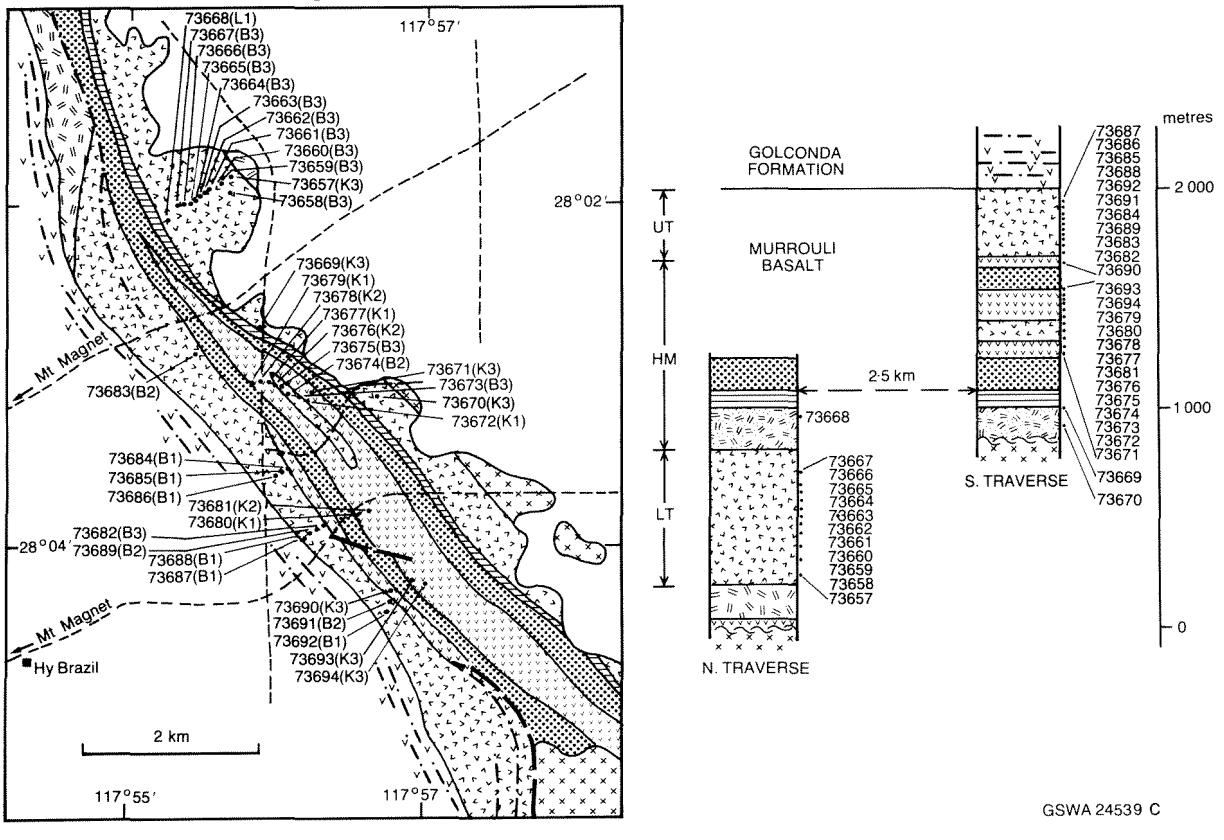


Figure 4C.

D. Traverse 52: Noongal

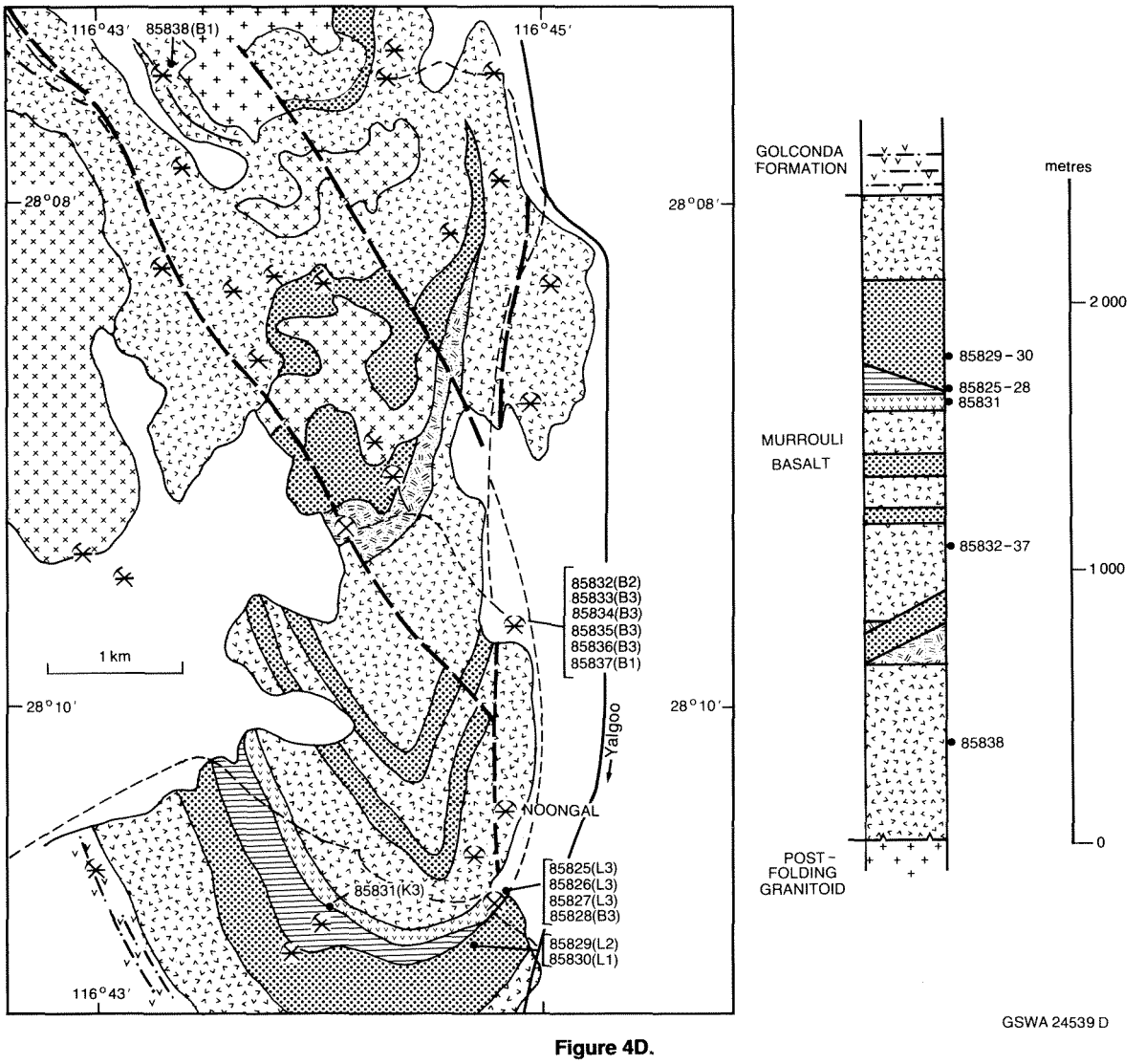


Figure 4D.

ite, are the main lithologies; tholeiitic basalt dominates. The proportion of high-Mg basalt varies from about 5% in the Murrouli Range to about 35% east of Mount Magnet. Approximately 20% of the formation is gabbro and dolerite. Rare, thin units of dacite schist, ferruginous chert, and fine-grained sedimentary rock are interlayered with the mafic volcanics east of Mount Magnet. The tholeiitic basalt is dark green to greenish grey, fine grained to aphanitic, and generally featureless. Most of the high-Mg basalt is dark green and has needle spinifex texture. Needle spinifex texture occurs in tholeiitic basalt in the lower part of the succession near Mount Magnet. Gabbro and dolerite sills are ubiquitous: they are medium to coarse grained, generally massive, and undifferentiated; however, peridotite and/or pyroxenite form the lower parts of some sills east of Mount Magnet. The margins of these intrusions are sheared in some places. In high-strain zones all mafic rocks have become amphibolite. There are very few morphological flow features in basalt, and little field evidence of the extent or thickness of individual lava flows, or of flow differentiation. Pillow lava has been identified at a few localities. Two thin (<50 m) volcaniclastic units occur in the Murrouli Range (Fig. 4B). The lower is a breccia containing irregularly shaped blocks of basalt, up to 15 cm across, in a fine-grained tuffaceous matrix. The upper unit is heavily altered and was probably tuff. Sporadic outcrops of chlorite–tremolite–talc schist occur 5 km west of Mount Magnet.

A strong foliation is developed throughout much of the formation; it is particularly intense adjacent to recrystallized monzogranite. Metamorphic grade is mainly greenschist facies in the Murrouli Range, and lower amphibolite facies east of Mount Magnet (Plate 3). The grade is amphibolite facies adjacent to recrystallized monzogranite. Greenschist-facies mineral assemblages in tholeiitic basalt, gabbro, and dolerite include actinolite, albite–oligoclase, epidote, sphene, and opaque phases; amphibolite-facies assemblages include hornblende, clinopyroxene, oligoclase–andesine, sphene, and opaque phases. The same phases are present in high-Mg basalts, although the mafic phases are more magnesian; tremolite, for example, occurs instead of actinolite in the greenschist facies. In unfoliated rocks, metamorphic phases pseudomorph igneous textures. In foliated rocks, metamorphic phases overgrow, and are partly aligned with, the tectonic fabric.

Many rocks are altered, particularly those in the Noongal area (Fig. 4D; Appendix II). Silicification and epidotization appear to be the dominant types of alteration.

Geochemistry

Sampling

Seventy-five samples of basalt were collected for geochemical analysis, from three traverses across the Murrouli Basalt (Fig. 4). Chemical analyses are listed in Appendix II. Samples from the Noongal traverse (Fig. 4D) are intensely altered and their geochemistry is not discussed here.

Compositional characteristics

Four chemically distinct basalt units have been recognized in the Murrouli Range traverse — lower, middle, and upper tholeiites, and high-Mg basalt. Three units were recognized in the Mount Magnet traverse — lower and upper tholeiites, and high-Mg basalt (Table 3, Fig. 4). Most samples have compositions typical of Archaean basalts (Fig. 5) (Basaltic Volcanism Study Project, 1981). However, the Mount Magnet lower tholeiite is unusual in that it is enriched in SiO_2, Ba, and Sr, and depleted in FeO^* (all Fe as FeO), TiO_2, and V, and has high Zr/(Zr+Y), 100 mol MgO/(MgO+FeO) (Mg number), and Cr/V ratios compared with the other tholeiites. The Mount Magnet upper tholeiite has high FeO^*, TiO_2, P_2O_5, and V contents, typical of Fe-rich tholeiite (Basaltic Volcanism Study Project, 1981, p. 13). Except for SiO_2-rich lower tholeiite and Fe-rich upper tholeiite from the Mount Magnet traverse, Murrouli Basalt tholeiites plot in the high-Mg tholeiite field on a Jensen diagram (Fig. 5). High-Mg basalt is clearly distinguished from tholeiitic basalt by its higher MgO, Cr, and Ni contents, and lower Al_2O_3, Nb, Sr, V, and Zr contents (Table 3, Fig. 5).

Chemostratigraphy

Tholeiitic basalt seen along sample traverses in the field appears monotonous; however, it is clear that stratigraphic

TABLE 3. MEAN COMPOSITIONS OF MURROULI BASALT THOLEIITE UNITS

	Murrouli Range traverse				*Mount Magnet traverse*		
	Lower tholeiite n=7	*Middle tholeiite n=4(a)*	*Upper tholeiite n=12*	*High-Mg basalt n=2*	*Lower tholeiite n=10(altered)*	*Upper tholeiite n=10*	*High-Mg basalt n=9*
				Percentage			
SiO_2	50.1	51.4	50.9	49.4	56.4	50.4	50.7
Al_2O_3	13.5	14.1	14.2	10.7	14.4	12.9	10.2
Fe_2O_3	2.31	1.70	1.95	1.25	0.99	2.61	1.61
FeO	8.35	8.05	7.64	7.77	5.58	10.2	8.25
FeO*(b)	10.43	9.57	9.38	8.92	6.47	12.55	9.69
MgO	6.92	6.96	7.37	14.35	6.63	6.48	12.55
CaO	11.97	11.85	11.73	10.0	11.45	10.25	11.05
Na_2O	2.24	2.12	1.74	1.15	1.34	2.21	1.08
K_2O	0.24	0.25	0.15	0.06	0.07	0.19	0.10
TiO_2	1.40	0.76	0.76	0.40	0.64	1.45	0.56
P_2O_5	0.17	0.11	0.10	0.08	0.10	0.21	0.09
MnO	0.19	0.19	0.18	0.20	0.20	0.21	0.18
LOI	1.97	2.04	2.74	3.90	1.42	2.10	2.94
S	0.006	0.015	0.036	0.003	0.014	0.006	0.004
				Parts per million			
Ba	85	68	43	39	163	114	51
Cr	395	144	266	1304	365	114	1166
Co	58	59	56	64	80	65	67
Cu	90	95	204	158	100	82	65
Ni	127	112	116	365	137	82	278
Nb	6	6	4	3	6	6	3
Rb	9	10	4	2	1	4	2
Sr	122	98	82	57	131	100	70
V	359	281	281	222	196	334	227
Y	30	19	20	15	25	33	15
Zn	100	70	97	114	93	105	77
Zr	87	50	47	32	87	93	35
Mg number(c)	59.5	60.6	63.2	76.6	67.8	51.9	72.6
Cr/V	1.14	0.51	0.94	5.86	1.87	0.38	5.23
Zr/(Zr+Y)	0.74	0.72	0.70	0.68	0.78	0.74	0.70

(a) Basaltic andesite 81442 is omitted from the mean (b) All Fe calculated as FeO (c) 100mol Mg0/(MgO + FeO)
Except for Mount Magnet lower tholeiite, samples assigned to alteration class 3 (see Appendix II) are omitted from the means.
For most of the analyses averaged in this table Pb<10 ppm, and Th<5 ppm.

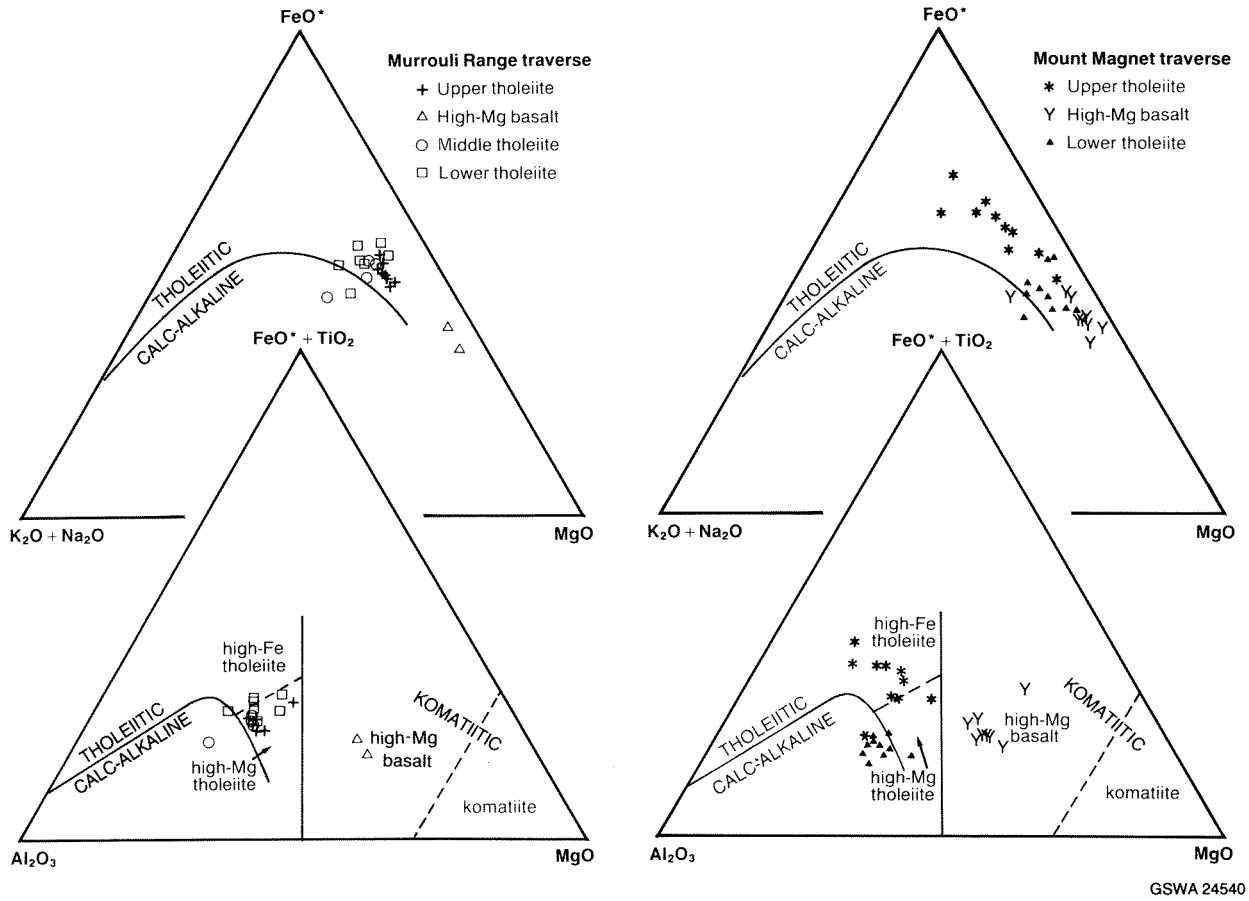


Figure 5. Murrouli Basalt analyses plotted on AFM diagrams (above), and Jensen diagrams (below). Irvine and Baragar's (1971) tholeiite trend is plotted on the AFM diagrams. Compositional fields on the Jensen diagrams are modified from Jensen (1976).

units can be distinguished on a chemical basis (Fig. 6). In the Murrouli Range the lower tholeiite is distinguished from the other tholeiite units by higher mean TiO_2, P_2O_5, V, Cr, Y, Zr, and lower mean Al_2O_3. The middle and upper tholeiites are distinguished because of their different Cr and Cu contents (Table 3, Fig. 6). In the Mount Magnet region the two tholeiite units are separated by a thick high-Mg basalt unit. The upper Fe-rich tholeiite is chemically similar to the lower tholeiite in the Murrouli Range, except for different FeO*, Cr, Ni, and Cu contents. The lower SiO_2-rich tholeiite is altered (Appendix II), but its unusual composition may be due in part to crustal contamination (cf. Arndt and Jenner, 1986; Barley, 1986). High-Mg basalts from both traverses are closely similar in composition (Table 3). Except for the lower tholeiite in the Murrouli Range, and the upper tholeiite near Mount Magnet, there is little systematic chemical variation within the basalt units (Fig. 6). It is unlikely that basalt units can be correlated between traverses, in a lithostratigraphic sense, because those which are similar are at different stratigraphic levels in each traverse. In addition, the traverses are more than 150 km apart.

Petrogenesis

Petrogenesis of basaltic rocks is complex (Basaltic Volcanism Study Project, 1981) and is often difficult to interpret, particularly for metamorphosed and altered rocks (Floyd and Winchester, 1978). In this chapter, much petrogenetic interpretation is based on relations between high-field-strength (HFS) elements (i.e. elements with high charge/radius ratios, such as Y, Ti, Zr) and the rare-earth elements (REE). These reflect igneous processes, and are thought to be relatively immobile during metamorphism and alteration (Pearce and Cann, 1973; Floyd and Winchester, 1975; Pearce and Norry, 1979). Metamorphism and alteration may sometimes result in absolute-abundance changes, but generally, ratios of HFS elements will be unaffected (Ludden and Gelinas, 1982). In addition, relations between Ni, Cr, and MgO, and between Cr and Y are described, as these are also important for understanding partial melting and crystal fractionation processes (Jahn et al., 1980; Arndt and Nisbet, 1982; Pearce, 1980, 1982). However, abundances of Ni, Cr, and MgO are more susceptible to alteration than those of the HFS elements. Element distributions are discussed in terms of Zr–Y, Ti–Y, Zr/Y–Zr, Cr–Y, Cr–MgO, Ni–MgO, and REE diagrams, because a strong theoretical base exists for interpreting basalt petrogenesis in terms of these plots (Pearce and Norry, 1979; Jahn et al., 1980; Pearce, 1980, 1982; Cullers and Graf, 1984a, and references therein). Sm–Nd isotopes were determined for a number of samples, and the petrogenetic significance of these results are also discussed.

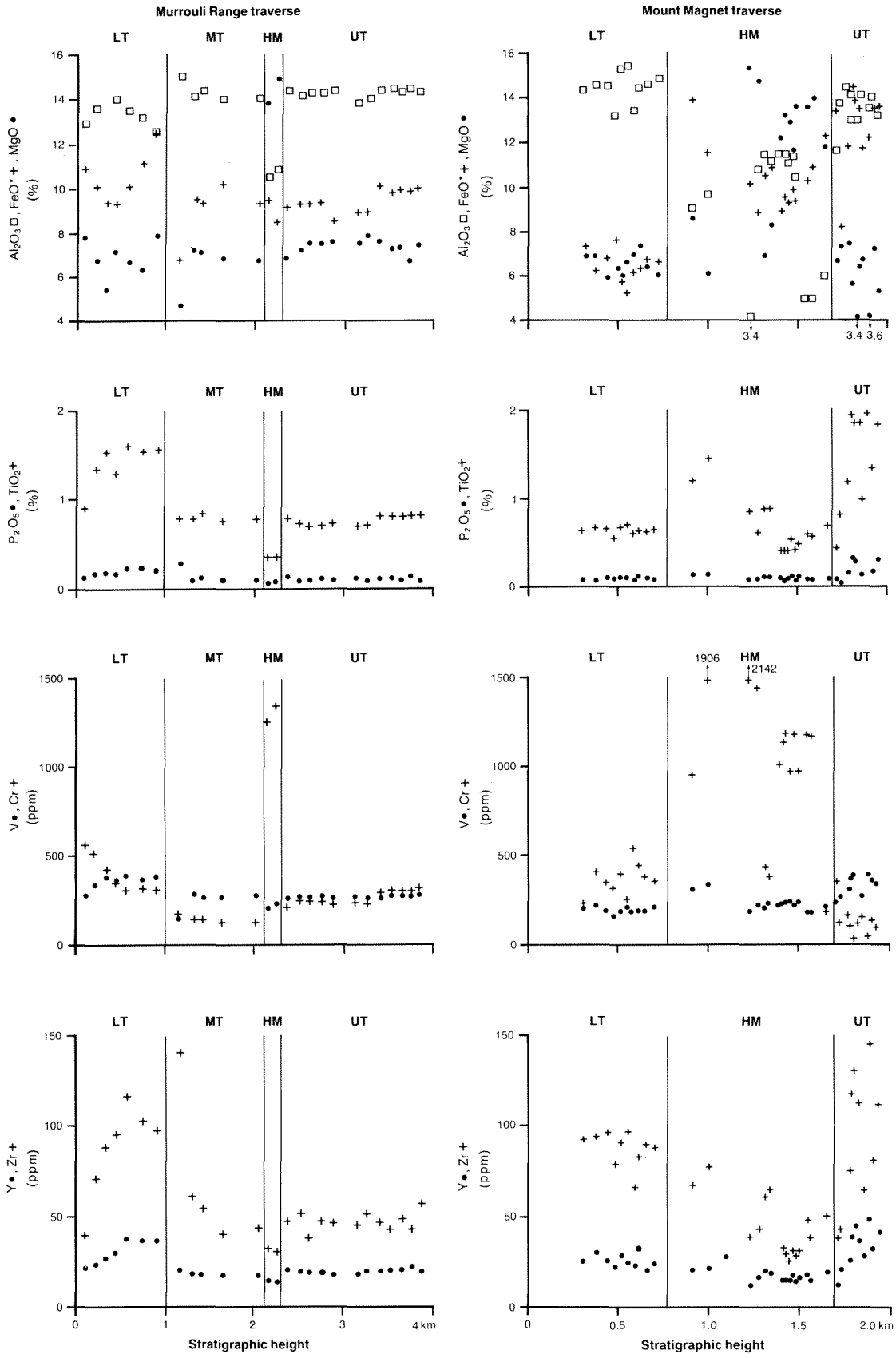


Figure 6. Chemostratigraphic variation in two of the Murrouli Basalt traverses. With the exception of the lower tholeiite in the Mount Magnet traverse, only samples in alteration classes 1 and 2 (Appendix II) are plotted. All samples in the Mount Magnet lower tholeiite are in alteration class 3.

Zr, Y, and Ti: With some exceptions, most basalt samples have Y/Zr and Ti/Zr ratios similar to that of the Archaean mantle (Fig. 7) (Sun and Nesbitt, 1977; Sun, 1982), clearly indicating derivation by melting of an upper mantle source (Nesbitt and Sun, 1976). Furthermore, the near-chondritic Y/Zr ratios indicate that garnet was not an important refractory phase in the source (Ludden and Gelinas, 1982), because Y is strongly partitioned into garnet (Henderson, 1982, table 5.2a). Fractional-crystallization trends can be interpreted from the variation of Ti and Y with Zr (Pearce and Norry, 1979).

There are two distinct patterns of element distribution for Murrouli Basalt units on Zr–Y and Ti–Y diagrams (Fig. 7). Data from the lower tholeiite in the Murrouli Range and the upper tholeiite from near Mount Magnet plot linearly along mantle-ratio trends. Data from other units plot in distinct clusters, on or near mantle-ratio trends. The cluster of points for the Mount Magnet lower tholeiite plots away from the mantle ratio on the Ti–Zr diagram. Sample 81442, a basaltic andesite from the middle tholeiite in the Murrouli Range, is chemically distinct and plots away from the main trend. Different degrees of olivine and pyroxene crystal fractionation, from an upper mantle source partial melt, are indicated for Murrouli Range middle and upper tholeiites and high-Mg basalt, and for Mount Magnet lower tholeiite and high-Mg basalt. The Murrouli Range lower tholeiite and the Mount Magnet upper tholeiite have undergone closed-system crystal fractionation of pyroxene and plagioclase in magma chambers from which successive increments of evolving magma were erupted onto the surface. Although most samples from these two units show progressive fractionation with increasing stratigraphic height, a significant proportion do not (Fig. 6). This fact implies that some flows could have been tapped from slightly different levels within compositionally zoned magma chambers (Cox, Bell, and Pankhurst, 1979, p. 272; Basaltic Volcanism Study Project, 1981, p. 399).

Compositions of the basaltic andesite sample 81442, and samples from the Mount Magnet lower tholeiite, cannot be explained easily in terms of crystal fractionation as they have anomalously high Zr contents relative to Ti (Fig. 7). It is possible that the basalt magmas from which these rocks crystallized were contaminated by assimilation of felsic crustal material (Arndt and Jenner, 1986; Barley, 1986). Mount Magnet lower tholeiite samples are intensely altered, and do not show all the features generally ascribed to crustal contamination. However, crustal contamination is an important process in Murchison Supergroup basalts (see 'Origin and crystallization of mafic magmas', p. 97) and it is possible that these rocks have been affected by both crustal contamination and alteration.

Pearce and Norry (1979) established that basalt compositions on a Zr/Y–Zr diagram were characterized by two common vectors, one with an approximate slope of unity, the other subparallel to the Zr axis. They modelled compositional variations along these vectors in terms of several petrogenetic processes, and concluded that variations along the first vector (a slope of unity) were due mainly to addition and extraction of magma in the source region, provided that garnet, a strong fractionator of Y, could be excluded as an important phase in the process (Pearce and Norry, 1979, fig. 4c). The subhorizontal vector is due to closed-system fractionation of mafic phases and plagioclase (Pearce and Norry, 1979, fig. 4d).

Data for the Murrouli Range middle and upper tholeiites, and the Mount Magnet lower tholeiite, plot on a 'first vector' trend which intersects the partial-melting curve of a plagioclase-lherzolite source at about 20% partial melting (Fig. 8). Such a degree of melting is considered typical for tholeiites (Basaltic Volcanism Study Project, 1981). The Murrouli Range lower tholeiite and the Mount Magnet upper tholeiite have 'second vector' trends, indicating closed-system crystal fractionation of mafic phases and plagioclase.

It is difficult to interpret the petrogenesis of high-Mg basalt on this diagram, in terms of the source compositions modelled, because of the low Zr content of these rocks. High-Mg basalt compositions are generally displaced to the left of 'first-vector' tholeiite trends, which possibly indicates a higher degree of partial melting of a depleted source. The diagram is generally used only for tholeiites (Pearce and Norry, 1979), and high-Mg basalts are not plotted.

Ni, Cr, and MgO: Compositional differences between tholeiitic and high-Mg basalts are emphasized on Ni–MgO and Cr–MgO diagrams (Fig. 9). With a few exceptions, Ni and Cr contents vary systematically with MgO content in high-Mg basalt. There are no clear trends for tholeiitic basalt. Data for these rocks plot in a cluster on the Ni–MgO diagram and show a large variation in Cr content on the Cr–MgO diagram. Variation in Ni and Cr with MgO at high MgO contents is due to crystal fractionation of olivine. At lower MgO values, fractionation of pyroxene increases the range of Cr variation relative to MgO (Jahn et al., 1980; Drury, 1983).

Cr–Y relations: Pearce (1980, 1982) pointed out that source regions for most basaltic magmas probably contained abundances of Y and Cr that were similar to those of the primordial mantle. Variations in these elements can be attributed, for the most part, to differences in their partial melting and/or fractional-crystallization histories. The partial-melting trend on an Y–Cr diagram (Fig. 10) lies subparallel to the Y axis, for less than 50% partial melting, because Cr will be concentrated in refractory phases such as pyroxenes, spinels, and olivine, during melting. These phases will be the first to crystallize during fractional crystallization, causing much depletion of Cr from the residual liquid, and nearly vertical trends on the Y–Cr diagram (Pearce, 1980, 1982). A flatter trend, where Y increases rapidly with small decrease in Cr, occurs when plagioclase, which contains no Y, becomes a liquidus phase. Thus, petrogenetic pathways can be inferred for suites of basalt samples, using these general principles, on an Y–Cr diagram (Fig. 10).

Murrouli Basalt tholeiites have been derived by about 15–20% partial melting of an upper mantle source, followed by varying amounts of crystal fractionation. Murrouli Range middle and upper tholeiite units, and the Mount

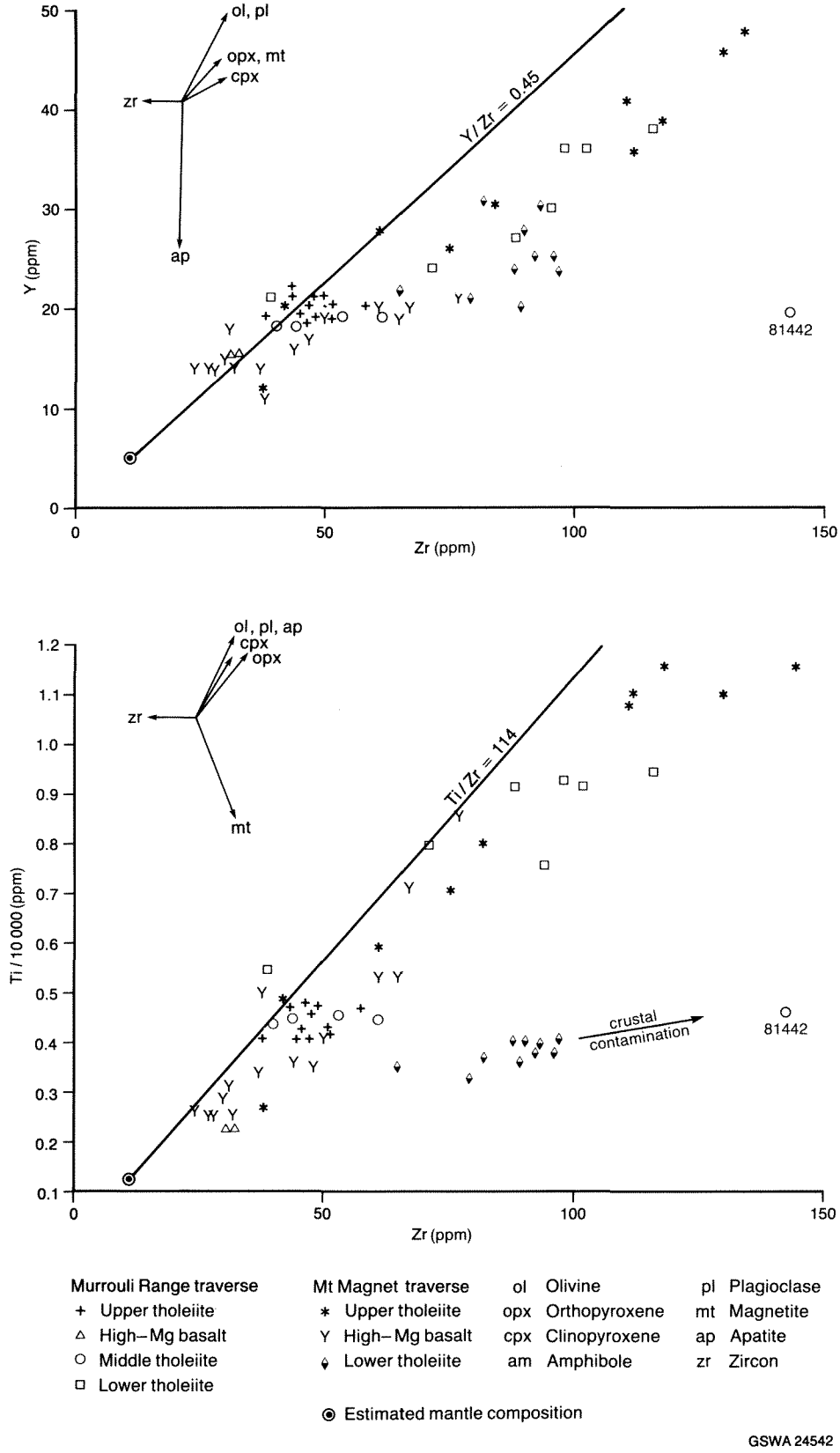


Figure 7. Y–Zr and Ti–Zr diagrams for Murrouli Basalt samples. Estimated mantle compositions (Sun and Nesbitt, 1977) and ratios are shown. Relative crystal-fractionation vectors for various minerals in equilibrium with a mafic melt, for up to 50% fractional crystallization (Pearce and Norry, 1979), are also shown.

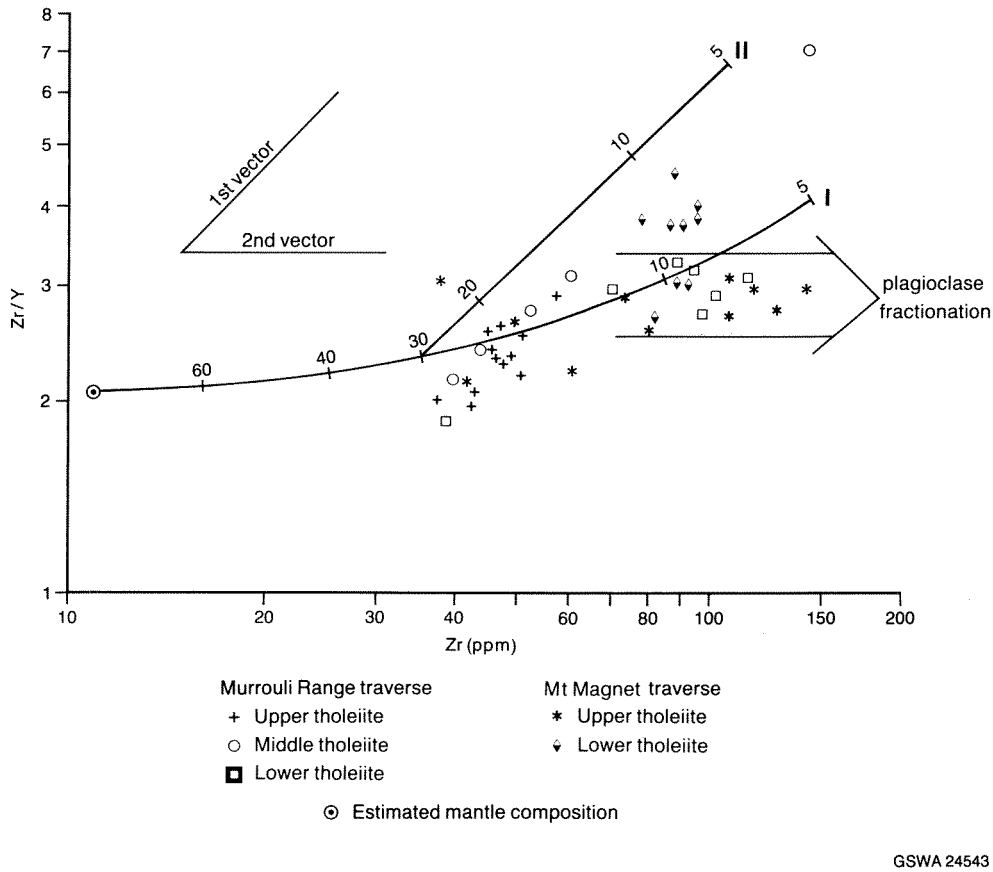


Figure 8. Zr/Y–Zr diagram for Murrouli Basalt samples. Two partial melting curves are shown: I — plagioclase-lherzolite source, consisting of olivine (0.6), orthopyroxene (0.2), clinopyroxene (0.1), and plagioclase (0.1); II — garnet-lherzolite source, consisting of olivine (0.6), orthopyroxene (0.2), clinopyroxene (0.1), and garnet (0.1), (mole fractions in brackets). For both sources, melting of mineral phases is in proportions 3:1:4:4, and clinopyroxene is completely melted after 30% melting (Pearce and Norry, 1979). Numbers indicate degree of partial melting (per cent). Mantle source Zr/Y–Zr composition from Sun and Nesbitt (1977).

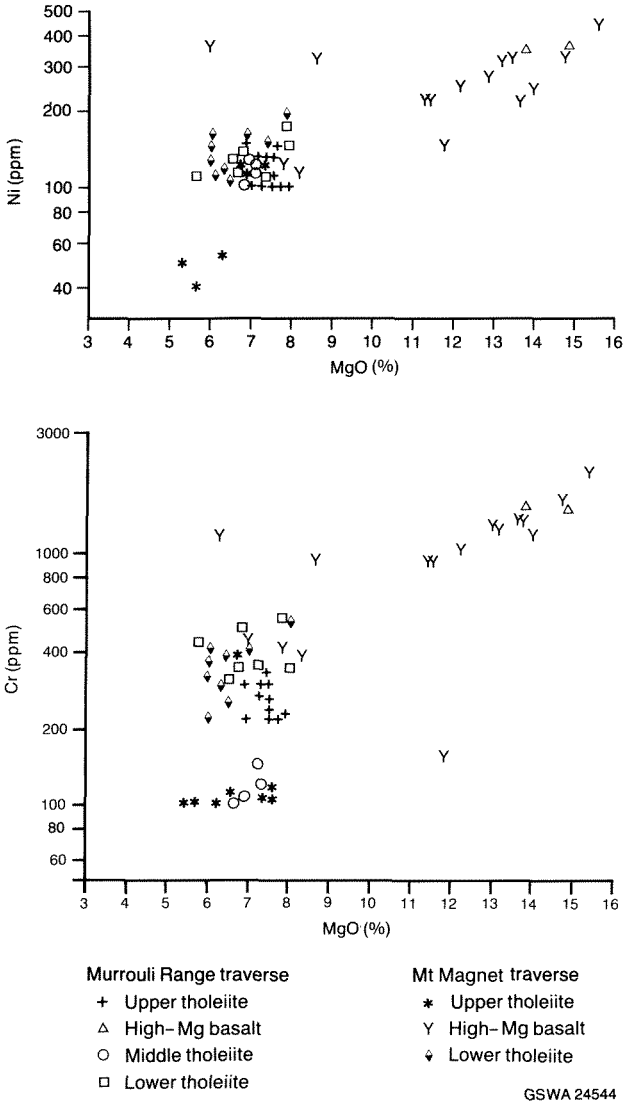


Figure 9. Ni–MgO and Cr–MgO plots for the Murrouli Basalt.

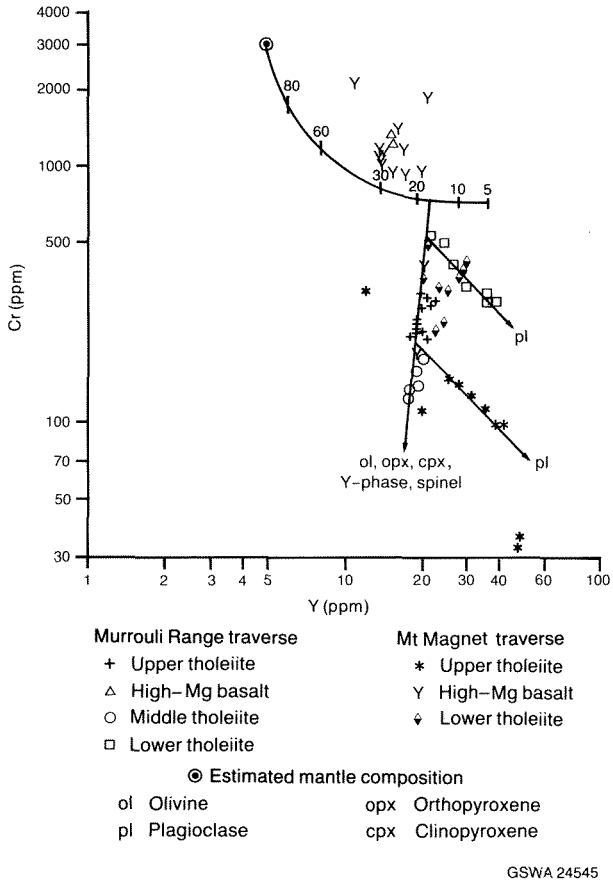


Figure 10. Y–Cr diagram for Murrouli Basalt samples. A model partial-melting curve is shown. The mantle source is plagioclase lherzolite (Sun and Nesbitt, 1977), consisting of olivine (0.6), orthopyroxene (0.2), clinopyroxene (0.1), and plagioclase (0.1) (mole fractions in brackets). Melting of mineral phases is in the proportions 3:1:4:4 (Pearce, 1980); after 30% melting, clinopyroxene is completely melted. Numbers indicate degree of partial melting (per cent). Model calculations follow the methods of Wood and Fraser (1977), and Cox, Bell, and Pankhurst (1979). Partition coefficients for Cr and Y are taken from Pearce and Norry (1979) and Pearce (1980). Straight lines are crystal-fractionation trends of liquid compositions following extraction of the phases indicated (Pearce and Norry, 1979; Pearce, 1980, 1982).

Magnet lower tholeiite unit, show no evidence of progressive fractionation in relation to stratigraphic level, either between or within units. It is likely that these units had separate source magmas from which spinel, pyroxenes, and olivine fractionated during ascent from the upper mantle. A small amount of an Y-bearing phase, such as apatite, zircon, or sphene, also fractionated from the melt and resulted in a slightly negative fractionation trend on the Y–Cr diagram (compare Fig. 10 with Pearce, 1982, fig. 4). The Murrouli Range lower tholeiite and Mount Magnet upper tholeiites underwent different amounts of spinel, pyroxenes, and olivine crystal fractionation, followed by plagioclase fractionation. Compositional trends of basalts along sample traverses in these units (Fig. 6) suggests that lavas were progressively tapped from liquids undergoing plagioclase crystal fractionation in magma chambers.

The origin of high-Mg basalt magmas is problematical (Arndt and Nisbet, 1982). High-Mg basalts in the Murrouli Basalt have Cr-rich compositions, and plot above the model curve derived by partial melting of the mantle composition represented in Figure 10. Plots of Cr–MgO and Ni–MgO (Fig. 9) for these rocks indicate that crystal fractionation of olivine was an important process in their genesis (Jahn et al., 1980). The mantle source could have been a residue rich in Mg-olivine (Drury, 1983).

Rare-earth elements: REE contents were determined for four samples from the Murrouli Range traverse, one from each of the basalt units. Chondrite-normalized REE patterns are shown in Figure 11. In addition, Sm–Nd isotope abundances were determined on three of these samples (Appendix III). The REE patterns and Sm/Nd ratios are typical of Archaean basalts (Basaltic Volcanism Study Project, 1981; Hawkesworth and Van Calsteren, 1984).

The lower tholeiite is slightly depleted in HREE (heavy

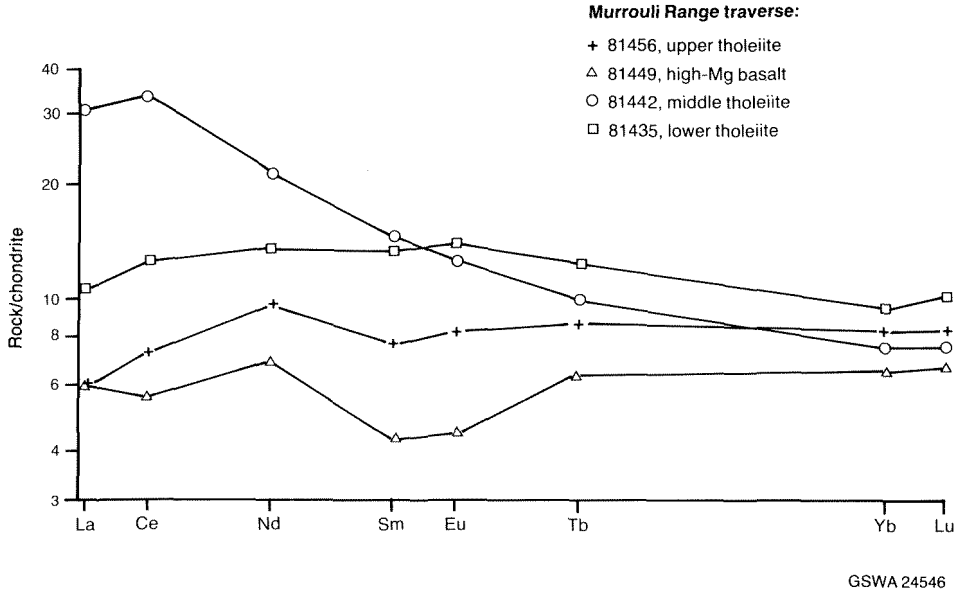


Figure 11. REE patterns for basalts from the Murrouli Range traverse. Original data have been normalized using values from Evensen et al. (1978) for type I carbonaceous chondrites, multiplied by 1.5 to give volatile-free values. Normalizing factors are listed in Taylor and McLennan (1985, appendix 2).

REE); this fact probably indicates minor residual garnet or clinopyroxene in the source region; small amounts (<5%) of these phases in the residue would have little effect on Ti–Zr and Y–Zr ratios (Sun and Nesbitt, 1978). This sample is depleted in LREE (light REE), which is a common feature of Archaean basalts, as it is of normal modern mid-ocean ridge basalts (MORB) (Jahn et al., 1980). If depletion is not due to alteration (Jahn and Sun, 1979), it may indicate a previous melt-extraction event in the source region (Basaltic Volcanism Study Project, 1981). Alternatively, it could be due to metasomatic processes (Hanson, 1981; Bailey, 1982). The sample is from near the base of the progressively fractionated lower tholeiite (Fig. 4B) but the REE pattern shows no evidence of fractionation, such as a Eu anomaly. However, about 15–20% plagioclase fractionation is necessary to produce a small negative Eu anomaly (Cullers and Graf, 1984a).

The middle tholeiite sample is a basaltic andesite and is unrepresentative of this unit. The REE pattern (Fig. 11) shows strong fractionation of LREE and HREE which may be due to crustal contamination (Barley, 1986), although inheritance of LREE enrichment from primary melts (Sun and Nesbitt, 1978) cannot be ruled out. The value of -0.4 for $\varepsilon_{Nd}(T)^*$ (Appendix III) is consistent with some degree of crustal contamination. The upper tholeiite sample is depleted in LREE and has a flat HREE pattern, indicating the absence of a garnet residue in the source region.

The high-Mg basalt has a flat HREE pattern, again indicating absence of a garnet residue in the source. The LREE are strongly depleted, suggesting considerable previous melt extraction or metasomatism; however, their irregular abundances may indicate some alteration (Jahn and Sun, 1979). The low REE abundance suggests that this rock was derived by a higher degree of partial melting than the other rocks (Cullers and Graf, 1984a). The near-chondritic values of Sm/Nd preclude calculation of reliable model ages.

In summary, it is clear that petrogenesis of the Murrouli Basalt was complex. Tholeiitic units were generated by partial melting of a plagioclase-lherzolite source, which in the case of the lower tholeiite from the Murrouli Range may have contained some residual garnet or clinopyroxene. The composition of the source region itself was being modified by addition and extraction of magma (Pearce and Norry, 1979; Bailey, 1982). Following partial melting, crystal fractionation of olivine, pyroxene, and spinel occurred, probably during ascent of magma to the upper crust. Some magmas then erupted onto the surface, while others underwent closed-system fractionation of mafic phases and plagioclase in magma chambers, from which lava was periodically tapped and erupted onto the surface. High-Mg basalts were derived by partial melting of a depleted mantle source of unknown composition, followed by olivine and spinel crystal fractionation.

Golconda Formation

Definition and distribution

The Golconda Formation is defined here as a succession of quartz–hematite BIF units interlayered with mafic and ultramafic extrusive and intrusive rocks, overlying the Murrouli Basalt. The formation is a distinctive stratigraphic marker which occurs throughout the northern and

*$\varepsilon_{Nd}(T)$ is the deviation (in parts/10^4) of the $^{143}Nd/^{144}Nd$ composition of the sample from $^{143}Nd/^{144}Nd$ of CHUR, calculated for time T. CHUR is the Chondritic Uniform Reservoir (an estimate of average earth composition)

central parts of the Murchison Province (Plate 2). In common with the Murrouli Basalt, it does not occur in the westernmost greenstone belts, or south of 28° 50'. The formation was either not developed in these regions or was excised from the greenstone belts by granitoid intrusions.

The formation is thickest near Golconda Well on CUE, where it is exposed in large outcrops in an anticlinal structure in and around Lake Austin (Watkins et al., 1987). It is more than 3 km thick in this region. The formation is overlain by well-exposed Gabanintha Formation mafic and ultramafic rocks. However, this is not designated as the type area as the rocks in the core of the anticline, underlying the Golconda Formation, are not exposed. The type area for the Golconda Formation is near the old railway siding and mining centre of Nannine, about 42 km south of Meekatharra between Butcher Well and Five Mile Well (Fig. 12, Plate 2). Here the formation consists of a 1000 m-thick succession of abundant quartz–hematite BIF units, 1–5 m-thick, interlayered with basalt, gabbro, dolerite, and minor amounts of ultramafic and sedimentary rocks. The rocks between the BIF units are very poorly exposed. Along the track between Butcher Well and Five Mile Well the formation is underlain by gabbro and tholeiitic basalt of the Murrouli Basalt, and overlain by serpentinite and tholeiitic basalt of the Gabanintha Formation. On a regional scale the thickness of the formation varies from a few hundred metres to several kilometres; the average thickness is about 1.5 km (Fig. 3).

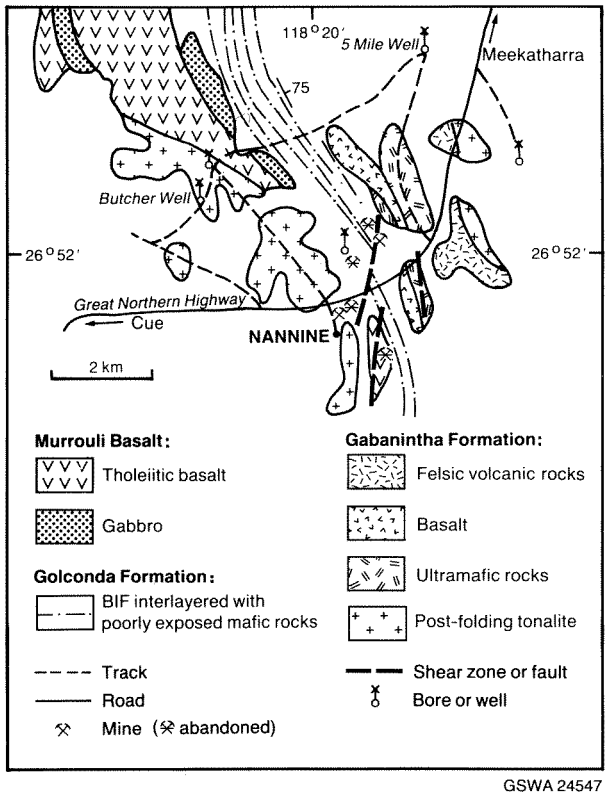


Figure 12. Geology of the type area for the Golconda Formation.

Lithostratigraphy

The Golconda Formation consists of numerous 1–5 m-thick quartz–hematite BIF units, interlayered with 10–50 m-thick units of mafic extrusive and intrusive rock, and minor amounts of ultramafic rock. BIF units generally form topographically prominent ridges and ranges of hills; the intervening rocks are poorly exposed and generally covered by BIF scree. Both BIF and the intervening rock units are deeply weathered in most areas. At the surface, BIF units comprise alternating recrystallized quartz-rich and hematite-rich bands, and occasional white chert bands a few millimetres to one centimetre thick. In the greenschist facies, mineral phases include quartz, magnetite, chamosite, stilpnomelane, minnesotaite, riebeckite, ankerite, calcite, and a fibrous amphibole which is probably actinolite. Hematite and goethite have largely replaced magnetite during weathering. The texture is fine grained granoblastic. In the amphibolite facies, BIF is coarsely recrystallized, and banding is less prominent, probably because of the quartz-consuming nature of many of the prograde metamorphic reactions (Gole, 1981). The texture is granoblastic, and generally medium to coarse grained; common mineral phases include quartz, magnetite, grunerite, and hornblende.

Rocks interlayered with BIF units comprise dolerite, gabbro, tholeiitic and high-Mg basalts, amphibolite, and mafic and ultramafic schists, and some fine-grained sedimentary rocks. The proportion of intrusive to extrusive rock is much higher than in the underlying Murrouli Basalt. The formation has clearly been intruded selectively by sills. The high, and variable, proportion of intrusive rock accounts for much of the variation in thickness of the formation. As in the Murrouli Basalt, flow features in basalt are extremely rare. However, as BIF units are generally 10–50 m apart, a maximum flow thickness of about 50 m (ignoring the effects of any tectonism) can be inferred, although most flows are probably much thinner.

Geochemistry

Sampling

Seventy-six samples were collected for geochemical analysis from a number of traverses and localities. Of these, 66 are BIF, and 10 are basalt. The small number of basalt samples reflects the degree of weathering of these rocks. Maps of sample localities are not shown as there is little chemostratigraphic variation; most samples were taken from short, very closely spaced traverses, or from single localities. Most BIF samples are from the Mount Magnet area (30); other BIF samples are from east of the Murrouli Range (6); The Island on CUE (8); Swan Bore, north of Mount Yagahong on GLENGARRY (7); Noongal (9), and Mugga Mugga Hill on YALGOO (6). In addition to surface samples, seven samples of BIF were obtained from diamond-drill core from The Island. The basalt samples are from Swan Bore (3), Kylie Hill (4), and Noongal (3). Sample grid references and chemical analyses are listed in Appendix II.

Compositional characteristics

BIF: All surface samples of BIF are almost completely oxidized and, with the exceptions of SiO_2 and Fe_2O_3, contain low and variable abundances of oxides and trace elements (Table 4). There is no apparent systematic variation with stratigraphic height and, generally, there is as much variation at a single sample locality as between localities. Drill-core samples from The Island are less oxidized and more hydrated than the surface samples. However, apart from differences in Fe_2O_3/FeO ratio, and MgO, CaO, LOI, Ba, Cr, Cu, and V contents, overall abundances of oxides and elements are similar. Most differences can be attributed to weathering, and to a volcaniclastic component in some of the drill-core samples (see 'Petrogenesis' below).

Basalt: Noongal and Kylie Hill tholeiitic basalts have very similar compositions and are distinctly different from those from Swan Bore (Table 5). The basalt from Swan Bore is a high-Fe tholeiite (Fig. 13) with typically high TiO_2 and V contents, similar to the Mount Magnet upper tholeiite in the Murrouli Basalt. Basalts from Noongal and Kylie Hill have much lower FeO*, TiO_2, V, Y, and Zr values, and higher MgO, Cr, and Ni values. Both tholeiites have affinities with high-Mg basalt, although only one sample (81365) is classed as a high-Mg basalt; the others plot in the high-Mg tholeiite field (Fig. 13, Table 5). There are too few samples to characterize any chemical variation within these units.

TABLE 4. MEAN COMPOSITIONS OF GOLCONDA FORMATION BANDED IRON-FORMATIONS

	All surface samples n=66	*The Island surface samples n=8*	*The Island drill-core samples n=7*
	Percentage		
SiO_2	51.0	47.8	41.7
Al_2O_3	0.19	<0.1	1.5
Fe_2O_3	43.6	47.4	18.9
FeO	1.7	1.7	20.6
FeO* (a)	40.9	44.3	37.6
MgO	0.25	0.03	3.2
CaO	0.27	0.04	2.0
Na_2O (b)	0.02	0.02	0.13
K_2O (b)	0.01	0.01	0.20
TiO_2 (b)	0.06	<0.01	0.09
P_2O_5	0.13	0.07	0.19
MnO	0.03	0.01	0.07
LOI	2.40	2.31	10.20
S	nd	0.013	0.050
	Parts per million		
Ba (b)	172	<10	58
Cr (b)	47	<10	21
Cu	50	43	11
Ni (b)	7	14	17
V	11	<5	33
Y	6	<5	7
Zn	52	28	69
Zr (b)	8	<10	13
Ce (b)	6	<10	9
La (b)	7	<10	7

(a) All Fe calculated as FeO
(b) Some values used to calculate the mean are below the detection limit; for these determinations the value 'detection limit/2' was used.
nd: not determined

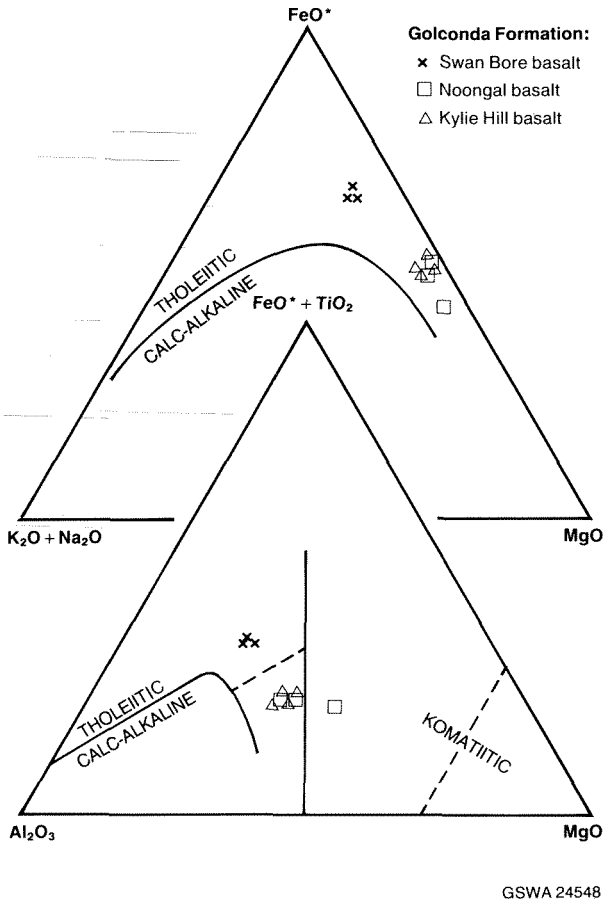


Figure 13. Golconda Formation basalts plotted on an AFM diagram (above) and a Jensen diagram (below).

Petrogenesis

BIF: Most Archaean BIF is thought to have originated by some mechanism of chemical precipitation (e.g. Condie, 1981). As a result, iron-formations generally have very low contents of most trace elements (Gole, 1981; Davy, 1983). However, some BIFs have higher HFS element contents, as well as higher Al_2O_3 and TiO_2 contents, indicating a volcaniclastic or epiclastic component (Ewers and Morris, 1981; Davy, 1983). Some drill-core samples show this type of enrichment (Fig. 14). Zr–Al_2O_3 ratios of these samples are comparable with those for tholeiitic basalt. The source of the volcaniclastic or epiclastic component in the BIF was probably mafic.

Basalt: The ten basalt samples are compared with basalts from the Murrouli Basalt on Y–Zr, Ti–Zr, Zr/Y–Zr, and Cr–Y diagrams in Figure 15. On most of these diagrams Noongal and Kylie Hill samples plot in, or near, the high-Mg basalt field. The Swan Bore samples generally plot just inside the 'more-fractionated tholeiite' field. Both groups have Y/Zr and Ti/Zr ratios similar to those for estimated Archaean mantle compositions (Sun and Nesbitt, 1977; Sun, 1982), indicating derivation by melting of an upper mantle source. The positions of the data points on these plots, relative to mantle source compositions, indicate that partial melting was followed by different degrees of crystal

TABLE 5. MEAN COMPOSITIONS OF GOLCONDA FORMATION BASALTS

	Swan Bore tholeiite n=3	*Noongal tholeiite n=2*	*Noongal high-Mg basalt n=1*	*Kylie Hill tholeiite n=4*
		Percentage		
SiO_2	50.6	51.1	49.8	50.6
Al_2O_3	13.0	13.0	11.7	11.7
Fe_2O_3	2.8	1.6	1.2	3.0
FeO	12.0	8.3	9.1	7.6
FeO* (a)	14.5	9.73	10.2	10.3
MgO	5.29	8.73	12.2	8.84
CaO	10.10	12.90	9.58	12.76
Na_2O	1.88	0.59	0.99	0.77
K_2O	0.13	0.05	0.07	0.03
TiO_2	0.99	0.45	0.43	0.55
P_2O_5	0.12	0.19	0.16	0.09
MnO	0.22	0.16	0.17	0.19
LOI	1.87	1.94	2.53	1.78
S	0.003	0.55	0.005	nd
		Parts per million		
Ba	31	<25	50	47
Cr	86	570	880	414
Co	74	nd	nd	87
Cu	70	56	67	39
Ni	87	141	215	159
Sr	83	142	76	40
V	324	205	211	214
Y	25	15	14	19
Zn	97	76	77	69
Zr	59	26	24	32
La	6	<5	6	nd
Ce	9	<5	<5	nd
Mg number (b)	39.4	61.5	68.1	60.5
Cr/V	0.27	2.78	4.17	1.93
Zr/(Zr+Y)	0.70	0.63	0.63	0.63

(a) All Fe calculated as FeO (b) 100mol MgO/(MgO + FeO)
Samples assigned to alteration class 3 (see Appendix II) are omitted from the means.
For most analyses averaged in this table Rb<2ppm, Th<5ppm, Nb<5ppm and Pb<10ppm.
nd: not determined

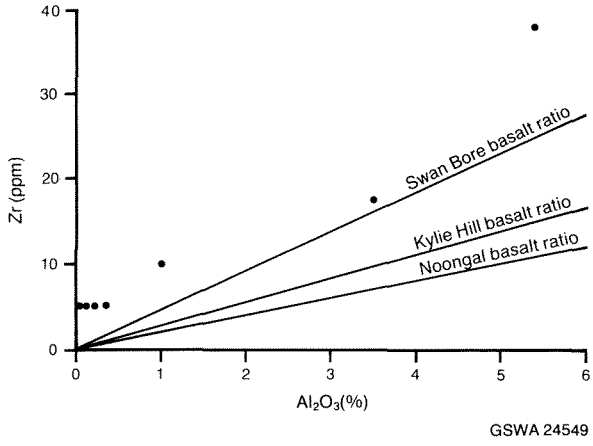


Figure 14. $Zr–Al_2O_3$ plot for banded iron-formation drill-core samples from The Island on CUE. $Zr–Al_2O_3$ ratios for Golconda Formation basalts are shown for comparison.

fractionation of olivine, pyroxenes, and possibly plagioclase (compare Figs 15A and B with Fig. 7). There are insufficient data to characterize trends on the other plots. However, when compared with data from the Murrouli Basalt, it appears that basalts from Noongal and Kylie Hill may have had a source and derivation process similar to high-Mg basalt in the Murrouli Basalt. The basalt from Swan Bore was probably derived from a similar source and by processes similar to those that produced the Murrouli Range lower tholeiite and Mount Magnet upper tholeiite. Swan Bore compositions correspond to least-fractionated members of these tholeiites.

Two of the Swan Bore basalt samples have remarkably similar middle and heavy REE (referred to as MREE and HREE, respectively) patterns (Fig. 16). La and Ce abundances appear to have been altered (Jahn and Sun, 1979). The flat, almost coincident HREE patterns suggest that both samples were derived by the same degree of partial melting of a plagioclase-lherzolite source. The MREE abundances of about 12 times chondrite are similar to those of the Murrouli Range lower tholeiite shown in Figure 11.

In summary, Golconda Formation basalts appear to have been generated by similar processes to those that

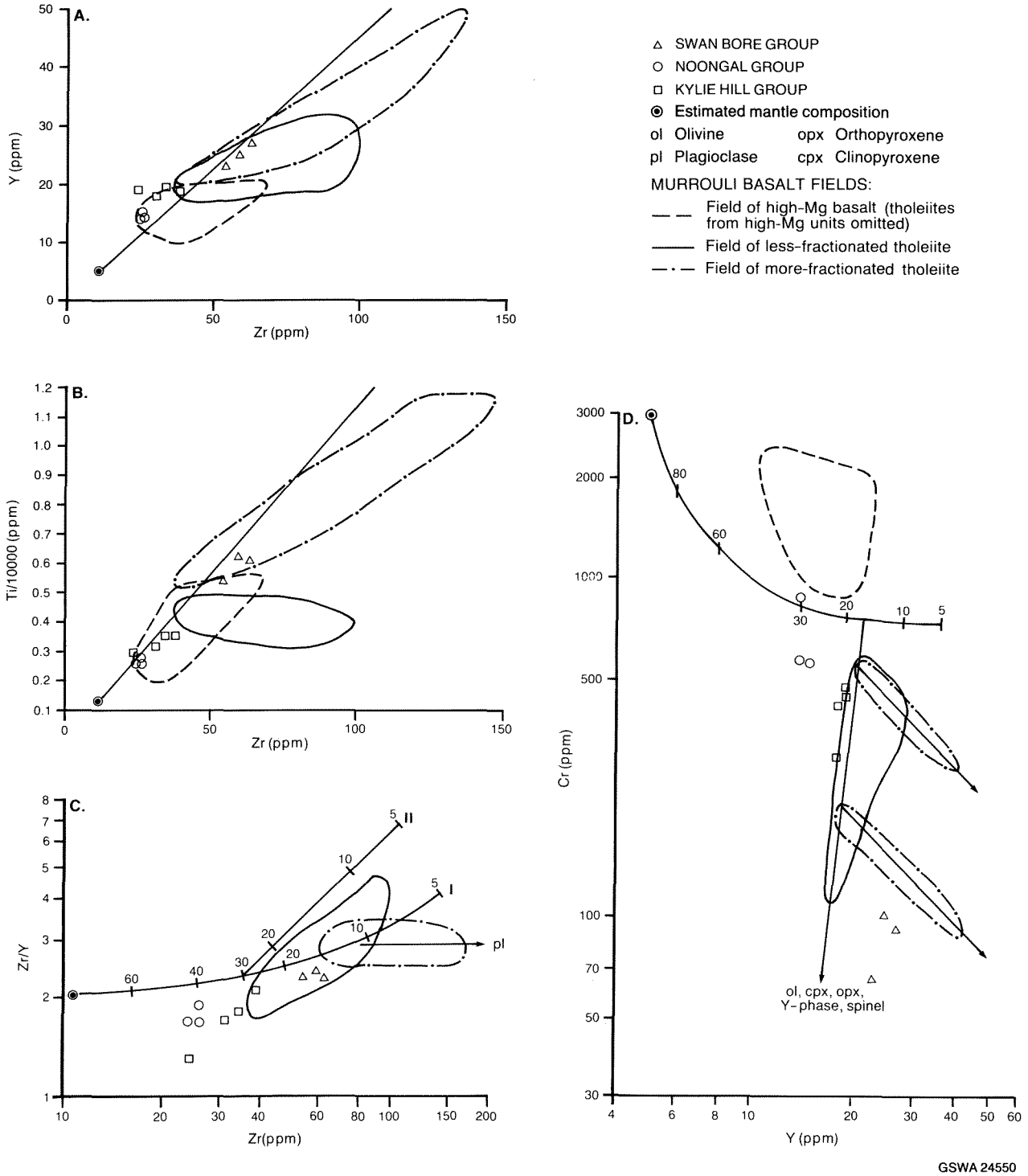


Figure 15. High field strength element interrelationships for Golconda Formation basalts. Murrouli Basalt compositional fields are shown for comparison. Data for partial-melting curves are given in Figures 8 and 10.

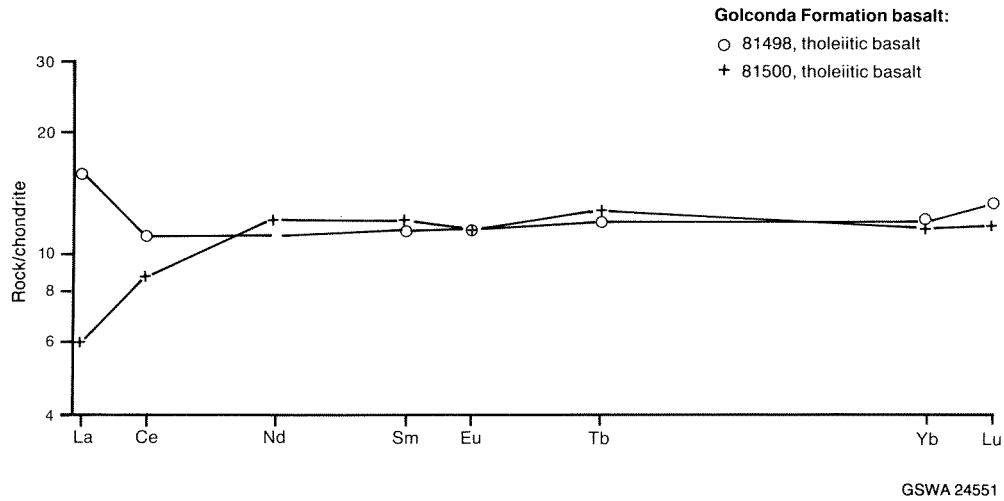


Figure 16. REE patterns for Golconda Formation basalt from Swan Bore.

formed the underlying Murrouli Basalt. This observation, combined with the relative paucity and limited thickness (10–50 m) of flows, suggests that the basalts represent the waning stages of the same overall, laterally extensive, volcanic episode. The presence of extensive, interlayered, chemically precipitated BIF, with a limited pyroclastic and/or epiclastic component, supports this conclusion and indicates that the Golconda Formation was deposited in relatively quiescent conditions.

Gabanintha Formation

Definition and distribution

The Gabanintha Formation is defined here as a bimodal succession of mafic and ultramafic rocks, felsic volcanic and volcaniclastic rocks, and sedimentary rocks, overlying the Golconda Formation. The formation is the most voluminous and widespread in the Murchison Supergroup. It accounts for almost half the thickness of the Luke Creek Group (Fig. 3) and comprises a substantial part of every greenstone belt in the Murchison Province (Plate 2). It is the lowest stratigraphic formation identified south of latitude 28° 50'.

The type area for the Gabanintha Formation is in the vicinity of the Gabanintha mining centre (Plates 1 and 2). Here the formation consists of a 1400 m-thick sequence of intrusive and extrusive ultramafic rocks at the base, overlain successively by interlayered high-Mg and tholeiitic basalt, 1100 m thick, and felsic volcanic and volcaniclastic rocks, 400 m thick. The succession in this area is intruded by a layered gabbro sill, about 1000 m thick, which has metamorphosed the immediately surrounding rocks to granulite facies (equivalent to the pyroxene-hornfels facies of Turner, 1981) (Plate 3). The succession is also cut by major northwest-trending shear zones (Plates 1 and 2). The Gabanintha Formation overlies the Golconda Formation north of Mount Yagahong, at Swan Bore, and is overlain by the Windaning Formation, 3.5 km west-northwest of the Gabanintha mining centre, at Star Bore. On a regional scale there is considerable variation in the thickness of the Gabanintha Formation, and in some areas the felsic component of the mafic–felsic bimodal sequence is missing. The mean thickness of the formation over the whole province is estimated to be 5000 m (Fig. 3).

Lithostratigraphy

Lithologies in the Gabanintha Formation comprise a bimodal sequence (e.g. Thurston and Fryer, 1983; Thurston et al., 1985; Jensen, 1985). Mafic and ultramafic rocks are overlain by felsic volcanic and volcaniclastic rocks interlayered with mafic rocks.

A laterally extensive ultramafic unit occurs locally at, and elsewhere close to, the base of the formation in the Meekatharra–Wydgee greenstone belt, between Meekatharra and Mount Magnet (compare Plates 1 and 2). Where it does not directly overlie the Golconda Formation, it is underlain by up to 500 m of basalt, e.g. at Yaloginda. This unit consists mainly of serpentinite, often with relic cumulate texture, talc–chlorite(–amphibole) schist, talc–carbonate schist, some ultramafic pyroclastic rocks, and rare, thin BIF units. Textures are generally poorly preserved because of deformation and metamorphism. Many outcrops are silicified and are now covered by a light-brown siliceous caprock. The unit is a volcanic–intrusive complex, with laterally variable proportions of volcanic and intrusive rocks. Its thickness varies from a few hundred metres to about 1400 m near the Gabanintha mining centre, where intrusive components appear to dominate. The ultramafic complex hosts much of the gold mineralization of the region (see Chapter 7). The complex is overlain by interlayered high-Mg and tholeiitic basalts with rare, thin BIF units; towards the top of the formation felsic volcanic rocks are interlayered with mafic rocks (Plate 1).

In the Meekatharra–Wydgee greenstone belt, south of Mount Magnet, and in other greenstone belts, the mafic–ultramafic portion of the bimodal formation consists of interlayered tholeiitic and high-Mg basalts together with relatively minor ultramafic units, mainly talc–chlorite–

amphibole schist and serpentinite, and rare, thin BIF units. The ultramafic units are not concentrated at the base of the formation in these regions. The mafic–ultramafic portion of the formation consists of approximately 60% tholeiitic basalt, 30% high-Mg basalt and 10% ultramafic rocks, excluding major sills. Apart from textural variations between high-Mg basalt and tholeiite, basalt sequences are generally monotonous and lack morphological volcanic features, as do basalts in underlying formations. However, pillow lava and mafic pyroclastic rocks are developed at a few localities, e.g. Trenton Hill, Cue Hill, and Pirgan Hill. Thin, rare, and discontinuous BIF units are developed in some regions; these are thought to represent interflow sediments. The basalts form accumulations up to several kilometres thick (Plate 1).

Felsic volcanic and volcaniclastic rocks form thin units in the upper part of the Gabanintha Formation throughout the Murchison Province. However, accumulations several kilometres thick were developed at local centres (Table 6). These probably represent the partly eroded, deformed, and metamorphosed remnants of central felsic volcanic complexes. Felsic rocks are interlayered with mafic rocks on a regional scale (compare Plates 1 and 2), which indicates that mafic and felsic volcanism were broadly contemporaneous in the upper part of the formation. Overall, felsic rocks comprise about 15% of the Gabanintha Formation. Most are now strongly foliated and thoroughly recrystallized fine-grained schists; igneous textures are preserved only rarely. Mineral assemblages include quartz, K-feldspar, plagioclase, epidote, biotite, amphibole, chlorite, and sphene.

Epiclastic and volcanogenic sandstone units occur in the

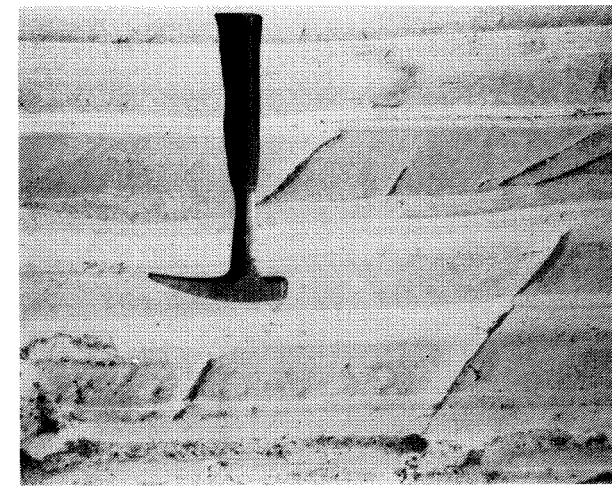
TABLE 6. CENTRAL FELSIC VOLCANIC CENTRES IN THE GABANINTHA FORMATION

Location	*Approximate thickness*	*Approximate lateral extent*	*Lithology*	*Stratigraphic and structural relationships*
Mingah Range greenstone belt (BELELE)	1800 m	30 km	Felsic crystal-lithic tuff, generally fine grained and schistose	Underlain and overlain by mafic rocks; intruded by thick (up to 500 m) mafic and ultramafic sills; tightly folded and intensely sheared
Abbotts greenstone belt (BELELE)	3000 m	30 km	Mainly schistose felsic tuff and volcanogenic sedimentary rocks; andesite lava and tuff occur in the western part of the complex	Complex occupies core of syncline; underlain by mafic rocks, and intruded by gabbro and dolerite sills; contains minor basalt units
Mindoolah (BELELE)	?2500 m	13 km	Schistose felsic tuff and agglomerate; abundant felsic porphyry; volcanogenic sedimentary rocks in the southern portion ofthe complex	Structure poorly understood, probably antiformal; contains minor basalt units; overlain by Beebynganna Formation; intruded by a post-folding granitoid
Weebacarry Bore (BELELE)	3000 m	15 km	Schistose felsic tuff and agglomerate	Complex occupies the core of a syncline; underlain by basalt and intruded by post-folding granitoid plutons
Reedy (CUE)	3500 m	35 km	Fine-grained quartz–K-feldspar - plagioclase–epidote–amphibole–chlorite–biotite–sphene schist; chiefly andesite and dacite, with minor rhyolite and basalt	Complex is bounded by shear zones and the rocks are intensely sheared; intruded by a post-folding tonalite and felsic porphyry
Cuddingwarra (CUE)	1500 m	30 km	Fine-grained and porphyroclastic rhyolite and dacite; quartz–K–feldspar–plagioclase–chlorite–biotite schists	Underlain and overlain by by mafic rocks; upper portion intruded by layered mafic sills; base intruded by post-folding tonalite
Eelya Hill (CUE)	?5000 m	15 km	Fine-grained and porphyroclastic rhyolite and dacite; quartz–K–feldspar–plagioclase–chlorite–biotite schists	Interlayered with mafic rocks in the south and east of the complex; intruded by post-folding granodiorite in the central part; complex may have been thickened by faulting and folding

TABLE 6. (continued)

Location	*Approximate thickness*	*Approximate lateral extent*	*Lithology*	*Stratigraphic and structural relationships*
Wydgee (KIRKALOCKA)	2000 m	15 km	Schistose dacite, crystal and lithic tuffs, agglomerate, and porphyritic lava; minor flow-banded rhyolite	Complex is folded by a tight F_3 syncline; interlayered with mafic rocks and intruded by recrystallized and post-folding monzogranite
Golden Grove (YALGOO)	2500 m	25 km	Schistose fine-grained volcanogenic sedimentary rocks, felsic tuff, lava and agglomerate (see Frater, 1983a, for detailed description)	Underlain by sandstone; overlain by mafic rocks to the south, and Beebynganna Formation to the north; intruded by post-folding granitoid to the north
Twin Peaks greenstone belt (MURGOO)	1500 m	22 km	Banded felsic tuff, volcanogenic sedimentary rocks	Underlain by basalt; overlain by Beebynganna Formation
Paynes Find (NINGHAN)	2500 m	9 km	Schistose rhyolite and dacite lava, agglomerate and tuff; minor volcanogenic sedimentary rocks; minor mafic rocks	Underlain by basalt; overlying rocks not exposed; intruded by post-folding granitoids

upper part of the Gabanintha Formation at Jillewarra (BELELE); in the Cuddingwarra to Sparrow Well area (CUE); and underlying the Golden Grove felsic volcanic complex. At Jillewarra, a white, cross-bedded quartz-sandstone unit, up to 400 m thick, occurs in an isoclinal fold bounded by shear zones (Plates 1 and 2); its stratigraphic position is therefore uncertain. A belt of poorly exposed sandstone and shale, locally up to 1000 m thick, extends from Cuddingwarra, south to Sparrow Well. These rocks are generally foliated or schistose; however, west of Trenton Hill, graded bedding is well preserved in water-worn pavements in creeks on the margin of Lake Austin (Fig. 17). The rocks consist of about 70% subrounded to angular quartz and (less abundant) plagioclase grains in a matrix of fine-grained quartz, sericite, and kaolinite. Some outcrops near Sparrow Well contain rounded cobbles of vein quartz several centimetres across. A unit of weathered and very poorly exposed sandstone underlies the Golden Grove felsic volcanic complex. The precise thickness of the unit is unknown, but is probably of the order of a few hundred metres.



GSWA 24552

Figure 17. Graded bedding in Gabanintha Formation epiclastic sandstone, 3 km west-northwest of Trenton Hill. The hammer handle is 30cm long.

The Gabanintha Formation is intruded by numerous gabbro and dolerite sills. Some sills are layered, and have peridotite or pyroxenite bases and leucogabbro tops. Many thicker gabbro units (shown on Plates 1 and 2) consist of multiple gabbro sills, several hundred metres thick, separated by thin screens of country rock, most of them basalt. These sill complexes are particularly well developed in the southern Murchison where they attain combined thicknesses of several kilometres (Plate 1).

Geochemistry

Sampling

Three hundred and ninety one rock samples were collected from the Gabanintha Formation for chemical analysis. Of these, 310 are mafic, 78 are felsic, and 3 are BIF. Most samples were collected along traverses across only part of the formation (Table 7, Fig. 18). Simplified geological maps and stratigraphic columns for traverses containing more than ten samples are shown in Figure 19. Stratigraphic columns are not shown for mono-lithological traverses, or where structural complexities obscure the way-up of all or part of the sequence traversed. No map is shown for traverse 31 (Table 7) as most samples are from an exploratory shaft sunk into the Scuddles massive sulphide deposit at Golden Grove. Chemical analyses are listed in Appendix II.

Bimodal compositions

Samples collected from the Gabanintha Formation comprise rocks with a broad compositional range from high-Mg basalt to rhyolite (Fig. 20). Basalts have a broad

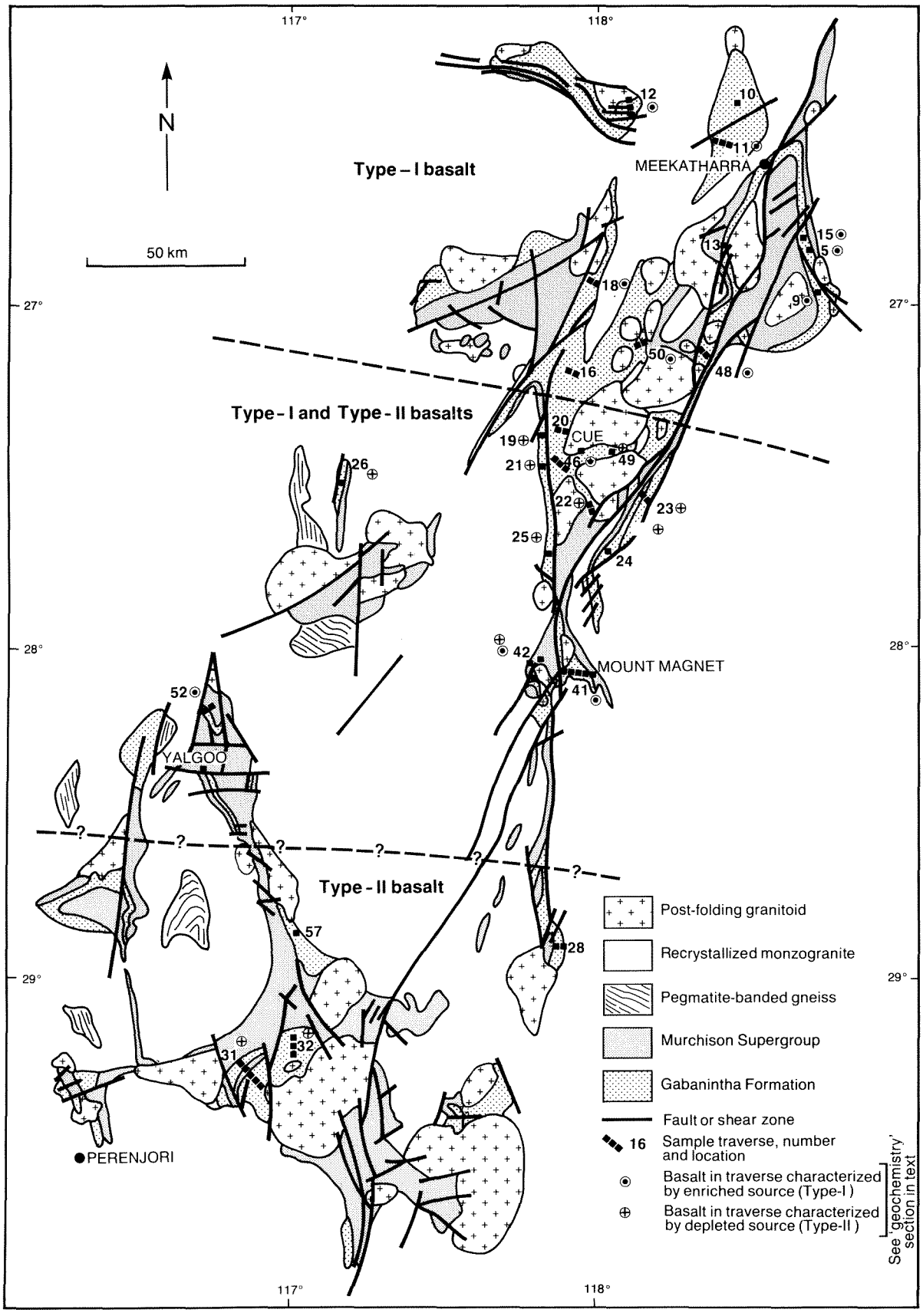


Figure18. Locations of sample traverses in the Gabanintha Formation. Province is subdivided to show occurrence of Type-I and Type-II basalts.

Windaning Formation:

- BIF, felsic volcanic and felsic volcanogenic sedimentary rocks
- Gabbro
- Pyroxenite

Gabanintha Formation:

- Tholeiitic basalt
- High-Mg basalt
- Interlayered high-Mg and tholeiitic basalt
- Ultramafic rocks
- Pyroxenite
- Gabbro and dolerite
- Felsic volcanic rocks
- Volcanogenic sedimentary rocks
- Epiclastic sedimentary rocks
- Felsic porphyry
- BIF and chert

Golconda Formation:

- BIF and mafic rocks

Granitoids:

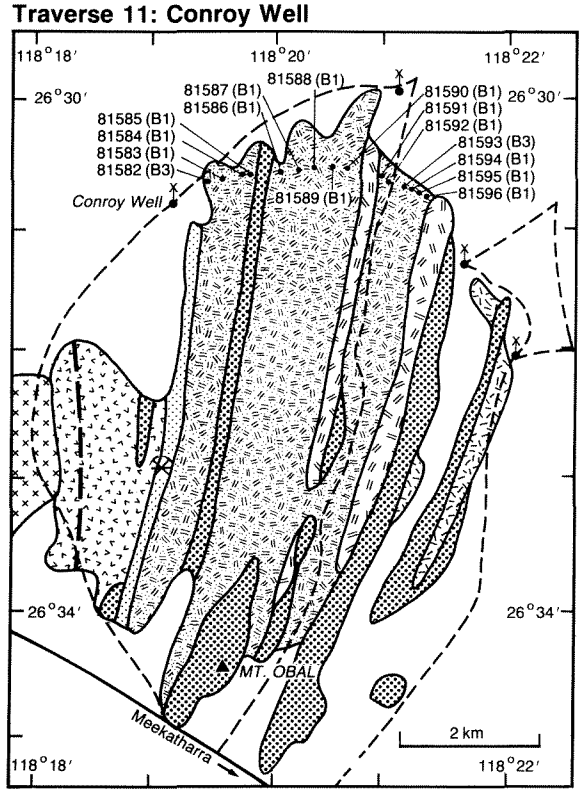
- Post-folding granitoid
- Recrystallized monzogranite
- Shear zone or fault
- Sheared granitoid contact
- Intrusive granitoid contact
- Mine
- Abandoned mine
- Road
- Track
- Homestead
- Well or bore

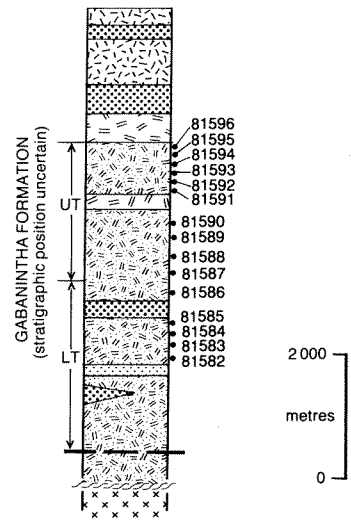
Geochemically distinct units (not correlated between traverses):

UT	Upper tholeiite	UB	Upper basalt
MT	Middle tholeiite	MB	Middle basalt
LT	Lower tholeiite	LB	Lower basalt
HM	High-Mg basalt	BA	Basaltic andesite

Note: Codes in brackets following sample numbers refer to 'rock type' and 'degree of alteration' as defined in Appendix II.

Traverse 11: Conroy Well





GSWA 24554 A

Figure 19. Geological maps and stratigraphic columns of areas traversed for geochemical samples in the Gabanintha Formation. Geochemically distinct units are distinguished in the stratigraphic columns. Note that map and stratigraphic column scales are not uniform.

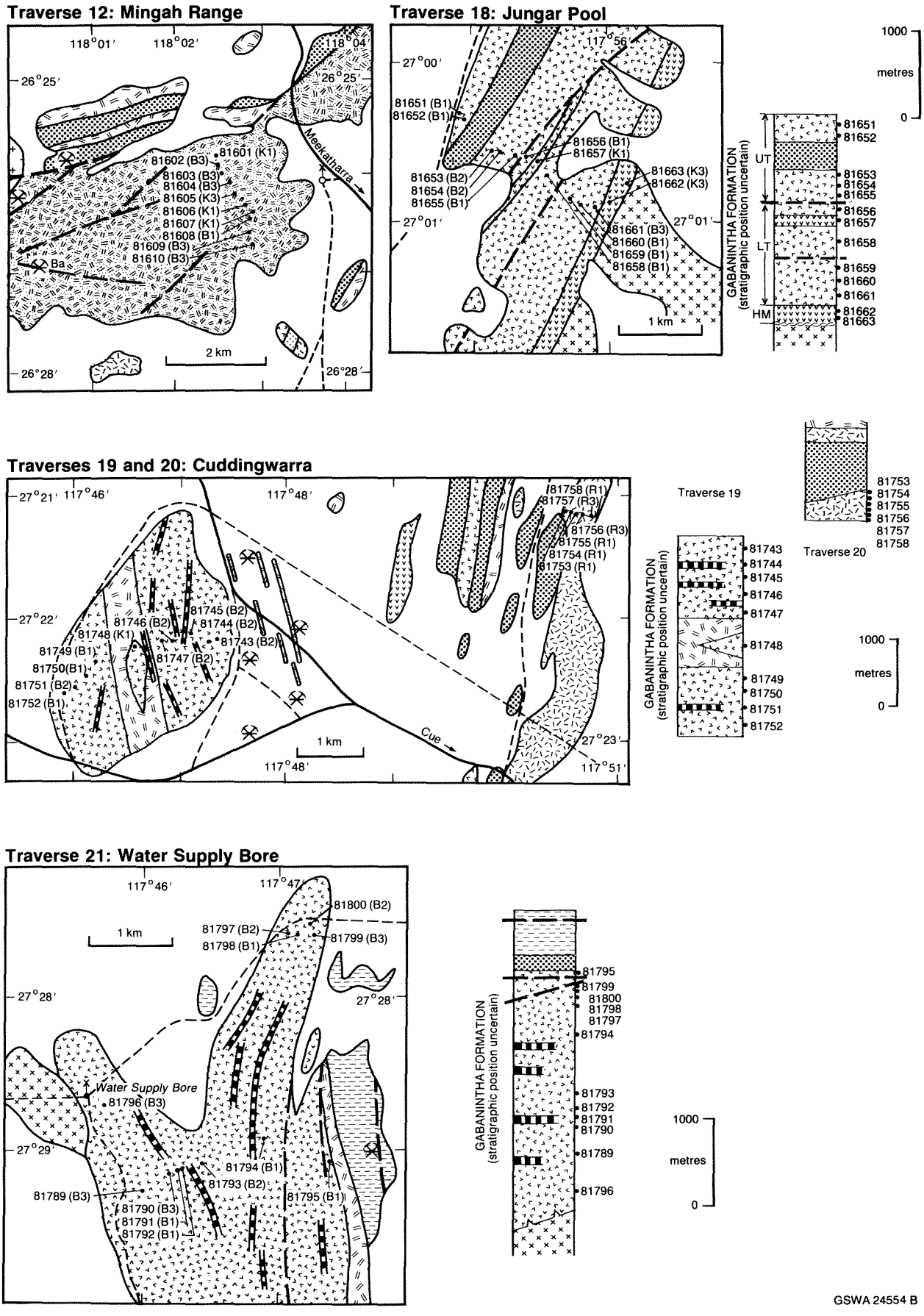
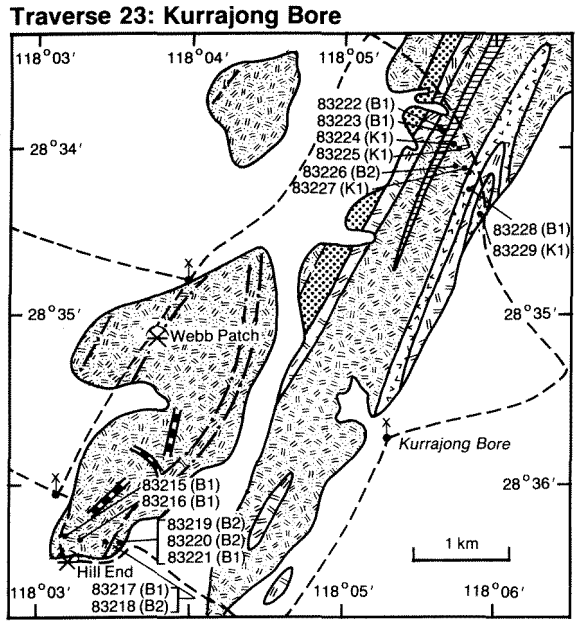
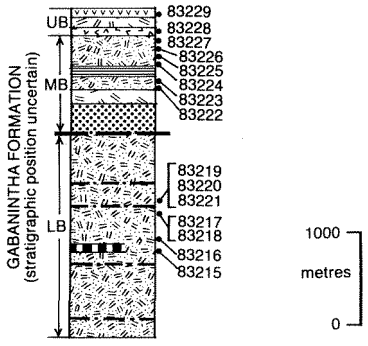


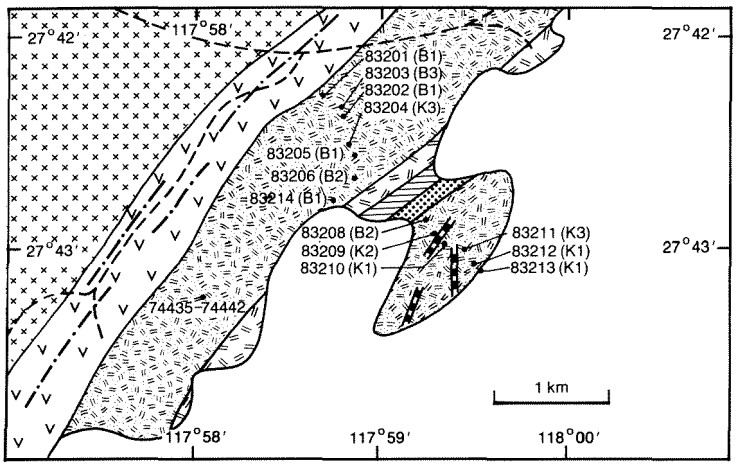
Figure 19. (continued)

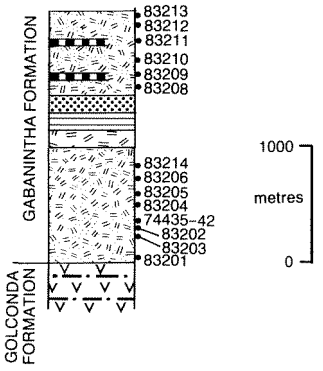
Traverse 23: Kurrajong Bore



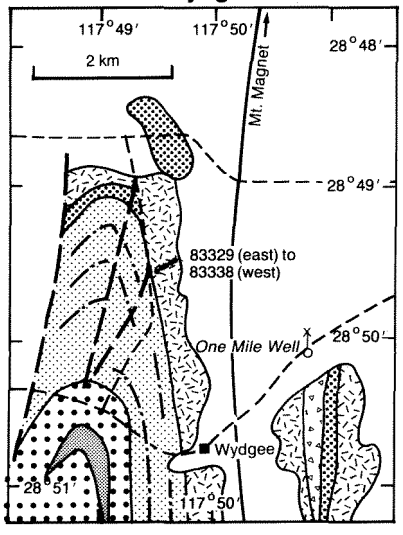


Traverse 24: Jean Well





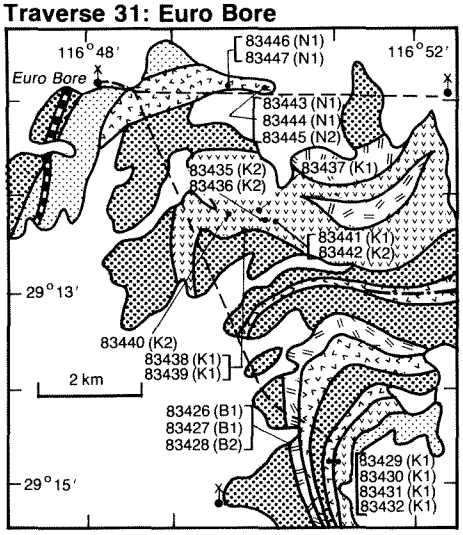
Traverse 28: Wydgee



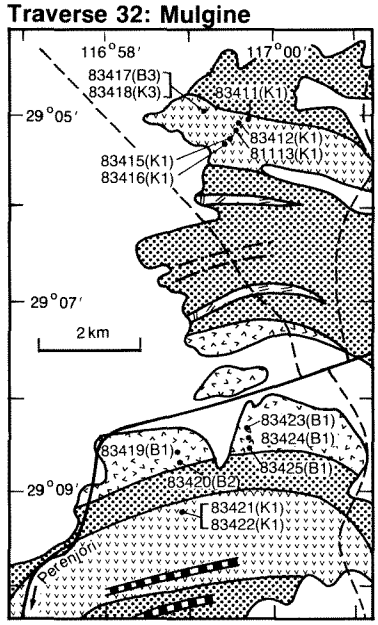
GSWA 24554 C

Figure 19. (continued)

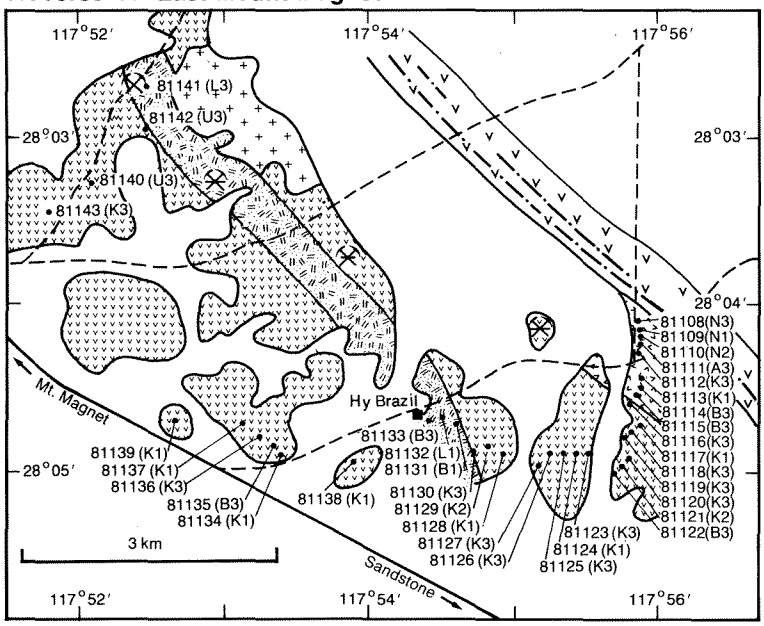
Traverse 31: Euro Bore

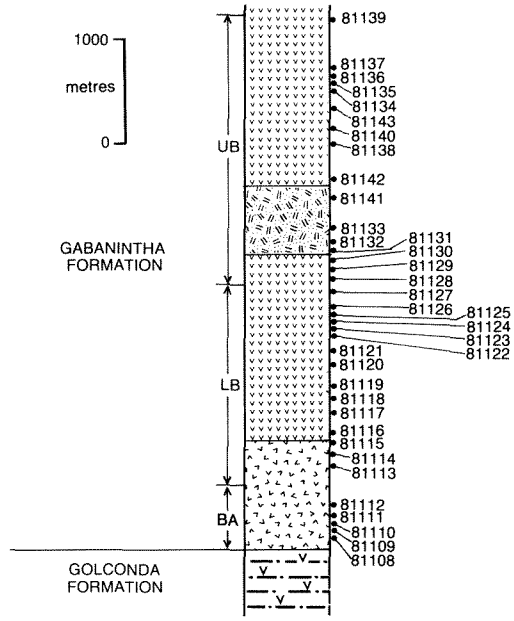


Traverse 32: Mulgine

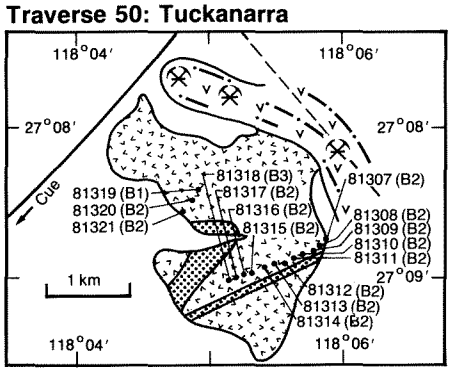


Traverse 41: East Mount Magnet





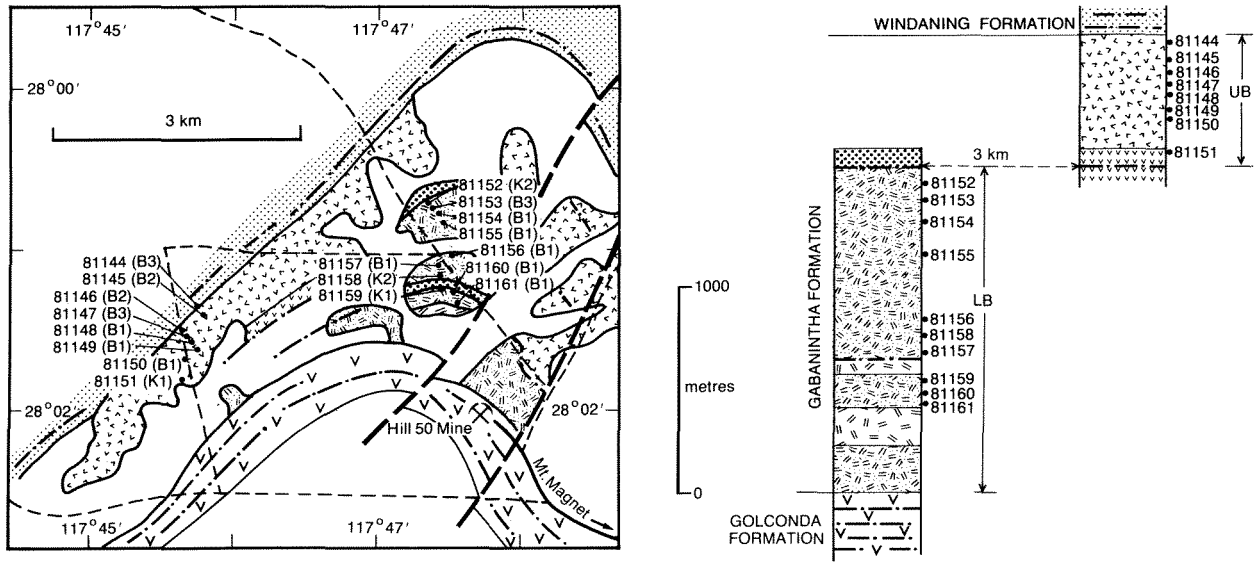
Traverse 50: Tuckanarra



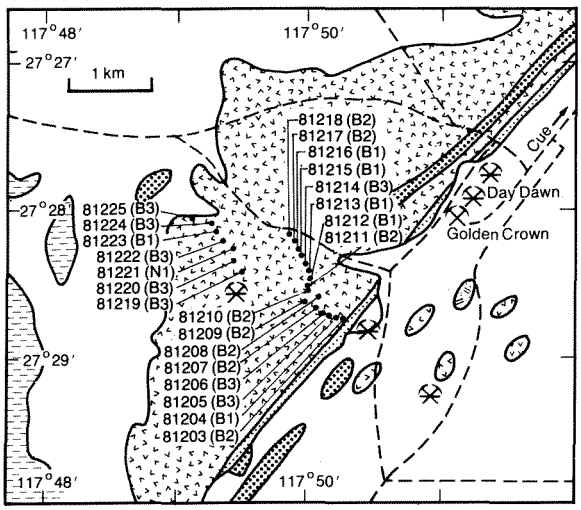
GSWA 24554 D

Figure 19. (continued)

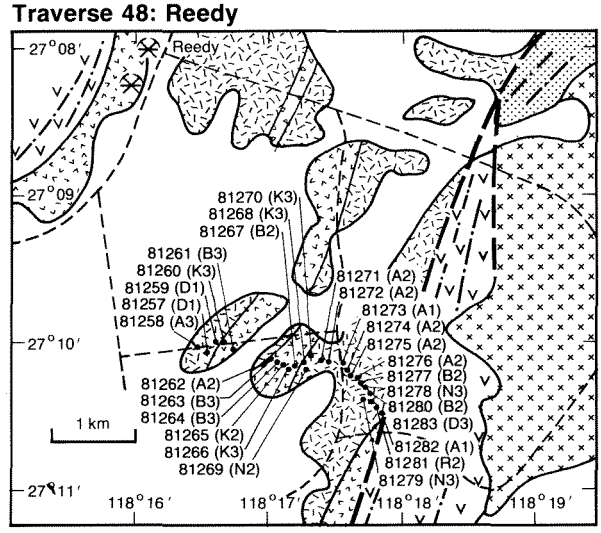
Traverse 42: West Hill 50



Traverse 46: Trenton Hill



Traverse 48: Reedy



GSWA 24554 E

Figure 19. (continued)

TABLE 7. SAMPLE TRAVERSES ON THE GABANINTHA FORMATION

Traverse number	*Location*	*GSWA 1:250000 map sheet*	*GSWA sample numbers*	*No. of samples*	*Rock type*
5	Swan Bore	GLENGARRY	81503 - 09	7	Basalt
9	Gabanintha	GLENGARRY	81569 - 76	8	Basalt
10	Abbotts	BELELE	81578 - 81	7	Felsic volcanics
11	Conroy Well	BELELE	81582 - 96	15	Basalt
12	Mingah Range	BELELE	81601 - 10	10	Basalt
13	Nannine	BELELE	81613 - 16	4	Dacite and andesite
15	Talval Pool	GLENGARRY	81664 - 69	6	Basalt
16	Wattagee	CUE	81618 - 23	6	Andesite and dacite
18	Jungar Pool	CUE	81651 - 63	13	Basalt
19	Cuddingwarra-1	CUE	81743 - 52	10	Basalt
20	Cuddingwarra-2	CUE	81753 - 58	6	Rhyolite
21	Water Supply Bore	CUE	81789 - 800	12	Basalt
22	Mainland	CUE	81784 - 88	5	Basalt
23	Kurrajong Bore	CUE	83215 - 29	15	Basalt
24	Jean Well	CUE	74435 - 42 83201 - 14	22	Basalt
25	Sparrow Well	CUE	81777 - 83	7	Basalt
26	Warda Warra	CUE	83266 - 75	6	Basalt
28	Wydgee	KIRKALOCKA	83329 - 38	10	Andesite and dacite
31	Euro Bore	PERENJORI	83426 - 47	22	Basalt
32	Mulgine	PERENJORI	83411 - 25	15	Basalt
41	East Mt Magnet	KIRKALOCKA	81108 - 43	36	Basalt
42	West Hill 50	KIRKALOCKA	81144 - 61	18	Basalt
46	Trenton Hill	CUE	81203 - 25	23	Basalt
48	Reedy	CUE	81257 - 85	29	Basalt, felsic volcanics, and BIF
49	Cue Hill	CUE	81301 - 06	6	Basalt
50	Tuckanarra	CUE	81307 - 21	15	Basalt
52	Noongal	YALGOO	81345 - 53	9	Basalt
57	Golden Grove	YALGOO	85758 - 59 85762 - 84 85789 - 94	31	Felsic volcanics
59	Gnows Nest	YALGOO	85816 - 20	5	Basalt
-	Miscellaneous	-	81162, 83235, 84434, 85811 - 12, 85727 - 29, 85755, 85845 - 48	13	Basalt, felsic volcanics, and BIF

tholeiitic trend, but most felsic rocks are calc-alkaline (Fig. 20). The formation is compositionally bimodal; this is only weakly reflected in SiO_2 content, but is better shown by trace-element abundances (Fig. 21). It is unlikely that mafic and felsic components of the sequence were derived from similar magmas by simple fractional crystallization, as they have distinctly different trends on incompatible element plots (Thurston and Fryer, 1983), e.g. Fig. 21B.

Compositional characteristics and petrogenesis of basalts

Two distinct types of tholeiitic and high-Mg basalts have been recognized, mainly on the basis of Zr/(Zr + Y) ratios. These are termed Type-I and Type-II basalts (Table 8). Type-I tholeiitic and high-Mg basalts are characterized by higher mean Zr/(Zr + Y), Zr, Sr, LREE, and lower mean Y values than Type-II tholeiitic and high-Mg basalts (Tables 8, 9, 10, 11, and 12). Apart from these distinctions, compositions of individual tholeiitic and high-Mg basalt units are highly variable. There is no systematic, statistically significant difference in major element geochemistry between the two tholeiitic basalt types, or between the two high-Mg basalt types, although compositional differences between tholeiitic and high-Mg basalts are marked (Table 8).

Y, Zr, and Ti: Type-I basalts plot on the high-Zr, low-Y side of Sun and Nesbitt's (1977) estimated mantle ratio, on an Y–Zr diagram (Figs 22A and B). There is a substantial overlap between the compositional fields of tholeiitic and high-Mg basalt. The high-Mg basalt field is displaced towards Sun and Nesbitt's (1977) estimated mantle composition relative to the tholeiite field, which suggests derivation from a more primitive melt. Trends in the data indicate that compositional variation in both basalts is due mainly to pyroxene fractionation. It is likely that the tholeiite melt was somewhat depleted in olivine prior to pyroxene fractionation (Fig. 22A).

Basalt samples from traverse 48 plot on Zr-enrichment

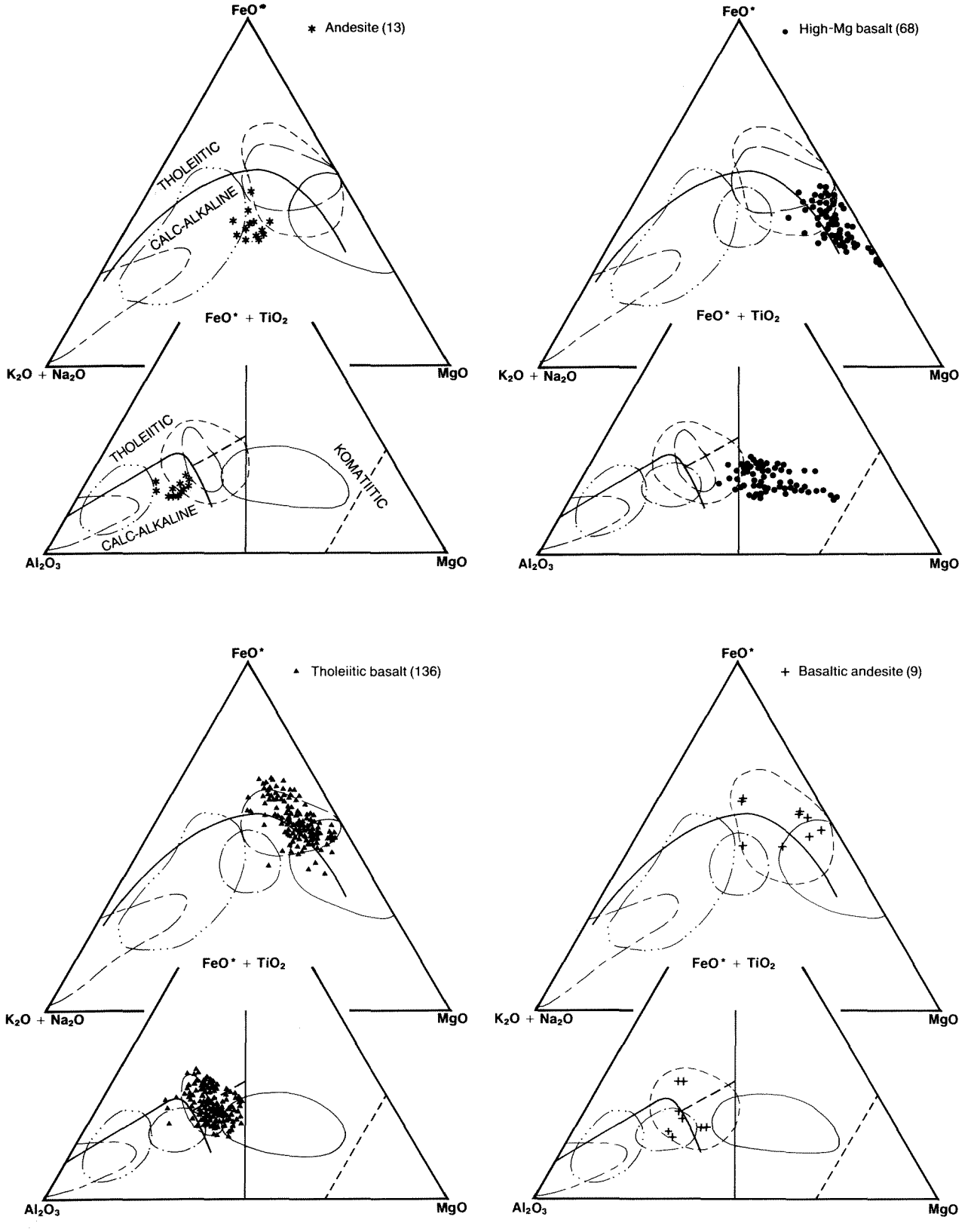
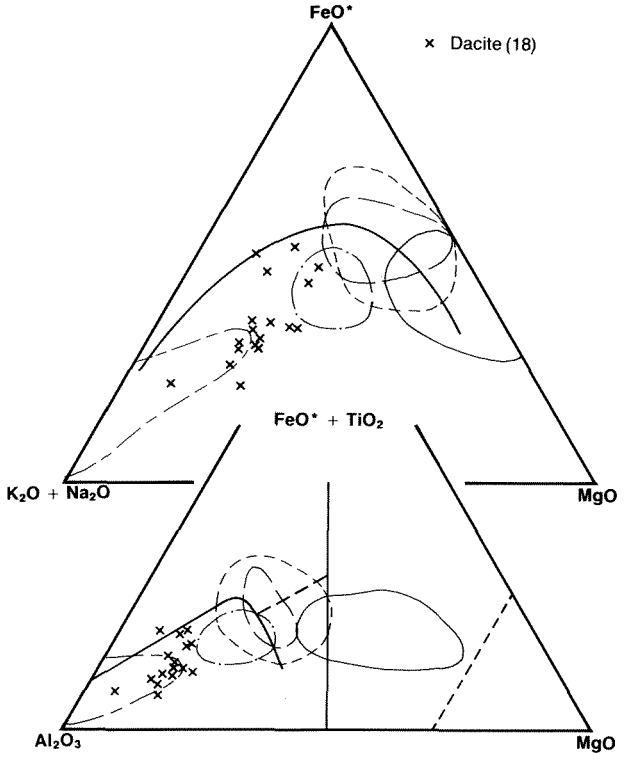
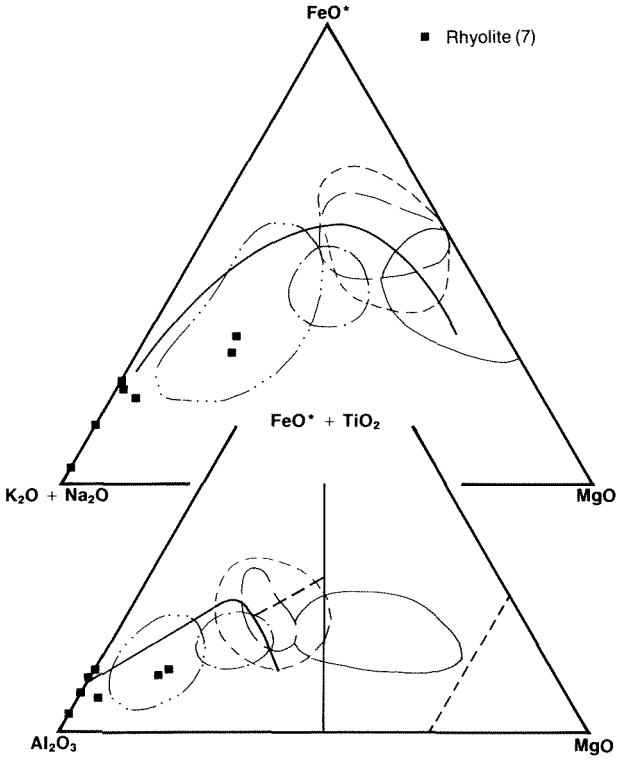


Figure 20. Gabanintha Formation volcanic rocks plotted on AFM (above) and Jensen (below) diagrams. Tholeiite trend on AFM diagram after Irvine and Baragar (1971). Compositional fields on the Jensen diagram are modified from Jensen (1976). Numbers of samples given in brackets.





GSWA 24555

Gabanintha Formation volcanic rocks

- High - Mg basalt (68)
- Tholeiitic basalt (136)
- Basaltic andesite (9)
- Andesite (13)
- Dacite (18)
- Rhyolite (7)

trends on Figure 22. Zr-rich basalts from this traverse contain anomalously high contents of Ba, Rb, Sr, Li, La, and Ce, and low contents of V and TiO_2 (Appendix II) which are characteristic of crustal contamination of magma during ascent from the mantle or eruption over siliceous rocks (Arndt and Jenner, 1986; Barley, 1986).

Type-II tholeiitic basalt data plot on the high-Y, low-Zr side of Sun and Nesbitt's (1977) estimated mantle ratio on an Y–Zr diagram (Fig. 22C). Tholeiitic basalt from traverse 21 is particularly depleted in Zr, and plots away from the main trend. Some basalts from traverses 19, 22, 23, and 25 are more fractionated than the others and are slightly displaced from the main trend at high Zr and Y values. The main trend, which is similar to that for Type-I basalt, indicates that pyroxene fractionation is mainly responsible for compositional variation.

Type-II high-Mg basalt data plot in a relatively small compositional field which substantially overlaps that of Type-II tholeiite (Fig. 22D). Two rocks from traverse 32 (83411 and 83412), and one rock from traverse 22 (81787) plot away from the main compositional field on a Zr-enrichment trend. These rocks contain anomalous abundances of Ba, Rb, Sr, Li, La, and Ce (Appendix II), in common with Type-I basalts from traverse 48, and may also have been contaminated with silicic material.

Type-I and Type-II tholeiitic basalt data plot in distinctly different compositional fields on Zr/Y–Zr diagrams (Fig. 23). The positions and broad trends of these fields indicate that Type-I tholeiite was derived by about 20–30% partial melting of incompatible-element-enriched plagioclase lherzolite, and that Type-II tholeiite was derived by about 10–20% partial melting of incompatible-element-depleted plagioclase lherzolite (Pearce and Norry, 1979). The fractionated Type-II tholeiites from traverses 19, 22, 23, and 25, noted above, and Type-I tholeiite from traverse 18, show evidence of plagioclase crystal fractionation (Fig. 23).

Ni, Cr, and MgO: Compositional differences between tholeiitic and high-Mg basalt are emphasized on Ni–MgO and Cr–MgO diagrams (Fig. 24). Ni and Cr abundances are positively correlated with variation in MgO, although there is much scatter. The diagrams show clearly the influence of olivine and pyroxene crystal fractionation on variation in basalt chemistry. Ni is most strongly partitioned into olivine (Henderson, 1982, table 5.2a) and most of the Ni–MgO variation can be attributed to olivine fractionation (Jahn et al., 1980). Ni abundance is largely independent of MgO for Type-II tholeiite (Fig. 24A) which suggests that

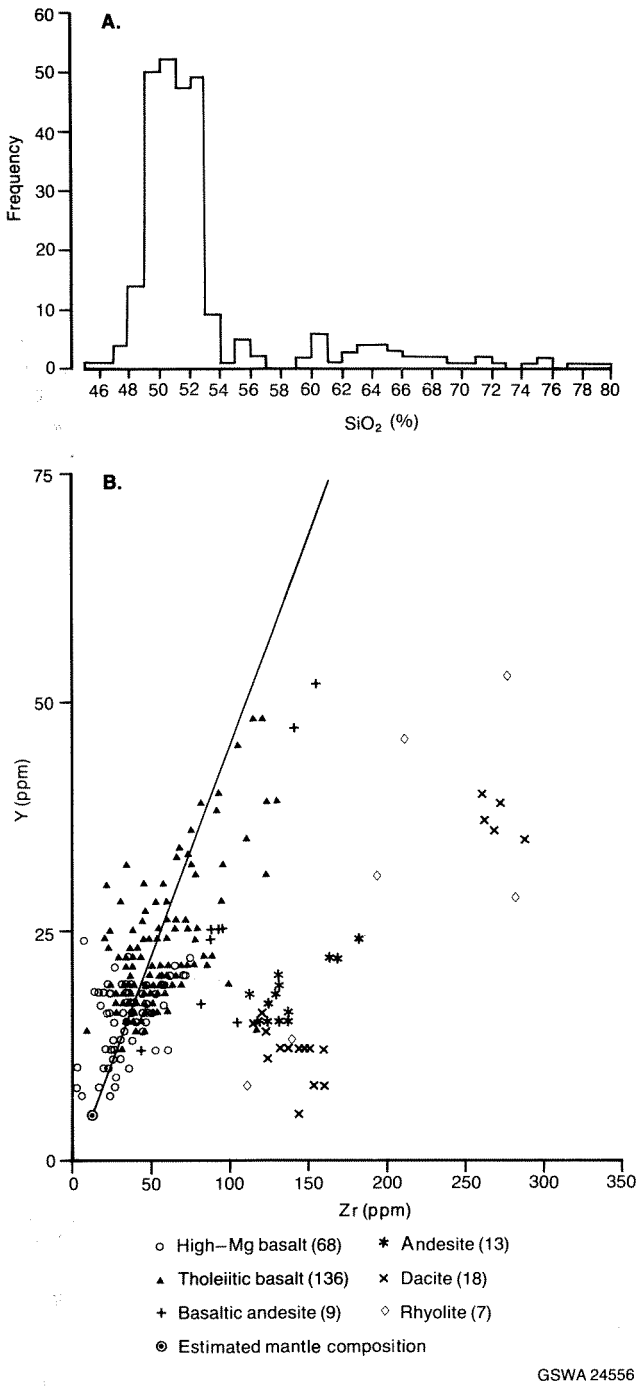


Figure 21. Bimodal compositions of Gabanintha formation volcanic rocks: A–histogram of SiO_2 content; B–Y–Zr diagram, estimated mantle composition and ratio as in Figure 7. Numbers of samples given in brackets.

olivine was not an important fractionating phase in this basalt. Cr is partitioned most strongly into pyroxenes (Henderson, 1982, table 5.2a) and most of the variation in Figure 24B can be attributed to fractionation of ortho- and clinopyroxene (Jahn et al., 1980). There is a change in slope in the Cr–MgO trend at about 9% MgO, which indicates a change in the types and/or proportions of phases crystallizing from the magma, possibly from orthopyroxene-dominated (MgO>9%) to clinopyroxene-dominated (MgO<9%) fractionation.

Cr–Y relations: Neither Cr or Y are thought to be involved in processes that cause mantle heterogeneities (Pearce, 1982; Drury, 1983) such as enrichments and depletions of incompatible elements (Pearce and Norry, 1979). Thus, source regions for most magmas contained Cr and Y abundances similar to those estimated for the primordial mantle (e.g. Sun and Nesbitt, 1977; Wood, 1979; Sun, 1982); compositional variations have been attributed mainly to differences in their partial-melting and fractional-crystallization histories (Pearce, 1982). The slightly higher Y abundances of Type-II tholeiite compared with Type-I tholeiite are thought, therefore, to reflect igneous processes rather than enrichment of Y in the source region prior to partial melting. If this reasoning is correct, petrogenetic pathways on Cr–Y diagrams for Type-I and Type-II tholeiites indicate derivation by 20–30%, and 10–20% partial melting, respectively, of a plagioclase-lherzolite source (Fig. 25) (Pearce, 1980, 1982), which is consistent with trends on Zr/Y–Zr diagrams (Fig. 23). For both basalts, partial melting was followed by fractionation of pyroxene and some olivine, and, in more differentiated units, plagioclase.

Most Type-I and Type-II high-Mg basalt data plot above the plagioclase-lherzolite model melting curve in Cr-rich compositions on Cr–Y diagrams (Figs 25C and D). There is no significant trend for Type-I high-Mg basalt; Type-II high-Mg basalt shows a linear trend intersecting the model melting curve at about 20% melting. The trend reflects pyroxene and olivine fractionation, although the significance of the model melting curve intersection is dubious since most data plot above it (Drury, 1983). Simple models of basalt genesis cannot be invoked for these rocks.

Rare-earth elements: REE patterns for Type-I high-Mg basalt from traverse 5 indicate fractionation with enriched LREE contents of up to 18 times chondrite, and HREE contents of 8–9 times chondrite (Fig. 26A). Depletion of La may reflect alteration (Bartley, 1986). These patterns are consistent with enrichment of the basalt source in incompatible elements. REE patterns for Type-II tholeiite and high-Mg basalts from traverse 24 are virtually identical. They show LREE depletion with values of 5–6 times chondrite, and flat HREE of about 8 times chondrite. These patterns indicate depletion of the basalt source in incompatible elements, consistent with other trace-element data.

In summary, trace- and rare-earth element data indicate that Type-I and Type-II basalts were derived from source regions which had been enriched and depleted, respectively, in incompatible elements prior to, or during, partial melting. The chemical similarities between tholeiitic and high-Mg basalt, within each basalt type, suggest that high-Mg basalts were derived from the same source regions as tholeiites. However, the high Cr and Ni contents require a different mode of genesis for high-Mg basalts, possibly by higher degrees of partial melting of olivine-rich residues (Drury, 1983). Enrichment and depletion of source regions of Type-I and Type-II basalts could have been accomplished by addition and extraction of melt fractions from

TABLE 8. MEAN COMPOSITIONS OF GABANINTHA FORMATION TYPE-I AND TYPE-II BASALTS

	THOLEIITES		*HIGH-Mg BASALT*	
	Type-I n=78	*Type-II n=58*	*Type-I n=32*	*Type-II n=34*
		Percentage		
SiO_2	51.2	50.5	50.3	50.8
Al_2O_3	14.3	13.8	11.1	10.4
Fe_2O_3	2.4	3.5	1.6	1.5
FeO	8.3	8.5	8.4	8.5
FeO* (c)	10.5	11.6	9.8	9.8
MgO	6.6	7.1	12.8	14.1
CaO	10.8	11.2	8.7	8.6
Na_2O	2.1	1.8	1.8	1.0
K_2O	0.25	0.11	0.13	0.06
TiO_2	0.79	0.89	0.51	0.46
P_2O_5	0.13	0.13	0.09	0.08
MnO	0.18	0.18	0.19	0.17
LOI	2.4	2.2	3.5	3.7
		Parts per million		
Ba	125	77	96	76
Cr	197	220	1264	1455
Co	57	57	69	89
Cu	141	87	112	49
Ni	99	132	352	367
Rb	6	<5	<5	<5
Sr	126	87	105	55
V	267	282	207	202
Y	19	29	14	15
Zn	83	77	74	71
Zr	59	50	44	35
La	7	(a) 5	(a) 6	6
Ce	10	(a) 5	(a) 7	(a) 5
Mg number (b)	52.8	52.2	69.9	71.9
Cr/V	0.74	0.78	6.11	7.20
Zr/(Zr+Y)	0.76	0.63	0.76	0.70

(a) Some values used to calculate the means are below the detection limit; for these determinations the value 'detection limit/2' was used. (b) 100mol MgO/(MgO + FeO) (c) All Fe calculated as FeO
Samples assigned to alteration class 3 (see Appendix II) are omitted from the means.
For most of the analyses averaged in this table, Nb<5ppm, Pb<10ppm, and Th<5ppm.

previous or concurrent melting episodes (Pearce and Norry, 1979), and/or by metasomatic introduction or removal of incompatible elements (Bailey, 1982). However, the differences between source regions may be of a more fundamental and large-scale nature (see next section). Following partial melting, during ascent of magma to the surface, various amounts of olivine, pyroxene, and plagioclase fractionated from the melt, causing most of the compositional variation within each basalt type. Ortho- and clinopyroxene were the most important fractionating phases. Some samples, particularly those from traverse 48, show trace-element enrichment and depletion that is characteristic of crustal contamination.

Chemostratigraphic variation in basalt

There is a systematic regional distribution of Type-I and Type-II basalts (Fig. 18). In the northern Murchison Province Gabanintha Formation basalt is exclusively Type-I. In the central portion of the province both Type-I and Type-II basalts occur; six traverses are in Type-II basalt, while three are in Type-I basalt. In traverse 42, near Mount Magnet, Type-II basalt overlies Type-I basalt (Fig. 19). In the southern Murchison Province, only two sample traverses were undertaken; both of these were in Type-II basalt. With the exception of traverse 42, this distribution appears to be independent of stratigraphic level within the formation. Bearing in mind the distribution of sample traverses, it appears that the upper mantle beneath the northern, central, and southern parts of the Murchison Province had fundamentally different geochemical characteristics at the time the Gabanintha Formation developed. The upper mantle under the northern and southern parts of the province was enriched and depleted, respectively, in incompatible elements; a zone of chemically heterogeneous mantle separated these two regions. Alternatively, the distribution of basalt types could be interpreted in terms of vertical

TABLE 9. MEAN COMPOSITIONS OF GABANINTHA FORMATION TYPE-I THOLEIITIC BASALT

Traverse	*5*	*9*	*11L*	*11U*	*12*	*15*	*18L*	*18U*	*41*	*42L*	*46*	*48*	*50*	*52*
	n=1	*n=5*	*n=3*	*n=8*	*n=1*	*n=3*	*n=4*	*n=5*	*n=1*	*n=7*	*n=15*	*n=3*	*n=14*	*n=8*
								Percentage						
SiO_2	49.5	50.9	49.9	52.5	51.6	51.0	52.0	49.4	52.4	49.4	51.6	52.0	50.8	51.3
Al_2O_3	12.5	14.5	12.7	13.9	14.6	14.7	13.7	14.2	15.4	12.1	14.5	14.4	14.2	15.1
Fe_2O_3	2.1	1.8	3.1	2.6	1.6	2.0	1.9	2.6	2.4	2.9	3.0	1.4	2.4	1.6
FeO	10.70	8.50	9.12	7.24	7.67	8.23	8.46	11.34	6.47	9.05	8.6	7.33	7.99	7.53
FeO*(c)	12.6	10.1	11.9	9.6	9.1	10.0	10.2	13.7	8.6	11.7	11.3	8.6	10.1	9.0
MgO	7.47	8.00	7.86	6.69	8.04	6.62	8.00	4.99	7.11	7.77	4.93	7.79	7.20	7.21
CaO	9.58	9.58	9.25	9.92	9.23	11.10	11.50	10.6	7.62	10.72	9.04	12.67	12.70	11.59
Na_2O	2.74	2.09	2.93	2.02	2.71	2.19	1.77	2.37	4.87	2.02	2.79	2.22	1.25	1.58
K_2O	0.27	0.36	0.47	0.45	0.33	0.39	0.15	0.19	0.12	0.12	0.34	0.08	0.07	0.25
TiO_2	1.60	0.63	1.07	0.57	0.56	0.64	0.61	1.68	0.41	1.33	0.77	0.63	0.76	0.57
P_2O_5	0.19	0.10	0.13	0.10	0.09	0.11	0.09	0.21	0.16	0.16	0.13	0.18	0.10	0.19
MnO	0.23	0.17	0.19	0.19	0.17	0.17	0.19	0.28	0.10	0.19	0.18	0.20	0.18	0.14
LOI	2.27	2.55	3.14	3.34	3.22	2.32	1.91	2.31	2.29	2.91	3.22	1.42	1.69	1.84
								Parts per million						
Ba	89	93	148	267	141	113	91	99	513	64	163	81	(37)	134
Cr	156	416	204	184	121	363	237	150	201	327	65	392	178	293
Co	65	59	59	54	51	59	61	71	46	60	48	56	63	nd
Cu	68	77	194	137	94	89	127	127	278	254	203	152	161	41
Ni	100	166	130	94	120	137	93	70	120	153	43	193	120	106
Rb	22	10	9	14	8	11	(a)2	(a)2	<2	<2	6	<2	<2	<2
Sr	229	101	107	91	85	127	112	113	342	218	141	203	119	115
V	362	238	317	233	244	254	256	438	204	297	272	179	273	205
Y	31	20	20	19	16	19	19	34	17	23	19	16	16	17
Zn	107	76	96	82	80	64	86	121	71	89	88	82	73	71
Zr	124	55	73	55	54	52	54	105	39	72	59	89	42	51
La	8	5	9	9	<5	<5	(a)8	13	6	7	8	13	<5	9
Ce	19	(a)7	12	13	10	<5	(a)8	16	16	(a)8	(a)9	20	<5	10
Mg number(b)	51.4	58.5	54.1	55.4	61.2	54.1	58.3	39.4	59.6	54.2	43.7	61.7	55.9	58.8
Cr/V	0.43	1.75	0.64	0.79	0.50	1.43	0.93	0.34	0.99	1.10	0.24	2.19	0.65	1.43
Zr/(Zr+Y)	0.80	0.73	0.78	0.74	0.77	0.73	0.74	0.75	0.70	0.76	0.76	0.85	0.72	0.75

(a) Some values used to calculate the means are below the detection limit; for these determinations the value 'detection limit/2' was used.
(b) 100 mol MgO/(MgO + FeO) (c) All Fe calculated as FeO
For the analyses averaged in this table, Nb<5 ppm, Pb<10 ppm and Th<5 ppm.
Samples assigned to alteration class 3 (see Appendix II) are omitted from the mean.
In the traverse identification, U and L refer to upper and lower parts of the traversed stratigraphy.
nd: not determined

chemical zonation in the upper mantle in Gabanintha Formation times, partial melts in the north being extracted from a different depth interval to those in the south. More sampling is necessary in the southern Murchison Province to be certain of this distribution.

Although many traverses sample only one basalt unit, some cross two or more chemically distinct basalt units (Figs 19 and 27). As in the Murrouli Basalt, these units generally have different partial melting and/or crystal-fractionation histories. It is impossible to correlate the individual basalt units between adjacent traverses. Thus, it appears that, although there is a relatively simple regional distribution of basalt types, on a smaller scale the volcanic stratigraphy of individual units is complex.

Compositional characteristics of felsic volcanic rocks

Mean compositions of felsic volcanic units sampled in the Gabanintha Formation are given in Table 13. Two broad groups of calc-alkaline felsic volcanic rocks can be distinguished — a high-(Zr+Y) group and a low-(Zr+Y) group (Fig. 28). These are not associated with Type-I and Type-II basalts. Chemically distinct units can be recognized within these broad groupings (Table 13, Fig. 29). With the exception of dacite from the Golden Grove centre, samples of low-(Zr+Y) felsic volcanics plot in distinct clusters along broad calc-alkaline differentiation trends on Harker variation diagrams (Fig. 29). The Golden Grove dacite has lower Ni, TiO_2, and FeO^* than other low-(Zr+Y) felsic rocks. The samples were collected in and around a mineralized zone (Frater, 1983b) and may have been metasomatized prior to deformation and metamorphism. Some important crystal-fractionation trends are evident in low-(Zr+Y) felsic volcanics on the Harker diagrams. The chief control of TiO_2 depletion with increasing SiO_2 in the calc-alkaline series is thought to be magnetite fractionation (Ewart, 1976); this also affects FeO^* and V abundances (Gill, 1978). The trend of decreasing Y with increasing differen-

TABLE 10. MEAN COMPOSITIONS OF GABANINTHA FORMATION TYPE-I HIGH-Mg BASALT

Traverse	*5* *n=4*	*9* *n=3*	*12* *n=3*	*15* *n=1*	*18* *n=1*	*41L* *n=8*	*41U* *n=6*	*42L* *n=3*	*48* *n=3*
					Percentage				
SiO_2	48.4	51.0	51.9	51.5	48.8	51.5	50.2	49.5	52.6
Al_2O_3	8.1	11.6	11.5	13.0	10.9	13.0	10.8	10.7	11.6
Fe_2O_3	1.6	1.3	1.9	1.6	1.5	1.6	1.8	2.3	1.0
FeO	10.29	8.1	8.03	8.5	9.29	6.39	7.78	8.8	6.782
FeO* (c)	11.7	9.3	9.7	9.9	10.6	7.8	9.4	10.9	7.68
MgO	14.7	14.4	10.5	9.41	13.2	11.10	13.24	10.38	10.5
CaO	9.41	8.07	9.93	8.93	10.8	10.26	6.95	10.80	12.15
Na_2O	1.33	1.31	1.53	1.89	1.14	1.44	2.99	1.86	1.98
K_2O	0.07	0.14	0.17	0.50	0.08	0.18	0.08	0.08	0.10
TiO_2	0.76	0.26	0.54	0.53	0.58	0.25	0.63	1.02	0.54
P_2O_5	0.09	0.06	0.09	0.10	0.08	0.09	0.09	0.12	0.17
MnO	0.21	0.17	0.18	0.20	0.19	0.21	0.18	0.19	0.20
LOI	3.90	2.65	3.11	3.15	3.52	2.77	4.16	3.11	1.76
					Parts per million				
Ba	63	30	52	123	39	106	174	64	120
Cr	1553	1961	737	780	1134	1101	1243	803	677
Co	82	73	64	61	67	68	66	60	53
Cu	114	55	126	79	87	74	195	212	107
Ni	395	464	210	280	320	340	343	283	295
Sr	57	45	150	97	89	200	132	195	262
V	229	174	213	217	246	155	233	270	150
Y	19	9	13	18	19	8	13	18	13
Zn	108	58	75	63	85	59	71	80	81
Zr	62	27	46	55	58	26	40	52	83
La	<5	<5	<5	7	<5	9	6	7	14
Ce	<5	<5	9	<5	5	14	(a)9	<5	15
Mg number (b)	69.1	73.3	65.9	62.9	68.9	71.7	71.5	62.9	70.9
Cr/V	6.78	11.27	3.46	3.59	4.61	7.10	5.33	2.97	4.51
Zr/(Zr+Y)	0.77	0.75	0.78	0.75	0.75	0.76	0.75	0.74	0.86

(a) Some values used to calculate the means are below the detection limit; for these determinations the value 'detection limit/2' was used.
(b) 100 mol MgO/(MgO + FeO) (c) All Fe calculated as FeO
For analyses averaged in this table, Rb<2 ppm, Nb<5 ppm, Pb<10 ppm, and Th<5 ppm.
Samples assigned to alteration class 3 (see Appendix II) are omitted from the means.
In the traverse identification, U and L refer to upper and lower parts of the traversed stratigraphy.
nd: not determined

tiation is controlled by amphibole fractionation (Lambert et al., 1974). Zr shows little variation with SiO_2; Zr abundance is thus likely to reflect source composition rather than crystal-fractionation processes (Pearce and Norry, 1979). High-(Zr+Y) felsic volcanics plot along similar trends to low-(Zr+Y) felsic volcanics for many elements, although MgO and Cr values are lower, and TiO_2, Zr, and Y values are markedly higher at similar SiO_2 contents. Chemical compositions of Gabanintha Formation felsic volcanic rocks are broadly similar to those elsewhere in the Yilgarn Craton (Fig. 29), although they have lower Al_2O_3, and higher Cr and Ni contents, compared with Cainozoic calc-alkaline rocks (Giles, 1981).

Petrogenesis of felsic volcanic rocks

Models for petrogenesis of silicic volcanic rocks are complex compared with those for mafic rocks, and often require two or more stages of melting and/or crystal fractionation, and even metasomatism, to explain geochemical and isotopic data. There are four main models of petrogenesis:

(a) Partial melting of large-ion-lithophile (LIL) enriched upper mantle (Giles, 1981, 1982; Barley et al., 1984; Hallberg and Giles, 1986);
(b) Fractional crystallization of basaltic magma (Arth et al., 1978);
(c) Partial melting of mafic crustal sources, such as amphibolite and eclogite (Taylor and Hallberg, 1977; Jahn et al., 1981; Condie, 1982);
(d) High degrees of partial melting of sialic crust (Condie, 1978).

For sources that involve partial melting, various amounts of crystal fractionation are usually required to explain trace-element chemistry and HREE depletions. The observed enrichment of LREE (e.g. Fig. 30) is difficult to explain (Cullers and Graf, 1984b); recent models invoke LREE enrichment in the source by previous addition of melt fractions (e.g. Hawkesworth, 1982), and/or enrichment by ascending hydrous fluids (e.g. Dostal et al., 1977).

Partial melting of both mafic crustal and upper mantle sources have been proposed for felsic volcanic rocks in the

TABLE 11. MEAN COMPOSITIONS OF GABANINTHA FORMATION TYPE-II THOLEIITIC BASALT

Traverse	*19*	*21*	*22*	*23L*	*23M*	*23U*	*24*	*25*	*31*	*32*	*42U*	*49*
	n=9	*n=7*	*n=1*	*n=7*	*n=3*	*n=1*	*n=9*	*n=2*	*n=3*	*n=5*	*n=5*	*n=6*
						Percentage						
SiO_2	49.8	50.9	50.9	49.0	50.9	50.1	51.6	51.9	49.5	51.8	51.5	50.7
Al_2O_3	13.8	14.8	14.6	13.5	12.7	14.0	13.4	14.0	14.8	13.7	15.0	13.8
Fe_2O_3	4.2	3.6	4.5	4.6	4.7	3.7	3.1	4.1	2.0	1.9	2.3	2.1
FeO	8.97	8.46	7.01	9.06	6.18	8.86	8.00	8.59	9.3	7.5	7.23	9.83
FeO*(c)	12.7	11.7	11.1	13.2	10.4	12.2	10.8	12.3	11.1	9.2	9.3	11.7
MgO	7.04	7.04	6.52	6.31	8.98	5.19	7.87	5.66	7.32	8.58	6.25	5.46
CaO	11.04	11.17	10.87	10.60	9.26	9.40	11.37	10.25	11.7	12.22	12.32	11.98
Na_2O	1.83	1.67	2.26	2.15	2.45	2.13	1.25	2.08	1.66	1.44	1.80	2.29
K_2O	0.10	0.08	0.20	0.13	0.26	0.13	0.08	0.18	0.08	0.04	0.15	0.12
TiO_2	1.18	0.55	1.48	1.42	0.63	1.46	0.70	1.27	0.77	0.44	0.64	0.82
P_2O_5	0.18	0.09	0.18	0.19	0.10	0.15	0.10	0.14	0.10	0.08	0.10	0.12
MnO	0.15	0.19	0.20	0.19	0.15	0.24	0.16	0.24	0.20	0.16	0.21	0.24
LOI	2.18	1.87	2.19	2.54	3.15	4.41	2.01	1.67	1.74	1.74	1.38	1.66
						Parts per million						
Ba	80	48	133	100	123	86	92	135	85	63	72	46
Cr	188	129	251	131	477	90	300	102	300	420	229	80
Co	46	46	42	47	35	51	45	43	103	102	60	70
Cu	125	77	99	117	52	238	89	63	35	66	148	61
Ni	144	112	102	133	142	136	121	88	173	149	98	70
Rb	<5	<5	6	<5	10	<5	<5	6	<5	<5	2	<2
Sr	134	64	132	104	71	92	71	126	72	81	104	59
V	339	247	320	311	275	409	267	324	255	211	240	300
Y	33	24	38	34	22	39	23	35	24	17	23	24
Zn	86	78	90	82	64	104	69	79	82	62	73	75
Zr	65	21	93	73	40	82	48	83	53	32	38	49
La	nd	nd	nd	nd	nd	nd	nd	nd	<5	<5	6	(a)6
Ce	nd	nd	nd	nd	nd	nd	nd	nd	<5	<5	(a)6	(a)6
Mg number(b)	49.7	51.7	51.1	46.0	60.6	43.1	56.5	45.1	54.0	62.4	54.5	45.4
Cr/V	0.55	0.52	0.78	0.42	1.73	0.22	1.12	0.31	1.18	1.99	0.95	0.27
Zr/(Zr+Y)	0.66	0.47	0.71	0.68	0.65	0.68	0.68	0.70	0.69	0.65	0.62	0.67

(a) Some values used to calculate the means are below the detection limit; for these determinations the value 'detection limit/2' was used.
(b) 100 mol MgO/(MgO + FeO) (c) All Fe calculated as FeO
For the analyses averaged in this table, Nb<5 ppm, Pb<10 ppm and Th<5 ppm.
Samples assigned to alteration class 3 (see Appendix II) are omitted from the means.
In the traverse identification, U, M and L refer to upper, middle and lower portions of the traversed stratigraphy.
nd: not determined

Yilgarn and Pilbara Cratons. Hallberg et al. (1976a) and Taylor and Hallberg (1977) proposed varying degrees of partial melting of a mafic crustal source to explain compositions of calc-alkaline felsic volcanic rocks from the Marda Complex in the Southern Cross Province. Jahn et al. (1981) invoked partial melting of a basaltic crustal source, followed by crystal fractionation, to form silicic volcanic rocks in the Pilbara. Giles (1981, 1982), Giles and Hallberg (1982), and Hallberg and Giles (1986) proposed hydrous melting of a non-chondritic upper mantle LIL-enriched source, followed by extensive amphibole and plagioclase fractionation, to explain the chemistry of felsic, and some mafic, volcanic rocks from several centres in the Eastern Goldfields Province. Barley et al. (1984) invoked a similar origin for chemically contiguous basalt, andesite, dacite, and rhyolite in the Pilbara. For sequences with proposed mantle sources, felsic volcanic rocks are chemically and spatially associated with basalt and/or basaltic andesite (Giles, 1981, 1982; Giles and Hallberg, 1982; Barley et al., 1984; Hallberg and Giles, 1986). However, for felsic volcanic rocks from proposed crustal sources, mafic and felsic volcanics are not chemically associated, and felsic volcanics from these sources have higher mean contents of SiO_2 than those from proposed mantle sources (Hallberg et al., 1976a; Taylor and Hallberg, 1977; Jahn et al., 1981).

Y–Zr relationships (Fig. 28), calc-alkaline trends (Fig. 29), and LREE enrichment (Fig. 30), indicate that Gabanintha Formation felsic volcanic rocks could not have been derived by partial melting of chondritic mantle, or by crystal fractionation of tholeiitic magma. In addition, large compositional differences between incompatible-element-enriched basalt (Type-I tholeiite) and felsic volcanics in the Gabanintha Formation, and the contemporaneity of their eruption, suggest that spatially associated sources in the upper mantle are unlikely. No chemically associated basalt or basaltic andesite occurs with the felsic volcanic rocks, which generally have high mean SiO_2 contents (Table 13). Thus, it is likely that the source regions for basalts and felsic volcanic rocks were spatially separated as well as compositionally different.

Low-(Zr+Y) felsic volcanic rocks have variable, but generally high, MgO, Cr, and Ni contents (Table 13),

TABLE 12. MEAN COMPOSITIONS OF GABANINTHA FORMATION TYPE-II HIGH-Mg BASALT

Traverse	*19* *n=1*	*25* *n=4*	*26* *n=6*	*31A* *n=4*	*31B* *n=10*	*32A* *n=2*	*32B* *n=6*	*42U* *n=1*
				Percentage				
SiO_2	50.6	50.3	50.6	48.9	51.5	51.3	52.2	50.2
Al_2O_3	10.2	9.7	12.2	10.4	9.2	12.4	9.1	13.5
Fe_2O_3	3.6	3.1	2.3	1.3	1.1	1.9	1.4	1.0
FeO	7.80	7.06	8.0	10.7	8.3	8.07	7.98	8.32
FeO* (c)	11.0	9.8	10.1	11.9	9.3	9.8	9.24	9.2
MgO	11.80	14.13	11.95	11.83	16.08	11.60	15.92	11.00
CaO	12.15	9.00	11.21	11.76	6.67	10.14	6.64	8.76
Na_2O	1.14	1.41	1.03	0.67	0.97	1.80	0.99	2.20
K_2O	0.08	0.15	0.04	0.04	(0.01)	0.02	0.19	0.07
TiO_2	0.50	0.49	0.36	0.86	0.38	0.49	0.43	0.30
P_2O_5	0.12	0.07	0.05	0.11	0.08	0.08	0.08	0.06
MnO	0.19	0.17	0.17	0.20	0.17	0.17	0.17	0.20
LOI	2.36	4.01	1.97	2.42	4.74	1.97	5.15	2.24
				Parts per million				
Ba	49	57	(a)54	56	61	90	150	114
Cr	914	1291	719	932	2014	683	1903	1040
Co	52	40	89	96	88	110	79	69
Cu	23	89	109	64	44	96	60	184
Ni	302	377	246	314	454	255	413	270
Sr	68	41	74	74	39	61	(a)46	119
V	214	227	206	250	188	224	184	196
Y	16	19	17	17	14	17	15	18
Zn	67	62	59	86	66	65	84	67
Zr	24	29	(a)20	49	34	33	45	21
La	<5	<5	<5	10	(a)5	<5	(a) 7	<5
Ce	<5	<5	<5	(a)6	<5	<5	(a) 7	<5
Mg number (b)	65.7	72.0	67.8	63.9	75.5	67.8	75.4	68.1
Cr/V	4.27	5.69	3.49	3.70	10.7	3.05	10.34	5.31
Zr/(Zr+Y)	0.60	0.60	0.54	0.74	0.71	0.66	0.75	0.54

(a) Some values used to calculate the means are below the detection limit; for these determinations the value 'detection limit/2' was used.
(b) 100 mol MgO/(MgO + FeO) (c) All Fe calculated as FeO
For most of the analyses averaged in this table Nb<5 ppm, Th<5 ppm, Rb<2 ppm, and Pb<10 ppm.
Samples assigned to alteration class 3 (see Appendix II) are omitted from the means.
In the traverse identification, U and L refer to upper and lower parts of the traversed stratigraphy. A and B refer to distinct units within a traverse, the relative stratigraphic positions of which are unknown.

suggesting a mafic source. REE patterns, with no Eu anomaly, and high LREE/HREE ratio (Fig. 30), combined with relatively low Y and Zr values, require that garnet and/or amphibole form a residue in the source region. In addition, it is likely that amphibole and magnetite crystal fractionation occurred during magma ascent (Figs 28 and 29). Plagioclase fractionation may also have occurred; the positive and negative Eu anomalies produced by amphibole and plagioclase fractionation, respectively (Hanson, 1978), would have effectively cancelled each other (Fig. 30) (Giles and Hallberg, 1982). Variation in composition of andesitic units within this group, particularly in MgO, Cr, and Ni contents, may be attributed to different degrees of partial melting of the mafic source. Low-(Zr+Y) dacite and rhyolite formed by crystal fractionation — principally of amphibole — from andesitic melts, which resulted in depletion of HREE and Y (Figs 29, and 30). The dominance of amphibole in controlling HREE and Y abundances indicates relatively high fluid pressures during partial melting and crystal fractionation (Green, 1972), and suggests an amphibolite source rather than anhydrous eclogite. The limited REE data plot on amphibolite partial-melting trends on the petrogenetic diagrams of Jahn et al. (1981, figs 6 and 8).

In summary, low-(Zr+Y) felsic volcanic rocks are believed to have formed by hydrous partial melting of crustal amphibolite, followed by various amounts of crystal fractionation, principally of amphibole. The basaltic source rocks were themselves derived by partial melting of the upper mantle.

High-(Zr+Y) felsic volcanic rocks from Cuddingwarra (traverse 20) and Golden Grove (traverse 57) plot on the same trend on an Y–Zr diagram; those from Wydgee (traverse 28) generally have lower Y values (Fig. 28). The Cuddingwarra and Wydgee samples have different mean compositions (Table 13); the mean composition of Golden Grove high-(Zr+Y) rocks was not calculated as they are considered to be altered (Appendix II). The REE pattern of a high-(Zr+Y) rhyolite from the base of the Cuddingwarra sequence shows slight HREE enrichment, a negative Eu anomaly, and strong LREE enrichment (sample 81758 in Fig. 30). This pattern suggests that neither garnet nor

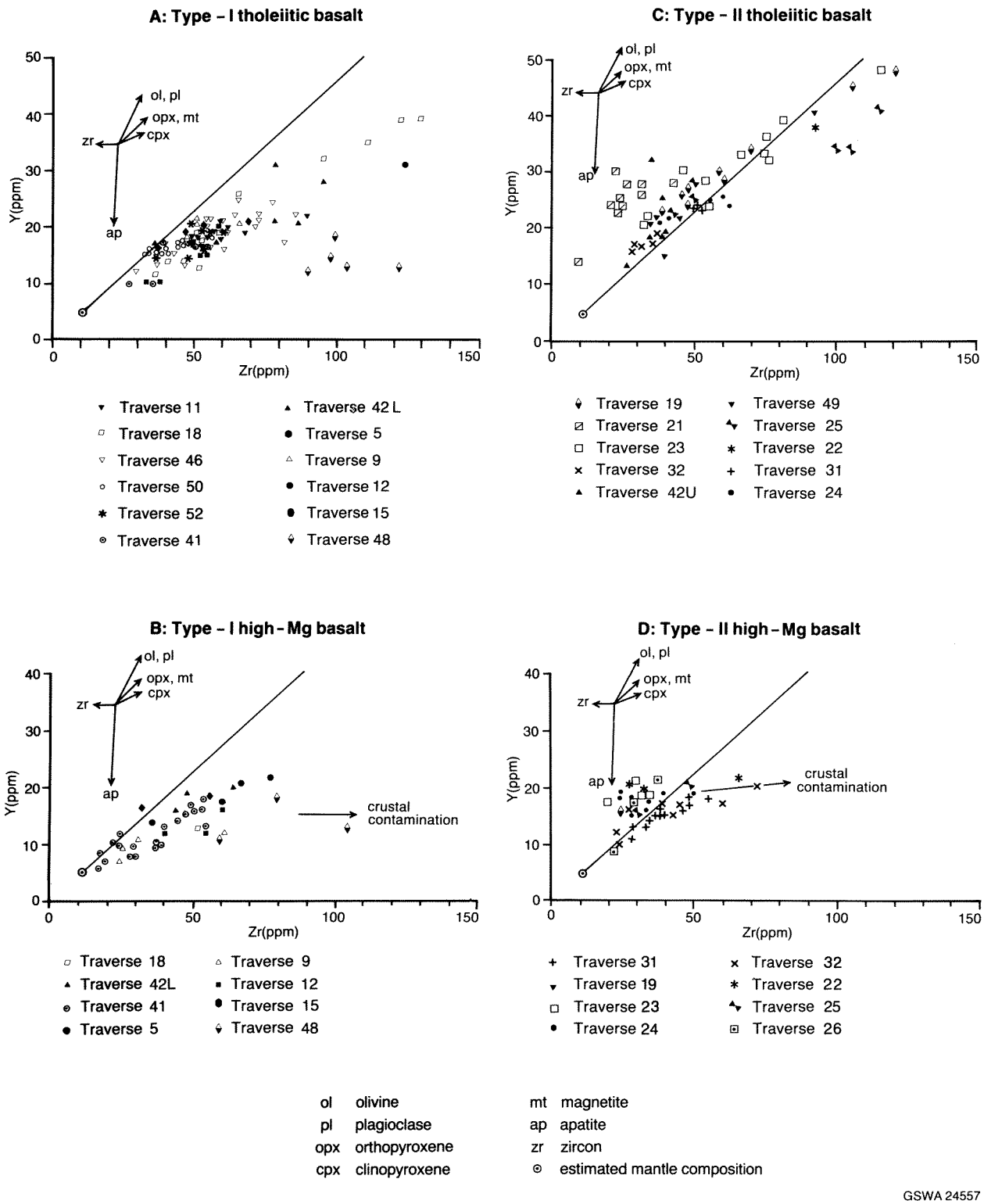


Figure 22. Y–Zr diagrams for Gabanintha Formation basalts. Estimated mantle composition and ratio, and crystal-fractionation vectors as in Figure 7.

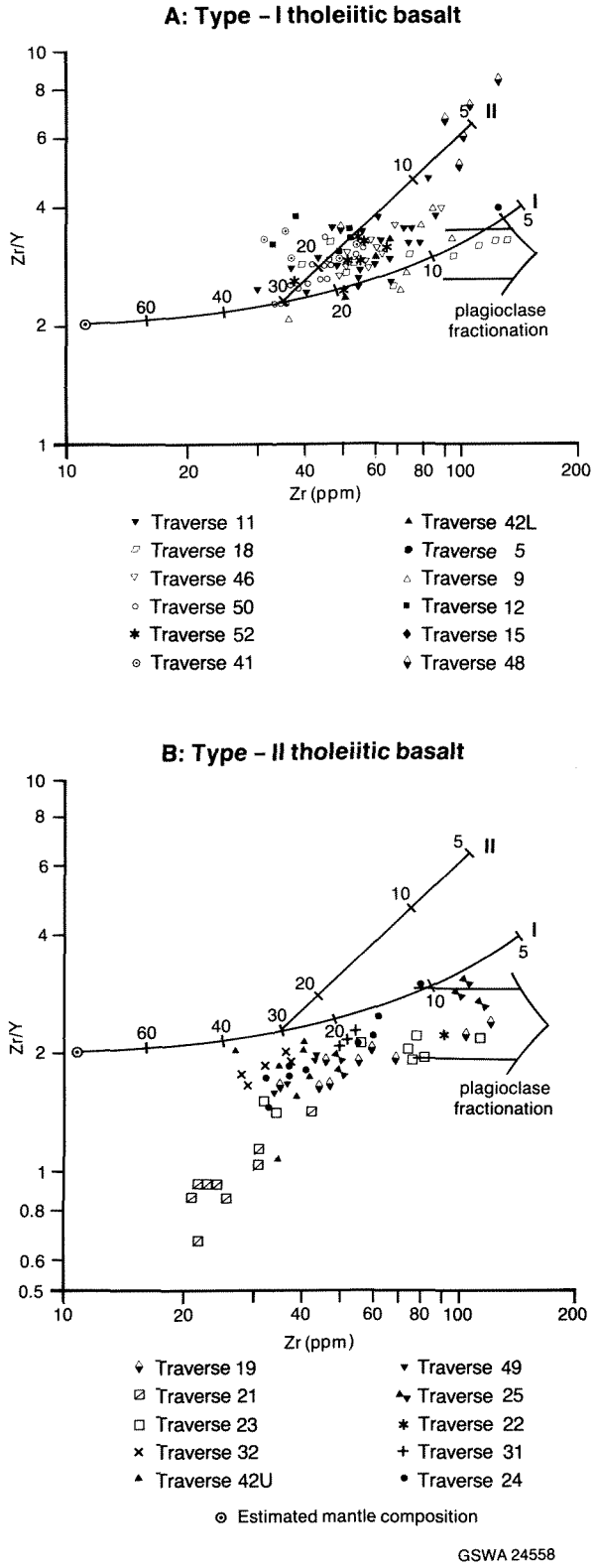


Figure 23. Zr/Y–Zr diagrams for Gabanintha formation tholeiitic basalt. Model partial-melting curves and estimated mantle composition as in Figure 8.

amphibole is important, either as residual or as fractionating phases. In addition, the negative Eu anomaly and low Sr values (Table 13) indicate that plagioclase was removed from the melt by crystal fractionation, or that the source region was depleted in plagioclase. One possible source for these rocks may be siliceous pyroxene–plagioclase granulite (Condie, 1978). The very low MgO, Cr, and Ni contents of these felsic rocks are additional evidence for a siliceous source. Clinopyroxene, magnetite, and plagioclase fractionated from the melt, causing the observed compositional variation (Figs 28 and 30). The relatively high Cr and Ni contents of the Wydgee high-(Zr+Y) felsic volcanic rocks (Table 13) suggest that they were generated from a more mafic source than the Cuddingwarra rocks; however, the high Y contents also preclude garnet or amphibole in the source or as fractionating phases.

Chemostratigraphy of felsic volcanic rocks

There appears to be little systematic chemical variation with stratigraphic level within individual felsic volcanic centres; samples from each centre tend to form clusters on Harker variation diagrams (Fig. 29). There are two exceptions to this pattern. In the Wydgee centre (Table 6, Figs 18 and 19) low-(Zr+Y) andesite is overlain by high-(Zr+Y) dacite (Table 13); the chemical distinction between the two sequences is marked (Fig. 28). In the Cuddingwarra centre (Table 6, Figs 18 and 19), high-(Zr+Y) rhyolite shows a trend of increasing, then decreasing, Y and Zn with increasing Zr, stratigraphically upwards (Fig. 28; Appendix II). In the latter case, the stratigraphic variation was probably caused by plagioclase and magnetite fractionation, followed by apatite fractionation. Both low- and high-(Zr+Y) dacites occur in the Golden Grove centre (Fig. 28); unfortunately, the relative stratigraphic positions of these samples is unknown.

The lack of chemostratigraphic variation is surprising, given the lithostratigraphic complexity of most centres (e.g. Frater, 1983a). It appears that eruption processes and products were complex, yet magma compositions for individual centres were fairly homogeneous. Direct correlation of felsic volcanic units between individual centres is not feasible (Table 13, Fig. 29). Moreover, there appears to be no regional chemical division of felsic volcanic rocks as there is for basalts (Fig. 19); this is consistent with derivation from the crust rather than from the upper mantle. The abundance of felsic volcanic centres in the upper part of the Gabanintha Formation suggests that some fundamental regional process was responsible for their contemporaneous generation.

Geochronology

Several age determinations of Gabanintha Formation rocks and minerals have been published (Table 14). Most of these have been made on felsic volcanic rocks or on minerals associated with these rocks. U–Pb zircon ages of three felsic volcanic rocks, with overlapping uncertainties, indicate that felsic volcanism in the Gabanintha Formation occurred at about 3.0 Ga. The mean age of syngenetic galenas from Pb–Zn massive-sulphide deposits in the Golden

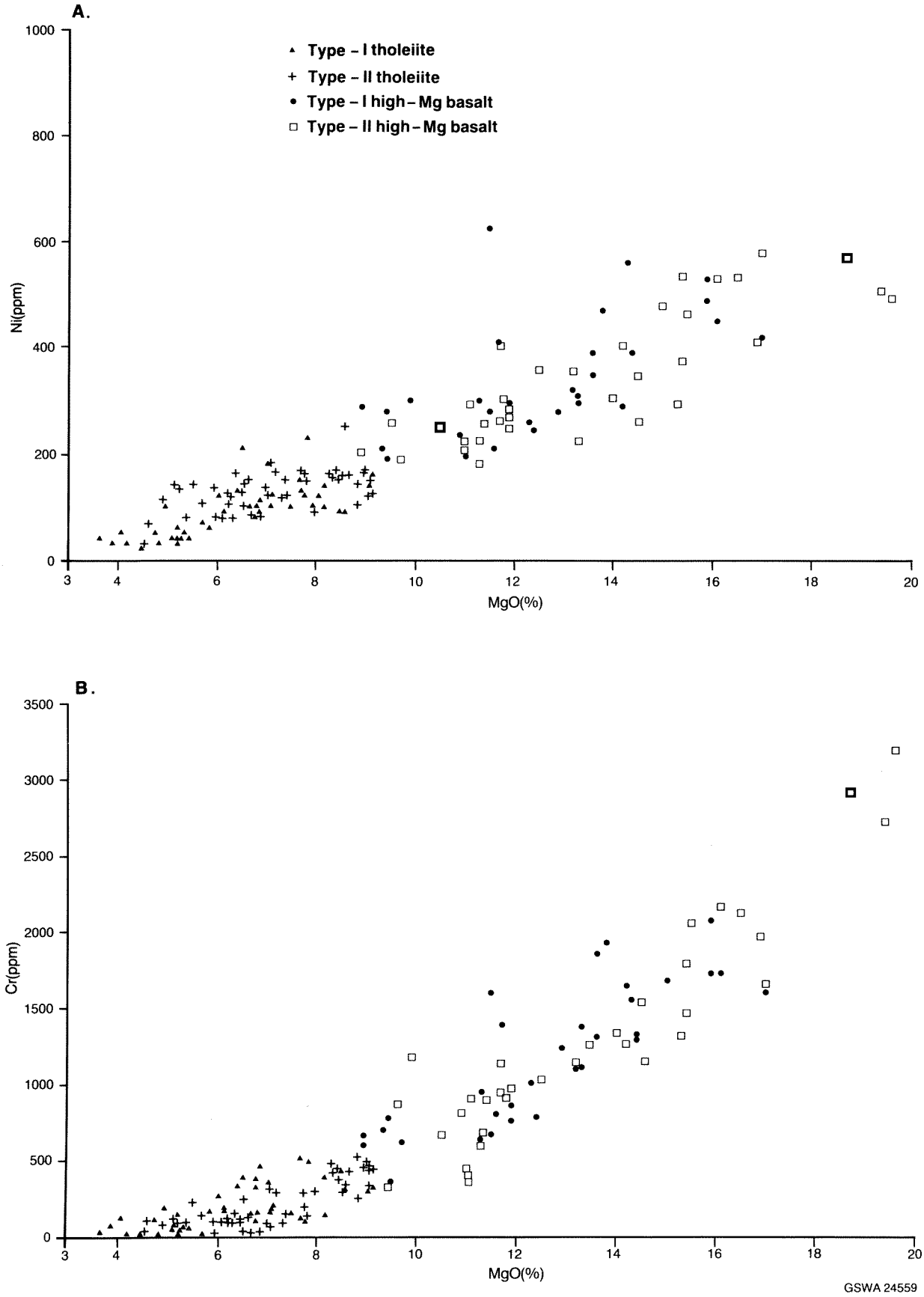


Figure 24. Ni–MgO and Cr–MgO diagrams for Gabanintha Formation basalt.

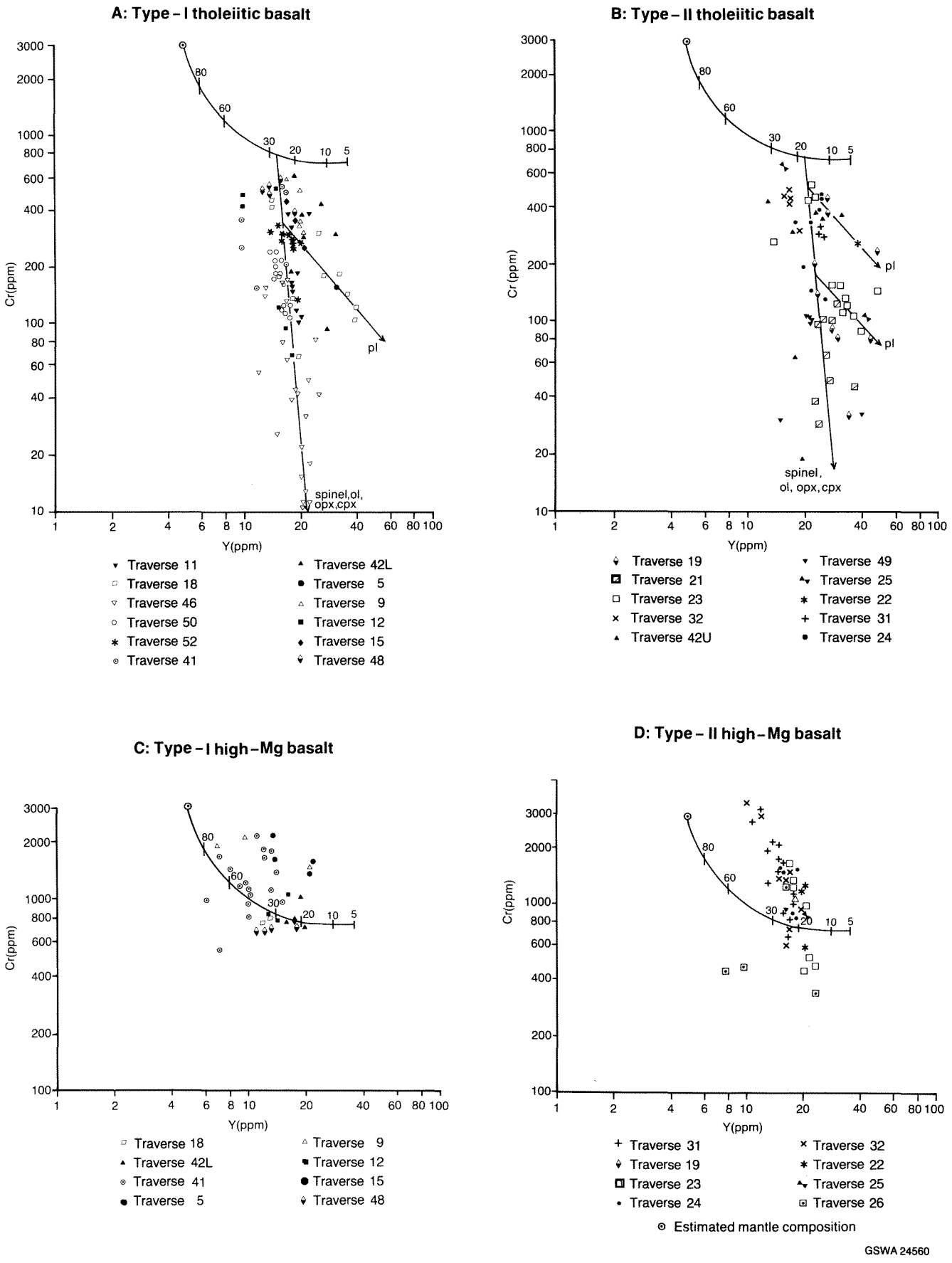


Figure 25. Cr–Y diagrams for Gabanintha Formation basalt. Data for model partial-melting curve, estimated mantle composition, and crystal-fractionantion trends as for Figure 10.

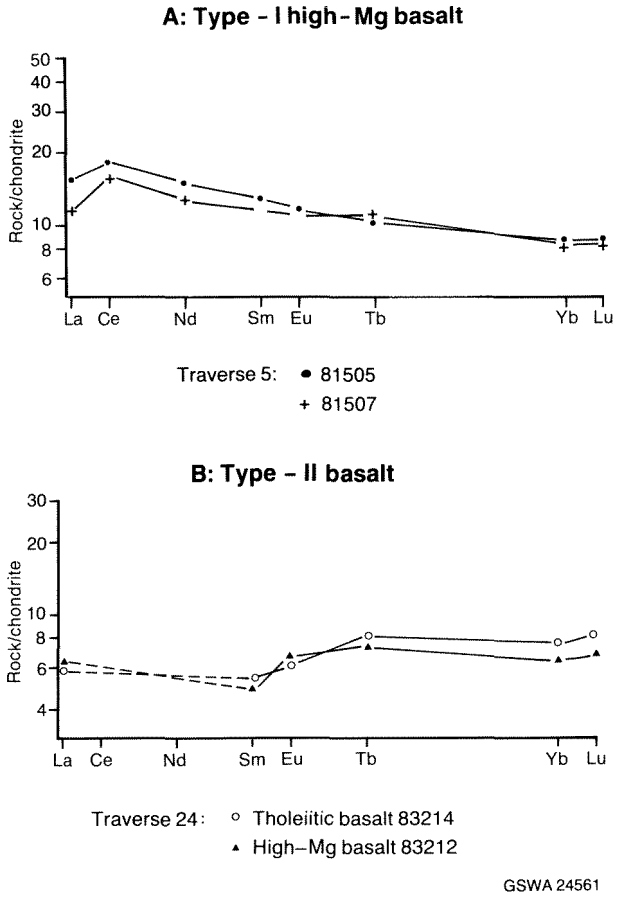


Figure 26. REE patterns for Gabanintha Formation basalts.

Grove felsic volcanic centre is 3044 Ma; however, many of the uncertainties overlap with the U–Pb zircon determinations (Table 14). Fletcher et al. (1984) determined a Sm–Nd isochron age of 2980±120 Ma from a variety of lithologies in the Yalgoo–Singleton greenstone belt, 25 km north of the Golden Grove mineral deposits. However, it is unlikely that these lithologies have a common REE fractionation history. Sm–Nd model ages (T_{DM}*, de Paolo, 1981) cluster in the range 3.0–3.1 Ga.

Sm–Nd isotope abundances and model ages have been determined on two andesites (samples 81618 from traverse 16, and 83329 from traverse 28) from the Gabanintha Formation (Appendix III). Sample 81618 is a split of the U–Pb zircon sample from Wattagee Hill listed in Table 14. The high initial $\varepsilon_{Nd}(T)$ values indicate short crustal residence times for the amphibolite precursors of these rocks. Thus, the sequence of mantle partial melting to produce basalt, hydration to form amphibolite, and further partial melting to produce andesite was not long lived and may even have been a continuous serial process.

*T_{DM} (Sm–Nd model age) is an estimate of 'crust formation' age or 'crustal residence' age, calculated as the time of fractionation from a hypothetical, continuously depleting mantle (DM), which is constrained to evolve from chondritic composition at the formation of the earth to the composition of the source of 'average' MORB (mid-ocean ridge basalt) at present.

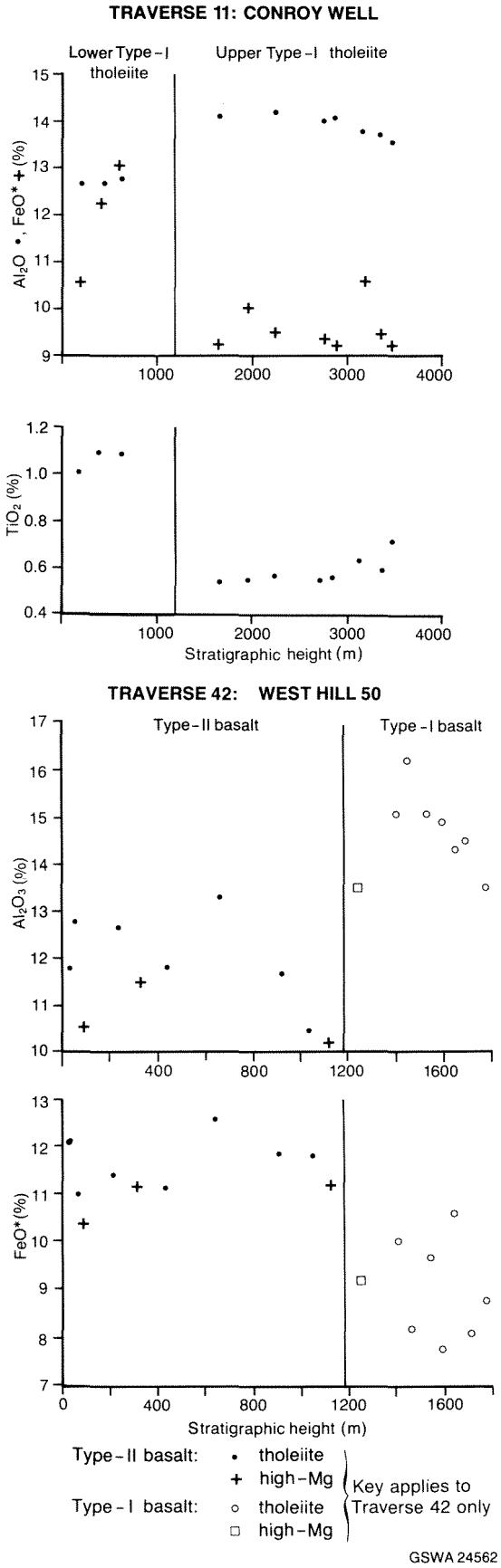


Figure 27. Examples of stratigraphic variation in Gabanintha Formation basalt chemistry in individual sample traverses.

TABLE 13. MEAN COMPOSITIONS OF GABANINTHA FORMATION FELSIC VOLCANIC ROCKS

Traverse	*10*	*13*	*16*	*20*	*28*	*28*	*48*	*48*	*57*	*57*
Location	*Abbotts*	*Nannine*	*Wattagee*	*Cuddingwarra*	*Wydgee*	*Wydgee*	*Reedy*	*Reedy*	*Golden Grove*	*Golden Grove*
Rock type	*Dacite*	*Dacite*	*Andesite*	*Rhyolite(c)*	*Andesite*	*Dacite(c)*	*Dacite*	*Andesite*	*Porphyry*	*Dacite*
	n=5	*n=4*	*n=6*	*n=5*	*n=3*	*n=5*	*n=2*	*n=5*	*n=4*	*n=4*
					Percentage					
SiO_2	68.6	66.1	59.3	76.6	60.8	64.2	65.8	61.4	74.5	64.2
Al_2O_3	13.7	15.3	16.2	11.3	14.2	14.5	15.2	14.7	14.0	14.3
Fe_2O_3	1.2	1.6	1.9	1.5	2.6	2.3	1.3	1.1	0.9	0.6
FeO	2.31	2.23	3.87	0.78	4.81	3.41	2.58	4.50	0.55	2.48
FeO*(b)	3.4	3.7	5.6	2.1	7.1	5.5	3.8	5.5	1.4	3.0
MgO	1.95	2.10	3.14	0.20	4.94	2.04	2.36	4.73	0.27	2.21
CaO	3.85	4.48	6.70	0.44	3.13	6.54	4.85	5.84	1.01	2.92
Na_2O	4.05	4.46	3.90	4.10	5.06	3.36	3.96	3.43	5.40	1.78
K_2O	1.25	1.30	0.80	2.98	0.32	0.57	1.25	0.94	1.43	2.05
TiO_2	0.44	0.49	1.18	0.23	0.71	0.76	0.44	0.54	0.11	0.38
P_2O_5	0.14	0.18	0.28	0.05	0.15	0.18	0.18	0.18	0.14	0.25
MnO	0.06	0.06	0.10	(a)0.03	0.09	0.10	0.07	0.12	0.01	0.22
LOI	2.05	1.55	2.81	0.80	2.67	1.14	1.12	1.69	1.25	4.48
					Parts per million					
Ba	379	537	299	573	120	153	675	371	1027	1409
Cr	31	59	125	<10	189	58	62	196	nd	nd
Co	43	46	50	28	71	95	53	47	<5	10
Cu	73	81	79	30	45	37	129	113	11	11
Pb	<10	<10	<10	<10	(a)12	<10	<10	<10	<10	<10
Li	10	10	9	3	31	9	76	65	5	4
Mo	1	1	nd	<1	<1	<1	<1	<1	<1	<1
Ni	28	30	82	26	144	71	50	116	7	(a)9
Nb	(a)8	7	15	9	8	12	8	9	<5	7
Rb	40	42	26	44	16	35	61	47	41	73
Sr	256	383	382	51	78	145	293	294	334	52
Th	<5	<5	<5	<10	<10	<10	5	(a)5	<10	<10
Sn	6	7	nd	5	5	8	7	7	<5	<5
U	<1	<1	nd	<1	<1	<1	<1	<1	<1	<1
V	82	77	169	<10	120	75	83	123	24	53
Y	12	9	18	55	23	37	15	16	6	12
Zn	55	43	84	58	77	109	44	59	28	43
Zr	126	146	138	249	171	271	122	130	94	149
La	13	13	18	nd	nd	nd	19	19	9	15
Ce	23	27	37	nd	nd	nd	35	32	15	28
Zr/(Zr+Y)	0.91	0.94	0.88	0.82	0.88	0.88	0.89	0.89	0.94	0.93

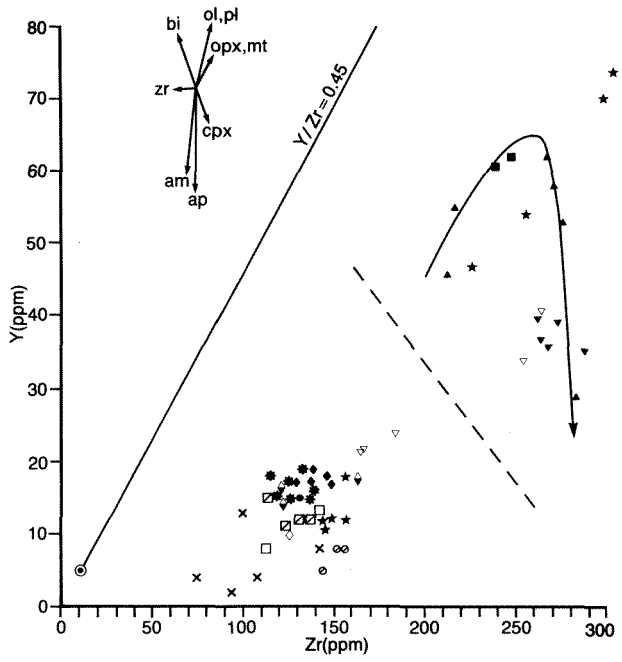
(a) Some values used to calculate the means are below the detection limit; for these determinations the value 'detection limit/2' was used.
(b) All Fe calculated as FeO (c) High-(Zr+Y) felsic volcanic rocks, other tabulated means are of low-(Zr+Y) rocks
Samples assigned to alteration class 3 (see Appendix II) are omitted from the means
nd: not determined

Windaning Formation

Definition and distribution

The Windaning Formation is defined here as a succession of abundant jaspilitic BIF and grey-white chert units interlayered with felsic volcanic, volcaniclastic, and volcanogenic rocks, and minor amounts of basalt, overlying the Gabanintha Formation. It is the uppermost formation in the Luke Creek Group. The formation is named after Windaning Hill in the southern part of the Yalgoo–Singleton greenstone belt, where prominent outcrops of the formation are complexly folded (Plates 1 and 2). The Windaning Formation is a distinct stratigraphic marker that occurs throughout the Murchison Province. The formation is thickest in the northern part of the Meekatharra–Wydgee greenstone belt, and in the central and southern parts of the Yalgoo–Singleton greenstone belt, but is relatively thin in the central and western regions of the province (Plate 2). Gabbro and dolerite sills selectively intrude the formation, resulting in considerable thickening in some regions. The mean thickness of the formation, excluding intrusive rocks, is about 1.5 km (Fig. 3).

The type area of the Windaning Formation is between Minjar Hill and Mougooderra Hill, near Golden Grove in the Yalgoo–Singleton greenstone belt (Fig. 31). Here the formation consists of prominent ridges of jaspilitic BIF



Traverse 10: ⧄ dacite ◘ rhyolite
Traverse 13: • andesite ⌀ dacite
Traverse 16: ♦ andesite ◇ dacite
Traverse 20: ▲ rhyolite ⟶ fractionation trend, arrow at top of sequence
Traverse 28: ▽ andesite ▼ dacite
Traverse 48: ✱ andesite ◆ dacite
Traverse 57: ★ dacite ■ rhyolite × rhyolite porphyry
◉ Estimated mantle composition

ol	olivine	am	amphibole
opx	orthopyroxene	bi	biotite
cpx	clinopyroxene	mt	magnetite
pl	plagioclase	zr	zircon
		ap	apatite

GSWA 24563

Figure 28. Y–Zr diagram for Gabanintha Formation felsic volcanic rocks. Estimated mantle composition and ratio (Sun and Nesbitt, 1977) are shown. Relative crystal-fractionation vectors for various minerals in equilibrium with a felsic melt, for up to 50% fractional crystallization (Pearce and Norry, 1979) are also shown. The dashed line separates a high-(Zr+Y) field from a low-(Zr+Y) field.

units, 1–5 m thick, interlayered with fine- to medium-grained volcanogenic sedimentary rocks and felsic tuff. The succession is 1000 m thick east of Mougooderra Hill, and becomes thinner to the north. Most of the underlying rocks are concealed by lateritic gravel and sand. However, a few weathered exposures, and drilling by mining companies exploring the Golden Grove region, reveal them to be fine- to medium-grained volcanogenic sedimentary rocks, and small amounts of basalt, intruded by gabbro and dolerite sills (Harris et al., 1982; Frater, 1983a). The conformable contact between these Gabanintha Formation rocks and the Windaning Formation is poorly exposed on the eastern slopes of the BIF ridges south of Minjar Hill. Conglomerate and medium- to coarse-grained lithic wackes of the Mougooderra Formation unconformably overlie the Windaning Formation. Clasts of Windaning Formation BIF are abundant in the conglomerate. The angular unconformity is reasonably well exposed at a number of localities between Minjar and Mougooderra Hills (Fig. 31).

Lithostratigraphy

Windaning Formation BIF and chert units form topographically prominent ridges and ranges of hills. The intervening rocks are poorly exposed and weathered, and most are covered by BIF and chert scree. Jaspilitic BIF comprises interlayered red jasper bands, black hematite- and/or magnetite-rich bands, and white chert bands, from a few millimetres to a few centimetres thick (Fig. 32A). The BIF units range from a few metres to 150 m in thickness. In some outcrops they contain fine-grained felsic tuff units from a few centimetres to a few metres thick. In the field, Windaning Formation BIF is easily distinguished from Golconda Formation BIF by its colour (red, black, and white bands); thickness (up to 150 m); and association with felsic rocks rather than mafic rocks. However, distinction between BIF types is difficult in deeply weathered or highly metamorphosed regions. Mineral phases in greenschist-facies jaspilitic BIF include quartz (cryptocrystalline or granoblastic), magnetite, hematite, minnesotaite, stilpnomelane, greenalite, siderite, pyrite, chamosite, ankerite, calcite, and riebeckite (also see Gole, 1980). Hematite and goethite replaced magnetite during weathering. The red colour of jaspilitic chert bands is due to finely disseminated dusty hematite. Grey-white chert is much less abundant than jaspilitic BIF. It occurs as 1–5 m-thick units comprising alternating bands of light- to dark-grey chert, and milky-white chert, up to a few centimetres thick (Fig. 32B). Some of these units are silicified, fine-grained, clastic sedimentary rocks.

A variety of felsic lithologies are interlayered with BIF. These are mainly siliceous, very fine-grained, laminated, distal tuff; fine- to medium-grained well-bedded and often reworked tuff with sedimentary structures; rare coarse-grained fragmental rocks; aphanitic to porphyritic felsic lava; and volcanogenic sedimentary rocks, mainly shale and sandstone with minor amounts of conglomerate. Felsic lava and volcaniclastic rocks are more common in the northern part of the province; in the south, volcanogenic sediments are more abundant. In the vicinity of Polelle Homestead, a 2.5 kilometre-thick lens-shaped sequence of andesite and dacite occurs (Plate 1). The basal part of this sequence is interlayered with jaspilitic BIF, but most overlies the BIF. A number of lithologies are exposed, including fine-grained plagioclase- and pyroxene-phyric andesite and dacite lavas, fine-grained vesicular andesite, hyaloclastite, and thin units of volcanogenic sedimentary rocks. Most felsic volcanic rocks are carbonatized and silicified. At one locality near the homestead a 50 m-thick tuff breccia (Williams and McBirney, 1979) is exposed. It consists of monolithological fragments of vesicular andesite in a matrix of crystal-lithic tuff. These lithologies are characteristic of the proximal facies of volcanic rocks, viz. 5–15 km from the central vent (Williams and McBirney, 1979). The rocks immediately around Polelle Homestead are the most proximal, but the main vent is not exposed.

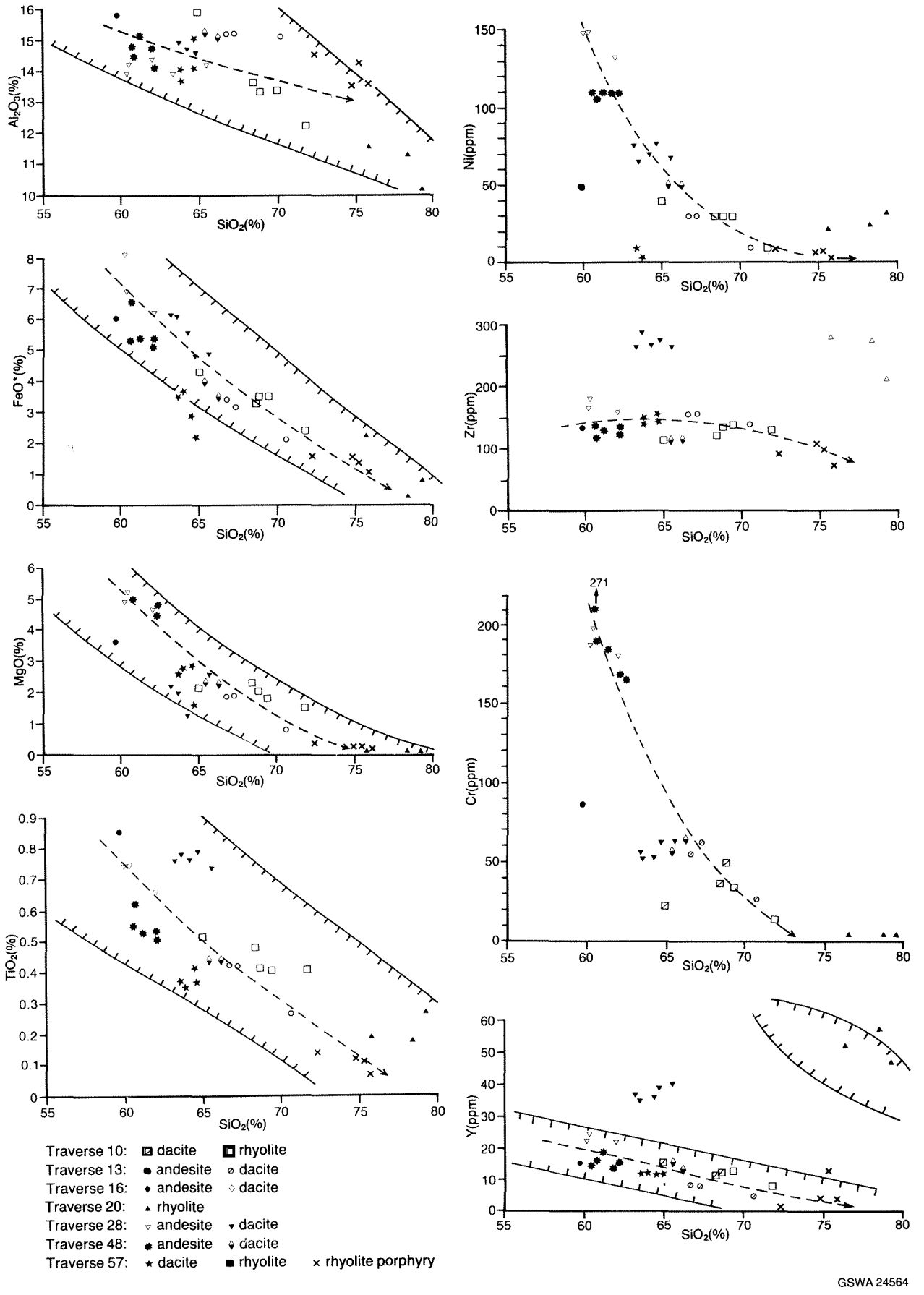


Figure 29. Harker variation diagrams for Gabanintha Formation felsic volcanic rocks. Dashed line is a calc-alkaline differentiation trend for these rocks. Solid lines with ticks define the compositional field of Yilgarn Craton felsic volcanic rocks described by Giles (1981).

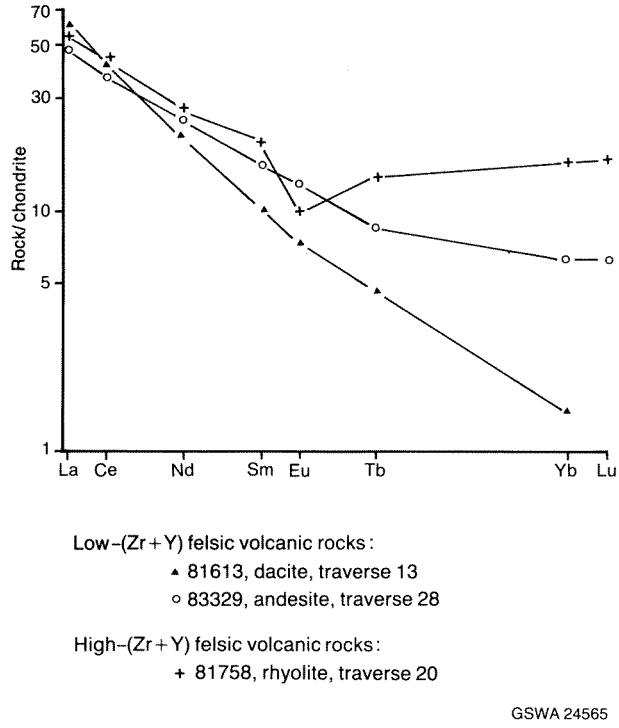


Figure 30. REE patterns for Gabanintha Formation felsic volcanic rocks.

Hallberg et al. (1976b) referred to these rocks as the 'Polelle andesites', and correlated them with andesites and dacites in the cores of two synclines, several kilometres to the west and northwest, which are now assigned to the Woolgra Formation (Fig. 3).

Minor units of basalt occur in laterally restricted deposits in the Windaning Formation; for example, in the southwestern part of the Weld Range and 10 km south of Meekatharra (Plates 1 and 2). In these areas, units of basalt more than 1 km thick pass laterally into felsic lava and volcaniclastic rocks. The basalts probably represent waning stages of the mafic volcanism which dominated development of the Luke Creek Group. The Windaning Formation is selectively intruded by gabbro and dolerite sills. In the Weld Range, dolerite sills of a few hundred metres thickness have successively intruded jaspilitic BIF and felsic volcaniclastic rocks. In the central part of the range, dolerite makes up more than 90% of the sequence (Plate 1). In the central part of the Yalgoo–Singleton greenstone belt, in the vicinity of the Blue Hill Range, thick gabbro and dolerite bodies comprising many sills dominate the Windaning Formation, although they also form a major component of the underlying Gabanintha Formation in this region (Plate 2). Gabbro and dolerite sills are abundant elsewhere in the Windaning Formation, particularly where it is well developed.

Geochemistry

Sampling

One hundred and thirteen samples were collected for chemical analysis from a number of traverses and localities. Of these, 85 are jaspilitic BIF, 11 are felsic volcanic rocks, 11 are sedimentary rocks (including grey-white chert), and 6 are mafic rocks. Maps of sample localities are not shown as there is little chemostratigraphic variation, and most samples were taken from short, very closely spaced traverses, or from single localities. Jaspilitic BIF samples were collected from near Polelle Homestead (13); the Weld Range (12); Mount Magnet (9); Quinns mining centre (8); Noongal (6); Tallering greenstone belt (9); Koolanooka greenstone belt (8); Mount Gibson (17); Reedy (2); and the Joker mine in the Yalgoo–Singleton greenstone belt (1). Felsic volcanic samples were collected from two short traverses, one 5 km north of Polelle Homestead (6 samples), and the other 5 km east of the homestead (5 samples). Sedimentary rocks were collected from Quinns mining centre (4); Tallering greenstone belt (3); Koolanooka greenstone belt (1); the Gnows Nest mine in the Yalgoo–Singleton greenstone belt (2); and Noongal (1). Tholeiitic basalt (4); high-Mg basalt (1); and dolerite (1) samples were collected from Noongal. At Mount Gibson, 34 samples of BIF were collected from two diamond-drill holes. Locations of samples and chemical analyses are listed in Appendix II.

Compositional characteristics

BIF: All surface samples of BIF are oxidized, and with the exceptions of SiO_2 and Fe_2O_3, contain low and variable abundances of oxides and trace elements (Table 15). There is no systematic stratigraphic or regional variation in chemical composition. The drill-core samples of BIF from Mount Gibson are less oxidized, and contain more MgO, CaO, MnO, Ni, and volatiles, than those at the surface (Table 15). Like Golconda Formation BIF, most differences between surface sample and drill-core sample geochemistry can be attributed to weathering. Weathered Golconda and Windaning Formation BIFs are very similar in composition, except that Ba and Cr contents are significantly lower in the latter. For unweathered drill-core samples, Windaning Formation BIF, on average, contains significantly more Ce and La, and less TiO_2, Ba, Cr, V, Zn, and volatiles, than Golconda Formation BIF (compare Tables 4 and 15).

Felsic volcanic rocks: On Harker variation diagrams, Windaning Formation felsic volcanic rocks (Table 16) exhibit different trends, for most elements, than those from the Gabanintha Formation (Fig. 33). Samples from the two Windaning Formation units have significantly different contents of Al_2O_3, FeO^*, Ni, Cr, Zr, and Y (Figs 33 and 34). REE patterns are also distinct (Fig. 35), and together with the other data suggest disparate origins for these units.

Basalt: The high-Mg basalt and dolerite samples from Noongal are altered (Appendix II). The mean composition of four unaltered tholeiitic basalt samples from this locality is given in Table 17. These plot on estimated Y/Zr and Ti/Zr upper mantle composition ratios in Figure 34.

Petrogenesis

BIF: BIF is thought to have originated by chemical

TABLE 14. PUBLISHED GEOCHRONOLOGY OF THE GABANINTHA FORMATION

Technique	*Rock type or mineral*	*Approximate location*	*Date (Ma)*	*Event*	*Source*
U–Pb zircon	Felsic volcanic	Twin Peaks greenstone belt	3046^{+45}_{-31}	Eruption	Pidgeon (1986)
	Felsic volcanic	Golden Grove	2952^{+90}_{-37}	Eruption	Pidgeon (1986)
	Andesite (81618)	Wattagee Hill Meekatharra–Wydgee greenstone belt	c. 2976	Eruption	Pidgeon (1986)
Pb–Pb model	Galena	Gossan Hill Golden Grove	3046 ± 23	Mineralization	Browning et al., (1987)
	Galena	Golden Grove	3052 ± 26	Mineralization	Browning et al., (1987)
	Galena	Scuddles Golden Grove	3052 ± 29	Mineralization	Browning et al., (1987)
	Pyrite	Golden Grove	3020 ± 34	Mineralization	Dahl et al., (1987)
	Pyrite	Golden Grove	3050 ± 34	Mineralization	Dahl et al., (1987)
	Pyrite	Golden Grove	3030 ± 34	Mineralization	Dahl et al., (1987)
	Galena	Golden Grove	3050 ± 34	Mineralization	Dahl et al., (1987)
	Galena	Golden Grove	3050	Mineralization	Fletcher et al., (1984)
Sm–Nd isochron	Ultramafic, mafic, and felsic lithologies	Yalgoo–Singleton greenstone belt	2980± 120	Mantle extraction	Fletcher et al., (1984)

precipitation (Condie, 1981), resulting in very low contents of most trace elements (Gole, 1981; Davy, 1983). However, in many outcrops chert and Fe-oxide bands in BIF are interlayered with thin units of felsic tuff and volcanogenic sedimentary rocks. Some unweathered BIF samples have higher contents of HFS elements and Al_2O_3 (Appendix II), indicating a volcanogenic component (Ewers and Morris, 1981; Davy, 1983). Zr/Al_2O_3 ratios of these samples are comparable with those for Windaning Formation felsic volcanics, and distinct from those for basalt and Golconda Formation BIF (Fig. 36). The origin of hematite in the red jasper of Windaning Formation BIF is conjectural. If the dusty hematite is primary it indicates high oxygen fugacity during precipitation and/or diagenesis. However, the hematite may have been derived by metamorphism and/or weathering of primary magnetite or siderite. Whichever process occurred, it rendered Windaning Formation BIF visually distinct from Golconda Formation BIF. Differences between some element abundances and ratios in unweathered samples of BIF from the two formations indicate that these formations were precipitated in different volcanic environments, albeit by similar depositional processes.

Felsic volcanic rocks: Andesite and dacite from traverse 2 have relatively high MgO, Ni, and Cr contents (Table 16), indicating a mafic source. High V and Sr values, and the absence of a Eu anomaly (Fig. 35), suggest that magnetite and plagioclase were not important fractionating phases. In addition, the high LREE/HREE ratio indicates fractionation of amphibole. On Harker variation diagrams these rocks have higher total REE, and slightly different trends than low-(Zr+Y) felsic volcanic rocks from the Gabanintha Formation. However, the source characteristics are very similar and, for reasons discussed previously, it is likely that they were derived from a crustal amphibolite source — possibly by a lower degree of partial melting than for Gabanintha Formation rocks — followed by crystal fractionation. In contrast, rhyolite samples from traverse 8 have low abundance of MgO, Cr, and Ni (Table 16). Low Sr values and a negative Eu anomaly (Fig. 35) indicate much plagioclase fractionation. In addition, the distribution of data on Y–Zr and Ti–Zr plots (Fig. 34), combined with low TiO_2 and V abundance, are consistent with substantial fractionation of magnetite. Enrichment of HREE, and high Y contents, suggest that neither amphibole nor garnet were residual or fractionating phases. Zr, Y, and total REE contents are high compared with other felsic volcanic rocks described so far, which suggests derivation by relatively low degrees of partial melting of a fractionated crustal source such as siliceous granulite (Condie, 1978). The relatively high $\varepsilon_{Nd}(T)$ value of +2.0 for one rhyolite sample (Appendix III) indicates a short crustal residence time for the source rock.

Basalt: Windaning Formation tholeiitic basalt from Noongal (traverse 52) plots on the estimated upper mantle composition ratio (Sun and Nesbitt, 1977) on an Y–Zr

diagram (Fig. 34). Trends on Zr/Y–Zr and Cr–Y diagrams (Fig. 37) indicate that this tholeiite was derived by about 20% partial melting of a plagioclase-lherzolite source which was slightly depleted in incompatible elements. Compositional variation was controlled by olivine and pyroxene fractionation. Although the tholeiite is compositionally similar to underlying Gabanintha Formation tholeiite, it contains more FeO* and V, and has a lower Zr/(Zr+Y) ratio (compare Tables 9 and 17). It has affinities with Gabanintha Formation Type-II tholeiite, rather than with Type-I tholeiite at Noongal (compare Tables 11 and 17).

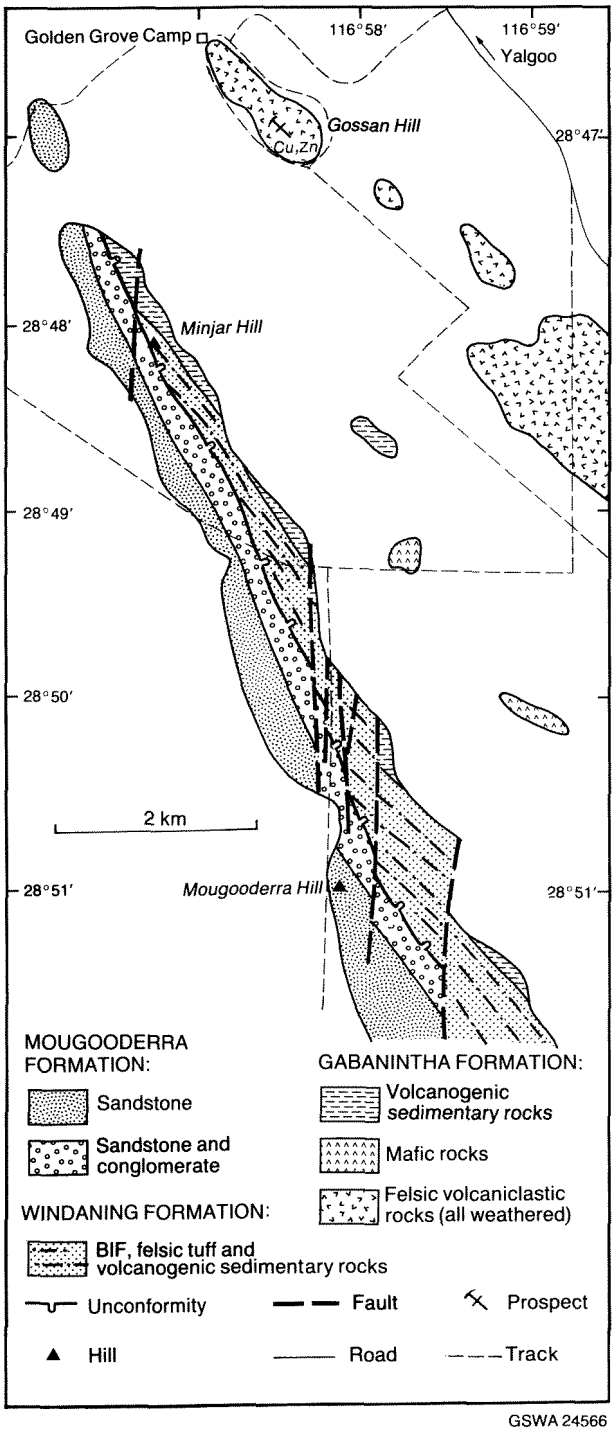


Figure 31. Outcrop geology of the type area for the Windaning Formation.

Mount Farmer Group

The Mount Farmer Group consists of two subgroups — one comprising three formations, the other two — and eight other formations (Fig. 3). The two subgroups and eight formations are thought to be broadly contemporaneous; each overlies the Windaning Formation (Plate 2). They are of limited lateral extent, each being confined to a part of one greenstone belt, except for the Mougooderra Formation which forms parts of two adjacent greenstone belts. The formations are distributed throughout the Murchison Province. All except the Mougooderra Formation

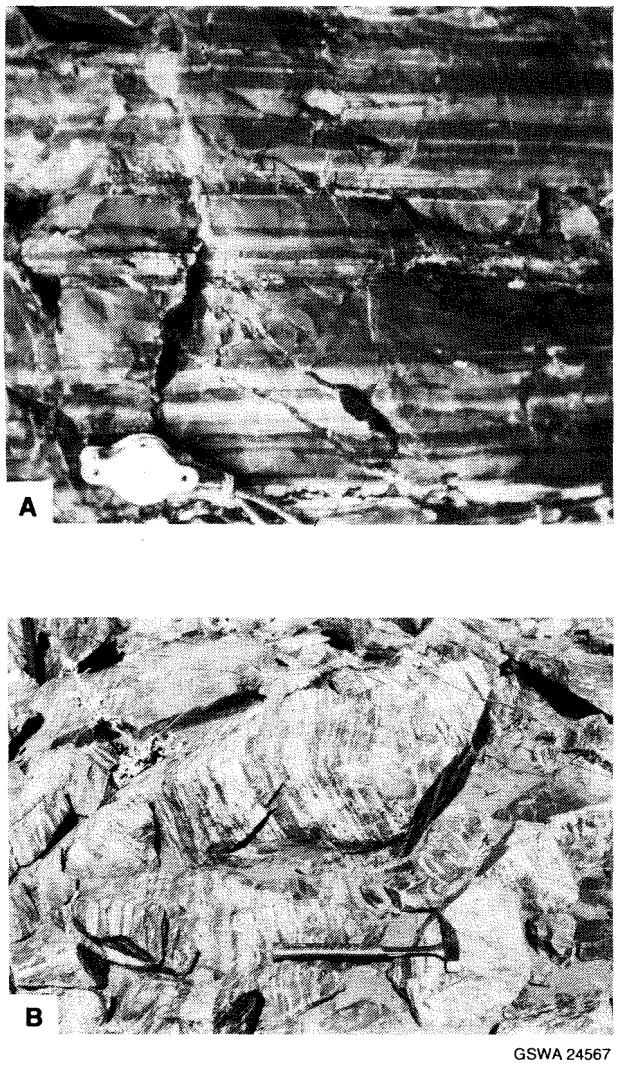


Figure 32. A — Windaning Formation jaspilitic banded iron - formation; the hand lens is 4cm long. B — Windaning Formation grey-white chert; the hammer handle is 30cm long.

TABLE 15. MEAN COMPOSITIONS OF WINDANING FORMATION BANDED IRON-FORMATION

	All surface samples n=85	*Mount Gibson surface samples n=17*	*Mount Gibson core samples n=32*
	Percentage		
SiO_2	50.5	44.1	44.1
Al_2O_3	0.4	0.4	0.5
Fe_2O_3	45.8	52.1	29.1
FeO	0.94	0.80	16.9
FeO*(c)	42.1	47.6	43.1
MgO	0.08	0.02	2.80
CaO	0.03	0.01	1.20
Na_2O	0.01	0.06	0.07
K_2O	0.01	0.08	0.09
TiO_2	0.01	<0.01	<0.01
P_2O_5	0.16	0.17	0.19
MnO	0.02	0.01	0.17
LOI	1.80	2.32	4.10
S	0.03	0.02	0.09
	Parts per million		
Ba	37	<20	<20
Cr	10	7	<10
Cu	37	12	(b)22
Ni	6	5	(b)22
V	13	5	10
Y	5	5	6
Zn	38	31	(b)32
Zr	7	6	(a) 9
Ce	9	15	(a)(b)14
La	8	5	(b)25

(a) Some values used to calculate the means are below the detection limit; for these determinations the value 'detection limit/2' was used.
(b) Mean for 12 samples only (c) All Fe calculated as FeO

TABLE 16. MEAN COMPOSITIONS OF WINDANING FORMATION FELSIC VOLCANIC ROCKS

	TRAVERSE 2 (NORTH POLELLE)		*TRAVERSE 8 (EAST POLELLE)*
	Andesite n=3	*Dacite n=3*	*Rhyolite n=5*
	Percentage		
SiO_2	58.5	64.4	75.0
Al_2O_3	16.1	14.9	10.8
Fe_2O_3	2.7	1.6	1.4
FeO	4.16	3.75	3.01
FeO* (b)	6.6	5.2	4.3
MgO	3.12	1.41	0.98
CaO	5.25	2.93	0.99
Na_2O	3.23	5.26	3.01
K_2O	1.90	1.47	1.06
TiO_2	0.81	0.73	0.22
P_2O_5	0.29	0.26	0.05
MnO	0.11	0.07	0.08
LOI	2.89	2.42	2.71
	Parts per million		
Ba	744	446	229
Cr	39	(a)20	(a) 5
Co	30	23	48
Cu	95	105	37
Pb	<10	<10	<10
Li	11	5	6
Mo	(a) 1	(a) 1	2
Ni	30	(a) 8	<10
Nb	16	19	24
Rb	57	36	29
Sr	485	289	42
Th	8	10	6
Sn	(a) 3	5	9
U	<1	<1	<1
V	132	53	<5
Y	27	30	162
Zn	81	87	53
Zr	182	231	495
La	27	32	29
Ce	54	65	68
Zr/(Zr+Y)	0.87	0.89	0.75

(a) Some values used to calculate the means are below the detection limit; for these determinations the value 'detection limit/2' was used.
(b) All Fe calculated as FeO
Samples assigned to alteration class 3 (see Appendix II) are omitted from the means.

are volcanic, and represent individual volcanic centres developed on an infrastructure of Luke Creek Group rocks. The Mougooderra Formation represents the only large epiclastic sedimentary basin in the Murchison Supergroup. The contact between the Mount Farmer and Luke Creek Groups was discussed earlier in this chapter. The Mount Farmer Group is named after a prominent hill in the central part of the Murchison Province.

Porlell Subgroup

The Porlell Subgroup overlies the Windaning Formation and occupies the core of a major double-syncline fold structure between Meekatharra and Reedy (Plate 2). It has an elongate north-northeasterly trending outcrop, about 50 km long by 8 km wide, and consists of three formations — the Lordy Basalt, Stockyard Basalt, and Woolgra Formation — which have a combined thickness of about 4.6 km (Fig. 3).

Definition and distribution of formations

Lordy Basalt

The Lordy Basalt is defined here as a succession of high-Mg basalt flows interlayered with small amounts of tholeiitic basalt, ultramafic rock, and volcanogenic sedimentary rock,

TABLE 17. MEAN COMPOSITIONS OF FOUR WINDANING FORMATION THOLEIITIC BASALTS FROM NOONGAL

Percentage		*ppm*		*Ratio*	
SiO_2	51.1	Ba	99	Mg number(b)	53.6
Al_2O_3	14.3	Cr	244	Cr/V	0.95
Fe_2O_3	1.8	Cu	89	Zr/(Zr+Y)	0.69
FeO	9.34	Ni	107		
FeO*(a)	10.9	Rb	<2		
MgO	7.06	Sr	91		
CaO	10.64	V	257		
Na_2O	1.62	Y	20		
K_2O	0.11	Zn	85		
TiO_2	0.69	Zr	45		
P_2O_5	0.19	La	7		
MnO	0.16	Ce	8		
LOI	1.90				

(a) All Fe calculated as FeO (b) 100 mol MgO/(MgO + FeO)
Samples assigned to alteration class 3 (see Appendix II) are omitted from the mean.

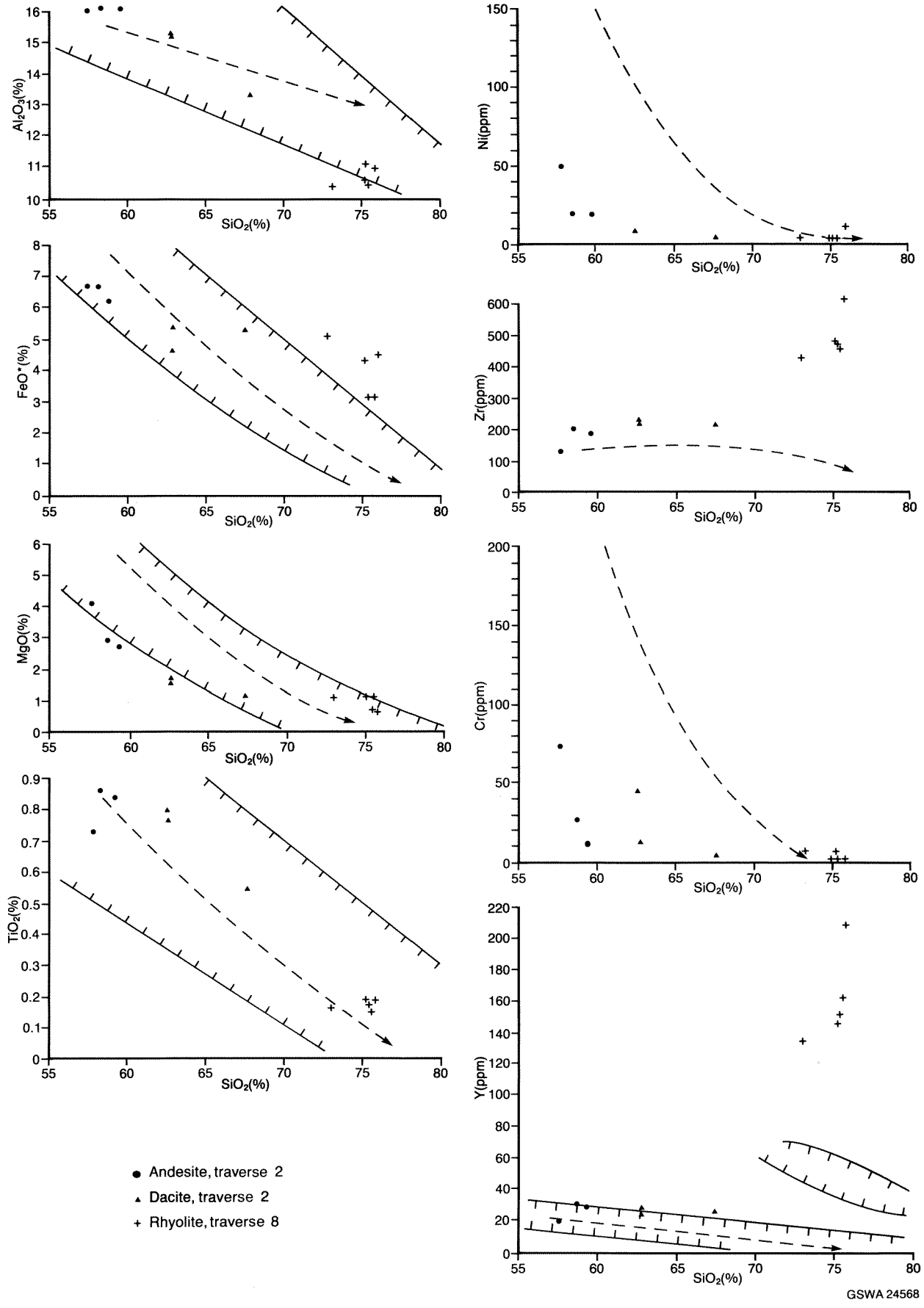
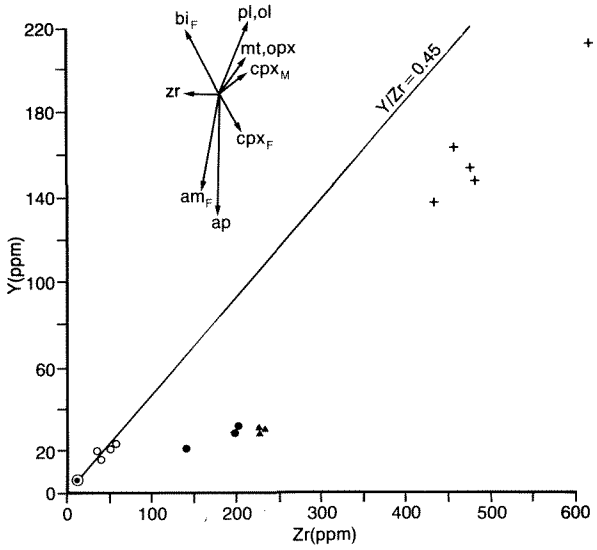
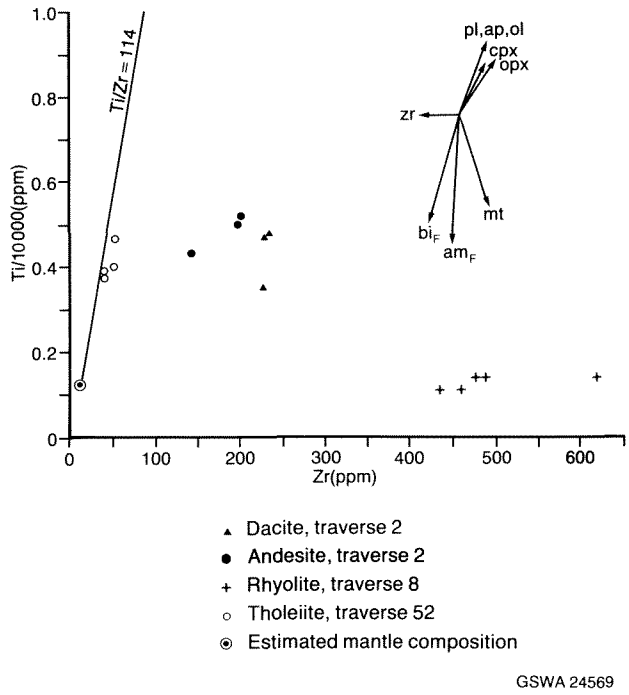


Figure 33. Harker variation diagrams for Windaning Formation felsic volcanic rocks. The dashed line is the calc-alkaline trend of Gabanintha Formation felsic volcanic rocks. The solid lines with ticks define the compositional field of Yilgarn Craton felsic volcanic rocks described by Giles (1981).





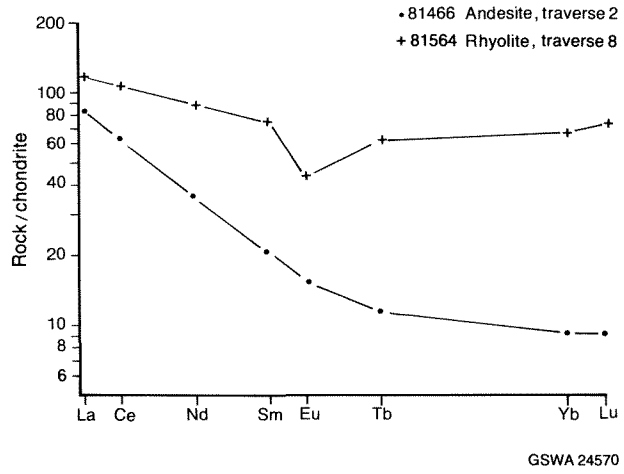


Figure 35. REE patterns for Windaning Formation felsic volcanic rocks.

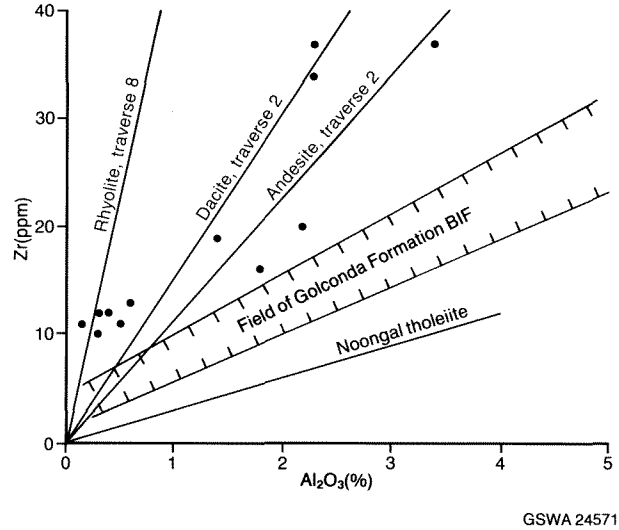


Figure 34. Y–Zr and Ti–Zr diagrams for Windaning Formation volcanic rocks. Estimated mantle composition and ratios, and relative crystal-fractionation vectors as in Figures 7 and 28. Subscripts F and M indicate mineral phases in equilibrium with felsic and mafic melts respectively.

Figure 36. Zr–Al_2O_3 plot for unweathered Windaning Formation jaspilitic banded iron-formation. Mean Zr–Al_2O_3 ratios of other Windaning Formation rocks are plotted for comparison. The compositional field of unweathered Golconda Formation banded iron-formation is also shown.

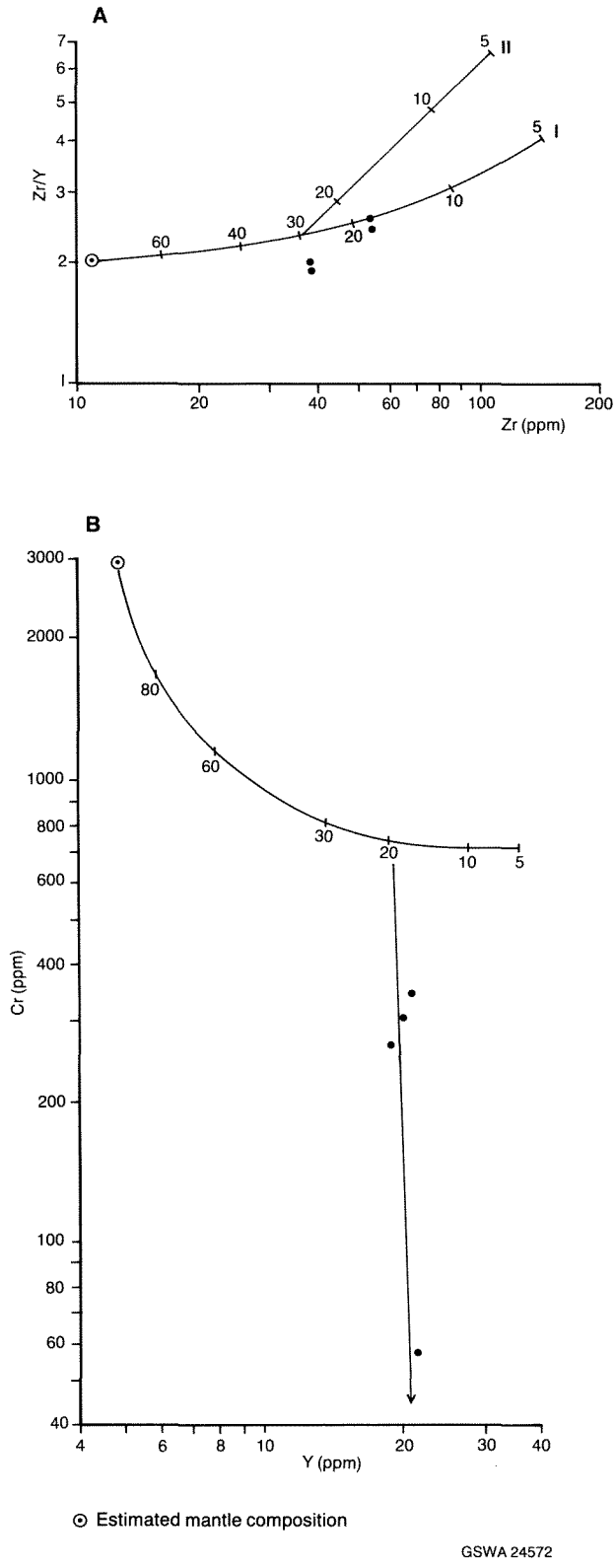


Figure 37. Zr/Y–Zr and Cr–Y diagrams for Windaning Formation tholeiitic basalt from Noongal (traverse 52). Model partial melting curves and source compositions as in Figures 8 and 10.

overlying the Windaning Formation. It is the basal formation in the Porlell Subgroup and is distributed as shown in Figure 38. It derives its name from Lordy Bore which is sited on the formation in the eastern limb of the fold structure. The type area is in the northern part of the fold structure between the Meekatharra–Murchison Downs and Meekatharra–Sandstone roads (Fig. 38A). The formation here varies in thickness from 800 m in the western limb of the fold to 2300 m in its tectonically thickened hinge zone. It overlies weathered, fine-grained volcanogenic sedimentary rocks, and jaspilitic BIF of the Windaning Formation (Plate 1), and is overlain by Stockyard Basalt. The lower contact is concealed beneath laterite. The upper contact is marked by a change from spinifex-textured high-Mg basalt of the Lordy Basalt to fine-grained and aphanitic tholeiitic basalt of the Stockyard Basalt.

Stockyard Basalt

The Stockyard Basalt is defined here as a succession of tholeiitic basalt flows, interlayered in the upper part with high-Mg basalt flows. It overlies the Lordy Basalt and is overlain by the Woolgra Formation (Figs 3 and 38). The type area is immediately south of Stockyard Bore (Fig. 38B). The formation here is 1100 m thick, comprising 800 m of monotonous tholeiitic basalt overlain by 300 m of interlayered high-Mg and tholeiitic basalt. A fine-grained ferruginous chert is exposed, in some places, at the lower contact with the needle spinifex-textured high-Mg basalt of the Lordy Basalt. The upper contact is between basalt and fine-grained laminated volcanogenic sedimentary rocks of the Woolgra Formation.

Woolgra Formation

The Woolgra Formation is defined here as a succession of felsic volcaniclastic rocks, dacite and andesite lava, and rare basalt units, overlying the Stockyard Basalt. It is the uppermost formation of the Murchison Supergroup in this region (Fig. 38). The Woolgra Formation derives its name from Woolgra Bore which is sited on the formation near the centre of the subgroup. The type area is between Lordy and Stockyard Bores (Fig. 38C) where the formation is 1200 m thick. At the base, fine-grained laminated volcanogenic sedimentary rocks overlie basalt of the Stockyard Basalt.

Lithostratigraphy

The Porlell Subgroup is a bimodal volcanic sequence; the lowest two formations are mafic but the uppermost is felsic (Fig. 3). The subgroup has been metamorphosed in prehnite–pumpellyite facies; igneous textures are generally well preserved, and some igneous mineral phases have survived metamorphism. An outcrop geology map and a schematic representation of the stratigraphy are shown in Figure 38.

Lordy Basalt

The Lordy Basalt consists mainly of massive needle spinifex-textured high-Mg basalt and minor fine-grained

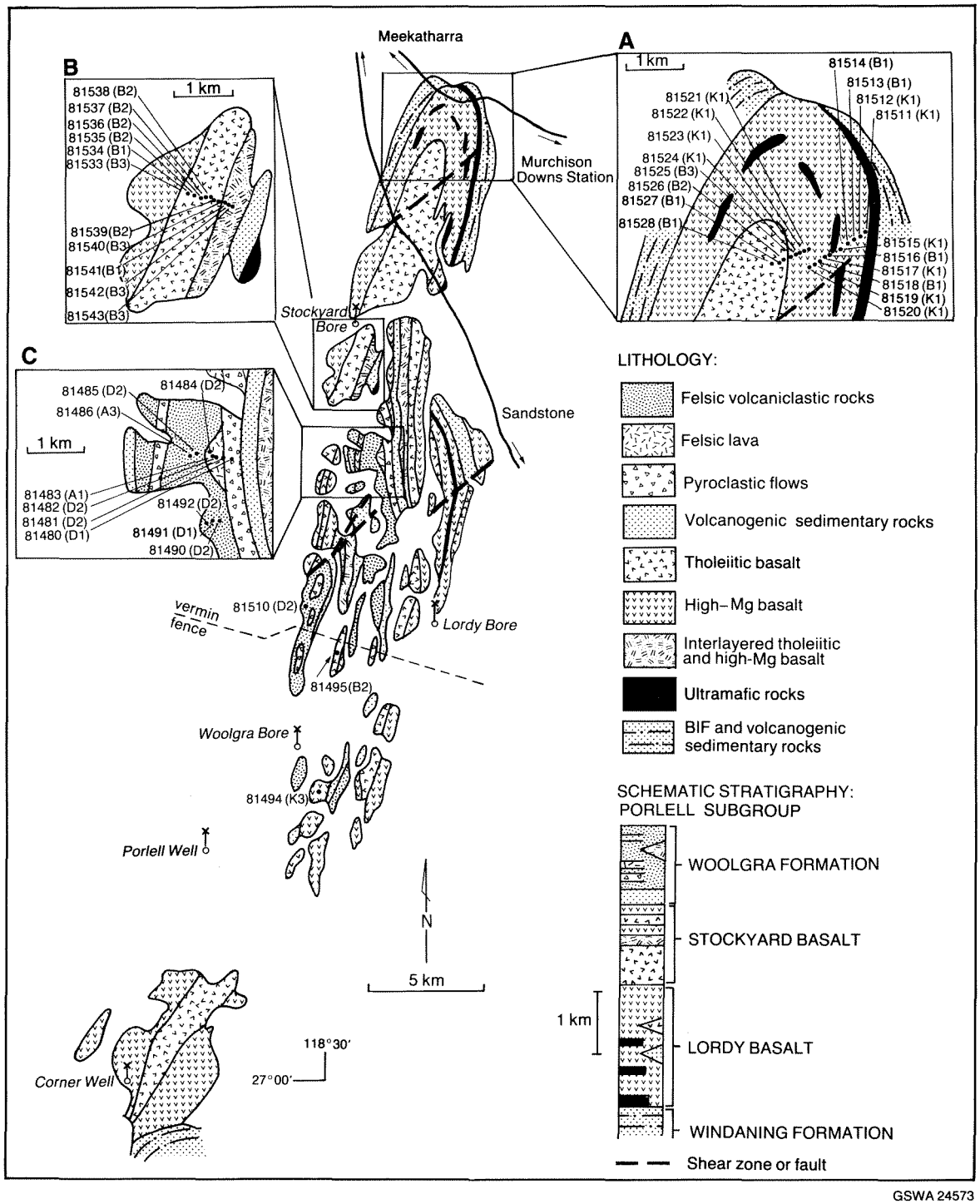
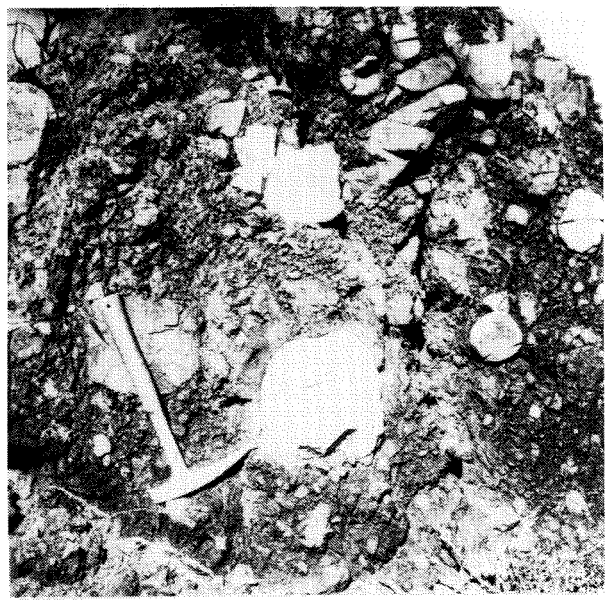


Figure 38. Geological outcrop map of the Porlell Subgroup showing sample locations (traverse 3) and stratigraphic relations. Codes in brackets following sample numbers refer to 'rock type' and 'degree of alteration' as defined in Appendix II.



GSWA 24574

Figure 39. Pyroclastic flow deposit in the Lordy Basalt; the hammer handle is 30cm long.

tholeiitic basalt. Ultramafic bladed spinifex-textured komatiite occurs at the base of the formation in the north-eastern limb of the fold (Fig. 38A). The formation is intruded by semiconformable sills and pods of peridotite (now serpentinite), pyroxenite, and gabbro; some sills are laterally continuous for several kilometres. At one locality near Corner Well on CUE, individual lava flows, about 50 m thick, can be distinguished. Many of these have peridotite (now serpentinite) bases, overlain successively by gabbro and needle spinifex-textured high-Mg basalt.

On the eastern side of the outcrop, about 6 km north of Lordy Bore, pyroclastic and sedimentary rocks are interlayered with high-Mg basalt near the base of the formation (Fig. 38). Two types of pyroclastic units occur. One contains angular fragments of high-Mg basalt, up to 15 cm across, in a matrix of small basalt fragments and (?secondary) quartz. The other consists of a mixture of subrounded high-Mg basalt and andesite fragments, up to 40 cm across, in a matrix of small angular fragments of these rocks (Fig. 39). The andesite fragments (generally 2–20 cm across) are more abundant than the high-Mg basalt fragments (generally 1–5 cm across), and are plagioclase- and pyroxene-phyric rocks with a grey-blue fine-grained matrix. The 15–30 m-thick pyroclastic units are not abundant. Sedimentary rocks range from poorly sorted, coarse-grained lithic wackes to very fine-grained siliceous banded rocks; all appear to be volcanogenic in origin. No other significant occurrences of sedimentary or pyroclastic rocks have been found in the Lordy Basalt.

Mineral phases in high-Mg basalt include clinopyroxene, serpentine (pseudomorphing orthopyroxene), Fe–Ti oxides, labradorite, devitrified glass, chlorite, talc, sphene, epidote, prehnite, pumpellyite, and carbonate. In some places, particularly in the south, the basalt is carbonatized and contains several modal percent carbonate. As there is little penetrative deformation, and the metamorphic grade



GSWA 24575

Figure 40. Well preserved pyroxene needle-spinifex texture with plagioclase crystals and altered glass (dark areas) in Lordy Basalt high-Mg basalt sample 81518.

is low, the spinifex textures are the best preserved in the Murchison Province (Fig. 40).

Stockyard Basalt

The Stockyard Basalt consists of fine-grained to aphanitic tholeiitic basalt and minor units of high-Mg basalt, interlayered with tholeiite near the top of the formation, particularly in the central part of the outcrop (Fig. 38). North of Stockyard Bore, the formation attains a thickness of 1200 m. South of Stockyard Bore the formation is 400–1100 m thick and contains units of high-Mg basalt in its upper part. Tholeiitic basalt is massive, blocky and featureless, except for ubiquitous concentric spherical fractures, many filled with carbonate and quartz. However, pillow lava, hyaloclastite, and vesicular lava are abundant in some outcrops. Units of 1–3 m-thick, fine-grained, laminated, siliceous interflow sedimentary rocks occur near the top of the formation; many separate tholeiitic and high-Mg basalt units.

Mineral phases in tholeiitic basalt include clinopyroxene, plagioclase, Fe–Ti oxides, chlorite, epidote, prehnite, pumpellyite, sphene, carbonate, quartz, and sericite. The Stockyard Basalt is characteristically carbonatized and partly silicified, and generally contains 2–5% (but up to 10%) post-metamorphic carbonate, abundant (<1 mm wide) quartz veins, and cryptocrystalline patches of silica. Basaltic textures are well preserved because of low metamorphic grade and weak development of foliation (Fig. 41).



Figure 41. Well-preserved basaltic texture consisting of interlocking clinopyroxene and plagioclase crystals with altered interstitial glass in Stockyard Basalt tholeiite sample 81528.

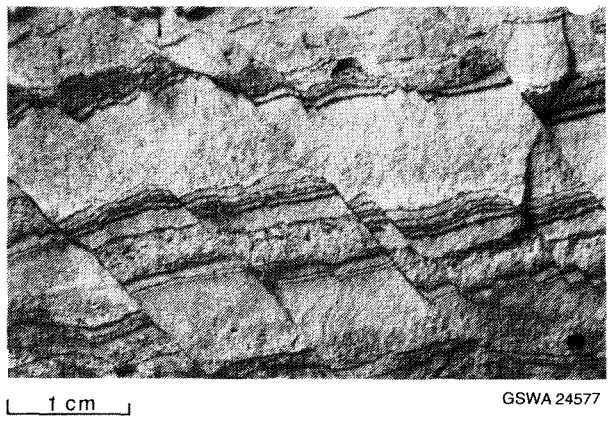


Figure 42. Fine-grained, cherty volcanogenic sedimentary rock from the Woolgra Formation, showing microfaulting and graded bedding.

Woolgra Formation

The Woolgra Formation consists mainly of volcaniclastic rocks and small amounts of dacite and andesite lava. A few thin basalt units occur near Stockyard Bore (Fig. 38). There are three main volcaniclastic lithologies:

(a) Fine-grained, laminated cherty rocks (Fig. 42). These contain bedding on a scale of less than 1 mm to a few centimetres. Microfaulting, domains of chaotic syndepositional slump structures, and graded bedding, are common features. Units of crystal-lithic tuff and volcanogenic sandstone, 1–50 cm thick, are interlayered with these rocks.

(b) Dacite and andesite tuff. These tuffs contain silt- and sand-size lithic fragments and/or crystals. Most are bedded, but when massive they resemble lava-flow rocks. Sedimentary structures other than bedding are rare.

(c) Coarse pyroclastic flow deposits. These contain fragments of all the lithologies seen in the Woolgra Formation, although clasts of lava and tuff dominate. The fragments are subangular to subrounded and range in size from less than 1 cm to 2 m across. The matrix is tuffaceous and consists of smaller lithic fragments and crystals. These deposits are thought to be lahars (Williams and McBirney, 1979). They grade upwards into coarse volcaniclastic rocks containing fragments less than 2 cm across.

Porphyritic dacite and andesite lava flows, 1–10 m thick, are interlayered with the volcaniclastic rocks. The proportion of volcaniclastic rocks to lava-flow rocks is approximately 5:1.

Stratigraphic relationships between these lithologies are shown schematically in Figure 43. The base of the formation is a laterally persistent unit of fine-grained, laminated cherty volcaniclastic rocks, generally 200 m (but up to 400 m) thick. These rocks grade upwards into tuffaceous volcaniclastic rocks and then into a zone of laterally impersistent lahar deposits, lava flows, and tuff. Two kilometres east of Stockyard Bore the laminated cherty rocks are overlain by about 200 m of interlayered tholeiitic and high-

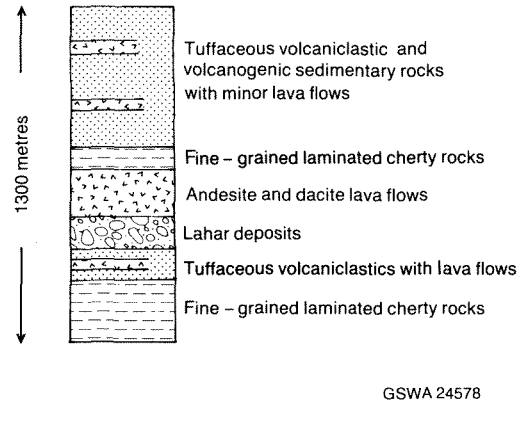


Figure 43. Schematic stratigraphy of the Woolgra Formation.

Mg basalt. Most of the lava flows in the sequence occur above the zone of lahar deposits; they generally form lens-like bodies in tuffaceous rocks. In one area, about 7 km north-northwest of Lordy Bore, a 500 m-thick pile of massive dacite and andesite lavas is developed (Fig. 38). Another laterally persistent unit of laminated cherty rocks, about 100 m thick, occurs above the zone of abundant lava flows. It is overlain by a thick sequence of tuffaceous volcaniclastic rocks, and silty and sandy volcanogenic sedimentary rocks with minor amounts of lava, which occupy the core of the eastern syncline (Plate 2). In the core of the western syncline the sequence is preserved only to the level of the lahars (Figs 38 and 43). These lithologies are characteristic of distal regions of volcanic complexes (Williams and McBirney, 1979, p. 313) i.e. more than 15 km from the central vent.

Hallberg at al. (1976b) thought that rocks comprising the Woolgra Formation could be correlated with dacite and andesite volcanics in the vicinity of Polelle Homestead. However, the lower units of the 'Polelle andesites' are interlayered with jaspilitic BIF of the Windaning Formation about 5 km north of Polelle Homestead, and are therefore assigned to this formation.

Mineral phases in the dacite and andesite lavas include clinopyroxene, orthopyroxene (generally pseudomorphed by aggregates of chlorite and serpentine), oscillatory-zoned plagioclase, hornblende, quartz, chlorite, epidote, sericite, sphene, carbonate, prehnite, pumpellyite, and Fe–Ti oxides. The mineralogy of the tuffaceous rocks is similar. Some rocks are altered and contain a few percent of post-metamorphic carbonate. Igneous textures are generally well preserved.

Geochemistry

Sampling

Forty-two samples of Porlell Subgroup rocks were collected for chemical analysis along a number of traverses; they comprise 15 Lordy Basalt, 16 Stockyard Basalt, and 11 Woolgra Formation samples. Sample locations are shown on Figure 38.

Bimodal compositions

The Porlell Subgroup is compositionally bimodal; there is a marked compositional gap between basalts and felsic volcanic rocks (Fig. 44). The basalts have tholeiitic and komatiitic affinities, but the felsic volcanics are calc-alkaline. Data for mafic and felsic rocks plot in distinctly different fields on Y–Zr and Ti–Zr diagrams (Fig. 45), indicating that they were derived by different petrogenetic processes.

Compositions and petrogenesis of mafic volcanic rocks

Mean compositions of Lordy and Stockyard Basalts are given in Tables 18 and 19. Rocks from the Lordy Basalt and the upper part of the Stockyard Basalt, where tholeiitic and high-Mg basalts are interlayered, share the same trends on Y–Zr and Ti–Zr diagrams (Fig. 45). In addition, tholeiites from the Lordy Basalt and upper Stockyard Basalt have very similar mean compositions (compare Tables 18 and 19). In contrast, tholeiites from the lower, monotonously tholeiitic part of the Stockyard Basalt plot in markedly different fields on Figure 46, and have clearly different mean compositions compared with the other tholeiites. It is unlikely that the two types of basalt are related by fractional crystallization. However, a feature that all Porlell Subgroup basalts have in common is a relatively high Rb content compared with Luke Creek Group basalts. This may reflect uniform alteration or enrichment of the source region in incompatible elements (Bailey, 1982).

Most basalt samples are enriched in Zr, relative to Y and Ti, compared with Sun and Nesbitt's (1977) estimated upper mantle ratio (Fig. 45). The division between the two types of tholeiite is clear on Zr/Y–Zr and Cr–Y diagrams (Fig. 46). Data for the Lordy Basalt and upper Stockyard Basalt tholeiite plot on trends indicating derivation by 20–30% partial melting of a plagioclase-lherzolite source enriched in incompatible elements, followed by crystal fractionation of olivine and pyroxene. Lower Stockyard Basalt samples plot in clusters on these diagrams. How-

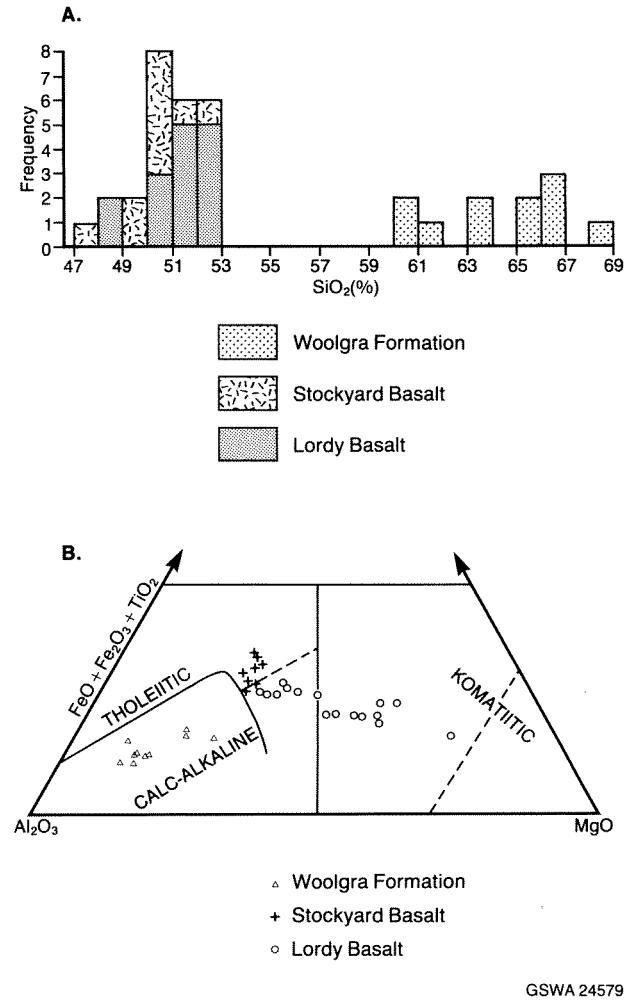


Figure 44. Bimodal composition of the Porlell Subgroup: A — SiO_2–frequency histogram; B — Jensen diagram.

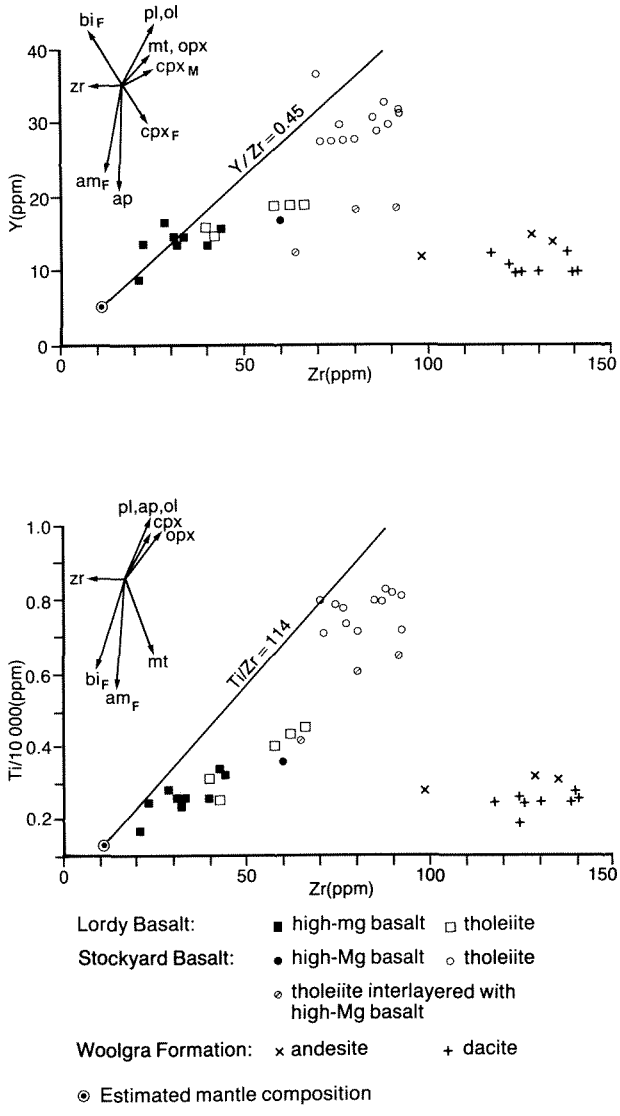


Figure 45. Y–Zr and Ti–Zr diagrams for Porlell Subgroup rocks. Estimated mantle composition and ratios, relative crystal-fractionation vectors, and mineral phases as in Figures 7 and 28. Subscripts F and M indicate mineral phases in equilibrium with felsic and mafic melts, respectively.

ever, the data are consistent with derivation by about 10% partial melting of a plagioclase-lherzolite source, followed by significant olivine and/or pyroxene fractionation prior to eruption as a relatively homogeneous suite of lavas. It is unlikely that plagioclase fractionation was important in lower Stockyard Basalt rocks, as Sr and CaO contents are comparable with those of the other tholeiite samples.

Lordy and Stockyard Basalts have distinctive REE patterns (Fig. 47). Three high-Mg basalt samples from the Lordy Basalt have low total REE contents, with flat HREE patterns of 6–7 times chondrite. Two of these samples have depleted MREE, although the patterns are incomplete, as Ce and Nd were not determined. The other sample, from the base of the formation, has enriched LREE with a $(La/Lu)_N$ value of 1.7. Three Stockyard Basalt samples have flat REE patterns of 14–16 times chondrite, except for consistent depletion of La and Ce. One sample of tholeiite from the upper Stockyard Basalt has a fractionated REE pattern with a $(La/Lu)_N$ value of 2.5. These patterns emphasise the differences between the Lordy and upper Stockyard Basalts and the lower Stockyard Basalt. The source of the Lordy Basalt and upper Stockyard Basalt appears to have undergone complex enrichments, and some depletions, of incompatible elements (cf. Pearce and Norry, 1979; Bailey, 1982). The flat HREE pattern indicates that garnet was not an important residual phase, and confirms plagioclase lherzolite as a suitable source material. The source of the other basalts had chondritic element ratios, with the possible exceptions of La and Ce. It is not clear whether abundances of these elements reflect petrogenetic processes, or alteration (Jahn and Sun, 1979). Again, plagioclase lherzolite is the most likely source material.

In summary, there are two unrelated types of mafic volcanic rocks in the Porlell Subgroup. The Lordy Basalt and the upper Stockyard Basalt are related by crystal fractionation, the latter being the more fractionated (Fig. 45). Extrusion of the compositionally distinct lower Stockyard Basalt interrupted the sequential eruption of these basalts.

TABLE 18. MEAN COMPOSITIONS OF LORDY BASALT

	High-Mg basalt n=11	*Tholeiitic basalt n=4*
	Percentage	
SiO_2	50.8	51.6
Al_2O_3	10.5	12.6
Fe_2O_3	1.9	2.8
FeO	7.86	7.38
FeO* (a)	9.6	9.9
MgO	14.30	8.92
CaO	8.10	9.46
Na_2O	1.04	1.67
K_2O	0.16	0.35
TiO_2	0.44	0.66
P_2O_5	0.07	0.10
MnO	0.16	0.15
LOI	4.11	3.76
	Parts per million	
Ba	(c) 31	57
Cr	1350	364
Co	65	56
Cu	82	112
Li	9	8
Ni	316	108
Rb	8	12
Sr	25	61
V	226	260
Y	15	18
Zn	61	64
Zr	33	57
La	<5	5
Ce	<5	8
Mg number (b)	72.6	61.6
Cr/V	5.97	1.40
Zr/(Zr+Y)	0.69	0.76

(a) All Fe calculated as FeO (b) 100 mol MgO/(MgO + FeO)
(c) Some values used to calculate the means are below the detection limit; for these determinations the value 'detection limit/2' was used.
Samples assigned to alteration class 3 (see Appendix II) are omitted from the means.
For the analyses averaged in this table Nb<5 ppm, Pb<10 ppm, and Th<5 ppm.

TABLE 19. MEAN COMPOSITIONS OF STOCKYARD BASALT

	Lower tholeiite n=11	*Upper tholeiite n=1*
	Percentage	
SiO_2	50.3	52.0
Al_2O_3	13.7	12.9
Fe_2O_3	2.5	1.5
FeO	8.47	8.20
FeO*(a)	10.7	9.5
MgO	5.67	8.39
CaO	10.25	7.71
Na_2O	2.18	1.81
K_2O	0.23	0.44
TiO_2	1.29	1.03
P_2O_5	0.17	0.11
MnO	0.21	0.18
LOI	4.47	5.10
	Parts per million	
Ba	67	66
Cr	96	493
Co	54	60
Cu	207	156
Li	9	21
Ni	95	140
Rb	9	20
Sr	106	98
V	360	277
Y	30	19
Zn	109	102
Zr	80	80
La	(c) 5	5
Ce	(c) 6	10
Mg number (b)	48.6	61.1
Cr/V	0.27	1.78
Zr/(Zr+Y)	0.73	0.81

(a) All Fe calculated as FeO (b) 100 mol MgO/(MgO + FeO)
(c) Some values used to calculate the means are below the detection limit; for these determinations the value 'detection limit/2' was used.
Samples assigned to alteration Åclass 3 (see Appendix II) are omitted from the means.
For most of the analyses averaged in this table, Nb<5 ppm, Pb<10 ppm and Th<5 ppm.

Compositions and petrogenesis of felsic volcanic rocks

Woolgra Formation dacite and andesite are closely comparable in composition to low-(Zr+Y) felsic volcanic rocks from the Gabanintha Formation (compare Tables 20 and 13). They also plot along similar trends on Harker variation diagrams (Fig. 48), although Cr contents are slightly higher, and FeO*, TiO_2, Zr, and Y contents are slightly lower at similar SiO_2 contents in Woolgra Formation rocks. In addition, REE patterns of Woolgra Formation rocks are virtually identical to those of Gabanintha Formation low-(Zr+Y) felsic volcanic rocks (compare Figs 49 and 30). In contrast, there are important differences between Woolgra Formation rocks and Windaning Formation rocks from traverse 2, north of Polelle Homestead (Fig. 48, and compare Tables 20 and 16) which were correlated by Hallberg et al. (1976b). Distinct trends of increasing MgO, Ni, and Cr are shown along one traverse through dacite and andesite lavas in the Woolgra Formation (Fig. 50). No other systematic chemostratigraphic variations have been discerned.

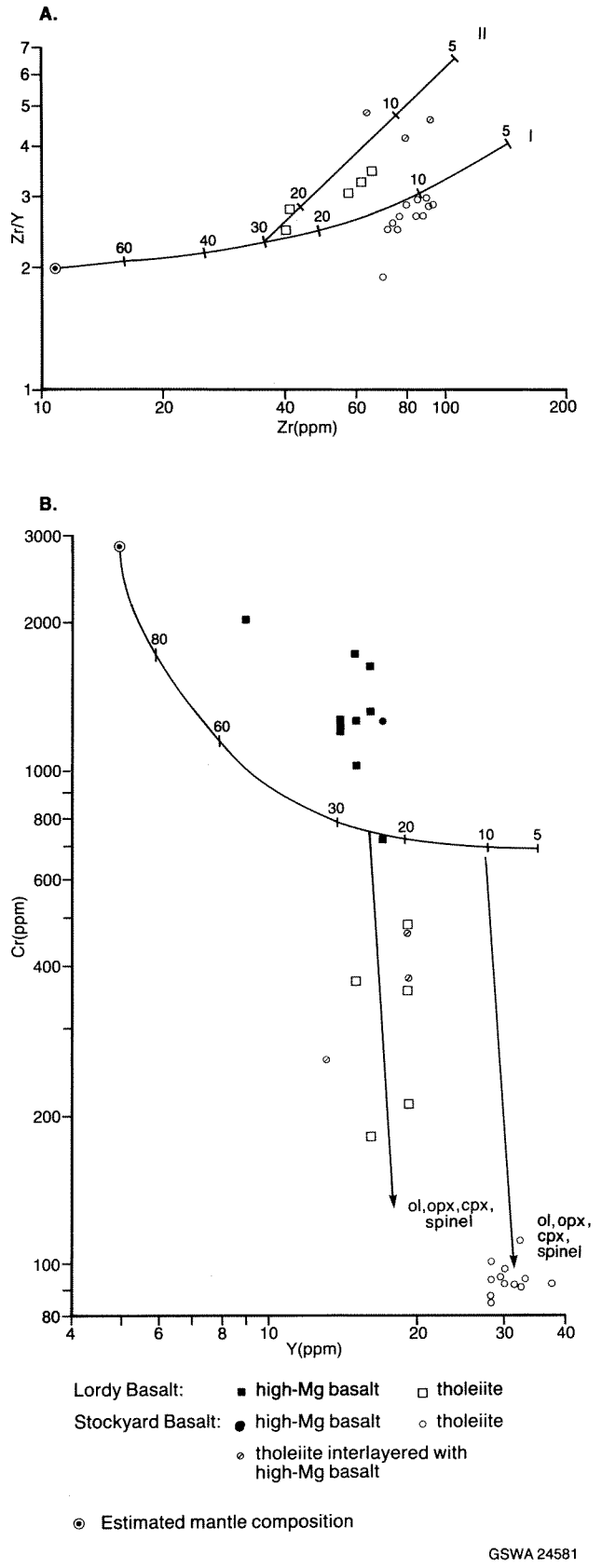


Figure 46. A—Zr/Y–Zr diagram for Porlell Subgroup tholeiitic basalt; model partial-melting curves and estimated mantle composition as in Figure 8. B—Cr–Y diagram for Porlell Subgroup basalt; model partial-melting curve, crystal-fractionation trends, and estimated mantle composition as in Figure 10.

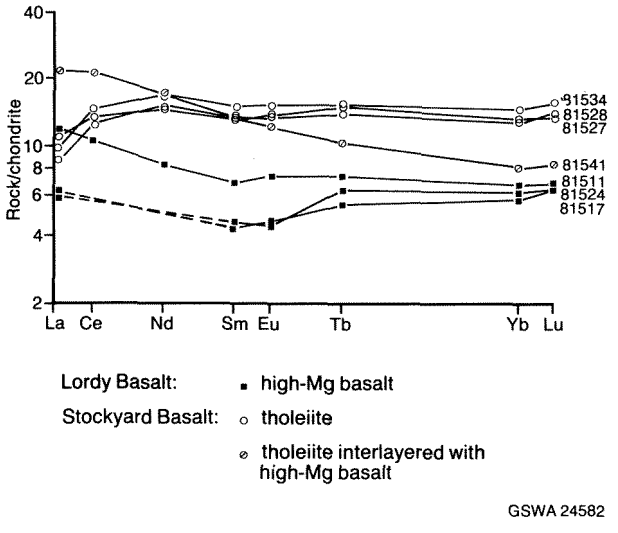


Figure 47. REE patterns for Porlell Subgroup basalt. Sample numbers are shown.

The close similarities in composition, Harker variation trends, REE patterns, and Sm–Nd isotope abundances (Appendix III) between Woolgra Formation rocks and Gabanintha Formation low-(Zr+Y) felsic volcanic rocks suggests that they both were formed by partial melting of LREE-enriched crustal amphibolite. Fractionated REE patterns, combined with relatively low Y, V, and FeO*, suggest that crystal fractionation of amphibole and magnetite followed partial melting. Sample 81480 has a small negative Eu anomaly, but the other samples have no anomalies (Fig. 49). These patterns, and the high Sr contents (Table 20), indicate that fractionation of plagioclase was not important. The increase of MgO, Ni, and Cr with stratigraphic height may indicate increasing degrees of partial melting — or alternatively, extraction of magma from the top, towards the bottom, of a zoned felsic magma chamber (Cox, Bell, and Pankhurst, 1979).

Sm–Nd geochronology

Sm–Nd isotope abundances have been determined for two samples (81491 and 81492) from the Woolgra Formation (Appendix III) and for mineral and material separates from sample 81492. This sample contains relatively fresh igneous clinopyroxene and plagioclase phenocrysts. The separates are composed of plagioclase, clinopyroxene, and magnetic, non-magnetic, and HCl-leach fractions of crushed rock. Data for sample 81492 and the separates plot on an isochron giving a date of 2818±57 Ma, which is interpreted as the crystallization age of the rock (Fig. 51), although the altered mineralogy of the sample necessitates caution in the use of this date. The initial $\varepsilon_{Nd}(T)$ of 1.3±0.6 given by the isochron is consistent with the interpreted origin of these rocks by partial melting of a mafic crustal source. However, it is also consistent with direct derivation from a mantle source, although it precludes a felsic source.

Yalgoo Subgroup

The Yalgoo Subgroup overlies the Windaning Formation in a fault-bounded anticline north of the town of Yalgoo (Plate 2) where it outcrops over an area of about 150 km². It is a bimodal volcanic sequence comprising two formations, the Wadgingarra Basalt, and the overlying Camberathunun Formation, which have a combined thickness of about 5 km.

TABLE 20. MEAN COMPOSITIONS OF DACITE AND ANDESITE LAVA FROM THE WOOLGRA FORMATION

	Dacite *n=6*	*Andesite* *n=2*
	Percentage	
SiO_2	66.3	61.3
Al_2O_3	15.0	15.2
Fe_2O_3	0.7	1.3
FeO	2.36	3.56
FeO*(a)	3.0	4.9
MgO	2.15	3.67
CaO	3.74	5.38
Na_2O	4.74	3.54
K_2O	1.35	1.67
TiO_2	0.41	0.53
P_2O_5	0.16	0.24
MnO	0.06	0.08
LOI	2.06	2.62
	Parts per million	
Ba	352	460
Cr	129	164
Co	36	34
Cu	114	113
Pb	<10	<10
Li	8	16
Mo	<1	<1
Ni	62	85
Nb	9	9
Rb	36	45
Sr	499	602
Th	<5	<5
Sn	8	8
U	<1	<1
V	69	102
Y	11	15
Zn	49	62
Zr	130	130
La	14	18
Ce	27	33
Zr/(Zr+Y)	0.92	0.90

(a) All Fe calculated as FeO
Samples assigned to alteration class 3 (see Appendix II) are omitted from the means

Definition and distribution of formations

Wadgingarra Basalt

The Wadgingarra Basalt is defined here as a succession of interlayered high-Mg and tholeiitic basalts, together with minor amounts of ultramafic rocks, and associated gabbro and dolerite intrusions. It overlies the Windaning Formation and is distributed as shown on Plate 2 and Figure 52A. The formation is named after Wadgingarra Hill. The type area is in the western part of the outcrop, from the hinge

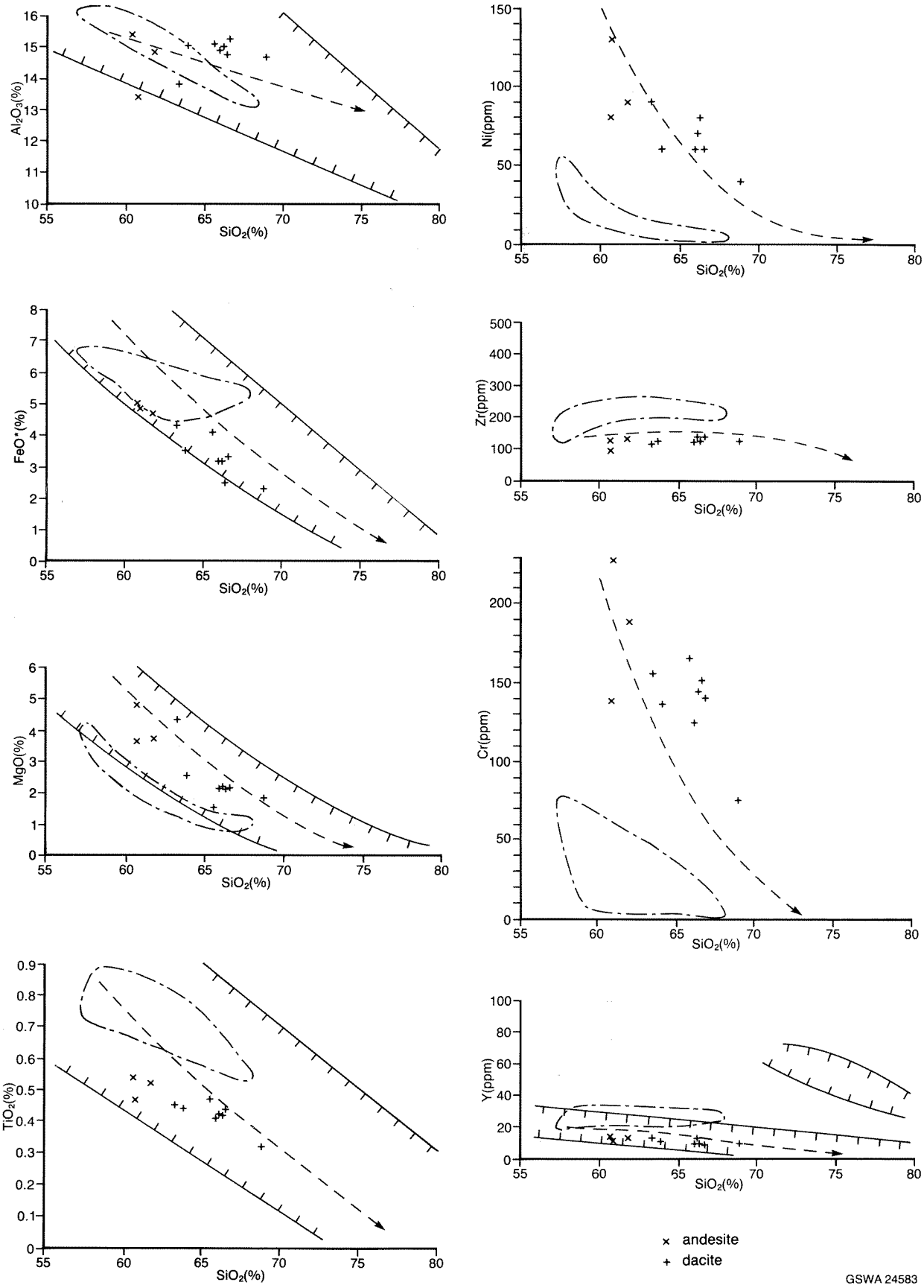


Figure 48. Harker variation diagrams for Woolgra Formation felsic volcanic rocks. Dashed line is the calc-alkaline differentiation trend for Gabanintha Formation felsic volcanic rocks. Dash-dot line defines the field of felsic volcanic rocks from traverse 2 (Hallberg et al., (1976b) 'Polelle andesites'). Solid lines with ticks define the compositional field of Yilgarn Craton felsic volcanic rocks described by Giles (1981).

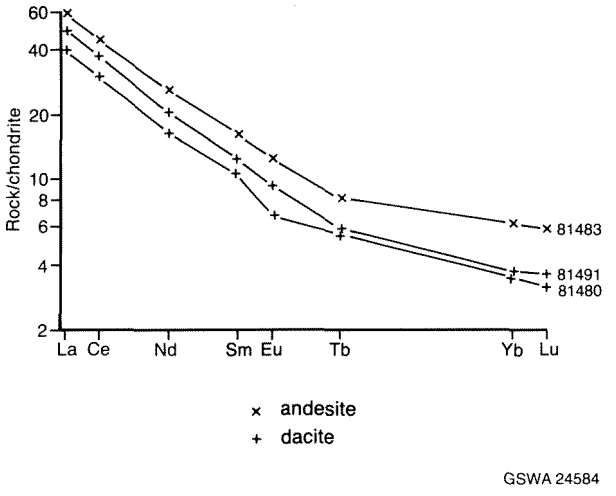


Figure 49. REE patterns for Woolgra Formation felsic volcanic rocks.

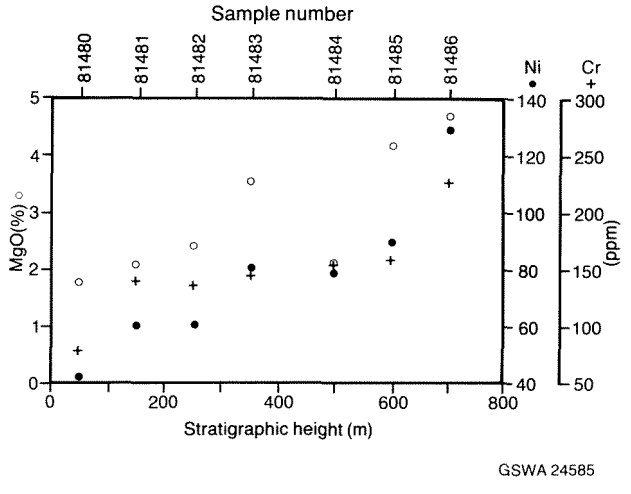


Figure 50. Chemostratigraphic variation in the Woolgra Formation.

zone of the anticline, where the Basalt overlies the Windaning Formation, to the contact with the Camberathunun Formation, 4 km east of Camberathunun Hill (Fig. 52A, Plate 2). At the lower contact, high-Mg basalt of the Wadgingarra Basalt overlies fine-grained volcanogenic sedimentary rocks and BIF of the Windaning Formation. East of Camberathunun Hill, tholeiitic basalt is overlain by felsic schist of the Camberathunun Formation. The succession is about 4 km thick in this area.

Camberathunun Formation

The Camberathunun Formation is defined here as a succession of sheared and weathered felsic volcanic rocks, together with small amounts of basalt and peridotite. Its type area is at Camberathunun Hill, northwest of Yalgoo, where it overlies the Wadgingarra Basalt (Fig. 52A). The top of the formation is bounded by a shear zone separating the felsic volcanic rocks from recrystallized monzogranite to the west (Plate 2). The original thickness is difficult to estimate because of intense deformation and lack of marker units. Its present thickness is about 1 km.

Lithostratigraphy

The Yalgoo Subgroup is a bimodal volcanic sequence (Fig. 52A) similar to the Porlell Subgroup. The lower formation, the Wadgingarra Basalt, consists of interlayered tholeiitic and high-Mg basalt, and small amounts of ultramafic rocks; it is intruded by sills of gabbro, felsic porphyry, and peridotite (now serpentinite). The lower 1800 m of this formation is dominantly spinifex-textured high-Mg basalt, while the upper 2200 m is mainly tholeiitic basalt. No stratigraphic subdivision has been made because the boundary between the lower and upper parts is indistinct. Pillow lava occurs in the lower part of the Wadgingarra Basalt, about 300–400 m above the base, but elsewhere lava-flow features are rare. Metamorphic grade ranges from greenschist to lower amphibolite facies. The mineralogy is dominated by tremolite–actinolite and oligoclase–andesine, together with minor amounts of chlorite, biotite, Fe–Ti oxide phases, sphene, and quartz. Hornblende replaces the tremolite–actinolite series in the amphibolite facies. The thickness of the Wadgingarra Basalt varies considerably along strike from the limbs to the hinge zone of the anticline (Fig. 52A and Plate 2). Rocks in the centre of the hinge zone are intensely sheared, and the thickness here was probably tectonically modified. Thick gabbro sills intrude the eastern part of the formation.

The intensely sheared and weathered felsic volcanic rocks of the Camberathunun Formation are generally cream-coloured, banded quartz–oligoclase–hornblende–chlorite rocks with fragmental textures. Banding is caused by alternating hornblende-rich and quartz–plagioclase-rich layers. The rocks are andesitic in composition (Muhling and Low, 1977, table 4) and probably pyroclastic in origin. They are interlayered with minor amounts of tholeiitic basalt, and intruded by peridotite (Fig. 52A).

Geochemistry

Sampling

Forty-six samples of basalt were collected along two traverses, about 8 km apart, across the Wadgingarra Basalt (Figs 52B and C). No samples were collected from the Camberathunun Formation because of its extensive alteration.

Compositions and petrogenesis

Most samples of Wadgingarra Basalt are mildly silicified and contain thin quartz veins and patches of cryptocrystalline silica; SiO_2 contents range from 48.9% to 55.8%, with a mean value of 53.3%. Mean compositions are given in Table 21. Ratios of HFS elements and major oxides seem unaffected by silicification and these data plot on clearly defined trends (Fig. 53). There is no systematic chemostratigraphic variation of element abundance along either of the two sample traverses. On Y–Zr and Ti–Zr diagrams (Figs 53A and B), basalts from the lower and upper portions of

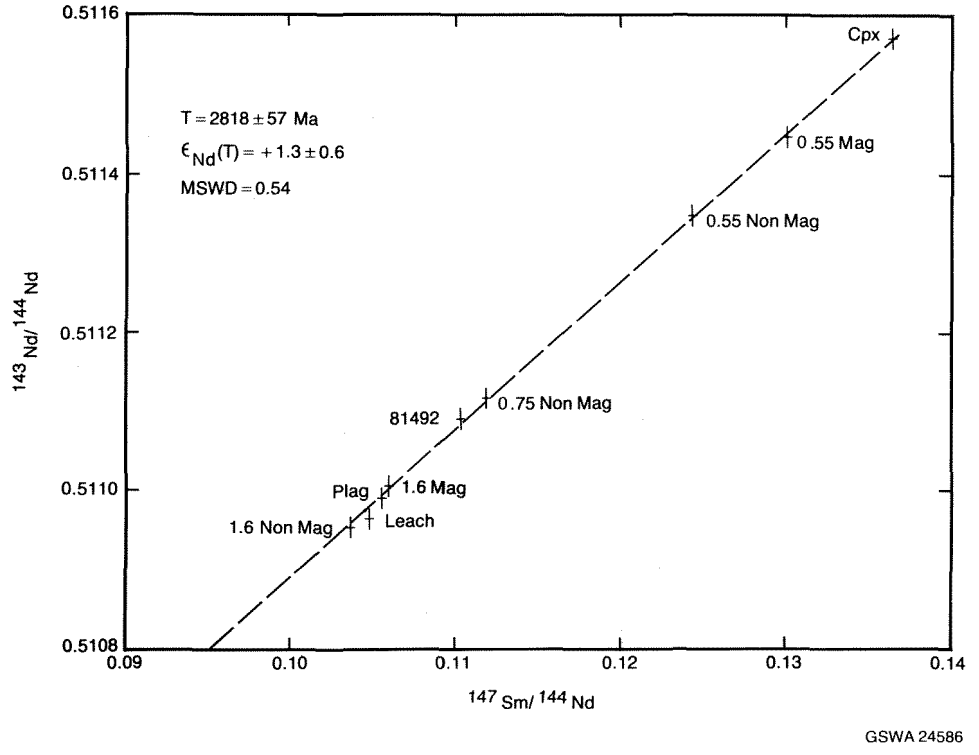


Figure 51. Sm–Nd isochron plot for Woolgra Formation sample 81492 whole rock, and mineral and material separates. The numbers 0.55, 0.75, and 1.6 denote Franz Magnetic Separator settings. Mag = magnetic separate, Nonmag = non-magnetic separate, Leach = HCl leach fraction (not used in isochron fit), plag = plagioclase, cpx = clinopyroxene.

the Wadgingarra Basalt have different, but overlapping, compositional fields. The upper basalts have a more restricted range in composition confined to more fractionated parts of the trends. On Ni–MgO and Cr–MgO diagrams (Figs 53C and D), lower tholeiitic basalts are richer in MgO, Cr, and Ni than upper tholeiitic basalts. However, there is substantial overlap of compositional fields, and nearly all data plot on the same well-defined trends, indicating that the basalts are probably comagmatic. The upper basalts, particularly the tholeiites, are more fractionated, on average, than the lower basalts. The geochemical data support the decision, made on the basis of field evidence alone, not to subdivide the Wadgingarra Basalt into two formations.

Most basalts are enriched in Zr, relative to Y and Ti, compared with Sun and Nesbitt's (1977) estimated upper mantle composition (Figs 53A and B). It is clear from the well-defined trends on Y–Zr and Ti–Zr diagrams, as well as the covariation of Ni, Cr, and MgO, that much compositional variation of basalt is controlled by crystal fractionation of olivine and pyroxenes. However, the trends cannot be explained completely in this way, as they are not parallel to single phase crystal-fractionation vectors, or reasonable phase-assemblage crystallization vectors (Pearce and Norry, 1979). Trends in both diagrams show marked enrichment in Zr compared with that expected from crystal fractionation alone. The basalts contain anomalously high abundances of K_2O (up to 1.1%), Ba (up to 357 ppm), Rb (up to 52 ppm), La (up to 21 ppm), and Ce (up to 32 ppm); and low abundances of Ti and V compared with most basalts in the Luke Creek Group and Porlell Subgroup (Table 21, Appendix II). These anomalous element abundances are characteristic of contamination of basalt magma with felsic crustal material (Arndt and Jenner, 1986; Barley, 1986). The simplest way to explain Y–Zr and Ti–Zr trends in the Wadgingarra Basalt is to invoke such contamination, followed by crystal fractionation of olivine and pyroxenes. Most of the silica enrichment can probably be ascribed to crustal contamination rather than later silicification. Some of this silica could have undergone secondary mobilization to give the observed alteration.

Wadgingarra Basalt data plot on a well-defined trend on a Zr/Y–Zr diagram (Fig. 53E), indicating derivation by 10–20% partial melting of a plagioclase-lherzolite source. The data plot in a part of the diagram that indicates enrichment in incompatible elements. This is usually interpreted in terms of processes in the source region (Pearce and Norry, 1979), although in this case it is probably due to crustal contamination. Because of this, the estimated degree of partial melting should be regarded with caution. A similar degree of partial melting of plagioclase lherzolite is indicated by the trend of data on a Cr–Y diagram (Fig. 53F), but there is much scatter in these data at high Cr contents. High-Mg basalts from the lower part of the Wadgingarra Basalt generally have lower Y contents which may reflect higher degrees of partial melting (Pearce, 1980, 1982).

In summary, Wadgingarra Basalt was probably derived by 10–20% partial melting of upper mantle plagioclase

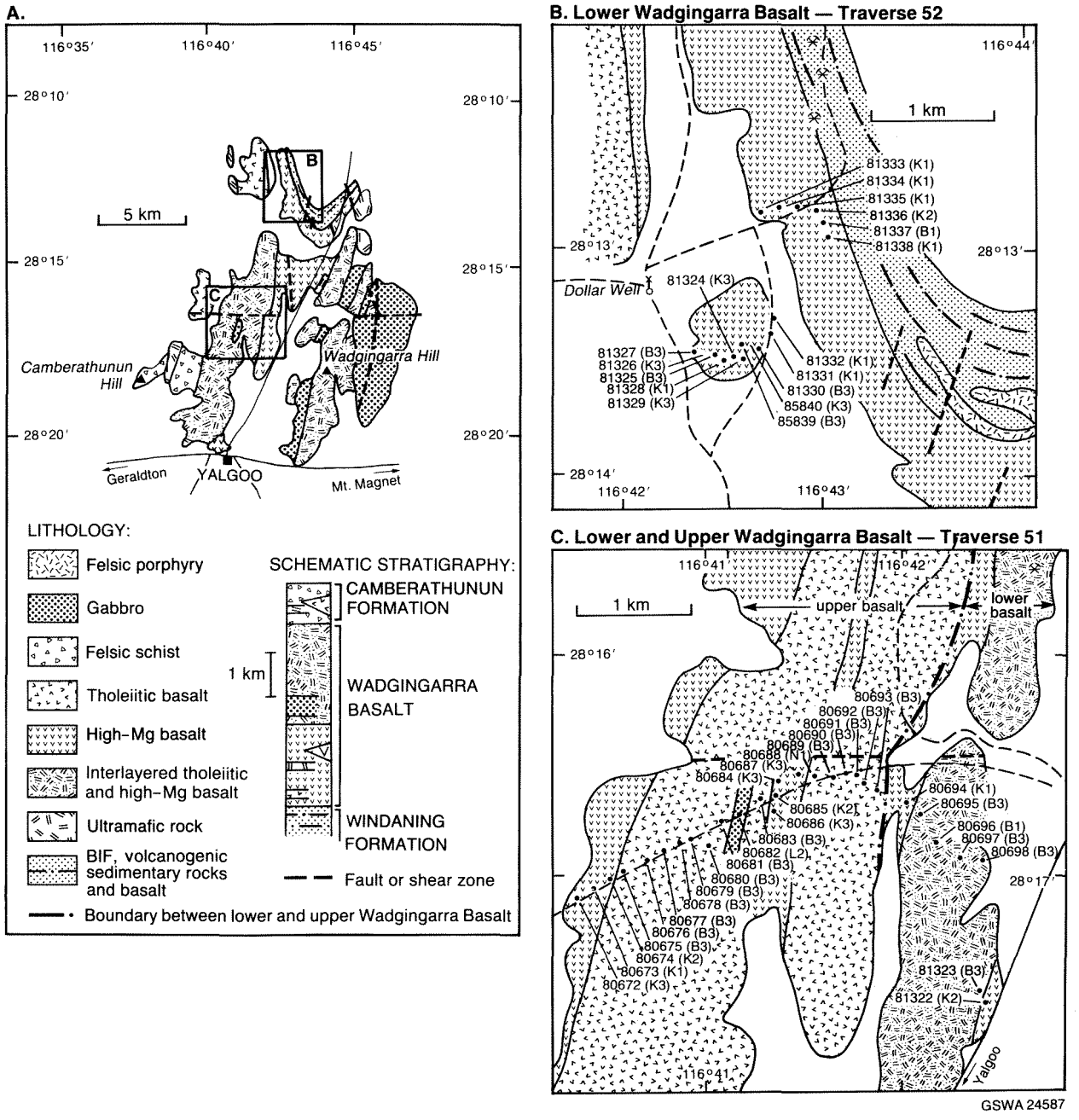


Figure 52. A — Outcrop geology and schematic stratigraphy of the Yalgoo Subgroup; B and C — locations of sample traverses in the Wadgingarra Basalt. Codes in brackets following sample numbers refer to 'rock type' and 'degree of alteration' as defined in Appendix II.

lherzolite. The basalt magma was subsequently contaminated by assimilation of felsic crustal material, followed by crystal fractionation of olivine and pyroxenes.

Quinns Basalt

Definition and distribution

The Quinns Basalt is defined here as a succession of interlayered high-Mg basalt, tholeiitic basalt, basaltic andesite, and dolerite, overlying the Windaning Formation in the core of a syncline in the type area, north of the old Quinns mining centre (Plate 2). Exposure is limited; hence the extent and disposition of the formation is not known in detail (Fig. 54). The upper contact was not observed; however, aeromagnetic data (1969 BMR survey) indicate the presence of a granitoid pluton to the north (also see Hallberg et al., 1976b, fig. 1). It is likely, from the shape and size of the body, that it is a post-folding granitoid pluton (Plate 2). At the lower contact, Quinns Basalt rocks overlie felsic volcanic and volcanogenic sedimentary rocks, and jaspilitic BIF of the Windaning Formation. Layering is rarely seen; the thickness of the exposed rocks is therefore difficult to estimate. However, using regional structure as a guide, it is thought that the exposed sequence is about 2500 m thick.

TABLE 21. MEAN COMPOSITIONS OF WADGINGARRA BASALT

	Lower high-Mg basalt n=13	*Upper high-Mg basalt n=7*	*Lower tholeiitic basalt n=9*	*Upper tholeiitic basalt n=13*
		Percentage		
SiO_2	52.4	52.2	53.5	54.3
Al_2O_3	11.5	12.3	12.5	13.0
Fe_2O_3	1.2	1.4	1.4	1.5
FeO	8.01	7.12	7.48	7.04
FeO*(a)	9.1	8.4	8.7	8.4
MgO	11.38	10.68	8.19	7.46
CaO	8.52	8.67	8.37	9.01
Na_2O	1.51	1.42	1.80	1.86
K_2O	0.26	0.25	0.76	0.49
TiO_2	0.57	0.54	0.48	0.62
P_2O_5	0.18	0.19	0.20	0.20
MnO	0.14	0.14	0.13	0.13
LOI	3.17	3.80	2.68	2.74
		Parts per million		
Ba	158	113	264	207
Cr	899	842	542	404
Cu	39	50	63	82
Li	8	11	9	8
Ni	207	195	151	127
Nb	<5	<5	<5	6
Rb	9	12	30	19
Sr	97	81	100	96
V	207	200	197	193
Y	17	20	23	25
Zn	69	76	68	76
Zr	51	76	87	101
La	8	10	14	15
Ce	(c)11	19	23	26
Mg number (b)	69.0	69.4	62.6	61.3
Cr/V	4.34	4.21	2.75	2.09
Zr/(Zr+Y)	0.75	0.79	0.79	0.80

(a) All Fe calculated as FeO (b) 100 mol MgO/(MgO + FeO)
(c) Some values used to calculate the mean are below the detection limit; for these determinations the value 'detection limit/2' was used.
For most of the analyses averaged in this table Pb <10 ppm and Th<10 ppm.

Lithostratigraphy

The Quinns Basalt consists predominantly of scattered outcrops of tholeiitic basalt, interlayered with high-Mg basalt in the west and basaltic andesite in the east (Fig. 54). The basalts are generally massive, and some flows show porphyritic or needle spinifex textures; variolitic and amygdaloidal textures also occur (Tingey, 1985). The rocks are thoroughly, and often coarsely, recrystallized in upper greenschist and lower amphibolite facies (Plate 3), and generally silicified and epidotized to some extent. Textures are metamorphic, with growth of sheaves of randomly oriented acicular actinolite–tremolite and hornblende which mimic needle spinifex texture in tholeiitic basalt and basaltic andesite. It is very difficult, given the degree of recrystallization, to distinguish these textures from pseudomorphed pyroxene needle spinifex texture, either in hand specimen or in thin section, even in high-Mg basalt. Both tholeiitic basalt and basaltic andesite are quartz- and plagioclase-rich. Most rocks contain 3–5% (but up to 10%) modal quartz, generally as small, recrystallized interstitial grains. Much quartz appears to be original, or a metamorphic reaction product; however, some silicification and concomitant epidotization is evident from replacement textures.

Geochemistry

Sampling

Nineteen samples of tholeiitic basalt and basaltic andesite were collected from the Quinns Basalt along a traverse north of Quinns mining centre (Fig. 54). All the basaltic andesite samples were collected from the lower part of the traversed stratigraphy where they were interlayered with tholeiitic basalt. The upper part of the traversed stratigraphy is tholeiitic basalt.

Composition and petrogenesis

Quinns Basalt tholeiitic basalt and basaltic andesite samples are characterized by fractionated compositions

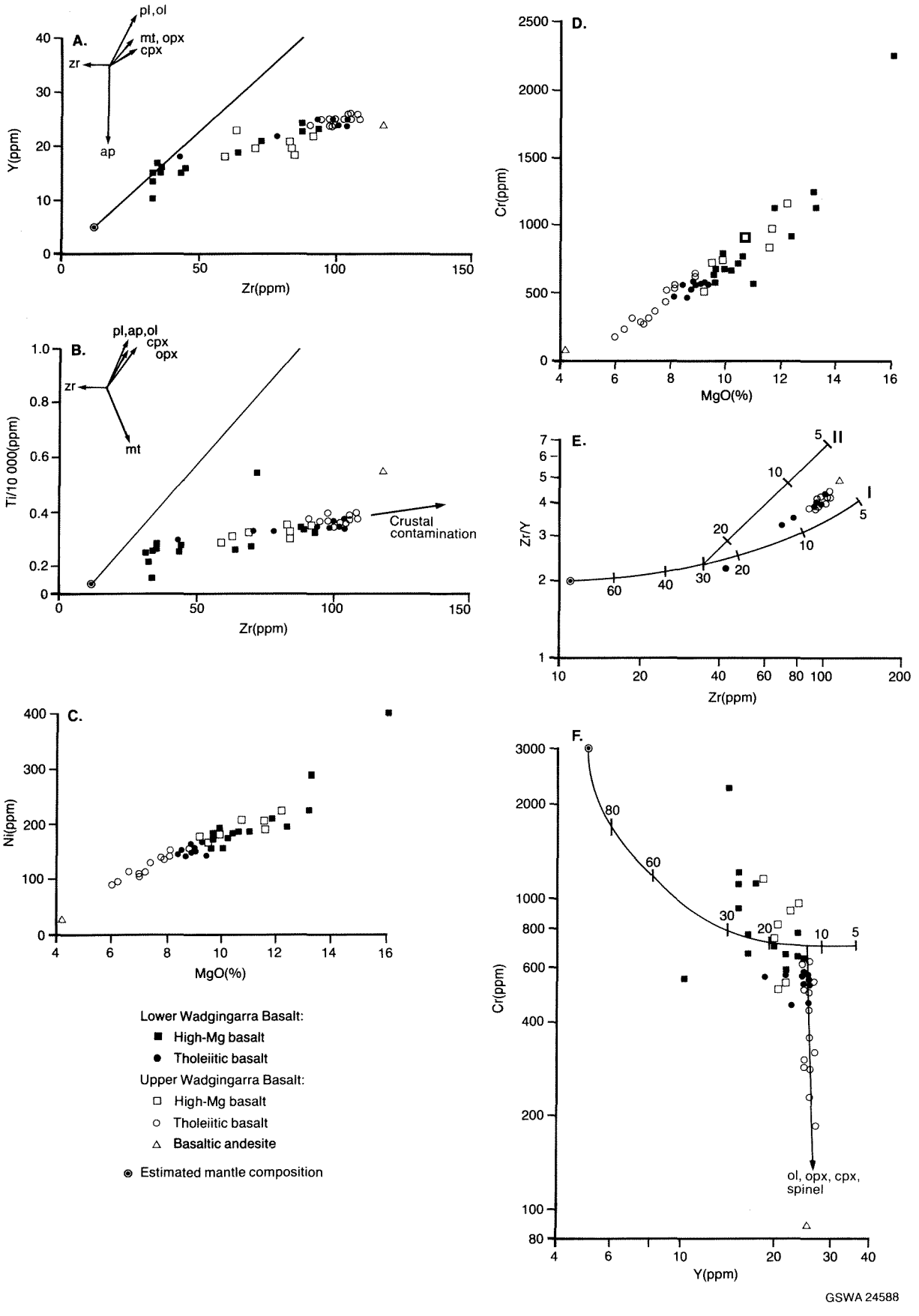


Figure 53. Geochemistry of the Wadgingarra Basalt. Estimated mantle composition and ratios, relative crystal-fractionation vectors, mineral phases, and model partial-melting curves as in Figures 7, 8 and 10.

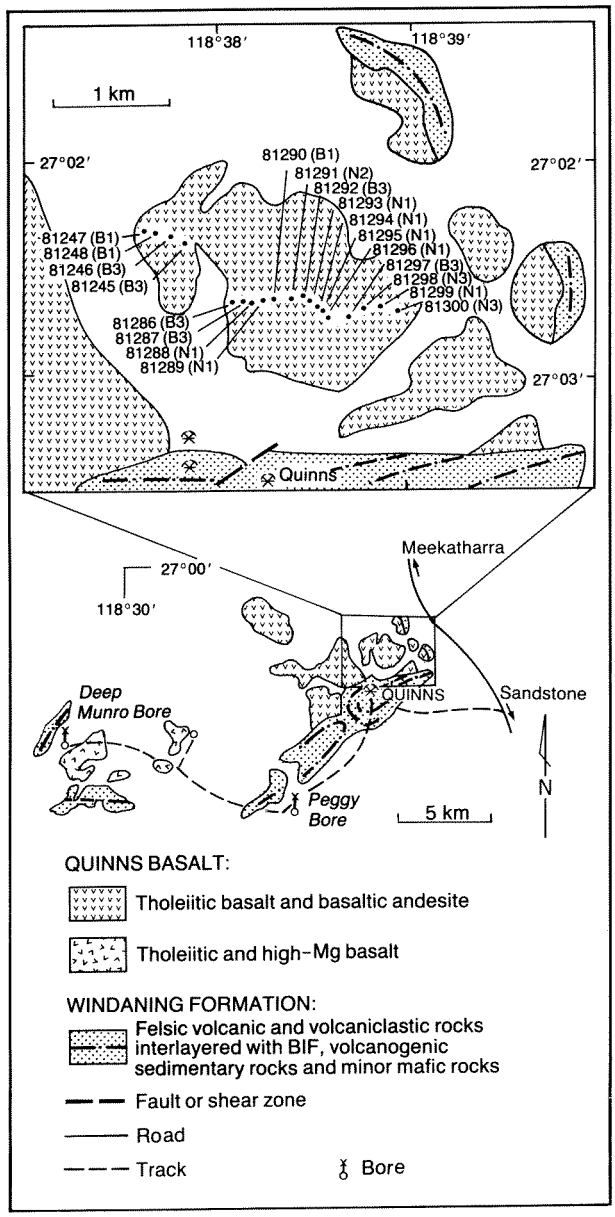


Figure 54. Outcrop geology of the Quinns Basalt and location of geochemistry samples. Codes in brackets following sample numbers refer to 'rock type' and 'degree of alteration' as defined in Appendix II.

with high SiO_2, TiO_2, P_2O_5, Y, Zr, and LREE contents, and low Cr and Ni contents (Table 22). About 40% of the samples were slightly, or moderately, silicified and epidotized (Appendix II). The samples are enriched in Zr relative to Y and Ti, compared with Sun and Nesbitt's (1977) estimated upper mantle composition (Figs 55A and B). Tholeiite and basaltic andesite data plot on the same trends in Figure 55, but are compositionally distinct. The trend of data on the Y–Zr diagram indicates control of compositional variation mainly by fractionation of clinopyroxene, and possibly of some plagioclase. The trend on the Ti–Zr diagram is difficult to interpret. Fractionation of rocks derived from mafic magmas usually results in trends of concurrent Ti and Zr enrichment in a proportion of about 1:1 (Pearce and Norry, 1979). Quinns Basalt data show strong enrichment of Zr relative to Ti, probably reflecting contamination of basaltic magma by assimilation of felsic crustal material, as appears to be so for the Wadgingarra Basalt. However, not all the element enrichments and depletions proposed for this type of contamination (Arndt and Jenner, 1986; Barley, 1986) have occurred. According to these authors, crustal contamination is characterized by enrichment of Rb, Ba, Th, K, Zr, and LREE, and depletion of V and Ti, relative to normal fractionation indices. In Quinns Basalt rocks only Zr, Ce, and La are enriched in a systematic way (Table 22). Trends on Zr/Y–Zr and Cr–Y diagrams (Figs 55C and D) indicate substantial plagioclase fractionation (Pearce and Norry, 1979; Pearce, 1980, 1982). It is difficult to estimate the degree of partial melting of source material from these diagrams. However, the positions of data points for least fractionated samples indicate

TABLE 22. MEAN COMPOSITIONS OF QUINNS BASALT

	Tholeiitic basalt n=3	*Basaltic andesite n=8*
	Percentage	
SiO_2	52.7	55.5
Al_2O_3	13.7	13.5
Fe_2O_3	2.3	2.3
FeO	7.15	7.20
FeO*(a)	9.2	9.3
MgO	6.87	5.54
CaO	9.61	9.07
Na_2O	1.97	2.16
K_2O	0.26	0.14
TiO_2	1.13	1.27
P_2O_5	0.26	0.31
MnO	0.14	0.13
LOI	3.05	2.11
	Parts per million	
Ba	149	64
Cr	143	71
Co	46	51
Cu	137	115
Ni	87	55
Rb	7	(c) 2
Sr	94	114
V	256	270
Y	32	47
Zn	69	74
Zr	117	178
La	7	13
Ce	15	28
Mg number (b)	57.1	51.5
Cr/V	0.56	0.26
Zr/(Zr+Y)	0.79	0.79

(a) All Fe calculated as FeO (b) 100 mol MgO/(MgO + FeO)
(c) Some values used to calculate the means are below the detection limit; for these determinations the value 'detection limit/2' was used.
Samples assigned to alteration class 3 (see Appendix II) are omitted from the means.
For most analyses averaged in this table, Nb<5 ppm, Pb<10 ppm, and Th<5 ppm.

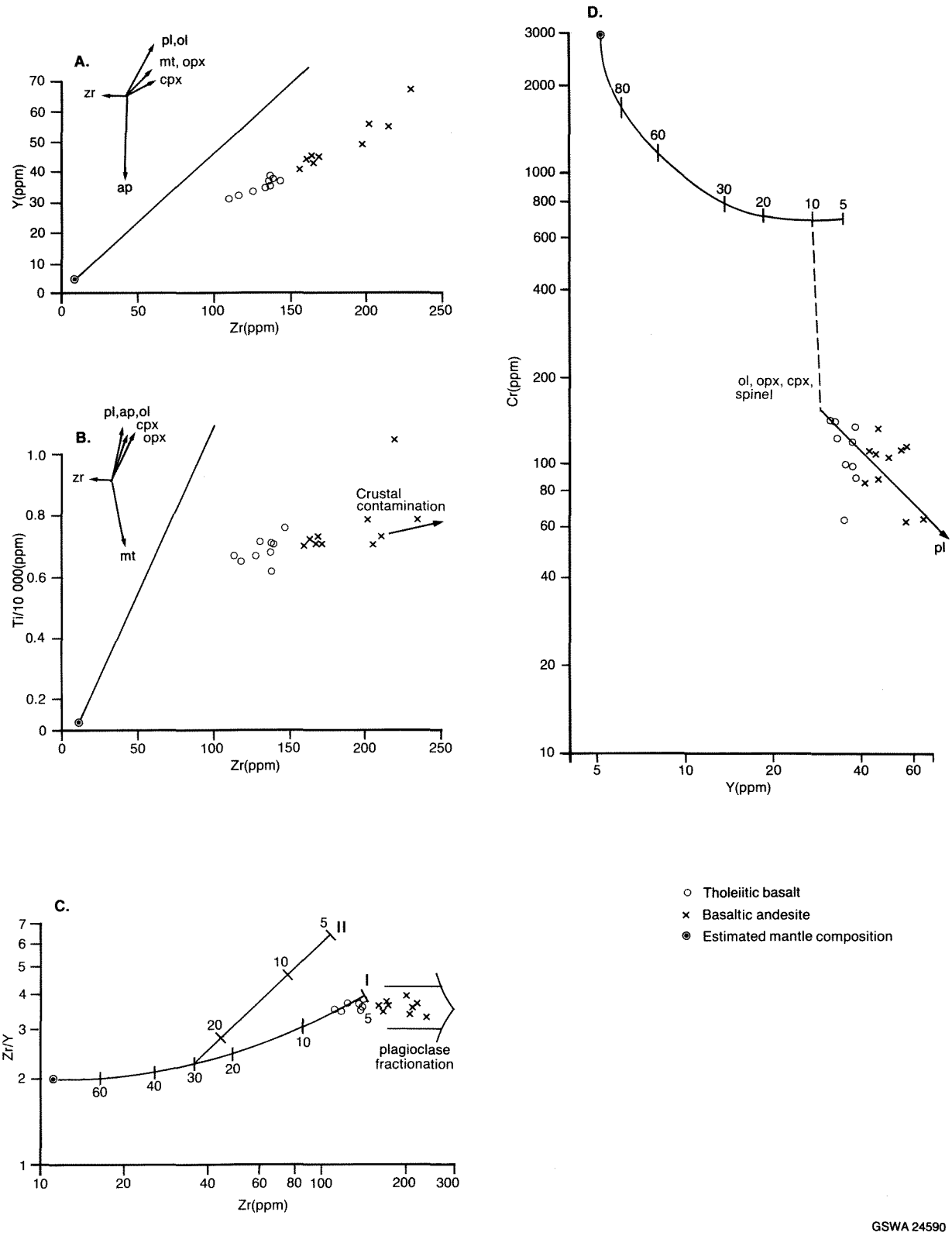


Figure 55. Geochemistry of the Quinns Basalt. Estimated mantle compositions and ratios, crystal-fractionation vectors, mineral phases, and model partial-melting curves as in Figures 7, 8 and 10.

about 5–10% partial melting of plagioclase lherzolite. This is consistent with the highly fractionated compositions of these rocks.

In summary, Quinns Basalt tholeiite and basaltic andesite are related by crystal fractionation of clinopyroxene and plagioclase. However, the original magma may have been contaminated to some extent by assimilation of felsic crustal material prior to crystal fractionation. It is likely that the magma was derived by a small degree of partial melting, of the order of 5–10%, of plagioclase lherzolite. More data, such as REE analyses and isotopic determinations, are required to elucidate the petrogenesis of these rocks with any confidence.

Mindoola Formation

Definition and distribution

The Mindoola Formation is defined here as a succession of high-Mg basalt, tholeiitic basalt, gabbro, dolerite, and ultramafic, sedimentary, and felsic volcanic rocks, overlying the Windaning Formation in the Weld Range greenstone belt (Plate 2, Fig. 56). It occurs in the core of a synclinal fold structure which defines the shape of the greenstone belt. The Mindoola Formation, named after Mindoola Bore, extends over an area of about 450 km^2; exposure is very limited in the northern part of the area, which is largely covered by laterite. The formation is intruded by recrystallized monzogranite in the south, and post-folding monzogranite in the north (Plate 1). The type area for the formation is around the old Ryansville mining centre (Fig. 56). Here the formation is about 3.5 km thick and overlies felsic volcanogenic sedimentary rocks of the Windaning Formation; the contact is not exposed.

Lithostratigraphy

The Mindoola Formation consists of interlayered fine-grained and needle spinifex-textured tholeiitic and high-Mg basalts. Minor units of bladed spinifex-textured komatiite occur near the base of the sequence near Ryansville (Fig. 56). In the core of the fold structure in the northeastern part of the outcrop, silicified and lateritic units of ultramafic, sedimentary, and felsic volcanic rocks are interlayered with the basalts. Apart from abundant spinifex texture and weak development of foliation, most of the basalt exposures are massive and featureless. However, pillow lava, hyaloclastic breccia, and variolitic basalt are abundant in some parts of the formation (Fig. 57). The basalts are intruded by many gabbro and dolerite sills ranging from less than 1 m to 200 m thick. The proportion of tholeiitic to high-Mg basalt increases towards the top of the formation.

The rocks are silicified and epidotized, and contain veins and cryptocrystalline aggregates of quartz, as well as crystals and crystal aggregates of epidote and zoisite. The alteration is post-metamorphic and imparts an unusual blue-green colour to both volcanic and intrusive mafic rocks (de la Hunty, 1973).

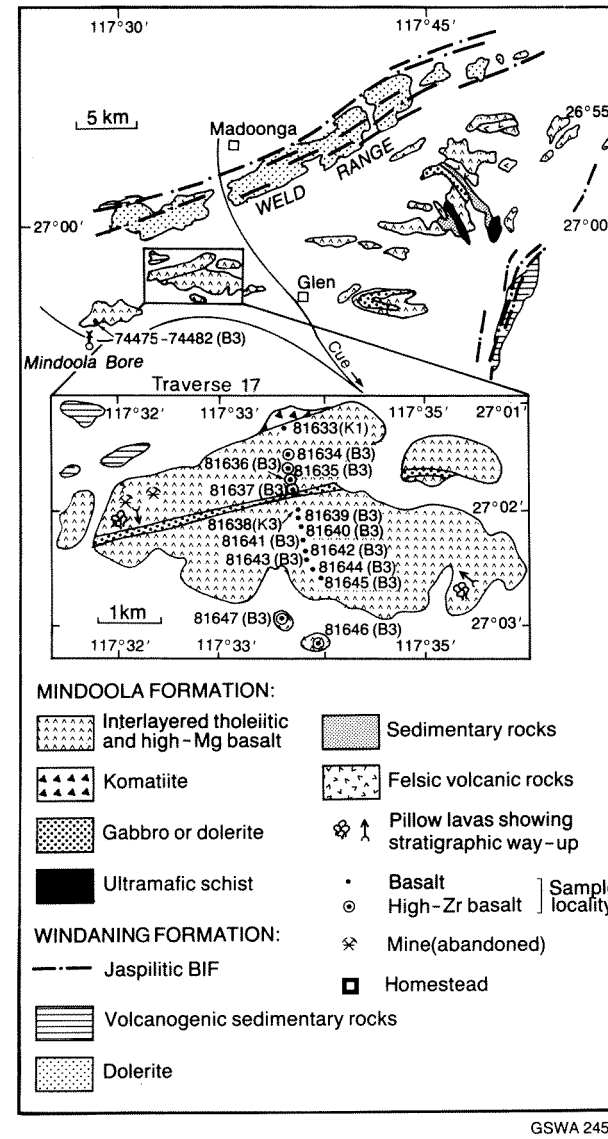


Figure 56. Outcrop geology of the Mindoola Formation showing locations of geochemistry samples in traverses 17 (samples 81633–81647) and 38 (samples 74475–74482). Codes in brackets following sample numbers refer to 'rock type' and 'degree of alteration' as defined in Appendix II.

Geochemistry

Sampling

Twenty-three samples of Mindoola Formation basalt were collected for geochemical analysis; 15 from a traverse in the Ryansville area, and 8 from a single locality near Mindoola Bore (Fig. 56).

Basalt compositions and petrogenesis

Mindoola Formation basalt samples have unusual compositions: high contents of SiO_2, K_2O, Ba, Li, Nb, Rb, La, and Ce, and low contents of V and TiO_2 (Table 23). All of the samples are enriched in silica, and have SiO_2 contents ranging from 52.9% to 55.5%. Two groups of tholeiitic basalt samples are distinguished on Y–Zr and Ti–Zr dia-



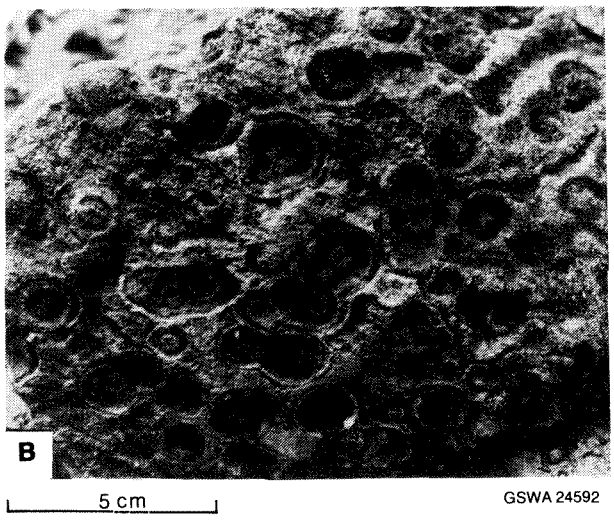


Figure 57. A — Mindoola formation high-Mg basalt pillow lava with interpillow breccia in the lower-middle part of the photograph; the hammer handle is 30cm long. B — variolitic texture in Mindoola Formation high-Mg basalt.

grams (Fig. 58). The high-Zr group has higher Zr, Rb, Y, Ti, and V contents, and lower Ni contents, than does the other group (Table 23). The high-Zr basalt occurs at two horizons within the traversed stratigraphy (Fig. 56). The two horizons may represent a single unit repeated by an east-northeasterly trending isoclinal fold (Plate 2).

Some enrichments and depletions of elements in basalts may be ascribed to post-metamorphic alteration. Certainly SiO_2, and probably K_2O, Ba, and Rb (Condie, 1981) have been enriched in this way to some extent. Some depletion of Ti, and enrichment of Zr, may also have occurred during silicification (Glikson and Hickman, 1981); although Dostal and Strong (1983) believe that silicification of basalt results only in dilution of immobile elements in proportion to the amount of silica added. Although absolute abundances of Ti and Zr may have been altered, it is generally thought that the ratios of these and other immobile elements, such as Y, Nb, P, and Ce are little affected by metamorphism and alteration (Pearce and Cann, 1973; Floyd and Winchester, 1978; Ludden et al., 1982; Hallberg, 1984). Thus, while anomalous contents of SiO_2, K_2O, Ba, and Rb may be ascribed, at least in part, to alteration, the ratios of Ti, Y, and Zr probably reflect igneous processes.

Trends of data on Y–Zr and Ti–Zr diagrams (Fig. 58) are similar to those for Wadgingarra Basalt and Quinns Basalt samples, and probably also reflect contamination of basalt

TABLE 23. MEAN COMPOSITIONS OF MINDOOLA FORMATION BASALTS

	High-Mg basalt n=2	*High-Zr tholeiitic basalt n=6*	*Low-Zr tholeiitic basalt n=15*
		Percentage	
SiO_2	53.5	54.3	54.2
Al_2O_3	9.1	14.0	14.9
Fe_2O_3	1.6	2.3	2.3
FeO	7.16	6.27	5.70
FeO*(a)	8.6	8.3	7.8
MgO	14.60	7.07	7.40
CaO	6.54	9.44	8.92
Na_2O	0.99	1.63	2.18
K_2O	0.48	0.76	0.56
TiO_2	0.43	0.66	0.50
P_2O_5	0.07	0.11	0.08
MnO	0.16	0.15	0.16
LOI	5.17	3.38	3.27
		Parts per million	
Ba	187	249	211
Cr	1435	280	339
Co	65	53	51
Cu	88	115	113
Li	17	12	10
Ni	300	113	188
Nb	<5	8	<5
Rb	20	28	19
Sr	50	130	162
V	212	232	176
Y	15	22	15
Zn	78	78	70
Zr	62	108	74
La	11	12	(c) 8
Ce	11	23	22
Mg number (b)	75.2	60.0	62.8
Cr/V	6.77	1.21	1.93
Zr/(Zr+Y)	0.81	0.83	0.83

(a) All Fe calculated as FeO (b) 100 mol MgO/(MgO + FeO)
(c) Mean of 7 analyses only
For most of the analyses averaged in this table, Th<5 ppm and Pb<10 ppm.

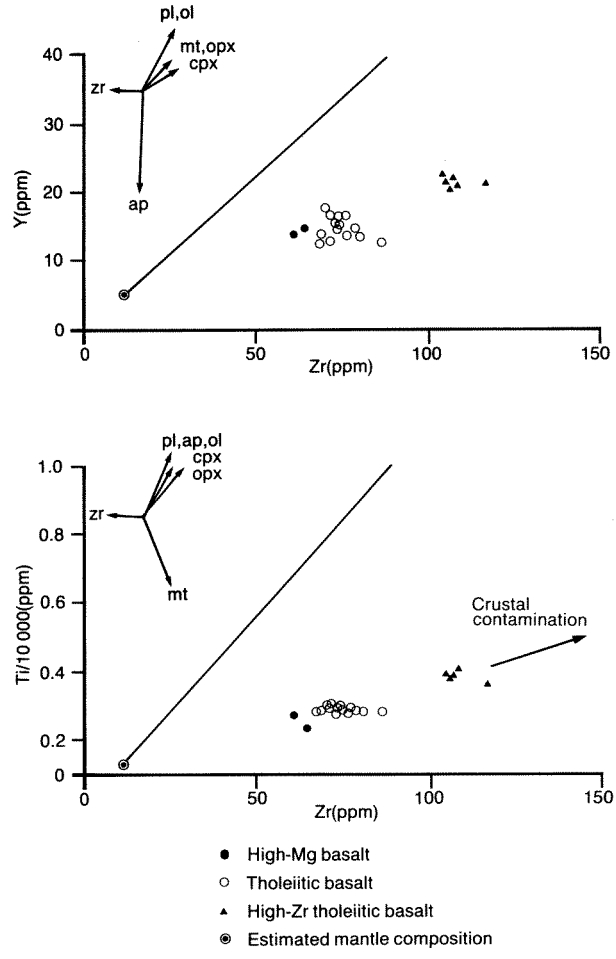


Figure 58. Y–Zr and Ti–Zr diagrams for the Mindoola Formation. Estimated mantle compositions and ratios, mineral phases, and relative crystal-fractionation vectors as in Figure 7.

magma by assimilation of felsic crustal material. These trends may represent mixing between original basalt magma and felsic contaminant; although compositions have probably been modified by subsequent crystal-fractionation processes. Except for basal flows, contamination by assimilation of felsic or sedimentary rocks at the surface (Huppert et al., 1984) is unlikely, as there is little evidence of interflow sedimentary material. Felsic material was probably assimilated during ascent of basalt magma from the upper mantle through the crust, and/or in near-surface magma chambers (Huppert and Sparks, 1985). At that stage in the development of the greenstone sequence, abundant felsic material existed in the upper crust beneath the Mount Farmer Group.

It is difficult to interpret with confidence source compositions and degrees of partial melting for these rocks, because original magma compositions have been changed significantly by crustal contamination and subsequent silicification and epidotization.

Dalgaranga Formation

Definition and distribution

The Dalgaranga Formation is defined here as a succession of dacite and rhyolite tuffs, volcanogenic sandstone, and conglomerate, overlying the Windaning Formation in the vicinity of the Dalgaranga mining centre (Plate 2). The formation is intruded by four large layered gabbro sills, part of the gabbroid complex near Dalgaranga (see Chapter 4), which disrupt the succession (Fig. 59). Both the top and bottom of the succession are intruded by post-folding granitoid plutons. The type area is between the Dalgaranga tantalite–beryl mine and Deep Well (Fig. 59). Here the formation overlies sedimentary rocks of the Windaning Formation; the exposed top of the formation is intruded by gabbro 1.5 km north-northeast of Deep Well. The succession is about 1300 m thick.

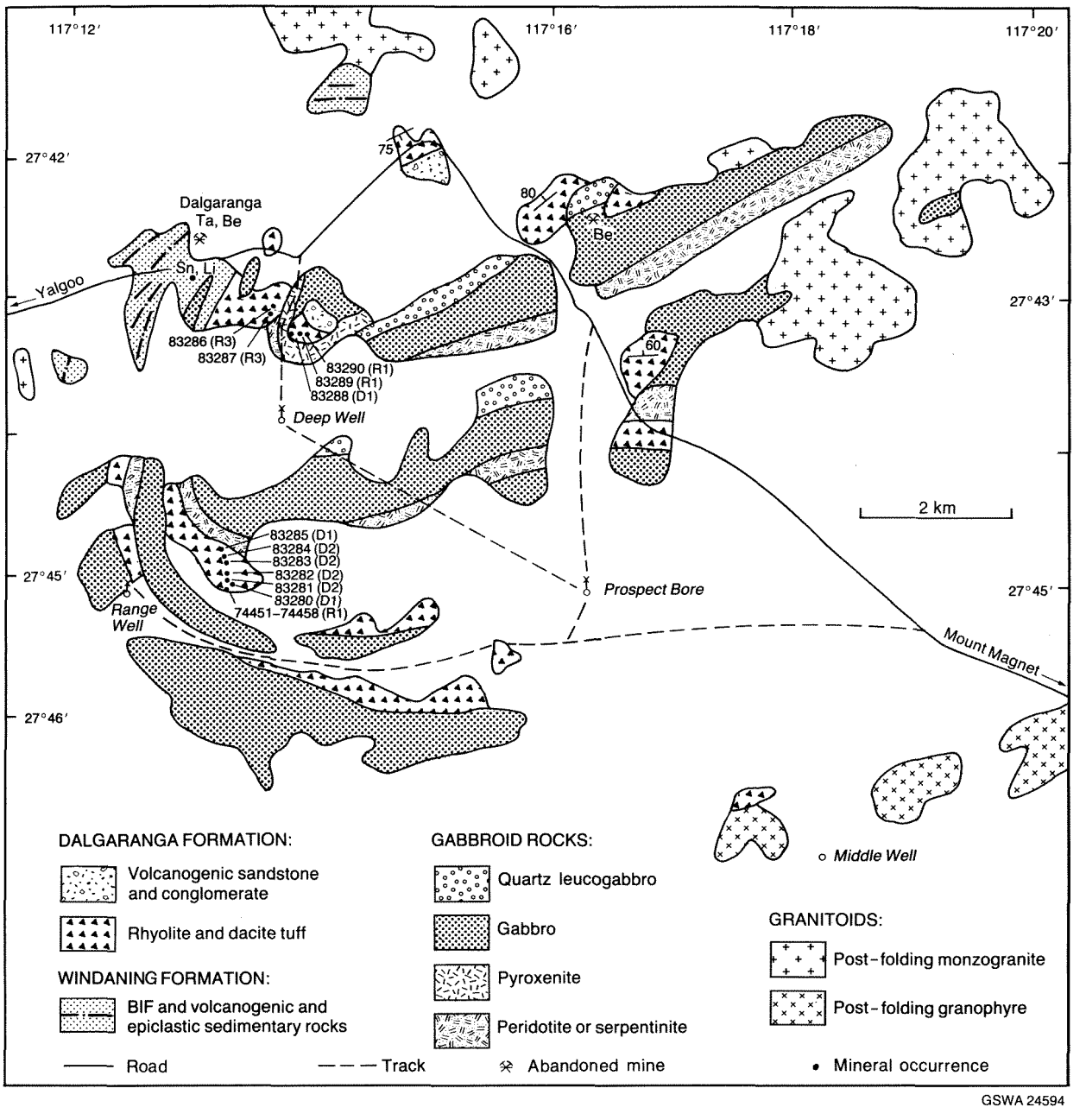


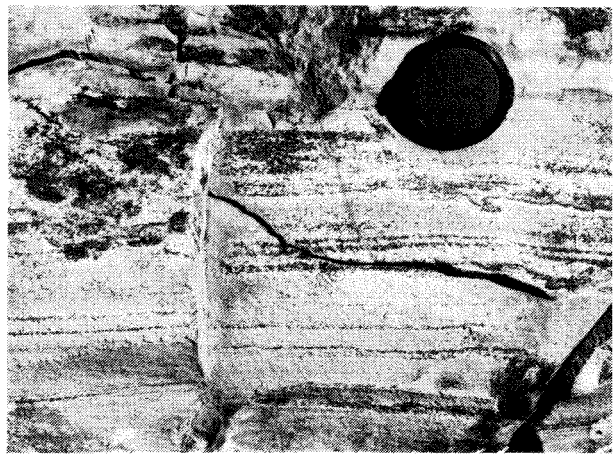
Figure 59. Outcrop geology of the Dalgaranga Formation showing locations of geochemistry samples in traverses 27 (samples 83280–83290) and 37 (samples 74451–74458). Codes in brackets following sample numbers refer to 'rock type' and 'degree of alteration' as defined in Appendix II.

Lithostratigraphy

The Dalgaranga Formation consists predominantly of about 1000 m of dacite tuff, and small amounts of rhyolite tuff, overlain by about 300 m of volcanogenic sandstone and conglomerate. The dacite tuff is a fine-grained, finely banded siliceous rock. It ranges in appearance from a very fine-grained, bluish-grey variety to an amphibole-phyric (possibly pseudomorphing pyroxene) and/or plagioclase-phyric variety. The phenocrysts may be disseminated, or concentrated in bands (Fig. 60). Some units contain ocelli, up to a few centimetres across, comprising concentric zones of plagioclase and amphibole. Rhyolite tuff is generally fine grained, quartz- and feldspar-phyric, or spherulitic with spherules up to a few millimetres in diameter.

The volcanogenic sandstone which overlies these tuffs is a medium- to coarse-grained, poorly sorted lithic wacke, containing minor lenses of conglomerate. The conglomerate consists of rounded cobbles of dacite and rhyolite tuff, up to 20 cm across, in a matrix of lithic wacke (Fig. 61). In thin section it is difficult to distinguish fine-grained lithic wacke from underlying tuff. The volcanogenic sandstone is probably reworked tuff.

Dalgaranga Formation rocks were metamorphosed in greenschist and lower-amphibolite facies (Plate 3). Min-



GSWA 24595

Figure 60. Compositional banding in Dalgaranga formation dacite tuff; the lens cap is 5cm across.



GSWA 24596

Figure 61. Volcanogenic sandstone and conglomerate in the Dalgaranga Formation; the lens cap is 5cm across.

eral assemblages in tuffs include quartz, oligoclase, K-feldspar, biotite, hornblende, chlorite (generally retrograded biotite and hornblende), carbonate, epidote, sphene, and opaque phases.

Geochemistry

Sampling

Nineteen samples of Dalgaranga Formation dacite and rhyolite were collected for geochemical analysis, 8 from a single locality and the others from a traverse through the middle and upper parts of the formation (Fig. 59). Chemical analyses are listed in Appendix II.

Compositions and petrogenesis

Two compositionally distinct felsic volcanic units occur in the Dalgaranga Formation. The lower part of the formation is dacite, but uppermost felsic volcanic units (samples 83288–83290, Fig. 59), underlying volcanogenic

TABLE 24. MEAN COMPOSITIONS OF DALGARANGA FORMATION FELSIC VOLCANIC ROCKS

	Dacite n=14	*Rhyolite n=2*
	Percentage	
SiO_2	70.9	71.9
Al_2O_3	11.7	14.2
Fe_2O_3	1.3	0.5
FeO	4.44	0.79
FeO*(a)	5.6	1.2
MgO	1.06	0.88
CaO	2.77	1.23
Na_2O	1.56	4.14
K_2O	3.63	3.87
TiO_2	0.33	0.17
P_2O_5	0.05	0.07
MnO	0.11	0.01
LOI	1.62	0.90
	Parts per million	
Ba	813	1552
Cr	(b) 36	44
Co	(b) 84	97
Cu	34	8
Li	21	30
Ni	37	32
Nb	12	7
Rb	144	89
Sr	90	193
Th	14	<10
Sn	(b) 7	9
U	2	1
V	37	22
Y	61	10
Zn	103	8
Zr	239	78
La	(b) 21	nd
Ce	(b) 61	nd
Zr/(Zr+Y)	0.80	0.89

(a) All Fe calculated as FeO
(b) Means of only six samples as these elements were not determined for all of the samples.
For analyses averaged in this table, Pb<10ppm and Mo<5ppm.
Samples assigned to alteration class 3 (see Appendix II) are omitted from the means.
nd: not determined

sandstone and conglomerate at the top of the formation, are rhyolite (Table 24). The mean dacite composition is close to the dacite–rhyolite compositional field boundary of Le Bas et al. (1986); however, it is compositionally distinct from the overlying rhyolite (Figs 62, 63, and 64). The dacite contains significantly less Al_2O_3, Na_2O, Ba, Li, and Sr, and more FeO*, Cu, Rb, Th, V, Y, Zn, and Zr, than the rhyolite (Table 24), although data from both lithologies plot on broad calc-alkaline trends (Fig. 63). The dacite and rhyolite have compositional features in common with high-(Zr+Y) and low-(Zr+Y) felsic volcanic rocks respectively, from the Gabanintha Formation. However, samples from the two formations have different trends on Harker variation diagrams (Fig. 63), particularly for Al_2O_3 and FeO*. In addition, Dalgaranga Formation rhyolite is more siliceous than low-(Zr+Y) felsic volcanic rocks from the Gabanintha Formation (compare Tables 13 and 24).

Dacite and rhyolite samples have distinctly different REE patterns (Fig. 64). The dacite has a higher total REE

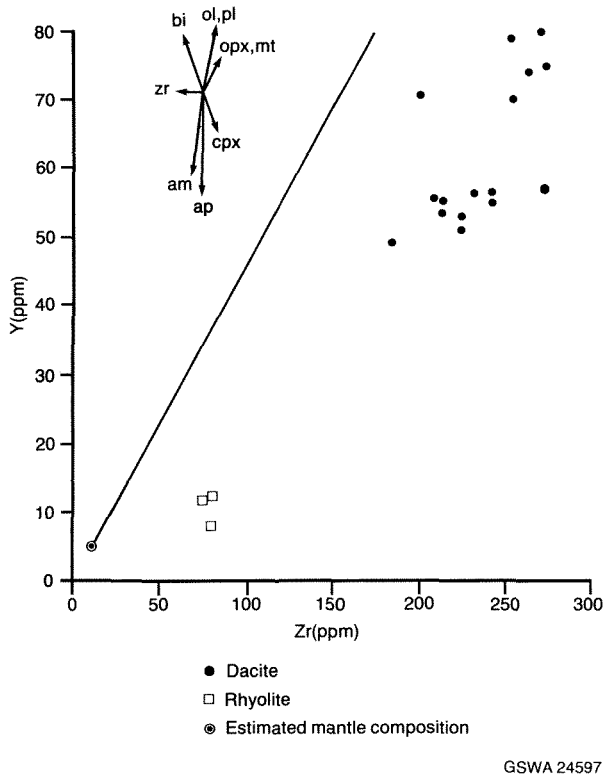


Figure 62. Y–Zr diagram for Dalgaranga Formation felsic volcanic rocks. Estimated mantle composition and ratio, mineral phases, and crystal-fractionation vectors as in Figures 7 and 28.

content, a negative Eu anomaly, and slightly enriched HREE. The negative Eu anomaly and low Sr content of the dacite sample indicate removal of plagioclase, either from the source, or by crystal fractionation. HREE enrichment suggests that neither garnet nor amphibole were important as residual or fractionating phases. As was suggested for Gabanintha Formation high-(Zr+Y) felsic volcanic rocks — which have similar REE patterns — a suitable source for these rocks would be a siliceous pyroxene–plagioclase granulite (Condie, 1978). In contrast, the rhyolite sample has a fractionated REE pattern with a very small negative Eu anomaly. The pattern is similar to those for low-(Zr+Y) felsic volcanic rocks in the Gabanintha Formation (Fig. 30), and a similar origin is postulated, namely hydrous partial melting of crustal amphibolite. However, differences in major-oxide and trace-element contents between low-(Zr+Y) felsic volcanic rocks from these formations indicate substantially more crystal fractionation in Dalgaranga Formation rocks, or alternatively, a more fractionated amphibolite source.

Wattle Creek Basalt

Definition and distribution

The Wattle Creek Basalt is defined here as a succession of tholeiitic basalt, together with minor amounts of high-Mg basalt, gabbro, ultramafic, and sedimentary rocks, overlying the Windaning Formation in the vicinity of Mount Magnet (Plate 2). There are two main regions of outcrop (Fig. 65). The larger is a northerly trending belt of rocks north of Mount Magnet; the lower part of this succession is poorly exposed. In the other region, 10 km southwest of Mount Magnet, Wattle Creek Basalt rocks are poorly exposed in the core of a vertically plunging fold. The formation is in tectonic contact with Gabanintha and Golconda Formation rocks in the northern part of the larger outcrop; elsewhere it overlies the Windaning Formation. The top of the formation was intruded by monzogranite that has since been recrystallized.

The name Wattle Creek Basalt is derived from the abandoned Wattle Creek Homestead, 12 km northwest of Mount Magnet. The type area for the formation is around the abandoned Burra Burra gold mine, 5 km northeast of Wattle Creek Homestead (Fig. 65). A thin sandstone unit occurs at the base of the formation in this area; although because of poor exposure it is not clear whether it is part of the Windaning Formation or of the Wattle Creek Basalt. A number of shear zones and faults cut the formation subparallel to its boundaries. Ignoring the effects of these, the thickness of the Wattle Creek Basalt in this area is about 2500 m.

Lithostratigraphy

The Wattle Creek Basalt consists predominantly of massive tholeiitic basalt together with subordinate pillow lava and pyroclastic rocks. Many lava flows are porphyritic or variolitic. The lower half of the succession contains several 10–20 m-thick units of fine- to medium-grained epiclastic and volcanogenic sedimentary rocks interlayered with the basalt (Fig. 66). A 100–200 m-thick pyroxenite sill intrudes the lower part of the basalt sequence 500 m west of the Burra Burra mine. A thick undifferentiated gabbro sill occurs in the core of the neutral fold structure in the very poorly exposed southern outcrop of the Wattle Creek Basalt (Fig. 65). Veins of microgranite and pegmatite are abundant near the upper contact of the formation with recrystallized monzogranite. In thin section, the actinolite–oligoclase dominated greenschist facies assemblages are partly replaced by quartz and epidote which are in crystalline aggregates and veins.

Geochemistry

Sampling

Twelve samples of tholeiitic basalt were collected along a traverse through the upper part of the Wattle Creek Basalt in its type area (Fig. 65). Chemical analyses are listed in Appendix II.

Compositional characteristics

The basalt samples are silicified and epidotized, and have up to 55.6% SiO_2, 15.7% CaO, and 5.2% Fe_2O_3; mean contents of these oxides are 54.8%, 12.0%, and 3.7% respectively. The Fe_2O_3/FeO ratio varies between 0.24 and 0.90, indicating oxidation during alteration. The rocks

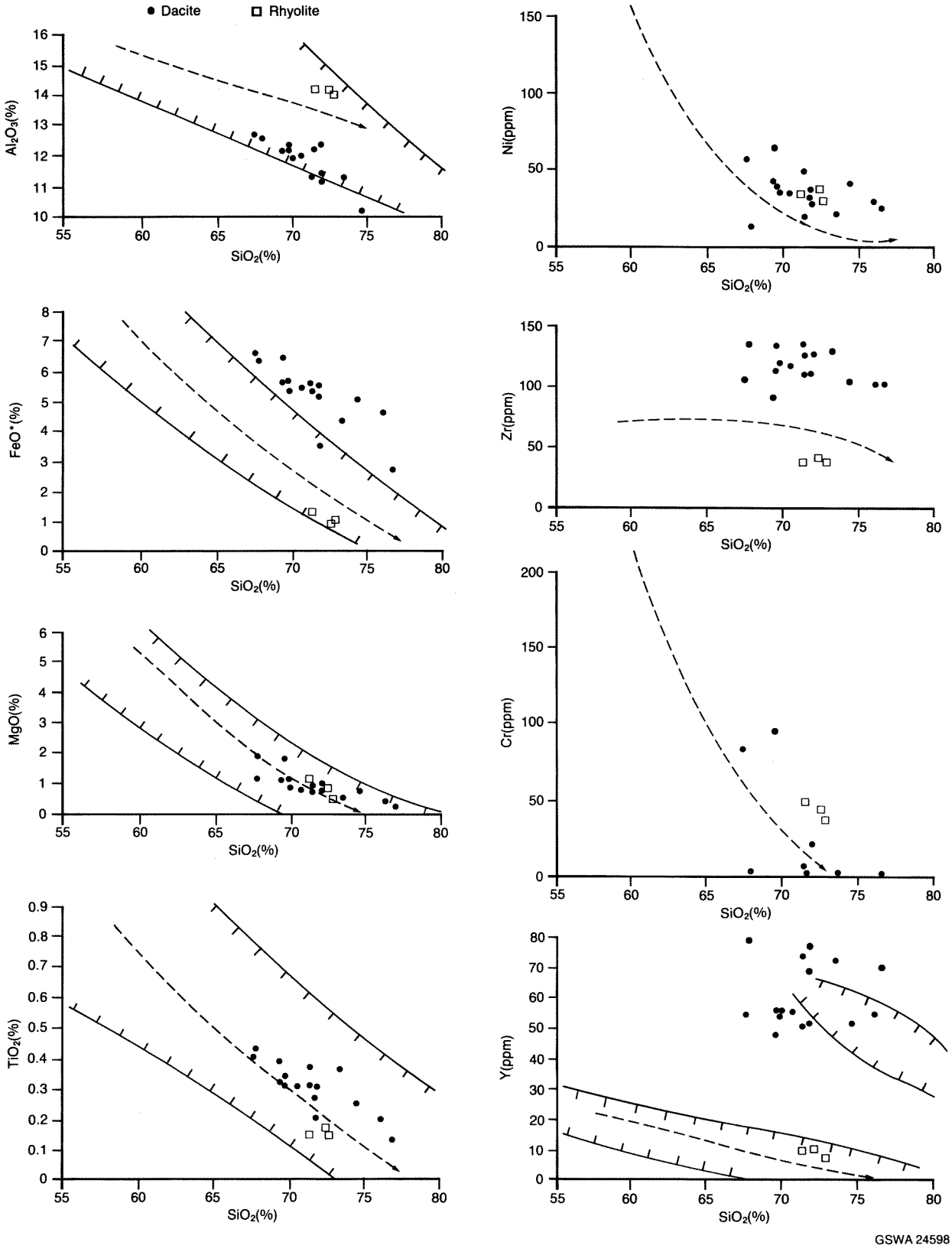


Figure 63. Harker variation diagrams for Dalgaranga Formation felsic volcanic rocks. The dashed line is the calc-alkaline differentiation trend for Gabanintha formation felsic volcanic rocks. Solid lines with ticks define the compositional field of Yilgarn Craton felsic volcanic rocks described by Giles (1981).

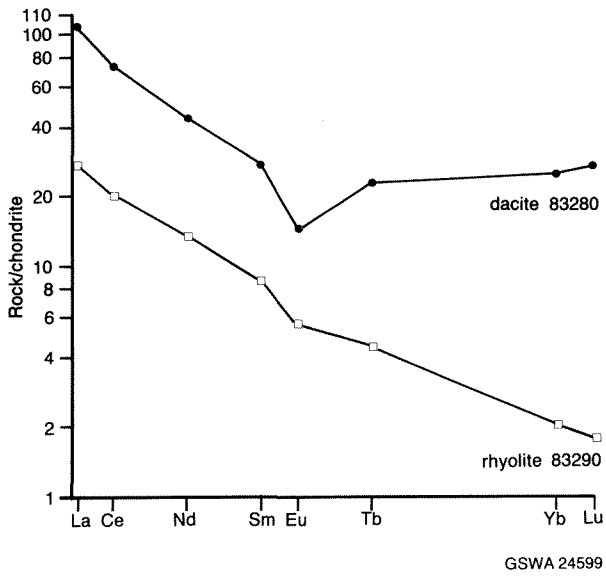


Figure 64. REE patterns for Dalgaranga Formation felsic volcanic rocks.

have abnormally low mean contents of MgO (4.32%), Ni (40 ppm), and Cr (8 ppm). Y contents range from 20 to 478 ppm (Appendix II). Some of these compositional features may reflect igneous processes; for example, low MgO, Ni, and Cr, and high Y are characteristic of extreme fractionation. It is difficult to assess to what degree alteration may have been responsible for further modification of these compositions, although petrographic evidence clearly indicates that the high values of SiO_2, CaO, Fe_2O_3, and Fe_2O_3/FeO are due to secondary development of quartz and epidote. In view of the intense alteration, and the small number of samples analysed, the petrogenesis of these rocks is not discussed.

Billabalong Basalt

Definition and distribution

The Billabalong Basalt is defined here as a succession of tholeiitic and high-Mg basalts, gabbro, and dolerite, and minor amounts of felsic volcanic rocks and chert, overlying the Windaning Formation in the Twin Peaks greenstone belt (Plate 2). The formation occurs on the northwestern side of the greenstone belt, in two main areas of outcrop separated by granitoid intrusions (Fig. 67). The best exposures are in the vicinity of Mount Hope; the northern exposures are weathered and lateritized. The formation derives its name from Billabalong Homestead, 15 km southwest of Mount Hope. The type area is in the vicinity of Mount Hope (Fig. 67). Here, at the base of the succession, high-Mg basalt overlies jaspilitic BIF, grey-white chert, and felsic volcaniclastic rocks of the Windaning Formation. The top of the formation is intruded by recrystallized monzogranite. The succession is 2500 m thick in its type area.

Lithostratigraphy

The stratigraphy of the Billabalong Basalt is shown schematically in Figure 68. At the base of the succession, a 150–200-m thick unit of needle spinifex-textured high-Mg basalt overlies Windaning Formation rocks. The contact is not exposed. A sequence of massive tholeiitic basalt overlies this unit and comprises most of the formation. The tholeiite is fine grained and almost featureless, although pillow lava is exposed poorly in a few places. Gabbro and dolerite sills are ubiquitous in this unit. Pyroclastic tholeiitic rocks are abundant in the upper 1000 m of the Billabalong Basalt, and range from coarse flow breccias to finely banded tuff (Fig. 69). In the lower half of this part of the succession the pyroclastic rocks are interlayered with tholeiitic basalt, gabbro, and dolerite. In the upper half, tholeiitic pyroclastics are interlayered with siliceous, aphanitic felsic volcanic rocks, and sparse units of grey-white chert which contain ferruginous bands. The uppermost part of the succession is intensely deformed, and is intruded by many quartz-porphyry sheets associated with the recrystallized monzogranite that intrudes the top of the formation.

Coocoowilya Formation

Definition and distribution

The Coocoowilya Formation is defined here as a succession of amphibolite, and felsic, pelitic and psammitic schists, overlying the Windaning Formation in the Barloweerie greenstone belt (Plate 2). The formation lies in the core of a tight fold; only its western limb and the region near the fold closure are exposed, in an area of about 4 km^2 (Fig. 70). The interpreted stratigraphic position of the Coocoowilya Formation is based on a single way-up determination, from a truncated slump structure in the northern part of the outcrop (Baxter, 1974), which places it above the Windaning Formation. Lithologies below the Windaning Formation are typical of the Gabanintha Formation at this level and are consistent with Baxter's (1974) way-up observation. The formation name is derived from Coocoowilya Well, about 6 km north of the greenstone belt.

The type area for the formation is in the centre of its outcrop, where its three units are all exposed in juxtaposition immediately south of an easterly trending fault (Fig. 70). The top and bottom of the formation are not exposed in this area. The base of the formation is in contact with the Windaning Formation about 2 km to the south, although the contact itself is obscured by scree from the prominent BIF ridges of the Windaning Formation. The top of the formation was intruded by recrystallized monzogranite which surrounds the Barloweerie greenstone belt. The formation is about 1200 m thick.

Lithostratigraphy

The Coocoowilya Formation consists of three units (Fig. 70) which are intensely deformed, intruded by numerous granitoid and pegmatite sheets, and metamorphosed in upper greenschist and lower amphibolite facies. The lowest unit is a fine- to medium-grained amphibolite, about

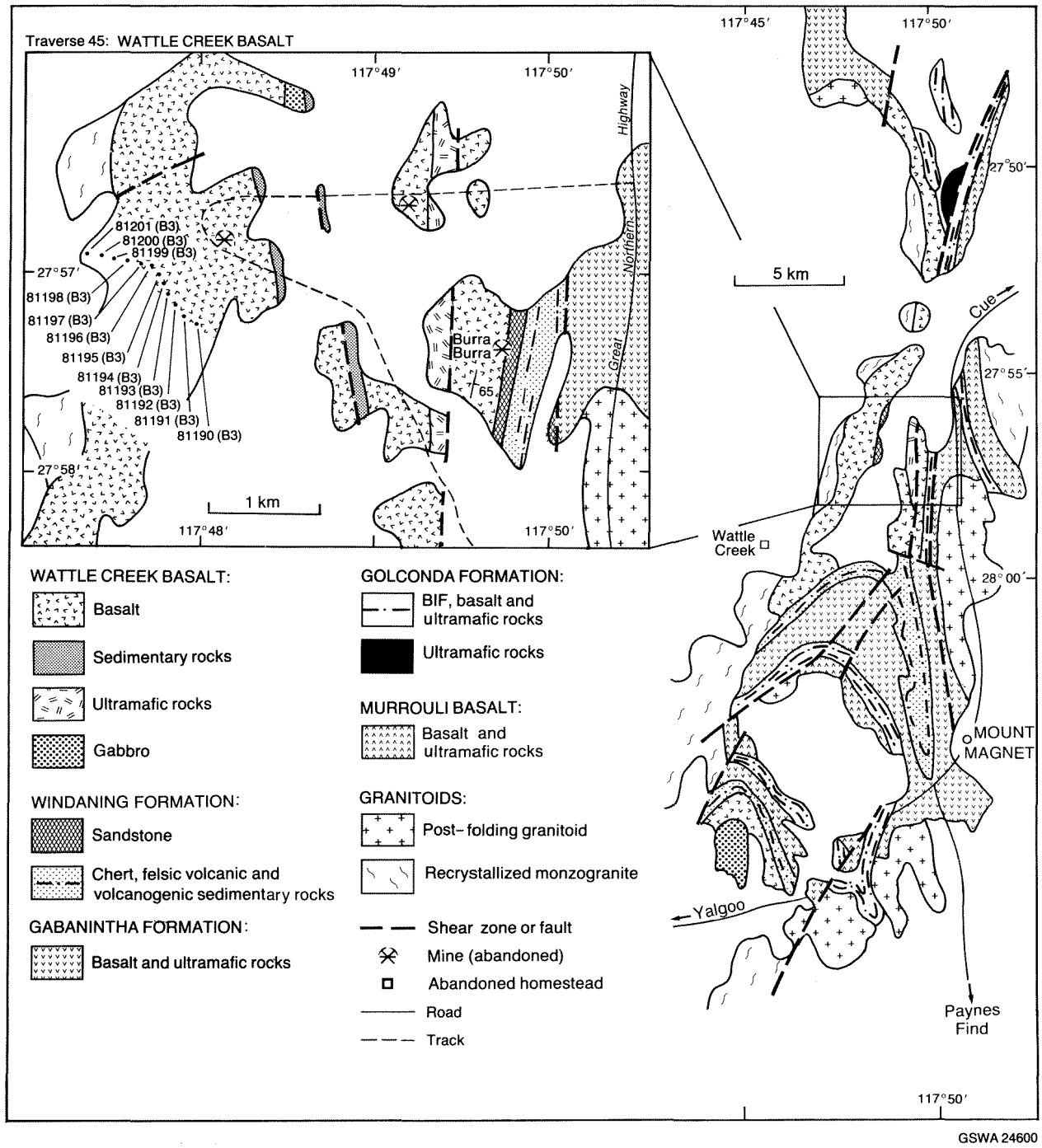


Figure 65. Outcrop geology of the Wattle Creek Basalt, sample locations are shown. Codes in brackets following sample numbers refer to 'rock type' and 'degree of alteration' as defined in Appendix II.

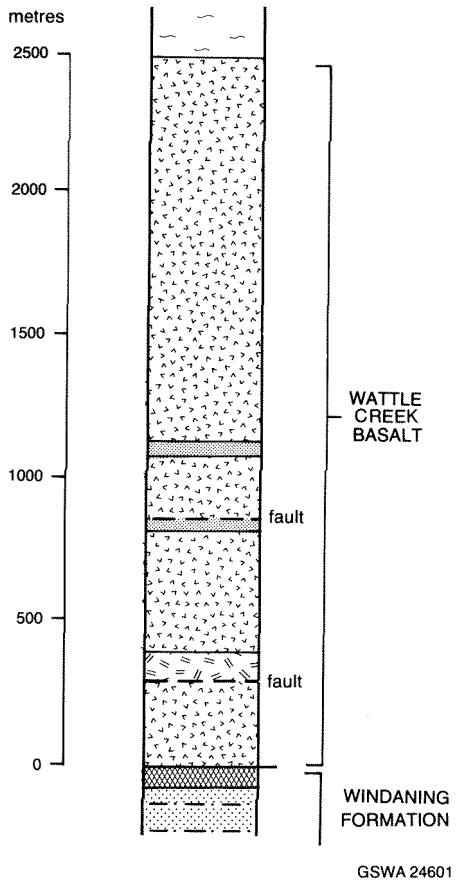
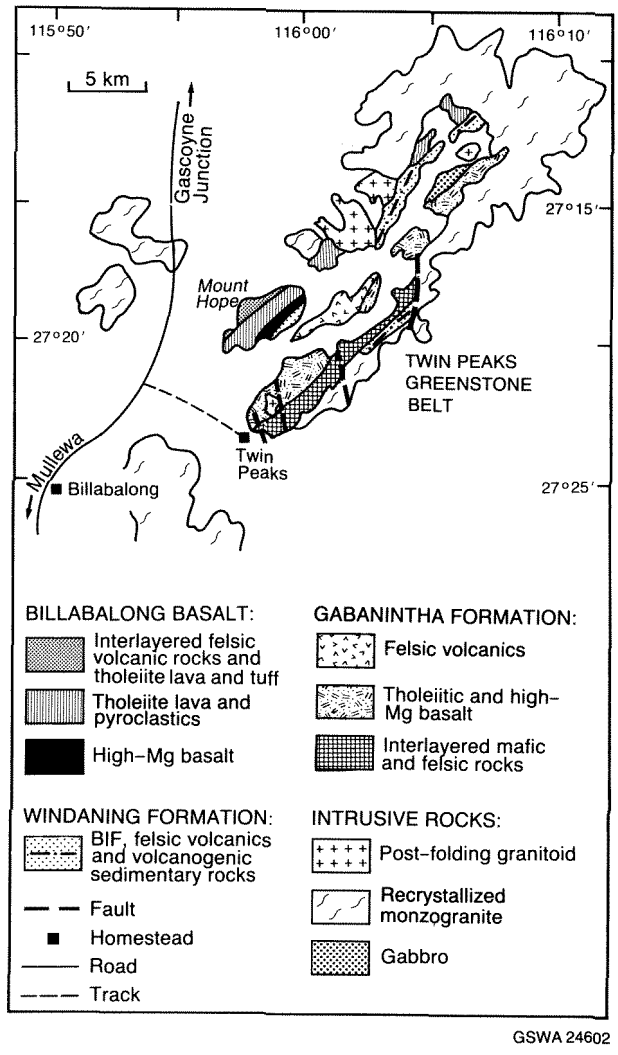


Figure 66. Stratigraphy of the Wattle Creek Basalt in the type area; ornament as in Figure 65.



Figures 67. Outcrop geology of the Billabalong Basalt.

350 m thick. The amphibolite was probably derived from basalt, dolerite, and gabbro. Remnants of fine-grained, porphyritic and vesicular basalt textures, and chilled pillow margins were seen in some parts of the outcrop. The amphibolite was intruded by a network of granitoid and pegmatite veins and dykes up to 5 m thick.

The amphibolite is overlain by a complex unit, about 300 m thick, of fine- to medium-grained pelitic and psammitic schists interlayered with siliceous, aphanitic to feldspar-phyric schists. These rocks were derived from a sequence of sedimentary and felsic volcanic rocks. Elongate pods of medium-grained buff-coloured rocks, up to 20 cm across, occur in the felsic schist. These are strongly foliated and recrystallized and are probably derived from felsic porphyry or granitoid rocks. They could be boudinaged (?pinch and swell) remnants of subvolcanic sills or deformed granitoid xenoliths. In thin section they appear to be coarser-grained variants of the surrounding felsic schist.

The uppermost unit is a 500 m-thick, fine- to medium-grained amphibolite containing abundant lenses, a few metres thick, of basaltic breccia. The breccia is composed of angular clasts of fine-grained amphibolite, 1–10 cm across, in a light-green tuffaceous matrix. The clasts are strongly elongated in the steep, northerly plunging lineation. The lenses of breccia probably represent pyroclastic flow deposits.

Singleton Basalt

Definition and distribution

The Singleton Basalt is defined here as a succession of tholeiitic and high-Mg basalts, mafic pyroclastic rocks, ultramafic rocks, gabbro, and dolerite, overlying the Windaning Formation in the southern part of the Yalgoo–Singleton greenstone belt. It is exposed in a number of hills and ranges, and forms a 100 km-long north-northwesterly trending belt from south of Mougooderra Hill to east of Mount Gibson Homestead (Plate 2, Fig. 71A). The formation derives its name from Mount Singleton, a prominent hill in the southern part of the belt.

The type area of the Singleton Basalt is in the Yeoh Hills to Mount Singleton region, where it attains a thickness of 3500 m. Here the Basalt has been folded into a double-plunging synclinal structure (Plate 2). The base of the formation occurs 1 km east of Ninghan woolshed, where gabbro and ultramafic rock are intruded by recrystallized monzogranite. The top of the formation is intruded by a post-folding syenogranite 25 km southeast of Mount Sin-

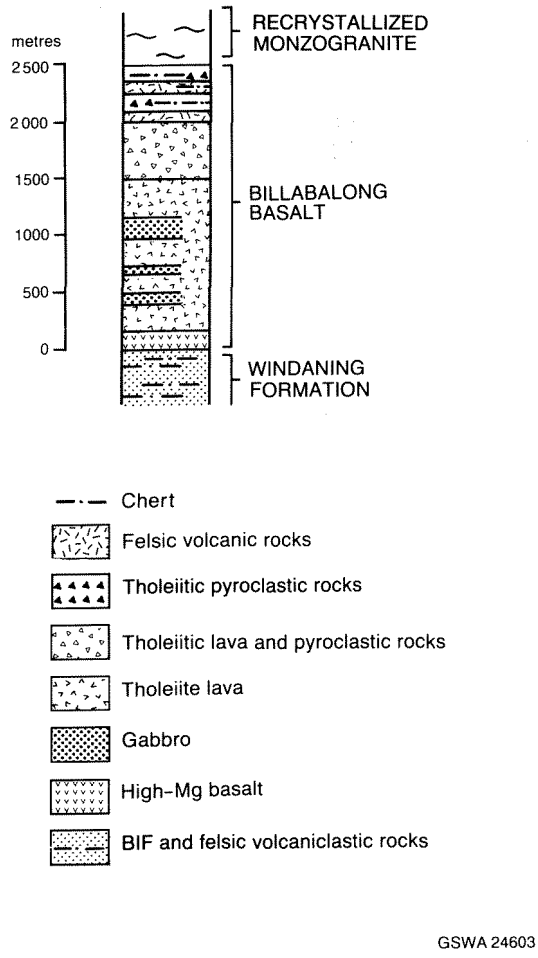


Figure 68. Schematic stratigraphy of the Billabalong Basalt.

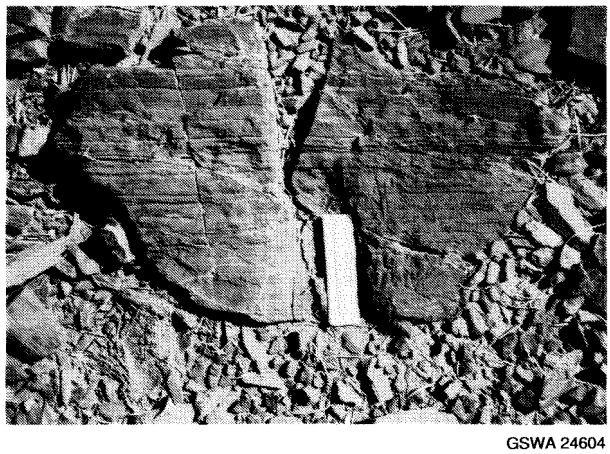


Figure 69. Fine layering in tholeiitic tuff in the Billabalong Basalt; the scale bar is 10cm.

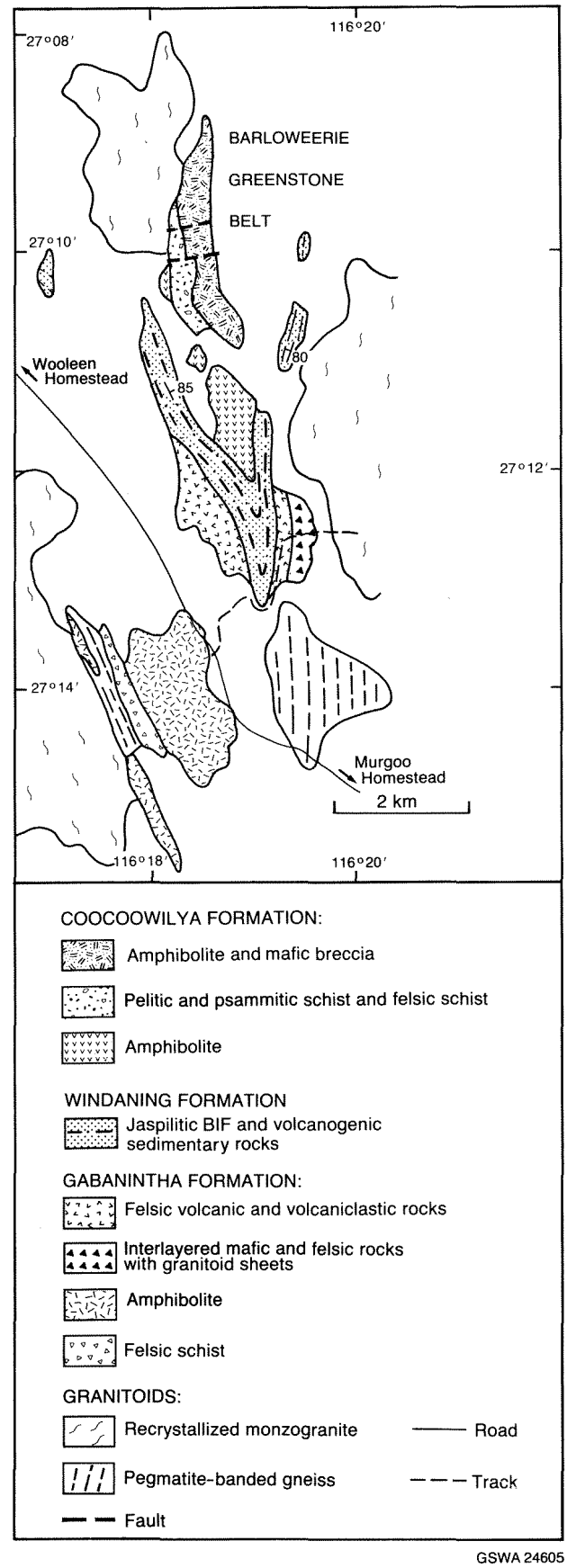


Figure 70. Outcrop geology of the Coocoowilya Formation.

gleton (Plate 2, Fig. 71A). The Singleton Basalt overlies the Windaning Formation 4 km south of Fields Find, but is separated from this formation to the south where it is intruded by granitoids (Plate 2). To the west, the Basalt is in tectonic contact with the Mougooderra Formation for much of its extent, and it is possible that this formation may have partly overlain the Singleton Basalt prior to faulting and shearing (Lipple, 1982a).

Lithostratigraphy

The lithostratigraphy of the Singleton Basalt is shown schematically in Figure 71B. The upper part of this stratigraphy is largely after Lipple (1982a). The succession is described in terms of six units, labelled a–f in Figure 71B.

(a) The lowest unit in the succession is exposed about 1 km east of Ninghan woolshed. It consists of ultramafic amphibole–chlorite(–talc) schist and serpentinite, interlayered with BIF and basalt. It is intruded by gabbro sills, particularly in its upper part.

(b) Fine-grained and needle spinifex-textured high-Mg basalt overlies the basal unit. Tholeiitic basalt flows are interlayered with the high-Mg basalt. The unit is massive and featureless.

(c) The next unit in the succession is a complex of gabbro and peridotite (now serpentinite) sills, with screens of basalt, and thin layers (<10 m) of mafic tuff and ferruginous chert. Some of the gabbro sills are differentiated, and have pyroxenite bases. Six kilometres west of Ninghan Homestead, the unit passes laterally into mafic pyroclastic rocks intruded by thin gabbro sills (Fig. 71A).

(d) The sill complex is overlain by a monotonous sequence of variolitic tholeiitic basalt containing abundant pillow lava, interlayered with minor amounts of high-Mg basalt. Spectacular exposures of pillow lava occur 1 km southwest of Greynight Bore (Fig. 71B). A 100 m-thick unit of ultramafic pyroclastic rocks, containing thin BIF and mafic tuff units, separates the basalt from a thick, overlying gabbro sill.

(e) A 500 m-thick undifferentiated gabbro sill intrudes the succession at this level. Its margins are fine-grained dolerite. Large xenoliths of mafic volcanic rocks occur in the sill, southeast of Coonigal Well and southwest of Mount Singleton (Fig. 71A). Lipple (1982a) reported small, partly assimilated granitoid xenoliths in this sill west of Mount Singleton.

(f) The upper part of the succession is dominated by mafic pyroclastic rocks. These are well exposed on the slopes of Mount Singleton as shallow-dipping to subhorizontal units of massive to poorly bedded, coarse breccia containing basalt lava fragments in a tuffaceous matrix; poorly bedded medium- to coarse-grained lithic tuffs; and fine-grained waterlain mafic tuffs showing sedimentary structures (Fig. 72). Thin units of aphanitic to fine-grained tholeiitic basalt are interlayered with the pyroclastic rocks. Pillow lava is abundant in these units. Well-formed pillows grade locally into pillows with brecciated margins, which grade with increasing fragmentation into chaotic hyaloclastite breccia (Lipple, 1982a). Much of the basalt is siliceous, and light-blue in colour, particularly in the upper part of the succession.

This stratigraphy records the evolution of a large basaltic volcano which, because of the extent of fresh outcrop and the weak deformation, is the best preserved volcanic edifice in the Murchison Province.

Geochemistry

Sampling

Forty-three samples of basalt were collected from two areas in the Singleton Basalt — 25 from the Yeoh Hills, and 18 from the vicinity of Mount Singleton (Figs 71A and B).

Compositions and petrogenesis

Compositions of tholeiitic basalt collected from the two regions are indistinguishable (Fig. 73). However, high-Mg basalt from the lower part of the Singleton Basalt in the Yeoh Hills region (samples 83456–83462 and 83470–83473, Fig. 71B) has a more primitive MgO-, Ni- and Cr-rich composition than does high-Mg basalt, interlayered with tholeiitic basalt, in the upper part of the formation in the Yeoh Hills and Mount Singleton regions (Table 25, Figs 73C, D, and F). Compositional fields for both high-Mg and tholeiitic basalts on Y–Zr and Ti–Zr diagrams are largely coincident (Figs 73A and B), indicating that they have common source characteristics. Trends on these diagrams do not show systematic crystal fractionation from high-Mg to tholeiitic basalts, although pyroxene and olivine fractionation exercised some control of compositional variation within each basalt type. Covariation of Ni, Cr, and MgO (Figs 73C and D) demonstrates that high-Mg basalt, and tholeiitic basalt from the upper part of the formation, are related by crystal fractionation of pyroxene and possibly olivine. High-Mg basalts from the lower part of the Singleton Basalt contain more Ni and Cr, relative to MgO, and have a steeper sloping trend on the Ni–MgO diagram, than the other basalts.

Tholeiitic basalt data plot on a well-defined trend on a Zr/Y–Zr diagram (Fig. 73E), indicating derivation by 15–20% partial melting of a plagioclase-lherzolite source. This is consistent with the trend shown by tholeiitic and high-Mg basalt data from the upper part of the formation on a Cr–Y diagram, which intersects the plagioclase-lherzolite model melting curve at about 20% melting, although there is much scatter in the data (Fig. 73F). High-Mg basalt data from the lower part of the formation plot above the model melting curve, but along the same trend as the other basalts.

The basalts plot close to the estimated upper mantle ratio of Sun and Nesbitt (1977), although most data fall on the Zr-rich side of this line. The spread of data on the Zr/Y–Zr diagram also suggests little, if any, enrichment or depletion of incompatible elements. REE patterns for three samples from the Mount Singleton region are inconsistent (Fig. 73G). One has a fractionated pattern with $(Ce/Lu)_N$=2.0; the other two, a tholeiite and a high-Mg

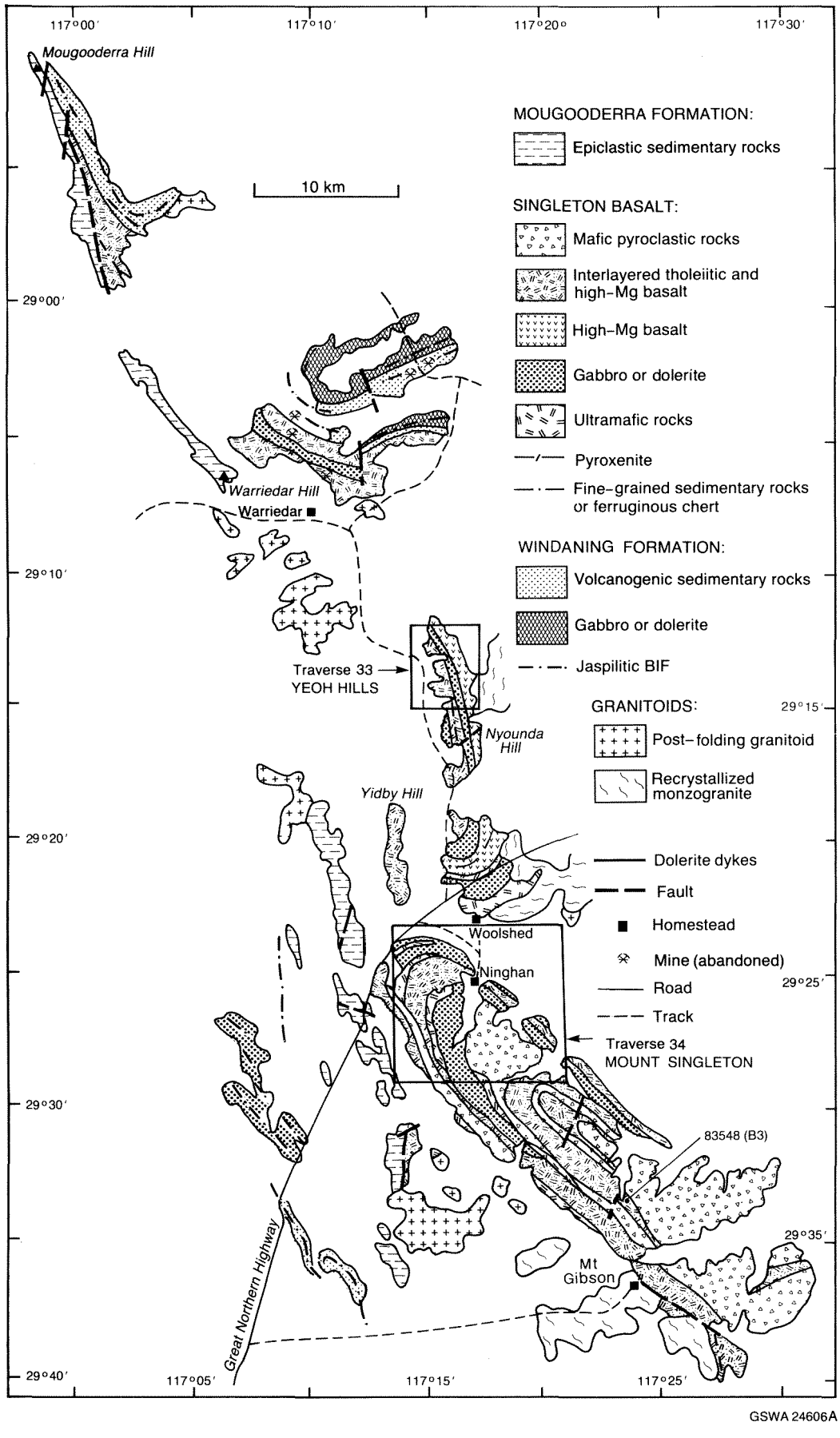
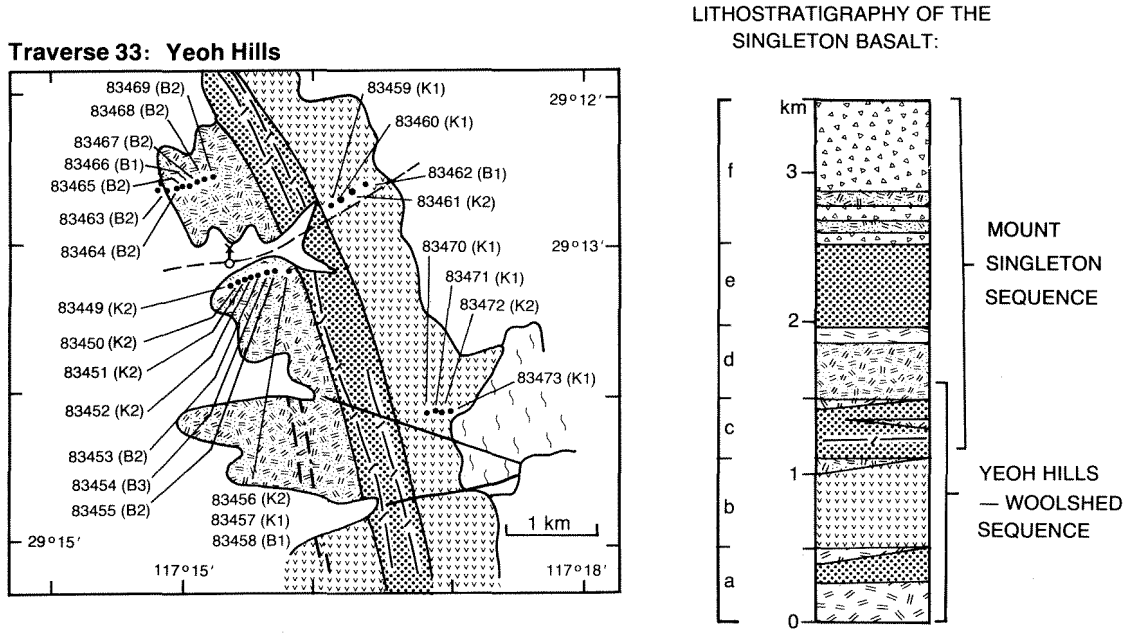


Figure 71A. Outcrop geology of the Singleton Basalt and location for Figure 71B.



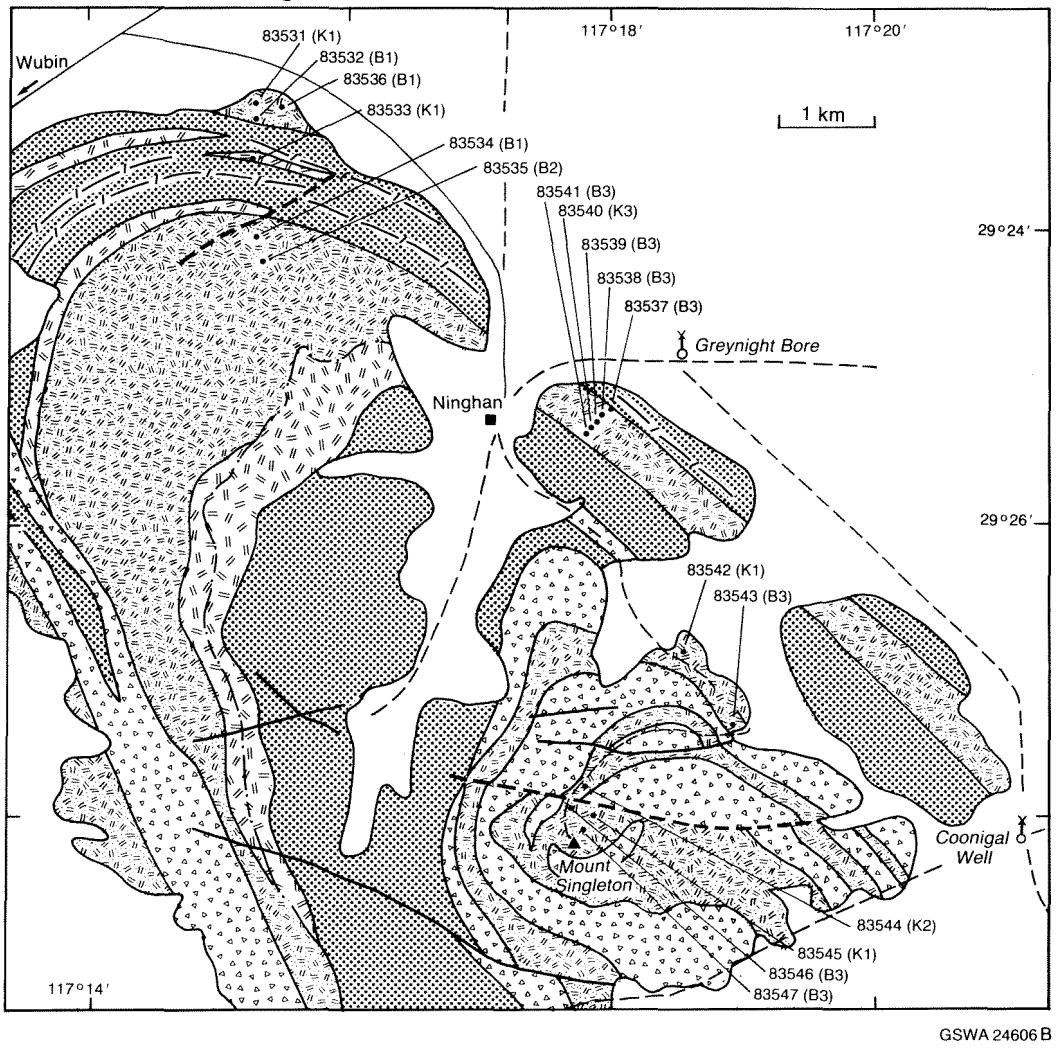


Figure 71B. Sample locations and schematic stratigraphy of the Singleton Basalt. Codes in brackets following sample numbers refer to 'rock type' and 'degree of alteration' as defined in Appendix II.

TABLE 25. MEAN COMPOSITIONS OF SINGLETON BASALT

	Tholeiitic basalt n=16	*Lower high-Mg basalt n=9*	*Upper high-Mg basalt n=9*
	Percentage		
SiO_2	51.9	48.2	50.3
Al_2O_3	13.5	8.0	10.9
Fe_2O_3	1.6	2.0	1.6
FeO	8.52	10.18	9.29
FeO*(a)	10.0	12.0	10.7
MgO	7.49	15.53	10.21
CaO	11.35	9.30	11.02
Na_2O	2.17	1.09	1.90
K_2O	0.07	0.07	0.13
TiO_2	0.76	0.71	0.84
P_2O_5	0.12	0.11	0.11
MnO	0.17	0.18	0.17
LOI	4.19	3.68	2.83
	Parts per million		
Ba	81	90	99
Cr	363	1771	700
Co	79	96	88
Cu	78	95	77
Li	2	7	3
Ni	160	701	249
Sr	136	99	140
V	233	214	250
Y	20	17	19
Zn	71	86	74
Zr	58	47	53
La	(b) 5	(b)(c) 5	(b) 6
Ce	(b) 8	(c) <5	(b) 5
Mg number (d)	57.2	69.8	63.0
Cr/V	1.56	8.28	2.80
Zr/(Zr+Y)	0.74	0.73	0.74

(a) All Fe calculated as FeO
(b) Some values used to calculate the means are below the detection limit; for these determinations the value 'detection limit/2' was used.
(c) Means exclude samples 83470–83473 which have means of 91 ppm La and 146 ppm Ce.
(d) 100 mol MgO/(MgO + FeO)
Samples assigned to alteration class 3 (see Appendix II) are omitted from the means.
For most of the analyses averaged in this table Nb<5 ppm, Rb<5 ppm, Th<5 ppm, and Pb<10 ppm.

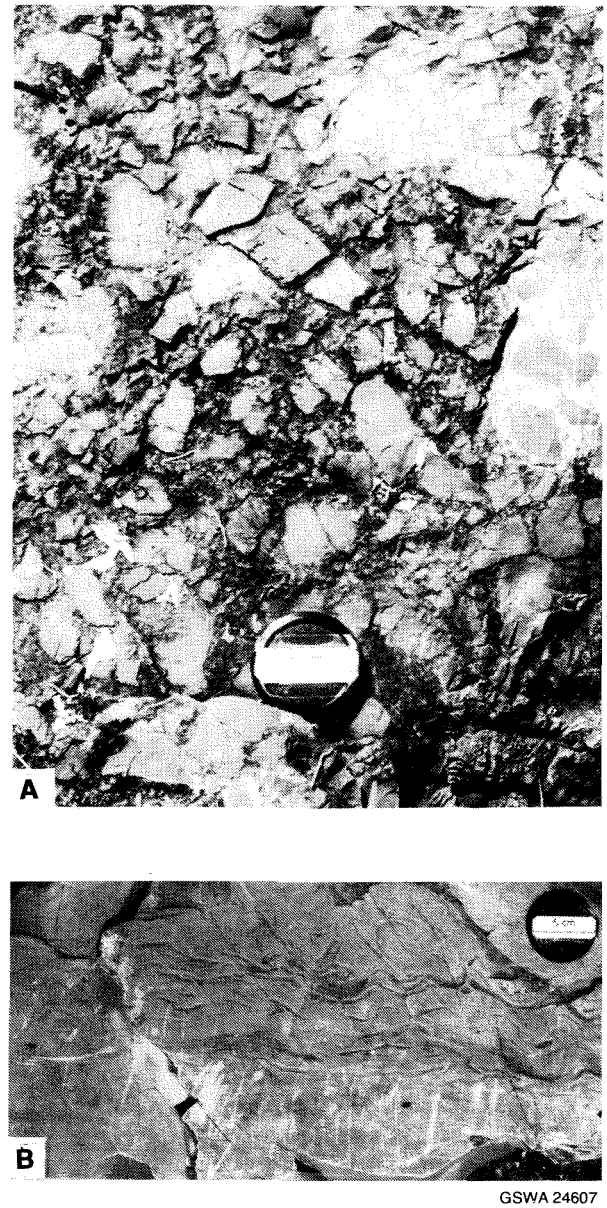
basalt, have fairly flat patterns and show slight depletion of Nd, Sm, and Eu in the high-Mg basalt sample. The sample with enriched LREE (83536) is atypical of the Singleton Basalt, and only one other sample (83532) has similar characteristics. These samples are fractionated high-Fe tholeiites with high abundances of FeO*, TiO_2, P_2O_5, V, Y, Zr, La, and Ce, and low abundances of MgO, Ni, and Cr (Appendix II). They were probably generated from the same plagioclase-lherzolite source as the other tholeiites, but by only 10% partial melting (Figs 73E and F). The similarity of the other two REE patterns is consistent with trends on the other diagrams, and suggests that tholeiitic and upper high-Mg basalt were derived from a near-chondritic source, and are related by crystal fractionation.

In summary, interlayered tholeiitic and high-Mg basalts from the middle and upper parts of the Singleton Basalt were derived by 10–20% partial melting of a plagioclase-lherzolite source. These basalts are related by olivine and pyroxene crystal fractionation. High-Mg basalt from the lower part of the Singleton Basalt is not directly related to the other basalts, although it has similar HFS element characteristics. There is no evidence for crustal contamination of these basalts.

Mougooderra Formation

Definition and distribution

The Mougooderra Formation is defined here as a succession of sedimentary rocks and minor amounts of basalt, overlying Luke Creek Group formations in the Yalgoo–Singleton and Gullewa greenstone belts (Plate 2). The formation occurs in a number of large outcrops, most of which occupy the cores of these synclinal greenstone belts



GSWA 24607

Figure 72. A — Pyroclastic basalt breccia with tuffaceous matrix; B — Fine grained basalt tuff; the lower part is laminated but the upper part shows slump structures. The lens cap is 5cm across.

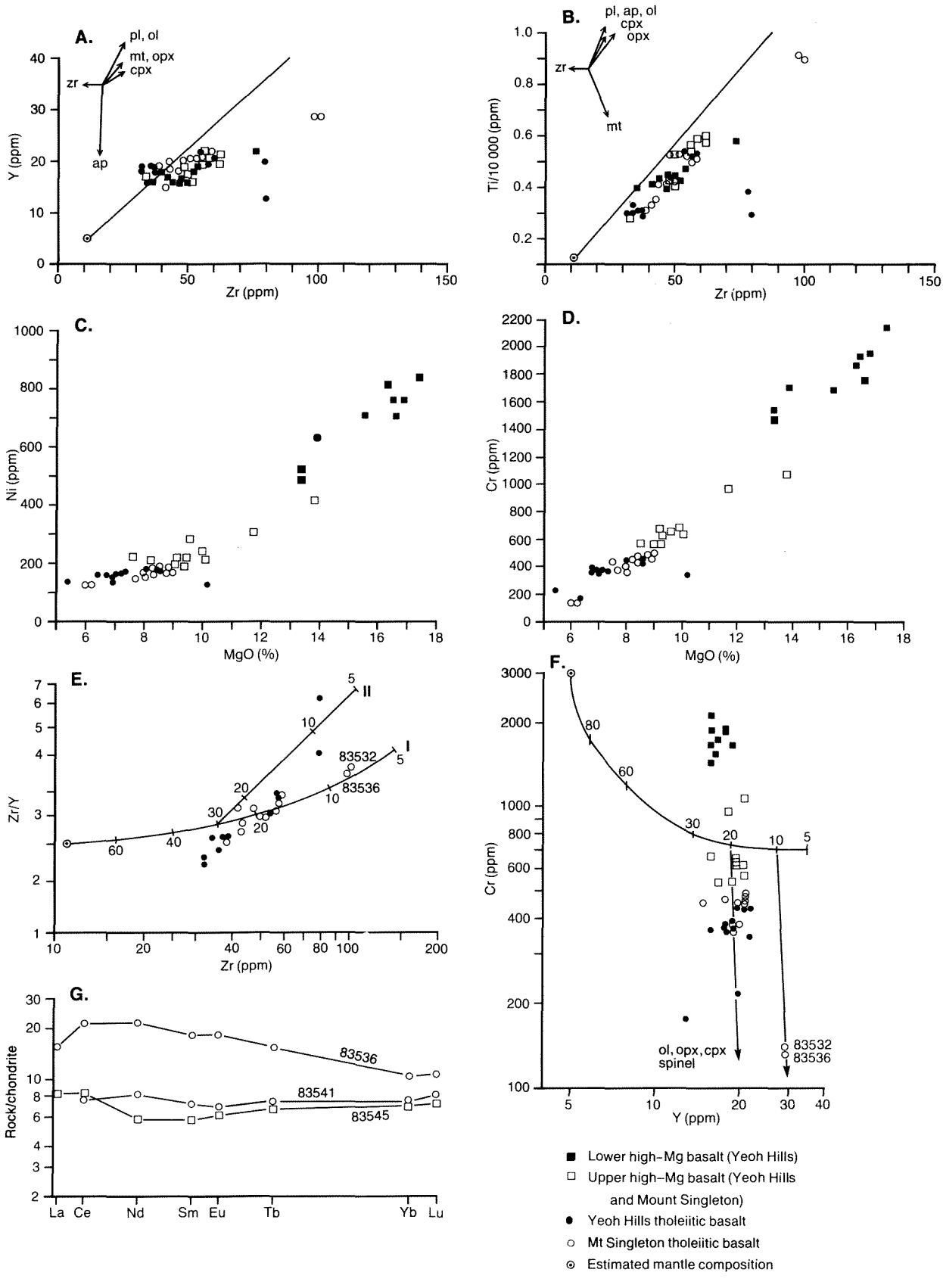


Figure 73. Geochemistry of the Singleton Basalt. Estimated mantle composition and ratios, relative crystal-fractionation vectors, mineral phases, and model partial-melting curves as in Figures 7, 8 and 10.

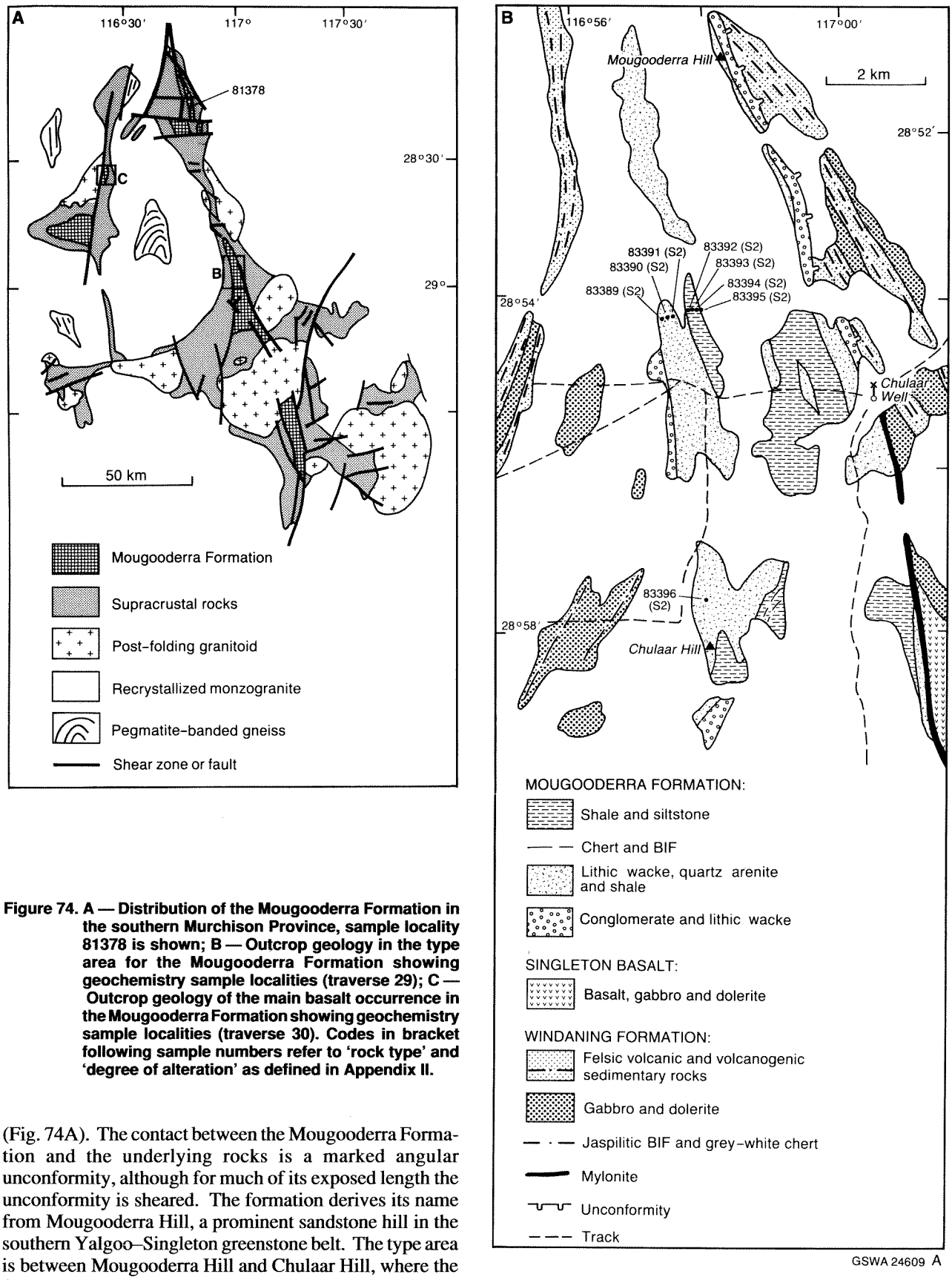


Figure 74. A — Distribution of the Mougooderra Formation in the southern Murchison Province, sample locality 81378 is shown; B — Outcrop geology in the type area for the Mougooderra Formation showing geochemistry sample localities (traverse 29); C — Outcrop geology of the main basalt occurrence in the Mougooderra Formation showing geochemistry sample localities (traverse 30). Codes in bracket following sample numbers refer to 'rock type' and 'degree of alteration' as defined in Appendix II.

(Fig. 74A). The contact between the Mougooderra Formation and the underlying rocks is a marked angular unconformity, although for much of its exposed length the unconformity is sheared. The formation derives its name from Mougooderra Hill, a prominent sandstone hill in the southern Yalgoo–Singleton greenstone belt. The type area is between Mougooderra Hill and Chulaar Hill, where the formation is 2000 m thick and comprises conglomerate, lithic wacke, quartz arenite, shale, chert, and BIF (Fig. 74B). North of Chulaar Well the basal contact with the Windaning Formation is an unconformity, but to the south it is a shear zone.

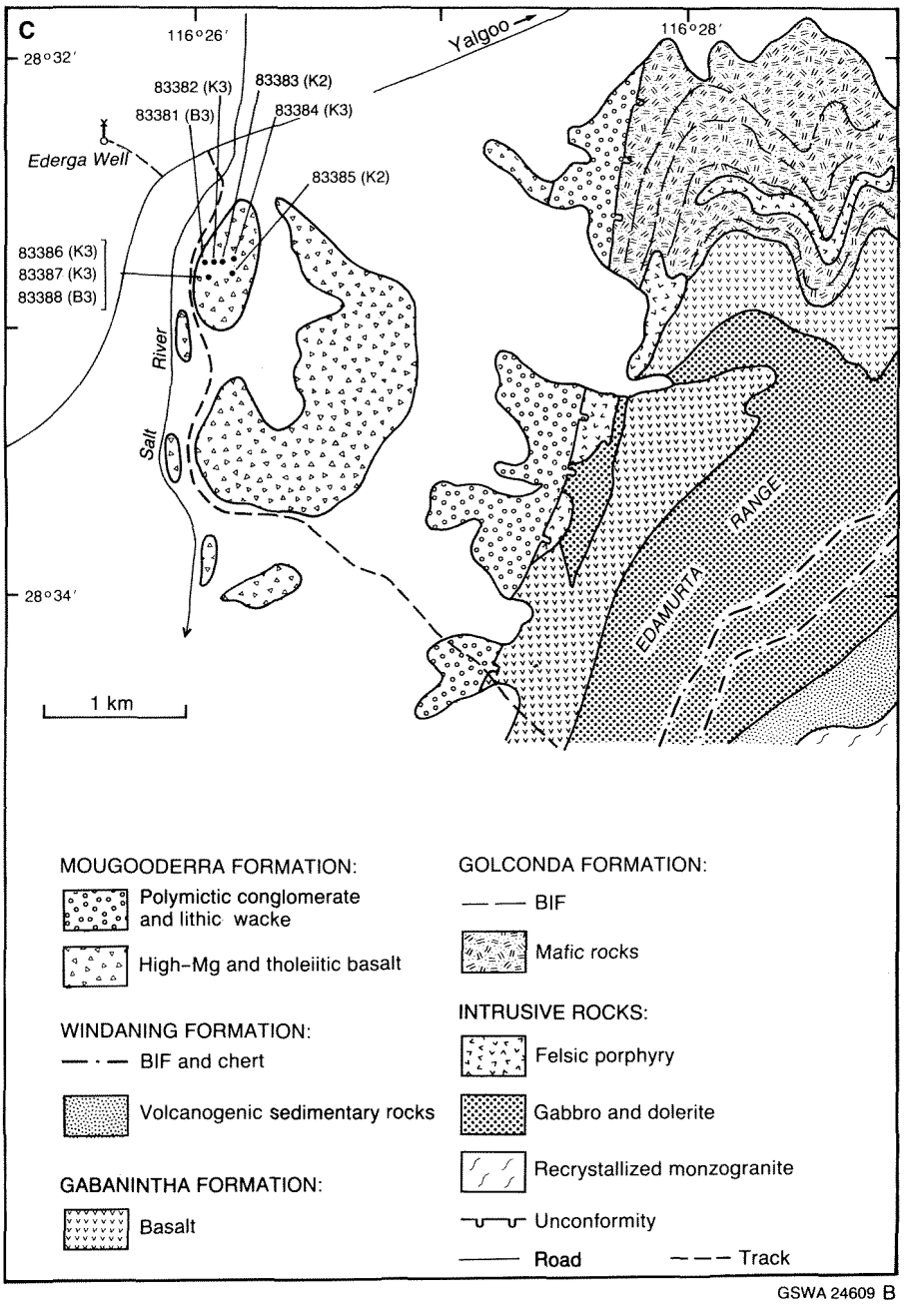


Figure 74. (continued)

Lithostratigraphy

The Mougooderra Formation unconformably overlies the Windaning, Gabanintha, and Golconda Formations and is in sheared contact with the Singleton Basalt. Its thickness is difficult to estimate because of extensive folding and faulting, and poor exposure; however, given the overall widths of outcrops and the regionally subvertical dip, a broad estimate of 2000 m is made. Lipple et al. (1983, table 2) estimated the maximum thickness as 3000 m. Most of the Mougooderra Formation comprises a large-scale upward-fining sequence of epiclastic sedimentary rocks. Three outcrops of basalt were found: 10 km west of Warriedar Homestead; 3 km northwest of the Edamurta Range adjacent to the Salt River (Plates 1 and 2, Fig. 74C); and a small occurrence 2 km west of the Wadgingarra mining centre (not shown on Plates 1 and 2).

Sedimentary rocks

The basal part of the formation consists of medium- to coarse-grained, poorly sorted, immature lithic wacke and pebbly lithic wacke, together with abundant lenticular beds of conglomerate up to 10 m thick. In addition, conglomerate units up to 500 m thick, containing minor units of lithic wacke, occur at Brandy Hill on YALGOO and 7 km northeast of Jasper Hill on PERENJORI. Conglomerate clasts are derived from the immediately underlying formations and consist of vein quartz, chert, jaspilitic BIF, felsic volcanics, sedimentary rocks, and basalt. No granitoid

clasts were seen. Locally, the sandstone matrix is pyritic, and pebbles of gossan are preserved, indicating erosion of massive sulphide deposits. Clasts are angular or subrounded and generally a few centimetres across (Fig. 75), but locally up to 50 cm across. Lithic wacke contains clasts of similar lithologies to those in the conglomerate, except that the proportion of felsic volcanic clasts to chert and BIF clasts is higher. The lithic wacke shows well-developed parallel stratification, due mainly to variations in grain size and clast types, and/or proportions of clast types. Beds range from several centimetres to several metres in thickness.

The lowermost coarse-grained unit passes upwards into a thin- to thick-bedded (a few centimeters to a few metres) unit of lithic wacke, quartz arenite, and shale. Fine- to medium-grained quartz arenites are graded and cross-stratified (sets about 30 cm thick) and have numerous scour surfaces. Ripple marks, including bifurcating, straight-crested symmetrical forms, are present locally, for example 1 km northeast of Warro Well on NINGHAN. The upper part of the succession is dominated by turbiditic siltstone and shale. Pyritic black shale occurs in some fresh exposures, but it is not known how representative these outcrops are as most rocks are bleached by weathering. Thin lenses of sandstone occur in some outcrops. BIF and ferruginous chert units also occur sporadically in this unit.

The upward-fining sedimentary succession of the Mougooderra Formation records a transition from shallow-marine shelf sedimentation to a deeper and more distal sedimentary environment. Conglomerate and parallel-stratified lithic wacke in the lower part of the succession are interpreted as streamflow and debris-flow deposits of proximal alluvial fans (Collinson, 1986). Well-sorted quartz arenites which display small- to medium-scale cross-stratification and symmetrical wave ripples are probably shoreline to shallow-marine shelf deposits, whereas the uppermost fine-grained unit records offshore sedimentation, in relatively deep water, from suspension currents (Johnson and Baldwin, 1986). There is little evidence to support Lipple's (1982a) contention that these sedimentary rocks developed in a graben filled by quartzose sediment derived principally from unroofed granitoid sources. The sedimentary rocks are metamorphosed in upper greenschist facies. Mineral assemblages include quartz, feldspar, white mica, chloritoid, andalusite, chlorite, rutile, and opaque phases. Chloritoid is particularly abundant in some samples.

Basalt

The basalt unit near Warriedar Homestead is poorly exposed and strongly foliated, and is now a fine-grained featureless amphibolite. It is about 200 m thick and occurs in the sandstone–shale part of the sedimentary sequence. The basalt west of Wadgingarra is also poorly exposed; it is a thin lenticular unit in the sandstone–shale sequence. The upper part of the basalt adjacent to the Salt River is well exposed (Fig. 74C); it consists of weakly deformed, fine-



GSWA 24610

Figure 75. Conglomerate at the base of the Mougooderra Formation; composed mainly of jaspilitic BIF, chert, and felsic volcanic clasts. The hand lens is 4cm in length.

TABLE 26. MEAN COMPOSITIONS OF MOUGOODERRA FORMATION SEDIMENTARY ROCKS

	Lithic wacke n=1	*Quartz arenite n=3*	*Shale n=4*
	Percentage		
SiO_2	79.1	91.3	74.5
Al_2O_3	10.5	5.7	13.3
Fe_2O_3	1.7	0.3	0.6
FeO	3.47	0.61	5.88
FeO* (a)	5.0	0.9	6.4
MgO	0.44	0.03	0.18
CaO	0.22	0.09	0.43
Na_2O	0.11	0.09	0.06
K_2O	0.39	0.18	0.26
TiO_2	0.55	0.31	0.55
P_2O_5	0.21	0.12	0.41
MnO	0.30	0.07	0.90
LOI	2.69	1.20	2.51
S	0.14	0.09	0.03
	Parts per million		
Ba	162	148	167
Cu	85	40	30
Pb	<10	(b) 12	13
Li	14	5	4
Mo	3	4	6
Ni	79	36	77
Nb	<10	<10	<10
Rb	25	12	14
Sr	45	46	44
Th	10	<10	<10
Sn	<5	<5	<5
U	1	<1	<1
V	96	38	108
Y	18	10	17
Zn	36	8	47
Zr	147	105	131
La	35	18	26
Ce	60	30	49
Zr/TiO_2	0.03	0.03	0.02

(a) All Fe calculated as FeO
(b) Some values used to calculate the mean are below the detection limit; for these determinations the value 'detection limit/2' was used.

TABLE 27. MEAN COMPOSITIONS OF MOUGOODERRA FORMATION BASALTS

	SALT RIVER SAMPLES		*WEST WADGINGARRA*
	Tholeiitic basalt n=2	*High-Mg basalt n=6*	*Tholeiitic basalt sample 81378*
	Percentage		
SiO_2	54.0	53.7	53.2
Al_2O_3	14.1	12.8	13.3
Fe_2O_3	1.4	1.4	1.4
FeO	6.77	6.98	7.26
FeO* (a)	8.0	8.2	8.5
MgO	7.82	10.37	7.55
CaO	10.21	7.99	11.2
Na_2O	1.87	1.38	1.86
K_2O	0.54	0.40	0.07
TiO_2	0.61	0.57	0.46
P_2O_5	0.11	0.10	0.18
MnO	0.17	0.15	0.13
LOI	1.98	3.53	1.86
	Parts per million		
Ba	228	234	192
Cr	391	694	449
Co	78	65	nd
Cu	37	14	102
Pb	15	<10	<10
Li	7	16	4
Ni	198	234	99
Rb	20	18	<2
Sr	122	95	168
V	189	200	216
Y	25	23	17
Zn	75	79	61
Zr	95	86	28
La	17	14	<5
Ce	25	22	5
Mg number (b)	63.5	69.3	61.3
Cr/V	2.07	3.47	2.08
Zr/(Zr+Y)	0.79	0.79	0.62

(a) All Fe calculated as FeO (b) 100 mol MgO/(MgO + FeO)
For most of the analyses averaged in this table Nb<10 ppm and Th<10 ppm.

grained and needle spinifex-textured, tholeiitic and high-Mg basalts. Pillow lavas are well developed in some exposures and give a consistent stratigraphic way-up to the west. The basalt is metamorphosed in lower amphibolite facies and contains hornblende, oligoclase, biotite, chlorite, and opaque phases. It also contains synmetamorphic quartz segregations and some thin (<1 mm) post-metamorphic quartz veins. The top of the succession is truncated by a major northerly trending shear zone which influences the course of the Salt River. The basalt occurs above the conglomerate–lithic wacke part of the sedimentary sequence. The base of the basalt was not observed. It is possible that it is not part of the Mougooderra Formation, but could be separated from it by a shear zone or fault, making the basalt a fault-bounded sliver of unknown stratigraphic affiliation.

Geochemistry

Sampling

Eight samples of sedimentary rock were collected, for chemical analysis, from the type area of the formation (Fig. 74B). In addition, eight samples of basalt were collected from the upper part of the unit near the Salt River, and one sample (81378) from the unit west of Wadgingarra (Figs 74A and C). Chemical analyses are listed in Appendix II.

Sedimentary rocks

Compositions of lithic wacke, quartz arenite, and shale are given in Table 26. Lithic wacke and shale samples have

broadly similar compositions; quartz arenite contains more silica and is proportionally depleted in other elements. Lithic wacke and shale do not contain the high combined MgO and FeO contents (> 8%) typical of Archaean greywackes; furthermore, they are relatively depleted in Na_2O, K_2O and Sr, although other trace element abundances are comparable (Ayres, 1983; McLennan, 1984; Ojakangas, 1985). Zr/TiO_2 ratios range from 0.02 to 0.03, corresponding to rhyolite and dacite compositions (Hallberg, 1984). This is consistent with the dominance of felsic volcanic clasts in lithic wacke. The high FeO^* content relative to MgO probably reflects the presence of BIF in the source region. The geochemistry of these samples is consistent with their derivation from the underlying Windaning and upper Gabanintha Formations (Fig. 74B).

Basalt

The nine basalt samples are all altered to some extent by post-metamorphic quartz veining; SiO_2 contents range from 52.3% to 55.0% (Appendix II). Most of the basalts have high-Mg characteristics with high abundances of MgO, Cr, Ni, and high Cr/V ratios. Samples from the Salt River outcrop have anomalously high contents of Ba, Li, Rb, Sr, La, and Ce, characteristic of crustal contamination (Table 27). It is unlikely that silicification is responsible for these anomalous values, as post-metamorphic quartz veining is only a minor feature of the rocks, and sample 81378, which also contains high silica, does not show these characteristics. However, silicification may have modified compositions to some extent. Mougooderra Formation basalt samples plot on the same trends on Y–Zr and Ti–Zr diagrams (Figs 76A and B); however, sample 81378 plots near the estimated mantle composition ratio, while the Salt River samples plot on Zr-enrichment trends. On a Cr–Y diagram the Salt River basalt data plot on a well-defined trend indicating derivation by about 15% partial melting of a plagioclase-lherzolite source, followed by crystal fractionation of olivine and pyroxene (Fig. 76C). However, this figure may not be reliable, because the effects of crustal contamination on Cr and Y abundances are unknown. The uncontaminated sample 81378 contains less Y than the contaminated samples (Table 27).

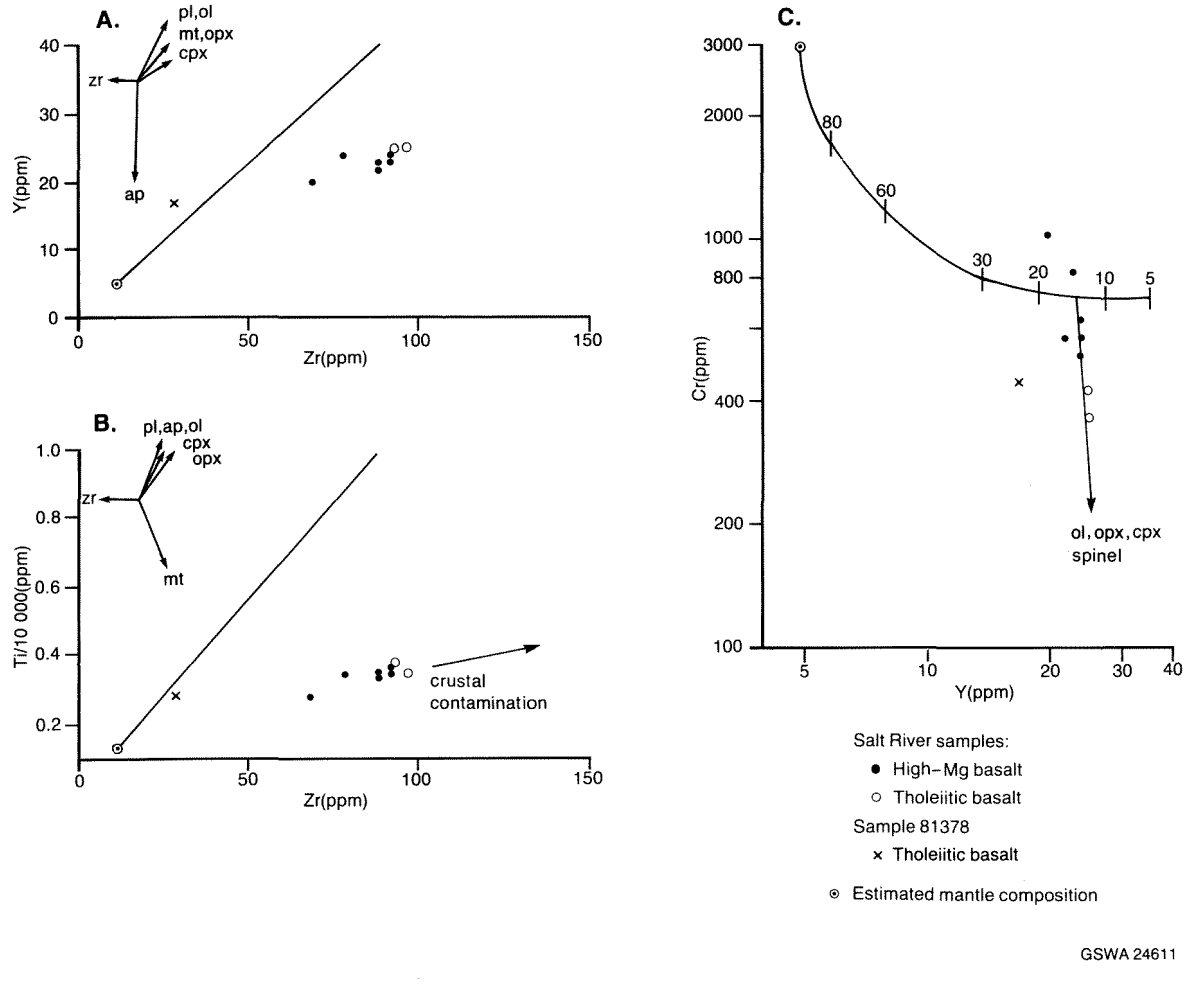


Figure 76. Geochemistry of Mougooderra Formation basalt. Estimated mantle compositon and ratios, crystal-fractionation vectors, mineral phases, and the model partial-melting curve as in Figures 7 and 10.

Wongan Hills greenstone belt

The Wongan Hills greenstone belt is south of the area shown in Figure 2, adjacent to rocks of the Jimperding Gneiss Complex at the southern tip of the Murchison Province as defined by Gee et al. (1981) (Fig. 77A). The belt was not mapped during this study and its rocks are therefore not included in the stratigraphic scheme described above, although correlation may be possible. This account is summarized partly from those of Carter and Lipple (1982) and Lipple (1982b).

The greenstone sequence consists of basalt, chert, BIF, schists derived from felsic volcanic and sedimentary rocks, and small amounts of ultramafic rock (Fig. 77B). The greenstone belt is intruded internally by a post-folding granitoid; the margins of the belt are in contact with porphyritic and equigranular recrystallized monzogranite to the east, and a complex of gneisses and deformed granitoids to the west. The greenstones have been metamorphosed in upper amphibolite facies. Psammo-pelitic schists may contain garnet, andalusite, sillimanite, and cordierite; mafic rocks contain clinopyroxene, hornblende, and andesine; BIF contains magnetite and grunerite. Metamorphic grade appears to increase southwards in the belt, and conditions of metamorphism in the southern part have been estimated as 640–680°C at 140–240 MPa (Blight, 1978, 1979).

The unit containing BIF and chert interlayered with felsic and psammo-pelitic schist is characteristic of the Windaning Formation. The underlying mafic rocks in the western part of the belt may be equivalent to the Gabanintha Formation.

Pidgeon and Wilde (1985, 1986) reported three U–Pb zircon ages from this region. A felsic porphyry, concordant with mafic volcanics in the northern part of the greenstone belt, gave an age of 3048 ± 25 Ma, similar to ages of rocks in the upper part of the Gabanintha Formation to the north. A gneiss west of the greenstone belt yielded

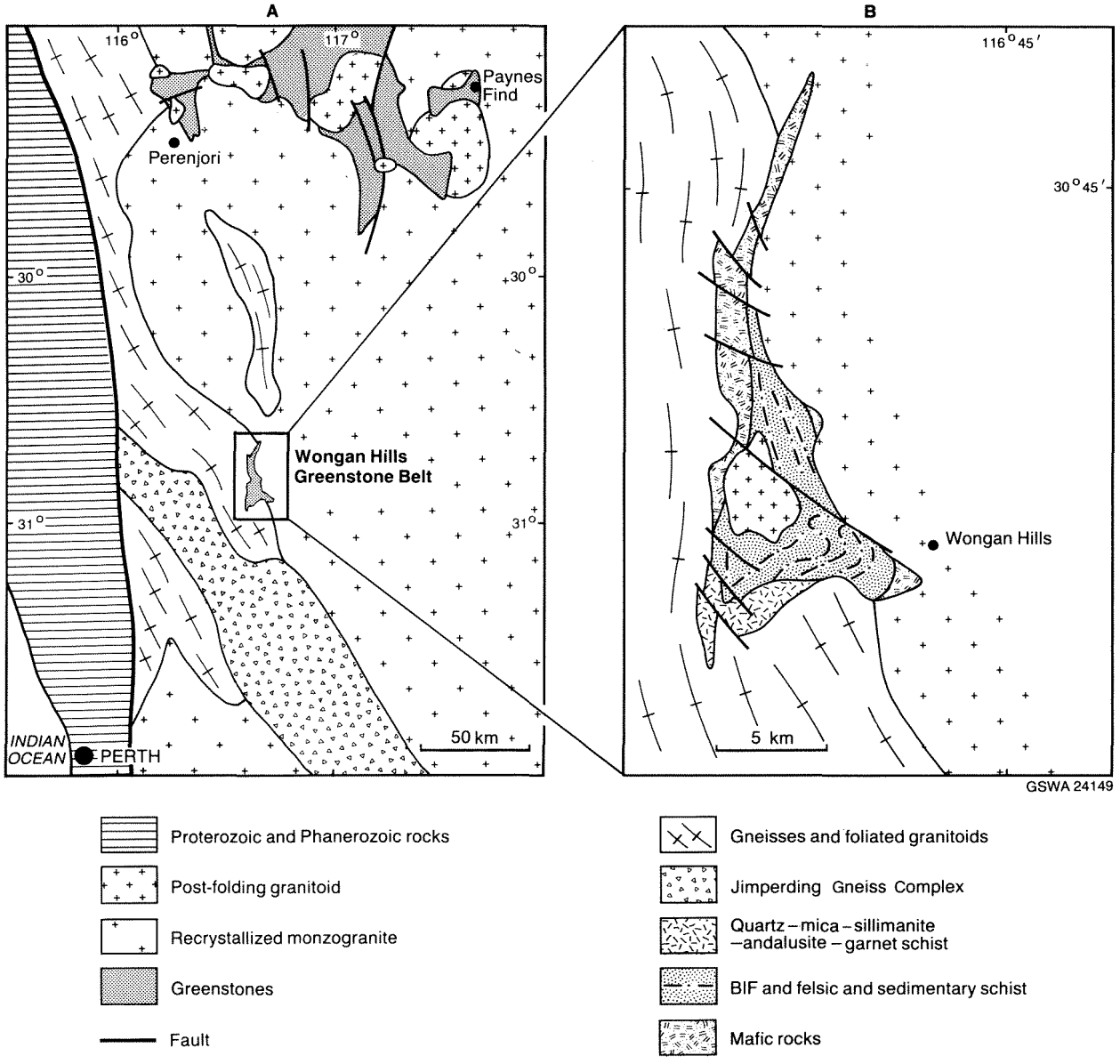


Figure 77. A — Regional setting of the Wongan Hills greenstone belt; B — Geology of the Wongan Hills greenstone belt.

an age of 2765 ± 25 Ma, and an undeformed porphyritic granitoid which intrudes the belt gave an age of 2620 ± 80 Ma.

Styles of volcanism

Three main styles of volcanism appear to have been important in development of the Murchison Supergroup: lava plains, shield volcanoes, and stratovolcanoes.

Lava plains are regionally extensive, monotonous sequences of tholeiitic and/or high-Mg basalt flows, several kilometres thick, within which volcanic centres (i.e. the main vent regions) are not recognized (Dimroth et al., 1982). In the Murchison Province, lava plains occur only in the Luke Creek Group. Although the Murrouli Basalt is not extensively preserved (because of subsequent intrusions of granitoids) it probably formed a lava plain over an unknown basement. The lower mafic part of the Gabanintha Formation also has the characteristics of a lava plain. These formations probably developed either by multiple fissure eruptions, forming flood basalts, or by interleaving of numerous, adjacent broad shield volcanoes of similar composition. Nearly all the lava is massive, and pillow lavas are rarely seen, making division into proximal (massive) and distal (pillowed) facies impossible. Pyroclastic rocks are extremely scarce. The absence of vesicles and pillow breccias, and the virtual absence of pyroclastic rocks, indicates eruption in deep water (McBirney, 1963; Moore, 1965; Dimroth et al., 1982, 1985). The scarcity of pillow lavas may reflect high eruption rates and flow volumes (Ayres and Thurston, 1985).

Shield volcanism is characterized by sequences of basaltic rocks, several kilometres thick, and generally from several tens to one hundred kilometres across (Williams and McBirney, 1979). In the Murchison Province the Mindoola Formation, Wattle Creek Basalt, Billabalong Basalt, Wadgingarra Basalt, and the lower parts of the Singleton Basalt and Porlell Subgroup, are thought to represent the remnants of shield volcanoes. Both pillow lavas and hyaloclastites occur, and it is often possible to separate small regions into massive and pillowed facies. Pyroclastic rocks are also seen, but are scarce. The presence of hyaloclastites and small amounts of pyroclastic rocks in some parts of these volcanic piles indicates eruption in water depths of only a few hundred metres (Sigurdsson, 1982a,b; Dimroth et al., 1985).

Stratovolcanoes are composite cones built partly of effusive rocks and partly of pyroclastic rocks (Williams and McBirney, 1979). In the Murchison Province, remnants of stratovolcanoes are thought to be represented by the Dalgaranga Formation, the upper parts of the Porlell Subgroup and Singleton Basalt, and by felsic volcanic complexes in the upper part of the Gabanintha Formation. With the exception of the upper Singleton Basalt, they consist of felsic to intermediate volcanic piles which were built on earlier lava plains or shield volcanoes. Most stratovolcanoes are poorly preserved because of erosion, which appears to have removed most of the edifices to form overlying and adjacent sedimentary rocks (Kuenzi et al., 1979; Sigurdsson et al., 1980; Ayres, 1983; Ojakangas, 1985). Despite erosion, some felsic volcanic piles attain thicknesses of a few kilometres and extend for several tens of kilometres along strike. Proximal and distal facies are recognizable in some volcanoes, and, in contrast to the other types of volcanism, a wide variety of volcanic rock morphologies are present, from proximal breccias and lava flows to distal fine-grained laminated tuffs. Rocks such as waterlain tuffs with depositional structures, and laharic deposits (Fisher, 1982), indicate that volcanism developed in shallow-water to subaerial environments, although there is evidence for some deep-water volcanism, e.g. at Golden Grove (B. Clifford, written communication, 1988). The upper part of the Singleton Basalt consists mainly of mafic pyroclastic rocks, which can only be formed subaerially or in water less than a few hundred metres deep (Sigurdsson, 1982a, b), usually by phreatomagmatic (Ayres, 1982) or phreatic eruptions (Williams and McBirney, 1979). Several stratovolcanoes have also been described from the Southern Cross and Eastern Goldfields Provinces; these include the Marda Complex (Hallberg et al., 1976a), and the Welcome Well, Spring Well, Bore Well, and Ida Hill complexes (Giles, 1981, 1982; Giles and Hallberg, 1982).

Synthesis

Greenstone stratigraphy

There is a systematic pattern of stratigraphic development in the Murchison Supergroup. The Luke Creek Group and Mount Farmer Group are characterized by different styles of volcanism and sedimentation (Fig. 78). In the Luke Creek Group, two episodes of lava-plain volcanism formed laterally extensive sequences, several kilometres thick, mainly of basalt. Regionally extensive banded iron-formations developed at the top of both sequences. These now form important markers for understanding the regional disposition of stratigraphic units. Felsic volcanism was widespread in the upper part of the Luke Creek Group. The group is subdivided into four formations — the two volcanic sequences, and the two BIF-dominated sequences (Fig. 3). In contrast, volcanism during formation of the Mount Farmer Group was characterized by contemporaneous development of nine distinct central volcanic complexes distributed through the Murchison Province. These were shield volcanoes and stratovolcanoes built on an infrastructure of Luke Creek Group rocks. One epiclastic sedimentary basin, the Mougooderra Formation, developed in the southern Murchison Province. It is not clear whether this basin developed contemporaneously with the volcanic complexes, or later. The contact between the Mougooderra Formation and the Luke Creek Group is an angular unconformity. Contacts between the volcanic complexes of the Mount Farmer Group and the Windaning Formation have not been observed, but are inferred to be unconformities mainly because the upper group was not deformed by the earliest phase of deformation (Chapter 5).

The lowest two formations, the Murrouli Basalt and the Golconda Formation, are not found south of latitude

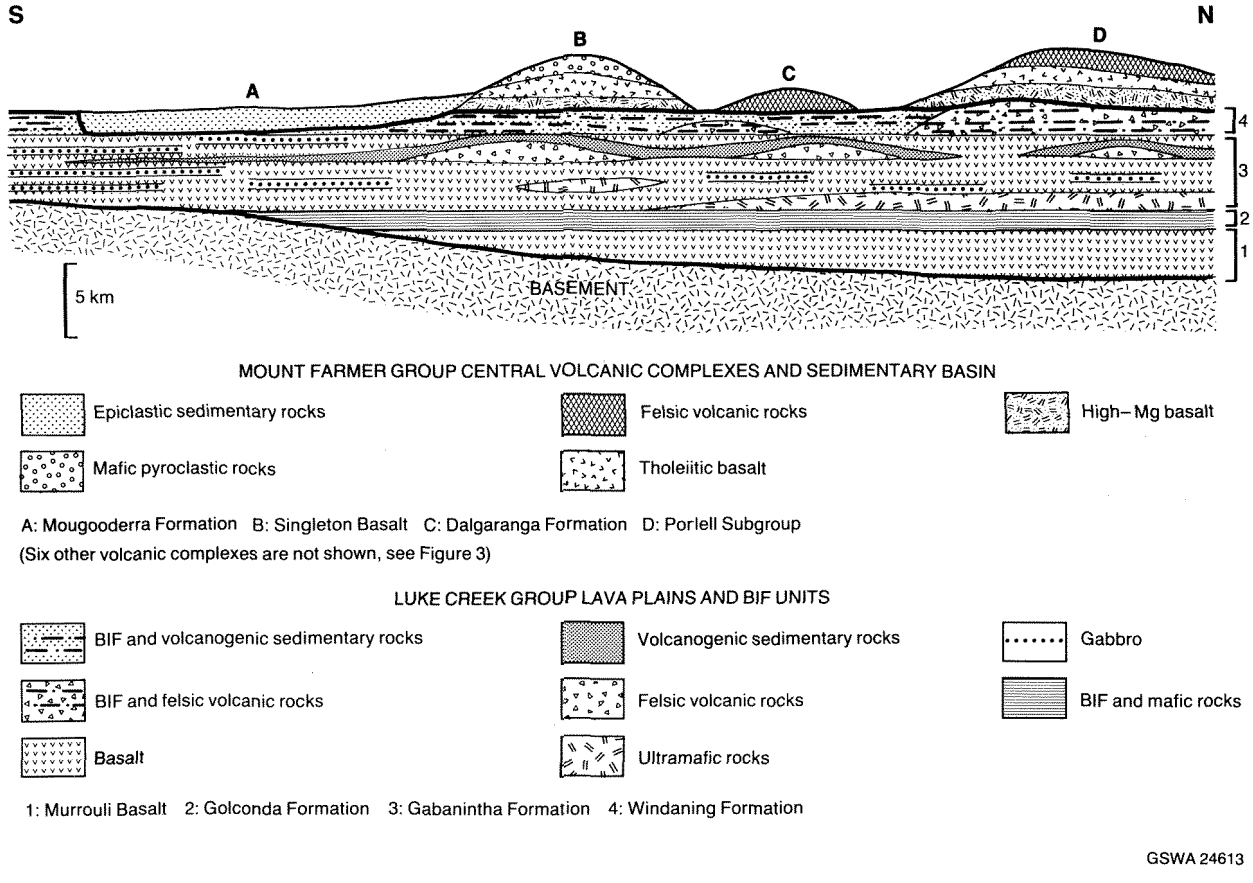


Figure 78. Schematic disposition of stratigraphic formations in the Murchison Supergroup. Not all Mount Farmer Group formations are shown.

28° 50'. It is possible that these were excised by intrusion of thick granitoid sheets into the base of the greenstone succession. These intrusions are now pegmatite-banded gneiss and recrystallized monzogranite (Chapter 3). However, xenoliths of rocks from these formations have not been identified in this region, and there is no aeromagnetic evidence to suggest that Golconda Formation BIF lies beneath the granitoids and gneiss. The alternative interpretation, that these formations were not developed south of 28° 50' is favoured in the absence of evidence to the contrary (Fig. 78).

The thickness of the Murchison Supergroup varies considerably throughout the province. This is due mainly to primary variations in stratigraphic thickness of individual formations, particularly those in the Mount Farmer Group. The thickest development is in the northern part of the Meekatharra–Wydgee greenstone belt where the Murchison Supergroup is about 15 km thick.

Geochemistry

Chemical compositions of 950 rock samples from the Murchison Supergroup have been documented and interpreted in this chapter. These analyses form the database (Appendix II) for one of the largest systematic regional geochemical surveys of Archaean greenstone belts undertaken to date in Western Australia. Several conclusions can be drawn from these data regarding the development of the Murchison Supergroup; these are summarized below.

Origin and crystallization of mafic magmas

Two groups of basalts have been distinguished; those with near-chondritic HFS element ratios, and those which show characteristics of crustal contamination. High-Mg and tholeiitic basalt occur in both groups.

Rocks from the first group were derived by partial melting of upper mantle rocks which were variably depleted or enriched in incompatible elements. Relatively simple REE patterns, with variably depleted or enriched LREE and flat HREE, suggest that garnet was not in equilibrium with the melt; thus, plagioclase lherzolite in the uppermost mantle is the most likely source. Tholeiitic compositions can be explained by simple models of 5–30% partial melting of plagioclase lherzolite followed by crystal fractionation of olivine, orthopyroxene, clinopyroxene, and, for more fractionated rocks, plagioclase and magnetite. However, the high MgO, Ni, and Cr contents of high-Mg basalt (e.g. Fig. 79) cannot be explained in the same way. High-Mg magma may have been generated by further partial melting of olivine-rich residue that remained after initial melting of plagioclase lherzolite had produced tholeiitic magma. Many high-Mg and tholeiitic basalt units

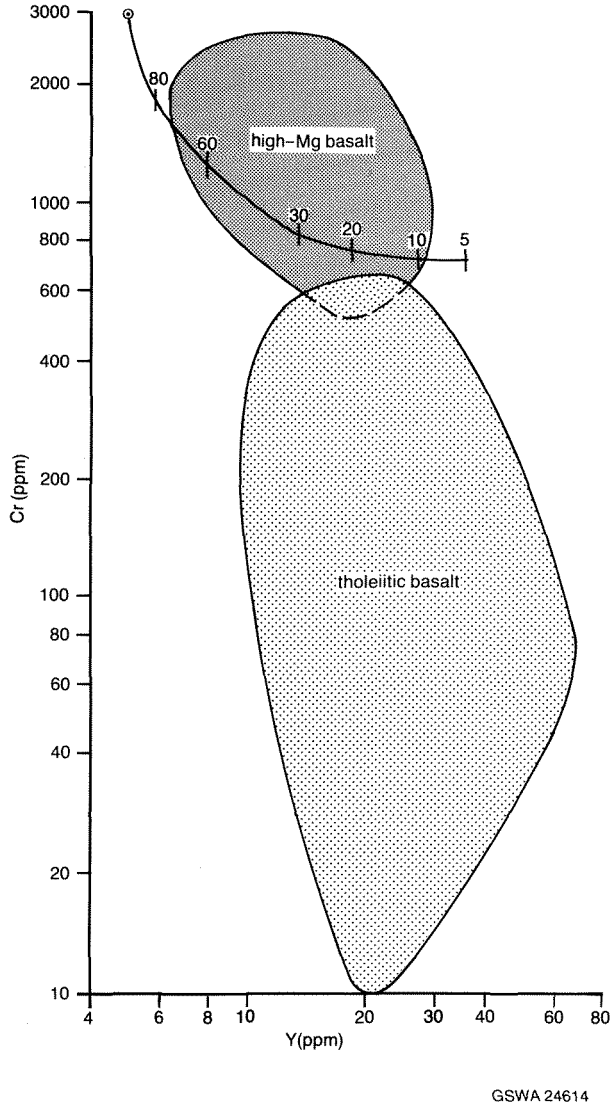


Figure 79. Compositional fields of Murchison Supergroup high-Mg basalt and tholeiitic basalt on a Cr–Y diagram. Estimated mantle compositon and ratio as in Figure 10.

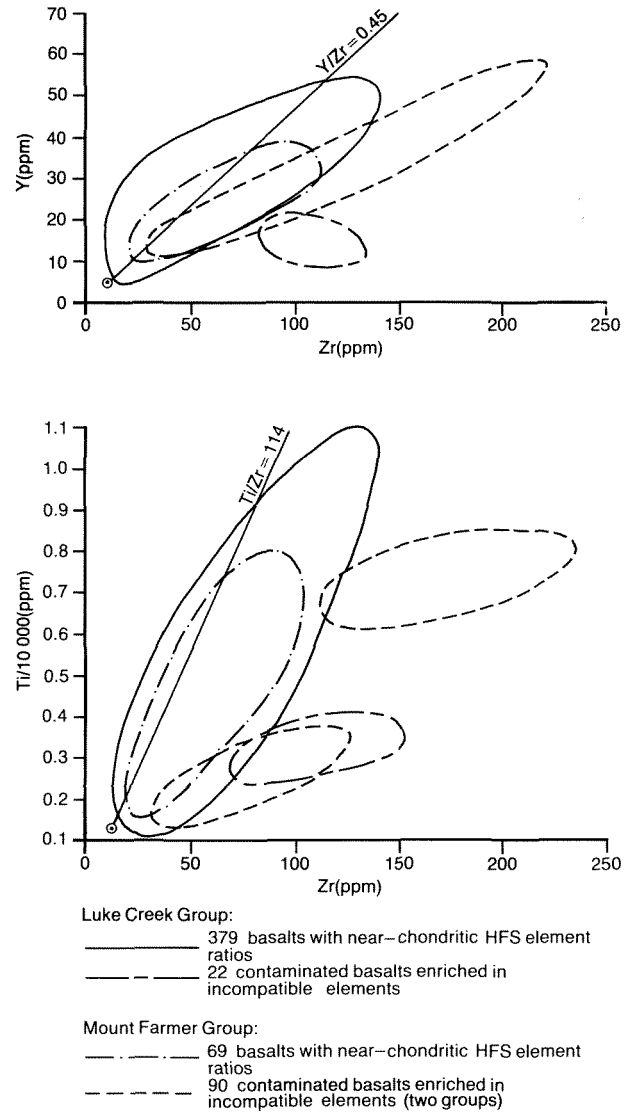


Figure 80. Compositional fields of the two types of Murchison Supergroup basalt plotted on Y–Zr and Ti–Zr diagrams. Estimated mantle composition and ratios as in Figure 7.

appear to be genetically linked, particularly when they are interlayered.

Rocks from the second group, those enriched in incompatible elements, were contaminated by assimilation of felsic crustal material. Most of these rocks show enrichment in SiO_2, K_2O, Ba, Rb, Zr, La, and Ce, and depletion of TiO_2 and V relative to basalts with near-chondritic HFS element ratios. They have trends on Y–Zr and Ti–Zr diagrams which cannot be explained by crystal fractionation. Apart from these enrichments and depletions, the basalts show evidence of primary derivation from upper mantle plagioclase lherzolite by degrees of partial melting similar to those for rocks of the other group. Most rocks in this group occur in the upper part of the Murchison Supergroup. Five of the eight basalt formations sampled in the Mount Farmer Group show evidence of crustal contamination, but few samples from the Luke Creek Group have these characteristics (Fig. 80). It is more likely that assimilation occurred during ascent of magma through the crust, rather than during eruption over felsic or sedimentary rocks, as most mafic piles are monotonous and have few felsic or sedimentary interlayers. Potential contaminants include the felsic complexes of the upper Luke Creek Group, and thick sheets of granitoid (now pegmatite-banded gneiss) emplaced in the base of the Murchison Supergroup prior to development of the Mount Farmer Group. Compositions of contaminated basalts were further modified by fractional crystallization of olivine and pyroxenes.

Origin and crystallization of felsic magmas

Markedly non-chondritic HFS element ratios, strong

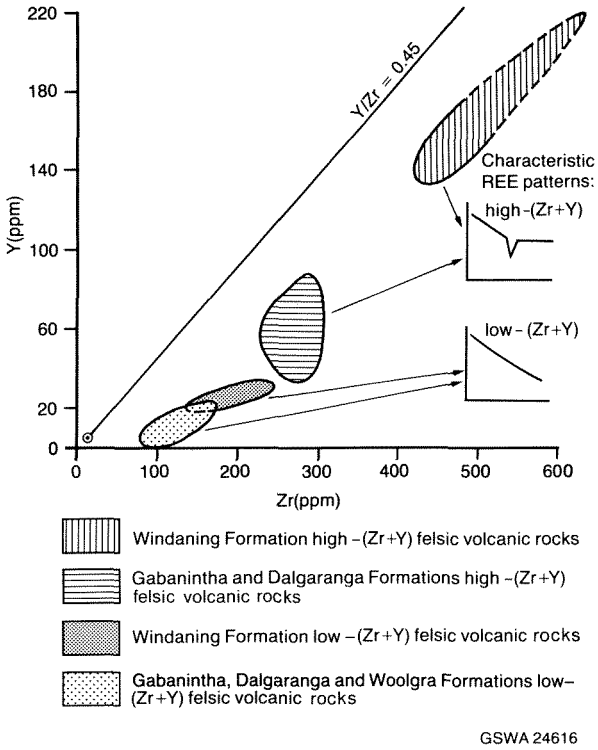


Figure 81. Compositional fields and REE pattern characteristics of the two types of Murchison Supergroup felsic volcanic rocks. Estimated mantle composition and ratios as in Figure 7.

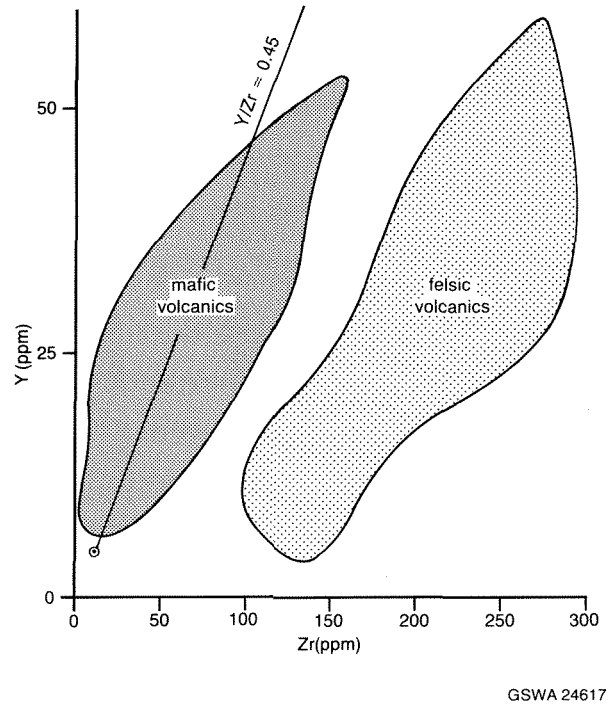


Figure 82. Compositional fields of mafic and felsic volcanic rocks from bimodal sequences in the Murchison Supergroup plotted on an Y–Zr diagram. Estimated mantle composition and ratios as in Figure 7.

LREE enrichments, and calc-alkaline trends of felsic volcanic rocks preclude a mantle source origin, either by partial melting of lherzolite, or crystal fractionation of mantle-derived tholeiite magma. Two types of compositionally distinct, crustally derived, felsic volcanic rocks have been identified — a high-(Zr+Y) type and a low-(Zr+Y) type (Fig. 81). The high-(Zr+Y) type is characterized by high Zr and Y contents, low MgO, Ni, and Cr contents, strong LREE enrichment, flat or slightly enriched HREE, and a negative Eu anomaly. The low-(Zr+Y) type characteristically has low Zr and Y contents, relatively high MgO, Ni, and Cr contents, and fractionated REE patterns with no Eu anomalies. Chemical compositions of the more abundant low-(Zr+Y) felsic volcanic rocks are consistent with a two-stage derivation process. Upper mantle lherzolite was partially melted to produce basalt or gabbro in the crust; this material was hydrated to form amphibolite. The amphibolite was subsequently partially melted to form low-(Zr+Y) felsic volcanic magma. High-(Zr+Y) felsic volcanic magma did not equilibrate with garnet or amphibole in the source, and was probably derived from a felsic crustal source such as pyroxene–plagioclase granulite. High $\varepsilon_{Nd}(T)$ values indicate that both mafic and felsic source rocks had short crustal residence times prior to partial melting. Most low-(Zr+Y) felsic volcanic rocks are andesite and dacite. Most high-(Zr+Y) rocks are rhyolite.

Bimodal volcanism

The Gabanintha Formation and the Porlell and Yalgoo Subgroups are characterized by bimodal volcanism. Basalt and minor amounts of ultramafic rock, which comprise about 70% of these sequences, are overlain by felsic volcanic rocks and associated volcanogenic sedimentary rocks. In the upper Gabanintha Formation, mafic and felsic volcanic rocks are interlayered on a regional scale (Fig. 78). Mafic and felsic rocks in these sequences are chemically unrelated (Fig. 82) and were derived from different sources — basalts from the upper mantle, and felsic volcanics from the crust. This type of compositional independence of associated mafic and felsic volcanic rocks is typical of Archaean bimodal sequences, and must reflect some fundamental process in their development. Felsic magma could have been derived by partial melting of lower crustal rocks caused by (?)local elevation of isotherms above solidus temperatures due to the passage of large quantities of mafic magma through the crust (cf. Huppert and Sparks, 1988). Differences in the rheological properties of the two types of magma would have controlled their relative rates of ascent. Mafic magma, being much less viscous (Scarfe and Hamilton, 1980), would have reached the surface before felsic magma, resulting in the observed distribution of rock types. Much mafic magma would have to pass through localized regions of the lower crust before isotherms were elevated sufficiently to cause partial melting.

Chemostratigraphic variation

There are a number of regional-scale variations in the chemistry of the Murchison Supergroup. The main chemical difference between the Luke Creek and Mount Farmer

Groups is the abundance in the latter of basalts enriched in incompatible elements. All basalts sampled in the Mount Farmer Group, except those from the Porlell Subgroup and Singleton Basalt, show evidence of crustal contamination. No other major differences in geochemistry have been recognized between the two groups. Systematic lateral variation of basalt chemistry occurs on a regional scale in the Gabanintha Formation. Basalts in the north are characteristically enriched in Zr, Sr, and LREE, and depleted in Y, compared with those in the south of the province. There is a zone separating these regions in which both basalt types occur. There are insufficient data to determine if this is a feature of other Luke Creek Group Formation basalts, although the available data suggest that it may be. These regional chemical differences are not propagated into the Mount Farmer Group. Incompatible element contents of uncontaminated Porlell Subgroup basalts in the north, and Singleton Basalt in the south, are broadly similar. There is no regional-scale lateral or vertical systematic variation of felsic volcanic geochemistry. Thus, it appears that there was probably a fundamental difference in the chemistry of the upper mantle, between the northern and southern parts of the Murchison Province, during development of the Luke Creek Group.

Volcanic chemostratigraphy is complex on a local scale. Chemically distinct volcanic units have been identified in lithologically monotonous sequences of both mafic and felsic volcanic rocks. These were not identified as distinct units in the field. It is not possible to correlate individual units on a chemical basis over distances larger than a few tens of kilometres. Data from traverses across mafic and felsic units generally plot on well-defined trends, indicating progressive fractionation of mineral phases. However, there is rarely a relationship between the stratigraphic positions of samples and the degree of fractionation. For most units it appears that, while individual lava flows may be related to others in the same pile by crystal fractionation, their order of extrusion is not systematic; this is also a common feature of Phanerozoic volcanoes (Cox, Bell, and Pankhurst, 1979). This type of volcanic chemostratigraphy can be explained in two ways. The magma chambers from which the volcanics were derived could have been chemically zoned; if magma was tapped from several different levels within such a chamber then a non-systematic volcanic chemostratigraphy would result (Cox, Bell and Pankhurst, 1979). Alternatively, progressively fractionating magma chambers could have been periodically refilled, from the upper mantle, by primitive unfractionated magma (O'Hara, 1977). Lava flows erupted from such magma chambers could have complex non-systematic chemical interrelationships. Both these processes may have been operating during development of the Murchison Supergroup. Flow differentiation, assimilation of crustal material, seafloor alteration, and tectonic repetition, may also have complicated the chemostratigraphy of these volcanic units.

Geochronology

The time span of greenstone belt development in the Murchison Province is very poorly constrained. Most published age determinations are on rocks from the upper part of the Gabanintha Formation, which consistently give ages of about 3.0 Ga (Table 14). Sm–Nd model ages of Luke Creek Group and Mount Farmer Group felsic volcanic rocks are indistinguishable. A Sm–Nd isochron on a Woolgra Formation felsic volcanic whole-rock sample, and igneous mineral and material separates from it, gave a date of 2818 ± 57 Ma for the top of the Supergroup in the northern Murchison Province. This date has been interpreted as a crystallization age.

The available geochronology thus hints at an appreciable time gap between development of the Luke Creek Group at about 3.0 Ga and development of at least the Porlell Subgroup of the Mount Farmer Group at about 2.8 Ga.

Chapter 3

Gneiss and granitoids

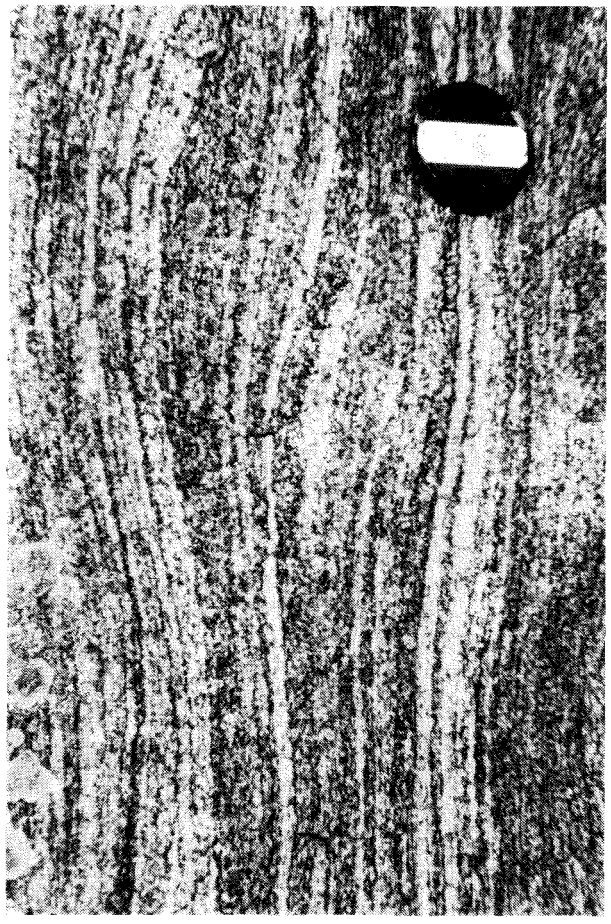
Most of the Murchison Province consists of gneiss or granitoids (Plate 1). These rocks occur mainly in large complexes between greenstone belts, although many of the later intrusions are within these belts. Previous GSWA mapping in the Murchison Province distinguished granitoid rocks on the basis of rock type and texture, usually from field observations. In this bulletin, granitoids are classified on the basis of relative chronology (from field relations and isotopic analysis) and geochemical characteristics; rock type and texture are considered as variants within this classification. Four suites of siliceous plutonic rocks have been distinguished. These are, in order of intrusion, pegmatite-banded gneiss, recrystallized monzogranite, and two broadly contemporaneous suites of post-folding granitoids. Pegmatite-banded gneiss and recrystallized monzogranite intruded the base of the Murchison Supergroup as extensive, thick, subhorizontal, tabular bodies; most post-folding granitoids were probably emplaced as steep-sided, cylindrical or inverted tear-drop shaped bodies. Each plutonic suite is described in terms of its field relations, petrography, geochemistry and petrogenesis, and geochronology.

Pegmatite-banded gneiss

Field relations

In the Murchison Province, outcrops of pegmatite-banded gneiss increase in abundance towards the west. The gneiss occurs as a broad northeasterly trending belt of rocks in the west; as abundant large enclaves and rafts in recrystallized monzogranite in the centre; and as occasional rafts and xenoliths in recrystallized monzogranite in the east of the province (Plate 2). The belt of pegmatite-banded gneiss in the west has been described by Myers (1990) as the Murgoo Gneiss Complex.

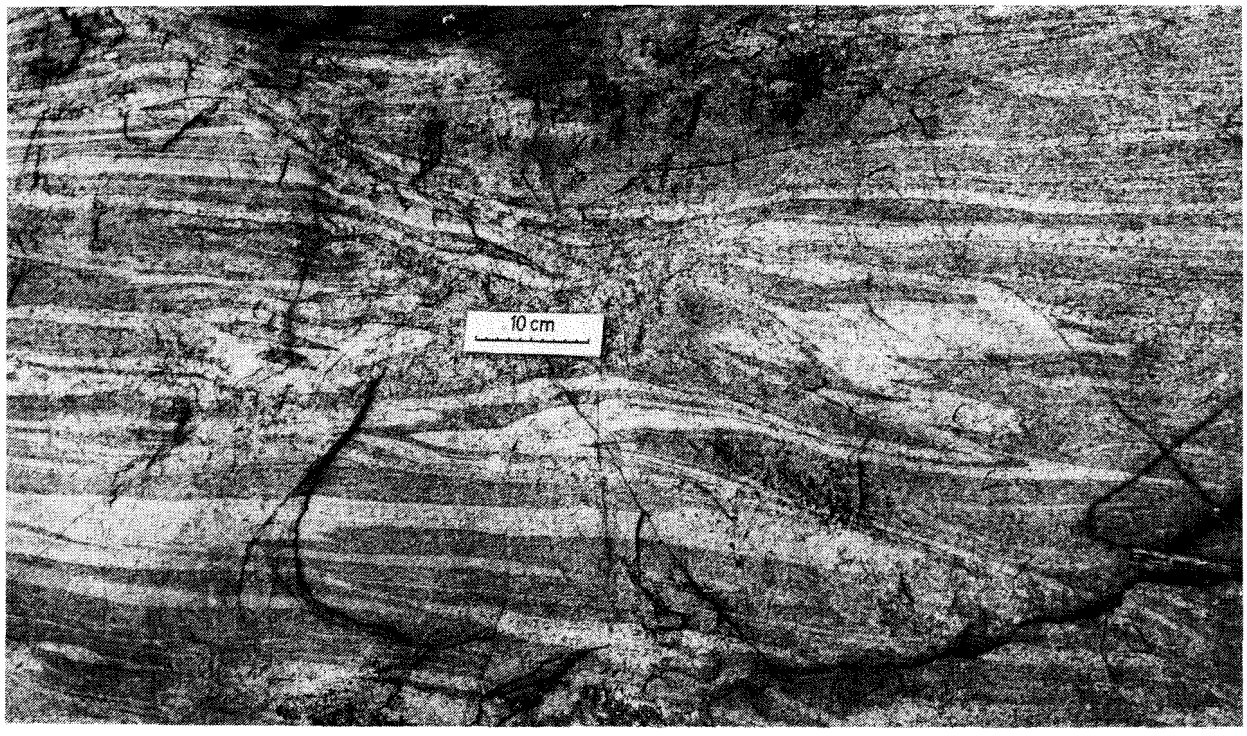
The gneiss has three components — two monzogranite–granodiorite phases and a pegmatite phase. The first monzogranite–granodiorite phase now consists of medium-grained, finely banded, biotite-rich and quartz–feldspar-rich layers, a few millimetres to 1 cm thick (Fig. 83). These layers are monzogranite or granodiorite in composition. The pegmatite phase consists of medium- to coarse-grained quartz–feldspar bands a few centimetres thick. These components are interlayered parallel to the



GSWA 24618

Figure 83. Monzogranite–granodiorite component of pegmatite-banded gneiss; the lens cap is 5cm across.

gneissosity (Fig. 84). Pegmatite bands are less abundant in the western than in the central part of the Murchison Province (Fig. 85). The overall gneissosity reflects intense deformation during which planar elements (such as pegmatites, aplite veins, mafic dykes, and schlieren) and other heterogeneities (such as feldspar phenocrysts, agmatites, and xenoliths) were rotated into subparallelism, and attenuated (cf. Myers, 1978). The second phase of monzogranite–granodiorite intruded the earlier components as veins and dykes during the deformation which formed the gneissosity. This phase also became banded, and it cuts the earlier components of gneiss at very low angles (Fig. 86). It is a minor component of pegmatite-



GSWA 24619

Figure 84. Interlayered monzogranite–granodiorite gneiss and pegmatite bands forming typical pegmatite-banded gneiss.



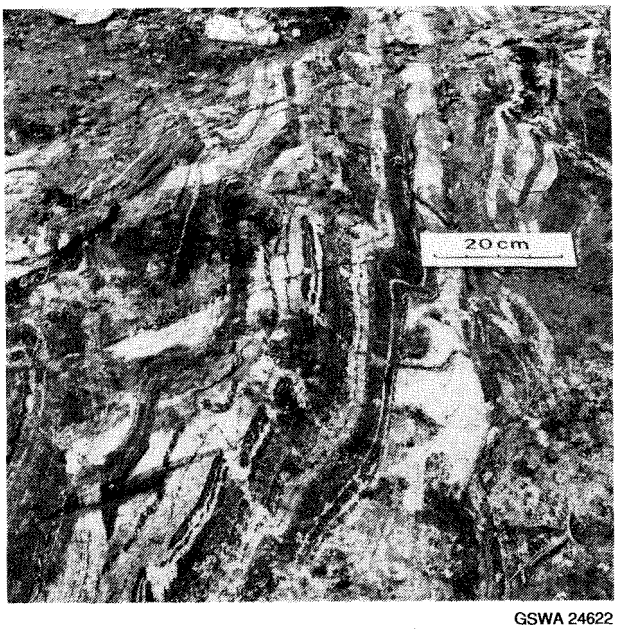
GSWA 24620

Figure 85. Raft of pegmatite-banded gneiss in recrystallized monzogranite from the western part of the Murchison Province. Note that pegmatite bands are relatively scarce in the gneiss (compare with Figure 84).



GSWA 24621

Figure 86. Two phases of monzogranite–granodiorite gneiss: a dyke of monzogranite gneiss runs from bottom left to top centre of the photograph (indicated by arrows), truncating banding in the surrounding gneiss at very low angles. the dyke is about 10cm wide. A prominent layer of leucocratic material occurs on its left side. The hammer head is 17cm across.



GSWA 24622

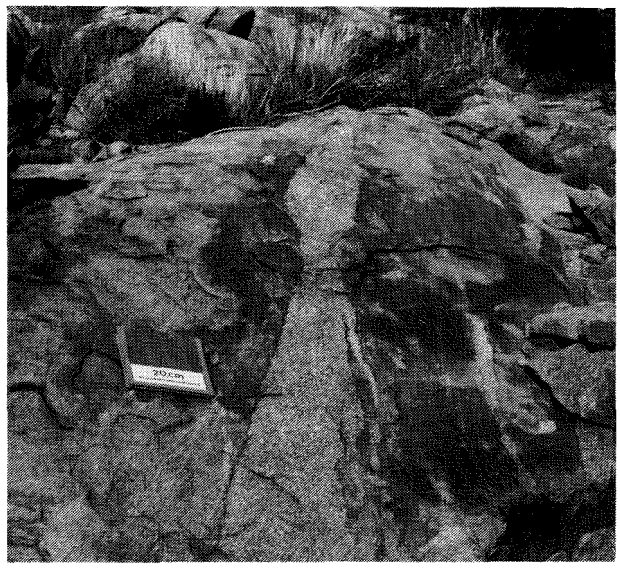
Figure 87. Pegmatite-banded gneiss (light grey) interlayered with amphibolite (dark grey) at the margin of a large amphibolite–BIF raft in the gneiss.

banded gneiss in the eastern and central parts of the province, but in the west of the province in the Murgoo Gneiss Complex (Myers, 1990), it is more voluminous, less deformed, and contains abundant remnants of the first two phases of gneiss.

Large rafts of amphibolite and BIF are interlayered with pegmatite-banded gneiss in some outcrops, for example, 20 km southwest of Badja Homestead, and 15 km northeast of Murdanna Rock (Plate 1). In a few outcrops, elongate pods and lenses of amphibolite up to a few tens of metres long, which may be remnants of mafic dykes or supracrustal xenoliths, occur subparallel to the gneissosity. These rocks generally record upper amphibolite facies conditions of metamorphism (Plate 3). The margins of these units are generally sheared against pegmatite-banded gneiss; however, in some outcrops the gneiss is intimately interlayered with amphibolite and BIF (Fig. 87), which suggests an originally intrusive relationship.

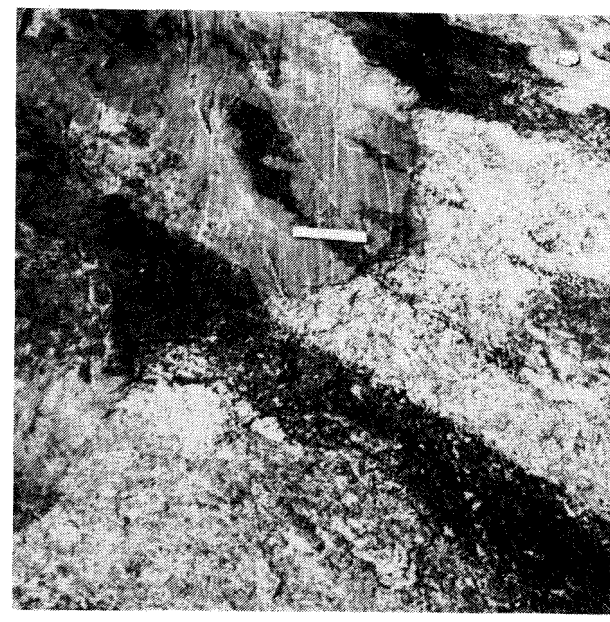
Pegmatite-banded gneiss is pervasively intruded by veins, dykes, and plutons of recrystallized monzogranite; many outcrops are a mixture of rocks from these two suites. The veins and dykes range from strongly foliated units which are difficult to distinguish from the gneiss, to weakly foliated units (Fig. 88). Most contacts between pegmatite-banded gneiss and recrystallized monzogranite are intrusive (Figs 88 and 89); however, many appear to be gradational (e.g. at Chiggarrie Rock on CUE), and some are sheared. Xenoliths of pegmatite-banded gneiss are abundant in recrystallized monzogranite. These range from large internally coherent rafts, several tens to hundreds of metres across and with sharp contacts (Fig. 89); through partially assimilated xenoliths, a few metres across, with indistinct contacts (Fig. 90); to patches of nebulitic banding which represent almost completely assimilated xenoliths (Fig. 91). In a few outcrops, pegmatite-banded gneiss grades into zones of stictolithic to schlieren structured injection migmatite (terminology after Mehnert, 1971, p. 11) (Fig. 92). Metamorphic grade in the paleosome is generally lower amphibolite facies, a fact which precludes partial melting of pegmatite-banded gneiss as the source of the neosome. The neosome is recrystallized and is probably a fractionated phase of recrystallized monzogranite.

In an outcrop 20 km southwest of Badja Homestead, amphibolite and BIF are interlayered with pegmatite-banded gneiss in dome-and-basin patterns (Fig. 93, and Chapter 5). When the effects of upright F_2 and F_3 folding are removed these units form a subhorizontal interlayered sequence. The simplest interpretation of field relations is that gneiss protoliths intruded the greenstones as thick subhorizontal sheets, and were further interleaved by tectonic processes which imparted a subhorizontal gneissosity; magmatism and tectonism were broadly coeval (cf. Myers, 1984). Amphibolite and BIF in this outcrop closely resemble (in grain size, mineralogy and appearance) rock units of the Windaning Formation which occur around the southern rim of the recrystallized monzogranite body 50



GSWA 24623

Figure 88. Recrystallized monzogranite dyke and veins intruding pegmatite-banded gneiss.



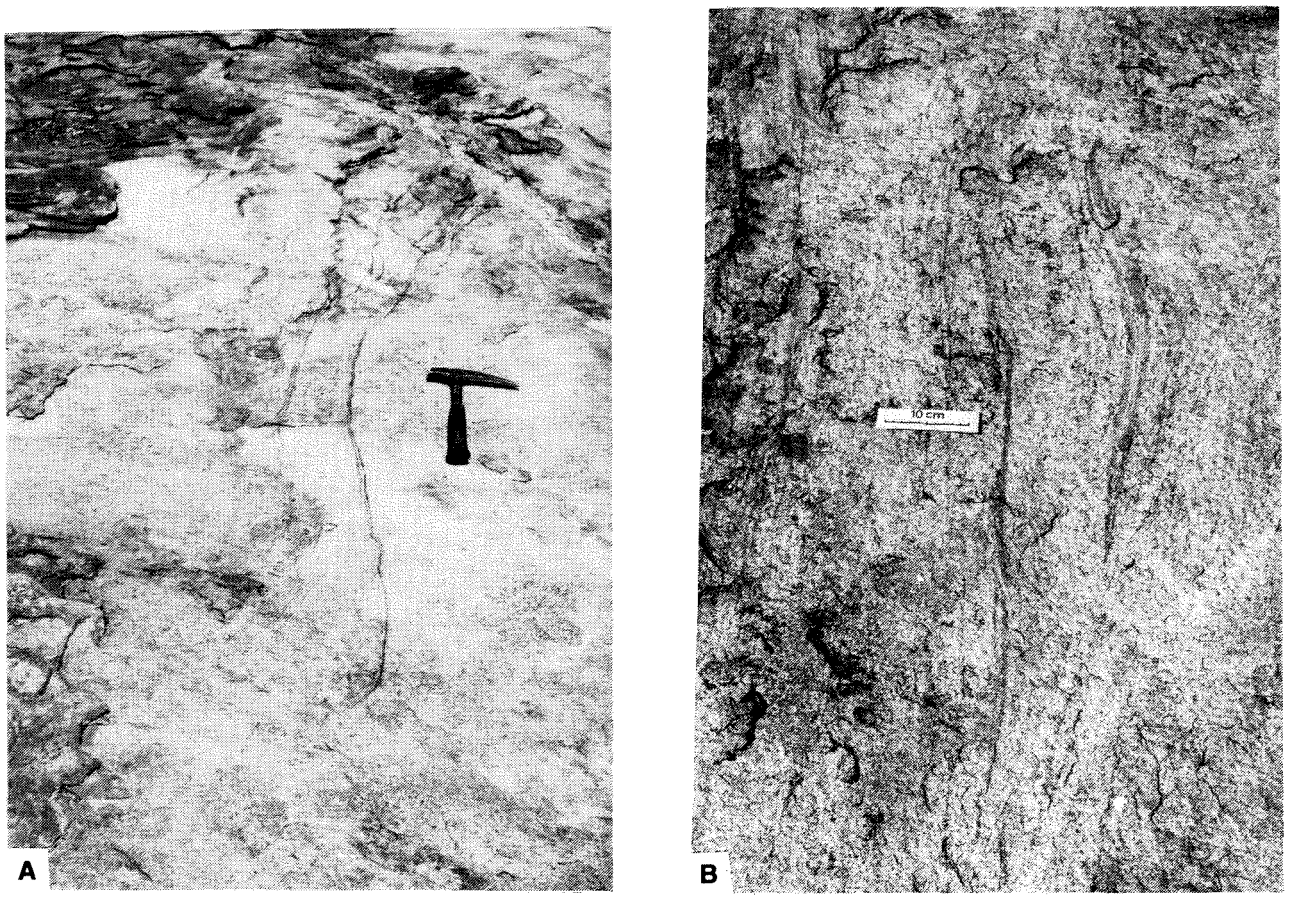
GSWA 24624

Figure 89. Intrusive contact between porphyritic recrystallized monzogranite and the margin of a large coherent raft of pegmatite-banded gneiss; the scale bar is 10cm long.



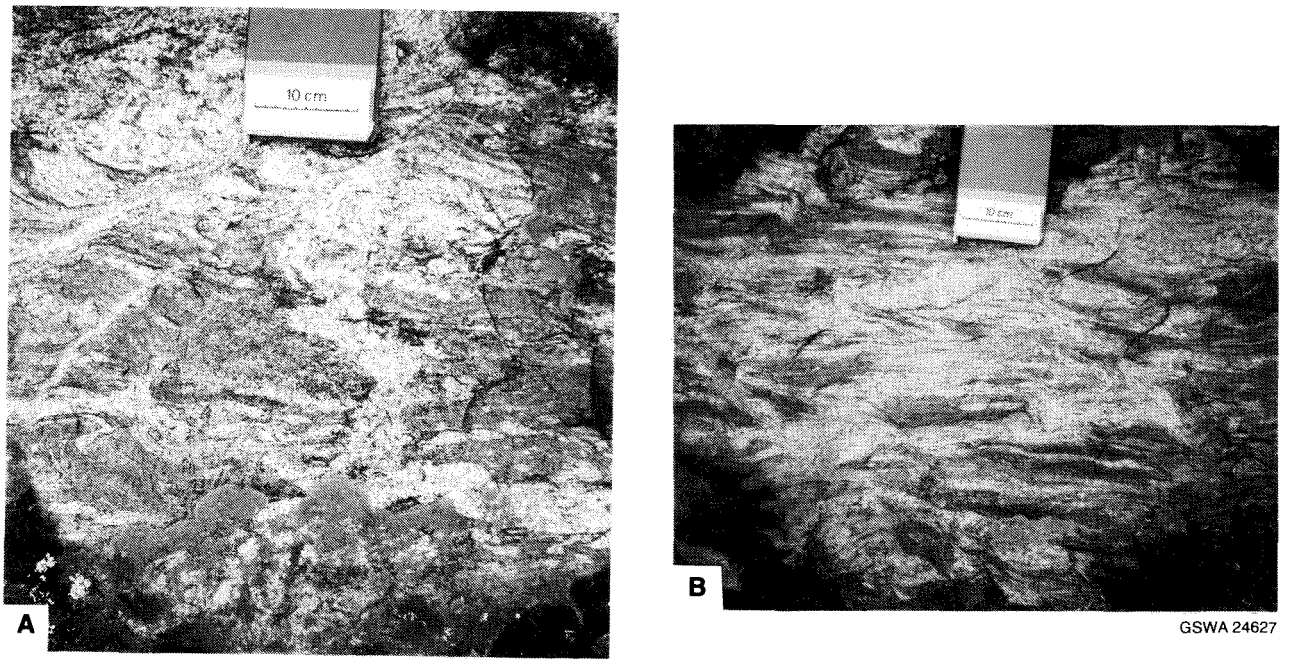
GSWA 24625

Figure 90. Partly assimilated xenolith of pegmatite-banded gneiss in equigranular recrystallized monzogranite. Note the indistinct contact.



GSWA 24626

Figure 91. Examples of nebulitic banding in recrystallized monzogranite after almost completely assimilated xenoliths of pegmatite-banded gneiss. The hammer is 30cm long.



GSWA 24627

Figure 92. Examples of injection migmatite formed by lit-par-lit intrusion of a fractionated phase of recrystallized monzogranite into pegmatite-banded gneiss. A — stictolithic structure; B — schlieren structure (Mehnert, 1971)

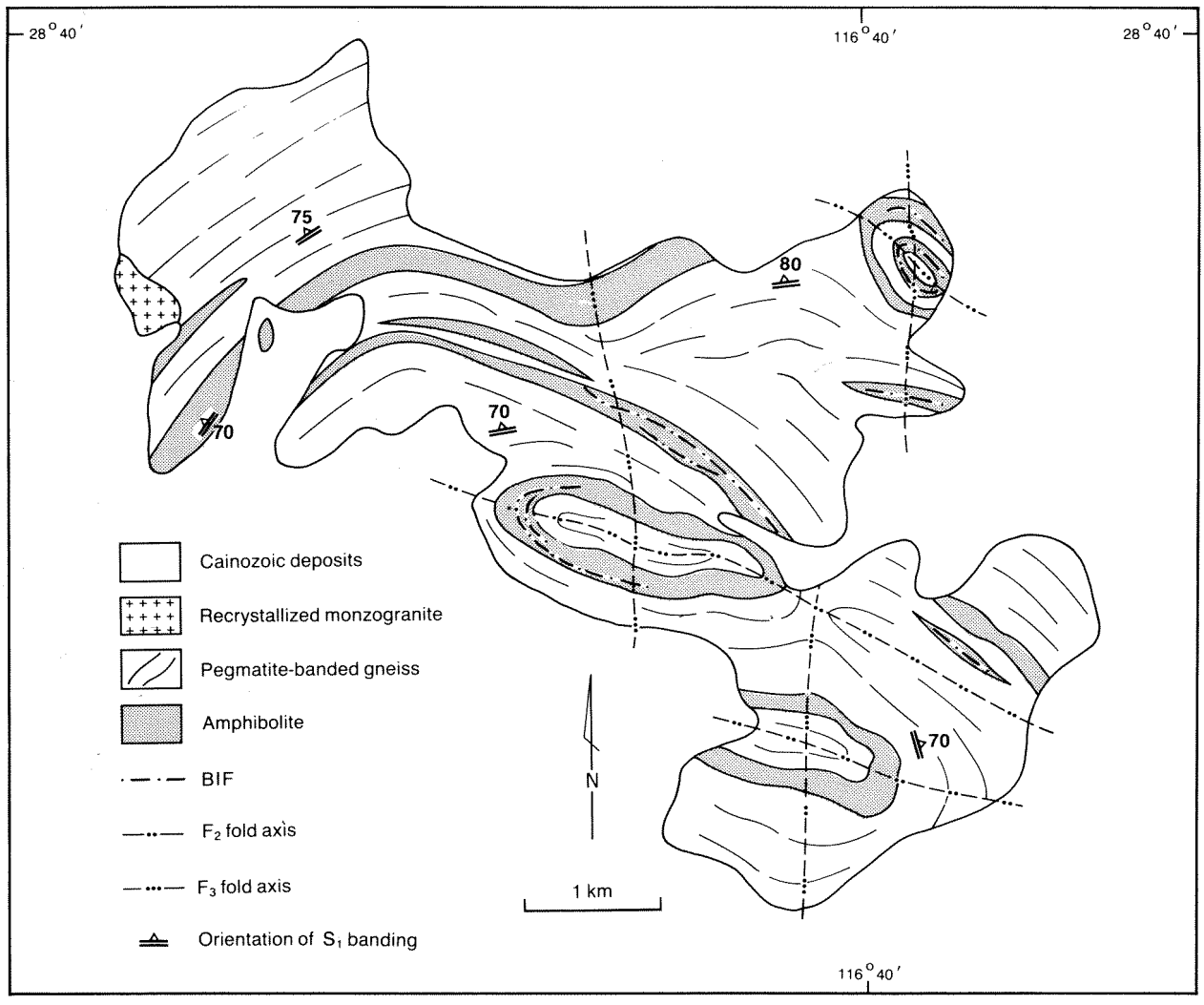


Figure 93. Outcrop geology of complexly folded and interlayered BIF, amphibolite, and pegmatite-banded gneiss 38 km south of Yalgoo.

km to the south, from north of the Blue Hill Range to northeast of Kadji Kadji Homestead (Plate 2). If this correlation is correct, then gneiss protoliths must have been emplaced into the greenstone succession after development of the Luke Creek Group. There is no evidence to suggest that pegmatite-banded gneiss intruded the Mount Farmer Group. The few exposed contacts between greenstone belts and gneiss (Plate 2) are strongly sheared.

Petrography

Pegmatite-banded gneiss generally comprises assemblages of quartz–oligoclase–microcline–biotite. Minor phases include opaque minerals, epidote, sphene, apatite, and zircon. K-feldspar is generally perthitic microcline, although perthite also occurs. Oligoclase is generally rimmed by albite and is weakly to moderately saussuritized. Myrmekite occurs in some samples. Biotite is partially retrograded to aggregates of chlorite and rutile in many samples. Monzogranite–granodiorite gneiss is generally leucocratic, with less than 10% phyllosilicates. Pegmatite bands comprise microcline, oligoclase, and quartz, with less than 1% phyllosilicates. Fabrics are granoblastic (Fig. 94) or lepidoblastic; gneissic layering is defined by variations in biotite content. Grain boundaries are interlobate and form a consertal texture. There are generally no remnants of igneous texture. Protomylonitic texture was developed in some regions of very high strain, but is now partly or completely recrystallized into mortar texture (Fig. 95).

Geochemistry and petrogenesis

Eleven samples of pegmatite-banded gneiss were collected for chemical analysis, 8 from the enclave 12 km west of the Warda Warra greenstone belt, the Buongnoo outcrop, and 3 from the enclave 20 km southwest of Badja Homestead, the Badja outcrop, (Plate 2, and units numbered 1 and 2, respectively, in Figure 96). The more obvious pegmatite-bands were avoided during sampling so that compositions reflect the first monzogranite–granodiorite phase of the gneiss.

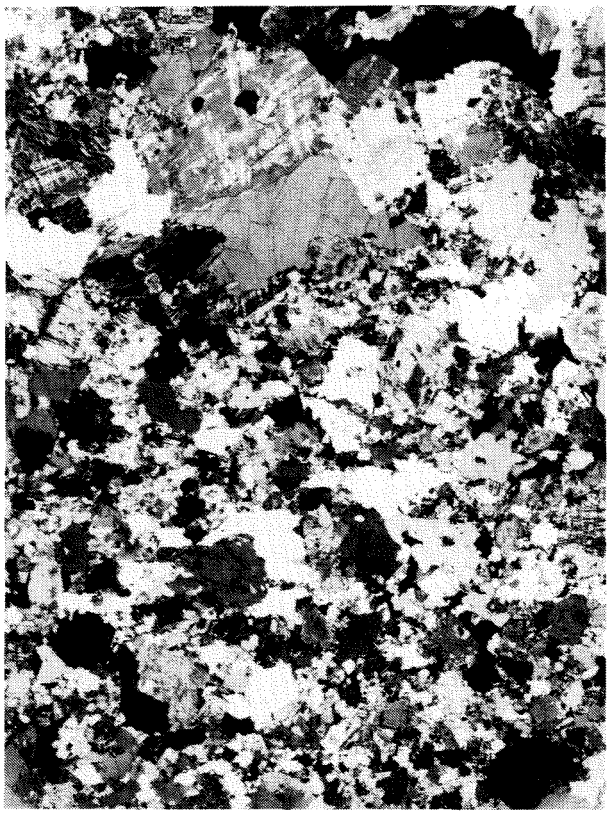


Figure 94. Photomicrograph of pegmatite-banded gneiss showing granoblastic texture. The coarse-grained region is part of a pegmatite band.

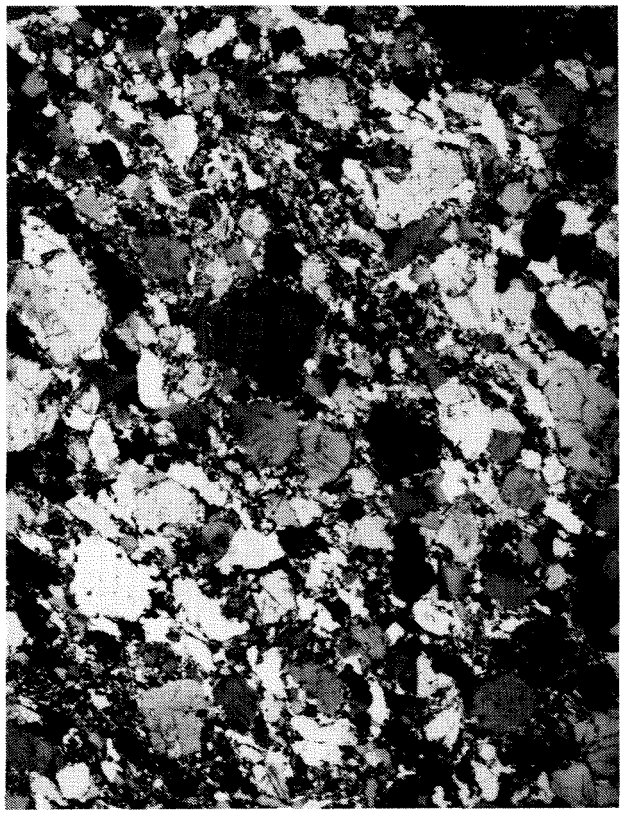


Figure 95. Photomicrograph of pegmatite-banded gneiss showing mortar texture.

Mean compositions of pegmatite-banded gneisses in the Buongnoo and Badja outcrops are given in Table 28. The gneiss in the Buongnoo outcrop is slightly more fractionated than that in the Badja outcrop. Compositions are broadly similar to other 'grey gneisses' of similar age elsewhere in the world (e.g. Condie, 1981; Martin et al., 1983; Taylor et al., 1984). Both sample groups have peraluminous compositions and are calcic according to Peacock's (1931) alkali–lime index (Fig. 97). They have a broadly calc-alkaline trend, although this is displaced towards Na-rich compositions (Fig. 98), in common with many ancient granitoid suites (Brown, 1981).

With the exception of Fe_2O_3, samples from the two groups have similar major-oxide compositions and colinear trends on Harker variation diagrams (Fig. 99). However, there are significant differences in Rb, Sr, Th, Nb, and Y contents (Table 28). Differences in Pb, Li, and La are not as significant, as there is large variation within each sample group for these elements (Appendix II). The mean Rb–Sr ratio for the Badja outcrop is 0.14 compared with 0.78 at Buongnoo, although Rb–Sr data for both gneiss bodies plot on the same trend (Fig. 100). Most trace elements can be correlated with other related trace elements and major oxides in a similar way. Thus, major and trace-element geochemistry is consistent with derivation of both gneiss bodies from similar sources; the minor compositional differences may be due to different degrees of partial melting, or differentiation during ascent of magma.

REE patterns for the three pegmatite-banded gneiss samples from the Badja outcrop are strongly fractionated with mean $(La/Yb)_N = 110.3$ (Fig. 101). Leucocratic and mesocratic bands separated from sample 83398 have positive and negative Eu anomalies respectively. The positive anomaly is due to the high feldspar content of leucocratic bands. Combining the REE contents of leucocratic and mesocratic bands would eliminate these anomalies. REE patterns of pegmatite-banded gneiss are more fractionated than most monzogranites and granodiorites, and the mean total REE content of 119.8 ppm is relatively low (Cullers and Graf, 1984). High LREE/HREE ratios require much residual garnet and/or amphibole in the source. Plagioclase was not an important residual or fractionating phase, although it may have been a relatively minor phase in the source which would account for the small negative Eu anomalies for samples 83339 and 83401. Monzogranites with no Eu anomalies, and with high LREE/HREE ratios, generally require eclogite or quartz-eclogite sources (Ewing, 1979, Jahn et al., 1980). However, the very small negative Eu anomalies probably indicate some involvement of plagioclase. Thus, it is more likely that the source material was mafic granulite, garnet amphibolite, or tonalite (e.g. Glikson, 1976; Drury, 1979; Cullers and Graf, 1984a), although distinction between various garnet-bearing sources of mafic composition is uncertain (Drury, 1978). Some sphene and/or allanite may have fractionated from the melt to reduce the total REE content (Gromet and Silver, 1983); alternatively, the source may have been depleted in REE.

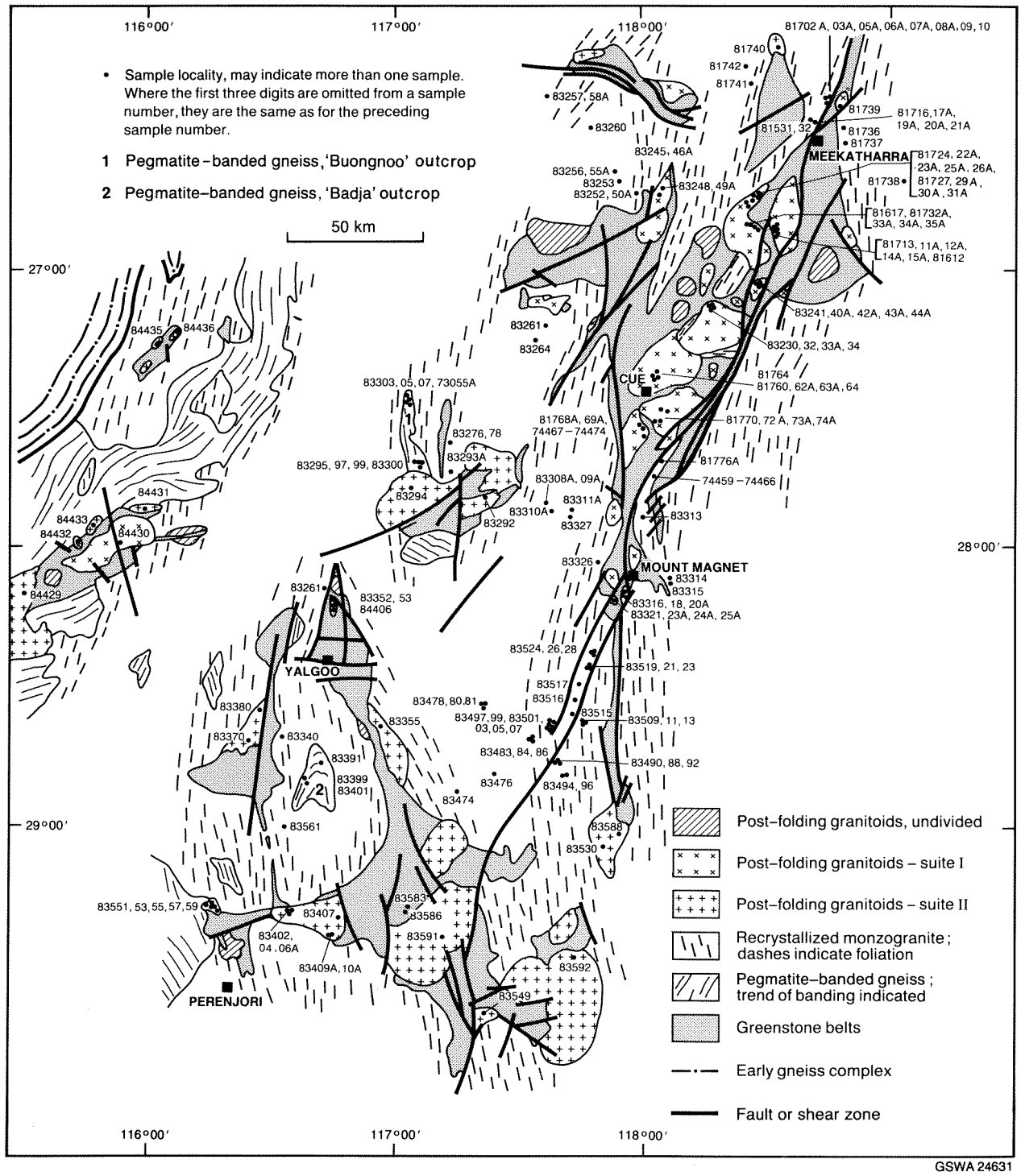


Figure 96. Granitoid geochemistry sample localities.

TABLE 28. MEAN COMPOSITIONS OF PEGMATITE-BANDED GNEISS

	Buongnoo n=8	*Badja n=3*
	Percentage	
SiO_2	72.2	71.1
Al_2O_3	14.3	15.2
Fe_2O_3	1.0	0.5
FeO	0.94	1.39
FeO* (a)	1.8	1.8
MgO	0.45	0.54
CaO	1.58	2.14
Na_2O	3.90	4.63
K_2O	3.48	2.26
TiO_2	0.22	0.23
P_2O_5	0.09	0.09
MnO	0.03	0.02
LOI	0.76	0.62
	Parts per million	
F	330	460
Ba	1067	1056
Cu	11	10
Pb	18	12
Li	30	90
Mo	<1	2
Ni	21	27
Nb	13	<10
Rb	183	78
Sr	236	546
Th	29	10
Sn	7	<5
U	2	<1
V	17	24
W	(b) <2	(c) <2
Y	8	<5
Zn	41	39
Zr	166	155
La	(b) 24	(c) 41
Ce	(b) 42	(c) 55

(a) All Fe calculated as FeO (b) One analysis only (c) Two analyses only

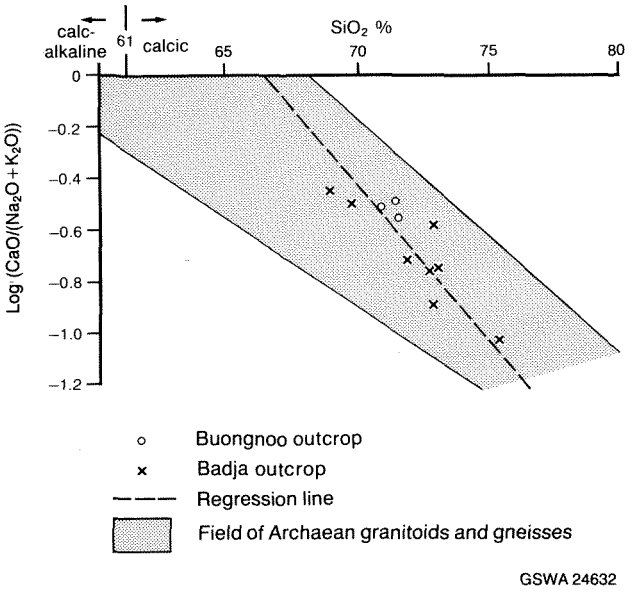


Figure 97. Log ($CaO/(Na_2O + K_2O)$) v. SiO_2 diagram for pegmatite-banded gneiss samples compared with a range of Archaean granitoids and gneisses from southern Africa (Anhaeusser and Robb, 1983; Robb, 1983; Robb et al., 1984); Canada (Frith and Fryer, 1985); India (Allen et al., 1986); the Pilbara Craton (Bickle et al., 1983; Davey and Lewis, 1986); and the Yilgarn Craton (Foden et al., 1984). The alkali-lime index is the SiO_2 concentration where $CaO = Na_2O+K_2O$, i.e. where log ($CaO/(Na_2O+K_2O)$) =0. The dashed line is a regression through the sample data.

Pegmatite-banded gneiss data partly straddle the plagioclase–K-feldspar cotectic on a CIPW-normative Ab–Or–An diagram, and plot in the low-temperature part of the plagioclase–quartz field on an Ab–Or–Qz diagram (Fig. 102). Gneiss protoliths initially crystallized with plagioclase and quartz on the liquidus, and K-feldspar crystallized from the melt later (Winkler, 1979). Biotite probably crystallized after initial plagioclase crystallization. During crystallization the degree of plagioclase solid-solution remained constant, at calcic oligoclase. Fluid pressure was probably high, resulting in the abundance of pegmatites. The gneiss from Badja plots in higher temperature regions of the diagram than that from Buongnoo, reflecting its less fractionated composition.

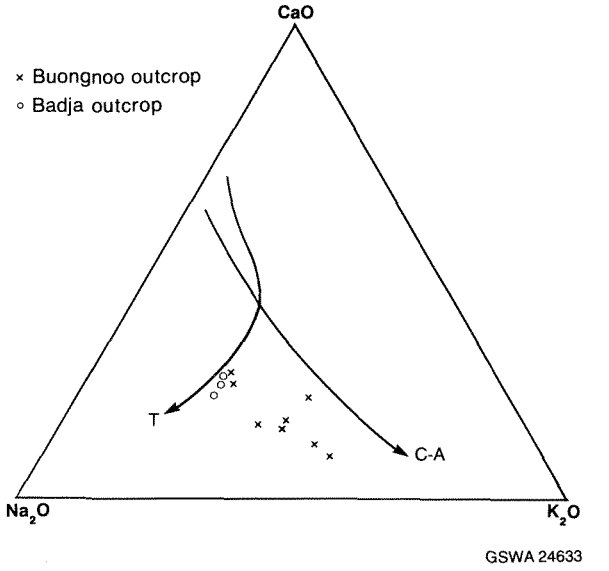


Figure 98. Pegmatite-banded gneiss compositions plotted on a $Na_2O–K_2O–CaO$ ternary diagram. C-A–calc-alkaline trend (Nockolds and Allen, 1953); T–trondhjemite trend (Barker and Arth, 1976).

Geochronology and isotope geochemistry

U–Pb zircon, Sm–Nd, and Rb–Sr isotopic data have been acquired for samples from the Buongnoo and Badja

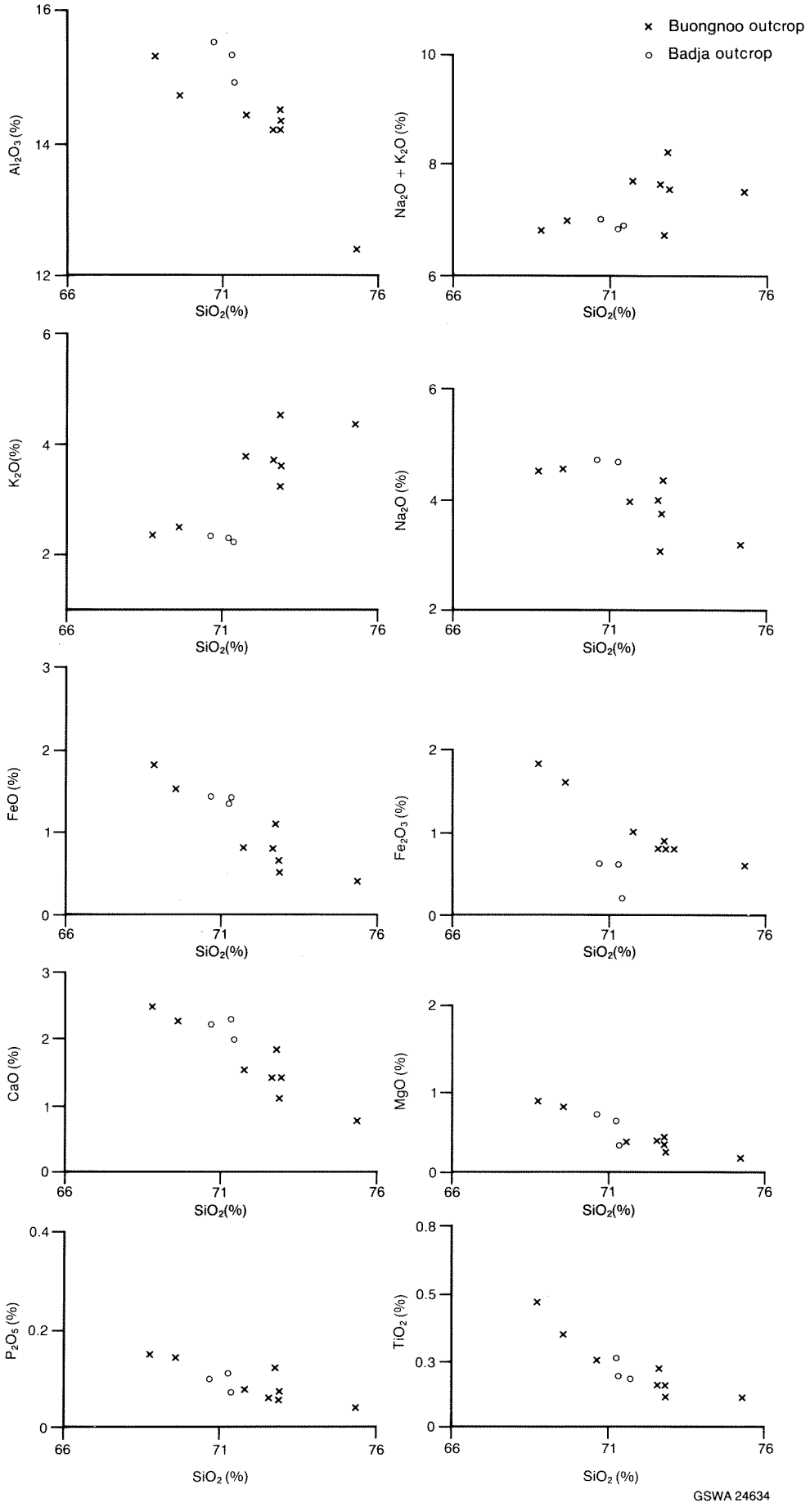


Figure 99. Major oxide Harker variation diagrams for pegmatite-banded gneiss samples.

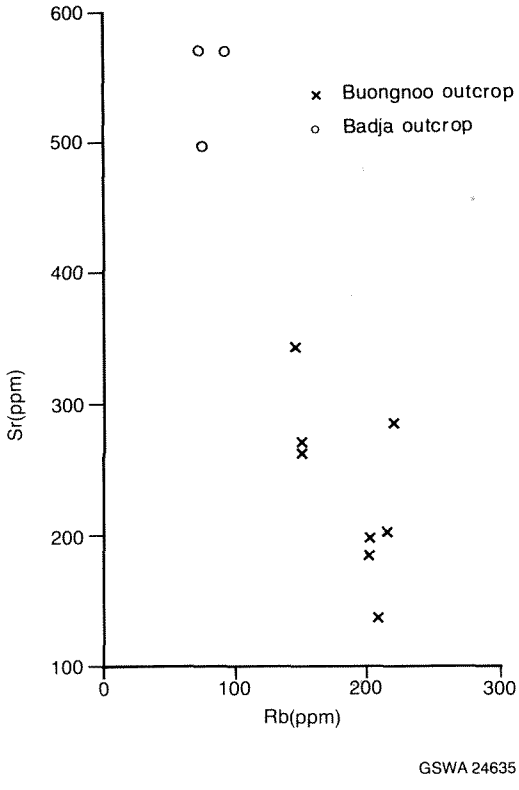


Figure 100. Pegmatite-banded gneiss compositions on a Rb–Sr plot.

outcrops (Figs 103 and 104). Zircon grains from sample 83339 were analysed, using the ion-microprobe at the Research School of Earth Sciences at the Australian National University, to determine U–Pb ages (Wiedenbeck and Watkins, in prep.). The interpreted crystallization age of the rock is 2918 Ma.

Sample 83305 from Buongnoo gave a Sm–Nd T_{DM} age of 2933 Ma; samples 83397 and 83398B from Badja gave different T_{DM} model ages of 3171 Ma and 2932 Ma, respectively (Appendix III, Figs 104A and B). The low values of $^{147}Sm/^{144}Nd$ require at least two fractionation events: probably the derivation of source rock from the mantle, and then partial melting of that source to form the gneiss protolith. T_{DM} model ages of 2933 Ma and 2932 Ma for the two samples 83305 and 83398B, respectively, are broadly comparable with the zircon age. The other sample, 83397, gives an older age of 3171 Ma, indicating that the gneiss precursors had a long crustal history.

Rb–Sr isochrons were determined for both pegmatite-banded gneiss bodies (Appendix III, Figs 104 and 105). The isochron ages are too young to date emplacement of gneiss protoliths, and they reflect homogenization of Sr during regional metamorphism (cf. Arriens, 1971; Faure, 1977; Chapman et al., 1981; Collerson, 1982). Muhling and de Laeter (1971) combined three pegmatite-banded gneiss samples, and two recrystallized monzogranite samples, on an isochron to date their 'outer granites' on CUE at 2550±51 Ma (Watkins et al., 1987, table 2). The two subsets of samples are isotopically indistinguishable, although there is a large difference in their crystallization ages — a further indication of isotopic homogenization during metamorphism.

Recrystallized monzogranite

Field Relations

Recrystallized monzogranite is the most voluminous of the four granitoid suites; it occupies most of the regions between greenstone belts (Plate 2). During regional metamorphism of the Murchison Province the suite was thoroughly recrystallized, mainly in greenschist facies (Plate 3). Although most rocks in the suite are monzogranite, some are granodiorite or syenogranite. Three main textural varieties occur — equigranular (Fig. 106A), porphyritic (Fig. 106B), and sparsely porphyritic (≤5% phenocrysts). All three are medium to coarse grained. An uncommon textural variety is fine grained and equigranular or sparsely porphyritic. The central parts of most recrystallized monzogranite bodies are porphyritic, but the margins are equigranular, although this distribution is not consistent (Plate 2). Most contacts between textural varieties are gradational, although intrusive contacts do occur. Intrusive relations generally show that porphyritic monzogranite intruded medium-grained equigranular monzogranite, and that the rare, fine-grained phase intruded the other textural variants. These textural varieties are broadly contemporaneous and, in many cases, where intrusive relations occur they probably result from intrusion of early crystallized fractions by later crystallized fractions of the same magma (cf. Groves and McCarthy, 1978).

Recrystallized monzogranite contains abundant cognate inclusions and accidental xenoliths (terminology follows Hughes, 1982, p. 133). Cognate inclusions have equilibrated with the host granitoid; they may represent restite material or fragments of deep wall rock which have been assimilated over long periods. Accidental xenoliths are fragments of wall rock which are not in equilibrium with the host granitoid. Cognate inclusions comprise schlieren and patches of mafic material (Fig. 107), and nebulitic banding after assimilated pegmatite-banded gneiss xenoliths (Figs 90 and 91). In porphyritic recrystallized monzogranite these inclusions contain phenocrysts (now porphyroblasts) of microcline (Fig. 107B). Accidental xenoliths comprise internally coherent blocks of pegmatite-banded gneiss (Fig. 89), and mafic or felsic rock fragments which occur as isolated blocks, in trains (Fig. 108A), and as aggregates of small blocks (Fig. 108B). Xenoliths and large rafts of country rock are abundant near recrystallized monzogranite margins.

Contacts between recrystallized monzogranite and greenstone belts are complex zones of high strain. In these zones, generally 50–1000 m wide, intensely deformed lenses and blocks of greenstones are interlayered with recrystallized monzogranite (Fig. 109A) which is strongly foliated and generally compositionally banded (Fig. 109B). Some intrusive relations are preserved despite the intense deformation; for example, in Figure 109C veins of monzogranite

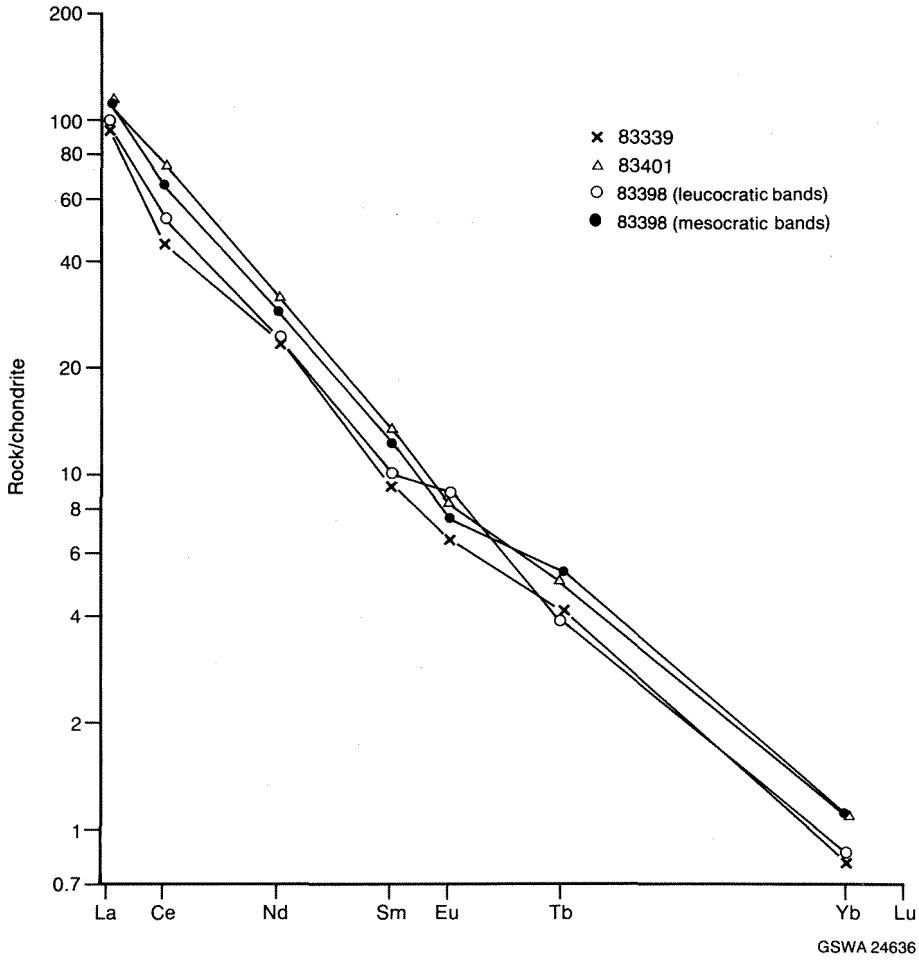


Figure 101. REE patterns for pegmatite-banded gneiss, Badja outcrop.

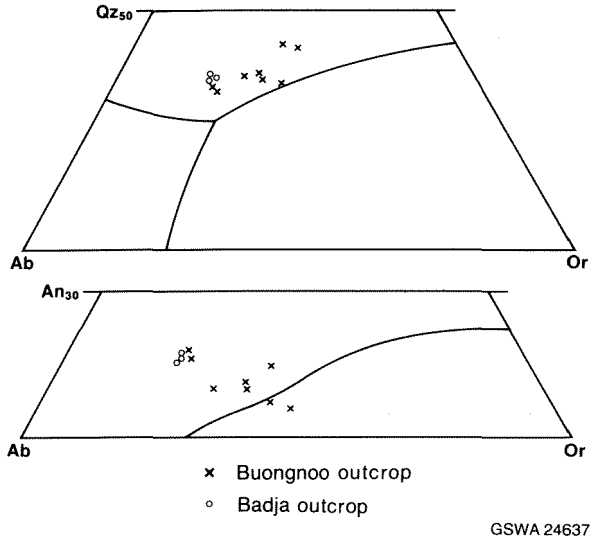


Figure 102. Pegmatite-banded gneiss compositions plotted on CIPW-norm diagrams. Cotectic lines are shown for P (H_2O)=500 Mpa, projected from An in the Ab–Or–Qz diagram, and from Qz in the Ab–Or–An diagram.

intruded basalt (now amphibolite) which was subsequently deformed. On a larger scale, dismembered elongate rafts of greenstone rocks, up to several kilometres in length, occur in marginal regions of recrystallized monzogranite bodies — for example, 15 km south of Yalgoo (Plate 1). On a regional scale, stratigraphic units are truncated at low angles by recrystallized monzogranite at the margins of greenstone belts (Plate 2).

Pegmatites and aplites are abundant throughout recrystallized monzogranite complexes, but particularly so adjacent to greenstone belt margins. Pegmatites comprise a large part of the outcrop in some places (Fig. 110). At Woolgerong Rock, on CUE, flat-lying pegmatites make up about 50% of the large granitoid monolith. Pegmatites range from a few tens of centimetres to tens of metres thick; most are not zoned and contain only K-feldspar, quartz, and mica, although some larger pegmatites are zoned and mineralized (Chapter 7). Quartz–feldspar porphyries, up to several metres thick, are abundant in greenstone belts within a kilometre of recrystallized monzogranite contacts.

The present outcrop distribution does not define the original shapes of individual monzogranite plutons — because of complex deformation since intrusion (Chapter 5). The greenstone belts appear to be enveloped by a mass

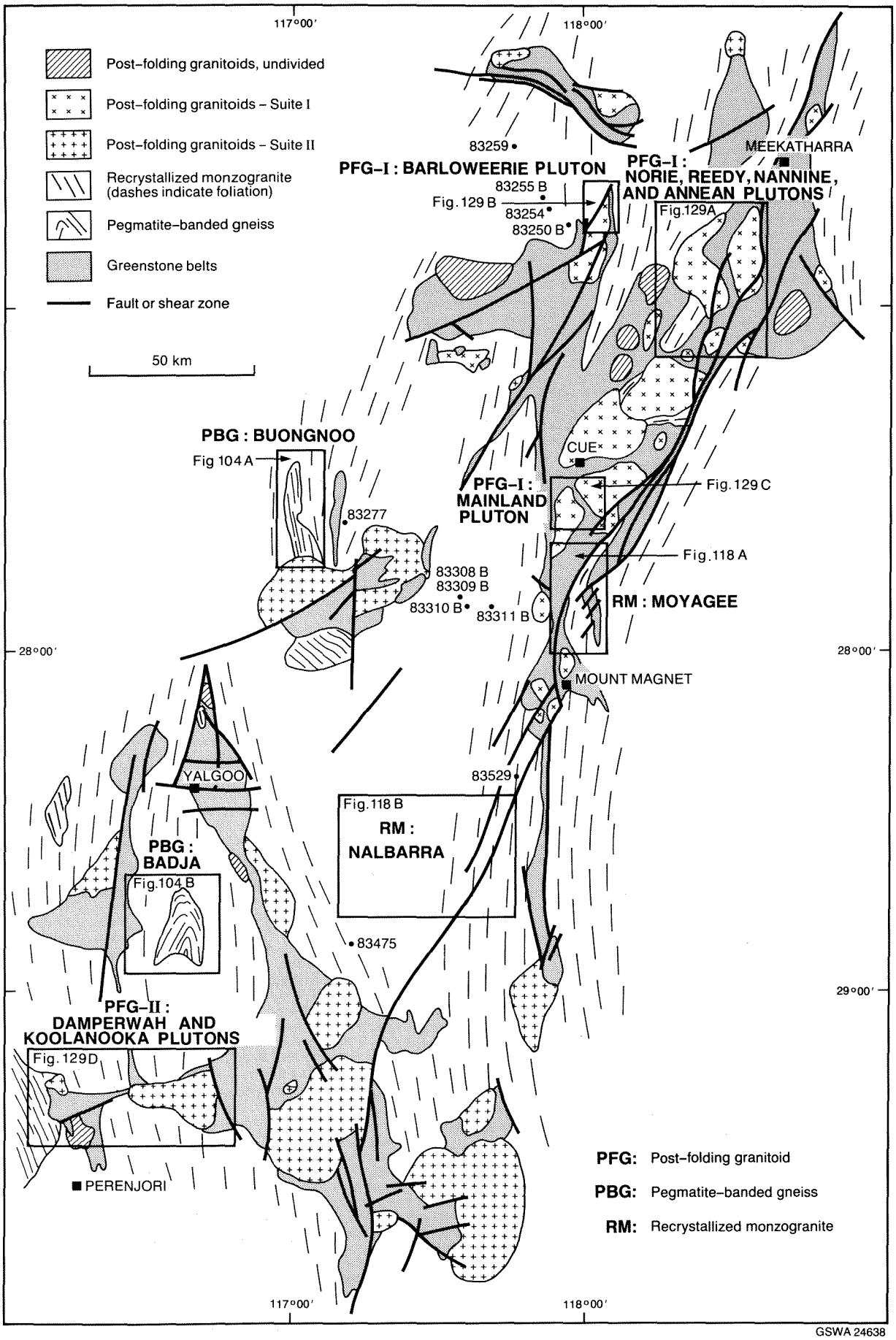
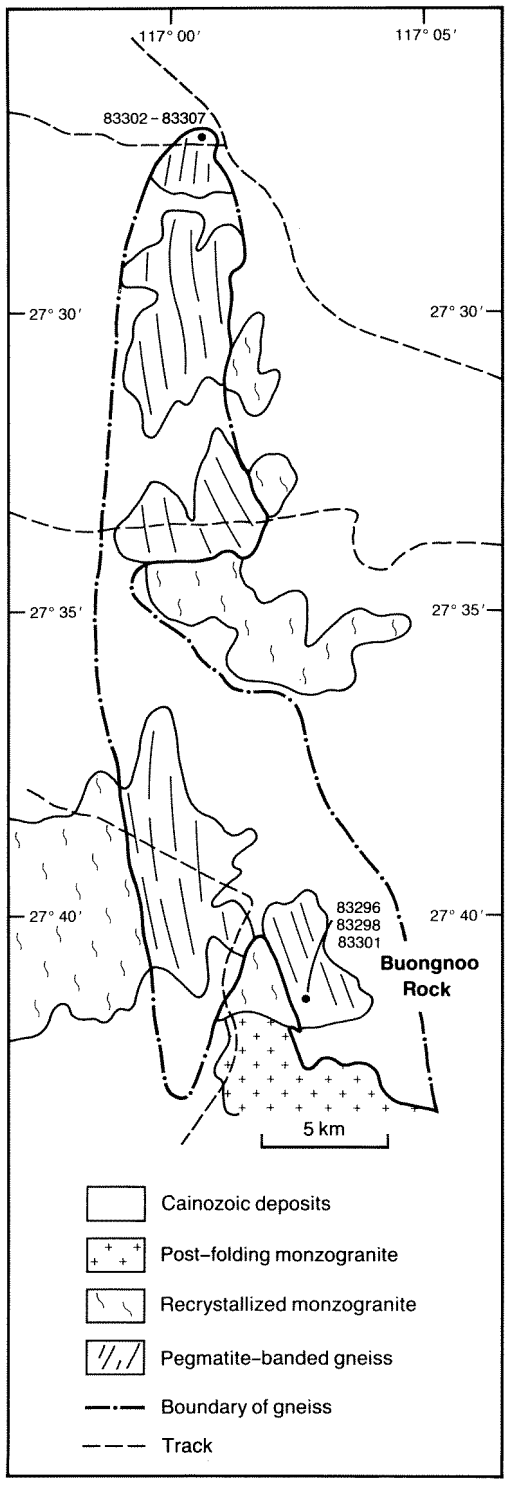


Figure 103. Distribution of map figures which show locations of granitoid geochronology samples. Locations of recrystallized monzogranite 'regional' samples are also shown.



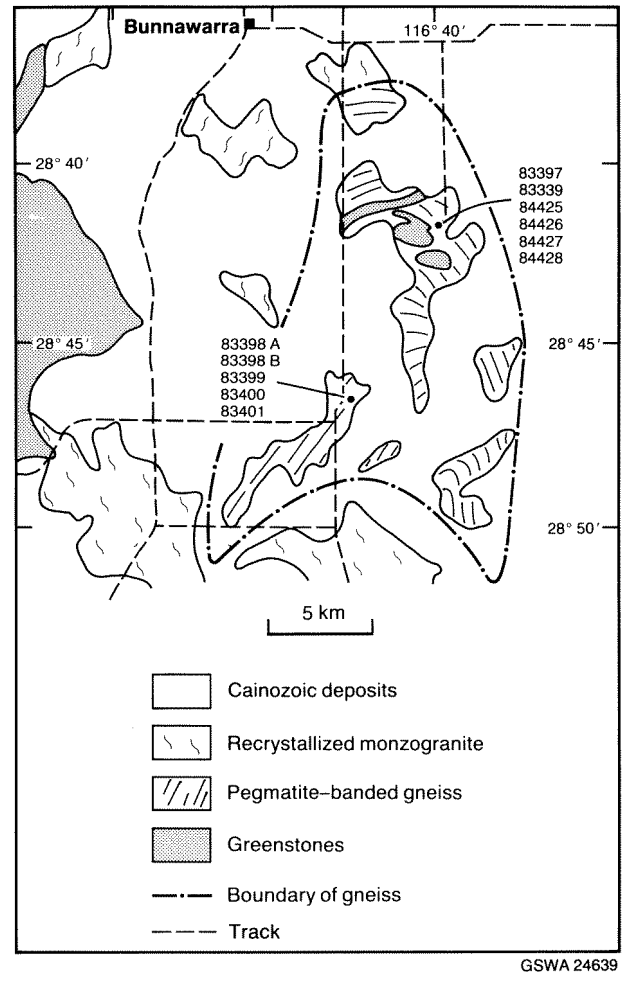
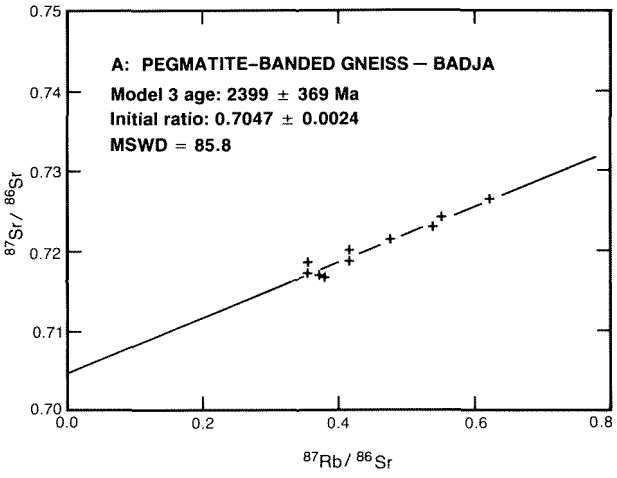
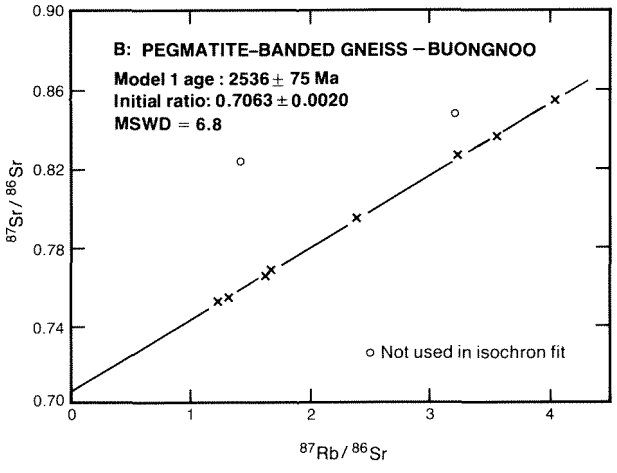


Figure 104. Locations of pegmatite-banded gneiss geochronology samples.

of recrystallized monzogranite. One exception is the monzogranite body south of Yalgoo which is almost enclosed by supracrustal rocks (Plate 2); a large outcrop of pegmatite-banded gneiss occurs in its core in an antiform–antiform culmination. Dips of banding in gneiss, and layering in greenstones, indicate that greenstones overlie recrystallized monzogranite which in turn overlies pegmatite-banded gneiss. Thus, prior to folding, the monzogranite body was tabular, and must have intruded the base of the greenstone succession as a thick tabular pluton or as a series of thin tablular plutons (Myers and Watkins, 1985). This mode of intrusion is thought to be typical, as gneisses also occur in core regions of some other recrystallized monzogranite bodies in or near antiformal culminations (Plates 1 and 2); however these gneisses are not as well exposed and their extents are uncertain.

Recrystallized monzogranite grades into granitoid gneiss which forms several large outcrops on CUE (Watkins et al., 1987) (Plate 1). This gneiss is dominantly monzogranitic in composition, strongly foliated, and compositionally banded. The banding consists of quartz–feldspar-rich and mica-rich bands, a few millimetres to several metres thick. The gneiss is typified by inclusions of supracrustal rocks and units of pegmatite-banded gneiss. Pods and bands of hornblende amphibolite (with or without clinopyroxene), up to several metres thick, are abundant. Larger units of metasedimentary rocks, up to 500 metres thick, occur in the





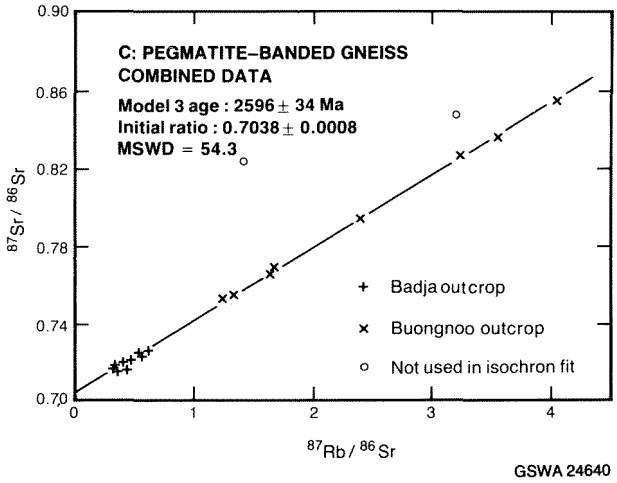
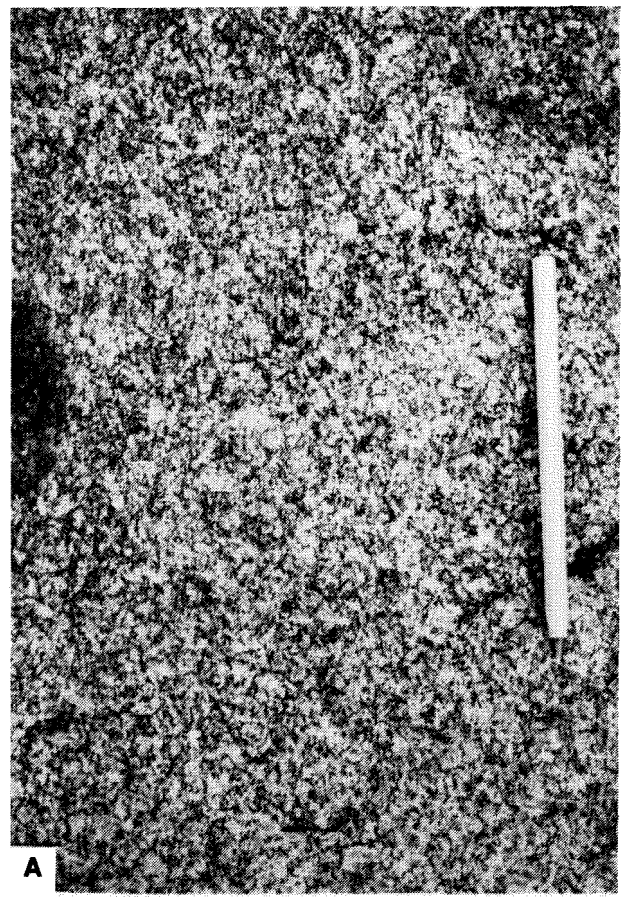


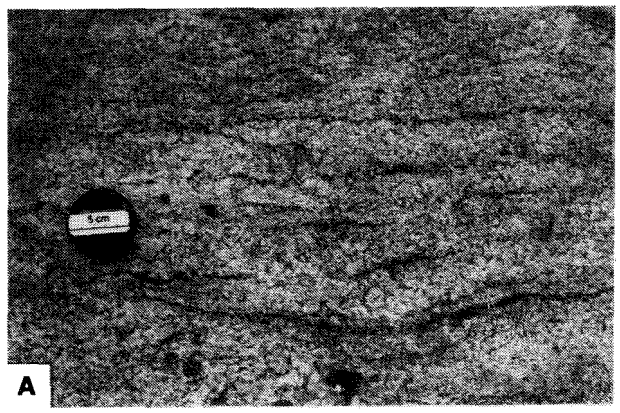
Figure 105. Rb–Sr isochron plots for pegmatite-banded gneiss.

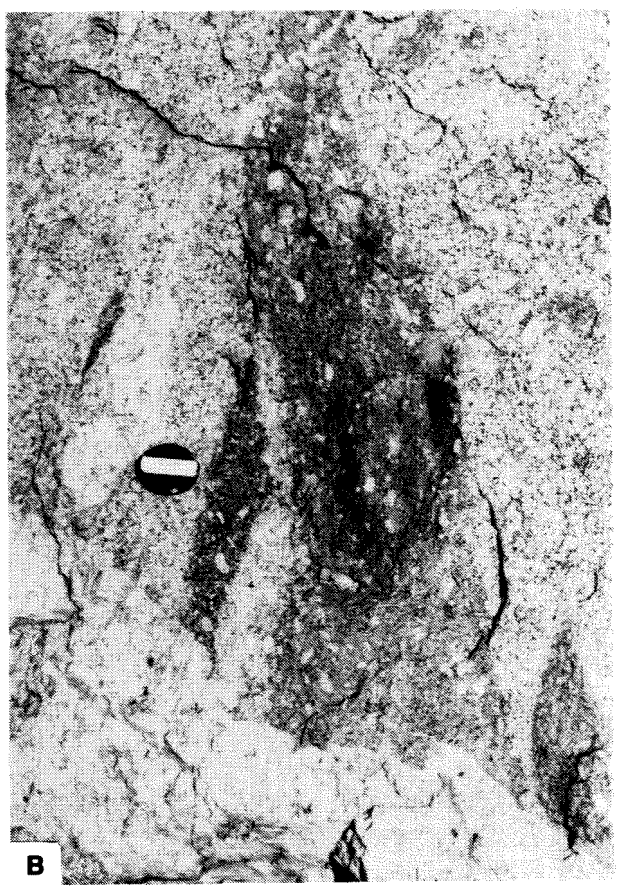




GSWA 24641

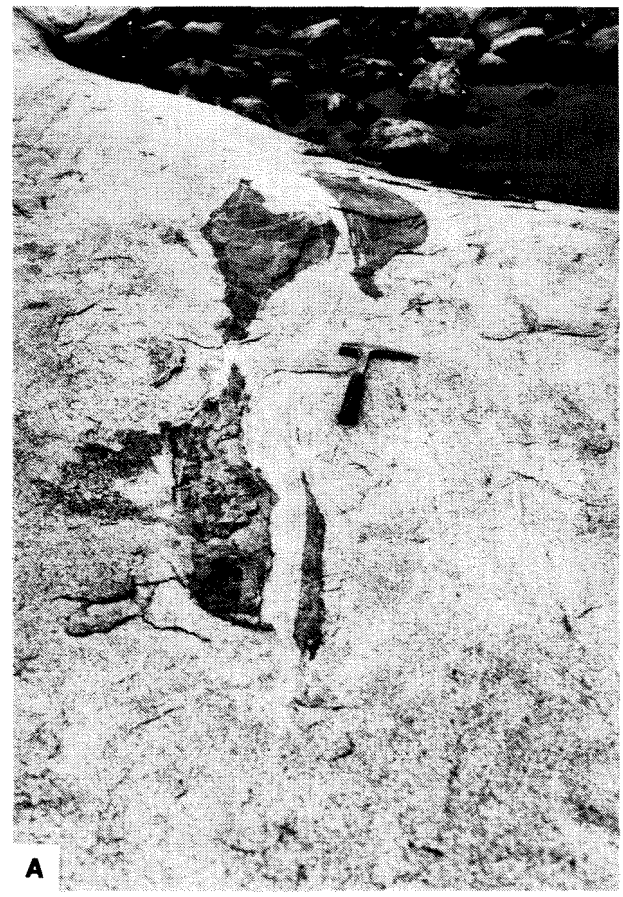
Figure 106. Textures of recrystallized monzogranite: A — medium-graned, foliated, equigranular; the pen is 14cm long; B — coarse-grained porphyritic; the lens cap is 5cm across.

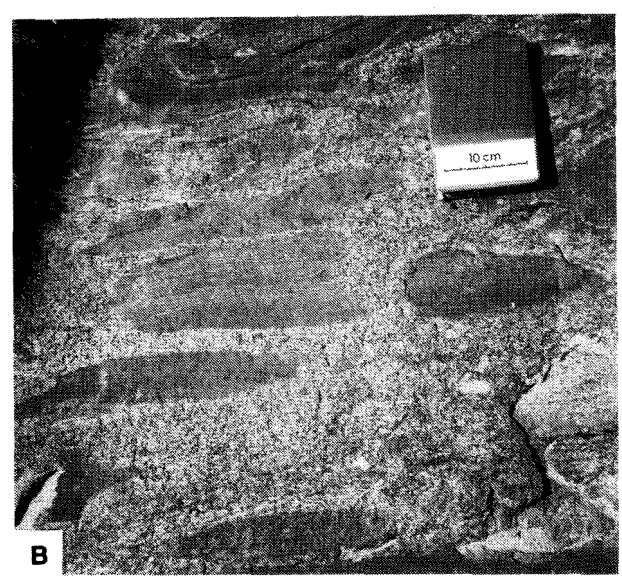




GSWA 24642

Figure 107. Cognate inclusions in recrystallized monzogranite: A — biotite-rich mafic schlieren; B — fragments of mafic rock, now a biotite-rich, quartz-poor aggregate, with phenocrysts of microcline.

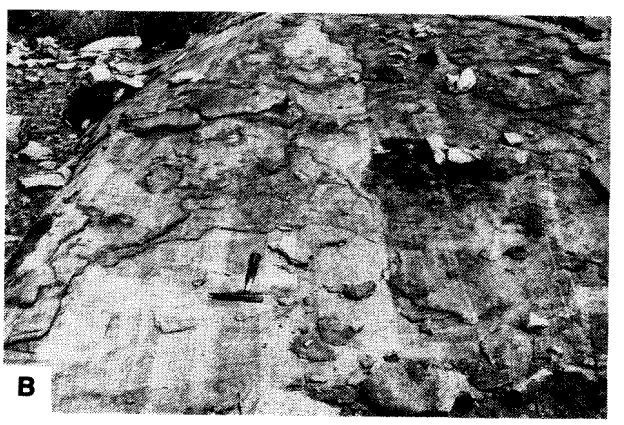


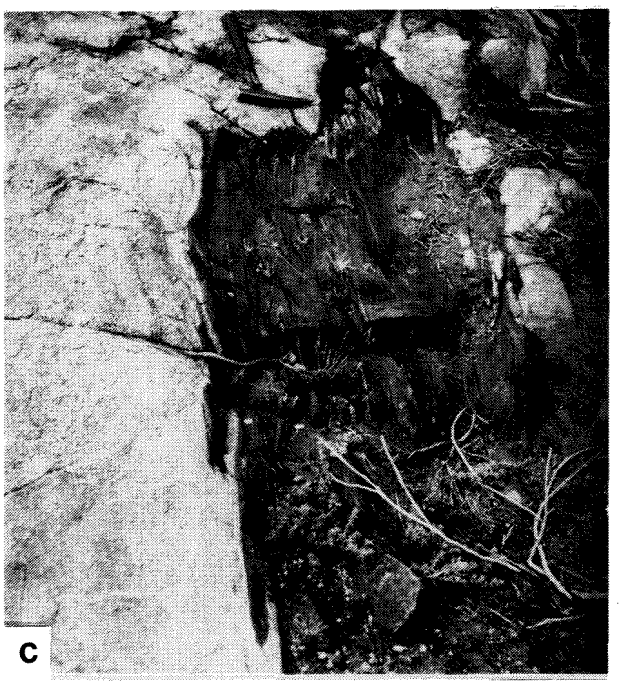


GSWA 24643

Figure 108. Accidental xenoliths in recrystallized monzogranite: A — train of amphibolite blocks, the hammer is 30cm long; B — aggregate of small blocks of banded felsic tuff.







GSWA 24644

Figure 109. Features of recrystallized monzogranite–greenstone belt contact zones: A — attenuated interlayered amphibolite and recrystallized monzogranite in a contact zone; B — compositionally banded and foliated recrystallized monzogranite near a greenstone belt contact; C — amphibolite infolded with recrystallized monzogranite; note the folded veins of microgranite in the amphibolite. The hammer handle in A is 1m in length, and in B and C, 30cm.



GSWA 24645

Figure 110. Pegmatites intruding recrystallized monzogranite; the hammer handle is 30cm long.

granitoid gneiss body near Yarraquin Homestead (Plate 1). These rocks include pelitic and psammitic schist containing staurolite or sillimanite, and BIF comprising quartz, magnetite, and amphibole. They may be remnants of the Windaning Formation (Plate 2). A discordant, near-vertical tabular body of quartz–plagioclase–epidote –amphibole–clinopyroxene gneiss in the granitoid gneiss east of Yarraquin Homestead is thought to have been a mafic intrusion (Watkins et al., 1987). The granitoid gneiss probably represents deformed and highly metamorphosed lower parts of tabular monzogranite plutons, originally in complex intrusive contact with lower greenstone units and pegmatite-banded gneiss.

Petrography

Mineral assemblages in recrystallized monzogranite are similar to those in pegmatite-banded gneiss. Quartz, oligoclase, K-feldspar (perthitic microcline and/or perthite) and biotite dominate; minor phases include chlorite, epidote, amphibole, white mica, opaques, sphene, apatite, zircon, and carbonates. Most assemblages are altered to some extent; biotite is partly retrograded to chlorite and rutile, and most oligoclase crystals have thin albite rims and moderately saussuritized cores. Myrmekite is developed in some plagioclase rims adjacent to grains of K-feldspar. Recrystallized monzogranite is generally leucocratic with 5–10% modal biotite and chlorite.

Igneous textures were recrystallized during regional metamorphism, and a variety of crystalloblastic textures developed. Remnants of igneous hypidiomorphic granular texture are occasionally preserved, particularly in porphyritic rocks. Two types of texture were developed in foliated recrystallized monzogranite. Lepidoblastic texture formed from alignment of phyllosilicates, and (sometimes) feldspars in weakly to moderately foliated rocks some distance from greenstone belt contacts (Fig. 111A). Protomylonitic texture formed in strongly foliated and sometimes banded rocks near greenstone belt contacts. Protomylonitic texture consists of ribboned quartz, and fine-grained feldspars and micas, wrapping large grains of feldspar (Fig. 111B); in





GSWA 24646

Figure 111. Photomicrographs of foliated recrystallized monzogranite: A — lepidoblastic texture; B — weakly recrystallized protomylonitic texture.

most cases this texture has been recrystallized to a mortar texture (Fig. 95). Unfoliated and very weakly foliated recrystallized monzogranite has a granoblastic texture similar to that in pegmatite-banded gneiss (Fig. 112A). In porphyritic rocks, large ragged microcline and perthite crystals are enclosed in a granoblastic matrix (Fig. 112B). Two facts indicate that these crystals were magmatic rather than metamorphic or metasomatic in origin:

(a) The crystals contain inclusions of euhedral, sometimes zoned, plagioclase and biotite which are unaffected by metamorphic textural degradation. These suggest that K-feldspar is a late magmatic phase.

(b) Small bodies of porphyritic monzogranite intruded equigranular monzogranite of identical composition. Both rock types are recrystallized, yet large K-feldspar crystals are confined to the intrusive body.

Thus, original magmatic phenocrysts were pseudomorphed, at least in part, by metamorphic microcline. K-feldspar crystals in cognate inclusions (Fig. 107B) indicate small-scale metasomatism during crystallization of monzogranite (Robb et al., 1983).

Geochemistry and petrogenesis

Ninety-one samples of recrystallized monzogranite were collected for chemical analysis; sample locations are shown in Figure 96. Of these samples, 67 are equigranular and mainly foliated; 24 are porphyritic and mainly unfoliated (Appendix II).

Mean compositions of recrystallized monzogranite samples are given in Table 29. Except for minor differences in F, Pb, Y, Zr, La, and Ce contents, equigranular and porphyritic recrystallized monzogranite are chemically indistinguishable. However, the minor differences suggest that, on average, the porphyritic variety is very slightly more fractionated than the equigranular variety. The samples have peraluminous compositions and are calcic according to Peacock's (1931) alkali–lime index (Fig. 113). The recrystallized monzogranite suite has a broad calc-alkaline trend which is displaced towards Na-rich compositions on a Na_2O–K_2O–CaO ternary diagram (Fig. 114). On Harker variation diagrams the data show well-defined linear trends for most major oxides (Fig. 115). The scatter of points about mean trends, particularly for Na_2O, K_2O, and Fe_2O_3, is attributed largely to redistribution of elements during regional metamorphism. Most trace elements do not correlate well with SiO_2, or with other major and trace elements. While some of this variation is undoubtably due to original compositional variation over the large area sampled, much is due to secondary mobilization during metamorphism. Petrographic evidence for such mobilization includes biotite partly retrograded to chlorite, with consequent loss of K and Rb from the rock, and albitization of calcic oligoclase grain rims and saussuritization of feldspars resulting in redistribution of Na, Ca, and Sr. However, despite mobility of some elements, trends on Harker

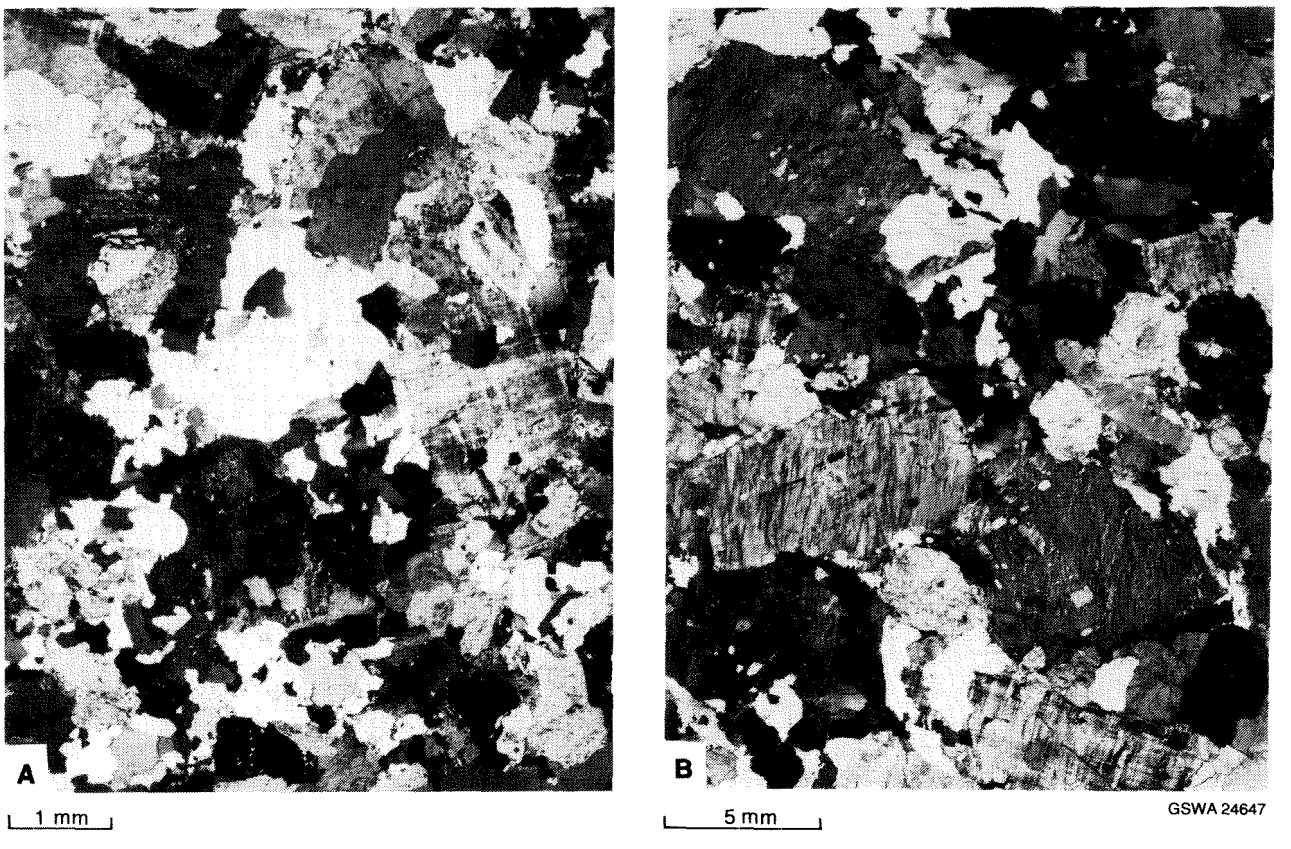


Figure 112. Photomicrographs of unfoliated recrystallized monzogranite: A — granoblastic texture; B — recrystallized porphyritic texture.

TABLE 29. MEAN COMPOSITIONS OF RECRYSTALLIZED MONZOGRANITE

	Equigranular n=67	*Porphyritic n=24*	*All n=91*
		Percentage	
SiO_2	71.2	70.9	71.1
Al_2O_3	14.4	14.7	14.5
Fe_2O_3	0.9	1.1	1.0
FeO	1.22	1.21	1.22
FeO*(a)	2.03	2.20	2.12
MgO	0.60	0.58	0.59
CaO	1.83	1.83	1.83
Na_2O	4.14	4.21	4.16
K_2O	3.31	3.08	3.24
TiO_2	0.27	0.30	0.28
P_2O_5	0.13	0.13	0.13
MnO	0.03	0.03	0.03
LOI	1.03	0.92	1.00
		Parts per million	
F	464	598	501
Ba	1314	1335	1319
Cu	19	21	20
Pb	20	11	18
Li	23	25	24
Mo	(b) 2	(b) 1	(b) 2
Ni	22	23	22
Nb	9	11	10
Rb	129	129	129
Sr	365	377	368
Th	27	26	27
Sn	(b) 3	(b) 5	(b) 4
U	2	2	2
V	21	26	22
W	<2	<2	<2
Y	9	14	11
Zn	53	50	52
Zr	177	220	189
La	(c) 53	(d) 77	(e) 56
Ce	(c) 95	(d)132	(e) 99
Zr/(Zr+Y)	0.95	0.94	0.95

(a) All Fe calculated as FeO

(b) Some values used to calculate the means were below the detection limit, the value 'detection-limit/2' was used for these.

(c) Mean of 46 analyses

(d) Mean of 9 analyses were below the detection limit, the value

(e) Mean of 55 analyses

variation diagrams are sufficiently well defined to indicate that recrystallized monzogranite samples are part of a chemically related suite of rocks with similar petrogeneses. Compositional fields of pegmatite-banded gneiss and recrystallized monzogranite coincide in Figures 113, 114, and 115. Mean major-oxide contents of recrystallized monzogranite are generally intermediate between those of the pegmatite-banded gneiss at Buongnoo and that at Badja; however, monzogranite contains more Ba, Cu, Zr, La, and Ce than gneiss (compare Tables 28 and 29).

REE patterns for seven recrystallized monzogranite samples are shown in Figure 116. They are moderately fractionated with a $(La/Lu)_N$ range of 24.1–124.4, and a mean value of 63.0. The total REE content ranges from 116 to 627 ppm, with a mean value of 345 ppm, which is normal for monzogranites and granodiorites (Cullers and Graf, 1984b). All samples except 83524 have slight to moderate negative Eu anomalies which require abundant feldspar in the source. The largest anomalies occur in porphyritic

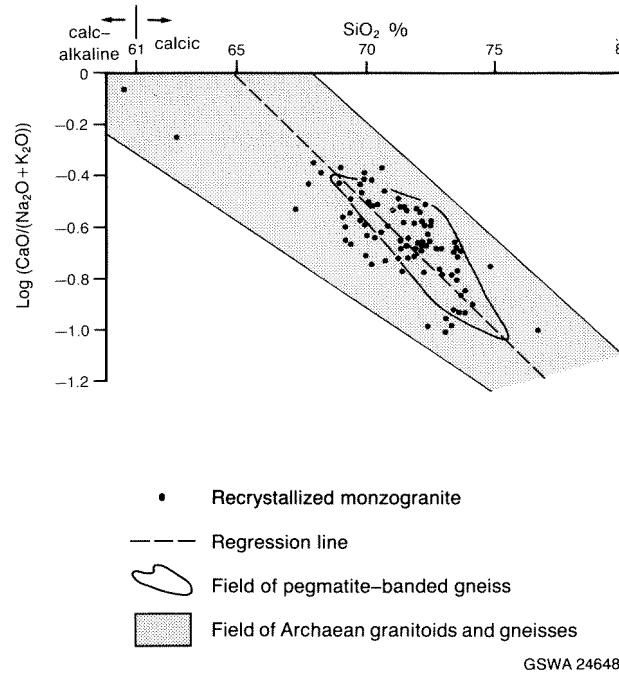


Figure 113. Log ($CaO/(Na_2O+K_2O)$) v. SiO_2 diagram for recrystallized monzogranite compared with pegmatite-banded gneiss and other Archaean granitoids and gneisses (sources of data given in caption for Figure 97). A regression line through the recrystallized monzogranite data is shown.

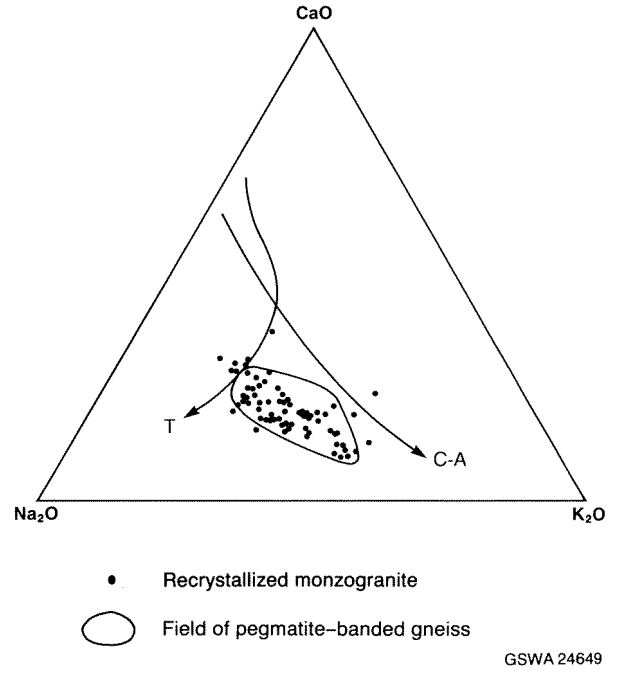


Figure 114. Recrystallized monzogranite compositions plotted on a Na_2O–K_2O–CaO ternary diagram. C-A — calc-alkaline trend (Nockolds and Allen, 1953); T — trondhjemite trend (Barker and Arth, 1976).

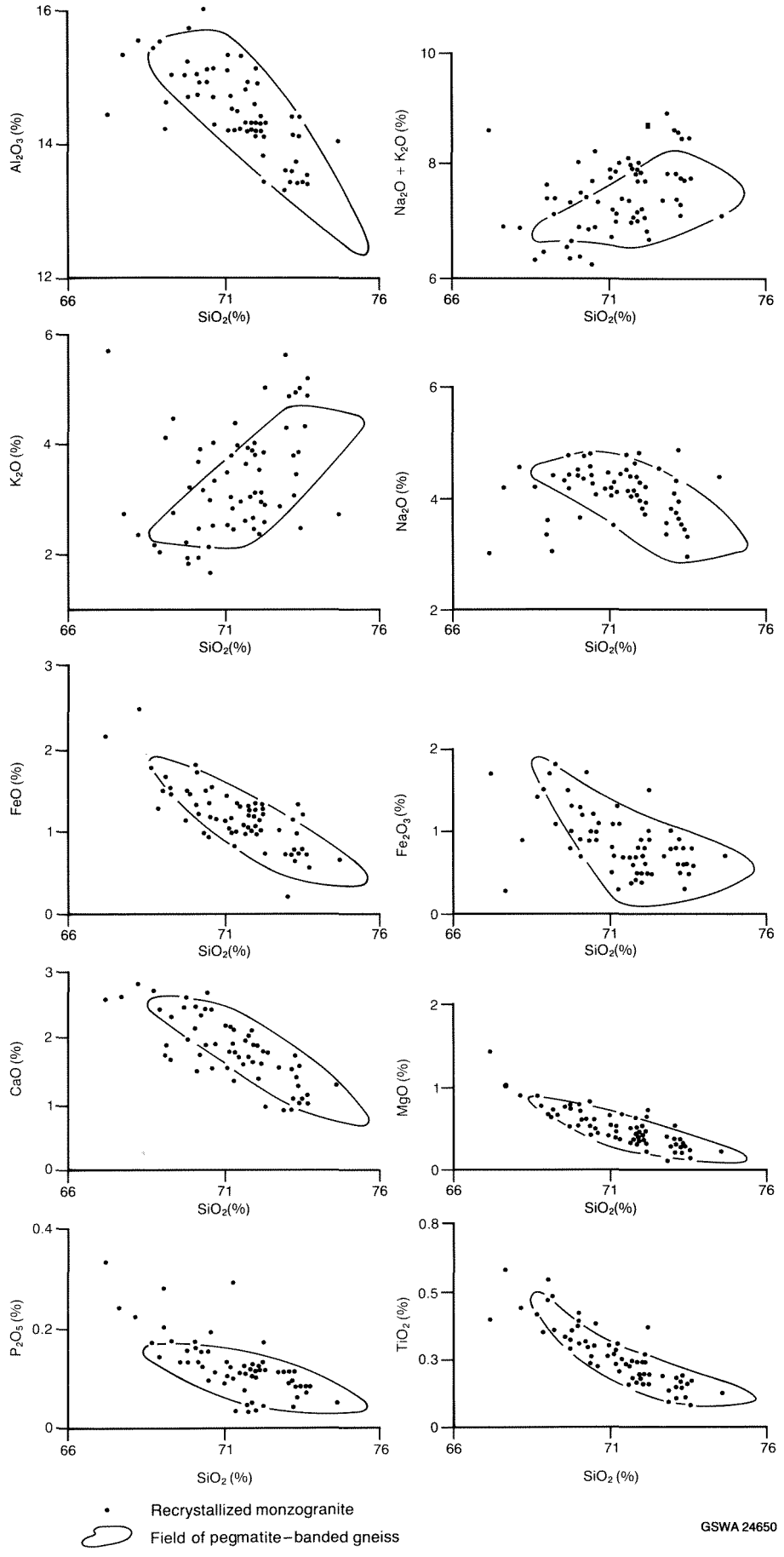


Figure 115. Major-oxide Harker variation diagrams for recrystallized monzogranite. Compositional fields for pegmatite-banded gneiss are shown.

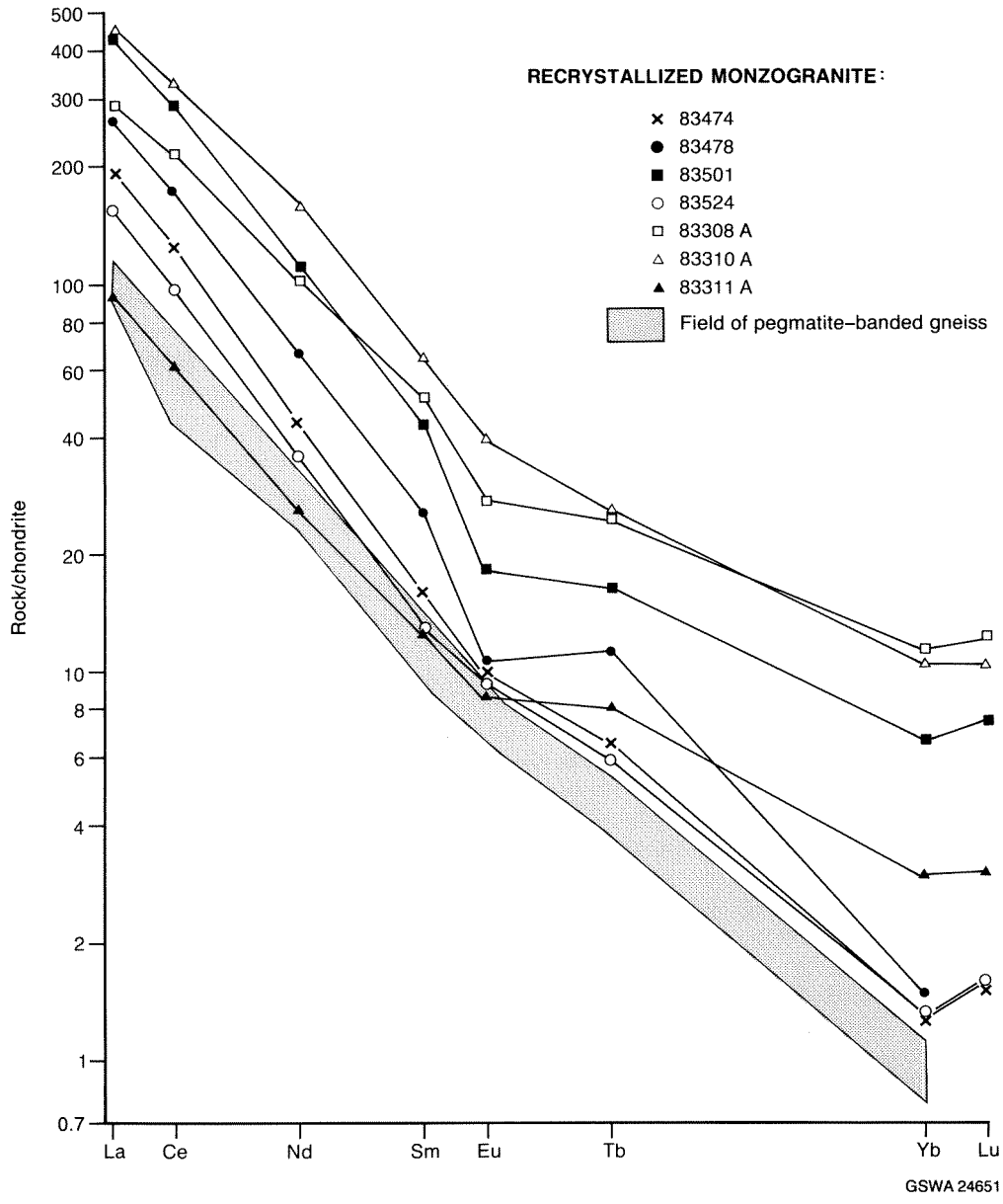


Figure 116. REE patterns for recrystallized monzogranite samples. Field of pegmatite-banded gneiss REE patterns is shown for comparison.

samples and probably indicate fractionation of plagioclase in these rocks. HREE patterns show upward deflections in Lu. It is not possible to distinguish whether these are due to anomalously positive Lu, or negative Yb contents, as Dy, Ho, Er, and Tm analyses are not available to precisely determine HREE trends. Recrystallized monzogranite contains larger amounts of REE, and has less fractionated REE patterns than pegmatite-banded gneiss (Fig. 116). The fractionated REE patterns indicate residual garnet and/or amphibole in the source. Source rocks are likely to have been similar to those for pegmatite-banded gneiss, although with a greater proportion of residual plagioclase, e.g. garnet amphibolite or tonalite. The higher REE contents which distinguish recrystallized monzogranite from pegmatite-banded gneiss can be explained by smaller degrees of partial melting or a more fractionated source-rock composition.

Recrystallized monzogranite and pegmatite-banded gneiss compositional fields coincide on CIPW normative Ab–Or–Qz and Ab–Or–An diagrams (Fig. 117). Thus the relative crystallization sequence in the Ab–Or–An–Qz vapour–liquid system is the same; calcic oligoclase and quartz crystallized first, followed by K-feldspar. This observation is consistent with the inclusions of plagioclase (and biotite) in microcline, noted previously. The constant Ab/An ratio of the trend of recrystallized monzogranite data indicates that the amount of plagioclase solid solution did not change during crystallization. Fluid pressure was probably high during crystallization (as in pegmatite-banded gneiss) resulting in abundant pegmatites.

The close compositional similarity of recrystallized monzogranite and pegmatite-banded gneiss, combined with their intimate field relations, suggests an association be-

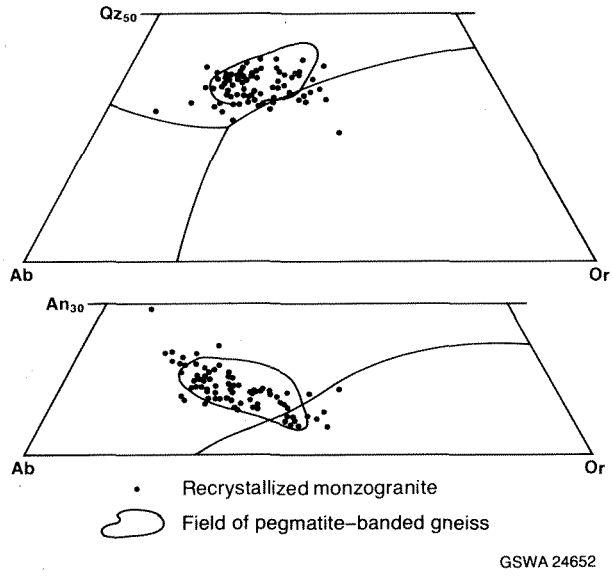


Figure 117. Recrystallized monzogranite compositions plotted on CIPW norm diagrams. Cotectic lines as in Figure 102.

tween them. It is unlikely that monzogranite was derived by anatexis of pegmatite-banded gneiss, because compositions of these suites are so similar that more than 90% of the gneiss would have had to be melted. Metamorphic grade of pegmatite-banded gneiss (greenschist and amphibolite facies) is too low for melting of the rocks now exposed to have occurred. Isotopic evidence also precludes this hypothesis (see next section). These suites were probably derived at different times by similar processes, from similar source rocks in the lower crust, and intruded to similar levels in the basal part of the greenstone succession.

Recrystallized monzogranite is chemically similar to monzogranites in the Lawlers region of the Yilgarn Craton (Foden et al., 1984). However, it is more fractionated than foliated monzogranites in the Pilbara Craton; for example, recrystallized monzogranite has higher Rb/Sr and K_2O/Na_2O ratios (Blockley, 1980; Davy and Lewis, 1981; Bickle et al., 1983; Hickman, 1983). However, the suite is less fractionated, and more calcic than Condie's (1981) averages of North American and South African Archaean monzogranites.

Geochronology and isotope geochemistry

U–Pb zircon, Sm–Nd and Rb–Sr ages have been determined on a number of recrystallized monzogranite samples (Figs 103 and 118). Zircons from two samples were analysed for U–Pb isotopes on the ion-microprobe at the Australian National University (Wiedenbeck and Watkins, in prep.). The samples were an equigranular, foliated marginal monzogranite (74459) and a porphyritic, unfoliated central monzogranite (83481) collected from sites over 100 km apart (Fig. 96). The interpreted crystallization ages of these samples are 2681 Ma and 2690 Ma, respectively.

Sm–Nd T_{DM} model ages have been determined on four samples: 84419 (2837 Ma), 83479 (2827 Ma), 83525 (2794 Ma), and 83475 (2846 Ma), which are splits of geochemistry samples 74459, 83481, 83524, and 83474, respectively (Fig. 96, Appendix III) (Watkins et al., in press). The low $^{147}Sm/^{144}Nd$ values require at least two fractionation events in the evolution of these samples from mantle sources, as was the case for pegmatite-banded gneiss. The T_{DM} model ages are considered to be minimum estimates of crustal residence age, and the precursor to the monzogranite could be as old as that for pegmatite-banded gneiss. Values of ε_{Nd} for recrystallized monzogranite and pegmatite-banded gneiss are quite distinct (Appendix III) and preclude derivation of monzogranite from gneiss by large degrees of partial melting. The similarities between the widely separated samples suggests derivation from a large, deep, laterally extensive and uniform source.

Some Rb–Sr studies on Murchison Province granitoids have been published (Table 30); isochron ages for this suite vary between 2535 Ma and 2706 Ma, with initial ratios in the range from 0.702–0.704. For this study, Rb–Sr isotopes were measured on 34 samples of recrystallized monzogranite (Appendix III, Figs 118 and 119). Most Rb–Sr isochron ages are in agreement with the published data for this granitoid suite, and are younger than U–Pb zircon crystallization ages. They date homogenization of Sr, or radiogenic ^{87}Sr loss, during regional metamorphism, as was the case for pegmatite-banded gneiss. The ages reflect closure of the Rb–Sr isotope system in the principal Rb- and Sr-bearing phases in recrystallized monzogranite, over a range of temperatures during post-peak metamorphic cooling. The Rb–Sr age is therefore likely to be younger than the true age of peak regional metamorphism, although the difference between the two ages is probably spanned by the uncertainties in the radiometric age determination. The 'combined data' model 3 age of 2603 ± 27 Ma thus represents a post-peak metamorphic cooling age. The similarity in Rb–Sr ages of recrystallized monzogranite and pegmatite-banded gneiss confirm that these reflect metamorphic rather than igneous processes. Initial ratios of the two suites are also similar; this may reflect similarity in the nature of crustal source materials as well as similar metamorphic effects.

Post-folding granitoids

Field relations

Fifty-seven plutons of post-folding granitoids have been recognized. The plutons have been divided, where possible, into two suites on the basis of petrology and geochemistry. These are distinguished as suite I and suite II on Plate 2. Suite I consists of tonalite, granodiorite, monzogranite, syenogranite, and trondhjemite; suite II consists of quartz-rich monzogranite and syenogranite. Most suite I plutons are in the northeastern part of the Murchison Province, whereas most suite II plutons occur in the south-

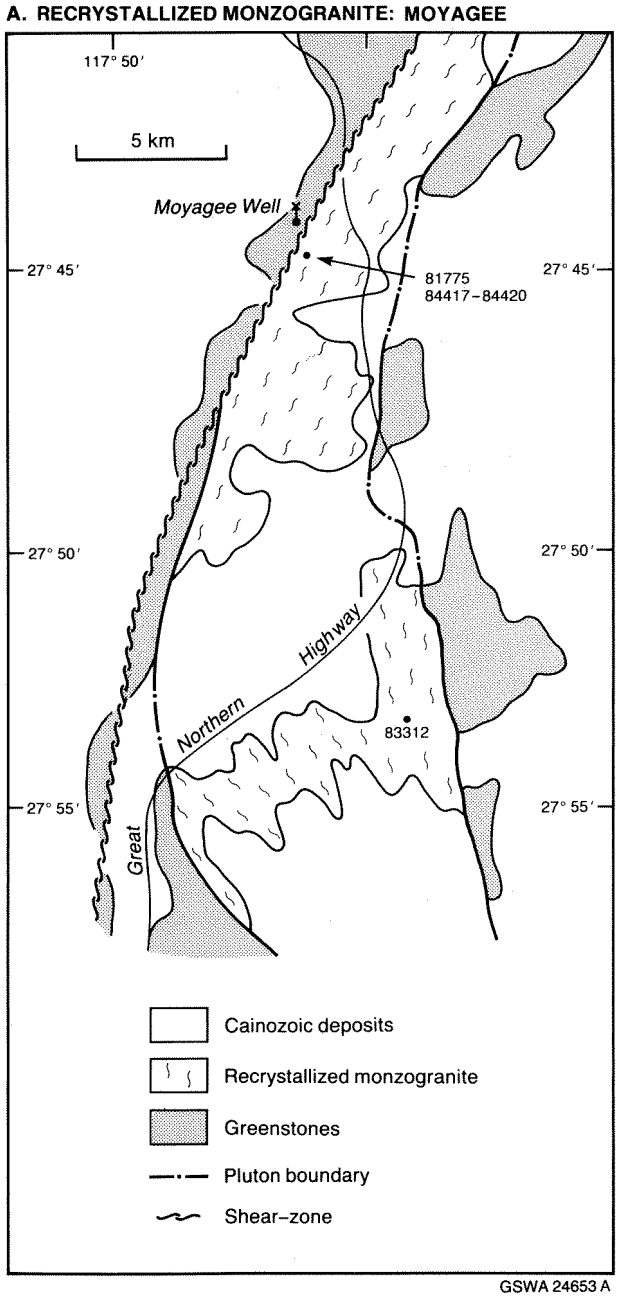


Figure 118A. Locations of recrystallized monzogranite geochronology samples — Moyagee area.

west. The exceptions to this distribution are the two northernmost plutons which are assigned to suite II, and suite I and II plutons which intrude the Tallering and Twin Peaks greenstone belts. Both suites have similar field relations, and it is not possible to consistently distinguish suite I and II plutons on this basis alone.

Post-folding granitoids generally have subcircular to oval-shaped outcrops. They are discordant, and truncate stratigraphic units and tectonic features associated with folding. However, they are cut by most D_4 shear zones, although they truncate some others. Plutons occur only in three situations: interiors of greenstone belts, contacts between recrystallized monzogranite and greenstone belts, and apices of greenstone belts in recrystallized monzogranite (Plate 2). No post-folding granitoid pluton has been identified wholly within a recrystallized monzogranite body, unlike in the Pilbara Craton (Hickman, 1983).

Most plutons appear to be compositionally and texturally homogeneous, apart from abundant xenoliths. However, three plutons in the Weld Range greenstone belt, west of the Murrouli Range and east of the Dalgaranga mining centre, are composite and contain compositionally distinct phases. It is not clear whether these phases represent different intrusions or are products of compositional zoning. Most plutons are medium grained and equigranular or porphyritic. Cognate inclusions a few centimetres across, consisting of aggregates of amphibole and biotite, are disseminated throughout most plutons. Accidental xenoliths of wall rock are also abundant, particularly near the margins of plutons; most of these are angular to rounded blocks of amphibolite, although many are recognizably basaltic (Fig. 120A). Other lithologies also occur (Fig. 120B). Some xenoliths are quite large; for example, blocks of gabbro in the post-folding monzogranite east of the Dalgaranga mining centre are several tens of metres across (Plate 1). North of Cue, large xenoliths of mafic and ultramafic rock, in post-folding tonalite, host gold deposits (Chapter 7).

Contacts with country rocks are sharp. Contact aureoles a few hundred metres wide were developed in the albite–epidote and hornblende hornfels facies (Turner, 1980). A parting cleavage, parallel to the granitoid contact, is weakly developed in some aureoles; minor faulting occurs at high angles to many contacts. In marginal zones of some plutons there are cataclastic shear zones, a few metres wide and of limited extent, subparallel to the contacts. Pegmatites and aplites intruded marginal zones of some plutons and adjacent country rocks, usually subparallel or subperpendicular to the contacts. These are much less abundant than pegmatites associated with recrystallized monzogranite.

Post-folding granitoid plutons were emplaced with very little distortion of the country rocks (Plate 2). One exception is the tonalite east of Nannine, which has split the greenstone sequence. Outcrop shapes, contact features, and timing of intrusion of post-folding granitoids are characteristic of emplacement by stoping into a relatively brittle crust (Pitcher, 1979).

Petrography

The compositional variation of post-folding granitoid rocks is reflected in their mineralogy. Syenogranite and monzogranite contain assemblages of quartz, K-feldspar, plagioclase, and biotite (in decreasing order of abundance) which in some rocks are accompanied by hornblende or muscovite. Tonalite and trondhjemite contain assemblages of plagioclase, quartz, hornblende, biotite, and K-feldspar. Chlorite, epidote, opaque minerals, apatite, sphene, zircon, carbonates, and fluorite occur as minor phases in most rocks. The monzogranite of the Damperwah

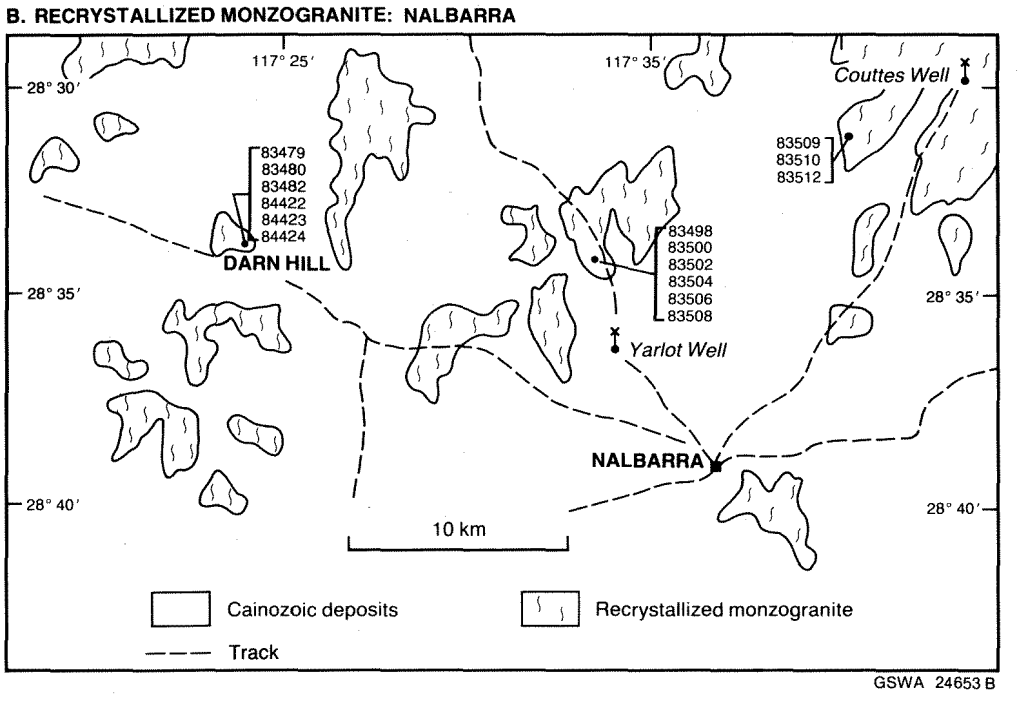


Figure 118B. Locations of recrystallized monzogranite geochronology samples — Nalbarra area.

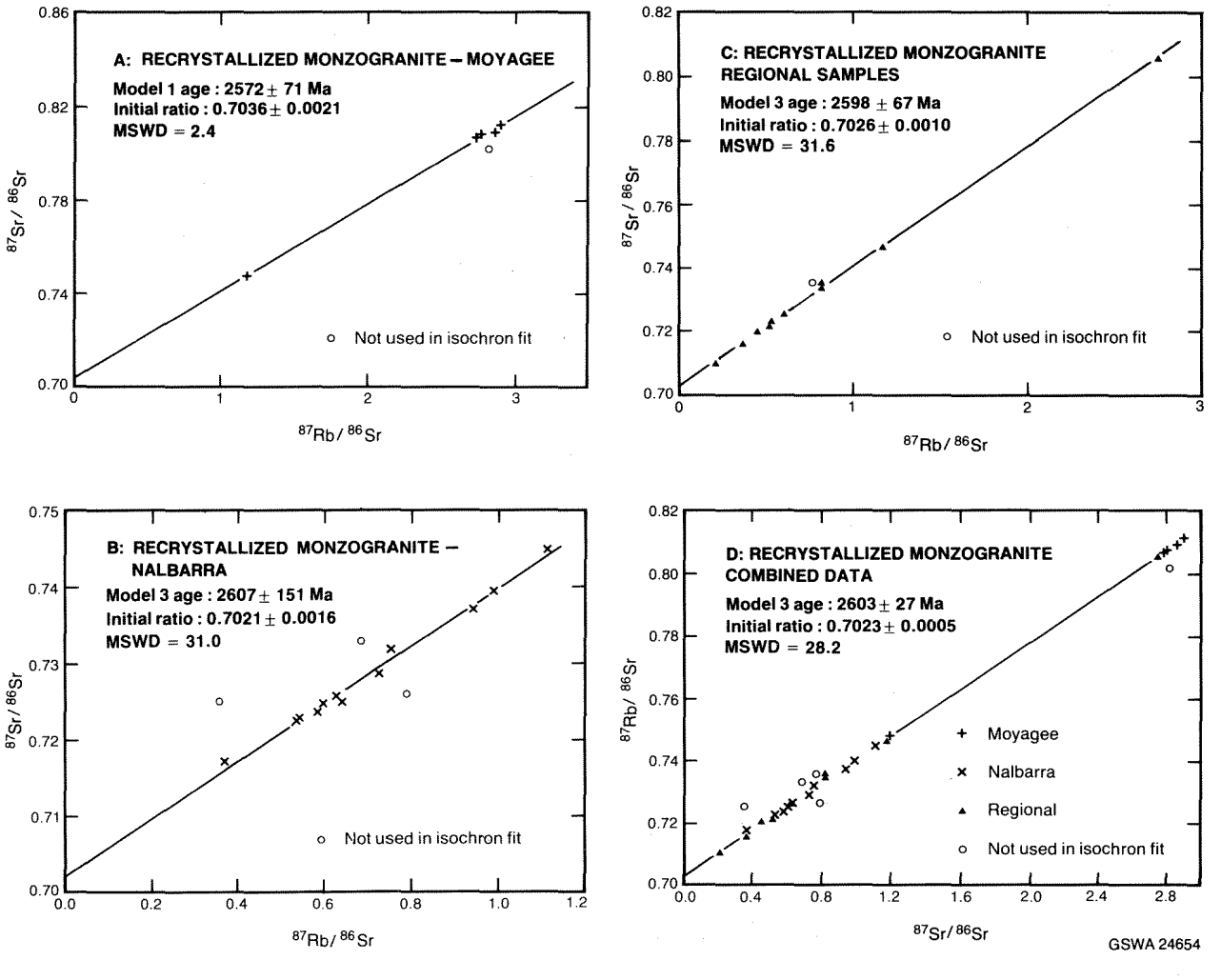


Figure 119. Rb–Sr isochron plots for recrystallized monzogranite.

TABLE 30. PUBLISHED Rb–Sr ISOCHRONS OF MURCHISON PROVINCE GRANITOIDS

Rock type	*Region*	*Age (a) (Ma)*	*$^{87}Sr/^{86}Sr$*	*Number of samples*	*Source*
RM	Cue–Paynes Find	2608 ± 68	0.702 ± 0.006	6	Arriens, 1971
RM	Perenjori–Paynes Find	2706 ± 264	0.704 ± 0.01	5	Arriens, 1971
RM	Koolanooka	2549 ± 117	0.704 ± 0.005	7	Arriens, 1971
RM	Cue (inner granitoids)	2535 ± 46	0.703 ± 0.001	7	Muhling and de Laeter, 1971
RM and PBG	Cue (outer granitoids)	2550 ± 102	0.703 ± 0.001	5	Muhling and de Laeter, 1971
RM	Mulgine	2684 ± 79	0.701 ± 0.005	7	de Laeter and Baxter, 1987
PFG-II	Koolanooka	2508 ± 28	0.707 ± 0.013	8	Arriens, 1971
Late porphyries	Koolanooka	2194 ± 38	0.747 ± 0.043	6	Arriens, 1971
PFG-II	Mulgine	2596 ± 35	0.704 ± 0.004	10	de Laeter and Baxter, 1987

(a) Dates published in 1971 have been recalculated using the decay constant of 1.42 x 10^{-11} a^{-1} (Steiger and Jager, 1971).
Uncertainties: 2σ to tσ. RM: recrystallized monzogranite PBG: pegmatite-banded gneiss PFG-II: post-folding granitoids, suite II

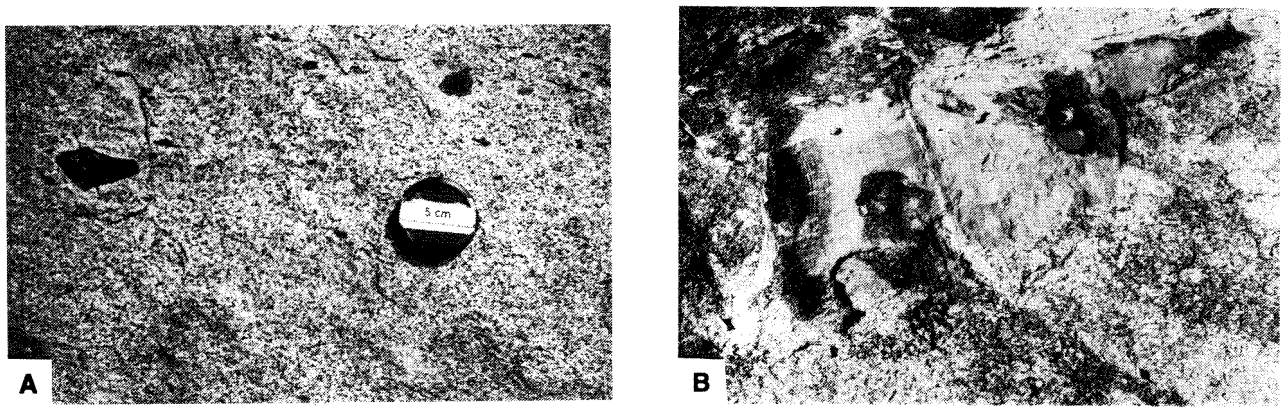


Figure 120. Xenoliths in post-folding granitoids: A — fragments of basalt and clots of mafic material in post-folding granodiorite; B — block of fine-grained, layered quartzo-feldspathic rock in porphyritic post-folding monzogranite. The open compass is 15cm long.

pluton, which outcrops near Karara Homestead in the southern Murchison Province (Plate 1), contains clinopyroxene and olivine, usually in a corona texture with hornblende. In general, post-folding granitoid rocks contain a higher proportion of ferromagnesian phases than either recrystallized monzogranite or pegmatite-banded gneiss.

Most post-folding granitoid rocks have an igneous hypidiomorphic granular texture (Fig. 121). However, some plutons are partly recrystallized, generally in greenschist facies (Plate 3). Plagioclase is euhedral to subhedral and has strong, complex, multiple or oscillatory zoning. Plagioclase crystals generally form glomerocrysts, some of them apparently of broken grains (e.g. Fig. 121). White and Chappell (1977) have suggested that zoned plagioclase such as this represents modified restite material. Overgrowths of unzoned plagioclase on these complex grains, and the coexistence of unzoned, or weakly and simply zoned grains of the same composition as the overgrowths, support this hypothesis. The presence of abundant cognate inclusions in most plutons also suggests that some restite material was transported upwards with granitoid magma.

Three plutons have unusual textures. A hornblende granophyre, 10 km southeast of the Dalgaranga mining centre, has a well-developed granophyric texture, regarded as a product of eutectic crystallization (Cox et al., 1979). Monzogranite of the Damperwah pluton consists of corroded bipyramidal phenocrysts of quartz, up to 6 mm across, and porphyritic zoned plagioclase with poikilitic hornblende and perthite in a finer grained matrix of quartz and feldspar. Quartz also occurs as numerous blebs in the matrix, and in perthite and hornblende (Fig. 122). The syenogranite at the northern end of the Koolanooka greenstone belt has a similar bimodal grain-size distribution. Broken euhedral phenocrysts of bipyramidal quartz, and K-feldspar and zoned plagioclase, are suspended in a fine-grained granular matrix of the same phases (Fig. 123). The rock contains about 3% modal biotite. Cobbing et al. (1986) recognized similar textures, commonly associated with tin mineralization, in some Malaysian granites. They considered that the textures were generated by late, high-



Figure 121. Photomicrograph of post-folding granitoid with igneous hypidiomorphic granular texture.

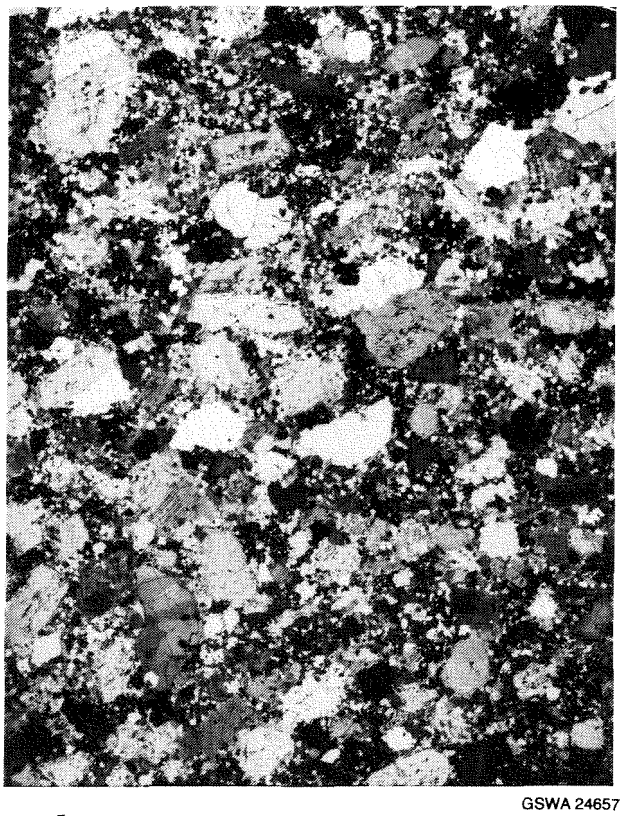


Figure 122. Photomicrograph of post-folding syenogranite of the Damperwah pluton, showing two-phase textural development of quartz. Corroded bipyramidal quartz phenocrysts represent the first phase, and tiny quartz blebs the second phase.

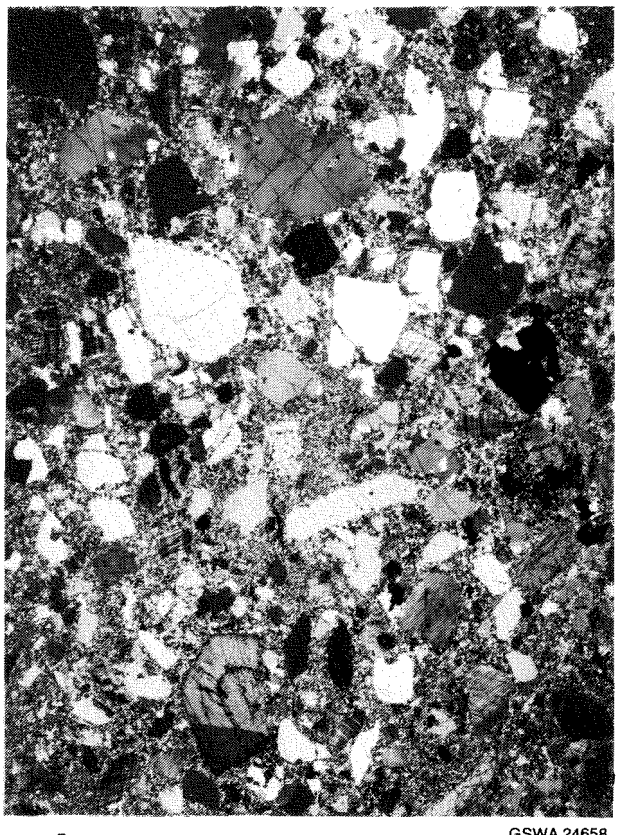


Figure 123. Photomicrograph of post-folding syenogranite of the Koolanooka pluton, showing bimodal grain-size distribution. Note the broken and fractured quartz bipyramids.

level pervasive emplacement of highly fractionated residual magmatic fluids into an already coarsely crystallized and essentially consolidated primary granitoid host.

Strong saussuritization of feldspar, and degradation of ferromagnesian phases, are characteristic of marginal zones of post-folding granitoids. Samples from core regions are much less altered. This suggests intense deuteric alteration in marginal zones by infiltrating hydrothermal fluids.

Geochemistry and petrogenesis

Of the 89 samples of post-folding granitoids collected for chemical analysis, 63 were from suite I and 26 from suite II (Appendix II). Between one and 14 samples were collected from each pluton (Fig. 96).

Post-folding granitoids have a broad range in composition, from syenogranite to trondhjemite (Table 31). They have distinctly different compositions compared with recrystallized monzogranite and pegmatite-banded gneiss. Tonalite is metaluminous, but the other granitoids are peraluminous. Both suites are calcic according to Peacock's alkali–lime index (Fig. 124). However, there are significant chemical differences between the two suites. Suite II rocks contain more F, Ba, Pb, Nb, Rb, Y, Zr, La, and Ce, and

TABLE 31. MEAN COMPOSITIONS OF POST-FOLDING GRANITOIDS

	SUITE I						*SUITE II*	
	High-Mg tonalite	*Low-Mg tonalite*	*Granodiorite*	*Monzogranite*	*Granophyre*	*Trondhjemite*	*Monzogranite*	*Syenogranite*
	n=11	*n=24*	*n=3*	*n=18*	*n=1*	*n=5*	*n=8*	*n=18*
				Percentage				
SiO_2	64.8	66.4	69.7	71.7	71.7	76.0	70.6	74.0
Al_2O_3	14.0	14.9	14.8	14.7	12.6	12.4	13.3	12.6
Fe_2O_3	1.8	1.7	1.2	1.3	0.8	1.6	1.3	0.8
FeO	2.64	2.39	1.44	1.32	0.78	1.63	2.63	1.62
FeO*(a)	4.3	3.9	2.5	1.9	4.3	2.0	3.8	2.3
MgO	3.63	1.74	1.01	0.53	0.33	0.25	0.84	0.24
CaO	4.55	3.59	2.58	1.93	2.07	1.42	2.23	1.16
Na_2O	4.04	4.23	4.62	4.77	4.30	4.57	3.17	3.02
K_2O	1.25	1.66	1.98	2.39	2.38	1.41	3.76	4.44
TiO_2	0.53	0.41	0.34	0.21	0.27	0.12	0.44	0.24
P_2O_5	0.17	0.16	0.18	0.09	0.06	0.09	0.27	0.11
MnO	0.06	0.06	0.03	0.03	0.05	0.03	0.07	0.04
LOI	1.90	1.85	1.09	1.17	0.71	1.19	0.95	0.79
				Parts per million				
F	355	409	433	379	420	158	1035	972
Ba	523	652	727	742	1040	552	1574	1007
Cu	37	33	24	19	8	12	11	17
Pb	(b)10	(b)19	(b)15	27	<10	9	31	31
Li	10	24	23	49	1	13	24	32
Mo	(b) 2	(b) 2	(b) 2	(b) 2	<1	2	<5	<5
Ni	106	49	34	23	25	23	27	16
Nb	(b) 7	(b) 7	<10	(b) 7	11	(b) 7	20	20
Rb	47	75	78	98	62	55	197	225
Sr	283	324	515	348	73	135	270	108
Th	<10	<10	(b)13	(b)12	14	10	20	46
Sn	<5	<5	<5	(b) 3	7	(b) 3	<5	<5
U	<1	<1	1	2	8	(b) 1	(b) 2	(b) 2
V	94	66	39	18	<10	(b) 5	(b) 30	(b) 9
W	(b)(c) 6	<2	<2	<10	nd	<10	(b) 3	(b) 5
Y	21	15	7	5	104	12	48	61
Zn	40	50	55	50	22	35	76	55
Zr	163	136	151	127	238	130	341	267
La	(c) 20	(d)15	(e)35	(f)23	nd	(g)29	(h) 88	(j)126
Ce	(c) 35	(d)41	(e)68	(f)45	nd	(g)45	(h)170	(j)240

The albitized tonalite 81739 is not included in this table (Appendix II)

(a) All Fe calculated as FeO (b) Some values used to calculate the means are below the detection limit; for these analyses the value 'detection-limit/2' was used. (c) mean of 9 analyses (d) mean of 15 analyses (e) mean of 2 analyses (f) mean of 17 analyses (g) mean of 4 analyses (h) mean of 5 analyses (j) mean of 11 analyses nd: not determined

have higher Rb/Sr and K_2O/Na_2O ratios than do suite I rocks (Table 31). The suites plot in distinctly different fields on a Na_2O–K_2O–CaO ternary diagram (Fig. 125). Tonalite, granodiorite, and monzogranite from suite I show a broad calc-alkaline differentiation trend of increasing K_2O/Na_2O ratio with decreasing CaO; however, the trend is displaced towards Na-rich compositions, and the K_2O/Na_2O ratio changes only slightly with increasing differentiation. Trondhjemite plots on the trondhjemite trend of Barker and Arth (1976) towards the Na_2O apex of the diagram. Suite II rocks plot along the calc-alkaline trend towards fractionated K-rich compositions. The two suites are also clearly distinguished by well-defined separate trends on Harker variation diagrams (Fig. 126), particularly on Al_2O_3, K_2O, Na_2O, FeO, and TiO_2 versus SiO_2 plots.

REE patterns for eight suite I samples and five suite II samples are shown in Figure 127. LREE contents of suite I rocks are enriched, and increase with degree of granitoid differentiation. Total REE contents range from 87 ppm and 103 ppm for the two low-Mg tonalite samples, to 159 ppm and 183 ppm for the two monzogranite samples. HREE contents of these rocks are variably depleted according to degree of differentiation; $(Tb/Yb)_N$ values are around unity for tonalites, and around four for monzogranites. Small negative Eu anomalies occur in tonalites, but not in the other suite I granitoids. HREE depletion was probably controlled by amphibole fractionation. Progressive HREE depletion and LREE enrichment, with increasing differentiation, can be explained in terms of both fractional crystallization and partial melting models. The range of patterns observed could be produced by crystal fractionation of amphibole from a large-percentage partial melt of a mafic source with residual plagioclase, but little residual amphibole or clinopyroxene. Europium enrichment of the melt due to amphibole crystallization, would cancel negative Eu

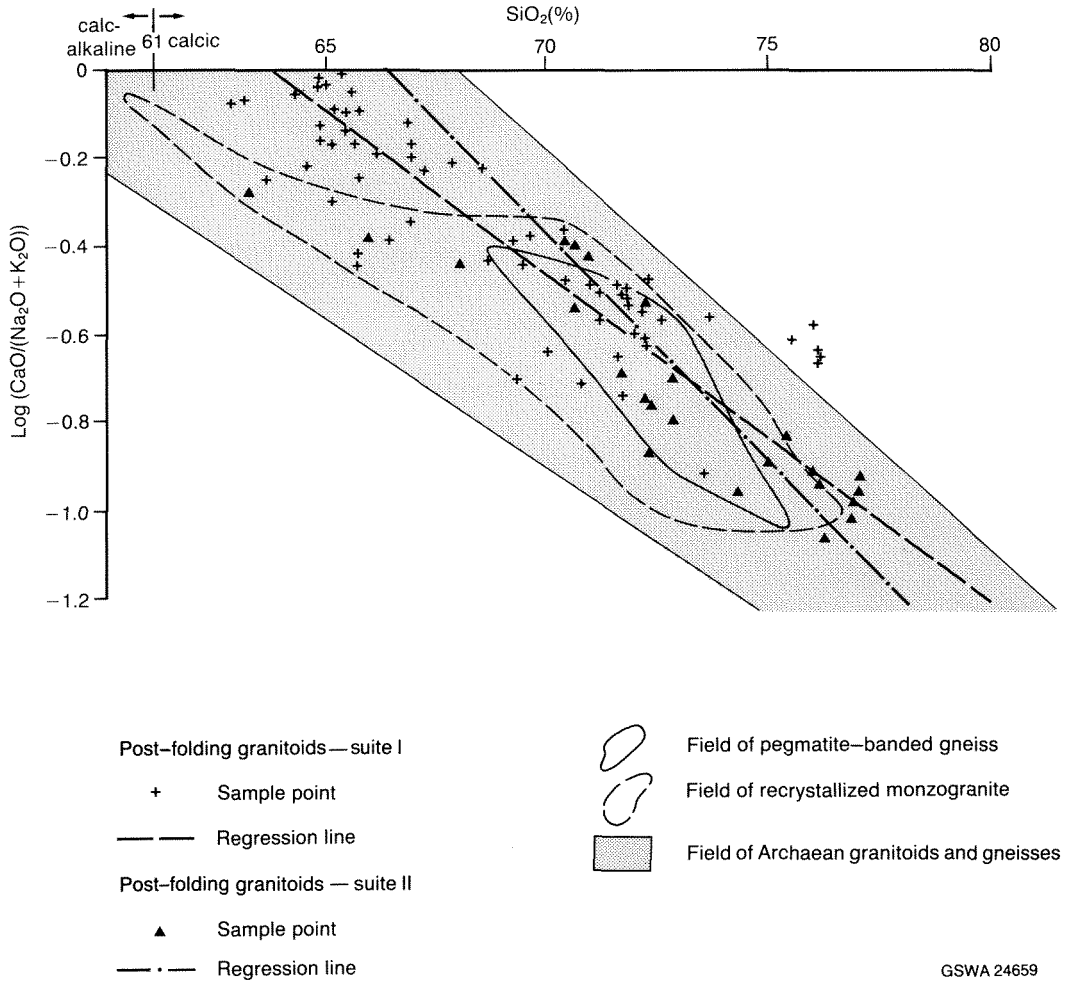


Figure 124. Log (CaO/(Na$_2$O+K$_2$O)) v. SiO$_2$ diagram for post-folding granitoids compared with recrystallized monzogranite, pegmatite-banded gneiss, and other Archaean granitoids and gneisses (sources of these data are given in Figure 97). Regression lines through the data for each post-folding granitoid suite are shown.

anomalies caused by residual plagioclase in more fractionated liquids. Alternatively, progressive degrees of partial melting of similar source rocks could also produce these patterns. However, the Eu anomalies in less differentiated rocks are difficult to explain in this model, as this would require residual plagioclase in high-percentage partial melts, producing tonalite; but no residual plagioclase in low-percentage partial melts, producing monzogranite.

REE patterns of suite II samples are distinctly different from suite I patterns and show less consistent variation with degree of differentiation (Fig. 127). Total REE contents of southern Murchison Province suite II samples, in the range 229–355 ppm, are higher than those of suite I samples. However, the northern Murchison Province suite II syenogranite (sample 81740) has an anomalously low REE content of 48 ppm. Except for this sample, suite II syenogranite samples have similar REE patterns, although sample 83407 has a much smaller negative Eu anomaly than other samples. These patterns require considerable residual feldspar in the source. It is unlikely that amphibole or garnet were important residual or fractionating phases as HREE patterns are relatively undepleted. However, some hornblende is present in two samples (83407 and 83551) and may originate from a small amount of hornblende which was completely melted in the source, or from clinopyroxene melted from the source and converted to amphibole in the more hydrous conditions of the melt. REE patterns of these syenogranite samples resemble those of high-(Zr+Y) felsic volcanic rocks described in Chapter 2, and suggest a similar siliceous granulite source. Although major and trace-element characteristics of the monzogranite 83380 and the syenogranite 81740 indicate that they are part of the same igneous suite as the other samples, their REE patterns indicate a different derivation. The patterns show evidence of amphibole and/or garnet involvement, either as residual or fractionating phases. Sample 83380 retains about 5% modal hornblende, so the source must have contained abundant hornblende or garnet and was probably mafic. Removal of REE-rich phases such as sphene and/or allanite may have reduced the REE content of sample 81470 (Gromet and Silver, 1983).

Post-folding granitoid suites plot in two discrete groups on Ab–Or–Qz and Ab–Or–An CIPW norm diagrams (Fig. 128). Suite I rocks plot in the plagioclase–quartz field in Ab–An–Or–Qz space, with reasonably good separation between tonalite, trondhjemite, and monzogranite. Suite II

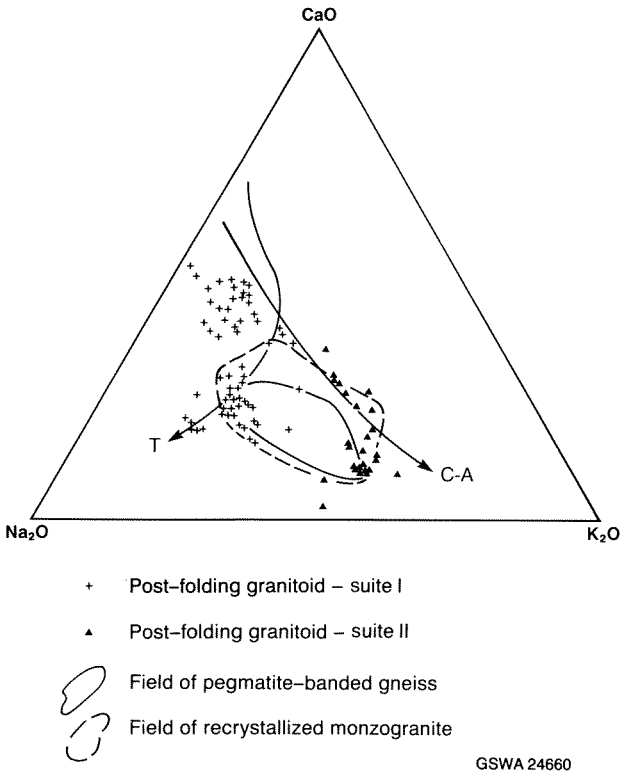


Figure 125. Post-folding granitoid compositions plotted on a Na_2O–K_2O–CaO ternary diagram. C–A — calc–alkaline trend (Nockolds and Allen, 1953); T — trondhjemite trend (Barker and Arth, 1976).

data straddle the plagioclase–alkali-feldspar cotectic on the Ab–Or–An diagram, and partly straddle the quartz–alkali-feldspar cotectic on the Ab–Or–Qz diagram. This distribution supports other geochemical data that indicate two distinct magma sources for these suites. The abundance in these granitoids of restite phases (such as cognate inclusions and zoned plagioclase) indicates that temperatures of magma genesis were not significantly higher than those required to produce melts on the pertinent cotectic surfaces (Winkler, 1979). These temperatures are about 700–740°C for tonalite, 680–700°C for monzogranite and trondhjemite, and under 670°C for syenogranite at $P(H_2O)$ = 500 MPa, with lower temperatures at higher water pressures (Winkler, 1979, fig. 18-8).

Geochronology and isotope geochemistry

U–Pb zircon, Sm–Nd, and Rb–Sr ages have been determined on a number of post-folding granitoids (Fig. 103). Zircons in rock samples from the suite II monzogranite of the Damperwah pluton (83407, a split of geochemistry sample 83408) and syenogranite of the Koolanooka pluton (83551, a split of geochemistry sample 83552) (Fig. 129D) were analysed for U–Pb isotopes on the ion-microprobe at the Australian National University (Wiedenbeck and Watkins, in prep.). These samples gave crystallization ages of 2641 Ma and 2617 Ma, respectively.

Sm–Nd model ages have been determined on two suite I and two suite II samples (Appendix III). Suite I samples gave T_{DM} model ages of 2820 Ma and 2870 Ma, which are considerably older than their assumed (c. 2630 Ma) emplacement age and indicate derivation of suite I source rocks from the mantle up to a few hundred million years before their remelting to form granitoid magma. Model ages for suite II rocks of 3153 Ma and 3301 Ma are much older than their emplacement ages, and older than suite I Sm–Nd model ages. The crustal source rocks for suite II plutons are very much older than those for suite I plutons, and are of different compositions. They were derived from the mantle at least 500 million years before granitoid magma genesis.

Rb–Sr isochrons for two suite II plutons have been published (Arriens, 1971; de Laeter and Baxter, 1987) (Table 30). The Rb–Sr date for syenogranite from the Mulgine pluton concurs broadly with the U–Pb zircon dates, although it also corresponds to the regional metamorphic resetting event recorded at about 2600 Ma in recrystallized monzogranite and pegmatite-banded gneiss. Rb–Sr dates for the Koolanooka pluton are much younger than the 2617 Ma U–Pb zircon crystallization age; the reason for this is not known.

Rb–Sr isotopes were measured on 30 samples of suite I granitoids, and 19 samples of suite II granitoids collected for this study (Appendix III, Figs 103, 129, and 130). Rb–Sr dates should reflect crystallization ages, as post-folding granitoids retain most of their igneous mineralogies. However, the metamorphic resetting event (c. 2600 Ma) recorded in earlier granitoids may have affected the distribution of Sr in these rocks also. Because of large uncertainties in the dates, these two events cannot be resolved with the Rb–Sr data.

Suite I tonalite and trondhjemite give ages, with large uncertainties, which are broadly consistent with both crystallization ages and metamorphic resetting. Initial ratios of about 0.702 are compatible with derivation of magma from a crustal source. The suite I monzogranite of the Mainland pluton yields a much younger age than other suite I plutons, albeit with a very large uncertainty. Most samples from this pluton were collected from its margin near a large quartz vein (samples 74467 to 74474, 81766 and 81767, Fig. 129C). Late hydrothermal activity associated with vein formation could have affected the Rb–Sr isotope system in the adjacent monzogranite.

Two suite II plutons dated by the Rb–Sr method give quite different ages (Appendix III). The monzogranite from the Damperwah pluton gives a model 3 Rb–Sr age of 2867 ± 82 Ma, consistent with both the U–Pb zircon date and metamorphic resetting. The high Rb/Sr syenogranite of the Koolanooka pluton gives a much younger model 1 Rb–Sr age of 2402 ±149 Ma, which is inconsistent with the U–Pb zircon date of 2617 Ma. The initial ratio of 0.7330 for this intrusion is very high, indicating a crustal melt.

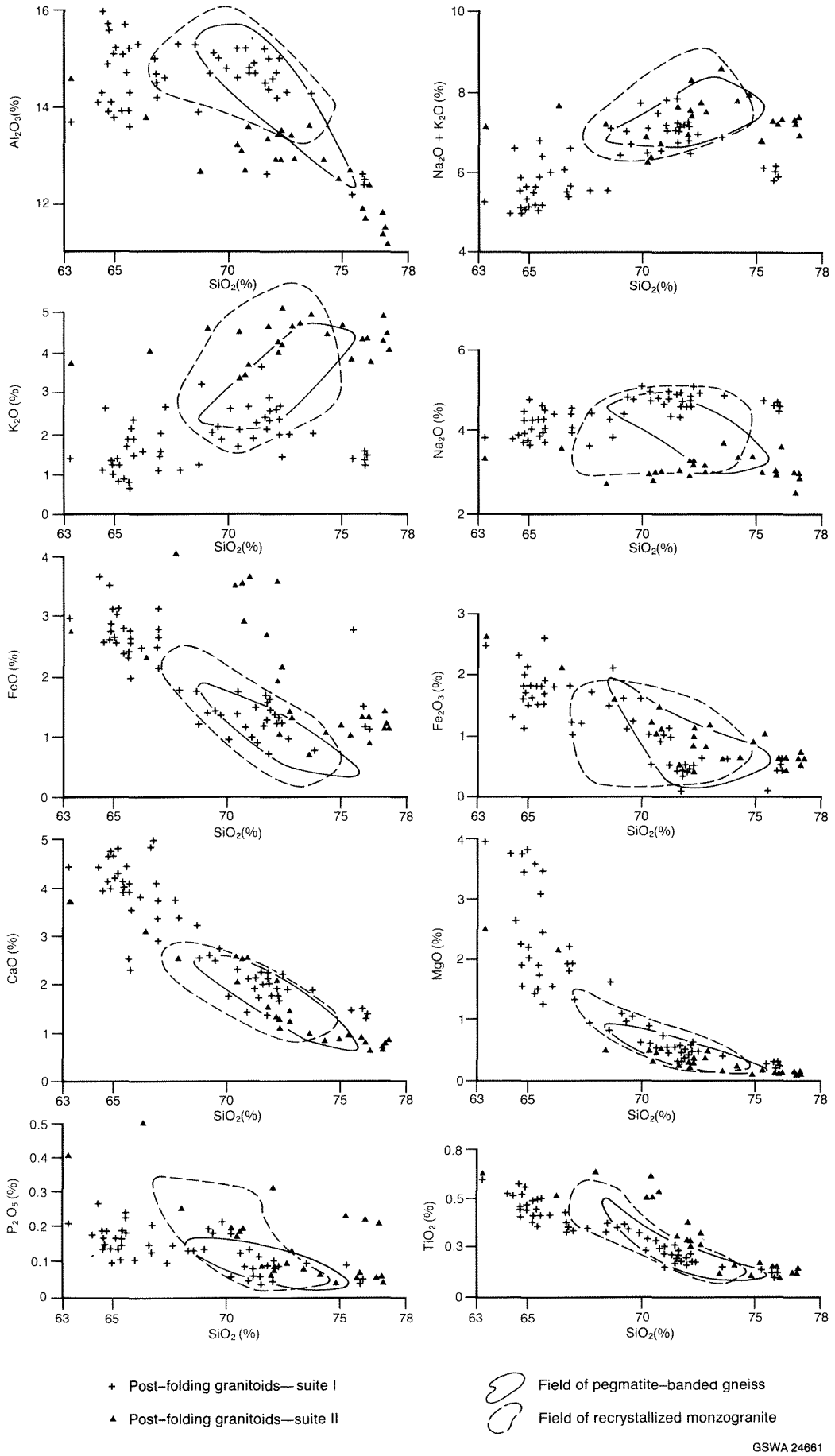


Figure 126. Major-oxide Harker variation diagrams for post-folding granitoids. Compositional fields for pegmatite-banded gneiss and recrystallized monzogranite are shown.

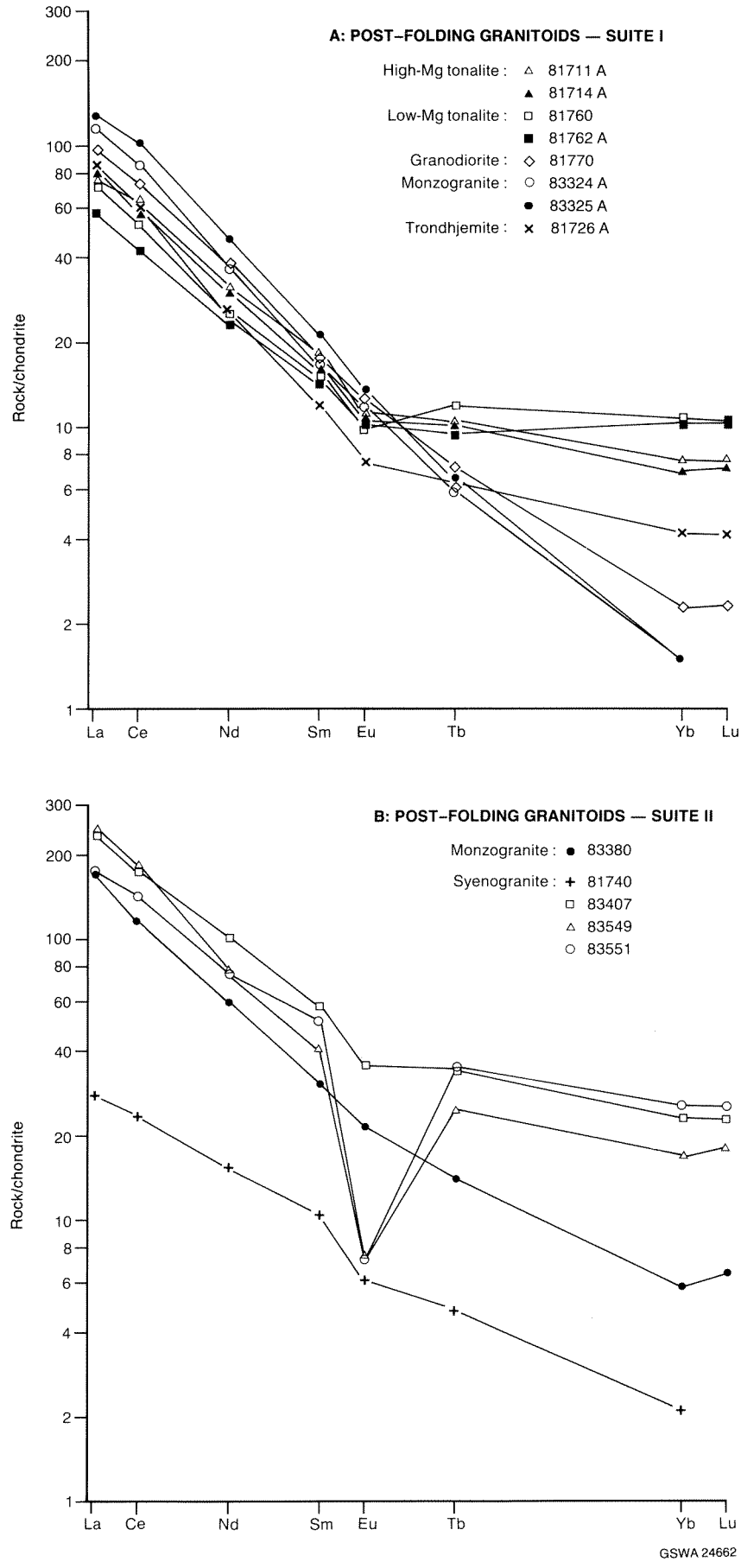


Figure 127. REE patterns for post-folding granitoid samples.

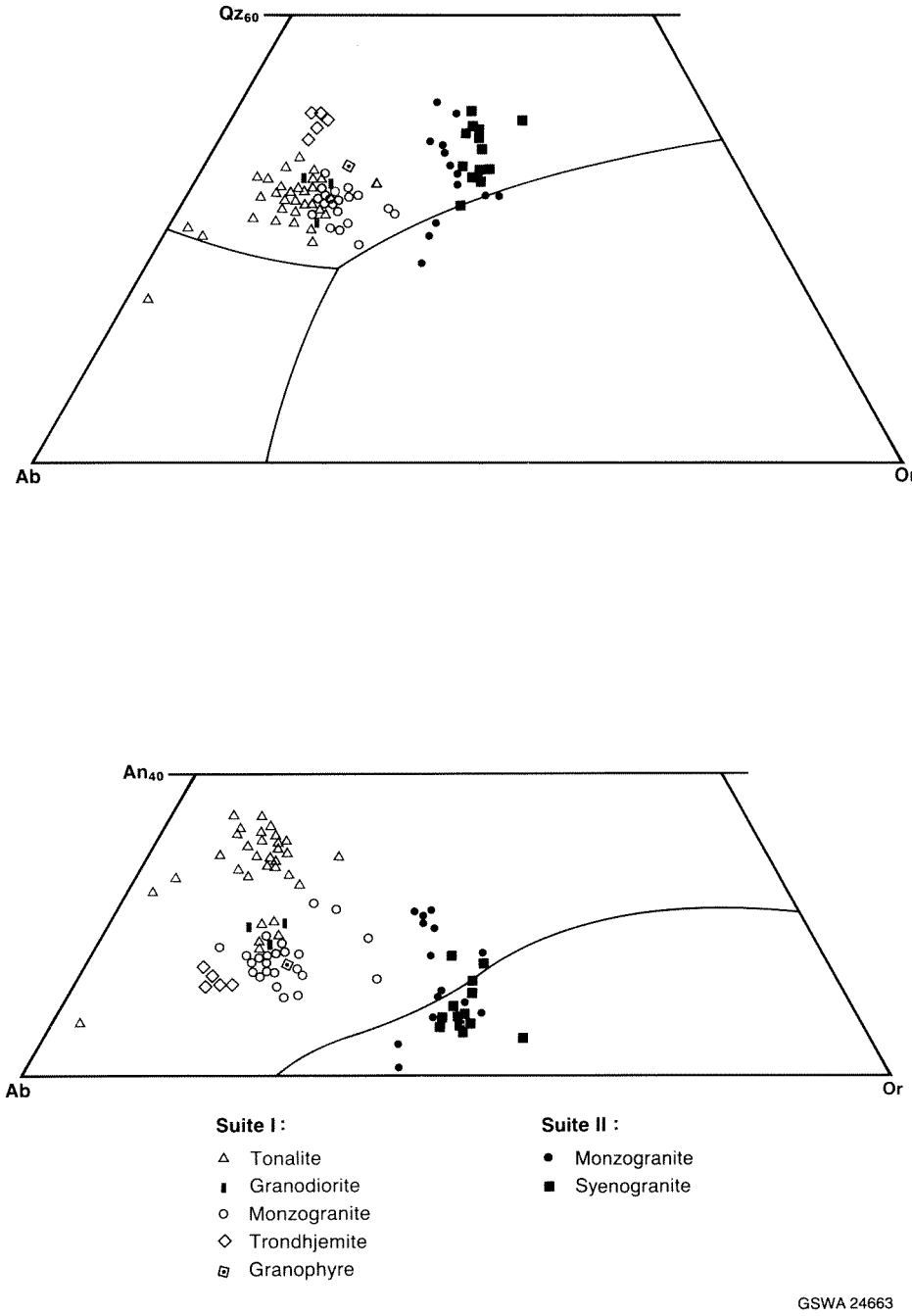


Figure 128. Post-folding granitoid compositons plotted on CIPW norm diagrams. Cotectic lines as in Figure 102.

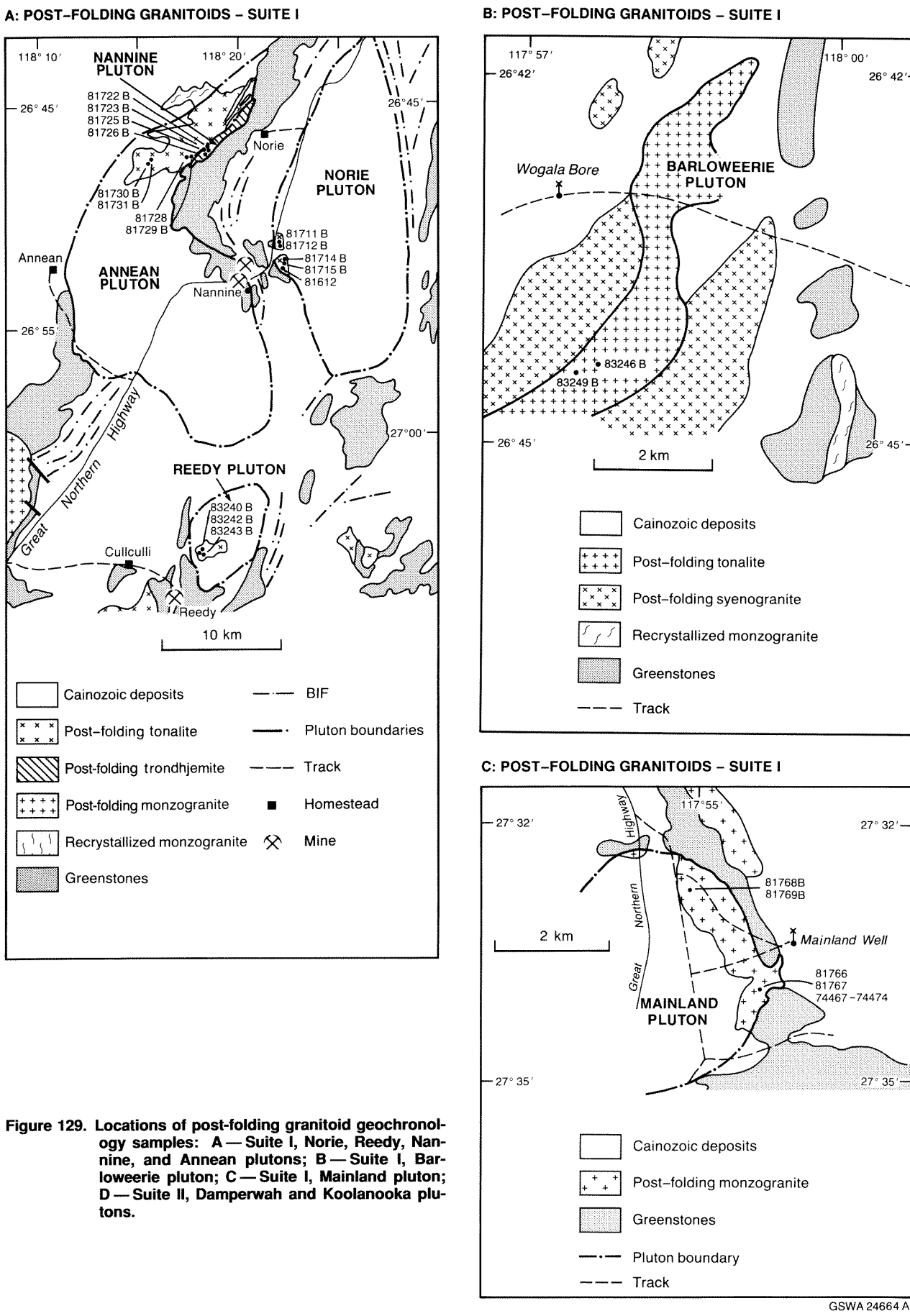


Figure 129. Locations of post-folding granitoid geochronology samples: A — Suite I, Norie, Reedy, Nannine, and Annean plutons; B — Suite I, Barloweerie pluton; C — Suite I, Mainland pluton; D — Suite II, Damperwah and Koolanooka plutons.

D: POST-FOLDING GRANITOIDS – SUITE II

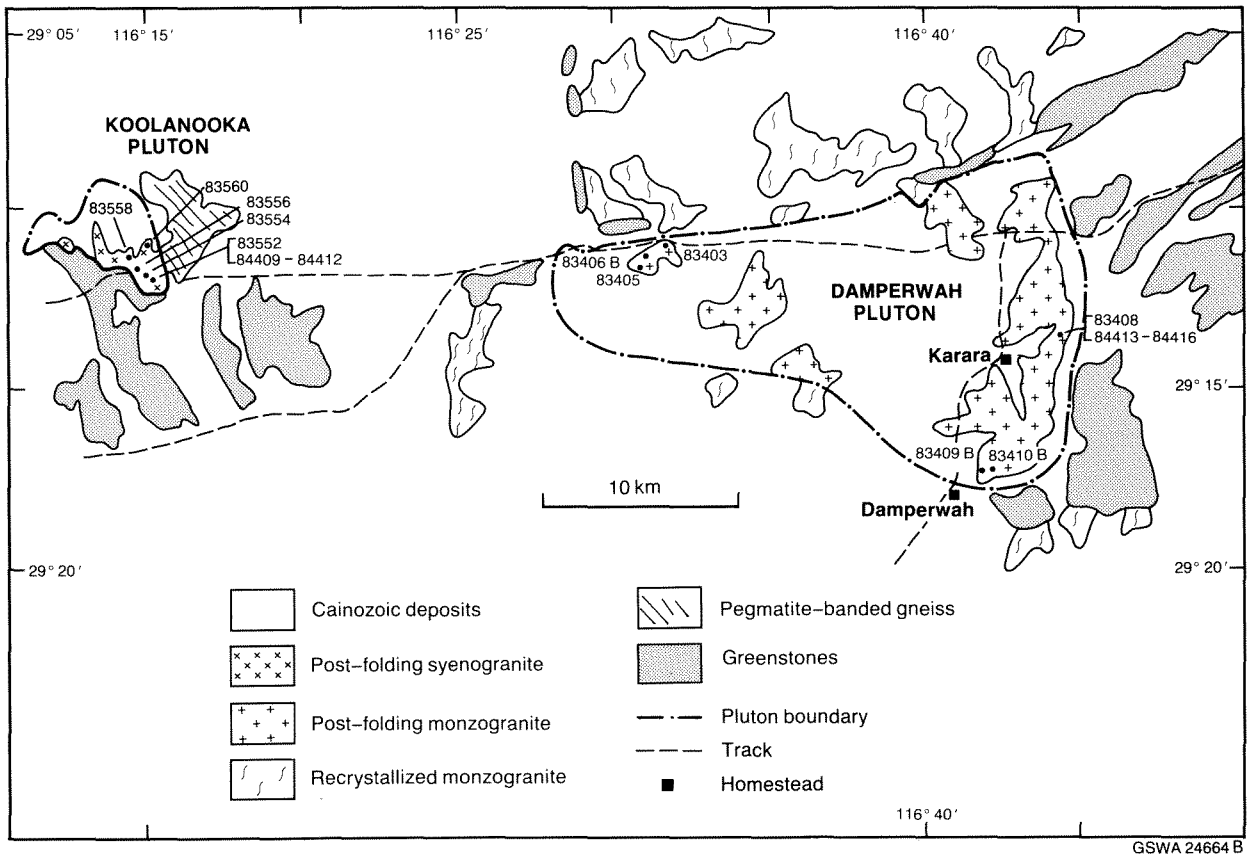


Figure 129. (continued)

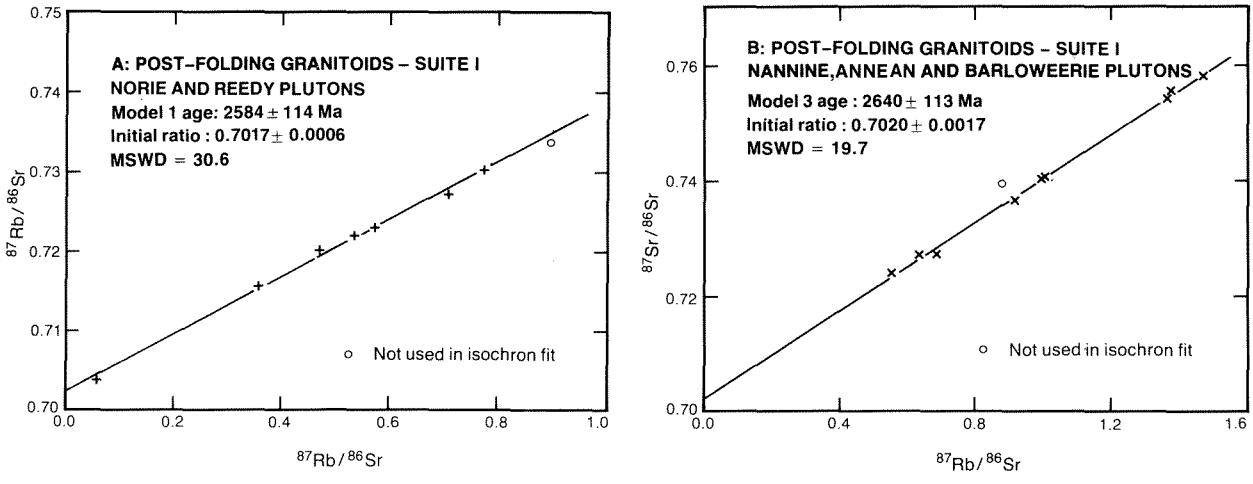
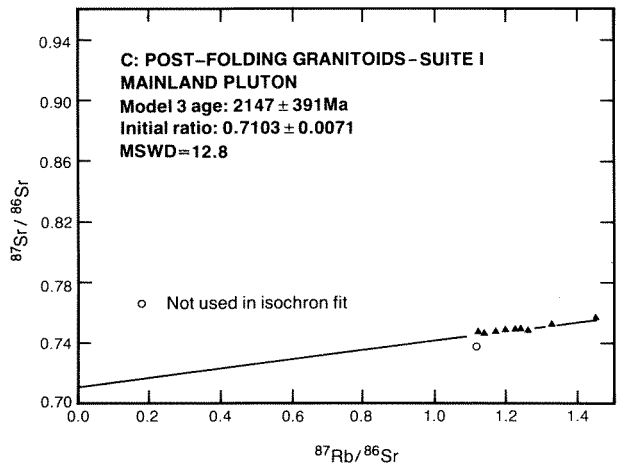
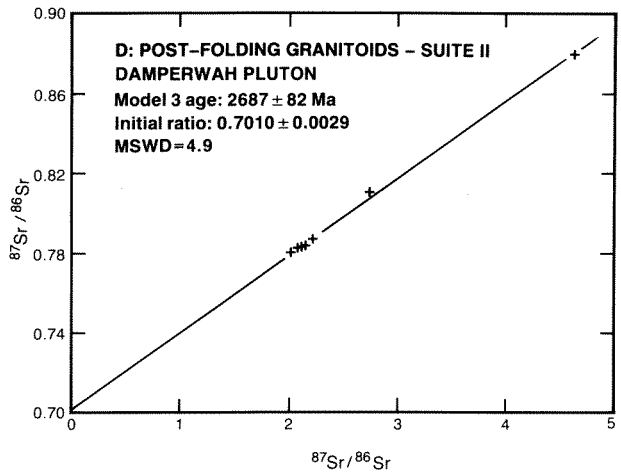


Figure 130. Rb–Sr isochron plots for post-folding granitoids.





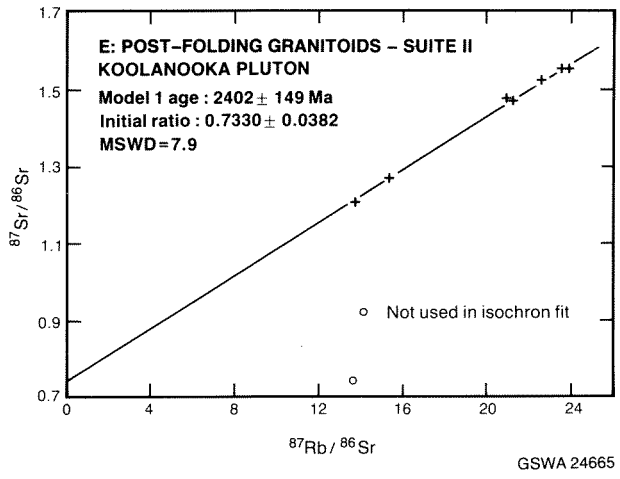


Figure 130. (continued)

Synthesis

Three episodes of felsic plutonism produced four suites of granitoid rocks in the Murchison Province:

1. Monzogranite, granodiorite, and pegmatite intruded the base of the Luke Creek Group as subhorizontal sheet-like plutons, during D_1 deformation, at about 2920 Ma. There were two phases of monzogranite and granodiorite intrusion, and an intervening phase of pegmatite injection. These intrusive phases were tectonically interleaved and attenuated to form pegmatite-banded gneiss. Intrusion and deformation were broadly coeval. Pegmatite-banded gneiss protoliths were derived by partial melting of lower crustal mafic rocks. The gneiss now occurs in a broad belt in the western part of the province; elsewhere it forms enclaves, rafts, and xenoliths in recrystallized monzogranite.

2. Thick, subhorizontal tabular plutons of monzogranite successively intruded the base of the Murchison Supergroup over the period of at least 2690–2681 Ma. These rocks are compositionally similar to pegmatite-banded gneiss and were derived by similar processes, and from similar source rocks, in the lower crust. Monzogranite complexes were folded into domes during D_2 and D_3, and were then regionally metamorphosed and thoroughly recrystallized in greenschist and lower amphibolite facies. Recrystallized monzogranite now forms vast, domal, composite plutonic complexes, which occupy most of the regions between greenstone belts.

3. Two suites of post-folding granitoids intruded the Murchison Supergroup over the period of at least 2641–2617 Ma. These granitoids are confined to greenstone belts, and contacts between these belts and older granitoids; none have been found wholly within older granitoids. Post-folding granitoids have subcircular and oval-shaped outcrops, and truncate stratigraphic units and tectonic features associated with folding. Suite I post-folding tonalite, granodiorite, monzogranite, syenogranite, and trondhjemite plutons were mainly confined to the northern half of the province, but suite II post-folding granitoids, comprising quartz-rich monzogranite and syenogranite, were mainly confined to the southern half. Both suite I and II plutons occur together in the extreme western and northern parts of the province. Suite I granitoids were derived by partial melting of mafic crustal rocks which probably intruded or underplated the crust at about 2.8 Ga. Suite II granitoids are chemically and isotopically distinct from suite I granitoids and were derived mainly by partial melting of siliceous granulite which was at least as old as basal greenstones (>3.0 Ga). The parent magmas of post-folding granitoids were probably generated in synformal regions of the deep crust by partial melting associated with regional metamorphism, which at higher crustal levels recrystallized greenstones and earlier granitoids in greenschist and lower amphibolite facies.

Chapter 4

Mafic and ultramafic intrusive rocks

Mafic and ultramafic intrusions constitute a significant proportion of Murchison Province rocks. Mafic intrusive rocks are much more abundant than ultramafic intrusive rocks, and many ultramafic units are derived from mafic magmas by differentiation *in situ*. Two broad types of mafic–ultramafic intrusions are abundant: concordant and subconcordant sills in greenstone belts, and cross-cutting intrusions in greenstone belts, granitoids, and gneiss. In addition, a major layered gabbroid complex intrudes the Dalgaranga greenstone belt (Watkins et al., 1987). The anorthositic Windimurra gabbroid complex, which outcrops over 2200 km^2 of CUE, KIRKALOCKA, SANDSTONE, and YOUANMI, is not described here. It lies near the poorly defined boundary between the Murchison and Southern Cross Provinces (Gee et al., 1981) and cannot, with present knowledge, be assigned to either. Ahmat (1986a, 1990) and Ahmat and de Laeter (1982) have described this intrusion.

Gabbroid complex near Dalgaranga

The Dalgaranga greenstone belt has been intruded and substantially thickened by a stack of seven broadly conformable and related gabbroid sills (Fig. 131, Plate 1). Six of the seven sills are at least 1 km thick, the other is a few hundred metres thick. The sills are described in ascending order from the base of the greenstone belt to the top.

The lowermost sill intrudes mafic volcanics at the base of the greenstone belt near Mount Farmer. The sill is a homogeneous, fine- to medium-grained, porphyritic olivine norite; its margin, where observed, is fine-grained foliated dolerite. The sill is intruded by post-folding monzogranite and hornblende granophyre.

The next sill in the sequence occurs at Dalgaranga Hill and intrudes a pelitic unit. Its lower part, forming the hill itself, is a medium- to coarse-grained, homogeneous gabbro norite. The upper part, northeast of Dalgaranga Hill, exhibits cyclic layering, 5 cm to several metres thick. The cycles consist of pyroxenitic gabbro bases grading to leucogabbro tops. Some pegmatoid layers occur.

The next sill in the sequence occurs west of Gum Well, and is separated from the Dalgaranga Hill sill, to the southwest, by pelitic rocks. It is a homogeneous, medium- to coarse-grained gabbro. A north-trending fault, west of Range Well, separates the two lower sills from those higher in the stratigraphic sequence to the northeast.

Two sills occur above the Gum Well sill near Range Well; these are separated by felsic tuffs. The lower sill is a homogeneous, medium- to coarse-grained gabbro, which is locally foliated near its margins. The upper sill shows large-scale differentiation layering, and has a peridotite (now serpentinite) to pyroxenite base, 200 m thick, which is overlain by up to 500 m of gabbro.

The two uppermost sills intrude felsic tuff and volcanogenic sandstone at the top of the greenstone sequence to the east and south of the Dalgaranga mining centre. They are strongly differentiated sills, each up to 1 km thick and comprising four layers: peridotite, pyroxenite, gabbro, and quartz leucogabbro, with gradational contacts. The margins of these sills, in contact with the greenstone sequence, are foliated. The uppermost sill is intruded along its northern and northeastern margins by a post-folding monzogranite. Xenoliths of gabbro occur in the monzogranite, and pegmatite and aplite intrude the margins of the sill.

There is an overall pattern of progressive upward differentiation within the sill sequence. Sills in the vicinity of Mount Farmer, Dalgaranga Hill, and Gum Well are olivine norite, gabbro norite, and gabbro, respectively. Those near Range Well are gabbro, the upper one being differentiated into three layers. The two uppermost sills in the sequence are each strongly differentiated into four layers.

Concordant sills

Concordant and subconcordant peridotite (now serpentinite), pyroxenite, gabbro, and dolerite sills are abundant in all basalt sequences in greenstone belts and were all deformed and metamorphosed with the surrounding volcanic rocks. Where the sills are undifferentiated they generally contain the same mineral assemblages as the associated volcanic rocks. Ultramafic intrusions are more abundant in high-Mg basalt units than in tholeiitic units, and conversely, gabbro and dolerite sills are more abundant in tholeiitic units. Most minor sills appear to be consanguineous and broadly contemporaneous with the volcanic

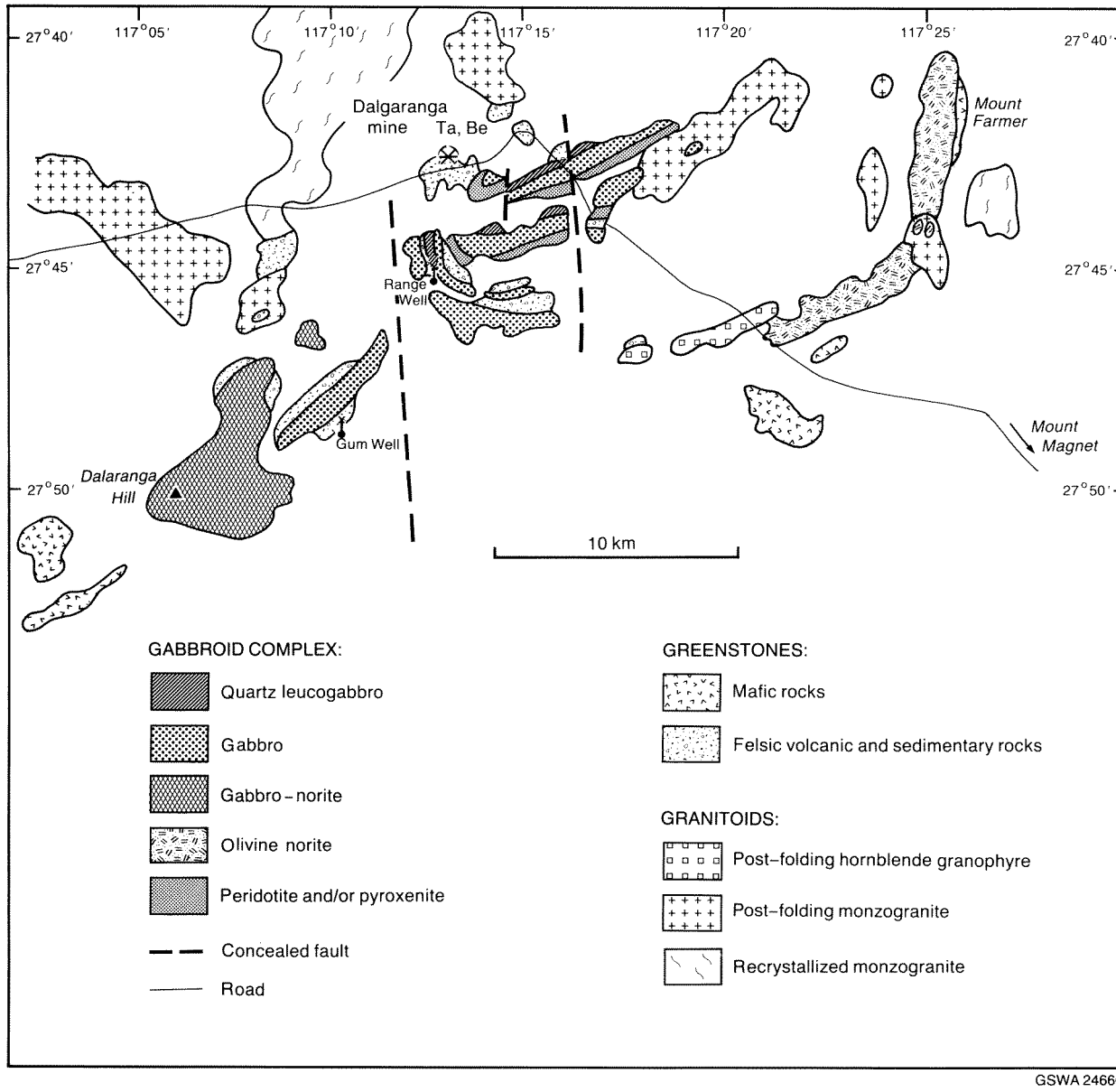


Figure 131. Geology of the gabbroid complex near Dalgaranga.

sequences in which they occur (cf. Jolly, 1977; Hallberg and Wilson, 1983).

Most of these intrusions are too small to be represented on the Plates. However, many are large composite bodies exceeding 1 km in total thickness and several tens of kilometres in strike-length. These composite bodies generally comprise numerous sills intruded into the same part of the greenstone succession; many are separated by screens of country rock. In the Weld Range, intrusion of multiple dolerite sills into Windaning Formation rocks has formed a composite dolerite body, up to 5 km thick, containing abundant screens of BIF. In the vicinity of the Blue Hill Range (Plate 1) numerous sills of dolerite and gabbro intrude the Gabanintha and Windaning Formations; many are separated by screens of basalt, felsic volcanic rocks, and BIF. Many sills, particularly the larger ones, contain differentiation layering, and have bases of peridotite (now serpentinite) or pyroxenite, and leucogabbro tops.

There appear to be more large gabbro sills in the southern part of the Murchison province than in the northern part (Plate 1); the reason for this is unknown. Throughout the province mafic sills selectively intrude the Golconda and Windaning Formations, the two formations which contain the most BIF.

Cross-cutting intrusions

Cross-cutting dykes and plugs of dolerite and gabbro are abundant in the Murchison Province (Plate 1). They are

more conspicuous in regions of granitoid and gneiss than in greenstone belts. The dykes intrude post-folding granitoids and therefore represent the last rock-forming event in this part of the Yilgarn Craton. There are several main trends of dykes which may represent different intrusive events. Westerly to west-southwesterly trending dykes dominate throughout most of the province. However, in the west of the province, southwesterly to south-southwesterly trending dykes dominate, and south of Perenjori, a conjugate set of southwesterly and southeasterly trending dykes occurs (Plate 1, Fig. 132). Flat-lying dolerite sills, several metres thick, intrude the greenstone succession and recrystallized monzogranite 10 km west-southwest of Noongal Homestead in the Yalgoo–Singleton greenstone belt.

The dykes range from a few metres to a few hundred metres wide; they are discontinuous, and vary in length from a few hundred metres to almost 100 km (Plate 1). They are neither deformed nor metamorphosed. Rock type varies from basalt to gabbro, depending on the width of the dyke. Most thin dykes (< 5m) are dolerite, but some are basalt; most thick dykes (> 20m) are gabbro, some of which is porphyritic. Gabbro and dolerite plugs are abundant in some areas (e.g. 15 km northwest of Chiggarrie Rock), but most are small and are not shown on the Plates. Westerly and west-southwesterly trending dykes have been correlated (de la Hunty, 1975) with the Widgiemooltha dyke suite (Soufolis, 1966), which gives a Rb–Sr isochron of 2420 ± 30 Ma (Turek, 1966).

Intrusions of lamprophyre have been identified near Cue (Miles, 1948a), and at a small number of other localities in Murchison Province greenstone belts (Rock et al., 1988).

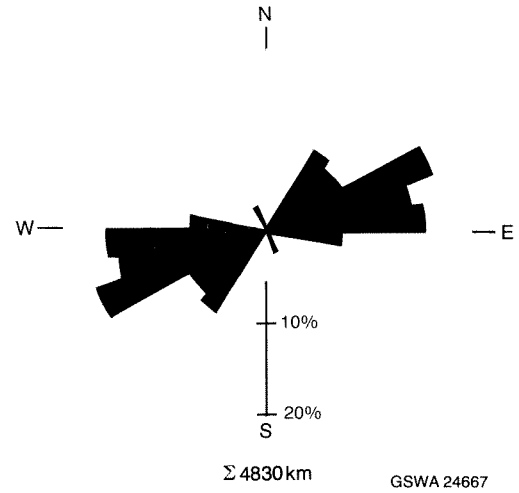


Figure 132. Azimuths of late, cross-cutting mafic dykes in the Murchison Province.

Chapter 5

Structure

Deformation scheme

The distribution of granitoids, gneisses, and greenstones in the Murchison Province forms a distinctive pattern typical of many Archaean granite–greenstone terranes (Condie, 1981). Linear arcuate belts of supracrustal rocks are separated by large regions of granitoids (Plate 1). This distribution is controlled by five major phases of deformation:

D_1: horizontal tectonic movements — recumbent folding and probably thrusting;
D_2: tight, upright folds with east-trending fold axes;
D_3: intense development of tight and isoclinal, upright folds with north-northeasterly to north-northwesterly trending fold axes;
D_4: extensive shear zone and fault development with mainly north to north-northeast trends;
D_5: shear zone and fault development in the northwestern portion of the Province, with mainly east to southeast trends.

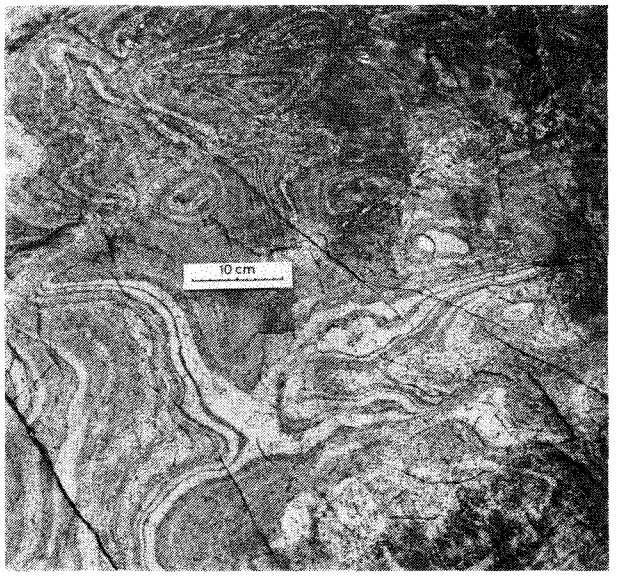
D_3 and D_4 are regarded as different phases of the same overall deformation event, driven by regional east–west compression.

D_1: horizontal structures

D_1 structures have been identified only in the Luke Creek Group and pegmatite-banded gneiss. The inference is that only these crustal components existed prior to D_1.

Pegmatite-banded gneiss

Pronounced banding developed during the earliest recognizable phase of deformation in pegmatite-banded gneiss (cf. Myers, 1978) (Fig. 84). In an outcrop 40 km south of Yalgoo, described in Chapter 3 (Fig. 93), amphibolite and BIF layering, and banding in gneiss, are folded by non-cylindrical F_2 and F_3 folds forming an irregular dome-and-basin fold pattern (Fig. 133). When the effects of these folds are removed, the attitude of amphibolite–BIF layering and gneiss banding is horizontal. Some form of horizontal tectonic movement formed the banding in this orientation (Myers and Watkins, 1985). As described in Chapter 3, the outcrop pattern (Fig. 93) indicates that pegmatite-banded gneiss protoliths and amphibolite–BIF units were interleaved as sheets. Banding and fabrics in amphibolite, BIF, and gneiss are broadly congruent and cognate. A few contacts preserve original intrusive relations; however, most are high strain zones which were initiated during D_1 and which developed further, by simple shear, during D_2 and particularly during D_3. It is thought that pegmatite-banded gneiss protoliths intruded the amphibolite–BIF units as sheets which were then further interleaved during D_1, magmatism and tectonism being broadly coeval (cf. Myers, 1984).



GSWA 24668

Figure 133. Dome-and-basin fold pattern in pegmatite-banded gneiss, from the outcrop shown in Figure 93.

Luke Creek Group

Major F_1 isoclinal fold structures have been identified in the Luke Creek Group. These folds are generally poorly preserved, and have been recognized at only five localities: near Mount Magnet; in the Wownaminya Hill and Rothsay–Red Hill regions of the Yalgoo–Singleton greenstone belt; in the southern part of the Koolanooka green-

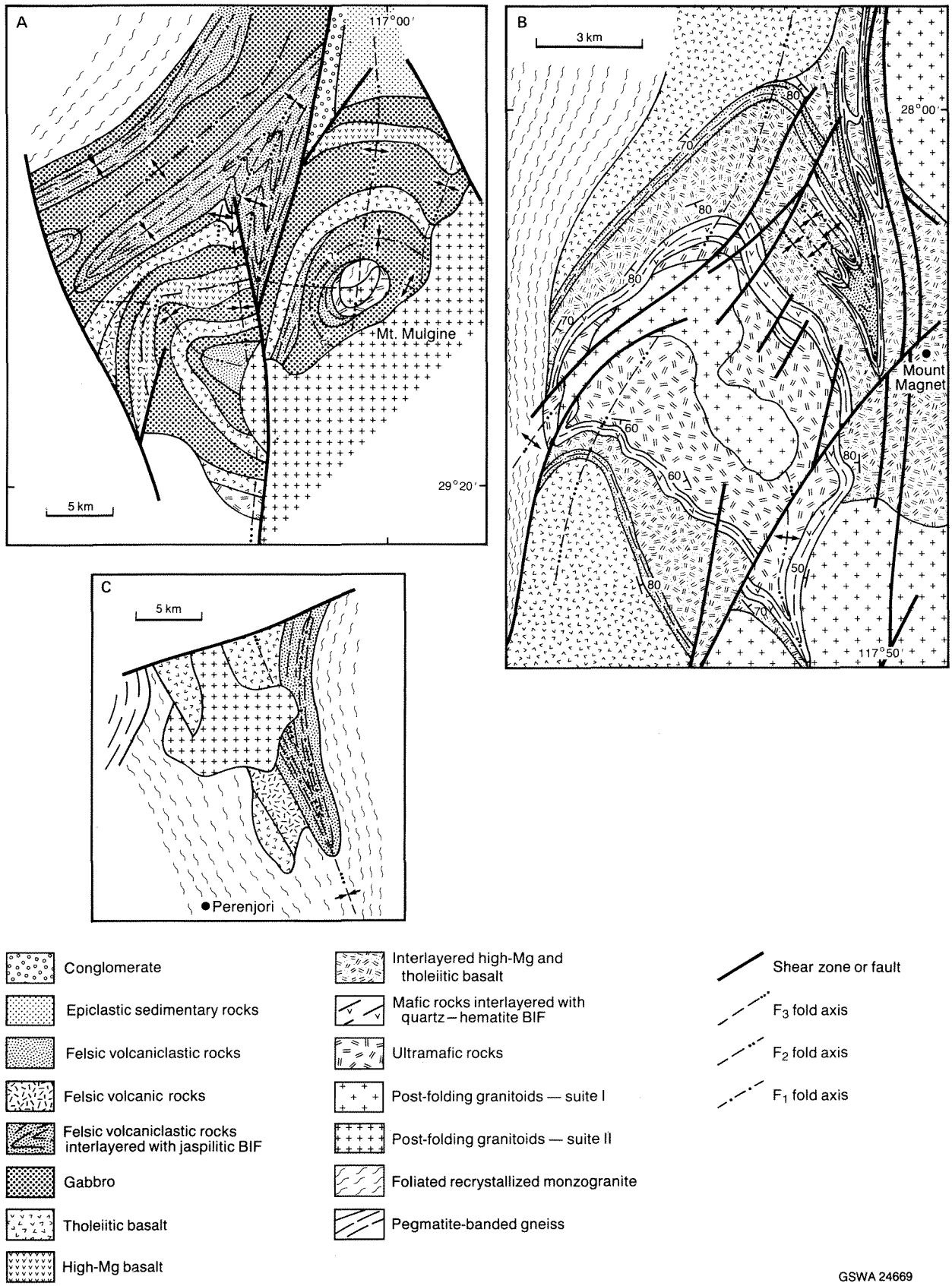


Figure 134. Fold patterns in greenstone belts: A — Rothsay-Red Hill region; B — Mount Magnet region; C — southern Koolanooka greenstone belt.

stone belt; and in the Meekatharra–Wydgee greenstone belt, 25 km south of Meekatharra (Fig. 134, Plate 2). Although their axial planes are now subvertical, due to refolding during D_2 and D_3, the forms of F_2–F_1 and F_3–F_1 fold-interference patterns indicate that F_1 folds must originally have had subhorizontal axial planes (Ramsay, 1967), i.e. they were recumbent.

Minor F_1 isoclinal folds, which are often rootless, are occasionally preserved in multilayered units, such as BIF and sedimentary rocks (Fig. 135). However, in zones of high D_3–D_4 strain, minor F_2 and F_3 tight folds are attenuated and can resemble F_1 folds.

In the northern Murchison Province, a layer-parallel sinistral shear zone, 100–400 m wide, occurs in the ultramafic unit near the base of the Gabanintha Formation. The shear zone extends from Gabanintha, through Meekatharra, Yaloginda, and Nannine, to Reedy (Plates 1 and 2). The shear zone is folded by F_2 and F_3 folds and is therefore assigned to D_1; however, it shows evidence of reactivation during folding and D_4 shearing. Movement probably began on a D_1 thrust. The structure of this shear zone in various mining centres is described in Chapter 7.

Layer-parallel fabrics are common in the Luke Creek Group, particularly near contacts between rheologically different units such as granitoids and greenstones; however, they are rare in the interiors of massive units such as mafic intrusives and thick basalt sequences. In most instances it is not clear which phase of deformation is responsible for these fabrics, as layer-parallel foliations were developed in limb regions of isoclinal F_1 and F_3 folds.

D_2: east–west folds

D_2 structures in greenstones

Several major easterly trending tight F_2 folds deform the Murchison Supergroup (Plate 2). De la Hunty (1973) also recognized these folds on CUE. F_2 folds were upright, with vertical axial planes and horizontal fold-axes. Fold shapes and fold axis orientations were intensely modified during D_3 and D_4. Major F_2 fold axes appear to be more widely spaced than F_3 fold axes (Plate 2), although many F_2 folds may not have been identified. Some F_2 fold axes on Plate 2 have been inferred on the basis of plunge reversals of F_3 fold axes. However, these plunge reversals could simply be associated with doubly plunging F_3 folds.

In general, S_2 fabrics were only weakly developed and have been obscured in regions of high D_3–D_4 strain (also see Frater, 1983a, p. 879; note that his f_1 is equivalent to F_2 of this bulletin). In the Tallering greenstone belt, S_2 fabrics are well preserved because D_3–D_4 structures were poorly developed. Minor F_2 folds are common in multilayered rocks such as BIF, for example in the northern part of the Gullewa greenstone belt and in the Tallering greenstone belt. Minor folds can be assigned to D_2 with confidence only when they can be related to a major structure; otherwise the problem of distinguishing minor F_1, F_2, and F_3 folds remains.



GSWA 24670

Figure 135. Minor F_1 rootless isocline in banded iron-formation, 10km north of Mount Yagahong on GLENGARRY. The compass is 8cm across.

D_2 structures in pegmatite-banded gneiss and recrystallized monzogranite

F_2 folds are well developed in pegmatite-banded gneiss. They were generally refolded during F_3 to form dome-and-basin fold patterns (Figs 93 and 133).

D_2 fabrics are the earliest recognized in recrystallized monzogranite, which indicates that these granitoids were folded, along with greenstones and pegmatite-banded gneiss, during D_2. However, the fabrics are poorly preserved due to overprinting by D_3 and thorough recrystallization during regional metamorphism. S_2 fabrics are preserved in small domains, from a few metres to several kilometres across, within the dominant S_3 fabric (Plate 2). Good examples of these domains occur 20 km east of Kadji Kadji Homestead, and west of the Paynes Find greenstone belt (Plate 2) (Lipple et al., 1983).

F_2–F_1 fold patterns

Because major F_1 folds are either rare, or obscured by later deformation, F_2–F_1 (and also F_3–F_1) fold-interference structures are correspondingly rare. F_2 folds are superimposed on F_1 folds in the Mount Magnet region, and also in the southwestern part of the Yalgoo–Singleton greenstone belt (Fig. 134). In both these regions the F_2–F_1 patterns are deformed by D_3–D_4 structures. The eastern limb of the F_2–F_1 structure near Mount Magnet contains intense planar fabrics developed near a major D_4 shear zone. In the southwestern Yalgoo–Singleton greenstone belt, F_1 structures are inferred from repetition of lithostratigraphic formations (Plate 2), which would be difficult to explain without early folding. These have been refolded by F_2 and F_3, and F_1 closures have been cut out by shear zones and faults. Minor F_2–F_1 interference folds are rare. Archibald (1982) reported small-scale 'arrowhead' fold structures in the Mount Magnet region which could be F_2–F_1 structures.

D_3: north–south folds

Major D_3 structures

Major north-northeasterly to north-northwesterly trending tight and isoclinal F_3 folds dominate the structure of the Murchison Province (Plate 2). This phase of folding was much more intense than D_2, and formed strong penetrative shear fabrics. Earlier structures were attenuated and a strong regional tectonic grain formed, accentuated by D_4 shear zones and faults. Fold axial planes are vertical and plunges of fold axes within these planes are controlled by the attitudes of S_2 form surfaces.

Both D_3 folds and D_4 shear zones are thought to have formed in response to an approximately east–west regional compression. North-northeasterly to north-northwesterly trending folds (F_3) formed first; and then as strain increased, shear zones (D_4) with dominantly northeast to north-northeast trends and dextral displacements were formed. Shear zones with north to north-northwest trends also developed. F_3 folds are attenuated in zones of strong D_4 shearing and become isoclinal.

F_3 folding is characterized by intense shearing in fold limbs, and generally weak deformation in fold cores. The folds were probably initiated by buckling, the fold limbs becoming modified by simple shear during progressive compression. Simple shear in fold limbs is most intense near contacts between major units of different competence, particularly granitoid–greenstone contacts, and to a lesser degree at contacts between major gabbro bodies and surrounding rocks.

Major F_3 fold axes are more widely spaced in granitoids than in greenstone belts (Plate 2). Folds in recrystallized monzogranite and pegmatite-banded gneiss are anticlines of broad, rounded aspect, with much larger wavelengths, and smaller amplitudes, than folds in greenstone belts. No major synclines have been identified in recrystallized monzogranite or pegmatite-banded gneiss. Both anticlines and synclines are common in greenstone belts, although the overall geometry of these belts is synformal.

Minor D_3 structures in greenstones

Tight to isoclinal F_3 folds dominate the structure of most greenstone belts (Plate 2). Fabrics that are parallel to F_3 fold axial surfaces are prominent, and generally obliterate earlier fabrics. Steep intersection lineations are developed where S_3 cuts these earlier fabrics. Crenulation cleavages occur in metasediments and schistose mafic units, particularly in hinge regions of some folds. Anastamosing fabrics are common in limb regions (Fig. 136); these are generally S–C fabrics (Berthe et al., 1979) near D_4 shear zones, but in other areas they may represent superimposed S_3 and S_2 fabrics. Foliation is intensely developed near granite–greenstone contacts, especially where these are subparallel to F_3 fold axes. Fabrics are also well developed near contacts between lithologies of differing competence within greenstone belts. In contrast, fabrics are weakly developed in axial regions of folds, particularly in massive units.

Minor F_3 folds are ubiquitous in multilayered rocks (Fig. 137); the geometry and vergence of most of these folds can be related to major folds. However, as noted previously, where minor folds cannot be related to a major structure, their relative chronology (F_1, F_2, or F_3) is often in doubt. In some outcrops of BIF, several fold styles with different vergence may occur; these are generally polyclinal and disharmonic in profile. Some may be slump folds deformed by tectonic folds, but most were probably caused by buckling of hematite–magnetite bands and chert bands of differing competence, and/or superimposition of minor folds (Ramsay, 1967). Some closed forms in high-strain D_4 shear zones are sheath folds (Cobbold and Quinquis, 1980).

Minor D_3 structures in recrystallized monzogranite

S_3 fabrics are intensely developed in northwest to northeasterly trending marginal zones of recrystallized monzogranite, subparallel to their contacts with greenstone belts (Plate 2). Compositional banding is developed within a few hundred metres to one kilometre of many



GSWA 24671

Figure 136. Anastamosing shear surfaces in high-Mg basalt; spinifex texture is preserved between the shears. The hand lens is 4 cm long.

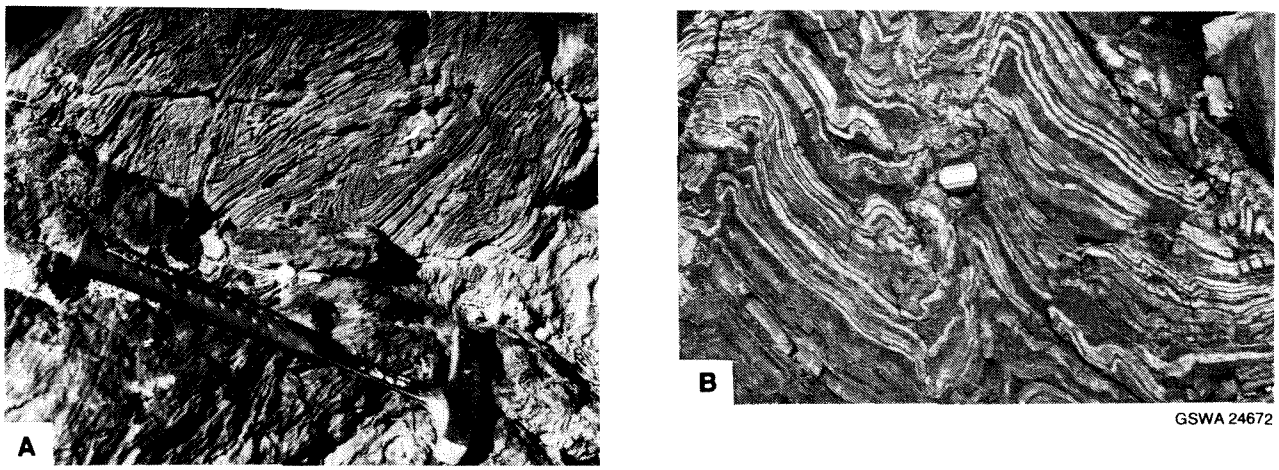


Figure 137. Minor F_3 folds: A — tight folds in lateritic banded iron-formation 13 km east of Poona on CUE; the hammer handle is 30 cm long. B — disharmonic folds in jaspilitic banded iron-formation, near Gnows Nest on YALGOO; a number of F_1 fold closures can be seen in this outcrop; the lens cap is 5cm across.

granitoid–greenstone contacts, because tabular intrusive units, such as pegmatites, aplites, quartz veins, and mafic dykes, were oriented into parallelism with S_3 (Fig. 109B). Greenstone xenoliths in these marginal zones became infolded with granitoids (Fig. 109C) and attenuated in the S_3 fabric, thus accentuating banding (Fig. 138). Away from these zones of intense deformation, compositional banding gives way to a strong foliation (Fig. 139), which weakens towards the centres of recrystallized monzogranite bodies where fabrics are either absent or very weakly developed (Plate 2).



Figure 138. Xenoliths of felsic volcanic rocks in the marginal zone of a recrystallized monzogranite, 15 km southeast of Pindathuna Homestead on YALGOO. The xenoliths have been attenuated in the S_3 foliation. The hammer handle is 30 cm long.

Minor D_3 structures in pegmatite-banded gneiss

Where pegmatite-banded gneiss is present in limb regions of major folds, S_1 banding and F_2 folds are re-oriented and strongly attenutated subparallel to F_3 fold axial planes. In some outcrops, where banding is at a large angle to S_3, subvertical shear zones may occur. These are parallel to F_3 fold axial planes, and may be a few centimetres to several metres wide. Banding was abruptly reoriented into the shear zones at their margins, and intense fabrics and banding developed. Steep mineral-elongation lineations occur along the intersection of S_3 and S_1, and less commonly, along S_3–S_2.

Fold patterns

F_3–F_1 fold patterns

Major F_3–F_1 interference folds were developed in the Mount Mulgine region of the Yalgoo–Singleton greenstone belt, and in the Koolanooka greenstone belt (Fig. 134). Minor interference folds have been recognized in these regions, and also in regions where no major interference folds are apparent, e.g. at The Island, on CUE (Fig. 140). Minor interference folds are generally confined to BIF units, as the massive nature of volcanic units precludes their development. These types of interference patterns form by superimposition of upright folds on folds with subhorizontal axial planes (Ramsay, 1967, figs 10-8 and 10-15). Thus, F_1 folds must originally have been flat-lying structures; parallelism of fold limbs indicates that these were recumbent folds. This interpretation is consistent with formation of originally subhorizontal S_1 banding in pegmatite-banded gneiss.

Dome-and-basin patterns

F_2 and F_3 fold axial planes are subvertical and approximately orthogonal; thus, interference patterns are dome-and-basin folds (Ramsay, 1967, fig. 10-3). De la Hunty (1973) first recognized that easterly trending folds preceded north-northeasterly trending folds on CUE, resulting in dome-and-basin patterns. Myers and Watkins (1985) described F_3–F_2 fold patterns in the Yalgoo region, and concluded that the granite–greenstone pattern in this part of the Murchison Province is due mainly to these structures.

Dome-and-basin structures are ubiquitous in the Murchison Province (Plate 2), although they are often difficult

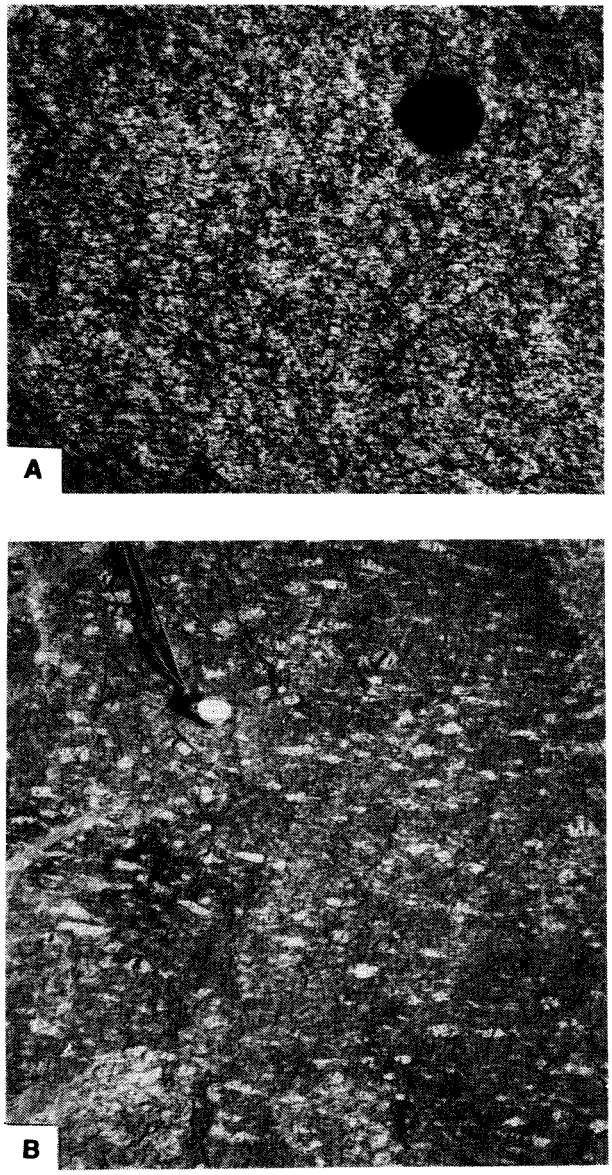


Figure 139. S_3 foliation in recrystallized monzogranite: A — equigranular (the lens cap is 5cm across); B — porphyritic (the hand lens is 4cm long).

to recognize as they are poorly exposed, cut by shear zones and faults, and intruded by post-folding granitoids. These patterns occur on all scales, and range from a few centimetres (Figs 133 and 141), through a few kilometres (Figs 93 and 134), to several tens of kilometres across (Fig. 142 and Plate 2). On all scales, limbs of dome-and-basin folds are subvertical and strongly sheared, while core regions of folds are only weakly deformed. In many cases these fold patterns were formed by straightforward interference between east–west (F_2) and north–south (F_3) folds. These patterns are generally quite irregular, possibly because both F_2 and F_3 folds are markedly non-cylindrical. However, some patterns, particularly near high-strain D_4 shear zones, are sheath folds developed during attenuation of both doubly plunging F_3 folds and F_3–F_2 interference folds. Some folds in the zone of major D_4 shearing between Meekatharra and Mount Magnet can be interpreted in this way.

Large-scale heterogeneous D_3 strains

Strain development was markedly heterogeneous on all scales during D_3. Immediately before F_2 folding, the upper crust in the Murchison Province consisted of two major layers with markedly different rheologies — a greenstone sequence, up to 15 km thick, but generally less, which overlay a thick complex of gneiss and granitoid sheets that had intruded the base of the greenstones. The rheological differences between these layers largely controlled the style of major folding during D_2 and D_3. Some important aspects of D_3 deformation styles are:

(a) Granitoid–gneiss bodies generally form broad, anticlinal structures, but greenstones belts are dominantly synclinal in overall shape.
(b) F_3 fold axes are much more closely spaced in greenstone belts than in granitoid–gneiss bodies.
(c) D_3 deformation is most intense near granitoid–greenstone contacts.

As Ramsay (1967, p. 382–386) pointed out, when two rock units of different viscosities suffer progressive compressive strain parallel to the boundary surface between them, a series of antiforms of broad rounded aspect develops; these have large wavelengths and small amplitudes, and are separated by much tighter synforms, with small wavelengths and large amplitudes. He later termed these cuspate-lobate folds (Ramsay and Huber, 1987, p. 397). In the Murchison Province, broad anticlines developed in the more competent granitoid–gneiss bodies, and tight synclinoria formed in the overlying, less competent greenstones. This style of deformation is similar to that developed in many basement–cover sequences (e.g. Ramsay, 1967, figs 7-43 and 7-44; Laubscher, 1983; Stanley and Ratcliffe, 1985; Ramsay and Huber, 1987, fig. 19-17). Zones of intense deformation occur between basement and cover in these situations, as is the case in the Murchison Province. It should be noted that in the Murchison Province, the granitoid–gneiss units form a basement to the greenstones in a structural, not a chronological, sense.

D_4: shear zones and faults

An extensive system of shear zones and faults, many of considerable length (> 100 km), developed in the Murchison Province in response to regional east–west compression. Shear zone development is related to F_3 folding in that these deformations occurred consecutively during the same compression event and must have overlapped somewhat. Attentuation of F_3 folds continued during D_4 shearing, particularly within and adjacent to the main shear zones. This anastamosing network of shear zones and faults generally trends northeast to northwest, but the dominant system is oriented north-northeast (Fig. 143, Plate 2). These structures are most prominent in greenstone

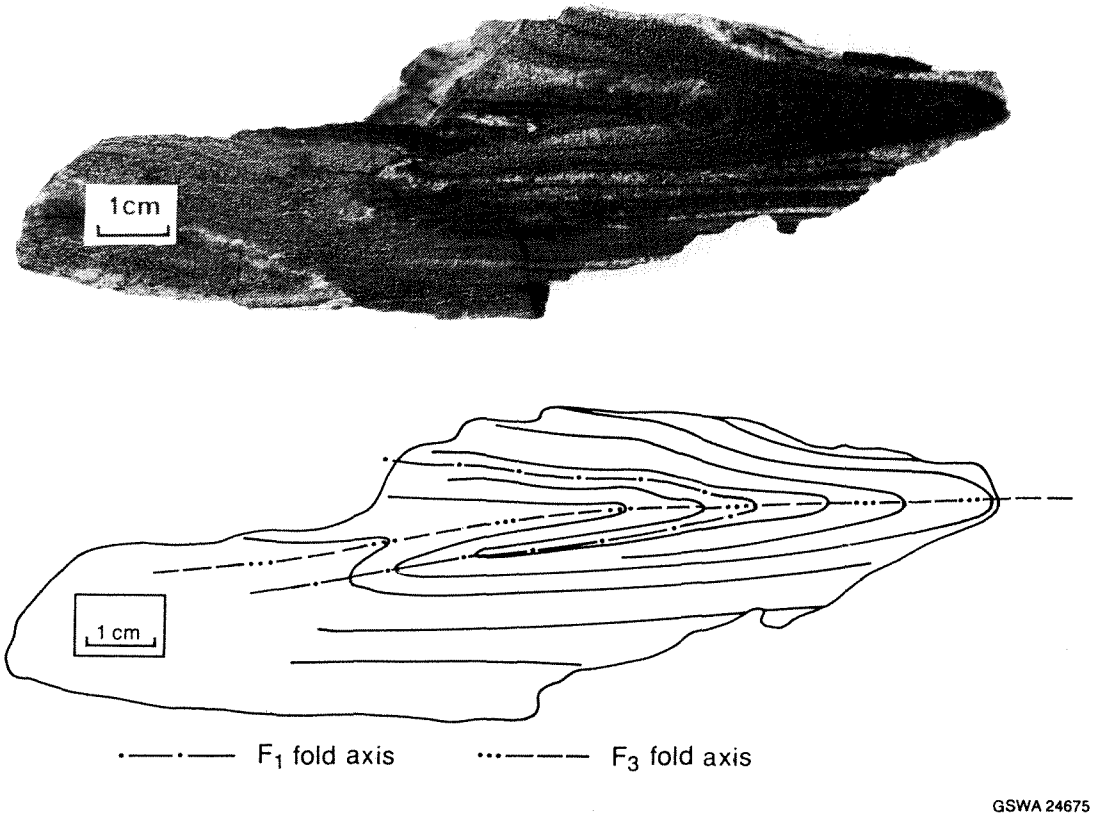


Figure 140. Minor F_3–F_1 interference fold in banded iron-formation from The Island on CUE.

belts, but most extend into adjacent granitoids (where recognition is more difficult).

Shear zones and faults are poorly exposed, although most contain quartz veins which often form prominent outcrops. Mylonites were developed in central parts of shear zones (Fig. 144). Fabrics are subvertical, with variably plunging lineations, but most are either vertical or horizontal. Most major shear zones are a few hundred metres wide, but some are up to 1 km in width. Faults and shear zones have not been distinguished on the maps (Plates 1 and 2) because the exposures of most are are not adequate to allow this. In general the larger features are brittle–ductile shear zones, particularly those trending north-northeast to north-northwest. Most smaller features, less than 10 km in length, are faults and are characterized by brittle fracturing in zones a few metres wide. Some shear zones may have been reactivated as faults at a late stage in the evolution of the craton.

Excellent exposures of shear zones, thought to be typical, occur for 6 km south-southeast of Chulaar Well on KIRKALOCKA, and 1 km northeast of Moyagee Well on CUE. The Chulaar Well Shear Zone (see Fig. 168) occurs at the basal unconformity of the Mougooderra Formation in coarse, immature sandstones containing conglomerate lenses (Plate 2). The shear zone is several hundred metres wide and about 35 km long; intensity of foliation increases towards its centre which is occupied by a 30–40 m-wide, topographically prominent, silicified, recrystallized, quartz–andalusite–white-mica mylonite (Fig. 144A). The mylonite has a ribbony banded appearance with subvertical foliation and a vertically plunging lineation. It contains lenses of conglomerate in which individual pebbles have been flattened in the foliation and elongated in the lineation. The Mount Magnet Shear Zone (see Fig. 168) near Moyagee Well is approximately 300–400 m wide and contains intensely foliated rocks and mylonite that have a subvertical foliation (Fig. 144B). This shear zone extends at least 250 km, from north of Meekatharra to south of Mount Magnet (Plate 2). Near Moyagee Well the shear zone occurs at a contact between a mafic sequence and recrystallized monzogranite. Lineations are dominantly subhorizontal, but zones of variably plunging lineations occur. Minor structures in this outcrop indicate dextral movement. The shear zone passes through the Havelock open-pit gold mine at Meekatharra, where the eastern wall of the pit is spectacularly striated with subhorizontal slickensides.

Minor structures that show the sense of displacement in shear zones are exposed in some underground workings at various mining centres. Movement directions can be interpreted locally from fracture patterns and from dilational quartz veins orientated *en echelon*, and oblique to shear zone trends. The dominant sense of displacement

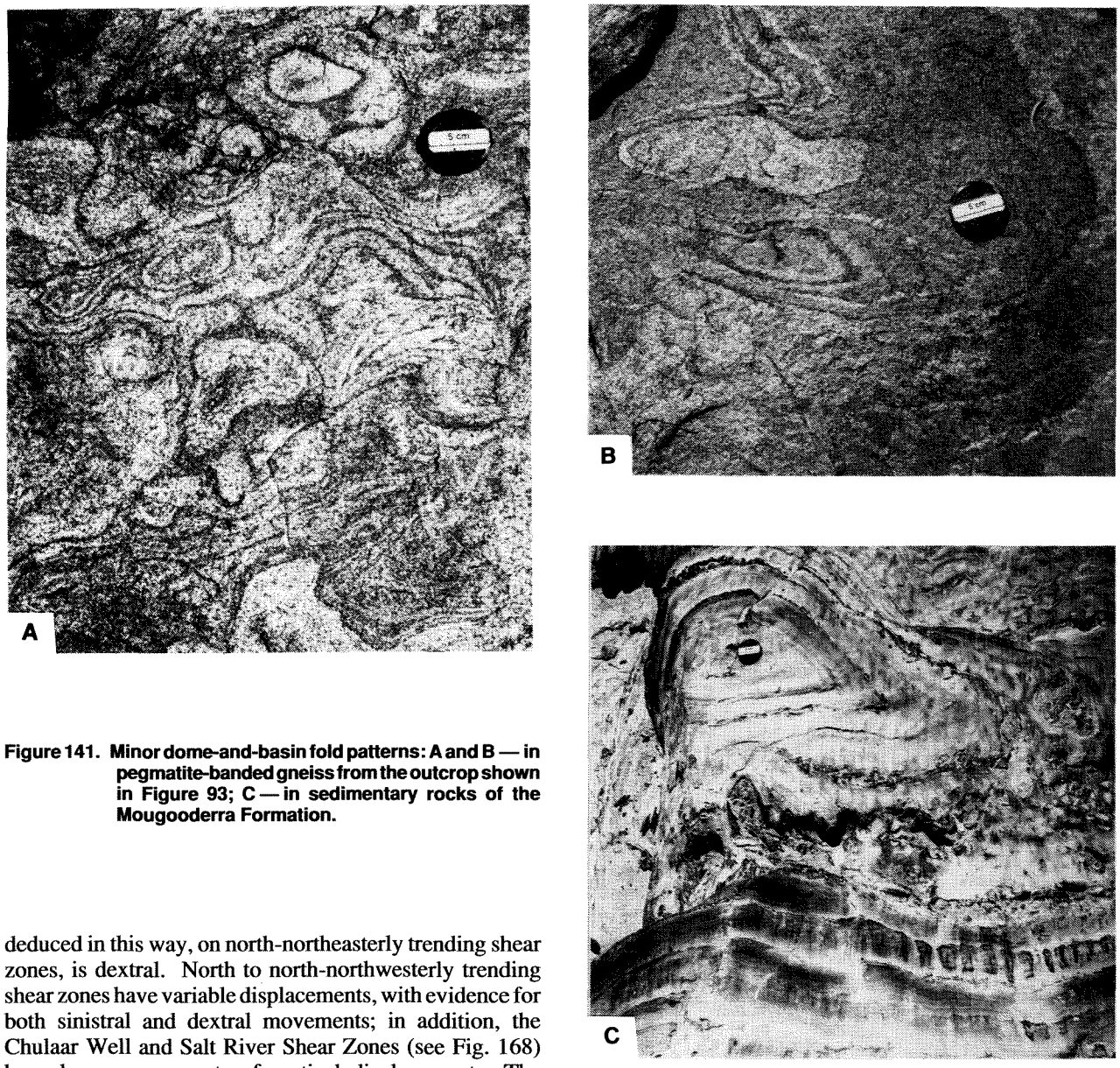


Figure 141. Minor dome-and-basin fold patterns: A and B — in pegmatite-banded gneiss from the outcrop shown in Figure 93; C — in sedimentary rocks of the Mougooderra Formation.

deduced in this way, on north-northeasterly trending shear zones, is dextral. North to north-northwesterly trending shear zones have variable displacements, with evidence for both sinistral and dextral movements; in addition, the Chulaar Well and Salt River Shear Zones (see Fig. 168) have large components of vertical displacement. The sinistral D_1 Gabanintha Shear Zone was reactivated, in places, during folding and D_4 shearing; it was displaced by the D_4 Mount Magnet Shear Zone near Meekatharra (Plate 2).

The duration of shearing and faulting is constrained by the following relations:

(a) Shear zones cut F_3 fold axial traces, although most were probably initiated during late F_3 folding;
(b) textures in shear zone rocks range from recrystallized to cataclastic;
(c) shear zones and faults cut post-folding granitoid plutons;
(d) some shear zones are intruded by albite porphyries, which are themselves sheared. These may be related to the post-folding granitoid suites.

These relations indicate that fault and shear zone activity began sometime between late D_3 and the peak of regional metamorphism, and continued until some time after intrusion of post-folding granitoid suites. Thus, shear zone and fault activity appears to have been long-lived.

Most shear zones contain quartz veins up to several metres thick, or are pervasively silicified, indicating massive precipitation of silica. Shear zones formed ideal conduits for rapid upward movement of magmatic and/or metamorphic dehydration fluid; the focused flow of these fluids precipitated the silica (cf. Fyfe et al., 1978). Fluid-inclusion studies of vein quartz in Yilgarn shear zones indicate that silica was precipitated from low salinity H_2O–CO_2 fluids at about 100–200 MPa and 250–350°C (Groves et al., 1984); that is, below peak metamorphic greenschist facies conditions (Turner, 1980). Many gold deposits in the Murchison Province are in shear zones and are thought to have been localized by hydrothermal activity. The detailed structure of shear zones and faults, and mineralization contained within them in various mining centres, is described in Chapter 7.

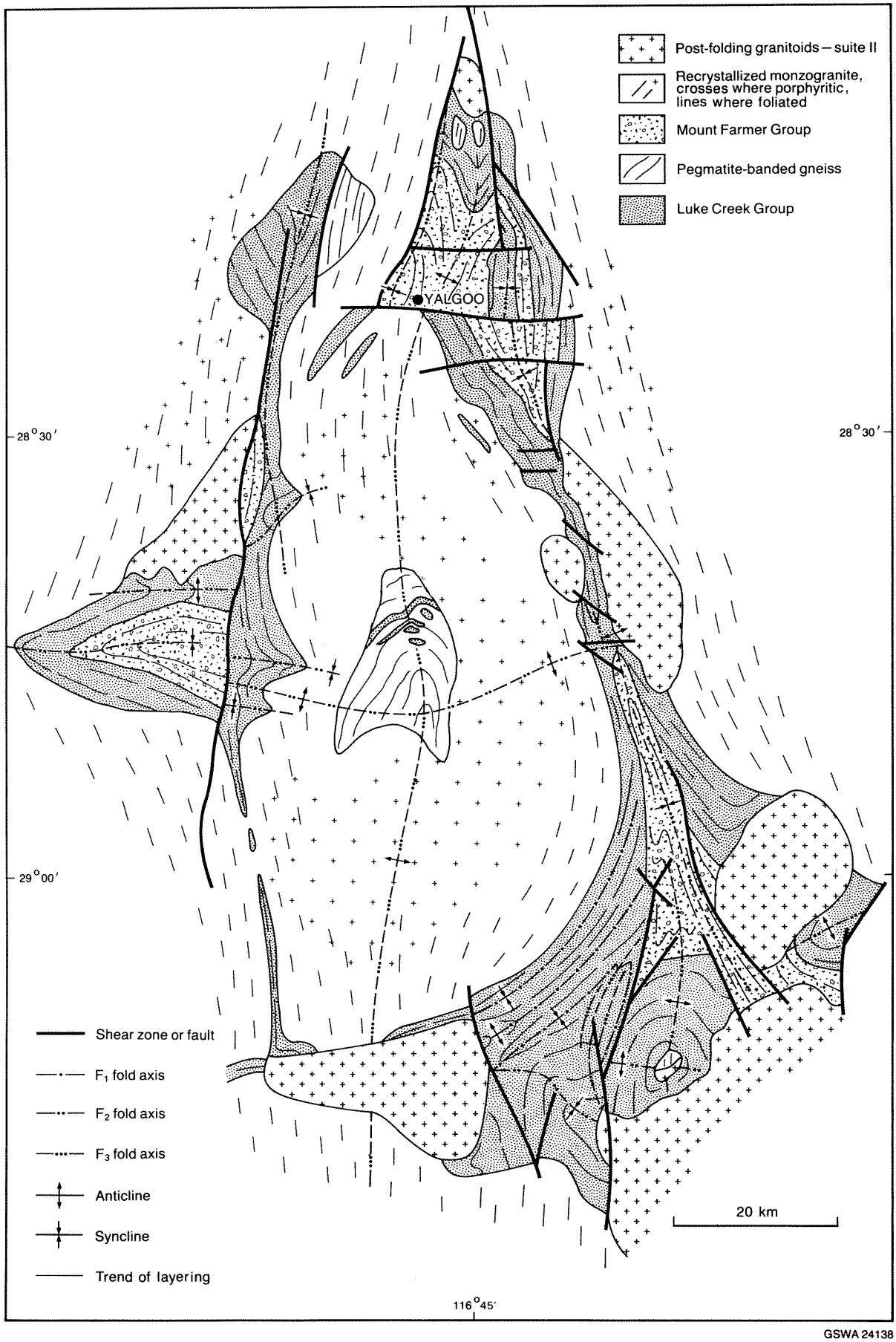


Figure 142. Simplified geology of the Yalgoo region.

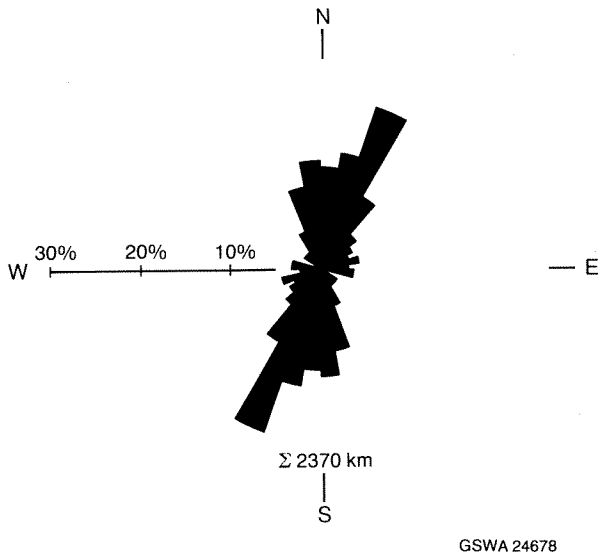


Figure 143. D_4 fault and shear-zone azimuths.

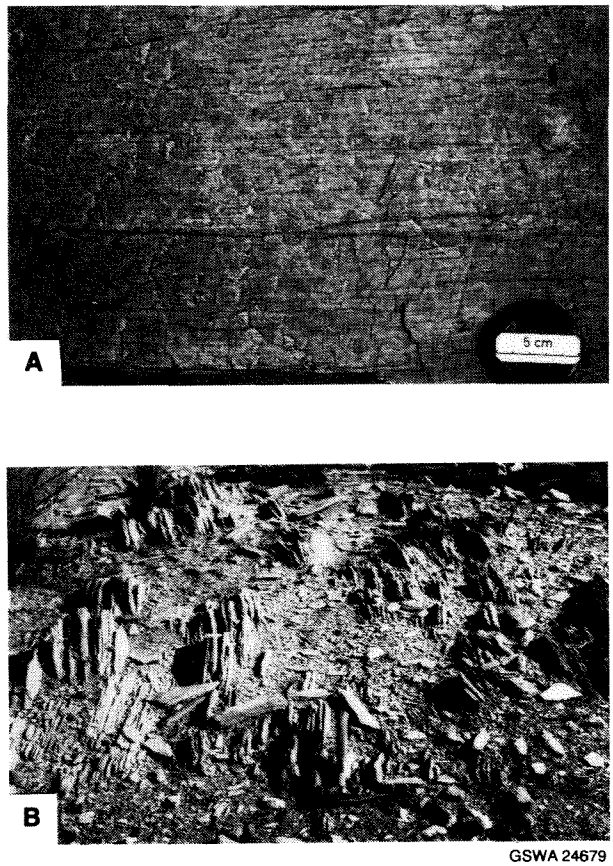


Figure 144. A — recrystallized, silicified, quartz–andalusite mylonite in the Chulaar Well Shear Zone, 12km west of Thundelarra Homestead on KIRKALOCKA. The protolith was a coarse immature sandstone with conglomerate lenses. B — cataclastic mylonite in the Mount Magnet Shear Zone, 1km northeast of Moyagee Well on CUE. The protolith was recrystallized monzogranite. The hammer handle is 30cm long.

D_5: Mingah Range fault and shear zone system

This system of mainly east-southeasterly trending faults and shear zones (Fig. 145) imbricates the Mingah Range greenstone belt into elongate slivers, each containing many minor faults (Plate 2). It also cuts the surrounding granitoids. These structures are parallel to major shear zones near the Yilgarn Craton–Gascoyne Province boundary to the northwest (Elias and Williams, 1980; Gee, 1979; Williams, 1986). Mylonite and quartz veins were developed in the shear zones; however, all fabrics are cataclastic, indicating post-metamorphic movement. The attitude of these structures is unknown.

A model Pb–Pb age of 2073 ± 14 Ma has been determined on galena from a D_5 fault breccia, 6 km west-southwest of Wadda Wadda Bore on BELELE (Browning et al., 1987). Although undue emphasis should not be placed on this single determination, it indicates that D_5 faulting (assumed to be broadly synchronous with mineralization) is probably significantly younger than D_4. The age of parallel shear zones to the northwest has not been determined. However, a major crust-forming event, at 2400–2000 Ma (and possibly later), has been postulated for the southern Gascoyne Province, on the basis of Sm–Nd model ages (Fletcher et al., 1983). Rb–Sr geochronology indicates a major orogenic event, the Capricorn Orogeny, in this region, between 1900 Ma and 1600 Ma (de Laeter, 1976; Williams et al., 1978). The 2073 Ma model age is broadly compatible with these events rather than with Archaean tectonism.

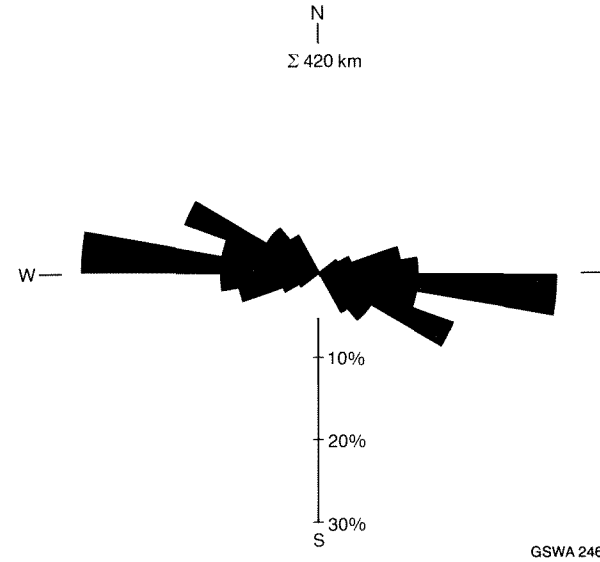


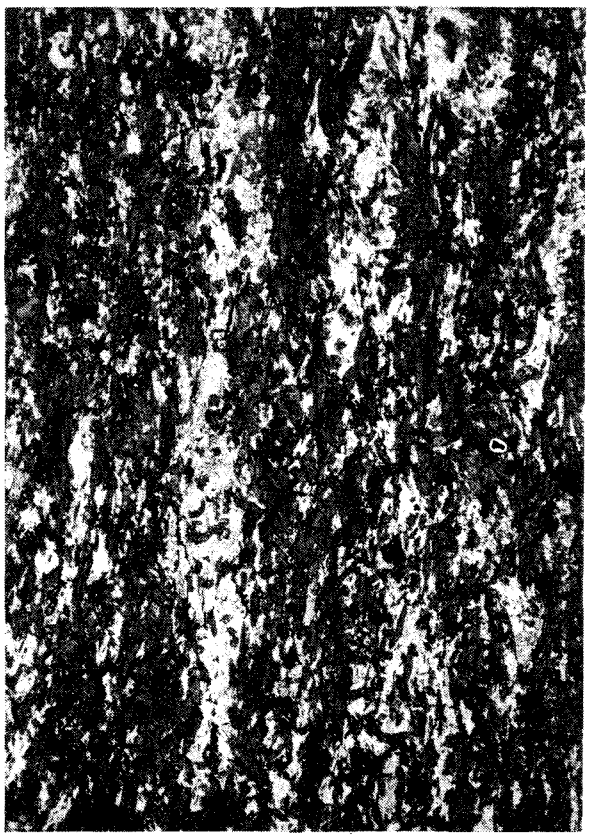
Figure 145. D_5 Mingah Range fault and shear zone azimuths.

Fabric development

Regional metamorphism outlasted D_3, which was the major fabric-forming event. Tectonic fabrics were generally recrystallized, and non-equant metamorphic mineral phases were aligned in, and overprinted, them.

Igneous textures are obliterated in high-strain zones of greenstone belts, generally near fold limbs and granitoid–greenstone contacts. Two types of fabric are common in these regions — a penetrative recrystallized L–S fabric (e.g. Fig. 146), and a fabric comprising anastamosing shear surfaces enclosing lenses which retain igneous textures, albeit pseudomorphed by metamorphic minerals (e.g. Fig. 136). In some cases it is not clear whether the anastamosing fabric is the product of one, or more, deformations. In high-strain zones of recrystallized monzogranite and pegmatite-banded gneiss, foliations are generally thoroughly recrystallized; they are either simple penetrative fabrics (e.g. Fig. 111A), or anastamosing protomylonitic fabrics which developed into mortar textures on recrystallization (Figs 95 and 111B).

In low-strain regions of greenstone belts, igneous textures are pseudomorphed by metamorphic minerals, and in low-strain regions of recrystallized monzogranite and pegmatite-banded gneiss, igneous textures are replaced by granoblastic metamorphic textures (Figs 94 and 112).



GSWA 24681

1 mm

Figure 146. Recrystallized penetrative foliation in amphibolite.

D_4 shear zone development began before the peak of regional metamorphism and continued for some time after it. Recrystallized mylonite fabrics in some shear zones (e.g. Fig. 147) indicate that movement on these structures ended before peak metamorphism. In other D_4 shear zones, cataclastic fabrics indicate that some movement occurred after the metamorphic peak. D_5 shear zone fabrics are cataclastic.

Structural control of granitoid emplacement

The distribution of granitoids, and their outcrop shapes, suggest that the modes and sites of intrusion of many were controlled either by active tectonic processes or by structural features of the crust.

Pegmatite-banded gneiss

Most pegmatite-banded gneiss occurs as enclaves in recrystallized monzogranite; however, in one important outcrop (Fig. 93) pegmatite-banded gneiss is interleaved with supracrustal rocks. Sheets of gneiss in this outcrop appear to have been ductile when deformed. Gneiss band-



1 mm

GSWA 24682

Figure 147. Recrystallized mylonite; andalusite forms ribbony porphyroblasts, subparallel to the fabric, in a matrix of quartz and white mica. The thin section was taken from the outcrop photographed in Figure 144A.

ing is parallel to sheet margins. The supracrustal rocks were more viscous during this deformation, which resulted in boudinaged amphibolite units in pegmatite-banded gneiss (Fig. 148). Near some contacts, amphibole is abundant for several metres into the gneiss (e.g. Fig. 148), which suggests partial assimilation of greenstone material by metasomatic reaction. It is unlikely that such ductile deformation and metasomatism would have occurred after substantial cooling of pegmatite-banded gneiss protoliths. Metamorphic grade is insufficient for ductility to have been enhanced by partial melting (cf. Arzi, 1978; McLellan, 1984). Evidence that intrusion and deformation were contemporaneous includes the ductile deformation of pegmatite-banded gneiss, metasomatic assimilation of greenstone material, and the abundance of pegmatite bands which intruded parallel to the gneissosity and were then deformed with the host gneiss. The mode of intrusion of pegmatite-banded gneiss was almost certainly controlled by D_1. It is possible that the magma was intruded along thrust planes (cf. Myers, 1984).

Recrystallized monzogranite

Recrystallized monzogranite also intruded the base of the Murchison Supergroup as tabular bodies. This mode of emplacement is clearly evident in the Yalgoo region (Fig. 142) where pegmatite-banded gneiss occupies the core of an anticline–anticline fold structure. Pegmatite-banded gneiss is overlain by recrystallized monzogranite, which in turn is overlain by greenstones (Myers and Watkins, 1985). Gneisses occur near the cores of other recrystallized monzogranite bodies (Plate 1), but relations are not as clear as in the Yalgoo region. Although the monzogranite originally formed thick subhorizontal sheets, it is not deformed by D_1; therefore, it is unlikely that the mode of intrusion was controlled by active D_1 processes. It is possible that the horizontal disposition of greenstones overlying pegmatite-banded gneiss (ignoring any true basement layer) controlled the mode of monzogranite intrusion in a manner similar to that envisaged by Hamilton and Myers (1967, 1974). They suggested that 'mesozonal batholiths' rise through the crust and spread out into tabular bodies beneath cover sequences several kilometres thick. In the Murchison Province the greenstone cover sequence may have formed a barrier to rising granitoid magma, causing it to intrude horizontally into basal greenstones. Other factors, such as magma composition, temperature, and volatile content, may also have influenced emplacement level of these intrusions (Pitcher, 1979; Hyndman, 1981).

It is difficult to estimate the original thickness of monzogranite bodies, as they were probably thickened by D_2 and D_3 folding. The amount of thickening may have been influenced by the viscosity contrast between monzogranite and greenstones (e.g. Deitrich, 1970). However, original thicknesses must have been of the order of several kilometres.



GSWA 24683

Figure 148. Boudinaged amphibolite unit in pegmatite-banded gneiss, 5m from a major contact with greenstones (Fig. 93). Note the amphibole-rich layers in the gneiss near the amphibolite unit. A late granitoid dyke intrudes the gneiss and the amphibolite.

Post-folding granitoids

There is a spatial association between post-folding granitoid plutons and greenstone belts which is difficult to explain. However, major D_4 shear zones are contemporaneous with intrusion of post-folding granitoids and occur mainly in greenstone belts. The large scale of these shear zones suggests that they are major crustal structures extending to great depths, probably to the lower crust or even to the upper mantle. It is conceivable that post-folding granitoids were localized by these structures. Deep shear zones may provide pathways to the upper crust for granitoid magmas. Such control is clearly evident in other geological settings (Pitcher, 1979); for example, for the Cordillera batholiths of the Andes (Pitcher and Bussell, 1977), and for some granites in Ireland (Leake, 1978). In the Yilgarn Craton, Gee (1979) and Hallberg (1983) thought that shear zones had controlled emplacement of some granitoids in the Eastern Goldfields Province. There are problems with this hypothesis in that post-folding granitoids have large subcircular shapes which are not obviously controlled by shear zone orientation; also, many plutons occur some distance from identified shear zones. It is possible that magma movement at depth was controlled by shear zones, but that the plutons became decoupled in the upper crust and continued upwards into their present sites by stoping and magma wedging.

Diapirism

The structural evolution of granite–greenstone terranes is controversial (Myers and Watkins, 1985). The classical model, resulting from MacGregor's (1951) work, is that greenstone belts formed downwarped synclinal structures between granitoid batholiths emplaced as magmatic, or solid-state, diapirs. This interpretation is based on the inferred gravitational instability of a dense greenstone sequence overlying less dense granitoid magmas or rocks. According to the model, granitoid–greenstone patterns

were formed by gravity-driven, vertical tectonic movements. This is a popular hypothesis which has gained widespread acceptance (e.g. Huddleston, 1976; Drury, 1977; Gee, 1979; Glikson, 1979; Coward, 1981; Schwerdtner, 1982; Anhaeusser, 1984; Hickman, 1984).

Much recent work has revealed that horizontal tectonic movements have played a major role in the structural evolution of many granite–greenstone terranes. Evidence for horizontal tectonic fabrics — and in some cases nappe structures, inverted successions, and thrusts — have been documented (Coward and James, 1974; Platt et al., 1978; Bickle et al., 1980; Fripp et al., 1980; Platt, 1980; De Wit, 1982; Sawyer, 1983; Drury et al., 1984; Lamb, 1984; Stowe, 1984; Spray, 1985; Myers and Watkins, 1985). Bickle et al., (1980) have proposed a combination of horizontal and vertical tectonic regimes to explain the structure of part of the Pilbara Craton. According to their model, early horizontal tectonic interleaving of granitoids and greenstones was followed by solid-state diapiric uprise of granitoids.

In some cases, structures indicate that the granite–greenstone pattern is not a response to vertical tectonic movements; instead it is a consequence of superimposition of two sets of upright folds (of both greenstones and granitoids) during regional horizontal tectonic compression (Snowden and Bickle, 1976; Dimroth et al., 1983; Snowden, 1984; Myers and Watkins, 1985).

Structures normally associated with diapirism do not occur in the Murchison Province. Such structures include radial extension lineations and subhorizontal foliations at high levels in the cores of domes; subvertical lineations and steep, outward dipping foliations at deeper levels; and concordant foliations near granite–greenstone contacts (Dixon, 1975; Schwerdtner et al., 1978; Ramberg, 1981). Concordant foliations are common along northeasterly to northwesterly trending contacts, but foliations are at high angles to east–west contacts (Plate 2). In some instances foliations indicate some degree of 'wrapping' of greenstone belts around recrystallized monzogranite bodies, probably in response to heterogeneous strain caused by the viscosity contrast between the two types of rocks. Where this is so, S_3 foliations converge towards southern and northern ends of recrystallized monzogranite bodies, but still cut east–west granitoid–greenstone contacts (Plate 2, Fig. 142). Lineations are rare in recrystallized monzogranite and pegmatite-banded gneiss; they are generally steep, but not radially plunging. Most appear to be S_2–S_3 intersection lineations.

In summary, no evidence for diapirism has been observed in the Murchison Province; all structures can be adequately explained in terms of regional horizontal tectonic compression. However, bearing in mind the density contrast between granitoids and greenstones, some gravitational influence on folding cannot be ruled out. It is conceivable that while the main driving force for deformation was horizontal compression, fold amplitudes were accentuated to some degree by gravity-driven vertical movements, so that recrystallized monzogranite rose relative to greenstone belts. Simple shear at granitoid–greenstone contacts could, in part, be due to such movement (Sims et al., 1985). It must be pointed out, however, that there is no field evidence to support this hypothesis; subvertical lineations which should have developed during such deformation are rare.

Synthesis

The structural history of the Murchison Province can be summarized in terms of five major events:

D_1: The earliest recognizable deformation produced subhorizontal banding in pegmatite-banded gneiss, and large isoclinal folds in the Luke Creek Group. Folding was recumbent and was probably accompanied by thrusting. Pegmatite-banded gneiss protoliths intruded the Luke Creek Group during this deformation.

D_2: Following deposition of the Mount Farmer Group, and intrusion of recrystallized monzogranite protoliths as thick sheets into the base of the Murchison Supergroup, east-trending tight folds developed. These were upright and had vertical axial planes and subhorizontal fold axes.

D_3: The easterly trending phase of folding was followed immediately by intense development of north-northeasterly to north-northwesterly trending tight and isoclinal folds. These were upright, with vertical axial planes. Strong penetrative fabrics formed during this deformation, imparting a regional tectonic grain to the province. Dome-and-basin fold patterns developed and formed the basis of the granite–greenstone pattern.

D_4: During this phase of deformation a system of shear zones and faults developed. These are of regional extent with mainly north-northeast to north-northwest trends. D_4 shear zone development is related to D_3 folding in that these deformations were consecutive responses to one regional east–west compression event. F_3 folds were attenuated near D_4 shear zones and became isoclinal; sheath folds developed in response to further attenuation in these zones. Shear zone activity continued until some time after the peak of regional metamorphism. Movements were complex and involved both vertical and horizontal displacements. Intrusion of post-folding granitoid plutons was probably controlled by these structures.

D_5: The final deformation phase developed in the northwestern part of the province. A system of east to southeasterly trending shear zones and faults imbricated the Mingah Range greenstone belt and surrounding granitoids. These shear zones and faults probably developed during the Proterozoic Capricorn Orogeny

In addition to the major deformation phases, several minor episodes of late, open folding, of local extent, have been identified (Lipple and Baxter, 1982; Frater, 1983; Watkins et al., 1987).

The structural history of the Murchison Province is similar to that proposed for the Zimbabwe Craton (Stowe, 1984; Snowden, 1984) and it contains elements similar to those documented in almost every granite–greenstone terrane (see references quoted above). The style of deforma-

tion — characterized by recumbent folding and thrusting followed by dome-and-basin fold patterns — is typical of Archaean high-grade gneiss terranes (Windley, 1984). The early gneiss complex to the north and west of the Murchison Province is characterized by such deformation (Myers and Williams, 1985; Myers, 1990). Thus, the major structures of Archaean granite–greenstone and high-grade gneiss terranes may not be as different as is widely believed (see, for example, references in Condie, 1981, and Windley, 1984).

Chapter 6

Metamorphism

All rocks in the Murchison Province are metamorphosed, with the exception of cross-cutting dykes and most post-folding granitoids; grades range from prehnite–pumpellyite to granulite facies (Plate 3). The metamorphic pattern results from a complex thermal history during which several metamorphic events were superimposed. The overall metamorphic pattern in the greenstone belts is similar to that in the eastern Yilgarn Craton, with higher grade, intensely deformed greenstone belt margins, and lower grade, weakly deformed greenstone belt cores (Binns et al., 1976; Ahmat, 1986b). High-grade rocks occur in the southwest of the Murchison Province (Plate 3); these form part of a large tract of amphibolite and granulite-facies rocks in the southwest Yilgarn Craton (Gee et al., 1981).

Previous work

Apart from short accounts in explanatory notes on GSWA 1:250 000 geological sheets, and brief statements in review articles based on these (e.g. Gee et al., 1981), there is no regional synthesis of metamorphism in the Murchison Province. Metamorphism and metasomatism of small regions around mineral deposits at Golden Grove (Frater, 1983a, b) and Big Bell (Chown et al., 1984; Phillips, 1985; Phillips and De Nooy, 1988) have been documented. Gole (1980) has described metamorphism of BIF from the Weld Range greenstone belt.

Regional metamorphic patterns in greenstone belts of the Southern Cross and Eastern Goldfields Provinces have been documented by Binns et al. (1976) and Ahmat (1986b). Binns et al. (1976) recognized two types of metamorphism:

(a) static metamorphism, characterized by weakly deformed prehnite–pumpellyite to lower amphibolite facies cores of greenstone belts; and
(b) dynamic metamorphism characterized by highly strained greenschist to uppermost amphibolite facies margins of greenstone belts.

These styles of metamorphism were considered by the authors to have developed contemporaneously during a single regional event. Archibald et al. (1978, 1981) presented further structural and metamorphic evidence in support of this model, and Ahmat (1986b) adopted a similar model for metamorphism of greenstone belts in the Southern Cross Province. Metamorphism of granitoid rocks was not considered by the authors cited above.

Compilation of Plate 3

Approximately 2500 thin sections were examined to determine mineral assemblages and textural relationships in Murchison Province rocks. These observations formed the basis for compilation of Plate 3. Most samples were collected during the course of this study and the remapping of the CUE 1:250 000 sheet (Watkins et al., 1987), although 650 samples were collected during previous 1:250 000 scale mapping, and by Hallberg (1976). The distribution of these samples is shown on Plate 3 (each point on the map may represent more than one sample).

Each of the examined samples was assigned to a metamorphic facies on the basis of its mineral assemblage according to the criteria shown on Plate 3. Retrograded samples were assigned to the highest metamorphic facies recorded. The metamorphic events responsible for these assemblages were also determined from field and microtextural relationships. The distribution of metamorphic facies on Plate 3 is based entirely on this information. Facies boundaries are uncertain in some parts of the map where sampling was inadequate. This is a particular problem near the margins of some greenstone belts. It is thought that nearly all greenstone belt margins have the same metamorphic characteristics, i.e. they are retrograded from amphibolite facies, but this has not been inferred on Plate 3 for unsampled greenstone belt margins.

Distribution of metamorphic facies

Distribution of metamorphic facies in the Murchison Province is controlled by three types of metamorphism, designated M_1, M_2, and M_3 (Plate 3). The first type, M_1, is caused by contact metamorphism of greenstone belt rocks during intrusion of large mafic bodies, and is only of local importance. Contact aureoles are up to a few hundred metres wide and are in amphibolite and granulite facies.

The second type, M_2, is also due to contact metamorphism. In this case metamorphism resulted from intrusion of pegmatite-banded gneiss and recrystallized monzogranite

protoliths, as thick sheets into the base of the greenstone sequence. Although intrusion of these granitoids was widely separated in time, the resulting metamorphic events are grouped together in M_2 as they are identical in style and grade. Contact metamorphic effects of pegmatite-banded gneiss protoliths are preserved in xenoliths and greenstone rafts, and along small segments of some greenstone belt margins in contact with the gneiss. Elsewhere, these effects have been obliterated by subsequent metamorphism and they contribute little to the overall metamorphic pattern. Recrystallized monzogranite contact metamorphic aureoles are generally in amphibolite facies, and are up to several hundred metres wide. However, in some greenstone belts they are several kilometres wide, probably indicating the presence of recrystallized monzogranite at relatively shallow depths beneath them.

The third type, M_3, is responsible for regional metamorphism of greenstone belts, pegmatite-banded gneiss, and recrystallized monzogranite, mainly in greenschist facies. In the northern part of the province, metamorphic grade decreases to prehnite–pumpellyite facies towards the centres of some greenstone belts. Elsewhere, any decrease in grade towards the centres of greenstone belts occurs within the greenschist facies and is not distinguished on Plate 3. For example, rocks in the core of the Weld Range greenstone belt are in lowermost greenschist facies, but those near the margins are in uppermost greenschist facies. Divisions like these for mafic rocks within the greenschist facies are based on relatively subjective petrographic criteria such as degree of crystallization of diagnostic mineral phases, and preservation of igneous texture. Formal divisions of the greenschist facies were not made on Plate 3, in the absence of more objective criteria such as mineral chemistry and chemical phase relations. However, lower and upper divisions of the greenschist facies have been indicated in Appendix II in the computer code classification for samples. A region of higher grade rocks, in amphibolite and granulite facies, occurs in the southwest of the province. The higher grades may reflect differential uplift or higher heat flow in this region.

It is important to note that the metamorphic pattern in the Murchison Province results from superimposition of metamorphic events. However, the pattern is similar to that in the eastern Yilgarn granite–greenstone terrane, which is interpreted as the result of one metamorphic event (Binns et al., 1976; Ahmat, 1986b). Contact metamorphic effects of post-folding granitoids are not shown on Plate 3; most aureoles are weak zones of albite–epidote and hornblende-hornfels facies metamorphism, up to a few hundred metres wide.

M_1: Contact metamorphism of greenstones by mafic intrusions

Distribution of M_1 metamorphism

Only one significant contact metamorphic aureole is well preserved in the Murchison Province — that around the layered mafic intrusion southwest of the Gabanintha mining centre (Plate 3). Other aureoles are narrow and extensively overprinted by later metamorphic events, although some high-grade assemblages are preserved. Basalts around the approximately 1700 m-thick northwest-trending layered mafic intrusion southwest of Gabanintha contain upper amphibolite-facies assemblages (equivalent to the hornblende-hornfels facies of Turner, 1980), in a zone several hundred metres wide. A thin zone, up to 150 m wide, on the northeast side of the intrusion records amphibolite–granulite transition and granulite-facies conditions (pyroxene-hornfels facies of Turner, 1980). The metamorphic aureole is wider on the northeastern side, probably indicating that the northeastern intrusive contact dips at a shallower angle to the northeast than the steeply dipping southwestern contact.

Granulite-facies rocks also occur 10 km north of Karara Homestead in the Yalgoo–Singleton greenstone belt, and in the Koolanooka greenstone belt (Plate 3). Exposure around these two small outcrops of granulite-facies rocks is very poor, and although there is much gabbro in the vicinity of these outcrops (Plate 3) it was not observed in direct contact with the high-grade rocks. The Karara occurrence is interpreted as being due to M_1, because of its textural and mineralogical similarity to better exposed rocks near the Gabanintha intrusion. Although the Koolanooka occurrence may also be due to M_1 metamorphism, it lies within the high-grade M_3 region in the southwest of the province, and could have developed during the latter metamorphism.

Some upper amphibolite-facies rocks in the Dalgaranga greenstone belt are thought to be remnants of an aureole around the gabbroid complex near Dalgaranga (Watkins et al., 1987).

Mineral assemblages and textures

Mineral assemblages in upper amphibolite-facies basalt comprise hornblende, andesine, clinopyroxene, biotite, quartz, and opaque phases; in the granulite facies they consist of andesine–bytownite, orthopyroxene, clinopyroxene, hornblende, quartz, and opaque phases. Most aureole rocks have granoblastic texture and remnants of igneous texture are not preserved (Fig. 149). Rocks in the mafic intrusions were metamorphosed in greenschist facies during M_3. Aureole rocks were slightly retrograded during this event, with development of epidote, talc, and chlorite. Orthopyroxene is usually the phase most affected by retrogression.

P–T conditions of M_1 metamorphism

Mineral phases in two granulite-facies samples were analysed on the MAC electron microprobe at the CSIRO, Floreat Park, Perth. Operating conditions and data reduction procedures were modified from those of Ware (1981).

Sample 81576 — Gabanintha

This mafic sample from the granulite-facies zone adja-

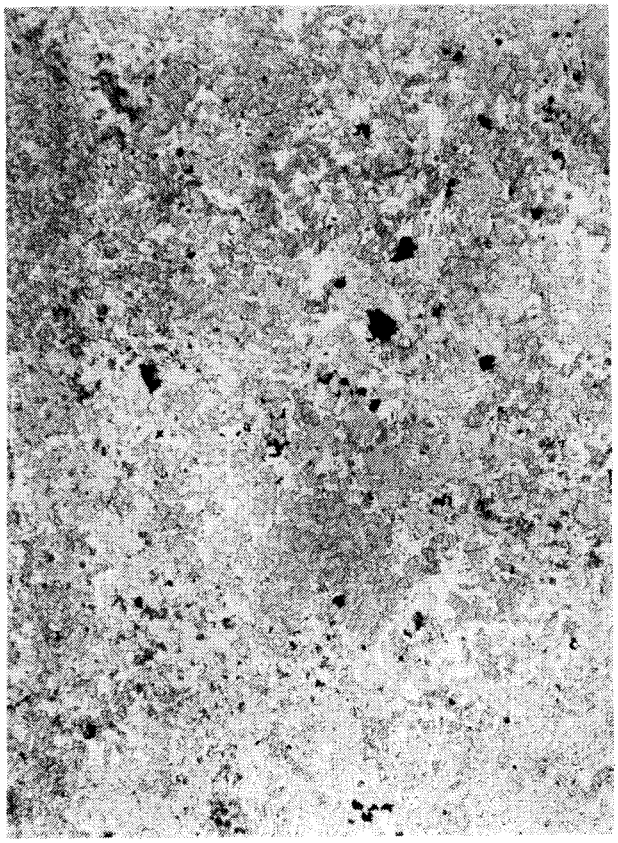


Figure 149. Granoblastic texture shown by poikiloblastic hypersthene, augite, labradorite–bytownite, hornblende, and opaque phases in mafic granulite from the M_1 contact aureole surrounding the layered mafic intrusion southwest of Gabanintha.

cent to the mafic intrusion southwest of Gabanintha contains labradorite (An_{54-65}), augite, hypersthene, hornblende, biotite, and ilmenite. Metamorphic temperatures of 710°C (orthopyroxene) and 800°C (clinopyroxene) have been calculated using Lindsley's (1983) two-pyroxene geothermometer. Estimates using Kretz's (1982) method gave higher temperatures for this sample, in the range 749–887°C (Table 32). These temperatures should be regarded as broad estimates, as two-pyroxene geothermometry is thought to be somewhat imprecise (Stephenson, 1984).

Sample 83596 — Karara

This sample from the outcrop in the Yalgoo–Singleton greenstone belt is a very fresh mafic granulite containing bytownite (An_{76-81}), augite, hypersthene, hornblende, ilmenite, magnetite, and apatite. The rock has an inequigranular texture formed by two types of pyroxene crystals. One type is characterized by medium-grained, elongate and poikiloblastic crystals with exsolution lamellae, and the other by fine-grained, unexsolved equant crystals. Compositions of medium- and fine-grained varieties of each pyroxene are similar (Table 32). The mean metamorphic temperature estimated for the medium-grained pyroxenes, using the methods of Kretz (1982) and Lindsley (1983), is 833°C; that for the fine-grained pyroxenes is 786°C (Table 32). This temperature difference is insignificant given the inaccuracies of the calculation; however, temperatures of 840°C and 650°C for medium- and fine-grained hypersthene, respectively, suggest a real difference in metamorphic temperatures for growth of the two textural types of pyroxene. The significance of these textural varieties is uncertain; the fine-grained pyroxene crystals may have developed after peak metamorphism and may reflect lower temperatures than the medium-grained pyroxene. The mean metamorphic temperature of Fe–Ti oxide phases, calculated using Stormer's (1983) method, is 719°C (Table 32). Metamorphic temperatures calculated for this rock are similar to those for the Gabanintha sample.

M_2: Contact metamorphism of greenstones by pegmatite-banded gneiss and recrystallized monzogranite protoliths

Distribution of M_2 metamorphism

Contact metamorphic effects of pegmatite-banded gneiss and recrystallized monzogranite protoliths are considered together, as they are identical and inseparable. This is due principally to the close similarities in granitoid compositions, pluton shapes, modes of emplacement, and levels of intrusion into basal greenstones which were already at elevated temperatures. Furthermore, monzogranite pervasively intruded pegmatite-banded gneiss, and most contact metamorphic assemblages associated with the gneiss were recrystallized during this event. Consequently, the contribution to the overall metamorphic pattern by the monzogranite is far greater than that by pegmatite-banded gneiss protoliths. The only pegmatite-banded gneiss contact effects preserved are those in the amphibolite-facies margins of the Tallering and southern Dalgaranga greenstone belts, and in rafts and xenoliths of supracrustal rocks in the gneiss. Most marginal zones of greenstone belts preserve greenschist–amphibolite transition, and amphibolite-facies remnants of assemblages developed during monzogranite contact metamorphism. Rafts and xenoliths of supracrustal rocks in recrystallized monzogranite have metamorphic characteristics identical to rocks in these marginal zones. Most M_2 contact metamorphic assemblages are overprinted to some extent by M_3 metamorphism.

The width of preserved contact aureoles varies from a few hundred metres to several kilometres, but most are less than 1 km wide. Zones of M_2 metamorphism are not shown as continuous features of greenstone belt margins on Plate 3. There are two reasons for this. Firstly, M_3 metamorphism completely overprinted some zones of M_2 metamorphism, particularly in the southwest of the province where M_3 is largely in amphibolite facies. Secondly, high-grade margins were not inferred on the map where there were no petrographic data or field observations to justify them — because of lack of samples, weathered outcrop, or poor

TABLE 32. CHEMISTRY OF MINERAL PHASES AND GEOTHERMOMETRY OF M_1 GRANULITE FACIES ROCKS

	Sample 81576 Gabanintha		*Sample 83596 Karara*					
	CPX	*OPX*	*CPX-mg*	*CPX-fg*	*OPX-mg*	*OPX-fg*	*MGT-bulk*	*ILM*
No. grains	2	3	2	2	2	3	2	1
No. analyses	4	8	3	2	3	3	3	2
				Percentage				
SiO_2	52.96	51.95	52.34	51.97	52.52	51.88	3.15	0.38
TiO_2	0.13	0.16	0.25	0.31	0.14	0.18	9.12	48.77
Al_2O_3	0.72	0.45	1.61	1.94	0.83	1.07	3.28	0.22
Cr_2O_3	0.23	<0.08	0.10	0.08	<0.09	<0.09	2.71	0.20
FeO (a)	10.08	24.91	10.38	9.93	23.50	24.63	74.59	48.83
MnO	0.21	0.54	0.15	0.17	0.41	0.54	0.26	0.68
NiO	<0.13	<0.13	<0.14	<0.14	<0.14	<0.14	<0.16	<0.16
MgO	14.02	20.38	13.60	13.66	21.26	21.02	1.74	0.32
CaO	21.19	0.97	20.92	20.88	1.20	0.68	0.54	0.09
Na_2O	0.25	0.14	0.23	0.29	<0.14	<0.14	-	-
K_2O	0.05	<0.05	<0.05	<0.05	<0.05	<0.05	-	-
Total	99.84	99.50	99.58	99.23	99.86	100.00	95.39	99.49
100Mg/(Mg+Fe)	71.3	59.3	70.0	71.0	61.7	60.3	-	-
mole % USP	-	-	-	-	-	-	34.6	-
mole % ILM	-	-	-	-	-	-	-	93.6
				Atomic %				
Ca	43.5	2.0	43.5	43.7	2.4	1.4	-	-
Mg	40.0	57.6	39.4	39.8	59.8	39.6	-	-
$Fe^{2+}+Fe^{3+}+Mn$	16.5	40.4	17.1	16.5	37.8	39.6	-	-
End-members for Lindsley and Andersen (1983) projection in Lindsley's (1983) two-pyroxene geothermometer:								
Wollastonite	42.3	2.0	41.0	40.9	2.5	1.5	-	-
Enstatite	41.3	58.8	41.3	42.1	60.6	60.6	-	-
Ferrosalite	16.4	39.2	17.7	17.0	36.9	37.9	-	-

	Lindsley's (1983) two-pyroxene geothermometer		*Kretz's (1982) two-pyroxene geothermometer*		*Stormer's (1983) Fe–Ti oxide geothermometer*
Sample	*CPX*	*OPX*	*solvus method (b)*	*K_D method(c)*	
81576	800°C	710°C	887°C	749°C	Sample 83596
83596(mg)	860°C	840°C	886°C	746°C	T = 719°C
83596(fg)	870°C	650°C	877°C	747°C	$f(O_2)$ = -16.5

Abbreviations: CPX: clinopyroxene, OPX: orthopyroxene, USP: ulvospinel, ILM: ilmenite, fg: fine-grained, mg: medium-grained,
(a) All Fe calculated as FeO
(b) $T(°K)=1000/[0.054+0.608X^{cpx}-0.304\ln(1-2(Ca)^{cpx})]$ (c) $T(°K)=1130/(\ln K_D+0.505)$
Where: $K_D = 2.0-0.45X^{opx}$; $X = Fe^{2+}/(Mg+Fe^{2+})$; and $(Ca)^{cpx} = Ca/(Ca+Mg+Fe^{2+})$ in cpx

exposure. The distribution and grade of M_2 metamorphism is similar to that documented in marginal regions of greenstone belts in other granite–greenstone terranes in the eastern Yilgarn (Binns et al., 1976; Ahmat, 1986b) and in the Abitibi belt in Canada (Jolly, 1978).

Mineral assemblages and textures

Mineral assemblages developed in M_2 contact metamorphic aureoles in mafic and sedimentary rocks are those listed on Plate 3 for the greenschist–amphibolite facies transition, and lower and upper amphibolite facies. Grunerite–cummingtonite, magnetite, and quartz assemblages developed in amphibolite-facies BIF.

Most greenstone belt margins are high-strain zones that developed during D_2 and D_3 folding, subsequent to intrusion of monzogranite. The timing of contact metamorphism due to monzogranite folding, and of regional metamorphism, is restricted to a period of about 40 million years, on the basis of emplacement ages of monzogranite (2681 and 2690 Ma) and post-folding granitoids (2641–2617 Ma). In most cases, M_2 assemblages are preserved in relatively undeformed lenses within the foliation; however, textures indicate that in some cases M_2 metamorphic mineral growth outlasted deformation in these marginal zones. This paradox can be simply explained if folding took place within a few million years of monzogranite intrusion. Because conduction of heat in rocks is very slow compared with deformation rates (England and Richardson, 1977), enough heat would be retained in contact aureoles (e.g. Turner, 1980, fig. 1-6) to allow textural annealing of metamorphic minerals during development of foliation. In

the rare regions of low strain, in marginal zones of greenstone belts, and more commonly in low-strain xenoliths and rafts of greenstones in recrystallized monzogranite, granoblastic texture developed during M_2 metamorphism (Fig. 150).

P–T conditions of M_2 metamorphism

Mineral phases in two samples of metasedimentary rock from the M_2 contact aureole in the Dalgaranga greenstone belt were analysed by electron-microprobe, for geothermometry. The samples were chosen because M_3 retrogression appears to be minimal in much of the aureole in this area. Calculated temperatures are given in Table 33. Hodges and Spear's (1982) adjustment to Ferry and Spear's (1978) calibration corrects for the effects of Mn and Ca substitution in garnet on the Fe–Mg equilibrium between garnet and biotite. The differences between the temperature estimates made by the two methods are within the uncertainties of the calculation, i.e. ±50°C. The temperatures are consistent with the lower amphibolite-facies mineral assemblages in the samples. Coexisting andalusite, garnet, and cordierite in pelitic rocks adjacent to these samples indicate metamorphic conditions of about 500–630°C at P <300 MPa (Hess, 1969).

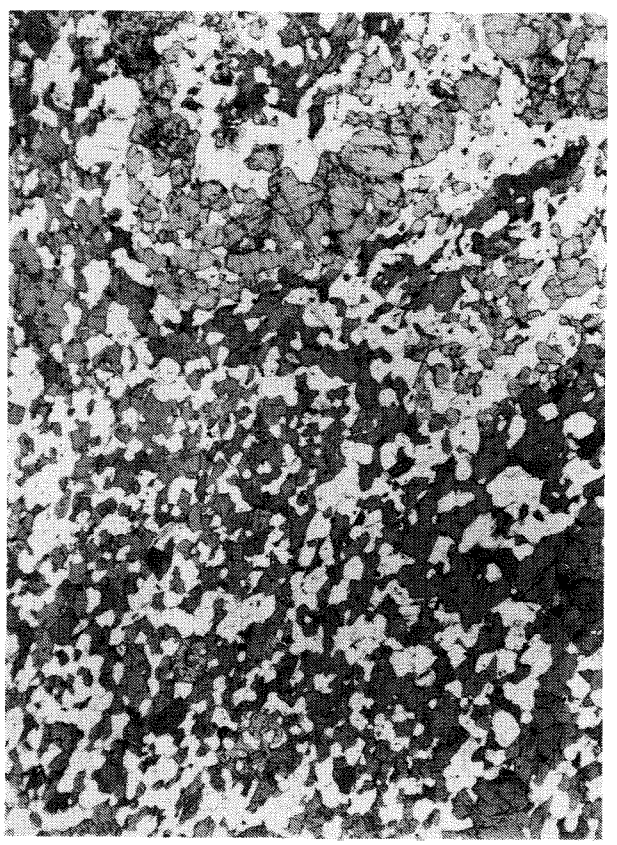


Figure 150. Granoblastic texture in a clinopyroxene–hornblende–andesine amphibolite (M_2) raft in monzogranite.

M_3: Regional metamorphism of greenstones, pegmatite-banded gneiss, and recrystallized monzogranite

Distribution of M_3 metamorphism

Regional metamorphism of supracrustal rocks, pegmatite-banded gneiss, and recrystallized monzogranite outlasted development of S_3 foliation and ended before the intrusion of most post-folding granitoids. Metamorphic grade ranges from prehnite–pumpellyite to granulite facies, although most rocks are in greenschist facies. In the Abbotts and northern Meekatharra–Wydgee greenstone belts, metamorphic grade is concentrically zoned from upper greenschist facies at the margins, to prehnite–pumpellyite facies in the cores. Facies boundaries are roughly parallel to these greenstone belt margins (Plate 3). In the remainder of the province, any variation in M_3 metamorphic grade between margins and cores of greenstone belts is subtle; except for the southwest of the province, this variation is generally only between upper and lower greenschist facies.

The southwest of the Murchison Province is in amphibolite facies and forms part of a large high-grade tract of granite–greenstone terrane in the southwest Yilgarn Craton (Fig. 1). The nature of the metamorphic boundary between this high-grade region and the remainder of the province is poorly understood. It appears in some areas to be gradational over several kilometres or even tens of kilometres. Granulite-facies conditions were attained in a small, poorly exposed part of the Koolanooka greenstone belt; however, as discussed previously, there is uncertainty about the timing of metamorphism here.

Pegmatite-banded gneiss and monzogranite were metamorphosed, along with the greenstones, in amphibolite facies in the southwest of the province, but in greenschist facies elsewhere. Few remnants of igneous minerals or textures survived metamorphism. There are no systematic differences in metamorphic grade between margins and cores of recrystallized monzogranite bodies, or between foliated and unfoliated recrystallized monzogranite.

M_3 regional metamorphism extensively overprinted M_2 mineral assemblages. The intensity of retrogression varied from very slight to complete re-equilibration.

Mineral assemblages and textures

Mineral assemblages for various facies in mafic and sedimentary rocks are given on Plate 3. Mineral assemblages in BIF, felsic volcanic rocks, and ultramafic rocks are not sufficiently diagnostic to assign them to the facies divisions used on Plate 3, although broad distinctions can be made, for example, between greenschist and amphibolite facies. Mineral assemblages for these lithologies at

TABLE 33. COMPOSITIONS OF GARNET AND BIOTITE, AND GEOTHERMOMETRY OF M_2 MINERAL ASSEMBLAGES

(A) COMPOSITIONS OF M_2 GARNET AND BIOTITE

Sample	*73095*		*73179*	
Mineral	*Biotite*	*Garnet rim*	*Biotite*	*Garnet rim*
No. of analyses	*7*	*7(a)*	*6*	*3(a)*
		Percentage		
SiO_2	33.78	36.76	34.51	36.72
TiO_2	1.74	<0.09	1.66	<0.08
Al_2O_3	19.90	20.75	17.13	20.84
FeO	25.17	36.85	23.75	36.15
MnO	<0.09	1.29	<0.09	1.50
MgO	5.68	1.68	8.27	2.50
CaO	0.10	1.73	0.25	2.04
Na_2O	<0.13	-	<0.13	-
K_2O	9.14	-	9.49	-
		Cations per formula unit		
	11(O)	12(O)	11(O)	12(O)
Si	2.64	3.01	2.71	2.99
Ti	0.10	-	0.10	-
Al	1.83	2.00	1.59	1.99
Fe	1.64	2.52	1.56	2.46
Mg	0.66	0.21	0.97	0.30
Ca	-	0.15	-	0.18
Mn	-	0.09	-	0.10
K	0.91	-	0.95	-

(a) Garnet rim with highest Mg/Fe ratio is given in table and used in geothermometry

(B) GARNET–BIOTITE GEOTHERMOMETRY

Sample	X_{ann}	X_{phl}	X_{alm}	X_{pyr}	X_{gr}	X_{sp}	lnK_1	lnK_2	$T_1(°C)$	$T_2(°C)$
73095	0.570	0.230	0.850	0.069	0.051	0.030	-4.811	-4.647	615	636
73179	0.534	0.331	0.809	0.099	0.058	0.034	-4.841	-4.654	611	635

Where:

X: mole fraction, ann: annite, phl: phlogopite, alm: almandine, pyr: pyrope, gr: grossular, sp: spessartine

$K_1 = [(X_{pyr})^3.(X_{ann})^3]/[(X_{phl})^3.(X_{alm})^3)]$

$K_2 = K_1\{\exp 3[(3300\text{-}1.5T).((X_{gr})^2+X_{alm}.X_{gr}+X_{gr}.X_{sp}+X_{pyr}.X_{gr})]/RT\}$

$0 = 12454\text{-}4.662T+0.57P+RTlnK$

T_1: Ferry and Spear's (1978) calibration, $K = K_1$

T_2:Hodges and Spear's (1982) correction to Ferry and Spear's calibration, $K = K_2$

P is taken as 300 MPa

various grades have been listed by Binns et al. (1976) and Ahmat (1986b).

Igneous textures are well preserved in weakly deformed greenstones in the prehnite–pumpellyite and lower greenschist facies. At the lowest grades some igneous mineral phases, particularly plagioclase and clinopyroxene, have survived metamorphism. At higher grades, in both weakly and strongly deformed rocks, textures become progressively more granoblastic, lepidoblastic, or porphyroblastic, and igneous textures and minerals are obliterated.

Most M_2 contact-metamorphic assemblages have been overprinted to some extent by M_3 metamorphism. In mafic rocks, pyroxene and hornblende crystals became ragged, and were patchily replaced by actinolite and chlorite; calcic plagioclase became albitized, with consequent growth of epidote. In metasedimentary rocks, biotite and garnet were partly chloritized, and cordierite was pinitized (Fig. 151).

Textures indicate that minerals in pegmatite-banded gneiss and recrystallized monzogranite were thoroughly recrystallized during M_3 (Figs 94 and 112); their mineral assemblages can thus be regarded as metamorphic rather than igneous. Recrystallization outlasted development of S_3 foliation, as in the greenstones. Igneous assemblages were downgraded, during and after F_2 and F_3 folding, to greenschist or lower amphibolite facies. Rock samples were assigned to metamorphic facies depending on the presence of some or all of the following minerals:

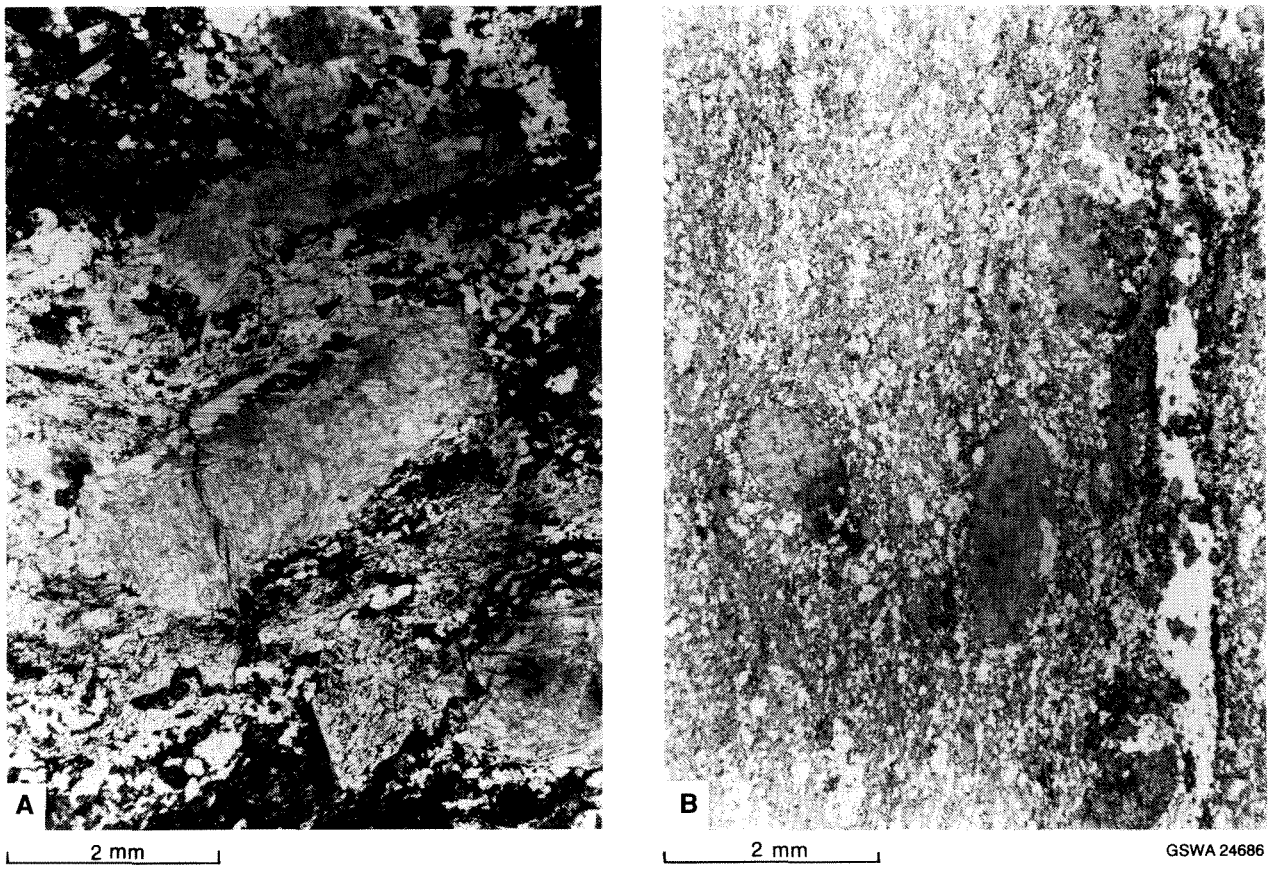


Figure 151. Partial retrogression due to overprinting of M_2 assemblages by M_3 metamorphism. A —Prismatic crystals of andalusite pseudomorphed by aggregates of phyllosilicates in metasedimentary rock. B — clinopyroxene crystals partially pseudomorphed by amphibole in amphibolite; the high-relief material in the porphyroblasts is clinopyroxene.

Greenschist facies: albite–oligoclase, chlorite, biotite, white mica, epidote, calcite;

Lower amphibolite facies: oligoclase–andesine,biotite, hornblende, garnet (rare).

Many granitoid rocks show textural evidence of retrogression to lowermost greenschist facies, with partial replacement of biotite by chlorite, rutile, and in some cases epidote. Plagioclase is partly replaced by fine-grained aggregates of white mica, epidote, calcite, and albite, indicating a reaction such as:

biotite + oligoclase —> chlorite + rutile + white mica + epidote + calcite + albite.

Ferry (1979) and Studemeister (1983, 1985) have documented similar assemblages and reactions in granitoids. In general, amphibolite facies assemblages are more thoroughly recrystallized and coarser grained than those in greenschist facies. More descriptive information on pegmatite-banded gneiss and recrystallized monzogranite textures is given in Chapters 3 and 5.

P–T conditions of M_3 metamorphism

There are no quantitative P–T data for M_3 assemblages. However, andalusite–chloritoid and andalusite –sillimanite–cordierite parageneses, in greenschist and amphibolite facies metasedimentary rocks respectively, indicate relatively low pressures of < 400 MPa (using the alumino-silicate triple point of Holdaway, 1971) throughout the province. Kyanite occurs rarely in low P–T kyanite–chlorite–muscovite–quartz assemblages. Regional metamorphic assemblages in other granite–greenstone provinces of the Yilgarn Craton also record relatively low pressures (Binns et al., 1976; Ahmat, 1986b, and references therein).

Timing of M_3 metamorphism

Timing of M_3 metamorphism is well constrained by U–Pb zircon ages of granitoids which intruded the Murchison Supergroup before and after metamorphism. Two monzogranite samples have been dated at 2690 Ma and 2681 Ma; these were recrystallized during M_3. Most post-folding granitoids have igneous texture and therefore post-date metamorphism; two of these have crystallization ages of 2641 Ma and 2617 Ma (Chapter 3). These relationships constrain M_3 within a period of about 40 million years.

Textures in greenstones and recrystallized monzogranite indicate that the peak of M_3 metamorphism occurred after D_2 and D_3 deformation. In addition, some post-folding

granitoid plutons are partly recrystallized in greenschist facies, particularly in the west of the province (Plate 3). These facts suggest that M_3 metamorphism climaxed immediately before intrusion of most post-folding granitoids.

Post-folding granitoids that intrude the Tallering and Twin Peaks greenstone belts are all recrystallized in greenschist facies, indicating that the metamorphic climax was diachronous, and was later in the west of the province than in the east. The alternative interpretation, that western post-folding granitoids were emplaced a little earlier than those to the east, relative to a synchronous metamorphism, is equally possible.

Rb–Sr systematics of pegmatite-banded gneiss and recrystallized monzogranite were disturbed during M_3 metamorphism. The Rb–Sr dates for these rocks (c. 2.6 Ga, see Chapter 3) reflect post-metamorphic cooling. These dates are indistinguishable from the intrusive ages of unmetamorphosed post-folding granitoids, the parent magmas of which were probably generated in the deep crust by partial melting associated with M_3 metamorphism (Watkins et al., in press).

Big Bell metamorphism

Rocks in the vicinity of the Big Bell gold mine contain high-grade mineral assemblages (Plate 3). Garnet–hornblende–cummingtonite–plagioclase–quartz amphibolite, and flaser-textured felsic schists containing andalusite, cordierite, garnet, and minor amounts of sillimanite (Chown et al., 1984) indicate middle to upper amphibolite-facies conditions of metamorphism. Rocks in the margin of the belt containing the Big Bell deposit were metamorphosed in lower amphibolite facies. Chown et al. (1984) suggested that this zonation was caused by hydrothermal metamorphism of the core of the belt (Plate 3). A major shear zone passes through this area (Plate 2) and it is possible that hot fluid was focused through this shear zone.

Phillips (1985) and Phillips and De Nooy (1988) argued convincingly that the high-grade assemblages result from high-temperature upper amphibolite-facies desulphidation and decarbonation reactions, with incipient partial melting forming quartz–K-feldspar veinlets. This event followed earlier greenschist-facies metasomatism which altered the rocks and localized the gold. They calculated peak metamorphic temperatures of 650–700°C at 400–500 MPa. Patchy retrogression of peak-metamorphic assemblages occurred as a result of fluid infiltration during cooling (Phillips, 1985). As a result of this work the words 'syntectonic hydrothermal' in the Plate 3 reference under 'BIG BELL METAMORPHISM' should be disregarded. It is difficult to relate metamorphism around Big Bell to the regional scheme proposed here; the style of metamorphism, and also the style of mineralization, appear to be unique in the Murchison Province.

Thermal model of metamorphism

Metamorphic models proposed by Binns et al. (1976) and Ahmat (1986b) for eastern Yilgarn greenstone belts cannot explain the distribution of metamorphic facies in the Murchison Province granite–greenstone terrane. In the model of Binns et al. (1976), two types of metamorphism (dynamic and static) developed simultaneously. Dynamic metamorphism is generally restricted to linear belts along the margins of greenstone belts; these were thought to represent deep-seated rocks uplifted relative to those in greenstone belt cores during diapiric emplacement of granitoids. Static metamorphism which occurred away from greenstone belt margins was related to structural height above a granitic substratum; the present distribution of metamorphic grade results from differential uplift of greenstones (Archibald et al., 1978, fig. 1B). Ahmat (1986b) reviewed this model in the light of his work in the Southern Cross Province. He preferred a model in which elevated isotherms were already present in greenstones, parallel to stratigraphic layering, before intrusion of granitoids. These isotherms were folded during diapiric emplacement of granitoids, and tilted by differential uplift, to give the present distribution of metamorphic grade. These models are shown schematically in Figure 152.

In the Murchison Province, M_1 and M_2 metamorphic events are the result of intrusion of igneous bodies. The widths and metamorphic temperatures of M_1 and M_2 contact aureoles are consistent with the sizes and types of intrusion that generated them (Jaeger, 1957, 1959; Turner, 1980). The main constraints for thermal modelling of M_3 regional metamorphism are the distribution of metamorphic facies, and the timing of metamorphism relative to granitoid intrusion and deformation events. These have been described in preceding sections. A qualitative model for Murchison Province metamorphism is shown schematically in four stages in Figure 153; each is described below.

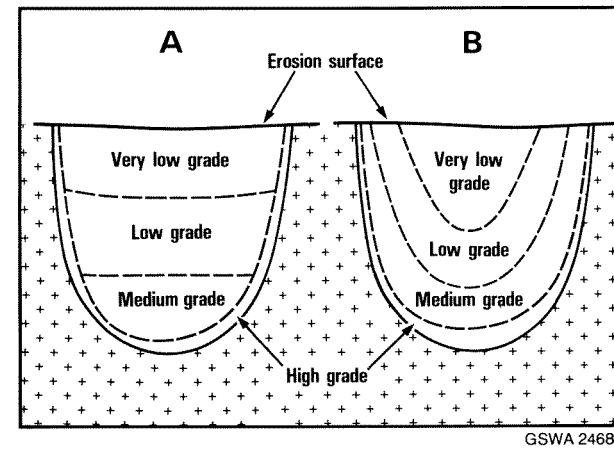


Figure 152. Metamorphic models for eastern Yilgarn greenstone belts: A — Binns et al., 1976; B — Ahmat, 1986.

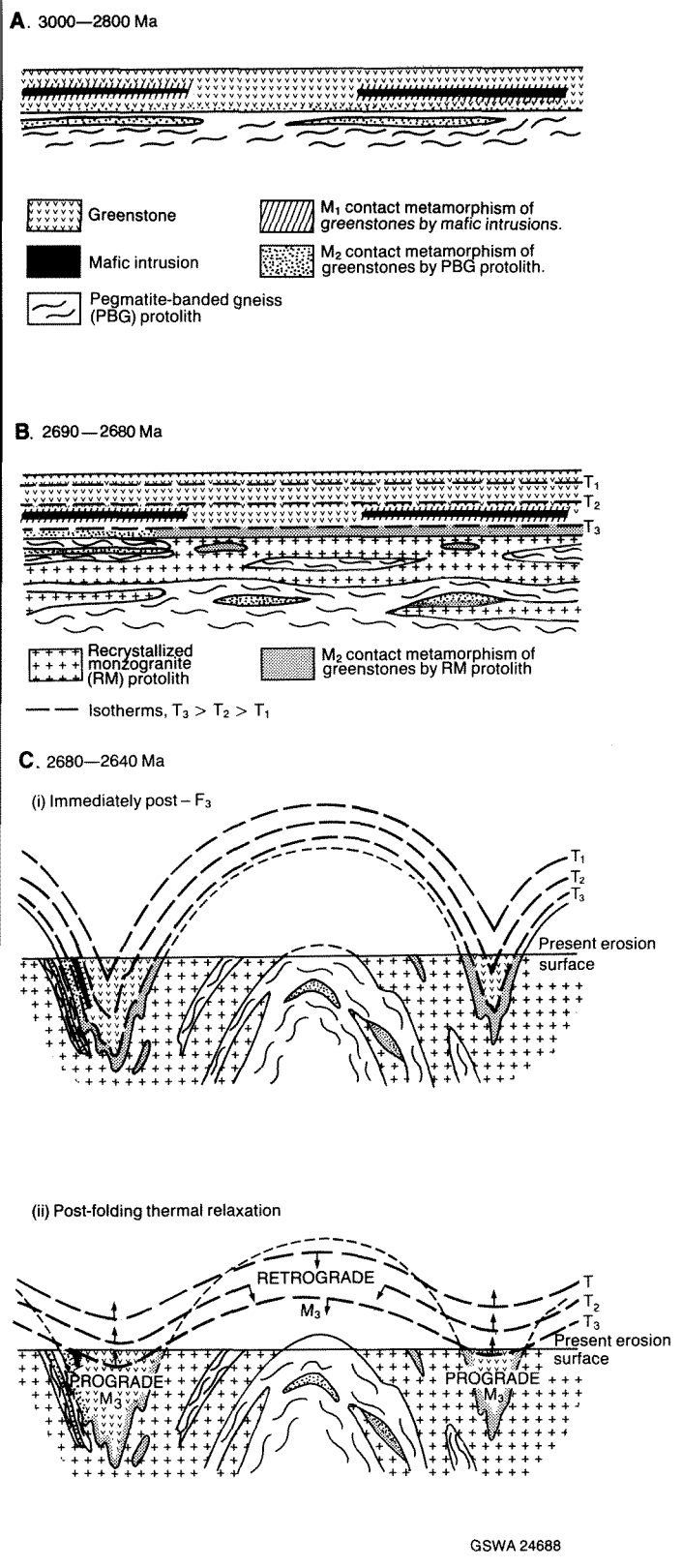


Figure 153. Qualitative thermal model for Murchison Province metamorphism.

A. 3000–2800 Ma

Emplacement of the Gabanintha layered mafic intrusion into the Luke Creek Group caused M_1 contact metamorphism of surrounding rocks in amphibolite and granulite facies. Other M_1 contact aureoles may have developed around this time. Intrusion of pegmatite-banded gneiss protoliths into basal greenstones at c. 2.9 Ga caused amphibolite-facies M_2 contact metamorphism of adjacent rocks.

B. 2690–2680 Ma

Intrusion of monzogranite sheets into basal greenstones and pegmatite-banded gneiss resulted in development of amphibolite-facies M_2 contact aureoles. The base of the (approximately 15 km thick) greenstone sequence would have been at elevated temperatures by this time if steady-state conditions had been attained, or even partly attained, after greenstone deposition. For example, in a thermal gradient of 30°C/km (equivalent to the present average geotherm) temperatures at the base of the sequence would have been 450°C at 430 MPa, that is, in greenschist facies. Higher thermal gradients, which may have characterized the Archaean (e.g. Condie, 1984) would have resulted in higher temperatures at the base of the greenstones. The crust was considerably thickened by monzogranite intrusion, and the thermal gradient below the greenstone sequence would have been significantly perturbed to higher temperatures because of this intrusion.

C. 2680–2640 Ma

(1) If D_2 and D_3 deformation rates were typical of Phanerozoic tectonic processes, isotherms would have been folded along with greenstones, monzogranite, and pegmatite-banded gneiss, and there would have been minimal thermal re-equilibration (cf. Sleep, 1979). The crust would have been substantially thickened by these folding events.

(2) After folding ceased the folded isotherms relaxed, over a period of several million years, towards steady-state conditions, causing cooling in anticlines and heating in synclines (e.g. Chamberlain, 1986; Chamberlain and Karabinos, 1987). Because most greenstone belts are in synclinal positions they record prograde metamorphism. M_2 assemblages in these belts, adjacent to recrystallized monzogranite and pegmatite-banded gneiss contacts, were partly retrograded to greenschist facies at this stage. Igneous assemblages and textures in monzogranite were retrograded to greenschist facies, and in the southwest of the province to amphibolite facies, as isotherms relaxed downwards. Marked zonation occurs only in the thickest greenstone belts in the north of the province, and indicates that thermal relaxation was almost completed before it was terminated by uplift and erosion (cf. England and Richardson, 1977). Post-folding

granitoids were intruded during the uplift stages, and were probably generated by metamorphic processes deep in the crust.

For most of the province, the present level of erosion exposes rocks of greenschist facies, although metamorphic grade in the southwest is amphibolite facies. Mineral assemblages indicate a temperature difference of about 100–150°C between these regions. If exposure of the higher grade region is due to differential uplift, a pressure increase of only 100–150 MPa would be expected in a 30°C/km thermal gradient, and less in a higher thermal gradient. This pressure difference is not big enough to cause marked development of higher pressure mineral parageneses. Thus, the two alternative hypotheses which might account for the higher grades in the southwest (i.e. differential uplift or higher heat flow) cannot be resolved by petrographic data alone. However, differential uplift is easier to explain in terms of the proposed model, and is the mechanism invoked in other studies of Yilgarn Craton metamorphism (Binns et al., 1976; Archibald et al., 1978, 1981; Ahmat, 1986b).

Chapter 7

Economic geology

The Murchison Province is Western Australia's second most productive gold-mining region after the Eastern Goldfields Province, and still presents major opportunities for further exploration and new discoveries. Production of other mineral commodities has been relatively insignificant, the only notable mining operation having been that at the Koolanooka iron-ore deposit between 1966 and 1972. However, the development of the Scuddles deposit at Golden Grove will make the province a significant producer of copper and zinc.

The area occupies most of the Murchison and Yalgoo Mineral Fields and, in the extreme southwest, part of the South West Mineral Field.

Gold

From the first authenticated discovery of economic gold mineralization at Yuin in 1890 to the end of 1987, the Murchison Province had yielded about 230 t of gold, representing about 10% of the State total. Gold mineralization is widespread in the province (Plate 2) and, unlike the Eastern Goldfields Province where about 3 km^2 of land at Kalgoorlie and Boulder has accounted for 75% of that region's total, no single mining area predominates in the Murchison. Even so, it must be noted that over half of the total production has come from just four deposits (Hill 50, Great Fingall, Big Bell, and Consols–Fenian), and only ten mining centres have individually contributed more than 1% of the province's production (Fig. 154).

One of the main aims of the investigation described in this bulletin has been to compile the first comprehensive account of gold mineralization throughout the Murchison Province. This has involved detailed field mapping of the more important gold-producing areas, supplemented by a collation of all available data from both published and unpublished sources.

The following account presents descriptions of all mining centres, and all mines which have recorded a total production in excess of 30 kg of gold. Smaller mines are also described where these occur outside the principal mining areas. This systematic documentation then permits examination of regional relationships of mineralization to lithology, structure, metamorphism, granitoid intrusions, and geochemical variations of the crust.

Important regional and local controls govern the location and size of gold deposits in the Murchison Province. The spatial distribution of known deposits can be explained in terms of these controls, and the resulting metallogenetic model can be used to recommend new areas for exploration.

Description of gold deposits

Production from Western Australian gold mines was first systematically recorded in 1897. In the Murchison Province significant gold production commenced in 1891. A considerable amount of gold extracted from alluvial deposits and near-surface supergene enrichments prior to 1897 was not documented. The gold deposits have been assigned to mining centres for statistical purposes and this section describes these mining centres in alphabetical order. Official total production figures for mining centres of the province during the period 1897 to 1987 are presented in Table 34. Production details for individual mines are presented in Tables 35–38 within mining centre descriptions. The geology of small mining centres and isolated deposits is summarized in Table 39.

Abbotts

The Abbotts mining centre is 30 km north-northwest of Meekatharra. The most productive mines have been New Murchison King (788 kg) and Mount Vranizan (391 kg), which are about 500 metres apart and are located in the same northerly striking shear zone. Country rocks are felsic tuffaceous and fine-grained metasediment, with minor dolerite, gabbro, and felsic porphyry units. Mining has been based on lenticular quartz veins, up to 2 m thick, which at New Murchison King dip steeply eastwards, and at Mount Vranizan dip both east and west. Free gold in the quartz is accompanied by minor amounts of pyrite and arsenopyrite, and less common tourmaline and carbonate.

Ellis (1936) stated that the quartz veins are parallel to the axial plane of a regional 'anticlinal' structure. However, the major fold forming the Abbotts belt has since been recognized as a syncline (Elias, 1982). The mines extended to depths of between 90 and 100 metres, and according to Ellis (1936) the orebodies terminated at about this level. Most production clearly came from the oxidized zone, and

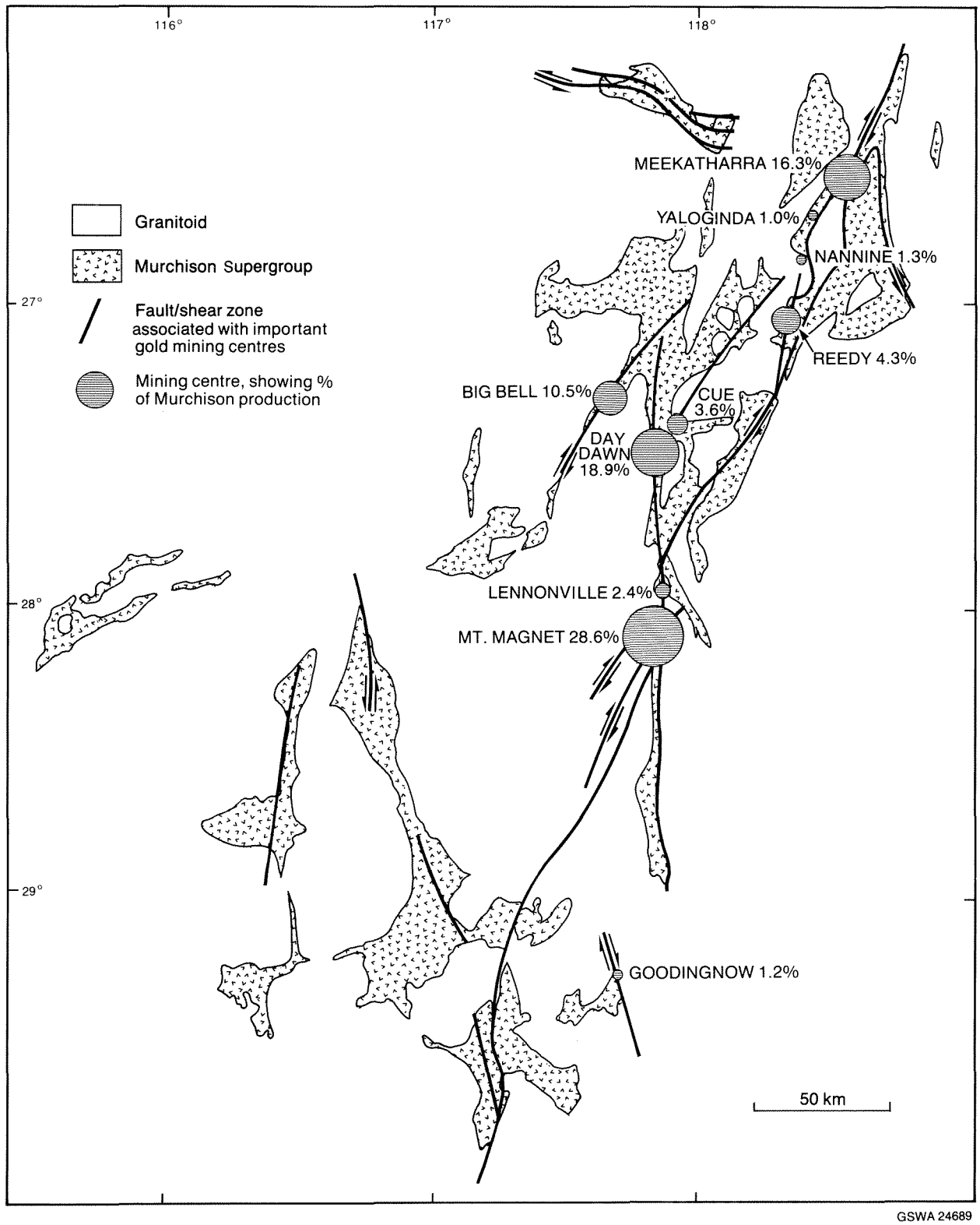


Figure 154. Distribution and relative productivity of the principal gold-producing centres in the Murchison Province.

TABLE 34. TOTAL PRODUCTION OF GOLD FROM THE MURCHISON PROVINCE PRIOR TO 31 DECEMBER 1987

Mining centre	*Alluvial (kg)*	*Dollied (kg)*	*Ore (t)*	*Gold (kg)*	*Total gold (kg)*
Abbotts	-	1.0	41 452	1 279.5	1 280.5
Big Bell	-	0.3	5 631 253	22 759.8	22 760.1
Bilberatha	0.1	3.0	6 563	101.0	104.1
Burnakura	3.4	105.0	248 812	1 520.6	1 629.0
Carlaminda	0.1	0.1	3 480	45.5	45.7
Chesterfield	5.1	15.2	13 374	294.9	315.2
Cuddingwarra	2.0	16.1	114 718	1 927.3	1 945.4
Cue	161.5	64.0	349 917	7 565.3	7 790.8
Day Dawn	18.5	45.4	2 112 313	42 015.1	42 079.0
Eelya	0.2	4.7	5 017	104.3	109.2
Fields Find	0.3	12.9	68 399	1 216.7	1 229.9
Gabanintha	3.8	7.5	145 108	954.9	966.2
Garden Gully	1.0	2.9	33 914	734.0	737.9
Goodingnow	22.0	16.6	113 749	2 454.8	2 493.4
Gullewa	-	5.9	45 036	711.8	717.7
Jillewarra	7.4	44.0	2 637	123.8	175.2
Jumbulyer	1.2	4.1	4 720	54.8	60.1
Kirkalocka	-	0.6	354	5.4	6.0
Lake Austin	82.3	126.6	41 204	1 630.6	1 839.5
Lennonville	4.9	104.7	611 843	5 982.6	6 038.2
Mainland	4.2	126.5	9 107	800.3	931.0
Meekatharra	35.5	120.7	4 890 541	36 360.1	36 516.3
Messenger Patch	17.6	21.4	42 342	908.8	947.8
Mindoolah–Ryansville	6.1	3.8	42 606	323.5	333.4
Mistletoe	3.8	33.3	444	15.2	52.3
Moyagee	0.4	6.2	14 321	624.9	631.5
Mount Farmer	-	-	535	5.8	5.8
Mount Gibson	0.2	1.6	752 041	2 444.7	2 446.5
Mount Magnet	61.8	422.0	6 265 865	63 238.2	63 722.0
Munarra Gully	0.7	1.5	14 561	215.8	218.0
Nannine	164.6	68.1	251 027	2 774.9	3 007.6
Ninghan	-	-	340	3.9	3.9
Noongal	3.0	11.6	20 371	292.8	307.4
Nyounda	-	7.7	1 671	13.2	20.9
Pinnacles	2.1	53.6	28 264	389.0	444.7
Pinyalling	0.1	13.9	3 931	65.5	79.5
Quinns	63.1	77.0	42 284	506.7	646.8
Reedy	8.0	11.5	1 463 433	10 604.6	10 624.1
Retaliation	-	-	6 282	69.0	69.0
Rothsay	-	0.8	47 974	415.0	415.8
Stake Well	2.6	7.3	22 725	315.7	325.6
Tuckabianna	25.3	56.2	23 581	400.1	481.6
Tuckanarra	10.7	135.6	30 851	1 032.2	1 178.5
Wadgingarra	-	-	2 884	38.8	38.8
Warda Warra	-	-	12 297	200.1	200.1
Warriedar	-	0.1	22 959	204.4	204.5
Weld Range	4.4	1.6	3 666	70.7	76.7
Winjangoo	0.1	13.2	613	5.3	18.6
Yalgoo	1.2	0.8	10 680	348.2	350.2
Yaloginda	6.0	82.0	866 840	2 607.5	2 695.5
Yuin	-	4.1	69 574	871.0	875.1
Sundry parcels:					
Murchison M.F.					
Cue District	164.0	35.1	9 166	2 044.0	2 243.1
Meekatharra Dist.	450.0	31.8	4 715	1 437.3	1 919.1
Day Dawn Dist.	69.6	2.8	1 004	413.2	485.6
Mount Magnet Dist.	82.1	15.1	999	1 929.7	2 026.9
Yalgoo M.F.	38.3	7.3	1 038	651.0	696.6
Total	**1539.3**	**1954.8**	**24 575 395**	**224 069.8**	**227 563.9**

available evidence suggests that the deposits were lenticular. The significance of dolerite and porphyry intrusions along strike, and dolerite and ultramafic intrusions to the west of the shear zone, are uncertain. Any future exploration should probably investigate the possibility of concealed mineralization along strike, particularly to the south where relatively thick superficial deposits may have precluded significant surface gold anomalies.

Big Bell

Big Bell is, in terms of contained gold, one of the largest individual gold deposits in Western Australia. Although prospecting and minor gold production took place early in the century it was not until 1937 that large- scale mining commenced. On closure of the mine in 1955 total production was 22.76 t of gold from 5.63 Mt of ore (average grade 4.04 g/t gold); in mid-1987 Australian Consolidated Minerals Ltd published a total reserve figure of 112.22 t of gold in ore averaging 3.36 g/t gold.

The Big Bell deposit is a pyritic quartz–muscovite–K-feldspar-schist lode, up to 40 m wide, about 500 m long, and extending to a depth of at least 1.5 km. The orebody is stratabound within the western part of a 200 m-wide flaggy quartzo-feldspathic unit, and plunges 70° to the east-southeast. To the west the orebody is structurally underlain by a thin graphite schist which overlies a thick amphibolite-facies metabasalt. East of the quartzo- feldspathic unit is another thick metabasalt, which, approaching the quartzo-feldspathic unit, has been intruded by sills of felsic porphyry. The lode is a flaggy, fine-grained quartzo-feldspathic rock with alternating thin (less than 3 mm) muscovite-rich and muscovite-poor laminae (Chown et al., 1984). Potassium feldspar and quartz occur with the muscovite, and in distinct thin bands; some zones contain abundant quartz lenses (less than 3 cm thick). According to Chown et al. (1984) andalusite, cordierite, and biotite are most common around the margins of the lode. Accessory minerals include tourmaline, which occurs in small lenses, and, on a larger scale, outlines a halo around the deposit. Sulphides and oxides form up to 10% of the lode and occur in laminae, parallel or subparallel to the main foliation. Pyrite is the dominant sulphide, and there are lesser amounts of pyrrhotite, sphalerite, chalcopyrite, molybdenite, stibnite, berthierite, arsenopyrite, tetrahedrite, ullmanite, and scheelite. Rutile occurs throughout most of the lode, and is particularly common in K-feldspar layers; ilmenite is associated with biotite schist at the southern end of the deposit. Gold is chiefly microscopic and occurs both as grains forming inclusions in silicates, and in blebs in pyrite. However, the sulphide fraction appears to also contain submicroscopic gold.

In a detailed description of the deposit and its local geological setting, Chown et al. (1984) stated that the mid- to upper-amphibolite facies metamorphism of the mine area post-dates gold mineralization. From petrographic and geochemical evidence they concluded that the quartzo-feldspathic unit hosting the deposit is an altered felsic volcanic rock, but that the lode itself, and associated thin units of biotite–andalusite–cordierite–garnet schist, are hydrothermally altered and metamorphosed mafic igneous rocks. The latter conclusion is largely dependent on the Ti and V contents of the rocks concerned, and should be treated with caution in the absence of data on trace elements such as Ni, Cr, and REE. The high Al_2O_3 content of the rock (16.3%) is most consistent with a shale, and shales commonly have high V values. The interpretation preferred here is that the host rock is of a metasomatized volcanogenic sedimentary origin.

Big Bell lies on the north-northeasterly striking Big Bell Shear Zone (Fig. 168), and all rocks, except late dykes, are strongly cleaved. A short distance to the south-southwest the greenstone succession terminates, but in the opposite direction its outcrop eventually expands into a wide greenstone belt in the Beebynbeebynganna Hill area. The main tectonic foliation at Big Bell dips steeply east-southeast on the western side of the belt, and steeply west-northwest on the eastern side. A second cleavage dips 65° towards the north. Subhorizontal pegmatite dykes that cross the main tectonic foliation are relatively undeformed. The felsic porphyry sills are strongly sheared and carry some gold mineralization within pyritic quartz veins and stringers.

Information presented by The Staff (1953, p. 228), concerning the geometry of the footwall, suggests that the orebody might occupy a local }'jog' (Sibson, 1986) in the shear zone. To the east of the orebody a set of easterly striking pegmatite veins and dykes have probably intruded dilational fractures that were produced during late-stage movement along the zone. Such movement would be dextral, but the sense of the main pre- and synmetamorphic shearing is currently unknown.

Chown et al. (1984) and Phillips and de Nooy (1988) discussed evidence bearing on the origin and age of the Big Bell deposit. Chown et al. (1984) concluded that mineralization pre-dated peak metamorphism and could either have been volcanogenic or post-volcanic to early metamorphic. Phillips and de Nooy (1988) stated that the high-grade metamorphism, which overprinted gold mineralization and low-grade metamorphism, included desulphidation around the margins of the deposit (producing biotite schist) and partial melting within the muscovite and K-feldspar schists. They concluded that melting was important because it provided a mechanism to remove water without the generation of a large volume of auriferous aqueous fluid which would have removed much of the gold.

The location of the deposit on a major shear zone, its shoot-like geometry, and the localized extensive hydrothermal alteration indicate an origin involving the passage of gold-bearing hydrothermal fluids along the shear zone, and the concentration of gold mineralization at a favourable site. The latter might have been a local dilational zone (possibly a 'jog' or open flexure) or the first available lithological trap where the shear zone passes from granitoids to greenstones. The atypical metamorphic grade of the host rocks could be due to this part of the greenstone belt, and the site of the deposit, being a conduit for hydrothermal solutions. Evidence relating to the relative timing of mineralization and metamorphism (Chown et al., 1984)

suggests that the shear zone may be the product of more than one phase of movement.

Burnakura

Production from the Burnakura mining centre has come chiefly from two mines, New Alliance and Federal City. These mines are separated by a distance of 3 km and the geological settings of the two groups of workings are different.

At the New Alliance mine a succession of felsic volcanogenic sedimentary rocks, tuff, shale, and jaspilitic BIF dips eastward at 30–40°, and has been intruded by concordant quartz veins. Low (1960) presented information to indicate that gold mineralization is concentrated in these veins, particularly in the most western, and structurally lowest, known as the 'Little Reef', and that highest grades occur at contacts with jaspilitic BIF. Montgomery (1910, p. 37) stated that the largest vein (about 4 metres thick) contains about 7 g/t gold; there may be scope for further mining of this body. Pyrite and galena occur in the quartz. The old workings extend to a depth of 60 metres.

The Federal City workings are located where quartz veins and stockworks have intruded sheared chlorite–carbonate rocks, basalt, dolerite, and microgranite. Montgomery (1910, p. 35–36) noted that the mine contains two parallel quartz veins, each about 1 metre thick, striking west-northwest, and dipping north-northeast at about 20°. The veins appear to occupy faults; intervening rocks are brecciated and contain numerous quartz veins cut by the main veins. Minor amounts of galena and copper carbonates are present in the quartz. The old workings extend to a depth of about 65 metres.

One of the factors impeding mining during the main production period (prior to 1909) was a significant inflow of water (about 50 kilolitres per hour) in both the Federal City and New Alliance mines. This may have been due to the location of both mines on fault zones. Drilling results included in Low's (1960) report suggest that the New Alliance area may still contain significant mineralization, and available evidence does not rule out future redevelopment of Federal City.

Chesterfield

Chesterfield is 50 km west-northwest of Meekatharra at the southeastern end of the Mingah Range. The mining centre is positioned in the axial region of an F_3 fold, which on the basis of minor structures and way-up criteria is an anticline. The principal mine is Margueritta (162 kg of gold from 9260 t of ore). Descriptions by Montgomery (1910, p. 59–60) and Connolly (1962) recorded that the early workings were based on a sulphidic (pyrite and pyrrhotite) 1 m-wide quartz vein, striking north-northwest and dipping 45–80° to the east-northeast. Ore shoots plunge northerly at about 25°. During a second phase of mining, which commenced in 1951, a parallel, eastern quartz vein was worked between levels at 25 and 38 m; Montgomery (1910, p. 59–60) also noted two parallel veins to the west. The main lithology of the wall rocks is carbonated chloritic schist (metamorphosed mafic tuff) which occurs within a succession of metabasalt, chert, graphitic slate, siltstone and quartzite (Blockley, 1962). Connolly (1962) stated that gold mineralization extends a short distance into the wall rocks. Sills of gabbro and pyroxenite intrude the succession and a dolerite dyke intrudes the mineralized zone. Descriptions by Connolly (1962) and Blockley (1962) indicate that the most productive quartz veins are those dipping at about 45° northeasterly. Such veins locally pass both upwards and downwards into narrower, subvertical veins which are parallel to the steep schistosity of the area and probably fill longitudinal fractures. It is therefore probable that the moderately dipping, most mineralized sections represent dilational tension fractures. Drilling by New Consolidated Goldfields (Australia) Pty Limited (Searl, 1961) intersected an auriferous quartz vein at about 100 m vertical depth, but it was narrow (intersection 0.75 m) and of low grade (less than 2 g/t gold).

Relatively late northeasterly and easterly striking faults displace the mineralization at several points, but appear to have had no other effect on the orebodies (Blockley, 1962).

Other significant gold producers of the Chesterfield mining centre have been the Dorothy, Dorothy North, and Big Ben mines. At Dorothy (59 kg of gold), about 2 km north-northwest of Margueritta, a 0.5–1 m-wide quartz vein has been mined to a depth of 35 m. The vein dips eastward at 30–75° and is discordant to the schistosity of the host rock which, as at Margueritta, is mafic tuff. About 100 m to the northwest of Dorothy, the Dorothy North (13.6 kg of gold) workings have exploited a subhorizontal quartz vein (Blockley, 1962). The Big Ben workings (15.5 kg of gold), about 8 km north of Margueritta, are based on a short, pipe-like shoot that forms part of a large quartz vein (Montgomery, 1910) within amphibolite, carbonaceous shale, and fine-grained granitoid intrusions. The vein is one of the easterly striking D_5 quartz veins in this area (Chapter 5).

Cuddingwarra

Cuddingwarra is near the northern end of the northerly striking Cuddingwarra Shear Zone (Fig. 168). Basalt, dolerite, and metasedimentary and ultramafic rocks contain two fracture sets, one striking north, and the other northeast. Each type of fracture contains lenticular quartz veins, and dykes of felsic porphyry. Gold mineralization appears to be confined to the fracture system; the highest grade material is in shoots at intersections of the two sets of fractures, or of either set with changes of lithology.

The principal mine is Victory United (production 1.0 t of gold at an average ore grade of 45.1 g/t) where a quartz vein, occupying a northeasterly striking fault, intersects northerly striking sheared basalt, and dykes of felsic porphyry. An open-cut reveals one ore horizon to consist of a felsic porphyry dyke and a 0.6 m-wide quartz vein, both inclined at about 80° to the northwest. Plans of underground

workings (Woodward, 1907, plate 15) establish that, at depth, the orebody dips steeply southeast and contains a shoot of ore, about 60 m long, which plunges steeply eastwards below the deepest workings (210 m). This shoot may coincide with the intersection of the quartz vein with either the easterly dipping host rock, or a northerly striking fracture. Some degree of fault control is indicated by the common occurrence of sheared amphibole–chlorite rock, talc–chlorite rock, and slickensided basalt, which are common on the mine dumps. The quartz is pyritic and also contains minor amounts of galena, sphalerite, and chalcopyrite. Minor amounts of pyrite also occur in the basalt and felsic porphyry. From dump material it is evident that several generations of quartz veins are present, some of which post-date the felsic porphyry. However, Woodward (1907, p. 89) indicated that the main orebody is intruded and crossed by at least one dyke of porphyry.

The only other mine to have recorded significant production is Golden Gate (about 140 kg of gold), which is situated about 100 m north of the Cue–Coodardy road. Here, the old workings follow northerly striking quartz veins and a felsic porphyry sill which are within talc–chlorite schist and metabasalt.

At both Victory United and Golden Gate, gold mineralization is partly associated with zones of brecciation. If, as seems probable, the two mineralized fracture sets are genetically related and the northeasterly striking fractures are tensional, the dominant movement direction in this section of the Cuddingwarra Shear Zone would be dextral. However, further southwest of Trenton Hill, minor structures suggest sinistral movement.

Present information suggests that gold mineralization at Cuddingwarra may be confined to relatively small discrete orebodies. Future large-scale mining appears unlikely unless exploration reveals larger orebodies or stockwork-style mineralization in a shatter zone.

Cue

Cue is atypical of mining centres in the Murchison Province in that most of its gold deposits are hosted by granitoid rocks (Fig. 155). On close examination, however, it is clear that many of the orebodies occur at faulted contacts with sheared greenstone enclaves. Mineralized faults and shear zones fall into two main sets: one strikes northeasterly to easterly and is parallel to the regional cleavage; the other strikes northerly to north-northwesterly and represents tensional fractures within a northeasterly trending zone of sinistral movement — the Day Dawn Shear Zone (Fig. 168). The northeasterly to easterly striking set dip northwestwards to northwards at low to moderate angles, whereas the north to north-northwest set generally dip moderately to steeply westwards. Ore shoots in veins occupying both systems generally plunge northwestwards, parallel to the most common intersection direction. The enclaves are assumed to have been stoped from the greenstone belt to the south, and may have acted as loci for shearing and for subsequent movement of hydrothermal fluids within the granitoids.

Almost all the mines at Cue are currently inaccessible, but descriptions of underground workings are available from earlier publications (Campbell, 1903; Woodward, 1907, 1912a, 1914). Gold production figures for the principal mines are presented in Table 35.

The Light of Asia, Queen of the May, and Mararoa mines are about 3 km north-northeast of Cue. The Light of Asia mine is based on a large quartz vein which dips to the west at about 45°. Dump material consists of hornblende granodiorite, amphibole–chlorite schist, and quartz which contains sulphides (pyrite, pyrrhotite, and minor amounts of chalcopyrite) and carbonate minerals. Drilling reported by Duggan (1958) indicates numerous mafic xenoliths or dykes, and several bodies of porphyry within the granitoid; Woodward (1907, p. 62) stated that the orebody is located between granodiorite and feldspar porphyry. The orientation of shoots probably represents an intersection of the westerly dipping vein with a north-northwesterly dipping mineralized fracture system at the adjacent mine, Queen of the May. Description by Woodward (1907, p. 63) indicates that gold mineralization at Queen of the May is related to quartz veining along the faulted contacts of a pyritic mafic unit, either a large elongate xenolith or a dolerite dyke. As at Light of Asia, ore shoots plunge northwestward at about 45°.

About 800 m to the south of Light of Asia, the Gem of Cue workings follow a vein dipping north at 35–50° along a granodiorite–greenstone contact (Woodward, 1907, p. 61). Dump material includes extensively carbonated amphibole–chlorite schist. Some 200 m further east, the Eclipse mine is located on the same fracture. Here the quartz vein dips north at 45° and is truncated to the east by a northerly striking hornblende porphyry dyke. However, abut 1 km further east a similar fracture, on strike with that at Gem of Cue and Eclipse, has been worked at Agamemnon. The Agamemnon orebody is a quartz vein dipping 30–40° north-northwestwards through granitoids, felsic schist, and carbonated amphibole–chlorite schist (western workings).

To the north of Agamemnon and to the east-northeast of Light of Asia, the Duke of York and Normanby mines show many of the features present in other workings of this area. At Duke of York, a west-southwesterly dipping quartz vein contains a northwesterly plunging shoot, whereas at Normanby, gold mineralization occurs in a north-northwesterly dipping quartz vein on strike with the Queen of the May deposit. Both mines contain feldspar porphyry which appears to have been intruded along the same fractures as auriferous quartz.

At Cue Victory (Fig. 155) a quartz vein dipping 20° to the north-northwest joins a vein dipping westwards at about 30° (Campbell, 1903 p. 9; Woodward, 1907, p. 57). Stopes indicate that the ore shoots plunge northerly and northwesterly. Woodward (1907, p. 57) stated that the westerly dipping vein is underlain by 'a very much altered basic dyke'; this may be a dolerite dyke or an elongate greenstone xenolith.

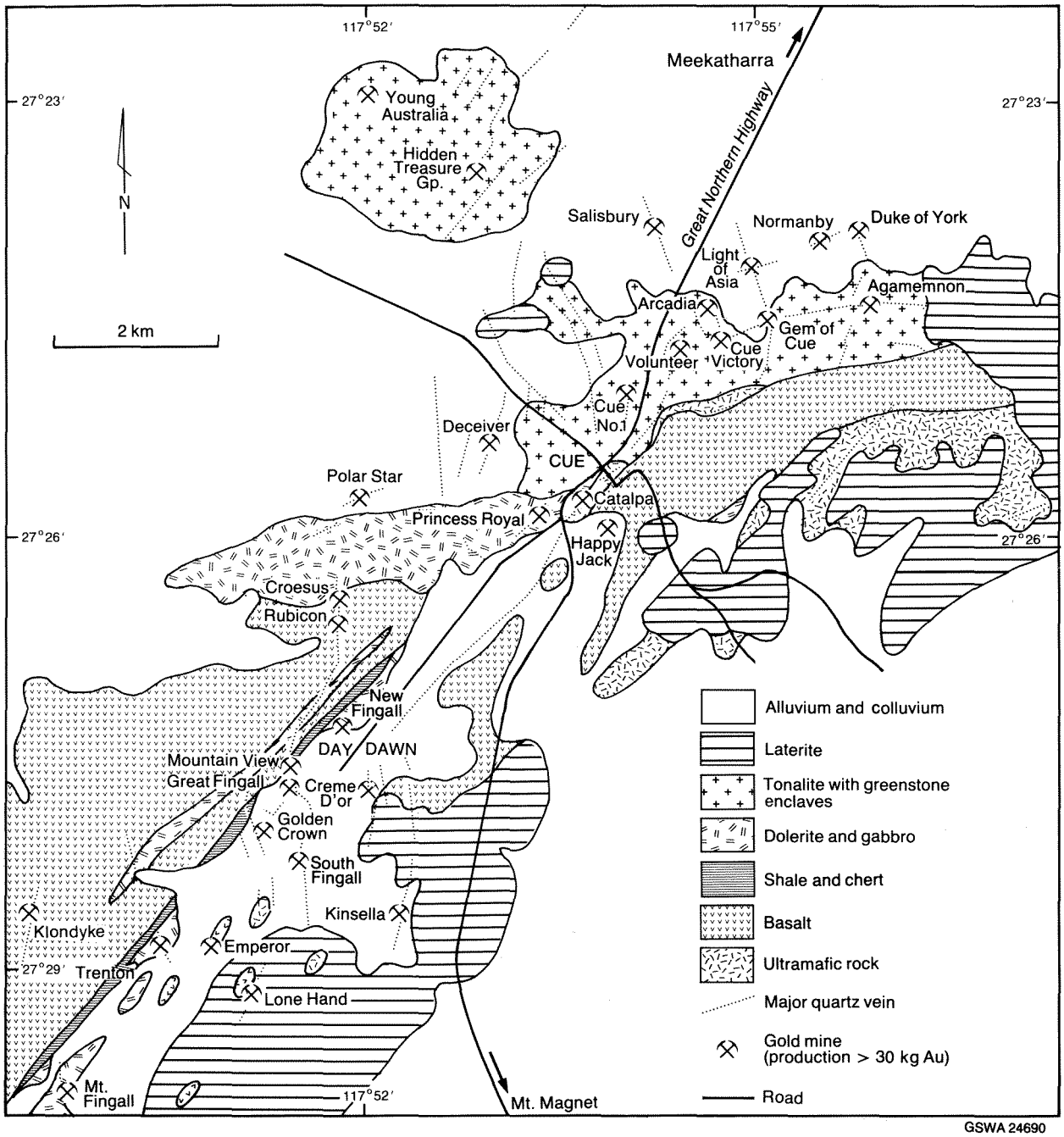


Figure 155. Geological setting of the principal mines at Cue and Day Dawn.

TABLE 35. TOTAL GOLD PRODUCTION FROM THE PRINCIPAL MINES AT THE CUE MINING CENTRE TO 31 DECEMBER 1987

Mine	*Alluvial and dollied (kg)*	*Ore (t)*	*Gold (kg)*	*Total gold (kg)*
Agamemnon	-	16 660	302.9	302.9
Arcadia/Countess	-	11 857	226.7	226.7
Catalpa/Cue No. 3	0.2	2 900	56.5	56.7
Cue No. 1 group	0.5	36 826	1 146.6	1 147.1
Cue Victory/Golden Stream	90.6	11 013	359.7	450.3
Deceiver/Lily	-	3 686	149.5	149.5
Duke of York/Normanby	-	9 145	175.4	175.4
Gem of Cue/Eclipse	-	18 645	462.0	462.0
Happy Jack	-	1 612	33.8	33.8
Hidden Treasure group	0.3	15 920	482.1	482.4
Light of Asia/ Queen of the May	-	67 336	1 670.4	1 670.4
Polar Star	-	957	33.1	33.1
Princess Royal	-	15 044	403.8	403.8
Salisbury	-	10 058	188.5	188.5
Volunteer group	0.9	53 539	941.6	942.5
Young Australia	-	1 651	45.5	45.5

To the north-northwest of Cue Victory are the Arcadia, Countess, and Salisbury mines (Fig. 155) which are located on a set of north-northwesterly striking pyritic quartz veins. These veins dip west-southwest at about 60–75°, and at Salisbury contain a northwesterly plunging ore shoot in contact with chloritic schist.

The Volunteer group of mines includes Volunteer, New Volunteer, Starlight, Princess Ada, Volunteer South, Twilight, Comforter, Lord Nolan, Golden Garter, Conscript, New Venture, Struggle, and South Volunteer, and extends over an area of about 30 ha, locally known as 'The Patch'. It is characterized by stacked, subhorizontal lenticular quartz veins within extensively kaolinized granitoid, and locally in contact with amphibolite schist. Where veins crop out they generally strike northeasterly, which suggests a possible correlation with the shallow-dipping, east-northeasterly striking veins of the Cue Victory–Normanby–Agamemnon area. At Princess Ada, on the southeastern side of the group, gold mineralization occurs in a vein dipping south at 30°, whereas at Volunteer South Extended, part of the mineralized vein dips to the east (Campbell, 1903, p. 12). It is uncertain if the veins have been folded or were formed in curved fractures.

The Cue No. 1 and Rising Sun mines are immediately north of Cue, and are based on a quartz vein which dips west at about 40°. Dump material is composed of sheared granitic rock, amphibole–chlorite rock (probably metabasalt) and vein quartz. Drilling reported by Noldart (1958, p. 107–119) revealed a close association between gold mineralization and the presence of sheared greenstone enclaves in the granitic rocks. About 150 m to the west of the Cue No. 1 vein, a parallel vein has been worked at the Lady Florence mine. Woodward (1907, p. 42) stated that this orebody consisted of a 'basic dyke' (probably a greenstone enclave) flanked by auriferous quartz veins. Drilling described by Noldart (1958) has established the presence of numerous greenstone xenoliths within the granitoids of the Cue No.1 area.

Small mines, such as Polar Star, Deceiver, Young Australia, and Hidden Treasure, to the west and northwest of Cue, are located on quartz veins within granitoids. Most of the veins dip westerly or northwesterly, and are commonly associated with thin units of mafic schist and feldspar porphyry dykes. The workings are described by Campbell (1903, p. 19–20), and Woodward (1907, p. 26–35; 1914, p. 43–48).

The Princess Royal mine, immediately to the southwest of Cue, is based on two quartz veins which dip 50° northwestward through sheared and silicified leucogabbro at, or close to, the intrusive contact of the hornblende tonalite–granodiorite of the Cue area. Drilling described by Noldart (1957, p. 205–215) established that the mineralized zone extends to a minimum vertical depth of 140 m, where it is a 9.5 m-wide zone of carbonated mafic schist containing quartz veins and stringers. The extent of quartz veining is greatest close to the surface where the main orebody (Royal Reef) was about 1 m thick. Stoping in the mine suggests that the main ore shoot plunged to the northwest.

The Catalpa, Vera, and Cue No. 3 workings are at the southern end of the town, immediately west of the old railway line. The quartz vein is about 1 m wide and dips northwest at about 80° and, according to Campbell (1903, p. 24), extends southwestwards almost to Day Dawn. The host rock is silicified talc–carbonate schist between metamorphosed pelitic wacke to the east, and gabbro and pyroxenite to the west.

On the opposite side of the old railway line from Catalpa, the Happy Jack mine is located on a quartz vein dipping 40° northeast within metabasalt. About 2.5 km further east smaller workings (including Pension) follow a 1.5 km-long zone of shearing and quartz veining within talc–chlorite and talc–carbonate schist; the veins dip 60° to the northwest.

Day Dawn

The Day Dawn mining centre is, like Cue, situated on the Day Dawn Shear Zone (Fig. 168); but gold mineralization at Day Dawn is chiefly hosted by dolerite and basalt. Two sets of mineralized fractures are present in the area: layer-parallel northeasterly striking shears, and northerly to northwesterly striking transverse shears. Almost all the Day Dawn mines are positioned on the latter type, particularly along the more northwesterly striking sections where considerable dilation is evident and thick lenticular quartz veins are developed. Northerly and northeasterly striking fractures are also veined by quartz, but such veins have generally proved to be too narrow or too low grade to be mined. Wall rocks in most of the mines show evidence of shearing, and at Mountain View a sinistral displacement of 100 m appears to be present along the Great Fingall fracture system. Therefore, the largest orebodies, such as those at Great Fingall and Golden Crown, do not occupy purely dilational fractures, but fractures involving a substantial degree of riedel shearing.

The most economically important geological unit at Day Dawn is a 600 m-thick sill of quartz dolerite (Fig. 155) which has intruded a 100 m-thick unit of shale and fine-grained clastic metasediment within the basalt pile in this area. Intrusion was not restricted to one horizon in the shale, consequently the sill contains numerous shale enclaves, particularly in its upper, northwestern section. As the northerly striking shears pass from the basalt into the dolerite–shale unit, they change strike to become oriented northwest or even west. This swing in strike is probably attributable to competency differences between the basalt and the dolerite, but may also be influenced by some degree of layer-parallel sinistral slip along shale beds.

About 90% of gold production at Day Dawn has come from the Great Fingall mine (Tables 34 and 36), the old workings of which extend to a vertical depth of 742 m. Plans of the mine are included in reports by Woodward (1907), Connolly (1936), Duggan (1958, 1960a), and Noldart (1960 a,b), and geological descriptions have been included in reports by Gray (1950), and McMath (1953).

Great Fingall is located on a major quartz vein that dips to the southwest at about 65° within the Day Dawn quartz-dolerite sill. To the north the vein narrows and passes through Mountain View where it splits, the more northerly branch continuing northwards and north-northeastwards towards the Rubicon and Croesus mines. Southeast from Great Fingall the vein appears to terminate fairly abruptly, but the host fracture passes into metabasalt below the sill and probably swings south to become host to the South Fingall vein (Campbell, 1903, p. 30). Although veining is discontinuous, the overall length of the Great Fingall fracture (or fracture zone), from Croesus to South Fingall, is about 5 km.

The main ore shoot at Great Fingall is up to 12 m wide, over 200 m long, and plunges west at 55–60°. Smaller shoots occur to the northwest and southeast of the main orebody. The ore is blue quartz, with minor amounts of white quartz, and contains pyrite, pyrrhotite, chalcopyrite, galena, arsenopyrite, sphalerite, and bornite. Wall-rock alteration in the dolerite includes silicification and carbonation, and within 1–3 m of the orebody the wall rocks contain pyrite, pyrrhotite, galena, and chalcopyrite, associated with numerous stringers of quartz and calcite.

TABLE 36. TOTAL GOLD PRODUCTION FROM THE PRINCIPAL MINES AT THE DAY DAWN MINING CENTRE TO 31 DECEMBER 1987

Mine	*Alluvial and dollied (kg)*	*Ore (t)*	*Gold (kg)*	*Total gold (kg)*
Creme D'Or	1.9	6 684	159.4	161.3
Croesus	-	1 368	52.7	52.7
Emperor	-	1 880	89.4	89.4
Golden Crown	-	117 193	2 087.6	2 087.6
Great Fingall	-	1 895 953	36 892.4	36 892.4
Kinsella	-	14 872	173.5	173.5
Klondyke	3.0	2 800	88.4	91.4
Lone Hand	6.3	2 366	86.8	93.1
Mountain View	3.3	27 557	1 595.5	1 598.8
Mount Fingall	-	1 838	34.3	34.3
New Fingall	0.4	3 824	57.2	57.6
Rubicon	-	6 521	93.8	93.8
South Fingall	-	2 470	43.8	43.8
Trenton	-	8 886	192.8	192.8

Drilling during the late 1950s and mid-1980s has shown that the main orebody extends to a vertical depth of at least 1100 m where it appears to have an average width of 4–5 m and contains ore grading 5–19 g/t gold (Australian Consolidated Minerals, 1987). Footwall alteration is more extensive than in the hanging wall and there are several subsidiary footwall veins which could contribute ore to future mining operations. A feature noted by Woodward (1907, p. 18), and apparently supported by the more recent drilling (Australian Consolidated Minerals, 1987), is that ore shoots in which ore grades are highest correspond to sections in which quartz veining is thickest. Woodward (1907, p. 18) noted the presence of three large shoots; a main central body, overlain to the northwest by the earliest worked shoot (the only outcropping orebody), and underlain to the southeast by a shoot commencing at a vertical depth of about 100 m. The plunge of the shoots is parallel to the intersection of the Great Fingall fracture, and bedding, and probably therefore to any compositional layering or internal boundary-parallel discontinuities within the quartz-dolerite sill, such as those recognized at Golden Crown (see below). Drill logs presented by Duggan (1958, 1960) and Noldart (1960 a,b) show that the sill contains numerous units of black shale and fine-grained metasediment (remnants of the sedimentary unit which the sill has intruded) and minor amounts of metabasalt. Some felsic porphyry was also intersected, but surface observations in the Day Dawn area suggest that these felsic intrusions are probably discordant.

Between the Great Fingall vein and the Golden Crown vein (720 m to the southwest) is the Fingall Cross Reef, which was worked as the Day Dawn West mine. Over most of its length this vein strikes north-northeastwards and dips steeply eastwards, but the most productive section has been at its southern end where it swings westward. According to Woodward (1907, p. 28) the ore shoot here is about 90 m long and was stoped above a vertical depth of 39 m.

Golden Crown mine (also previously known as 'West Fingall No. 3') is geologically very similar to Great Fingall. The main quartz vein is at least 300 m long and dips 60° southwest through the Day Dawn quartz-dolerite sill. Its true thickness ranges up to about 3 m and averages about 1 m. Where the vein narrows and terminates outside the ore zone its position is marked by a thin shear zone. Carbonation and silicification are the main types of wall-rock alteration and are evident up to 2–3 m away from the orebody. Sulphide mineralization is similar to that at Great Fingall.

Mine production at Golden Crown recommenced in April 1986; earlier recorded production was small, and partly included with that of Great Fingall. Recent exploration has revealed a footwall spur vein dipping 45° southwest and averaging 31.7 g/t gold over an average width of 0.83 m (Australian Consolidated Minerals, 1987). ACM

geologists consider that the position of the orebodies corresponds to a quartz- and iron-rich phase of the dolerite.

A map of the Cue and Day Dawn areas presented by Campbell (1903) indicates that the Golden Crown fracture may extend northwards to Pelican and southwards to Try Again, an overall strike length of 2 km. A parallel fracture, or zone of fractures, is located 200 m southwest of the Golden Crown veins.

The Mountain View mine is located on the Great Fingall fracture, immediately northwest of Great Fingall. Jones (1962) noted that the ore shoot occupies 'a pronounced "S" curve' and that the dolerite host has been displaced sinistrally along the fracture. The shoot plunges westward at 50° and is bounded by dolerite in the footwall and slate in the hanging wall. As at Great Fingall, the ore is blue quartz, but was higher grade at Mountain View (57.8 g/t), and contained abundant free gold. The Mountain View shoot can probably be best regarded as the most northerly shoot of the Great Fingall deposit.

The Rubicon and Croesus mines are about 2.5 km north of Great Fingall. The fracture zone linking the two mines strikes north, and quartz veins occupying it dip west at 50–80°. At Rubicon, two quartz veins, the footwall and hanging wall 'lodes', are separated by about 5 m of crushed and quartz-veined tholeiitic basalt. The eastern vein was about 1.7 m thick and the western vein 1.5–3.6 m. Woodward's (1907, p. 25–26) description suggests that ore grades diminish below about 150 m, although the 'crush zone' between the two orebodies is here also mineralized. Campbell (1903, p. 27) commented on the presence of high-grade gold mineralization at a point in the mine where the two veins meet, but the attitude of this intersection was not recorded. Campbell (1903, p. 27), Woodward (1907, p. 26), Hobson (1940), Low (1963, p. 130) and Yinnex (1986, p. 20) briefly noted the presence of associated copper mineralization at Rubicon and Croesus, and minor production has been recorded (see Table 44). Gold production at Croesus was obtained from a vein dipping steeply west within metagabbro. The vein crops out over a strike length of 300 m, but workings were limited to a vertical depth of 30 m.

The South Fingall mine is based on a 1 m-wide vein of dark-coloured quartz, dipping west at 53° and cropping out intermittently over a strike length of 1 km. The predominant host rock is carbonated and schistose metabasalt, but some talc–chlorite schist units are also crossed by the vein. The workings are relatively small and no underground information is available.

The Trenton mine, which lies about 1.5 km southwest of Golden Crown, is geologically similar to Great Fingall and Golden Crown. The sulphidic quartz vein, ranging in width up to 3.6 m, dips west-southwest at 40–55° (Woodward, 1907, p. 35) through the Day Dawn dolerite sill. Two ore shoots plunge west, and the larger northern one has been stoped to 58 m over a length of about 50 m. As noted by Woodward (1907, p. 36) there appears to be scope for further mining below the 58 m level.

The Emperor mine is located about half way between Trenton and South Fingall. The orebody is a 0.75 m-wide quartz vein, dipping 62° southwest through carbonated metabasalt and dolerite; it appears to be positioned on, or a short distance to the southeast of, the southeastern contact of the Day Dawn dolerite sill. Although the shaft extends to a vertical depth of 60 m, Woodward (1907, p. 33) stated that little ore was obtained below 14 m, and drilling to depth of 155 m revealed 'no values'.

Some 2.4 km southwest of Trenton, the Mount Fingall mine workings follow quartz veins in a narrow shear zone through metadolerite (almost certainly the Day Dawn sill as the intrusion is at least 500 m wide). This zone dips west-southwest at 70°; the principal orebody varies in thickness from 0.5 to 2 m, and averages about 1 m (Woodward, 1907, p. 31). The Mount Fingall shear zone may be related to a similar structure at the Klondyke mine, 2.5 km to the north. The Klondyke is based on northerly striking quartz veins cutting a dolerite sill within metabasalt.

The Lone Hand workings, 600 m southeast of Emperor, are based on sheared basalt, ultramafic, and metasedimentary rocks. Some of the orebodies are quartz veins, but mineralized schist also appears to have been mined. The shear zone dips 70° west to west-northwest and extends along a strike length of about 500 m. It may be the same fracture as that at Try Again, 700 m further north-northeast, where mining has been based on quartz veins dipping west at 80° through talc–carbonate–chlorite schist.

About 2.5 km southeast of Great Fingall, the Kinsella mine is located on a pyritic quartz vein, dipping 80° east-southeast through carbonated metabasalt. The vein varies in thickness up to 5 m (Woodward, 1907, p. 41–43) and extends over a strike length of at least 550 m. Stoping has been intermittent over 280 m of this length, but has been restricted to levels above a depth of 52 m. Wall rocks of the vein are carbonated, silicified, and sheared.

Relatively little information is available on the other two significant gold producers of the Day Dawn mining centre — Creme D'Or and New Fingall. Creme D'Or is based on a 0.4–1 m-wide quartz vein, dipping 55–70° southwest through metabasalt, and New Fingall (earlier known as White Horse) is located on an apparently shallow (Woodward, 1907, p. 37) quartz vein dipping south within the Day Dawn dolerite sill.

Fields Find

Fields Find is on the eastern side of the Yalgoo–Singleton greenstone belt, where the Gabanintha and Windaning Formations strike westerly and have been extensively intruded by granitoids (Plate 2). The principal rock types at the mining centre are basalt, chlorite schist (possibly basaltic tuff), dolerite, gabbro, BIF, and felsic volcanogenic metasediments. The main gold producers have been the Fields Find group (843 kg of gold from ore averaging 21 g/t gold) and the Browns Reward group (135 kg of gold from ore averaging 20 g/t gold).

The Fields Find group is based on a 0.5–1.5 m-wide sulphidic (pyrite, pyrrhotite, and minor amounts of chalcopyrite, arsenopyrite, galena, and sphalerite) quartz vein,

dipping 55° to subvertically north-northwest through carbonated mafic schist (metabasalt), quartzose dolerite, and felsic porphyry. The vein extends at least 1.2 km along strike and has been worked intermittently over about 700 m. Almost all production has been obtained from two northerly plunging shoots which have been stoped above a vertical depth of 100 m. The eastern shoot, which has accounted for most of the production, is about 70 m long and has been mined over 150 m down plunge. The western shoot is about 100 m long, and has been mined above a vertical depth of 70 m. Weatherall (1937) reported that the quartz vein is laminated, varied in colour, and dips in the opposite direction to the bedding of the basalt–chert–clastic sedimentary succession (approximately 60° towards the south-southeast). The vein appears to be one of a conjugate system, striking east-northeasterly and northerly. It post-dates the intrusive sills and dykes of dolerite and felsic porphyry; the eastern shoot being hosted by dolerite, and the western shoot by both mafic schist and felsic porphyry. At the eastern shoot, the vein changes direction slightly and bifurcates within the dolerite. From Weatherall's descriptions (1937) and accompanying mine plans, it appears that the eastern shoot is controlled by host rock, and by the quartz vein intersection direction. The vein itself appears to occupy a fault along relatively incompetent metabasalt and BIF between two large dolerite intrusions.

The Browns Reward workings extend 340 m along a south-southeasterly dipping unit of BIF and quartz–sericite schist which can be traced along strike for more than 600 m. This unit is about 60 m wide and is flanked to the north by metagabbro and to the south by dolerite. The principal workings — an open-cut at the western end of the unit — are located about 500 m to the north of the Fields Find eastern shoot. Two parallel lodes, mined to a depth of about 30 m, consist of massive sulphide (pyrite) mixed with laminated sulphidic quartz–carbonate rock and bands of schist. All production appears to have come from a zone of oxidation and supergene enrichment above the water table.

About 400 m southeast of the Fields Find line of workings is a 1.5 km-long zone of sheared pelitic schist and chert within a clastic sedimentary sequence. The shear zone, extending through the old Tobins and Boxlaffs leases, is about 80 m wide and contains a stockwork system of auriferous quartz–tourmaline veins. Grades reported by Weatherall (1937) are moderate to low (about 5 g/t gold over intervals of a few metres), but the zone is poorly exposed and probably justifies further examination.

The Rose Marie (also called 'Reids Ridge') is between the Fields Find and Warriedar mining centres. The mine is based on a 1 m-wide quartz vein within a 2 km-long, north-northeasterly striking fracture through metabasalt. Chalcopyrite is present in the quartz and in adjacent mafic rocks; Marston (1979, p. 142) recorded 9.5 t of copper-ore production in 1957. In December 1986, published resources were 2600 t of ore grading 16.5 g/t gold; production prior to 1988 was 157 kg of gold from 13 612 t of ore. Production of 43 kg of silver has also been recorded.

The only other significant gold producer of the Fields Find mining centre has been Golden Eagle (27 kg of gold from 1695 t of ore) which is 4 km northeast of Rose Marie on a northeasterly striking quartz vein through metagabbro.

Gabanintha

Gold mineralization at Gabanintha is associated with quartz veins and stockworks in sheared ultramafic (komatiitic) rocks, altered mafic rocks, and quartz–feldspar porphyry. The mafic and ultramafic rocks include tuff and thin BIF units; metasedimentary rocks are locally present.

The mining centre is near the southern end of the northerly striking Gabanintha Shear Zone (Fig. 168, Plate 2) which also extends through the New Australia and Bourke Find mining areas. At Gabanintha the shear zone is about 1 km wide and positioned between serpentinized peridotite to the west, and a prominent line of quartz veins to the east. Further north, the eastern boundary is marked by BIF and mafic rocks of the Golconda Formation. Quartz veining within the shear zone is somewhat erratic, but generally dominated by northwesterly to westerly striking veins which occupy a transverse fracture system. The orientation of these veins suggests that the main sense of movement along the Gabanintha Shear Zone is sinistral. This corresponds to the principal sense of shear at Paddys Flat (Meekatharra mining centre). Since the same stratigraphic level is involved in both areas it is concluded that the Gabanintha and Paddys Flat shear zones are contiguous.

The most productive mines at Gabanintha have been Tumbulgum, Mountain View, Golden Hope, and Mount Yagahong. Tumbulgum is based on a north-striking shear zone of actinolite–chlorite schist in which the orebody is a lenticular and limonitic quartz vein, locally attaining a thickness of 2.5 m (Gibson, 1904, p. 51). Here, and elsewhere at Gabanintha, talc–carbonate and talc–chlorite alteration is widespread, and pyrite is common in wall rocks.

At Mountain View, two zones of ultramafic schist carrying irregular masses of quartz intersect to produce what appears to have been a shoot. One of the mineralized zones strikes north and the other northwest. The Golden Hope workings are based on the southern section of a northwesterly striking quartz vein, where brecciation associated with late faulting has been accompanied by the development of a relatively small area of economic mineralization. The host rock for the stockwork gold mineralization at Golden Hope is a quartz–feldspar porphyry.

Some distance to the north of the main group of workings at Gabanintha is the Mount Yagahong deposit which is a northerly dipping, irregular and lenticular quartz vein within mafic schist, talc schist, and talc–chlorite schist. Copper mineralization is associated with gold at Tumbulgum and Mountain View, where host rocks include metadacite and ultramafic tuff (Marston, 1979, p. 139).

Garden Gully (Kyarra)

Situated about 17 km north-northwest of Meekatharra,

the Garden Gully mining centre is based on westerly to northwesterly striking siliceous orebodies within chlorite schist, fine-grained clastic sedimentary rocks, and felsic–intermediate volcanics within a larger area of mafic and ultramafic rocks. The only large producer has been the Kyarra mine which has recorded 628 kg of gold from 29 400 t of ore. Workings in the mine extend to a depth of almost 100 m and follow two principal siliceous zones which are folded and faulted. These zones are reported to include granular, ferruginous, sericitic, kaolinitic, and finely laminated material (Clarke, 1916) and, though described as quartz veins, may actually be strata which have been silicified and intruded by quartz stringers. Discrete veins do occur in the area, but these strike northeasterly and do not appear to be deformed. The siliceous zones are steeply inclined southwards and southwestwards and may locally occupy the core of a southerly plunging syncline, perhaps of the same generation as the main Abbotts syncline. No distinct shoots of ore are present and the average thickness of the main orebody is almost 3 m. The ore contains some pyrite and, locally, minor amounts of chalcopyrite and azurite. Yellow tourmaline is present and the wall rocks are bleached, sericitized, and albitized in the oxidized zone.

The Garden Gully area is poorly exposed and it is possible that concealed orebodies, similar to that mined at Kyarra, may be present. The relatively high grade of early production from above the 10 m level indicates that there has been significant supergene enrichment; further exploration will probably investigate the possibility of open-cut mining.

Goodingnow (Paynes Find)

The Goodingnow mining centre is located on sheared mafic amphibolite and tonalite on the eastern contact of the Paynes Find greenstone belt. Gold mineralization occurs in a system of lenticular quartz veins, arranged *en echelon*, which intrude the north-northwesterly striking Paynes Find Shear Zone along the granite–greenstone contact. The veins strike northerly to north-northeasterly, oblique to the main schistosity of the shear zone. If the veins are related to riedel shear, they indicate dextral movement along the zone.

Host rocks in the area of the largest mines are restricted to fine-grained amphibolite, biotite–hornblende tonalite, and a mixture of these rock types along the granite–greenstone contact.

The two principal groups of workings are the Ark–Sweet William group (0.70 t of gold from ore averaging 23 g/t gold) and the Marraposa–Lake View–Carnation line of workings (1.33 t of gold from ore averaging 27 g/t gold).

The Ark–Sweet William–Orchid group is located in foliated biotite–hornblende tonalite. Clarke (1925, p. 30–33) described southwesterly plunging shoots in veins which dip westerly at about 60°. The Carnation and Marigold mines are located about 300 m west of the Ark–Sweet William Group. Here the orebodies are sulphidic (pyrite and minor amounts of chalcopyrite) quartz veins, up to 0.5 m wide, dipping westerly or west-southwesterly at 60–70°. The host rocks are sheared tonalite and amphibolite, containing thin (1–2 mm) seams of mylonite. The amphibolite is extremely altered, containing quartz, and up to 20% biotite. Descriptions by Clarke (1925, p. 23–29) suggest that shoots of ore plunge to the southwest or south and are generally short; one, however, extends to a depth in excess of 76 m. At Lake View, a southwesterly plunging shoot occupies a vein that dips 80° towards 280°. It is notable that the main cleavage of the host amphibolite and tonalite at this mine dips 70° towards 260°, which emphasises the observation that the auriferous quartz veins at Goodingnow are not, in general, parallel to the principal schistosity. Further south, the Marraposa workings follow a quartz vein dipping 80° west-northwesterly within fine-grained amphibolite schist (metamorphosed amygdaloidal basalt, and possibly dolerite).

Other workings at the Goodingnow centre are the Aster Consolidated–Havela group (162 kg of gold) and mines such as Daffodil and Pansy in the southern part of the mining centre. At Aster Consolidated the auriferous quartz vein dips 45° west-southwesterly, parallel to the main foliation of the surrounding tonalite and amphibolite schist of the granite–greenstone contact zone. The Havela workings are now chiefly alluvial, although some old pits testify to earlier workings along a southern continuation of the Aster Consolidated mineralization (Clarke, 1925, p. 35). Daffodil is based on quartz veins along shears through tonalite containing isolated amphibolite xenoliths. Further south, Pansy and other small mines are variously positioned on amphibolite, chloritized and kaolinized felsic tuff, and pelitic metasedimentary rocks. Descriptions of some of the workings are provided by Woodward (1912b).

Simpson (1925, p. 39) recorded the presence of pyrite, sphalerite, chalcopyrite, and galena in the Goodingnow quartz veins. However, apart from locally significant amounts of sphalerite (Lake View), the dominant sulphide is pyrite. The presence of biotite in the mafic amphibolite adjacent to the quartz veins indicates that K- metasomatism and carbonation (siderite) is locally present. This alteration is probably not related to north-northwesterly striking pegmatite veins in the area because, as seen in the Daffodil open cut, these post-date shearing. Clarke (1925, p. 17) also stated that the pegmatites developed later than gold mineralization.

Gullewa

The principal mines of the Gullewa mining centre are King Soloman (previously 'Phoenix'), Monarch, Shannadoah, and Mugga King. These and other workings in the mining centre are located along a 20 km, east-northeasterly trending line from Mugga Mugga Hill to Cagacaroon Hill, about 40 km southwest of Yalgoo.

King Soloman (production, including that of Phoenix, 400 kg of gold from ore averaging 23 g/t gold) is at the northeastern end of the BIF ridge that extends from Mugga Mugga Hill to the old Gullewa townsite, and is about 100 m west of the Yalgoo–Morawa road. Department of Mines

plans show that the workings extend to a vertical depth of 95 m and follow three parallel orebodies dipping northwest at about 70°. The main orebody, a 40 m-long shoot that plunges northerly at about 50°, has been extensively stoped above 95 m. An unpublished report on Department of Mines files states that the shoot is a 'reef' (presumably a quartz vein) defined by diminishing grades and not by any lateral narrowing. At the 95 m level this orebody is about 1.4 m wide and was reported to average about 13.5 g/t gold. About 7 m to the southeast of the main orebody, the footwall orebody has been stoped above 30 m. The hanging wall orebody, 15 m to the northeast of the main orebody, has been partly worked to 88 m.

The mineralization is hosted by metabasalt with minor amounts of sulphidic BIF, metadolerite, pyroxenite, and felsic porphyry. The ore contains pyrite and pyrrhotite. Surface exposures around the mine are extremely limited and there has been no geological report on the underground workings. However, it is probable that the orebodies are quartz veins occupying a northeasterly striking fault zone. Shoots may be controlled by vein intersections with BIF or dolerite units.

About 700 m to the west-southwest of King Soloman, the Monarch mine (84 kg of gold from ore averaging 9.6 g/t gold) is based on a 0.5–1 m-wide zone of sheared BIF and psammopelitic schist within metabasalt. The lode contains quartz veins and stringers, is parallel to bedding, and dips 70° to the south-southeast. Chemical analyses (samples 85720–22, Appendix II) of the BIF reveal markedly elevated Ba (up to 0.6%), Sr, Cu, and V contents compared to BIF samples (85723–25) from the adjacent ridge. The average gold content of samples at the mine is 3.0 g/t, the highest value being 6.7 g/t (sample 85720). No information on the underground workings is available.

The Shannadoah mine (45 kg of gold from ore grading 15 g/t gold), 4 km southwest of King Soloman, is based on a 0.5–1 m-wide shear zone within amphibolite. The lode dips 60° southeast and contains 0.3–0.5 m-wide sulphidic quartz veins. A large body of felsic porphyry intrudes the mafic sequence on the northwestern side of the workings, and felsic porphyry is present in the mine dumps. Samples (85727–29, Appendix II) of pyritic amphibolite from the mineralized zone reveal silicification, K-metasomatism, and associated enrichment of Ba, Rb, Sr, Ce, and La. Samples of quartz (85731–32), collected from a surface exposure of the lode 50 m to the west-southwest, assayed 14.3 g/t and 5.5 g/t gold.

Mugga King (25 kg of gold from ore grading 18 g/t gold) is 5 km southwest of Shannadoah. Gold mineralization occurs in sheared felsic porphyry containing thin stringers of sulphidic quartz. The lode, where mined, is about 1.5 m wide and dips 60° southwards; slickenside lineations plunge 50° to the south-southwest, indicating substantially vertical relative movement. The porphyry is pyritic, and within the shear zone includes layers of mylonite. Chemical analyses (samples 85733–36) reveal slightly elevated Cu, Pb, and W levels in the porphyry. A massive 10 m-wide gossan across strike from the ore zone contains anomalous As, Cu, and Pb, but only minor gold (samples 85738A–B, Appendix II).

Other workings within the Gullewa mining centre include those at Golden Stream in the Cagacaroon Hills. Here a system of quartz veins, dipping 70° to the southeast through micaceous mafic–ultramafic rock, has been mined along a series of shallow pits.

The main zone of gold mineralization at Gullewa is clearly related to an east-northeasterly striking zone of shearing and faulting along the eastern side of Mugga Mugga Hill. Poor exposure in the area would have impeded early prospecting; thus the zone may contain additional concealed gold deposits.

Lake Austin

The Lake Austin mining centre is 25 km south of Cue on The Island, an 8 km^2 landmass in the centre of Lake Austin. The area contains a succession of intercalated mafic volcanics, BIF, chlorite schist, black shale, and minor occurrence of felsic rocks, intruded by sills and irregular bodies of dolerite and gabbro.

BIF constitutes about 20% of the pile, is predominantly of oxide facies (although minor sulphide–carbonate BIF is present), and forms units from 1 to 20 m in thickness at intervals of 10–50 m. X-ray diffraction investigation at the Chemistry Centre of Western Australia has revealed that below 75 m (common depth of weathering) the BIF consists of quartz–magnetite and stilpnomelane–chlorite–magnetite assemblages with minor amounts of siderite and minnesotaite, and trace pyrite, hematite, ankerite, and calcite.

Chloritized and carbonated mafic volcanic rocks, including tuff, are the predominant rock type, but dolerite sills also constitute a significant part of the sequence.

Bedding is vertical or inclined steeply westwards, and strikes almost due north. Minor folds of several generations are present, but are rarely large enough to provide significant deflections of strike.

Gold mineralization occurs in quartz veins, BIF–shale units, and in alluvial deposits. Most production has come from the Golconda and Eureka (also called Island Eureka) mines which, together with smaller mines such as Evening Star and Scottish Chief, are based on quartz veins in an area of faulting about 1 km east of the old railway station. Most of the quartz veins strike parallel or subparallel to bedding, but in cross section are discordant, and dip at steep to low angles westwards. However, one of the larger veins strikes northeast and has been deformed into an open fold pair (wavelength approximately 200 m) at Golconda. The Golconda workings intersected northerly plunging shoots of ore where this vein crossed the vertical, northerly striking BIFs. The same vein appears to extend southwestwards to Eureka. Other shoots of ore were located in fractured and quartz-injected BIF fold cores, and in the parallel quartz veins where these are in contact with BIF. Inspection of dumps at the various workings indicates that quartz and quartz–carbonate vein material was the predominant ore.

Pyrite occurs both in the quartz, and within basalt, dolerite, and BIF. Trace amounts of chalcopyrite and pyrrhotite also occur in the BIF.

The deepest workings at Lake Austin are in Eureka, where ore was mined to a depth of 76 m. The most productive workings were located in the zone of supergene enrichment, and grades generally diminished with increasing depth. The principal mines appear to have been largely worked out in the zone of oxidation.

Controls of gold mineralization at Lake Austin have not been firmly established. However, it appears that gold was concentrated where quartz veins of various orientations intersected BIF units. Most production has come from structurally complex areas bounded by northeasterly and west-northwesterly striking faults, and in close proximity to large discordant bodies of gabbro and course-grained dolerite. Several factors probably combined to create gold mineralization of economic grade.

Alluvial gold deposits have been worked at Lake Austin since the first discovery of gold, prior to 1894. Total recorded production understates actual production, but to what extent is uncertain. Most of the alluvial and colluvial deposits are located to the east and south of the Golconda–Eureka area, and some attempts have been made to locate deep leads under lake sediments.

Lennonville

The Lennonville and Mount Magnet mining centres are contiguous; Lennonville covers a group of mines about 10 km north of Mount Magnet. Gold mineralization at Lennonville is confined to the 1 km-wide Mount Magnet Shear Zone (Figs 168, 156) in which the Windaning Formation is deformed by southerly plunging folds, three sets of faults, and intraformational brecciation. All the gold deposits occur either in quartz veins occupying the faults, or in stratabound orebodies within chert, tuff, and shale of the Windaning Formation. The most extensive deposits are associated with northerly striking longitudinal veins in the shear zone (e.g. Long Reef, Lindsays Reward, Occidental–Souvenir, and Brooklyn), but important high-grade deposits occur in shorter, northeasterly striking veins (e.g. Wheel of Fortune North, Empress, and Golden Gem). Deposits in northwesterly to north-northwesterly striking veins (e.g. Last Chance and Gambier) are less common and have proved to be far less productive. Stratabound orebodies within chert (e.g. Galtee Moore, Welcome, and Ard Patrick) are invariably located close to large faults, and, in addition to disseminated sulphide mineralization, include auriferous quartz veins, stringers, and stockworks. Ore shoots within the veins generally plunge vertically or steeply, in most cases along intersections with bedding. In the central part of the area most quartz veins strike north-northwesterly, parallel to a cleavage which appears to have an axial-planar relationship with the southerly plunging folds. Another possible relationship to the fold structures is seen at Wheel of Fortune where the shape and orientation of the orebody is consistent with that of a saddle reef.

The Windaning Formation consists of two major chert units separated by a succession of metabasalt, basaltic tuff, talc–chlorite schist, and minor amounts of chert, and intruded by dolerite and ultramafic rocks. Between Galtee Moore and Wheel of Fortune this succession is almost 1 km thick, but to the south and north, tectonic attenuation (probably combined with a lower proportion of intrusions) reduces its thickness to between 200 and 300 m. The prevailing dip of the succession is 70–80° to the east, but way-up evidence, and regional geology, establish that it is overturned. The western, stratigraphically highest chert is immediately overlain by a thin unit of sandstone and grit, which in turn is overlain by basalt, komatiitic basalt, and locally by mafic and ultramafic sills. The eastern chert is stratigraphically underlain by the upper part of the Golconda Formation, containing basaltic tuff, basalt, and komatiitic basalt. Two northwesterly striking chert units to the north and south of the Empress mine dip southwesterly at about 60°, and are interpreted as central cherts within the middle limb of the major southerly plunging Z-shaped fold pair in this area (Fig. 156). This interpretation differs from that of Archibald (1982, p. 18) in its recognition of more than one chert in the Windaning Formation (Archibald's 'Warramboo Unit'); Archibald invoked duplication of a single chert by early isoclinal folding.

The structural geology of the area is relatively complex; poor exposure hinders determination of the precise genetic relationships between the different types of gold deposits and the various deformation episodes (Chapter 5). The orientations of the southerly plunging folds (interpreted as F_2) and the major D_4 shear zone, are such that individual fractures in the area could be related to either (particularly as the D_4 shear zone has a dominantly dextral sense of movement). Northerly striking veins could have formed in shears within the attenuated limbs of F_2 folds, or alternatively, in longitudinal D_4 shears. The northeasterly striking veins could occupy tension fractures in the F_2 folds, riedel fractures in the D_4 shear zone, or may be associated with faults of the Boogardie fault system (Mount Magnet). The north-northwesterly striking veins could occupy axial-plane fractures in the F_2 folds, or be pressure or riedel shears in the D_4 Mount Magnet Shear Zone.

The stratabound, chert-hosted gold deposits may include a primary, synvolcanic gold component, but it is notable that such deposits attain economic grades only where the sedimentary units have been extensively deformed and altered in the vicinity of faults. This, and the fact that the highest grade ore in such deposits is generally vein quartz, suggests that the stratabound deposits are partly or totally epigenetic.

Prior to redevelopment of the Galtee Moore mine in 1986, gold production from Lennonville had been dominated by the Long Reef, Wheel of Fortune, and Wheel of Fortune North mines (Table 37).

Long Reef, 500 m southwest of the railway station site, is based on a 0.5–2 m-wide, vertical quartz vein which strikes north-northeast to north over a distance of about 500 m. The vein is thickest in the northern part of the mine where it dips 80° to the west. Mine plans show four shoots

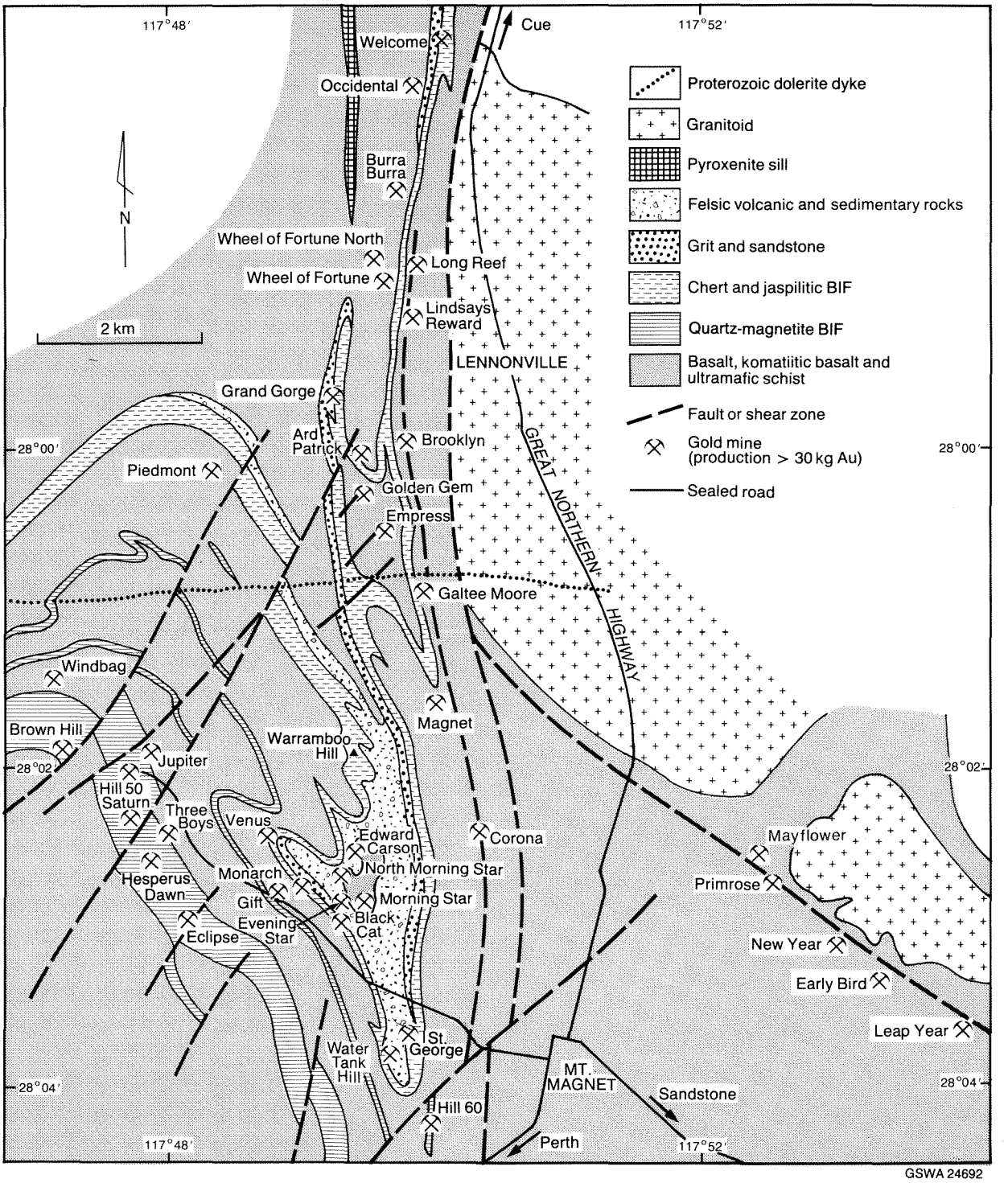


Figure 156. Geological setting of the principal mines at Mount Magnet and Lennonville.

TABLE 37. TOTAL GOLD PRODUCTION FROM THE PRINCIPAL MINES AT THE LENNONVILLE MINING CENTRE TO 31 DECEMBER 1987

Mine	*Alluvial and dollied (kg)*	*Ore (t)*	*Gold (kg)*	*Total gold (kg)*
Ard Patrick	0.3	5 142	41.0	41.3
Brooklyn	-	1 844	31.5	31.5
Burra Burra	0.4	2 292	188.5	188.9
Express	-	7 104	224.7	224.7
Galtee Moore	-	443 395	1 797.1	1 797.1
Golden Gem	6.3	1 144	51.9	58.2
Grand Gorge	-	770	33.2	33.2
Lindsays Reward	0.6	5 202	64.6	65.2
Long Reef/Wheel of Fortune	11.7	93 098	2 462.4	2 474.1
Occidental	1.4	4 463	75.0	76.4
Piedmont	-	5 168	90.4	90.4
Welcome	75.6	4 504	151.7	227.3

of ore, plunging vertically. The northern shoot is 60 m long and extends from the surface to below a vertical depth of 150 m; a note attached to the plans indicates that at this level the shoot is at least 30 m long and averages 13 g/t gold across a width of 1.6 m. The central shoot is up to 100 m long, but is narrower than the northern shoot, and is relatively low grade below 60 m. The two southern shoots are 20–40 m long; workings shown on mine plans extend only to the 60 m level. Host rocks at Long Reef are cleaved metabasalt and minor amounts of talc–chlorite schist, and probably stratigraphically underlie the eastern chert unit. The wall rocks contain quartz–carbonate veins, pyrite, and some biotite. De la Hunty (1958a, p. 39–41) provided additional information on the mine.

Wheel of Fortune is 300 m west-southwest of Long Reef and is based on a curved vein of quartz which could be a saddle reef plunging 45° to the southeast. The vein is generally 0.5–1.5 m wide, but stoping widths locally reach 4 m, possibly due to extraction of mineralized wall rock. The single fan-shaped stope appears to occupy most of the vein. The longest section of the stope is 60 m long at the 60 m level, and close to the surface (at the apex of the 'fan') economic mineralization occurs over a relatively short interval. It is uncertain why mining stopped at the 60 m level. According to de la Hunty (1958a, p. 41) a crosscut below the 60 m level failed to intersect ore, but such an abrupt termination of the deposit is surprising. Host rocks of the Wheel of Fortune deposit are cleaved metabasalt and talc–chlorite(–carbonate) schist. Carbonate veins are common and both quartz and carbonate veins also contain pyrite.

Some 200 m northwest of Wheel of Fortune, a similar east-northeasterly striking orebody has been mined at Wheel of Fortune North. A report by Bewick Moreing and Co. (1902) stated that to June 1902 this mine had produced 280 kg of gold from 3040 t of ore (average grade 92 g/t gold), and total production attributed to this and related leases is 937 kg from 25 884 t of ore. The vein is 1–1.5 m thick, dips to the south-southeast at 50°, and has been mined to a vertical depth of 93 m. The Bewick Moreing report described the vein as occupying a 'bulgy' fissure, which suggests a dilation structure. De la Hunty (1958a, p. 39) recorded quartz stockwork mineralization, particularly at the eastern end of the orebody. Mine-dump material is composed of talc–chlorite schist, pyritic metabasalt, and quartz–carbonate veins.

The Lindsays Reward mine is 800 m south of Long Reef and about 150 m east of the eastern chert unit of the Windaning Formation. Old workings on the same ground include Canterbury, Lady Audrey, Park, and Good Hope. Gold mineralization occurs in narrow (generally less than 0.5 m-wide) quartz veins along northerly striking shears through carbonated metabasalt, minor basaltic tuff, and dolerite. The shears dip easterly at about 80° and the deposits probably occupy structures constituting a southern continuation of the Long Reef zone. About 1.5 km south of Lindsays Reward is the Brooklyn group of workings which are also based on vertical, northerly striking quartz veins within basalt and mafic to intermediate tuff, about 200 m east of the eastern chert.

On the western side of the Windaning Formation, at the northern end of the mining centre, northerly striking quartz veins host gold mineralization at Occidental, Golden Treasure, Lily, Fair Play, and Souvenir. Host rocks here are metabasalt, chlorite schist, and minor units of ultramafic schist (further descriptions are provided by Gibson (1903, p. 25–26), Jutson (1914a, p. 114) and de la Hunty (1958a, p. 37–38).

In addition to Wheel of Fortune North (and possibly Wheel of Fortune, which may be a saddle reef), northeasterly striking quartz veins host important gold deposits at Empress and Golden Gem. The Empress vein dips northwesterly at 85° above a vertical depth of 78 m, below which its inclination is about 60°. Its width ranges from 0.5 to 1.5 m and is reportedly greatest in the lower levels close to the lowest workings at 126 m. Stoping indicates the presence of one main shoot, 40 m long and plunging west-northwesterly at about 60°. Wall rocks are pyritic metabasalt, basaltic tuff, dolerite, and talc–chlorite schist. Carbonation and silicification are widespread and the main sulphide minerals are pyrite and arsenopyrite. Jutson (1914a, p. 110) also recorded the presence of scheelite. Additional information is provided by de la Hunty (1958a, p. 43).

The Golden Gem vein, 500 m northwest of Empress, dips northwesterly at 80° (de la Hunty, 1958a, p. 43) and is hosted by mafic rocks.

The Galtee Moore mine is at the southern end of the Lennonville mining centre. Gold mineralization is in steeply plunging stratabound orebodies within the lower (eastern) chert of the Windaning Formation. The chert, which includes grey–white banded chert, fine-grained tuff, shale, and minor amounts of BIF, dips east at 70–80°. To the east it is stratigraphically underlain by mafic and ultramafic volcanic rocks of the Gabanintha Formation. In an account of the geology of the mine, Anderson (in press) reports that two types of ore are present: quartz veins in fractures, and stratabound concentrations of pyrite–pyrrhotite, chlorite, and carbonate. Two principal orebodies,

the Galtee and Spearmont deposits, plunge vertically to steeply southward, but are each composed of several shoots plunging vertically to steeply northwards. The orebodies are separated by a distance of about 300 m and appear to be located close to a north-northeasterly striking fault zone which extends southwards towards the Morning Star mine at Mount Magnet.

The Welcome, Ard Patrick, and Grand Gorge workings are in, or immediately adjacent to, grey–white chert. At Welcome, 2 km north of Lennonville townsite, only the western chert is exposed. The chert dips 85° to the east and contains quartz veins striking to the north and northeast. At Ard Patrick, 1 km northwest of Empress, the host chert is extensively folded and brecciated; gold mineralization is associated with layer-parallel, southwesterly dipping quartz veins, close to a major northeasterly striking fault. About 300 m north-northwest of the Ard Patrick are the Golden Hill and Grand Gorge mines, on either side of a northwesterly striking fault. The workings are associated with quartz veins and shears in sandstone and metabasalt on the western side of the western chert.

The Piedmont mine is geographically and geologically most closely related to mines of the Mount Magnet mining centre; its description is therefore given under Mount Magnet.

Mainland

The geology of Mainland is very similar to that of the Lake Austin mining centre, about 10 km to the southwest. The strike of the BIF–mafic unit (Golconda Formation) at Mainland is east-northeast and bedding is inclined steeply to the south-southeast. Gold mineralization is associated with north to north-northeasterly striking quartz veins which, as in the case of the veins at Lake Austin, contain high-grade shoots of ore at BIF–mafic contacts. A set of fractures striking northwest, and at one locality producing a marked dextral displacement, appears to contain some mineralization, but to date it has been of far less economic significance than the northerly to northeasterly striking veins.

Most gold production has come from Consols (727 kg from ore averaging 103 g/t gold) where Gibson (1904, p. 24–25) reported the presence of two pyritic quartz veins. The main vein strikes northeasterly to north-northeasterly and follows the northern contact of a BIF unit. It is 0.3–2.4 m wide and generally of low grade, but includes small shoots and pockets of extremely high-grade ore. The main shoot, which has been worked out, was 15 m long. It is not recorded if this structure, and the smaller shoots, are controlled by the intersections of the northeasterly and northwesterly striking fractures and veins. This seems probable, although Gibson's mapping (1904, plate 3) suggests that since the main vein occupies a major fault which crosses the BIF–mafic unit obliquely, the geometry of the orebody may relate to lithological variations in the wall rocks along the strike of the vein.

Gibson (1904, p. 24) stated that the cross vein at Consols is 0.3–0.9 m wide and dips to the northeast at a low angle. At Consols, and other smaller deposits at Mainland, gold mineralization is associated with carbonation, silicification, and sulphidation.

A major north-northeasterly striking dextral fault terminates the BIF–mafic unit to the east of Mainland. Mineral exploration in the vicinity of this structure has not yet revealed significant gold mineralization.

Meekatharra

Gold production (Table 34) from the Meekatharra mining centre has come mainly from two parallel north-northeasterly striking zones, one east of the town at Paddys Flat, and the other to the north at Haveluck (Fig. 157). Significant mineralization outside these zones is restricted to felsic porphyry at Pioneer–Savages (immediately east of the town), and faulted BIF at Prohibition (also called 'Queen of the Hill').

The Paddys Flat zone is 100–200 m wide and at least 7.5 km long. However, almost all gold production has been obtained from the central 4 km interval between Phar Lap and Halcyon (Fig. 158). The zone is composed of talc–carbonate and talc–chlorite schist, intruded by an almost continuous 10–20 m-wide sill of quartz–albite porphyry, and a complex system of quartz veins. Within 100–200 m of the porphyry the ultramafic schists contain variable carbonate, fuchsite, and quartz, which reflect carbonation and metasomatism. Gold mineralization is partly associated with the porphyry and its ultramafic wall rocks; contact zones commonly contain arsenopyrite and pyrite. The porphyry and ultramafic rocks contain disseminated, relatively low-grade gold mineralization, whereas higher grade gold deposits are developed in quartz veins.

From detailed plans presented by Clarke (1916), it is clear that both longitudinal and transverse quartz veins and, to a lesser extent, late subhorizontal quartz veins are mineralized. The transverse veins are steeply inclined, strike northerly to northwesterly, are commonly curved or sigmoid, and occur in the vicinity of northerly trending zones of sinistral displacement. The latter have the effect of deforming the mineralized zone into a series of contiguous lenses arranged slightly *en echelon*. The longitudinal veins generally dip steeply to the east-southeast, and parallel to bedding.

The structural geology of Paddys Flat, as currently understood, is consistent with a north-northeasterly striking sinistral shear zone, the northerly to northwesterly striking veins representing tensional fractures and R and R' riedel shears, whereas the longitudinal veins occupy D (displacement) shears. Easterly and northeasterly striking sinistral shears, locally developed in the vicinity of the Phar Lap deposit, probably represent pressure fractures. This shear zone is considered to be a continuation of the D_1 Gabanintha Shear Zone (Fig. 168).

The structural history of the Gabanintha Shear Zone at Paddys Flat is probably the product of at least three phases

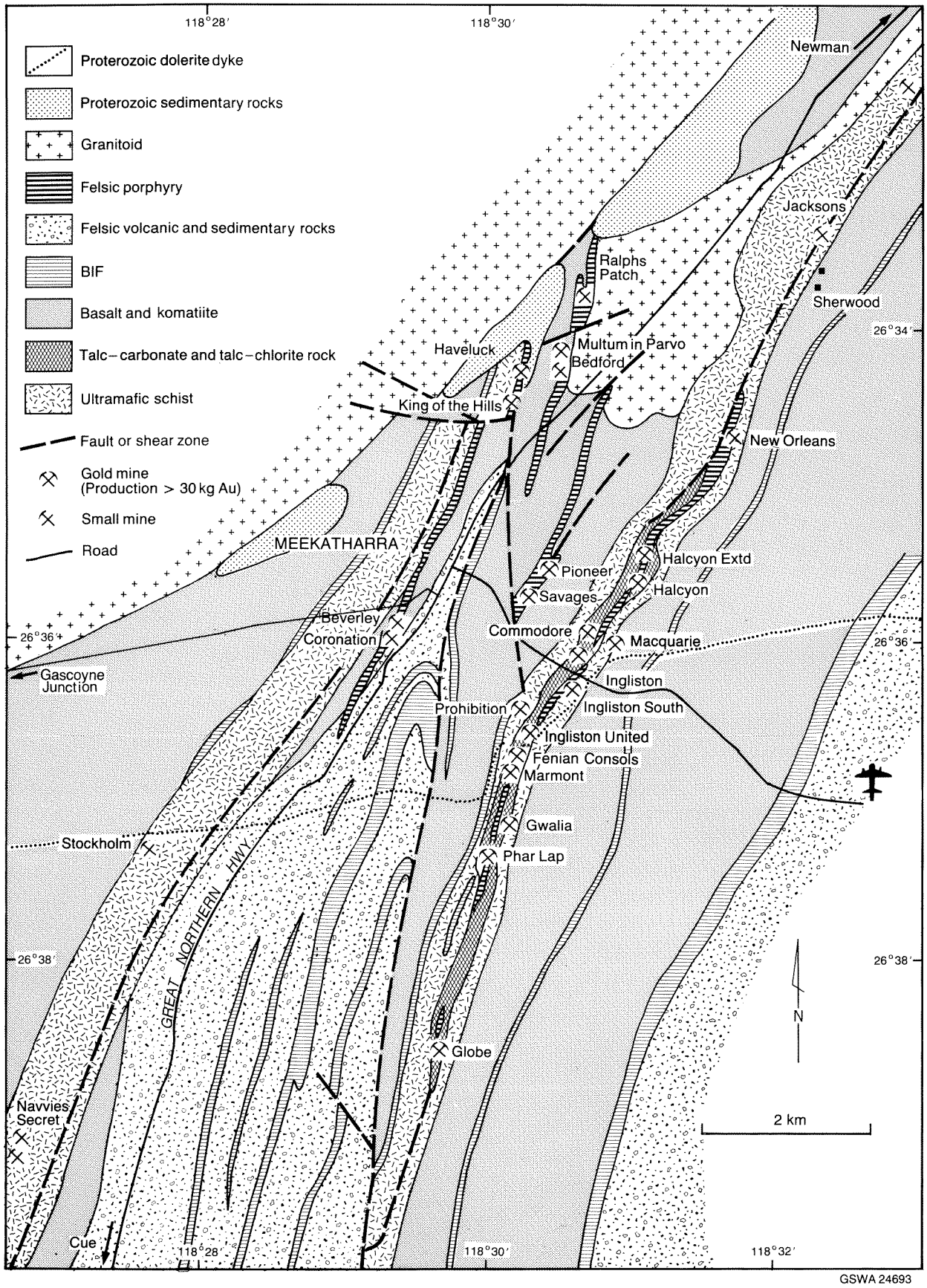


Figure 157. Geological setting of the principal mines at Meekatharra.

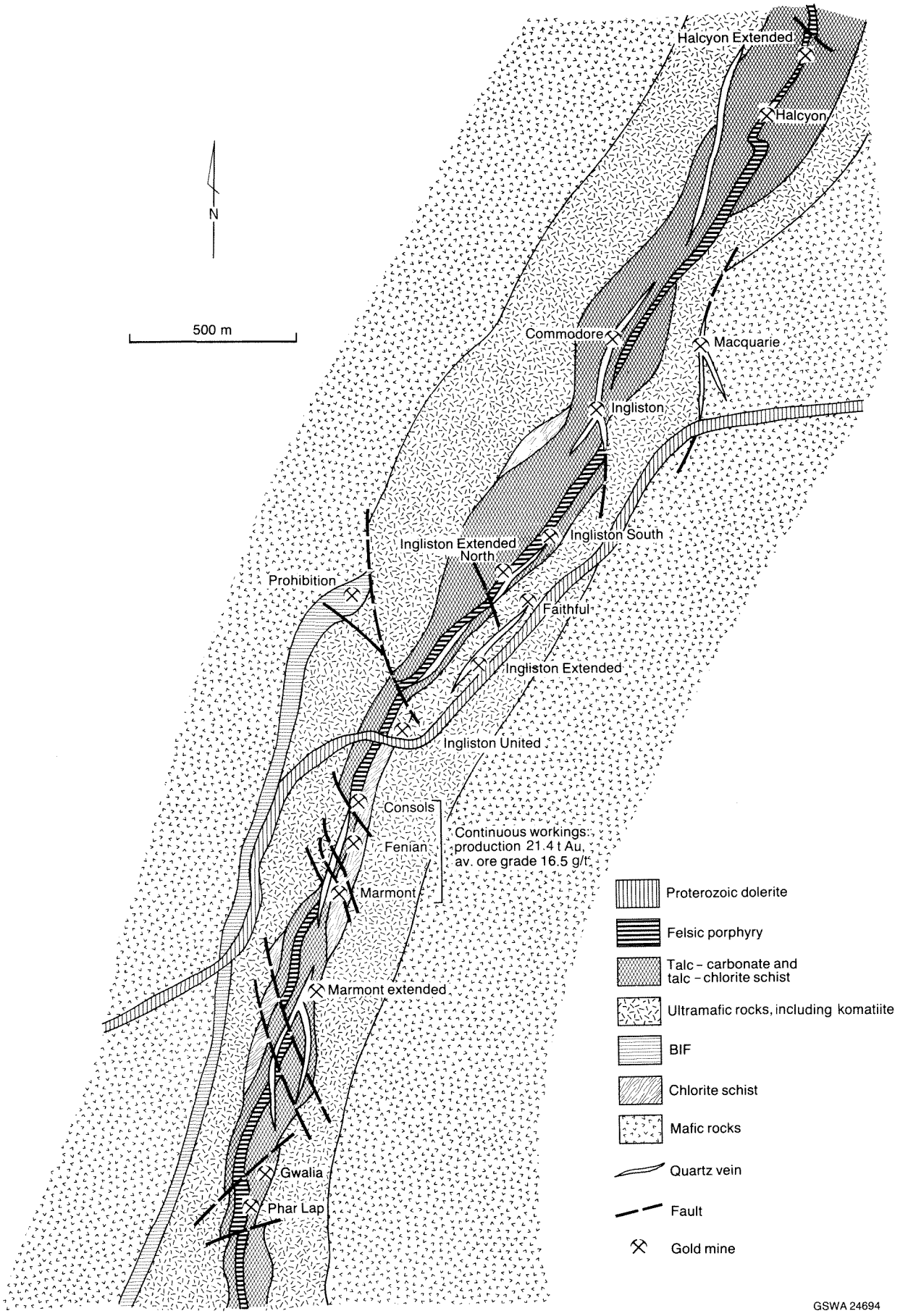


Figure 158. Geological map of Paddys Flat, Meekatharra.

of movement. Isolated remnants of extremely sheared chlorite schist occur along the contact of the fuchsitic talc–carbonate and talc–chlorite unit and surrounding amphibole–chlorite schists. These appear to date from the early stratoconformable D_1 shear zone which was later intruded by peridotite and felsic porphyry sills prior to a subsequent layer-parallel movement. The shear zone developed preferentially along a unit of peridotitic lava within the Gabanintha Formation. To the west, the Gabanintha Shear Zone is truncated by the northerly striking D_4 Mount Magnet Shear Zone. Displacement along this shear zone is essentially horizontal (Chapter 5), and at Meekatharra a dextral movement of about 10 km is involved. Various relatively late faults of several orientations affect the Gabanintha Shear Zone and are probably related to this major D_4 structure.

As almost all the underground workings are now inaccessible, Clarke's (1916) report remains the most comprehensive reference for information on the geometry of the deposits. Accordingly, the following summary of the principal features of the larger mines is based on Clarke's (1916) account, subsequent published and unpublished information, and surface observations made during field work in the preparation of this bulletin.

The Commodore mine (production prior to 1987 about 660 kg of gold at an average ore grade of 14.2 g/t) marks the site of the first gold discovery in the Paddys Flat area, in 1899. Mineralization is now known to occur in two longitudinal quartz veins, up to 1 m wide, which dip steeply west-northwest. These intrude variably fuchsitic talc–carbonate rock, and commonly contain fuchsite inclusions. No porphyry occurs at the surface, but the deepest workings reveal an adjacent chloritized albite porphyry. North-northwesterly and east-northeasterly striking minor faults, carrying short high-grade quartz veins, cross the main veins at several places; the intersections were probably occupied by short rich shoots. Fuchsitic rock, marginal to the veins, is locally pyritic and net-veined by quartz (Clarke, 1916, fig. 51). To the north-northeast, the Commodore veins terminate at what appears to be a northerly striking fracture zone containing some dilation veins, and which has produced a general sinistral displacement. Gibson (1904, p. 71) also refers to a low-grade 6 m-wide 'lode formation' which strikes westward through the workings. The precise position of this mineralized zone is uncertain, but, if Gibson's description of orientation is accurate, it may represent a pressure fracture occupied by brecciated and quartz-veined ultramafic rock.

Simpson (1916, p. 311) reported that Commodore ore was low in metallic sulphides (arsenopyrite and pyrite totalling 4.2%), but contained significant dolomite, mesitite (Mg, Fe carbonate), turgite–limonite, serpentine, chlorite, fuchsite, and sericite. The composition reported is consistent with a high proportion of altered ultramafic rock in the ore.

The Ingliston mine (about 1020 kg of gold at an average ore grade of 22.1 g/t, prior to 1988) is about 150 m to the south of Commodore and is based on several quartz veins in variably fuchsitic talc–carbonate and talc–chlorite rock. Descriptions by Clarke (1916, p. 138–140) indicate two main auriferous quartz veins. One is longitudinal, and probably a southern continuation of the eastern vein at Commodore, whereas the other is a northerly striking quartz vein, commonly 1 m wide, and appears to fill a major tensional dilation structure. At its northern end the vein swings north-northeasterly, whereas to the south it swings south-southwesterly. Shoots of ore appear to be partly controlled by intersections between the main veins and subsidiary veins, and on the transverse veins, plunge steeply south-southeasterly. Ingliston has been developed since Clarke's investigation, chiefly on the northerly striking vein which is persistent and dips steeply westward below the lowest workings at 200–250 m.

About 500 m south-southwest from Ingliston, the Ingliston Extended workings (production about 2.1 t of gold at an average ore grade of 17.0 g/t, prior to 1987) are located on longitudinal veins and quartz-veined lodes to the east of the felsic porphyry sill. The western deposit consists of quartz-veined porphyry and a discrete quartz vein along the eastern contact of the sill with fuchsitic quartz–carbonate rocks. Highest gold values were reported (Clarke, 1916) to have come from a 5 cm-wide vein of bluish quartz along the slickensided eastern contact of the porphyry. In places the main vein bifurcates around lenses of fuchsitic carbonate rock containing pyritic quartz stockworks. The eastern lode, which is parallel to, and about 80 m from, the western deposit, has poorly defined walls and consists of ultramafic rock containing numerous greenish quartz veins and stringers. It is in a subsidiary shear zone close to the western contact of a dolerite dyke that post-dates both shearing and gold mineralization. The southern section of the eastern lode swings westwards, away from the dyke, a feature that may reflect a change in the subsidiary shear zone from a longitudinal displacement fracture, to a pressure fracture. Both deposits dip steeply eastwards and contain ore shoots which plunge northwards at 30–40°.

A third orebody, situated between the eastern and western deposits, is a 1–2 m-wide quartz vein containing fuchsitic inclusions; Clarke (1916) commented that it is similar to the eastern vein at Commodore.

Simpson's (1916, p. 307–308) analyses of concentrates from the Ingliston Extended workings suggest that the dominant sulphides in the ore are arsenopyrite and pyrite. As at Commodore, it is clear that a large proportion of the ore was ultramafic rock, presumably net-veined by quartz.

Ingliston South–Ingliston United workings (about 510 kg of gold at an average ore grade of 26.9 g/t, prior to 1987) are 400 m south-southwest from Ingliston Extended, at a point where the post-shear dolerite dyke crosses the Gabanintha Shear Zone. Most production was recorded after 1913, and consequently Clarke's (1916) descriptions are limited. However, additional geological evidence was presented by Noldart (1961) based on drilling to a vertical depth of about 500 m. The main Ingliston United orebody appears to be located on the eastern contact of the quartz–albite porphyry sill. The drilling intersected the porphyry at about 450 m vertical depth, where it was about 15 m wide; the eastern part was extensively veined by quartz.

Noldart (1961) stated that pyrite and arsenopyrite occurred throughout the porphyry, but that pyrrhotite was associated with the ultramafic wall rocks and the quartz veins.

The most productive section at Paddys Flat has been the 700 m interval encompassing the Ingliston Consols, Fenian, and Marmont workings. Prior to 1953, when mining ceased, these mines had produced 21.4 t of gold at an average grade of 16.5 g/t gold. Detailed plans of the workings, as they existed in 1914, were presented by Clarke (1916); at that stage the workings had extended to a depth of about 250 m and had produced 7.2 t of gold at an average grade of 25.6 g/t gold. In 1934, Forman reported mining to a depth of 420 m. This section of Paddys Flat is distinctive in that the felsic porphyry sill does not extend to the surface. Insufficient evidence is available to determine if this is due to longitudinal shearing-out, down-faulting between transverse faults, or primary intrusive termination in this particular area. Whatever the reason for the absence of the sill near the surface, it is clear that the horizon that the sill elsewhere intrudes is also the mineralized horizon in this area. The sill is present at depth and becomes thicker downwards, (Forman, 1934). The main orebody occupies a shear zone in which a sinuous longitudinal lode consisting of carbonated and chloritized fuchsitic ultramafic rocks contains numerous quartz veins. Arsenopyrite is common in the ultramafic rock of the lode and dominates over pyrite. According to Clarke (1916, p. 159), the gold occurs in the quartz and as 'face gold' along shear planes in the ultramafic rock. Northwesterly striking 'spur' veins bifurcate southeastwards from the main lode, particularly in the central (Fenian) and southern (Marmont) sections of the deposit. These veins are high grade and appear to occupy fractures which are partly tensional, and partly of R and R' riedel type. R fractures predominate; movement is sinistral and commonly displaces longitudinal veins and the porphyry sill at depth.

The high productivity of the Ingliston Consols–Fenian–Marmont group appears to have resulted from the abundance of quartz veins in this section of the Gabanintha Shear Zone. The workings here probably occupy a higher structural level than elsewhere in the zone, and this may be associated with more extensive quartz veining and carbonation above the upper limit of the porphyry sill.

The Phar Lap open-cut and pre-existing minor workings had, to the end of 1987, produced about 5.0 t of gold at an average ore grade of 2.4 g/t. The fuchsitic talc–carbonate and talc–chlorite zone is relatively wide at Phar Lap, is extensively sheared, and contains numerous veins of quartz and porphyry. Many of the quartz veins strike east or east-northeast, which is uncommon in most other sections of the Gabanintha Shear Zone at Paddys Flat, and may reflect extensive local pressure fracturing.

Other significant gold producers from the Gabanintha Shear Zone are Halcyon–Halcyon Extended, Macquarie, and Globe. At the northern end of the zone, the New Orleans deposit is geologically significant, although recorded production has been minor.

At Halcyon–Halcyon Extended group of workings (about 160 kg of gold from 26 000 t of ore) gold has been mined from chloritized, pyritic albite porphyry in talc–carbonate and talc–chlorite schist containing veins and stringers of quartz. Clarke (1916, p. 133) reported that small, but rich, deposits occur where the quartz veins pass into the ultramafic rocks. Narrow fuchsitic and rare narrow gossanous zones strike parallel to the foliation of the schists. A sample (80611, Appendix II) of one of the gossanous zones contained 0.2 g/t gold, 580 ppm As, 4800 ppm Cr, 1280 ppm Ni, and 530 ppm Cu, which suggests the presence of arsenopyrite and chalcopyrite at depth.

The Macquarie workings (about 64 kg of gold from 8823 t of ore) lie on a northerly striking shear zone of similar structural affinities to the main vein at Ingliston, but situated on the eastern side of the Paddys Flat shear zone. The lode is subvertical to steeply eastward dipping and consists of sheared talc–carbonate and amphibole–chlorite rocks containing numerous small veins and stringers of quartz.

The Globe mine is at the southern end of the shear zone, about 2.5 km south-southwest of Phar Lap. The intervening ground contains no significant workings and outcrops are rare. Accordingly, its geology is less well understood than that of the ground to the north, but ultramafic cap rock and scattered pits that have brought up fuchsitic ultramafic schist, indicate geological continuity with the main mineralized zone. At Globe, quartz veins of various orientations intrude fuchsitic talc–carbonate and talc–chlorite rock. Sulphidic porphyry occurs in the southern workings; analyses (samples 80619, 80620, Appendix II) revealed up to 1.4 g/t gold. Northwestwards, quartz veins extend into a unit of BIF.

The New Orleans workings are based on a north- northwesterly striking quartz vein within fuchsitic ultramafic schist, close to the eastern contact of a felsic porphyry intrusion.

Apart from the steeply inclined lodes and quartz veins in the Paddys Flat shear zone, many of the workings also contain auriferous subhorizontal veins. In terms of overall production, these structures are of relatively minor importance, although at Ingliston Extended significant amounts of high-grade ore appear to have been obtained. Clarke (1916) noted the presence of other subhorizontal auriferous veins at Halcyon, Commodore, Ingliston, Gwalia, and Globe. Most subhorizontal veins appear to be late structures and occur in fractures displacing the steep veins.

Analyses of five samples of pyritic porphyry (Appendix II) from Halcyon and Globe, at opposite ends of the shear zone, reveal an average gold content of 1.8 g/t. Arsenic values range up to 2350 ppm but, at least in these areas, there does not appear to be a positive correlation between arsenic and gold. However, Clarke (1916, p. 160) reported a strong correlation between the two elements in most of the workings, and noted that pyrite (as opposed to arsenopyrite) was considered to be an unfavourable indicator.

The Haveluck zone of mineralization extends at least

5 km north-northeast from Beverley (immediately west of Meekatharra) to Ralphs Patch (4 km north of Meekatharra), and also includes areas of gold mineralization at King of the Hills, Haveluck, Lone Hand, and Bedford. As at Paddys Flat, gold is associated with sills of felsic porphyry within sheared ultramafic and mafic rocks in the D_1 Gabanintha Shear Zone; however, the D_1 structure is locally displaced by the D_4 Mount Magnet Shear Zone (Fig. 168 and Plate 1).

At Haveluck, King of the Hills, and Lone Hand, gold has been mined from sills of felsic porphyry containing numerous quartz stringers. These sills intrude extensively sheared ultramafic rocks in which foliation planes carry subhorizontal slickensides. Mineralization does not extend far into the ultramafic rocks, but is largely confined to the porphyry bodies and their associated quartz veins. Sericitization and kaolinization are pervasive so that original rock composition is commonly difficult to determine at the surface and within the 70 m-deep open-cut. Total production from contiguous ground at Haveluck, Lone Hand, and King of the Hills, prior to 1987, is imprecisely known due to bulking of production, but is estimated to be between 3.0 and 4.0 t of gold at an average grade of about 1.7 g/t.

Ralphs Patch and Bedford are situated a short distance to the east of Haveluck. Clarke (1916, p. 110–113) reported that the porphyry at Ralphs Patch contained few quartz veins and much of the gold was probably obtained from a single 5 cm-wide quartz vein. At Bedford, Clarke's (1916) report suggests that ultramafic rocks associated with the felsic porphyry contain some fuchsite, as in the Paddys Flat shear zone.

The Beverley workings are based principally on quartz stringers within felsic porphyry, especially in veins striking east. The Pioneer–Savages group of workings (about 340 kg gold at an average ore grade of 26.3 g/t, prior to 1987), immediately east of Meekatharra, exploit auriferous quartz veins in felsic porphyry and adjacent talc–chlorite schist. Fuchsite is developed along the porphyry–ultramafic contact. The veins occupy north-northeasterly striking faults and are extremely variable in thickness, measuring up to 15 m in width. Clarke (1916) considered that the quartz veins were genetically related to the porphyry and probably represented late-stage intrusions.

Prohibition (also called Queen of the Hills) is the only significant mine (1.9 t of gold at an average ore grade of 11.3 g/t) of the Meekatharra area that is located on BIF. Clarke's (1916, p. 167–173) descriptions of the underground workings indicated that gold mineralization occurs in shattered and sheared BIF between several faults dipping steeply to the west. The lode extends horizontally northwards for about 150 m and has been mined to a depth of about 150 m. The mine is positioned on faults forming part of the Mount Magnet Shear Zone, but is also situated at an intersection of this zone with a north-northwesterly striking shear which passes through the Ingliston South area. Clarke (1916, p. 173) also noted gold mineralization associated with the north-striking Prohibition fault at Fenian West, about 1 km to the south of Prohibition, and small workings are scattered along this structure southwards to the Globe.

Messenger Patch

The Messenger Patch mining centre encompasses several groups of old workings extending from Golden Grove to Gnows Nest — a distance of about 20 km. About 93% of the recorded production (Table 34) has come from the Gnows Nest mine. Gold mineralization at Gnows Nest occurs in a 3–10 m-wide shear zone in amphibole–chlorite schist, talc–carbonate schist, and metadolerite. This zone contains quartz stringers and lenticular quartz veins up to 1 m wide, and is confined between discontinuous auriferous quartz veins on the hanging wall and footwall (Arboyne N.L., 1987). The orebody dips west at between 60° and 75°, and production has been based on a shoot plunging north-northwest at about 60°. This shoot has been stoped to a vertical depth of 136 m; stoping widths increase downwards to reach 3 m at the lowest level. Surface workings extend about 400 m along strike. A sample of ferruginous quartz (85821) collected from the principal dump assayed 56.6 g/t gold and 73 ppm arsenic. Assay data reported by Arboyne N.L. (1987, p. 22–28) indicate the possibility of several shoots of ore along the 400-m shear zone. A short distance to the east of the mineralized zone a folded grey-white chert–jaspilite unit contains gossanous material, one sample (85824) of which assayed 0.5 g/t gold. This anomalous result suggests the possibility of parallel subsidiary zones of gold mineralization.

Whole-rock geochemical analysis of five samples (85816–20, Appendix II) from the ore zone reveals extensive alteration of mafic rock; K-metasomatism and Na, Ca, and Mg loss is particularly evident. Mafic schist from the hanging wall (sample 85816) and footwall (sample 85817) of the deposit, near the main shaft, exhibits markedly elevated As, Cu, and Pb contents, and galena (in addition to pyrite) is reported (Arboyne N.L., 1987) to be present in the orebody.

Gnows Nest is located at a point where the Yalgoo–Singleton greenstone belt is less than 3 km wide and flanked by post-folding granitoids (Plate 2). The mineralized shear zone strikes north to north-northwest, parallel to the axis of the belt; hydrothermal activity might be expected in such a position. Ore-shoot control has not been established, but the plunge of the orebody is approximately parallel to the local plunge of lineations on bedding. It should also be noted that the shear zone is not concordant with bedding; consequently lithological change may be a contributing factor.

Other productive mines of the mining centre include Crescent and the Marloo–Vatican group. Crescent is on the margin of a suite II post-folding granitoid, 3 km east of the Scuddles shaft. Gold mineralization occurs in a quartz vein which dips 55° in a direction slightly north of west, and appears to have been concentrated in a shoot plunging northwest at about 45°. The Marloo–Vatican group is 7 km north-northeast of Scuddles in an area of extensive laterite, silcrete, and kaolinization. Hard-rock mining was based on quartz veins dipping west-northwest at 70° through granitoid rocks and felsic schist. Clastic textures and bedding preserved in the schist suggest that it was originally pyro-

clastic, or composed of volcanogenic sediments. At the Marloo mine, extensively altered rocks, now almost wholly composed of phyllosilicate minerals, may represent mafic or ultramafic tuff. Extensive alluvial workings occur in the Marloo–Vatican area, although recorded alluvial production (Table 34) is relatively low.

Crescent, the Marloo–Vatican group, and small intervening mines are all along the intrusive contact of the large suite II post-folding granitoid (or group of post-folding granitoids) in this area, and all appear to be based on quartz veins occupying north to north-northeasterly striking faults and shears. These are probably of the same generation as the north-northeasterly striking faults which displace the base-metal mineralization at Golden Grove.

Moyagee

The Moyagee mining centre is 40 km north of Mount Magnet, and about 10 km along strike from, and to the south-southwest of, Lake Austin. The mines occur on the western side of a low ridge of BIF units intercalated with mafic rocks, and are distributed along two northerly striking zones of mineralization about 400 m apart. The western zone, which includes the Moyagee (491 kg of gold from ore averaging 48 g/t) and Louise (27 kg gold from ore averaging 21 g/t) mines, is composed of sheared metabasalt, talc–chlorite schist, felsic schist, and metasediments intruded by northerly striking quartz veins. Similar veins also host much of the mineralization in the eastern zone, which is located about 300 m to the west of the main BIF–mafic sequence of the ridge, and which consists of grey-white chert, mafic schist, felsic schist, and metasediments.

The old workings are inaccessible, but dump material at Louise consists of fine-grained quartz–chlorite–carbonate mafic schist which is quartz-veined parallel to the main foliation. This schist contains elongate, lenticular aggregates of Fe–Ti oxides and euhedral cubic sulphide (probably pyrite). At Moyagee, most of the waste from the mine is mafic schist, talc–chlorite schist, and vein quartz.

A short distance to the west of the Moyagee mining centre, a major north-striking shear zone(Cuddingwarra Shear Zone) extends about 90 km, from Cuddingwarra in the north to Blackman Find and Lennonville in the south. The Cuddingwarra Shear Zone produces a strong angular discordance between north-striking basalt to the west, and northeasterly striking volcanics and BIF to the east. The structure probably possesses a vertical throw component of several kilometres; dextral displacement is indicated at Cuddingwarra. The course of the fault is marked by quartz veins and it has probably been a relatively deep conduit for hydrothermal fluids.

Lithologically and structurally the Moyagee mining centre is similar to Lennonville. Although it is uncertain if the Cuddingwarra Shear Zone is directly linked to the Mount Magnet Shear Zone at Lennonville, it appears probable that gold mineralization in the two areas is related.

Mount Gibson

Prior to 1986, when mining commenced at the Mount Gibson laterite-hosted gold deposit, gold production at this mining centre was limited to small-scale mining at Tobias Find, Orion, Leakes Find, and Paynes Crusoe. In 1988, gold production commenced from oxide and sulphide orebodies in underlying sheared mafic and felsic rocks. Primary gold mineralization is associated with shear zones and quartz veins related to the Mount Gibson Shear Zone (Fig. 168). At Tobias Find and Orion, these strike northwards, parallel to bedding and tectonic foliation in felsic tuff and quartz–sericite schist. At Orion, and to the north-northeast at the Mount Gibson Well prospect, gold is closely associated with weak Cu–Pb–Zn mineralization. At Leakes Find, gold mineralization occurs in quartz veins through metabasalt and talc–chlorite schist, and at Paynes Crusoe the host rock is metabasalt close to BIF.

The Mount Gibson laterite-hosted gold mineralization has been defined over a strike length of 7 km. The Miocene laterite overlies altered mafic, felsic, and sedimentary rocks of the Windaning Formation, and is generally about 2–8 m thick; it consists chiefly of transported material containing secondary gold. Gold mining has initially been restricted largely to the upper 4 m of the laterite, and the ore is pisolitic, nodular, and massive ('hardcap' of Davy et al., 1988). The gold is fine grained (normally less than 10 microns) and contains no silver. Below the hardcap, gold mineralization in weathered bedrock is erratic and partly associated with quartz veins which appear to be remnants, *in situ*, of underlying Archaean veins.

Drilling along the Mount Gibson Shear Zone in 1988 revealed substantial gold mineralization below the laterite. Primary gold mineralization in the bedrock contains a significant amount of silver, and occurs in quartz veins and mineralized shear zones; it is partly associated with base-metal sulphides. Host rocks are predominantly mafic in composition, but some felsic porphyry chert and serpentinite is also present in the 300–700 m-wide zone of deformation. Individual orebodies are generally 10–50 m wide and coincide with shears.

Mount Magnet

With the exception of the Mayflower group of mines, all the significant gold deposits at Mount Magnet are restricted to the eastern limb of the Boogardie Synform (Fig. 157), and exhibit a combination of structural and lithological controls indicating that gold mineralization is epigenetic. The Boogardie Synform is a major fold plunging very steeply to the south-southwest and possessing a north-northeasterly striking axial-plane cleavage. From its western limb, west of Hill 50, to the Hillcrest area, south of Mount Magnet, it rotates S_2 through 150°. The orientation, size, and structural relations of the fold are consistent with it being the main D_3 structure of the Mount Magnet area (Fig. 134C). However, in detail the synform clearly owes part of its present geometry to superimposed D_4 structures; in particular, major north-northeasterly striking wrench

faults which occupy a 6–8 km-wide zone of chiefly dextral faulting, west of the northerly striking Mount Magnet Shear Zone. These faults, which exercise an important control over many of the ore deposits, have previously been referred to as the 'Boogardie Breaks'. The overall effect of the D_4 deformation was to attenuate the western limb of the synform (aligned parallel to the north-northeasterly faults) and to produce a fracture pattern, complicated by subsidiary stress systems, in the eastern limb. Minor D_4 structures include kink bands striking north-northeast, and conjugate folds with north-northeasterly and easterly striking axial planes. Fracture and strain-slip cleavages dipping steeply east-southeast to southeast are probably related mainly to the D_3 synform, but parallelism of D_3 and D_4 structures makes separation of S_3 and S_4 difficult.

The D_3 and D_4 structures are visibly superimposed on minor tight to isoclinal F_2 folds, and a bedding-parallel tectonic foliation — S_2. The orientation and vergence of F_2 folds in the Golconda and Windaning formations demonstrates rotation by the Boogardie Synform, and indicates the presence of a major F_2 antiformal axis to the south of the Hill 50 mine. Northwest of Mount Magnet, in the vicinity of Morning Star, large F_2 folds refold the western limb of a major F_1 isoclinal syncline, here referred to as the Warramboo Syncline (Fig. 156). Some of the minor isoclinal folds visible in BIF and chert outcrops of the area may also be F_1 structures, but in the absence of interference with F_2 folds this is impossible to establish.

The most detailed structural account of the Mount Magnet area has been presented by Archibald (1982). The present investigation confirmed many of his observations, but additional regional and local information shows that the succession youngs from the Golconda Formation ('Sirdar Unit', Archibald, 1982) to the Windaning Formation ('Warramboo Unit', Archibald, 1982), not vice versa as suggested by Archibald (1982). In addition, the recent mapping did not reveal evidence of the existence of major intraformational isoclines (Archibald's 'F_1' folds) within the BIF and chert units; thus, Archibald's 'F_2' folds are equivalent to the F_1 folds described in this bulletin.

Gold mineralization at Mount Magnet, as at Lennonville to the north, is chiefly related to D_4 structures, but pre-existing gold deposits associated with D_2 structures are also present. Thus, as elsewhere in the Murchison Province, more than one phase of gold mineralization is indicated. Supergene enrichment is an important feature of many of the deposits and led to high grades being obtained during initial mining.

About 70% of the total gold production from the Mount Magnet mining centre has been attributed to Hill 50 mine (Tables 34, 38). On closure of the mine in 1976, workings had extended to a vertical depth of 1065 m, making it the deepest mine in the Murchison Province and one of the deepest mines in the State. Prior to 1934, when Hill 50 Gold Mine N.L. was formed, the same ground had been worked on the Sirdar, Mount Zion, and Polar Star leases; descriptions of the pre-1934 workings were provided by Gibson (1903, p. 23–24), Jutson (1914a, p. 122–126, 131), Feldtmann (1920), and Forman (1933). The Hill 50 mine

TABLE 38. TOTAL GOLD PRODUCTION FROM THE PRINCIPAL MINES AT THE MOUNT MAGNET MINING CENTRE TO 31 DECEMBER 1987

Mine	*Alluvial and dollied (kg)*	*Ore gold (t)*	*Gold (kg)*	*Total (kg)*
Brown Hill–Boogardie View	42.3	9 859	124.9	167.2
Corona	0.5	5 839	144.5	145.0
Early Bird	3.5	1 246	55.2	58.7
Eclipse	15.3	45 064	1 594.0	1 609.3
Edward Carson	-	18 612	404.9	404.9
Evening Star/Black Cat	19.7	42 850	1 335.1	1 354.8
Gift–Revenue	26.1	3 328	260.4	286.5
Hesperus Dawn	9.6	4 059	221.0	230.6
Hill 50 group	80.8	3 318 733	43 119.1	43 199.9
Hill 60	-	359 556	1 832.3	1 832.3
Hillcrest	-	10 660	37.0	37.0
Jupiter	1.7	4 513	76.6	78.3
Leap Year	-	2 420	56.4	56.4
Magnet/Mabel Dorothy	0.4	4 744	80.5	80.9
Mayflower–Primrose	3.8	2 167	91.7	94.5
Monarch/Poverty Pot	2.0	1 093	42.9	44.9
New Year	0.1	1 892	81.9	82.0
Star/Water Tank Hill	1.0	1 808 019(a)	10 125.4(a)	10 126.4(a)
St George	1.5	504 132	2 006.1	2 007.6
Three Boys/Return	11.7	1 768	72.2	83.9
Venus	0.1	435	49.5	49.6
Windbag	-	4 434	52.2	52.2

(a) Recent reported production from Star and Water Tank Hill includes production from the Hill 50 Gold Mine N.L. deposits such as Saturn and Hill 50, but Star has been the principal producer.

was described by Johnson (1950b), Finucane (1953), de la Hunty (1958b, p. 63–65), Forman (1960a,b), and Lewis (1965).

Gold mineralization at Hill 50 is hosted by BIF of the Golconda Formation and is spatially controlled by intersecting north-northeasterly and north to north-northwesterly striking faults. Hydrothermal fluids passing along the faults have caused sulphide replacement of magnetite in adjacent oxide-facies BIF. This has produced steeply plunging stratabound shoots of massive gold-bearing pyrrhotite–pyrite ore containing variable amounts of BIF, chert, and vein quartz. According to de la Hunty (1958b, p. 64), gold is chiefly associated with pyrrhotite rather than pyrite. Dykes of feldspar porphyry have intruded many of the north-northeasterly striking faults in the vicinity of the mine, and particularly high-grade ore is developed along porphyry–BIF contacts; however, the porphyry intrusions are internally barren. Although individual shoots are bounded by north-northeasterly striking faults and associated porphyry intrusions, the most important structure controlling mineralization appears to be a north to north-northwesterly striking fault (Lewis, 1965, fig. 2). This fault is subparallel to bedding and represents the sheared-out central limb of a tight to isoclinal fold pair. Structural relationships in the Mount Magnet area suggest that such folding occurred during D_2 deformation, though a D_3 correlation cannot be ruled out from the limited evidence currently available. It is possible that some gold mineralization is directly associated with the north to north-northwesterly striking fault, but it may be that the main role played by this structure was that of a trap for hydrothermal fluids during the D_4 event.

There are about 20 individual BIF units in the Golconda Formation at Hill 50, and the largest orebody is in the thickest BIF, a 20–40 m-wide unit. The other rock types in the succession (mafic to ultramafic extrusives and intrusives) are not mineralized, except where veined by sulphidic quartz in close proximity to faulted BIF contacts.

The Hill 50 production figures (Table 38) include production from nearby mines such as Saturn, Neptune, Haveluck, and Mars, in addition to previous workings on the same ground at Mount Zion and Sirdar. In recent years production from the Hill 50 group has been bulked, but prior to 1975 official figures were as follows: Saturn, 284.4 kg of gold from 47 076 t of ore; Sirdar, 201.9 kg of gold from 18 868 t of ore; Neptune, 141.4 kg of gold from 3344 t of ore; Haveluck, 117.3 kg of gold from 9919 t of ore; Mars, 94.9 kg of gold from 14 059 t of ore; and Mount Zion, 44.0 kg of gold from 5129 t of ore. All these mines exploit orebodies in sulphidated BIF adjacent to north-northeasterly striking faults, but workings have generally been confined to the oxidized zone. Quartz veins, quartz-veined fault breccia, and feldspar-porphyry dykes and sills occur in some of the deposits, and late-stage horizontal quartz veins and fractures are present in the Saturn and Mars deposits. Gold mineralization at the neighbouring Jupiter mine is similar to that in the Hill 50 group.

The Three Boys, Hesperus Dawn, Hesperian, Golden Ridge, Eclipse, and Boomer mines are hosted by BIF of the Golconda Formation, from 1 to 2.5 km southeast of Hill 50. At Hesperus Dawn, Eclipse, and Boomer the orebodies are controlled by northeasterly striking D_4 faults, but are also partly stratabound and associated with zones of breccia. Within these zones shoots of medium- to high-grade ore plunge steeply southeast. At Eclipse the workings are based on two such shoots, about 70 m apart, which have been mined to a vertical depth of 290 m. Economic mineralization is confined to BIF and does not extend into the surrounding mafic schist; however, gold content in intrusive felsic porphyry is locally low to moderate, particularly along pyritic margins. The Three Boys (including Return and Lucknow) and Golden Ridge (including Hesperian) deposits are more closely associated with northeasterly striking faults and breccia zones that are veined by pyritic quartz. Other descriptions of the Three Boys–Boomer group are provided by Gibson (1903, p. 20–23), Jutson (1914a, p. 131–132), de la Hunty (1958a, p. 68–70; 1958b, p. 82–87) and Sofoulis (1958, p. 61–70, 75–82).

The Brown Hill–Boogardie View deposits are about 1 km west of Hill 50 and, like those in the Hill 50 area, are associated with epigentic sulphidation of BIF along fault zones through the Golconda Formation. However, at Brown Hill much of the recorded production has come from laterite developed on the BIF. At Windbag, 1 km to the north of Brown Hill, gold mineralization occurs in several sets of quartz veins in felsic porphyry and mafic schist.

The Morning Star mine, redeveloped in 1979, has recently been the most important gold producer of the Mount Magnet area. Gold mineralization is associated with quartz–carbonate–pyrite–stibnite–tourmaline veins stringers, and stockworks within extensively altered komatiitic metabasalt, intermediate to felsic volcanics, and minor amounts of both BIF and chert of the Windaning Formation. The geology of the mine area is extremely complex and involves F_2 refolding of the major F_1 Warramboo Syncline (Fig. 156) with subsequent D_3 and D_4 effects superimposed. The principal host rock is metabasalt which contains probable pillow structures, and now consists of quartz, chlorite, carbonate, sericite, and plagioclase, together with minor amounts of tourmaline, pyrite, and arsenopyrite. Archibald (1982), drawing on unpublished information by Henderson (1981), stated that the auriferous veins possess well-defined chlorite–sulphide (chiefly pyrite) alteration selvages. Fluid inclusion studies (Groves et al., 1984) indicate essentially homogeneous CO_2-rich (20 ±5 mole % CO_2), low salinity H_2O–CO_2 ore fluids, temperatures of about 400°C, and pressures of 100–200 MPa. Structural observations made by Henderson (1981) suggest that these veins are mainly of D_2 and pre-D_2 generation, and Jutson (1914a, p. 115) noted the presence of horizontal veins which may be late-stage unloading structures.

Published descriptions of the mine workings prior to recent redevelopment and extension (Gibson, 1903, p. 18; Jutson, 1914a, p. 115–116; de la Hunty, 1958a, p. 50–51) establish that in the upper 150 m of the mineralized zone there were three principal shoots of ore, the 'Star', 'Big', and 'Easter' lodes. The mineralized zone is about 200 m long, and over most of its length strikes northwest, parallel to S_2. The Easter Lode was at the southeastern end of this zone, whereas the Big Lode was to the northwest, at a point where the zone swings sharply southwestwards; the Star Lode is close to the Big Lode on the southwesterly striking section. Descriptions of these deposits are provided in the references cited above, but the generalization can be made that they are lenticular bodies of extensively veined and hydrothermally altered mafic schist, plunging southwards at about 60°. In the Easter Lode, part of the orebody was jaspilitic BIF and chert, and it is in this area that horizontal pyrrhotitic quartz veins are best developed.

The change in strike of the mineralized zone may result from the presence of an F_3 synclinal axis between the Star Lode and Big Lode; de la Hunty's (1958a, p. 51) comments indicate that the Star Lode does not lie on a D_4 fault.

The North Morning Star, Evening Star, and Late Comer deposits occupy a northerly trending zone of mineralization about 300 m west of Morning Star. Old mines previously occupying this ground included Cushie Doo, Cushie Doo South, Broken Bond, Fortune of War, Tattersalls, Ticket, Birthday, Planet, Meteor, Hallmark, and Bronzewing. Gold mineralization occurs in folded, sheared and extensively altered (carbonated, chloritized, and silicified) felsic to mafic volcanics, fine-grained clastic sedimentary rocks, and chert, and takes the form of lenticular concentrations of quartz, carbonate, and quartz–carbonate veins and stringers. The dominant host lithology is now quartz–sericite schist containing varying amounts of carbonate, chlorite, and disseminated sulphides (pyrite, pyrrhotite and, locally, molybdenite and stibnite). The lenticular orebodies are elongated in a northerly to north-northwesterly direction and plunge vertically to steeply southwards, probably along S_2–bedding intersections. Most

of the veins are approximately parallel to S_2, but an earlier set may be genetically related to the F_1 Warramboo Syncline, the axis of which lies a short distance to the east. North-northeasterly striking D_4 quartz veins are also present, but do not constitute orebodies; it appears that most of the gold mineralization pre-dates D_4 in this area. Late subhorizontal quartz veins, similar to those at Morning Star, locally disrupt the orebodies.

In 1988 the North Morning Star open-cut merged with the Morning Star–Evening Star open-cut to form the 'Star Pit' (Frontispiece and Fig. 159), the entire area having been found to be a more-or-less continuous zone of closely spaced orebodies.

The Black Cat mine is immediately south of the Evening Star–North Morning Star area, and contains similar mineralization. According to de la Hunty (1958a, p. 51) the orebody plunges south at 65°. The zone of mineralization dips west-southwest at 60–80°.

The Edward Carson deposit is about 500 m north of Morning Star, and like that mine is based on quartz veins in altered and sheared basalt in the core of the Warramboo Syncline (Fig. 156). The quartz veins, which strike mainly northeastwards and dip northwest at about 60°, contain pyrite and stibnite, and are flanked by wall rocks of quartz–chlorite–sericite schist. These veins may occupy D_4 faults, but two orebodies in west-northwesterly striking veins (de la Hunty, 1958a, p. 50) are probably controlled by D_2 shears.

About 500 m west of North Morning Star, the Monarch–Poverty Pot line of workings trends northwest along sheared sandstone, ferruginous chert, and kaolinized schist. Gibson's reference to the deposits (1903, p. 20) indicates that the main orebody is a schist lode containing quartz stringers, but no other information is available. At Venus (Fig. 156) gold mineralization occurs in folded units of BIF and ferruginous chert, containing northwesterly striking quartz veins. The deposits here appear to be small high-grade shoots along BIF margins, probably adjacent to faults.

The Gift–Revenue group of workings, 1.5 km west of Morning Star, follows a thin northwesterly striking shaly BIF unit within the Gabanintha Formation. The BIF is probably deformed by D_2 shear, parallel to bedding, but high-grade gold mineralization appears to be principally localized in, and immediately adjacent to, northeasterly striking D_4 faults (based on observations by Jutson, 1914a, p. 134).

The St George mine is located at a point where the Windaning Formation is folded and faulted on the eastern limb of the F_1 Warramboo Syncline (Fig. 156). The Windaning Formation locally strikes north-northwest, and consists of five chert units with associated quartzite, chloritized shale, black shale, and kaolinized rhyolite–dacite lava and pyroclastic units (Balde and Woolfe, in press). Economic gold mineralization is confined to the chert, which is grey-white banded, intensely folded and brecciated, and forms lenticular bodies with abrupt, irregular contacts. Orebodies are 25–150 m long and 5–28 m thick. Above the water table (40 m), in the oxidized zone, grades average about 6 g/t gold, although gold content is erratic, and the gold occurs as fine free particles. Below the water table, gold is associated with sulphides in chert and BIF, and also occurs in sulphidic quartz veins. Most north-northwesterly striking faults are probably D_2 structures, and northwesterly striking D_4 faults have been mapped at various places within the mineralized zone. Jutson (1914a, p. 120–122) recorded the presence of subhorizontal joints or fault planes, close to which gold contents are elevated. The old workings extend to a maximum depth of 95 m (Jutson, 1914a, p. 120–122; de la Hunty, 1958, p. 54–55).

Water Tank Hill, 400 m west of St George, is located in the Windaning Formation on the western limb of the F_1 Warramboo Syncline (Fig. 156). BIF is more common than at St George, and thin units of extensively carbonated and chloritized mafic tuff are also present. Gold mineralization is associated with stacked subhorizontal quartz–pyrrhotite–siderite/ankerite veins, and massive pyrrhotite zones in BIF. Both types of deposit occur a short distance to the east of a north-northwesterly striking fault zone. The veins occupy dilational fractures in BIF and chert, and post-date F_1–F_2 isoclinal folds plunging about 60° north-northwestwards. The massive sulphide deposits, in otherwise oxide-facies BIF, form lenticular shoots plunging about 70° to the southwest. An important feature of both types of deposit is the replacement of magnetite by pyrrhotite, which indicates localized sulphidation adjacent to faults and quartz veins (Groves et al., 1984; Lambert et al., 1984). Oxide-facies BIF and grey-white banded chert outside these areas of pyrrhotite alteration do not possess economic gold grades. Fluid inclusion studies (Groves et al., 1984) indicate mainly heterogeneous, CO_2-rich, low salinity H_2O–CO_2 ore fluids at temperatures above 370°C and pressures above 180 MPa. Nodules of inferred diagenetic pyrite in chert and carbonaceous shale contain no gold, and are isotopically different from pyrrhorite and pyrite in the veins and alteration haloes (Lambert et al., 1984). These observations indicate that although the Water Tank Hill deposits are stratabound, they are almost certainly entirely epigenetic. The age of gold mineralization is probably post-D_2, although it is possible that the subhorizontal veins occupy tension fractures related to the D_2 fault zone. The latter is displaced by several northeasterly striking D_4 faults (Groves et al., 1984, fig. 4D), but it is uncertain to what extent these are also mineralized.

Production figures for Water Tank Hill are not available, production having been bulked with other mines in the area, such as Morning Star, Saturn, and Hill 50.

The Piedmont mine, 4 km north of Hill 50, is based on quartz veins and stringers in basalt at the top of the Gabanintha Formation. Most of the veins strike north-northeast and probably occupy splay faults to the west of the Boogardie Fault (Figs 168 and 156). The quartz carries pyrite, and wall-rock alteration includes silicification and chloritization.

Faults within the north-striking Mount Magnet Shear Zone appear to be the main factor controlling gold mineralization at the Magnet, Corona, Hill 60, and Hillcrest



Figure 159. Vertical aerial photograph of the area between Mount Magnet and Star Pit.

mines. The Magnet and Mabel Dorothy workings are 5 km north of Mount Magnet. The orebodies are northerly striking pyritic quartz veins in sheared mafic and ultramafic rocks of the Gabanintha Formation. At Corona, 2 km south of the Magnet mine, the main host rock to the auriferous quartz veins is talc schist.

About 1.5 km southwest of Mount Magnet, the Hill 60 deposit is associated with a northerly striking shaly BIF within the Gabanintha Formation. The BIF dips vertically to steeply westwards within metabasalt and kaolinized sericitic schist. Mine plans indicate southerly plunging disharmonic folds in the area of the open-cut at Hill 60; and the eastern contact of the BIF is probably a fault. Miles (1948a) stated that the BIF ('banded chert') varies in width from 2.5 to 13 m and is lenticular, and that some of the higher grade ore was obtained from the thickest sections. This could reflect the presence of folds within the BIF, or be due to repetition by faulting. In general terms, the orebody can be described as stratabound, highest grades being along BIF–schist contacts. The dominant sulphide is pyrite, although a minor amount of pyrrhotite is also present. Quartz veining is not an important feature of the deposit, and is mainly confined to the wall rocks; felsic porphyry is present but not significantly mineralized (Miles, 1948a). The workings extend to a vertical depth of 152 m, but most production came from the upper 90 m of the deposit; this indicates the importance of supergene enrichment.

The Hillcrest (previously Worker and Royal Consols) deposit is 4 km south-southwest of Mount Magnet. Gold mineralization is in an intensely folded BIF unit within the Golconda Formation. According to Jutson (1914a, p. 126–127) the main orebody is located where a 9 m-wide north-northeasterly striking zone of brecciation and shearing crosses the BIF. Mine plans of the Royal Consols lease also indicate shearing, and the presence of felsic porphyry. Archibald (1982) indicated that pyrrhotite is the dominant sulphide associated with the mineralization. From the information available, it appears that the Hillcrest deposit is an irregular area of sulphidated BIF, immediately adjacent to a major north-northeasterly striking fault.

The Mayflower–Primrose, New Year, Early Bird, and Leap Year deposits are 3 km east-northeast of Mount Magnet. Gold mineralization occurs in numerous narrow quartz veins which occupy a 3 km-long, northwesterly to west-northwesterly striking shear zone through komatiite, basalt, and dolerite of the Gabanintha Formation. The intrusive contact of a post-folding granitoid intrusion is located about 200 m to the northeast of Mayflower, New Year, and Early Bird; this granitoid, which also contains northwesterly striking quartz veins, probably underlies the mineralized shear zone at relatively shallow depth. Descriptions by Jutson (1914a, p. 112–114) and de la Hunty (1958, p. 73–75) indicate that the deposits are lodes consisting of numerous quartz veins and leaders within schist. A subsidiary set of northerly striking quartz veins in the zone may reflect predominantly dextral shear, and the zone probably represents a splay structure related to the Mount Magnet Shear Zone.

Munarra Gully

The Munarra Gully mining centre is about 6 km northwest of Stake Well. Most of the recorded production was obtained from the After Many Years workings (Gibson, 1904, p. 37–39). A large easterly striking quartz vein intrudes a 2 km-wide belt of metabasalt that is intruded to the north and south by post-folding granitoid. Little production has been recorded since 1903 when Gibson (1904) reported mining to a vertical depth of about 30 m along the vein which dips north at 30–40°. The vein is up to 4 m wide (averages 2 m) and contains substantial quantities of pyrite, malachite, and chalcopyrite. Gibson's descriptions suggest potential for further open-cut mining and for mining below 30 m, where the vein was reported to be 3 m wide.

Nannine

Gold mineralization at Nannine occurs in quartz veins and lode structures occupying two main sets of fractures; one parallel to bedding and striking north to northwest, and the other striking northeast to north-northeast. The host rocks consist of (from west to east) metabasalt and minor basaltic tuff (Murrouli Basalt), BIF intercalated with mafic and ultramafic rocks (Golconda Formation), metabasalt, talc–chlorite and talc–carbonate schist, and metabasalt containing metasedimentary units (Gabanintha Formation). Most of the Murrouli Basalt and the upper part of the Gabanintha Formation have been excised by granitoids. Immediately to the south of Nannine mine the succession dips steeply east to east-southeast, whereas to the north it is inclined steeply northeast. This change in dip direction (Plate 2) is accompanied by northeasterly striking faults and a northerly to east-northeasterly striking cleavage. North-northeasterly plunging open folds have refolded isoclinal folds and layer-parallel cleavage within the BIF units. No detailed structural studies have been undertaken in this area, but it appears probable that the faults are related to the swing in strike, which suggests a sinistral rotation. If a north-northeasterly striking zone of sinistral movement extends through the Nannine area, it may represent a continuation of the Day Dawn Shear Zone (Fig. 168). However, the faults may also be related to the Reedy Shear Zone (Fig. 168 and Plate 2). A further complication is that some of the layer-parallel veins are folded by the north-easterly plunging open folds. Accordingly, more than one generation of quartz veining is present at Nannine; the earliest of the layer-parallel veins are possibly related to the refolded isoclinal folds, or to relatively early layer-parallel shearing along ultramafic members of the Gabanintha Formation (Gabanintha Shear Zone).

In 1891, Nannine was the site of one of the first reliably documented discoveries of payable gold in the Murchison Province, the other being at Yuin in 1890 (Woodward, 1895, p. 83; Maitland, 1919, p. 20, 32). By 1891, hundreds of miners were camped in the area, and much of the early production, particularly from nuggets, was not recorded. Four mines, Nannine, Champion, Caledonian, and Queen of the Lake (also known as 'Aladdin'), have been responsible for 90% of gold production recorded from ore in this area.

The Nannine mine (783 kg of gold from ore averaging 31.7 g/t) is close to the northern end of a 2 km-long north-northeasterly striking zone of quartz veining. In the southern section, the veins occur in granitoid and mafic rocks close to the granitoid–greenstone contact, but at the Nannine mine wall rocks are metabasalt, mafic tuff, and units of BIF and chert. Plans of the Nannine mine show two parallel zones of stoping, separated by a distance of about 25 m. The western workings ('Mount Hall Reef') extend to a vertical depth of about 70 m, whereas the eastern orebody ('Nannine Reef') has been developed to 150 m. The orebodies dip steeply west-northwest and, rather than being simple veins, are narrow zones occupied by closely packed quartz vein lenses and stringers, arranged *en echelon*. The width of the orebodies ranges from 0.5 to 5 m, and ore shoots plunge 35° to the north. These shoots, which are controlled by intersections between the vein system and the east- northeastward dipping BIF–chert units, are no more than 5–10 m long, but are fairly continuous down plunge. The mine workings extend 600 m along strike, and in the southern section there is a long zone of continuous stoping. This may partly reflect a different mining method, but the wall rocks of this section are principally metabasalt, and gold mineralization may be more evenly distributed than further north. Host rocks contain pyrite and pyrrhotite, but pyrite is most common in the mineralized veins, and in layers within chert.

The Caledonian (159 kg of gold from ore averaging 20.9 g/t) and Champion (861 kg of gold from ore averaging 19.6 g/t) mines are about 1 km northwest of the Nannine mine. They are positioned on a vein which at its southern end (Caledonian mine) is in two parts, strikes north and dips 70° to the west. Here the wall rocks are granitoid and carry quartz stockworks. The workings extend to a vertical depth of 55 m and stoping indicates a long ore shoot plunging 45° northwest. Northwards, in the Champion workings, the vein swings north-northwest and northwest, dips southwest at about 30°, and becomes more variable in thickness (0.5–5.0 m). The wall rocks are metabasalt at the surface, but probably include granitoid rocks at depth. The workings at Champion extend to a vertical depth of 98 m. Although the ore zone strikes parallel to bedding, it dips at a high angle to it and in the opposite direction. This may explain the reportedly erratic distribution of gold, since any lithologically controlled shoots would be horizontal, probably narrow, and laterally variable according to the lenticular nature of the veining.

The Aladdin (previously Queen of the Lake) mine (721 kg of gold from ore averaging 5.0 g/t) is 2 km north of the Nannine mine, in the lower section of the Gabanintha Formation. Gold mineralization occurs in a 50–100 m-wide northeasterly striking shear zone through metabasalt, talc–chlorite schist, and talc–carbonate schist. Within this broader zone of shearing, up to four or five parallel mineralized zones have either been mined, or confirmed by drilling. These zones are up to 20 m wide and carry numerous veins and stringers of quartz. Where they intersect thin units of BIF, chert, and graphitic shale, northwesterly plunging shoots of ore are developed. Complex variations in the size and orientation of the economically mineralized sections at the northeastern end of the zone may be due to the presence of northwesterly plunging tight to isoclinal folds in the BIF and shale units. Dykes of felsite occur in the vicinity of the workings, but their relationship to the mineralization is unknown.

In many respects the Aladdin deposits are similar to those of the Karangahaki–Romsey–Blue Bird zone (Gabanintha Shear Zone) at Yaloginda. However, the dominant structural control at Aladdin is currently considered to be relatively late-stage (D_4) transverse shear, rather than early layer-parallel shear.

About 1.5 km south-southeast of Aladdin and 600 m northeast of the Nannine mine is the Daisy mine and adjacent workings, which are based on a series of north-northeasterly striking quartz veins within talc–chlorite schist, talc–carbonate schist, and metabasalt. Felsic porphyry is also present in some of the workings and there are several thin BIF units. Immediately to the east of the Daisy, a major zone of north-northwesterly striking quartz veining is exposed. Quartz veins of this type, which extend northwards for about 3 km past the northeastern end of the Aladdin shear zone, probably represent longitudinal veins in the Gabanintha Shear Zone between Karangahaki and Blue Bird.

West of the Nannine, Caledonian, and Champion mines, numerous small abandoned workings are located on north-northeasterly striking quartz veins and quartz stockworks in foliated chloritic granitoid rocks close to the granitoid–greenstone contact. The veins are parallel to a northerly to northeasterly striking crenulation cleavage which deforms the main foliation of the granitoid rocks. South of the Nannine mine, the Baileys Island workings are located on layer-parallel and northeasterly striking quartz veins in the BIF–mafic unit.

About 15 km northwest of Nannine, the Wanganui mining area is based on a 5–10 m-wide zone of shearing in a post-folding granitoid. The zone dips west at 40–45° and consists of several narrow shears containing veins and stringers of pyritic quartz. Grades decrease with depth, which suggests supergene enrichment in the oxidized zone. Slickenside lineations plunge west-northwest, but the sense of movement has not been established.

Table 34 shows that at Nannine, production of gold from alluvial sources is the largest of any individual mining centre in the Murchison Province. Most of this production has come from colluvial and alluvial material on the western side of Lake Annean and on the southern and eastern sides of Baileys Island. The gold was presumably derived by weathering of the high-grade shoots at BIF–quartz vein intersections in the epigenetic deposits.

Noongal (Melville)

A substantial proportion (about 40%) of the Noongal mining centre production (Table 34) has been recorded under 'Sundry parcels'. Of the remainder, about 65% came from mines located on the northerly striking Noongal Shear Zone, (Figs 160, 168) extending from Don Bradman in the

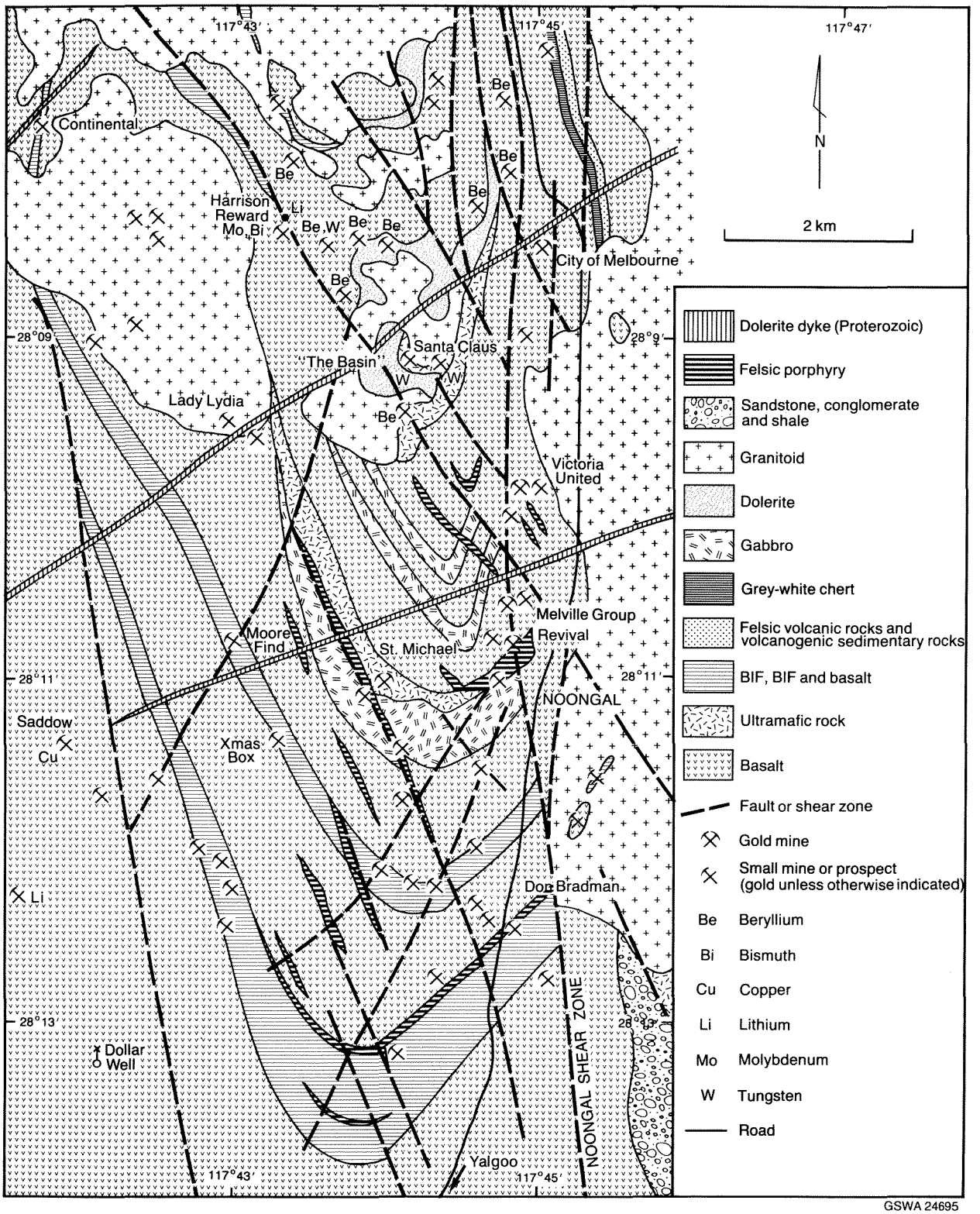


Figure 160. Geological map of Noongal.

south through Revival and Victoria United, to City of Melbourne in the north. To the west of this zone, numerous smaller workings occur on faulted, sheared BIF that has been quartz veined or intruded by felsic porphyry, quartz-veined granitoid, and quartz-veined basalt, dolerite and ultramafic rock.

The largest production has been recorded from the Melville group (including Revival) where about 120 kg of gold have been obtained from ore averaging 16 g/t gold (Johnson, 1950a, p. 72). At Revival, a system of quartz veins dips 80° southwest through metadolerite. Johnson (1950a, p. 72) stated that orebodies occurred at the contacts between the dolerite and quartz porphyry. Information on the deposit is limited due to collapse of the workings which left a hole 10 m deep, 10 m wide, and 20 m long. About 500 m to the south-southwest, another mine is based on a quartz vein dipping 80° west-southwest through felsic porphyry which intrudes cleaved amphibole–chlorite rock (metadolerite or metabasalt). Samples of pyritic metadolerite wall rock (85824–27, Appendix II) collected at Revival exhibit K-metasomatism, probable addition of Na, and low Ca/Sr ratios — presumably due to loss of Ca. Plagioclase has been partly replaced by K-feldspar, and biotite comprises up to 10% of the rock. A sample of ferruginous quartz (80655D, Appendix II) assayed 3.4 ppm Au, 54 ppm Ag, 1364 ppm Cu, and 120 ppm Pb.

About 200 m northwest of Revival, another group of workings has exploited gold mineralization along a shear dipping 50° to the west. The orebody appears to have been a lode composed of basaltic schist and quartz stringers.

Victoria United, 2 km north of Revival, is based on a somewhat lenticular, but generally 0.5 m-wide quartz vein occupying a 1–1.5 m-wide shear in amphibolite-facies metabasalt. The vein and shear dip at about 40° west, swinging to 60° west-northwest in the northern workings. Samples of wall rock (85833–85836, Appendix II) reveal K-metasomatism (with accompanying addition of Ba and Rb), Sr enrichment, and elevation of Cu and Pb contents. Petrographic examination establishes the presence of K-feldspar and minor amounts of biotite, and extensive retrogression of the amphibolite. However, significant chemical and mineralogical wall-rock alteration does not extend more than 1 m from the margins of the vein. Samples of quartz (80660A–C, Appendix II) collected from the vein, and from a vein in the footwall, assayed up to 2.2 ppm Au and showed slightly anomalous Cu and Pb contents.

About 2.5 km north of Victoria United, the City of Melbourne workings follow a quartz vein dipping 50° west-northwest within amphibolite-facies metabasalt. A short distance to the north of the main shaft the orebody is terminated by an east-northeasterly striking fault and parallel dolerite dyke. Johnson (1950a, p. 73) also reported intrusive quartz porphyry associated with the mineralization. The most northerly workings in the Noongal Shear Zone, about 2 km north of the City of Melbourne workings, are based on narrow (about 0.1 m) quartz veins in felsic tuff, adjacent to grey-white banded chert and BIF. The most southerly workings in the zone are those near Don Bradman, about 3 km south of Revival. At these mines, felsic porphyry dykes and quartz veins intrude BIF and felsic schist. The mineralization is partly stratabound in sheared BIF, but the auriferous quartz veins strike north-northwest, parallel to a swarm of felsic porphyry dykes which intrude the area to the west.

To the south of the Don Bradman, the Noongal Shear Zone continues southwards for about 10 km (Plate 2). However, the only known mineralization in this part of the zone is a copper deposit, 4 km east-southeast of Carlaminda Homestead. Lateral displacement of both the Wadgingarra layered intrusion and the Windaning Formation at Don Bradman indicates effective sinistral movement along the shear zone, and there is adequate information from mine workings to establish that it dips westwards at 40–60°. However, no direct structural evidence has been observed to indicate what component of vertical movement, if any, is present. North-northwesterly striking faults and fractures exhibiting negligible displacement are extremely common in the greenstone belt west of Revival (Fig. 160), and may be tensional and riedel fractures related to the shear zone. They are commonly intruded by dykes of felsic porphyry, but porphyry also intrudes bedding, particularly along BIF contacts. Local shearing in the porphyry dykes suggests a genetic relationship to the nearby tectonically foliated and sheared granitoid stocks, rather than post-folding granitoid to the north (Plate 2); Maitland (1919, Ch. II, p. 36) commented that the 'acid' dykes emanate from granitic rocks to the west.

Production records indicate that mines outside the Noongal Shear Zone individually produced less than 20 kg of gold. Some, such as Lady Lydia, exploited quartz veins and stockworks in granitoid rocks and felsic porphyry, whereas others (e.g. Xmas Box and Moore Find) are based on BIF. Mineralization in BIF is generally stratabound, either within BIF or adjacent mafic schist, and most of the mines are located close to north-northeasterly or north-northwesterly striking faults. At Saddow, a 1 m-wide quartz vein dips 80° southeast through actinolite schist (metabasalt and/or metadolerite), whereas the St Michael mine exploits auriferous quartz veins through amphibolite and talc–chlorite schist in a metapyroxenite. The amphibolite (sample 85831, Appendix II) has high Mg content, consists of hornblende, biotite, and plagioclase, and has been metasomatised (K_2O 2.47%, Ba 919 ppm, Rb 205 ppm).

The economic geology of the Noongal area is complex and includes a wide range of deposit types (including scheelite, beryl, and emerald). However, gold mineralization appears to be concentrated in the Noongal Shear Zone where it occurs in longitudinal and transverse quartz veins, and longitudinal lodes. In view of the length of the shear zone, and the widely distributed gold mineralization along it, the area still offers considerable scope for detailed exploration.

Pinnacles (Jasper Hill)

At the Pinnacles (formerly 'Jasper Hill') mining centre, gold mineralization occurs in Golconda Formation basalt,

dolerite, pyroxenite, and BIF. The mines are located on a low ridge, 4 km long and 1.5 km wide, which is bounded to the north and west by intrusive suite I post-folding granitoid, and to the south by recrystallized monzogranite (Plate 2). The Mount Magnet Shear Zone (Fig. 168) passes through unexposed ground immediately to the east, and a subsidiary north-northeasterly striking fault is occupied by a wide quartz vein on its northwestern side.

By far the largest mine of the Pinnacles area is the Comet mine, which is located at the northeast end of the ridge. Here, gold mineralization is stratabound and occurs in two parallel lodes. Feldtmann's description (1921a, p. 60–61) combined with that of Lord (1963) indicates that the orebody consists of strongly laminated (sheared) BIF alternating with fine-grained quartz–actinolite and talc–chlorite schist containing layers and veinlets of cryptocrystalline quartz, calcite, siderite, and disseminated pyrite. Mineralization appears to be associated with strong bedding-plane shear, and it is notable that the strike of bedding is parallel to that of the Mount Magnet Shear Zone. Drilling described by Lord (1963) established that significant gold mineralization extended to a vertical depth of at least 185 m along the mineralized BIF, which dips east-southeast at about 60°. Ore shoots in the mine plunge steeply northeastwards (Lord, 1963) which corresponds to the plunge of minor folds and crenulation lineations in BIF units of the Pinnacles area. The workings at Comet extend along strike for about 250 m, and further south the mineralized zone has been mined intermittently for a distance of about 2 km.

About 1 km south-southwest from Comet, the Eclipse workings occupy the same mineralized horizon which here dips east-southeast at about 45°; 1 km further south, gossanous samples (73609A–C) from the BIF returned gold grades up to 2.5 g/t (Appendix II). Workings at the southern end of the ridge include Venus and Kelly which are based on quartz-veined sulphidic BIF and amphibolite. Veins of fine-grained granitoid intrude the BIF, but do not appear to influence mineralization. The BIF at Venus lies to the west of that at Comet, and is structurally (and probably stratigraphically) about 200 m beneath it.

A short distance to the northwest from Eclipse are the Shamrock workings which consist of several small mines on a north-northeasterly striking sulphidic quartz vein through amphibolite and quartz–chlorite rock.

Gold mineralization at Pinnacles is fairly uniform in character, and clearly related to quartz veining and sulphidation of BIF and associated amphibolite. The deposits occur along shear planes which are parallel to, and probably genetically related to, the Mount Magnet Shear Zone. The mineralized BIF units are deformed by northeasterly plunging minor folds which appear to have controlled the more productive shoots of ore. Accordingly, any further exploration should be concentrated in areas where such minor folds are present.

Quinns

Gold mineralization at the Quinns mining centre (Fig. 161) is associated with east-northeasterly striking quartz veins in felsic volcanics, volcanogenic sedimentary rocks, jaspilitic BIF, and chert of the Windaning Formation. The structure of the area is dominated by an easterly to east-northeasterly trending D_2 isoclinal anticline which has been refolded by a northwesterly trending D_3 syncline. The resulting interference takes the form of an east-northeasterly plunging anticline passing eastwards into a westerly plunging anticline. The more productive mine groups (Two Jacks, Favourite, and Cornstalk) are in the westerly plunging section of the D_2 anticline, chiefly at the top of the thick felsic volcanic–sedimentary unit which occupies the core of the fold. Further southwest on the southern limb of the east-northeasterly plunging anticline, the Nowthanna mine is located at a slightly higher stratigraphic level. The Quinns mining centre has also recorded significant alluvial and dollied gold (Table 34), mostly from superficial deposits in close proximity to the underground mines.

The 'Two Jacks Reef' deposit (Gibson, 1904; Feldtmann, 1921a) is a laminated quartz vein which strikes east-northeast for at least 1 km and includes the Phoenix, Phoenix Extended, Commonwealth, and Two Jacks mines (total production prior to 1987 about 304 kg of gold from 29 540 t of ore). The vein is generally about 1 m wide and dips fairly constantly south-southeast at about 70°. Host rocks are chiefly felsic tuff and felsic agglomerate, but minor amounts of amphibole–chlorite schist and possible metapelite occur in the western workings (Commonwealth and Phoenix Extended), where the quartz vein is visibly pyritic and includes accessory chlorite. At several points the vein is displaced by northwesterly striking faults and quartz veins, which dip steeply southwest. These locally contain minor gold mineralization, but generally appear to have little effect on the distribution of gold within the main vein. From Feldtmann's (1921a, p. 27) comment that the vein is 'richest' along 'joints', it is considered possible that longitudinal shearing of the vein has led to some secondary gold concentration.

The Favourite group of workings (total production less than 50 kg of gold) is about 1.5 km southwest of the Quinns State Battery site, and consists of several small mines on an east-striking fault zone veined by quartz. The quartz veins vary in orientation, but most dip steeply southwards. The workings extend from felsic schist in the east, to grey-white banded chert and BIF in the west. Most production has been recorded from the BIF section.

The 'Cornstalk Reef' (total production less than 50 kg of gold) strikes east-northeast, parallel to, and about 500 m south of, the Two Jacks vein. The only significant mine is Princess Dagmar, in which the vein is laminated and its walls exhibit vertical striations (Feldtmann 1921a, p. 34). The vein contains southwesterly plunging shoots of ore Feldtmann (1921a, p. 34), but it is unknown if these are controlled by intersections with northwesterly striking veins, or with particular lithological units (bedding dips westerly). Wall rocks are fine- to medium-grained andalusite-bearing quartz–chlorite rocks, probably representing clastic metasediments.

The Nowthanna mine, about 5 km southwest of the Quinns Battery site, consists of a complex system of small

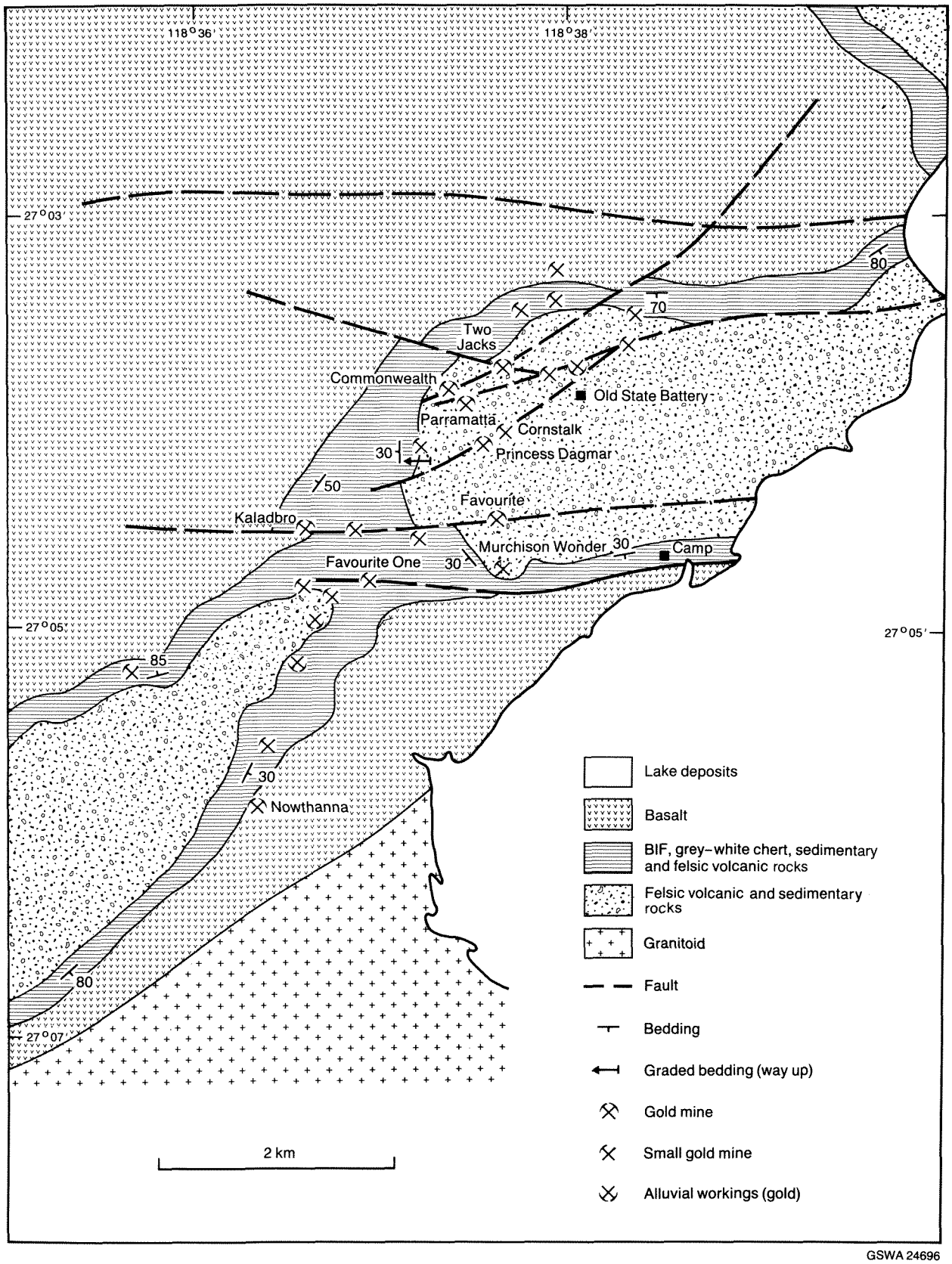


Figure 161. Geological map of Quinns.

workings on sulphidic quartz veins. Most of the veins dip either 30° southeast, or 30° northeast. The workings are situated in felsic schist and amphibole–chlorite schist, immediately adjacent to BIF.

Apart from the mines noted above, the Quinns mining centre includes numerous small mines and prospects located on jaspilitic BIF units, and several additional lines of workings along quartz veins within the felsic-sedimentary schist; descriptions are provided by Montgomery (1910, p. 15–30) and Feldtmann (1921a).

Most gold mineralization at Quinns is contained within the east-northeasterly striking quartz veins. Limited evidence (striations noted by Feldtmann, 1921a) suggest that these probably occupy faults with predominantly vertical movement. The faults are not axial planar to the F_2 folds, which they clearly post-date, and have the same orientation as most of the quartz veins in the Burnakura area, about 20 km to the west. The latter are probably splay structures related to the Mount Magnet Shear Zone; the Quinns faults may have the same origin.

There is considerable scope for further exploration at Quinns, particularly where the east-northeasterly striking quartz veins intersect BIF, and also adjacent to old workings where drilling may reveal additional mineralized veins.

Reedy

Gold mineralization at Reedy (Fig. 162) is structurally controlled and occurs along the sheared contacts of dolerite, basalt, ultramafic schist, quartz–feldspar porphyry and shale. The mining centre is situated on the Mount Magnet, Gabanintha, and Reedy Shear Zones (Fig. 168). Two main fracture zones are shown on Plate 2: a western zone (Reedy and Gabanintha Shear Zones) including the Triton, Rand ('Reedy' of Metana Minerals N.L.) and Kurara mines; and an eastern zone (Mount Magnet Shear Zone) hosting mineralization at Turn of the Tide and Cullculli North. In terms of gold production and known ore reserves the western zone is economically the most important by far (production and known reserves exceed 21 t of gold). Although differing host rock lithology (eastern zone: felsic to intermediate volcanics and metasediments; western zone: chiefly mafic and ultramafic rocks) may be a controlling factor, it is also evident that the western zone is structurally more complex. The ultramafic unit of the western zone is a southern continuation of the lower ultramafic member of the Gabanintha Formation which occurs at Gabanintha, Bourkes Find, Paddys Flat, Haveluck, and Yaloginda.

At Triton (7.116 t of gold from ore averaging 9.7 g/t gold) economic gold mineralization occurs in a 1.5–9 m-wide unit of altered mafic schist. The schist is composed of thin (less than 5 mm) layers containing varying proportions of carbonate, chlorite, quartz, phlogopite, pyrite, and pyrrhotite. Gold content is closely associated with pyrite, and rock in which pyrrhotite predominates over pyrite is of low grade. The schist dips steeply westwards above the 200 m level, and steeply eastwards below. It is bounded to the east by a dolerite sill and to the west by quartz–albite porphyry, amphibole–chlorite schist, and talc–chlorite (–carbonate) schist (metabasalt and ultramafic rock). The dolerite sill intrudes a black shale unit; all rocks contain quartz veins and are intruded by quartz–albite porphyry. The porphyry is itself deformed and contains quartz stockworks. Two ore shoots (North Emu and South Emu deposits) plunge steeply south (Campbell, 1953). Most production has come from the northern deposit which has been mined to a depth of about 500 m. Within the northern shoot, high-grade lenses plunge steeply south, or at a low angle towards the north. Campbell (1953, p. 198) stated that the attitude of these lenses corresponds to that of two sets of 'crumpling zones'. It is unknown if these sets are genetically related, but Campbell's (1953) descriptions suggest that they might be brittle structures resulting from layer-parallel movements. Triton is located at a point where the mineralized zone is narrowest and appears to have sustained maximum north–south extension.

Recent drilling at South Emu has shown that this shoot extends to a depth of at least 240 m; the upper levels of the deposit are being mined by open-cut methods. The orebody here is divided by a central sheet of felsic porphyry.

The Reedy mine (production, 1984–1987, 3.0 t of gold from ore averaging 4.3 g/t gold) was developed on the old Rand workings, about 1.2 km north of Triton, and on the same shear zone, which contains mafic and ultramafic rocks intruded by quartz–feldspar porphyry. All rocks show the effects of shearing but the porphyry is least deformed. The main lode is vertical, 10–15 m wide, extends about 400 m along strike, and is a pyritic quartz–biotite–carbonate–albite schist. The host rock is talc–chlorite–carbonate schist, tremolite–chlorite schist, pyritic metadolerite, and quartz-veined, pyritic porphyry. The main types of alteration are K-metasomatism, silicification, chloritization, and carbonation. Ore shoots plunge 30–70° south, parallel to fold structures in the schist. Supergene enrichment appears to have resulted in maximum gold concentrations between 5 m and 50 m depth. However, Metana Minerals N.L. (1986) have announced drilling results establishing that significant gold mineralization extends to a depth of at least 300m. Low-grade laterite-hosted gold mineralization is also locally developed near the shear zone.

The Kurara mine (1987 reserves 8.4 t of gold at an average ore grade of 2.9 g/t gold) is located 10 km north of Triton. The ore zone identified at Kurara is 1200 m long, 50–100 m wide, and contains two parallel lodes of carbonate–chlorite schist separated by about 20 m of barren talc–carbonate rock. The lodes dip west at about 70° and have been shown by drilling to extend to a depth of at least 300 m. Gold mineralization is associated with numerous quartz veins and stringers and is accompanied by pyrite and magnetite; thin dykes of felsic porphyry are also present in the lodes. In 1987 production was 518 kg of gold from ore averaging 2.5 g/t.

About 5 km to the east of the Triton–Rand–Kurara line of workings, the Mount Magnet Shear Zone contains

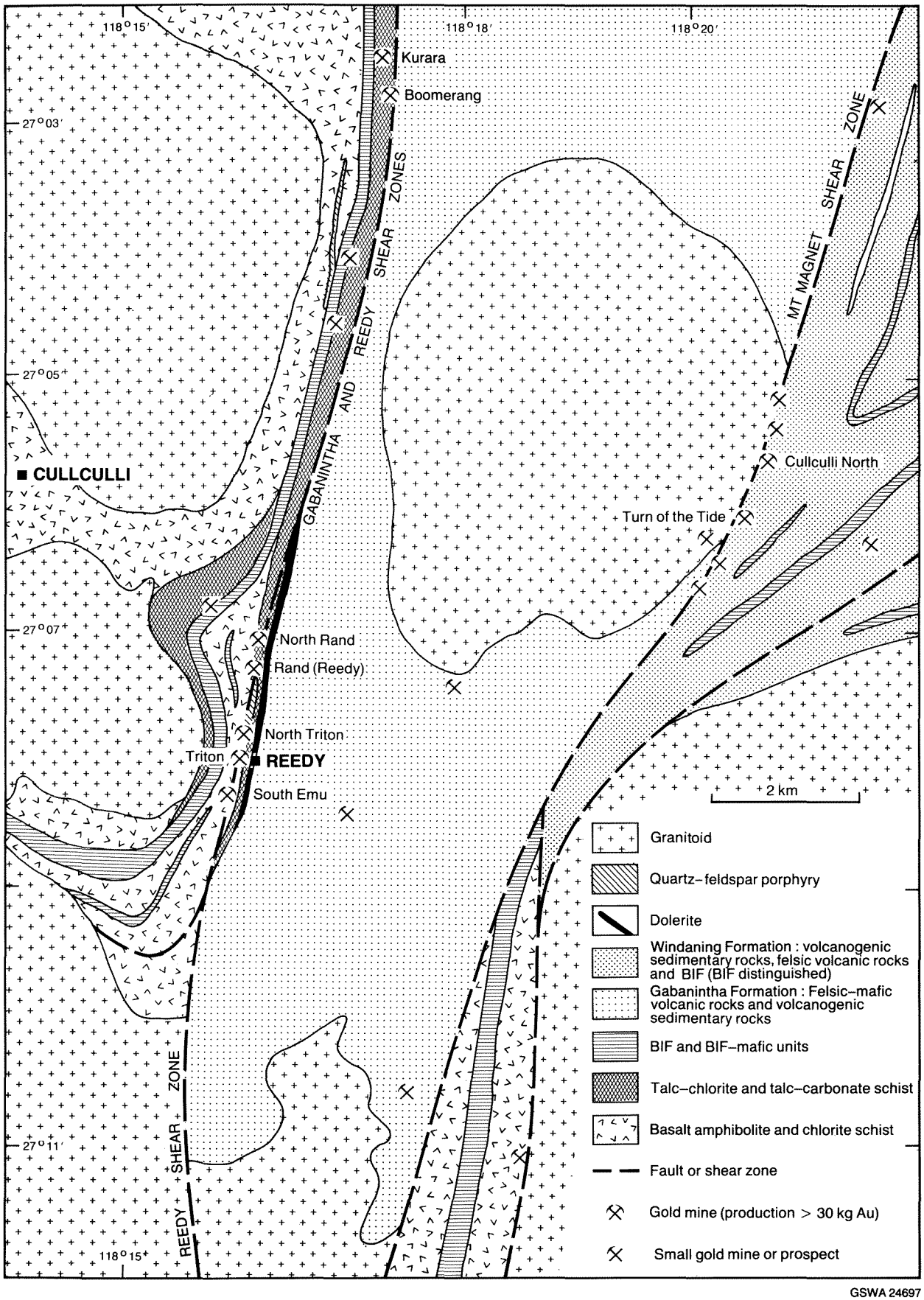


Figure 162. Geological map of Reedy.

significant gold deposits at Turn of the Tide (226 kg of gold from ore averaging 50 g/t gold) and Cullculli North (41 kg of gold from ore averaging 39 g/t gold). Gold mineralization occurs in variably pyritic quartz veins along a narrow shear in felsic to intermediate volcanics, quartz–feldspar porphyry, and less abundant mafic volcanics. Some of the workings extend into kaolinized granitoid forming the eastern margin of the post-folding granitoid between here and Kurara. Mine dumps suggest that carbonation is widespread in wall rocks; other alteration minerals include chlorite and biotite.

Rothsay

Gold mineralization at the Rothsay mining centre occurs in a number of quartz veins which intrude shear zones, parallel to layering and bedding, in a succession of high-Mg basalt and peridotite–gabbro sills. Clarke (1925, p. 11–14) described five parallel northwesterly trending lines of workings, but official records indicate that at least 85% of the gold production was obtained solely from British Queen and other workings on the 'Woodleys Reward Line' (Clarke, 1925). All the veins dip northeast at about 70°, and some range in thickness up to 2 m. Most are lenticular, and gold mineralization is erratic along their length. At British Queen the workings are 80 m deep and drives extend about 240 m. At the 40 m level, stoping is continuous for about 200 m along strike, except for a central low-grade interval of about 50 m. The orebody is a vein of blue and white quartz, generally about 1 m wide, and occupies a 1.5 m-wide shear zone. In some places the vein divides to form hanging wall and footwall orebodies separated by chloritic schists (Clarke, 1925). To the southwest of the orebody the country rock is relatively massive metagabbro, whereas to the northeast there is a unit of sheared serpentinized peridotite. This relationship indicates that shearing has been partly localized at boundaries between units of contrasting competence.

Gold at Rothsay contains significant quantities of copper, and the vein quartz commonly has about 1% chalcopyrite in addition to variable amounts of pyrite and pyrrhotite. Clarke (1925, p. 6) noted that treatment problems of the copper-rich gold ore constituted an important factor in leading to the closure of the mine in 1902.

The British Queen workings are located at the southern end of the Rothsay quartz vein system and adjacent to the intrusive contact of a large suite II post-folding granitoid to the southeast. Veins of pegmatite intrude the greenstones close to the intrusive contact; Clarke (1925, p. 10) recorded the presence of pegmatite about 50 m west of the British Queen workings. However, regional observations indicate that the shear zones hosting the mineralization post-date D_3, and may also completely post-date the post-folding granitoid. Moreover, had the shear zones existed prior to the intrusion of granitoid it can reasonably be expected that they would have been partly intruded by pegmatite. It is therefore possible that gold-bearing hydrothermal solutions that post-dated the granitoid moved through late fractures and precipitated gold on passing from the granitoid into the mafic–ultramafic assemblage of the greenstones.

Stake Well

About 263 kg of production at the Stake Well mining centre has come from Kohinoor South, where northeasterly striking BIF units within amphibole–chlorite schist are intruded by northwesterly striking quartz veins. The quartz veins dip steeply northeast whereas the BIFs dip at about 70° to the northwest. Shoots of ore plunge steeply northwards along the intersections between the veins and BIF–mafic schist contacts. The BIF is pyritic below the water table, and below this level gold content decreases (Woodward, 1912a, p. 129) to grades not economic in 1912 (less than 5–10 g/t). However, Woodward (1912a, p. 129) noted that in one deposit 'values' continued to 60 m depth. Plans to establish an open-cut mining operation were announced in 1987; reserves were reported as 0.105 Mt at a grade of 5.9 g/t gold.

The regional structural relationships of the quartz veins at Stake Well have not been investigated. However, it is notable that this area is situated in a north-northeasterly striking zone, extending from Nannine to Tuckanarra, in which bedding is locally rotated or 'kinked' southeastwards. This zone is probably a continuation of the Day Dawn Shear Zone (Fig. 168). This structure may be accompanied by northwesterly striking tension fractures providing sites for the development of quartz veins.

Supergene enrichment is a pronounced feature of the Stake Well deposits, and economic mineralization may be confined to relatively small, isolated shoots.

Star of the East

The Star of the East mine is 6 km west of Gabanintha, but for historical reasons its gold production (635 kg of gold from 27 812 t of ore) has been recorded under the Nannine mining centre. The mine is located on a west- striking quartz vein through felsic and mafic volcanic rocks of the Windaning Formation. According to Gibson (1904, p. 52) the vein ranges in thickness from 1 to 3 m, dips steeply south, and has been stoped to a depth of 50 m. Most production appears to have come from a shoot plunging steeply to the east, possibly located at the intersection of the vein with a particular lithological unit.

Tuckabianna

Tuckabianna is situated on the Mount Magnet Shear Zone about 30 km east of Cue. Gold mineralization occurs in sheared and brecciated jaspilitic BIF and volcanogenic sedimentary rocks of the Windaning Formation, which have been intruded by felsic porphyry. Quartz veining is absent or uncommon in most of the deposits, which consist of high-grade lodes in the oxidized zone. Most orebodies are less than 10 m in true width, and dip southeast at about 45°. Exploration by Australmin Holdings Limited has identified open-cut resources totalling 4.2 Mt of ore at an average grade of 3.1 g/t gold (including about 1.5 Mt of laterite-hosted gold mineralization).

At Webb Patch, 15 km south-southwest of Tuckabianna, gold-bearing sulphidic quartz veins occur in jaspilitic BIF, grey-white chert, and metabasalt. Quartz–feldspar porphyry veins are associated with some of the workings, the largest of which is the Hill End mine.

Early mining operations at Tuckabianna were briefly described by Blatchford (1918, p. 64).

Tuckanarra

Tuckanarra is situated 40 km north-northeast of Cue where an otherwise northerly striking BIF–mafic unit (Golconda Formation) is locally kinked east–west by two northeasterly trending folds (shown as F_3 folds on Plate 2). This local swing in strike appears to be related to the Day Dawn Shear Zone (Fig. 168), and is similar to another local sinistral strike rotation at Nannine, 35 km to the north-northeast. Within the east–west limb of the Tuckanarra fold-pair, or kink, a steep northwesterly dipping cleavage and northeasterly striking faults are superimposed on earlier tight to isoclinal folds with axial planes that are more or less parallel to bedding. These northeasterly striking structures may be directly related to the strike rotation.

Gold mineralization occurs in fractures at, or along, BIF–mafic contacts and within mafic and ultramafic rocks close to BIF units. The more productive mines (Fig. 163) have been the Anchor–Trilby–Cable group (270 kg of gold), Boyd Reward–Ensign–Union Jack group (282 kg of gold) and the Nemesis mine (231 kg of gold). Other deposits have individually yielded less than 100 kg of gold.

The Anchor–Trilby–Cable group of workings extends to a depth of 60 metres and is based on several north-northeasterly striking quartz veins within mafic schist (Gibson, 1904). The old workings are now inaccessible, but dump material consists of metabasalt, felsic porphyry, and vein quartz containing minor amounts of malachite. Gibson (1904) reported that the veins range up to 4 m in thickness and dip west-northwest at about 80°. He commented on the attitude of only one shoot, that in the Cable workings, which he said plunges southwards.

The Boyd Reward group exploits erratic but high-grade gold mineralization along a west-northwesterly striking quartz vein which has intruded at the contact between BIF and amphibolite. According to Gibson (1904) mining was largely restricted to the level above 30 m (i.e. above the water table). The grade of the ore produced from these deposits was extremely high (176 g/t from Boyd Reward, 125 g/t from Ensign, and 106 g/t from Union Jack) but productive shoots and 'pockets' were small. This may point to local gold enrichment at intersections of the vein with northeasterly striking faults. One such fault visibly displaces the BIF units at Blue Peter, about 500 m to the east of Ensign.

The Nemesis mine, about 6 km east of Tuckanarra Homestead, is based on three shoots which occur where east-northeasterly striking quartz veins cross a unit of BIF within sheared mafic schist (Woodward, 1912c). The resulting ore shoots plunge almost vertically and have been worked to a depth of 76 m. Above the water table (approx. 30 m) these shoots were wide and high grade, but mineralization rapidly diminished in the sulphide zone. A few metres to the south of the workings are outcrops of biotite granite, apparently in faulted contact with the mafic schist.

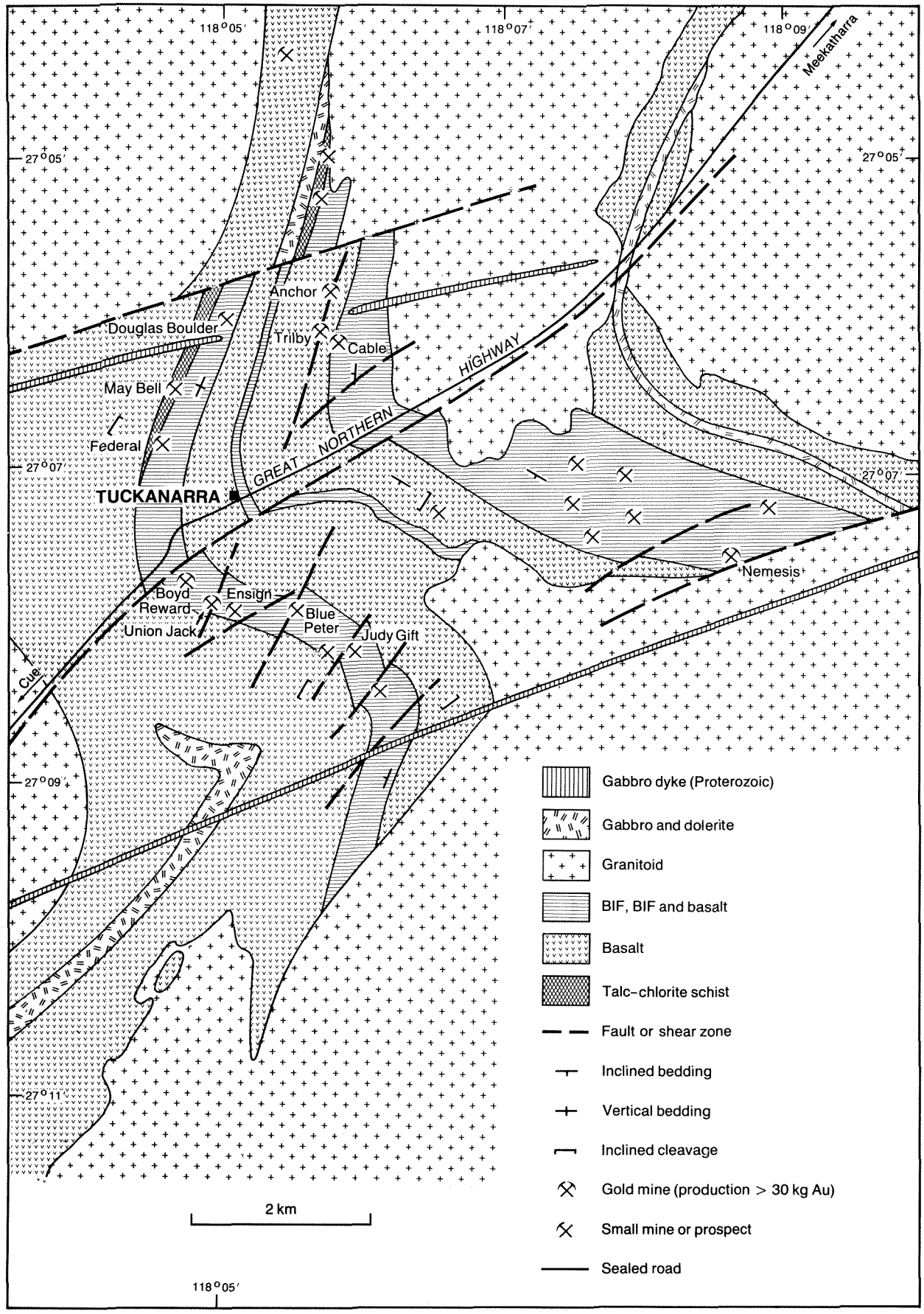
In summary, gold mineralization at the principal mines of the Tuckanarra mining centre is contained in quartz veins which occupy faults and shear zones. The higher grade deposits occur where these structures intersect BIF, but not all deposits are associated with BIF. Most of the quartz veins constituting the identifiable 'reefs' are more or less parallel to the strike of adjacent BIF units. Shoots of economic-grade gold mineralization are probably, at least partly, controlled by cross-cutting faults, and possibly by minor folds related to the Tuckanarra fold pair. Felsic porphyry intrusions in the mineralized areas may be related to adjacent post-folding granitoids (Plate 2). An observation by Gibson (1904, p. 32) suggests that felsic porphyry post-dates at least some of the quartz veins.

Almost all production at Tuckanarra has come from the zone of supergene enrichment (above about 30 m) and has been obtained from small, widely scattered high-grade shoots and lenses. Such mineralization would not sustain modern mining operations, but it is possible that larger low-grade deposits, amenable to open-cut mining, could still remain, particularly northeast and northwest of Tuckanarra Homestead. The east-northeasterly trending Nemesis fault zone may also prove to be mineralized along strike from the existing workings.

Warda Warra

About 90% of gold production recorded at Warda Warra has been obtained at the Western Queen mine, almost all the balance coming from the Trixie and Mistake workings. At Western Queen, gold mineralization occurs in a narrow unit of quartz–hornblende–mica schist, flanked to the west by ultramafic rocks and to the east by metabasalt. Closely associated with the quartz–mica schist, which may represent a metamorphosed chert, are units of quartzite and magnetite-bearing quartzite (Yinnex, 1986), and chlorite–amphibole–talc schist. Mining was concentrated on three shoots on the hanging wall and footwall of the quartz–mica schist. Mine plans suggest that these shoots plunge steeply northeastwards, but drilling by Monarch Petroleum N.L. in 1980 cast some doubt on this (Yinnex, 1986). Within about 10–15 m of the mineralized zone the chlorite–amphibole–talc schists are extensively hydrothermally altered to bright green chlorite–biotite–talc schist containing vertical 'stringers' and sheets of biotite-rich material. At the contact with the quartz–mica schist there are large books of muscovite, greater than 1 cm thick. These features are consistent with K-metasomatism and hydrothermal activity, which may be related to the suite of pegmatite dykes intruding the Warda Warra Belt.

At Trixie, gold mineralization occurs in a quartz vein carrying azurite and malachite and intruding metabasalt, metagabbro, and ultramafic rock (Johnson, 1950a p. 73;



GSWA 24698

Figure 163. Geological map of Tuckanarra.

Yinnex, 1986). The area within 300 m of the main shaft contains numerous subhorizontal quartz veins, many of which are folded by northerly striking anticlines and synclines (Yinnex, 1986).

To the west of Warda Warra Hill, a number of small shafts have been sunk at the contact between a mafic–ultramafic sill and mafic schist containing several thin BIF units. At the contact, auriferous quartz stringers occur in a zone of sheared chlorite–talc–iron carbonate rock, ferruginous siltstone, and sheared metaperidotite (Yinnex, 1986).

Yalgoo

About 87% of production from the Yalgoo mining centre (Table 34) came from the Emerald Reward mine. Reed (1896, p. 41) stated that about 125 kg of gold was initially obtained from a 30 m-long 'boat-like' body of quartz. Unpublished reports suggest that the vein was inclined at a low angle southwards and was irregular, varying in thickness from 0.3 to 1 m. Subsequent mining was based on ground which had underlain the vein and formed an east-northeasterly striking zone containing quartz veins and stockworks. Most gold occurs in the quartz, but it is also erratically distributed within the talc–chlorite (–phlogopite) and talc–carbonate schist which hosts the veins. To the northwest and southeast, the mineralized unit is bounded by tremolite–chlorite rock (high-Mg basalt of the Wadgingarra Basalt). Carbonation, silicification, and K-metasomatism are the chief types of alteration. Sulphide minerals occur in places in the quartz, but are not a significant feature of the deposit. Northwesterly striking faults and shears cross the lode and contain some auriferous quartz veins. Drilling to a depth of 90 m in 1926 (Larcombe, 1927) failed to locate the Emerald Reward orebody at the projected intersection depth of 60 m. However, at 45 m, one hole (No. 3) included a 3.65 m intersection (true thickness unknown) of quartz with an average grade of 2.4 g/t gold. The drilling results suggest either that the stockwork-alteration zone is very shallow, or that it dips at a moderate to low angle in a direction not explored by the holes (unfortunately, precise hole positions were not recorded).

About 200 m west-southwest from Emerald Reward there are further workings on a quartz stockwork in ultramafic schist. The mined zone is extensively altered talc–chlorite–amphibole schist which, on the basis of adjacent less-altered rocks, probably represents high-Mg basalt. The mineralized unit occurs at the same stratigraphic level as that in the Emerald Reward mine, which suggests that the mineralization is stratabound, probably in a relatively incompetent ultramafic unit. Some 500 m to the south of these workings a quartz-vein orebody has been open-cut mined. The strike of the vein curves through 60°, from dipping 45° towards 070° in the north, to dip 80° towards 130° in the south. The vein is 0.25–0.5 m wide and is hosted by tremolite–chlorite rock.

The Yalgoo mining centre is located on the crest of the major anticline which occupies the western part of the greenstone belt at Yalgoo (Plate 2). To the south of Yalgoo greenstones have been intruded by granitoid rocks; Johnson (1950a, p. 70) recorded the presence of felsic porphyry close to the area of mineralization. Available evidence suggests that the Emerald Reward mineralization is both structurally and stratigraphically controlled, and that the orebody could be a saddle-reef lode.

Yaloginda

The Yaloginda mining centre is about 12 km southwest of Meekatharra, and consists of numerous old workings scattered along a north-northeasterly trending zone about 8 km long and 2 km wide (Fig. 164). Prior to development of Blue Bird in 1985, the more significant gold producers had been the Revenue–Rocklee group (293 kg), Karangahaki (200 kg), Black Jack (50 kg), and Romsey (38 kg). The principal workings are along two parallel zones: a western zone (including Black Jack, Monte Carlo, Revenue, Rocklee, and Kelpy) containing mineralized shears within BIF and metabasalt; and an eastern zone (including Blue Bird, Romsey, Gibraltar, and Karangahaki) of sheared ultramafic rocks veined by quartz and felsic porphyry. Workings in the western zone are located on quartz veins, whereas the eastern zone is characterized by lode deposits and forms part of the Gabanintha Shear Zone (Fig. 168).

The Black Jack group of workings is based on generally stratiform limonitic quartz veins at contacts with BIF, metasediments, and mafic schist. According to Clarke (1916) the veins are erratic, and economic mineralization is limited to a depth of 10 m. Further north along the western zone, deposits such as Revenue, Rocklee, Ecrin, Two Bells, and Monte Carlo occur as narrow (mostly less than 0.3 m) and commonly lenticular quartz veins occupying shear zones within the mafic rocks. Most of the veins occupy sheared mafic rocks and are flanked by slickensided fault planes. According to Clarke (1916, p. 184), the striae plunge north at about 45°. Clarke (1916, p. 184) also reported that the auriferous quartz veins post-date earlier quartz stringers which, in turn, post-date the main shearing. At the Revenue mine, a laterally extensive vein system has been worked to a depth of 70 m; most gold has come from a narrow high-grade (about 200 g/t gold) shoot plunging southwards at about 80°.

The Karangahaki–Romsey–Blue Bird zone of gold mineralization has proved more productive than the western zone and appears to offer more scope for future development. At Karangahaki, gold was obtained from deformed lenticular quartz and quartz–carbonate veins in a north-northeasterly striking zone of pyritic talc–chlorite schist and talc–carbonate–serpentine rock; the latter exhibits relict cumulate olivine (Farquharson, 1916, p. 256). According to Montgomery (1910, p. 40–41) the lenses of quartz range up to 6 m in width and occur in brecciated country rock, underlain to the west by shale and BIF. The structural geology of the deposit is relatively complex; the auriferous quartz veins appear to have intruded a shear zone and been subsequently deformed by further shearing and faulting. Available descriptions of the old workings indicate that the ore shoots at Karangahaki plunge vertically or very

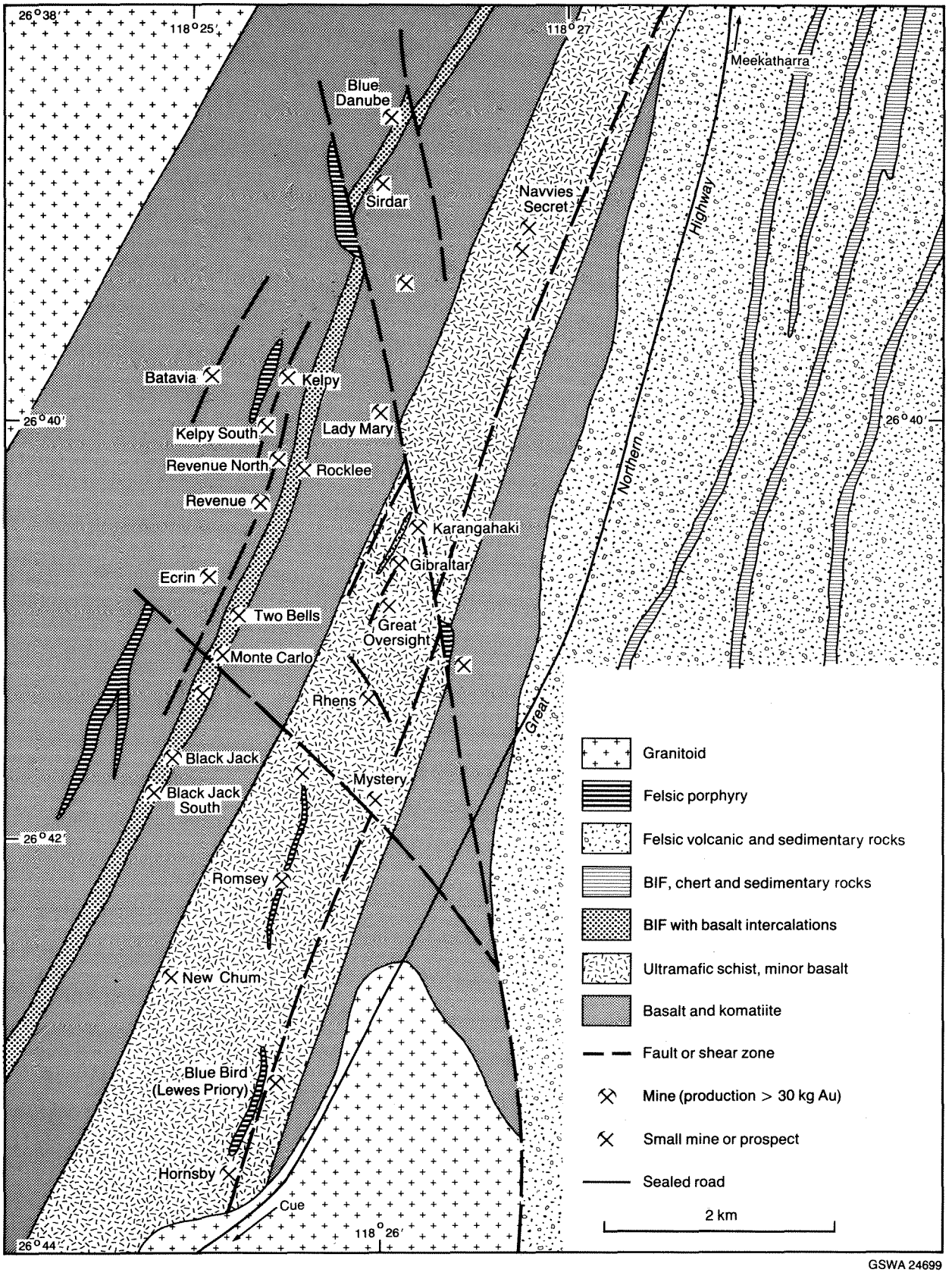


Figure 164. Geological map of Yaloginda.

steeply northwards. The controls of these shoots are uncertain, but they may be related to the relatively late deformation of the north-northeasterly striking veins.

The Gibraltar workings, about 400 m to the south-southwest of Karangahaki, are located in a 10 m-wide zone of quartz-vein stockworks within talc–chlorite schist and kaolinized felsic porphyry. The mineralized zone is inclined at about 60° east-southeast and is underlain, at a distance of about 35 m, by BIF (Montgomery, 1910 p. 43). Montgomery (1910, p. 42) described the Gibraltar deposit as a 'large quartz lode', about 13 m wide, and averaging about 8 g/t gold; however, Clarke's evidence suggests that the Gibraltar lode is a stockwork deposit rather than a single vein.

About 3 km to the south-southwest of Gibraltar are the Romsey workings, which are based on quartz veins and stockworks in a sericitized albite-porphyry dyke which has intruded sheared talc–chlorite and talc–carbonate schist. The porphyry is up to 20 m wide, extends north-northeast for more than 1 km, and locally trangresses the foliation of the schists. According to Clarke (1916, p. 197, 199) highest gold grades occur where cross-cutting quartz veins intersect longitudinal veins.

To the 31st December 1987, the Blue Bird deposit had produced 1915 kg of gold from ore averaging 2.3 g/t; published resources were 2.4 Mt of ore at 2.5 g/t gold. In addition to this production, a few kilograms of gold were produced from the Lewes Priory, Lewes Castle, Port Philip, Problem, Hornsby, and Edin Hope leases, which previously occupied part of the same ground, and dated back to 1909. Clarke (1916, p. 199–202) reported that gold mineralization in this area was associated with felsic porphyry at Lewes Priory, and with a north-northeasterly striking quartz vein through sheared 'amphibolite' (possibly including dolerite) at Hornsby. The Lewes Priory porphyry, which extends at least 1 km towards Hornsby, strikes north-northeasterly over most of its length, but at Lewes Priory it swings northwards and is flanked by north-striking shears. However, the surrounding schists continue to strike north-northeasterly and contain north-northeasterly striking shear zones. Exploration and mine development at the Blue Bird open-cut has shown gold mineralization to be in a north-striking, 40 m-wide vertical shear zone in talc–carbonate–chlorite schist. The principal orebodies are two marginal zones, 4–12 m wide, containing quartz vein stockworks and appreciable hematite after pyrite. Rocks between these zones show development of fuchsite, feldspar, and minor amounts of chert.

Other minor deposits of the Yaloginda mining centre were described by Clarke (1916) and Montgomery (1910, p. 38–46). Old workings at some of these deposits (e.g. Rhens, Mystery, and Lady Mary) show that gold mineralization is partly associated with a set of north to north-westerly striking quartz veins.

At least some of the gold deposits at Yaloginda are located at fault or quartz vein intersections; for example, Karangahaki is located at or close to, the intersection of the north-northeasterly striking vein system with a north-northwesterly trending silicified fault zone. Apart from veins parallel to the Gabanintha Shear Zone, the most commonly veined fractures strike north to northwest. This north to northwest set is probably dilational, and may be related to sinistral movement along the Gabanintha Shear Zone.

Yuin

Virtually all production recorded at the Yuin mining centre (Table 34) has come from the Royal Standard mine. The principal workings are located on a 1–2 m-wide quartz vein which dips 70° to the north and extends laterally for almost 1 km. The host rocks are sheared metabasalt and metadolerite within a sequence which, several hundred metres to the south, includes felsic volcanogenic sedimentary rocks and grey-white chert, and which is intruded by gabbro to the north. The margins of the quartz vein are lenticular, indicating late shear. An open crenulation of the tectonic foliation in the mafic host plunges east-northeast at about 50°, and is approximately aligned with elongation of the quartz lenses. The quartz contains minor amounts of sulphide and garnet. Stopes, which extend to the surface, are about 50 m deep and continuous for about 200 m in an east–west direction. According to Jutson (1914b, p. 144–145) the workings extend to a maximum depth of about 80 m and the ore shoots plunge east-northeast at a 'high angle' (i.e. parallel to the tectonic crenulation noted above). At a vertical depth of about 80 m in the main shaft, the quartz vein and the mafic schist are abruptly terminated by non-foliated microcline–biotite granite which is at least 10 m thick. The contact is tectonic and almost horizontal, and dips east-southeast at 5–10° (Jutson, 1914b, p. 146). This granite is probably part of the post-folding granitoid body which crops out to the south and east of the mine. Dykes of felsite and microgranite which intrude the mafic schist and the orebody, and strike predominantly northerly or north-northeasterly, are probably related to the granite, although no physical connection has been observed.

The auriferous quartz vein at Yuin has clearly intruded a shear zone which pre-dates the post-folding granitoid of the area. Minor deformation of the vein, related to late movement along the shear zone, appears to have influenced the geometry of ore shoots, and may have established a system of tensional fractures that was later intruded by microgranite. Subhorizontal faulting was probably the latest tectonic event.

As Jutson (1914b) noted, there appears to be scope for locating extensions of the Royal Standard mineralization, either along strike, or at depth along and beneath the subhorizontal fault.

Minor gold mining centres and localities

Table 39 summarizes the main geological features of those mining centres and isolated mines which have recorded only minor gold production. Some of these deposits were not investigated during the present study.

TABLE 39. MINOR GOLD MINING CENTRES AND LOCALITIES

Mining centre or locality	*Description*	*Reference*
Albury Heath	Sulphidic quartz veins along a northeasterly striking fault through fuchsitic talc–chlorite and talc–carbonate schist; production included in Meekatharra mining centre	-
Blackman Find	Gold mineralization occurs in a quartz vein within grey and white banded chert and volcanogenic metasediments adjacent to mafic schist	-
Bonnie Venture	Gold mineralization occurs in pyritic conglomerate and in quartz veins where these cross conglomerate units within a sandstone–shale–conglomerate sequence (Mougooderra Formation); associated tungsten mineralization	Maitland, 1919, p. 36–37; Baxter, 1978, p. 46–49; Woodward, 1915
Bourkes Find	Principal mine was 'Golden Bracelet' which produced 31.3 kg of gold from 1188 t of ore; numerous quartz veins intrude northerly striking shear zone in talc–carbonate and talc–chlorite schist of Gabanintha Formation; production included in Meekatharra mining centre	-
Bilberatha	Quartz veins and stringers in extensively altered mafic schist adjacent to jaspilitic BIF; host rocks may include mafic tuff and fine-grained volcanogenic sedimentary rocks; some lode material, probably sulphidic at depth	-
Carlaminda	'Reliance' — quartz vein intrudes tremolite–chlorite(–talc) schist and metadolerite; copper minerals common; 'Dollar' — 0.5 m quartz vein carrying minor pyrite intrudes talc–chlorite and talc–carbonate schist	Johnson, 1950
Eelya	'Jasper Queen' — sulphidic quartz veins intrude metadolerite; 'Eaglehawk' — pyrite and chalcopyrite-rich metabasalt and metadolerite contain quartz veins; 'Eelya Reward' and 'Eelya North' — gold–copper mineralization in sheared suite I post-folding granitoid	Woodward, 1914, p. 96–97; Low, 1963; Duggan, 1960b
Jillewarra - Carwell	Stratabound quartz veins in metabasalt, metadolerite, quartzite, BIF, and chloritic schist; some deposits in felsic porphyry; northwesterly striking shear zones (Mingah Shear Zone System) control most of the deposits	Johnson, 1950; Money Mining NL, 1986, p. 35–36; Elias, 1982, p. 18
Jumbulyer	Quartz veins in metabasalt and metadolerite close to BIF; quartz veins in suite I post-folding granitoid	Hobson, 1948
Kirkalocka	'April Fool' mine — gold mineralization along shear zone in metabasalt and high-Mg basalt; zone of quartz–sericite schist containing quartz stringers and iron oxide probably reflects metasomatic alteration of the mafic rock	Baxter et al., 1983
Meeka Pool	Production recorded in 1910–11 from Meeka Eldorado (GML 1054N); location data are imprecise, but Meekatharra residents advise that Meeka Pool is only a short distance south of Paddys Flat	-
Mindoolah	Quartz veins in felsic porphyry close to an intrusive contact with a post-folding granitoid	Woodward, 1914, p. 66–69; Johnson, 1950; Elias, 1982
Mistletoe	*En echelon* sulphidic quartz veins strike north to northeast in enclave of amphibole–chlorite schist (metabasalt) within granitoid rocks	-

TABLE 39. (continued)

Mining centre or locality	*Description*	*Reference*
Mount Farmer	'Lindville' mine based on quartz veins developed parallel to the foliation of mafic amphibolite; extensive alteration obscures primary lithology	-
New Australia	Northerly and northeasterly striking quartz veins in carbonated and sheared mafic and ultramafic rocks; Gabanintha Shear Zone	-
Nyounda	Shear zones, locally occupied by quartz veins, in metabasalt and metadolerite; at Kings Find part of the mineralization is hosted by BIF	Hallberg, 1976
Pinyalling	Partly in quartz veins through BIF, metasediments, and metabasalt, and partly as stratiform sulphide zones in BIF	-
Retaliation	'Julie' gold mineralization in narrow stratabound zone of silicified and brecciated shale and mudstone within a sequence of mafic schist, metadolerite, and BIF; elsewhere most workings are residual–alluvial	-
Ryansville	Gold mineralization in westerly striking quartz veins within komatiitic basalt; veins dip north at about 60° and occupy a zone of shear and tension fracturing	Johnson, 1950, p. 75
Tal Val	Quartz veins along northeasterly striking fault in ultramafic schist and BIF; Gabanintha Shear Zone and northeasterly striking Albury Heath Fault	-
Wadgingarra	Quartz veins through a variety of lithologies, including talc–chlorite schist, metabasalt, metagabbro and BIF (minor); western workings based on quartz veins through pyritic conglomerate (Mougooderra Formation)	Johnson, 1950
Warriedar	Sulphidic (pyrite and arsenopyrite) quartz veins in metabasalt, metagabbro and BIF; quartz veins are oblique to bedding, and locally bifurcate to form lodes of mafic rock with quartz stringers; at 'Highland Chief' felsic porphyry (associated with a suite II post-folding granitoid) and BIF host an auriferous quartz vein	Feldtmann, 1921; Maitland, 1919, p. 34–36; Woodward, 1915
Weld Range	Quartz vein through BIF and dolerite; highest grades at BIF contacts	Woodward, 1914, p. 70–74
Winjangoo	Western deposits consist of massive quartz veins in altered, well-foliated amphibolite near granitoid contact; southwestern deposits occur in BIF	-

Additional gold occurrences

Table 40 describes gold occurrences unrelated to existing mines or prospects, that were identified by the program of gossan analysis (Appendix II). New areas of exploration suggested by these results include Tallering Range (previously the subject of exploration for iron ore) and the Mougooderra Formation between Wadgingarra and Yalgoo. An old 1.5 m-deep test pit at the southern end of the West Wadgingarra vein revealed very early prospecting, but grades were apparently too low to encourage development.

Discussion and interpretation

Regional distribution of gold deposits

Plate 2 shows the distribution, size, host lithology, and style of gold deposits in relation to regional stratigraphy and structure. On a regional scale, economic gold mineralization is concentrated in a limited range of geological environments:

1. Almost all the gold deposits are situated in the **green-**

TABLE 40. NEW GOLD OCCURRENCES IDENTIFIED IN THE MURCHISON PROVINCE

Locality (lat., long)	*GSWA sample*	*Gold (ppm)*	*Geology*
Coombeloona Rock (27° 08' 50"S; 117° 36' 00"E)	87627	1.2	Quartz vein in BIF adjacent to intrusive contact of pegmatitic monzogranite. Associated anomalies: Mo, 33 ppm; W, 4 ppm; Zn, 170 ppm
Poona (27° 08' 20"S, 117° 26' 15"E) About 50 m north of the Poona beryl-emerald open cut (near exploration camp)	87612	0.4	Quartz vein in mafic schist; vein is large and contains narrow sulphidic zones. Associated anomalies: Zn, 4.47%; Pb, 1.5%; Cu, 1650 ppm; Ag, 36 ppm
South Cullculli (27° 07' 30"S, 118° 19' 40"E) About 2 km south of Turn of the Tide	73619	0.8	Pyritic quartz vein in clastic sedimentary rocks, chert, and BIF of the Windaning Formation.
South Pinnacles (27° 33' 20"S, 118° 01' 40"E) About 1.5 km southwest of Zadow Bore	73609C	2.5; averages 1.0 in 3 samples (A–C)	Gossan in BIF unit between dolerite and pyroxenite in Golconda Formation. Associated anomalies: As, up to 10 ppm; Cu, up to 370 ppm
Tallering Range (28° 06' 35"S, 115° 37' 30"E) Iron ore deposit T1	85709	2.0	Ferruginous chert within BIF of Windaning Formation. Associated Ba anomaly indicates metasomatism
West Wadgingarra (28° 16' 50"S, 116° 47' 25"E) About 1 km west of Wadgingarra mining centre	81379E, 85878 A–Y	Up to 9.7; averages 1.2 over 26 samples	Locally sulphidic quartz vein, about 1 m wide and 150 m long, strikes parallel to bedding of sandstone and conglomerate in Mougooderra Formation. Associated anomalies: W, up to 4250 ppm; As, up to 121 ppm; Cu, up to 600 ppm

Note: All samples are listed in Appendix II (Data File II.4), except sample 85709 (Data File II.3).

stone belts, although these occupy only 12 per cent of the province.

2. Most gold deposits are located on, or within 1 km of, the area's **major faults and shear zones**.

3. Gold deposits generally occur within 2 to 3 km of granite–greenstone contacts, and there appears to be a strong correlation between gold deposits and the location of **post-folding granitoids**.

4. Almost 90 per cent of mines with production exceeding 30 kg of gold occur in the Golconda, Gabanintha, and Windaning Formations of the **Luke Creek Group**.

Less immediately evident from Plate 2, is a major difference in the historical productivities of the northeastern and southwestern halves of the province. The northeast, including the important mining areas of Mount Magnet, Cue–Day Dawn, and Meekatharra, has a total recorded gold production which, when averaged over the area of greenstones, exceeds 31 kg Au/km^2; however, the equivalent figure for the southwest is only 1.7 kg Au/km^2. These regional observations have important metallogenetic implications for gold mineralization in the province.

Lithological associations of gold deposits

Studies in other Archaean granite–greenstone terranes have established that certain lithologies host far more gold deposits than others (Groves et al., 1986; Colvine et al., 1988). Figure 165 presents a statistical comparison between the overall lithological composition of Murchison Province greenstone belts, and gold deposit (>30 kg Au) host lithology. All post-folding granitoid intrusions have been included in this analysis because these also host several deposits. It is immediately evident that, when the entire province is considered, BIF–chert and ultramafic rocks are the preferred host rocks to gold deposits; this is true both with respect to deposit frequency and productivity. Felsic porphyry also emerges as a preferred host despite the fact that its outcrop area is far too limited to be shown on the areal distribution diagram. However, data in Figure 165 represent the lithological distribution for the province as a whole and it is clear from field evidence that

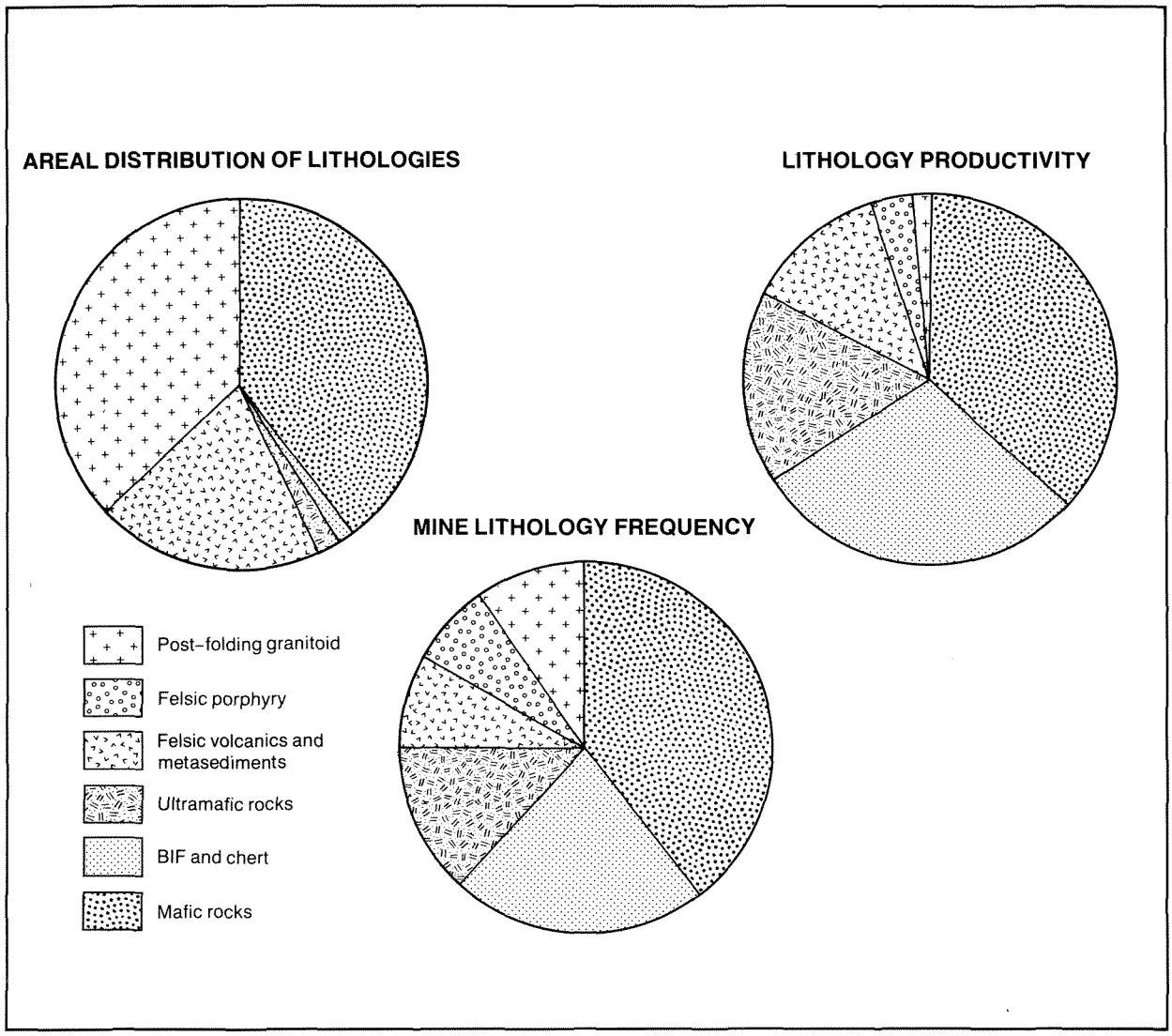


Figure 165. Lithological associations of Murchison Province gold deposits (production >30 kg Au).

there are significant regional differences in preferred host lithology and mineralization style. Based on these differences the province is divided into four areas on Figure 166, referred to as 'metallogenetic domains'. The statistical treatment undertaken in Figure 165 is repeated for each of these domains in Figure 167.

Although the compositions of the four domains are broadly similar there are major differences in preferred host lithology and appreciable differences in productivity per km^2 of greenstones. The Meekatharra domain is dominated by shear-zone deposits in a thin ultramafic member near the base of the Gabanintha Formation. In contrast, the Mount Magnet domain contains principally BIF- and chert-hosted deposits within the Golconda Formation, whereas the Cue domain is, with the exception of Big Bell, dominated by deposits in mafic rocks of the Gabanintha Formation. The general characteristics of ultramafic-, BIF–chert-, and mafic-hosted gold deposits are described later ('Gold deposit types and associated alteration'). Figure 167 also demonstrates the extremely low productivity of the Yalgoo domain, equivalent to the southwestern half of the province (Fig. 166). In terms of gold metallogeny, there is probably a strong case for further subdivision of the Yalgoo domain since geological controls at its various component mining centres differ considerably; however, the small number of significant deposits, and consequently the limited geological information available, currently makes this impractical.

Discussion of possible reasons for the differences outlined above is deferred until factors such as structural controls and ore-fluid sources have been described.

Structural controls

The spatial association of gold deposits with major faults and shear zones appears to be a more or less universal feature of Archaean granite–greenstone terranes (e.g. Phillips and Groves, 1983; Colvine et al., 1988), and has been recognized in Western Australia for many years (e.g.

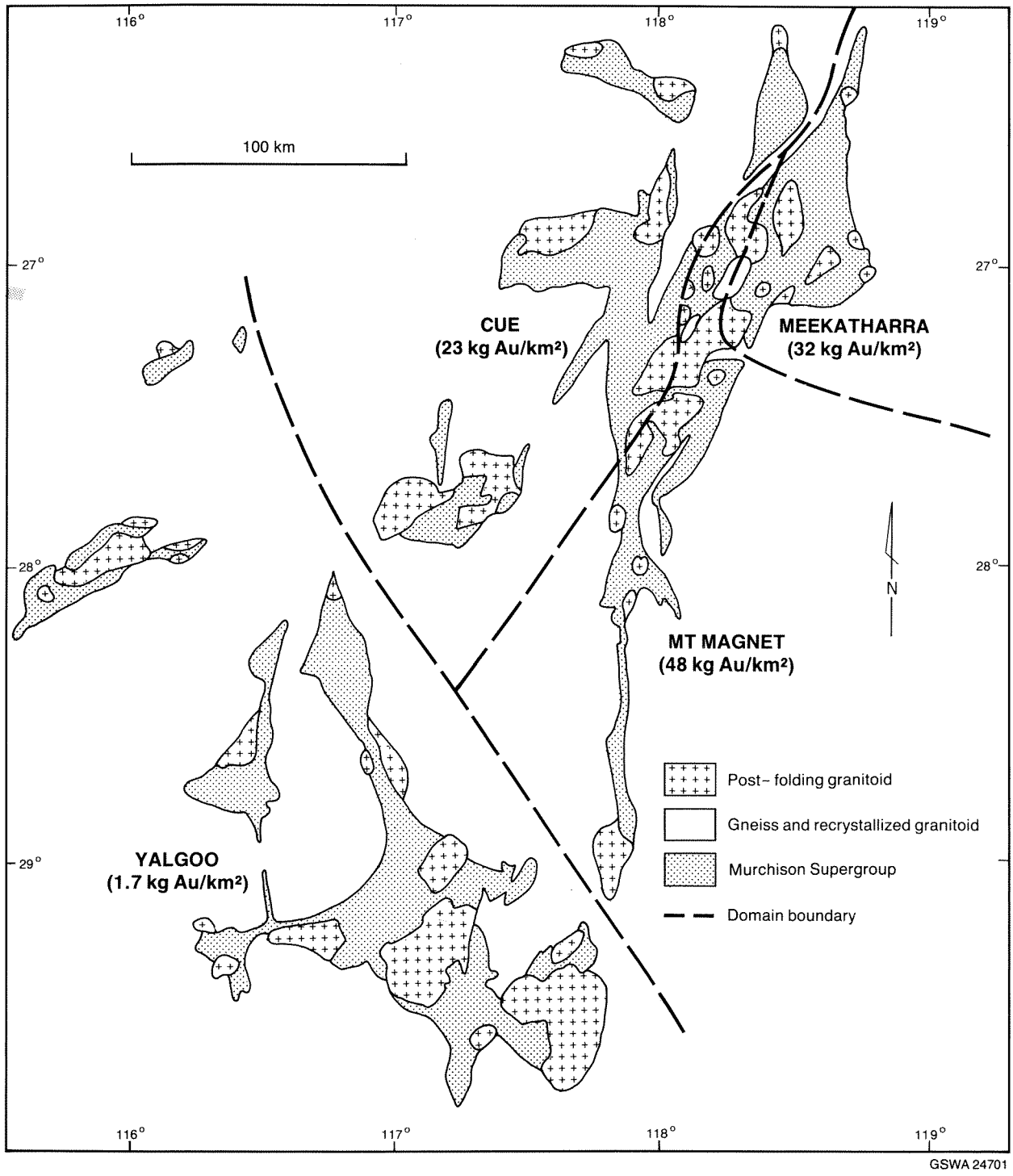


Figure 166. Metallogenetic domains (gold) of the Murchison Province.

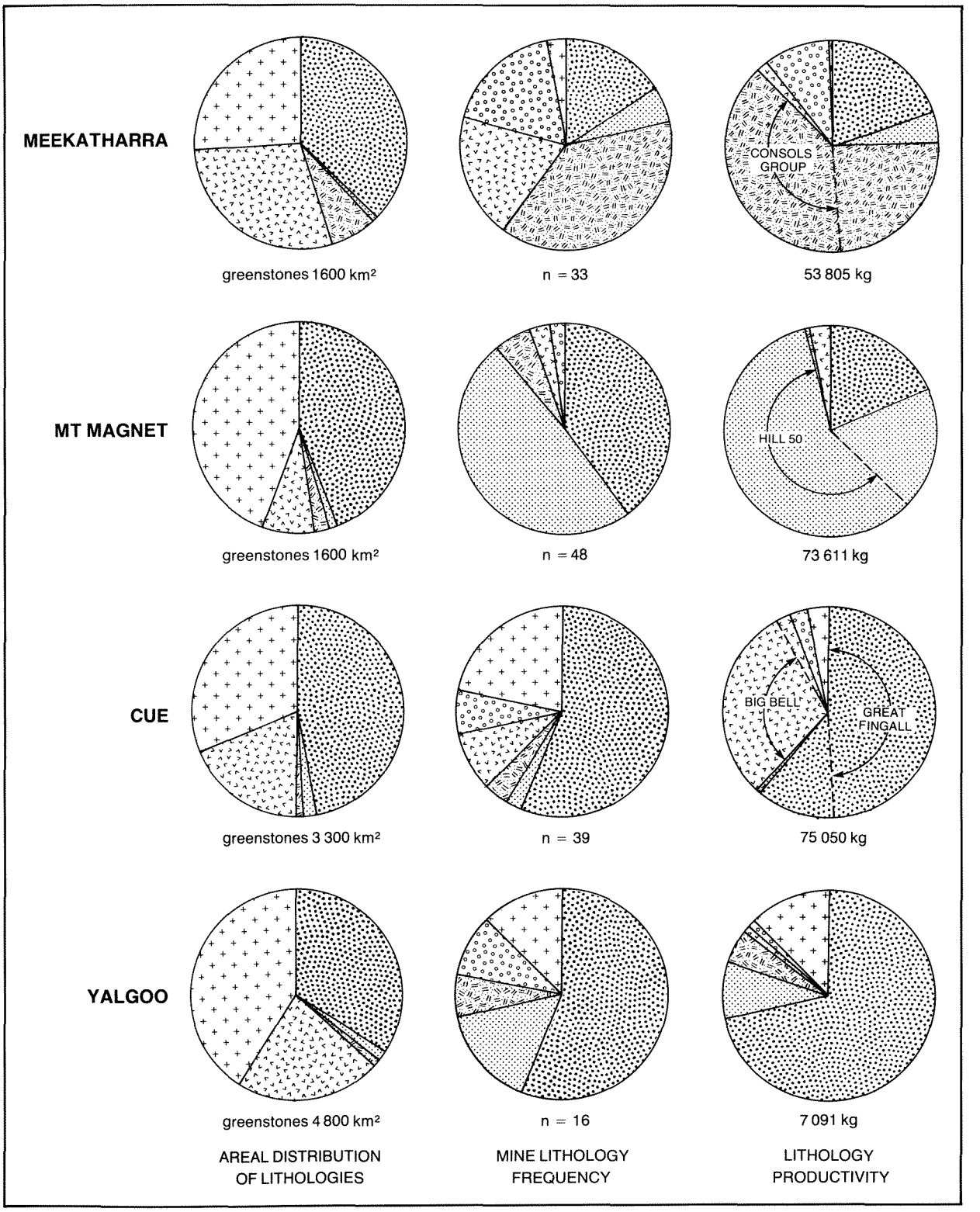


Figure 167. Host lithologies of the four metallogenetic domains of the Murchison Province, showing domain composition, host-rock frequency in mines, and relative productivity. Legend as for Figure 165.

Maitland, 1919). The proximity of gold mineralization to faults and shear zones, combined with evidence from mine geology, strongly supports an epigenetic origin for almost all the gold deposits. Here, as in other granite–greenstone terranes, it is considered that the major crustal fractures have acted as conduits for gold-bearing hydrothermal fluids.

The distribution, structure, and tectonic relationships of the major faults and shear zones are discussed in Chapter 5. Because the precise location; form, and size of gold deposits within these deformation zones is largely dependent on relatively small-scale structures, and structure–lithology relationships, further description is now appropriate. For ease of reference, the major faults and shear zones are named on Figure 168. The total historical productivities of all deposits on, and within 1 km of, each of the deformation zones are presented in Table 41. Ninety-one percent of total gold production in the Murchison Province has come from these 13 productive zones.

The major faults and shear zones are mainly of D_4 age, but the Gabanintha Shear Zone is a D_1 layer-parallel structure which has been folded by the large F_3 syncline southeast of Meekatharra, and displaced some 10 km by the D_4 Mount Magnet Shear Zone. In detail, certain of the other shear zones show evidence of more than one sense of movement and it is possible that some have a history predating D_4. Progressive or multiphase deformation is locally evident from mine geology (e.g. Paddys Flat at Meekatharra) where early veins are deformed and cross-cut by later ones.

The width of the shear zones, degree of deformation, and stratigraphic displacement across them suggest relative movement of kilometres or tens of kilometres. Where major movement of this magnitude is involved it must be predominantly subhorizontal, as metamorphic grade on either side of the dominantly post-metamorphic shear zones is not appreciably different. This conclusion is supported by mine geology in which fracture systems are generally consistent with dextral strike-slip movement; only the Day Dawn and Noongal Shear Zones are clearly sinistral. However, some shear zones and faults do record vertical movements (Chapter 5). The Chulaar Well and Salt River shear zones have dominantly vertical movements (Fig. 168), which on the Chulaar Well shear zone, at least, were pre-metamorphic (Chapter 5).

TABLE 41. HISTORICAL GOLD PRODUCTION (TO 31 DECEMBER 1987) OF DEPOSITS ASSOCIATED WITH THE MAJOR FAULTS AND SHEAR ZONES OF THE MURCHISON PROVINCE

Fault/shear zone	*Gold production (kg)*
Boogardie	45 758
Big Bell	22 760
Cuddingwarra	2 577
Salt River	-
Chulaar Well	-
Day Dawn	51 375
Fields Find	1 230
Gabanintha	40 178
Jumbulyer	60
Mingah	175
Mount Gibson	2 447
Mount Magnet	25 202
Noongal	307
Paynes Find	2 493
Reedy	13 365
Total	**207 927**

Gold deposition in, and adjacent to, the major faults and shear zones would have occurred preferentially in those sections containing highly permeable local structures, particularly dilational structures such as tension gashes, riedel shears, jogs, and pull-aparts at fault bends. Locally dilational sections of longitudinal shears and oblique P (pressure) shears (e.g. Paddys Flat) also provided conduits for ore fluids, as did dilational jogs (? Big Bell) and breccia zones (Mount Magnet). High permeability would have permitted the passage of large volumes of hydrothermal fluid, thereby increasing the potential for gold precipitation through fluid–wallrock interaction. Within these areas of high permeability economic-grade gold mineralization generally formed in ore shoots following the intersections between the conduits (fractures) and particular lithological units (e.g. dolerite at Day Dawn, BIF units at Nannine, and mafic xenoliths in post-folding tonalite at Cue).

Almost all of the epigenetic gold deposits in the Murchison Province are genetically related to major faults and shear zones, but some deposits, such as the D_2 shear-hosted lodes at Star (Mount Magnet), are associated with more local structures. Though apparently few in number, these deposits, like those in the D_1 Gabanintha Shear Zone, are significant in establishing epigenetic gold mineralization prior to D_4.

Association with post-folding granitoids and minor intrusions

The 57 identified post-folding granitoid plutons occupy a total area of 6600 km^2; all occur within, or at the margins of, greenstone belts, but, given this constraint, are otherwise evenly distributed across the province (Fig. 167). There are few areas in the greenstone belts more distant than 10 km from an exposed post-folding granitoid contact (Plate 2) and some of these areas may be underlain by post-folding granitoid plutons. About 40% of the greenstones occur within 3 km of an exposed post-folding granitoid contact, but 70% of gold production has come from these marginal zones.

The spatial association between gold deposits and the contacts of post-folding granitoid intrusions is considered to be at least partly coincidental in that the tectonic and metamorphic environments responsible for the generation and migration of granitic magma and gold-bearing hydrothermal fluids were probably similar. As noted in Chapter 5, emplacement of the post-folding granitoids was, like gold deposits, partly controlled by the location of the major faults and shear zones.

Gold deposits in the Superior Province of Canada have a close spatial association with late plutonic intrusions

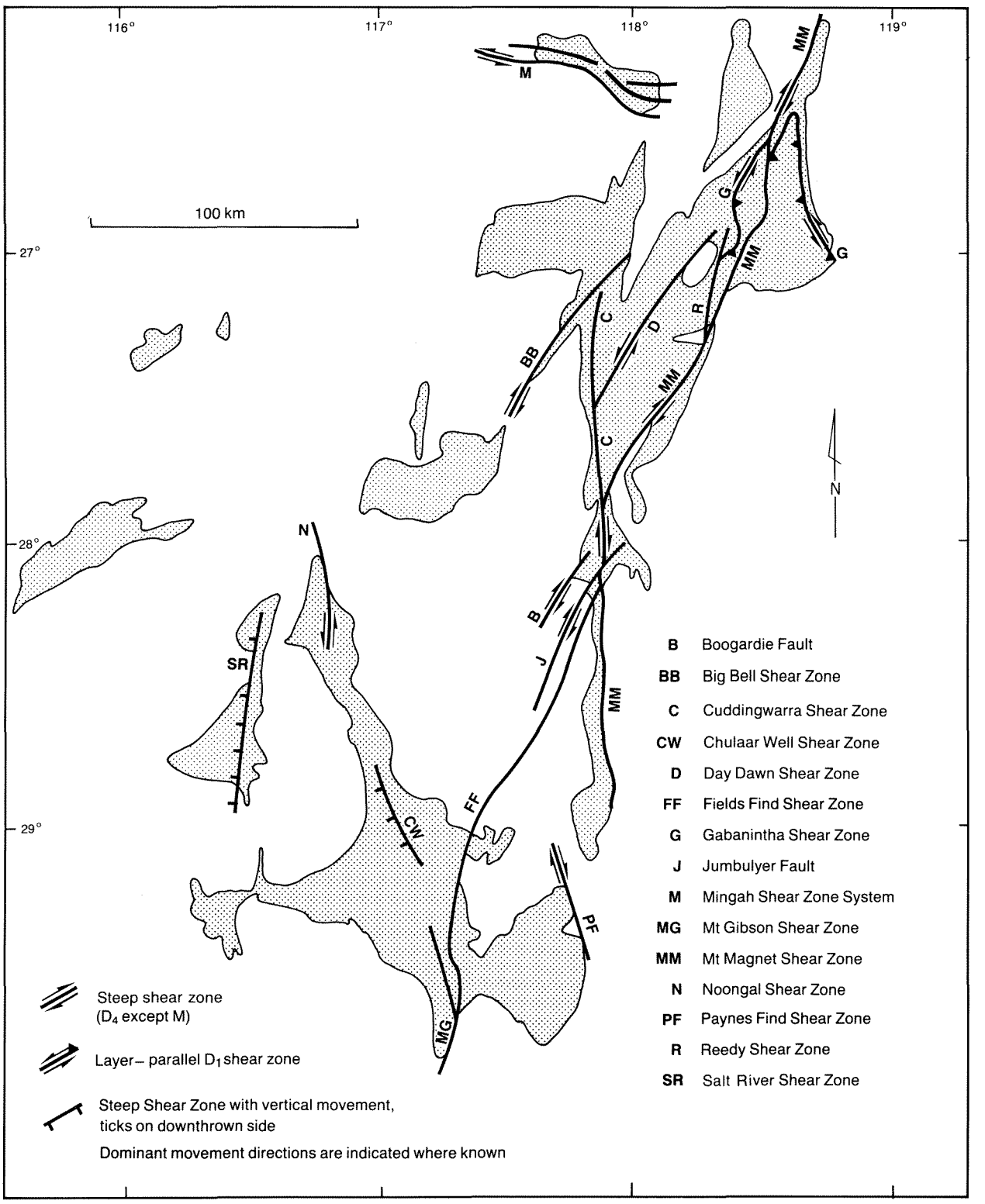


Figure 168. Major shear zones and faults of the Murchison Province.

including silica-undersaturated varieties (Colvine et al., 1988), although a clear genetic link has not yet been established. None of the post-folding granitoid intrusions in the Murchison Province are silica-undersaturated, but the suite I post-folding granitoids of the northeastern area contain much less free quartz and are markedly more sodic than suite II intrusions in the southwest (see Chapter 3).

The low average gold contents of granitic rocks provides some evidence against granitic magma being a primary source of gold in epigenetic deposits. However, granitic magma may have played a role in transporting metamorphically derived gold-bearing fluids from the lower crust. With reductions in pressure and temperature as the magma entered the upper crust, such fluids would have been released (Colvine et al., 1988). It is also possible that the post-folding granitoid plutons generated gold-rich metamorphic fluids by dehydration of greenstones along their paths of ascent (a process postulated by Andrews et al., 1986; Skwarnecki, 1987). The plutons may have provided sufficient heat during ascent and emplacement to drive large-scale convection of fluids produced by regional metamorphism. Perring et al. (1987) have suggested that thermal convective circulation of metamorphic fluids (Etheridge et al., 1983) could continue for some time after peak metamorphism.

The presence of sills and dykes of felsic porphyry in many gold deposits could provide some indirect evidence of a link to the post-folding granitoid plutons. Although no detailed mapping or geochemical studies have been undertaken to show that the felsic porphyry intrusions represent peripheral phases of post-folding granitoids, a marked spatial relationship suggests that this is commonly the case (e.g. Paddys Flat, where porphyry becomes more common northeastwards towards the post-folding granitoid intrusion between Meekatharra and Sherwood, Fig. 158). In all granite–greenstone terranes, the presence of felsic porphyry in faults and shear zones is regarded as an indication of gold potential, although these late-stage felsic intrusions are unlikely to have contributed significant gold to the zones of mineralization in which they occur. Their relationship to gold deposits may centre on common structural control of emplacement, combined with either contact metamorphic concentration of existing gold mineralization, or provision of physically suitable host rocks during later mineralization. Where felsic porphyry hosts economic gold mineralization this usually occurs in quartz stockworks or stringers in zones of brittle deformation (e.g. at Ingliston Extended, Ingliston South, Ingliston United, Paddys Flat), showing porphyry intrusion to pre-date gold mineralization.

The debate over the relationship between gold mineralization and felsic intrusions is similar to that concerning the genetic importance of lamprophyres within and adjacent to epigentic gold deposits (Rock et al., 1987, 1988; Rock and Groves, 1988; Wyman and Kerrich, 1988). The present study identified no lamprophyres in the Murchison Province, but Rock et al. (1988) stated that a 0.45 m-wide altered spessartite dyke occurs in drill core at Day Dawn; recrystallized and metamorphosed minette has also been found in mine dumps at Yalgoo. Field identification of extensively altered lamprophyres is extremely difficult, but if future geochemical studies were to reliably establish the widespread occurrence of such intrusions in faults and shear zones of the Murchison Province it would indicate that these structures almost certainly extend through the crust into the mantle. This would support the possibility of mantle-derived ore fluids, but not necessarily imply that the lamprophyres themselves constituted a source of gold (Wyman and Kerrich, 1988).

Stratigraphic controls

Of the 136 epigenetic gold deposits which have yielded more than 30 kg of gold, four are hosted by the Mount Farmer Group, and 19 by granitoid rocks and felsic porphyry. Within the Luke Creek Group, three deposits occur in the Murrouli Basalt, 24 in the Golconda Formation, 66 in the Gabanintha Formation, and 20 in the Windaning Formation. The concentration of gold deposits in the Luke Creek Group is predictable, assuming that channelling of ore fluids along the fault and shear zone conduits was essentially upward. Gold precipitation would have occurred in the lowest crustal material providing favourable pressure–temperature conditions, suitable chemistry (e.g. Fe-rich composition for sulphidation reactions) and structural traps. Across most of the province only the Luke Creek Group satisfied all these requirements. Evidence from individual mining centres, such as Mount Magnet, indicates that within the Luke Creek Group, gold deposition occurred over substantial vertical intervals of particular fracture systems, with certain lithologies and structures being selectively mineralized.

The observation that only three significant gold deposits occur in the basal formation can be partly explained by the restricted distribution of this unit (Plate 2), and by the fact that at the surface it is rarely intersected by major faults or shear zones.

No evidence has been obtained to suggest any syngenetic gold concentrations, other than in the Cu–Zn deposit at Golden Grove. Geochemical analyses of BIF units outside the immediate vicinity of gold deposits reveal gold contents of less than 10 ppb. For example, of 39 BIF samples from the Mount Magnet area, only one (sample 81188) contained significant gold (0.33 g/t), and this was collected within 100 m of the Eclipse mine.

Gold deposit types and associated alteration

Epigenetic

Almost all of the gold deposits in the Murchison Province are clearly epigenetic in origin. Subdivision of epigenetic gold deposits into types or classes can be achieved on the basis of host lithology, structure, or metamorphic grade (Groves et al., 1985). In the Murchison Province, the simplest and most widely applicable subdivision is one based on a combination of lithological and structural features. This subdivision is particularly appropriate because

it also serves to highlight the main differences between the Meekatharra, Mount Magnet, and Cue metallogenetic domains (Figs 166 and 167).

Three main types of epigenetic gold deposit can be recognized in the Murchison Province (Fig. 169):

Type 1: basalt-hosted and, less commonly, dolerite-hosted quartz vein deposits;
Type 2: ultramafic schist-hosted, and less commonly mafic schist-hosted, shear zone deposits;
Type 3: BIF-hosted and chert-hosted deposits.

Basalt- and dolerite-hosted quartz vein deposits

Basalt- and dolerite-hosted deposits are typically single quartz veins, or simple quartz or quartz–carbonate vein systems, occupying tensional fractures, faults or narrow shears. Country rocks are massive or only weakly foliated, and wall-rock alteration (sulphidation, silicification, carbonation, chloritization, and K-metasomatism) is confined to very narrow (generally less than 1 or 2 m) zones of localized shear and veining. Economic gold mineralization is generally restricted to the main vein(s), where it is medium- to high-grade, and occurs in narrow shoots (commonly vein width) with strike lengths up to about 100 m (e.g. Long Reef at Lennonville). Where several shoots occur in one vein their plunge orientations are generally similar, reflecting repetitions of wall rock, or structural control along strike. Highest grades are commonly located in the thickest sections of veins (e.g. Great Fingall at Day Dawn), which probably indicates the importance of ore-fluid volumes and greater wall-rock interaction. Wall rocks show retrograde alteration consistent with gold mineralization occurring after peak metamorphism. Limited geological data (e.g. Victoria United, Noongal and Gnows Nest, Messenger Patch) show wall-rock enrichment in K, Ba, Rb, Sr, Pb, and H_2O and depletion in Na, Ca, and Mg.

Ultramafic-hosted shear zone deposits

Ultramafic-hosted epigenetic gold deposits occur in wide (0.5–1 km), regionally extensive and pervasively sheared zones. Mafic rocks may form a minor component, but in areas where mafic rocks predominate deformation is typically non-pervasive and gold deposits are of the basalt-

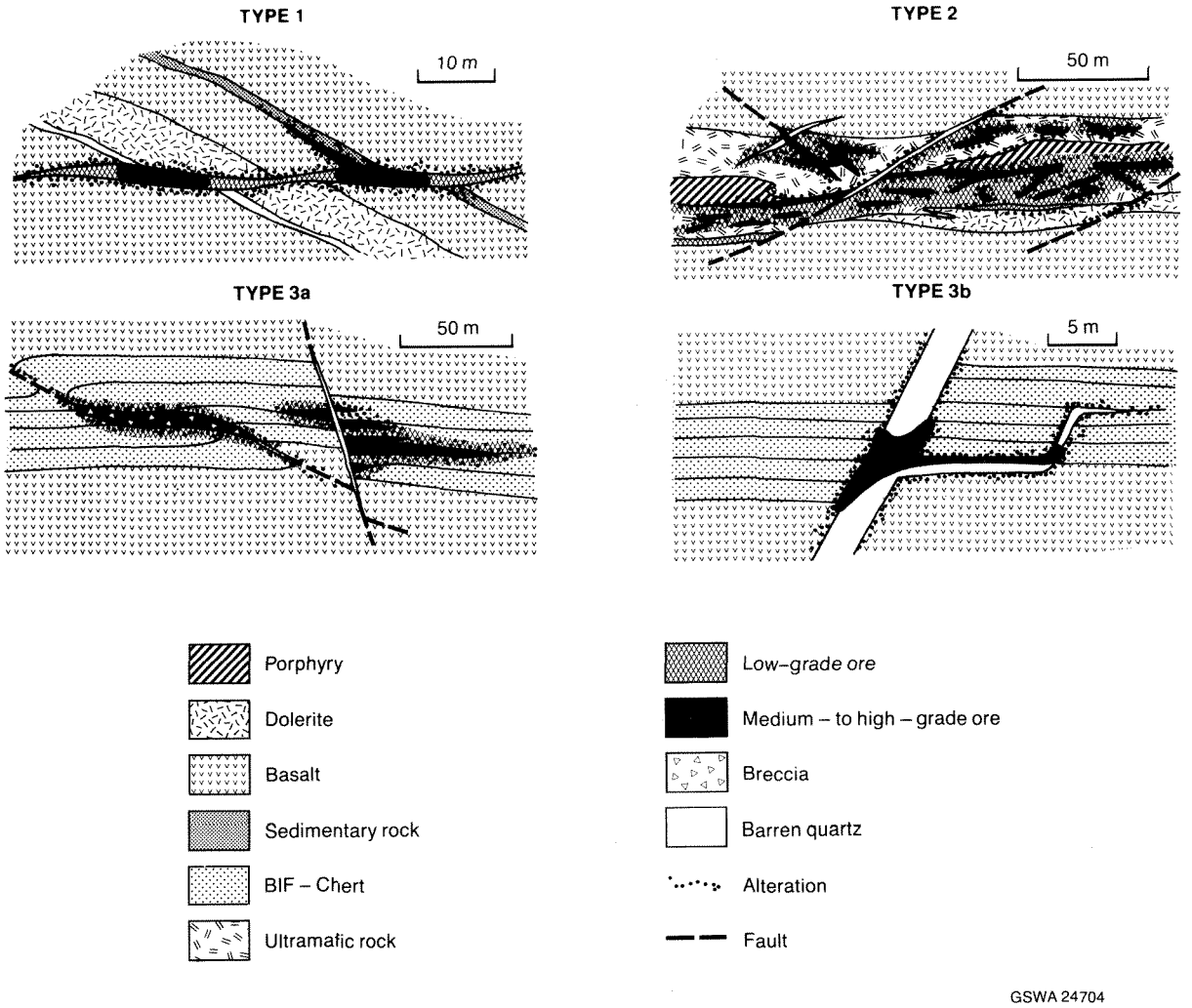


Figure 169. Principal types of Murchison Province gold deposits.

and dolerite-hosted type (e.g. Day Dawn and Lennonville). All the major ultramafic-hosted deposits are located in the Meekatharra–Reedy area (Fig. 167). They are composed of extensively altered rocks including talc–chlorite, talc–carbonate, talc–tremolite, and tremolite–talc–phlogopite schists. Numerous quartz veins and veinlets are present, but are generally lenticular and discontinuous. Quartz–feldspar porphyry intrusions are common, and high gold grades occur locally at the margins of these intrusions where pyrite, arsenopyrite, fuchsite (chrome mica) and sericite are well developed. Gold mineralization is not confined to the quartz veins and porphyry contacts, but extends into the ultramafic schist — a feature which has recently permitted large-scale open-cut mining (e.g. Phar Lap, Bluebird, and Gabanintha).

BIF- and chert-hosted deposits

BIF- and chert-hosted gold deposits take two forms:

(a) stratabound sulphide-rich and commonly brecciated lenses; and
(b) erratic high-grade shoots at intersections with fault and quartz veins (Fig. 169).

In both cases, gold precipitation was structurally controlled, and triggered by sulphidation of oxide-facies BIF (Phillips et al., 1984), or, where chert is the host, ore-fluid interaction with some other lithology such as tuff or carbonaceous shale. Stratabound orebodies are commonly wide, and extend to depths of several hundred metres (e.g. deposits in the Hill 50 area at Mount Magnet), whereas the narrow shoots associated with cross-cutting faults are typically short, isolated, and sub-economic below the zone of supergene enrichment (e.g. Lake Austin, Mainland, and Yaloginda). Alteration is largely confined to the orebodies and their immediate wall rocks.

Other epigenetic deposits

Other types of epigenetic gold deposit are hosted by felsic porphyry, granitoid rocks, felsic-volcanogenic sedimentary rocks, and sandstone–conglomerate.

Sills and semi-concordant sheets of felsic porphyry within ultramafic schist locally contain quartz-stockwork gold deposits. These probably orginated by pressure fracturing when hydrothermal fluids were preferentially injected along the conduits provided by sheared porphyry–schist contacts. At Paddys Flat, pyrrhotite is intimately associated with the quartz stockworks; pyrite and arsenopyrite occur throughout the porphyry sills and in adjacent schist. The main types of alteration are sericitization, carbonation, and chloritization; fuchsite is common close to sill margins.

Felsic porphyry also hosts gold mineralization within mafic rocks (e.g. Cuddingwarra, Noongal, and at the Windbag mine, Mount Magnet) and granitoids (Cue); all these deposits are associated with quartz veins. Extensively sheared porphyry has been mined at Mugga King (Gullewa), where associated elevated Cu, Pb, and W levels, and a nearby massive sulphide (Cu–Pb) gossan, indicate that gold mineralization is atypical and may be genetically related to porphyry intrusion.

Granitoids host significant (>30 kg Au) gold deposits at Cue, Goodingnow, and Nannine. Mineralization takes the form of quartz veins developed in transverse tensional fractures and minor shears within major shear zones. Ore shoots are generally controlled by vein intersections with the main, longitudinal schistosity of the shear zones, with other veins, or with mafic xenoliths. Associated mafic rocks are carbonated, chloritized, and K-metasomatized, but the granitoids are less altered.

Gold deposits hosted by felsic volcanic and fine- to medium-grained clastic rocks occur at Abbotts, Garden Gully, Reedy (Turn of the Tide and Cullculli North) and Quinns. Big Bell is also included in this group, although extensive alteration and metamorphism makes the protolith of this deposit uncertain. The orebodies at Abbotts, Reedy, and Quinns are relatively simple quartz veins, whereas that at Garden Gully is a silicified shear. Wall-rock alteration in these deposits includes albitization, sericitization, carbonation, chloritization, and local development of tourmaline.

The Big Bell deposit is unique in the Murchison Province. It is a pyritic quartz–muscovite–K-feldspar schist lode hosted by upper-amphibolite facies metasediments, felsic volcanic rocks, and basalt. Mineralogical and geochemical evidence (Chown et al., 1984; Phillips and de Nooy, 1988) establishes that gold mineralization occurred before peak metamorphism, and is assumed to have occurred in greenschist facies. The deposit is located in a major shear zone, probably in a dilational jog. A notable feature of the deposit is the absence of carbonate alteration, which reflects metamorphic decarbonation (Phillips and de Nooy, 1988).

Sandstone- and conglomerate-hosted auriferous quartz veins occur in the Mougooderra Formation at Bonnie Venture and Wadgingarra. Mining has been on a small scale and restricted to sections where the veins are hosted by pyritic conglomerate. Anomalous gold contents in the conglomerate units remote from the old workings suggest that the deposits may contain mobilized placer gold (see below).

Syngenetic

Evidence of syngenetic gold mineralization is extremely limited in the Murchison Province. Apart from gold which will be obtained as a by-product of mining the stratabound Cu–Zn mineralization at Golden Grove, it appears that if syngenetic concentrations do exist they are at levels far too low to be economic.

Archaean placers

Conglomerate-hosted gold mineralization occurs in the Mougoodera Formation of the Yalgoo–Singleton green-

stone belt. As noted above, those deposits which have been mined are associated with quartz veins and minor shears, but high background gold contents are present in the pyritic conglomerate units along strike. Detrital gold is assumed to have been derived by erosion of early epigenetic, and possibly syngenetic, deposits in the Luke Creek Group.

Cainozoic placers

Table 34 shows total 'alluvial' gold production to be 1539.3 kg, which represents 0.68% of total gold production in the Murchison Province. The most productive alluvial deposits have been those at Cue, Lake Austin, and Nannine. At Cue, a large amount of coarse gold was obtained from residual sand and locally derived colluvium in the Volunteer–Gem of Cue–Light of Asia area. This gold originated through weathering and breakdown of epigenetic deposits hosted by quartz veins in granitoid rocks. The Lake Austin and Nannine deposits represent colluvial outwash from nearby BIF-hosted epigenetic deposits. Supergene enrichment of the latter produced exceptionally high-grade gold concentrations close to the surface; a large quantity of unrecorded gold production, in the form of nuggets and grains obtained during the early years of prospecting (1890–1897), must have come from both areas. No deep leads have been mined, but it seems probable that this type of deposit exists in areas such as Lake Austin, Nannine, Mount Magnet, and Meekatharra where large amounts of gold have been eroded from epigenetic deposits.

Laterite-hosted deposits

Laterite-hosted gold mineralization occurs at Mount Gibson, Retaliation, Reedy, Tuckabianna, and Cuddingwarra. The main producer is currently Mount Gibson, but significant production is also anticipated from Tuckabianna and from deposits adjacent to Kurara and Rand at Reedy.

It is significant that all the known laterite-hosted gold deposits occur within 1 km of Archaean epigenetic deposits. Lateral transport of gold has been minimal and some of the deposits are partly residual. Gold enrichment zones in laterite profiles are largely the result of precipitation at water-table redox barriers (Hickman and Keats, 1990).

Supergene enrichment

Supergene gold enrichment, associated with chemical weathering (Mann, 1984a, 1984b), is a common feature in Murchison gold deposits. This secondary concentration of gold in the zone of weathering explains the observation that many mines proved to be uneconomic below a depth of about 100 m. Reprecipitation of gold has produced discrete high-grade zones associated with quartz vein- or fault-hosted deposits, or larger, irregular shaped areas of low-grade enrichment in the wide shear zones.

Regional productivity variation

The differences in historical gold production between the northeastern and southwestern parts of the province (Fig. 167) suggest that the greenstones of the northeast contain more gold. Information already presented on relationships between the epigenetic gold deposits and lithology, structure, granitoid intrusion, and stratigraphy indicates that this difference cannot be entirely attributed to any single factor. Rather, it is probably best explained as due to a combination of variables such as ore-fluid source and composition, availability of conduits and suitable depositional sites, and, with respect to the extreme southwest, regional differences in erosion level.

Geochemical and isotopic differences between the post-folding granitoid plutons of the northeast and southwest indicate significant compositional and age differences in the crustal source rocks for these granitoids. Post- folding granitoid intrusions in the southwest were mainly derived by partial melting of siliceous granulite whereas those in the northeast originated by partial melting of mafic crustal material (Chapter 3). Since most of the epigenetic gold deposits were emplaced in the same areas and at essentially the same time as the post-folding granitoid intrusions, it is likely that the gold-bearing hydrothermal fluids and granitic magmas came from the same general source regions. If this is the case, the more mafic source material in the northeast would have contributed more gold to hydrothermal fluids than would the siliceous granulite of the southwest. The low background levels of gold in granitoids and granitic gneisses, and the mineralogical setting of gold in such rocks, significantly downgrades them as potential source rocks (Saager and Meyer, 1984). Mafic rocks generally contain more gold, which tends to occur in sulphides; gold is far more easily liberated from sulphides than from the rock-forming silicate and oxide minerals (Keays and Scott, 1976; Keays, 1984; Groves et al., 1984).

The northeastern part of the province contains more major faults and shear zones than the southwest (Plate 2, Fig. 168). Therefore, a better 'plumbing system' for migration of gold-bearing hydrothermal fluids existed in the northeast.

Although the general lithological compositions of greenstones in the northeast and southwest are similar (Plate 1 and Fig. 167), the greenstone belts of the southwest possess fewer mafic and Fe-rich formations because of the absence of the Murrouli Basalt and Golconda Formation in this area. Tectonic duplication of the succession may also be more significant in the northeast. Figure 170 shows that the greenstone belts of the northeast are thicker, with more abundant BIF, and mafic and ultramafic rocks, and that (particularly in view of the greater frequency of conduits noted above) there are more numerous potential depositional sites.

Fluid inclusion studies in various areas of the Yilgarn Craton have indicated that epigenetic gold mineralization generally occurred over a P–T range of 100–250 MPa and 250–350°C (Ho, 1987). Almost all greenstones in the Murchison Province exhibit regional metamorphic (M_3) grades above this range. Epigenetic gold mineralization, on the basis of its relations to post-folding granitoid intrusions, occurred after peak metamorphism. P–T conditions

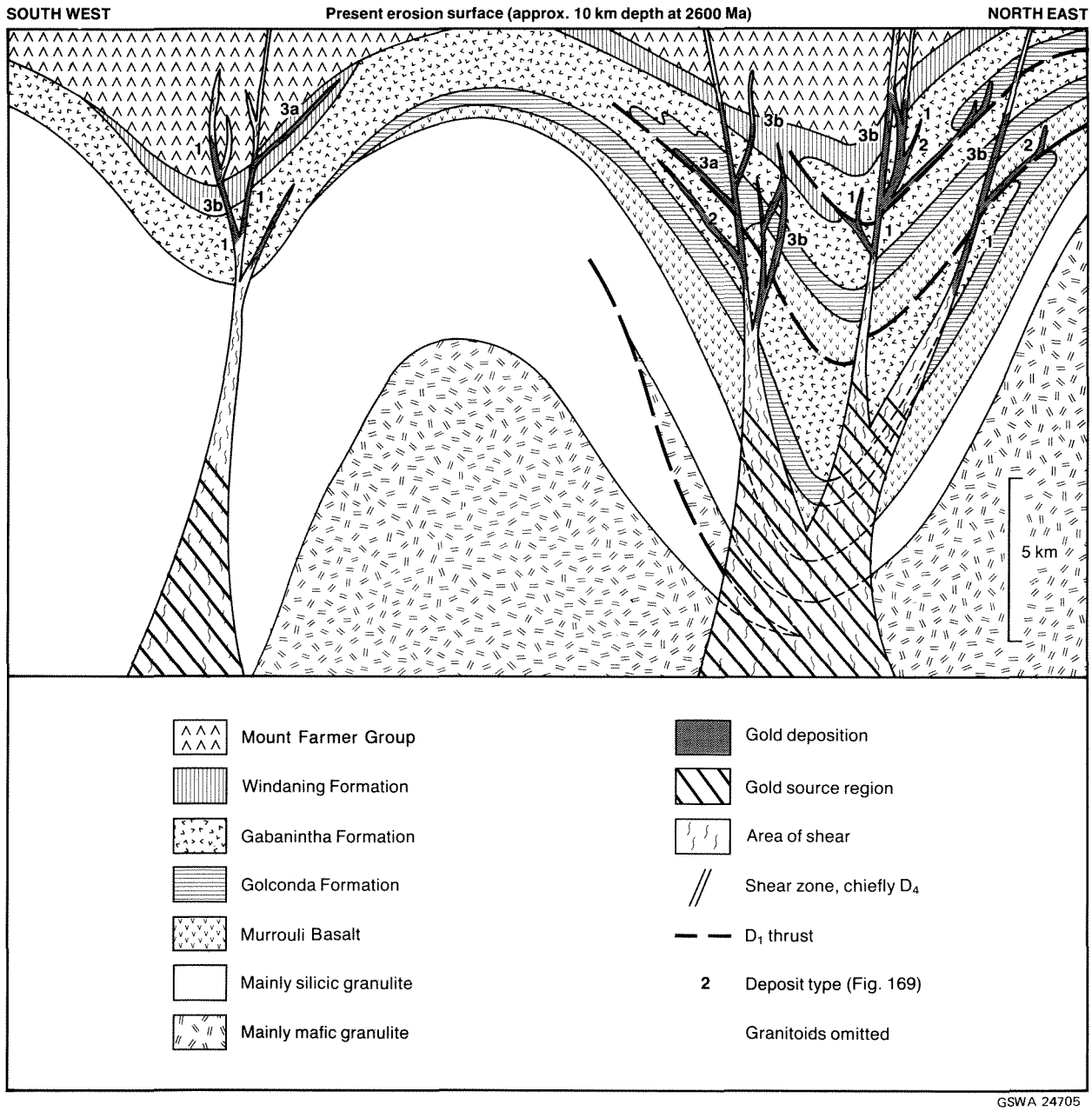


Figure 170. Differences in gold mineralization, northeastern and southwestern parts of the Murchison Province.

of mineralization, indicated by fluid inclusions and mineral assemblages in gold deposits, were retrograde with respect to the metamorphic grade of surrounding greenstones. Metamorphic grades in the extreme southwest of the province are higher than those in the northeast (Plate 3), and may reflect deeper erosion, and possibly removal of some gold deposits from this area.

Relations to crustal evolution

Field relations and isotopic data establish that Archaean gold mineralization in this part of the Yilgarn Craton was not a single event, but spanned a period of 400 Ma (Table 42). The age of syngenetic base-metal associated gold mineralization at Golden Grove is well constrained by Pb–Pb and Sm–Nd data at c. 3000 Ma (Chapter 2). Part of the gold mineralization in the Gabanintha Shear Zone is probably the same age as the shear system because it is contained in geometrically related quartz veins. However, the zone was reactivated during D_3 and D_4 and much of the gold mineralization could be of D_4 age. Placer gold mineralization in the Mougooderra Formation must have occurred at about 2800 Ma (the inferred age of the Mount Farmer Group).

The main period of tectonism, metamorphism, and granitoid intrusion associated with gold mineralization in the Murchison Province spanned an interval of approxi-

TABLE 42. GOLD MINERALIZATION DURING THE ARCHAEAN CRUSTAL EVOLUTION OF THE MURCHISON PROVINCE

Age (Ma)	*Event*	*Gold mineralization*
c. 3000	Deposition of the Luke Creek Group (volcanics, BIF, and clastic sedimentary rocks) in a province-wide ensialic basin	Synvolcanic; associated with massive Cu–Zn sulphide deposits
c. 2920	D_1 deformation: recumbent folds and thrusts; contemporaneous intrusion of monzogranite and granodiorite sheets (pegmatite-banded gneiss protoliths)	Late- or post-D_1 epigenetic deposits in bedding-parallel shear zones
c. 2800	Local erosion of Luke Creek Group followed by deposition of the Mount Farmer Group (volcanics and clastic sedimentary rocks) in separate volcanic centres and basins	Placer Au–W deposits in pyritic conglomerate
c. 2690–2680	Intrusion of voluminous monzogranite sheets; amphibolite-facies contact metamorphism of adjacent greenstones	
c. 2680–2640	D_2 deformation: east-trending tight upright folds (F_2)	Epigenetic deposits in fractures related to F_2 folds
	D_3 deformation: north-northeast to north-northwest-trending tight to isoclinal folds (F_3)	
	Regional metamorphism with partial melting in the lower crust	
c. 2650–2600	D_4 deformation: regional north-northeast to north-northwest-striking faults and shear zones; local kink folds (F_4); contemporaneous intrusion of post-folding granitoid plutons	Main episode of epigenetic gold mineralization

mately 60 Ma, between about 2680 and 2620 Ma. It is notable that this period falls within the only significant, world-wide episode of Precambrian gold mineralization (Woodall, 1988), and corresponds to a period of cratonization which can be recognized in many Archaean granite–greenstone terranes. D_2 appears to be a distinct episode of deformation, but D_3 and D_4 overlap and coincide with regional metamorphism and post-folding granitoid intrusion. Gold mineralization of D_2 and pre-M_3 age includes the F_2-related epigenetic deposits at Star (Mount Magnet) and possibly the high-grade regionally metamorphosed deposit at Big Bell (the age of the high-grade metamorphism at Big Bell is still uncertain). The Hill 50 deposit occupies a probable F_2 structure and could also be 'partly' D_2 in age (mineralized D_4 faults and dykes of felsic porphyry also occur at Hill 50).

Most of the epigenetic gold deposits in the province are clearly related to D_4 faults and shear zones, some of which locally deform post-folding granitoids, as well as sills of felsic porphyry that are probably related to those intrusions.

Potential sources of gold-bearing fluids in Archaean granite–greenstone terranes have recently been reviewed by Perring et al. (1987), Colvine et al. (1988) and Groves et al. (1986). Evidence from fluid inclusions indicates that the ore fluids were of low salinity (typically <2 wt% NaCl equivalent), contained moderate levels of CO_2 (generally 10–25% CO_2), and were at relatively low pressure (commonly 100–200 MPa) and moderate temperature (normally 250–350°C). This combination of properties distinguishes Archaean gold-bearing fluids from meteoric–epithermal, diagenetic, volcanogenic, and high-level magmatic fluids, all of which exhibit lower CO_2 contents, lower pressures, and generally higher salinities. The temperature range of Archaean gold-bearing fluids is higher than for diagenetic fluids, and lower than in magmatic fluids associated with high-level granitoid-related mineralization (e.g. porphyry copper). Stable isotope evidence (oxygen, deuterium, carbon, and sulphur) is compatible with derivation of the Archaean gold-bearing fluids from either magmatic or metamorphic sources.

Other granite–greenstone terranes have not yet revealed any unequivocal criteria to determine if the ore fluids responsible for Archaean epigenetic gold deposits were derived magmatically (from either the crust or mantle), or metamorphically (Perring et al., 1987; Colvine et al., 1988, p. 84). The source of 2650–2600 Ma gold-bearing hydrothermal fluids in the Murchison Province is considered to have been the lower crust, possibly with contributions from the upper mantle. The source material was principally mafic to ultramafic, but its precise nature is less certain.

The main period of gold mineralization in the Murchison Province occurred during the waning stages of regional metamorphism (M_3). Prior to D_2–D_3, the Murchison Province crust consisted of an upper layer (10–15 km thick) of volcanic and sedimentary rocks (Murchison Supergroup) above a substratum of gneiss and granitoid. D_2–D_3 deformation resulted in local downfolding of the upper layer to form major synclines, the upper levels of which now form the greenstone belts. Upward relaxation of folded isotherms in these structures led to metamorphic devolatilization and partial melting in the lower crust. This resulted in the generation of post-folding granitoid magmas and gold-bearing hydrothermal fluids, and explains the observed spatial association of gold deposits with post-folding granitoids and greenstone belts. Other possible causes of devolatilization and partial melting, such as mantle diapirism (Colvine et al., 1988), less satisfactorily explain the virtual restriction of gold deposits and post-folding granitoids to greenstone belts.

The timing of gold mineralization (after peak metamorphism) is consistent with the above model. As discussed earlier, thermal convective circulation of metamorphic fluids could have continued for some time after peak metamorphism, perhaps partly driven by heat from the post-folding granitoids. It is also likely that metamorphism in the lower crust continued to produce ore fluids beyond the period of peak metamorphism in the upper crust. The timing of gold mineralization does not closely agree with Pb-model ages of galena from the Don Bradman, Nannine, Morning Star, and Golden Crown gold deposits (Browning et al., 1987); these, and unpublished Pb–Pb isotopic data from Victory United, suggest that gold mineralization in the Murchison Province occurred at about 2850–2750 Ma. However, if the gold-bearing hydrotherml fluids were derived by partial melting of older crustal material the Pb-model ages may not accurately reflect the age of mineralization. It is interesting that the Pb-model ages are broadly similar to the estimated age of source material for suite I post-folding granitoids in the northeastern Murchison Province (Chapter 3).

Metamorphically derived ore fluids, possibly combined with mantle-derived volatiles (especially CO_2), were channelled along the D_4 faults and shear zones. At present erosion levels the shear zones are generally less than 1 km wide, but in the lower crust they are possibly much wider (Colvine et al., 1988, p. 20) and capable of abstracting gold-bearing fluids from very large volumes of rock. On the assumption that the original gold content of the source material was about 1–2 ppb (average content of mafic rocks), extremely large volumes of such material must have been metamorphosed to produce the amount of gold precipitated in epigenetic deposits; for example, assuming 50% gold liberation from a 2 ppb Au source, the volume of the source necessary to account for total past gold production from Mount Magnet (64 t of Au) would have been about 25 cubic kilometres.

Future exploration

Given the information now available on controls of gold mineralization in the Murchison Province, it should be possible to identify those areas with the greatest potential for future discoveries. Total possible gold resources of the province can be very approximately estimated from the generalization that the 230 t of Au already produced has come from those parts of the greenstone belts that contain outcrop or shallow subcrop (about 10 per cent). Future exploration will be partly aimed at investigating depth extensions of known surface mineralization, but will increasingly employ metallogenetic models to predict the existence of totally concealed mineralization in areas unsuitable for earlier prospecting and exploration. Remote sensing technology will be used to establish general bedrock geology and to identify target areas where favourable factors such as structure, lithology, and geological setting are combined. The location and investigation of hydrothermal alteration haloes will also be important in those types of gold deposit accompanied by significant alteration (e.g. ultramafic-hosted deposits in shear zones).

Metallogenetic models will be used not only to find new gold deposits, but also to determine the probability of significant mineralization at depth. An example is the depositional model described by Colvine et al. (1988, p. 71–77) in which a typical vertical zonation of deposit characteristics is related to depth variation beneath the palaeosurface. This model is based on vertical variations in P–T conditions and structure, but cannot include the important interrelationship between structure and lithology. Another model, based on gold mineralization in Western Australian greenstone belts, was proposed by Phillips and Groves (1983). This 'metamorphic-replacement' model is generally consistent with observations in the Murchison Province, except that, because gold mineralization occurred largely after peak metamorphism, the metamorphic grade of host rocks is not directly related to gold deposition. Gold deposits can occur in either greenschist- or amphibolite-facies host rocks.

Evidence from the Murchison Province indicates that the regional location of economic gold mineralization is directly related to:

(a) the composition of source regions in the lower crust;
(b) the distribution of areas of crustal subsidence at about 2650 Ma (broadly equivalent to the present distribution of greenstone belts);
(c) the location and frequency of major faults and shear zones; and
(d) a crustal palaeodepth at 2650–2600 Ma consistent with pressure conditions of 100–250 MPa (about 3–9 km depth).

The precise location and style of gold deposition was controlled by wall-rock lithology and local structure. Deposition within any particular mineralization system occurred spasmodically over a considerable vertical interval (up to 2 or 3 km) according to the vertical distribution of preferred host lithologies. This last observation has considerable significance for exploration in the vicinity of established deposits because gold potential at depth, or laterally, can be assessed on the basis of local stratigraphy.

Gold-related metals

Silver

About 18 t of silver have been produced as a by- product of gold mining, the most important centres being Big Bell, Day Dawn, and Mount Magnet (Table 43). Future silver production will continue to come from gold mines (particularly Big Bell), but a significant resource (about 1500 t, Table 45) also lies in the Golden Grove Cu–Zn deposits. The silver content of gold ores is extremely variable, and no regional studies of silver distribution or geological controls have been undertaken. Analyses of concentrates from gold ores at Meekatharra (Simpson, 1916, p. 307–312) reveal gold to silver ratios varying from 3:1 to 10:1.

TABLE 43. TOTAL PRODUCTION OF SILVER FROM THE MURCHISON PROVINCE TO 31 DECEMBER 1987

Mining centre	*Silver (kg)*
Abbotts	0.005
Big Bell	7 825.107
Burnakura	5.837
Carlaminda	0.103
Chesterfield	0.913
Cuddingwarra	4.183
Cue	6.759
Day Dawn	5 526.914
Eelya	0.064
Fields Find	24.704
Gabinintha	29.118
Garden Gully	34.306
Goodingnow	2.402
Gullewa	3.556
Jillewarra	0.101
Jumbulyer	0.695
Lake Austin	1.513
Lennonville	61.271
Mainland	0.005
Meekatharra	94.041
Messenger Patch	33.762
Mindoolah–Ryansville	63.394
Moyagee	23.569
Mount Gibson	45.727
Mount Magnet	3 188.404
Munarra Gully	0.187
Nannine	15.088
Noongal	0.179
Nyounda	0.017
Pinnacles	0.158
Pinyalling	0.007
Quinns	4.436
Reedy	689.141
Stake Well	0.095
Tuckabianna	1.297
Tuckanarra	5.498
Wadgingarra	0.082
Warda Warra	0.265
Warriedar	0.401
Winjangoo	0.047
Yalgoo	0.083
Yaloginda	0.461
Yuin	4.097
Sundry parcels:	
Murchison M.F.	
Cue District	68.466
Meekatharra District	19.185
Day Dawn District	99.651
Mount Magnet District	36.221
Yalgoo M.F.	18.245
Total	**17 939.760**

Antimony

Stibnite, berthierite, tetrahedrite, ullmanite, native antimony, aurostibnite, and breithauptite have been recognized at Big Bell (Stillwell, 1948; Chown et al., 1984), and various minor occurrences of stibnite, cervantite, tennantite, tetrahedrite, and valentinite were recorded by Simpson (1948, p. 406; 1952, p. 599–600, 656, 684). At Big Bell the antimony minerals occur as small segregations within quartz veinlets and lenticles in the quartz–muscovite–K-feldspar schist, and are generally associated with pyrite and sphalerite; stibnite also occurs along grain boundaries and as minute particles along the cleavages of feldspar (Stillwell, 1948). Simpson (1952, p. 599) stated that the gold orebody contains about 0.13% antimony. Other occurrences of antimony minerals have been recorded from various mines at Mount Magnet, particularly Morning Star. None of the Murchison antimony occurrences have been worked for the metal.

Arsenic

Arsenopyrite is relatively common in Murchison gold deposits, but only at Meekatharra has arsenious oxide been produced as a commercial by-product of gold mining (Simpson, 1948, p. 145–147). Most production came from the Consols–Fenian gold deposit where arsenopyrite is the dominant sulphide. The arsenious oxide was used locally as a pesticide for treating timber; recorded exports are less than 100 t.

Copper–zinc

Copper occurs in two main types of deposit in the Murchison Province: stratabound Cu–Pb–Zn deposits and in local shears and quartz veins (commonly auriferous). The stratabound deposits are typically massive sulphide lenses in volcano-sedimentary units, whereas the vein deposits are generally hosted by mafic or ultramafic rocks. Minor production of copper ore and cupreous ore has been recorded from a number of deposits; (Low, 1963; Marston, 1979), but so far only two reasonably large deposits (Scuddles and Gossan Hill at Golden Grove) have been identified; no zinc production has been recorded from the province. Table 44 summarizes the main features of the minor deposits, based largely on descriptions by Low (1963) and Marston (1979). Stratabound deposits at Golden Grove and Mount Mulcahy, and the Gabanintha vein deposits merit separate description.

TABLE 44. MINOR COPPER DEPOSITS OF THE MURCHISON PROVINCE

Deposit (location)	*Type*	*Host rock*	*Metallic minerals*	*Production Cu (t)*	*References, comments*
Abbotts (26° 17' 20"S 118° 23' 10"E)	Limonitic vein along shear	Sedimentary schist	Chrysocolla, malachite, limonite	1.3	(a),(e)
Blaneys (28° 31' 00"S 116° 50' 30"E)	Quartz vein; associated gold	Basalt	Malachite, azurite, chalcopyrite	–	
Buddadoo (28° 44' 00"S 116° 29' 00"E)	?Disseminated	Gabbro	Malachite	–	Occurrence only
Bunnawarra (28° 34' 10"S 116° 29' 00"E)	Stratabound quartz veins and breccia; disseminated sulphides	Quartz – chlorite – sericite schist and quartzite	Pyrrhotite, sphalerite, chalcopyrite, pyrite	0.8	(a)
Burnakura (27° 01' 10"S 118° 26' 30"E)	Stratabound sulphides	Felsic volcanics, chert, and clastic sedimentary rocks	Pyrite, chalcopyrite, sphalerite, malachite, chalcocite	–	
Carlaminda (28° 16' 00"S 116° 44' 00"E)	Quartz vein; associated gold	Basalt	Pyrite, chalcopyrite, native copper, malachite, azurite	–	(d)
Chunderloo (26° 42' 30"S 118° 21' 50"E)	Stratabound goethitic contact between amphibolite and schist	Ampbibolite and quartz – mica – chlorite – hornblende schist	Malachite, azurite, chrysocolla, cuprite	28	(a)
Cuddingwarra (27° 18' 30"S 117° 47' 30"E)	Stratabound limonite lenses	Felsic volcaniclastic rocks and phyllite in contact with basalt	Cupriferous limonite	–	(a)
Day Dawn (Croesus, 27° 26' 30"S 117° 51'30"E)	Quartz veins in shear zone; associated gold	Basalt	Malachite, azurite, chalcocite, chalcopyrite, limonite	13	(a),(b) See 'Croesus' under 'Gold'
Eelya North (27° 18' 20"S 118° 07' 30"E)	Stratabound massive sulphides	Felsic volcanics	Pyrrhotite, pyrite, chalcopyrite	–	(a)
Fields Find (29° 02' 20"S 117° 14' 30"E)	Quartz vein; associated gold	Basalt, dolerite, and felsic porphyry	Pyrite, pyrrhotite, chalcopyrite, arsenopyrite, galena, sphalerite	4.1	(a) See 'Fields Find' under 'Gold'
Mount Charles (27° 42' 30"S 117° 25' 00"E)	Disseminated	Gabbro	Chalcopyrite	–	(c) Occurrence only
Mount Eelya (27° 21' 30"S 118° 09' 40"E)	Shear zone	Granodiorite and felsic volcanics		0.3	
Mount Gibson (29° 43'S 117° 11'E)	Stratabound massive sulphides and quartz veins; associated gold	Felsic volcanics and chert	Pyrite, chalcopyrite, sphalerite, galena, pyrrhotite	1.1	

TABLE 44. (continued)

Deposit (location)	*Type*	*Host rock*	*Metallic minerals*	*Production Cu (t)*	*References, comments*
Mount Singleton (29° 28' 40"S 117° 17' 40"E)	Stratabound lenticular sulphide bodies	Ultramafic (fragmental); underlain by BIF and quartzite	Pyrite, pyrrhotite, chalcopyrite, sphalerite, malachite, azurite	–	(f)
Munarra Gully (26° 59' 20"S 118° 08' 20"E)	Quartz vein; associated gold	Basalt	Malachite, chalcopyrite, pyrite		See 'Munarra Gully' under 'Gold'
Paynes Find (29° 13' 30"S 117° 39' 10"E)	Sulphidic quartz veins in shears	Amphibolite schist	Malachite, chalcopyrite, cerussite, galena, acanthite, goethite	–	Pb – Pb model age 2865 ± 19, Browning et al., 1987
Quinns (27° 03' 30"S 118° 38' 30"E)	Stratabound	BIF and volcanogenic sedimentary rocks	Pyrite, pyrrhotite, chalcopyrite	–	(a)
Reliance (28° 18' 30"S 116° 41' 30"E)	Quartz vein; associated gold	Komatiitic basalt and dolerite	Malachite	–	
Rose Marie (29° 04' 50"S 117° 07' 50"E)	Quartz vein; associated gold	Basalt	Malachite	1.3	(a) see 'Rose Marie' under 'Gold'
Saddows (28° 11' 40"S 116° 42' 10"E)	Quartz vein; associated gold	Actinolite schist	Chrysocolla, malachite	–	(e) (p. 21, under Melville); see 'Noongal' under 'Gold'
Tuckabianna (27° 30' 50"S 118° 07' 00"E)	Stratabound; partly mobilized syngenetic	Argillaceous unit within volcanogenic sedimentary rocks	Pyrrhotite, sphalerite, chalcopyrite, marcasite, galena	–	(g)
Twin Peaks (27° 22' 30"S 115° 58' 50"E)	Silicified shear zone	Volcanogenic sedimentary rock	Malachite, azurite, chrysocolla	8.5	(a), (b)
Wadgingarra (28° 17' 00"S 116° 48' 10"E)	Quartz veins	Gabbro and basalt	Chalcopyrite, chrysocolla, malachite	1.3	(a)
Wandarrie (27° 52' 10"S 117° 51' 00"E)	Shear zone	Mafic schist (sheared gabbro)	Malachite	–	
Warriedar (29° 05' 20"S 117° 07' 40"E)	Quartz vein	Basalt	Malachite, azurite, chrysocolla, cuprite, chalcocite, chalcopyrite, pyrite, pyrrhotite	217	(a)
Wattagee (27° 12' 30"S 117° 52' 00"E)	Stratabound massive sulphides	Volcanogenic sedimentary rocks	Pyrrhotite, sphalerite, chalcopyrite	–	(a)

References: (a) Marston, 1979 (b) Low, 1963 (c) de la Hunty, 1973 (d) Simpson, 1952 (e) Simpson, 1951 (f) Marlow, 1973 (g) Penzoil of Australia Ltd, 1976

Golden Grove

Exploration of the Golden Grove area commenced in 1970 and was initially centred on the prominent gossans at Gossan Hill. However, following extensive regional exploration, a totally blind orebody was successfully located at Scuddles, about 4 km to the north of Gossan Hill. Published 1988 resources for the two deposits are presented in Table 45.

Base-metal mineralization at Golden Grove is hosted by the Gabanintha Formation. The lower part of this formation has been intruded by monzogranite, before and after regional metamorphism, so that only the upper part of the succession is preserved. This consists of a lower quartz arenite overlain by a 1–1.5 km-thick succession of fine to coarse felsic volcaniclastic sedimentary rocks, felsic lava, and minor chemical sedimentary units. Between this sequence and the overlying Windaning Formation is an upper member of tholeiitic basalt containing mafic sills and dykes of felsic porphyry.

Stratabound massive sulphide mineralization is situated about 400–500 m below the base of the tholeiitic basalt at a stratigraphic level where volcaniclastic sedimentary rock and chert are overlain by andesite. The Scuddles and Gossan Hill orebodies occur on different horizons separated by a vertical interval of about 50 m. At Scuddles the mineralized unit is 10–90 m thick and dips 70° to the west. It consists of fine- to medium-grained volcaniclastic sedimentary rocks of rhyolite to dacite composition. The rocks are well bedded and graded bedding is common. Numerous narrow chloritic shear zones, parallel or subparallel to bedding, disrupt the succession and probably cause repetition of strata. Mineralization is vertically zoned and consists of a lower zone of disseminated and stringer pyrite–chalcopyrite, a central zone of massive magnetite–pyrite–chalcopyrite–pyrrhotite, and an upper zone of stratabound sphalerite–pyrite–galena capped by chert. Three separate lenses of such mineralization occur over a strike length of 600 m, but most exploration has been undertaken on the southern 'main' lens. In 1984, a 370 m-deep shaft of 4 m diameter was sunk on this orebody, and 150 m-long drives were cut at the 310 and 370 m levels. The drives run across strike and are almost entirely confined to the orebody and its footwall. The footwall succession is composed of chloritized, brecciated and sheared medium-grained volcanogenic sedimentary rock of rhyolite to dacite composition (samples 85767–84, Appendix II).

The structural geology of the mineralized unit at Scuddles is incompletely understood. Two cleavages are present: the first could be termed 'regional schistosity' and is parallel or subparallel to bedding (striking north-northwest), whereas the second is a north-northeasterly striking strain-slip or crenulation cleavage. Shear, parallel to the first cleavage, is evidenced by zones of chloritic schist within the sedimentary rock, and appears to have broken the primary sulphide zones into a series of lenses. The mineralized zone is further complicated by faults, parallel to the second cleavage, and various dolerite dykes which effectively 'dilute' the sulphide orebodies.

The Gossan Hill mineralization extends over a strike length of 550 m and consists of several sulphide–magnetite orebodies separated by pyritic and chloritic sedimentary schist. The dominant sulphides are generally pyrite, chalcopyrite, and pyrrhotite, but sphalerite and galena occur in the upper part of the mineralized unit. Chalcopyrite is associated with pyrite in disseminated or massive sulphide–magnetite lenses, but also occurs alone or with pyrite, pyrrhotite, or quartz in veins through massive sulphide magnetite pods or in sedimentary schist. The zinc zone, at the top of the mineralized unit, includes pyrite–sphalerite in chert breccia, and bedded pyrite–sphalerite–galena. As at Scuddles, the mineralization is complicated by faulting and dolerite intrusions.

Sedimentological evidence currently available (Clifford, 1987) suggests that the Cu–Zn mineralization at Golden Grove is a product of hydrothermal discharge and subsurface replacement processes in a deep subaqueous environment. The host rocks are probably distal turbiditic sediments and debris flows in rift or caldera settings. More detailed descriptions of Golden Grove are provided by Harris et al. (1982), Frater (1983a), and Clifford (1987).

TABLE 45. IDENTIFIED RESOURCES AT GOLDEN GROVE, 1988

Deposit	*Million tonnes*	*Cu (%)*	*Pb (%)*	*Zn (%)*	*Ag (g/t)*	*Au (g/t)*
Gossan Hill						
Zn zone	2.3	0.5	1.2	10.6	92	1.7
Cu zone	14.1	3.8	-	0.1	15	0.2
Scuddles						
Massive Zn zone	9.3	0.5	1.3	15.8	108	1.2
Massive Cu zone	1.3	5.1	0.1	1.7	44	1.3
Stringer Cu zone	4.0	2.9	-	0.2	10	0.3

Mount Mulcahy

The Mount Mulcahy Cu–Zn mineralization, 5 km east of Glen Homestead, is stratabound within thin units of chert, shale, phyllite, and tuff in mafic rocks of the Mindoola Formation. At the surface it is expressed as two gossans about 750 m apart. Production of 49.24 t of cupreous ore prior to 1966 had a total copper content of 3.54 t.

The gossans are limonitic and contain chrysocolla. Marston (1979, p. 127–128) summarized the results of exploration between 1969 and 1974. Drilling has established zoned massive sulphide mineralization consisting chiefly of pyrrhotite with subordinate chalcopyrite, sphalerite, and minor amounts of galena and pyrite; sphalerite is concentrated in the upper section of the massive sulphide section. Disseminated or veinlet sulphides, in which pyrite locally predominates, underlie the massive sulphides. Further drilling between 1981 and 1983 did not substantially change estimates of available resources, previously reported (Marston, 1979) as 250 000 t averaging 3.77% Cu and 2.75% Zn.

Gabanintha

Mines at Gabanintha have yielded almost 7000 t of ore containing 352.5 t of copper. Two groups of workings are present: the northwestern group, including Mountain View and Tumbulgum, consists of gold mines in which copper was a by-product; and the southeastern group, including Lady Alma and small mines near Copper Hills Well, which has produced relatively little gold. The Au–Cu deposits at Mountain View and Tumbulgum are described under 'Gold'; previous reports are provided by Gibson (1904, p. 44–53), Simpson (1952, p. 166), Low (1963, p. 123–128) and Marston (1979, p. 139). The Lady Alma deposit is a 7.5 m-wide shear zone between gabbro and serpentinite, that has been worked over a strike length of 46 m. The sheared and brecciated material contains veins and lenses of quartz, with local concentrations of chalcocite, cuprite, bornite, chrysocolla, malachite, azurite, and minor amounts of chalcopyrite. An *en echelon* shear, 145 m to the south-southwest of Lady Alma, was worked as Copper King. Massive, copper-stained limonite gossans and quartz–malachite–azurite–chrysocolla veins are present at the surface (Marston, 1979, p. 140). At Copper Hills Well, copper mineralization takes the form of cupriferous limonite–quartz bodies along a sheared gabbro–ultramafic contact, but relatively little production has come from the small workings in this area. Bunting et al. (1981) recorded the existence of an old copper mine at Hillview woolsheds, 5 km north of Copper Hills Well, but no descriptions are available.

The copper and gold–copper deposits at Gabanintha are located in the Gabanintha Shear Zone which is locally complicated by later (probably D_4) parallel faulting.

Iron ore

Supergene enrichment hematite–goethite iron-ore deposits are associated only with BIF of the Windaning Formation; Golconda Formation BIF does not host economically significant iron enrichments. This is probably partly because the Windaning Formation BIF units are generally far thicker than those in the Golconda Formation, but it also appears that the BIF–felsic volcanic–sediment association of the Windaning Formation is more permeable than the BIF–mafic succession of the Golconda Formation. Permeability is important because supergene concentration of iron has resulted from groundwater leaching of silica and carbonate minerals. Iron-ore deposits tend to be located where outcrops of thick, fractured and permeable BIF units were exposed during long periods of weathering. The ore typically consists of hematite inherited from the BIF progenitor, martite after primary magnetite, goethite replacing chert and silicates, and secondary hematite.

The principal iron-ore deposits of the Murchison Province are Koolanooka, Mungada, Weld Range, Mount Gibson, and Tallering Range. Similar deposits at Jack Hills in the eastern part of the Narryer Gneiss Complex, are not described here.

Koolanooka

The Koolanooka iron-ore mine operated between 1966 and 1972, by which time ore-grade material had been removed. Total production was 6.7 Mt of ore averaging 60.2% Fe and 0.129% P; during the latter years of mining this production was supplemented by additional ore from Mungada, 65 km to the east. The Koolanooka orebody was a supergene enrichment of Windaning Formation BIF at the northwestern end of the Koolanooka Hills. At this locality the BIF is faulted against clastic sedimentary rocks to the west, and intruded by a post-folding syenogranite to the north. Groundwater flowing along strike from higher ground to the southeast may have been barred at these western and northern contacts to locally produce an environment favouring Fe-enrichment. McKay (1975) described four types of ore at Koolanooka: massive magnetite–hematite–goethite, goethite–hematite, goethite–hematite–limonite, and goethite-cemented scree. Magnetite is primary, hematite is largely secondary after magnetite, and goethite has replaced chert, iron silicates, iron carbonates, and hematite. Limonite probably formed from very fine-grained iron-silicate bands within the BIF. Outside the area of Fe-enrichment, the BIF, which has been metamorphosed to lower amphibolite facies, consists of quartz, magnetite, grunerite, and anthophyllite–gedrite. The average Fe content of BIF to the southeast of the mine is 35.5% (samples 85744, 85746–50, Appendix II) A sample of ore (85742, Appendix II) assaying 63.2% Fe also contained 671 ppm Cu, 85 ppm Pb, and 6 ppm Ag.

Mungada

The Mungada (also called 'Blue Hills') deposits are small lenses of hematite–goethite ore hosted by the Windaning Formation of the Yalgoo–Singleton greenstone belt. The largest deposit at Mungada is located in a zone of minor folding, which has probably caused local thickening of the BIF and aided groundwater movement. Exploration by Western Mining Corporation between 1962 and 1973 established total reserves of 260 000 t of iron ore, of which about 200 000 t were subsequently mined. The BIFs have also been evaluated as a source of taconite, but although separation of magnetite is technically feasible, it has been ruled out by cost.

Mount Gibson

Three deposits of high-grade iron ore have been identified at Mount Gibson. Reported reserves (>60% Fe) for the northern deposit at Extension Hill are 2.7 Mt, whereas deposits at Iron Hill and Mount Gibson, 5 km to the south, contain a total of 5.6 Mt (Blockley, 1985, unpublished). The Windaning Formation here is composed of jaspilitic BIF and minor grey-white banded chert associated with clastic sedimentary and felsic volcanic rocks. The ore deposits crop out on the top of the Mount Gibson–Extension Hill ridge, and drilling has shown them to be shallow. BIF samples from core at Extension Hill (74520–32, 85849–

68, Appendix II) are predominantly composed of quartz and magnetite with minor amounts of Fe-rich talc, stilpnomelane, siderite, ankerite, chlorite, pyrite, and riebeckite; surface samples (85881–96, 87601, 87602, Appendix II) are composed of quartz, hematite, and goethite.

Former holders of the deposit carried out limited drilling of the BIF to test for possible beneficiable ore. During 1985, the Engineering Chemistry Laboratory of the Chemistry Centre of Western Australia carried out tests on quartz–magnetite BIF from the Extension Hill core. It was found that excessively fine grinding was required to achieve acceptable liberation of magnetite, and that the resulting extra costs would prohibit economic production.

Weld Range

The largest resources of high-grade iron ore in the Murchison Province are located in the Weld Range. Here, BIF of the Windaning Formation hosts both magnetite–goethite and hematite–goethite orebodies (Jones, 1963). The BIF is jaspilitic and possesses normal greenschist-facies mineral phases (Chapter 2, and Gole, 1980). Although the range is about 5 km wide, most of this interval is composed of dolerite and gabbro sills, and to a lesser extent felsic volcanic and volcaniclastic sedimentary rocks intercalated with the BIF.

Iron-ore deposits exceeding 5 Mt at 60% Fe are confined to two areas, Madoonga and Limestone Well. The Madoonga deposit (W14) is 3 km southeast of Madoonga Homestead, and consists of a massive stratabound goethite replacement of BIF on the northern margin of the range. Some 25 km to the east-northeast, a series of lenticular hematite–goethite and magnetite orebodies (W7–12) occur along another BIF unit about 3 km southwest of Limestone Well (Jones, 1963). Available information indicates that total high-grade (approximately 60% Fe) iron-ore resources of the two areas, assuming open-cut mining with normal stripping ratios (i.e. mining to depths of 50–75 m), are between 30 and 50 Mt. Available information on intervening deposits (Jones, 1963) indicates that none of these possess high-grade resources exceeding 5 Mt.

Jones (1963) suggested that some of the deposits are related to iron enrichment close to faults. This is probably an important contributory factor, but the fact that the larger goethitic deposits extend for several kilometres along strike indicates extensive groundwater movement parallel to bedding. Johnson (1950a, p. 88–89) presented analyses of ore samples from deposits W1–6.

Tallering Range

The Tallering Range iron-ore deposits are hosted by greenschist- to lower amphibolite-facies BIF of the Windaning Formation. The deposits have previously been described by Johnson (1950a, p. 84), Connolly (1959, p. 61–63, 1960a) and Blockley (1985); analyses of ore were presented by Johnson (1950a , p. 88). Five orebodies, T1–5, have been identified, and consist of lenses of supergene hematite in BIF. Drilling has indicated a general decline in grade with depth, although a hole through T3 intersected high-grade ore at a depth of 140 m. The oxidized zone extends to about 100 m, below which the BIF consists of quartz, magnetite, and accessory chlorite and pyrite. Samples (85707, 85709–13, 85715–18, Appendix II) of BIF analysed in this study contained up to 44.6% Fe, and one sample of ore (85706A, Appendix II) contained 66.9% Fe. Apart from silica, other constituents were minor, although one sample of BIF (85709) from the adit into T1 assayed 2.0 ppm Au, and contained 165 ppm Ba (indicative of metasomatism).

The orebodies are interpreted as supergene iron enrichments produced by silica removal beneath an ancient weathering surface. Blockley (1985) stated that total ore reserves for the T3–4 orebodies at Trig Hill are 18 Mt grading 64.5% Fe; the other deposits contain less than 1 Mt ore.

Lead

Economically significant lead mineralization in the Murchison Province appears to be confined to syngenetic stratabound Cu–Zn deposits at Golden Grove. Similar mineralization at Mount Mulcahy also contains a minor amount of lead (Marston, 1979, p. 127–128), but this deposit appears unlikely to be developed in the near future. Galena is relatively common as a trace sulphide constituent of Murchison gold deposits (Simpson, 1951, p. 330–333) and is associated with Cu–Zn mineralization at Paynes Find and Au–Cu mineralization at Fields Find (Table 44). Considerable amounts of galena occur in the Chesterfield barite deposit (see 'Barite'), where quartz veins through amphibolite and gabbro also carry sphalerite and fluorite. Galena samples from ten localities in the Murchison Province were dated by Browning et al. (1987); these included samples from additional occurrences at Twin Peaks, Morning Star and Golden Crown. A sample of gossanous quartz (87612, Appendix II) from Poona contained 1.5% Pb and 4.47% Zn, indicating local galena–sphalerite mineralization (Table 40).

Tungsten–molybdenum–bismuth

Tungsten and molybdenum mineralization are closely associated at Mount Mulgine, Noongal (Santa Claus and Harrisons Reward) and Callie Soak; tungsten has been mined from quartz veins at Bonnie Venture (Yandhanoo King and Wolfram Queen), and minor molybdenite occurrences are located at Gullewa (Davys Reward) and Mount Farmer (Already Well and Keygo Well). Bismuth minerals occur at Mount Mulgine and Noongal.

Mount Mulgine

Two main areas of mineralization have been identified

at Mount Mulgine, namely the 'Hill' and 'Trench' deposits. The Hill deposit is located in a zone at the northern contact of a small composite body of recrystallized monzogranite and post-folding syenogranite. The granitoids occupy the core of a D_2–D_3 dome (Plate 2), and are surrounded by felsic, mafic, and ultramafic schist of the Gabanintha and Windaning Formations. The main mineralized zone consists of quartz–muscovite greisen and veined phlogopite–pyrite schist. Scheelite is present both as disseminations, and in quartz veins, and is accompanied by molybdenite, chalcopyrite, and fluorite. It appears to be stratabound along a contact between tremolite–chlorite–talc schist and an overlying unit of quartz–microcline–muscovite rock. Baxter (1978) interpreted the upper unit as either a hydrothermally altered felsic igneous rock, or an aluminous sedimentary rock, but noted that it could also be a greisen.

The Trench deposit is situated 1.5 km west of the Hill deposit and consists of a 2 km-long, north-northeasterly striking zone of quartz-stockwork scheelite and molybdenite mineralization, hosted by greenstones. The latter consist of felsic schist, mafic schist, and BIF intruded by aplite, microgranite, and quartz porphyry. The deposit is stratabound and about 130 m thick, with a tungsten dominated zone overlying a tungsten–molybdenum zone. The mineralized zone dips west-northwest at about 35°, and underlies a unit of tholeiitic basalt. Sulphides other than molybdenite include pyrite, chalcopyrite, pyrrhotite, stibnite, bismuth sulphides, and minor amounts of galena. The deposit contains sufficient gold and silver to justify feasibility studies into development for these commodities. Total reserve estimates for tungsten- and molybdenum-bearing material range from about 35 to 85 Mt, depending on WO_3 cut-off levels (usually 0.1–0.5% WO_3). Tonnages of potential gold ore are much less, and exploration in 1988 was aimed at proving up 1 Mt with an average grade of 2–3 g/t gold.

Molybdenite mineralization at Mount Mulgine also occurs in southeasterly striking quartz veins through the granitoids south of the Hill deposit. The molybdenite is concentrated along vein margins and is associated with some fluorite and scheelite. More details were provided by Maitland (1919) and Matheson (1944a).

Callie Soak

The Callie Soak tungsten deposits were described by Woodward (1914, p. 53–54), Maitland (1919), Matheson (1944b), and Baxter (1978, p. 44–46). Wolframite and minor amounts of scheelite are hosted by vertical, northeast-striking quartz and pegmatitic quartz veins within recrystallized porphyritic biotite monzogranite. Molybdenite occurs in quartz veins at the 'Recovery' and 'Molybdenite' workings (Baxter, 1978, p. 17–18). The presence of numerous pegmatite veins in the Callie Soak area suggest that the recrystallized monzogranite might have been intruded very close to a granite–greenstone contact. Although Callie Soak is remote from present outcrops of greenstones, it is possible that the present erosion level is only a short distance below a previous contact; the pegmatites and quartz veins could have formed as a result of late-stage, metal-enriched fluid emanations.

Noongal

Scheelite mineralization at Noongal occurs in north-northwesterly striking narrow shear zones through mafic and ultramafic rocks of the Murrouli Basalt. The main deposit has been referred to both as 'Nevilles Scheelite' and 'Santa Claus', and is about 5 km north-northwest of Noongal townsite in an area termed 'The Basin'. This is situated in the core of a southerly plunging F_3 anticline intruded by a strongly foliated recrystallized biotite monzogranite and a post-folding granitoid (Plate 2). The area has thus been subjected to more than one phase of granitoid intrusion, and intrusion has been highly discordant to local stratigraphy. Pegmatite veins are common and the metamorphic grade is lower amphibolite facies (Plate 3). The mineralized shears strike parallel to numerous closely spaced north-northwesterly striking faults, many of which are intruded by felsic porphyry. However, the scheelite at Santa Claus is not generally associated with porphyry, pegmatite, or quartz veining, but is principally contained in chlorite–talc–tremolite schist. The scheelite is irregularly distributed and locally forms masses weighing over 4 kg (Ellis, 1953). Simpson (1952, p. 532) noted that bismutite is associated with the scheelite in some deposits. Bismuth carbonate, molybdenite, and minor scheelite occur at Harrisons Reward (Fig. 160) where mineralization occupies quartz in the core of a pegmatite intruded into pyroxenite.

The north-northwesterly striking shear zones post-date the F_3 anticline and are probably genetically related to the D_4 Noongal Shear Zone. Thus, tungsten mineralization must have occurred during, or subsequent to, D_4.

Bonnie Venture

Wolframite has been mined at Bonnie Venture where it occurs in quartz and quartz–pegmatite veins within ferruginous conglomerate and sandstone of the Mougooderra Formation. The deposits are lenticular, and appear to be concentrated where quartz veins cross conglomerate units. Further description is provided by Simpson (1951, p. 278–279) and Baxter (1978, p. 46–49).

Other minor occurrences

Minor molybdenite occurrences at Gullewa and Mount Farmer were described by Baxter (1978). Tungsten minerals are present in several gold mines, including Galtee Moore and Empress (Lennonville), Ark, Astor, and Sweet William (Goodingnow), Homeward Bound and Welcome (Cue), Warriedar, and conglomerate-hosted gold deposits at Wadgingarra.

Vanadium–titanium

Vanadium mineralization in the Murchison Province is associated with titaniferous magnetite deposits in layered mafic intrusions at Gabanintha and Buddadoo. The vanadiferous magnetite zones occur at the bases of cyclically differentiated layers, and are characterized by abrupt bases and disseminated upper contacts. Ilmenite is a common accessory, and sulphides include pyrite and chalcopyrite.

Gabanintha

The Gabanintha vanadiferous magnetite deposits have been described by Connolly (1959), Jones (1965) and Baxter (1978, p. 91–92). Titaniferous magnetite units occur in medium- to coarse-grained anorthositic gabbro, about 2 km west of Gabanintha mining centre. The intrusion is essentially concordant with the mafic and ultramafic rocks of the Gabanintha Formation, and is exposed over a strike length of about 7 km. Faulting has fragmented the magnetite-rich zone into numerous lenses, the largest of which is 421.5 m long, 15.3 m wide, and contains 1.22% V_2O_5 (Baxter, 1978, p. 92). Drilling by Mangore (Australia) Pty Ltd in 1961 indicated total reserves of 8.56 Mt averaging 1.24% V_2O_5 and 15.5% TiO_2.

Buddadoo

The gabbro at Buddadoo intrudes the Golconda Formation and is intruded by recrystallized monzogranite (Plate 1). Titaniferous, vanadiferous magnetite was first reported by Muhling and Low (1977) following GSWA mapping of YALGOO. Vanadium is associated with a zone of martite (after titaniferous magnetite), anorthosite, and gabbro within a series of zones containing varying proportions of gabbro, dolerite, pyroxenite, anorthosite, and granophyre. The martite, or 'oxide zone', has been traced along a strike length of 4.6 km and varies in width from 1 to 190 m. In the thickest section there are 24 layers, consisting of basal martite below gabbro, and an upper unit of anorthosite. The martite units are 0.3–3.7 m thick, with an average composition of 0.72% V_2O_5 and 18.68% TiO_2 (based on ten samples).

Nickel and chromium

Compared to other granite–greenstone terranes of Western Australia, the Murchison Province is deficient in mineral commodities related to thick ultramafic units or major ultramafic–mafic intrusions. Nickel and chromium contents of mafic and ultramafic rocks in the province are within the normal range for Archaean rocks, but the region lacks very thick flows and intrusions of peridotite–dunite composition. The reason for this probably lies in the depositional environment of the Murchison Supergroup (see Chapter 8).

Pegmatite metals

Pegmatites containing economic concentrations of tin, tantalum, niobium, beryllium, and lithium are largely restricted to the central western part of the Murchison Province, between Poona and Noongal. The reason for this restricted distribution has not been established; but it implies some as yet unrecognized characteristic of granitoid–greenstone contacts in this area. Davy et al. (1986) discussed the geochemistry of the recrystallized monzogranite in the Poona–Dalgaranga area, and presented evidence of significant Ba, Li, Nb, and Sn anomalies.

Only two localities outside the Poona–Noongal area are known to contain economically significant pegmatite deposits: Rothsay and Goodingnow. In each case pegmatite intrusion is confined to small areas.

Beryllium

About 579 t of beryl ore, containing 67.9 t of BeO, have been mined from the Murchison Province (Table 46).

At Rothsay, production was obtained from three northeasterly striking quartz-cored pegmatite intrusions within mafic amphibolite, 2 km southwest of the old townsite. A crude zoning is present, and most of the beryl is located between 45 and 300 cm from the amphibolite contact (Blockley and Gibson, 1973).

Production from Warda Warra came from several localities, but particularly Kylie, where quartz veins and quartz-cored pegmatite intrude mafic amphibolite and ultramafic schist near the margin of the Warda Warra greenstone belt (de la Hunty, 1962, p. 70). Beryl and emerald are concentrated in marginal reaction zones of phlogopite–biotite schist. Darragh and Hill (1983, p. 134) considered that beryllium was transported in an alkali-carbonate complex within a potassium-rich pneumatolytic-hydrothermal fluid.

TABLE 46. TOTAL PRODUCTION OF BERYLLIUM (AS BeO) TO 31 DECEMBER 1987

Centre	*Ore* (*t*)	*Contained BeO* (*kg*)
Big Bell	0.45	38
Dalgaranga	32.49	3 657
Edah	4.10	475
Goodingnow	5.85	692
Lakeside	1.14	125
Noongal	15.97	1 911
Poona	38.39	4 781
Rothsay	296.69	35 450
Warda Warra	175.97	19 834
Wydgee	8.10	894
Total	**579.15**	**67 857**

The Dalgaranga deposits were described by Blockley (1980, p. 92–93) and de la Hunty (1962, p. 69–70). The orebodies are zoned pegmatites containing beryl, tantalite, tapiolite, and, locally, cassiterite.

In the Poona area, beryl and emerald are associated with northwesterly and north-northeasterly striking pegmatite dykes where these intrude greenstones. The beryl is located in the pegmatite and in marginal reaction zones of phlogopite schist; Woodward (1914, p. 54–65), Wilson (1926), and Simpson (1948, p. 202–204) described these deposits.

The Noongal (Melville) beryl deposits occur in a suite of microcline–quartz pegmatite dykes intruding the northern end of the Yalgoo–Singleton greenstone belt. Simpson (1948, p. 200–202) described the more important beryl localities in this area (see also 'Tungsten–molybdenum–bismuth').

Minor beryl deposits briefly described in previous publications include those at Coodardy, near Big Bell (Simpson, 1948, p. 200; Blockley 1980, p. 91–92), Edah and Wydgee (Baxter et al., 1983, p. 21) and Goodingnow (Lipple et al., 1983, p. 20).

Lithium

The lithium-bearing minerals, lepidolite, spodumene, zinnwaldite, and petalite, are confined to pegmatites, and are commonly associated with other economic minerals such as cassiterite, tantalite, and beryl. No production of lithium minerals has been recorded from the Murchison Province, and they are comparatively uncommon in this part of the Yilgarn Craton. The main occurrences are at Noongal, Poona, Dalgaranga, and Warda Warra; that is, in the rare-metal pegmatite domain of the province.

Blockley and Gibson (1973) recorded zinnwaldite at the Rothsay beryl deposit, and Simpson (1952, p. 60) referred to a minor occurrence of lepidolite east of Ninghan Homestead. Lipple et al. (1983) stated that lepidolite has been reported from the Goodingnow feldspar quarry. In the Noongal area, minor amounts of lepidolite occur in pegmatite veins near the Santa Claus Scheelite deposit (see 'Tungsten–molybdenum–bismuth'), but the mineral is most common at a locality 3 km north-northwest of Dollar Well. Here it locally makes up about 25% of a 1 km-long, west-northwesterly striking pegmatite dyke. The lepidolite is best exposed 2 km north-northwest of Dollar Well.

At Poona, minor amounts of lepidolite are present in pegmatite at 'Olivers' (PA 1486, Simpson, 1926, p. 177) 1 km west-northwest of Ryans Prospect (immediately south of Poona exploration camp); and Simpson (1952, p. 60) also stated that it is common at 'Doreen' (ML 48). Blockley (1980, p. 91) observed rare spodumene at Ryans Prospect where 'spheroidal mica' noted by Simpson (1926) is probably zinnwaldite. Blockley (1980, p. 91) referred to a 'lithium-bearing pegmatite', 500 m northwest of Ryans Prospect; Montgomery (1910, p. 87) previously described this deposit, under the name of 'Patons Lode', as an east-striking quartz-rich pegmatite.

The Dalgaranga pegmatite deposits are described under 'Tin–tantalum', and by de la Hunty (1962) and Blockley (1980, p. 92). Zinnwaldite occurs in some of the zoned pegmatites at this locality. At the southern end of the Warda Warra greenstone belt, minor amounts of lepidolite are associated with tantalite and beryl in pegmatite immediately south of the vermin-proof fence.

Tin–tantalum

Descriptions of tin and tantalum deposits of the province have been provided by Blockley (1980, p. 89–93) and Miles et al. (1945, p. 38–39, 96, 110, 126) and are not repeated here. Mining of tantalite–columbite terminated at Dalgaranga in 1981, and small amounts of ore were obtained from Goodingnow and Warda Warra in the late 1970s. Blockley (1980, p. 90) presented production figures for tin concentrate, which still apply, the last production being recorded from Poona in 1969. All the deposits except those at Coodardy are associated with zoned pegmatite veins which have intruded the margins of greenstone belts; the Coodardy pegmatites belong to the layered category (Blockley, 1980).

The factors controlling the metallic mineral composition of pegmatites are not fully understood. Therefore, it is unclear why tantalite, tapiolite, and cassiterite are common at Dalgaranga, but are rare or absent in other areas. It is possible that many of the pegmatites at Dalgaranga are related to post-folding granitoid magma, and this contained more tin and tantalum than the earlier magma responsible for the recrystallized monzogranite. However, more detailed geochemical and geochronological work would be necessary to determine such a relationship.

Other metals

Minor occurrences of economic metallic minerals other than those described above have been listed by Carroll (1945) and described by Simpson (1948, 1951, 1952). Most of these 'occurrences' amount to nothing more than mineral observations, and are not included on Plate 2. Two metallic mineral commodities not already discussed are uranium and platinum-group elements. The Murchison Province is not known to contain economic deposits of either, but available evidence suggests limited potential; some discussion is therefore included.

Uranium

The uranium occurrences shown on Plate 2 were described by Butt et al. (1977). On the classification used by these authors most of the uranium occurrences of the

Murchison Province are hosted by 'trunk valley calcrete'. This type of calcrete forms sinuous, lenticular sheets along the main drainage courses. Uranium deposits within the calcrete and associated sedimentary rocks take the form of carnotite films along fractures and cavity walls, and carnotite disseminations or grain coatings. All the deposits occur in granitoid terrain and are assumed to have been derived by deep weathering of granitoids, many of which have uranium contents of 5–10 ppm. Groundwater flowing from the granitoids into the calcrete has been locally 'ponded' by subsurface drainage obstructions, to result in partial evaporation and concentration of uranyl and potassium ions. Groundwater salinity is generally in the range 2000–20000 ppm (total dissolved solids) and uranium is carried in the form of soluble uranyl carbonate complexes. Oxidation of vanadium is probably the main cause for precipitation of carnotite.

'Playa lake' uranium deposits are most common in the southern part of the province. Uranium enrichments occur close to the surface within gypsiferous and calcareous clays, or more rarely in carbonaceous sediments.

Limited exploration has so far failed to identify reserves of economic-grade uranium mineralization in the Murchison Province.

Platinum-group elements

Platinum-group elements may yet be found in major mafic intrusions separating the Murchison Province from the Southern Cross Province (i.e. the Windimurra and Narndee Complexes). Within the province, the gabbroid complex near Dalgaranga probably offers most scope for platinum-group element exploration, although its individual component sills (Chapter 4) may be too thin (about 1 km) to host significant concentrations.

Non-metallic and industrial minerals

Asbestos (chrysotile)

The Murchison Province contains several chrysotile occurrences, but is not known to possess any commercial deposits. Veins of the mineral occur in serpentinite at Tuckabianna, and de la Hunty (1973) noted the presence of chrysotile at Lennonville and Cullculli Trig.

Barite

The most important barite deposits in the Murchison Province occur at Chesterfield, Badja, and Jillewarra. The Chesterfield deposit takes the form of a quartz–barite vein system in amphibolite and gabbro of the Gabanintha Formation. Two sets of fractures are developed, one striking west-northwest (probably belonging to the D_5 fracture system of this area (Chapter 5)), and the other striking northeast, parallel to bedding. Based on the extent of the old workings, most of the recorded barite production (5845 t) has come from the west-northwesterly striking vein system. This consists of a fault breccia mineralized by quartz, barite, and galena, with minor amounts of sphalerite, fluorite, epidote, and pyrolusite. A Pb-model age of 2073 ±14 Ma has been obtained on the galena (Browning et al., 1987), supporting field evidence that mineralization at this locality is late in the evolutionary history of the province.

A pegmatite vein intruding recrystallized monzogranite 10 km northwest of Badja Homestead yielded 51 t of barite in 1967. Muhling and Low (1977) stated that the barite forms patches within a weathered quartz–feldspar–muscovite pegmatite.

During GSWA mapping of BELELE, a previously undocumented barite deposit was discovered about 18 km east of Jillewarra, near Quartzite Hill. Elias (1982, p. 19) stated that the barite occurs in a quartz vein and is present over a width of about 40 m. Individual barite zones are about 1 m wide and the mineralization extends along a strike length of about 200 m. The quartz–barite vein system occupies a D_5 fault belonging to the Mingah Shear Zone System, and is probably genetically related to the Chesterfield barite deposit.

Minor occurrences of barite are associated with some gold deposits (e.g. Warda Warra; Simpson, 1948, p. 189) and a small deposit occurs in association with copper-stained volcanogenic sedimentary rocks east of Quinns.

Construction material

The engineering properties of rocks, which include such features as strength, suitability for foundations, stability on slopes and in excavations, and suitability as construction materials, depend on physical and chemical composition, freshness, and mode of occurrence. Granitoids are strong and stable when fresh, but in surface exposures are generally weakened and less stable due to weathering. Proterozoic dolerite is generally massive, and presents fewer engineering problems than Archaean dolerite and gabbro, which have been variably metamorphosed and deformed. Rocks such as schist and bedded sedimentary rocks are susceptible to failure along foliation planes, and plans for excavations or heavy constructions must take this into account. Conglomerate and sandstone may be highly jointed and are thus susceptible to failure in several directions.

Weathering in the Murchison Province commonly reaches depths of about 100 m. Fresh rock for construction purposes must generally be sought in hilly outcrops or from rock pavements. The few existing quarries are shown on GSWA 1:250 000 geological sheets.

All the principal settlements of the province are located close to hilly areas with available rock outcrops and gravel

deposits from colluvial material. However, in more remote areas where the regolith is limited to sand, clay, and salt lake deposits, road construction may present problems. Satisfactory road materials, such as crushed rock or laterite gravel, may have to be transported for considerable distances. The location of potential sources of such materials is indicated on the GSWA 1:250 000 geological sheets.

White quartz, for aggregate, decorative stone, or even as a source of silica, is available from several large quartz veins in the province (e.g. Eelya Hill).

Emerald

Emerald has been obtained from Poona, Warda Warra, and Noongal, although significant production has been recorded only at Poona. The gemstone is associated with pegmatite veins containing beryl, and owes its richer green colour to high chromium contents derived from intruded ultramafic rocks. The Poona deposits were described by Woodward (1914) and Wilson (1926); emerald at Noongal was discussed by Simpson (1948, p. 200–202), and the Warda Warra emerald occurrence was described by Darragh and Hill (1983).

Feldspar

Feldspar has been mined at Goodingnow and Bald Hill, 30 km west of Mount Gibson. According to Lipple et al. (1983), 1023 t of feldspar was obtained from the pegmatite quarry 1.5 km south of Goodingnow; no information is available on the Bald Hill deposit.

Gypsum

Gypsum deposits occur in the Lake Moore area in the southeastern part of the Murchison Province. Known deposits have high silt contents, but it is possible that higher quality material occurs on the lakes or within marginal dunes.

Kaolin

Kaolinitic saprolite is a common product of deep Tertiary weathering of felsic igneous rocks and quartzo- feldspathic sedimentary rocks. Some of these deposits elsewhere in the State are sufficiently high grade to be used in ceramics or fillers. The largest known kaolin deposit in the province is located just north of Carlinga well, 29 km east-northeast from Tallering Range. Lipple (1976) described the deposit as up to 40 m thick and averaging 20 m thick. It was reported to contain 60% kaolin, together with 40% quartz and other silicate minerals; resources inferred from drilling are 130 Mt, but total resources of this area may be about 500 Mt. Lipple (1976) noted production of 42 t of kaolin from Cue, but the precise location of this deposit was not recorded.

Magnesite

Magnesite is a common weathering product of ultramafic rocks, above which it forms residual caps or nodules. The mineral occurs near Abbotts, and several other deposits were briefly described by Simpson (1952, p. 77–86).

Ochre

Wilgie Mia, in the Weld Range, is the oldest and largest ochre mine in Western Australia. The deposit has been worked by Aborigines for several thousand years and it is estimated that during this period about 46 500 t ('15 000 cubic yards') of ochre were removed (Woodward, 1914, p. 74–89). The ochre is of high quality and was reportedly traded across Australia as far as Queensland.

The ochre forms veins and lenses within a supergene deposit of massive hematite developed in BIF of the Windaning Formation (see 'Iron ore, Weld Range'). The workings form a cavernous open-cut, about 30 m deep and 50 m across. The ochre is chiefly bright red, but close to the surface there are narrow veins of yellow ochre. Smaller ochre deposits along the Weld Range include Little Wilgie Mia, 3 km west-southwest of Wilgie Mia, and a deposit of yellow ochre 5 km south of Mindoolah. Since 1944, ochre production from Wilgie Mia and the smaller Weld Range deposits has totalled 10 738 t. Gibson (1976, p. 295–296) stated that minor production has also been recorded from Pinnacles and Rothsay, and that yellow ochre is available near Meekatharra.

Talc

Talc is widespread as an important constituent of altered ultramafic rocks, but no production of the mineral has been recorded from the Murchison Province. The most significant occurrences are at Garden Gully, where a unit of altered peridotite within the Gabanintha Formation has been tested, and at Poona where Simpson (1952, p. 617) noted the existence of a 0.15 m-wide vein of talc.

Chapter 8

Crustal evolution

Previous models of granite–greenstone evolution

Windley (1984) has succinctly described the historical development of models for crustal evolution of Archaean granite–greenstone terranes. Most are variations of three principal models:

(1) Lower parts of greenstone successions represent oceanic crust (Glikson, 1972, 1979; Glikson and Lambert, 1976). Subsidence and partial melting of this crust resulted in diapiric intrusion of Na-rich granites. Upper greenstone sequences were then developed in troughs between the major granite intrusions. Deformation and metamorphism were followed by intrusion of late potassic granites.

(2) Greenstones developed in ensialic basins and/or rifts in extensional tectonic regimes (Groves et al., 1978; Archibald et al., 1981; Groves and Batt, 1984; Ayres and Thurston, 1985). The basins were filled with extensive, laterally continuous volcanic and associated sedimentary rocks. Rifts may have developed by further extension of basins or may represent new depositories. Rifts in older basins are dominated by trough sediments, while those in younger terrains contain abundant komatiites (Groves and Batt, 1984).

(3) A number of plate-tectonic models have been proposed in which analogies to modern plate-margin volcanism are drawn (Windley, 1984, p. 52–57). The most popular of these is the marginal basin model in which greenstones formed in back-arc spreading centres (Burke et al., 1976; Tarney et al., 1976; Drury, 1983). Other models include greenstones forming over proto-oceanic ridge systems, involving only small amounts of continental separation (Windley, 1973), and over island-arcs (Condie, 1981; Dimroth et al., 1982). In most of these models greenstones form in linear depositories and show chemical and temporal asymmetry in development of plutonic, volcanic, and sedimentary rocks.

It is clear from this summary that the nature of the basement is a critical factor in formulating a model for granite–greenstone evolution.

Nature of the basement

One of the main problems in constructing tectonic models for most Archaean granite–greenstone terranes is that the basement upon which the greenstones developed is not exposed and its nature is poorly understood. Two types of basement have been inferred in most previous models, a simatic 'oceanic' type (e.g. Glikson, 1972; Glikson and Lambert, 1976), and a sialic 'continental' type (e.g. Archibald et al., 1981; Gee et al., 1981, Groves and Batt, 1984). Several lines of evidence suggest that the basement to the Murchison Supergroup was an assemblage of much older rocks comprising siliceous granulite, mafic granulite, garnet amphibolite, and tonalite. This evidence is summarized below.

Lithological evidence

Greenstones that were formed in a simatic setting should be underlain by peridotite and, by analogy with Phanerozoic ophiolites, would have an entirely igneous stratigraphy (except for uppermost cherty sedimentary rocks) with abundant pillow lavas and sheeted dykes. Some geologists have argued that Archaean oceanic crust would not contain sheeted dykes or abundant pillow lava because of higher heat flow, resulting in faster spreading rates and increased magma supply (Dalziel et al., 1974; Tarney et al., 1976). However, probable remnants of Archaean oceanic crust do contain these features in at least one instance (Helmstaedt et al., 1986).

In Luke Creek Group rocks, pillow lavas are rare and restricted to small areas; sheeted dykes are not evident. Further, although sedimentary and felsic volcanic units are abundant towards the top of this group, they also occur throughout the succession. Epiclastic sandstone units in the Gabanintha Formation indicate the presence of exposed sialic basement during development of lower greenstone formations.

Geophysical evidence

The present crustal structure of the Yilgarn Craton has been investigated by regional gravity surveys, deep seismic refraction, and heat-flow studies (see references in Archibald

et al., 1981, and Gee et al., 1981). These data indicate a three-layer stratification of crust beneath the granite–greenstone terrane (Drummond, 1979; Archibald et al., 1981, fig. 1). Granitoids dominate the upper layer (density = 2.78 g/cm^3), and granulite forms the middle layer (density = 2.94 g/cm^3). These layers have acid to intermediate composition and a combined thickness of about 32 km, in the Eastern Goldfields Province, which thins to 14 km beneath the Western Gneiss Terrane. The lowermost layer of mafic granulite (density = 3.1 g/cm^3) is up to 32 km thick beneath the Western Gneiss Terrane and thins towards the east to a few kilometres thickness beneath the Eastern Goldfields Province (Archibald et al., 1981, fig. 1).

Geochemical and isotopic evidence

(a) Some Murrouli Basalt units in the Mount Magnet region show enrichment of incompatible elements, suggesting assimilation of felsic crustal material.

(b) High-(Zr+Y) felsic volcanic rocks (c. 3000 Ma) in the Gabanintha Formation have REE and other trace-element characteristics that suggest a siliceous granulite source; but more abundant low-(Zr+Y) felsic volcanic rocks from the same formation were derived from mafic crust.

(c) Most suite II post-folding granitoids in the southern Murchison Province have geochemical characteristics consistent with derivation by partial melting of siliceous granulite. U–Pb zircon ages of these rocks give emplacement ages of 2641 Ma and 2617 Ma, but Sm–Nd model ages indicate that the source rocks resided in the crust for at least 500 million years before partial melting. Suite I post-folding granitoids in the northern Murchison Province were derived by partial melting of mafic rocks with crustal residence times of a few hundred million years.

(d) Pegmatite-banded gneiss protoliths emplaced at 2920 Ma were derived by partial melting of mafic to intermediate crustal granulite. The antiquity of the source is indicated by Sm–Nd model ages of 2932 Ma, 2933 Ma, and 3171 Ma.

Evidence for ancient crustal rocks in adjacent terranes

Old zircon ages have been reported from eastern Yilgarn granite–greenstone provinces. Compston et al. (1984) reported U–Pb ages of 2700 Ma, 3100 Ma, and 3500 Ma from zircon xenocrysts in basalts at Kambalda in the Eastern Goldfields Province. Detrital zircons from the Maynard Hills quartzite at the base of the greenstone succession in the Southern Cross Province gave two groups of U–Pb ages in the ranges 3700–3600 Ma and 3400–3300 Ma (Froude et al., 1983). Both studies indicated the presence of crust significantly older than the granite–greenstone terrane in the eastern Yilgarn Craton.

The oldest crust identified in the Yilgarn Craton is the 3630–3350 Ma Narryer Gneiss Complex to the northwest of the Murchison Province (Myers and Williams, 1985). This terrane is in tectonic contact with the Murchison Province (Myers, 1990). It does not contain the 2.9 Ga pegmatite-banded gneiss, but its boundary with the Murchison Province is intruded by recrystallized monzogranite protoliths. The inference is that the Narryer Gneiss Complex may have been a considerable distance from the Murchison Province at the time of greenstone development, but was adjacent to the province by about 2690 Ma. Thus, it cannot be assumed that the Narryer Gneiss Complex extended beneath the Murchison Province granite–greenstone terrane to form its basement.

Tectonic considerations

Large-scale tectonic considerations support the hypothesis of ensialic greenstone development. Generation of oceanic crust was probably an important rock-forming process in the Archaean (Arndt, 1983; Nisbet and Fowler, 1983); however, the nature of this simatic crust is conjectural (Nisbet, 1982). As in the Phanerozoic, Archaean oceanic crust would only be preserved in unusual circumstances (e.g. obduction in marginal basins); most of this crust would be subducted and little would be preserved. Preservation of Archaean greenstones requires that they be erupted onto buoyant sialic crust, thereby preventing their destruction by subduction (Nisbet and Fowler, 1983).

Conclusion

From the evidence above, it seems that the basement was an assemblage of siliceous granulite, mafic granulite, garnet amphibolite, and tonalite. Siliceous granulite probably overlay mafic granulite, but these layers were probably quite heterogeneous and contained significant units of garnet amphibolite and tonalite. The basement beneath granitoids and greenstones was thus a mixture of rock types and was broadly intermediate in bulk composition.

Model of crustal evolution for the Murchison Province

Constraints

The following facts and inferences constrain any model of crustal evolution and related mineralization for the Murchison Province:

(a) Earliest lavas were erupted in relatively deep water upon sialic basement.

(b) The lower greenstone group has a 'layer-cake' style of stratigraphy developed over a very large area; it was not confined to a linear trough.

(c) The upper greenstone group developed unconformably on the lower group, as a number of shallow-water to subaerial volcanic centres and one large sedimentary basin. These were distributed over a region as wide as that for the lower group.

(d) Mafic and felsic volcanic rocks were derived by partial melting of uppermost mantle, and crustal rocks, respectively.

(e) Granitoids were derived by partial melting of crustal rocks; their emplacement was largely structurally controlled.

(f) Deformation was due to externally imposed lateral compression and was not due to vertical gravity-driven tectonics.

(g) In the Murchison Province there was northeast–southwest asymmetry in aspects of stratigraphic development, composition of some units, metamorphic grade, and epigenetic gold mineralization. The two lowest greenstone formations, the Murrouli Basalt and Golconda Formation, do not occur in the southwest. Furthermore, the large epiclastic sedimentary basin of the upper greenstone group is confined to the southwest. Gabanintha Formation basalts are depleted in incompatible elements in the southwest, but enriched in these in the northeast. Suite I post-folding granitoids occur mainly in the northeast, but suite II plutons occur mainly in the southwest. Metamorphic grade in the extreme southwest is amphibolite facies; in the remainder of the province it is mainly greenschist facies. Gold mineralization is more abundant in the northeastern half of the province. The boundaries between these northeast–southwest asymmetrical features are not coincident. Pegmatite-banded gneiss is also asymmetrically disposed; most occurs in the west of the province and outcrops decrease in abundance to the east.

(h) The main episode of gold mineralization was after the peak of regional metamorphism; most gold deposition occurred over a P–T range of 100–250 MPa and 250–350°C. Gold-related alteration assemblages are typically retrograde.

(i) Ore fluids responsible for gold mineralization were chiefly derived from the lower crust, probably by granulitization and partial melting of predominantly mafic material beneath the lower levels of greenstone belts.

Tectonic setting

Models involving development of greenstones on, or as, oceanic crust can be excluded because most indicators point to a sialic basement to greenstones. Plate-margin models are difficult to justify as no linear controls are evident in development of lithostratigraphy (see also Groves et al., 1978). There is a certain asymmetry in development of some rock units, but it is not of the type generally associated with plate margins (Windley, 1984). Moreover, there is little evidence of temporal variation of rock-forming events across the Murchison Province. However, some form of plate-tectonic process probably influenced the tectonic environment of greenstone deposition, but this would have operated on a scale much larger than that of the Murchison Province.

The most appropriate tectonic setting for initial development of the Murchison Supergroup appears to be an extensional ensialic basin. Stages in the development of an ensialic model for the Murchison Province are shown schematically in Figure 171, and are described below.

Stages of crustal development

A. Basement extension and development of the Luke Creek Group — c. 3000 Ma

The ensialic depository for the Murchison Supergroup developed by extension and consequent thinning and subsidence of the basement. From the present distribution of greenstones, and the nature of basal lavas, the basin was probably at least of the order of 600–800 km long, 300–400 km wide, and 2 km deep. Plate-tectonic processes were probably responsible for development of such a large crustal structure. Partial melting of uppermost mantle rocks beneath the basin generated mafic and ultramafic magma which intruded the crust through major fractures. Magma erupted rapidly on the deep basin floor and formed vast lava plains. Basin development began in the northeastern and central parts of the province with deposition of the Murrouli Basalt and Golconda Formation. These units were not deposited in the southwest, which indicates delayed basin development, possibly because the crust was more buoyant in this region, due to a thicker silicic granulite layer.

The basement was already deeply submerged before eruption of basal lavas. Basement subsidence would have continued, due to loading of the crust by dense lava plains (cf. Ayres and Thurston, 1985). Elevation of isotherms in the crust because of subsidence, and local heating due to rising mafic magma, caused partial melting of crustal rocks, generating felsic magma. Subsidence did not keep pace with eruption, as felsic volcanic and sedimentary depositional structures indicate shallow water over most of the region when development of the Luke Creek Group ended.

Mafic volcanic rocks were derived by partial melting of uppermost mantle rocks, followed by crystal fractionation, mainly of olivine and pyroxenes. The uppermost mantle beneath the northeastern Murchison Province was enriched in incompatible elements, but that beneath the southwestern part of the province was depleted in these elements during volcanic development of the Luke Creek Group. Felsic volcanic rocks were derived from partial melting of various lower crustal rocks, generally with low crustal-residence times, and do not show regional differences in chemistry. Syngenetic copper–lead–zinc–silver–gold

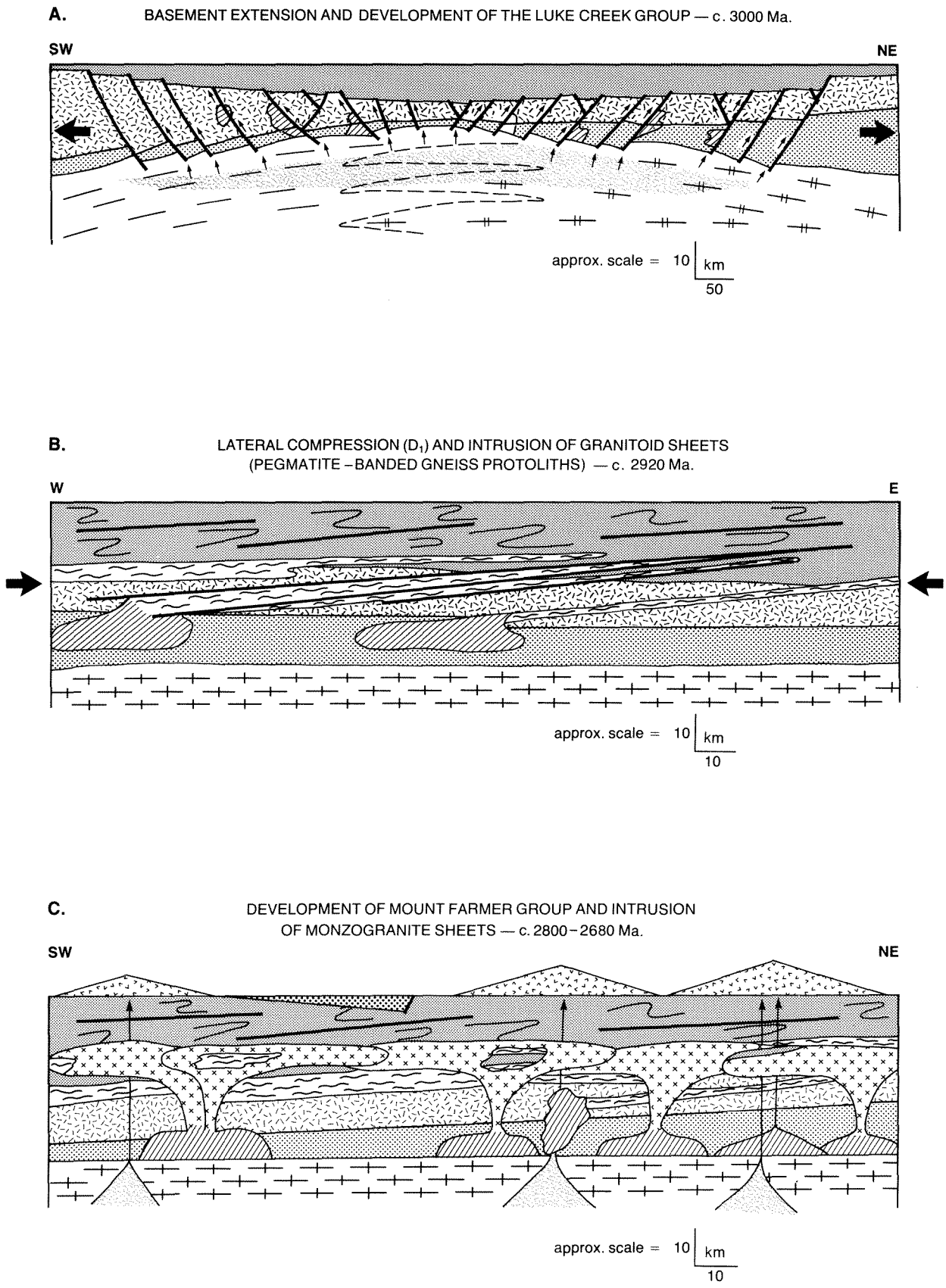


Figure 171. Crustal evolution in the Murchison Province.

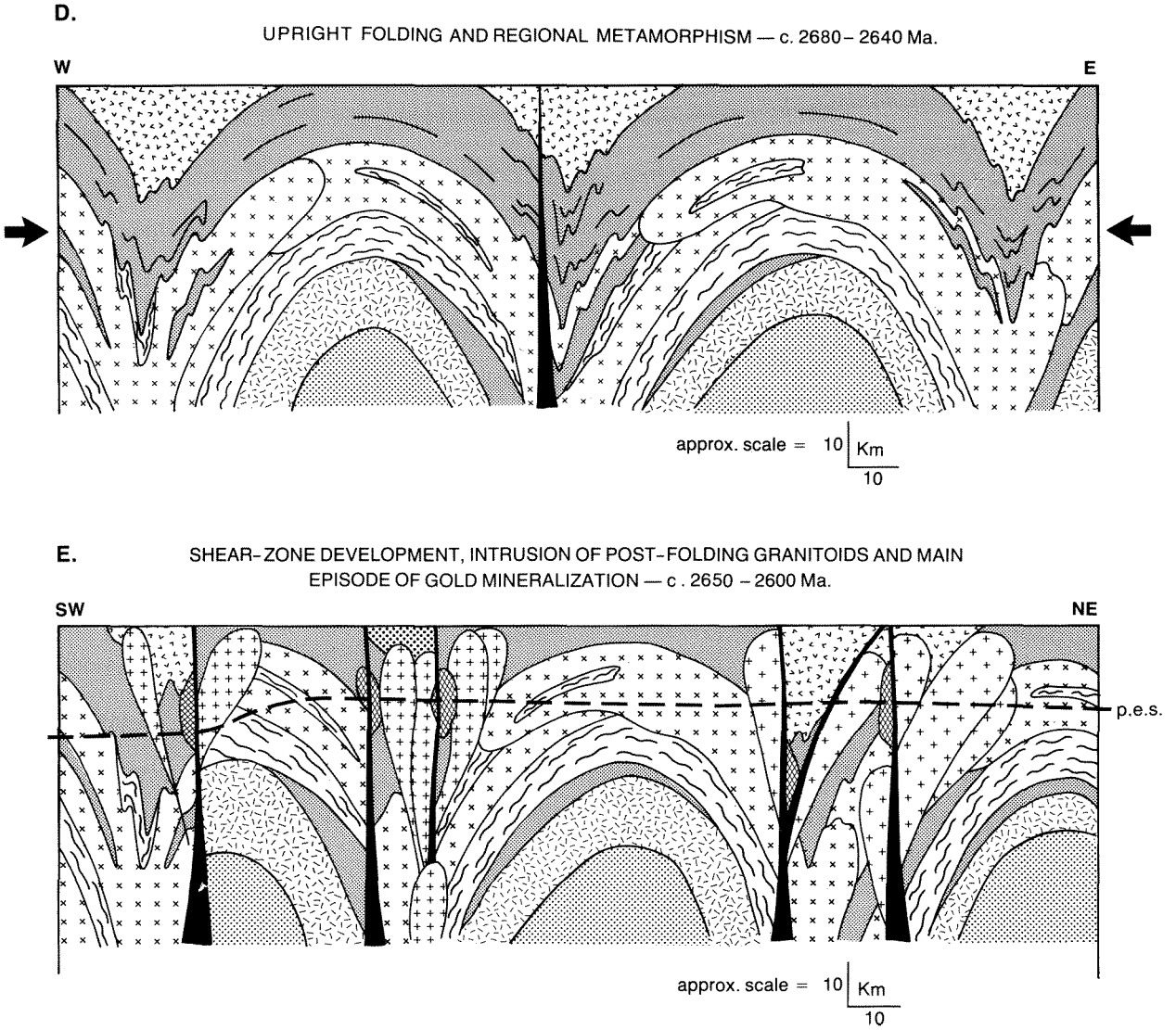


Figure 171. (continued)

mineralization was associated with some felsic volcano-sedimentary complexes (e.g. Golden Grove).

B. Lateral compression and intrusion of granitoid sheets (pegmatite-banded gneiss protoliths) c. 2920 Ma

Following development of the Luke Creek Group, a phase of horizontal compressional deformation formed large recumbent folds and thrusts, particularly in the relatively thick succession of the northeast. Subhorizontal monzogranite, granodiorite, and pegmatite sheets intruded the base of the Luke Creek Group during this deformation at about 2920 Ma. The granitoids were deformed along with the greenstones and formed pegmatite-banded gneiss. The crust was considerably thickened during these events.

Granitoid melts were derived by partial melting of lower crustal mafic granulite, garnet amphibolite and/or tonalite. Partial melting was a consequence of rising isotherms in subsiding basement. The subsidence was caused by loading of the crust by the Luke Creek Group and/or D_1 tectonic thickening.

Epigenetic gold mineralization resulted from upward migration of fluids derived from lower crustal granulitization and partial melting, and formed stratabound orebodies along layer-parallel thrusts. In detail, many of these deposits occupy structures which are locally discordant to lithological layering.

C. Development of the Mount Farmer Group and intrusion of monzogranite sheets c. 2800–2680 Ma

Shield volcanoes and stratovolcanoes that form individual formations in the Mount Farmer Group developed on an infrastructure of Luke Creek Group rocks. These volcanic rocks erupted in shallow-water to subaerial environments. Their distribution suggests that there were no linear tectonic controls of deposition. Mount Farmer Group mafic volcanic rocks were derived from uppermost mantle sources similar to their Luke Creek Group counterparts. There appear to be no regional differences in basalt chemistry; however, most Mount Farmer Group basalts show evidence of assimilation of felsic material during ascent through the crust. Felsic volcanic rocks in this group were derived by similar processes and from similar crustal sources as those in the Luke Creek Group.

A major epiclastic sedimentary basin developed in the southern Murchison Province in the Mount Farmer Group. From present outcrop distribution the basin was at least 170 km long, 90 km wide, and the sedimentary sequence was about 2 km thick. Some of the margins of this basin may have been fault controlled. The maximum preserved thickness of the Mount Farmer Group is 5 km. Subsidence of basement, Luke Creek Group rocks, and pegmatite-banded gneiss due to loading by Mount Farmer Group rocks kept pace with development of this succession.

The base of the Murchison Supergroup was intruded by numerous thick subhorizontal sheets of monzogranite over a period of time, at least 2690–2681 Ma, following development of the Mount Farmer Group. These minimum-melt intrusions generated amphibolite-facies contact metamorphic aureoles in adjacent greenstones. The monzogranite was subsequently recrystallized, and the contact aureoles retrograded, during regional metamorphism. Recrystallized monzogranite is compositionally very similar to pegmatite-banded gneiss and was derived by partial melting of similar crustal source rocks. Partial melting may have been caused by upward relaxation of isotherms in subsiding crust loaded by the Mount Farmer Group.

Gold–tungsten placer deposits accumulated locally in the pyritic conglomerate units of the Mount Farmer Group as a result of erosion of syngenetic and epigenetic deposits in the Luke Creek Group. Titanium – vanadium – magnetite deposits are associated with large layered mafic intrusions; some of these intrude the Mount Farmer Group but others could be older than 2800 Ma. Stratabound Cu–Zn mineralization developed locally in tuff and volcanogenic sedimentary rocks of the Mount Farmer Group (e.g. Mount Mulcahy).

D. Upright folding and regional metamorphism c. 2680–2640 Ma

Within a 40 million-year period following intrusion of the recrystallized monzogranite protolith, several events occurred. F_2 and F_3 folding of greenstones, gneiss, and granitoids was followed by regional metamorphism, shear-zone development, intrusion of post-folding granitoids, and the main episode of epigenetic gold mineralization. Easterly trending, upright, tight F_2 folds were refolded by more intense north-northwest to north-northeasterly trending, upright, tight to isoclinal F_3 folds; these events formed dome-and-basin fold patterns on all scales from a few centimetres to 100 km across. High-strain zones developed at monzogranite–greenstone contacts due to simple shear modification of fold limbs, enhanced by the ductility contrast between these rock types. The folding resulted from lateral compression and was largely responsible for the present granite–greenstone pattern in the Murchison Province.

The Murchison Supergroup, pegmatite-banded gneiss, and monzogranite were regionally metamorphosed as a consequence of dome-and-basin folding of isotherms and subsequent thermal relaxation towards steady-state conditions. The metamorphic grade of rocks now exposed across most of the province is greenschist facies, but cores of some greenstone belts in the northern part of the province are in prehnite–pumpellyite facies, and rocks in the extreme southwest of the province are in amphibolite facies. Thermal relaxation, and hence regional metamorphism, was terminated by uplift and erosion before isotherms achieved steady-state horizontal attitudes. This preserved the lower metamorphic grades in cores of thicker greenstone belts in the northern Murchison Province. Amphibolite-facies rocks in the southwest may reflect greater post-metamorphic uplift in this region due to the buoyancy of a thicker silicic basement granulite layer in this region.

Shear zones and fracture systems related to D_2 folds (e.g. at Mount Magnet) contain epigenetic gold deposits which have been subsequently deformed by D_3 and D_4 structures.

E. Shear-zone development, intrusion of post-folding granitoids, and gold mineralization c. 2650–2600 Ma

Major north-northwest to north-northeasterly trending faults and shear zones developed over a long time period from late D_3 to some time after intrusion of post-folding granitoids. Shear zones are most recognizable in the greenstone belts, but also extend into the granitoids. Many of these structural breaks are zones of highly strained rock and mylonite, several hundreds of metres wide (and in a few cases up to 1 km wide) and over 200 km long. These very large-scale structures probably extend to the lower crust, or even to the upper mantle. Most displacements were dextral, although a few were sinistral or vertical. The shear zones probably developed in response to continued regional compression in the same stress field which caused F_3 folding.

Post-folding granitoid plutons intruded greenstone belts and earlier granite–greenstone contacts during shear-zone development. They have not been recognized wholly within recrystallized monzogranite or pegmatite-banded gneiss. Intrusion of most plutons post-dated the peak of regional metamorphism, but some were recrystallized. Shear zones may have localized intrusion into greenstone belts at deep levels by acting as pathways to the upper crust for granitoid melts. At higher levels, plutons became decoupled from shear zones and were emplaced by stoping and magma-wedging into brittle crust.

Two suites of post-folding granitoids, suite I and suite II, intruded greenstone belts and recrystallized monzogranite–greenstone contacts. Suite I plutons occur in the northeastern half of the province and intrude the Tallering and Twin Peaks greenstone belts in the west. They consist of tonalite, granodiorite, monzogranite, and trondhjemite and were derived by partial melting of mafic crustal source rocks. Suite II plutons occur mainly in the southwestern half of the province, but they also occur, mixed with suite I plutons, in the Tallering and Twin Peaks greenstone belts in the west, and in the Mingah Range and Abbotts greenstone belts in the north. They consist of quartz-rich syenogranite and monzogranite and were derived by partial melting of siliceous granulite, but some intrusions may have been derived from source rocks of more mafic character. Limited Sm–Nd isotope data indicate that sources of suite II granitoids were several hundred million years older than suite I source rocks. Suite II partial melts probably formed from a variety of sources, but mainly from a thick siliceous basement granulite layer in the southwest. In the northeast, suite I partial melts were generated in mafic crust which underplated or intruded the basement. Sm–Nd dates from suite I granitoids and the Woolgra Formation (both about 2.8 Ga) indicate that these mafic source rocks were temporally associated with volcanic rocks in the Mount Farmer Group. Partial melting was induced by crustal thickening and warping during dome-and-basin folding and consequent upward relaxation of isotherms.

Gold-bearing hydrothermal fluids were generated in the lower crust, and possibly upper mantle, in response to elevated P–T conditions beneath regional synclines. At these levels the D_4 shear zones were probably many kilometres wide, permitting extensive fluid liberation and channelling to the upper crust. Gold precipitation occurred under P–T conditions of 100–250 MPa and 250–350°C, as a result of chemical reactions with wall rocks in structurally favourable sites. Sulphidation reactions were most important, and Fe-rich rocks were the preferred host lithologies. Where BIF units were intersected by the fluid conduits, gold deposition occurred preferentially in them; if BIF was not available, ultramafic rocks were preferentially mineralized, and in the absence of ultramafic rocks mafic rocks became the principal hosts. This is consistent with the main gold transporting agents being reduced-sulphur complexes which precipitated gold during fluid sulphidation of Fe-rich rocks.

The fact that most gold mineralization occurred after peak regional metamorphism could indicate thermal convective circulation of metamorphic fluids in the shear zones for some time after peak metamorphism, possibly driven by heat from cooling post-folding granitoid plutons.

In summary, the Murchison Supergroup was deposited in an extensional ensialic basin that developed as a result of large-scale plate-tectonic processes. Subsidence of the crust under loading from greenstones, and tectonic compression, controlled further development of greenstones and intrusion of granitoids. Compression events were externally imposed, probably by large-scale plate-tectonic processes. Eventually, the crust was sufficiently thick and buoyant, as a result of tectonic compression and intrusion of granitoids, to form a stable cratonic region.

References

AHMAT, A. L., 1986a, Petrology, structure, regional geology and age of the gabbroic Windimurra Complex, Western Australia: University of Western Australia, PhD Thesis (unpublished).

AHMAT, A. L., 1986b, Metamorphic patterns in the greenstone belts of the Southern Cross Province, Western Australia: Western Australia Geological Survey, Report 19, p. 1–21.

AHMAT, A. L., 1990, Windimurra Complex, *in* Geology and Mineral Resources of Western Australia: Western Australia Geological Survey, Memoir 3, p. 120–124.

AHMAT, A. L., and de LAETER, J. R., 1982, Rb–Sr isotopic evidence for Archaean–Proterozoic crustal evolution of part of the central Yilgarn Block, Western Australia — constraints on the age and source of the anorthositic Windimurra Gabbroid: Geological Society of Australia, Journal, v. 29, p. 177–190.

ALLEGRE, C. J., and OTHMAN, D. B., 1980, Nd–Sr isotopic relationship in granitoid rocks and continental crust development — a chemical approach to orogenesis: Nature, v. 286, p. 335–342.

ALLEN, P., CONDIE, K., and BOWLING, G. P., 1986, Geochemical characteristics and possible origins of the southern Closepet Batholith, south India: Journal of Geology, v. 94, p. 283–299.

ANDERSON, I. G., in press, The Galtee More gold mine, Mount Magnet, Western Australia, *in* Geology of the mineral deposits of Australia and Papua New Guinea *edited by* F. E. HUGHES: Australasian Institute of Mining and Metallurgy, Monograph 14.

ANDREWS, A. J., HUGON, H., DUROCHER, M., CORFU, F., and LEVIGNE, M. J., 1986, The anatomy of a gold bearing greenstone belt — Red Lake, Northwestern Ontario, Canada; *in* Gold '86, An International Symposium on the Geology of Gold Deposits, Toronto, Proceedings, p. 3–22.

ANHAEUSSER, C. R., 1984, Structural elements of Archaean granite–greenstone terrains as exemplified by the Barberton Mountainland, southern Africa, *in* Precambrian Tectonics Illustrated *edited by* A. KRÖNER and R. GREILING: Stuttgart, E. Schweizerbart'sche Verlagsbuchhandlung, p. 57–78.

ANHAEUSSER, C. R., and ROBB, 1983, Chemical analyses of granitoid rocks from the Barberton Mountain Land: Geological Society of South Africa, Special Publication No. 9, p. 189–219.

ARBOYNE, N.L., 1987, Prospectus, Arboyne N.L., 6 March 1987: Perth.

ARCHIBALD, N., 1982, Structure, lithological association units and gold mineralization, Mt. Magnet area, *in* Archaean geology of the southern Murchison *edited by* J. L. BAXTER: Geological Society of Australia (W.A. Division), Excursion Guide, p. 15–27.

ARCHIBALD, N. J., and BETTENAY, L. F., 1977, Indirect evidence for tectonic reactivation of a pre-greenstone sialic basement in Western Australia: Earth and Planetary Science Letters, v. 33, p. 370–378.

ARCHIBALD, N. J., BETTENAY, L. F., BINNS, R. A., GROVES, D. I., and GUNTHORPE, R. J., 1978, The evolution of Archaean greenstone terrains, Eastern Goldfields Province, Western Australia: Precambrian Research, v. 6, p. 103–131.

ARCHIBALD, N. J., BETTENAY, L. F., BICKLE, M. J., and GROVES, D. I., 1981, Evolution of Archaean crust in the Eastern Goldfields Province of the Yilgarn Block, *in* Archaean Geology *edited by* J. E. GLOVER and D. I. GROVES: International Archaean Symposium, 2nd, Perth, W.A., 1980, Proceedings; Geological Society of Australia, no. 7, p. 491–504.

ARNDT, N. T., 1983, Role of a thin, komatiite-rich oceanic crust in the Archean plate-tectonic process: Geology, v. 11, p. 372–375.

ARNDT, N. T., and JENNER, G. A., 1986, Crustally contaminated komatiites and basalts from Kambalda, Western Australia: Chemical Geology, v. 56, p. 229–255.

ARNDT, N. T., and NISBET, E. G., 1982, What is a komatiite?, *in* Komatiites *edited by* N. T. ARNDT and E. G. NISBET: London, George Allen and Unwin, p. 19–27.

ARRIENS, P. A., 1971, The Archaean geochronology of Australia, *in* Symposium on Archaean Rocks *edited by* J. E. GLOVER: Geology Society of Australia, Special Publication no. 3, p. 11–23.

ARTH, J. G., BARKER, F., PETERMAN, Z. E., and FRIEDMAN, I., 1978, Geochemistry of the gabbro–diorite–tonalite–trondhjemite suite of southwest Finland and its implications for the origin of tonalite and trondhjemite magmas: Journal of Petrology, v. 19, p. 289–316.

ARZI, A. A., 1978, Critical phenomena in the rheology of partially melted rocks: Tectonophysics, v. 44, p. 173–184.

AUSTIN, R., 1855, Journal of an expedition sent by the Government to explore the interior of western Australia north and east of the settled districts for extensive tracts of fertile land available for pastoral and agricultural purposes: Perth, Government Printer, 59p.

AUSTRALIAN CONSOLIDATED MINERALS LTD, 1987, Annual Report: Perth.

AYRES, L. D., 1982, Pyroclastic rocks in Precambrian greenstone belt volcanoes, *in* Pyroclastic volcanism and deposits of Cenozoic intermediate to felsic volcanic islands with implications for Precambrian greenstone-belt volcanics *edited by* L. D. AYRES: Geological Society of Canada, Short Course Notes, v. 2, p. 343–365.

AYRES, L. D., 1983, Bimodal volcanism in Archaean greenstone belts exemplified by greywacke composition, Lake Superior Park, Ontario: Canadian Journal of Earth Science, v. 20, p. 1168–1194.

AYRES, L. D., and THURSTON, P. C., 1985, Archean supracrustal sequences in the Canadian Shield — an overview: Geological Association of Canada, Special Paper 28, p. 343–380.

BAILEY, D. K., 1982, Mantle metasomatism–continuing chemical change within the Earth: Nature, v. 296, p. 525–530.

BALDE, R., and WOOLFE, T. I., in press, St. George Gold Mine, Mt. Magnet, Western Australia, *in* Geology of the mineral deposits of Australia and Papua New Guinea *edited by* F. E. HUGHES: Australasian Institute of Mining and Metallurgy Monograph 14.

BARKER, F., and ARTH, J. G., 1976, Generation of trondhjemitic–tonalitic liquids and Archean bimodal trondhjemite–basalt suites: Geology, v. 4, p. 596–600.

BARLEY, M. E., 1986, Incompatible-element enrichment in Archaean basalts — A consequence of contamination by older sialic crust rather than mantle heterogeneity: Geology, v. 14, p. 947–950.

BARLEY, M. E., SYLVESTER, G. C., and GROVES, D. I., 1984, Archaean calc-alkaline volcanism in the Pilbara Block, Western Australia: Precambrian Research, v. 24, p. 285–319.

BARTLEY, J. M., 1986, Evaluation of REE mobility in low-grade metabasalts using mass-balance calculations: Norsk Geologisk Tidsskrift, v. 66, p. 145–152.

BASALTIC VOLCANISM STUDY PROJECT, 1981, Basaltic volcanism on the terrestrial planets, New York, Pergamon Press Inc., 1286p.

BAXTER, J. L., 1974, Murgoo, Western Australia: Western Australia Geological Survey, 1:250 000 Geological Series Explanatory Notes.

BAXTER, J. L., 1978, Molybdenum, tungsten, vanadium and chromium in Western Australia: Western Australia Geological Survey, Mineral Resources Bulletin 11.

BAXTER, J. L., 1982, The regional setting of the southern Murchison, *in* Archaean geology of the southern Murchison *edited by* J. L. BAXTER: Geological Society of Australia (W.A. division), Excursion Guide, p. 1–5.

BAXTER, J. L., LIPPLE, S. L., and MARSTON, R. J., 1983, Kirkalocka, Western Australia: Western Australia Geological Survey, 1:250 000 Geological Series Explanatory Notes.

BAXTER, J. L., and LIPPLE, S. L., 1985, Perenjori, Western Australia: Western Australia Geological Survey, 1:250 000 Geological Series Explanatory Notes.

BEARD, J. S., 1976, Vegetation survey of Western Australia, Murchison 1:1 000 000 Vegetation Series, Explanatory Notes to Sheet 6: University of Western Australia Press.

BERTHE, D., CHOUKROUNE, P., and JEGOUZO, P., 1979, Orthogneiss, mylonite and non-coaxial deformation of granites — the example of the South Amorican Shear Zone: Journal of Structural Geology, v. 1, p. 31–42.

BEWICK MOREING AND CO., 1902, Brief report on Wheel of Fortune North, Lennonville, Western Australia: Engineer's Report, 15 November 1902, Kalgoorlie (unpublished).

BICKLE, M. J., BETTENAY, L. F., BARLEY, M. E., CHAPMAN, H. J., GROVES, D. I., CAMPBELL, I. H., and De LAETER, J. R., 1983, A 3500 Ma plutonic and volcanic calc-alkaline province in the Archaean east Pilbara Block: Contributions to Mineralogy and Petrology, v. 84, p. 25–35.

BICKLE, M. J., BETTENAY, L. F., BOULTER, C. A., GROVES, D. I., and MORANT, P., 1980, Horizontal tectonic interaction of an Archaean gneiss belt and greenstones, Pilbara Block, Western Australia: Geology, v. 8, p. 525–529.

BINNS, R. A., GUNTHORPE, R. J., and GROVES, D. I., 1976, Metamorphic patterns and development of greenstone belts in the eastern Yilgarn Block, Western Australia, *in* The Early History of the Earth *edited by* B. F. WINDLEY: London, Wiley-Interscience, p. 303–313.

BLATCHFORD, T., 1918, Notes on the Tuckabianna Mining Centre: Western Australia Department of Mines, Annual Report 1917, p. 64.

BLIGHT, D. F., 1978, Petrological evidence for an unusually high Archaean geothermal gradient in the Wongan Hills area, Western Australia: Western Australia Geological Survey, Annual Report 1977, p. 64–65.

BLIGHT, D. F., 1979, Aspects of amphibole chemistry and metamorphic gradient in the Wongan Hills area, Western Australia: Western Australia Geological Survey, Annual Report 1978, p. 105–108.

BLOCKLEY, J. G., 1962, Notes on the regional geology and mineralization, Chesterfield gold mining centre, Murchison Goldfield, Western Australia: New Consolidated Goldfields (Australasia) Pty Ltd, (unpublished).

BLOCKLEY, J. G., 1980, The tin deposits of Western Australia with special reference to the associated granites: Western Australia Geological Survey, Mineral Resources Bulletin 12.

BLOCKLEY, J. G., 1985, Report on Ministerial Iron Ore Temporary Reserves in the Yilgarn Block: Western Australia Geological Survey, Mineral Resources Report 177 (unpublished).

BLOCKLEY, J. G., and GIBSON, A. A., 1973, The Rothsay beryl deposits: Western Australia Geological Survey, Mineral Resources Report 33 (unpublished).

BROWN, G. C., 1981, Space and time in granite plutonism: Philosophical Transactions of the Royal Society, London, v. A301, p. 321–336.

BROWNING, P., GROVES, D. I., BLOCKLEY, J. G., and ROSMAN, K. J. R., 1987, Lead isotopic constraints on the age and source of gold mineralization in the Archaean Yilgarn Block, Western Australia: Economic Geology, v. 82, p. 971–986.

BUNTING, J. A., COMMANDER, D. P., ELIAS, M., and WHARTON, P. H., 1981, Glengarry, Western Australia: Western Australia Geological Survey, 1:250 000 Geological Series.

BURKE, K., DEWEY, J. F., and KIDD, W. S. F., 1976, Dominance of horizontal movements, arc and microcontinental collisions during the later permobile regime, *in* The Early History of the Earth *edited by* B. F. WINDLEY: London, Wiley-Interscience, p. 113–129.

BUTT, C. R. M., 1981, The nature and origin of the lateritic weathering mantle, with particular reference to Western Australia, *in* Geophysical prospecting in deeply weathered terrains *edited by* H. A. DOYLE, J. E. GLOVER and D. I. GROVES: University of Western Australia, Geology Department and Extension Service, Publication No. 6, p. 11–29.

BUTT, C. R. M., HORWITZ, R. C., and MANN, A. W., 1977, Uranium occurrences in calcrete and associated sediments in Western Australia: Australia CSIRO, Division of Mineralogy, Mineral Research Laboratory, Report FP 16.

CAMPBELL, J. D., 1953, The Triton gold mine, W.A. *in* Geology of Australian ore deposits *edited by* A. B. EDWARDS: Fifth Empire Mining and Metallurgy in Australia and New Zealand Congress, v. 1, p. 195–207.

CAMPBELL, W. D., 1903, Notes on the auriferous reefs of Cue and Day Dawn: Western Australia Geological Survey, Bulletin 7.

CARROLL, D., 1945, Census of Western Australian minerals: Western Australia Department of Mines, Mineral Resources Bulletin 1.

CARTER, J. D., and LIPPLE, S. L., 1982, Moora, Western Australia: Western Australia Geological Survey, 1:250 000 Geological Series Explanatory Notes.

CHAMBERLAIN, C. P., 1986, Evidence for repeated folding of isotherms during regional metamorphism: Journal of Petrology, v. 27, p. 63–89.

CHAMBERLAIN, C. P., and KARABINOS, P., 1987, Influence of deformation on pressure–temperature paths of metamorphism: Geology, v. 15, p. 42–44.

CHAPMAN, H. J., BICKLE, M. J., de LAETER, J. R., BETTENAY, L. F., GROVES, D. I., ANDERSON, L. S., BINNS, R. A., and GORTON, M., 1981, Rb–Sr geochronology of granitic rocks from the Diemals area, central Yilgarn Block, Western Australia, *in* Archaean Geology *edited by* J. E. GLOVER and D. I. GROVES: International Archaean Symposium, 2nd, Perth, W.A., 1980, Proceedings; Geological Society of Australia, Special Publication, no. 7, p. 173–186.

CHOWN, E. H., HICKS, J., PHILLIPS, G. N., and TOWNSEND, R., 1984, The disseminated Archaean Big Bell gold deposit, Murchison Province, Western Australia–an example of pre-metamorphic hydrothermal alteration, *in* Gold '82–The Geology, Geochemistry and Genesis of Gold Deposits *edited by* R. P. FOSTER: Rotterdam, A. A. Balkema Pub.; Geological Society of Zimbabwe, Special Publication, no. 1, p. 305–324.

CLARKE, E. de C., 1916, The geology and ore-deposits of Meekatharra, Murchison Goldfield: Western Australia Geological Survey, Bulletin 68.

CLARKE, E. de C., 1920, Melville (Noongal), Yalgoo Goldfield: Western Australia Geological Survey, Annual Report 1919, p. 95–96.

CLARKE, E. de C., 1925, The geology and mineral resources of the Yalgoo Goldfield, Part II, The mining centres of Rothsay and Goodingnow (Paynes Find): Western Australia Geological Survey, Bulletin 86.

CLARKE, E. de C., and TEICHERT, C., 1948, Cretaceous stratigraphy of the lower Murchison River area, Western Australia: Journal of the Royal Society of Western Australia, v. 32, p. 19–47.

CLIFFORD, B. A., 1987, Volcanic-sedimentary facies associations hosting the volcanogenic massive sulphide mineralization at Golden Grove, Western Australia, *in* The geology, structure, mineralization and economics of the Pacific Rim: Pacific Rim Congress, Queensland, August, 1987: Australasian Institute of Mining and Metallurgy Extended Abstracts.

COBBING, E. J., MALLICK, D. I. J., PITFIELD, P. E. J., and TEOH, L. H., 1986, The granites of the Southeast Asian Tin Belt: Journal of the Geological Society, London, v. 143, p. 537–550.

COBBOLD, P. R., and QUINQUIS, H., 1980, Development of sheath folds in shear regimes: Journal of Structural Geology, v. 2, p. 119–126.

COLLERSON, K. D., 1982, The Archaean gneiss complex of northern Labrador, 2 — mineral ages, secondary isochrons, and diffusion of strontium during polymetamorphism of the Uivak gneisses: Canadian Journal of Earth Science, v. 20, p. 707–718.

COLLINSON, J. D., 1986, Alluvial Sediments, *in* Sedimentary Environments and Facies (2nd edition) *edited by* H. G. READING: Oxford, Blackwell Scientific Publications, p. 20–62.

COLVINE, A. C., FYON, J. A., HEATHER, K. B., MARMONT, S., SMITH, P. M., and TROOP, D. G., 1988, Archaean Lode Gold Deposits in Ontario: Ontario Geological Survey, Miscellaneous Paper 139.

COMPSTON, W., WILLIAMS, I. S., and CLEMENT, S. W., 1982, U–Pb ages with single zircons using a sensitive high mass-resolution ion microprobe (abstr.): American Society of Mass Spectrometry, 30th Conference, Honolulu, p. 593–595.

COMPSTON, W., WILLIAMS, I. S., CAMPBELL, I. H., and GRESHAM, J., 1984, Xenocrystic zircons in the Kambalda volcanics: Australian National University, Research School of Earth Sciences, Annual Report 1984, p. 94–95.

CONDIE, K. C., 1978, Geochemistry of Proterozoic granitic plutons from New Mexico, U.S.A.: Chemical Geology, v. 21, p. 131–149.

CONDIE, K. C., 1981, Archaean greenstone belts — Developments in Precambrian Geology 3: Amsterdam, Elsevier Scientific Publishing Company, 434p.

CONDIE, K. C., 1982, Archaean andesites, *in* Orogenic andesites *edited by* R.S. THORPE: New York, John Wiley & Sons, p. 575–589.

CONDIE, K. C., 1984, Archaean geotherms and supracrustal assemblages: Tectonophysics, v. 105, p. 29–41.

CONNOLLY, H. J. C., 1936, A contour method of revealing some ore structures (preliminary contour test of the Great Fingall mine): Economic Geology, v. 31, p. 262–263.

CONNOLLY, R. R., 1959, Iron ores in Western Australia: Western Australia Geological Survey, Mineral Resources Bulletin 7.

CONNOLLY, R. R., 1960a, Report on exploratory drilling of the Tallering Range iron deposits: Western Australia Geological Survey, Annual Report 1959, p. 38–47.

CONNOLLY, R.R., 1960b, Notes on the occurrence of iron ore at Tallering Peak, Yalgoo Goldfield: Western Australia Geological Survey, Bulletin 114, p. 186–189.

CONNOLLY, R. R., 1962, Report on examination of GML 1942N, Margueritta G. M., Chesterfield, Murchison Goldfield: Western Australia Mines Department, Annual Report 1960, p. 99–100.

COWARD, M. P., 1981, Diapirism and gravity tectonics — Report on a Tectonic Studies Group conference held at Leeds University, 25–26 March 1980: Journal of Structural Geology, v. 3, p. 89–95.

COWARD, M. P., and JAMES, P. R., 1974, The deformation patterns of two Archaean greenstone belts in Rhodesia and Botswana: Precambrian Research, v. 1, p. 235–258.

COX, K. G., BELL, J. D., and PANKHURST, R. J., 1979, The interpretation of igneous rocks: London, George Allen and Unwin, 450p.

CULLERS, R. L., and GRAF, J. L., 1984a, Rare earth elements in igneous rocks of the continental crust — predominantly basic and ultrabasic rocks, *in* Rare earth element geochemistry *edited by* P.HENDERSON: Amsterdam, Elsevier, p. 237–274.

CULLERS, R. L., and GRAF, J. L., 1984b, Rare earth elements in igneous rocks of the continental crust — intermediate and silicic rocks — ore petrogenesis, *in* Rare earth element geochemistry *edited by* P. HENDERSON: Amsterdam, Elsevier, p. 275–316.

DALZIEL, I. W. D., DE WIT, M. J., and PALMER, K. F., 1974, Fossil marginal basin in the southern Andes: Nature, v. 250, p. 291–294.

DAHL, N., McNAUGHTON, N. J., and GROVES, D. I., 1987, Trace-element and lead isotopic composition of pyrites as guides to gold and base-metal mineralization — a pilot study: Western Australia Mineral and Petroleum Research Institute, Report 22, 57p.

DARRAGH, P. J., and HILL, R. E. T., 1983, The mineralogy and genesis of an emerald occurrence at Warda Warra near Yalgoo, Western Australia: Australia CSIRO, Division of Mineralogy, Research Review, 1983, p. 134–136.

DAVY, R., 1983, A contribution on the chemical composition of Precambrian iron-formations, *in* Iron-formation — facts and problems *edited by* A. F TRENDALL and R. C. MORRIS: Amsterdam, Elsevier, p. 325–343.

DAVY, R., and LEWIS, J. D., 1981, The geochemistry of the Mount Edgar batholith, Pilbara area, Western Australia: Geological Society of Australia, Special Publication no. 7, p. 373–384.

DAVY, R., and LEWIS, J. D., 1986, The Mount Edgar batholith, Pilbara area, Western Australia — Geochemistry and petrography: Western Australia Geological Survey, Report 17, 43p.

DAVY, R., HICKMAN, A. H., WATKINS, K. P., and MUHLING, P. C., 1986, Economic significance of geochemical data from granitoids in the Poona–Dalgaranga area, Murchison Province: Western Australia Geological Survey, Record 1986/9.

DAVY, R., CLARKE, R. M., SALE, M., and PARKER, M., 1988, The nature and origin of the gold bearing laterite at Mount Gibson, Western Australia: Second International Conference on Prospecting in Arid Terrains, Australasian Institute of Mining and Metallurgy, Abstracts Volume, p. 45–48.

DEITRICH, J. H., 1970, Computer experiments on mechanics of finite amplitude folds: Canadian Journal of Earth Science, v. 7, p. 467–476.

de la HUNTY, L. E., 1958a, The mining groups of the Mount Magnet disrict, Murchison goldfield: Western Australia Geological Survey, Bulletin 109, p. 30–76.

de la HUNTY, L. E., 1958b, Summary report on exploratory drilling for gold, Mount Magnet district, Murchison Goldfield: Western Australia Geological Survey, Bulletin 113, p. 59–98.

de la HUNTY, L. E., 1962, Report on some pegmatites north of Yalgoo: Western Australia Department of Mines, Annual Report 1961, p. 69–70.

de la HUNTY, L. E., 1973, Cue, Western Australia: Western Australia Geological Survey, 1:250 000 Geological Series Explanatory Notes.

de la HUNTY, L. E., 1975, Murchison Province, *in* Geology of Western Australia, Western Australia Geological Survey, Memoir 2, p. 54–65.

de LAETER, J. R., 1976, Rb–Sr whole-rock and mineral ages from the Gascoyne Province: Western Australia Geological Survey, Annual Report 1975, p. 126–130.

de LAETER, J. R., WILLIAMS, I. R., ROSMAN, K. J. R., and LIBBY, W. G., 1981, A definitive 3350 Ma age from banded gneiss, Mount Narryer area, Western Gneiss Terrain: Western Australia Geological Survey, Annual Report 1980, p. 94–98.

de LAETER, J. R., and BAXTER, J. L., 1987, Rb–Sr geochronology of granitoids from Mount Mulgine, Western Australia: Journal of the Royal Society of Western Australia, v. 69, p. 113–116.

DE PAOLO, D. J., 1981, Nd isotopes in the Colorado Front Range and crust–mantle evolution in the Proterozoic: Nature, v. 291, p. 193–196.

DE PAOLO, D. J., and WASSERBURG, G. J., 1976, Nd isotopic variations and petrogenetic models: Geophysical Research Letters, v. 3, p. 249–252.

DE WIT, M. J., 1982, Gliding and overthrust nappe tectonics in the Barberton greenstone belt: Journal of Structural Geology, v. 4, p. 117–136.

DIMROTH, E., IMREH, L., ROCHELEAU, M., and GOULET, N., 1982, Evolution of the south-central part of the Archaean Abitibi belt, Quebec, Part I — Stratigraphy and paleogeographic model: Canadian Journal of Earth Science, v. 19, p. 1729–1758.

DIMROTH, E., IMREH, L., GOULET, N., and ROCHELEAU, M., 1983, Evolution of the south-central segment of the Archean Abitibi belt, Quebec. Part II — Tectonic evolution and geomechanical model: Canadian Journal of Earth Science, v. 20, p. 1355–1373.

DIMROTH, E., IMREH, L., COUSINEAU, P., LEDUC, M., and SANSCHAGRIN, Y., 1985, Paleogeographic analysis of mafic submarine flows and its use in the exploration for massive sulphide deposits: Geological Association of Canada, Special Paper 28, p. 203–222.

DIXON, J. M., 1975, Finite strain and progressive deformation in models of diapiric structures: Tectonophysics, v. 28, p. 89–124.

DOSTAL, J., and STRONG, D. F., 1983, Trace-element mobility during low-grade metamorphism and silicification of basaltic rocks from Saint John, New Brunswick: Canadian Journal of Earth Sciences, v. 20, p. 431–435.

DOSTAL, J., ZENTILLI, M., CAELLES, J. C., and CLARK, A. H., 1977, Geochemistry and origin of volcanic rocks of the Andes (26°- 28°S): Contributions to Mineralogy and Petrology, v. 63, p. 113–128.

DRUMMOND, B. J., 1979, A crustal profile across the Archaean Pilbara and northern Yilgarn Cratons, northwest Australia: Australia BMR, Journal of Australian Geology and Geophysics, v. 4, p. 171–180.

DRURY, S. A., 1977, Structures induced by granite diapirs in the Archaean greenstone belt at Yellowknife, Canada — implications for Archaean geotectonics: Journal of Geology, v. 85, p. 345–358.

DRURY, S. A., 1978, REE distributions in a high grade Archaean gneiss complex in Scotland — implications for the genesis of ancient sialic crust: Precambrian Research, v. 7, p. 237–257.

DRURY, S. A., 1979, Rare-earth and other trace element data bearing on the origin of Archaean granitic rocks from Yellowknife, Northwest Territories: Canadian Journal of Earth Sciences, v. 4, p. 809–815.

DRURY, S. A., 1983, The petrogenesis and setting of Archaean metavolcanics from Karnataka State, South India: Geochimica et Cosmochimica Acta, v. 47, p. 317–329.

DRURY, S. A., HARRIS, N. B. W., HOLT, R. W., REEVES-SMITH, G. J., and WIGHTMAN, R. T., 1984, Precambrian tectonics and crustal evolution in south India: Journal of Geology, v. 92, p. 3–20.

DUGGAN, J. W., 1958, Report on diamond drilling on 'Great Fingall' quartz reef in depth: Western Australia Geological Survey, Bulletin 113, p. 98–106.

DUGGAN, J. W., 1960a, Report on diamond drilling of 'Great Fingall' quartz reef in depth: Western Australia Geological Survey, Bulletin 114, p. 153–157.

DUGGAN, J. W., 1960b, Report on diamond drilling of abandoned gold shows DDH No. 9, site D1, GML 2241, 'Eagle Hawk' GM, Eelya, Murchison Goldfield: Western Australia Geological Survey, Bulletin 114, p. 158–161.

ELIAS, M., 1982, Belele, Western Australia: Western Australia Geological Survey, 1:250 000 Geological Series Explanatory Notes.

ELIAS, M., and WILLIAMS, S. J., 1980, Robinson Range, Western Australia: Western Australia Geological Survey, 1:250 000 Geological Series Explanatory Notes.

ELIAS, M., BUNTING, J. A., and WHARTON, P. H., 1982, Glengarry, Western Australia: Western Australia Geological Survey, 1:250 000 Geological Series Explanatory Notes.

ELLIS, H. A., 1936, The geology and ore deposits of the Abbotts mining centre (Murchison Goldfield): Western Australia Geological Survey, Bulletin 96, p. 1–49 (unpublished).

ELLIS, H. A., 1953, Report on Nevilles scheelite prospect P.A. 2476, Noongal, Yalgoo G.F.: Western Australia Geological Survey, Annual Report 1951, p. 13.

ELLIS, H. A., 1954, Report on a wolfram deposit on P.A. 2472 about six miles N.E. of Mount Gibson, Yalgoo Goldfield: Western Australia Mines Department, Annual Report 1951, p. 49–50.

ENGLAND, P. C., and RICHARDSON, S. W., 1977, The influence of erosion upon the mineral facies of rocks from different metamorphic environments: Journal of the Geological Society, London, v. 134, p. 201–213.

ESSON, A. G. D., 1923, Notes on Yalgoo, Noongal and Mugga Mugga, Yalgoo Goldfield: Western Australia Geological Survey, Annual Report 1922, p. 10–11.

ETHERIDGE, M. A., WALL, V. J., and VERNON, R. H., 1983, The role of the fluid phase during regional metamorphism and deformation: Journal of Metamorphic Geology, v. 1, p. 205–226.

EVENSEN, N. M., HAMILTON, P. J., and O'NIONS, R. K., 1978, Rare-earth abundances in chondritic meteorites: Geochimica et Cosmochimica Acta, v. 42, p. 1199–1212.

EWART, A., 1976, Mineralogy and chemistry of modern orogenic lavas — some statistics and implications: Earth and Planetary Science Letters, v. 31, p. 417–432.

EWERS, W. E., and MORRIS, R. C., 1981, Studies on the Dales Gorge Member of the Brockman Iron Formation, Western Australia: Economic Geology, v. 77, p. 1929–1953.

EWING, T. E., 1979, Two calc-alkaline volcanic trends in the Archean — trace element evidence: Contributions to Mineralogy and Petrology, v. 71, p. 1–7.

FARQUHARSON, R. A., 1916, Petrology, *in* The geology and ore deposits of Meekatharra, Murchison Goldfield: Western Australia Geological Survey, Bulletin 68, p. 206–287.

FAURE, G., 1977, Principles of isotope geology, New York, John Wiley and Sons, 464p.

FELDTMANN, F. R., 1920, The Mount Zion GML 1183M, Boogardie, Murchison Goldfield: Western Australia Geological Survey, Annual Report 1919, p. 30–34.

FELDTMANN, F. R., 1921a, The mining centres of Quinns and Jasper Hill, Murchison Goldfield: Western Australia Geological Survey, Bulletin 80.

FELDTMANN, F. R., 1921b, The geology and mineral resources of the Yalgoo Goldfield — Part I, The Warriedar gold mining centre: Western Australia Geological Survey, Bulletin 81.

FERRY, J. M., 1979, Reaction mechanisms, physical conditions, and mass transfer during hydrothermal alteration of mica and feldspar in granitic rocks from south-central Maine, U.S.A.: Contributions to Mineralogy and Petrology, v. 68, p. 125–139.

FERRY, J. M., and SPEAR, F. S., 1978, Experimental calibration of the partitioning of Fe and Mg between biotite and garnet: Contributions to Mineralogy and Petrology, v. 66, p. 113–117.

FINUCANE, K. J., 1953, The Hill 50 gold mine, Boogardie, *in* Geology of Australian ore deposits: Fifth Empire Mining and Metallurgy Congress, Australia and New Zealand, Publications, v. 1, p. 231–235.

FISHER, R. V., 1982, Debris flows and lahars: Geological Society of Canada, Short Course Notes, v. 2, p. 136–220.

FLETCHER, I. R., WILLIAMS, S. J., GEE, R. D., and ROSMAN, K. J. R., 1983, Sm–Nd model ages across the margins of the Archaean Yilgarn Block, Western Australia; northwest transect into the Proterozoic Gascoyne Province: Geological Society of Australia, Journal, v. 30, p. 167–174.

FLETCHER, I. R., ROSMAN, K. J. R., WILLIAMS, I. R., HICKMAN, A. H., and BAXTER, J. L., 1984, Sm–Nd geochronology of greenstone belts in the Yilgarn Block, Western Australia: Precambrian Research, v. 26, p. 333–361.

FLEUTY, M. J., 1964, The description of folds: Proceedings of the Geological Association, v. 75, p. 461–489.

FLOYD, P. A., and WINCHESTER, J. A., 1975, Magma type and tectonic setting discrimination using immobile elements: Earth and Planetary Science Letters, v. 27, p. 211–218.

FLOYD, P. A., and WINCHESTER, J. A., 1978, Identification and discrimination of altered and metamorphosed volcanic rocks using immobile elements: Chemical Geology, v. 21, p. 291–306.

FODEN, J. D., NESBITT, R. W., and RUTLAND, R. W. R., 1984, The geochemistry and crustal origin of the Archaean acid intrusive rocks of the Agnew Dome, Lawlers, Western Australia: Precambrian Research, v. 23, p. 247–272.

FORMAN, F. G., 1933, Report on inspection of the Mount Magnet district: Western Australia Geological Survey, Annual Report 1932, p. 11–12.

FORMAN, F. G., 1934, Ingliston Consols Extended and Fenian gold mines, Meekatharra: Western Australia Geological Survey, Annual Report 1933, p. 8–12.

FORMAN, D. J., 1958, The stratigraphy of the Boogardie Group and geology of the Hill 50 gold mine: University of Western Australia Honours thesis (unpublished).

FORMAN, D. J., 1960a, Geological structure of the Hill 50 gold mine: Australasian Institute of Mining and Metallurgy, Proceedings, 195, p. 147–160.

FORMAN, D. J., 1960b, Stratigraphy of the Boogardie Group: Royal Society of Western Australia, Journal, v. 43, p. 83–96.

FORREST, J., 1875, Explorations in Australia: Sampson Low, Marston Howard Searle, London, p. 27–31, 60–64 (facsimile reprint by Greenwood Press, 1969, New York).

FRATER, K. M., 1983a, Geology of the Golden Grove prospect, Western Australia — a volcanogenic massive sulphide–magnetite deposit: Economic Geology, v. 78, p. 875–919.

RATER, K. M., 1983b, Effects of metasomatism and development of quartz 'eyes' in intrusive rocks at Golden Grove Cu–Zn deposit, Western Australia: Institute of Mining and Metallurgy, Transactions, v. 92, p. B121–B131.

FRIPP, R. E. P., VAN NIEROP, D. A., CALLOW, M. J., LILLY, P. A., and DU PLESSIS, L. U., 1980, Deformation in part of the Archaean Kapvaal Craton, South Africa: Precambrian Research, v. 13, p. 241–251.

FRITH, R. A., and FRYER, B. J., 1985, Geochemistry and origin of the Regan Intrusive Suite and other granitoids in the northeastern Slave Province, northwest Canadian Shield: Canadian Journal of Earth Science, v. 22, p. 1048–1065.

FROUDE, D. O., COMPSTON, W., and WILLIAMS, I. S., 1983, Early Archaean zircon analyses from the central Yilgarn Block: Research School of Earth Sciences, Australian National University, Canberra, Annual Report 1983, p. 124–126.

FYFE, W. S., PRICE, N. J., and THOMPSON, A. B., 1978, Fluids in the Earth's crust, Amsterdam, Elsevier.

GEE, R. D., 1979, Structure and tectonic style of the Western Australian shield: Tectonophysics, v. 58, p. 327–369.

GEE, R. D., BAXTER, J. L., WILDE, S. A., and WILLIAMS, I. R., 1981, Crustal development in the Yilgarn Block, Western Australia: Geological Society of Australia, Special Publication No. 7, p. 43–56.

GIBSON, A. A., 1976, Pigments (mineral)–Western Australia, *in* Economic geology of Australia and Papua New Guinea, 4. Industrial Minerals and Rocks *edited by* C. L. KNIGHT: Australasian Institute of Mining and Metallurgy, Monograph 8, p. 295–296.

GIBSON, C. G., 1903, Lennonville, Mount Magnet and Boogardie, Murchison Goldfield: Western Australia Geological Survey, Bulletin 8.

GIBSON, C. G., 1904, The geology and mineral resources of a part of the Murchison Goldfield: Western Australia Geological Survey, Bulletin 14.

GILES, C. W., 1981, Archaean calc-alkaline volcanism in the Eastern Goldfields Province, Western Australia: Geological Society of Australia, Special Publication No. 7, p. 275–286.

GILES, C. W., 1982, The geology and geochemistry of the Archaean Spring Well felsic volcanic complex, Western Australia: Geological Society of Australia, Journal, v. 29, p. 205–220.

GILES, C. W., and HALLBERG, J. A., 1982, The genesis of the Archaean Welcome Well volcanic complex, Western Australia: Contributions to Mineralogy and Petrology, v. 80, p. 307–318.

GILES, E., 1889, Australia twice traversed — the romance of exploration being a narrative compiled from the journals of five exploring expeditions into and through central South Australia and Western Australia from 1872-1876: London, Sampson Low, Marston, Searle and Rivington Ltd., v. 2.

GILL, J. B., 1978, The role of trace element partition coefficients in models of andesite genesis: Geochimica et Cosmochimica Acta, v. 42, p. 709–724.

GLIKSON, A. Y., 1972, Early Precambrian evidence of a primitive ocean crust and island nuclei of sodic granite: Geological Society of America, Bulletin, v. 83, p. 3323–3344.

GLIKSON, A. Y., 1976, Trace element geochemistry and origin of early Precambrian acid igneous series, Barberton Mountain Land, Transvaal: Geochimica et Cosmochimica Acta, v. 40, p. 1261–1280.

GLIKSON, A. Y., 1979, Early Precambrian tonalite-trondhjemite sialic nuclei: Earth Science Reviews, v. 15, p. 1–73.

GLIKSON, A. Y., and HICKMAN, A. H., 1981, Geochemistry of Archaean volcanic successions, eastern Pilbara Block, Western Australia: Australia BMR, Record 1981/36, 83p.

GLIKSON, A. Y., and LAMBERT, I. B., 1973, Relations in space and time between major Precambrian shield units — an interpretation of West Australian data: Earth and Planetary Science Letters, v. 20, p. 395–403.

GLIKSON, A. Y., and LAMBERT, I. B., 1976, Vertical zonation and petrogenesis of the early Precambrian crust in Western Australia: Tectonophysics, v. 30, p. 55–89.

GOLE, M. J., 1980, Mineralogy and petrology of very-low- metamorphic grade Archaean banded iron-formations, Weld Range, Western Australia: American Mineralogist, v. 65, p. 8–25.

GOLE, M. J., 1981, Archean banded iron-formations, Yilgarn Block, Western Australia: Economic Geology, v. 76, p. 1954–1974.

GRAY, N. M., 1950, Report on the proposed diamond drilling of the Great Fingall ore body, Day Dawn, Murchison Goldfield: Western Australia Geological Survey, Annual Report 1948, p. 68–69.

GREEN, T. H., 1972, Crystallization of calc-alkaline andesite under controlled, high-pressure hydrous conditions: Contributions to Mineralogy and Petrology, v. 34, p. 150–166.

GREGORY, A. C., and GREGORY, F. T., 1884, Journals of Australian explorations: Brisbane, Government Printer.

GRIFFIN, T. J., 1990, Southern Cross Province, *in* Geology and Mineral Resources of Western Australia, Western Australia Geological Survey, Memoir 3, p. 60–77.

GROMET, L. P., and SILVER, L. T., 1983, Rare earth element distributions among minerals in a granodiorite and their petrogenetic implications: Geochimica et Cosmochimica Acta, v. 47, p. 925–939.

GROVES, D. I., ARCHIBALD, N. J., BETTENAY, L. F., and BINNS, R. A., 1978, Greenstone belts as ancient marginal basins or ensialic rift zones: Nature, v. 273, p. 460–461.

GROVES, D. I., and McCARTHY, T. S., 1978, Fractional crystallization and the origin of tin deposits in granitoids: Mineralium Deposita, v. 13, p. 11–26.

GROVES, D. I., and BATT, W. D., 1984, Spatial and temporal variations of Archaean metallogenic associations in terms of evolution of granitoid–greenstone terrains with particular emphasis on the Western Australian shield, *in* Archaean Geochemistry — the origin and evolution of the Archaean continental crust *edited by* A. KRÖNER, G. N. MANSON, and A. M. GOODWIN: Berlin, Springer-Verlag, p. 73–98.

GROVES, D. I., PHILLIPS, G. N., HO, S. E., HENDERSON, C. A., CLARK, M. E., and WOAD, G. M., 1984, Controls on distribution of Archaean hydrothermal gold deposits in Western Australia, *in* Gold '82 — The Geology, Geochemistry and Genesis of Gold Deposits *edited by* R. P. FOSTER: Rotterdam, A.A. Balkema Publ.; Geological Society of Zimbabwe, Special Publication, no. 1, p. 689–712.

GROVES, D. I., PHILLIPS, G. N., HO, S. E., and HOUSTON, S. M., 1985, The nature, genesis and regional controls of gold mineralization in Archaean greenstone belts of the Western Australian shield — a brief review: Geological Society of South Africa, Transactions, v. 88, p. 135–148.

GROVES, D. I., PHILLIPS, G. N., FOSTER, R. P., and VILJOEN, M. J., 1986, Regional controls of Archaean gold mineralization in Western Australia and Southern Africa — a comparative review: Geological Society of South Africa, Geocongress '86, Extended Abstracts, p. 287–290.

GROVES, R. H., 1981, (Ed.) Australian Vegetation: Cambridge University Press.

HALLBERG, J. A., 1976, A petrochemical study of a portion of the Yilgarn Block, Australia: Australia CSIRO Mineral Resource Laboratory Report No. FP13, 35p.

HALLBERG, J. A., 1983, Geology and mineral deposits of the Leonora–Laverton area, northeastern Yilgarn Block, Western Australia: Western Australia Geological Survey, Record 1983/8.

HALLBERG, J. A., 1984, A geochemical aid to igneous rock type identification in deeply weathered terrain: Journal of Geochemical Exploration, v. 20, p. 1–8.

HALLBERG, J. A., CARTER, D. N., and WEST, K. N., 1976b, Archaean volcanism and sedimentation near Meekatharra, Western Australia: Precambrian Research, v. 3, p. 577–595.

HALLBERG, J. A., and GILES, C. W., 1986, Archaean felsic volcanism in the northeastern Yilgarn Block, Western Australia: Australian Journal of Earth Science, v. 33, p. 413–427.

HALLBERG, J. A., JOHNSTON, C., and BYE, S. M., 1976a, The Archaean Marda igneous complex, Western Australia: Precambrian Research, v. 3, p. 111–136.

HALLBERG, J. A., and WILSON, P., 1983, Relative timing of intrusion in the Eucalyptus area, northeastern Yilgarn Block, Western Australia: Geological Society of Australia, Journal, v. 30, p. 383–392.

HALLIDAY, A. N., 1984, Coupled Sm–Nd and U–Pb systematics in late Caledonian granites and the basement under northern Britain: Nature, v. 307, p. 229–233.

HAMILTON, P. J., O'NIONS, R. K., and PANKHURST, R. J., 1980, Isotopic evidence for the provenance of some Caledonian granites: Nature, v. 287, p. 279–284.

HAMILTON, W., and MYERS, W. B., 1967, The nature of batholiths: United States Geological Survey, Professional Paper 554-C, 30p.

HAMILTON, W., and MYERS, W. B., 1974, Nature of the Boulder batholith of Montana: Geological Society of America, Bulletin, v. 85, p. 365–378.

HANSON, G. N., 1978, The application of trace elements to the petrogenesis of igneous rocks of granitic composition: Earth and Planetary Science Letters, v. 38, p. 26–43.

HANSON, G. N., 1981, Geochemical constraints on the evolution of the early continental crust: Philosophical Transactions of the Royal Society, London, v. A301, p. 423–442.

HARRIS, M. F., ASHLEY, P. M., DUDLEY, R. J., LESH, R. H., MARR, J. M., and RYALL, A. W., 1982, The Gossan Hill and Scuddles volcanogenic massive sulphide deposits of Golden Grove, Western Australia, *in* Archaean geology of the southern Murchison *edited by* J. L. BAXTER: Geological Society of Australia, Western Australian Division, Excursion Guide, p. 41–73.

HAWKESWORTH, C. J., 1982, Isotopic characteristics of magmas erupted along destructive plate margins, *in* Orogenic andesites *edited by* R. S. THORPE, New York, J. Wiley and Sons, p. 549–571.

HAWKESWORTH, C. J., and VAN CALSTEREN, P. W. C., 1984, Radiogenic isotopes–some geological applications, *in* Rare earth element geochemistry *edited by* P. HENDERSON, Amsterdam, Elsevier, p. 375–422.

HELMSTAEDT, H., PADGHAM, W. A., and BROPHY, J. A., 1986, Multiple dikes in the Lower Kam Group, Yellowknife greenstone belt — evidence for Archean sea-floor spreading?: Geology, v. 14, p. 562–566.

HENDERSON, C. A., 1981, The nature and genesis of quartz gold systems at the Morning Star deposit, Mount Magnet, Western Australia: University of Western Australia, BSc Honours Thesis (unpublished).

HENDERSON, P., 1982, Inorganic geochemistry, Oxford, Pergamon Press, 353p.

HESS, P. C., 1969, The metamorphic paragenesis of cordierite in pelitic rocks: Contributions to Mineralogy and petrology, v. 24, p. 191–207.

HICKMAN, A. H., 1983, Geology of the Pilbara Block and its environs: Western Australia Geological Survey, Bulletin 127.

HICKMAN, A. H., 1984, Archaean diapirism in the Pilbara Block, Western Australia, *in* Precambrian Tectonics Illustrated *edited by* A. KRÖNER and R. GREILING: Stuttgart, E. Schweizerbart'sche Verlagsbuchhandlung, p. 113–127.

HICKMAN A. H., and KEATS, W., 1990, Gold, *in* Geology and Mineral Resources of Western Australia: Western Australia Geological Survey, Memoir 3, p. 645–668.

HO, S. E., 1987, Fluid inclusions — their potential as an exploration tool for Archaean gold deposits, *in* Recent advances in understanding Precambrian gold deposits *edited by* S. E. HO, and D. I. GROVES: University of Western Australia, Department of Geology and University Extension Service, Publication 11, p. 239–263.

HOBSON, R. A., 1940, Copper mineralization in the Murchison and Yalgoo Goldfields: Western Australia Geological Survey, Annual Report 1940.

HOBSON, R. A., 1948, P.A. 3094 (late P. A. 2968), Jumbulyer, near Mount Magnet: Western Australia Mines Department, Annual Report 1946, p. 60.

HODGES, K. V., and SPEAR, F. S., 1982, Geothermometry, geobarometry and the Al_2SiO_5 triple point at Mt. Moosilauke, New Hampshire: American Mineralogist, v. 67, p. 1118–1134.

HOLDAWAY, M. J., 1971, Stability of andalusite and the aluminosilicate phase diagram: American Journal of Science, v. 271, p. 97–131.

HUDDLESTON, P. J., 1976, Early deformation history of Archaean rocks in the Vermillion District northeastern Minnesota: Canadian Journal of Earth Science, v. 13, p. 579–592.

HUGHES, C. J., 1982, Igneous Petrology, Amsterdam, Elsevier Scientific Publishing Company, 551p.

HUPPERT, H. E., and SPARKS, R. S. J., 1985, Cooling and contamination of mafic and ultramafic lavas during ascent through the continental crust: Earth and Planetary Science Letters, v. 74, p. 371–386.

HUPPERT, H.E., and SPARKS, R.S.J., 1988, The generation of granitic magmas by intrusion of basalt into continental crust: Journal of Petrology, v. 29, p. 599–624.

HUPPERT, H. E., SPARKS, R. S. J., TURNER, J. S., and ARNDT, N. T., 1984, Emplacement and cooling of komatiite lava: Nature, v. 309, p. 19–22.

HYNDMAN, D. W., 1981, Controls on source and depth of emplacement of granitic magma: Geology, v. 9, p. 244–249.

IRVINE, T. N., and BARAGAR, W. R. A., 1971, A guide to the chemical classification of the common volcanic rocks: Canadian Journal of Earth Science, v. 8, p. 317–324.

JAEGER, J. C., 1957, The temperature in the neighborhood of a cooling intrusive sheet: American Journal of Science, v. 255, p. 306–318.

JAEGER, J. C., 1959, Temperatures outside a cooling intrusive sheet: American Journal of Science: v. 257, p. 44–54.

JAHN, B. M., and SUN, S. S., 1979, Trace element distribution and isotopic composition of Archaean greenstones: Physics and Chemistry of the Earth, v. 11, p. 597–618.

JAHN, B. M., AUVRAY, B., BLAIS, S., CAPDEVILA, R., CORNICHET, J., VIDAL, F., and HAMEURT, J., 1980, Trace element geochemistry of Finnish greenstone belts: Journal of Petrology, v. 21, p. 201–244.

JAHN, B. M., GLIKSON, A. Y., PEUCAT, J. J., and HICKMAN, A. H., 1981, REE geochemistry and isotopic data of Archean silicic volcanics and granitoids from the Pilbara Block, Western Australia — implications for early crustal evolution: Geochimica et Cosmochimica Acta, v. 45, p. 1633–1652.

JENSEN, L. S., 1976, A new cation plot for classifying subalkalic volcanic rocks: Ontario Division of Mines, Miscellaneous Paper No. 66.

JENSEN, L. S., 1985, Stratigraphy and petrogenesis of Archean metavolcanic sequences, southwestern Abitibi subprovince, Ontario: Geological Association of Canada, Special Paper 28, p. 65–88.

JOHNSON, W., 1950a, A geological reconnaissance survey of part of the area included between the limits Lat. 24° 00' S and Lat. 29° 00' S and between Long. 115° 30' E and Long. 118° 30' E including parts of Yalgoo, Murchison, Peak Hill and gascoyne Goldfields: Western Australia Geological Survey, Bulletin 106.

JOHNSON, W., 1950b, Report on Hill 50 goldmine, Boogardie, Murchison Goldfield: Western Australia Geological Survey, Annual Report 1947, p. 46–50.

JOHNSON, H. D., and BALDWIN, C. T., 1986, Shallow Siliciclastic Seas, *in* Sedimentary Environments and Facies (2nd edition) *edited by* H. G. READING: Oxford, Blackwell Scientific Publications, p. 229–282.

JOHNSTONE, D., CONDON, M. A., and PLAYFORD, P. E., 1958, Stratigraphy of the lower Murchison River area and Yaringa North station: Royal Society of Western Australia, Journal, v. 41, p. 13–16.

JOHNSTONE, M. H., LOWRY, D. C., and QUILTY, P. G., 1973, The geology of southwestern Australia — a review: Royal Society of Western Australia, Journal, v. 56, p. 5–15.

JOLLY, W. T., 1977, Relations between Archaean lavas and intrusive bodies of the Abitibi greenstone belt, Ontario–Quebec: Geological Association of Canada, Special Paper 16, p. 311–330.

JOLLY, W. T., 1978, Metamorphic history of the Archaean Abitibi Belt: Geological Survey of Canada, Paper 78-10, p. 63–78.

JONES, W. R., 1962, Report on subsidised diamond drilling, Mountain View North Prospect, GMLs 573D, 671D, 674D, Day Dawn, Murchison Goldfield: Western Australia Geological Survey, Annual Report 1960, p. 50–53.

JONES, W. R., 1963, The iron ore deposits of the Weld Range, Murchison Goldfield: Western Australia Geological Survey, Annual Report 1962, p. 54–60.

JONES, W. R., 1965, Vanadium deposits of Western Australia, *in* Geology of Australian Ore Deposits (2nd edition) *edited by* J. McANDREW: Commonwealth Mining and Metallurgy Congress, 8th, Australia and New Zealand, Publications, v. 1, p. 154–155.

JUTSON, J. T., 1914a, Geological observations and remarks on the present state of mining in the districts of Mount Magnet, Lennonville and Boogardie, Murchison Goldfield; Western Australia Geological Survey, Bulletin 59, p. 91–139.

JUTSON, J. T., 1914b, Notes on the geology of Yuin, Yalgoo Goldfield: Western Australia Geological Survey, Bulletin 59, p. 140–149.

JUTSON, J. T., 1950, The physiography of Western Australia (3rd edition): Western Australia Geological Survey, Bulletin 95.

KEAYS, R. R., 1984, Archaean gold deposits and their source rocks — the upper mantle connection, *in* Gold '82 — The Geology, Geochemistry and Genesis of Gold Deposits *edited by* R. P. FOSTER: Rotterdam, A. A. Balkema Publ., Geological Society of Zimbabwe, Special Publication, no. 1, p. 17–51.

KEAYS, R. R., and SCOTT, R. B., 1976, Precious metals in ocean-ridge basalts — implications for basalts as source rocks for gold mineralization: Economic Geology, v. 71, p. 705–720.

KRETZ, R., 1982, Transfer and exchange equilibria in a portion of the pyroxene quadrilateral as deduced from natural and experimental data: Geochimica et Cosmochimica Acta, v. 46, p. 411–421.

KUENZI, W. D., HORST, O. H., and McGHEE, R. V., 1979, Effects of volcanic activity on fluvial-deltaic sedimentation in a modern arc-trench gap, southwestern Guatemala: Geological Society of America, Bulletin, v. 90, p. 827–838.

LAJOIE, J., 1984, Volcaniclastic rocks, *in* Facies Models (2nd edition) *edited by* R. G. WALKER: Geoscience Canada, Reprint Series 1, p. 39–51.

LAMB, S. H., 1984, Structures on the eastern margin of the Archaean Barberton greenstone belt, northwest Swaziland, *in* Precambrian Tectonics Illustrated, *edited by* A. KRÖNER, and R. GREILING: Stuttgart, E. Schweizerbart'sche Verlagsbuchhandlung, p. 19–40.

LAMBERT, I. B., PHILLIPS, G. N., and GROVES, D. I., 1984, Sulphur isotope compositions and genesis of Archaean gold mineralization, Australia and Zimbabwe, *in* Gold '82 — The Geology, Geochemistry and Genesis of Gold Deposits *edited by* R. P. FOSTER: Geological Society of Zimbabwe, Special Publication 1, p. 373–387.

LAMBERT, R. St. J., HOLLAND J. G., and OWEN, P. F., 1974, Chemical petrology of a suite of calc-alkaline lavas from Mt Ararat, Turkey: Journal of Geology, v. 82, p. 419–438.

LARCOMBE, C. O. G., 1927, Boring at Yalgoo, petrological work: Western Australia Mines Department, Annual Report 1926, p.137–138.

LAUBSCHER, H. P., 1983, Detachment, shear and compression in the central Alps: Geological Society of America, Memoir 158, p. 191–211.

LEAKE, B. E., 1978, Granite emplacement — the granites of Ireland and their origin, *in* Crustal evolution in northwest Britian and adjacent regions *edited by* D. R. BOWES and B. E. LEAKE: Geological Journal Special Issue, v. 10, p. 221–248.

LE BAS, M. J., LE MAITRE, R. W., STRECKEISEN, A., and ZANETTIN, B., 1986, A chemical classification of volcanic rocks based on the total alkali-silica diagram: Journal of Petrology, v. 27, p. 745–750.

LE MAITRE, R. W., 1976, A new approach to the classification of igneous rocks using the basalt–andesite–dacite–rhyolite suite as an example: Contributions to Mineralogy and Petrology, v. 56, p. 191–203.

LEWIS, B. R., 1965, Gold deposits of the Hill 50 mine, *in* Geology of Australian ore deposits *edited by* J. McANDREW: Eighth Commonwealth Mining and Metallurgical Congress, Australia and New Zealand, p. 98–100.

LIBBY, W. G., 1978, Regional variation in granitic rock, *in* Contributions to the geology of the Eastern Goldfields Province of the Yilgarn Block: Western Australia Geological Survey, Report 9, p. 53–110.

LINDSLEY, D. H., 1983, Pyroxene thermometry: American Mineralogist, v. 68, p. 477–493.

LINDSLEY, D. H., and ANDERSEN, D. J., 1983, A two-pyroxene thermometer, *in* Proceedings of the Thirteenth Lunar and Planetary Science Conference, Part 2: Journal of Geophysical Research, v. 88, Supplement, A887–A906.

LIPPLE, S. L., 1976, Kaolin–Western Australia, *in* Economic Geology of Australia and Papua New Guinea, 4. Industrial Minerals and Rocks *edited by* C. L. KNIGHT: Australasian Institute of Mining and Metallurgy, Monograph 8, p. 295–296.

LIPPLE, S. L., 1982a, Geology of the Ninghan fold belt, Mt. Singleton, Western Australia, *in* Archaean Geology of the Southern Murchison *edited by* J. L. BAXTER: Geological Society of Australia, Western Australian Division, Geological Excursion Guide, p. 6–14.

LIPPLE, S. L., 1982b, Geology of the Wongan Hills: Western Australia Geological Survey, Record 1982/4.

LIPPLE, S. L., and BAXTER, J. L., 1982, The Koolanooka synform, *in* Archaean geology of the southern Murchison *edited by* J. L. BAXTER: Geological Society of Australia, Western Australian Division, Geological Excursion Guide, p. 79–80.

LIPPLE, S. L., BAXTER, J. L., and MARSTON, R. J., 1983, Ninghan, Western Australia: Western Australia Geological Survey, 1:250 000 Geological Series Explanatory Notes.

LORD, J. H., 1963, Report on diamond drilling on the Pinnacles group of leases, near Cue, Murchison Goldfield: Western Australia Geological Survey, Annual Report 1962, p. 42–44.

LOW, G. H., 1960, Report on drilling for gold on the New Alliance leases, Burnakura centre, Murchison Goldfield: Western Australia Geological Survey, Bulletin 114, p. 123–133.

LOW, G. H., 1963, Copper deposits of Western Australia: Western Australia Geological Survey, Mineral Resources Bulletin 8.

LUDDEN, J. N., and GELINAS, L., 1982, Trace element characteristics of komatiites and komatiitic basalts from the Abitibi metavolcanic belt of Quebec, *in* Komatiites *edited by* N. T. ARNDT, and E. G. NISBET: London, George Allen and Unwin, p. 331–346.

LUDDEN, J., GELINAS, L., and TRUDEL, P., 1982, Archean metavolcanics from the Rouyn–Noranda district, Abitibi Greenstone Belt, Quebec, 2 — Mobility of trace elements and petrogenetic constraints: Canadian Journal of Earth Sciences, v. 19, p. 2276–2287.

MACGREGOR, A. M., 1951, Some milestones in the Precambrian of southern Rhodesia: Geological Society of South Africa, Transactions, v. 54, p. 27–71.

MAITLAND, A. G., 1919, The gold deposits of Western Australia, *in* The Mining Handbook: Western Australia Geological Survey, Memoir 1, p. 24, 26.

MAITLAND, A. G., 1924, Notes on the iron ore deposits of Tallering Range, Yalgoo Goldfield: Western Australia Geological Survey, Annual Report 1923, p. 4–6.

MANN, A. W., 1984a, Mobility of gold and silver in lateritic weathering profiles — some observations from Western Australia: Economic Geology v. 79, p. 38–49.

MANN, A. W., 1984b, Redistribution of gold in the oxidized zone of some Western Australian deposits, *in* Gold-mining, metallurgy and geology: Australasian Institute of Mining and Metallurgy, Regional Conference, 1984, Geology Paper 8.

MARLOW, N. H., 1973, Termination report on exploration of the Mount Singleton prospect, Yalgoo Goldfield, W.A.: Hawkestone Minerals Ltd. (unpublished company report).

MARSTON, R. J., 1979, Copper mineralization in Western Australia: Western Australia Geological Survey, Mineral Resources Bulletin 13.

MARTIN, H., CHAUVEL, C., and JAHN, B. M., 1983, Major and trace element geochemistry and crustal evolution of Archean granodioritic rocks from eastern Finland: Precambrian Research, v. 21, p. 159–180.

MATHESON, R. S., 1944a, The molybdenite deposits on P.A.s 2323 and 2324, Mt. Mulgine: Western Australia Geological Survey, Annual Report 1943, p. 22–24.

MATHESON, R. S., 1944b, The tungsten deposits on M.C.s 24 and 25, Callie Soak, Murchison Goldfield: Western Australia Geological Survey, Annual Report 1943, p. 21–22.

McBIRNEY, A. R., 1963, Factors governing the nature of submarine volcanism: Bulletin of Volcanology, v. 2, p. 455–469.

McCULLOCH, M. T., in press, Sm–Nd isotopic constraints on the evolution of Precambrian crust in the Australian Continent: Interunion Commission on the Lithosphere, Working Group 3 — Proterozoic Lithosphere Evolution.

McKAY, J. H., 1975, Koolanooka iron ore mine, W.A., *in* Economic geology of Australia and Papua New Guinea, 1. Metals *edited by* C. L. KNIGHT: Australasian Institute of Mining and Metallurgy Monograph 5, p. 936–940.

McLELLAN, E., 1984, Deformational behaviour of migmatites and problems of structural analysis in migmatite terrains: Geological Magazine, v. 121, p. 339–345.

McLENNAN, S. M., 1984, Petrological characteristics of Archaean greywackes: Journal of Sedimentary Petrology, v. 54, p. 889–898.

McMATH, J. C., 1953, Report on the Great Fingall venture: Western Australia Geological Survey, Annual Report 1950, p. 23–27.

MEHNERT, K. R., 1971, Migmatites and the origin of granitic rocks: Amsterdam, Elsevier Scientific Publishing Company, 405p.

METANA MINERALS N.L., 1986, Audited consolidated financial statements: Metana Minerals N.L. and subsidiary companies, 30 June, 1986, Perth.

MILES, K. R., 1948a, Report on the Hill 60 lode, Mount Magnet Gold Mines Ltd., Mount Magnet: Western Australia Geological Survey, Annual Report 1945, p. 41–43.

MILES, K. R., 1948b, Some Western Australian lamprophyres: Royal Society of Western Australia, Journal, v. 31, p. 1–15.

MILES, K. R., CARROLL, D., and ROWLEDGE, H. P., 1945, Tantalum and niobium: Western Australia Geological Survey, Mineral Resources Bulletin 3, p. 39, 104, 126.

MONEY MINING N.L., 1986, Prospectus, Money Mining N.L., December, 1986, Perth.

MONTGOMERY, A., 1910, Report on the state of mining progress in certain centres in the Murchison and Peak Hill Goldfields: Western Australia Department of Mines, Perth.

MOORE, J. G., 1965, Petrology of deep sea basalt near Hawaii: American Journal of Science, v. 263, p. 40–52.

MUHLING, P. C., and de LAETER, J. R., 1971, Ages of granitic rocks in the Poona–Dalgaranga area of the Yilgarn Block, Western Australia: Western Australia Geological Survey, Annual Report 1970, p. 68–73.

MUHLING, P. C., and LOW, G. H., 1977, Yalgoo, Western Australia: Western Australia Geological Survey, 1:250 000 Geological Series Explanatory Notes.

MYERS, J. S., 1978, Formation of banded gneisses by deformation of igneous rocks: Precambrian Research, v. 6, p. 43–64.

MYERS, J. S., 1984, Archaean tectonics in the Fiskenaesset region of southwest Greenland, *in* Precambrian Tectonics Illustrated *edited by* A. KRÖNER, and R. GREILING: Stuttgart, Schweizerbart'sche Verlagsbuchhandlung, p. 95–112.

MYERS, J. S., 1988, Early Archaean Narryer Gneiss Complex, Yilgarn Craton, Western Australia: Precambrian Research, v. 38, p. 297–308.

MYERS, J. S., 1990, Western Gneiss Terrane, *in* Geology and Mineral Resources of Western Australia: Western Australia Geological Survey, Memoir 3, p. 13–31.

MYERS, J. S., and WATKINS, K. P., 1985, Origin of granite–greenstone patterns, Yilgarn Block, Western Australia: Geology, v. 13, p. 778–780.

MYERS, J. S., and WILLIAMS, I. R., 1985, Early Precambrian crustal evolution at Mount Narryer, Western Australia: Precambrian Research, v. 27, p. 153–164.

NESBITT, R. W., and SUN, S. S., 1976, Geochemistry of Archaean spinifex-textured peridotites and magnesian and low-magnesian tholeiites: Earth and Planetary Science Letters, v. 31, p. 433–453.

NISBET, E. G., 1982, The tectonic setting and petrogenesis of komatiites, *in* Komatiites *edited by* N. T. ARNDT, and E. G. NISBET: London, Allen and Unwin, p. 501–521.

NISBET, E. G., and FOWLER, C. M. R., 1983, Model for Archean plate tectonics: Geology, v. 11, p. 376–379.

NOCKOLDS, S. R., and ALLEN, R., 1953, The geochemistry of some igneous rock series: Geochimica et Cosmochimica Acta, v. 4, p. 105–142.

NOLDART, A. J., 1957, Report on exploratory diamond drilling of abandoned gold shows in the Murchison Goldfield: Western Australia Geological Survey, Bulletin 112, p. 205–215.

NOLDART, A. J., 1958, Report on exploratory diamond drilling of abandoned gold shows, Cue, Murchison Goldfield: Western Australia Geological Survey, Bulletin 113, p. 107–131.

NOLDART, A. J., 1960a, Report on diamond drilling of "Great Fingall" quartz reef in depth, D.D.H. No. G.F. 5 and 6: Western Australia Mines Department, Annual Report 1959, p. 68–72.

NOLDART, A. J., 1960b, Historical summary of exploratory diamond drilling of the "Great Fingall" quartz reef in depth: Western Australia Mines Department, Annual Report 1959, p. 75–78.

NOLDART, A. J., 1961, Report on exploratory diamond drill hole No. PF1, Site A, Paddys Flat, Meekatharra, Murchison Goldfield: Western Australia Mines Department, Annual Report 1960, p. 89–90.

O'HARA, M. J., 1977, Geochemical evolution during fractional crystallization of a periodically refilled magma chamber: Nature, v. 266, p. 503–507.

OJAKANGAS, R. W., 1985, Review of Archaean clastic sedimentation, Canadian Shield — major felsic volcanogenic contributions to turbidite and alluvial fan-fluvial facies associations: Geological Association of Canada, Special Paper 28, p. 23–47.

PEACOCK, M. A., 1931, Classification of igneous rock series: Journal of Geology, v. 39, p. 54–67.

PEARCE, J. A., 1980, Geochemical evidence for the genesis and eruptive setting of lavas from Tethyan ophiolites, *in* International Ophiolite Symposium, Cyprus, 1979: Proceedings of the Geological Survey, Nicosia, 1980, p. 261–272.

PEARCE, J. A., 1982, Trace element characteristics of lavas from destructive plate boundaries, *in* Andesites *edited by* R. S. THORPE: New York, John Wiley, p. 525–548.

PEARCE, J. A., and CANN, J. R., 1973, Tectonic setting of basic volcanic rocks determined using trace element analyses: Earth and Planetary Science Letters, v. 19, p. 290–300.

PEARCE, J. A., and NORRY, M. J., 1979, Petrogenetic implications of Ti, Zr, Y and Nb variations in volcanic rocks: Contributions to Mineralogy and Petrology, v. 69, p. 33–47.

PENNZOIL OF AUSTRALIA LIMITED, 1976, Tuckabianna Project–Progress Report: Western Australia Geological Survey, M Series open file, Microfilm roll 153, Item 340 (unpublished).

PERRING, C. S., GROVES, D. I., and HO, S. E., 1987, Constraints on the source of auriferous fluids for Archaean gold deposits, *in* Recent advances in understanding Precambrian gold deposits *edited by* S. E. HO, and D.I. GROVES: University of Western Australia, Geology Department and University Extension, Publication 11, p. 287–306.

PETTIJOHN, E. J., 1975, Sedimentary rocks (3rd edition): New York, Harper and Row, 628p.

PHILLIPS, G. N., 1985, Interpretation of Big Bell/Hemlo-type gold deposits — precursors, metamorphism, melting and genetic constraints: Geological Society of South Africa, Transactions, v. 88, p. 159–173.

PHILLIPS, G. N., and DE NOOY, D., 1988, High-grade metamorphic processes which influence Archaean gold deposits, with particular reference to Big Bell, Australia: Journal of Metamorphic Geology, v. 6, p. 95–114.

PHILLIPS, G. N., and GROVES, D. I., 1983, The nature of Archaean gold-bearing fluids as deduced from gold deposits of Western Australia: Geological Society of Australia, Journal, v. 30, p. 25–39.

PHILLIPS, G. N., GROVES, D. I., and MARTYN, J. E., 1984, An epigenetic origin for Archaean banded iron-formation hosted gold deposits: Economic Geology, v. 79, p. 162–171.

PIDGEON, R. T., 1986, The correlation of acid volcanics in the Archaean of Western Australia: Western Australia Mineral and Petroleum Research Institute, Report 27.

PIDGEON, R. T., and WILDE, S. A., 1985, Geochronology of granite and granite greenstone terrain — three year progress report to ARGS: Western Australian Institute of Technology, Department of Geology and Geophysics.

PIDGEON, R. T., and WILDE, S. A., 1986, Geochronology of the Wongan Hills greenstone belt, Western Gneiss Terrain, Yilgarn Block, Western Australia: Geological Society of Australia, Abstracts, No. 15, p. 155–156.

PITCHER, W. S., 1979, The nature, ascent and emplacement of granitic magmas: Journal of the Geological Society, London, v. 136, p. 627–662.

PITCHER, W. S., and BUSSELL, M. A., 1977, Structural control of batholith emplacement in Peru — a review: Journal of the Geological Society, London, v. 133, p. 249–256.

PLATT, J. P., 1980, Archaean greenstone belts — a structural test of tectonic hypotheses: Tectonophysics, v. 65, p. 127–150.

PLATT, J. P., ALLCHURCH, P. D., and Rutland, R. W. R., 1978, Archaean tectonics in the Agnew supracrustal belt, Western Australia: Precambrian Research, v. 7, p. 3–30.

RAMBERG, H., 1981, Gravity, deformation and the Earth's crust (2nd edition): London, Academic Press, 452p.

RAMSAY, J. G., 1967, Folding and fracturing of rocks: New York, McGraw-Hill, 568p.

RAMSAY, J. G., and HUBER, M. I., 1987, The techniques of modern structural geology, Volume 2 — folds and fractures: London, Academic Press, 391p.

REED, F., 1896, Report on geological features and state of development of principal mines on the Yalgoo Goldfield: Western Australia Department of Mines, Annual Report 1895, p. 37.

ROBB, L. J., 1983, Geological and chemical characteristics of late granite plutons in the Barberton region and Swaziland with an emphasis on the Dalmein pluton–a review: Geological Society of South Africa, Special Publication No. 9, p. 153–167.

ROBB, L. J., ANHAEUSSER, C. R., and VAN NIEROP, D. A., 1983, The recognition of the Nelspruit Batholith north of the Barberton Greenstone Belt and its significance in terms of Archaean crustal evolution: Geological Society of South Africa, Special Publication No. 9, p. 117–130.

ROBB, L. J., BARTON, J. M., KABLE, E. J. D., and WALLACE, R. C., 1984, Geological, geochemical and isotopic characteristics of the Archaean Kaap Valley pluton, Barberton Mountain Land, South Africa: University of the Witwatersrand, Economic Geology Research Unit, Information Circular, no. 167, 45p.

ROCK, N. M. S., DULLER, P., HASZELDINE, R. S., and GROVES, D. I., 1987, Lamprophyres as potential gold exploration targets — some preliminary observations and speculations: University of Western Australia, Geology Department and University Extension, Publication No. 11, p. 271–286.

ROCK, N. M. S., and GROVES, D. I., 1988, Do lamprophyres carry gold as well as diamonds?: Nature, v. 332, p. 253–255.

ROCK, N. M. S., HALLBERG, J. A., GROVES, D. I., and MATHER, P. J., 1988, Archaean lamprophyres in the goldfields of the Yilgarn Block, Western Australia — new indications of their widespread distribution and significance: University of Western Australia, Geology Department and University Extension, Publication No. 12, p. 245–275.

SAAGER, R., and MEYER, M., 1984, Gold distribution in Archaean granitoids and supracrustal rocks from southern Africa — a comparison, *in* Gold '82 — the geology, geochemistry and genesis of gold deposits *edited by* R. P. FOSTER: Geological Society of Zimbabwe, Special Publication No. 1, p. 53–70.

SAWYER, E. W., 1983, The structural history of a part of the Archaean Quetico metasedimentary belt, Superior Province, Canada: Precambrian Research, v. 22, p. 271–294.

SCARFE, C. M., and HAMILTON, T. S., 1980, Viscosity of lavas from the Level Mountain volcanic centre, northern British Columbia: Carnegie Institute of Washington, Yearbook no. 79, p. 318–320.

SCHMID, R., 1981, Descriptive nomenclature and classification of pyroclastic deposits and fragments — recommendations of the IUGS Subcommission on the Systematics of Igneous Rocks: Geology, v. 9, p. 41–43.

SCHWERDTNER, W. M., 1982, Salt stocks as natural analogues of Archaean gneiss diapirs: Geologische Rundschau, v. 71, p. 370–379.

SCHWERDTNER, W. M., SUTCLIFFE, R. H., and TROENG, B., 1978, Pattern of total strain in the crestal regions of immature diapirs: Canadian Journal of Earth Science, v. 15, p. 1437–1447.

SEARL, R. A., 1961, Final report on Chesterfield prospect, Western Australia: New Consolidated Goldfields (Australasia) Pty. Ltd. (unpublished).

SIBSON, R. H. 1986, Earthquakes and lineaments infrastructure: London, Philosophical Transactions Royal Society A317, p. 63–79.

SIGURDSSON, H., 1982a, Volcanogenic sediments in island arcs: Geological Association of Canada, Short Course Notes v. 2, p. 221–293.

SIGURDSSON, H., 1982b, Subaqueous volcanogenic sediments in ocean basins: Geological Association of Canada, Short Course Notes v. 2, p. 294–342.

SIGURDSSON, H., SPARKS, R. S. J., CAREY, S. N., and HUANG, T. C., 1980, Volcanic sedimentation in the Lesser Antillies arc: Journal of Geology, v. 88, p. 523–540.

SIMPSON, E. S., 1916, The minerals of the Meekatharra District: Western Australia Geological Survey, Bulletin 68, p. 288–312.

SIMPSON, E. S., 1925, Determinations of some minerals collected during the geological survey of Goodingnow: Western Australia Geological Survey, Bulletin 86, p. 39.

SIMPSON, E. S., 1926, The occurrence of common and precious beryl at Poona: Western Australia Department of Mines, Annual Report 1925, p. 177.

SIMPSON, E. S., 1948, Minerals of Western Australia, Volume 1: Perth, Western Australia, Government Printer.

SIMPSON, E. S., 1951, Minerals of Western Australia, Volume 2: Perth, Western Australia, Government Printer.

SIMPSON, E. S., 1952, Minerals of Western Australia, Volume 3: Perth, Western Australia, Government Printer.

SIMS, P. K., PETERMAN, Z. E., and SHULZ, K. J., 1985, The Dunbar gneiss-granitoid dome — implications for early Proterozoic tectonic evolution of northern Wisconsin: Geological Society of America, Bulletin, v. 96, p. 1101–1112.

SKWARNECKI, M. S., 1987, Controls on Archaean gold mineralization in the Leonora district, Western Australia, *in* Recent advances in understanding Precambrian gold deposits: Geology Department and University Extension, University of Western Australia, Publication no. 11, p. 109–135.

SLEEP, N. H., 1979, A thermal constraint on the duration of folding with reference to Acadian geology, New England (USA): Journal of Geology, v. 87, p. 583–589.

SNOWDEN, P. A., 1984, Non-diapiric batholiths in the north of the Zimbabwe shield, *in* Precambrian tectonics illustrated *edited by* A. KRÖNER and R. GREILING: E. Schweizerbart'sche Verlagsbuchhandlung, p. 135–146.

SNOWDEN, P. A., and BICKLE, M. J., 1976, The Chinamora batholith — a diapiric intrusion or interference fold?: London, Journal of the Geological Society, v. 132, p. 131–137.

SOFOULIS, J., 1958, Summary reports on exploratory drilling for gold, Mt. Magnet, Murchison Goldfield: Western Australia Geological Survey, Bulletin 113, p. 61–82.

SOUFOLIS, J., 1966, Widgiemooltha, Western Australia: Western Australia Geological Survey, 1:250 000 Geological Series Explanatory Notes.

SPRAY, J. G., 1985, Dynamothermal transition zone between Archaean greenstone and granitoid gneiss at Lake Dundas, Western Australia: Journal of Structural Geology, v. 7, p. 187–204.

STAINES, H. R. E., 1985, Field geologists guide to lithostratigraphic nomenclature in Australia: Australian Journal of Earth Sciences, v. 32, p. 83–106.

STANLEY, R., and RATCLIFFE, N., 1985, Tectonic synthesis of the Taconian Orogeny in western New England: Geological Society of America, Bulletin, v. 96, p. 1227–1250.

STEIGER, R. H., and JAGER, E., 1977, Subcommission on geochronology–convention on the use of decay constants in geo- and cosmochronology: Earth and Planetary Science Letters, v. 36, p. 359–362.

STEPHENSON, N. C. N., 1984, Two-pyroxene thermometry of Precambrian granulites from Cape Riche, Albany-Fraser Province, Western Australia: Journal of Metamorphic Geology, v. 2, p. 297–314.

STILLWELL, F. L., 1948, Ore specimens from Big Bell, W.A.: Australia, CSIRO, Minerographic Report 392.

STORMER, J. C., 1983, The effects of recalculation on estimates of temperature and oxygen fugacity from analyses of multicomponent iron-titanium oxides: American Mineralogist, v. 68, p. 586–594.

STOWE, C. W., 1984, The early Archaean Selukwe Nappe, Zimbabwe, *in* Precambrian tectonics illustrated *edited by* A. KRÖNER and R. GREILLING: Stuttgart, E. Schweizerbart'sche Verlagsbuchhandlung, p. 41–56.

STRECKEISEN, A. L., 1974, Classification and nomenclature of plutonic rocks: Geolische Rundschau, v. 63, p. 773–786.

STRECKEISEN, A. L., 1976, To each plutonic rock its proper name: Earth Science Reviews, v. 12, p. 1–33.

STRECKEISEN, A. L., 1980, Classification and nomenclature of volcanic rocks, lamprophyres, carbonatites and melilitic rocks, IUGS Subcommission on the Systematics of Igneous Rocks: Geolische Rundschau, v. 69, p. 194–207.

STUDEMEISTER, P. A., 1983, The greenschist facies of an Archean assemblage near Wawa, Ontario: Canadian Journal of Earth Science, v. 20, p. 1409–1420.

STUDEMEISTER, P. A., 1985, The greenschist metamorphism of Archaean synvolcanic stocks near Wawa, Ontario, Canada: Journal of Metamorphic Geology, v. 3, p. 79–90.

SUN, S. S., 1982, Chemical composition and origin of the earth's primitive mantle: Geochimica et Cosmochimica Acta, v. 46, p. 179–192.

SUN, S. S., and NESBITT, R. W., 1977, Chemical heterogeneity of the Archaean mantle, composition of the earth and mantle evolution: Earth and Planetary Science Letters, v. 35, p. 429–448.

SUN, S. S., and NESBITT, R. W., 1978, Petrogenesis of Archaean ultrabasic and basic volcanics — evidence from rare earth elements: Contributions to Mineralogy and Petrology, v. 65, p. 301–325.

TARNEY, J., DALZIEL, I. W. D., and DE WIT, M. J., 1976, Marginal basin 'Rocas Verdes' complex from S. Chile — a model for Archaean greenstone belt formation, *in* The Early History of the Earth *edited by* B. F. WINDLEY: London, Wiley-Interscience, p. 131–146.

TAYLOR, S. R., and HALLBERG, J. A., 1977, Rare-earth elements in the Marda calc-alkaline suite — an Archaean geochemical analogue of Andean-type volcanism: Geochimica et Cosmochimica Acta, v. 41, p. 1125–1129.

TAYLOR, P. N., MOORBATH, S., CHADWICK, B., RAMAKRISHNAN, M., and VISWANATHA, M. N., 1984, Petrography, chemistry and isotope ages of Peninsula Gneiss, Dharwar acid volcanic rocks and the Chitradurga Granite with special reference to the late Archaean evolution of the Karnataka craton, southern India: Precambrian Research, v. 23, p. 349–376.

TAYLOR, S. R., and McLENNAN, S. M., 1985, The continental crust — its composition and evolution: Oxford, Blackwell Scientific Publications, 312p.

THE STAFF, 1953, The Big Bell Goldmine, *in* Geology of Australian ore deposits *edited by* A. B. EDWARDS: Fifth Empire Mining and Metallurgy in Australia and New Zealand Congress, v. 1, p. 224–230.

THURSTON, P. C., AYRES, L. D., EDWARDS, G. R., GELINAS, L., LUDDEN, J. N., and VERPLAELST, P., 1985, Archaean bimodal volcanism: Geological Association of Canada, Special Paper 28, p. 7–22.

THURSTON, P. C., and FRYER, B. J., 1983, The geochemistry of repetitive cyclical volcanism from basalt through rhyolite in the Uchi-Confederation greenstone belt, Canada: Contributions to Mineralogy and Petrology, v. 83, p. 204–226.

TINGEY, R. J., 1985, Sandstone, Western Australia: Western Australia Geological Survey, 1:250 000 Geological Series Explanatory Notes.

TUREK, A., 1966, Rubidium-strontium isotopic studies in the Kalgoorlie-Norseman area, Western Australia: Australian National University PhD Thesis, (unpublished).

TURNER, F. J., 1981, Metamorphic petrology — mineralogical, field and tectonic aspects: New York, McGraw-Hill Book Co.

van de GRAAFF, W. J. E., CROWE, R. W. A., BUNTING, J. A., and JACKSON, M. L., 1977, Relict early Cainozoic drainages in arid Western Australia: Zeitschrift für Geomorphologie N. F., v. 21, p. 379–400.

WALLER, D. R., and BEATTIE, 1971, Airborne magnetic and radiometric survey of Belele, Cue, Kirkalocka, and the eastern parts of Byro, Murgoo, and Yalgoo 1:250 000 sheet areas, Western Australia, 1969: Australia, BMR, Record 1971/28.

WARE, N. G., 1981, Computer programs and calibration with the PIBS technique for quantitative electron probe analysis using a lithium drifted silicon detector: Computers and Geosciences, v. 7, p. 167–184.

WATKINS, K. P., 1990, Murchison Province, *in* Geology and Mineral Resources of Western Australia: Western Australia Geological Survey, Memoir 3, p. 32–60.

WATKINS, K. P., FLETCHER, I. R., and de LAETER, J. R., in press, Crustal evolution of Archaean granitoids in the Murchison Province, Western Australia: Precambrian Research.

WATKINS, K. P., and TYLER, I. M., 1985, Structural and stratigraphic relationships in the Archaean granite–greenstone terrain around Cue, Western Australia: Western Australia Geological Survey, Report 14, p. 46–56.

WATKINS, K. P., TYLER, I. M., and HICKMAN, A. H., 1987, Cue, Western Australia, (2nd edition): Geological Survey of Western Australia, 1:250 000 Geological Series Explanatory Notes.

WEATHERALL, M. V., 1937, Fields Find Gold Mine: Bewick Moreing and Co. (unpublished).

WHITE, A. J. R., and CHAPPELL, B. W., 1977, Ultrametamorphism and granitoid genesis: Tectonophysics, v. 43, p. 7–22.

WIEDENBECK, M., and WATKINS, K. P., in prep., A time scale for granitoid emplacement in the Archaean Murchison Province, Western Australia, by single zircon geochronology.

WILDE, S. A., and PIDGEON, R. T., 1986, Geology and geochronology of the Saddleback Greenstone Belt in the Archaean Yilgarn Block, southwestern Australia: Australian Journal of Earth Science, v. 33, p. 491–502.

WILLIAMS, H., and McBIRNEY, A. R., 1979, Volcanology: San Fransisco, Freeman Cooper and Co., 397p.

WILLIAMS, I. R., 1975, Eastern Goldfields Province, *in* Geology of Western Australia: Western Australia Geological Survey Memoir 2, p. 33–54.

WILLIAMS, S. J., 1986, Geology of the Gascoyne Province, Western Australia: Western Australia Geological Survey, Report 15.

WILLIAMS, S. J., ELIAS, M., and de LAETER, J. R., 1978, Geochronology and evolution of the eastern Gascoyne Province and the adjacent Yilgarn Block: Western Australia Geological Survey, Annual Report 1977, p. 50–56.

WILSON, R. C., 1926, The beryl deposits of Poona and Ferndale: Western Australia Mines Department, Annual Report 1925, p. 81–82.

WINDLEY, B. F., 1973, Crustal development in the Precambrian: London, Philosophical Transactions of the Royal Society, v. A273, p. 321–341.

WINDLEY, B. F., 1984, The evolving continents (2nd edition): Chichester, John Wiley and sons, 399p.

WINKLER, H. G. F., 1979, Petrogenesis of metamorphic rocks (5th edition): New York, Springer-Verlag, 348p.

WOOD, B. J., and FRASER, D. G., 1977, Elementary thermodynamics for geologists: Oxford University Press, 303p.

WOOD, D. A., 1979, A variably veined suboceanic upper mantle — Genetic significance for mid-ocean ridge basalts from geochemical evidence: Geology, v. 7, p. 499–503.

WOODALL, R., 1988, Gold in 1988 *in* Bicentennial Gold 88, Extended Abstracts Oral Programme: Geological Society of Australia Abstracts Series, no. 22, p. 1–12.

WOODWARD, H.P., 1895, Mining handbook to the colony of Western Australia (2nd edition): Perth, Government Printer.

WOODWARD, H. P., 1907, A report upon the geology, together with a description of the productive mines of the Cue and Day Dawn districts, Murchison Goldfield; Part I, Cue and Cuddingwarra centres; Part II, Day Dawn centre: Western Australia Geological Survey, Bulletin 29.

WOODWARD, H. P., 1912a, Miscellaneous Reports 23, 24, 28 and 29: Western Australia Geological Survey, Bulletin 48, p. 112–114, 128–137.

WOODWARD, H. P., 1912b, Payne's recent gold discovery near Goodingnow, Yalgoo Goldfield: Western Australia Geological Survey, Bulletin 48, p. 90–94.

WOODWARD, H. P., 1912c, The Nemesis gold mine, Tuckanarra, Murchison Goldfield: Western Australia Geological Survey, Bulletin 48, p. 100–104.

WOODWARD, H. P., 1914, A geological reconnaissance of a portion of the Murchison Goldfield: Western Australia Geological Survey, Bulletin 57.

WOODWARD, H. P., 1915, Certain mining centres at the south end of the Yalgoo Goldfield: Western Australia Geological Survey, Bulletin 64, p. 46–51.

WYMAN, D., and KERRICH, R., 1988, Lamprophyres — a source of gold: Nature, v. 332, p. 209–210.

YINNEX, N. L., 1986, Prospectus, Yinnex N.L., 12 March 1986: Perth.

Appendix I

Localities referred to in the text

Locality	1:250 000 Map sheet	Latitude ° ' "	Longitude ° ' "
Abbotts (mining centre)	BELELE	26 20 00	118 24 00
Badja Homestead	YALGOO	28 36 10	116 46 35
Bald Hill	PERENJORI	29 40 43	116 51 19
Beebynbeebynganna Hill	CUE	27 01 56	117 49 21
Big Bell	CUE	27 19 16	117 39 10
Billabalong Homestead	MURGOO	27 25 15	115 50 00
Blue Hill Range	PERENJORI	29 09 00	116 47 00
Bonnie Venture	NINGHAN	29 31 43	117 13 44
Brandy Hill	YALGOO	28 46 15	116 24 00
Buddadoo	YALGOO	28 43 00	116 28 00
Bunnawarra Homestead	YALGOO	28 36 30	116 34 00
Buongnoo Rock	CUE	27 41 25	117 02 20
Burnakura (mining centre)	CUE	27 03 15	118 27 50
Burra Burra	CUE	27 57 20	117 50 00
Butcher Well	BELELE	26 52 00	118 18 35
Cagacaroon Hill	YALGOO	28 38 00	116 25 00
Callie Soak	CUE	27 18 15	117 32 05
Camberathunun Hill	YALGOO	28 18 15	116 37 30
Carlaminda Homestead	YALGOO	28 17 00	116 43 00
Carlaminda Well	YALGOO	28 17 00	116 43 00
Chesterfield (mining centre)	BELELE	26 31 00	117 59 00
Chiggarrie Rock	CUE	27 18 45	117 05 10
Chulaar Hill	YALGOO	28 58 00	116 58 10
Coocoowilya Well	MURGOO	27 06 40	116 19 20
Coodardy	CUE	27 15 20	117 39 00
Coonigal Well	NINGHAN	29 27 50	117 20 40
Copper Hills Well	GLENGARRY	26 58 00	118 42 00
Corner Well	CUE	27 00 45	118 25 20
Cuddingwarra (mining centre)	CUE	27 22 00	117 47 15
Cue	CUE	27 25 40	117 53 30
Cue Hill	CUE	27 25 20	117 54 20
Cullculli Homestead	CUE	27 05 50	118 13 50
Cullculli Trig	CUE	27 02 36	118 23 09
Dalgaranga Hill	CUE	27 50 05	117 06 05
Dalgaranga (mining centre)	CUE	27 42 30	117 13 00
Damperwah Homestead	PERENJORI	29 18 00	116 40 20
Day Dawn (mining centre)	CUE	27 27 35	117 51 35
Deep Well	CUE	27 58 40	117 14 00
Dollar Well	YALGOO	28 13 10	116 42 00
Edah Homestead	KIRKALOCKA	28 16 00	117 09 00
Eelya Hill	CUE	27 22 00	118 10 00
Fields Find (mining centre)	NINGHAN	29 02 18	117 14 43
Five Mile Bore	BELELE	26 50 15	118 21 20
Gabanintha (mining centre)	GLENGARRY	26 55 50	118 38 45
Garden Gully (mining centre)	BELELE	26 27 00	118 28 00
Glen Homestead	CUE	27 03 05	117 33 50
Gnows Nest	YALGOO	28 35 15	116 52 00
Golconda Well	CUE	27 40 00	117 54 00
Golden Grove	YALGOO	28 46 40	116 57 50
Goodingnow (mining centre)	NINGHAN	29 16 09	117 41 33
Greynight Bore	NINGHAN	29 25 00	117 18 05
Gullewa (mining centre)	YALGOO	28 39 40	116 18 40
Gum Well	CUE	27 48 30	117 10 15

Locality	1:250 000 Map sheet	Latitude ° ' "	Longitude ° ' "
Jasper Hill	PERENJORI	29 05 35	116 54 05
Jillewarra (mining centre)	BELELE	26 20 00	117 44 00
Joker	YALGOO	28 26 30	116 45 10
Kadji Kadji Homestead	PERENJORI	29 06 30	116 20 45
Karara Homestead	PERENJORI	29 11 05	116 42 10
Kirkalocka Homestead	KIRKALOCKA	28 33 20	117 46 45
Koolanooka	PERENJORI	29 16 09	116 04 24
Kylie Hill	CUE	27 31 30	117 08 45
Lake Austin	CUE	27 53 00	117 38 00
Lake Austin (mining centre)	CUE	27 53 00	117 38 00
Lake Moore	NINGHAN	29 35 00	117 35 00
Lennonville (mining centre)	CUE	27 58 20	117 50 00
Limestone Well	BELELE	26 51 20	117 50 10
Lordy Bore	GLENGARRY	26 49 25	118 32 50
Madoonga Homestead	BELELE	26 56 00	117 36 00
Mainland (mining centre)	CUE	27 35 06	117 55 33
Meekatharra	BELELE	26 35 30	118 29 30
Messenger Patch (mining centre)	YALGOO	28 41 00	116 57 00
Mindoolah (mining centre)	BELELE	26 56 00	117 29 00
Mindoola Bore	CUE	27 04 45	117 28 35
Mingah Range	BELELE	26 28 00	117 57 00
Minjar Hill	YALGOO	28 47 30	116 56 50
Morawa	PERENJORI	29 12 35	116 00 30
Mougooderra Hill	YALGOO	28 51 10	116 58 15
Mount Farmer	CUE	27 41 25	117 25 10
Mount Hope	MURGOO	27 19 00	115 58 10
Mount Gibson	NINGHAN	29 35 45	117 11 15
Mount Magnet	KIRKALOCKA	28 03 50	117 50 50
Mount Mulcahy	CUE	27 03 15	117 42 30
Mount Mulgine	PERENJORI	29 11 15	116 58 40
Mount Singleton	NINGHAN	29 27 50	117 17 20
Mount Yagahong	GLENGARRY	26 53 50	118 39 30
Moyagee (mining centre)	CUE	27 41 51	117 49 46
Moyagee Well	CUE	27 44 20	117 49 00
Mugga Mugga Hill	YALGOO	28 41 30	116 14 45
Mullewa	YALGOO	28 32 30	115 30 45
Munarra Gully (mining centre)	BELELE	26 59 00	118 09 00
Mungada	PERENJORI	29 08 00	116 53 00
Murdanna Rock	MURGOO	27 32 20	116 53 30
Nannine	BELELE	26 53 30	118 20 35
Ninghan Homestead	NINGHAN	29 25 25	117 16 50
Ninghan woolshed	NINGHAN	29 22 30	117 16 50
Noongal Homestead	YALGOO	28 07 30	116 49 30
Noongal (mining centre)	YALGOO	28 10 00	116 45 00
Paynes Find	NINGHAN	29 15 45	117 40 45
Perenjori	PERENJORI	29 26 30	116 17 00
Pindar	YALGOO	28 28 45	115 47 15
Pinnacles (mining centre)	CUE	27 33 00	118 02 00
Pirgan Hill	CUE	27 12 20	118 02 05
Polelle Homestead	GLENGARRY	26 54 50	118 33 00
Poona (mining centre)	CUE	27 08 00	117 28 00
Quartzite Hill	BELELE	26 19 00	117 27 00
Quinns (mining centre)	SANDSTONE	27 04 00	118 38 00
Range Well	CUE	27 45 10	117 12 30
Red Hill	PERENJORI	29 05 00	116 50 50
Reedy	CUE	27 07 20	118 16 30
Rothsay (mining centre)	PERENJORI	29 17 20	116 52 40
Ryansville (mining centre)	CUE	27 02 10	117 32 00
Southern Cross Bore	NINGHAN	29 03 20	117 02 40
Sparrow Well	CUE	27 45 15	117 48 50
Stake Well (mining centre)	CUE	27 01 25	118 11 50
Star Bore	GLENGARRY	26 55 10	118 37 15
Star of the East	GLENGARRY	26 57 00	118 36 00

Locality	1:250 000 Map sheet	Latitude ° ' "	Longitude ° ' "
Stockyard Bore	GLENGARRY	26 42 40	118 30 40
Swan Bore	GLENGARRY	26 48 30	118 53 45
Tallering Range	YALGOO	28 06 56	115 37 17
The Island (mining centre)	CUE	27 38 00	117 52 30
Trenton Hill	CUE	27 28 40	117 49 45
Tuckabianna (mining centre)	CUE	27 28 45	118 08 00
Tuckanarra Homestead	CUE	27 07 15	118 05 00
Tuckanarra (mining centre)	CUE	27 07 00	118 04 30
Twin Peaks Homestead	MURGOO	27 23 09	115 57 54
Wadda Wadda Bore	BELELE	26 26 25	118 03 45
Wadgingarra Hill	YALGOO	28 18 15	116 43 50
Warda Warra Hill	CUE	27 35 01	117 08 05
Warda Warra (mining centre)	CUE	27 35 01	117 08 05
Warriedar (mining centre)	NINGHAN	29 06 13	117 00 18
Warriedar Homestead	NINGHAN	29 07 50	117 10 00
Warro Well	NINGHAN	29 25 00	117 09 20
Wattle Creek Homestead (abandoned)	CUE	27 59 20	117 45 20
Weebacarry Bore	BELELE	26 55 50	118 04 50
Weld Range	CUE	27 01 53	117 24 11
Wilgie Mia	BELELE	26 57 00	117 42 00
Windaning Hill	PERENJORI	29 09 35	116 54 20
Woolgerong Rock	CUE	27 23 40	117 22 45
Woolgra Bore	BELELE	26 52 20	118 29 40
Wownaminya Hill	YALGOO	28 27 35	116 49 40
Wydgee Homestead	KIRKALOCKA	28 51 00	117 49 35
Yalgoo	YALGOO	28 20 50	116 40 45
Yaloginda (mining centre)	BELELE	26 39 45	118 25 00
Yarraquin Homestead	CUE	27 32 50	118 12 50
Yeoh Hills	NINGHAN	29 13 00	117 16 00
Yuin (mining centre)	MURGOO	27 56 00	116 10 00

Appendix II

Geochemical analyses

Analyses for major oxides and/or trace elements were performed on 1395 rock samples. All samples were assigned to one of four groups:

(1) volcanic rocks (including a small number of clastic sedimentary rocks);
(2) granitoids;
(3) banded iron-formations; and
(4) miscellaneous mineral deposit and prospect samples.

A fifth group consists of the basic data for 54 samples from groups (1) and (2), but with additional rare-earth and some other minor-element data.

Locations of traverses and samples are shown on Figure AII.1.

Sample preparation and analysis

After cleaning and removal of weathered material, a thin section was made of each rock sample in groups 1–3. For all samples a reference chip, and in most cases a hand specimen, was retained. The remainder of each sample was crushed for analysis. Most ultramafic–mafic rocks and banded iron-formation were crushed in a tungsten-carbide mill, whereas most felsic, sedimentary, and granitoid rocks were crushed in a chrome-steel mill. Tungsten- carbide and chrome-steel mills cause W and Co, and Cr contamination of samples respectively; some samples were halved and crushed in both mills to facilitate analysis of W, Co, and Cr.

Samples in groups 1–3 were analysed for major oxides and up to 21 trace elements by X-ray fluorescence (XRF), atomic absorption spectroscopy (AAS), inductively coupled plasma atomic emission spectroscopy (ICP-AES), and wet chemical methods, at the Geological Survey of Western Australia (GSWA) and the Chemistry Centre of Western Australian (CCWA). In addition, 54 samples from groups 1 and 2 were analysed for Th, U, Ta, Hf, Rb, Cs, Sc, Co, Cr, and the rare-earth elements (REE) La, Ce, Nd, Sm, Eu, Tb, Yb, and Lu by instrumental neutron activation analysis (INAA) at the Open University in England. Samples in group 4 were analysed for trace metals only.

Major oxides (except Na_2O and K_2O) were determined at the CCWA by XRF after fusion of samples with lithium tetraborate. Initially the CCWA determined Na_2O and K_2O by AAS, but subsequently these oxides were determined by ICP-AES. Most trace elements were determined by XRF at the CCWA on pressed powder briquettes. Initially, determinations of Cu, Pb, Zn, Mn, Co, Ni, and Li were made at the GSWA by AAS, but subsequently these elements were determined at the CCWA by ICP-AES. Uranium was analysed by paper chromatography. Fluorine was determined using a specific ion-electrode. Sulphur was measured by titrating sulphur dioxide after its release by ignition, with potassium iodate solution, in an induction furnace. Boron was determined initially by a colorimetric method, but subsequently by ICP-AES. Ferrous oxide was determined by titration with $K_2Cr_2O_7$. Volatile content is reported as loss-on-ignition.

For samples from group 4, determinations were made for some, or all, of Ag, As, Au, Co, Cr, Cu, Fe, Mn, Mo, Ni, Pb, Sn, W, and Zn at the CCWA. Au was determined by fire-assay, Pb by AAS, W by a colorimetric method; other metals were analysed by XRF or ICP-AES.

Composite samples of banded iron-formation from each surface traverse, and from each drill-core site, were analysed for Au by fire assay. For composite samples with anomalous gold values, individual samples comprising the composite were also analysed for Au. In addition, bulk mineral determinations were carried out at the CCWA on the drill-core samples by X-ray diffraction.

Computing methods

Each sample analysed chemically has been assigned an alphanumeric classification code which, for supracrustal rocks, classifies samples in terms of rock type, sampling traverse number, stratigraphic unit, alteration state, and metamorphic grade. For granitoids it classifies samples in terms of rock type, texture, intrusive suite, and alteration state.

Geochemical data were stored in five direct-access data files on a Department of Lands Administration VAX-780 computer. The data files correspond to the group classifications, i.e.(1) volcanic rocks, (2) granitoids, (3) banded iron-formations, (4) miscellaneous mineral deposit and prospect samples, and (5) samples analysed for rare-earth elements. Each file comprises sample numbers, classification codes, metric northings and eastings, and the numerical data. Listings of these data files are given on the microfiche in the pocket at the back of this bulletin. A guide for each data file follows.

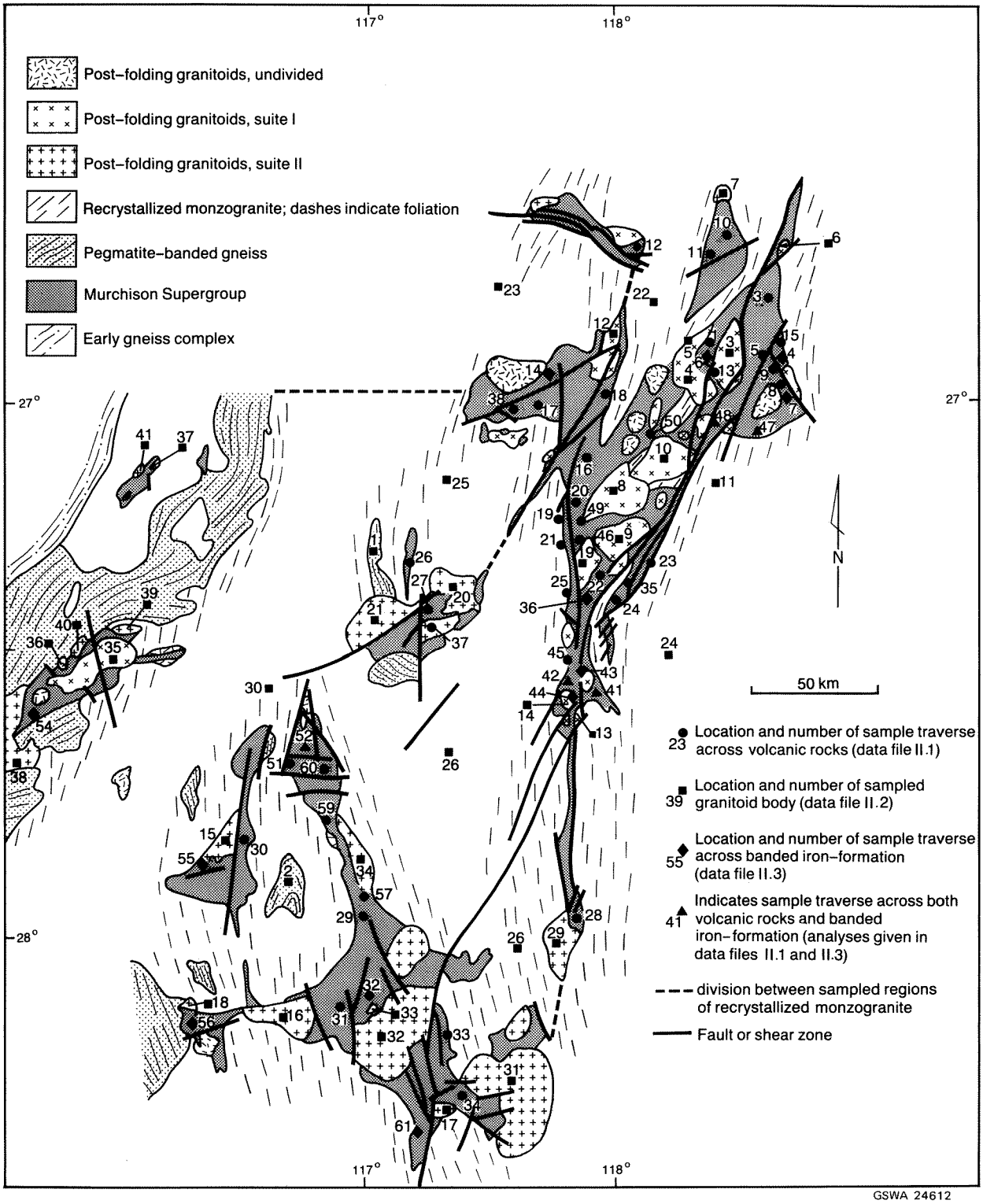


Figure A-II.1. Locations of sample traverses for supracrustal rocks (data files II.1 and II.3) and sampled granitoid bodies (data file II.2). The numbers are those used in the data-file code, for each sample, to identify its location.

DATA FILE II.1 — Analyses of volcanic rocks

Data headings:

SAMPLE Geological Survey of Western Australia sample number

CODE The code has six characters; these are, from left to right: 1, rock type; 2–3, traverse number; 4, stratigraphic formation; 5, degree of alteration; 6, metamorphic grade.

(1) Rock type:
- S clastic sedimentary rock
- P felsic porphyry
- R rhyolite
- D dacite
- A andesite
- N basaltic andesite
- B tholeiitic basalt
- K high-Mg basalt
- L dolerite
- U ultramafic rock
- X protolith unknown

(2–3) Traverse number:
Locations of traverses are shown in Figure AII.1. Isolated samples not taken from formal traverses are indicated by 00.

(4) Stratigraphic unit:
- A Murrouli Basalt
- B Golconda Formation
- C Gabanintha Formation
- D Windaning Formation
- E Lordy Basalt
- F Stockyard Basalt
- G Woolgra Formation
- H Dalgaranga Formation
- I Mindoola Formation
- J Wattle Creek Basalt
- K Singleton Basalt
- L Mougooderra Formation
- M Wadgingarra Basalt
- N Camberathunun Formation
- Q Quinns Basalt

(5) Degree of alteration:
- 1 Little visible alteration in thin section, geochemical analysis typical of rock type
- 2 Evidence of some alteration in thin section, geochemical analysis typical of rock type.
- 3 Clear evidence of alteration in thin section and/or anomalous geochemistry.

(6) Metamorphic grade:
- 0 prehnite–pumpellyite facies
- 1 lower greenschist facies
- 2 upper greenschist facies
- 3 greenschist–amphibolite facies transition
- 4 lower amphibolite facies
- 5 upper amphibolite facies

EAST and NORTH Eastings and Northings are based on the Australian Metric Grid, longitude group 50, and are given to the nearest 100 m.

Oxides and sulphur are given in percentages, the remaining analyses are in parts per million. Blank spaces or dashes indicate that no determination was made.

DATA FILE II.2 — Analyses of granitoid rocks

Data headings:

SAMPLE Geological Survey of Western Australia sample number

CODE The code has six characters; these are, from left to right: 1, rock type; 2, texture; 3, intrusive suite; 4–5, granitoid location; 6, degree of alteration.

(1) Rock type:
- A albitized granitoid
- S syenogranite
- M monzogranite
- G granodiorite
- T tonalite
- J trondhjemite
- Y granophyre

(2) Texture:
- 1 equigranular, unfoliated
- 2 porphyritic, unfoliated
- 3 equigranular, foliated
- 4 porphyritic, foliated
- 5 banded

(3) Intrusive suite:
- 1 Pegmatite-banded gneiss
- 2 Recrystallized monzogranite
- 3 Post-folding granitoids, suite I
- 4 Post-folding granitoids, suite II

(4–5) Granitoid location:
Each granitoid body sampled is numbered and located on Figure AII.1.

(6) Degree of alteration:
- 1 Little visible alteration in thin section, chemical analysis typical of rock type.
- 2 Minor alteration in thin section, chemical analysis typical of rock type.
- 3 Clear evidence of alteration in thin section and/or anomalous geochemistry.

CLASS granitoid classification
- 1 Pegmatite-banded gneiss
- 2 Recrystallized monzogranite
- 3 Post-folding granitoids, suite I
- 4 Post-folding granitoids, suite II

Eastings and Northings and rock analyses are expressed in the same way as in the previous data file.

DATA FILE II.3 — Analyses of banded iron-formation

Results are presented by traverse number.

Data headings:

SAMPLE Geological Survey of Western Australia sample number

CODE The code has six characters and is the same as that in the volcanic rocks data file, except that there are only three rock types:

- H quartz–hematite–magnetite banded iron-formation
- J jaspilitic banded iron-formation
- I ferruginous chert or undivided banded iron-formation

TRAVERSE	Traverse locations are shown on Figure AII.1	

Eastings and Northings and rock analyses are expressed in the same way as in previous data files.

DATA FILE II.4 — Analyses of miscellaneous samples from mineral deposits and prospects

Samples are classified in terms of type of material (CLASS) and host rock (HOST). Results are reported in parts per million.

Data headings:

CLASS	AMPH	amphibolite
	B	breccia
	BAS	basalt
	C	conglomerate
	CARB	carbonate/carbonated
	FC	ferruginized conglomerate
	FE	ironstone
	FELS	felsic volcanic rock
	FSH	ferruginized shale
	FSLT	ferruginized siltstone
	FSST	ferruginized sandstone
	G	gossan
	GRAN	granitoid
	LAT	laterite
	M	mylonite
	MICA	micaceous rock
	Q	quartz and/or chert
	S	sulphide
	SCH	schist
	SH	shale
	SIL	silicified
	SST	sandstone
	UM	ultramafic rock

These may be used in combination where two types of material are present, e.g. Q/S: chert and sulphide.

HOST	BAS	basalt
	BIF	banded iron-formation
	BREC	breccia
	CARB	carbonate
	CH	chert or quartzite
	CONG	conglomerate
	DOL	dolerite
	FEL	felsic volcanic rocks
	FELTF	felsic tuff
	GAB	gabbro
	GRAN	granitoid
	LAT	laterite
	SCH	schist
	SH	shale
	SST	sandstone
	UM	ultramafic rock

DATA FILE II.5

Analyses of samples with rare-earth element determinations. Data headings are as for DATA FILE II.1 (volcanic rocks) and DATA FILE II.2 (granitoids).

Variation in sample composition at a single locality

Forty samples were collected for an investigation of compositional variation of the major rock types at single sample localities. Eight samples were collected from each of five sites, which were generally less than 9 m^2 in area. Each site was sampled at random, but each sample was typical of the outcrop. Lithologies sampled in this way were high-Mg basalt, tholeiitic basalt, dacite, recrystallized monzogranite, and post-folding granodiorite.

Arithmetic means and coefficients of variation for each of the sampled lithologies are shown in Table AII-1. An indication of compositional variation at sample sites is provided by the coefficient of variation (CV):

$$\text{coefficient of variation} = \frac{100 \times \text{standard deviation}}{\text{arithmetic mean}}$$

A high value for the CV indicates a large variation in composition. However, this coefficient characteristically increases as the mean approaches the detection limit, reflecting the high analytical imprecision in the vicinity of that limit. Where the mean is substantially above the detection limit, the value of the CV reflects the compositional variation of rock at a sample site and normally includes only a small analytical component. Thus, a high CV value near the detection limit may be due to analytical imprecision, but a high CV value well above the detection limit indicates compositional heterogeneity at the sample site. To minimize the effects of analytical variations, only CVs for those components with mean values at least five times their detection limits are shown in Table AII-1.

The data shown in Table AII-1 indicate that tholeiitic basalt and recrystallized monzogranite are relatively homogeneous with respect to major oxides. In contrast, the dacite and post-folding granodiorite are less homogeneous, and the high-Mg basalt is relatively heterogeneous. Among the major oxides Fe_2O_3, FeO, MgO, K_2O, and Na_2O show surprisingly large values of CV in several lithologies. Variations in Fe_2O_3 may reflect the two-stage analytical procedure: Fe_2O_3 is calculated from the difference between all of the iron calculated as Fe_2O_3, and ferrous iron determined separately. K_2O, Na_2O, and MgO may have been affected by alteration processes. High values of CV for S and P_2O_5, which are present in low abundances, may still reflect the proximity of the detection limit. Values of CV for trace elements are generally higher than those for oxides. CV values for some trace elements are high even though the mean values are well above the detection limit. For example, Ba, Cr, Cu, Ni, Sr, and Zr in high-Mg basalt; Ba in tholeiitic basalt; Cu, F, Li and Rb in dacite; Ce and Th in recrystallized monzogranite; and Cu and Li in post-folding granodiorite are almost certainly quite variable in their distribution.

The data suggest that, for most components, tholeiitic basalt and recrystallized monzogranite have homogeneous compositions at the sample sites. Compositions of other rock types sampled may show some variation due to sam-

ple-site heterogeneity, particularly high-Mg basalt. These results were taken into consideration during interpretation of geochemical data for this bulletin. In most cases, enough samples were taken of a given rock unit for the average values to accurately represent the composition of that unit. In addition, chemical trends are considered valid where abundances of major oxides and/or trace elements indicate consistent patterns.

TABLE AII-1. MEANS AND COEFFICIENTS OF VARIATION OF SAMPLED LITHOLOGIES AT FIVE LOCALITIES

	Detection limit (a)	*High-Mg basalt* *35 (b)*		*Tholeiitic basalt* *38*		*Dacite* *37*		*Post-folding granodiorite* *31*		*Recrystallized monzogranite* *22*	
		X	*CV*	*X*	*CV*	*X*	*CV*	*X*	*CV*	*X*	*CV*
SiO_2(%)	0.05	51.3	1.9	53.9	0.6	71.6	3.4	71.7	0.8	72.1	0.8
Al_2O_3	0.05	11.7	11.3	14.7	1.4	11.4	9.4	14.6	2.5	14.3	0.9
Fe_2O_3	0.05	2.1	7.9	2.5	10.9	0.89	12.7	0.43	16.6	0.44	17.0
FeO	0.01	9.0	4.0	6.0	2.3	4.6	7.1	1.5	9.7	1.2	5.3
MgO	0.01	9.7	12.4	7.1	1.4	0.92	17.5	0.52	11.2	0.36	3.6
CaO	0.01	11.9	10.2	9.1	5.2	2.7	19.5	2.0	12.1	1.7	0.9
Na_2O	0.01	1.1	42.7	2.0	16.5	1.1	17.2	4.7	2.4	4.1	1.6
K_2O	0.01	0.07	29.8	0.52	24.0	4.5	14.5	2.4	7.7	3.8	1.8
TiO_2	0.01	0.65	17.3	0.50	0.9	0.30	12.6	0.20	12.1	0.18	2.8
P_2O_5		0.01	0.07	29.0	0.07	10.5	0.03	-	0.05	-	0.04
-											
MnO	0.01	0.18	14.0	0.16	2.2	0.12	10.3	0.03	-	0.03	-
LOI	0.01	2.1	7.2	3.4	5.4	1.5	15.9	1.5	6.4	1.2	8.7
S	0.005	0.01	-	0.05	17.4	-	-	-	-	-	-
Ba (ppm)	10	61	83.0	215	31.4	1089	12.9	535	12.8	905	1.8
Ce	10	-	-	26	-	61	15.1	37	-	84	50.2
Co	3	71	19.4	50	13.0	7	-	3	-	6	-
Cr	10	1051	44.0	366	14.8	-	-	-	-	-	-
Cu	2	91	64.0	113	12.0	38	45.5	17	55.3	10	-
F	10	97	15.0	177	8.0	698	28.4	273	9.6	222	7.4
La	10	-	-	-	-	21	-	14	-	38	-
Li	1	4	-	10	4.5	20	37.7	43	36.1	41	2.9
Nb	5	-	-	4	-	10	-	8	-	9	-
Ni	5	260	40.2	191	4.2	39	15.0	23	-	15	-
Pb	10	-	-	11	-	29	-	30	-	55	9.6
Rb	5	-	-	16	-	171	25.0	92	5.7	186	1.2
Sn	5	-	-	-	-	6	-	-	-	-	-
Sr	5	65	44.2	170	3.9	75	8.6	221	3.8	197	1.8
Th	5	7	-	9	-	16	-	15	-	34	28.2
U	1	-	-	-	-	2	-	3	-	6	9.7
V	5	260	5.7	168	3.9	37	18.0	15	-	9	-
Y	5	20	-	17	-	55	4.0	6	-	8	-
Zn	1	76	14.9	73	4.4	106	10.9	52	7.4	51	9.3
Zr	10	58	63.2	73	2.5	233	8.8	114	7.2	152	5.1

(a) detection limits are specific for this group of analyses only
(b) sample site number (= traverse or rock-body number in data files)
X arithmetic mean
CV coefficient of variation (= 100 x standard deviation/mean)

Appendix III

Geochronology

Sample Preparation and analysis

Splits of geochemistry samples were generally used for Sm–Nd and Rb–Sr geochronology. Sample splits were crushed at the Geological Survey of Western Australia (GSWA) and analysed by I. R. Fletcher and J. R. de Laeter at Curtin University. Methods used for Sm–Nd analysis were similar to those outlined in Fletcher et al. (1984), and methods for Rb–Sr analysis were those of de Laeter et al. (1981). Results of Sm–Nd and Rb–Sr analyses follow in Tables AIII-1 to AIII-10.

Nineteen samples were collected for U–Pb zircon geochronology. Each of these comprised 60–70 kg of fresh material collected from one block of rock in the field. Fourteen samples were crushed at the Western Australian Chemical Engineering Laboratory (CEL). Crushed material was passed over a Wilfley Table for gravity concentration of heavier minerals; the magnetic fraction was then removed. The remaining material was cleaned by heavy-liquid separation to produce a zircon residue. Individual zircons from five of these samples were analysed by M. Wiedenbeck at the Research School of Earth Sciences, Australian National University on the high resolution ion-microprobe (Compston et al., 1982; Wiedenbeck and Watkins, in prep.). The five remaining rock samples were sent to R. T. Pidgeon at the Department of Physics and Geosciences, Curtin University, for preparation (by similar methods to those used at CEL) and analysis of zircon aggregates by standard mass spectrometric techniques (e.g. Wilde and Pidgeon, 1986). Sufficient zircon for isotopic determination was found in only one of these samples (GSWA no. 81618, Pidgeon, 1986; see Table 14 in main text).

Sm–Nd GEOCHRONOLOGY — SUPRACRUSTAL ROCKS

TABLE AIII-1. Sm–Nd ISOTOPE DATA FOR MURROULI BASALT SAMPLES

Sample no.	*Sm* (μg/g)	*Nd*	*Sm/Nd*	$^{147}Sm/^{144}Nd$	$^{143}Nd/^{144}Nd$	$\varepsilon_{Nd}(T)$ (a)
81435	2.8	8.5	0.33	0.1975 ±10	0.512725 ±21	+1.7
81442	2.8	11.0	0.25	0.1537 ±6	0.511750 ±17	-0.4
81449	1.0	2.9	0.34	0.2057 ±10	0.512776 ±27	-0.5

(a) computed to T = 3000 Ma

TABLE AIII-2. Sm–Nd ISOTOPIC DATA FOR GABANINTHA FORMATION ANDESITE

Sample	*Sm* (μg/g)	*Nd*	*Sm/Nd*	$^{147}Sm/^{144}Nd$	$^{143}Nd/^{144}Nd$	$\varepsilon_{Nd}(T)$ (a)	T_{DM} (Ma)
81618	4.7	25.7	0.18	0.11071 ±19	0.511100 ±10	+3.6	2855
83329	3.2	15.5	0.21	0.12489 ±31	0.511351 ±10	+3.0	2884

(a) computed to T = 3000 Ma

TABLE AIII-3. Sm–Nd ISOTOPIC DATA FOR WINDANING FORMATION RHYOLITE (SAMPLE NO. 81564)

	Sm (μg/g)	*Nd*	*Sm/Nd*	$^{147}Sm/^{144}Nd$	$^{143}Nd/^{144}Nd$	$\varepsilon_{Nd}(T)$ (a)
	15.5	57.6	0.27	0.16248 ±35	0.512046 ±15	+2.0

(a) computed to T = 3000 Ma

TABLE AIII-4. Sm–Nd ISOTOPIC DATA FOR THE WOOLGRA FORMATION

		Sm (μg/g)	Nd	Sm/Nd	$^{147}Sm/^{144}Nd$	$^{143}Nd/^{144}Nd$ (a)	$\varepsilon_{Nd}(T)$ (Ma)	T_{DM}
Rock samples								
81491		2.4	13.1	0.18	0.11158 ±28	0.511098 ±15	+1.0	2883
81492		3.6	19.9	0.18	0.11039 ±27	0.511085 ±14	+1.2	2868
Material separates from sample 81492								
0.55(b)	Nonmag	4.4	21.4	-	0.12421 ±12	0.511336 ±12	-	-
0.55	Mag	5.1	23.7	-	0.12996 ±13	0.511439 ±12	-	-
0.75	Nonmag	3.9	20.8	-	0.11193 ±11	0.511111 ±20	-	-
1.6	Nonmag	2.6	14.9	-	0.10365 ±10	0.510949 ±15	-	-
1.6	Mag	3.3	18.8	-	0.10595 ±11	0.511001 ±10	-	-
	Leach	1.7	9.8	-	0.10471 ±10	0.510959 ±10	-	-
Mineral separates from sample 81492								
Plag		3.1	18.0	-	0.10551 ±11	0.510985 ±12	-	-
Cpx		5.5	24.3	-	0.13632 ±14	0.511563 ±13	-	-

Isochron data: T = 2818 ±57 Ma, $\varepsilon_{Nd}(T)$ = +1.3 ±0.6, MSWD = 0.54

(a) computed to T = 2800 Ma
(b) The numbers 0.55, 0.75, and 1.6 denote Franz Magnetic Separator settings. Mag = magnetic separate; Leach = HCl leach fraction (not used in isochron fit); plag = plagioclase; cpx = clinopyroxene

Sm–Nd GEOCHRONOLOGY — GRANITOID ROCKS

TABLE AIII-5. Sm–Nd GEOCHRONOLOGY OF PEGMATITE-BANDED GNEISS

Sample	Sm	Nd (μg/g)	$^{147}Sm/^{144}Nd$	$^{143}Nd/^{144}Nd$	$\varepsilon_{Nd}(T)$ (a)	T_{DM} (Ma)
83305	4.6	33.0	0.08518 ±9	0.510554 ±16	+1.7	2933
83397	1.6	11.3	0.08789 ±20	0.510416 ±15	-2.1	3171
83398B	2.9	22.2	0.07828 ±17	0.510418 ±15	-	-
83398B	3.3	26.0	0.07816 ±14	0.510422 ±11	+1.7	2932

(a) computed to T = 2920 Ma

TABLE AIII-6. Sm–Nd MODEL AGES OF RECRYSTALLIZED MONZOGRANITE

Sample	Sm	Nd (μg/g)	$^{147}Sm/^{144}Nd$	$^{143}Nd/^{144}Nd$	$\varepsilon_{Nd}(T)$ (a)	T_{DM} (Ma)
83475	3.2	29.0	0.06603 ±7	0.510266 ±12	-0.8	2846
83479	-	43.0	-	0.510325 ±12	-	-
83479	5.5	49.2	0.06790 ±18	0.510319 ±16	-0.4	2827
83525	2.7	24.3	0.06788 ±16	0.510350 ±15	+ 0.2	2794
84419	3.7	25.0	0.09052 ±9	0.510733 ±18	-0.1	2837

(a) computed to T = 2685 Ma

TABLE AIII-7. Sm–Nd GEOCHRONOLOGY OF POST-FOLDING GRANITOIDS

Sample	Sm	Nd (μg/g)	$^{147}Sm/^{144}Nd$	$^{143}Nd/^{144}Nd$	$\varepsilon_{Nd}(T)$ (a)	T_{DM} (Ma)
SUITE I						
74474	2.2	11.8	0.11197 ±39	0.511145 ±16	-0.1	2820
81711B	3.9	22.0	0.10755 ±21	0.511030 ±10	-0.9	2870
SUITE II						
83408	12.5	67.6	0.11215 ±26	0.510936 ±15	-4.3	3153
83552	11.4	53.1	0.12998 ±30	0.511231 ±15	-4.5	3301

(a) computed to T = 2630 Ma

Rb–Sr GEOCHRONOLOGY

TABLE AIII-8. Rb–Sr GEOCHRONOLOGY OF PEGMATITE-BANDED GNEISS

Sample	*Rb* (μg/g)	*Sr*	*Rb/Sr*	$^{87}Rb/^{86}Sr$	$^{87}Sr/^{86}Sr$	*Isochron age (Ma)*	*Initial ratio*
BUONGNOO OUTCROP							
83296(a)	198	181	1.095	3.20	0.84681		
83298(b)	290	211	1.380	4.04	0.85403	MODEL 1	MODEL 1
83301(c)	241	293	0.822	2.39	0.79402	2536 ±75 Ma	0.7063
83302A(a)(d)	154	320	0.484	1.41	0.82287		±0.0020
83302B(d)	162	355	0.486	1.32	0.75379	MSWD = 6.8	
83303	145	347	0.424	1.23	0.75210		
83304	151	270	0.560	1.63	0.76563	MODEL 3	MODEL 3
83305	151	266	0.567	1.65	0.76761	2531 ±57 Ma	0.7065
83306	231	189	1.215	3.55	0.83533		±0.0020
83307	225	203	1.105	3.23	0.82611		
BADJA OUTCROP							
83339	61	503	0.123	0.356	0.71849		
83397 (e)	63	486	0.128	0.370	0.71693		
83398A(f)	82	644	0.128	0.370	0.71700	MODEL 1	MODEL 1
83398B(f)	77	533	0.144	0.416	0.71881	2514 ±492 Ma	0.7040
83399	71	497	0.144	0.416	0.71986		±0.0031
83400	87	531	0.165	0.477	0.72136	MSWD = 85.8	
83401	99	525	0.191	0.552	0.72418		
84425	72	563	0.129	0.373	0.71677	MODEL 3	MODEL 3
84426	104	553	0.186	0.538	0.72302	2399 ±369 Ma	0.7047
84427	77	360	0.215	0.621	0.72625		±0.0024
84428	61	458	0.123	0.355	0.71725		

COMBINED DATA (19 analyses)
Isochron age : MODEL 1 2630 ±89 Ma (MSWD = 54.3); MODEL 3 2596 ±34 Ma
Initial ratio: MODEL 1 0.7034 ±0.0007; MODEL 3 0.7038 ±0.0008

(a) Sample omitted from isochron
(b) Split of geochemistry sample 83297
(c) Split of sample 83300
(d) Split of sample 83303
(e) Split of sample 83339
(f) Split of sample 83399

Sample numbers ending in A are from leucocratic bands, B from mesocratic bands

TABLE AIII-9. Rb–Sr GEOCHRONOLOGY OF RECRYSTALLIZED MONZOGRANITE

Sample	*Geochem. sample split*	*Rb*	*Sr* (μg/g)	*Rb/Sr*	$^{87}Rb/^{86}Sr$	$^{87}Sr/^{86}Sr$	*Isochron age*	*Initial ratio*
MOYAGEE AREA								
81775		199	204	0.797	2.85	0.80848	MODEL 1	MODEL 1
83312		137	336	0.408	1.18	0.74747	2572 ±71 Ma	0.7036 ±0.0021
84417		198	200	0.990	2.89	0.81096	MSWD = 2.4	
84418(a)		198	205	0.963	2.81	0.80104		
84419		195	206	0.951	2.77	0.80731	MODEL 3	MODEL 3
84420		193	204	0.948	2.76	0.80678	2570 ±103 Ma	0.7036 ±0.0038
NALBARRA AREA								
Darn Hill outcrop								
83479	83478	81	374	0.217	0.628	0.72555		
83480		70	381	0.187	0.541	0.72259		
83482	83481	74	338	0.219	0.633	0.72518		
84422		75	365	0.206	0.596	0.72462		
84423(a)		61	503	0.123	0.356	0.72482		
84424		70	376	0.186	0.538	0.72239	MODEL 1	MODEL 1
Yarlot Well outcrop							2539 ±166 Ma	0.7028 ±0.0015
83498	83497	82	644	0.128	0.370	0.71700		
83500	83499	135	676	0.202	0.584	0.72361	MSWD = 31.0	
83502	83501	133	535	0.251	0.726	0.72855		
83504	83503	115	444	0.260	0.752	0.73165		
83506(a)	83505	92	390	0.236	0.683	0.73277	MODEL 3	MODEL 3
83508(a)	83507	112	419	0.272	0.787	0.72586	2607 ±151 Ma	0.7021 ±0.0016
Couttes Well outcrop								
83509		120	371	0.324	0.938	0.73690		
83510		117	343	0.340	0.985	0.73931		
83512	83511	104	274	0.382	1.110	0.74468		
REGIONAL SAMPLES — BELELE 1:250 000 SHEET								
83250B	83250A	101	390	0.283	0.819	0.73409		
83254	83253	78	375	0.208	0.602	0.72477		
83255B	83255A	74	406	0.184	0.532	0.72255		
83259(a)	83260	75	283	0.265	0.767	0.73506		
REGIONAL SAMPLES — CUE 1:250 000 SHEET							MODEL 1	MODEL 1
83277	83276	96	616	0.156	0.451	0.71988	2704 ±115 Ma	0.7016 ±0.0008
83308B	83308A	152	538	0.282	0.816	0.73503		
83309B	83309A	157	166	0.941	2.743	0.80517	MSWD = 31.6	
83310B	83310A	65	864	0.075	0.216	0.70979		
83311B	83311A	105	261	0.403	1.170	0.74623	MODEL 3	MODEL 3
							2598 ±67 Ma	0.7026 ±0.0010
REGIONAL SAMPLES — KIRKALOCKA 1:250 000 SHEET								
83475	83474	62	496	0.127	0.367	0.71605		
83529	83528	70	384	0.181	0.523	0.72174		

COMBINED DATA (27 analyses)
Isochron age: MODEL 1 2635 ±56 Ma (MSWD = 28.2), MODEL 3 2603 ±27 Ma
Initial ratio: MODEL 1 0.7020 ±0.0005, MODEL 3 0.7023 ±0.0005

(a) Sample omitted from isochron

TABLE AIII-10. Rb–Sr GEOCHRONOLOGY OF POST-FOLDING GRANITOIDS

Sample	*Geochem. sample split*	*Rb*	*Sr* (μg/g)	*Rb/Sr*	$^{87}Rb/^{86}Sr$	$^{87}Sr/^{86}Sr$	*Isochron age*	*Initial ratio*
POST-FOLDING GRANITOIDS SUITE I								
NORIE PLUTON (TONALITE)								
81612		80	260	0.309	0.894	0.73336		
81711B	81711A	58	313	-	0.535	0.72189		
81712B	81712A	59	297	0.198	0.573	0.72292	MODEL 1	MODEL 1
81714B	81714A	72	271	0.267	0.773	0.73016	2584 ±114 Ma	0.7017 ±0.0006
81715B	81715A	60	118	0.244	0.706	0.72709		
							MSWD = 30.6	
REEDY PLUTON (TONALITE)							MODEL 3	MODEL 3
83240B	83240A	46	280	0.162	0.468	0.71991	2508 ±162 Ma	0.7022 ±0.0013
83242B	83242A	6	299	0.020	0.059	0.70386		
83243B	83243A	42	312	0.133	0.358	0.71548		
NANNINE AND ANNEAN PLUTONS								
Tonalite								
81728	81727	52	271	0.190	0.549	0.72369		
81729B	81729A	59	212	0.219	0.633	0.72663		
81730B	81730A	80	427	0.342	0.991	0.73979		
81731B	81731A	77	228	0.343	0.993	0.73999	MODEL 1	MODEL 1
Trondhjemite							2617 ±142 Ma	0.7023 ±0.0018
81722B	81722A	63	134	0.469	1.360	0.75406		
81723B	81723A	150	385	0.318	0.921	0.73609	MSWD = 19.7	
81725B	81725A	99	217	0.506	1.470	0.75768	MODEL 3	MODEL 3
81726B	81726A	61	143	0.472	1.370	0.75512	2640 ±113 Ma	0.7020 ±0.0017
BARLOWEERIE PLUTON (TONALITE)								
83246B(a)	83246A	125	416	0.302	0.875	0.73902		
83249B	83249A	103	443	0.236	0.683	0.72703		
NORIE, REEDY, NANNINE, ANNEAN, AND BARLOWEERIE DATA COMBINED Isochron age: MODEL 1 2644 ±59 Ma (MSWD = 29.2), MODEL 3 2663 ±74 Ma Initial ratio: MODEL 1 0.7016 ±0.0004, MODEL 3 0.7014 ±0.0009								
MAINLAND PLUTON (MONZOGRANITE)								
74467		92	221	0.413	1.200	0.74795		
74468		109	221	0.499	1.450	0.75568		
74469(a)		95	245	0.386	1.120	0.73680		
74470		97	227	0.429	1.240	0.74841	MODEL 1	MODEL 1
74471		92	229	0.405	1.170	0.74721	2221 ±436 Ma	0.7090 ±0.0079
74472		97	230	0.424	1.230	0.74819		
74473		92	210	0.436	1.260	0.74782	MSWD = 12.8	
74474		99	233	0.424	1.230	0.74816	MODEL 3	MODEL 3
81766		92	222	0.459	1.330	0.75182	2147 ±391 Ma	0.7103 ±0.0071
81767(a)		103	238	0.427	1.260	0.93873		
81768B	81768A	96	246	0.391	1.130	0.74595		
81769B	81769A	89	225	0.393	1.140	0.74532		
POST-FOLDING GRANITOIDS SUITE II								
DAMPERWAH PLUTON (MONZOGRANITE)								
83403	83402	219	139	1.57	4.61	0.87963		
83405	83404	154	163	0.941	2.74	0.80966		
83406B	83406A	151	212	0.711	2.07	0.78182	MODEL 1	MODEL 1
83408	83407	150	204	0.735	2.14	0.78371	2704 ±118 Ma	0.7004 ±0.0039
83409B	83409A	158	221	0.715	2.08	0.78243		
83410B	83410A	152	218	0.692	2.01	0.78001	MSWD = 4.9	
84413		147	202	0.734	2.14	0.78346	MODEL 3	MODEL
84414		152	210	0.721	2.10	0.78253	32687 ±82 Ma	0.7010 ±0.0029
84415		156	214	0.728	2.12	0.78236		
84416		161	211	0.760	2.21	0.78597		
KOOLANOOKA PLUTON (SYENOGRANITE)								
83552	83551	251	38	6.76	20.98	1.47339		
83554	83553	256	38	6.82	21.17	1.46861	MODEL 1	MODEL 1
83556	83555	232	46	5.03	15.33	1.26782	2402 ±149 Ma	0.7330 ±0.0382
83558	83557	215	47	4.54	13.74	1.20354		
83560(a)	83559	197	42	4.68	13.56	0.73962	MSWD = 7.9	
84409		256	34	7.56	23.62	1.54900	MODEL 3	MODEL 3
84410		268	37	7.26	22.63	1.52031	2365 ±161 Ma	0.7416 ±0.0492
84411		273	36	7.60	23.76	1.54690		
84412		263	35	7.55	23.55	1.53025		

(a) sample omitted from isochron

GEOLOGICAL SURVEY OF WESTERN AUSTRALIA

BULLETIN 137 PLATE 1

MURCHISON PROVINCE

PRECAMBRIAN GEOLOGY AND MINERAL DEPOSITS



HON. JEFF CARR, M.L.A.
MINISTER OF MINES
D.R. KELLY, DIRECTOR GENERAL OF MINES

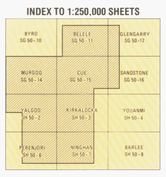
P.E. PLAYFORD
DIRECTOR, GEOLOGICAL SURVEY
OF WESTERN AUSTRALIA

SCALE 1:500 000

5000 0 10 20 30 40 50
Metres Kilometres

Geology by K.P. Watkins and A.H. Hickman 1982-86

INDEX TO 1:250,000 SHEETS



SYMBOLS

- Geological boundary
- Fault or shear-zone
- Primary layering in supracrustals
  - inclined
  - vertical
- Foliation
  - inclined
  - vertical
- Banding in gneiss
  - inclined
  - vertical
- Trend of foliation in granitoid
- Trend of banding in gneiss
- Porphyritic texture in Agr
- Highway
- Road
- Townsite — YALGOO
- Homestead — Coodardy
- Watercourse, intermittent
- Salt lake
- Mining locality — REEDY

Mine (gold unless otherwise indicated)	
Mine (not being worked)	
Open cut	
Alluvial workings	
Prospect	
Mineral occurrence	
Antimony	Sb
Asbestos	Ac
Barite	Ba
Beryl	Be
Copper	Cu
Crushed rock	Rc
Emerald	Em
Feldspar	Fs
Gemstones (excluding Em)	Gs
Gypsum	Gp
Iron ore	Fe
Kaolin/clay	Ck
Lead	Pb
Lithium	Li
Magnesite	Ms
Molybdenum	Mo
Ochre	Oc
Silver	Ag
Talc	T
Tantalum	Ta
Tin	Sn
Titanium	Ti
Tungsten	W
Uranium	U
Vanadium	V
Zinc	Zn

Note: uranium and gypsum occur in surficial deposits overlying Precambrian bedrock

REFERENCE

All rocks are metamorphosed unless stated otherwise.

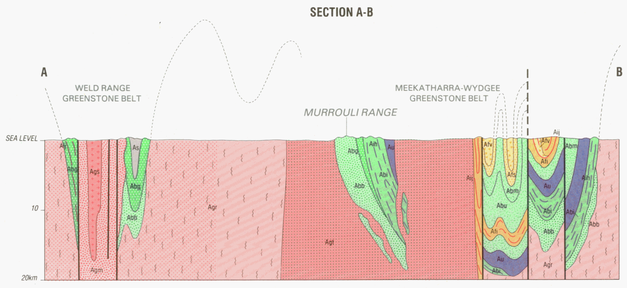
- Ps — Sedimentary rocks unconformably overlying granitoids and greenstone belts, may be weakly metamorphosed
- b — Cross-cutting mafic intrusions, mainly dykes, generally unmetamorphosed
- As — Sedimentary rocks, undivided
- Asp — Shale, may include some sandstone
- Asa — Sandstone, may include some shale and/or conglomerate
- Asc — Conglomerate, may include some sandstone
- Ai — Banded iron-formation, undivided
- Aih — Quartz and hematite banded iron-formation, may contain magnetite and/or chert
- Aij — Red jasper and hematite banded iron-formation, may contain magnetite and/or chert
- Aic — Grey and white banded chert
- Af — Felsic volcanic rocks, undivided
- Afv — Rhyolite, dacite and/or andesite lava and tuff
- Afs — Volcanogenic sedimentary rocks of rhyolite, dacite and/or andesite composition
- Afi — Volcanogenic sedimentary rocks, felsic lava and tuff, and minor mafic rocks, interlayered with banded iron-formation (mainly Aij and Aic)
- Ab — Mafic rocks, undivided
- Abb — Tholeiitic basalt, includes amphibolite and schist derived from tholeiitic basalt, may contain some high-Mg basalt and minor mafic intrusive rocks
- Abu — High-Mg basalt, often with pyroxene needle-spinifex texture (generally pseudomorphed by amphibole), includes schist derived from high-Mg basalt, may contain some tholeiitic basalt and minor mafic and ultramafic intrusive rocks
- Abm — Interlayered tholeiitic and high-Mg basalts, may contain minor mafic and ultramafic intrusive rocks
- Abi — Mafic and ultramafic rocks interlayered with banded iron-formation (mainly Aih)
- Abp — Mafic pyroclastic rocks
- Abg — Gabbro and dolerite, includes layered sills
- Au — Ultramafic rocks, undivided
- Ag — Granitoids, undivided
- Agv — Granophyre
- Ags — Syenogranite
- Agm — Monzogranite
- Agg — Granodiorite
- Agt — Tonalite
- Agi — Trondhjemite

  (Ag, Agv, Ags, Agm, Agg, Agt, Agi: Unmetamorphosed, or very low metamorphic grade)
- Agr — Recrystallized monzogranite, may include some syenogranite and/or granodiorite; commonly contains rafts, xenoliths and recrystallized remnants of Anb
- An — Gneiss, undivided
- Ang — Granitoid gneiss with supracrustal enclaves
- Anb — Pegmatite-banded quartz-microcline-plagioclase-biotite gneiss pervasively intruded by veins, dykes and plutons of Agr
- Ane — Early gneiss complex

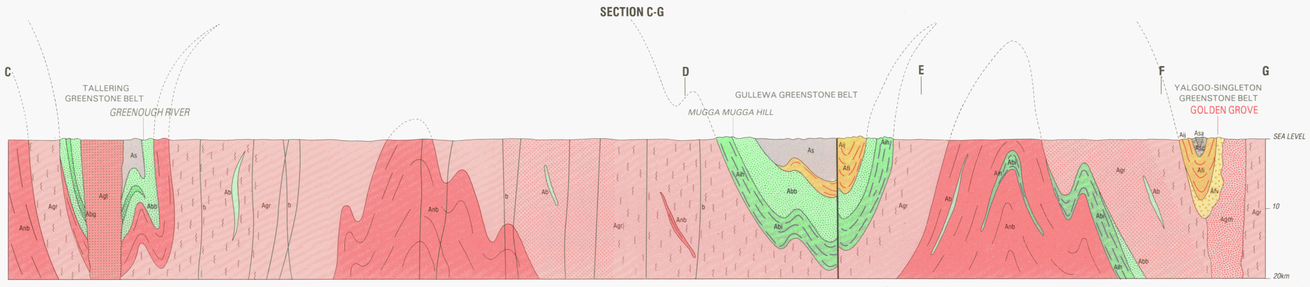
DIAGRAMMATIC SECTIONS

NATURAL SCALE

SECTION A-B



SECTION C-G



Cartography by the Surveys and Mapping Division, Department of Mines, Western Australia.
Topographic information supplied by the Department of Land Administration, Western Australia.
Published by and available from the Geological Survey Division of the Department of Mines, 100 Plain Street, Perth, Western Australia.

Printed by Mercury-Walch, Hobart, Australia

© Western Australia 1988

MURCHISON PROVINCE

PRECAMBRIAN GEOLOGY AND MINERAL DEPOSITS

GEOLOGICAL SURVEY OF WESTERN AUSTRALIA

BULLETIN 137 PLATE 2

MURCHISON PROVINCE

STRATIGRAPHY, STRUCTURE AND MINERALIZATION

HON. JEFF CARR, M.L.A.
MINISTER OF MINES
D.R. KELLY, DIRECTOR GENERAL OF MINES

P.E. PLAYFORD
DIRECTOR, GEOLOGICAL SURVEY
OF WESTERN AUSTRALIA

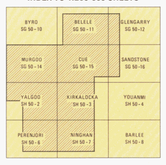


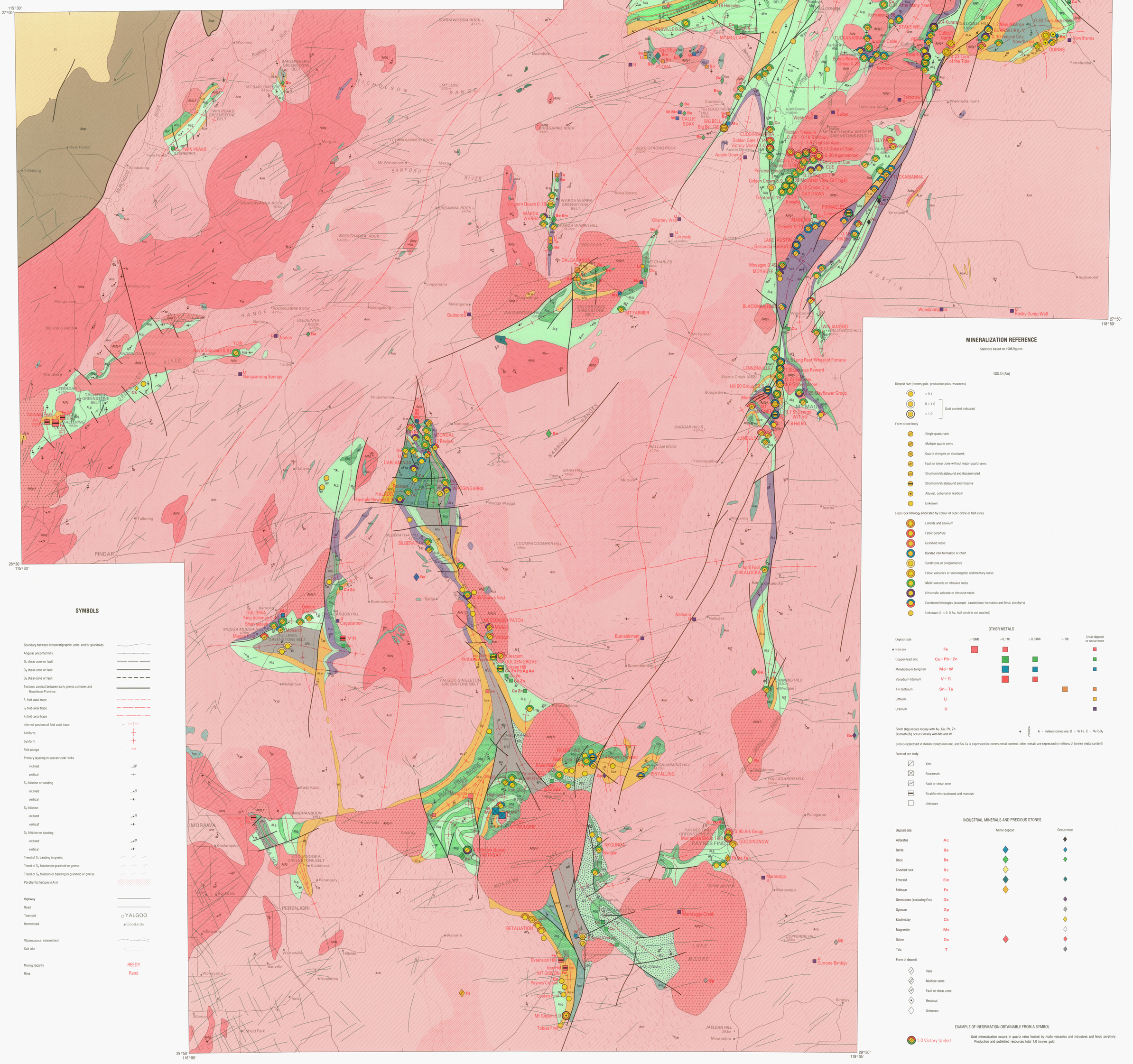
SCALE 1:500 000

5000 0 10 20 30 40 50
Metres Kilometres

Geology by K.P. Watkins and A.H. Hickman 1982-86

INDEX TO 1:250 000 SHEETS




115°30'
27°00'
118°50'
26°10'
117°10'
26°10'
28°30'
115°30'
27°50'
118°50'
29°50'
116°00'
29°50'
118°05'
Hope River
Koonmarra
Jillewarra
JILLEWARRA-CARWELL
Mileura
Belele
MINGAH RANGE GREENSTONE BELT
MINGAH RANGE
MISTLETOE
Mt Sarra
ABBOTTS
0.39 Mt Vranizan
0.79 New Murchison King
ABBOTTS GREENSTONE BELT
0.63 Kyarra
GARDEN GULLY
Havelock 3.0
Prohibition 5.3
MEEKATHARRA
Phar Lap 4.0
Revenue Group 0.23
YALGONDA
Chunderloo Consols
6.6 Eldorado
GNAWEEDA GREENSTONE BELT
Bourkes Find
Tal Val
New Australia
WANGANO
Nannine Aurora
Aladdin Group 6.0
NANNINE
4 Nannine
MT YAGAHONG
Gabanintha
GABANINTHA
Star of the East 5.0
MUNARRA GULLY
Konkoro 0.69
Only After Many Years
STAKE WELL
Culcuth North
Culcuth
Reedy
Rand
Bonds Reward Group 0.79
Nemesis
TUCKANARRA
Cable
Karbar
Nowthanna
QUINNS
1.2 New Alliance
BURNAKURA
0.30 Federal City
0.30 Two Jacks Reef
Yarrabubba
Wanmulla (ruin)
Tom Crow
Hidden Treasure
MEEKATHARRA-WYDGEE GREENSTONE BELT
1.97 Light of Asia
0.17 Duke of York
0.30 Agamemnon
0.46 Gem of Cue
CUE
Princess Royal
Golden Crown 0.9
Trenton 0.19
DAY DAWN
PINNACLES
MAINLAND
Consols 0.7
LAKE AUSTIN
Golconda Eureka
Moyagee 0.45
MOYAGEE
BLACKMAN FIND
Wandarra
WINJANGOO
WINJANGOO HILL
Inglewood
Wondinong
Rocky Dump Well
Mt Farmer
LENNONVILLE
Wattle Creek (Abd)
Hill 50 Group 2.8
Boogardie
Mount Maguet
0.25 Mayflower Group
MT MAGUET
9.7 St George
W.H Hill
8 Hill 60
JUMBUL
Coodardy
TELEGOOTHERE HILL
544m
BIG BELL
Big Bell 3.5
CUDDINGWARRA
Golden Gate 0.14
Victory United 1.0
Austin Downs
Austin Downs Irrigation
Webb West
Nallan
Nalbarra
Burnabinmah
Killarney Well
Lakeside
Lake
DALGARANGA
DALGARANGA GREENSTONE BELT
MT CHARLES
MT FARMER
Western Queen 0.18
WARDA WARRA
WARDA WARRA GREENSTONE BELT
WARDA WARRA HILL
MURDANNA ROCK
BOOLTHARDA ROCK
CURDAWOODA ROCK
CUNDIANNOO ROCK
GNAROWANNA ROCK
WOOLGERONG ROCK
BARLOWEERIE GREENSTONE BELT
MT BARLOWEERIE
TWIN PEAKS GREENSTONE BELT
TWIN PEAKS
NICHOLSON RANGE
MT LUKE
SANFORD RIVER
MURCHISON RIVER
Roderick River
Wooleen
New Forest
Yallalong
Billabalong
Murgoo
Twin Peaks
Mt Wittenoom
Meka
Bulla Dutcana
Jingemarra
Melangata
Dudoorow
Woogalong
Mellenbye
Thundelarra
Burnerbinmah
Pinegrove
Woolgorong
Bullardoo (Abd)
Narloo
Nangcarrong Springs
Yuin
Wandina
Tardie
Pindathuna
Noongal
Gabyon
Tallering
Badja
Bunnawarra
Barnong
Golden Crown
Monarch
Mugga Mugga Hill
Mugga Mugga
Cagacaroon Hill
Cagacaroon
Mt Wittenoom Gap
Kadji Kadji
Koolanooka
Koolanooka Hill
Koolanooka Greenstone Belt
Kooldesak
Perangery
Rockdale
Lucknow
Kalbalya
Ninghanboun Hill
Morawa
PERENJORI
Killawarra
Warrawilla
Hillside
Sanville
Wongyarra
Noalimba
Iona
Billeroo
Enfield Park
Wanarra
Wyggarny
Yowergabbie
Murrum
Edah
Edah Hill
Wagga Wagga
Tallering
PINDAR
Eeradar
Tallering Peak
Tallering Greenstone Belt
Gheenanger River
Polkadin Range
Poondarrie Rock
Beedenna Rock
Underong Rock
Yalgoo Peak
Gnanagooragoo Peak
Weld Range
Weld Range Greenstone Belt
Mindoolah
Ryansville 0.26
Ryansville
Mt Mulcahy
Glenburgh
Bearing Creek
Poona
Siga Khan
Emu
Bonanza
Coodardy
Callie Soak
Big Bell
Cuddingwarra
Golden Gate
Victory Union
Princess Royal
Golden Crown
Trenton
Day Dawn
Pinnacles
Mainland
Lake Austin
Golconda
Eureka
Moyagee
Blackman Find
Wandarra
Winjangoo
Winjangoo Hill
Lennonville
Wattle Creek
Hill 50 Group
Boogardie
Mount Maguet
Jumbul
Mt Farmer
Dalgaranga
Dalgaranga Greenstone Belt
Mt Charles
Western Queen
Warda Warra
Warda Warra Greenstone Belt
Killarney Well
Lakeside
Nalbarra
Burnabinmah
Cuddingwarra
Austin Downs
Webb West
Nallan
Meekatharra-Wydgee Greenstone Belt
Tuckanarra
Karbar
Nowthanna
Quinns
Burnakura
Culcuth
Reedy
Rand
Stake Well
Munarra Gully
Nannine
Wangano
Yalgonda
Mt Yagahong
Gabanintha
Mistletoe
Abbotts
Abbotts Greenstone Belt
Garden Gully
Gnaweeda Greenstone Belt
Meekatharra
Mt Gibson
Mt Gibson-Sons
Tobias Find
Lookes Find
Paynes Find
Paynes Find Greenstone Belt
Marrakesa Group
Goodingnow
Maranalgo
Gunyidi
Gunyidi Creek
Retaliation
Extension Hill
Irony Hill
Fe
Cu Zn
Cu Zn Pb Ag Au
Cu Pb Zn
Au
Ba
Be
Mo
W
Ta
Sn
Li
Ga
Re
Gp
Cp
Yalgoo-Singleton Greenstone Belt
Yalgoo
Singleton
Emerald Reward 0.8
Golden Crown
Messenger Patch
Marion
Vatican
Scimitar
Crescent
Golden Grove
Gossan Hill
Blue Hills Range
Mangada
Iron Chief
Iron Clad
Patrick Find
Fairfield Find
Rose Marie
Mt Singleton
Mt Fitzgerald
Mt Gregory
Mt Gregory Greenstone Belt
Mt Gregory Hill
Mt Gregory Nth
Mt Gregory Sth
Iron Duke
Iron Knight
Iron Prince
Iron Monarch
Iron Baron
Iron Chief
Iron Clad
Iron Duke
Iron Knight
Iron Prince
Iron Monarch
Iron Baron
Mt Singleton Hill
Mt Singleton
Nyngan
Nyounda
Nyounda Hill
Paynes Find Greenstone Belt
Paynes Find
Goodingnow
Maranalgo
Currone-Bimbijy
Bimbijy
Jaelean Hill
Mouroubra
Pullagaroo
Pullagaroo Hill
Quobbunna
Gunyidi
Gunyidi Creek
Tuckanarra
Karbar
Nowthanna
Quinns
Burnakura
Culcuth
Reedy
Rand
Stake Well
Munarra Gully
Nannine
Wangano
Yalgonda
Mt Yagahong
Gabanintha
Mistletoe
Abbotts
Abbotts Greenstone Belt
Garden Gully
Gnaweeda Greenstone Belt
Meekatharra
Mt Gibson
Lookes Find
Tobias Find
Paynes Find
Paynes Find Greenstone Belt

GEOLOGICAL SURVEY OF WESTERN AUSTRALIA

BULLETIN 137 PLATE 3

MURCHISON PROVINCE

METAMORPHIC FACIES



HON. JEFF CARR, M.L.A.
MINISTER OF MINES
D.R. KELLY, DIRECTOR GENERAL OF MINES

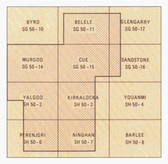
P.E. PLAYFORD,
DIRECTOR, GEOLOGICAL SURVEY
OF WESTERN AUSTRALIA

SCALE 1:500 000

5000 0 10 20 30 40 50
Metres Kilometres

Geology by K.P. Watkins and A.L. Ahmat 1982-86

INDEX TO 1:250 000 SHEETS



117°10' 26°10' 118°50'

115°30' 27°00' 28°30' 29°50' 116°00' 118°05' 27°50'

SYMBOLS

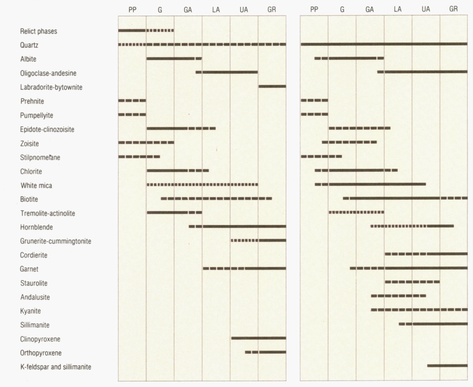
- Boundary between lithological units
- Angular unconformity
- D_1 shear-zone or fault
- D_4 shear-zone or fault
- D_5 shear-zone or fault
- Tectonic contact between early gneiss complex and Murchison Province
- F_1 fold-axial trace
- F_3 fold-axial trace
- F_5 fold-axial trace
- Inferred position of fold-axial trace
- Antiform
- Synform
- Fold plunge
- Primary layering in supracrustal rocks
  - inclined
  - vertical
- S_1 foliation or banding
  - inclined
  - vertical
- S_3 foliation
  - inclined
  - vertical
- S_5 foliation or banding
  - inclined
  - vertical
- Trend of S_1 banding in gneiss
- Trend of S_3 foliation in granitoid or gneiss
- Trend of S_5 foliation or banding in granitoid or gneiss
- Highway
- Road
- Townsite ○ CUE
- Homestead ▪ Coodardy
- Watercourse, intermittent
- Salt lake

Cartography by the Surveys and Mapping Division, Department of Mines, Western Australia.
Topographic information supplied by the Department of Land Administration, Western Australia.
Published by and available from the Geological Survey Division of the Department of Mines, 100 Plain Street, Perth, Western Australia.

Printed by Mercury-Walch, Hobart, Australia

© Western Australia 1988

MINERALOGICAL CRITERIA FOR METAMORPHIC FACIES



PP Prehnite-pumpellyite facies
G Greenschist facies
GA Greenschist-amphibolite facies transition
LA Lower amphibolite facies
UA Upper amphibolite facies
GR Granulite facies

Mineral phase generally present
Mineral phase sometimes present
Mineral phase rarely present

REFERENCE

METAMORPHIC FACIES OF SAMPLE LOCALITIES

- Unmetamorphosed or weakly metamorphosed
- Prehnite-pumpellyite facies
- Greenschist facies
- Greenschist-amphibolite facies transition
- Lower amphibolite facies
- Upper amphibolite facies
- Granulite facies

Each point represents one or more samples

METAMORPHIC FACIES

Metamorphic facies boundary

M_3: Regional metamorphism of supracrustal rocks, pegmatite-banded gneiss and recrystallized monzogranite

- pp Prehnite-pumpellyite facies
- g Greenschist facies
- ga Greenschist-amphibolite facies transition
- la Lower amphibolite facies
- ua Upper amphibolite facies
- gr Granulite facies

M_3: Contact metamorphism of supracrustal rocks by recrystallized monzogranite and pegmatite-banded gneiss protoliths. M_3 assemblages were generally partially retrograded during M_5

- gga Greenschist-amphibolite facies transition, generally partially retrograded to M_5 greenschist facies
- gla Lower amphibolite facies, generally partially retrograded to M_5 greenschist facies
- gua Upper amphibolite facies, generally partially retrograded to M_5 greenschist or lower amphibolite facies

M_5: Contact metamorphism of supracrustal rocks by layered gabbro intrusions. M_3 and M_5 retrograde effects are rare

- cua Upper amphibolite facies
- cgr Granulite facies

POST-FOLDING GRANITOIDS

- um Unmetamorphosed or weakly metamorphosed
- pr Partially recrystallized, generally in low greenschist facies, remnants of igneous texture are preserved

Contact effects of post-folding granitoids are minor and are not shown

BIG BELL METAMORPHISM

- hua Upper amphibolite facies syntectonic hydrothermal metamorphism

LITHOLOGICAL UNITS

- Boundary between major lithological units
- Proterozoic sedimentary rocks
- Post-folding granitoid
- Recrystallized monzogranite
- Pegmatite-banded gneiss
- Metagabbro or metadolerite
- Luke Creek Group supracrustal rocks
- Mount Farmer Group supracrustal rocks
- Unassigned supracrustal rocks
- Early gneiss complex

ARCHAEAN ROCKS

MURCHISON PROVINCE

METAMORPHIC FACIES

BULLETIN 137 PLATE 3



GEOLOGICAL SURVEY OF WESTERN AUSTRALIA

GEOLOGICAL SURVEY OF WESTERN AUSTRALIA

BULLETIN 137

GEOLOGICAL EVOLUTION AND MINERALIZATION OF THE MURCHISON PROVINCE WESTERN AUSTRALIA

BY
KEITH P. WATKINS AND ARTHUR H. HICKMAN

APPENDIX II

LISTING OF GEOCHEMICAL ANALYSIS DATA FILES

FICHE 1:

DATA FILE II.1 ANALYSES OF VOLCANIC ROCKS

FICHE 2:

DATA FILE II.1 (CONTINUED)

DATA FILE II.2 ANALYSES OF GRANITOID ROCKS

DATA FILE II.3 ANALYSES OF BANDED IRON-FORMATION

FICHE 3:

DATA FILE II.4 ANALYSES OF MISCELLANEOUS SAMPLES FROM MINERAL DEPOSITS AND PROSPECTS

DATA FILE II.5 ANALYSES OF SAMPLES WITH RARE-EARTH ELEMENT DETERMINATIONS

FIGURE AII.1 LOCATIONS OF SAMPLE TRAVERSES FOR SUPRACRUSTAL ROCKS AND SAMPLED GRANITOID BODIES

DATA FILE II.1

ANALYSES OF VOLCANIC ROCKS

DATA FILE II.1 -- Analyses of volcanic rocks

Data headings:

SAMPLE - Geological Survey of Western Australia sample number

CODE - the code has six characters; these are, from left to right: 1, rock type; 2 - 3, traverse number; 4, stratigraphic formation; 5, degree of alteration; 6, metamorphic grade.

(1) Rock type:

S	clastic sedimentary rock
P	felsic porphyry
R	rhyolite
D	dacite
A	andesite
N	basaltic andesite
B	tholeiitic basalt
K	high-Mg basalt
L	dolerite
U	ultramafic rock
X	protolith unknown

(2 - 3) Traverse number:

Locations of traverses are shown in Figure AII.1. Isolated samples not taken from formal traverses are indicated by 00.

(4) Stratigraphic unit:

A	Murrouli Basalt
B	Golconda Formation
C	Gabanintha Formation
D	Windaning Formation
E	Lordy Basalt
F	Stockyard Basalt
G	Woolgra Formation
H	Dalgaranga Formation
I	Mindoola Formation
J	Wattle Creek Basalt
K	Singleton Basalt
L	Mougooderra Formation

M Wadgingarra Basalt

W Camberathunun Formation

Q Quinns Basalt

(5) Degree of alteration:

1 Little visible alteration in thin section, geochemical analysis typical of rock type.

2 Evidence of some alteration in thin section, geochemical analysis typical of rock type.

3 Clear evidence of alteration in thin section and/or anomalous geochemistry.

(6) Metamorphic grade:

0 prehnite - pumpellyite facies

1 lower greenschist facies

2 upper greenschist facies

3 greenschist - amphibolite facies transition

4 lower amphibolite facies

5 upper amphibolite facies

EAST and NORTH - Eastings and Northings are based on the Australian Metric Grid, longitude group 50, and are given to the nearest 100 m.

Oxides and sulphur are given in percentages, the remaining analyses are in parts per million. Blank spaces or dashes indicate that no determination was made.

SAMPLE	73657	73658	73659	73660	73661	73662	73663	73664	73665	73666
CODE	X41A33	B41A33	B41A33	B41A33	B41A33	B41A33	B41A33	B41A33	B41A33	B41A33
TRAVERSE	41	41	41	41	41	41	41	41	41	41
EAST	5915	5912	5905	5898	5897	5897	5897	5896	5897	5897
NORTH	68994	68987	68988	68991	68989	68989	68989	68991	68991	68991
SiO_2 (%)	60.1	56.5	56.0	57.0	57.1	55.4	56.8	57.1	55.8	56.0
Al_2O_3	14.1	14.3	14.5	14.4	13.1	15.3	15.4	13.2	14.4	14.5
Fe_2O_3	0.9	1.0	1.0	1.3	1.2	0.7	0.6	0.8	1.0	1.1
FeO	4.66	6.43	5.31	5.61	6.52	5.11	4.81	5.35	5.44	5.69
MgO	5.67	6.01	6.90	5.95	6.27	6.02	6.55	7.88	7.38	6.37
CaO	11.1	12.2	10.7	10.7	12.2	12.2	12.5	11.8	11.6	11.4
Na_2O	0.88	0.58	2.26	1.48	0.42	1.08	0.83	0.68	1.34	1.28
K_2O	0.05	0.07	0.08	0.09	0.05	0.05	0.05	0.04	0.05	0.07
H_2O	1.17	1.34	1.56	1.42	1.57	1.30	1.27	1.68	1.46	1.45
TiO_2	0.64	0.64	0.66	0.65	0.56	0.68	0.70	0.60	0.63	0.63
P_2O_5	0.11	0.10	0.09	0.10	0.10	0.11	0.11	0.09	0.12	0.10
MnO	0.18	0.24	0.23	0.22	0.15	0.23	0.18	0.17	0.16	0.26
S	0.006	0.004	0.010	0.010	0.014	0.014	0.010	0.010	0.006	0.016
Ba (ppm)	130	83	433	258	73	233	108	44	179	101
Ce	27	28	17	20	20	22	24	19	21	15
Co	86	81	87	79	73	73	73	85	85	74
Cr	288	238	405	349	310	398	253	531	426	380
Cu	106	75	107	77	134	97	96	136	79	99
F	-	-	-	-	-	-	-	-	-	-
La	14	15	13	18	11	20	12	12	18	8
Li	3	3	4	5	2	3	3	3	3	4
Mn	1290	1790	1670	1620	1100	1710	1280	1220	1130	1870
Mo	-	-	-	-	-	-	-	-	-	-
Nb	10	5	8	7	8	6	6	<5	<5	<5
Ni	126	110	157	131	117	137	125	181	145	114
Pb	20	20	10	<10	<10	10	10	10	<10	10
Rb	<2	<2	<2	<2	<2	<2	<2	<2	<2	<2
Sn	-	-	-	-	-	-	-	-	-	-
Sr	120	108	132	114	283	111	134	93	111	106
Th	15	5	<5	6	<5	5	6	<5	<5	<5
U	-	-	-	-	-	-	-	-	-	-
V	213	211	203	197	166	192	206	190	189	199
W	-	-	-	-	-	-	-	-	-	-
Y	30	25	30	25	21	28	24	22	31	20
Zn	239	167	104	88	76	79	88	81	77	82
Zr	98	92	93	96	79	90	97	84	82	89

SAMPLE	73667	73668	73669	73670	73671	73672	73673	73674	73675	73676
CODE	B41A33	L41A12	K41A33	K41A34	K41A33	K41A13	B41A33	B41A23	B41A33	K41A23
TRAVERSE	41	41	41	41	41	41	41	41	41	41
EAST	5897	5896	5916	5925	5916	5915	5915	5912	5912	5915
NORTH	68991	68986	68978	68969	68969	68969	68971	68974	68974	68972
SiO_2 (%)	56.3	49.9	53.8	48.7	52.5	50.5	52.9	51.9	53.9	51.0
Al_2O_3	14.9	17.3	9.7	9.0	3.4	10.3	11.4	11.1	9.6	11.2
Fe_2O_3	1.2	1.2	1.5	1.7	1.3	1.0	3.5	2.0	4.2	2.0
FeO	5.51	5.23	10.2	12.4	8.85	8.10	7.37	9.12	3.06	7.08
MgO	6.03	8.30	6.08	8.64	15.4	14.7	6.93	8.16	7.78	12.2
CaO	10.7	13.6	11.7	13.0	12.6	6.83	14.0	12.3	15.9	12.5
Na_2O	1.75	1.73	1.90	0.96	0.59	1.53	0.90	1.13	0.11	0.76
K_2O	0.11	0.07	0.34	0.86	0.14	0.09	0.17	0.11	0.04	0.16
H_2O	1.34	1.57	1.51	2.02	2.46	4.71	1.92	1.86	1.38	2.55
TiO_2	0.66	0.36	1.44	1.20	0.84	0.61	0.89	0.89	0.72	0.43
P_2O_5	0.09	0.06	0.14	0.14	0.08	0.10	0.11	0.12	1.66	0.10
MnO	0.20	0.12	0.25	0.28	0.17	0.14	0.18	0.19	0.17	0.20
S	0.046	0.010	0.024	0.004	0.004	0.002	0.004	0.004	0.008	0.002
Ba (ppm)	121	219	218	204	52	33	119	<20	79	76
Ce	24	6	<5	<5	<5	<5	10	16	350	<5
Co	86	58	123	91	74	74	60	67	65	67
Cr	362	424	1906	971	2162	1665	413	384	419	1068
Cu	105	81	157	95	42	85	79	40	98	74
F	-	-	-	-	-	-	-	-	-	-
La	15	<5	8	5	<5	6	10	7	169	<5
Li	4	2	8	9	4	26	2	2	2	4
Mn	1440	870	1690	1950	1240	1110	1310	1320	1200	1370
Mo	-	-	-	-	-	-	-	-	-	-
Nb	8	<5	<5	<5	<5	<5	<5	6	9	<5
Ni	159	85	383	322	444	341	121	117	123	255
Pb	<10	<10	<10	<10	<10	<10	<10	<10	<10	<10
Rb	<2	<2	4	19	2	<2	2	<2	<2	4
Sn	-	-	-	-	-	-	-	-	-	-
Sr	119	101	101	86	40	67	266	155	232	95
Th	<5	<5	<5	<5	<5	<5	<5	<5	48	<5
U	-	-	-	-	-	-	-	-	-	-
V	211	157	342	305	197	222	210	224	151	225
W	-	-	-	-	-	-	-	-	-	-
Y	24	11	21	20	11	16	20	19	45	14
Zn	77	45	109	108	99	92	126	91	45	66
Zr	88	22	77	67	38	44	61	65	216	32

SAMPLE	73677	73678	73679	73680	73681	73682	73683	73684	73685	73686
CODE	K41A13	K41A23	K41A13	K41A13	K41A23	B41A36	B41A23	B41A13	B41A13	B41A12
TRAVERSE	41	41	41	41	41	41	41	41	41	41
EAST	5913	5912	5912	5928	5931	5921	5909	5920	5919	5917
NORTH	68967	68966	68966	68957	68957	68954	68974	68960	68960	68958
SiO_2 (%)	49.9	50.9	49.9	49.9	50.0	54.9	52.3	50.3	51.8	48.2
Al_2O_3	11.4	11.0	10.4	11.3	11.4	11.7	13.8	14.0	13.5	14.0
Fe_2O_3	1.7	1.8	1.7	1.6	1.4	2.0	2.2	2.0	2.6	2.2
FeO	7.82	8.36	8.87	7.89	8.22	11.7	6.14	12.5	9.81	11.8
MgO	12.9	11.4	11.4	13.6	13.2	6.57	7.16	5.66	3.64	7.35
CaO	10.8	12.0	12.7	9.72	10.0	8.56	11.9	6.78	9.78	9.81
Na_2O	1.24	1.03	1.15	1.08	1.22	0.76	2.85	1.85	3.56	1.94
K_2O	0.10	0.07	0.07	0.13	0.07	0.19	0.05	0.33	0.16	0.19
H_2O	2.97	2.83	2.18	3.54	3.32	2.36	1.62	2.97	2.13	2.44
TiO_2	0.44	0.52	0.49	0.43	0.43	0.46	0.82	1.94	1.95	1.34
P_2O_5	0.09	0.10	0.10	0.07	0.09	0.08	0.03	0.32	0.32	0.19
MnO	0.18	0.18	0.21	0.18	0.20	0.23	0.19	0.15	0.22	0.22
S	0.004	0.005	0.004	0.004	0.004	0.002	0.006	0.004	0.004	0.004
Be (ppm)	43	61	52	84	48	29	57	88	38	22
Ce	<5	<5	<5	<5	<5	<5	<5	21	35	19
Co	63	68	70	61	62	62	40	60	67	69
Cr	1196	968	973	1185	1140	336	119	101	37	132
Cu	72	67	67	69	72	39	61	73	45	103
F	-	-	-	-	-	-	-	-	-	-
La	5	6	6	<5	<5	5	<5	15	11	6
Li	8	7	3	15	12	22	3	14	5	15
Mn	1340	1320	1490	1320	1460	1670	1350	1150	1710	1710
Mo	-	-	-	-	-	-	-	-	-	-
Nb	<5	<5	<5	<5	<5	<5	<5	8	11	6
Ni	289	215	220	316	312	116	90	42	50	84
Pb	<10	<10	<10	<10	<10	<10	<10	<10	<10	<10
Rb	2	<2	<2	6	2	4	<2	10	<2	3
Sn	-	-	-	-	-	-	-	-	-	-
Sr	48	79	54	41	51	20	82	116	40	100
Th	<5	<5	<5	<5	<5	<5	<5	<5	<5	<5
U	-	-	-	-	-	-	-	-	-	-
V	237	241	244	227	227	232	263	378	393	358
W	-	-	-	-	-	-	-	-	-	-
Y	14	18	15	14	14	12	20	39	48	31
Zn	69	73	71	68	66	132	88	117	133	90
Zr	24	31	30	27	28	38	42	118	144	82

SAMPLE	73687	73688	73689	73690	73691	73692	73693	73694	74635	74636
CODE	B41A13	B41A13	B4 .A24	K41A32	B41A24	B41A16	K41A36	K41A34	K35C36	K35C14
TRAVERSE	41	41	41	41	41	41	41	41	35	35
EAST	5917	5919	5920	5931	5931	5929	5932	5933	5950	5950
NORTH	68956	68955	68957	68947	68946	68944	68947	68947	69346	69346
SiO_2 (%)	50.4	50.2	48.6	51.5	51.2	49.8	51.6	52.6	53.1	51.5
Al_2O_3	13.2	14.1	14.4	6.0	12.9	12.9	4.9	4.9	10.9	11.3
Fe_2O_3	3.5	2.5	2.4	2.0	3.4	3.3	1.8	1.9	2.0	1.8
FeO	10.5	9.51	9.66	10.6	10.9	10.6	9.36	9.16	8.80	8.35
MgO	5.41	6.67	7.42	11.8	3.37	6.27	13.7	14.0	10.1	9.93
CaO	9.44	11.8	10.6	12.2	10.2	9.96	14.0	14.2	9.95	12.92
Na_2O	2.66	1.56	2.07	1.21	2.27	2.08	0.69	0.74	1.72	0.67
K_2O	0.18	0.13	0.29	0.19	0.31	0.11	0.16	0.13	0.10	0.05
H_2O	1.73	1.84	2.42	2.22	1.81	1.86	2.54	2.18	2.28	1.92
TiO_2	1.83	0.99	1.19	0.70	1.84	1.85	0.60	0.58	0.67	0.56
P_2O_5	0.31	0.14	0.16	0.09	0.30	0.26	0.09	0.09	0.07	0.06
MnO	0.23	0.22	0.19	0.21	0.27	0.21	0.21	0.20	0.15	0.19
S	0.010	0.004	0.008	0.006	0.006	0.008	0.006	0.004	0.010	0.004
Ba (ppm)	337	58	75	126	89	38	123	73	120	34
Ce	5	5	11	<5	25	15	<5	<5	<10	<10
Co	61	68	65	78	71	70	75	77	57	88
Cr	107	150	159	189	33	120	1191	1137	970	1243
Cu	73	133	80	98	45	104	145	117	66	54
F	-	-	-	-	-	-	-	-	120	100
La	9	5	8	11	16	14	8	<5	<10	<10
Li	10	9	34	10	13	34	22	20	5	3
Mn	1660	1630	1330	1550	1900	1480	1390	1370	-	-
Mo	-	-	-	-	-	-	-	-	<5	<5
Nb	<5	<5	5	<5	8	9	<5	<5	5	<5
Ni	50	113	125	165	49	55	226	250	253	299
Pb	<10	<10	<10	<10	<10	<10	<10	<10	<10	<10
Rb	<2	<2	14	3	3	<2	<2	<2	<5	<5
Sn	-	-	-	-	-	-	-	-	<5	<5
Sr	110	183	103	62	73	135	57	55	49	52
Th	<5	<5	<5	<5	<5	<5	<5	<5	7	7
U	-	-	-	-	-	-	-	-	-	-
V	355	287	306	202	393	410	171	172	242	253
W	-	-	-	-	-	-	-	-	12	132
Y	41	28	26	19	46	36	17	14	22	18
Zn	129	86	85	92	125	111	92	83	67	73
Zr	111	61	75	50	130	112	47	37	138	34

SAMPLE	74437	74438	74439	74440	74441	74442	74451	74452	74453	74454
CODE	K35C14	B35C14	K35C14	K35C14	B35C14	K35C14	R37H13	R37H13	R37H13	R37H13
TRAVERSE	35	35	35	35	35	35	37	37	37	37
EAST	5950	5950	5950	5950	5950	5950	5211	5211	5211	5211
NORTH	69346	69346	69346	69346	69346	69346	69305	69305	69305	69305
SiO_2 (%)	50.4	50.8	50.0	51.3	52.0	51.5	70.4	71.2	76.0	71.7
Al_2O_3	10.4	13.8	10.6	11.1	13.6	12.0	12.0	11.4	9.4	11.3
Fe_2O_3	2.0	2.2	2.2	2.0	2.2	2.3	0.8	0.8	0.9	0.8
FeO	9.25	9.05	9.17	9.27	8.51	9.22	4.83	4.65	3.96	4.52
MgO	10.9	8.09	10.9	9.93	7.66	10.2	0.93	0.98	0.59	1.01
CaO	13.00	11.69	12.68	12.85	11.65	10.29	3.01	3.68	2.49	2.62
Na_2O	0.61	1.60	0.85	0.68	1.27	1.76	0.96	1.32	1.32	0.91
K_2O	0.05	0.09	0.08	0.05	0.07	0.10	5.13	3.71	3.63	4.74
H_2O	2.27	2.08	2.22	1.87	2.11	2.14	1.39	1.40	1.02	1.63
TiO_2	0.55	0.81	0.54	0.56	0.80	0.68	0.31	0.32	0.22	0.31
P_2O_5	0.05	0.08	0.04	0.05	0.09	0.09	0.03	0.04	0.02	0.03
MnO	0.21	0.16	0.21	0.20	0.15	0.18	0.13	0.14	0.12	0.12
S	0.004	0.011	0.005	0.005	0.009	0.007	-	-	-	-
Ba (ppm)	16	132	21	<10	55	101	1183	1313	968	1031
Ce	<10	<10	<10	<10	<10	<10	79	62	61	69
Co	75	63	75	85	68	74	5	9	7	5
Cr	1518	396	1464	1536	468	811	181	262	230	227
Cu	56	95	64	56	226	114	60	62	18	23
F	108	102	97	88	90	71	855	921	335	543
La	<10	<10	<10	<10	<10	<10	16	<10	30	20
Li	2	7	3	3	7	5	22	14	5	19
Mn	-	-	-	-	-	-	-	-	-	-
Mo	<5	<5	6	<5	<5	<5	<5	<5	<5	<5
Nb	<5	<5	6	<5	<5	<5	10	13	8	9
Ni	349	107	357	368	112	235	36	50	30	37
Pb	<10	<10	<10	<10	<10	<10	29	26	27	32
Rb	<5	<5	<5	<5	<5	<5	183	137	87	191
Sn	<5	<5	<5	<5	13	<5	5	14	8	<5
Sr	38	110	43	46	105	73	81	68	83	72
Th	10	5	5	6	8	6	15	18	21	19
U	-	-	-	-	-	-	2	2	2	2
V	244	281	259	264	281	259	41	43	24	41
W	<10	85	<10	64	<10	79	18	17	11	17
Y	15	24	16	19	25	19	57	51	56	53
Zn	91	67	79	75	63	94	105	105	82	106
Zr	28	62	34	39	80	49	244	225	210	225

SAMPLE	74455	74456	74457	74458	74475	74476	74477	74478	74479	74480
CODE	R37H13	R37H13	R37H13	R37H13	B38I32	B38I32	338I32	B38I32	B38I32	B38I32
TRAVERSE	37	37	37	37	38	38	38	38	38	38
EAST	5211	5211	5211	5211	5475	5475	5475	5475	5475	5475
NORTH	69305	69305	69305	69305	70060	70060	70060	70060	70060	70060
SiO_2 (%)	69.9	69.3	69.5	74.4	53.6	53.9	53.6	54.0	54.0	54.1
Al_2O_3	12.0	12.2	12.4	10.1	14.8	14.9	14.6	14.5	14.5	14.6
Fe_2O_3	0.9	0.8	1.1	1.0	2.8	2.1	2.6	2.3	2.8	2.5
FeO	4.56	4.99	4.67	4.26	5.87	6.23	5.85	6.04	5.82	5.98
MgO	0.92	1.04	1.11	0.81	7.08	7.16	6.98	7.05	7.03	7.18
CaO	3.00	2.76	2.32	1.91	9.51	8.73	9.47	9.28	9.55	9.45
Na_2O	0.97	1.18	1.06	0.84	2.01	2.61	2.14	2.03	1.63	1.70
K_2O	5.11	4.99	4.98	3.92	0.36	0.44	0.56	0.46	0.45	0.51
H_2O	1.32	1.68	1.68	1.74	3.51	3.26	3.37	3.24	3.56	3.38
TiO_2	0.31	0.32	0.34	0.27	0.50	0.50	0.50	0.50	0.50	0.50
P_2O_5	0.04	0.03	0.04	0.03	0.07	0.06	0.08	0.06	0.07	0.07
MnO	0.13	0.12	0.11	0.10	0.16	0.16	0.16	0.16	0.16	0.16
S	-	-	-	-	0.050	0.055	0.065	0.055	0.053	0.046
Ba (ppm)	1184	1131	1031	871	133	168	256	204	189	160
Ce	62	56	53	67	19	25	30	37	36	14
Co	6	8	11	<5	43	61	45	56	45	55
Cr	223	227	230	235	430	326	414	330	429	306
Cu	36	26	50	28	100	132	102	113	108	115
F	850	695	792	589	155	171	182	185	163	196
La	24	24	15	31	<10	<10	<10	<10	<10	<10
Li	22	21	30	23	11	10	10	10	10	10
Mn	-	-	-	-	-	-	-	-	-	-
Mo	<5	<5	5	<5	<5	<5	<5	<5	<5	<5
Nb	9	11	12	11	6	<5	<5	7	<5	<5
Ni	36	42	38	41	188	193	190	184	184	189
Pb	34	31	29	24	12	12	11	10	10	11
Rb	183	193	229	164	12	14	17	14	13	17
Sn	9	8	<5	<5	6	<5	<5	<5	<5	<5
Sr	82	73	77	66	176	166	176	169	176	169
Th	19	14	17	18	<5	9	9	10	8	9
U	3	3	3	2	-	-	-	-	-	-
V	34	38	42	31	169	174	161	167	173	155
W	11	12	13	<10	<10	85	<10	70	<10	65
Y	55	57	57	54	16	18	15	17	16	17
Zn	107	108	122	116	71	77	68	71	71	72
Zr	242	233	274	213	74	70	73	74	73	76

SAMPLE	74481	74482	80672	80673	80674	80675	80676	80677	80678	80679
CODE	B38I32	B38I32	B51M22	K51M12	K51M22	B51M32	B51M31	B51M31	B51M32	B51M32
TRAVERSE	38	38	51	51	51	51	51	51	51	51
EAST	5475	5475	4673	4676	4679	4680	4683	4684	4687	4688
NORTH	70060	70060	68712	68713	68714	68715	68715	68715	68716	68717
SiO_2 (%)	53.4	54.3	50.9	49.4	52.7	54.8	54.2	53.6	53.3	55.8
Al_2O_3	15.0	14.9	12.8	11.9	11.2	14.0	13.2	13.9	12.9	12.6
Fe_2O_3	2.7	2.2	1.8	1.1	1.4	1.4	1.2	1.1	1.6	1.4
FeO	6.04	6.10	7.28	7.80	6.82	7.16	7.34	7.09	7.25	6.67
MgO	7.25	7.24	9.18	11.6	12.2	6.26	7.76	7.37	8.11	8.10
CaO	8.83	8.24	11.5	11.0	8.18	8.90	9.34	10.1	8.75	8.02
Na_2O	1.73	2.54	1.12	1.39	1.20	2.26	1.62	1.74	1.70	1.82
K_2O	0.77	0.57	0.12	0.08	0.10	0.42	0.18	0.36	0.87	0.70
H_2O	3.75	3.23	2.79	2.85	3.97	2.39	2.75	2.28	2.82	2.81
TiO_2	0.51	0.51	0.54	0.52	0.49	0.66	0.62	0.64	0.60	0.60
P_2O_5	0.07	0.06	0.19	0.18	0.18	0.20	0.20	0.20	0.21	0.20
MnO	0.17	0.16	0.15	0.17	0.14	0.13	0.13	0.13	0.13	0.12
S	0.034	0.056	0.005	0.005	0.010	0.045	0.020	0.010	0.010	0.040
Ba (ppm)	281	330	84	66	72	185	104	260	303	241
Ce	32	17	21	17	14	18	23	28	27	29
Co	46	52	-	-	-	-	-	-	-	-
Cr	382	309	516	990	1179	233	444	368	507	541
Cu	98	132	95	12	26	70	68	63	42	129
F	194	174	-	-	-	-	-	-	-	-
La	<10	<10	8	9	9	12	9	12	20	18
Li	11	10	5	6	14	10	8	6	10	8
Mn	-	-	1258	1326	1162	1014	1065	1098	1093	1094
Mo	<5	<5	-	-	-	-	-	-	-	-
Nb	<5	6	<5	<5	<5	5	5	7	6	9
Ni	192	209	175	196	226	98	137	131	142	153
Pb	17	<10	<10	<10	<10	10	<10	<10	<10	<10
Rb	25	17	4	<2	5	15	6	13	39	26
Sn	<5	<5	-	-	-	-	-	-	-	-
Sr	168	157	95	71	77	97	83	88	94	97
Th	11	10	<10	<10	<10	<10	<10	<10	<10	<10
U	-	-	-	-	-	-	-	-	-	-
V	169	172	193	207	199	203	198	191	195	191
W	<10	51	-	-	-	-	-	-	-	-
Y	17	16	20	23	18	25	25	25	25	26
Zn	76	76	74	67	67	74	84	87	74	70
Zr	71	73	70	63	59	98	95	109	103	105

SAMPLE	80680	80681	80682	80683	80684	80685	80686	80687	80688	80689
CODE	B51M32	B51M32	L51M21	B51M31	K51M31	K51M22	K51M31	K51M31	N51M12	B51M31
TRAVERSE	51	51	51	51	51	51	51	51	51	51
EAST	4689	4692	4694	4696	4698	4698	4698	4700	4702	4703
NORTH	68717	68718	68719	68720	68722	68721	68720	68723	68723	68723
SiO_2 (%)	54.5	54.0	52.7	54.4	53.8	52.1	52.5	54.1	56.1	54.3
Al_2O_3	12.2	12.3	8.7	12.8	12.1	12.4	12.7	12.8	16.5	12.8
Fe_2O_3	1.3	1.3	1.0	2.0	1.5	1.4	1.3	1.4	2.0	1.5
FeO	6.99	6.93	7.62	6.64	6.54	7.44	6.94	7.02	6.96	7.23
MgO	8.91	8.86	15.1	6.96	9.93	11.6	10.7	9.54	4.12	7.87
CaO	7.94	7.72	6.32	11.0	7.75	7.30	7.43	7.56	8.55	8.86
Na_2O	1.88	2.13	0.76	1.32	1.91	1.56	1.58	1.15	2.41	1.79
K_2O	0.59	0.59	0.17	0.41	0.34	0.35	0.23	0.51	0.63	0.16
H_2O	3.18	3.32	5.33	2.37	3.96	4.58	4.32	4.14	2.24	3.08
TiO_2	0.58	0.58	0.41	0.60	0.52	0.54	0.58	0.58	0.92	0.61
P_2O_5	0.19	0.20	0.16	0.20	0.19	0.18	0.18	0.20	0.48	0.21
MnO	0.13	0.13	0.15	0.14	0.13	0.14	0.12	0.13	0.12	0.12
S	0.035	0.070	0.010	0.035	0.005	0.010	0.010	0.015	0.30	0.025
Be (ppm)	235	229	150	130	133	153	101	181	258	138
Ce	29	25	14	23	18	25	17	24	26	32
Co	-	-	-	-	-	-	-	-	-	-
Cr	613	638	1590	290	742	836	909	719	88	522
Cu	99	69	47	184	50	62	61	44	102	73
F	-	-	-	-	-	-	-	-	-	-
La	21	14	13	11	7	12	10	14	21	15
Li	7	11	12	5	15	14	13	13	9	8
Mn	1220	1298	1307	1311	1168	1125	995	1063	839	926
Mo	-	-	-	-	-	-	-	-	-	-
Nb	<5	6	5	8	<5	5	7	<5	5	6
Ni	156	155	304	112	181	207	209	168	29	141
Pb	10	<10	<10	11	<10	<10	<10	13	<10	<10
Rb	26	18	6	16	13	11	8	44	24	5
Sn	-	-	-	-	-	-	-	-	-	-
Sr	98	93	24	103	72	73	91	86	173	91
Th	<10	<10	<10	<10	<10	<10	<10	<10	<10	<10
U	-	-	-	-	-	-	-	-	-	-
V	187	189	171	190	188	194	211	206	171	197
W	-	-	-	-	-	-	-	-	-	-
Y	24	25	17	24	19	20	22	21	24	24
Zn	77	73	94	76	77	82	72	94	94	74
Zr	100	100	63	99	84	84	92	83	118	91

SAMPLE	80690	80691	80692	80693	80694	80695	80696	80697	80698	81108
CODE	B51M31	B51M31	B51M31	B51M31	K51M12	B51M32	B51M12	B51M31	B51M31	M41C33
TRAVERSE	51	51	51	51	51	51	51	51	51	41
EAST	4704	4705	4706	4707	4710	4711	4713	4715	4718	5916
NORTH	68723	68723	68723	68722	68720	68720	68717	68715	68714	68951
SiO_2 (%)	54.6	54.7	53.5	54.5	50.4	53.5	52.7	54.6	54.8	53.4
Al_2O_3	13.7	14.3	13.6	13.8	13.6	12.9	12.7	12.2	12.5	16.4
Fe_2O_3	1.5	1.9	2.0	1.8	0.6	1.4	1.2	1.4	1.4	2.4
FeO	7.09	6.77	7.10	6.70	7.43	7.73	7.98	7.16	7.31	6.32
MgO	6.61	5.96	7.21	7.00	11.0	8.58	9.28	8.72	8.41	4.28
CaO	8.68	9.49	9.51	8.87	10.5	8.79	8.81	7.89	7.92	10.7
Na_2O	2.09	2.19	1.49	2.18	1.55	1.43	1.40	1.94	1.97	2.43
K_2O	0.36	0.47	0.45	0.87	0.18	0.86	1.10	0.94	0.64	0.24
H_2O	2.72	2.40	2.98	2.55	3.10	2.99	2.89	2.85	3.00	1.44
TiO_2	0.65	0.67	0.61	0.64	0.27	0.55	0.55	0.60	0.59	0.50
P_2O_5	0.19	0.22	0.21	0.23	0.15	0.19	0.19	0.19	0.20	0.19
MnO	0.13	0.13	0.14	0.13	0.14	0.13	0.13	0.12	0.12	0.16
S	0.020	0.025	0.025	0.015	0.005	0.010	0.010	0.020	0.0..	0.008
Ba (ppm)	145	212	187	324	73	303	301	350	255	142
Ce	27	27	20	26	7	18	20	27	32	42
Co	-	-	-	-	-	-	-	-	-	88
Cr	321	187	304	284	574	474	582	530	557	48
Cu	73	74	71	53	13	76	42	70	61	65
F	-	-	-	-	-	-	-	-	-	-
La	13	18	18	14	(5	16	13	14	18	19
Li	7	7	10	8	5	9	8	9	11	4
Mn	926	944	1016	918	1065	1071	1118	1071	1083	1090
Mo	-	-	-	-	-	-	-	-	-	-
Nb	7	5	5	6	(5	6	(5	5	(5	7
Ni	115	94	112	111	187	156	167	149	147	28
Pb	(10	(10	(10	(10	(10	(10	(10	(10	(10	(10
Rb	12	15	18	35	7	37	52	38	21	2
Sn	-	-	-	-	-	-	-	-	-	-
Sr	80	105	104	115	98	101	88	116	103	290
Th	(10	(10	(10	(10	(10	(10	(10	(10	(10	(5
U	-	-	-	-	-	-	-	-	-	-
V	204	190	186	192	178	199	200	185	183	187
W	-	-	-	-	-	-	-	-	-	-
Y	26	26	24	25	10	22	21	24	25	15
Zn	73	75	81	67	51	73	67	69	58	84
Zr	106	108	98	106	33	78	70	101	99	74

SAMPLE	81109	81110	81111	81112	811.	81114	81115	81116	81117	81118
CODE	N41C13	N41C23	A41C33	X41C33	K41C13	B41C33	B41C32	K41C32	K41C12	K41C32
TRAVERSE	41	41	41	41	41	41	41	41	41	41
EAST	5916	5916	5917	5918	5914	5914	5914	5913	5917	5913
NORTH	68949	68947	68944	68943	68466	68946	68944	68943	68941	68941
SiO_2 (%)	55.5	54.2	57.6	55.1	50.2	56.6	54.2	51.8	51.7	53.1
Al_2O_3	12.7	13.0	11.7	11.3	12.4	14.8	15.1	14.0	11.7	12.4
Fe_2O_3	3.2	3.6	5.1	5.4	2.1	1.1	1.4	1.3	1.5	1.9
FeO	8.27	8.76	7.31	7.91	6.26	4.96	6.09	6.35	6.40	5.99
MgO	3.97	4.25	2.55	3.01	11.5	7.86	8.17	10.3	11.7	10.4
CaO	7.70	7.95	6.67	10.6	11.8	11.4	9.76	12.2	12.4	11.2
Na_2O	3.26	3.32	3.91	1.44	1.64	1.29	1.54	0.68	0.72	1.38
K_2O	0.15	0.22	0.06	0.14	0.08	0.14	0.09	0.09	0.07	0.10
H_2O	1.33	1.36	1.51	1.54	2.50	2.40	2.67	2.73	2.00	2.21
TiO_2	1.74	1.65	2.12	2.03	0.08	0.31	0.28	0.24	0.25	0.25
P_2O_5	0.30	0.30	0.34	0.32	0.07	0.13	0.11	0.09	0.09	0.10
MnO	0.17	0.22	0.18	0.12	0.21	0.21	0.14	0.23	0.20	0.21
S	0.006	0.006	0.024	0.012	0.004	0.002	0.004	0.004	0.006	0.002
Ba (ppm)	160	147	535	188	72	73	97	67	110	81
Ce	14	21	29	21	14	33	19	9	11	15
Co	87	85	76	79	80	68	65	64	67	75
Cr	25	21	13	7	1602	267	352	1194	1396	1061
Cu	61	31	33	70	79	74	121	58	63	72
F	-	-	-	-	-	-	-	-	-	-
La	7	6	6	11	10	14	<5	9	8	5
Li	5	9	3	5	7	5	8	5	4	5
Mn	1160	1550	1280	900	1410	1490	1000	1550	1380	1470
Mo	-	-	-	-	-	-	-	-	-	-
Nb	7	7	11	12	<5	<5	<5	<5	<5	<5
Ni	30	38	27	9	625	130	155	335	403	310
Pb	<10	<10	<10	<10	<10	<10	<10	<10	<10	<10
Rb	<2	<2	<2	<2	<2	3	<2	<2	<2	2
Sn	-	-	-	-	-	-	-	-	-	-
Sr	75	138	83	110	94	96	171	159	144	210
Th	<5	<5	<5	<5	<5	5	<5	<5	<5	<5
U	-	-	-	-	-	-	-	-	-	-
V	425	397	366	475	128	133	168	168	153	161
W	-	-	-	-	-	-	-	-	-	-
Y	47	52	72	51	7	10	10	9	8	10
Zn	66	64	50	100	63	54	64	54	55	57
Zr	141	156	180	162	7	27	35	31	18	22

SAMPLE	81119	81120	81121	81122	81123	81124	81125	81126	81127	81128
CODE	K41C32	K41C32	K41C22	B41C32	K41C32	K41C12	K41C32	K41C32	K41C32	K41C12
TRAVERSE	41	41	41	41	41	41	41	41	41	41
EAST	5912	5912	5913	5914	5909	5907	5906	5905	5903	5899
NORTH	68940	68937	68937	68935	68938	68938	68938	68938	68937	68938
SiO_2 (%)	52.8	53.0	51.8	54.9	52.4	49.8	51.6	56.8	51.0	50.4
Al_2O_3	12.3	12.7	13.7	15.0	14.0	13.1	12.9	9.7	13.2	10.4
Fe_2O_3	1.6	1.6	1.2	1.5	2.2	1.4	1.8	1.3	1.4	1.6
FeO	5.52	6.59	7.06	6.00	6.48	7.40	5.61	6.01	6.61	8.28
MgO	10.4	12.8	12.4	8.14	8.09	13.3	11.1	10.9	11.4	13.6
CaO	11.6	6.46	6.32	8.93	11.1	6.69	10.2	7.20	10.7	6.58
Na_2O	1.36	1.08	1.15	2.24	2.49	1.28	2.20	2.46	2.22	2.69
K_2O	0.09	0.17	0.26	0.15	0.14	0.28	0.46	0.22	0.66	0.04
H_2O	2.08	2.21	3.82	1.55	1.73	4.89	2.39	3.06	3.03	4.20
TiO_2	0.26	0.31	0.33	0.29	0.26	0.25	0.16	0.66	0.17	0.64
P_2O_5	0.11	0.10	0.10	0.12	0.11	0.08	0.08	0.08	0.08	0.08
MnO	0.24	0.15	0.16	0.14	0.23	0.18	0.19	0.15	0.16	0.18
S	0.004	0.002	(0.002	0.002	0.002	0.016	0.004	0.012	0.004	0.006
Ba (ppm)	76	108	129	78	104	134	156	604	196	194
Ce	13	17	16	26	24	9	15	6	11	(5
Co	58	65	61	65	79	66	55	67	63	74
Cr	1005	912	793	157	1152	1122	546	2110	954	1316
Cu	89	86	68	108	100	92	61	93	94	109
F	-	-	-	-	-	-	-	-	-	-
La	11	7	16	14	9	5	6	5	(5	(5
Li	4	12	13	3	1	20	5	7	3	8
Mn	1580	1020	1030	970	1640	1250	1310	1080	1100	1220
Mo	-	-	-	-	-	-	-	-	-	-
Nb	(5	(5	(5	(5	(5	(5	(5	(5	(5	(5
Ni	316	255	244	132	321	297	177	246	317	348
Pb	(10	(10	(10	(10	(10	(10	(10	(10	(10	(10
Rb	(2	4	8	3	2	11	25	7	29	(2
Sn	-	-	-	-	-	-	-	-	-	-
Sr	270	193	225	159	389	128	192	334	297	92
Th	(5	(5	(5	7	(5	(5	(5	(5	(5	(5
U	-	-	-	-	-	-	-	-	-	-
V	143	168	180	158	155	186	145	226	131	237
W	-	-	-	-	-	-	-	-	-	-
Y	10	10	10	12	8	8	7	11	6	14
Zn	62	63	67	61	68	66	54	46	39	75
Zr	37	39	37	36	29	28	19	28	17	45

SAMPLE	81129	81130	81131	81132	81133	81134	81135	81136	81137	81138
CODE	K41C22	K41C32	B41C12	L41C12	B41C32	K41C12	B41C32	K41C32	K41C12	K41C12
TRAVERSE	41	41	41	41	41	41	41	41	41	41
EAST	5898	5897	5895	5891	5886	5872	5869	5867	5864	5877
NORTH	68940	68938	68941	68943	68943	68939	68940	68943	68945	68938
SiO_2 (%)	48.6	50.7	52.4	52.0	53.5	48.4	52.1	52.7	50.3	52.0
Al_2O_3	9.5	8.6	15.4	11.9	10.9	9.7	11.8	10.8	12.1	10.4
Fe_2O_3	1.0	2.9	2.4	2.2	2.4	2.2	3.7	3.3	2.3	2.1
FeO	9.24	6.95	6.47	8.88	6.65	7.96	5.68	6.66	7.91	7.66
MgO	15.9	13.2	7.11	8.24	8.27	16.1	8.66	12.0	9.32	11.3
CaO	7.48	8.52	7.62	8.27	7.91	6.44	6.71	5.33	8.34	7.77
Na_2O	1.90	2.81	4.87	4.03	5.27	1.96	4.34	2.97	3.64	3.43
K_2O	0.04	0.03	0.12	0.10	0.04	0.06	0.07	0.04	0.16	0.10
H_2O	4.51	4.00	2.29	2.33	4.44	4.82	5.38	4.43	3.49	3.05
TiO_2	0.65	0.61	0.41	1.06	0.97	0.53	0.82	0.77	0.88	0.75
P_2O_5	0.09	0.08	0.10	0.11	0.12	0.08	0.10	0.08	0.12	0.09
MnO	0.18	0.17	0.16	0.18	0.18	0.18	0.17	0.17	0.18	0.18
S	0.006	0.006	0.006	0.006	0.008	0.004	0.034	0.010	0.014	0.006
Ba (ppm)	20	<20	513	53	<20	<20	55	68	322	188
Ce	8	6	16	10	<5	<5	13	<5	8	5
Co	79	68	46	52	46	69	47	57	57	60
Cr	1733	1599	201	357	502	1733	549	1088	705	957
Cu	226	265	278	236	241	151	348	267	264	250
F	-	-	-	-	-	-	-	-	-	-
La	8	7	6	8	8	5	<5	5	7	6
Li	7	4	6	3	3	19	13	19	10	12
Mn	1240	1250	1130	1250	1350	1250	1220	1180	1310	1270
Mo	-	-	-	-	-	-	-	-	-	-
Nb	<5	<5	<5	5	<5	<5	<5	5	<5	<5
Ni	489	440	120	90	100	450	160	310	210	300
Pb	<10	<10	<10	<10	<10	<10	<10	<10	<10	<10
Rb	<2	<2	<2	<2	<2	2	<2	<2	<2	2
Sn	-	-	-	-	-	-	-	-	-	-
Sr	68	89	342	98	105	93	161	153	169	98
Th	<5	<5	<5	<5	<5	<5	<5	<5	<5	<5
U	-	-	-	-	-	-	-	-	-	-
V	230	206	204	318	275	220	252	260	261	241
W	-	-	-	-	-	-	-	-	-	-
Y	13	12	17	18	17	12	16	13	16	15
Zn	80	71	71	80	86	77	82	60	59	70
Zr	40	25	39	54	49	25	53	54	51	47

SAMPLE	81139	81140	81141	81142	81143	81144	81145	81146	81147	81148
CODE	K41C12	U41C32	L41C32	U41C32	K41C32	B42C34	B42C24	B42C24	B42C34	B42C14
TRAVERSE	41	41	41	41	41	42	42	42	42	42
EAST	5871	5856	5863	5854	5846	5764	5765	5764	5765	5767
NORTH	68934	68971	68982	68967	68963	68998	68998	68995	68993	68993
SiO_2 (%)	51.6	44.2	52.6	47.9	55.8	53.6	52.8	52.0	52.7	49.6
Al_2O_3	12.7	7.3	12.9	6.6	8.1	13.5	16.5	16.3	14.9	15.1
Fe_2O_3	1.6	0.9	2.8	1.0	1.2	1.2	1.6	2.1	2.1	4.2
FeO	7.12	9.92	6.95	8.82	6.68	7.70	6.71	8.70	5.87	5.89
MgO	12.3	22.8	5.36	26.7	12.7	7.12	6.68	6.27	6.73	7.27
CaO	5.11	2.44	4.05	0.17	7.23	11.9	13.2	11.6	16.0	12.4
Na_2O	3.00	0.33	1.34	0.12	3.02	1.59	1.42	1.46	0.92	1.95
K_2O	0.07	0.01	0.04	<0.01	0.08	0.10	0.08	0.12	0.08	0.14
H_2O	4.88	9.50	6.29	7.67	3.71	1.46	1.46	1.62	1.06	1.39
TiO_2	0.30	0.58	0.80	0.68	0.43	0.52	0.66	0.66	0.63	0.66
P_2O_5	0.08	0.04	0.13	0.07	0.07	0.09	0.10	0.09	0.10	0.11
MnO	0.17	0.12	0.16	0.07	0.16	0.20	0.21	0.21	0.19	0.21
S	0.042	0.024	1.6	0.030	0.012	0.006	0.006	0.004	0.006	0.006
Ba (ppm)	308	<20	67	<20	70	33	39	70	22	48
Ce	19	<5	12	<5	6	<5	7	9	8	<5
Co	54	97	57	77	54	55	65	60	60	55
Cr	1013	3338	97	2204	992	627	65	19	297	346
Cu	89	97	175	68	129	105	83	143	187	175
F	-	-	-	-	-	-	-	-	-	-
La	10	5	14	<5	<5	<5	6	7	<5	5
Li	14	8	3	11	3	5	5	6	4	5
Mn	1200	810	1150	530	1140	1450	1440	1470	1370	1500
Mo	-	-	-	-	-	-	-	-	-	-
Nb	<5	<5	<5	<5	<5	<5	<5	<5	<5	<5
Ni	260	1200	70	950	270	100	70	60	100	140
Pb	<10	<10	<10	<10	<10	<10	<10	<10	<10	<10
Rb	<2	<2	<2	<2	2	<2	3	3	<2	<2
Sn	-	-	-	-	-	-	-	-	-	-
Sr	274	80	225	8	122	71	97	87	76	109
Th	<5	<5	<5	<5	<5	<5	<5	<5	<5	<5
U	-	-	-	-	-	-	-	-	-	-
V	210	243	349	216	186	230	259	273	214	218
W	-	-	-	-	-	-	-	-	-	-
Y	9	7	23	9	9	13	18	19	18	25
Zn	67	72	74	71	50	73	64	82	70	83
Zr	29	28	57	25	28	27	35	40	40	39

SAMPLE	81149	81150	81151	81152	81153	81154	81155	81156	81157	81158
CODE	B42C14	B42C14	K42C14	K42C13	B42C32	B42C12	B42C12	B42C12	B42C12	K42C22
TRAVERSE	42	42	42	42	42	42	42	42	42	42
EAST	5767	5765	5765	5767	5769	5770	5771	5774	5773	5773
NORTH	68992	68992	68986	69010	69008	69007	69005	69004	69002	69004
SiO_2 (%)	53.0	50.2	50.2	49.7	47.8	49.7	49.6	49.9	50.2	49.2
Al_2O_3	16.2	15.1	13.5	10.2	10.4	11.7	13.3	11.9	12.7	11.5
Fe_2O_3	1.6	2.1	1.0	2.4	3.2	2.3	3.3	2.7	3.1	2.5
FeO	6.72	8.14	8.32	8.96	8.91	9.84	9.60	8.67	8.56	8.97
MgO	4.59	6.65	11.0	9.82	9.3[illegible]	8.24	6.07	8.31	7.56	9.93
CaO	12.7	11.7	8.76	11.8	14.3	10.7	9.10	10.2	9.92	10.1
Na_2O	1.89	2.27	2.20	1.41	0.96	1.66	2.87	2.17	2.31	2.27
K_2O	0.20	0.21	0.07	0.06	0.08	0.08	0.09	0.06	0.14	0.08
H_2O	1.17	1.55	2.24	2.88	2.95	2.95	2.73	3.05	2.80	3.11
TiO_2	0.70	0.64	0.30	0.88	0.91	1.12	1.69	1.44	1.43	1.16
P_2O_5	0.10	0.10	0.06	0.10	0.13	0.13	0.19	0.15	0.17	0.15
MnO	0.22	0.23	0.20	0.19	0.19	0.23	0.19	0.17	0.17	0.19
S	0.002	0.004	0.012	0.004	0.004	0.002	0.006	0.004	0.004	0.004
Ba (ppm)	72	131	114	<20	27	33	22	57	76	37
Ce	6	12	<5	<5	<5	<5	14	5	10	12
Co	49	69	69	62	65	60	55	59	64	60
Cr	364	351	1040	732	597	192	95	431	301	688
Cu	171	170	184	237	204	380	330	189	202	188
F	-	-	-	-	-	-	-	-	-	-
La	5	5	<5	7	<5	7	9	8	9	7
Li	13	6	5	4	3	5	5	5	5	6
Mn	1480	1590	1330	1370	1350	1330	1630	1360	1240	1380
Mo	-	-	-	-	-	-	-	-	-	-
Nb	<5	<5	<5	<5	<5	<5	6	<5	6	<5
Ni	80	140	270	190	170	110	80	240	160	280
Pb	<10	<10	<10	<10	<10	<10	<10	<10	<10	<10
Rb	2	2	<2	<2	<2	<2	<2	<2	<2	<2
Sn	-	-	-	-	-	-	-	-	-	-
Sr	83	145	119	256	149	155	145	325	266	156
Th	<5	<5	<5	<5	<5	<5	<5	<5	<5	<5
U	-	-	-	-	-	-	-	-	-	-
V	229	219	196	260	266	287	336	314	294	289
W	-	-	-	-	-	-	-	-	-	-
Y	23	32	18	16	17	18	28	26	31	20
Zn	73	84	67	80	73	79	108	88	89	82
Zr	42	35	21	44	36	57	95	72	78	64

SAMPLE	81159	81160	81161	81162	81189	81190	81191	81192	81193	81194
CODE	K42C12	B42C12	B42C12	B43C12	B42J24	B45J32	B45J32	B45J33	B45J33	B45J33
TRAVERSE	42	42	42	43	42	45	45	45	45	45
EAST	5777	5778	5780	5808	5761	5781	5781	5780	5780	5779
NORTH	68999	68998	68996	68985	69025	69075	69075	69076	69078	69079
SiO_2 (%)	49.5	50.3	50.4	69.9	52.8	54.7	54.6	55.5	54.9	54.0
Al_2O_3	10.5	12.8	11.8	14.6	13.4	13.1	13.1	12.7	13.4	13.1
Fe_2O_3	2.0	2.9	3.0	2.1	1.9	3.2	2.6	4.7	2.8	4.6
FeO	8.55	8.35	9.44	8.18	9.23	8.33	8.84	6.42	8.55	6.17
MgO	11.6	7.35	7.49	7.80	5.33	4.62	4.85	3.90	4.72	4.09
CaO	10.5	10.8	10.0	11.0	8.26	9.68	9.27	12.7	9.51	14.3
Na_2O	1.90	1.55	2.65	1.77	4.28	2.68	2.78	0.38	2.19	0.23
K_2O	0.11	0.32	0.08	0.10	0.18	0.20	0.17	0.10	0.19	0.06
H_2O	3.34	3.11	2.78	3.25	1.60	1.75	1.55	2.10	1.78	1.99
TiO_2	1.01	1.42	1.29	0.70	1.95	0.59	0.55	0.54	0.57	0.56
P_2O_5	0.12	0.17	0.15	0.13	0.23	0.11	0.10	0.11	0.10	0.11
MnO	0.19	0.18	0.20	0.19	0.22	0.19	0.20	0.18	0.18	0.20
S	0.006	0.008	0.004	0.006	0.008	0.012	0.006	0.004	0.006	0.006
Ba (ppm)	119	180	55	41	99	215	<20	<20	66	<20
Ce	<5	11	12	7	21	7	9	5	28	6
Co	60	53	64	50	73	75	74	72	70	74
Cr	988	295	379	363	46	11	23	9	13	5
Cu	210	335	138	247	310	104	58	67	56	61
F	-	-	-	-	-	-	-	-	-	-
La	7	7	6	<5	14	8	<5	<5	51	5
Li	9	9	7	5	4	2	3	3	3	2
Mn	1320	1280	1460	1330	1500	1390	1440	1310	1290	1470
Mo	-	-	-	-	-	-	-	-	-	-
Nb	<5	<5	5	<5	10	7	<5	<5	<5	<5
Ni	380	150	160	160	100	40	40	40	40	40
Pb	<10	<10	<10	<10	<10	<10	<10	<10	<10	<10
Rb	<2	6	<2	2	2	14	<2	4	<2	<2
Sn	-	-	-	-	-	-	-	-	-	-
Sr	174	215	274	90	105	108	57	186	171	39
Th	<5	<5	<5	<5	<5	<5	<5	<5	<5	<5
U	-	-	-	-	-	-	-	-	-	-
V	262	288	294	231	423	283	266	242	278	250
W	-	-	-	-	-	-	-	-	-	-
Y	19	21	21	24	30	32	27	31	478	35
Zn	77	89	96	81	128	99	90	71	85	76
Zr	48	86	78	46	116	50	49	39	20	47

SAMPLE	81195	81196	81197	81198	81199	81200	81201	81203	81204	81205
CODE	B45J33	B45J33	B45J32	B45J32	B45J32	B45J32	B45J32	B46C22	B46C12	B46C32
TRAVERSE	45	45	45	45	45	45	45	46	46	46
EAST	5779	5780	5779	5777	5775	5773	5771	5830	5830	5829
NORTH	69081	69082	69084	69085	69085	69085	69085	69597	69597	69599
SiO_2 (%)	54.7	55.6	55.2	55.6	53.3	55.0	54.4	50.0	50.3	46.9
Al_2O_3	13.0	13.0	13.2	13.1	13.4	12.8	12.8	14.8	12.7	16.5
Fe_2O_3	2.3	2.3	4.4	4.7	5.2	5.0	3.1	2.7	3.8	3.4
FeO	9.62	9.19	5.40	5.72	5.75	5.66	8.15	8.13	10.0	6.08
MgO	4.86	4.77	3.52	3.92	4.21	4.06	4.59	6.10	5.22	6.02
CaO	9.08	9.08	14.6	14.1	15.7	14.2	12.0	11.2	10.7	14.0
Na_2O	2.88	2.82	0.20	0.20	0.08	0.22	1.38	2.69	1.57	1.97
K_2O	0.14	0.12	0.06	0.05	0.02	0.04	0.09	0.10	0.04	0.10
H_2O	1.56	1.58	2.49	1.93	2.02	1.83	1.57	2.77	3.57	3.70
TiO_2	0.59	0.57	0.57	0.57	0.55	0.55	0.56	0.72	1.07	0.68
P_2O_5	0.11	0.11	0.11	0.11	0.11	0.10	0.11	0.11	0.13	0.07
MnO	0.20	0.19	0.18	0.19	0.21	0.17	0.22	0.19	0.25	0.19
S	0.004	0.008	0.043	0.044	0.009	0.006	0.009	0.020	0.026	0.004
Ba (ppm)	68	76	26	62	102	24	46	54	<20	75
Ce	10	10	11	10	5	12	<5	9	13	<5
Co	71	70	73	74	72	72	75	68	61	48
Cr	16	5	<5	<5	<5	<5	8	168	41	139
Cu	75	61	89	132	199	62	94	254	288	123
F	-	-	-	-	-	-	-	-	-	-
La	<5	44	7	7	6	7	5	5	7	5
Li	4	3	2	2	2	3	3	7	8	8
Mn	1400	1370	1290	1330	1520	1230	1540	1400	1750	1340
Mo	-	-	-	-	-	-	-	-	-	-
Nb	<5	<5	<5	<5	<5	<5	<5	11	5	10
Ni	40	40	40	40	40	40	40	90	40	80
Pb	<10	<10	<10	<10	<10	<10	<10	<10	<10	<10
Rb	2	2	<2	<2	<2	<2	<2	2	<2	3
Sn	-	-	-	-	-	-	-	-	-	-
Sr	72	64	27	26	25	51	51	113	90	237
Th	<5	<5	<5	<5	<5	<5	<5	<5	<5	<5
U	-	-	-	-	-	-	-	-	-	-
V	291	295	241	252	233	250	258	258	357	193
W	-	-	-	-	-	-	-	-	-	-
Y	28	224	22	21	22	20	24	17	25	13
Zn	108	94	71	80	79	76	92	77	119	69
Zr	41	35	51	45	45	45	48	40	66	37

SAMPLE	81206	81207	81208	81209	81210	81211	81212	81213	81214	81215
CODE	B46C32	B46C22	B46C22	B46C22	B46C22	B46C22	B46C12	B46C12	B46C32	B46C12
TRAVERSE	46	46	46	46	46	46	46	46	46	46
EAST	5826	5823	5821	5818	5819	5819	5819	5818	5818	5818
NORTH	69599	69599	69604	69602	69605	69607	69608	69610	69611	69613
SiO_2 (%)	53.3	53.0	51.3	52.8	52.3	51.5	52.8	50.0	52.1	52.2
Al_2O_3	14.2	14.1	17.1	14.5	13.1	16.5	14.3	15.0	15.9	16.1
Fe_2O_3	2.8	3.7	3.5	2.4	3.5	3.5	2.2	3.2	3.7	2.5
FeO	8.67	8.20	9.96	9.21	9.73	7.95	8.69	9.32	7.56	8.12
MgO	6.24	6.43	6.80	6.46	5.19	3.62	5.61	5.07	3.73	3.85
CaO	8.52	8.86	9.10	7.15	9.01	8.65	8.69	8.83	9.78	7.95
Na_2O	2.57	2.14	2.50	3.97	2.14	2.83	3.20	2.95	2.34	3.57
K_2O	0.50	0.41	0.26	0.32	0.16	0.63	0.60	0.27	0.05	0.17
H_2O	3.40	3.28	3.19	3.12	3.30	3.28	2.77	3.42	3.20	4.05
TiO_2	0.83	0.84	0.80	0.85	0.81	0.60	0.61	1.03	0.76	0.72
P_2O_5	0.14	0.14	0.16	0.15	0.13	0.10	0.07	0.14	0.12	0.11
MnO	0.19	0.18	0.21	0.19	0.20	0.15	0.16	0.18	0.15	0.17
S	0.013	0.004	0.042	0.024	0.012	0.015	0.006	0.008	0.004	0.008
Ba (ppm)	218	187	123	171	62	327	212	76	(20	70
Ce	11	13	(5	8	6	7	(5	9	11	9
Co	45	40	53	43	47	52	50	52	36	30
Cr	22	10	13	11	11	26	55	43	39	70
Cu	193	201	176	195	165	169	196	197	265	202
F	-	-	-	-	-	-	-	-	-	-
La	11	7	7	12	5	7	5	8	7	8
Li	8	9	7	7	8	10	7	10	8	10
Mn	1340	1330	1570	1370	1480	1160	1230	1310	1160	1150
Mo	-	-	-	-	-	-	-	-	-	-
Nb	8	7	7	9	7	5	(5	7	8	5
Ni	20	20	30	20	30	40	40	40	20	30
Pb	(10	(10	(10	(10	(10	(10	(10	(10	(10	(10
Rb	10	8	3	5	2	12	10	6	(2	2
Sn	-	-	-	-	-	-	-	-	-	-
Sr	178	153	162	96	77	322	168	201	137	89
Th	(5	(5	(5	(5	(5	(5	(5	(5	(5	(5
U	-	-	-	-	-	-	-	-	-	-
V	292	277	279	272	267	261	226	341	274	258
W	-	-	-	-	-	-	-	-	-	-
Y	20	21	21	22	21	15	12	19	18	19
Zn	91	88	99	101	98	87	72	89	60	59
Zr	72	73	55	86	55	43	30	62	59	58

SAMPLE	81216	81217	81218	81219	81220	81221	81222	81223	81224	81225
CODE	B46C12	B46C22	B46C22	B46C32	B46C32	N46C12	B46C32	B46C12	B46C32	B46C32
TRAVERSE	46	46	46	46	46	46	46	46	46	46
EAST	5816	5817	5817	5812	5811	5811	5809	5809	5808	5807
NORTH	69614	69616	69617	69608	69610	69611	69613	69613	69614	69616
SiO_2 (%)	50.4	50.2	52.6	54.9	51.8	53.6	54.8	51.8	56.1	53.1
Al_2O_3	14.8	14.0	14.8	14.4	13.8	15.0	13.2	14.9	13.3	14.3
Fe_2O_3	3.1	3.3	3.0	2.4	3.9	2.0	4.2	3.1	3.3	2.5
FeO	8.60	8.98	8.43	7.08	8.57	7.28	7.08	7.09	6.44	8.22
MgO	5.30	5.16	4.15	5.16	4.41	5.31	3.86	5.82	5.26	5.30
CaO	9.20	9.83	9.04	8.04	9.83	7.44	12.1	9.69	13.6	7.54
Na_2O	3.26	2.26	2.55	2.96	2.36	3.75	0.16	2.54	0.36	3.76
K_2O	0.35	0.43	0.17	0.25	0.25	1.05	0.04	0.16	0.06	0.22
H_2O	2.99	3.45	3.32	3.00	3.09	2.59	2.89	3.26	2.27	3.11
TiO_2	0.93	0.98	0.75	0.59	0.89	0.78	0.82	0.87	0.49	0.76
P_2O_5	0.16	0.17	0.12	0.11	0.13	0.15	0.13	0.16	0.10	0.13
MnO	0.16	0.17	0.18	0.15	0.18	0.13	0.16	0.16	0.14	0.17
S	0.012	0.012	0.005	0.008	0.005	0.007	0.003	0.007	0.003	0.006
Ba (ppm)	240	219	64	96	81	551	24	84	32	87
Ce	10	9	7	7	10	19	8	11	<5	11
Co	51	49	43	39	43	38	39	36	36	42
Cr	64	82	15	79	18	132	32	166	153	49
Cu	249	196	243	243	407	234	110	85	131	247
F	-	-	-	-	-	-	-	-	-	-
La	8	9	6	10	7	10	<5	10	<5	8
Li	9	10	8	11	9	10	8	11	4	10
Mn	1270	1340	1310	1100	1350	1040	1230	1050	1040	1260
Mo	-	-	-	-	-	-	-	-	-	-
Nb	6	<5	7	<5	5	6	<5	6	<5	5
Ni	50	40	30	40	20	80	20	60	50	40
Pb	<10	<10	<10	<10	<10	<10	<10	<10	<10	<10
Rb	5	5	4	6	5	20	<2	3	<2	5
Sn	-	-	-	-	-	-	-	-	-	-
Sr	118	126	48	85	80	128	42	240	62	68
Th	<5	<5	<5	<5	<5	<5	<5	<5	<5	<5
U	-	-	-	-	-	-	-	-	-	-
V	302	284	268	215	294	200	255	226	184	269
W	-	-	-	-	-	-	-	-	-	-
Y	17	24	20	16	22	17	21	16	13	22
Zn	85	104	95	77	95	83	78	67	58	92
Zr	48	78	55	56	65	82	60	61	47	73

SAMPLE	81233	81234	81235	81236	81265	81246	81247	81248	81257	81258
CODE	S47D12	S47D12	S47D12	S47D12	B47D32	B47D32	B47D32	B47D32	D48C12	X48C32
TRAVERSE	47	47	47	47	47	47	47	47	48	48
EAST	6617	6617	6623	6628	6621	6619	6616	6617	6262	6260
NORTH	70062	70051	70059	70059	70034	70090	70090	70090	69965	69965
SiO_2 (%)	94.0	76.1	75.0	78.7	53.8	53.6	52.8	52.2	66.2	69.0
Al_2O_3	2.9	11.0	10.5	3.9	13.8	14.2	13.9	13.8	15.1	22.9
Fe_2O_3	<0.1	0.4	0.3	0.6	2.6	2.2	2.5	2.1	1.3	1.6
FeO	0.27	1.28	2.23	3.57	7.06	6.67	6.98	7.10	2.34	4.58
MgO	0.98	6.71	0.15	4.01	5.91	6.41	6.56	6.72	2.31	4.14
CaO	0.05	0.02	0.01	<0.01	8.27	9.50	9.90	9.32	4.66	10.8
Na_2O	0.08	0.08	6.78	0.06	2.83	1.91	2.00	2.48	4.28	3.02
K_2O	0.02	0.03	0.07	0.03	0.08	0.21	0.24	0.26	1.11	0.76
H_2O	0.95	3.48	4.07	3.14	2.94	3.39	3.09	2.98	1.26	2.16
TiO_2	0.04	0.17	0.21	0.13	1.16	1.05	1.14	1.12	0.44	0.33
P_2O_5	0.02	0.03	0.04	0.03	0.29	0.25	0.25	0.26	0.18	0.05
MnO	<0.01	<0.01	<0.01	<0.01	0.14	0.14	0.15	0.14	0.06	0.12
S	0.011	0.009	0.006	0.015	0.011	0.010	0.008	0.007	0.007	0.006
Ba (ppm)	<20	43	27	<20	120	130	116	132	711	307
Ce	18	51	56	44	19	23	13	17	34	5
Co	101	67	46	67	50	47	44	45	48	48
Cr	<5	<5	<5	<5	102	123	131	122	65	65
Cu	195	102	105	60	116	137	146	141	102	111
F	-	-	-	-	-	-	-	-	-	-
La	6	19	19	18	13	9	8	6	16	7
Li	2	5	11	10	5	6	5	4	55	90
Mn	20	30	30	40	990	1020	1040	1050	490	790
Mo	2	1	1	2	-	-	-	-	<1	1
Nb	13	21	18	20	9	10	7	6	9	<5
Ni	<5	<5	<5	<5	70	80	80	80	50	60
Pb	<10	<10	<10	<10	<10	<10	<10	<10	<10	<10
Rb	<2	<2	2	<2	<2	4	5	6	45	92
Sn	10	9	9	7	-	-	-	-	6	7
Sr	2	4	6	3	107	84	97	100	327	237
Th	<5	7	<5	5	<5	<5	<5	<5	5	<5
U	<1	<1	<1	<1	-	-	-	-	<1	<1
V	<5	<5	<5	5	273	239	258	253	83	143
W	-	-	-	-	-	-	-	-	-	-
Y	31	97	101	86	35	37	31	32	14	16
Zn	8	20	27	295	70	68	69	66	39	49
Zr	129	420	365	301	135	138	111	116	123	22

SAMPLE	81259	81260	81261	81262	81263	81264	81265	81266	81267	81268
CODE	D68C13	K68C32	B68C32	A68C24	B68C32	B68C32	K68C22	K68C34	B68C22	K68C32
TRAVERSE	68	68	68	68	68	68	68	68	68	68
EAST	6263	6266	6267	6270	6271	6273	6273	6274	6274	6276
NORTH	69965	69964	69963	69960	69961	69960	69960	69960	69960	69960
SiO_2 (%)	65.4	51.8	57.4	59.0	55.7	55.7	52.4	52.4	52.4	52.7
Al_2O_3	15.3	13.6	12.3	12.8	12.4	12.8	10.6	9.2	14.5	12.5
Fe_2O_3	1.3	1.1	1.4	1.0	1.4	1.5	0.9	1.4	0.9	1.0
FeO	2.82	6.62	5.70	5.13	6.45	5.61	6.98	6.73	6.46	6.57
MgO	2.41	9.99	6.80	5.50	7.72	7.43	11.5	10.5	7.82	9.50
CaO	5.04	11.8	11.2	8.98	11.0	11.3	12.6	13.6	12.7	11.7
Na_2O	3.63	1.05	1.48	3.31	1.96	2.22	1.67	2.02	1.97	2.29
K_2O	1.38	0.37	0.12	1.14	0.13	0.13	0.07	0.28	0.06	0.12
H_2O	0.97	2.33	1.43	1.08	1.44	1.45	1.79	2.24	1.47	1.73
TiO_2	0.44	0.59	0.54	0.55	0.57	0.59	0.46	0.42	0.62	0.61
P_2O_5	0.17	0.08	0.18	0.26	0.19	0.18	0.12	0.11	0.25	0.22
MnO	0.07	0.16	0.28	0.16	0.15	0.15	0.25	0.30	0.15	0.14
S	0.008	0.011	0.007	0.014	0.009	0.008	0.009	0.006	0.004	0.006
Ba (ppm)	638	170	75	1238	88	86	69	85	89	170
Ce	35	22	20	27	18	20	8	<5	37	22
Co	57	60	53	48	57	46	53	51	49	53
Cr	59	696	562	425	526	522	674	663	490	680
Cu	155	354	127	125	112	101	135	91	75	79
F	-	-	-	-	-	-	-	-	-	-
La	22	12	14	18	14	10	10	9	20	13
Li	97	19	16	10	12	11	9	19	9	15
Mn	540	1100	1990	1160	1130	1110	1740	2290	1050	980
Mo	<1	-	1	2	-	-	-	-	-	-
Nb	7	7	10	9	<5	8	<5	5	6	8
Ni	50	210	160	140	250	200	280	90	230	310
Pb	<10	<10	<10	<10	<10	<10	<10	<10	<10	<10
Rb	76	22	5	26	4	5	2	9	<2	4
Sn	7	-	7	6	-	-	-	-	-	-
Sr	258	111	142	534	410	432	279	173	298	265
Th	5	<5	<5	5	<5	<5	<5	<5	6	5
U	<1	-	<1	<1	-	-	-	-	-	-
V	82	194	122	112	151	146	135	134	138	165
W	-	-	-	-	-	-	-	-	-	-
Y	16	18	16	18	13	14	12	11	14	13
Zn	49	70	84	68	69	68	81	102	90	80
Zr	121	81	98	131	90	103	62	60	121	104

SAMPLE	81269	81270	81271	81272	81273	81274	81275	81276	81277	81278
CODE	N48C22	X48C32	A48C32	A48C33	A48C13	A48C23	A48C23	A48C22	B48C22	N48C32
TRAVERSE	48	48	48	48	48	48	48	48	48	48
EAST	6276	6276	6277	6277	6278	6278	6278	6280	6280	6280
NORTH	69940	69940	69940	69940	69940	69940	69940	69940	69940	69940
SiO_2 (%)	55.9	57.5	60.4	60.1	62.1	61.2	60.7	62.1	51.8	60.3
Al_2O_3	14.6	13.6	15.2	14.2	16.7	15.1	14.8	14.1	15.1	14.1
Fe_2O_3	1.2	3.2	2.6	(0.1	0.9	1.1	1.2	1.1	2.2	1.3
FeO	6.11	2.92	3.92	6.32	4.26	4.37	4.26	4.22	5.90	4.34
MgO	5.71	5.55	3.17	5.35	4.83	4.58	4.84	4.57	6.50	5.05
CaO	11.2	12.3	9.24	6.19	5.45	5.41	5.80	7.44	12.5	10.8
Na_2O	2.26	1.81	2.87	2.36	3.21	3.45	3.23	3.35	2.72	1.79
K_2O	0.10	0.07	0.15	1.24	0.88	1.45	1.01	0.38	0.11	0.06
H_2O	1.44	1.46	1.11	2.22	1.80	1.99	1.73	1.19	1.59	1.17
TiO_2	0.65	0.49	0.68	0.56	0.53	0.54	0.55	0.51	0.73	0.52
P_2O_5	0.21	0.17	0.30	0.20	0.17	0.19	0.18	0.18	0.21	0.07
MnO	0.15	0.16	0.09	0.11	0.07	0.09	0.08	0.09	0.18	0.11
S	0.004	0.003	0.009	0.013	0.007	0.010	0.010	0.013	0.084	0.002
Ba (ppm)	120	122	176	522	397	513	444	226	107	43
Ce	31	33	58	39	31	37	28	37	19	29
Co	44	44	46	47	40	40	39	45	56	48
Cr	261	257	107	248	167	187	190	166	386	175
Cu	74	84	117	111	86	94	112	152	293	71
F	-	-	-	-	-	-	-	-	-	-
La	16	14	29	24	16	20	20	19	14	14
Li	8	6	9	68	65	58	61	28	7	10
Mn	1050	1100	730	860	610	690	650	710	1520	810
Mo	-	-	(1	1	(1	2	2	(1	-	1
Nb	11	8	9	8	7	9	12	6	6	10
Ni	130	140	70	160	110	110	110	110	210	120
Pb	(10	(10	(10	(10	(10	(10	(10	(10	(10	(10
Rb	(2	3	3	80	32	103	35	25	4	2
Sn	-	-	7	7	8	6	5	9	-	6
Sr	200	268	529	354	351	336	333	184	206	250
Th	(5	5	7	6	(5	6	6	6	(5	(5
U	-	-	(1	(1	(1	(1	(1	(1	-	(1
V	152	100	149	125	125	120	118	106	154	108
W	-	-	-	-	-	-	-	-	-	-
Y	15	12	17	18	15	19	16	15	19	12
Zn	77	66	51	72	68	61	61	55	78	60
Zr	105	103	127	115	135	133	139	125	99	108

SAMPLE	81279	81280	81281	81282	81283	81286	81287	81288	81289	81290
CODE	N48C32	B48C22	R48C22	A48C12	D48C32	B47032	B47032	N47012	N47012	B47012
TRAVERSE	48	48	48	48	48	47	47	47	47	47
EAST	6281	6281	6284	6281	6281	6626	6627	6628	6630	6631
NORTH	69940	69940	69940	69940	69940	70082	70082	70083	70083	70083
SiO_2 (%)	56.7	51.8	77.2	60.7	67.8	53.8	53.7	55.4	55.5	53.0
Al_2O_3	13.6	13.6	12.3	14.6	16.0	13.6	13.8	13.7	13.7	13.4
Fe_2O_3	1.5	1.2	0.3	1.4	1.2	2.3	2.2	2.6	2.5	2.2
FeO	5.45	6.06	0.96	5.38	2.60	7.42	7.67	7.10	6.92	7.36
MgO	6.3	9.04	0.32	4.85	0.85	6.45	6.21	5.59	5.51	7.34
CaO	10.31	12.8	2.38	5.12	6.18	8.75	9.77	9.42	9.25	9.62
Na_2O	3.11	1.97	2.96	3.90	1.75	2.84	2.17	1.66	2.17	1.44
K_2O	0.12	0.07	2.22	0.96	1.67	0.12	0.17	0.17	0.14	0.29
H_2O	1.28	1.62	0.43	1.74	0.96	2.18	2.24	2.43	2.14	3.07
TiO_2	0.56	0.55	0.18	0.62	0.46	1.21	1.21	1.24	1.22	1.13
P_2O_5	0.21	0.09	0.06	0.17	0.17	0.29	0.28	0.29	0.29	0.27
MnO	0.16	0.26	0.05	0.11	0.13	0.15	0.16	0.12	0.14	0.14
S	0.003	0.004	0.002	0.015	0.014	0.005	0.010	0.003	0.007	0.007
Ba (ppm)	105	67	324	276	698	92	37	61	79	200
Ce	36	<5	102	29	52	17	15	21	23	16
Co	46	62	43	73	67	60	52	54	52	50
Cr	268	301	<5	271	6	98	99	81	79	176
Cu	76	89	41	123	53	90	65	91	111	125
F	-	-	-	-	-	-	-	-	-	-
La	14	6	33	19	29	9	10	12	12	8
Li	5	7	51	112	114	4	4	5	3	5
Mn	1050	1850	450	830	910	1060	1000	940	1000	1050
Mo	-	-	<1	<1	<1	-	-	-	-	-
Nb	8	5	16	10	17	12	10	11	12	11
Ni	130	140	<5	110	20	80	70	60	60	100
Pb	<10	<10	20	<10	40	<10	<10	<10	<10	<10
Rb	<2	<2	67	41	97	<2	2	3	<2	9
Sn	-	-	3	6	6	-	-	-	-	-
Sr	358	104	107	265	123	104	89	87	102	84
Th	<5	<5	11	<5	9	<5	<5	<5	<5	<5
U	-	-	<1	<1	<1	-	-	-	-	-
V	145	264	6	147	70	272	269	264	263	258
W	-	-	-	-	-	-	-	-	-	-
Y	15	14	31	15	18	38	35	45	44	33
Zn	71	77	52	68	129	83	62	70	72	72
Zr	103	46	195	120	163	138	137	169	161	125

SAMPLE	81291	81292	81293	81294	81295	81296	81297	81298	81299	81300
CODE	M47022	B47032	M47012	M47012	M47012	M47012	B47032	M47032	M47013	M47032
TRAVERSE	47	47	47	47	47	47	47	47	47	47
EAST	6633	6634	6634	6635	6635	6637	6639	6641	6643	6645
NORTH	70083	70083	70082	70080	70080	70079	70080	70080	70080	70080
SiO_2 (%)	54.9	54.0	56.4	57.4	55.1	54.5	54.4	57.7	55.1	56.4
Al_2O_3	13.7	13.8	13.2	13.4	13.6	13.8	13.4	11.9	12.8	12.6
Fe_2O_3	2.4	2.1	2.3	2.3	2.1	2.1	2.1	4.5	2.5	3.0
FeO	6.93	7.34	6.95	6.88	7.17	7.27	7.57	5.22	8.40	8.13
MgO	5.81	6.11	5.17	5.22	5.84	6.24	5.90	3.66	4.97	3.86
CaO	9.60	9.80	8.46	8.00	8.99	9.59	10.4	11.6	9.25	8.30
Na_2O	1.80	2.35	2.61	2.40	2.35	2.12	1.96	1.05	2.15	2.97
K_2O	0.18	0.18	0.14	0.10	0.10	0.16	0.16	0.10	0.15	0.13
H_2O	2.50	2.22	2.04	2.20	2.13	2.01	1.68	1.72	1.43	1.65
TiO_2	1.21	1.22	1.23	1.26	1.20	1.24	1.28	1.36	1.57	1.79
P_2O_5	0.29	0.30	0.31	0.31	0.30	0.30	0.32	0.36	0.41	0.43
MnO	0.14	0.13	0.13	0.12	0.13	0.14	0.14	0.12	0.15	0.15
S	0.006	0.008	0.054	0.006	0.006	0.006	0.008	0.007	0.084	0.007
Ba (ppm)	96	126	40	64	65	96	257	56	37	37
Ce	24	14	36	30	26	33	22	38	31	30
Co	50	55	48	45	48	52	54	54	62	60
Cr	88	101	64	59	98	91	76	53	21	11
Cu	130	137	117	115	137	113	100	66	108	63
F	-	-	-	-	-	-	-	-	-	-
La	14	12	9	15	15	11	7	21	18	19
Li	4	4	4	5	5	4	3	2	3	3
Mn	1010	1000	950	930	960	990	1070	940	1140	1120
Mo	-	-	-	-	-	-	-	-	-	-
Nb	13	8	15	15	12	13	11	15	13	12
Ni	60	60	50	50	70	60	60	30	30	20
Pb	<10	<10	<10	<10	<10	<10	<10	<10	<10	<10
Rb	4	3	2	<2	<2	<2	2	<2	<2	<2
Sn	-	-	-	-	-	-	-	-	-	-
Sr	108	97	120	142	137	101	106	95	114	105
Th	<5	<5	<5	<5	<5	<5	<5	<5	<5	<5
U	-	-	-	-	-	-	-	-	-	-
V	263	268	262	268	261	272	287	264	309	363
W	-	-	-	-	-	-	-	-	-	-
Y	41	38	57	55	45	43	37	67	49	56
Zn	69	70	71	68	69	72	71	66	101	78
Zr	157	139	202	206	164	166	144	231	199	215

SAMPLE	81301	81302	81303	81304	81305	81306	81307	81308	81309	81310
CODE	B49C14	B49C12	B49C12	B49C12	B49C12	B49C22	B50C24	B50C24	B50C24	B50C24
TRAVERSE	49	49	49	49	49	49	50	50	50	50
EAST	5895	5895	5895	5896	5898	5899	6087	6086	6084	6084
NORTH	69665	69665	69665	69665	69663	69662	69969	69969	69968	69968
SiO_2 (%)	50.2	49.6	50.0	49.9	50.8	53.6	49.0	50.2	50.3	49.5
Al_2O_3	13.3	13.7	14.1	14.0	14.4	13.4	14.6	14.3	14.4	14.3
Fe_2O_3	2.3	3.1	1.9	1.8	1.7	1.6	2.4	2.2	2.4	2.1
FeO	11.6	10.1	9.36	9.79	9.07	9.07	8.57	8.54	8.49	8.70
MgO	4.58	4.59	6.09	6.30	5.36	5.94	7.77	7.17	7.41	7.73
CaO	11.3	13.0	12.5	12.0	12.1	11.0	13.0	13.4	12.4	12.3
Na_2O	2.50	1.90	2.30	2.27	2.76	2.00	1.21	0.98	1.26	1.65
K_2O	0.15	0.11	0.10	0.12	0.10	0.11	0.04	0.03	0.02	0.09
H_2O	1.58	1.76	1.68	1.77	1.52	1.67	1.60	1.68	1.63	1.69
TiO_2	1.42	0.73	0.76	0.77	0.81	0.43	0.76	0.76	0.74	0.76
P_2O_5	0.20	0.10	0.12	0.11	0.11	0.07	0.09	0.10	0.10	0.11
MnO	0.26	0.25	0.23	0.24	0.23	0.21	0.17	0.18	0.18	0.17
S	0.004	0.003	0.009	0.009	0.007	0.003	0.010	0.011	0.012	0.047
Ba (ppm)	51	27	46	43	62	47	29	46	<20	80
Ce	7	<5	6	7	10	<5	<5	11	11	<5
Co	63	76	74	67	67	70	64	64	70	65
Cr	33	111	104	103	100	31	182	170	177	183
Cu	37	49	63	70	71	78	145	139	189	164
F	-	-	-	-	-	-	-	-	-	-
La	7	<5	10	7	<5	7	<5	10	6	5
Li	3	2	2	2	2	2	11	15	13	17
Mn	1890	1930	1810	1820	1810	1700	1290	1340	1280	1270
Mo	-	-	-	-	-	-	-	-	-	-
Nb	5	<5	5	7	<5	5	5	5	<5	<5
Ni	30	70	80	80	80	80	140	140	140	140
Pb	<10	<10	<10	<10	<10	<10	<10	<10	<10	<10
Rb	<2	2	<2	<2	<2	<2	<2	<2	<2	<2
Sn	-	-	-	-	-	-	-	-	-	-
Sr	78	69	51	48	56	53	138	120	114	105
Th	<5	<5	<5	<5	<5	<5	<5	<5	<5	<5
U	-	-	-	-	-	-	-	-	-	-
V	372	283	299	303	305	235	276	264	268	262
W	-	-	-	-	-	-	-	-	-	-
Y	40	21	22	22	22	15	16	17	15	15
Zn	69	69	78	83	83	70	73	72	76	76
Zr	93	34	37	44	44	40	46	44	34	37

SAMPLE	81311	81312	81314	81315	81316	81317	81318	81319	81320	81321
CODE	B50C24	B50C24	B50C24	B50C24	B50C24	B50C26	B50C34	B50C14	B50C24	B50C26
TRAVERSE	50	50	50	50	50	50	50	50	50	50
EAST	6083	6082	6080	6076	6076	6078	6075	6069	6068	6067
NORTH	69966	69966	69965	69963	69963	69963	69962	69977	69976	69974
SiO_2 (%)	50.1	50.7	50.9	52.6	53.9	51.9	53.2	50.5	49.9	50.5
Al_2O_3	14.4	14.3	14.2	14.2	13.4	13.9	14.0	14.4	14.3	14.4
Fe_2O_3	2.8	2.5	2.4	2.3	2.6	2.6	2.2	2.5	2.2	2.1
FeO	8.13	7.92	8.58	7.64	6.65	7.06	7.65	7.76	8.14	7.80
MgO	7.60	7.65	7.30	6.14	6.27	6.48	7.04	7.06	7.28	7.26
CaO	12.4	12.7	12.1	12.0	12.4	13.2	11.4	13.1	12.8	13.3
Na_2O	0.97	0.9[illegible]	1.35	1.42	1.11	1.09	1.09	1.58	1.63	1.24
K_2O	0.08	0.02	0.09	0.07	0.06	0.06	0.09	0.11	0.11	0.10
H_2O	1.81	1.77	1.74	1.64	1.54	1.64	1.64	1.76	1.87	1.69
TiO_2	0.75	0.68	0.81	0.85	0.82	0.85	0.85	0.74	0.73	0.74
P_2O_5	0.10	0.08	0.11	0.10	0.11	0.11	0.10	0.10	0.10	0.10
MnO	0.18	0.17	0.17	0.16	0.16	0.17	0.13	0.19	0.19	0.19
S	0.034	0.007	0.002	0.002	0.011	0.015	0.015	0.003	0.007	0.027
Ba (ppm)	33	95	<20	<20	61	39	148	52	36	<20
Ce	<5	<5	6	<5	<5	7	<5	<5	<5	5
Co	71	62	62	55	57	55	58	64	64	65
Cr	179	203	127	122	113	109	130	220	241	264
Cu	179	225	140	128	169	184	173	92	182	185
F	-	-	-	-	-	-	-	-	-	-
La	<5	<5	6	5	6	<5	<5	5	<5	<5
Li	21	11	11	11	8	7	16	6	7	6
Mn	1300	1280	1220	1190	1150	1240	1000	1430	1450	1408
Mo	-	-	-	-	-	-	-	-	-	-
Nb	6	5	<5	5	5	6	8	5	<5	8
Ni	140	120	120	100	90	90	100	110	120	120
Pb	<10	<10	<10	<10	<10	<10	<10	<10	<10	<10
Rb	<2	<2	<2	<2	<2	<2	<2	2	<2	<2
Sn	-	-	-	-	-	-	-	-	-	-
Sr	121	126	132	198	135	106	163	117	106	75
Th	<5	<5	<5	<5	<5	<5	<5	<5	<5	<5
U	-	-	-	-	-	-	-	-	-	-
V	270	266	277	304	285	292	279	257	266	271
W	-	-	-	-	-	-	-	-	-	-
Y	15	15	17	16	17	18	17	16	15	14
Zn	77	72	71	70	63	71	69	73	84	77
Zr	35	34	45	45	52	56	47	40	38	46

SAMPLE	81322	81323	81324	81325	81326	81327	81328	81329	81330	81331
CODE	K51M21	B51M31	K52M32	B52M32	K52M32	B52M32	K52M12	K52M32	B52M32	K52M12
TRAVERSE	51	51	52	52	52	52	52	52	52	52
EAST	4714	4713	4717	4717	4717	4716	4717	4718	4719	4727
NORTH	68704	68706	68778	68778	68778	68778	68777	68777	68778	68775
SiO_2 (%)	48.9	55.0	53.3	54.7	54.3	54.6	52.7	54.2	54.6	52.3
Al_2O_3	9.0	12.8	12.1	12.7	12.3	12.4	12.0	12.1	12.4	10.4
Fe_2O_3	1.3	1.3	1.1	1.3	1.2	1.2	1.1	1.3	1.3	1.3
FeO	8.03	7.28	7.81	7.27	7.38	7.46	7.54	7.15	7.24	8.57
MgO	16.1	8.10	10.2	8.93	9.64	9.01	10.4	9.56	8.90	13.2
CaO	8.19	8.15	8.28	7.86	8.12	7.97	8.05	7.92	7.60	7.42
Na_2O	0.99	1.97	1.64	2.04	1.79	2.00	2.42	1.98	2.38	0.83
K_2O	0.08	0.89	0.68	0.96	0.32	0.81	0.28	0.82	0.55	0.06
H_2O	5.09	2.87	3.03	2.29	2.99	2.41	3.05	2.81	2.63	4.52
TiO_2	0.36	0.60	0.47	0.59	0.59	0.59	0.45	0.58	0.59	0.42
P_2O_5	0.17	0.20	0.19	0.21	0.20	0.20	0.18	0.19	0.19	0.17
MnO	0.16	0.13	0.14	0.13	0.14	0.13	0.12	0.13	0.12	0.16
S	0.005	0.020	0.005	0.015	0.010	0.010	0.005	0.005	0.010	0.010
Ba (ppm)	58	338	271	295	273	275	119	357	227	114
Ce	<5	32	21	25	26	26	23	26	25	<5
Co	-	-	-	-	-	-	-	-	-	-
Cr	2273	470	687	558	655	546	713	636	598	1225
Cu	6	59	18	75	61	66	25	21	54	36
F	-	-	-	-	-	-	-	-	-	-
La	8	15	13	16	19	16	14	11	14	<5
Li	10	12	8	9	7	9	8	10	6	7
Mn	1471	1112	1172	1094	1145	1121	1014	1021	1003	1267
Mo	-	-	-	-	-	-	-	-	-	-
Nb	<5	6	<5	5	5	8	5	7	7	<5
Ni	403	137	178	150	167	155	185	161	154	228
Pb	<10	<10	<10	<10	<10	<10	<10	<10	<10	<10
Rb	2	34	26	35	18	32	11	31	21	<2
Sn	-	-	-	-	-	-	-	-	-	-
Sr	103	114	87	103	102	98	135	106	111	43
Th	<10	<10	<10	<10	<10	<10	<10	<10	<10	<10
U	-	-	-	-	-	-	-	-	-	-
V	191	187	179	186	182	189	179	181	186	196
W	-	-	-	-	-	-	-	-	-	-
Y	14	25	21	25	23	25	19	24	24	15
Zn	55	68	77	70	77	74	55	69	65	64
Zr	32	104	70	94	88	99	64	88	99	31

SAMPLE	81332	81333	81334	81335	81336	81337	81338	81339	81340	81341
CODE	K52M12	K52M12	K52M12	K52M12	K52M22	B52M11	K52M12	L52032	K52032	B52012
TRAVERSE	52	52	52	52	52	52	52	52	52	52
EAST	4727	4722	4723	4726	4729	4729	4730	4733	4734	4737
NORTH	68778	68788	68788	68789	68789	68786	68784	68784	68781	68781
SiO_2 (%)	51.8	51.0	52.4	50.6	51.9	53.0	52.7	53.6	53.1	50.6
Al_2O_3	10.7	11.3	12.5	11.1	10.7	12.2	11.7	13.4	12.1	16.9
Fe_2O_3	1.3	1.6	0.9	1.0	1.4	1.7	1.7	3.1	1.2	1.6
FeO	8.65	9.78	7.85	8.12	8.01	7.91	7.87	9.15	7.84	9.21
MgO	11.8	9.70	10.6	13.3	12.4	9.43	10.0	5.36	9.85	6.93
CaO	7.10	10.2	8.72	8.72	9.01	10.3	10.8	10.5	9.08	10.9
Na_2O	1.86	1.39	1.72	1.46	0.96	1.09	0.99	0.92	2.07	1.69
K_2O	0.21	0.07	0.22	0.08	0.07	0.11	0.07	0.11	0.10	0.09
H_2O	4.17	2.17	2.59	3.30	3.42	2.17	2.30	1.61	2.54	1.89
TiO_2	0.44	0.91	0.46	0.44	0.45	0.50	0.47	1.01	0.53	0.76
P_2O_5	0.17	0.21	0.18	0.18	0.18	0.19	0.19	0.26	0.19	0.19
MnO	0.15	0.16	0.15	0.14	0.13	0.14	0.15	0.15	0.16	0.15
S	0.005	0.015	0.005	0.010	0.010	0.090	0.035	0.010	0.010	0.035
Ba (ppm)	117	103	131	54	171	35	25	127	74	103
Ce	7	13	<5	<5	<5	<5	7	14	10	7
Co	-	-	-	-	-	-	-	-	-	-
Cr	1126	580	773	1127	926	562	678	46	678	347
Cu	48	128	14	57	47	68	47	72	62	123
F	-	-	-	-	-	-	-	-	-	-
La	<5	12	8	7	5	<5	5	8	9	7
Li	6	5	6	7	11	8	6	12	8	6
Mn	1264	1316	1297	1262	1167	1246	1321	1246	1317	1345
Mo	-	-	-	-	-	-	-	-	-	-
Nb	5	5	<5	<5	<5	<5	<5	<5	<5	<5
Ni	214	181	186	296	195	142	157	63	160	131
Pb	<10	<10	<10	<10	<10	<10	<10	<10	<10	<10
Rb	4	<2	10	6	4	3	<2	<2	3	<2
Sn	-	-	-	-	-	-	-	-	-	-
Sr	151	158	53	34	26	70	49	166	82	88
Th	<10	<10	<10	<10	<10	<10	<10	<10	<10	<10
U	-	-	-	-	-	-	-	-	-	-
V	204	229	249	240	232	255	260	334	196	253
W	-	-	-	-	-	-	-	-	-	-
Y	15	21	16	17	15	18	16	28	15	21
Zn	48	97	93	67	72	66	75	90	76	83
Zr	43	72	35	34	35	43	44	81	53	51

SAMPLE	81342	81343	81344	81345	81346	81347	81348	81349	81350	81351
CODE	B52D12	B52D12	B52D12	B52C12	B52C12	B52C12	B52C12	B52C32	B52C12	B52C12
TRAVERSE	52	52	52	52	52	52	52	52	52	52
EAST	4738	4740	4741	4742	4742	4745	4751	36	4753	4753
NORTH	68781	68781	68781	68781	68797	68795	68792	68797	68800	68799
SiO_2 (%)	51.4	50.9	51.6	51.4	52.7	51.5	51.7	53.1	51.1	51.5
Al_2O_3	14.3	14.2	13.9	14.5	14.7	15.2	15.4	14.6	15.3	15.3
Fe_2O_3	1.4	1.7	2.4	1.6	1.6	1.2	1.7	2.4	2.1	1.4
FeO	9.60	9.25	9.30	8.21	7.19	7.94	7.48	7.07	6.88	6.97
MgO	7.87	7.05	6.40	7.50	6.77	7.86	6.86	6.50	7.15	6.66
CaO	9.86	11.5	10.3	11.8	11.5	10.4	11.2	10.2	11.9	12.5
Na_2O	1.58	1.47	1.74	1.34	1.49	2.31	1.82	1.36	1.60	1.36
K_2O	0.08	0.14	0.14	0.12	0.26	0.12	0.09	0.34	0.21	0.12
H_2O	1.79	1.95	1.97	1.96	1.75	1.61	1.71	2.66	1.76	1.62
TiO_2	0.65	0.65	0.68	0.49	0.60	0.56	0.58	0.62	0.59	0.59
P_2O_5	0.18	0.19	0.20	0.18	0.18	0.18	0.20	0.20	0.18	0.19
MnO	0.15	0.17	0.15	0.15	0.13	0.13	0.13	0.13	0.14	0.14
S	0.005	0.005	0.005	0.005	0.005	0.005	0.090	0.005	0.005	0.005
Ba (ppm)	108	47	136	96	151	163	76	262	134	66
Ce	6	9	9	5	13	11	9	11	15	12
Co	-	-	-	-	-	-	-	-	-	-
Cr	302	268	59	343	285	307	288	141	269	276
Cu	96	6	129	84	9	101	91	11	5	17
F	-	-	-	-	-	-	-	-	-	-
La	6	7	6	<5	18	5	8	10	10	12
Li	4	4	8	4	6	4	5	12	6	2
Mn	1284	1551	1339	1401	1147	1151	1170	1142	1195	1310
Mo	-	-	-	-	-	-	-	-	-	-
Nb	<5	<5	<5	<5	<5	5	<5	<5	6	5
Ni	117	100	80	103	79	132	98	74	108	102
Pb	<10	<10	11	<10	17	<10	<10	14	<10	<10
Rb	<2	<2	<2	<2	8	<2	<2	12	9	3
Sn	-	-	-	-	-	-	-	-	-	-
Sr	81	106	87	64	137	161	126	127	137	103
Th	<10	<10	<10	<10	<10	<10	<10	<10	<10	<10
U	-	-	-	-	-	-	-	-	-	-
V	255	251	269	228	202	197	202	220	214	201
W	-	-	-	-	-	-	-	-	-	-
Y	20	19	21	15	18	16	16	19	18	20
Zn	86	88	82	68	70	79	70	64	65	70
Zr	38	38	52	37	54	55	53	61	54	50

SAMPLE	81352	81353	81364	81365	81366	81373	81378	81397	81433	81434
CODE	B52C12	B52C22	B52B12	K52B12	B52B12	S00031	B00L32	S53032	B01A34	301A14
TRAVERSE	52	52	52	52	52	00	00	53	01	01
EAST	4753	4753	4742	4742	4742	4809	4793	5359	6268	6269
NORTH	68801	68802	68811	68812	68814	68742	68702	71342	70337	70337
SiO_2 (%)	49.9	50.3	50.0	49.8	52.2	98.6	53.2	92.9	49.0	49.0
Al_2O_3	15.2	14.9	13.1	11.7	12.8	0.5	13.3	0.1	12.9	12.8
Fe_2O_3	1.9	1.4	1.7	1.2	1.5	0.5	1.4	5.8	4.4	2.1
FeO	7.79	7.76	8.60	9.10	8.05	0.09	7.26	0.61	8.07	8.98
MgO	7.25	7.64	9.34	12.2	8.12	0.03	7.55	0.03	5.56	7.88
CaO	11.9	11.5	12.3	9.58	13.4	0.04	11.2	(0.01	12.4	13.2
Na_2O	2.00	0.75	0.79	0.99	0.39	0.01	1.86	(0.01	2.15	1.30
K_2O	0.13	0.94	0.06	0.07	0.03	0.01	0.07	(0.01	0.52	0.22
H_2O	1.86	2.46	2.12	2.53	1.76	0.56	1.86	0.33	2.03	2.23
TiO_2	0.60	0.56	0.46	0.43	0.44	0.01	0.46	(0.01	1.67	0.92
P_2O_5	0.19	0.19	0.19	0.16	0.18	0.13	0.18	0.13	0.24	0.12
MnO	0.16	0.14	0.16	0.17	0.16	(0.01	0.13	(0.01	0.27	0.22
S	0.005	0.005	0.105	0.005	0.005	0.010	0.015	0.005	0.034	0.005
Ba (ppm)	86	303	(25	50	34	88	192	(25	294	91
Ce	8	8	(5	(5	(5	(5	5	(5	13	(5
Co	-	-	-	-	-	-	-	-	61	66
Cr	276	300	562	880	577	13	449	(10	2524	561
Cu	5	20	80	67	32	9	102	10	50	37
F	-	-	-	-	-	-	-	-	-	-
La	12	6	(5	6	(5	(5	(5	8	13	(5
Li	3	6	4	2	1	(1	4	(1	2	5
Mn	1305	1236	1462	1501	1363	33	1330	83	2600	1670
Mo	-	-	-	-	-	-	-	-	-	-
Nb	(5	(5	(5	(5	(5	(5	(5	(5	8	(5
Ni	102	127	138	215	143	(5	99	8	100	170
Pb	(10	(10	23	18	(10	(10	(10	14	(10	(10
Rb	(2	31	(2	(2	(2	(2	(2	(2	17	8
Sn	-	-	-	-	-	-	-	-	-	-
Sr	118	70	166	76	137	(5	168	(5	206	89
Th	(10	(10	(10	(10	(10	(10	(10	(10	(5	(5
U	-	-	-	-	-	-	-	-	-	-
V	202	197	206	211	203	19	216	(5	339	286
W	-	-	-	-	-	-	-	-	-	-
Y	18	17	15	14	14	7	17	2	36	21
Zn	70	75	77	77	75	3	61	15	89	118
Zr	56	49	26	24	26	13	28	(10	124	39

SAMPLE	81435	81436	81437	81438	81439	81440	81441	81442	81443	81444
CODE	B01A14	B01A24	B01A14	B01A14	B01A14	N01A13	B01A32	N01A33	B01A13	B01A12
TRAVERSE	01	01	01	01	01	01	01	01	01	01
EAST	6270	6271	6272	6273	6275	6276	6278	6279	6280	6281
NORTH	70337	70337	70337	70337	70337	70337	70337	70337	70337	70337
SiO_2 (%)	50.9	50.7	51.1	50.7	49.4	49.2	54.3	57.3	51.3	51.5
Al_2O_3	13.6	15.0	14.0	13.5	13.1	12.5	15.1	15.0	14.1	14.3
Fe_2O_3	2.1	1.9	2.3	2.5	2.9	2.4	1.2	1.5	2.0	1.5
FeO	8.21	7.58	7.12	7.85	8.42	10.3	5.79	5.28	7.72	7.99
MgO	6.86	5.55	7.18	6.61	6.37	7.97	6.34	4.71	7.12	7.12
CaO	11.9	12.1	10.4	12.0	13.1	11.1	11.8	9.21	12.4	10.9
Na_2O	2.33	2.96	3.17	2.18	2.20	1.55	2.29	3.28	2.49	1.99
K_2O	0.11	0.14	0.57	0.32	0.17	0.15	0.08	0.12	0.14	0.65
H_2O	1.86	1.53	2.40	1.94	1.91	1.93	1.40	1.49	2.30	1.89
TiO_2	1.35	1.53	1.27	1.60	1.54	1.56	0.81	0.78	0.76	0.77
P_2O_5	0.16	0.16	0.16	0.21	0.21	0.20	0.11	0.27	0.10	0.12
MnO	0.20	0.18	0.17	0.20	0.19	0.19	0.14	0.13	0.20	0.18
S	0.006	0.004	0.009	0.011	0.004	(0.001	(0.001	(0.001	0.012	0.004
Ba (ppm)	75	52	178	108	42	46	63	86	99	66
Ce	7	8	10	11	13	9	8	27	6	9
Co	59	54	54	50	56	65	55	49	57	60
Cr	510	421	347	303	310	314	173	185	163	144
Cu	152	157	135	61	41	50	36	36	109	44
F	-	-	-	-	-	-	-	-	-	-
La	(5	9	9	10	5	(5	(5	8	(5	5
Li	3	3	13	5	2	3	2	3	8	3
Mn	1560	1330	1240	1480	1440	1450	1020	900	1610	1260
Mo	-	-	-	-	-	-	-	-	-	-
Nb	(5	5	7	8	6	9	(5	9	6	6
Ni	130	110	110	110	120	140	120	120	120	110
Pb	(10	(10	(10	(10	(10	(10	(10	(10	(10	(10
Rb	2	2	36	13	3	2	(2	2	36	2
Sn	-	-	-	-	-	-	-	-	-	-
Sr	113	164	146	105	109	128	117	303	124	98
Th	(5	(5	(5	(5	(5	(5	(5	(5	(5	(5
U	-	-	-	-	-	-	-	-	-	-
V	335	371	356	397	372	394	285	156	293	271
W	-	-	-	-	-	-	-	-	-	-
Y	24	27	30	38	36	36	19	20	19	19
Zn	100	138	73	94	75	102	48	41	71	69
Zr	71	88	94	116	102	98	56	142	61	53

SAMPLE	81445	81446	81447	81448	81449	81450	81451	81452	81453	81454
CODE	B01A12	B01A32	B01A13	K01A12	K01A12	B01A12	B01A12	B01A12	B01A12	B01A12
TRAVERSE	01	01	01	01	01	01	01	01	01	01
EAST	6283	6286	6286	6288	6289	6290	6291	6292	6293	6294
NORTH	70337	70337	70337	70337	70337	70337	70337	70337	70337	70337
SiO_2 (%)	50.9	53.3	51.9	48.8	50.0	52.2	51.3	51.4	51.7	52.1
Al_2O_3	14.0	14.4	14.0	10.5	10.8	14.4	14.1	14.2	14.2	14.3
Fe_2O_3	1.4	2.2	1.9	1.3	1.2	2.2	2.0	1.6	1.7	1.6
FeO	8.85	7.10	7.62	8.22	7.31	7.08	7.46	7.82	7.82	7.06
MgO	6.87	6.40	6.72	13.8	14.9	6.91	7.23	7.47	7.47	7.57
CaO	12.1	11.2	12.0	10.8	9.21	12.7	11.7	11.7	11.8	12.1
Na_2O	2.17	1.85	1.83	1.14	1.15	1.61	1.60	1.84	1.83	1.81
K_2O	0.14	0.34	0.08	0.06	0.06	0.06	0.30	0.16	0.10	0.08
H_2O	1.84	2.55	2.12	3.66	4.14	1.98	2.58	2.58	2.23	2.18
TiO_2	0.75	0.78	0.76	0.39	0.40	0.78	0.72	0.70	0.70	0.73
P_2O_5	0.10	0.10	0.10	0.08	0.08	0.11	0.09	0.09	0.11	0.09
MnO	0.19	0.16	0.18	0.21	0.19	0.20	0.18	0.18	0.18	0.16
S	0.042	0.007	0.003	0.003	0.003	0.019	0.013	0.029	0.009	0.007
Ba (ppm)	25	66	102	29	49	31	75	26	129	52
Ce	<5	<5	7	<5	<5	<5	5	<5	<5	9
Co	62	54	57	67	60	52	54	54	58	56
Cr	139	102	130	1250	1358	219	260	248	242	225
Cu	125	94	103	84	231	157	240	145	140	88
F	-	-	-	-	-	-	-	-	-	-
La	7	9	<5	7	6	7	<5	6	<5	<5
Li	4	8	4	12	14	4	7	7	4	4
Mn	1350	1120	1300	1550	1320	1470	1300	1270	1250	1150
Mo	-	-	-	-	-	-	-	-	-	-
Nb	5	5	6	<5	<5	6	8	<5	<5	<5
Ni	120	100	100	360	370	110	100	110	100	100
Pb	<10	<10	<10	<10	<10	<10	<10	<10	<10	<10
Rb	<2	15	<2	2	2	<2	16	5	<2	<2
Sn	-	-	-	-	-	-	-	-	-	-
Sr	92	108	77	57	56	103	82	76	75	78
Th	<5	<5	<5	<5	<5	<5	<5	<5	<5	<5
U	-	-	-	-	-	-	-	-	-	-
V	275	294	286	212	233	275	275	274	283	271
W	-	-	-	-	-	-	-	-	-	-
Y	18	19	18	15	15	21	19	19	19	18
Zn	81	57	59	84	143	59	113	70	75	68
Zr	40	45	44	32	31	48	51	38	48	46

SAMPLE	81455	81456	81457	81458	81459	81460	81461	81462	81463	81464
CODE	B01A12	B01A12	B01A12	B01A12	B01A12	B01A22	B01A12	B01A31	A02D21	A02D11
TRAVERSE	01	01	01	01	01	01	01	01	02	02
EAST	6297	6298	6299	6301	6302	6304	6305	6306	6528	6528
NORTH	70337	70337	70337	70337	70337	70337	70337	70337	70272	70272
SiO_2 (%)	51.2	50.9	50.1	50.2	49.7	50.3	49.8	47.3	59.3	58.6
Al_2O_3	13.8	14.0	14.3	14.4	14.2	14.4	14.2	13.9	16.1	16.2
Fe_2O_3	2.0	2.0	2.0	1.8	1.9	2.5	2.1	3.1	2.7	2.7
FeO	7.08	7.09	8.24	8.15	8.18	7.73	8.00	8.70	3.80	4.26
MgO	7.45	7.85	7.66	7.21	7.25	6.87	7.44	8.37	2.59	2.81
CaO	11.6	11.6	11.0	11.5	11.7	12.0	11.4	10.8	5.18	4.60
Na_2O	1.85	1.61	1.62	1.99	1.66	1.58	1.73	2.26	3.81	3.30
K_2O	0.20	0.11	0.24	0.13	0.17	0.09	0.14	0.19	1.63	2.39
H_2O	3.28	3.02	2.88	2.93	3.02	2.84	3.31	3.40	2.52	2.81
TiO_2	0.70	0.71	0.81	0.81	0.80	0.82	0.80	0.90	0.84	0.86
P_2O_5	0.10	0.09	0.10	0.11	0.10	0.12	0.09	0.11	0.30	0.32
MnO	0.18	0.17	0.17	0.18	0.18	0.17	0.17	0.18	0.10	0.10
S	0.044	0.019	0.027	0.078	0.078	0.078	0.034	0.050	0.017	0.008
Ba (ppm)	24	57	49	33	22	<20	<20	37	517	1099
Ce	6	<5	<5	<5	<5	7	<5	7	62	55
Co	55	67	57	60	55	58	51	67	29	29
Cr	234	233	298	304	302	306	319	163	12	30
Cu	137	171	257	307	255	302	248	570	78	68
F	-	-	-	-	-	-	-	-	-	-
La	6	<5	7	<5	9	<5	<5	7	31	29
Li	6	5	8	6	6	6	7	20	11	12
Mn	1250	1190	1260	1210	1250	1180	1220	1270	740	740
Mo	-	-	-	-	-	-	-	-	<1	2
Nb	5	5	<5	<5	<5	7	<5	<5	19	18
Ni	100	100	140	130	130	140	130	140	20	20
Pb	<10	<10	<10	<10	<10	<10	<10	<10	<10	<10
Rb	6	<2	7	2	5	2	5	5	64	64
Sn	-	-	-	-	-	-	-	-	<3	3
Sr	84	73	82	82	76	96	83	182	525	486
Th	<5	<5	<5	<5	<5	<5	<5	<5	8	7
U	-	-	-	-	-	-	-	-	<1	<1
V	280	267	293	289	283	284	292	306	130	126
W	-	-	-	-	-	-	-	-	-	-
Y	19	20	20	21	21	22	20	23	28	31
Zn	69	78	123	138	117	134	118	113	73	76
Zr	45	51	47	43	49	43	58	56	200	203

SAMPLE	81466	81467	81478	81479	81480	81481	81482	81483	81484	81485
CODE	A02011	D02011	D02021	D02020	D03610	D03620	D03620	A03610	D03620	D03620
TRAVERSE	02	02	02	02	03	03	03	03	03	03
EAST	6533	6534	6532	6532	6524	6523	6521	6520	6518	6516
NORTH	70270	70269	70270	70270	70378	70378	70378	70378	70378	70378
SiO_2 (%)	57.5	67.5	62.8	62.8	68.9	66.6	63.9	60.7	66.4	63.3
Al_2O_3	16.1	13.5	15.6	15.6	14.7	15.3	15.1	15.4	14.8	13.8
Fe_2O_3	2.6	1.5	1.7	1.5	0.4	0.8	0.9	1.4	0.5	0.9
FeO	4.42	4.04	3.18	4.02	1.92	2.60	2.70	3.72	2.07	3.46
MgO	3.97	1.10	1.52	1.60	1.78	2.08	2.49	3.60	2.13	4.29
CaO	5.98	1.86	3.48	3.44	2.68	3.80	4.18	5.78	3.83	3.87
Na_2O	2.58	4.89	5.50	5.39	5.80	4.68	4.61	3.36	4.60	4.02
K_2O	1.68	1.63	1.52	1.27	0.84	1.37	1.79	2.03	1.58	1.25
H_2O	3.35	2.29	2.63	2.33	1.78	2.06	2.16	2.51	2.27	4.08
TiO_2	0.72	0.59	0.79	0.80	0.32	0.44	0.44	0.54	0.42	0.45
P_2O_5	0.24	0.16	0.30	0.31	0.12	0.16	0.20	0.23	0.17	0.19
MnO	0.12	0.08	0.07	0.07	0.04	0.05	0.07	0.08	0.07	0.09
S	0.007	0.004	0.006	0.008	0.007	0.005	0.005	0.008	0.015	0.009
Ba (ppm)	616	521	439	377	262	296	390	438	372	387
Ce	44	68	66	63	21	28	30	32	26	29
Co	32	19	17	34	37	39	40	35	33	29
Cr	74	<5	15	41	76	141	137	139	152	155
Cu	138	98	67	151	135	129	125	119	129	104
F	-	-	-	-	-	-	-	-	-	-
La	22	29	34	30	9	13	14	19	14	18
Li	9	4	5	6	6	6	9	15	8	15
Mn	870	630	540	570	340	390	550	610	510	680
Mo	<1	1	3	<1	<1	<1	<1	<1	<1	<1
Nb	11	19	19	18	8	8	8	9	10	9
Ni	50	<5	10	10	40	60	60	80	80	90
Pb	<10	<10	<10	<10	<10	<10	<10	<10	<10	<10
Rb	62	40	37	30	22	36	45	52	43	30
Sn	3	3	4	9	8	8	11	7	7	5
Sr	526	193	367	308	275	610	647	700	550	399
Th	7	11	10	10	<5	7	5	5	5	<5
U	<1	<1	<1	<1	<1	<1	<1	<1	<1	<1
V	141	16	76	68	47	78	82	102	67	85
W	-	-	-	-	-	-	-	-	-	-
Y	21	31	28	30	10	10	11	15	10	13
Zn	96	125	69	66	33	52	53	63	51	54
Zr	143	229	229	234	124	140	122	128	130	117

SAMPLE	81486	81490	81491	81492	81494	81495	81498	81500	81501	81503
CODE	A03630	D03620	D03610	A03610	K03E30	B03F20	B05B14	B05B14	B05B14	K05C13
TRAVERSE	03	03	03	03	03	03	05	05	05	05
EAST	6515	6520	6518	6517	6491	6499	6631	6630	6628	6627
NORTH	70378	70389	70389	70389	70249	70311	70337	70337	70337	70337
SiO_2 (%)	60.8	66.2	66.0	61.8	49.9	49.2	50.5	50.3	51.1	46.8
Al_2O_3	13.8	15.0	14.9	14.9	9.9	13.0	13.1	12.8	13.0	6.9
Fe_2O_3	1.7	0.8	0.9	1.1	1.9	2.8	2.7	2.7	2.9	1.8
FeO	3.39	2.45	2.41	3.73	7.87	10.0	12.4	12.0	11.6	10.4
MgO	4.80	2.27	2.13	3.73	12.3	5.56	5.15	5.53	5.20	17.0
CaO	4.98	3.93	4.20	4.97	7.29	9.44	10.1	10.4	9.81	9.37
Na_2O	3.92	4.76	4.17	3.73	1.35	2.14	1.72	1.83	2.09	0.59
K_2O	0.87	1.14	1.35	1.30	0.21	0.44	0.10	0.15	0.13	0.03
H_2O	3.77	2.05	2.03	2.72	7.45	4.48	1.78	1.91	1.91	4.35
TiO_2	0.47	0.42	0.41	0.52	0.60	1.21	1.02	1.04	0.90	0.68
P_2O_5	0.24	0.17	0.16	0.24	0.09	0.17	0.13	0.13	0.11	0.09
MnO	0.08	0.05	0.05	0.08	0.23	0.18	0.21	0.25	0.19	0.22
S	0.015	0.003	0.004	0.020	0.020	0.11	0.003	0.003	0.003	0.003
Ba (ppm)	418	290	500	480	176	65	31	27	36	49
Ce	31	28	30	34	<5	9	10	7	11	<5
Co	29	31	34	33	57	53	76	68	77	93
Cr	228	165	125	189	1285	114	91	102	66	1612
Cu	86	77	89	107	122	243	81	69	61	49
F	-	-	-	-	-	-	-	-	-	-
La	13	17	19	17	6	6	6	8	<5	<5
Li	16	7	11	16	15	11	6	8	11	20
Mn	670	390	400	580	1510	1410	1610	2000	1660	1710
Mo	<1	<1	<1	1	-	-	-	-	-	-
Nb	9	10	10	9	8	9	<5	7	8	<5
Ni	130	70	60	90	230	100	80	100	80	420
Pb	<10	<10	<10	<10	<10	<10	<10	<10	<10	<10
Rb	21	32	38	37	7	18	<2	<2	2	<2
Sn	5	6	10	9	-	-	-	-	-	-
Sr	458	439	472	503	131	128	83	85	81	20
Th	<5	<5	<5	<5	<5	<5	<5	<5	<5	<5
U	<1	<1	<1	<1	-	-	-	-	-	-
V	87	72	67	102	198	375	331	328	312	201
W	-	-	-	-	-	-	-	-	-	-
Y	12	13	10	14	17	32	27	25	23	17
Zn	65	51	53	60	87	107	110	105	77	118
Zr	98	138	125	134	60	92	63	59	54	60

SAMPLE	81504	81505	81506	81507	81508	81509	81510	81511	81512	81513
CODE	B05C14	K05C12	K05C12	K05C22	U05C12	B05C12	D03620	K03E10	K03E10	B03E10
TRAVERSE	05	05	05	05	05	05	03	03	03	03
EAST	6626	6625	6626	6620	6618	6617	6483	6561	6560	6559
NORTH	70337	70337	70337	70337	70337	70337	70416	70513	70513	70513
SiO_2 (%)	49.5	48.5	50.3	48.1	45.3	48.4	65.6	48.6	48.9	52.2
Al_2O_3	12.5	9.4	6.9	9.1	7.8	9.5	15.1	10.2	9.0	12.1
Fe_2O_3	2.1	1.4	1.9	1.3	1.3	1.5	1.72	2 2	2.3	2.2
FeO	10.7	10.4	9.35	11.0	10.5	11.1	2.59	9.28	8.83	8.12
MgO	7.47	14.3	14.2	13.3	18.5	12.9	1.90	14.5	15.5	9.63
CaO	9.58	8.71	11.7	7.84	8.51	9.03	3.56	8.16	7.19	8.61
Na_2O	2.74	1.43	1.23	2.10	0.37	1.94	4.13	0.72	1.18	1.36
K_2O	0.27	0.13	0.10	(0.01	(0.01	0.12	1.80	0.17	0.09	0.61
H_2O	2.27	3.96	2.78	4.69	5.52	3.68	2.05	5.80	5.84	3.76
TiO_2	1.60	0.84	0.61	0.90	0.68	0.93	0.47	0.56	0.55	0.68
P_2O_5	0.19	0.10	0.08	0.12	0.09	0.13	0.15	0.08	0.09	0.11
MnO	0.23	0.19	0.21	0.21	0.21	0.21	0.05	0.18	0.17	0.14
S	0.002	0.005	0.003	0.009	0.006	0.005	(0.01	0.029	0.007	0.10
Ba (ppm)	89	118	55	28	33	25	404	(20	60	81
Ce	19	(5	8	(5	(5	10	-	(5	(5	8
Co	65	77	78	78	89	76	-	75	75	57
Cr	156	1562	1653	1383	2260	1245	169	1315	1608	699
Cu	68	58	81	270	56	140	-	148	104	129
F	-	-	-	-	-	-	-	-	-	-
La	8	6	5	9	(5	6	-	5	6	6
Li	15	19	5	10	5	8	-	14	14	9
Mn	1710	1420	1500	1510	1500	1480	-	1260	1280	1060
Mo	-	-	-	-	-	-	-	-	-	-
Nb	8	8	(5	5	5	6	8	(5	(5	5
Ni	100	560	290	310	790	280	-	610	340	110
Pb	(10	(10	(10	(10	(10	(10	-	(10	(10	(10
Rb	22	8	(2	(2	(2	(2	44	6	(2	21
Sn	-	-	-	-	-	-	-	-	-	-
Sr	229	61	85	61	39	85	484	24	17	63
Th	(5	(5	(5	(5	(5	(5	(5	(5	(5	(5
U	-	-	-	-	-	-	-	-	-	-
V	362	23(	210	273	220	274	68	238	228	299
W	-	-	-	-	-	-	-	-	-	-
Y	31	22	14	21	14	20	10	16	16	19
Zn	107	127	79	109	100	83	-	75	75	77
Zr	124	77	45	67	36	71	139	43	44	58

SAMPLE	81514	81515	81516	81517	81518	81519	81520	81521	81522	3
CODE	B03E10	K03E10	B03E10	K03E10	B03E10	K03E10	K03E10	K03E10	K03E10	K03E10
TRAVERSE	03	03	03	03	03	03	03	03	03	03
EAST	6558	6557	6556	6556	6555	6554	6553	6552	6551	6550
NORTH	70513	70512	70512	70512	70512	70512	70512	70512	70512	70512
SiO_2 (%)	51.0	52.9	51.1	50.2	52.0	50.5	51.3	51.4	50.5	52.3
Al_2O_3	13.1	7.3	12.6	10.7	12.6	10.8	11.1	11.2	10.7	12.3
Fe_2O_3	3.6	1.3	2.7	1.7	2.8	2.3	2.2	2.1	1.6	1.9
FeO	7.35	7.48	6.66	7.84	7.38	7.21	7.32	7.61	7.82	7.47
MgO	7.67	20.2	10.9	14.5	7.67	14.4	12.6	12.6	14.7	11.1
CaO	10.2	5.72	8.63	8.31	10.4	8.47	8.73	8.79	7.46	9.37
Na_2O	1.71	0.67	1.50	1.18	2.09	1.04	1.38	1.12	0.74	1.25
K_2O	0.35	0.19	0.37	0.16	0.05	0.22	0.10	0.07	0.45	0.06
H_2O	3.98	3.12	4.00	4.09	3.30	3.49	3.85	3.86	4.43	3.23
TiO_2	0.76	0.28	0.44	0.42	0.74	0.44	0.43	0.44	0.42	0.47
P_2O_5	0.11	0.04	0.07	0.07	0.11	0.08	0.07	0.07	0.07	0.07
MnO	0.16	0.17	0.16	0.16	0.15	0.16	0.16	0.16	0.16	0.15
S	0.013	0.016	0.009	0.034	0.067	0.021	0.019	0.026	0.008	0.012
Ba (ppm)	73	<20	39	43	34	28	40	33	38	38
Ce	11	<5	<5	<5	9	<5	<5	<5	<5	<5
Co	52	69	55	65	58	64	63	61	63	58
Cr	219	2027	377	1262	361	1275	1269	1747	1268	734
Cu	133	53	64	67	120	77	78	70	77	78
F	-	-	-	-	-	-	-	-	-	-
La	6	<5	<5	<5	5	<5	<5	<5	<5	<5
Li	11	5	6	10	5	7	8	9	10	7
Mn	1140	1220	1200	1200	1190	1120	1130	1120	1120	1120
Mo	-	-	-	-	-	-	-	-	-	-
Nb	5	<5	<5	<5	8	<5	<5	<5	<5	<5
Ni	70	360	170	340	80	330	310	280	330	180
Pb	<10	<10	<10	<10	<10	<10	<10	<10	<10	<10
Rb	9	12	15	5	<2	14	3	3	22	2
Sn	-	-	-	-	-	-	-	-	-	-
Sr	65	22	36	30	79	35	23	25	19	29
Th	<5	<5	<5	<5	<5	<5	<5	<5	<5	<5
U	-	-	-	-	-	-	-	-	-	-
V	275	182	234	229	272	219	233	226	227	253
W	-	-	-	-	-	-	-	-	-	-
Y	19	9	15	14	19	14	15	15	14	17
Zn	69	59	64	53	73	56	57	56	57	61
Zr	66	21	42	32	62	40	32	33	23	29

SAMPLE	81524	81525	81526	81527	81528	81533	81534	81535	81536	81537
CODE	K03E10	B03E30	B03F20	B03F10	B03F10	B03F30	B03F10	B03F20	B03F20	B03F20
TRAVERSE	03	03	03	03	03	03	03	03	03	03
EAST	6550	6549	6547	6546	6545	6504	6505	6506	6507	6508
NORTH	70511	70511	70511	70511	70511	70427	70426	70426	70425	70425
SiO_2 (%)	51.2	52.6	50.0	50.5	50.7	46.7	47.9	49.7	50.6	51.3
Al_2O_3	11.4	14.1	13.9	13.4	13.3	14.6	13.7	13.5	13.8	14.4
Fe_2O_3	1.4	2.1	2.2	2.6	2.6	2.0	3.7	2.8	2.4	1.9
FeO	7.98	6.51	8.19	9.25	9.09	8.52	9.54	8.88	7.30	7.16
MgO	12.9	7.63	5.08	6.10	5.55	5.91	5.55	5.86	5.51	5.76
CaO	8.80	9.03	10.4	10.4	10.6	11.0	10.6	10.4	10.2	9.84
Na_2O	0.82	1.52	2.65	2.08	2.13	2.37	1.73	1.82	2.36	2.14
K_2O	0.12	1.06	0.20	0.24	0.23	0.20	0.29	0.16	0.26	0.19
H_2O	3.39	4.19	5.40	3.51	4.11	6.47	4.49	4.38	4.92	4.85
TiO_2	0.43	0.53	1.24	1.19	1.21	1.39	1.30	1.33	1.34	1.37
P_2O_5	0.08	0.09	0.17	0.17	0.17	0.19	0.17	0.16	0.16	0.16
MnO	0.17	0.16	0.22	0.25	0.24	0.25	0.21	0.22	0.21	0.18
S	0.026	0.017	0.087	0.084	0.12	0.051	0.10	0.11	0.085	0.098
Ba (ppm)	<20	101	62	55	24	23	137	53	95	73
Ce	<5	9	<5	<5	10	10	6	8	6	8
Co	60	50	46	57	56	58	56	57	52	56
Cr	1013	188	101	88	85	95	99	91	93	93
Cu	68	61	205	204	214	208	207	219	225	233
F	-	-	-	-	-	-	-	-	-	-
La	<5	<5	5	6	5	7	<5	<5	6	6
Li	8	10	8	8	6	11	8	8	9	11
Mn	1230	1200	1580	1730	1690	1740	1530	1610	1640	1260
Mo	-	-	-	-	-	-	-	-	-	-
Nb	<5	<5	5	<5	10	7	6	5	5	9
Ni	280	100	90	100	90	110	110	100	90	90
Pb	<10	<10	<10	<10	<10	<10	<10	<10	<10	<10
Rb	8	57	7	7	9	7	10	5	10	6
Sn	-	-	-	-	-	-	-	-	-	-
Sr	21	57	90	95	94	87	125	107	122	99
Th	<5	<5	<5	<5	<5	<5	<5	<5	<5	<5
U	-	-	-	-	-	-	-	-	-	-
V	229	277	340	323	329	380	364	385	373	369
W	-	-	-	-	-	-	-	-	-	-
Y	15	16	28	28	28	33	30	37	31	30
Zn	59	57	91	101	83	142	111	136	115	127
Zr	31	40	77	71	80	88	76	70	85	89

SAMPLE	81538	81539	81540	81541	81542	81543	81559	81561	81563	81564
CODE	B03F20	B03F30	B03F30	B03E10	B03E30	B03E30	R08D21	R08D21	R08D10	R08D11
TRAVERSE	03	03	03	03	03	03	08	08	08	08
EAST	6508	6509	6510	6511	6512	6513	6596	6599	6601	6603
NORTH	70424	70424	70424	70423	70423	70422	70220	70220	70220	70220
SiO_2 (%)	50.6	52.7	54.3	52.0	55.5	53.4	73.0	75.5	75.4	75.2
Al_2O_3	13.7	13.8	13.8	12.9	13.0	12.1	10.4	10.6	10.8	11.2
Fe_2O_3	2.1	2.2	2.0	1.5	1.3	2.5	1.0	0.9	1.2	1.3
FeO	7.72	7.60	6.68	8.20	7.28	8.16	4.33	2.74	2.42	3.18
MgO	6.04	5.71	5.28	8.39	6.67	8.40	1.16	1.12	0.82	1.02
CaO	10.8	9.62	9.80	7.71	7.38	7.03	1.56	0.93	1.26	0.59
Na_2O	2.60	2.30	2.24	1.81	2.69	1.98	2.60	2.78	3.63	6.16
K_2O	0.12	0.12	0.27	0.44	0.64	0.82	1.00	1.33	1.24	0.89
H_2O	6.94	3.76	3.54	5.10	3.46	4.40	3.49	2.87	2.71	2.34
TiO_2	1.32	1.34	1.35	1.03	1.08	0.71	0.20	0.19	0.23	0.23
P_2O_5	0.17	0.17	0.18	0.11	0.12	0.11	0.11	0.03	0.05	0.04
MnO	0.20	0.20	0.18	0.18	0.17	0.12	0.11	0.11	0.05	0.05
S	0.082	0.073	0.076	0.025	0.007	0.016	0.013	0.014	0.012	0.014
Ba (ppm)	52	52	72	66	89	168	180	270	228	262
Ce	<5	7	6	10	14	9	59	86	69	78
Co	53	53	55	60	54	56	37	61	46	47
Cr	94	95	89	493	387	261	7	<5	9	<5
Cu	211	232	239	156	155	116	35	41	44	56
F	-	-	-	-	-	-	-	-	-	-
La	7	8	6	5	12	9	22	39	23	31
Li	9	9	8	21	17	14	8	5	5	7
Mn	1400	1390	1260	1260	1170	910	780	790	390	330
Mo	-	-	-	-	-	-	1	1	2	4
Nb	7	<5	6	7	9	<5	20	29	23	23
Ni	100	80	90	140	120	90	<10	<10	<10	<10
Pb	<10	<10	<10	<10	<10	<10	<10	<10	<10	<10
Rb	8	8	10	20	34	33	33	41	31	22
Sn	-	-	-	-	-	-	7	8	7	10
Sr	101	102	110	98	124	129	49	36	47	37
Th	<5	<5	<5	<5	<5	<5	5	6	5	7
U	-	-	-	-	-	-	<1	<1	<1	<1
V	366	379	378	277	274	222	<5	<5	<5	<5
W	-	-	-	-	-	-	-	-	-	-
Y	28	29	32	19	19	13	137	163	153	167
Zn	106	115	102	102	100	80	59	55	50	36
Zr	74	86	92	80	91	64	435	460	478	484

SAMPLE	81569	81570	81571	81572	81573	81574	81575	81576	81578	81579
CODE	B09C12	B09C12	B09C12	K09C12	K09C14	K09C16	K09C16	B09C15	D10C11	R10C11
TRAVERSE	09	09	09	09	09	09	09	09	10	10
EAST	6625	6624	6623	6622	6620	6619	6618	6617	6361	6363
NORTH	70216	70215	70214	70213	70212	70212	70211	70210	70658	70638
SiO_2 (%)	50.5	51.5	51.4	50.1	49.2	52.2	51.7	51.1	65.0	71.7
Al_2O_3	14.5	15.0	15.0	13.3	11.4	12.3	11.2	14.7	15.9	12.2
Fe_2O_3	2.3	1.5	2.2	1.8	1.2	1.4	1.4	1.4	2.0	0.9
FeO	7.69	7.32	7.89	9.96	8.12	8.54	7.62	9.84	2.54	1.60
MgO	7.91	7.66	6.39	8.93	15.9	13.6	13.8	9.11	2.11	1.52
CaO	10.0	10.2	10.8	9.16	8.16	7.19	8.87	8.79	4.14	4.26
Na_2O	2.19	2.53	1.92	1.88	0.91	1.32	1.69	1.93	4.71	3.68
K_2O	0.63	0.23	0.26	0.24	0.25	0.04	0.12	0.46	1.07	0.89
H_2O	3.02	2.56	2.44	2.90	3.49	2.02	2.44	1.82	2.01	2.07
TiO_2	0.71	0.69	0.60	0.55	0.28	0.22	0.29	0.61	0.51	0.40
P_2O_5	0.12	0.12	0.11	0.09	0.06	0.05	0.08	0.08	0.17	0.13
MnO	0.14	0.14	0.17	0.21	0.17	0.18	0.16	0.20	0.06	0.06
S	0.005	0.004	0.008	0.006	0.009	0.003	0.003	0.003	0.010	0.012
Ba (ppm)	77	62	97	94	36	<20	43	137	601	185
Ce	11	7	6	<5	<5	<5	<5	6	24	19
Co	57	52	55	70	72	74	72	62	47	49
Cr	308	513	330	601	2079	1866	1938	327	22	13
Cu	50	62	80	90	61	55	48	132	67	73
F	-	-	-	-	-	-	-	-	-	-
La	<5	6	<5	5	6	<5	6	<5	12	11
Li	6	5	5	5	6	1	2	6	9	8
Mn	940	990	1210	1400	1140	1230	1170	1640	670	630
Mo	-	-	-	-	-	-	-	-	1	1
Nb	<5	<5	7	6	<5	<5	<5	<5	10	8
Ni	100	150	130	290	530	390	470	160	40	10
Pb	<10	<10	<10	<10	<10	<10	<10	<10	<10	10
Rb	18	6	6	7	6	<2	2	13	32	32
Sn	-	-	-	-	-	-	-	-	4	5
Sr	112	123	84	78	47	32	57	108	156	325
Th	<5	<5	<5	<5	<5	<5	<5	<5	<5	<5
U	-	-	-	-	-	-	-	-	<1	<1
V	254	235	243	227	180	174	169	229	87	71
W	-	-	-	-	-	-	-	-	-	-
Y	21	20	20	19	10	7	11	18	15	8
Zn	53	53	77	59	50	59	66	136	60	49
Zr	51	66	50	58	25	25	31	48	115	113

SAMPLE	81580	81581	81582	81583	81584	81585	81586	81587	81588	81589
CODE	R10C11	S10C32	B11C32	B11C12	B11C12	B11C12	B11C32	B11C32	B11C12	B11C12
TRAVERSE	10	10	11	11	11	11	11	11	11	11
EAST	6363	6389	6321	6323	6325	6327	6328	6330	6332	6334
NORTH	70638	70864	70659	70659	70659	70659	70659	70659	70659	70659
SiO_2 (%)	69.3	63.1	46.7	52.4	49.5	47.8	50.4	54.4	52.3	51.7
Al_2O_3	13.3	14.4	14.4	12.7	12.7	12.8	12.9	14.2	14.1	14.0
Fe_2O_3	1.1	1.4	9.1	2.3	3.3	3.6	3.8	2.9	2.2	2.5
FeO	2.47	3.15	3.50	8.37	9.22	9.78	7.76	5.80	7.24	7.79
MgO	1.83	3.57	2.19	8.14	7.69	7.75	5.49	6.49	6.64	6.76
CaO	3.31	2.83	18.6	7.82	9.74	10.2	10.0	9.23	9.87	9.87
Na_2O	4.11	2.72	0.06	3.98	2.77	2.04	2.28	1.97	2.24	2.42
K_2O	1.43	3.21	0.12	0.23	0.27	0.91	0.38	0.73	0.38	0.37
H_2O	2.08	4.58	3.22	2.79	3.18	3.44	3.42	3.23	3.55	3.17
TiO_2	0.40	0.42	1.98	1.01	1.10	1.09	2.16	0.51	0.53	0.53
P_2O_5	0.12	0.12	0.22	0.14	0.12	0.12	0.24	0.10	0.09	0.09
MnO	0.06	0.06	0.16	0.16	0.20	0.22	0.17	0.15	0.20	0.19
S	0.008	0.39	0.007	0.014	0.006	0.008	0.009	0.023	0.049	0.094
Ba (ppm)	320	460	64	105	61	277	208	440	210	146
Ce	26	30	16	14	11	10	19	16	12	12
Co	43	24	32	58	62	57	43	43	55	55
Cr	35	28	42	387	118	107	150	195	149	321
Cu	76	73	97	221	184	176	242	125	118	124
F	-	-	-	-	-	-	-	-	-	-
La	15	15	13	11	6	11	9	15	9	10
Li	12	19	2	7	8	10	9	9	9	9
Mn	400	400	1130	1190	1410	1460	1270	1090	1550	1490
Mo	1	1	-	-	-	-	-	-	-	-
Nb	10	9	11	6	<5	<5	6	<5	<5	7
Ni	30	30	10	140	130	120	90	100	100	100
Pb	10	10	<10	<10	<10	<10	<10	<10	<10	<10
Rb	47	119	2	4	5	19	6	18	11	10
Sn	9	7	-	-	-	-	-	-	-	-
Sr	227	177	1151	101	106	114	297	128	84	82
Th	5	<5	<5	<5	<5	<5	<5	<5	<5	<5
U	<1	<1	-	-	-	-	-	-	-	-
V	75	87	372	280	340	330	464	205	222	231
W	-	-	-	-	-	-	-	-	-	-
Y	13	14	23	22	19	20	34	18	18	18
Zn	49	72	45	88	100	100	100	69	77	80
Zr	141	138	111	89	68	62	127	80	69	59

SAMPLE	81590	81591	81592	81593	81594	81595	81596	81597	81598	81601
CODE	B11C12	B11C12	B11C12	B11C32	B11C12	B11C12	B11C12	D10C11	D10C11	K12C14
TRAVERSE	11	11	11	11	11	11	11	10	10	12
EAST	6336	6338	6340	6342	6344	6345	6348	6363	6363	6032
NORTH	70659	70659	70659	70659	70659	70659	70659	70638	70638	70747
SiO_2 (%)	52.5	52.6	52.9	53.2	52.8	52.1	53.0	67.3	68.8	50.7
Al_2O_3	14.2	14.0	14.1	13.4	13.8	13.7	13.6	14.8	13.3	9.5
Fe_2O_3	2.5	2.4	2.7	3.5	3.3	2.8	2.2	1.1	1.2	2.4
FeO	7.27	7.10	6.77	7.98	7.62	6.88	7.23	0.90	2.40	9.37
MgO	6.76	7.06	6.80	6.07	5.69	6.75	7.08	2.01	1.99	10.2
CaO	9.78	9.77	10.2	9.29	10.5	10.4	8.93	6.77	4.01	12.3
Na_2O	2.01	2.18	2.00	1.95	1.33	1.51	2.48	4.83	3.95	1.67
K_2O	0.46	0.60	0.31	0.35	0.44	0.47	0.53	0.20	1.15	0.13
H_2O	3.39	3.03	3.26	3.21	3.96	3.32	3.06	1.25	2.29	2.24
TiO_2	0.54	0.53	0.54	0.62	0.63	0.58	0.71	0.47	0.41	0.82
P_2O_5	0.09	0.09	0.09	0.10	0.10	0.10	0.11	0.17	0.12	0.12
MnO	0.19	0.17	0.18	0.18	0.20	0.19	0.17	0.04	0.07	0.18
S	0.057	0.068	0.052	0.017	0.018	0.022	0.011	0.008	0.007	0.002
Ba (ppm)	171	298	107	142	727	218	262	61	331	21
Ce	11	9	12	10	20	15	14	23	25	11
Co	53	55	54	53	54	53	53	37	41	72
Cr	381	163	157	13	17	103	187	39	50	776
Cu	116	138	139	127	192	124	146	48	71	178
F	-	-	-	-	-	-	-	-	-	-
La	7	7	8	12	11	11	10	8	11	(5
Li	11	9	10	13	12	11	9	1	10	5
Mn	1450	1350	1430	1390	1570	1330	1230	35[illegible]	550	1230
Mo	-	-	-	-	-	-	-	[illegible]	1	-
Nb	5	(5	6	8	7	(5	6	8	(5	(5
Ni	100	100	100	70	70	80	100	20	30	230
Pb	(10	(10	(10	(10	(10	(10	(10	(10	(10	(10
Rb	16	21	12	12	15	14	15	5	38	(2
Sn	-	-	-	-	-	-	-	5	6	-
Sr	87	83	90	102	100	105	97	85	285	311
Th	(5	(5	(5	(5	(5	(5	(5	(5	(5	(5
U	-	-	-	-	-	-	-	(1	(1	-
V	238	227	225	261	243	234	249	81	82	253
W	-	-	-	-	-	-	-	-	-	-
Y	17	18	18	20	21	20	19	12	12	14
Zn	84	76	86	86	85	84	84	20	55	81
Zr	52	54	51	64	59	62	57	132	136	45

SAMPLE	81602	81603	81604	81605	81606	81607	81608	81609	81610	81611
CODE	B12C34	B12C34	B12C34	K12C34	K12C14	K12C14	B12C14	B12C34	B12C34	D10C11
TRAVERSE	12	12	12	12	12	12	12	12	12	10
EAST	6033	6033	6034	6035	6036	6037	6033	6039	6040	6363
NORTH	70745	70742	70740	70738	70736	70734	70732	70729	70727	70638
SiO_2 (%)	53.8	49.2	51.1	54.4	52.8	52.3	51.6	53.7	53.1	68.4
Al_2O_3	9.6	12.1	13.3	10.6	12.9	12.0	14.6	14.5	14.4	13.6
Fe_2O_3	2.4	1.7	2.0	2.3	1.7	1.6	1.6	1.9	1.4	0.9
FeO	9.43	7.18	7.11	8.57	7.22	7.50	7.67	6.61	7.56	2.56
MgO	8.16	8.60	8.73	7.88	9.70	11.6	3.04	6.71	7.24	2.32
CaO	10.4	13.9	12.8	11.0	9.01	8.69	9.23	11.7	9.06	3.55
Na_2O	1.92	2.09	1.68	1.43	1.78	1.13	2.71	1.85	2.96	3.81
K_2O	0.12	0.09	0.12	0.24	0.13	0.25	0.33	0.13	0.37	1.72
H_2O	2.13	4.08	2.70	2.60	3.16	3.93	3.22	1.81	2.39	1.79
TiO_2	0.90	0.56	0.57	0.85	0.42	0.38	0.56	0.55	0.58	0.48
P_2O_5	0.11	0.08	0.07	0.07	0.08	0.06	0.09	0.09	0.09	0.16
MnO	0.20	0.20	0.20	0.26	0.17	0.18	0.17	0.18	0.18	0.06
S	0.007	0.004	0.007	0.006	0.003	0.003	0.004	0.006	0.003	0.006
Ba (ppm)	31	86	47	56	82	52	161	117	194	458
Ce	7	6	<5	<5	9	9	10	11	8	23
Co	69	55	60	85	62	57	51	56	60	35
Cr	507	482	428	1093	627	807	121	93	66	36
Cu	185	130	124	157	110	90	94	115	114	90
F	-	-	-	-	-	-	-	-	-	-
La	<5	7	<5	9	<5	<5	<5	<5	6	14
Li	8	4	5	7	13	20	8	1	5	11
Mn	1390	1350	1390	1860	1200	1220	1100	1140	1080	450
Mo	-	-	-	-	-	-	-	-	-	1
Nb	6	7	5	7	5	<5	<5	<5	5	7
Ni	110	140	120	210	190	210	120	110	100	30
Pb	<10	<10	<10	<10	<10	<10	<10	<10	<10	<10
Rb	<2	<2	<2	3	2	10	8	<2	10	50
Sn	-	-	-	-	-	-	-	-	-	4
Sr	99	63	114	105	74	66	85	126	86	288
Th	<5	<5	<5	<5	<5	<5	<5	<5	<5	<5
U	-	-	-	-	-	-	-	-	-	<1
V	279	191	208	274	202	184	244	221	259	94
W	-	-	-	-	-	-	-	-	-	-
Y	15	10	10	16	12	13	16	17	19	11
Zn	86	63	68	88	74	70	80	66	74	63
Zr	52	38	33	60	54	40	54	50	58	124

SAMPLE	81613	81614	81615	81616	81618	81619	81620	81621	81622	81623
CODE	D13C11	D13C11	D13C11	A13C11	A16C32	A16C32	A16C32	A16C32	A16C32	D16C32
TRAVERSE	13	13	13	13	16	16	16	16	16	16
EAST	6347	6347	6347	6347	5858	5858	5858	5855	5855	5855
NORTH	70287	70287	70287	70287	69897	69897	69897	69899	69899	69899
SiO_2 (%)	70.6	67.2	66.8	59.7	56.2	61.5	56.6	59.9	59.0	62.5
Al_2O_3	15.1	15.2	15.2	15.8	17.3	16.1	15.7	16.3	16.8	15.2
Fe_2O_3	1.0	1.4	1.3	2.8	2.3	1.7	1.9	2.3	1.5	1.6
FeO	1.18	1.98	2.2	3.47	4.32	2.45	5.58	2.90	4.07	3.89
MgO	0.87	1.98	1.96	3.58	3.21	2.23	3.77	2.69	4.36	2.56
CaO	2.60	4.40	4.13	6.79	7.69	8.00	6.39	9.05	4.36	4.72
Na_2O	5.14	4.40	4.58	3.71	3.57	4.02	3.67	3.69	3.87	4.60
K_2O	1.45	1.43	1.31	0.99	1.44	1.19	0.40	0.23	0.88	0.64
H_2O	1.30	1.36	1.15	2.37	2.48	1.40	4.80	2.14	3.45	2.59
TiO_2	0.27	0.42	0.42	0.85	1.21	1.11	1.07	1.13	1.15	1.39
P_2O_5	0.12	0.19	0.19	0.23	0.31	0.29	0.28	0.30	0.30	0.20
MnO	0.04	0.05	0.05	0.09	0.11	0.08	0.09	0.11	0.13	0.07
S	0.006	0.009	0.011	0.004	0.032	0.021	0.019	0.005	0.005	0.008
Ba (ppm)	535	767	561	306	449	415	258	181	272	220
Ce	29	23	29	25	46	41	41	34	37	26
Co	42	48	48	45	58	68	44	51	41	36
Cr	28	63	55	88	122	118	123	109	127	149
Cu	79	76	81	87	112	103	105	64	50	40
F	250	-	-	-	-	-	-	-	-	-
La	12	9	15	16	23	17	23	17	18	11
Li	8	9	11	12	6	1	10	4	23	11
Mn	250	360	380	700	820	630	660	840	960	570
Mo	1	2	-	-	-	-	-	-	-	-
Nb	5	5	7	12	15	15	14	16	15	16
Ni	10	30	30	50	130	70	40	90	100	60
Pb	<10	<10	<10	<10	<10	<10	<10	<10	10	<10
Rb	51	37	40	39	63	52	8	4	19	9
Sn	7	7	8	-	-	-	-	-	-	-
Sr	431	389	371	340	493	488	413	280	344	275
Th	<5	5	<5	<5	<5	<5	<5	<5	<5	<5
U	<1	<1	<1	-	-	-	-	-	-	-
V	28	75	70	136	166	146	166	166	175	197
W	-	-	-	-	-	-	-	-	-	-
Y	5	8	8	15	18	17	17	17	19	18
Zn	43	34	37	59	86	74	61	40	610	160
Zr	143	156	154	131	146	148	130	139	140	123

SAMPLE	81633	81634	81635	81636	81637	81638	81639	81640	81641	81642
CODE	K17I13	B17I31	B17I31	B17I31	B17I31	K17I31	B17I31	B17I31	B17I31	B17I31
TRAVERSE	17	17	17	17	17	17	17	17	17	17
EAST	5559	5559	5559	5559	5558	5558	5558	5558	5558	5558
NORTH	70111	70109	70107	70104	70102	70000	70097	70095	70092	70087
SiO_2 (%)	52.9	54.4	54.2	54.5	54.8	54.0	54.7	54.1	54.5	54.9
Al_2O_3	8.1	13.3	13.9	14.3	14.5	10.1	14.9	14.8	15.4	15.1
Fe_2O_3	1.5	2.5	2.4	2.6	2.2	1.6	1.6	2.4	1.6	2.1
FeO	7.86	6.14	6.47	6.15	5.85	6.45	6.15	4.82	5.30	5.59
MgO	15.9	7.31	7.35	6.52	6.67	13.3	7.84	8.11	7.75	7.34
CaO	5.89	9.87	9.98	9.44	9.22	7.18	8.05	8.16	8.49	8.49
Na_2O	0.87	1.41	1.19	1.41	1.78	1.10	2.56	2.14	2.91	2.55
K_2O	0.37	0.65	0.58	0.72	1.19	0.59	0.39	0.86	0.90	0.69
H_2O	5.60	3.56	3.50	3.40	3.09	6.73	3.11	3.52	2.95	3.10
TiO_2	0.40	0.61	0.66	0.69	0.68	0.46	0.69	0.69	0.51	0.69
P_2O_5	0.08	0.12	0.13	0.10	0.11	0.06	0.09	0.09	0.09	0.10
MnO	0.17	0.15	0.15	0.14	0.14	0.15	0.16	0.16	0.15	0.15
S	0.007	0.046	0.022	0.014	0.018	0.007	0.041	0.15	0.007	0.014
Ba (ppm)	93	197	135	207	362	281	168	361	283	224
Ce	10	22	19	30	19	12	16	23	14	16
Co	69	53	56	54	53	60	54	57	34	55
Cr	1461	395	316	184	239	1408	321	333	309	305
Cu	75	102	117	120	128	101	104	120	112	126
F	-	-	-	-	-	-	-	-	-	-
La	13	12	11	10	14	8	8	5	12	6
Li	19	11	14	16	8	16	10	12	10	10
Mn	1100	1020	1030	980	1040	1070	1160	1120	700	1120
Mo	-	-	-	-	-	-	-	-	-	-
Nb	6	6	8	8	9	<5	6	<5	<5	<5
Ni	340	140	120	90	100	260	200	200	130	190
Pb	<10	<10	<10	<10	<10	<10	<10	<10	<10	<10
Rb	20	25	24	26	40	19	12	36	35	22
Sn	-	-	-	-	-	-	-	-	-	-
Sr	61	126	177	163	105	59	153	164	132	146
Th	<5	<5	<5	<5	<5	<5	<5	<5	<5	<5
U	-	-	-	-	-	-	-	-	-	-
V	201	214	236	245	242	222	194	180	183	185
W	-	-	-	-	-	-	-	-	-	-
Y	15	22	21	23	22	14	15	14	13	14
Zn	83	72	82	78	76	72	72	69	65	71
Zr	64	116	106	106	108	60	78	68	71	76

SAMPLE	81643	81644	81645	81646	81647	81651	81652	81653	81654	81655
CODE	B17I31	B17I31	B17I31	B17I31	B17I31	B18C14	B18C14	B18C24	B18C24	B18C14
TRAVERSE	17	17	17	17	17	18	18	18	18	18
EAST	5558	5558	5558	5560	5553	5909	5911	5912	5913	5915
NORTH	70085	70084	70082	70073	70078	70125	70124	70123	70122	70121
SiO_2 (%)	54.6	55.5	54.4	53.8	54.1	49.6	48.2	49.9	49.5	50.0
Al_2O_3	16.9	16.8	15.3	13.8	14.4	13.9	14.1	15.2	13.7	14.0
Fe_2O_3	2.1	2.3	1.8	2.2	2.1	2.6	1.8	2.4	2.8	3.2
FeO	5.61	4.96	5.32	6.70	6.32	11.4	11.8	10.8	11.1	11.6
MgO	7.93	7.60	7.52	7.80	6.79	6.11	5.17	4.92	6.03	6.71
CaO	9.39	8.96	9.14	9.15	8.99	10.6	11.8	10.6	10.6	9.47
Na_2O	1.74	2.00	2.68	2.04	1.96	1.89	2.06	2.38	2.66	2.85
K_2O	0.70	0.25	0.44	0.25	1.18	0.14	0.17	0.21	0.20	0.21
H_2O	3.20	3.39	2.94	3.45	3.30	2.02	1.83	2.17	3.31	2.23
TiO_2	0.69	0.68	0.69	0.65	0.67	1.21	1.85	1.49	1.91	1.96
P_2O_5	0.11	0.09	0.10	0.10	0.10	0.15	0.25	0.18	0.22	0.24
MnO	0.15	0.15	0.15	0.15	0.14	0.22	0.44	0.26	0.27	0.21
S	0.036	0.015	0.027	0.013	0.022	0.12	0.041	0.007	0.006	0.007
Ba (ppm)	184	97	141	59	535	21	62	52	267	91
Ce	19	21	15	27	22	12	12	16	19	20
Co	55	54	54	51	53	76	68	78	64	67
Cr	315	292	291	335	213	183	145	189	124	111
Cu	111	111	111	95	130	200	53	145	112	127
F	-	-	-	-	-	-	-	-	-	-
La	8	7	11	14	11	6	12	17	14	15
Li	10	10	11	12	10	21	12	9	8	8
Mn	1090	1100	1110	1090	1090	1530	3300	1920	2030	1590
Mo	-	-	-	-	-	-	-	-	-	-
Nb	5	7	9	6	8	6	10	7	9	12
Ni	190	190	190	130	100	90	60	100	50	50
Pb	<10	<10	<10	<10	<10	<10	180	<10	<10	<10
Rb	29	8	17	11	44	2	<2	<2	<2	<2
Sn	-	-	-	-	-	-	-	-	-	-
Sr	169	171	162	151	60	80	116	98	154	118
Th	<5	<5	<5	<5	<5	<5	<5	<5	<5	<5
U	-	-	-	-	-	-	-	-	-	-
V	180	180	195	228	226	365	431	421	466	507
W	-	-	-	-	-	-	-	-	-	-
Y	13	13	14	22	23	26	35	32	39	39
Zn	73	68	68	82	77	107	104	116	137	142
Zr	68	86	80	105	104	66	111	96	123	130

SAMPLE	81656	81657	81658	81659	81660	81661	81662	81663	81664	81665
CODE	B18C14	K18C14	B18C14	B18C14	B18C14	B18C34	K18C34	K18C34	K15C32	B15C12
TRAVERSE	18	18	18	18	18	18	18	18	15	15
EAST	5916	5917	5918	5920	5921	5923	5924	5925	6591	6590
NORTH	70120	70120	70119	70118	70117	70116	70115	70114	70318	70319
SiO_2 (%)	53.0	48.8	52.1	52.9	50.0	55.1	50.9	49.9	47.3	50.6
Al_2O_3	12.3	10.9	12.9	14.3	15.1	14.3	10.1	11.0	12.4	14.3
Fe_2O_3	2.1	1.5	1.7	1.8	1.8	1.6	3.1	1.7	2.0	2.0
FeO	8.17	9.29	8.36	8.67	8.62	6.20	8.13	9.06	8.22	8.25
MgO	8.47	13.2	8.54	6.84	8.15	6.68	8.56	9.69	11.4	6.85
CaO	12.0	10.8	10.7	11.5	11.7	12.1	14.9	13.3	10.7	11.5
Na_2O	1.35	1.14	2.25	1.42	2.04	1.72	0.44	1.31	1.55	2.30
K_2O	0.1	0.08	0.10	0.18	0.16	0.13	0.13	0.12	0.78	0.62
H_2O	2.2	3.52	1.94	1.67	1.77	1.45	2.23	1.95	3.10	2.40
TiO_2	0.53	0.58	0.81	0.56	0.56	0.48	0.73	0.66	0.55	0.56
P_2O_5	0.09	0.08	0.11	0.09	0.07	0.07	0.09	0.09	0.08	0.08
MnO	0.18	0.19	0.17	0.20	0.20	0.17	0.26	0.20	0.16	0.13
S	0.015	0.008	0.067	0.067	0.016	0.012	0.013	0.007	0.006	0.008
Ba (ppm)	109	39	<20	88	156	150	58	27	292	140
Ce	5	5	<5	15	10	7	5	6	7	<5
Co	62	67	54	61	67	62	71	71	71	62
Cr	437	1134	303	68	139	650	778	729	1344	466
Cu	167	87	120	88	133	116	93	97	57	106
F	-	-	-	-	-	-	-	-	-	-
La	8	<5	8	12	<5	5	9	<5	<5	<5
Li	6	15	10	21	27	15	11	9	5	1
Mn	1340	1400	1270	1440	1440	1190	2000	1530	1140	1020
Mo	-	-	-	-	-	-	-	-	-	-
Nb	90	320	90	90	100	160	220	210	640	110
Ni	<5	8	9	<5	5	6	<5	<5	5	<5
Pb	<10	<10	<10	<10	<10	<10	<10	<10	<10	<10
Rb	5	2	<2	2	<2	3	8	3	26	17
Sn	-	-	-	-	-	-	-	-	-	-
Sr	127	89	101	97	122	138	138	157	86	133
Th	<5	<5	<5	<5	<5	<5	<5	<5	<5	<5
U	-	-	-	-	-	-	-	-	-	-
V	224	246	294	247	259	219	256	262	233	269
W	-	-	-	-	-	-	-	-	-	-
Y	14	19	25	19	18	14	13	12	17	17
Zn	82	85	94	85	83	61	93	80	56	48
Zr	40	58	74	51	52	66	52	37	32	39

SAMPLE	81666	81667	81668	81669	81743	81744	81745	81746	81747	81748
CODE	B15C12	B15C32	B15C12	K15C12	B19C22	B19C22	B19C22	B19C22	B19C22	K19C12
TRAVERSE	15	15	15	15	19	19	19	19	19	19
EAST	6589	6588	6587	6586	5777	5775	5773	5770	5768	5765
NORTH	70320	70321	70322	70324	69722	69722	69722	69722	69722	69722
SiO_2 (%)	51.5	50.9	51.0	51.5	50.0	50.1	51.5	49.1	50.8	50.6
Al_2O_3	15.6	13.7	14.2	13.0	12.9	13.3	13.3	13.1	14.0	10.2
Fe_2O_3	2.0	1.8	1.9	1.6	3.4	3.9	4.8	5.4	4.1	3.6
FeO	7.26	9.20	9.18	8.50	8.55	8.09	8.96	9.64	9.24	7.80
MgO	6.00	7.16	7.02	9.41	8.41	8.45	5.48	6.89	6.52	11.80
CaO	11.5	11.3	10.3	8.93	10.17	10.25	10.07	11.59	9.88	12.15
Na_2O	2.12	1.79	2.15	1.89	2.17	2.10	2.10	2.21	1.86	1.14
K_2O	0.27	0.21	0.29	0.50	0.08	0.07	0.15	0.14	0.08	0.08
H_2O	2.38	2.39	2.19	3.15	2.69	2.81	1.83	2.43	2.27	2.36
TiO_2	0.73	0.73	0.64	0.53	0.93	0.96	1.96	1.69	1.28	0.50
P_2O_5	0.13	0.11	0.12	0.10	0.16	0.16	0.27	0.24	0.19	0.12
MnO	0.16	0.20	0.21	0.20	0.13	0.12	0.13	0.14	0.16	0.19
S	0.003	0.003	0.005	0.005	-	-	-	-	-	-
Ba (ppm)	78	74	121	123	70	72	138	137	83	49
Ce	13	(5	9	(5	-	-	-	-	-	-
Co	54	63	60	61	44	40	47	46	50	52
Cr	268	340	355	780	443	377	233	81	48	914
Cu	69	143	93	79	159	102	89	106	196	23
F	-	-	-	-	-	-	-	-	-	-
La	(5	(5	5	7	-	-	-	-	-	-
Li	2	1	2	5	3	4	4	3	4	2
Mn	1140	1570	1560	1520	1310	1200	1250	1390	1300	1560
Mo	-	-	-	-	-	-	-	-	-	-
Nb	5	(5	(5	(5	5	(5	10	6	5	(5
Ni	120	100	180	280	170	152	143	115	143	302
Pb	(10	(10	(10	(10	(10	(10	30	(10	(10	(10
Rb	6	5	9	22	(5	(5	(5	(5	(5	(5
Sn	-	-	-	-	-	-	-	6	5	6
Sr	142	131	107	97	59	91	158	145	144	68
Th	(5	(5	(5	(5	(10	(10	(10	(10	(10	(10
U	-	-	-	-	-	-	-	-	-	-
V	244	281	249	217	272	270	400	377	344	214
W	-	-	-	-	-	-	-	-	-	-
Y	21	20	19	18	26	27	48	45	34	16
Zn	55	86	89	69	77	78	89	99	96	67
Zr	69	59	47	51	45	47	120	105	69	24

SAMPLE	81749	81750	81751	81752	81753	81754	81755	81756	81757	81758
CODE	B19C12	B19C12	B19C22	B19C12	R20C32	R20C12	R20C12	R20C32	R20C32	R20C12
TRAVERSE	19	19	19	19	20	20	20	20	20	20
EAST	5763	5760	5758	5755	5831	5832	5834	5835	5837	5838
NORTH	69722	69722	69722	69722	69744	69744	69744	69744	69745	69745
SiO_2 (%)	69.9	50.0	47.0	69.6	74.0	75.7	78.3	75.0	74.8	79.1
Al_2O_3	14.4	14.0	14.5	14.4	13.0	11.6	11.3	11.7	11.9	10.1
Fe_2O_3	3.5	6.1	6.4	3.8	<0.1	1.7	0.8	2.8	1.3	0.9
FeO	8.78	9.67	9.50	8.33	0.31	0.80	0.30	0.23	1.69	0.86
MgO	7.76	6.99	7.03	7.80	0.02	0.05	0.04	0.26	0.56	0.11
CaO	11.89	10.72	13.43	11.35	0.04	0.16	0.13	1.04	0.52	0.33
Na_2O	1.44	1.76	1.27	1.57	0.63	3.51	4.95	3.17	4.85	4.00
K_2O	0.09	0.11	0.10	0.06	9.93	4.68	2.30	3.81	1.71	2.38
H_2O	1.86	1.91	1.97	1.87	1.04	0.51	0.47	0.92	1.38	0.71
TiO_2	0.81	1.04	1.09	0.85	0.23	0.19	0.18	0.21	0.28	0.27
P_2O_5	0.13	0.16	0.17	0.15	0.09	0.04	0.03	0.06	0.07	0.05
MnO	0.15	0.16	0.18	0.15	<0.01	0.02	<0.01	0.06	0.03	<0.01
S	-	-	-	-	-	-	-	-	-	-
Ba (ppm)	43	68	59	47	1593	861	562	644	577	620
Ce	-	-	-	-	-	-	-	-	-	-
Co	48	47	49	45	27	33	32	27	26	24
Cr	201	91	81	141	<10	<10	<10	<10	<10	<10
Cu	110	214	27	118	10	37	42	24	26	19
F	-	-	-	-	-	-	-	-	-	-
La	-	-	-	-	-	-	-	-	-	-
Li	3	4	3	2	4	<1	2	5	6	2
Mn	1230	1310	1520	1310	10	184	48	541	462	67
Mo	-	-	-	-	<1	<1	<1	<1	<1	<1
Nb	<5	5	7	6	12	6	11	9	8	11
Ni	165	136	23	149	46	22	27	38	13	32
Pb	20	<10	10	<10	<10	<10	<10	<10	<10	<10
Rb	<5	<5	<5	<5	162	73	26	47	46	27
Sn	2	3	3	3	4	4	5	4	5	5
Sr	155	170	130	86	49	27	27	144	35	23
Th	<10	<10	<10	<10	<10	<10	<10	<10	<10	<10
U	-	-	-	-	<1	<1	<1	<1	<1	<1
V	270	306	322	273	<10	<10	<10	<10	<10	<10
W	-	-	-	-	-	-	-	-	-	-
Y	23	28	30	24	29	53	58	62	55	44
Zn	79	87	88	81	11	49	50	104	55	34
Zr	38	60	58	47	283	277	271	269	218	212

SAMPLE	81777	81778	81779	81780	81781	81782	81783	81784	81785	81786
CODE	B25C22	K25C12	B25C12	B25C12	K25C12	B25C32	B25C32	K22C32	K22C32	B22C12
TRAVERSE	25	25	25	25	25	25	25	22	22	22
EAST	5775	5765	5781	5782	5786	5790	5794	5917	5917	5916
NORTH	69330	69295	69295	69358	69358	69358	69358	69492	69492	69497
SiO_2 (%)	52.8	49.9	52.9	50.9	49.8	58.3	57.5	49.5	52.6	50.9
Al_2O_3	13.9	11.2	14.0	14.0	9.9	12.4	13.3	11.0	12.8	14.6
Fe_2O_3	4.0	4.8	3.8	4.3	4.2	6.8	5.7	3.3	3.5	4.5
FeO	9.03	7.05	8.91	8.26	9.97	6.19	7.85	6.79	6.05	7.01
MgO	5.51	8.99	5.70	5.61	9.52	2.71	3.31	13.80	10.00	6.52
CaO	9.90	13.40	9.58	10.91	9.61	10.09	6.80	7.85	7.24	10.87
Na_2O	2.33	0.87	2.23	1.92	2.01	0.92	3.34	1.40	2.14	2.26
K_2O	0.19	0.06	0.21	0.14	0.09	0.12	0.31	0.12	0.16	0.20
H_2O	1.73	1.93	1.72	1.62	2.99	1.73	1.63	5.03	4.53	2.19
TiO_2	0.64	0.66	0.62	1.92	0.91	1.01	1.04	0.44	0.53	1.48
P_2O_5	0.10	0.09	0.09	0.19	0.11	0.14	0.13	0.07	0.08	0.18
MnO	0.17	0.16	0.19	0.28	0.20	0.14	0.15	0.17	0.14	0.20
S	-	-	-	-	-	-	-	-	-	-
Ba (ppm)	83	42	129	141	103	243	227	50	77	133
Ce	-	-	-	-	-	-	-	-	-	-
Co	42	41	43	42	48	44	46	37	39	42
Cr	<10	655	<10	102	885	<10	<10	1277	588	251
Cu	66	29	67	59	141	16	12	48	60	99
F	-	-	-	-	-	-	-	-	-	-
La	-	-	-	-	-	-	-	-	-	-
Li	2	1	1	2	2	2	3	6	5	2
Mn	1450	1480	1490	2350	1620	1080	1150	1270	1060	1610
Mo	-	-	-	-	-	-	-	-	-	-
Nb	<5	5	5	6	<5	5	6	<5	<5	<5
Ni	84	213	92	84	271	43	47	378	157	102
Pb	<10	<10	<10	<10	<10	<10	<10	<10	20	30
Rb	<5	<5	<5	<5	<5	<5	8	<5	<5	6
Sn	-	-	-	-	-	-	-	-	-	-
Sr	95	197	88	163	105	43	81	41	70	132
Th	<10	<10	<10	<10	<10	<10	<10	<10	<10	<10
U	-	-	-	-	-	-	-	-	-	-
V	257	199	260	388	278	274	303	228	274	320
W	-	-	-	-	-	-	-	-	-	-
Y	24	16	28	42	21	34	34	19	22	38
Zn	73	67	78	79	94	44	51	55	44	90
Zr	69	32	50	115	48	105	100	32	28	93

SAMPLE	81787	81788	81789	81790	81791	81792	81793	81794	81795	81796
CODE	K22C32	B22C32	B21C32	B21C32	B21C12	B21C12	B21C22	B21C12	B21C22	B21C32
TRAVERSE	22	22	21	21	21	21	21	21	21	21
EAST	5914	5913	5755	5761	5764	5766	5768	5774	5781	5752
NORTH	69501	69508	69599	69599	69601	69599	69595	69596	69598	69607
SiO_2 (%)	53.2	60.0	49.7	51.6	51.7	50.7	52.4	69.0	50.0	51.6
Al_2O_3	10.6	16.9	14.0	14.1	14.0	15.7	16.0	16.1	12.7	14.0
Fe_2O_3	2.6	2.6	4.4	4.2	3.8	2.7	3.4	4.2	7.0	3.7
FeO	6.79	6.13	7.95	7.79	8.24	5.86	8.85	11.08	10.70	7.83
MgO	12.90	5.81	6.11	6.74	6.88	8.83	6.69	7.31	6.58	5.40
CaO	5.91	4.95	16.59	12.95	12.06	13.19	10.11	9.23	8.81	14.82
Na_2O	1.68	2.04	0.33	0.95	1.12	1.11	2.11	1.96	2.34	0.30
K_2O	0.21	0.06	0.03	0.04	0.04	0.04	0.11	0.10	0.28	0.02
H_2O	4.57	3.55	1.96	1.74	1.56	1.64	1.80	2.55	1.86	2.05
TiO_2	0.52	0.69	0.63	0.52	0.53	0.28	0.55	0.72	2.34	0.65
P_2O_5	0.08	0.14	0.10	0.08	0.08	0.07	0.08	0.10	0.22	0.10
MnO	0.15	0.09	0.22	0.20	0.20	0.14	0.20	0.21	0.19	0.20
S	-	-	-	-	-	-	-	-	-	-
Ba (ppm)	426	127	30	<30	33	<30	53	74	300	65
Ce	-	-	-	-	-	-	-	-	-	-
Co	33	36	45	48	47	35	51	50	53	44
Cr	1307	174	69	29	38	257	32	96	65	65
Cu	69	145	82	99	72	44	45	100	178	83
F	-	-	-	-	-	-	-	-	-	-
La	-	-	-	-	-	-	-	-	-	-
Li	9	8	1	2	1	3	2	5	4	<1
Mn	1150	733	1780	1570	1610	1130	1650	1680	1470	1510
Mo	-	-	-	-	-	-	-	-	-	-
Nb	5	7	<5	<5	<5	<5	<5	<5	9	<5
Ni	305	135	103	77	82	105	84	118	86	108
Pb	10	30	<10	20	<10	<10	<10	<10	<10	20
Rb	9	<5	<5	<5	<5	<5	<5	<5	5	<5
Sn	-	-	-	-	-	-	-	-	-	-
Sr	66	61	28	42	46	62	55	84	202	40
Th	<10	<10	<10	<10	<10	<10	<10	<10	<10	<10
U	-	-	-	-	-	-	-	-	-	-
V	193	166	265	239	248	147	257	289	644	260
W	-	-	-	-	-	-	-	-	-	-
Y	22	25	28	24	23	14	139	28	37	26
Zn	71	408	79	73	78	52	81	89	113	67
Zr	65	130	26	24	23	9	24	31	125	31

SAMPLE	81797	81798	81799	81800	83201	83202	83203	83204	83205	83206
CODE	B21C22	B21C12	B21C32	B21C22	B24C14	B24C33	B24C13	K24C33	B24C13	B24C23
TRAVERSE	21	21	21	21	24	24	24	24	24	24
EAST	5773	5775	5777	5779	5945	5946	5948	5950	5951	5953
NORTH	69621	69622	69624	69625	69352	69351	69351	69350	69349	69348
SiO_2 (%)	48.8	52.3	52.8	49.6	49.2	53.1	52.2	53.4	51.9	51.8
Al_2O_3	14.0	15.2	14.9	14.4	14.1	13.1	12.4	11.3	13.7	12.0
Fe_2O_3	4.0	3.8	2.7	3.8	4.6	4.0	4.1	3.9	1.7	3.4
FeO	10.00	8.66	6.43	8.84	9.97	7.93	8.37	6.74	7.22	6.77
MgO	6.21	5.12	4.56	6.47	6.62	7.71	8.28	10.40	8.53	9.07
CaO	11.99	10.22	9.78	10.66	11.56	11.96	10.99	10.61	11.66	12.30
Na_2O	1.47	2.47	2.50	1.97	1.48	1.04	1.09	1.38	1.09	0.82
K_2O	0.10	0.14	0.05	0.10	0.07	0.07	0.10	0.10	0.10	0.05
H_2O	3.04	1.71	4.70	2.72	2.09	1.80	2.02	2.26	1.95	1.85
TiO_2	0.58	0.66	0.76	0.62	1.04	0.78	0.75	0.46	0.61	0.48
P_2O_5	0.08	0.09	0.10	0.09	0.13	0.11	0.11	0.09	0.10	0.09
MnO	0.22	0.21	0.23	0.21	0.19	0.16	0.18	0.18	0.15	0.16
S	-	-	-	-	-	-	-	-	-	-
Ba (ppm)	<30	71	147	55	88	115	116	44	84	57
Ce	-	-	-	-	-	-	-	-	-	-
Co	47	52	48	50	46	42	45	37	43	36
Cr	97	124	101	99	132	411	485	880	297	360
Cu	60	92	93	99	183	69	65	40	51	69
F	-	-	-	-	-	-	-	-	-	-
La	-	-	-	-	-	-	-	-	-	-
Li	1	2	4	3	4	2	3	4	2	2
Mn	1800	1730	1970	1700	1470	1210	1340	1510	1260	1370
Mo	-	-	-	-	-	-	-	-	-	-
Nb	<5	<5	6	<5	7	5	<5	6	<5	<5
Ni	106	142	119	128	152	144	162	258	157	149
Pb	10	<10	20	30	10	<10	<10	<10	<10	<10
Rb	<5	<5	<5	<5	<5	<5	<5	<5	<5	<5
Sn	-	-	-	-	-	-	-	-	-	-
Sr	49	65	72	127	103	105	111	29	59	60
Th	<10	<10	<10	<10	<10	<10	<10	<10	<10	<10
U	-	-	-	-	-	-	-	-	-	-
V	254	303	280	269	272	266	260	236	262	220
W	-	-	-	-	-	-	-	-	-	-
Y	24	30	28	25	26	24	25	18	20	18
Zn	83	92	78	89	79	63	70	65	62	60
Zr	21	22	42	24	60	55	55	28	37	32

SAMPLE	83207	83208	83209	83210	83211	83212	83213	83214	83215	83216
CODE	B24C23	B24C23	K24C23	K24C13	K24C33	K24C13	K24C13	B24C13	B23C13	B23C13
TRAVERSE	24	24	24	24	24	24	24	24	23	23
EAST	5956	5956	5958	5959	5959	5963	5964	5949	6038	6038
NORTH	69347	69346	69346	69345	69344	69343	69342	69347	69463	69463
SiO_2 (%)	51.8	52.7	50.1	50.4	49.9	69.7	69.8	51.6	69.9	69.0
Al_2O_3	14.9	13.7	11.9	11.0	10.6	10.7	10.0	12.3	13.2	13.9
Fe_2O_3	3.5	3.1	3.5	1.2	3.5	3.4	4.1	3.3	4.9	4.5
FeO	7.03	6.47	7.12	8.06	8.34	8.35	8.32	8.29	9.73	8.81
MgO	7.40	8.58	9.89	11.70	10.30	10.90	11.40	9.11	5.91	5.67
CaO	11.44	11.29	13.07	12.11	13.08	11.77	12.25	9.77	9.99	10.23
Na_2O	1.70	1.03	0.85	1.03	0.87	1.24	0.95	1.37	1.95	2.61
K_2O	0.09	0.05	0.07	0.08	0.03	0.06	0.06	0.08	0.12	0.15
H_2O	1.69	1.73	1.87	2.29	2.00	2.11	2.13	2.52	2.58	2.58
TiO_2	0.60	0.58	0.67	0.64	0.51	0.56	0.50	0.62	1.41	2.00
P_2O_5	0.10	0.10	0.08	0.08	0.09	0.10	0.09	0.09	0.17	0.28
MnO	0.14	0.14	0.24	0.19	0.22	0.19	0.24	0.15	0.19	0.17
S	-	-	-	-	-	-	-	-	-	-
Ba (ppm)	68	73	61	64	96	117	60	125	101	265
Ce	-	-	-	-	-	-	-	-	-	-
Co	40	42	41	40	--	43	45	42	50	41
Cr	167	344	1178	1136	746	815	899	437	108	145
Cu	35	53	18	17	24	45	23	68	60	144
F	-	-	-	-	-	-	-	-	-	-
La	-	-	-	-	-	-	-	-	-	-
Li	1	3	3	4	2	5	7	8	3	2
Mn	1190	1210	2190	1640	1980	1660	1940	1260	1550	1250
Mo	-	-	-	-	-	-	-	-	-	-
Nb	6	<5	<5	<5	<5	<5	<5	<5	8	8
Ni	121	251	301	408	226	235	256	125	137	108
Pb	<10	<10	<10	10	<10	20	<10	10	20	<10
Rb	<5	<5	<5	<5	<5	<5	<5	<5	<5	<5
Sn	-	-	-	-	-	-	-	-	-	-
Sr	65	65	55	57	92	94	66	50	124	131
Th	<10	<10	<10	<10	<10	<10	<10	<10	<10	<10
U	-	-	-	-	-	-	-	-	-	-
V	276	259	220	213	221	260	221	299	336	365
W	-	-	-	-	-	-	-	-	-	-
Y	22	22	19	18	18	19	18	21	36	48
Zn	58	64	63	51	72	65	69	66	91	83
Zr	41	33	26	24	23	35	28	37	76	116

SAMPLE	83217	83218	83219	83220	83221	83222	83223	83224	83225	83226
CODE	B23C13	B23C22	B23C22	B23C22	B23C12	B23C12	B23C12	K23C12	K23C12	B23C22
TRAVERSE	23	23	23	23	23	23	23	23	23	23
EAST	6046	6047	6047	6047	6047	6080	6082	6083	6085	6086
NORTH	69463	69463	69463	69463	69463	69512	69512	69511	69510	69509
SiO_2 (%)	69.0	67.6	69.0	69.6	69.6	69.9	50.7	69.6	50.5	52.1
Al_2O_3	13.8	14.2	13.6	13.6	13.2	12.1	12.1	10.8	11.9	13.8
Fe_2O_3	4.5	3.7	4.7	4.8	5.1	5.3	5.1	2.9	3.1	3.8
FeO	8.88	9.63	8.90	8.58	8.91	7.01	6.79	7.08	6.31	6.73
MgO	6.35	7.37	6.65	6.20	6.26	9.05	8.82	14.20	11.90	9.06
CaO	10.20	11.55	10.84	10.81	10.58	9.03	9.64	8.00	8.49	9.11
Na_2O	1.67	2.30	2.24	2.19	2.06	2.73	1.92	1.95	1.99	2.69
K_2O	0.16	0.12	0.12	0.11	0.14	0.40	0.13	0.10	0.15	0.24
H_2O	2.38	2.81	2.66	2.59	2.15	3.15	3.19	4.56	3.94	3.13
TiO_2	2.02	1.06	1.15	1.15	1.14	0.72	0.62	0.45	0.47	0.54
P_2O_5	0.28	0.13	0.16	0.15	0.15	0.11	0.10	0.08	0.08	0.09
MnO	0.19	0.20	0.20	0.19	0.19	0.18	0.16	0.16	0.16	0.12
S	-	-	-	-	-	-	-	-	-	-
Ba (ppm)	59	60	65	68	79	205	107	66	44	56
Ce	-	-	-	-	-	-	-	-	-	-
Co	48	47	46	44	50	32	41	37	62	31
Cr	153	152	122	123	114	669	526	1366	976	637
Cu	140	115	166	74	163	64	62	31	252	31
F	-	-	-	-	-	-	-	-	-	-
La	-	-	-	-	-	-	-	-	-	-
Li	2	3	2	2	3	2	3	5	5	4
Mn	1520	1640	1610	1440	1580	1570	1350	1320	1250	875
Mo	-	-	-	-	-	-	-	-	-	-
Nb	<5	<5	6	5	<5	<5	<5	<5	<5	<5
Ni	164	151	128	125	119	121	143	403	297	162
Pb	<10	<10	<10	<10	<10	<10	<10	<10	10	<10
Rb	<5	<5	<5	<5	<5	11	<5	<5	6	15
Sn	-	-	-	-	-	-	-	-	-	-
Sr	86	100	103	102	86	89	55	33	62	70
Th	<10	<10	<10	<10	<10	<10	<10	<10	<10	<10
U	-	-	-	-	-	-	-	-	-	-
V	284	283	302	303	301	275	285	230	256	266
W	-	-	-	-	-	-	-	-	-	-
Y	28	30	33	33	32	24	22	18	21	21
Zn	76	82	79	77	85	59	60	59	68	73
Zr	56	46	67	74	76	56	34	34	29	33

SAMPLE	83227	83228	83229	83235	83265	83266	83267	83268	83269	83270
CODE	K23C12	B23C12	K23C32	A00C12	R08022	K26C13	K26C12	K26C12	K26C32	K26C12
TRAVERSE	23	23	23	00	08	26	26	26	26	26
EAST	6087	6089	6090	6282	6597	5128	5130	5133	5136	5139
NORTH	69509	69508	69508	69949	70225	69557	69557	69557	69557	69557
SiO_2 (%)	48.8	50.1	52.2	61.4	75.9	49.5	49.6	49.7	51.6	52.5
Al_2O_3	9.5	14.0	6.4	14.9	11.1	15.1	14.9	14.8	5.3	12.0
Fe_2O_3	3.1	3.7	3.1	2.1	2.5	2.4	2.0	1.9	2.5	2.5
FeO	6.98	8.86	7.86	4.18	2.39	7.89	7.27	7.64	7.85	8.96
MgO	17.00	5.19	13.40	4.55	0.77	9.42	11.00	11.00	14.60	11.30
CaO	7.27	9.40	12.24	5.66	0.61	12.03	11.70	11.85	13.66	9.23
Na_2O	0.76	2.13	0.95	3.04	1.90	1.37	1.23	1.00	0.69	1.18
K_2O	0.24	0.13	0.13	1.10	0.85	0.05	0.03	0.02	0.13	0.01
H_2O	5.25	4.41	2.30	1.68	2.16	1.84	1.78	1.78	2.38	1.87
TiO_2	0.43	1.46	0.61	0.59	0.23	0.29	0.17	0.17	0.52	0.53
P_2O_5	0.05	0.15	0.08	0.17	0.03	0.04	0.04	0.04	0.07	0.09
MnO	0.16	0.24	0.19	0.08	0.06	0.16	0.15	0.18	0.19	0.15
S	-	-	-	-	-	-	-	-	-	-
Ba (ppm)	74	86	45	411	224	67	<30	<30	160	69
Ce	-	-	-	-	-	-	-	-	-	-
Co	44	51	35	36	51	101	103	93	66	85
Cr	1666	90	1257	177	<10	333	453	444	1137	665
Cu	19	238	75	45	8	11	8	44	550	31
F	-	-	-	300	-	-	-	-	-	-
La	-	-	-	-	-	-	-	-	-	-
Li	8	6	1	41	3	24	31	27	10	17
Rb	1320	2050	1580	622	415	1130	1080	1260	1320	1130
Mo	-	-	-	1	<1	-	-	-	-	-
Nb	<5	7	<5	6	23	<5	<5	<5	<5	<5
Ni	578	136	229	151	16	191	223	207	280	182
Pb	20	30	<10	<10	<10	<10	10	20	40	<10
Rb	8	<5	<5	46	20	<5	<5	<5	<5	<5
Sn	-	-	-	<5	12	-	-	-	-	-
Sr	17	92	72	320	43	106	103	101	64	38
Th	<10	<10	<10	<10	<10	<10	<10	<10	<10	<10
U	-	-	-	-	1	-	-	-	-	-
V	216	409	206	107	<10	197	172	177	201	262
W	-	-	-	-	-	-	-	-	-	-
Y	17	39	18	20	210	24	10	8	17	22
Zn	60	104	59	56	65	64	44	57	63	55
Zr	20	82	34	133	620	9	<7	<7	29	37

SAMPLE	83271	83272	83273	83274	83275	83280	83281	83282	83283	83284
CODE	B26[illegible]2	K26C12	B26B13	B26B13	B26B16	D27H16	D27H24	D27H23	D27H24	D27H24
TRAVERSE	26	26	26	26	26	27	27	27	27	27
EAST	5141	5139	5128	5147	5147	5216	5213	5212	5212	5211
NORTH	69555	69554	69554	69563	69545	69306	69308	69309	69311	69312
SiO_2 (%)	51.2	50.6	50.7	48.9	51.6	71.9	67.3	69.2	73.2	67.7
Al_2O_3	14.1	10.8	14.1	13.2	13.0	11.5	12.7	12.1	11.4	12.7
Fe_2O_3	2.8	2.3	3.1	3.1	2.9	1.3	2.3	1.7	1.6	2.1
FeO	7.02	8.32	7.91	8.01	7.32	4.54	4.67	5.07	3.04	4.52
MgO	7.89	14.60	8.95	9.63	8.89	0.90	2.00	1.93	0.50	1.19
CaO	13.61	8.77	11.68	13.42	12.93	2.29	2.52	3.18	1.84	3.50
Na_2O	0.39	0.71	1.28	0.63	0.79	1.17	2.25	1.28	4.00	3.80
K_2O	0.02	0.01	0.04	0.02	0.02	3.54	2.69	2.00	1.45	2.07
H_2O	1.68	2.22	1.80	1.89	1.75	1.65	2.54	2.21	1.56	1.40
TiO_2	0.59	0.45	0.52	0.58	0.49	0.28	0.41	0.40	0.37	0.43
P_2O_5	0.09	0.08	0.09	0.09	0.08	0.06	0.07	0.06	0.07	0.78
MnO	0.15	0.16	0.17	0.22	0.20	0.11	0.12	0.13	0.06	0.11
S	-	-	-	-	-	-	-	-	-	-
Ba (ppm)	<30	<30	42	44	37	894	695	281	684	410
Ce	-	-	-	-	-	-	-	-	-	-
Co	89	96	94	85	79	77	95	78	86	78
Cr	299	1301	627	449	482	21	83	98	<10	<10
Cu	12	13	69	44	32	63	39	42	11	10
F	-	-	-	-	-	-	-	-	-	-
La	-	-	-	-	-	-	-	-	-	-
Li	4	5	10	21	24	32	25	27	13	3
Mn	1120	1250	1290	1650	1560	829	965	984	672	819
Mo	-	-	-	-	-	<1	<1	<1	<1	<1
Nb	<5	<5	<5	<5	<5	14	12	10	13	13
Ni	115	391	178	167	177	32	58	65	21	13
Pb	10	<10	<10	10	30	<10	<10	<10	20	<10
Rb	<5	<5	<5	<5	<5	184	102	94	61	70
Sn	-	-	-	-	-	7	6	5	9	13
Sr	61	33	49	24	28	70	181	84	104	132
Th	<10	<10	<10	<10	<10	14	10	<10	13	14
U	-	-	-	-	-	1	1	1	2	2
V	209	228	221	227	198	27	73	79	<10	24
W	-	-	-	-	-	-	-	-	-	-
Y	18	19	18	19	19	70	55	49	76	80
Zn	65	71	74	69	66	86	120	113	86	102
Zr	38	35	31	34	24	255	215	186	265	273

SAMPLE	83285	83286	83287	83288	83289	83290	83328	83329	83330	83331
CODE	D27H14	R27H34	R27H34	R27H35	R27H10	R27H10	D00026	A28C16	A28C12	A28C13
TRAVERSE	27	27	27	27	27	27	00	28	28	28
EAST	5211	5222	5222	5223	5225	5226	5756	5800	5799	5799
NORTH	69314	69342	69338	69334	69334	69334	68978	68116	68115	68115
SiO_2 (%)	71.2	76.6	71.9	72.2	71.1	72.7	69.5	62.0	60.3	60.1
Al_2O_3	12.2	9.5	12.5	14.4	14.2	14.1	15.2	14.4	14.2	13.9
Fe_2O_3	2.0	1.3	1.5	0.5	0.5	0.4	0.6	2.4	2.3	3.0
FeO	3.90	1.76	2.23	0.54	0.81	0.77	0.57	4.04	4.88	5.52
MgO	0.98	0.39	1.14	0.92	1.07	0.69	0.25	4.67	5.18	4.98
CaO	3.66	3.14	2.29	5.18	1.38	1.08	2.32	3.13	3.22	3.05
Na_2O	0.76	1.60	2.71	4.39	3.59	4.68	5.44	5.38	5.19	4.61
K_2O	2.79	2.30	2.49	0.14	4.37	3.36	1.57	0.22	0.21	0.53
H_2O	1.47	1.94	1.51	0.56	0.96	0.86	2.63	2.69	2.76	2.77
TiO_2	0.38	0.16	0.22	0.19	0.16	0.17	0.11	0.66	0.74	0.74
P_2O_5	0.08	0.05	0.05	0.07	0.06	0.07	0.07	0.14	0.16	0.15
MnO	0.08	0.07	0.07	0.02	0.01	0.01	0.02	0.09	0.07	0.11
S	-	-	-	-	-	-	-	-	-	-
Ba (ppm)	460	889	1503	51	1524	1580	418	107	101	152
Ce	-	-	-	-	-	-	-	-	-	-
Co	92	73	72	139	101	92	107	67	65	80
Cr	<10	<10	11	46	50	38	<10	181	198	187
Cu	16	20	21	8	8	7	12	44	47	45
F	-	-	-	-	-	-	-	-	-	-
La	-	-	-	-	-	-	-	-	-	-
Li	24	23	51	4	47	13	2	23	35	35
Mn	635	599	538	121	56	86	177	669	547	821
Mo	<1	<1	<1	<1	<1	<1	<1	<1	<1	<1
Nb	13	13	14	7	8	5	6	8	9	7
Ni	20	26	29	38	33	30	41	132	149	150
Pb	<10	<10	10	10	<10	<10	<10	10	20	<10
Rb	143	112	148	<5	109	68	42	10	11	20
Sn	4	6	8	5	9	9	10	7	6	5
Sr	55	46	343	108	278	108	260	55	91	87
Th	13	19	24	<10	<10	<10	<10	<10	<10	<10
U	2	2	4	1	1	1	<1	<1	<1	<1
V	11	15	20	21	22	22	<10	113	125	121
W	-	-	-	-	-	-	-	-	-	-
Y	75	71	79	12	11	8	5	22	24	22
Zn	90	75	97	10	8	8	21	75	79	78
Zr	276	202	256	80	76	79	80	166	18.	165

SAMPLE	83332	83333	83334	83335	83336	83337	83338	83381	83382	83383
CODE	D28C24	D28C24	A28C34	D28C24	A28C34	D28C13	D28C13	B30L32	K30L32	K30L32
TRAVERSE	28	28	28	28	28	28	28	30	30	30
EAST	5798	5798	5798	5798	5797	5797	5797	4443	4446	4446
NORTH	68115	68114	68114	68114	68113	68113	68113	68420	68420	68420
SiO_2 (%)	63.5	64.1	62.5	63.2	62.1	64.7	65.5	55.3	55.0	53.0
Al_2O_3	16.9	14.7	14.0	13.9	14.0	14.6	14.2	14.4	12.8	10.7
Fe_2O_3	2.5	2.4	3.5	2.5	3.7	1.7	2.5	1.7	1.7	1.8
FeO	3.86	3.41	2.41	3.89	2.99	3.24	2.66	6.38	6.29	6.82
MgO	1.93	1.20	1.18	2.06	1.53	2.56	2.46	7.51	9.96	13.10
CaO	4.90	6.44	10.30	7.41	10.15	7.16	6.77	10.78	8.36	6.87
Na_2O	4.45	2.56	2.24	3.42	2.46	3.43	2.94	2.07	1.19	1.01
K_2O	0.69	1.77	0.10	0.24	0.10	0.07	0.06	0.55	0.36	0.10
H_2O	1.49	1.21	1.17	1.20	1.20	0.97	0.82	1.77	3.01	4.73
TiO_2	0.78	0.76	0.77	0.76	0.77	0.79	0.73	0.63	0.57	0.66
P_2O_5	0.20	0.18	0.19	0.18	0.18	0.19	0.17	0.12	0.10	0.08
MnO	0.07	0.09	0.28	0.16	0.27	0.10	0.09	0.18	0.14	0.15
S	-	-	-	-	-	-	-	0.002	0.002	0.002
Ba (ppm)	167	236	76	203	106	69	88	258	173	202
Ce	-	-	-	-	-	-	-	28	27	14
Co	83	99	105	102	98	82	110	86	64	62
Cr	54	54	57	56	63	61	63	362	832	1016
Cu	22	52	15	25	12	47	10	16	13	14
F	-	-	-	-	-	-	-	-	-	-
La	-	-	-	-	-	-	-	16	14	9
Li	18	17	2	3	2	2	5	7	8	21
Mn	699	578	2210	1070	2160	685	668	1480	991	1290
Mo	<1	<1	2	-	<1	<1	<1	-	-	-
Nb	13	14	11	11	14	11	10	<10	<10	<10
Ni	65	68	80	76	79	78	69	191	222	311
Pb	<10	10	<10	<10	10	<10	20	20	10	<10
Rb	41	122	<5	7	<5	<5	<5	22	14	<5
Sn	8	6	47	10	18	8	7	<5	<5	<5
Sr	176	71	99	161	131	156	162	127	62	87
Th	<10	<10	<10	<10	<10	<10	<10	<10	<10	<10
U	<1	<1	<1	<1	<1	<1	<1	-	-	-
V	75	68	69	73	70	76	82	196	211	194
W	-	-	-	-	-	-	-	-	-	-
Y	35	36	36	37	41	39	40	25	23	20
Zn	75	130	241	186	194	85	71	80	61	89
Zr	289	269	253	263	265	273	262	93	88	69

SAMPLE	83384	83385	83386	83387	83388	83389	83390	83391	83392	83393
CODE	K30L32	K30L32	K30L32	K30L32	B30L32	S29L21	S29L21	S29L21	S29L21	S29L21
TRAVERSE	30	30	30	30	30	29	29	29	29	29
EAST	4447	4447	4443	4443	4443	4956	4957	4957	4958	4958
NORTH	68420	68417	68419	68419	68419	68028	68028	68028	68028	68028
SiO_2 (%)	53.2	52.3	54.4	53.4	54.7	93.7	90.9	89.2	78.8	70.8
Al_2O_3	13.4	13.8	13.1	13.2	13.7	4.1	6.8	6.3	14.4	14.0
Fe_2O_3	1.4	1.3	1.0	1.0	1.1	0.1	0.1	0.7	1.1	0.5
FeO	6.96	7.58	7.24	7.00	7.16	0.38	0.39	1.06	1.17	8.68
MgO	9.95	9.96	9.68	9.78	8.12	0.02	0.02	0.04	0.06	0.24
CaO	8.67	7.91	7.98	8.16	9.64	0.01	<0.01	0.27	0.11	0.68
Na_2O	1.62	1.76	1.57	1.12	1.67	0.08	0.11	0.07	0.16	0.01
K_2O	0.35	0.20	0.63	0.76	0.52	0.15	0.18	0.20	0.61	0.06
H_2O	3.12	3.67	3.07	3.57	2.19	1.00	1.32	1.29	2.24	2.78
TiO_2	0.58	0.61	0.58	0.60	0.59	0.25	0.36	0.33	0.59	0.56
P_2O_5	0.09	0.10	0.10	0.10	0.09	0.04	0.06	0.27	0.20	0.46
MnO	0.16	0.16	0.15	0.14	0.16	<0.01	0.01	0.19	0.34	1.24
S	0.002	0.002	0.003	0.002	0.078	0.079	0.017	0.17	0.003	0.013
Ba (ppm)	200	248	237	344	197	120	169	155	266	77
Ce	22	20	23	28	22	30	29	32	56	61
Co	63	66	78	57	69	13	14	33	26	68
Cr	521	586	582	629	419	418	335	364	325	617
Cu	15	15	13	14	57	62	30	29	30	25
F	-	-	-	-	-	-	-	-	-	-
La	14	16	10	15	20	19	16	18	28	24
Li	13	18	16	17	6	5	5	3	6	3
Mn	1180	1170	1140	1040	1250	10	61	1380	2120	6290
Mo	-	-	-	-	-	5	4	3	5	5
Nb	<10	<10	<10	<10	<10	<10	10	<10	11	<10
Ni	195	213	235	229	205	26	23	60	35	99
Pb	20	10	<10	<10	10	<10	10	20	10	20
Rb	12	7	22	48	18	9	14	14	23	<5
Sn	<5	<5	<5	<5	<5	<5	<5	<5	<5	<5
Sr	91	112	93	103	116	42	62	34	89	10
Th	<10	<10	<10	<10	<10	<10	<10	<10	12	<10
U	-	-	-	-	-	<1	<1	<1	<1	<1
V	204	204	189	195	183	33	42	38	101	128
W	-	-	-	-	-	-	-	-	-	-
Y	24	24	22	26	25	7	12	10	16	18
Zn	83	92	75	71	70	7	7	11	20	58
Zr	78	92	88	92	97	86	119	109	143	127

SAMPLE	83394	83395	83396	83411	83412	83413	83414	83415	83416	83417
CODE	S29L21	S29L21	S29L21	K32C13	K32C12	K32C22	K32C12	K32C12	K32C12	K32C32
TRAVERSE	29	29	29	32	32	32	32	32	32	32
EAST	4959	4959	4966	5008	5007	5005	5005	5004	5001	5001
NORTH	68028	68028	67971	67825	67824	67823	67823	67821	67820	67826
SiO_2 (%)	72.2	76.1	79.1	53.0	52.7	49.7	48.4	52.1	51.4	54.7
Al_2O_3	13.5	11.1	10.5	12.0	9.6	7.7	7.2	9.1	9.2	15.2
Fe_2O_3	0.4	0.5	1.7	1.3	1.3	1.6	1.2	1.7	1.5	1.0
FeO	7.61	6.24	3.47	7.51	7.42	8.03	8.13	8.19	8.60	6.13
MgO	0.21	0.22	0.44	11.70	15.40	18.70	20.40	15.30	16.00	6.11
CaO	0.51	0.63	0.22	6.63	5.44	6.60	6.92	7.21	7.05	12.31
Na_2O	0.02	0.03	0.11	1.90	1.55	0.20	0.11	1.08	1.09	1.00
K_2O	0.22	0.34	0.39	0.39	0.19	0.02	<0.01	0.09	0.42	0.13
H_2O	2.64	2.37	2.69	3.94	5.15	6.12	6.26	4.77	4.70	1.56
TiO_2	0.57	0.47	0.55	0.52	0.44	0.31	0.27	0.51	0.51	0.66
P_2O_5	0.45	0.53	0.21	0.09	0.07	0.07	0.05	0.09	0.09	0.11
MnO	1.17	0.82	0.30	0.14	0.15	0.20	0.17	0.18	0.18	0.14
S	0.019	0.092	0.14	0.003	0.012	0.002	0.003	0.003	0.003	0.064
Be (ppm)	144	179	162	256	151	55	44	91	304	56
Ce	54	45	60	17	8	<5	<5	5	6	26
Co	46	35	42	74	49	86	85	84	77	123
Cr	372	402	372	964	1474	2920	3418	1320	1361	256
Cu	26	39	85	88	55	16	9	159	31	84
F	-	-	-	-	-	-	-	-	-	-
La	28	24	35	14	11	5	<5	<5	6	12
Li	2	5	14	11	16	6	6	16	15	5
Mn	5980	4880	2060	1030	1060	1450	1340	1310	1290	1070
Mo	5	9	3	-	-	-	-	-	-	-
Nb	10	<10	<10	<10	<10	<10	<10	<10	<10	<10
Ni	105	68	79	262	375	569	671	294	305	178
Pb	10	10	<10	10	<10	20	50	30	30	40
Rb	10	19	25	17	7	<5	<5	<5	18	<5
Sn	<5	<5	<5	<5	<5	<5	<5	6	<5	<5
Sr	26	52	45	120	86	<5	<5	33	35	82
Th	<10	<10	10	<10	<10	<10	<10	<10	<10	<10
U	1	1	1	-	-	-	-	-	-	-
V	109	94	96	202	195	168	152	194	190	205
W	-	-	-	-	-	-	-	-	-	-
Y	19	16	18	20	17	12	10	16	15	24
Zn	54	57	36	95	97	82	69	81	79	97
Zr	130	126	147	72	60	23	24	65	63	94

SAMPLE	83418	83419	83420	83421	83422	83423	83424	83425	83426	83427
CODE	K32C32	B32C12	B32C22	K32C12	K32C12	B32C13	B32C12	B32C12	B31C12	B31C12
TRAVERSE	32	32	32	32	32	32	32	32	31	31
EAST	5001	4980	4980	4980	4980	4995	4995	4995	4862	4846
NORTH	67826	67760	67757	67754	67754	67769	67768	67765	67646	67646
SiO_2 (%)	53.8	51.2	52.8	52.6	49.9	52.4	51.3	51.4	49.9	49.6
Al_2O_3	13.2	13.8	13.0	11.9	12.8	14.3	14.0	13.3	15.0	14.8
Fe_2O_3	1.3	2.0	1.6	1.9	1.9	1.9	2.0	2.1	2.0	1.9
FeO	7.68	7.51	7.65	7.36	8.77	7.45	7.67	7.30	9.15	9.16
MgO	8.91	8.65	8.95	11.30	11.90	7.96	8.33	8.99	7.18	7.72
CaO	9.97	12.00	12.69	10.69	9.78	12.64	12.13	11.65	11.68	11.66
Na_2O	0.61	1.85	0.79	1.94	1.65	0.89	2.06	1.61	1.67	1.74
K_2O	0.07	0.04	0.01	0.01	0.03	0.03	0.07	0.03	0.07	0.09
H_2O	3.10	1.68	1.69	1.84	2.10	1.72	1.76	1.86	1.72	1.75
TiO_2	0.57	0.64	0.61	0.68	0.50	0.47	0.64	0.62	0.76	0.77
P_2O_5	0.11	0.08	0.08	0.07	0.09	0.10	0.08	0.08	0.10	0.10
MnO	0.17	0.17	0.17	0.17	0.18	0.15	0.17	0.17	0.20	0.19
S	0.002	0.003	0.075	0.008	0.007	0.036	0.003	0.003	0.002	0.006
Be (ppm)	104	71	68	77	103	62	63	72	74	114
Ce	23	<5	7	<5	<5	<5	<5	<5	6	<5
Co	84	106	112	110	111	96	98	100	104	102
Cr	595	432	459	599	767	301	421	487	293	292
Cu	10	64	78	93	99	81	46	68	37	34
F	-	-	-	-	-	-	-	-	-	-
La	10	8	<5	5	<5	<5	<5	<5	<5	5
Li	13	3	4	8	10	6	2	8	6	5
Mn	1260	1430	1580	1300	1470	996	1670	1360	1780	1670
Mo	-	-	-	-	-	-	-	-	-	-
Nb	<10	<10	<10	<10	<10	<10	<10	<10	<10	<10
Ni	182	161	164	225	285	91	157	170	167	169
Pb	30	<10	<10	<10	<10	<10	<10	<10	<10	<10
Rb	<5	<5	<5	<5	<5	<5	<5	<5	<5	<5
Sn	<5	<5	<5	<5	<5	<5	<5	<5	<5	<5
Sr	67	78	99	46	75	106	75	87	64	71
Th	<10	<10	<10	<10	<10	<10	<10	<10	<10	<10
U	-	-	-	-	-	-	-	-	-	-
V	220	215	200	211	237	225	210	207	255	255
W	-	-	-	-	-	-	-	-	-	-
Y	21	17	16	16	17	19	17	17	24	24
Zn	111	68	59	56	74	55	66	64	83	80
Zr	79	29	28	27	38	37	36	32	50	52

SAMPLE	83428	83429	83430	83431	83432	83433	83434	83435	83436	83437
CODE	B31C22	K31C12	K31C12	K31C12	K31C13	K31C13	K31C13	K31C23	K31C23	K31C13
TRAVERSE	31	31	31	31	31	31	31	31	31	31
EAST	6846	6850	6850	6850	6850	6874	6874	6850	6850	6847
NORTH	67646	67646	67646	67646	67646	67671	67671	67700	67663	67701
SiO_2 (%)	48.9	49.1	48.8	49.4	48.5	49.1	49.0	52.4	51.1	52.5
Al_2O_3	15.2	10.6	11.4	9.8	9.7	10.9	10.8	9.1	8.9	7.5
Fe_2O_3	2.1	2.0	0.6	1.2	1.4	1.1	1.1	0.8	1.1	1.2
FeO	9.66	10.24	12.00	10.21	10.24	8.92	8.98	8.63	8.34	7.86
MgO	7.05	11.10	10.50	12.50	13.20	15.40	15.00	15.50	16.50	16.90
CaO	...76	12.03	11.17	12.17	11.65	8.13	8.54	6.69	6.40	6.27
Na_2O	1.78	1.06	0.91	0.35	0.35	1.00	1.12	1.83	1.15	0.25
K_2O	0.07	0.04	0.03	0.04	0.03	0.01	0.02	(0.01	0.01	(0.01
H_2O	1.75	2.23	2.54	2.22	2.69	3.97	3.72	4.02	4.99	5.73
TiO_2	0.78	0.83	0.90	0.87	0.84	0.45	0.45	0.38	0.37	0.33
P_2O_5	0.10	0.09	0.11	0.12	0.10	0.07	0.09	0.08	0.08	0.06
MnO	0.20	0.20	0.19	0.21	0.21	0.17	0.18	0.16	0.18	0.19
S	0.003	0.065	0.010	0.004	0.004	0.026	0.025	0.005	0.003	0.005
Ba (ppm)	68	52	70	53	47	48	43	44	61	54
Ce	(5	(5	8	9	6	(5	(5	(5	(5	(5
Co	104	97	98	95	93	95	89	91	87	86
Cr	316	908	672	1036	1113	1797	1688	2063	2129	1973
Cu	33	102	99	25	28	56	61	115	20	19
F	-	-	-	-	-	-	-	-	-	-
La	5	13	9	9	7	7	5	5	(5	7
Li	6	3	4	3	4	15	13	5	9	8
Mn	1620	1670	1690	1760	1680	1380	1430	1320	1530	1710
Mo	-	-	-	-	-	-	-	-	-	-
Nb	(10	(10	(10	(10	(10	(10	(10	(10	(10	(10
Ni	182	293	269	358	355	534	479	464	532	611
Pb	(10	(10	(10	(10	(10	16	(10	(10	(10	(10
Rb	(5	(5	(5	(5	(5	(5	(5	(5	(5	(5
Sn	(5	(5	(5	(5	(5	(5	(5	(5	(5	(5
Sr	80	105	83	57	50	52	63	49	34	6
Th	(10	(10	(10	(10	(10	(10	(10	(10	(10	(10
U	-	-	-	-	-	-	-	-	-	-
V	255	261	268	234	238	211	219	187	185	170
W	-	-	-	-	-	-	-	-	-	-
Y	24	16	17	18	18	15	16	15	13	13
Zn	84	82	114	74	75	71	66	63	61	66
Zr	55	46	48	55	48	37	38	39	33	29

SAMPLE	83438	83439	83440	83441	[illegible]		83444	83445	83446	83447
CODE	K31C12	K31C12	K31C22	K31C12	K31C22	N31C12	N31C12	N31C22	N31C12	N31C32
TRAVERSE	31	31	31	31	31	31	31	31	31	31
EAST	4846	4846	4843	4853	4853	4826	4826	4826	4826	4815
NORTH	67698	67698	67701	67700	67700	67717	67717	67717	67717	67717
SiO_2 (%)	52.5	52.1	52.5	51.7	51.6	56.0	56.2	55.9	55.0	55.8
Al_2O_3	11.9	7.0	9.8	8.8	7.2	15.6	14.9	14.7	14.4	14.3
Fe_2O_3	1.4	1.0	0.9	0.9	1.0	1.3	1.3	1.1	1.2	1.0
FeO	8.33	7.99	8.33	8.62	7.53	6.83	7.43	7.51	7.10	7.45
MgO	11.90	19.40	14.50	16.10	19.60	5.73	5.53	5.61	6.71	7.28
CaO	7.58	4.73	6.58	6.58	5.42	12.05	11.22	11.19	11.46	11.15
Na_2O	1.58	0.07	1.64	1.00	0.06	0.75	0.88	0.91	0.97	0.48
K_2O	0.08	(0.01	0.01	(0.01	(0.01	0.03	0.05	0.05	0.03	0.03
H_2O	3.66	6.07	4.11	5.10	5.03	1.43	1.43	1.62	1.50	1.69
TiO_2	0.47	0.28	0.41	0.36	0.30	0.69	0.68	0.67	0.64	0.63
P_2O_5	0.08	0.06	0.08	0.08	0.06	0.11	0.12	0.11	0.11	0.11
MnO	0.16	0.16	0.16	0.17	0.17	0.19	0.17	0.16	0.22	0.25
S	0.002	0.005	0.061	0.007	0.003	0.055	0.091	0.13	0.003	0.005
Ba (ppm)	110	116	58	64	(30	66	84	94	66	(30
Ce	8	(5	(5	(5	(5	29	21	32	24	23
Co	91	88	91	80	88	123	97	85	87	89
Cr	865	2724	1540	2168	3192	138	128	130	227	164
Cu	30	26	71	17	23	211	84	95	26	28
F	-	-	-	-	-	-	-	-	-	-
La	5	(5	(5	7	5	12	11	8	17	12
Li	5	8	7	8	8	5	8	8	5	3
Mn	1390	1300	1180	1390	1350	1560	1380	1320	1710	1960
Mo	-	-	-	-	-	-	-	-	-	-
Nb	(10	(10	(10	(10	(10	(10	(10	(10	(10	(10
Ni	248	505	346	529	493	121	95	97	136	165
Pb	(10	(10	20	(10	(10	(10	(10	(10	(10	(10
Rb	(5	(5	(5	(5	(5	(5	(5	(5	(5	(5
Sn	(5	(5	(5	(5	(5	(5	(5	(5	(5	(5
Sr	95	(5	59	30	(5	100	92	98	85	20
Th	(10	(10	(10	(10	(10	(10	(10	(10	(10	(10
U	-	-	-	-	-	-	-	-	-	-
V	210	153	193	186	161	200	206	206	199	100
W	-	-	-	-	-	-	-	-	-	-
Y	17	11	15	14	12	25	25	24	25	12
Zn	52	68	89	60	62	91	101	103	65	62
Zr	41	28	38	35	26	95	93	88	99	65

SAMPLE	83448	83449	83450	83451	83452	83453	83454	83455	83456	83457
CODE	K00L32	K33K22	K33K22	K33K22	K33K22	B33K22	B33K32	B33K22	K33K23	K33K13
TRAVERSE	00	33	33	33	33	33	33	33	33	33
EAST	5196	5268	5249	5249	5250	5251	5252	5252	5255	5255
NORTH	67798	67672	67672	67672	67673	67673	67673	67673	67674	67674
SiO_2 (%)	48.1	51.1	50.9	51.5	50.4	52.3	53.1	52.8	50.9	50.5
Al_2O_3	12.0	10.4	10.2	10.6	10.4	11.6	11.5	11.9	9.2	9.1
Fe_2O_3	1.6	1.9	1.8	2.0	2.0	2.3	1.8	1.9	1.4	1.8
FeO	13.03	9.12	9.01	9.17	9.10	8.51	8.51	8.52	10.15	9.56
MgO	11.00	9.26	9.97	9.33	10.10	8.47	8.04	8.48	13.40	13.40
CaO	8.25	13.23	12.93	11.95	12.16	11.41	11.69	11.89	9.99	10.32
Na_2O	0.53	1.68	1.64	1.48	1.79	2.05	1.74	1.76	1.40	1.31
K_2O	0.48	0.05	0.04	0.08	0.10	0.05	0.03	0.03	0.04	0.05
H_2O	2.93	1.80	1.93	1.83	1.95	1.83	1.80	1.80	2.37	2.37
TiO_2	1.26	0.94	0.93	0.96	0.92	0.89	0.87	0.90	0.69	0.67
P_2O_5	0.15	0.13	0.12	0.12	0.12	0.12	0.12	0.12	0.10	0.09
MnO	0.26	0.21	0.20	0.18	0.17	0.16	0.18	0.19	0.19	0.19
S	0.040	0.004	0.003	0.005	0.002	0.002	0.003	0.003	0.023	0.044
Ba (ppm)	114	72	76	119	79	89	100	70	127	74
Ce	24	7	<5	10	<5	<5	5	8	<5	<5
Co	101	88	91	96	93	94	90	75	86	102
Cr	130	613	630	612	630	436	432	434	1544	1458
Cu	245	19	18	94	23	26	29	33	166	320
F	-	-	-	-	-	-	-	-	-	-
La	16	6	6	6	<5	<5	6	<5	6	<5
Li	18	1	<1	1	1	2	1	1	2	3
Mn	2080	1590	1590	1480	1370	1350	1530	1508	1520	1430
Mo	-	-	-	-	-	-	-	-	-	-
Nb	10	<10	<10	<10	<10	<10	<10	<10	<10	<10
Ni	130	203	217	198	211	183	182	179	528	690
Pb	<10	<10	12	<10	<10	<10	<10	<10	<10	<10
Rb	25	<5	<5	<5	<5	<5	<5	<5	<5	<5
Sn	<5	<5	<5	<5	<5	<5	<5	<5	<5	<5
Sr	208	148	122	139	135	134	112	102	86	115
Th	<10	<10	<10	<10	<10	<10	<10	<10	<10	<10
U	-	-	-	-	-	-	-	-	-	-
V	264	257	274	267	263	260	260	267	234	233
W	-	-	-	-	-	-	-	-	-	-
Y	25	20	20	21	20	21	20	22	17	16
Zn	131	85	81	61	63	58	72	69	86	82
Zr	90	56	56	58	62	58	57	54	42	36

BULLETIN 137

APPENDIX II

LISTING OF GEOCHEMICAL ANALYSIS DATA FILES

(CONTINUED)

DATA FILE II.1

ANALYSES OF VOLCANIC ROCKS

(CONTINUED)

SAMPLE	83458	83459	83460	83461	83462	83463	83464	83465	83466	83467
CODE	B33K33	K33K12	K33K12	K33K22	B33K32	B33K22	B33K24	B33K26	B33K16	B33K26
TRAVERSE	33	33	33	33	33	33	33	33	33	33
EAST	5255	5259	5260	5262	5263	5239	5240	5241	5241	5242
NORTH	67674	67680	67681	67683	67684	67686	67686	67686	67686	67686
SiO_2 (%)	53.0	48.1	48.0	46.5	54.2	50.6	51.2	51.2	52.3	51.2
Al_2O_3	11.1	7.9	7.6	7.4	15.8	14.2	14.4	14.2	15.9	14.3
Fe_2O_3	1.0	1.8	2.1	2.1	1.9	1.3	1.2	1.4	1.5	1.2
FeO	14.41	10.34	10.23	10.28	7.01	6.89	6.69	7.48	7.03	7.91
MgO	10.20	16.60	15.50	17.60	6.41	7.28	7.05	6.76	5.39	7.15
CaO	7.01	8.86	9.65	8.52	6.72	15.46	14.86	14.96	12.23	13.24
Na_2O	0.81	1.22	1.22	0.69	4.80	1.73	1.75	1.30	2.31	1.53
K_2O	(0.01	0.10	0.05	0.13	0.04	0.04	0.07	0.08	0.08	0.13
H_2O	1.68	3.58	3.60	4.79	1.50	1.37	1.53	1.65	1.30	1.62
TiO_2	0.96	0.74	0.72	0.73	0.49	0.49	0.50	0.50	0.63	0.50
P_2O_5	0.14	0.11	0.11	0.11	0.13	0.11	0.10	0.09	0.15	0.10
MnO	0.15	0.17	0.18	0.20	0.12	0.21	0.20	0.22	0.17	0.18
S	0.003	0.005	0.004	0.006	0.007	0.001	0.002	0.002	0.002	0.004
Ba (ppm)	68	96	92	108	116	36	35	37	106	63
Ce	6	(5	5	(5	18	(5	6	(5	20	7
Co	87	96	94	97	71	69	64	74	77	72
Cr	348	1746	1685	2132	178	367	368	380	218	378
Cu	21	91	28	60	84	18	16	22	18	77
F	-	-	-	-	-	-	-	-	-	-
La	9	7	6	(5	9	5	(5	(5	12	(5
Li	2	5	10	9	6	1	1	1	2	1
Mn	1220	1580	1390	1610	816	1830	1720	1910	1640	1650
Mo	-	-	-	-	-	-	-	-	-	-
Nb	(10	(10	(10	(10	(10	(10	(10	(10	(10	(10
Ni	127	713	719	852	161	172	160	158	169	166
Pb	(10	(10	(10	(10	(10	(10	(10	(10	(10	(10
Rb	(5	(5	(5	7	(5	(5	(5	(5	(5	(5
Sn	(5	(5	(5	(5	(5	(5	(5	(5	(5	(5
Sr	134	224	245	42	668	82	72	78	162	66
Th	(10	(10	(10	(10	(10	(10	(10	(10	(10	(10
U	-	-	-	-	-	-	-	-	-	-
V	258	218	209	200	168	196	192	203	173	211
W	-	-	-	-	-	-	-	-	-	-
Y	22	17	16	16	13	18	16	18	20	19
Zn	83	91	87	84	45	74	76	73	65	67
Zr	76	48	44	50	80	38	34	32	79	32

SAMPLE	83468	83469	83470	83471	83472	83473	83531	83532	83533	83534
CODE	B33K24	B33K24	K33K13	K33K13	K33K23	K33K13	K34K12	B34K12	K34K12	B34K12
TRAVERSE	33	33	33	33	33	33	34	34	34	34
EAST	5243	5243	5269	5269	5269	5270	5253	5253	5253	5251
NORTH	67686	67686	67658	67658	67658	67658	67486	67484	67483	67475
SiO_2 (%)	51.9	51.6	47.5	48.0	48.0	46.7	48.1	50.5	49.6	52.5
Al_2O_3	14.7	14.8	7.6	7.0	8.5	7.7	8.0	13.2	8.8	11.3
Fe_2O_3	1.2	1.3	2.0	2.3	2.3	2.1	1.9	2.1	2.7	1.8
FeO	7.50	6.80	10.20	9.58	10.96	10.36	11.44	11.23	10.95	8.76
MgO	6.92	6.90	16.80	16.30	13.90	16.50	13.80	6.08	11.70	8.88
CaO	12.98	13.91	9.07	9.30	8.96	9.04	9.81	8.06	10.49	9.24
Na_2O	1.37	1.49	1.07	0.70	1.51	0.73	1.12	3.72	1.50	2.70
K_2O	0.09	0.10	0.10	0.09	0.06	0.03	0.03	0.10	0.05	0.05
H_2O	1.56	1.61	4.05	4.46	3.57	4.50	4.02	2.36	3.42	2.96
TiO_2	0.51	0.51	0.71	0.66	0.78	0.72	0.97	1.51	0.88	0.86
P_2O_5	0.09	0.11	0.11	0.11	0.11	0.10	0.12	0.18	0.12	0.11
MnO	0.18	0.18	0.18	0.18	0.18	0.19	0.18	0.17	0.15	0.16
S	0.002	0.003	0.007	0.010	0.002	0.004	0.004	0.004	0.070	0.11
Ba (ppm)	69	52	84	112	57	58	68	178	54	68
Ce	<5	7	93	200	155	135	<5	9	10	<5
Co	80	74	89	103	99	94	103	95	93	82
Cr	395	388	1915	1858	1697	1904	1074	140	964	675
Cu	72	53	44	105	24	39	88	104	154	148
F	-	-	-	-	-	-	-	-	-	-
La	<5	<5	63	120	92	87	6	7	<5	<5
Li	1	<1	7	9	6	10	4	3	5	3
Mn	1580	1690	1550	1540	1450	1470	1610	1530	1310	1470
Mo	-	-	-	-	-	-	-	-	-	-
Nb	<10	<10	<10	<10	<10	<10	<10	<10	<10	<10
Ni	138	156	775	824	638	772	413	126	303	173
Pb	<10	<10	<10	<10	<10	<10	<10	<10	<10	<10
Rb	<5	<5	5	<5	<5	<5	<5	<5	<5	<5
Sn	<5	<5	<5	<5	<5	<5	<5	<5	<5	<5
Sr	83	80	63	27	67	22	75	181	80	76
Th	<10	<10	<10	<10	<10	<10	<10	<10	<10	<10
U	-	-	-	-	-	-	-	-	-	-
V	210	203	209	197	223	206	252	309	261	273
W	-	-	-	-	-	-	-	-	-	-
Y	19	18	18	16	19	18	21	29	18	21
Zn	77	66	87	87	82	89	80	84	86	69
Zr	36	37	49	47	54	52	62	101	49	57

SAMPLE	83535	83536	83537	83538	83539	83540	83541	83542	83543	83544
CODE	B34K22	B34K12	B34K32	B34K32	B36K32	K34K32	B34K32	K34K32	B34K32	B36K3
TRAVERSE	34	34	34	34	34	34	34	34	34	34
EAST	5251	5256	5290	5289	5288	5287	5287	5295	5303	5281
NORTH	67473	67486	67452	67451	67450	67449	67449	67426	67419	67410
SiO_2 (%)	52.0	50.4	52.8	51.5	52.0	52.1	51.1	49.8	52.4	50.6
Al_2O_3	11.7	12.4	11.7	11.7	11.6	11.1	14.3	12.4	12.9	13.9
Fe_2O_3	1.4	2.3	1.7	1.7	2.3	2.1	1.6	1.3	1.4	0.8
FeO	8.98	11.23	8.67	8.75	8.32	8.68	7.77	8.16	7.29	8.55
MgO	8.61	6.13	8.47	8.41	8.29	8.97	7.73	9.59	8.89	9.02
CaO	9.16	8.45	10.51	12.02	11.15	10.52	11.71	8.42	12.10	9.29
Na_2O	2.97	3.29	2.26	1.81	1.92	1.91	1.45	3.87	1.09	2.72
K_2O	0.05	0.22	0.05	0.05	0.04	0.07	0.18	0.15	0.02	0.16
H_2O	3.04	2.33	2.30	2.33	2.60	2.72	2.29	4.71	2.55	3.03
TiO_2	0.89	1.52	0.87	0.86	0.88	0.86	0.58	0.70	0.68	0.71
P_2O_5	0.11	0.18	0.11	0.12	0.11	0.11	0.09	0.10	0.10	0.11
MnO	0.17	0.17	0.16	0.16	0.16	0.16	0.16	0.15	0.13	0.15
S	0.10	0.004	0.067	0.055	0.080	0.037	0.006	0.018	0.015	0.010
Ba (ppm)	68	150	67	55	57	57	87	133	57	148
Ce	5	15	7	8	<5	6	7	7	14	5
Co	85	96	84	78	82	80	81	76	74	79
Cr	478	132	455	445	445	573	378	686	478	548
Cu	110	198	114	85	121	114	87	118	262	91
F	-	-	-	-	-	-	-	-	-	-
La	6	9	<5	<5	5	6	<5	6	<5	7
Li	4	3	3	2	3	4	4	7	2	4
Mn	1550	1490	1410	1390	1350	1380	1330	1360	1190	1430
Mo	-	-	-	-	-	-	-	-	-	-
Nb	<10	<10	<10	<10	<10	<10	<10	<10	<10	<10
Ni	181	122	181	179	180	199	146	293	186	203
Pb	<10	<10	<10	<10	<10	<10	<10	<10	<10	<10
Rb	<5	<5	<5	<5	<5	<5	11	<5	<5	<5
Sn	<5	<5	<5	<5	<5	<5	<5	<5	<5	<5
Sr	46	155	72	60	57	105	80	365	56	107
Th	<10	<10	<10	<10	<10	<10	<10	<10	<10	<10
U	-	-	-	-	-	-	-	-	-	-
V	280	308	266	259	257	260	218	226	209	238
W	-	-	-	-	-	-	-	-	-	-
Y	21	29	21	20	21	21	19	16	18	19
Zn	85	87	72	70	67	78	67	70	59	72
Zr	51	99	58	48	55	56	43	50	47	48

SAMPLE	83545	83546	83547	83548	84434	85708	85716	85727	85728
CODE	K34K32	B34K32	B34K33	B34K33	B00C32	S54D31	S56D31	B00C32	B00C33
TRAVERSE	34	34	34	34	00	54	56	00	00
EAST	5277	5283	5280	5382	4309	3649	3647	4292	4292
NORTH	67406	67403	67400	67301	69963	68899	68896	68281	68281
SiO_2 (%)	51.1	53.9	51.1	50.8	56.1	97.4	98.1	54.1	58.9
Al_2O_3	13.6	12.6	14.4	14.2	12.9	0.2	0.2	11.3	12.8
Fe_2O_3	1.3	2.2	1.5	1.3	1.5	1.8	1.1	2.4	1.6
FeO	8.15	5.93	7.57	8.37	6.38	0.20	0.24	6.01	5.19
MgO	9.11	7.66	8.03	8.06	8.12	0.02	0.02	6.08	6.05
CaO	10.96	13.38	11.28	12.26	13.8	0.01	0.04	5.93	5.20
Na_2O	1.37	0.31	1.71	1.46	0.79	<0.01	<0.01	1.12	3.42
K_2O	0.52	0.04	0.28	0.15	0.16	<0.01	<0.01	6.08	1.71
H_2O	2.76	2.83	2.59	2.04	1.5	0.27	0.25	1.52	1.66
TiO_2	0.68	0.55	0.69	0.52	0.39	<0.01	<0.01	0.96	0.85
P_2O_5	0.09	0.10	0.10	0.10	0.09	0.13	0.14	0.91	0.80
MnO	0.15	0.13	0.15	0.15	0.18	<0.01	<0.01	0.12	0.08
S	0.014	0.008	0.005	0.003	-	0.020	0.005	0.57	1.1
Ba (ppm)	166	47	108	72	43	<25	66	3654	1658
Ce	<5	7	160	118	10	7	<5	116	75
Co	75	72	84	86	40	-	-	-	-
Cr	541	427	391	386	606	<10	<10	195	102
Cu	89	46	97	57	12	15	<3	121	303
F	-	-	-	-	-	-	-	-	-
La	8	<5	86	55	5	<5	<5	58	39
Li	5	2	4	3	8	<1	<1	20	13
Mn	1510	1160	1360	1470	-	54	32	942	638
Mo	-	-	-	-	<5	-	-	-	-
Nb	<10	<10	<10	<10	<5	<5	<5	7	9
Ni	199	211	171	151	310	<5	<5	116	74
Pb	12	<10	<10	<10	<15	40	<10	<10	<10
Rb	19	<5	10	<5	<5	<2	<2	226	82
Sn	<5	<5	<5	<5	<10	-	-	-	-
Sr	85	46	108	65	114	<5	<5	558	333
Th	<10	<10	<10	<10	<10	<10	<10	15	11
U	-	-	-	-	-	-	-	-	-
V	209	166	221	216	115	<5	<5	138	136
W	-	-	-	-	-	-	-	-	-
Y	17	15	20	19	10	12	2	23	19
Zn	69	57	68	75	60	8	<1	99	50
Zr	33	41	43	38	72	<10	11	187	193

SAMPLE	85729	85730	85733	85734	85735	85736	85745	85756	85758	85759
CODE	B00C34	P00012	P00032	P00032	P00032	P00012	S56031	B00K31	P57C11	P57C21
TRAVERSE	00	00	00	00	00	00	56	00	57	57
EAST	4292	4292	4251	4251	4251	4251	4264	5004	5084	5084
NORTH	68281	68281	68244	68244	68246	68246	67699	67798	68049	68049
SiO_2 (%)	56.2	64.1	70.3	73.3	75.8	74.1	90.1	49.4	71.9	74.8
Al_2O_3	9.6	16.3	13.0	12.7	11.9	13.9	0.3	12.0	16.0	13.5
Fe_2O_3	2.4	2.9	2.4	2.4	1.5	1.2	8.2	2.6	0.9	1.4
FeO	5.14	1.94	1.35	0.46	0.43	0.38	0.67	12.8	0.93	0.36
MgO	6.80	2.07	0.40	0.11	0.06	0.21	0.02	7.06	0.26	0.22
CaO	9.62	2.66	0.89	0.38	0.20	0.97	0.01	6.63	1.46	0.52
Na_2O	1.76	3.28	3.39	3.58	2.80	5.08	<0.01	1.40	3.46	5.56
K_2O	0.72	4.56	4.35	4.37	5.18	1.54	0.01	2.32	4.92	1.08
H_2O	2.16	1.41	1.93	1.15	0.96	1.66	0.74	2.82	0.96	1.66
TiO_2	0.86	0.55	0.12	0.11	0.11	0.15	<0.01	1.20	0.13	0.12
P_2O_5	0.22	0.48	0.27	0.20	0.18	0.14	0.15	0.23	0.30	0.13
MnO	0.14	0.06	0.03	0.02	<0.01	<0.01	<0.01	0.15	0.03	<0.01
S	1.0	-	-	-	-	-	0.010	0.005	-	-
Ba (ppm)	475	2533	2503	1805	2180	1499	<25	298	2269	919
Ce	14	192	24	23	25	9	<5	23	30	<5
Co	-	15	5	<5	<5	<5	-	-	<5	<5
Cr	606	-	-	-	-	-	<10	137	-	-
Cu	123	56	291	151	33	14	6	19	22	12
F	-	910	420	190	90	80	-	-	250	50
La	6	107	9	11	8	<5	<5	13	19	<5
Li	2	19	11	3	1	3	1	13	5	3
Mn	1125	380	169	52	20	24	40	1298	196	70
Mo	-	<1	<1	<1	<1	<1	-	-	<1	<1
Nb	<5	11	8	6	7	<5	<5	7	6	5
Ni	50	33	6	8	<5	7	<5	165	9	7
Pb	<10	18	97	56	132	<10	48	<10	22	<10
Rb	20	161	128	147	168	62	<2	146	145	37
Sn	-	<5	<5	<5	<5	<5	-	-	<5	<5
Sr	210	841	119	133	126	464	<5	134	126	207
Th	<10	33	10	10	13	<10	<10	<10	11	<10
U	-	2	1	4	1	<1	-	-	3	<1
V	231	94	24	27	9	47	5	247	30	51
W	-	2	8	44	19	<2	-	-	17	2
Y	14	13	8	9	5	3	2	19	8	4
Zn	62	63	24	30	2	13	51	164	19	17
Zr	68	207	122	126	124	91	<10	86	141	108

SAMPLE	85762	85763	85764	85765	85766	85767	85768	85769	85770	85771
CODE	P57C21	P57C11	S57C31	P57C11	S57C31	R57C31	D57C31	D57C31	R57C31	D57C31
TRAVERSE	57	57	57	57	57	57	57	57	57	57
EAST	5076	5065	5057	5061	5024	4951	4951	4951	4951	4951
NORTH	68029	68029	68077	68083	68098	68185	68185	68185	68185	68185
SiO_2 (%)	75.2	72.3	82.1	75.7	88.2	76.3	72.8	69.1	74.4	72.7
Al_2O_3	14.3	14.6	7.8	13.6	6.6	7.6	10.2	13.7	9.1	8.9
Fe_2O_3	0.8	0.7	5.1	0.7	1.0	2.7	2.5	0.6	1.2	2.3
FeO	0.49	1.00	0.35	0.36	0.27	5.29	5.34	2.73	6.37	5.85
MgO	0.25	0.46	0.16	0.15	0.16	2.38	2.09	2.28	2.96	3.96
CaO	0.44	2.08	0.02	0.98	0.02	0.12	0.10	1.46	0.06	0.07
Na_2O	5.26	5.39	0.12	5.37	0.16	0.17	0.31	0.75	0.12	0.12
K_2O	1.58	1.71	1.87	1.35	1.76	0.52	1.10	2.84	0.76	0.53
H_2O	1.36	0.85	2.05	1.12	1.53	4.09	4.18	5.06	3.91	4.53
TiO_2	0.11	0.14	0.31	0.07	0.12	0.17	0.23	0.38	0.19	0.20
P_2O_5	0.13	0.17	0.13	0.14	0.14	0.14	0.15	0.22	0.15	0.15
MnO	0.01	0.02	<0.01	<0.01	<0.01	0.05	0.05	0.17	0.15	0.09
S	-	-	-	-	-	-	-	-	-	-
Ba (ppm)	658	688	604	2045	333	106	204	566	171	97
Ce	28	16	12	12	23	66	64	28	38	35
Co	<5	<5	<5	<5	<5	7	9	10	<5	6
Cr	-	-	-	-	-	-	-	-	-	-
Cu	19	9	7	5	4	758	966	30	18	438
F	170	200	120	90	150	250	300	310	230	180
La	18	7	9	7	13	20	22	18	19	24
Li	6	5	<1	5	1	10	10	4	9	14
Mn	74	205	50	58	19	464	386	1643	1266	770
Mo	<1	<1	<1	<1	<1	<1	1	1	<1	2
Nb	5	<5	8	<5	5	5	10	7	8	7
Ni	8	9	5	<5	<5	<5	<5	9	<5	<5
Pb	<10	<10	<10	<10	19	<10	<10	<10	<10	<10
Rb	64	64	37	37	35	10	24	73	15	11
Sn	<5	<5	<5	<5	<5	<5	<5	<5	<5	<5
Sr	377	504	9	249	27	16	25	33	10	11
Th	<10	<10	<10	<10	<10	<10	<10	<10	<10	<10
U	<1	<1	<1	<1	<1	<1	<1	<1	<1	<1
V	16	12	10	15	<5	<5	5	51	<5	<5
W	<2	<2	<2	<2	<2	<2	<2	<2	<2	<2
Y	13	2	20	4	28	51	54	18	62	57
Zn	28	36	15	30	7	91	105	66	125	110
Zr	100	96	156	75	172	189	251	157	248	212

SAMPLE	85772	85773	85774	85775	85776	85777	85778	85779	85780	85781
CODE	D57C31	D57C31	D57C31	R57C31	D57C31	D57C21	D57C21	D57C21	D57C21	D57C31
TRAVERSE	57	57	57	57	57	57	57	57	57	57
EAST	4951	4951	4951	4951	4951	4951	4951	4951	4951	4951
NORTH	68185	68185	68185	68185	68185	68185	68185	68185	68185	68185
SiO_2 (%)	72.2	64.0	72.9	75.6	72.5	63.7	66.5	64.7	63.9	70.6
Al_2O_3	11.2	12.7	10.5	9.2	11.1	16.0	15.2	14.1	13.8	10.9
Fe_2O_3	1.2	1.6	3.0	1.0	1.0	0.6	0.8	0.6	0.5	1.1
FeO	6.16	6.83	3.46	4.93	4.06	3.01	2.13	1.66	3.13	5.64
MgO	3.00	6.00	2.56	3.50	3.66	2.62	1.89	1.56	2.76	4.20
CaO	0.09	0.18	0.07	0.08	0.41	2.79	2.58	3.49	2.80	0.19
Na_2O	0.19	0.08	0.29	0.11	0.32	1.83	1.42	1.92	1.96	0.10
K_2O	1.12	1.29	1.41	0.92	1.30	2.37	3.22	2.91	2.18	1.38
H_2O	4.01	5.37	4.50	3.68	4.32	6.74	6.39	7.28	6.80	4.65
TiO_2	0.23	0.48	0.24	0.23	0.25	0.37	0.41	0.37	0.36	0.40
P_2O_5	0.17	0.20	0.17	0.18	0.17	0.24	0.24	0.26	0.23	0.20
MnO	0.15	0.06	0.06	0.16	0.23	0.29	0.12	0.16	0.31	0.08
S	-	-	-	-	-	-	-	-	-	-
Ba (ppm)	272	128	267	211	301	467	2036	2704	430	322
Ce	55	43	37	60	68	30	27	30	23	38
Co	<5	10	7	<5	<5	10	11	7	10	7
Cr	-	-	-	-	-	-	-	-	-	-
Cu	6	6	235	23	10	25	3	5	10	69
F	200	330	320	280	280	250	280	260	290	310
La	25	22	18	21	23	14	15	12	17	22
Li	10	11	9	10	11	6	6	3	5	6
Mn	1264	519	439	1266	1798	2289	1204	1560	2474	700
Mo	<1	5	<1	<1	3	<1	<1	2	<1	2
Nb	11	12	10	10	11	7	7	7	7	9
Ni	<5	<5	<5	<5	<5	9	10	<5	10	<5
Pb	<10	<10	<10	<10	<10	<10	<10	<10	<10	<10
Rb	23	33	33	23	35	62	90	82	57	34
Sn	<5	<5	<5	<5	<5	<5	<5	<5	<5	<5
Sr	18	9	22	9	25	46	56	63	66	11
Th	<10	<10	<10	<10	<10	<10	<10	<10	<10	<10
U	<1	<1	<1	<1	<1	<1	<1	<1	<1	<1
V	<5	<5	<5	<5	6	51	56	51	52	21
W	3	3	<2	<2	3	<2	<2	<2	<2	13
Y	70	56	63	61	74	12	12	12	12	47
Zn	145	106	56	187	140	58	36	13	63	68
Zr	302	256	251	240	307	146	159	169	145	224

SAMPLE	85782	85783	85784	85789	85790	85791	85792	85793	85794	85811
CODE	D57C31	057C31	057C31	S57C31	S57C31	R57C31	X57C31	X57C31	X57C31	858C31
TRAVERSE	57	57	57	57	57	57	57	57	57	58
EAST	4951	4951	4951	4962	4962	4962	4962	4962	4962	4750
NORTH	68185	68185	68185	68166	68166	68166	68166	68166	68166	68517
SiO_2 (%)	64.7	69.9	70.5	93.5	96.7	87.9	66.7	72.1	56.0	59.6
Al_2O_3	11.8	10.3	10.0	1.2	0.7	3.4	12.6	8.8	16.3	16.4
Fe_2O_3	1.7	1.9	9.8	2.7	3.0	6.2	12.6	12.6	17.1	14.3
FeO	8.26	7.11	0.21	0.23	0.27	0.24	0.24	0.35	0.25	0.15
MgO	4.50	3.32	3.44	0.06	0.04	0.14	0.09	0.09	0.02	0.02
CaO	0.25	0.13	0.15	0.01	(0.01	(0.01	0.01	0.09	0.01	0.02
Na_2O	0.12	0.07	0.06	0.01	(0.01	(0.01	0.01	0.08	0.02	0.01
K_2O	0.92	1.02	0.86	0.03	(0.01	0.01	0.02	0.72	0.01	(0.01
H_2O	5.36	4.66	3.66	1.14	0.65	1.91	6.65	4.28	8.96	7.97
TiO_2	0.56	0.39	0.37	0.03	0.07	0.10	0.71	0.26	0.77	1.21
P_2O_5	0.28	0.22	0.23	0.14	0.14	0.16	0.15	0.15	0.13	0.14
MnO	0.23	0.14	0.16	(0.01	(0.01	(0.01	(0.01	(0.01	(0.01	0.04
S	-	-	-	0.26	0.010	-	-	-	-	0.015
Ba (ppm)	187	180	148	(25	(25	(25	(25	130	36	123
Ce	29	29	33	7	6	6	(5	7	(5	(5
Co	15	11	11	-	-	(5	9	(5	7	-
Cr	-	-	-	(10	(10	-	-	-	-	224
Cu	42	216	152	59	32	16	33	23	167	15
F	310	280	280	-	-	40	90	90	60	-
La	19	16	14	5	(5	6	7	5	6	6
Li	10	9	8	1	(1	(1	3	1	3	3
Mn	1860	1273	1583	54	30	28	43	26	29	374
Mo	2	(1	1	-	-	1	(1	(1	4	-
Nb	5	8	9	(5	(5	7	6	(5	8	6
Ni	(5	(5	(5	(5	(5	(5	17	(5	9	79
Pb	(10	(10	(10	113	(10	(10	(10	(10	(10	(10
Rb	18	21	20	(2	(2	(2	(2	14	(2	(2
Sn	(5	(5	(5	-	-	(5	(5	(5	(5	-
Sr	9	9	8	(5	(5	(5	(5	10	(5	(5
Th	(10	(10	(10	(10	(10	(10	(10	(10	(10	(10
U	(1	(1	(1	-	-	(1	(1	(1	(1	-
V	56	7	5	(5	8	(5	333	8	206	433
W	(2	(2	(2	-	-	(2	3	3	4	-
Y	40	45	44	9	6	37	21	22	30	22
Zn	2136	96	100	32	17	6	32	28	36	33
Zr	175	197	192	36	28	149	91	165	222	125

SAMPLE	85812	85816	85817	85818	85819	85820	85822	85823	85825	85826
CODE	858C31	859C31	859C31	L59C31	859C31	859C31	559031	559031	L52A32	L52A33
TRAVERSE	58	59	59	59	59	59	59	59	52	52
EAST	4750	4861	4861	4861	4861	4861	4861	4861	4751	4751
NORTH	68517	68377	68377	68377	68377	68377	68377	68377	68825	68825
SiO_2 (%)	47.9	47.7	51.3	49.0	69.8	64.5	95.8	93.7	52.6	51.4
Al_2O_3	14.2	24.0	22.8	17.2	15.4	20.9	2.0	1.4	14.4	14.1
Fe_2O_3	26.1	13.1	11.7	2.5	4.5	1.8	0.6	3.0	2.9	4.2
FeO	0.39	0.34	0.28	6.27	0.10	0.21	0.17	0.25	6.77	6.57
MgO	0.13	0.75	0.56	6.60	0.42	0.39	0.04	0.02	5.69	4.75
CaO	0.10	0.05	0.04	10.6	0.08	0.13	0.03	0.03	6.62	6.73
Na_2O	0.05	0.10	0.14	2.11	0.08	0.11	0.01	0.01	4.30	4.80
K_2O	0.06	5.14	3.79	0.26	2.29	2.29	0.05	0.01	2.08	1.21
H_2O	9.38	6.89	7.55	3.58	5.87	8.04	1.15	1.19	2.05	1.50
TiO_2	1.03	0.41	0.39	0.38	0.33	0.43	0.03	(0.01	0.62	1.00
P_2O_5	0.25	0.13	0.12	0.17	0.15	0.16	0.13	0.14	0.20	0.22
MnO	0.16	0.01	0.01	0.13	(0.01	(0.01	(0.01	(0.01	0.14	0.15
S	0.035	0.010	0.030	-	0.005	0.010	0.010	0.010	0.19	0.75
Ba (ppm)	341	1331	740	123	273	243	57	55	605	256
Ce	10	(5	5	(5	6	(5	(5	(5	5	7
Co	-	-	-	38	-	-	-	-	-	-
Cr	35	255	163	-	328	465	21	53	85	(10
Cu	65	215	308	52	49	18	25	92	64	144
F	-	-	-	60	-	-	-	-	-	-
La	23	(5	(5	(5	(5	5	(5	(5	7	7
Li	3	5	6	8	6	6	(1	(1	11	7
Mn	1288	126	94	1283	75	29	18	20	1157	1143
Mo	-	-	-	(1	-	-	-	-	-	-
Nb	(5	(5	(5	(5	(5	(5	(5	(5	(5	(5
Ni	32	46	23	74	60	71	22	16	59	31
Pb	(10	46	67	(10	(10	(10	(10	(10	46	29
Rb	(2	103	84	8	63	75	(2	(2	125	80
Sn	-	-	-	(5	-	-	-	-	-	-
Sr	21	14	13	92	10	20	(5	(5	316	541
Th	(10	(10	(10	(10	(10	(10	(10	(10	(10	(10
U	-	-	-	(1	-	-	-	-	-	-
V	428	309	290	192	256	277	11	27	247	330
W	-	-	-	(2	-	-	-	-	-	-
Y	30	4	4	16	13	15	4	3	18	27
Zn	60	33	28	80	43	20	12	15	84	88
Zr	94	31	30	30	25	60	10	14	36	59

SAMPLE	85827	85828	85829	85830	85831	85832	85833	85834	85835	85836
CODE	L52A33	B52A33	L52A23	L52A12	K52A32	B52A23	B52A34	B52A36	B52A33	B52A33
TRAVERSE	52	52	52	52	52	52	52	52	52	52
EAST	4751	4751	4748	4748	4738	4753	4753	4753	4751	4751
NORTH	68825	68825	68821	68821	68823	68843	68843	68843	68863	68863
SiO_2 (%)	51.7	54.5	49.0	50.8	48.7	51.3	53.2	50.8	72.4	53.0
Al_2O_3	14.1	12.1	12.6	13.9	10.2	14.2	12.6	13.8	8.2	12.1
Fe_2O_3	2.7	13.2	1.9	1.9	2.2	2.1	3.1	6..	5.2	6.7
FeO	7.56	0.62	7.28	6.43	7.37	8.04	6.0[illegible]	4.83	1.12	3.71
MgO	6.12	0.11	10.3	9.03	13.5	7.09	6.86	6.04	1.76	5.52
CaO	7.20	0.27	12.2	11.5	9.27	11.7	9.56	9.36	6.91	11.0
Na_2O	3.80	2.27	1.44	2.17	0.93	1.27	1.53	1.28	0.30	0.85
K_2O	1.94	2.73	0.28	0.27	2.47	0.13	2.81	1.77	0.91	1.74
H_2O	1.89	7.39	2.64	2.19	3.06	1.72	2.38	4.61	2.51	3.06
TiO_2	0.63	0.96	0.41	0.43	0.37	0.57	0.43	0.52	0.21	0.53
P_2O_5	0.19	0.22	0.18	0.16	0.17	0.19	0.17	0.16	0.15	0.15
MnO	0.15	0.08	0.14	0.14	0.16	0.16	0.19	0.19	0.11	0.19
S	0.125	1.5	0.01	0.01	0.015	0.015	0.015	0.016	0.005	0.045
Ba (ppm)	329	1535	102	73	919	175	1407	1696	1318	3743
Ce	<5	13	8	5	<5	<5	<5	5	6	11
Co	-	-	-	-	-	-	-	-	-	-
Cr	35	<10	637	289	1038	290	213	273	105	257
Cu	38	1035	76	16	6	169	26	149	107	188
F	-	-	-	-	-	-	-	-	-	-
La	<5	7	8	<5	6	5	6	6	<5	7
Li	-	-	3	6	33	5	<1	<1	<1	2
Mn	-	-	1148	1126	1296	1424	1503	1490	810	1476
Mo	-	-	-	-	-	-	-	-	-	-
Nb	5	<5	<5	<5	<5	<5	<5	<5	<5	<5
Ni	57	9	172	122	255	106	55	42	39	62
Pb	69	6690	282	<10	11	21	149	185	171	65
Rb	123	56	16	10	205	2	61	47	26	37
Sn	-	-	-	-	-	-	-	-	-	-
Sr	276	343	56	100	199	67	180	333	363	336
Th	<10	108	<10	<10	<10	<10	<10	<10	10	<10
U	-	-	-	-	-	-	-	-	-	-
V	265	532	216	215	183	211	172	213	89	175
W	-	-	-	-	-	-	-	-	-	-
Y	20	12	15	14	10	21	5	5	5	20
Zn	76	26	78	59	73	87	121	142	52	115
Zr	39	56	29	20	24	41	33	35	17	28

SAMPLE	85837	85838	85839	85840	85841	85842	85843	85844	85845	85846
CODE	852A13	852A14	852M32	K52M31	X00U34	B60M31	B60M31	U00U31	L00C31	L00C31
TRAVERSE	52	52	52	52	00	60	60	00	00	00
EAST	4753	4746	4718	4718	4760	4747	4755	4777	4809	4815
NORTH	68843	68871	68778	68778	68797	68709	68709	68723	68720	68721
SiO_2 (%)	50.7	51.8	56.9	54.5	48.4	54.8	54.7	56.7	59.7	53.1
Al_2O_3	14.4	12.8	12.4	11.8	11.2	13.7	12.9	6.7	6.3	13.7
Fe_2O_3	2.5	1.7	1.2	1.0	2.6	1.3	1.8	0.7	0.4	11.0
FeO	7.60	7.93	7.36	7.96	6.16	7.11	6.71	8.23	8.69	1.51
MgO	7.11	8.47	8.87	9.88	6.45	6.87	7.56	22.3	3.20	1.87
CaO	10.9	13.5	7.86	7.06	22.6	9.79	8.27	3.62	6.11	1.89
Na_2O	2.04	0.41	1.82	1.96	0.44	1.66	2.05	0.71	0.29	0.69
K_2O	0.23	0.08	0.92	0.60	1.11	0.15	0.65	0.08	0.18	2.09
H_2O	2.19	1.89	2.37	3.05	1.47	2.46	2.64	1.83	1.19	10.8
TiO_2	0.57	0.42	0.57	0.55	0.41	0.65	0.62	0.37	0.28	0.97
P_2O_5	0.18	0.18	0.20	0.19	0.21	0.21	0.19	0.18	0.16	0.18
MnO	0.16	0.14	0.13	0.12	0.27	0.12	0.12	0.16	0.16	0.09
S	0.01	0.010	0.015	0.005	-	0.015	0.030	0.030	3.8	0.015
Ba (ppm)	157	341	317	196	371	53	548	97	25	1131
Ce	7	<5	24	23	10	20	24	<5	21	43
Co	-	-	-	-	121	-	-	-	-	-
Cr	290	612	590	783	-	380	418	2562	30	117
Cu	68	30	62	7	15	73	61	16	32312	10021
F	-	-	-	-	100	-	-	-	-	-
La	5	<5	19	17	14	13	12	9	15	16
Li	5	16	8	7	4	7	5	5	8	7
Mn	1255	1288	1109	1025	2306	1108	1029	1415	1478	628
Mo	-	-	-	-	<1	-	-	-	-	-
Nb	<5	<5	5	6	<5	6	6	6	<5	5
Ni	107	159	152	188	679	123	133	506	10	62
Pb	25	<10	<10	<10	<10	<10	<10	<10	<10	25
Rb	9	7	34	22	35	4	16	2	9	70
Sn	-	-	-	-	<5	-	-	-	-	-
Sr	96	212	95	85	292	96	112	47	37	53
Th	<10	<10	<10	<10	<10	<10	<10	<10	<10	<10
U	-	-	-	-	<1	-	-	-	-	-
V	211	196	182	180	103	200	193	178	84	286
W	-	-	-	-	2	-	-	-	-	-
Y	24	17	24	23	21	24	25	12	16	17
Zn	130	56	73	83	69	73	71	57	224	96
Zr	38	23	104	93	37	92	102	47	14	103

SAMPLE	85847	85848
CODE	B00C32	B00C32
TRAVERSE	00	00
EAST	4815	4815
NORTH	68721	68721
SiO_2 (%)	49.5	56.0
Al_2O_3	18.6	12.7
Fe_2O_3	11.3	2.3
FeO	0.10	9.39
MgO	0.98	6.48
CaO	0.60	8.60
Na_2O	0.25	1.31
K_2O	0.88	0.26
H_2O	14.6	2.27
TiO_2	1.12	0.95
P_2O_5	0.19	0.22
MnO	0.04	0.19
S	0.015	0.005
Ba (ppm)	668	174
Ce	8	14
Co	-	-
Cr	160	11
Cu	5675	923
F	-	-
La	12	14
Li	15	6
Mn	161	1627
Mo	-	-
Nb	7	5
Ni	35	29
Pb	<10	<10
Rb	46	7
Sn	-	-
Sr	65	41
Th	<10	<10
U	-	-
V	398	292
W	-	-
Y	17	31
Zn	95	142
Zr	115	89

DATA FILE II.2

ANALYSES OF GRANITOID ROCKS

DATA FILE II.2 -- Analyses of granitoid rocks

Data headings:

SAMPLE - Geological Survey of Western Australia sample number

CODE - the code has six characters; these are, from left to right: 1, rock type; 2, texture; 3, intrusive suite; 4 - 5, granitoid location; 6, degree of alteration.

(1) Rock type:

A	albitized granitoid
S	syenogranite
M	monzogranite
G	granodiorite
T	tonalite
J	tronchjemite
Y	granophyre

(2) Texture:

1	equigranular, unfoliated
2	porphyritic, unfoliated
3	equigranular, foliated
4	porphyritic, foliated
5	banded

(3) Intrusive suite:

1	Pegmatite-banded gneiss
2	Recrystallized monzogranite
3	Post-folding granitoids, suite I
4	Post-folding granitoids, suite II

(4 - 5) Granitoid location:

Each granitoid body sampled is numbered and located on Figure AII.1.

(6) Degree of alteration:

1	Little visible alteration in thin section, chemical analysis typical of rock type.

3 Clear evidence of alteration in thin section and/or anomalous geochemistry.

CLASS - granitoid classification

1 Pegmatite-banded gneiss

2 Recrystallized monzogranite

3 Post-folding granitoids, suite I

4 Post-folding granitoids, suite II

Eastings and Northings and rock analyses are expressed in the same way as in the previous data file.

SAMPLE	74459	74460	74461	74462	74463	74464	74465	74466	74467	74468
CODE	M32241	M32241	M32241	M32241	M32261	M32261	M32261	M32261	M13192	M13192
CLASS	2	2	2	2	2	2	2	2	3	3
EAST	5880	5880	5880	5880	5880	5880	5880	5880	5909	5909
NORTH	69302	69302	69302	69302	69302	69302	69302	69302	69516	69516
SiO_2 (%)	72.3	73.3	72.0	71.4	72.0	71.8	71.9	72.0	71.8	71.2
Al_2O_3	14.3	14.4	14.2	14.5	14.1	14.2	14.3	14.3	15.0	14.2
Fe_2O_3	0.50	0.50	0.50	0.30	0.50	0.40	0.40	0.40	0.50	0.60
FeO	1.22	1.13	1.27	1.33	1.16	1.28	1.22	1.26	1.63	1.34
MgO	0.33	0.36	0.35	0.36	0.36	0.37	0.36	0.37	0.59	0.68
CaO	1.70	1.70	1.70	1.74	1.71	1.69	1.72	1.71	2.25	1.76
Na_2O	3.93	4.09	4.08	4.14	4.07	4.13	4.07	4.10	4.75	4.57
K_2O	3.79	3.76	3.94	3.92	3.80	3.88	3.84	3.79	2.34	2.66
H_2O	1.30	1.15	1.13	1.29	1.11	1.01	1.07	1.15	1.68	1.56
TiO_2	0.19	0.18	0.19	0.19	0.18	0.18	0.18	0.18	0.23	0.18
P_2O_5	0.04	0.04	0.05	0.03	0.03	0.04	0.03	0.05	0.05	0.05
MnO	0.03	0.03	0.03	0.03	0.06	0.03	0.03	0.03	0.03	0.03
S	-	-	-	-	-	-	-	-	-	-
Ba (ppm)	901	907	911	926	876	929	897	899	516	603
Ce	81	50	71	65	183	64	95	63	36	26
Co	5	5	<5	11	12	6	<5	<5	<5	<5
Cr	174	179	184	187	186	186	177	186	260	274
Cu	10	42	6	6	5	6	5	5	16	19
F	234	246	231	228	219	202	199	213	280	253
La	35	27	17	23	97	28	41	39	14	15
Li	41	39	40	42	39	42	41	41	65	22
Mn	-	-	-	-	-	-	-	-	-	-
Mo	<5	<5	<5	<5	<5	<5	<5	<5	<5	<5
Nb	7	9	8	9	10	11	10	9	7	10
Ni	15	16	12	13	17	13	16	16	23	19
Pb	55	51	56	52	56	56	50	67	31	29
Rb	186	185	185	187	182	189	188	186	94	102
Sn	<5	<5	<5	<5	<5	<5	<5	<5	<5	<5
Sr	198	200	197	197	189	197	200	200	229	211
Th	34	31	28	30	57	28	34	30	15	13
U	6	6	6	6	5	5	5	5	3	2
V	10	10	11	10	5	9	8	9	15	13
W	<10	<10	<10	11	<10	<10	<10	<10	<10	<10
Y	8	7	8	7	14	6	8	8	6	<5
Zn	52	53	53	54	54	56	50	40	52	47
Zr	153	146	147	159	167	151	147	144	115	117

SAMPLE	74469	74470	74471	74472	74473	74476	81531	81532	81599	81600
CODE	M13192	M13192	M13192	M13192	M13192	M13192	132223	631222	632222	M32222
CLASS	3	3	3	3	3	3	2	2	2	2
EAST	5909	5909	5909	5909	5909	5909	6456	6456	6586	6579
NORTH	69516	69516	69516	69516	69516	69516	70689	70589	70762	70762
SiO_2 (%)	70.4	71.8	72.2	72.0	71.8	71.2	60.5	73.5	71.2	71.7
Al_2O_3	15.2	14.4	14.2	14.6	14.6	14.7	15.4	14.2	14.2	14.3
Fe_2O_3	0.50	0.30	0.40	0.40	0.40	0.50	3.10	0.70	0.70	0.70
FeO	1.75	1.50	1.33	1.42	1.60	1.54	4.10	1.28	1.13	1.03
MgO	0.61	0.48	0.45	0.48	0.53	0.55	2.05	0.69	3.62	0.35
CaO	2.35	2.10	1.70	1.79	2.16	2.17	4.69	1.71	2.16	1.58
Na_2O	4.92	4.62	4.73	4.58	4.68	4.75	4.56	4.68	4.19	4.53
K_2O	2.11	2.56	2.37	2.60	2.37	2.27	0.77	2.92	3.00	3.59
H_2O	1.56	1.35	1.61	1.55	1.38	1.43	2.20	1.16	1.13	1.21
TiO_2	0.24	0.20	0.17	0.18	0.21	0.22	1.62	0.25	0.27	0.23
P_2O_5	0.06	0.04	0.05	0.06	0.05	0.05	0.57	0.11	0.10	0.07
MnO	0.04	0.03	0.03	0.03	0.03	0.03	0.11	0.03	0.03	0.03
S	-	-	-	-	-	-	0.067	0.005	0.006	0.002
Ba (ppm)	438	528	491	655	551	494	397	729	866	1646
Ce	37	40	24	57	36	40	-	-	-	-
Co	<5	<5	<5	5	<5	5	22	5	6	5
Cr	241	235	251	285	247	232	124	194	196	203
Cu	11	11	12	13	38	12	66	25	38	30
F	302	277	265	239	289	301	1370	670	390	393
La	17	18	17	17	11	<10	-	-	-	-
Li	54	54	22	31	57	57	53	24	26	19
Mn	-	-	-	-	-	-	820	220	280	240
Mo	<5	<5	<5	<5	<5	<5	<1	3	3	6
Nb	10	7	8	5	7	9	29	10	10	7
Ni	19	25	22	20	27	25	10	10	10	<10
Pb	34	25	39	24	26	32	10	20	20	30
Rb	90	92	86	85	92	91	73	111	96	108
Sn	<5	5	<5	<5	6	<5	4	<3	3	<3
Sr	236	220	218	212	220	223	445	265	306	433
Th	19	14	11	16	15	15	13	29	13	45
U	2	3	2	2	3	4	4	2	2	3
V	21	12	11	17	18	16	92	15	24	12
W	<10	<10	<10	<10	<10	<10	9	14	18	19
Y	8	6	7	6	6	7	20	8	15	6
Zn	52	47	57	57	52	50	206	63	56	50
Zr	130	112	107	102	116	114	327	103	132	173

SAMPLE	81612	81617	81709	81710	81713	81716	81724	81727	81736	81737
CODE	T13032	T33043	632222	S32222	T13032	S32221	J13052	T13053	T32243	632242
CLASS	3	3	2	2	3	2	3	3	2	2
EAST	6355	6436	6586	6586	6354	6445	6298	6273	6621	6627
NORTH	70285	70278	70761	70761	70288	70587	70364	70363	70588	70519
SiO_2 (%)	65.6	64.8	69.3	73.0	63.1	72.3	75.5	64.8	69.9	70.5
Al_2O_3	13.9	15.6	15.0	13.3	13.7	13.8	12.2	15.7	15.2	15.1
Fe_2O_3	1.50	1.60	1.10	1.00	2.50	1.00	0.05	1.80	1.20	1.00
FeO	2.80	2.64	1.67	0.20	2.96	0.72	2.81	2.89	0.89	0.90
MgO	3.10	1.54	0.74	0.14	3.98	0.24	0.25	1.92	0.60	0.54
CaO	3.91	3.99	2.29	0.88	4.43	2.92	1.48	4.11	1.79	1.89
Na_2O	3.92	4.68	4.63	3.38	3.84	3.75	4.69	4.26	5.13	4.79
K_2O	1.91	1.34	2.70	5.56	1.39	4.97	1.40	1.25	2.43	2.93
H_2O	1.86	3.04	1.28	0.82	2.14	0.77	1.25	2.08	1.27	1.04
TiO_2	0.50	0.64	0.36	0.09	0.61	0.16	0.14	0.61	0.26	0.24
P_2O_5	0.15	0.14	0.17	0.11	0.21	0.11	0.13	0.15	0.17	0.15
MnO	0.08	0.06	0.01	0.01	0.05	0.01	0.02	0.06	0.02	0.01
S	0.006	0.015	-	-	-	-	-	-	-	-
Ba (ppm)	593	381	1178	1590	521	1050	665	323	894	1243
Ce	-	-	-	-	-	-	-	-	-	-
Co	17	20	31	30	35	29	32	39	36	36
Cr	313	176	<10	<10	189	<10	<10	63	<10	<10
Cu	98	77	16	6	42	8	12	52	15	16
F	390	180	310	120	360	380	150	240	570	600
La	-	-	-	-	-	-	-	-	-	-
Li	13	23	11	5	6	10	11	13	16	22
Mn	570	680	151	71	510	122	119	530	216	140
Mo	2	3	<1	<1	<1	<1	<1	<1	<1	<1
Nb	9	8	7	<5	10	14	8	8	7	11
Ni	80	20	23	32	141	18	28	63	22	31
Pb	10	<10	10	<10	<10	20	10	20	10	30
Rb	79	59	93	162	47	175	68	52	84	103
Sn	3	4	5	<5	<5	<5	<5	<5	5	<5
Sr	255	338	319	337	275	164	156	288	535	557
Th	9	<5	31	47	<10	51	<10	<10	13	14
U	1	<1	1	6	1	4	1	<1	2	3
V	90	83	26	13	102	<10	<10	71	21	23
W	14	8	-	-	-	-	-	-	-	-
Y	20	11	6	<5	25	14	13	15	6	6
Zn	67	56	100	43	51	55	46	61	57	50
Zr	186	121	270	138	160	148	136	121	162	138

SAMPLE	81738	81739	81740	81741	81742	81760	81764	81770	83230	83232
CODE	S12242	A13063	S14072	S32222	S12222	T13082	T13082	G13092	T13102	M13103
CLASS	2	3	4	2	2	3	3	3	3	3
EAST	6911	6638	6393	6309	6292	5865	5872	5910	6123	6123
NORTH	70379	70753	70949	70873	70917	69700	69712	69581	69975	69975
SiO_2 (%)	73.2	69.3	73.6	67.7	73.3	66.1	65.1	69.2	71.0	71.6
Al_2O_3	13.6	14.5	13.6	15.3	13.6	15.3	15.2	14.7	14.8	15.2
Fe_2O_3	0.80	0.70	0.60	0.30	0.90	1.80	1.80	1.60	1.00	0.60
FeO	0.69	1.89	0.77	3.56	0.63	2.50	3.16	1.52	1.04	1.25
MgO	0.55	1.06	0.15	1.02	0.21	1.56	2.03	1.12	0.74	0.56
CaO	0.90	1.58	1.01	2.60	1.03	3.82	6.31	2.61	2.13	2.26
Na_2O	3.82	7.57	3.64	4.22	3.74	4.39	4.02	4.37	4.61	4.86
K_2O	4.83	0.39	4.91	2.70	4.87	1.58	1.25	2.04	1.90	2.13
H_2O	0.97	0.36	0.64	1.41	0.99	1.23	1.18	0.91	0.70	0.77
TiO_2	0.15	0.34	0.12	0.58	0.10	0.42	0.46	0.36	0.25	0.22
P_2O_5	0.11	0.15	0.09	0.24	0.11	0.12	0.10	0.14	0.09	0.12
MnO	0.01	0.02	0.01	0.03	0.01	0.06	0.06	0.02	0.03	0.02
S	-	-	-	-	-	-	-	-	-	-
Ba (ppm)	726	2010	561	1542	781	562	686	596	698	713
Ce	-	-	-	-	-	-	-	-	-	29
Co	35	32	33	37	36	29	32	31	40	37
Cr	<10	<10	<10	12	<10	13	44	17	<10	185
Cu	11	22	8	31	13	24	31	25	9	16
F	550	160	-	1030	200	360	300	420	410	350
La	-	-	-	-	-	-	-	-	-	17
Li	39	5	10	41	8	6	8	11	32	64
Mn	125	116	111	262	172	410	521	247	75	158
Mo	<1	<1	<1	<1	<1	<1	<1	<1	<1	1
Nb	17	7	11	15	11	11	8	8	9	<10
Ni	15	42	17	29	31	61	58	39	37	27
Pb	10	<10	20	<10	30	10	30	<10	10	30
Rb	258	<5	225	115	197	57	67	84	81	89
Sn	<5	5	-	5	9	5	6	5	8	<5
Sr	113	414	76	319	112	168	182	428	399	435
Th	42	<10	37	41	52	<10	<10	<10	<10	10
U	3	<1	6	<1	1	1	<1	2	2	4
V	<10	49	<10	39	18	63	81	40	23	21
W	-	-	-	-	-	-	-	-	-	22
Y	26	8	38	23	13	27	29	8	<5	<5
Zn	39	51	46	76	41	42	50	57	48	48
Zr	164	163	112	398	113	168	165	121	100	133

SAMPLE	83234	83241	83245	83248	83252	83253	83256	83257	83260	83261
CODE	M13102	T13113	T13122	T13123	G42233	M22232	M22232	M22231	M22232	M22253
CLASS	3	3	3	3	2	2	2	2	2	2
EAST	6123	6285	5952	5949	5866	5809	5789	5532	5666	5575
NORTH	69975	70026	70413	70418	70396	70416	70438	70768	70726	69839
SiO_2 (%)	72.3	62.7	68.7	63.6	71.2	68.9	69.7	68.7	70.3	74.0
Al_2O_3	15.0	16.3	13.9	14.2	14.3	15.5	15.0	15.4	16.0	13.5
Fe_2O_3	0.50	2.80	2.10	3.50	1.20	1.50	1.50	1.40	1.70	1.10
FeO	1.28	2.98	1.25	1.89	0.71	1.26	1.11	1.75	0.98	0.80
MgO	0.67	3.91	1.62	2.73	0.52	0.78	0.76	0.90	0.62	0.29
CaO	2.20	4.34	2.55	3.56	1.51	2.42	2.42	2.70	2.33	0.95
Na_2O	5.03	3.87	3.81	3.59	4.14	4.47	4.33	4.22	4.35	3.28
K_2O	1.43	1.39	3.24	2.79	3.07	1.98	2.21	2.11	3.11	4.20
H_2O	0.62	2.05	1.44	1.92	1.38	1.02	0.87	0.90	0.78	0.82
TiO_2	0.21	0.55	0.38	0.58	0.23	0.35	0.33	0.41	0.31	0.20
P_2O_5	0.11	0.16	0.16	0.20	0.08	0.14	0.13	0.17	0.12	0.06
MnO	0.03	0.07	0.04	0.07	0.03	0.04	0.03	0.06	0.03	0.05
S	-	-	-	-	-	-	-	-	-	-
Ba (ppm)	588	451	1002	930	667	769	1080	711	958	610
Ce	18	-	-	-	-	-	-	-	-	-
Co	33	69	101	68	108	106	103	100	96	126
Cr	215	172	42	75	<10	<10	<10	<10	<10	<10
Cu	50	13	15	27	11	22	19	15	25	9
F	220	400	570	830	520	620	370	530	370	900
La	12	-	-	-	-	-	-	-	-	-
Li	62	19	32	30	19	36	23	20	12	58
Mn	187	467	321	482	223	289	256	280	258	334
Mo	2	<1	1	<1	<1	<1	<1	<1	<1	<1
Nb	<10	9	9	11	10	11	5	15	7	26
Ni	29	115	39	64	16	18	25	24	21	24
Pb	20	20	30	<10	20	30	20	10	<10	10
Rb	74	46	136	163	117	79	70	90	75	423
Sn	<5	6	6	5	5	6	<5	6	8	10
Sr	434	268	312	385	249	381	409	251	287	80
Th	<10	<10	26	24	18	12	12	46	11	61
U	2	<1	1	2	2	<1	<1	<1	<1	8
V	19	95	51	93	43	31	35	62	24	28
W	<2	-	-	-	-	-	-	-	-	-
Y	<5	21	14	20	20	12	16	24	9	40
Zn	51	40	43	63	41	60	54	70	68	69
Zr	114	161	146	155	144	228	198	291	191	207

SAMPLE	83264	83276	83278	83292	83294	83295	83297	83299	83300	83303
CODE	M22251	M32253	M32253	Y13201	S16212	M51012	M51012	M51012	G51012	M51011
CLASS	2	2	2	3	6	1	1	1	1	1
EAST	5529	5148	5148	5327	5036	5062	5062	5062	5062	5008
NORTH	69788	69695	69695	69286	69340	69366	69366	69366	69366	69634
SiO_2 (%)	69.3	69.8	69.0	71.7	72.3	71.8	72.9	75.4	72.7	68.8
Al_2O_3	14.2	14.9	14.6	12.6	13.5	14.4	14.3	12.4	14.2	15.3
Fe_2O_3	1.80	1.90	1.60	3.90	1.10	1.00	0.80	0.60	0.80	1.80
FeO	1.45	0.88	0.87	0.78	1.08	0.79	0.66	0.41	0.80	1.79
MgO	0.69	0.93	0.88	0.33	0.35	0.38	0.32	0.18	0.37	0.85
CaO	1.64	2.26	2.08	2.07	1.11	1.52	1.38	0.74	1.37	2.47
Na_2O	3.03	4.13	4.91	6.30	3.16	3.96	4.32	3.17	3.98	4.48
K_2O	4.39	2.58	2.61	2.38	5.08	3.75	3.21	4.34	3.67	2.32
H_2O	1.41	1.36	1.34	0.71	1.11	0.73	0.56	0.67	1.13	0.70
TiO_2	0.48	0.34	0.31	0.27	0.26	0.18	0.16	0.11	0.22	0.46
P_2O_5	0.16	0.12	0.11	0.06	0.09	0.08	0.07	0.04	0.06	0.15
MnO	0.04	0.02	0.02	0.05	0.04	0.03	0.04	0.02	0.03	0.04
S	-	-	-	-	-	-	-	-	-	-
Ba (ppm)	1671	1655	1316	1042	778	924	759	928	1541	1108
Ce	-	-	-	-	-	-	-	-	-	-
Co	106	82	112	108	121	115	145	126	119	116
Cr	<10	<10	<10	<10	<10	<10	<10	<10	<10	<10
Cu	16	16	13	8	6	5	9	6	10	14
F	980	600	590	420	110	360	240	150	370	500
La	-	-	-	-	-	-	-	-	-	-
Li	26	14	23	1	51	56	42	47	43	20
Mn	298	162	179	360	248	261	401	131	203	365
Mo	<1	<1	<1	<1	<1	<1	<1	<1	<1	<1
Nb	17	<5	<5	11	22	13	22	8	9	10
Ni	21	16	31	25	12	15	27	16	17	25
Pb	10	30	20	<10	20	10	10	30	10	20
Rb	256	100	95	62	326	199	198	206	217	163
Sn	10	8	11	7	8	7	11	6	9	7
Sr	162	624	596	73	103	198	185	138	286	364
Th	75	<10	<10	14	78	27	26	31	60	21
U	3	2	2	8	1	2	6	2	1	2
V	27	34	27	<10	21	10	<10	<10	20	33
W	-	-	-	-	-	-	-	-	-	-
Y	40	<5	<5	104	38	12	11	5	5	10
Zn	63	48	47	22	43	40	42	26	60	63
Zr	476	121	120	238	267	147	160	84	160	273

SAMPLE	83305	83307	83313	83314	83315	83316	83318	83321	83326	83327
CODE	G51011	M51012	M22242	M42242	M32242	T13133	T13133	M13142	G42263	T22263
CLASS	1	1	2	2	2	3	3	3	2	2
EAST	5007	5008	5914	5990	5997	5795	5794	5776	5713	5593
NORTH	69636	69637	69147	68901	68894	68897	68894	68867	68976	69116
SiO_2 (%)	69.6	72.9	71.3	71.2	73.0	65.7	65.6	71.7	71.6	69.3
Al_2O_3	14.7	14.5	14.5	14.7	13.6	15.2	14.7	14.5	14.4	14.9
Fe_2O_3	1.60	0.80	1.10	1.10	0.80	2.60	1.50	0.05	1.20	1.10
FeO	1.50	0.52	0.97	1.00	0.69	2.01	2.34	1.69	0.88	1.17
MgO	0.78	0.27	0.55	0.56	0.29	1.27	1.76	0.31	0.55	0.61
CaO	2.25	1.08	1.89	1.76	0.87	2.32	2.55	1.42	1.96	2.10
Na_2O	4.52	3.73	4.30	4.05	3.57	4.68	4.59	4.87	4.50	4.58
K_2O	2.47	4.50	2.82	3.73	4.27	1.90	2.15	2.92	2.33	2.62
H_2O	0.77	0.84	0.80	0.76	0.91	2.34	2.73	1.23	1.21	1.66
TiO_2	0.34	0.12	0.30	0.28	0.13	0.42	0.36	0.18	0.25	0.33
P_2O_5	0.14	0.06	0.10	0.12	0.06	0.23	0.19	0.07	0.11	0.11
MnO	0.04	0.02	0.03	0.02	0.03	0.05	0.07	0.03	0.02	0.02
S	-	-	-	-	-	-	-	-	-	-
Be (ppm)	802	1188	1195	1750	978	725	1027	1015	779	819
Ce	-	-	-	-	-	-	-	-	-	-
Co	118	131	119	110	118	96	99	138	125	118
Cr	<10	<10	<10	<10	<10	70	68	<10	<10	<10
Cu	11	10	20	13	7	10	18	15	14	13
F	650	150	460	340	170	600	530	500	260	340
La	-	-	-	-	-	-	-	-	-	-
Li	21	2	38	22	30	9	22	61	22	18
Mn	354	112	220	162	231	360	481	261	202	164
Mo	<1	<1	<1	1	<1	<1	<1	<1	<1	<1
Nb	11	10	8	8	10	10	8	10	5	14
Ni	20	17	21	22	14	68	65	27	31	39
Pb	30	<10	<10	10	30	20	<10	10	<10	<10
Rb	145	212	123	122	210	88	110	126	86	109
Sn	6	6	6	5	10	6	7	7	12	12
Sr	264	203	325	350	135	467	479	424	354	263
Th	37	25	26	25	50	20	20	<10	24	17
U	2	2	2	2	3	2	2	2	4	1
V	25	20	20	22	<10	69	60	13	16	38
W	-	-	-	-	-	-	-	-	-	-
Y	10	12	10	9	21	13	11	8	7	13
Zn	58	21	52	43	37	45	52	45	41	56
Zr	258	111	207	186	142	149	126	110	143	199

SAMPLE	83339	83340	83352	83353	83355	83361	83370	83380	83399	83401
CODE	G51022	M32272	M32303	G32303	M16343	M12273	M64152	M24152	G51022	G51022
CLASS	1	2	2	2	4	2	4	4	1	1
EAST	4669	4515	4738	4738	4853	4715	4304	4354	4626	4626
NORTH	68253	68385	68864	68865	68458	68866	68310	68686	68166	68166
SiO_2 (%)	71.4	70.5	70.9	71.1	78.5	71.5	66.4	63.1	71.3	70.7
Al_2O_3	14.9	15.1	14.8	15.4	12.9	15.0	13.8	16.6	15.3	15.5
Fe_2O_3	0.20	1.20	1.8	0.9	0.4	1.5	2.1	2.60	0.60	0.60
FeO	1.42	1.32	0.77	1.51	0.34	0.67	2.35	2.76	1.35	1.41
MgO	0.35	0.45	0.48	0.52	0.05	0.51	2.15	2.50	0.59	0.68
CaO	1.97	2.66	2.16	2.24	0.11	1.55	3.11	3.72	2.26	2.20
Na_2O	4.66	4.59	5.00	4.78	3.35	5.20	3.55	3.36	4.57	4.68
K_2O	2.22	1.60	2.40	2.09	3.57	2.87	4.03	3.70	2.26	2.31
H_2O	0.68	0.91	1.10	1.07	1.11	1.07	1.21	1.36	0.55	0.64
TiO_2	0.19	0.25	0.22	0.22	0.02	0.23	0.52	0.63	0.25	0.25
P_2O_5	0.07	0.09	0.30	0.29	0.20	0.29	0.51	0.41	0.11	0.10
MnO	0.02	0.04	0.05	0.03	<0.01	0.02	0.05	0.08	0.02	0.02
S	-	-	-	-	-	-	-	-	-	-
Ba (ppm)	1193	645	5288	1749	833	1979	2051	2251	966	1010
Ce	-	-	-	-	-	-	-	76	50	59
Co	117	119	6	6	<5	<5	16	45	38	33
Cr	<10	<10	<10	<10	<10	<10	65	176	171	164
Cu	6	10	5	10	<3	10	12	27	16	9
F	360	270	380	609	87	477	813	1420	390	630
La	-	-	-	-	-	-	-	48	43	39
Li	23	19	-	-	-	-	-	38	125	123
Mn	105	246	-	-	-	-	-	587	140	151
Mo	<1	<1	<5	<5	<5	11	<5	4	2	2
Nb	<5	6	5	<5	11	<5	11	<10	<10	<10
Ni	25	22	5	<5	<5	6	40	40	30	25
Pb	10	20	<10	<10	14	34	34	30	<10	20
Rb	73	61	126	84	157	184	176	199	71	91
Sn	5	7	<5	<5	<5	<5	<5	<5	<5	<5
Sr	497	317	613	768	46	918	565	632	571	570
Th	<10	<10	<10	<10	<10	<10	28	18	12	12
U	<1	<1	<1	<1	<1	<1	<1	2	<1	<1
V	16	19	21	22	<5	32	67	95	26	30
W	-	-	10	<2	<2	3	<2	2	<2	<2
Y	<5	6	8	7	14	<2	13	16	<5	<5
Zn	34	51	26	21	4	34	56	73	38	39
Zr	133	137	142	116	53	114	187	153	159	172

SAMPLE	83402	83404	83407	83674	83676	83678	83680	83681	83683	83684
CODE	S14162	S14163	S14161	G32262	G22261	M22262	M22262	M22261	M32262	M32262
CLASS	4	4	4	2	2	2	2	2	2	2
EAST	4533	4530	4731	5244	5427	5385	5383	5383	5664	5672
NORTH	67716	67704	67678	68106	68185	68404	68404	68404	68359	68356
SiO_2 (%)	71.7	72.3	72.2	70.1	70.1	72.1	71.1	73.4	76.7	72.2
Al_2O_3	13.3	12.9	12.9	15.0	14.7	14.3	15.1	14.1	14.0	14.6
Fe_2O_3	0.50	1.00	0.40	0.70	1.30	0.90	0.80	0.60	0.70	0.60
FeO	2.71	2.18	3.59	1.77	1.71	0.98	1.09	0.73	0.66	0.99
MgO	0.28	0.31	0.31	0.79	0.76	0.62	0.64	0.31	0.24	0.46
CaO	1.53	1.30	1.34	2.46	2.12	1.35	1.51	1.24	1.25	1.59
Na_2O	2.98	3.21	3.23	4.47	4.48	4.39	4.47	3.97	4.39	4.29
K_2O	4.60	4.19	4.23	1.89	2.42	3.47	3.45	3.81	2.70	2.92
H_2O	0.93	1.21	0.57	1.07	0.83	0.67	0.57	0.59	0.48	0.89
TiO_2	0.31	0.29	0.29	0.41	0.39	0.24	0.26	0.15	0.12	0.19
P_2O_5	0.09	0.08	0.07	0.16	0.17	0.11	0.09	0.06	0.05	0.12
MnO	0.04	0.05	0.09	0.02	0.02	0.02	0.02	0.01	0.01	0.02
S	-	-	-	-	-	-	-	-	-	-
Ba (ppm)	1738	1571	1613	1649	2133	1813	2091	2167	2148	1955
Ce	511	608	142	75	-	-	-	-	38	37
Co	25	31	30	36	33	30	27	25	21	29
Cr	176	154	224	212	210	199	160	180	235	186
Cu	10	12	14	31	36	31	30	23	38	26
F	940	730	790	470	550	480	590	320	340	210
La	254	281	73	68	-	-	-	-	25	31
Li	34	7	20	18	8	13	12	8	8	9
Mn	260	361	641	160	261	169	161	116	119	132
Mo	3	4	5	3	2	2	2	3	3	2
Nb	21	21	19	<10	<10	<10	<10	<10	<10	<10
Ni	21	24	25	26	23	19	20	18	19	20
Pb	30	30	30	<10	<10	<10	<10	<10	<10	<10
Rb	199	130	142	58	51	81	75	76	69	91
Sn	<5	<5	<5	<5	<5	<5	<5	<5	<5	<5
Sr	133	155	200	567	606	393	635	388	512	458
Th	97	135	20	22	11	40	16	21	20	26
U	2	4	4	2	<1	<1	<1	<1	<1	<1
V	<10	<10	<10	32	29	16	12	<10	<10	14
W	2	3	4	<2	<2	<2	<2	<2	<2	2
Y	68	58	68	<5	<5	5	5	<5	<5	<5
Zn	63	74	98	68	60	39	40	25	24	30
Zr	378	319	420	261	303	237	203	125	96	168

SAMPLE	83486	83488	83490	83492	83494	83496	83497	83499	83501	83503
CODE	M32263	M32263	M32263	M32263	M32262	M32262	M22262	M22262	M22263	M32263
CLASS	2	2	2	2	2	2	2	2	2	2
EAST	5472	5619	5619	5620	5655	5655	5522	5522	5522	5522
NORTH	68356	68264	68285	68283	68258	68258	68399	68399	68399	68399
SiO_2 (%)	72.6	72.7	73.2	73.5	72.1	72.0	70.6	70.1	69.9	69.7
Al_2O_3	14.5	14.0	13.7	14.7	14.9	15.1	14.7	15.0	14.7	14.7
Fe_2O_3	0.60	0.80	0.80	0.60	0.50	0.70	0.90	0.90	1.40	1.40
FeO	0.91	0.84	0.82	0.70	0.98	1.00	1.15	1.29	1.39	1.36
MgO	0.43	0.30	0.28	0.28	0.44	0.43	0.50	0.55	0.65	0.58
CaO	1.51	1.34	1.26	1.57	1.84	1.60	1.53	1.46	1.53	1.99
Na_2O	4.26	3.57	3.49	3.71	4.82	4.62	4.29	4.45	4.32	4.26
K_2O	3.03	4.12	4.18	3.91	2.35	3.08	3.97	3.62	3.60	3.12
H_2O	0.96	1.16	1.11	0.76	0.81	0.79	0.81	0.70	0.81	1.10
TiO_2	0.17	0.08	0.08	0.08	0.17	0.17	0.38	0.38	0.36	0.29
P_2O_5	0.10	0.06	0.05	0.05	0.10	0.10	0.19	0.17	0.15	0.13
MnO	0.02	0.03	0.02	0.02	0.02	0.03	0.03	0.05	0.04	0.03
S	-	-	-	-	-	-	-	-	-	-
Ba (ppm)	1905	908	839	1028	667	697	1870	1651	2189	3228
Ce	39	69	63	45	17	24	150	143	312	273
Co	22	18	20	26	30	32	32	36	34	38
Cr	196	176	217	174	180	197	162	140	167	169
Cu	24	22	20	21	22	24	20	36	25	27
F	190	310	240	200	380	270	950	830	1160	880
La	32	39	37	32	12	12	77	87	168	157
Li	8	16	12	13	25	22	26	29	30	26
Mn	140	215	183	185	191	243	225	342	284	243
Mo	2	1	3	2	3	3	2	4	4	2
Nb	<10	15	14	10	<10	13	16	13	14	<10
Ni	21	20	22	21	23	24	21	29	26	22
Pb	<10	<10	<10	<10	<10	<10	12	<10	<10	<10
Rb	95	204	204	162	122	143	142	140	156	115
Sn	<5	<5	<5	<5	<5	<5	<5	<5	<5	<5
Sr	413	155	142	236	310	311	781	747	667	680
Th	27	48	49	40	<10	<10	20	13	31	29
U	<1	4	2	2	2	2	2	1	2	1
V	<10	<10	<10	20	15	16	22	19	24	19
W	<6	<2	3	<2	<2	<2	<2	<2	<2	<2
Y	<5	10	10	<5	<5	7	7	10	16	10
Zn	28	26	115	34	52	40	47	58	65	55
Zr	155	126	121	69	113	95	200	208	329	312

SAMPLE	83505	83507	83509	83511	83513	83515	83516	83517	83519	83521
CODE	M32262	M32262	M32261	M32262	M32262	M22262	M32262	M32262	M32262	M32262
CLASS	2	2	2	2	2	2	2	2	2	2
EAST	5522	5522	5652	5652	5652	5605	5620	5620	5635	5635
NORTH	68399	68399	68458	68458	68458	68472	68518	68537	68561	68561
SiO_2 (%)	69.8	70.7	72.0	72.8	73.3	72.3	71.3	70.2	69.1	73.7
Al_2O_3	14.7	14.3	14.6	14.3	14.1	13.4	14.2	14.9	16.2	13.4
Fe_2O_3	1.30	1.10	0.80	0.70	0.60	1.50	1.30	1.20	1.70	0.80
FeO	1.35	1.13	1.02	0.99	0.75	1.33	0.80	1.19	1.63	0.72
MgO	0.55	0.48	0.51	0.40	0.32	0.70	0.63	0.61	0.68	0.26
CaO	1.94	1.89	1.85	1.56	1.51	1.76	1.32	1.72	1.85	1.10
Na_2O	4.18	4.07	4.62	4.54	4.35	3.81	3.55	3.67	3.36	2.98
K_2O	3.16	3.27	2.40	2.84	3.03	2.86	4.31	3.84	4.87	4.81
H_2O	1.07	1.25	0.65	0.59	0.68	0.68	0.99	0.78	0.97	0.66
TiO_2	0.29	0.[illegible]	0.24	0.18	0.16	0.36	0.28	0.31	0.56	0.17
P_2O_5	0.13	0.11	0.12	0.11	0.09	0.17	0.11	0.13	0.28	0.08
MnO	0.03	0.03	0.03	0.03	0.02	0.04	0.02	0.03	0.04	0.02
S	-	-	-	-	-	-	-	-	-	-
Ba (ppm)	2832	2382	1438	963	912	1684	2490	2805	2638	2949
Ce	268	168	55	60	36	233	102	103	222	110
Co	33	34	35	34	31	33	39	40	37	30
Cr	154	152	156	147	153	183	155	154	152	156
Cu	20	19	23	21	20	20	15	28	45	38
F	890	730	360	290	260	870	750	740	1060	370
La	148	96	30	52	22	138	66	62	113	54
Li	29	19	29	20	15	14	10	17	14	5
Mn	252	209	203	223	164	302	159	227	331	138
Mo	3	3	2	1	1	2	1	<1	<1	<1
Nb	13	<10	<10	<10	<10	13	13	10	16	10
Ni	23	19	20	21	20	22	22	27	26	21
Pb	<10	<10	<10	<10	12	<10	<10	<10	<10	<10
Rb	111	89	111	102	112	100	173	158	75	82
Sn	<5	<5	<5	<5	<5	<5	<5	<5	<5	<5
Sr	442	421	371	267	272	392	426	559	926	897
Th	28	25	19	23	17	34	39	44	15	<10
U	1	1	1	1	1	2	2	2	2	1
V	20	16	18	14	13	28	17	22	41	18
W	<2	2	<2	<2	<2	<2	<2	2	<2	<2
Y	10	8	5	8	<5	24	12	8	20	10
Zn	53	41	42	29	24	58	27	38	73	32
Zr	305	227	181	169	127	305	276	225	307	170

SAMPLE	83523	83524	83526	83528	83530	83549	83551	83553	83555	83557
CODE	M32262	M32262	M32262	M32262	S24293	S24172	S14182	S14182	S14182	S14182
CLASS	2	2	2	2	4	4	4	4	4	4
EAST	5637	5648	5648	5648	5730	5258	4271	4267	4263	4255
NORTH	68563	68586	68586	68586	67871	67273	67701	67704	67707	67713
SiO_2 (%)	69.1	69.8	71.8	71.1	72.8	74.3	76.9	77.0	76.1	77.1
Al_2O_3	14.6	15.7	14.9	15.3	13.6	12.9	11.4	11.5	11.7	11.2
Fe_2O_3	1.70	0.80	0.60	0.50	0.80	0.60	0.60	0.70	0.60	0.60
FeO	1.67	1.67	1.03	1.41	1.36	1.10	1.22	1.24	1.36	1.20
MgO	0.67	0.77	0.52	0.66	0.37	0.24	0.13	0.14	0.12	0.12
CaO	1.70	2.59	2.04	2.16	1.24	0.85	0.75	0.81	0.82	0.86
Na_2O	3.61	4.43	4.00	4.19	3.10	3.30	2.93	2.92	2.92	2.86
K_2O	4.05	1.89	2.98	2.48	4.60	4.43	4.29	4.42	4.30	4.07
H_2O	0.89	0.87	0.59	0.69	0.81	0.91	0.60	0.59	0.75	0.70
TiO_2	0.66	0.35	0.23	0.29	0.27	0.17	0.13	0.13	0.15	0.15
P_2O_5	0.20	0.15	0.11	0.13	0.10	0.07	0.06	0.06	0.07	0.05
MnO	0.04	0.03	0.02	0.02	0.04	0.03	0.03	0.03	0.04	0.03
S	-	-	-	-	-	-	-	-	-	-
Ba (ppm)	2737	1050	1167	1014	1073	584	341	417	451	469
Ce	332	85	50	77	177	145	137	-	130	-
Co	45	48	36	44	42	32	28	26	31	30
Cr	146	161	176	174	193	179	221	205	178	201
Cu	33	36	28	21	29	26	34	26	23	25
F	670	740	270	550	1650	1370	1080	1150	870	880
La	182	55	31	42	97	74	74	-	71	-
Li	12	36	20	28	42	53	42	38	8	31
Mn	352	223	125	186	319	215	246	230	319	294
Mo	1	<1	<1	<1	<1	<1	<1	<1	<1	<1
Nb	14	<10	<10	<10	20	21	19	21	18	14
Ni	23	32	27	31	29	22	21	19	22	20
Pb	<10	<10	<10	<10	32	24	48	20	28	24
Rb	95	79	75	77	276	388	234	245	214	196
Sn	<5	<5	<5	<5	<5	<5	<5	<5	<5	<5
Sr	735	523	419	453	158	81	36	37	63	64
Th	31	15	13	12	58	50	36	35	36	30
U	1	1	2	1	2	2	2	2	4	2
V	31	44	19	23	20	10	<10	<10	11	<10
W	<2	<2	<2	<2	2	<2	5	9	12	9
Y	30	<5	<5	<5	34	49	76	77	72	65
Zn	69	61	52	51	51	35	47	38	47	44
Zr	307	242	178	209	286	170	152	159	170	164

SAMPLE	83559	83561	83583	83586	83588	83591	83592	86406	73065A	817028
CODE	S14182	M22272	M12333	S24333	M14293	S24322	S24312	632302	M51012	M32222
CLASS	4	2	2	4	4	4	4	2	1	2
EAST	4260	4520	4974	4974	5877	5156	5627	6738	5007	6586
NORTH	67718	68085	67705	67694	66871	67591	67540	68861	69635	70761
SiO_2 (%)	76.0	73.6	76.6	75.4	76.3	76.9	72.2	71.5	72.8	73.9
Al_2O_3	11.9	13.4	13.1	12.7	12.4	11.8	13.6	15.5	14.2	14.2
Fe_2O_3	0.60	0.50	0.5	1.0	0.4	0.5	0.8	1.1	0.80	0.70
FeO	1.37	1.17	0.63	1.08	0.94	1.46	1.96	0.98	1.08	1.25
MgO	0.13	0.28	0.16	0.18	0.13	0.06	0.26	0.47	0.61	0.65
CaO	0.89	1.05	0.79	0.99	0.63	0.70	2.08	2.09	1.81	2.07
Na_2O	2.96	3.68	3.81	2.95	3.56	2.44	2.90	4.55	3.08	4.40
K_2O	6.29	4.26	4.09	3.82	3.73	4.86	3.99	2.61	3.60	2.63
H_2O	0.63	0.99	0.58	0.86	0.73	0.67	0.77	0.98	0.69	1.03
TiO_2	0.16	0.16	0.10	0.18	0.10	0.13	0.38	0.23	0.16	0.24
P_2O_5	0.06	0.08	0.23	0.24	0.23	0.22	0.32	0.29	0.12	0.12
MnO	0.03	0.04	0.03	0.03	0.04	0.03	0.05	0.02	0.02	0.03
S	-	-	-	-	-	-	-	-	-	-
Ba (ppm)	481	566	570	644	226	896	2129	2308	1287	812
Ce	172	78	-	-	-	-	-	-	42	42
Co	33	35	<5	<5	<5	<5	6	6	36	36
Cr	187	199	<10	<10	<10	<10	<10	<10	245	228
Cu	27	23	<3	6	<3	<3	<3	<3	26	11
F	960	1060	570	781	1364	389	922	356	620	360
La	97	48	-	-	-	-	-	-	24	23
Li	37	67	-	-	-	-	-	-	11	20
Mn	286	316	-	-	-	-	-	-	204	233
Mo	<1	<1	<5	<5	<5	<5	<5	<5	3	2
Nb	17	21	11	20	26	15	27	6	21	10
Ni	23	22	6	9	<5	<5	<5	<5	31	32
Pb	32	28	39	39	40	22	20	16	32	10
Rb	208	399	232	306	446	172	158	72	147	86
Sn	<5	<5	<5	<5	<5	<5	<5	<5	<5	<5
Sr	44	92	89	80	38	60	220	766	272	300
Th	35	45	23	46	38	19	25	<10	23	13
U	1	1	<1	<1	<1	<1	<1	<1	1	<1
V	<10	15	7	20	<5	<5	<5	20	17	28
W	7	<2	2	7	<2	3	6	<2	<2	<2
Y	78	31	4	40	27	69	72	<2	<5	9
Zn	48	37	28	75	33	57	62	18	36	61
Zr	181	153	84	198	111	240	431	317	134	120

SAMPLE	81703A	81705A	81706A	81707A	81708A	81711A	81712A	81714A	81715A	81717A
CODE	G32222	M32222	M32222	G32223	M32223	T13032	T13033	T13033	T13033	M32223
CLASS	2	2	2	2	2	3	3	3	3	2
EAST	6586	6586	6586	6586	6586	6352	6352	6352	6352	6352
NORTH	70761	70761	70761	70761	70761	70288	70284	70288	70273	70273
SiO_2 (%)	70.4	69.8	73.7	67.9	72.1	65.0	66.8	65.4	65.7	72.8
Al_2O_3	14.9	15.2	13.5	15.7	14.4	13.8	13.9	13.9	13.6	13.9
Fe_2O_3	1.90	1.00	0.60	1.40	1.00	2.10	2.00	1.50	1.70	0.70
FeO	1.46	1.46	0.58	1.57	1.11	2.67	2.77	2.83	2.59	1.08
MgO	0.85	0.80	0.16	1.03	0.71	3.82	3.77	3.59	3.48	0.52
CaO	2.42	2.59	1.00	3.00	2.13	4.23	4.65	4.02	4.09	1.24
Na_2O	4.77	4.80	3.36	5.02	4.38	3.65	3.71	3.85	3.69	3.76
K_2O	2.07	1.82	5.14	1.65	2.52	1.40	1.35	1.74	1.68	3.64
H_2O	1.30	1.20	0.92	1.49	1.06	2.29	2.19	1.89	2.10	1.28
TiO_2	0.30	0.32	0.08	0.39	0.27	0.56	0.57	0.49	0.50	0.18
P_2O_5	0.15	0.15	0.07	0.18	0.13	0.19	0.17	0.17	0.18	0.10
MnO	0.06	0.03	0.02	0.05	0.03	0.07	0.07	0.07	0.07	0.03
S	-	-	-	-	-	-	-	-	-	-
Ba (ppm)	605	643	1680	525	780	693	607	679	634	1237
Ce	42	33	38	39	29	45	37	36	43	81
Co	35	33	26	36	30	49	48	46	45	30
Cr	266	180	211	165	174	296	284	282	270	199
Cu	22	18	14	21	11	45	57	33	61	10
F	490	510	130	470	390	380	360	400	430	290
La	27	23	28	26	20	21	25	25	21	46
Li	27	29	6	33	20	7	7	8	7	16
Mn	267	249	101	387	221	503	495	477	508	200
Mo	2	2	3	2	2	3	3	3	3	2
Nb	10	<10	<10	<10	11	<10	11	<10	10	<10
Ni	28	26	22	31	25	112		96	99	26
Pb	20	10	20	10	20	10		20	10	20
Rb	81	76	159	77	87	53		68	63	142
Sn	<5	<5	<5	<5	<5	<5	<5	<5	<5	<5
Sr	317	458	349	496	307	312	290	266	266	267
Th	13	<10	17	<10	13	<10	<10	<10	<10	48
U	<1	<1	2	<1	1	<1	<1	<1	1	4
V	31	34	14	45	26	102	101	91	83	17
W	<2	9	13	5	6	8	11	6	13	<2
Y	11	6	<5	12	14	23	21	20	21	9
Zn	56	63	19	68	46	45	45	47	40	51
Zr	166	125	122	156	128	195	176	167	182	145

SAMPLE	81719A	81720A	81721A	81722A	81723A	81725A	81726A	81729A	81730A	81731A
CODE	M32223	M32222	M32222	J13053	J13053	J13053	J13052	T33043	T33043	T33043
CLASS	2	2	2	3	3	3	3	3	3	3
EAST	6454	6454	6454	6298	6298	6298	6298	6269	6265	6265
NORTH	70590	70590	70590	70364	70364	70364	70364	70357	70359	70359
SiO_2 (%)	73.4	72.3	72.2	76.1	76.0	76.1	76.1	64.8	66.9	66.9
Al_2O_3	13.7	14.1	14.2	12.4	12.6	12.5	12.5	14.9	14.5	14.7
Fe_2O_3	0.80	0.90	0.80	0.50	0.40	0.60	0.40	1.10	1.20	1.20
FeO	0.90	1.20	1.13	1.26	1.54	1.35	1.22	3.56	2.71	2.80
MgO	0.36	0.67	0.54	0.22	0.29	0.27	0.23	2.28	1.82	1.93
CaO	1.26	1.75	1.65	1.39	1.51	1.35	1.35	4.76	3.75	3.37
Na_2O	3.79	6.26	3.97	4.66	4.55	4.49	4.46	3.93	4.06	3.92
K_2O	3.61	2.56	3.07	1.48	1.25	1.38	1.52	1.04	1.56	1.48
H_2O	0.89	1.29	1.16	1.04	1.20	1.47	0.99	2.33	1.81	2.13
TiO_2	0.14	0.26	0.27	0.11	0.13	0.13	0.11	0.45	0.37	0.36
P_2O_5	0.08	0.13	0.11	0.06	0.06	0.05	0.06	0.15	0.13	0.13
MnO	0.03	0.03	0.04	0.03	0.04	0.03	0.03	0.07	0.06	0.06
S	-	-	-	-	-	-	-	-	-	-
Ba (ppm)	1407	813	994	622	548	690	633	467	696	505
Ce	80	64	89	44	48	47	40	25	25	27
Co	32	34	33	29	31	26	27	67	63	62
Cr	177	154	200	322	348	286	237	239	196	230
Cu	12	11	10	12	15	10	13	26	20	16
F	250	420	360	160	170	190	120	220	200	210
La	48	35	52	26	31	36	25	19	16	20
Li	10	28	18	11	16	19	12	33	37	27
Mn	178	251	265	199	240	217	181	524	638	641
Mo	2	2	3	3	2	3	1	4	2	3
Nb	<10	<10	<10	<10	<10	11	<10	<10	<10	<10
Ni	24	27	22	23	22	21	20	67	62	58
Pb	40	20	20	10	10	10	<10	10	10	20
Rb	132	103	115	58	46	60	62	67	69	73
Sn	<5	<5	<5	<5	<5	<5	<5	<5	<5	<5
Sr	267	264	296	132	157	93	136	265	225	229
Th	43	22	35	11	11	11	10	<10	<10	16
U	2	2	2	1	<1	<1	1	1	1	1
V	10	13	30	<10	<10	<10	<10	88	63	65
W	<2	<2	<2	<2	<2	2	<2	<2	2	<2
Y	<5	7	5	11	11	12	13	15	12	12
Zn	50	67	51	32	34	30	31	58	47	44
Zr	153	137	202	118	141	125	128	132	116	122

SAMPLE	81732A	81733A	81734A	81735A	81762A	81763A	81768A	81769A	81772A	81773A
CODE	T33043	T33043	T33043	T33043	T13082	T13082	M13091	M13092	T13092	613J93
CLASS	3	3	3	3	3	3	3	3	3	3
EAST	6316	6316	6303	6302	5865	5872	5900	5900	5910	5904
NORTH	70270	70270	70280	70280	69700	69712	69525	69525	69581	69560
SiO_2 (%)	67.8	68.6	65.4	65.5	66.8	65.1	73.7	72.6	69.6	70.4
Al_2O_3	15.3	15.3	15.1	15.7	15.0	15.1	14.3	14.3	15.0	14.6
Fe_2O_3	1.70	1.50	1.80	1.80	1.80	1.60	0.60	0.60	1.20	1.00
FeO	1.79	1.79	2.60	2.64	2.51	3.04	0.82	1.02	1.61	1.63
MgO	0.96	0.86	1.67	1.51	1.92	2.20	0.40	0.50	1.05	0.91
CaO	3.42	3.27	4.12	4.65	4.11	4.81	1.88	1.92	2.76	2.61
Na_2O	4.40	4.27	4.29	4.30	4.34	4.24	4.81	4.90	4.76	4.70
K_2O	1.13	1.26	0.86	0.73	1.12	0.88	2.04	2.03	1.90	1.71
H_2O	2.22	1.79	2.86	2.41	1.10	1.28	0.69	1.14	0.93	1.38
TiO_2	0.35	0.33	0.42	0.45	0.43	0.45	0.15	0.18	0.35	0.30
P_2O_5	0.15	0.14	0.14	0.17	0.15	0.16	0.10	0.09	0.19	0.19
MnO	0.05	0.05	0.06	0.07	0.07	0.07	0.02	0.02	0.04	0.04
S	-	-	-	-	-	-	-	-	-	-
Ba (ppm)	495	464	499	396	533	529	635	570	730	728
Ce	28	26	34	20	33	24	27	28	50	59
Co	43	40	41	43	45	50	34	33	39	38
Cr	180	180	178	140	186	186	193	216	199	223
Cu	24	25	165	69	25	29	17	20	23	22
F	230	250	220	330	330	190	240	470	430	660
La	16	17	9	13	16	17	15	17	33	31
Li	16	11	22	21	5	13	52	63	31	27
Mn	398	383	420	496	451	556	169	168	276	227
Mo	2	2	2	1	1	1	2	1	1	3
Nb	<10	<10	<10	<10	<10	<10	<10	<10	<10	<10
Ni	33	27	35	36	44	65	25	26	35	32
Pb	10	<10	10	20	20	20	20	<10	30	20
Rb	55	51	43	36	55	61	87	97	78	78
Sn	<5	<5	5	<5	<5	<5	<5	<5	<5	<5
Sr	306	287	339	329	171	187	255	256	460	496
Th	<10	<10	<10	<10	<10	<10	<10	11	<10	12
U	1	1	<1	<1	<1	<1	<1	1	4	1
V	69	66	76	71	67	78	15	15	52	53
W	<2	<2	<2	<2	<2	3	<2	<2	2	<2
Y	11	12	13	16	26	29	<5	5	8	7
Zn	66	58	53	52	63	69	34	48	53	51
Zr	125	121	122	122	137	144	115	117	150	169

SAMPLE	81774A	81776A	83233A	83269A	83242A	83243A	83246A	83266A	83269A	83250A
CODE	G13092	M32242	M13102	T13113	T13113	T13113	T13113	T13122	T13122	M32232
CLASS	3	2	3	3	3	3	3	3	3	2
EAST	5904	5909	6123	6285	6288	6288	6289	5940	5950	5865
NORTH	69540	69338	69975	70026	70040	70040	70037	70414	70418	70396
SiO_2 (%)	69.4	73.4	72.2	64.3	66.4	64.9	65.3	65.7	64.5	71.7
Al_2O_3	15.1	13.7	14.7	14.1	14.3	14.1	14.4	14.3	14.3	14.8
Fe_2O_3	1.10	0.80	0.40	1.30	1.50	1.70	1.00	1.90	2.30	0.70
FeO	1.46	0.93	1.27	3.68	0.75	3.14	1.90	2.63	2.60	0.97
MgO	0.99	0.32	0.59	3.76	3.19	3.47	3.83	2.45	2.64	0.38
CaO	2.51	1.37	1.95	4.45	5.90	4.67	5.39	3.56	3.96	1.94
Na_2O	4.79	3.71	4.80	3.83	5.30	3.73	5.01	4.06	3.90	4.78
K_2O	2.18	3.39	1.99	1.13	0.26	1.27	0.46	2.36	2.65	2.58
H_2O	0.97	0.94	0.83	1.82	1.02	1.96	1.54	1.25	1.40	0.94
TiO_2	0.37	0.19	0.19	0.53	0.50	0.53	0.50	0.50	0.52	0.15
P_2O_5	0.20	0.08	0.09	0.18	0.16	0.19	0.18	0.26	0.27	0.12
MnO	0.04	0.02	0.03	0.06	0.03	0.05	0.03	0.07	0.06	0.03
S	-	-	-	-	-	-	-	-	-	-
Ba (ppm)	856	1407	531	499	211	632	228	1079	1058	929
Ce	76	75	27	34	26	31	31	80	86	26
Co	38	32	35	68	37	47	41	43	45	31
Cr	173	147	208	313	350	299	302	231	218	217
Cu	26	8	26	14	10	16	13	30	31	14
F	220	450	340	280	270	300	330	1260	860	620
La	38	46	16	20	18	19	16	45	42	18
Li	30	26	68	18	3	19	5	61	23	28
Mn	242	167	205	468	213	375	283	485	502	214
Mo	1	<1	<1	1	1	1	2	2	2	2
Nb	<10	10	<10	<10	<10	<10	<10	10	11	10
Ni	30	25	26	110	83	102	119	69	72	22
Pb	20	40	20	10	10	<10	10	40	40	20
Rb	71	180	89	42	7	40	17	127	102	97
Sn	<5	<5	<5	<5	<5	<5	<5	<5	<5	<5
Sr	620	181	391	265	298	305	318	399	440	363
Th	23	36	<10	<10	<10	<10	<10	20	17	<10
U	1	1	4	<1	<1	1	<1	2	2	<1
V	44	<10	17	100	76	98	98	76	81	13
W	<2	4	<2	<2	<2	<2	<2	4	<2	<2
Y	6	6	<5	19	21	20	21	13	14	12
Zn	56	63	60	34	11	23	17	55	57	31
Zr	183	155	113	144	185	160	174	146	153	106

SAMPLE	83256A	83258A	83293A	83338A	83309A	83310A	83311A	83320A	83323A	83324A
CODE	M22232	M22232	M32252	S32261	M32262	M32262	G22263	T33133	M13142	M13142
CLASS	2	2	2	2	2	2	2	3	3	3
EAST	5789	5532	5137	5473	5477	5500	5593	5794	5776	5776
NORTH	70638	70768	69379	69207	69204	69204	69116	68891	68862	68858
SiO_2 (%)	70.6	68.2	73.4	67.2	73.5	62.6	70.0	66.9	70.0	71.2
Al_2O_3	15.1	15.5	14.4	14.4	13.4	16.7	15.1	14.2	14.8	14.9
Fe_2O_3	1.00	0.90	0.30	1.70	0.60	2.70	0.70	1.00	1.60	1.10
FeO	1.52	2.46	1.31	2.12	0.76	3.60	1.41	2.16	0.99	0.95
MgO	0.66	0.91	0.35	1.64	0.21	1.67	0.67	2.22	0.63	0.68
CaO	2.41	2.82	1.53	2.56	0.99	3.73	2.22	2.95	1.77	1.90
Na_2O	4.41	4.59	4.88	3.04	3.51	4.11	4.65	4.53	5.04	4.88
K_2O	2.48	2.29	2.41	5.63	4.96	2.55	2.45	2.03	2.63	2.25
H_2O	0.81	0.96	0.58	0.91	0.62	1.50	1.48	2.56	0.75	1.13
TiO_2	0.30	0.44	0.16	0.60	0.11	1.25	0.30	0.33	0.33	0.26
P_2O_5	0.14	0.22	0.09	0.33	0.08	0.68	0.12	0.21	0.22	0.14
MnO	0.03	0.04	0.06	0.09	0.02	0.07	0.02	0.05	0.04	0.03
S	-	-	-	-	-	-	-	-	-	-
Ba (ppm)	1260	752	902	3463	856	1886	716	1121	1365	1198
Ce	63	123	38	205	47	322	48	72	126	63
Co	32	38	25	39	27	45	32	40	34	38
Cr	217	221	207	162	235	209	185	265	188	205
Cu	18	22	10	21	9	31	16	20	18	18
F	430	700	680	930	100	1810	400	600	960	630
La	44	74	18	111	29	155	31	44	65	41
Li	19	25	52	10	5	25	18	24	69	46
Mn	192	276	283	635	96	507	138	361	248	213
Mo	2	2	2	2	3	3	<1	2	2	2
Nb	<10	16	16	16	<10	20	12	10	13	<10
Nd	27	32	21	31	19	30	22	58	22	21
Pb	20	20	40	50	30	30	20	30	40	30
Rb	73	98	212	158	145	61	98	92	107	88
Sn	<5	<5	<5	<5	<5	<5	<5	<5	<5	<5
Sr	413	244	199	568	167	911	266	537	726	622
Th	10	27	18	55	27	20	17	22	18	<10
U	1	1	2	4	2	2	1	2	2	1
V	26	66	13	64	<10	78	28	63	30	20
W	<2	2	<2	<2	<2	<2	<2	3	<2	<2
Y	9	20	8	29	9	32	11	9	8	<5
Zn	38	67	35	63	15	126	55	40	58	46
Zr	191	360	136	265	125	403	199	133	164	153

SAMPLE	83325A	83406A	83409A	83410A	84429	84430	84431	84432	84433
CODE	M33162	M14161	M14161	M14161	S24002	T13003	S24001	M23003	M24002
CLASS	3	4	4	4	4	3	4	3	4
EAST	5682	4531	4707	4711	3565	3934	4032	3776	3842
NORTH	68857	67707	67598	67596	68881	69060	69199	69083	69139
SiO_2 (%)	70.8	70.9	70.4	70.6	70.6	65.2	75.0	71.7	68.4
Al_2O_3	15.2	13.6	13.2	13.1	12.8	16.0	12.6	14.5	12.8
Fe_2O_3	0.90	1.10	1.20	1.00	1.4	1.5	0.9	1.0	1.6
FeO	1.21	3.66	3.56	3.56	2.93	2.68	1.15	1.22	3.92
MgO	0.53	0.55	0.47	0.31	0.52	1.96	0.16	0.60	0.52
CaO	1.44	2.54	2.59	2.55	2.01	3.82	1.04	1.76	2.60
Na_2O	4.77	2.98	2.90	2.95	2.66	4.72	3.32	4.20	2.70
K_2O	2.68	3.69	3.38	3.43	4.42	0.91	4.70	3.73	4.54
H_2O	0.90	0.62	0.58	0.59	0.85	2.66	0.76	1.08	1.41
TiO_2	0.29	0.54	0.51	0.51	0.59	0.62	0.17	0.24	0.70
P_2O_5	0.13	0.20	0.20	0.18	0.18	0.11	0.05	0.10	0.24
MnO	0.03	0.09	0.09	0.09	0.08	0.06	0.05	0.03	0.16
S	-	-	-	-	-	-	-	-	-
Ba (ppm)	1249	1657	1659	1660	2153	323	807	1222	2252
Ce	77	130	135	139	167	15	210	72	371
Co	40	35	34	31	10	16	3	7	10
Cr	209	190	212	212	<10	16	<10	12	<10
Cu	18	13	17	13	7	24	2	10	4
F	580	990	900	820	769	178	1662	451	1884
La	43	67	70	75	111	8	117	38	181
Li	34	23	21	25	28	18	42	12	14
Mn	171	640	682	667	-	-	-	-	-
Mo	2	3	5	5	<5	<5	<5	<5	<5
Nb	<10	22	20	20	24	5	32	10	47
Ni	28	26	27	30	6	20	4	6	2
Pb	40	40	30	30	30	<15	60	30	30
Rb	87	149	142	137	133	31	270	175	171
Sn	<5	<5	<5	<5	<10	<10	<10	<10	<10
Sr	599	213	215	208	176	609	106	343	262
Th	<10	11	18	17	<10	<10	46	23	28
U	1	2	4	4	1	<1	4	4	2
V	22	25	<10	<10	19	73	10	30	34
W	<2	<2	5	8	<10	<10	<10	<10	<10
Y	<5	62	65	64	63	8	65	8	121
Zn	70	97	101	112	82	60	56	38	130
Zr	163	449	435	428	583	122	250	186	914

SAMPLE	84435	84436
CODE	S24002	T13001
CLASS	4	3
EAST	4031	4120
NORTH	69830	69915
SiO_2 (%)	72.8	67.3
Al_2O_3	13.0	14.5
Fe_2O_3	1.2	1.2
FeO	1.68	3.17
MgO	0.52	1.24
CaO	1.52	3.68
Na_2O	3.00	3.52
K_2O	4.64	2.52
H_2O	0.80	1.26
TiO_2	0.41	0.41
P_2O_5	0.14	0.11
MnO	0.06	0.07
S	-	-
Ba (ppm)	1626	960
Ce	242	61
Co	7	14
Cr	<10	20
Cu	40	14
F	1475	698
La	138	33
Li	30	54
Mn	-	-
Mo	<5	<5
Nb	26	10
Ni	4	15
Pb	40	20
Rb	233	111
Sn	<10	<10
Sr	199	173
Th	45	15
U	2	1
V	19	55
W	<10	<10
Y	79	22
Zn	52	54
Zr	329	204

DATA FILE II.3

ANALYSES OF BANDED IRON-FORMATION

DATA FILE II.3 -- Analyses of Banded Iron-Formation

Results are presented by traverse number.

Data headings:

SAMPLE - Geological Survey of Western Australia sample number

CODE - the code has six characters and is the same as that in the volcanic rocks data file, except that there are only three rock types:

H quartz - hematite - magnetite banded iron-formation

J jaspilitic banded iron-formation

I ferruginous chert or undivided banded iron-formation

TRAVERSE - traverse locations are shown on Figure AII.1

Eastings and Northings and rock analyses are expressed in the same way as in previous data files.

SAMPLE	73695	73696	73697	73698	73699	73700	74443	74444	74445	74446
CODE	H61B33	H61B33	H61B33	H61B33	H61B33	H61B33	H36B32	H36B32	H36B32	H36B32
TRAVERSE	61	61	61	61	61	61	36	36	36	36
EAST	5898	5898	5901	5898	5898	5898	5866	5866	5866	5866
NORTH	68976	68972	68975	68976	68976	68976	69429	69429	69429	69429
SiO_2 (%)	38.8	39.4	38.3	33.4	44.7	48.1	45.6	47.2	45.5	52.9
Al_2O_3	0.1	0.2	0.1	0.1	0.1	0.2	0.1	<0.1	<0.1	<0.1
Fe_2O_3	57.6	53.2	49.3	60.0	51.3	48.4	49.4	49.0	50.0	42.8
FeO	0.62	2.56	0.45	0.73	0.66	0.75	1.60	0.90	1.90	1.94
MgO	0.10	1.76	1.95	0.04	0.03	0.02	0.10	0.06	0.02	0.02
CaO	0.11	1.71	3.14	0.08	<0.01	0.02	0.07	0.03	0.04	0.03
Na_2O	0.01	0.02	0.01	0.01	0.01	0.02	0.03	0.02	0.03	0.01
K_2O	<0.01	0.01	<0.01	<0.01	<0.01	<0.01	<0.01	<0.01	0.05	<0.01
H_2O	1.83	1.42	5.86	4.80	2.61	2.08	2.42	1.91	1.88	1.72
TiO_2	<0.01	<0.01	<0.01	<0.01	<0.01	<0.01	<0.01	<0.01	<0.01	<0.01
P_2O_5	0.14	0.06	0.19	0.10	0.15	0.16	0.07	0.07	0.01	0.08
MnO	0.02	0.03	0.07	0.11	0.02	0.01	0.01	0.01	0.01	0.01
S	0.008	0.010	0.026	0.046	0.016	0.010	0.009	0.009	0.018	0.011
As (ppm)	-	-	-	-	-	-	-	-	-	-
Au	-	-	-	-	-	-	-	-	-	-
Ba	<20	<20	<20	<20	<20	<20	<10	<10	<10	<10
Ce	10	<5	<5	15	<5	5	<10	<10	<10	<10
Co	45	47	36	50	51	98	<5	39	<5	65
Cr	13	<5	<5	<5	22	<5	550	<10	566	<10
Cu	67	38	152	56	36	143	60	30	64	34
La	7	<5	6	10	7	11	<10	<10	<10	<10
Li	3	1	5	1	2	2	<1	<1	<1	<1
Mn	100	190	510	770	120	50	-	-	-	-
Nb	<5	<5	<5	<5	<5	<5	<5	<5	<5	<5
Ni	<5	<5	<5	<5	<5	<5	20	9	16	7
Pb	<10	<10	<10	<10	<10	<10	15	11	<10	<10
Rb	<2	<2	<2	<2	<2	<2	<5	<5	<5	<5
Sr	3	3	7	<2	<2	<2	<5	<5	<5	<5
Th	<5	<5	<5	<5	<5	<5	<5	6	9	8
V	10	11	<5	12	21	13	8	<5	<5	<5
Y	5	4	5	8	7	5	5	5	<5	5
Zn	34	32	26	151	129	89	20	23	14	47
Zr	7	14	25	9	14	12	<10	<10	<10	<10

SAMPLE	74467	74468	74469	74470	74520	74521	74522	74523	74524	74525
CODE	H36832	H36832	H36832	H36832	J61D31	J61D11	J61D11	J61D11	J61D11	J61D11
TRAVERSE	36	36	36	36	61	61	61	61	61	61
EAST	5866	5866	5866	5866	5151	5151	5151	5151	5151	5151
NORTH	69429	69429	69429	69429	67284	67284	67284	67284	67284	67284
SiO_2 (%)	49.0	44.0	48.2	49.9	43.9	55.6	45.3	44.3	39.4	44.5
Al_2O_3	<0.1	<0.1	<0.1	<0.1	3.6	2.3	2.2	1.8	1.4	0.2
Fe_2O_3	46.1	53.4	44.4	44.0	35.2	21.3	21.6	21.3	17.0	30.6
FeO	1.18	0.49	4.13	1.08	3.91	8.87	13.1	18.1	21.7	16.2
MgO	0.01	0.01	0.02	0.01	1.84	2.66	6.20	4.13	5.89	1.85
CaO	0.03	0.05	0.02	0.03	0.11	0.22	0.16	0.23	0.78	1.36
Na_2O	0.03	0.01	0.02	0.02	0.44	0.15	0.14	0.06	0.17	0.03
K_2O	0.01	<0.01	<0.01	0.03	0.08	<0.01	0.06	0.02	0.07	0.04
H_2O	2.63	1.76	2.22	3.95	8.89	7.51	9.22	8.96	12.3	4.07
TiO_2	0.01	<0.01	<0.01	<0.01	0.13	0.08	0.07	0.05	0.06	0.01
P_2O_5	0.14	0.06	0.05	0.08	0.25	0.23	0.16	0.17	0.16	0.17
MnO	0.01	0.01	0.01	0.01	0.05	0.24	0.30	0.26	0.39	0.18
S	0.007	0.016	0.011	0.020	1.05	0.63	0.53	0.13	0.16	0.06
As (ppm)	-	-	-	-	64	18	29	10	23	8
Au	-	-	-	-	<0.1	<0.1	<0.1	<0.1	<0.1	<0.1
Ba	<10	<10	<10	<10	38	27	41	43	42	29
Ce	14	<10	<10	<10	20	21	23	<15	<15	<15
Co	<5	49	<5	47	-	-	-	-	-	-
Cr	555	<10	604	<10	160	116	76	66	47	18
Cu	47	41	47	43	96	22	96	20	34	10
La	<10	15	<10	<10	28	28	22	28	25	24
Li	<1	<1	<1	<1	2	4	2	6	2	<2
Mn	-	-	-	-	-	-	-	-	-	-
Nb	<5	<5	<5	<5	<5	<5	<5	<5	<5	<5
Ni	32	<5	6	18	130	60	40	30	25	5
Pb	<10	<10	<10	<10	<15	15	<15	<15	<15	<15
Rb	<5	<5	<5	<5	7	<5	7	8	12	7
Sr	<5	<5	<5	<5	8	8	<5	8	10	5
Th	5	5	9	<5	<10	<10	<10	<10	<10	<10
V	<5	<5	<5	<5	66	44	39	29	25	<5
Y	<5	<5	<5	<5	12	12	13	6	7	5
Zn	27	17	28	48	36	28	38	32	30	28
Zr	<10	<10	<10	<10	37	34	20	16	19	<10

SAMPLE	74526	74527	74528	74529	74530	74531	74532	81101	81102	81103
CODE	J61D11	J61D11	J61D11	J61D11	J61D11	J61D11	J61D11	M61833	M61833	M61833
TRAVERSE	61	61	61	61	61	61	61	61	61	61
EAST	5151	5151	5151	5151	5151	5151	5151	5898	5898	5898
NORTH	67284	67284	67284	67284	67284	67284	67284	68974	68974	68974
SiO_2 (%)	41.1	42.7	40.6	40.2	48.5	45.7	46.6	42.2	52.1	43.2
Al_2O_3	0.2	0.6	0.5	0.2	0.1	2.3	0.1	0.1	0.1	0.4
Fe_2O_3	30.6	27.4	20.1	21.2	27.4	25.1	31.5	51.4	44.1	52.0
FeO	19.2	20.6	18.8	19.9	16.0	16.8	14.9	2.26	1.74	0.83
MgO	1.78	3.49	4.10	3.07	4.43	4.79	1.80	0.02	0.02	0.03
CaO	0.18	0.24	0.68	1.84	0.18	0.46	1.76	0.01	0.02	0.06
Na_2O	0.02	0.03	0.05	0.03	0.03	0.03	0.10	0.01	0.02	0.03
K_2O	<0.01	0.04	0.09	0.03	<0.01	<0.01	0.09	<0.01	<0.01	<0.01
H_2O	5.75	3.34	12.6	11.7	2.32	3.57	2.47	3.30	1.91	2.49
TiO_2	<0.01	0.02	0.01	<0.01	<0.01	0.11	<0.01	<0.01	<0.01	0.01
P_2O_5	0.18	0.16	0.39	0.32	0.16	0.28	0.17	0.12	0.07	0.06
MnO	0.27	0.09	0.38	0.39	0.06	0.07	0.11	0.03	0.04	0.01
S	0.03	0.26	0.89	0.11	0.02	0.05	0.02	0.014	0.020	0.026
As (ppm)	6	14	44	6	2	8	<1	-	-	-
Au	<0.1	<0.1	<0.1	<0.1	<0.1	<0.1	<0.1	-	-	-
Ba	<25	26	33	<25	<25	<25	117	<20	<20	70
Ce	<15	17	<15	<15	15	32	<15	5	5	16
Co	-	-	-	-	-	-	-	65	95	83
Cr	11	11	<10	<10	<10	115	51	7	15	27
Cu	16	20	7	6	5	12	10	38	39	52
La	26	19	24	20	25	40	22	5	12	10
Li	<2	<2	<2	<2	<2	2	<2	1	1	1
Mn	-	-	-	-	-	-	-	230	280	90
Nb	<5	<5	<5	<5	<5	<5	<5	<5	<5	<5
Ni	5	10	25	10	<5	65	5	<5	<5	13
Pb	<15	<15	<15	<15	<15	<15	<15	80	<10	<10
Rb	<5	6	9	6	<5	5	21	<2	<2	<2
Sr	<5	<5	5	<5	<5	12	33	<2	<2	3
Th	<10	<10	<10	<10	<10	<10	<10	<5	<5	<5
V	<5	13	9	<5	<5	33	15	11	7	26
Y	5	7	11	8	4	7	5	6	6	5
Zn	30	32	30	30	36	38	32	554	94	73
Zr	11	13	11	<10	<10	37	<10	<5	<5	12

SAMPLE	81104	81105	81106	81107	81163	81164	81165	81166	81167	81168
CODE	H41B33	H41B33	H41B33	H41B33	J43D32	J43D32	J43D32	J43D32	J43D32	J43D32
TRAVERSE	41	41	41	41	43	43	43	43	43	43
EAST	5898	5893	5890	5889	5807	5807	5807	5807	5807	5807
NORTH	68974	68978	68975	68973	68991	68991	68991	68991	68991	68991
SiO_2 (%)	51.5	39.7	35.3	65.9	63.5	64.2	50.4	61.3	66.5	66.1
Al_2O_3	0.1	0.1	0.1	0.2	0.5	0.2	0.3	0.2	0.2	0.2
Fe_2O_3	44.4	55.5	53.3	49.4	31.6	30.6	46.8	36.8	29.7	49.3
FeO	1.76	0.99	5.59	3.59	1.66	2.37	0.55	0.31	0.83	1.09
MgO	0.08	0.01	0.05	0.02	0.26	0.08	0.03	0.03	0.03	0.02
CaO	<0.01	0.01	0.01	0.01	0.30	0.04	0.03	0.01	0.03	0.01
Na_2O	0.08	0.01	0.05	<.01	0.05	0.01	0.01	<.01	0.01	<.01
K_2O	<0.01	<0.01	<0.01	0.01	<0.01	<0.01	<0.01	<0.01	<0.01	<0.01
H_2O	1.36	2.78	4.77	0.97	1.18	1.28	0.99	0.52	1.53	2.13
TiO_2	<0.01	<0.01	<0.01	<0.01	0.02	<0.01	0.01	<0.01	<0.01	<0.01
P_2O_5	0.04	0.13	0.14	0.05	0.17	0.11	0.10	0.11	0.08	0.08
MnO	0.01	0.01	0.07	0.01	0.02	0.01	0.01	0.01	0.01	0.01
S	0.306	0.016	0.010	0.008	0.009	0.010	0.016	0.006	0.018	0.026
As (ppm)	-	-	-	-	-	-	-	-	-	-
Au	-	-	-	-	-	-	-	-	-	-
Ba	<20	<20	<20	<20	<20	<20	<20	29	27	<20
Ce	<5	12	18	<5	7	<5	<5	6	<5	<5
Co	124	60	57	92	37	51	63	54	60	33
Cr	<5	<5	<5	5	12	21	9	<5	<5	5
Cu	61	35	43	40	72	85	76	59	81	68
La	<5	10	12	8	6	7	<5	9	5	7
Li	<1	1	1	1	1	1	1	<1	1	1
Mn	70	70	560	40	120	100	60	40	100	80
Nb	<5	<5	<5	<5	6	<5	<5	<5	<5	<5
Ni	<5	<5	<5	<5	<5	<5	<5	<5	<5	<5
Pb	<10	<10	<10	<10	<10	<10	<10	<10	<10	<10
Rb	<2	<2	<2	<2	<2	<2	<2	<2	<2	<2
Sr	<2	<2	2	2	4	<2	<2	9	<2	2
Th	<5	7	<5	<5	<5	<5	<5	<5	<5	<5
V	<5	8	5	7	15	5	11	7	5	7
Y	<2	7	6	6	4	3	4	4	3	4
Zn	25	65	120	28	25	21	17	20	19	19
Zr	7	53	12	<5	15	10	11	5	<5	6

SAMPLE	81169	81170	81171	81172	81173	81174	81175	81176	81177	81178
CODE	J43D32	J43D32	J43D32	H42B32	H42B32	H42B32	H42B32	H42B32	H42B32	H42B32
TRAVERSE	43	43	43	42	42	42	42	42	42	42
EAST	5807	5807	5807	5764	5765	5765	5766	5766	5766	5767
NORTH	68991	68991	68991	68987	68989	68990	68992	68992	68993	68995
SiO_2 (%)	57.0	50.4	59.8	53.5	50.7	50.6	76.7	68.2	62.0	65.0
Al_2O_3	0.2	0.2	0.4	0.2	0.2	0.2	0.1	0.2	0.1	0.3
Fe_2O_3	39.4	46.2	36.8	42.4	46.7	46.6	20.4	44.8	53.5	48.8
FeO	0.61	0.52	0.58	0.80	0.42	1.07	0.65	1.13	0.62	0.34
MgO	0.02	0.03	0.02	0.01	0.01	0.01	0.01	0.21	0.02	0.03
CaO	0.02	0.02	0.01	0.01	0.01	0.02	0.03	0.04	0.01	0.07
Na_2O	<.01	<.01	0.01	<.01	<.01	<.01	<.01	0.01	<.01	<.01
K_2O	<0.01	<0.01	0.03	<0.01	<0.01	<0.01	<0.01	0.01	0.01	0.01
H_2O	1.91	1.91	1.57	2.56	1.54	1.06	1.20	6.79	3.20	5.05
TiO_2	<0.01	<0.01	<0.01	<0.01	<0.01	<0.01	<0.01	<0.01	<0.01	<0.01
P_2O_5	0.13	0.07	0.13	0.13	0.06	0.08	0.07	0.15	0.11	0.16
MnO	0.01	0.02	0.01	<0.01	0.01	0.01	<0.01	0.03	0.01	0.02
S	0.018	0.020	0.016	0.016	0.020	0.010	0.012	0.042	0.014	0.052
As (ppm)	-	-	-	-	-	-		-	-	-
Au	-	-	-	-	-	-	-	-	-	-
Ba	<20	<20	51	<20	342	90	<20	<20	<20	<20
Ce	25	<5	7	<5	<5	<5	11	<5	<5	5
Co	45	51	46	33	40	49	54	28	29	26
Cr	38	14	<5	33	20	41	21	44	6	6
Cu	63	23	27	40	33	25	31	33	24	23
La	10	<5	9	9	9	10	11	<5	10	8
Li	1	1	1	1	1	1	2	3	2	2
Mn	70	160	90	60	110	80	60	260	90	140
Nb	<5	<5	<5	<5	<5	5	<5	<5	<5	<5
Ni	<5	<5	<5	<5	<5	20	10	20	<5	<5
Pb	<10	<10	<10	<10	<10	<10	<10	<10	<10	<10
Rb	<2	<2	<2	<2	<2	<2	<2	<2	<2	<2
Sr	2	<2	2	<2	<2	<2	5	<2	<2	2
Th	<5	<5	<5	<5	<5	<5	<5	<5	<5	<5
V	11	13	12	7	12	12	10	11	5	8
Y	5	3	8	8	2	6	6	6	3	5
Zn	19	22	22	47	16	22	19	42	40	35
Zr	10	24	7	6	5	<5	<5	12	5	17

SAMPLE	81179	81180	81181	81182	81183	81184	81185	81186	81187	81188
CODE	H42B32	H42B32	H42B32	H44B32	H44B32	H44B32	H44B32	H44B32	H44B32	H44B32
TRAVERSE	42	42	42	44	44	44	44	44	44	44
EAST	5767	5767	5782	5761	5761	5761	5761	5761	5761	5761
NORTH	68995	68996	68996	68975	68975	68975	68975	68975	68975	68975
SiO_2 (%)	45.7	67.2	48.5	50.6	45.6	55.6	49.9	59.9	49.0	55.8
Al_2O_3	0.2	0.2	0.2	0.2	0.3	0.2	0.1	0.1	0.1	0.1
Fe_2O_3	47.4	30.0	47.3	46.4	47.9	41.5	47.7	36.4	43.5	39.7
FeO	0.50	0.56	2.27	0.38	0.62	0.50	0.37	0.95	2.97	0.48
MgO	0.02	0.02	0.02	0.01	0.02	0.03	0.02	0.01	0.03	0.01
CaO	0.10	0.03	0.04	(0.01	0.01	0.01	0.01	0.01	0.02	(0.01
Na_2O	(.01	(.01	(.01	(.01	(.01	(.01	(.01	(.01	0.01	(.01
K_2O	(0.01	0.01	(0.01	(0.01	(0.01	(0.01	(0.01	0.01	(0.01	(0.01
H_2O	5.29	1.89	1.79	2.14	5.05	1.95	1.67	1.80	3.88	3.58
TiO_2	(0.01	(0.01	(0.01	(0.01	(0.01	(0.01	(0.01	(0.01	(0.01	(0.01
P_2O_5	0.16	0.09	0.08	0.14	0.20	0.10	0.10	0.11	0.10	0.07
MnO	0.01	(0.01	0.01	(0.01	(0.01	0.02	0.02	0.01	0.01	0.01
S	0.064	0.014	0.024	0.012	0.016	0.016	0.014	0.082	0.006	0.026
As (ppm)	-	-	-	-	-	-	-	-	-	-
Au	-	-	-	0.03	0.02	0.02	(0.01	0.02	(0.01	0.33
Ba	(20	(20	(20	(20	69	52	(20	(20	(20	(20
Ce	(5	(5	(5	(5	6	8	14	8	(5	(5
Co	38	75	55	50	38	54	62	84	20	68
Cr	(5	(5	11	(5	8	267	18	(5	(5	(5
Cu	40	75	68	26	27	33	28	32	45	21
La	7	7	5	5	7	9	(5	8	8	6
Li	1	2	1	2	1	2	2	1	1	1
Mn	70	40	50	30	30	120	60	80	100	60
Nb	(5	(5	(5	(5	(5	(5	(5	(5	(5	(5
Ni	10	10	(5	(5	10	(5	(5	(5	(5	(5
Pb	(10	(10	(10	(10	(10	(10	(10	(10	(10	(10
Rb	(2	(2	(2	(2	(2	(2	(2	(2	(2	(2
Sr	(2	(2	2	(2	2	(2	(2	(2	(2	(2
Th	(5	(5	(5	(5	(5	(5	(5	(5	(5	(5
V	6	19	10	(5	10	6	7	(5	(5	5
Y	7	4	3	5	12	4	4	5	5	5
Zn	31	30	27	41	53	41	28	46	102	29
Zr	15	10	18	11	8	(5	(5	6	15	(5

SAMPLE	81237	81238	81239	81240	81241	81242	81243	81244	81284	81285
CODE	J47D32	J47D32	J47D32	J47D32	J47D32	J47D32	J47D32	J47D32	J48D32	J48D32
TRAVERSE	47	47	47	47	47	47	47	47	48	48
EAST	6620	6620	6620	6620	6629	6621	6621	6621	6292	6292
NORTH	70070	70070	70070	70070	70037	70034	70034	70034	69940	69940
SiO_2 (%)	55.1	47.5	44.3	52.3	43.7	44.3	42.3	40.7	43.2	48.1
Al_2O_3	0.3	0.4	0.7	0.7	0.2	0.2	0.4	0.3	0.2	<0.1
Fe_2O_3	40.7	49.6	52.3	44.1	52.9	52.1	54.9	56.5	52.6	49.2
FeO	0.54	0.63	0.56	0.56	1.15	1.37	0.62	1.88	0.57	0.61
MgO	0.04	0.02	0.02	0.02	0.09	0.02	0.01	0.02	0.02	0.01
CaO	<0.01	0.01	0.01	0.01	0.08	0.04	0.01	0.05	0.03	0.03
Na_2O	0.01	0.00	0.01	0.00	0.00	0.00	0.01	0.01	0.01	0.01
K_2O	<0.01	0.01	0.03	<0.01	<0.01	<0.01	0.01	<0.01	<0.01	<0.01
H_2O	2.42	1.20	1.38	1.57	1.46	1.64	1.27	1.71	3.13	1.72
TiO_2	<0.01	0.01	0.01	0.02	0.01	<0.01	<0.01	<0.01	<0.01	<0.01
P_2O_5	0.29	0.21	0.14	0.24	0.14	0.08	0.11	0.17	0.09	0.10
MnO	0.01	0.01	0.01	<0.01	<0.01	<0.01	<0.01	<0.01	0.16	0.15
S	0.021	0.020	0.057	0.011	0.065	0.037	0.022	0.060	0.025	0.021
As (ppm)	-	-	-	-	-	-	-	-	-	-
Au	-	-	-	-	-	-	-	-	-	-
Ba	<20	<20	<20	<20	21	43	104	<20	<20	34
Ce	5	11	5	<5	<5	5	<5	12	11	<5
Co	90	71	76	83	70	90	81	75	52	62
Cr	<5	<5	<5	23	23	<5	10	<5	5	19
Cu	94	45	50	100	37	33	66	37	72	26
La	8	8	7	9	14	12	8	7	5	6
Li	1	1	1	1	1	1	1	1	3	2
Mn	90	60	80	30	40	40	40	40	120	90
Nb	<5	7	5	<5	<5	<5	7	5	<5	<5
Ni	<5	<5	<5	<5	<5	<5	<5	10	10	20
Pb	<10	<10	<10	<10	<10	<10	<10	<10	<10	<10
Rb	<2	<2	<2	<2	<2	<2	<2	<2	<2	<2
Sr	2	3	15	2	4	3	2	8	<2	<2
Th	<5	<5	<5	<5	<5	<5	<5	<5	<5	<5
V	11	16	8	20	24	11	32	17	56	22
Y	7	3	4	8	5	6	5	4	4	4
Zn	35	19	15	33	19	48	76	139	77	79
Zr	12	7	<5	17	6	<5	14	6	6	<5

SAMPLE	81354	81355	81356	81357	81358	81359	81360	81361	81362	81363
CODE	J52D32	J52D32	J52D32	J52D32	J52D32	J52D32	H52B32	H52B32	H52B32	H52B32
TRAVERSE	52	52	52	52	52	52	52	52	52	52
EAST	4738	4738	4738	4736	4736	4736	4746	4746	4744	4744
NORTH	68781	68781	68781	68785	68785	68785	68812	68812	68809	68809
SiO_2 (%)	51.6	50.2	38.4	47.7	49.6	48.4	52.6	49.5	39.3	64.1
Al_2O_3	0.2	0.2	0.2	0.2	0.2	0.2	0.3	0.5	0.5	0.5
Fe_2O_3	44.0	44.6	57.3	46.7	47.6	46.7	43.6	47.1	57.4	32.0
FeO	1.62	1.17	0.66	0.26	1.67	2.85	0.26	0.39	0.44	0.33
MgO	0.09	0.08	0.04	0.13	0.04	0.02	0.01	0.01	0.04	0.03
CaO	0.08	0.05	0.04	0.09	0.05	0.07	0.12	0.02	0.03	0.07
Na_2O	0.01	0.01	<0.01	<0.01	<0.01	0.01	0.01	<0.01	0.01	0.01
K_2O	0.01	<0.01	<0.01	<0.01	0.03	<0.01	0.01	<0.01	0.04	0.01
H_2O	2.00	3.08	2.73	3.72	0.97	1.11	3.23	2.26	1.83	2.59
TiO_2	<0.01	<0.01	<0.01	<0.01	<0.01	<0.01	<0.01	<0.01	0.03	<0.01
P_2O_5	0.22	0.19	0.15	0.25	0.21	0.22	0.20	0.22	0.17	0.16
MnO	0.07	0.08	0.08	0.14	0.01	0.02	0.02	0.04	0.02	0.01
S	0.010	0.015	0.010	0.005	0.005	0.010	0.055	0.020	0.025	0.020
As (ppm)	-	-	-	-	-	-	-	-	-	-
Au	<0.01	<0.01	<0.01	<0.01	<0.01	<0.01	-	-	-	-
Ba	<25	<25	<25	<25	45	63	120	107	256	80
Ce	6	5	9	<5	5	<5	7	8	5	<5
Co	-	-	-	-	-	-	-	-	-	-
Cr	<10	<10	<10	<10	<10	<10	<10	16	17	13
Cu	8	28	30	7	8	12	109	78	89	42
La	13	9	7	9	14	14	6	8	<5	7
Li	1	1	1	<1	<1	<1	1	<1	<1	5
Mn	579	622	687	1136	139	181	185	309	166	99
Nb	<5	<5	<5	<5	<5	<5	<5	<5	<5	<5
Ni	5	8	6	<5	<5	7	9	7	13	20
Pb	11	<10	11	11	19	19	23	16	21	18
Rb	<2	<2	<2	<2	<2	<2	<2	<2	<2	<2
Sr	<5	<5	<5	<5	<5	<5	5	<5	<5	<5
Th	<10	<10	<10	<10	<10	<10	<10	<10	<10	<10
V	26	58	37	27	6	33	10	17	37	37
Y	5	6	4	6	5	7	5	2	2	4
Zn	57	67	162	52	46	46	40	35	36	60
Zr	<10	10	<10	10	<10	<10	<10	<10	14	<10

SAMPLE	81367	81368	81369	81370	81371	81387	81388	81389	81390	81391
CODE	H52B32	H52B32	H52B32	H52B32	H52B32	I53032	I53032	I53032	I53032	I53032
TRAVERSE	52	52	52	52	52	53	53	53	53	53
EAST	4735	4736	4736	4730	4730	5367	5367	5366	5366	5365
NORTH	68808	68808	68808	68817	68817	71338	71339	71340	71340	71340
SiO_2 (%)	45.9	61.4	75.8	51.4	53.2	82.4	55.2	61.1	55.9	78.0
Al_2O_3	0.2	0.3	0.3	0.3	0.2	0.3	0.2	0.2	0.3	0.1
Fe_2O_3	51.3	35.2	22.3	46.3	43.8	13.0	42.7	36.6	36.9	7.2
FeO	1.14	1.00	0.52	0.44	0.48	0.63	0.20	0.68	3.02	7.99
MgO	0.08	0.05	0.03	0.03	0.02	0.87	0.12	0.25	0.77	2.02
CaO	0.06	0.04	0.05	0.04	0.03	0.05	0.03	0.01	1.02	3.07
Na_2O	0.01	0.01	0.01	0.01	0.01	0.02	0.01	<0.01	0.01	0.01
K_2O	0.01	0.05	0.02	0.01	0.01	0.01	<0.01	<0.01	<0.01	<0.01
H_2O	1.20	1.37	0.65	1.49	1.62	2.13	0.86	0.88	1.84	1.04
TiO_2	<0.01	<0.01	<0.01	<0.01	<0.01	<0.01	<0.01	<0.01	<0.01	<0.01
P_2O_5	0.20	0.23	0.16	0.17	0.22	0.18	0.17	0.17	0.20	0.17
MnO	0.03	0.02	<0.01	0.01	0.01	0.02	0.02	0.02	0.07	0.20
S	0.010	0.020	0.010	0.045	0.050	0.015	0.010	0.015	0.030	0.005
As (ppm)	-	-	-	-	-	-	-	-	-	-
Au	-	-	-	-	-	-	-	-	-	-
Ba	173	128	294	60	70	<25	<25	555	54	<25
Ce	<5	<5	8	<5	<5	5	5	27	7	<5
Co	-	-	-	-	-	-	-	-	-	-
Cr	<10	<10	<10	23	<10	<10	<10	<10	<10	<10
Cu	22	11	16	40	102	9	5	6	12	6
La	8	<5	10	6	8	8	8	20	7	<5
Li	1	1	<1	1	<1	11	3	8	2	1
Mn	197	110	91	125	97	152	148	194	608	1623
Nb	<5	<5	<5	<5	<5	<5	<5	<5	<5	<5
Ni	6	10	8	<5	7	95	18	20	55	13
Pb	25	<10	<10	<10	<10	26	<10	<10	<10	<10
Rb	<2	<2	<2	<2	<2	<2	<2	<2	<2	<2
Sr	<5	32	5	6	<5	<5	<5	<5	<5	<5
Th	<10	<10	<10	<10	<10	<10	<10	<10	<10	<10
V	6	10	<5	27	13	7	<5	<5	<5	<5
Y	2	4	3	<2	<2	5	5	14	9	2
Zn	35	20	12	27	26	22	27	34	46	30
Zr	<10	11	<10	<10	<10	<10	<10	<10	<10	<10

SAMPLE	81392	81393	81394	81395	81396	81398	81399	81400	81496
CODE	I53U32	I53U32	I53U32	I53U32	I53U32	I53U32	I53U32	I53U32	H04834
TRAVERSE	53	53	53	53	53	53	53	53	04
EAST	5364	5364	5363	5363	5360	5350	5350	5349	6634
NORTH	71340	71340	71341	71340	71342	71335	71335	71335	70337
SiO_2 (%)	70.2	58.1	56.0	68.2	87.5	66.6	52.5	54.1	43.7
Al_2O_3	0.2	0.2	0.2	0.2	0.1	0.2	0.2	0.2	0.2
Fe_2O_3	13.9	28.1	33.5	28.9	10.6	30.0	39.3	34.2	38.6
FeO	6.65	3.91	4.63	0.32	0.83	1.33	1.55	6.86	11.4
MgO	2.96	2.98	1.97	0.09	0.10	0.01	2.36	1.57	1.70
CaO	3.65	3.15	1.98	0.05	0.01	0.03	1.89	1.44	2.19
Na_2O	0.03	0.02	0.01	<0.01	<0.01	<0.01	0.01	0.01	0.13
K_2O	<0.01	0.01	0.01	0.01	<0.01	<0.01	0.01	<0.01	0.01
H_2O	1.27	2.77	1.11	1.75	0.65	1.77	1.24	1.18	1.14
TiO_2	<0.01	<0.01	<0.01	<0.01	<0.01	<0.01	<0.01	<0.01	0.01
P_2O_5	0.16	0.20	0.18	0.15	0.14	0.15	0.16	0.19	0.15
MnO	0.25	0.19	0.08	0.07	0.02	0.03	0.16	0.07	0.16
S	0.015	0.005	0.010	0.015	0.010	0.020	0.015	0.005	0.005
As (ppm)	-	-	-	-	-	-	-	-	-
Au	-	-	-	-	-	-	-	-	-
Ba	<25	<25	<25	94	<25	<25	125	<25	<20
Ce	7	6	<5	<5	<5	<5	70	<5	<5
Co	-	-	-	-	-	-	-	-	19
Cr	<10	<10	<10	<10	<10	<10	<10	<10	<5
Cu	10	9	7	13	4	8	7	5	40
La	5	<5	10	6	6	7	37	<5	00
Li	3	6	2	6	<1	2	2	2	1
Mn	2029	1556	732	570	164	249	1365	625	1180
Nb	<5	<5	<5	<5	<5	<5	<5	<5	<5
Ni	27	23	29	38	15	13	24	26	<5
Pb	<10	<10	<10	<10	<10	<10	<10	<10	<10
Rb	<2	3	<2	<2	<2	<2	<2	<2	<2
Sr	<5	6	<5	<5	<5	<5	7	<5	4
Th	<10	<10	<10	<10	<10	<10	<10	<10	<5
V	13	<5	<5	6	<5	<5	<5	<5	16
Y	5	6	6	5	3	3	29	9	6
Zn	35	39	32	27	12	32	59	37	92
Zr	<10	<10	<10	<10	<10	<10	<10	<10	8

SAMPLE	81497	81499	81502	81544	81545	81546	81547	81548	81549	81550
CODE	H04834	H04834	H04834	H06832	H06831	H06831	H06831	H06831	H06832	J07030
TRAVERSE	04	04	04	06	06	06	06	06	06	07
EAST	6632	6629	6628	6312	6315	6317	6320	6320	6313	6473
NORTH	70337	70337	70337	70336	70336	70336	70336	70336	70336	70317
SiO_2 (%)	51.9	53.1	50.0	68.0	57.5	53.1	66.7	51.1	66.6	68.0
Al_2O_3	0.1	0.1	0.1	0.2	<0.1	<0.1	0.3	<0.1	<0.1	0.1
Fe_2O_3	35.1	38.4	32.0	28.5	38.9	42.2	29.6	44.3	30.0	48.1
FeO	6.66	4.59	9.91	0.51	0.28	0.27	0.62	0.33	0.87	0.68
MgO	1.91	1.04	2.53	0.12	0.01	0.01	0.02	0.02	0.02	0.01
CaO	2.05	1.27	3.18	0.06	0.01	<0.01	0.02	<0.01	0.03	<0.01
Na_2O	0.12	0.07	0.09	0.03	0.01	0.01	0.02	0.01	0.01	<0.01
K_2O	<0.01	<0.01	<0.01	0.01	<0.01	<0.01	0.01	<0.01	<0.01	<0.01
H_2O	1.18	0.95	1.15	2.12	3.10	4.13	3.10	4.46	2.18	2.06
TiO_2	<0.01	<0.01	<0.01	<0.01	<0.01	<0.01	<0.01	<0.01	<0.01	<0.01
P_2O_5	0.22	0.16	0.16	0.10	0.07	0.06	0.06	0.05	0.07	0.11
MnO	0.12	0.05	0.11	0.02	<0.01	<0.01	<0.01	<0.01	0.02	0.05
S	0.005	0.006	0.007	0.014	0.009	0.006	0.012	0.010	0.014	0.013
As (ppm)	-	-	-	-	-	-	-	-	-	-
Au	-	-	-	-	-	-	-	-	-	-
Ba	<20	<20	<20	<20	<20	<20	<20	<20	<20	<20
Ce	<5	<5	6	8	<5	11	10	5	<5	<5
Co	40	46	35	52	63	55	58	44	81	53
Cr	6	<5	<5	23	<5	<5	13	<5	<5	<5
Cu	47	65	46	106	53	40	169	40	47	46
La	8	8	5	9	8	13	6	10	5	6
Li	1	1	1	2	2	<1	13	<1	1	1
Mn	940	470	890	70	20	20	30	30	110	320
Nb	<5	<5	<5	<5	<5	<5	<5	<5	6	<5
Ni	<5	<5	<5	<10	<10	<10	60	<10	<10	20
Pb	<10	<10	30	<10	<10	<10	<10	<10	<10	<10
Rb	<2	<2	<2	<2	<2	<2	<2	<2	<2	<2
Sr	3	<2	7	<2	<2	<2	<2	<2	<2	<2
Th	<5	<5	<5	<5	<5	<5	<5	<5	<5	<5
V	7	8	7	10	7	<5	18	5	9	9
Y	6	6	6	7	5	53	12	6	9	5
Zn	33	47	37	60	42	18	81	44	33	29
Zr	19	<5	<5	<5	<5	<5	<5	6	<5	5

SAMPLE	81551	81552	81553	81554	81555	81556	81557	81558	81560	81562
CODE	J07030	J07030	J07030	J07030	J07030	J07030	J07030	J07030	J07030	J07030
TRAVERSE	07	07	07	07	07	07	07	07	07	07
EAST	6525	6526	6527	6528	6528	6529	6595	6595	6597	6600
NORTH	70275	70275	70274	70273	70273	70272	70220	70220	70220	70220
SiO_2 (%)	61.5	54.4	51.3	51.2	50.1	51.7	51.1	63.9	80.0	53.1
Al_2O_3	0.2	(0.1	0.1	0.1	0.1	0.1	1.8	0.2	0.5	1.6
Fe_2O_3	37.0	43.8	46.5	46.9	48.6	46.0	43.2	36.0	17.5	41.7
FeO	0.32	0.53	0.64	0.60	0.20	0.27	0.71	0.67	0.97	1.38
MgO	(0.01	(0.01	(0.01	(0.01	(0.01	(0.01	0.03	0.01	0.03	0.05
CaO	0.07	(0.01	0.05	(0.01	0.07	0.01	0.02	0.02	0.05	(0.01
Na_2O	(0.01	(0.01	0.04	(0.01	(0.01	(0.01	0.02	0.01	0.02	0.02
K_2O	(0.01	(0.01	0.01	(0.01	(0.01	(0.01	0.06	(0.01	0.05	0.01
H_2O	0.60	0.74	1.06	1.13	0.43	1.17	1.90	0.85	0.69	1.66
TiO_2	(0.01	(0.01	(0.01	(0.01	(0.01	(0.01	0.07	(0.01	0.01	0.05
P_2O_5	0.07	0.09	0.08	0.17	0.09	0.16	0.17	0.13	0.11	0.12
MnO	0.01	(0.01	(0.01	(0.01	(0.01	(0.01	0.04	0.01	0.01	0.02
S	0.015	0.012	0.009	0.011	0.023	0.013	0.044	0.022	0.033	0.030
As (ppm)	-	-	-	-	-	-	-	-	-	-
Au	-	-	-	-	-	-	-	-	-	-
Ba	28	22	(20	(20	52	22	751	(20	93	311
Ce	15	(5	(5	18	30	12	20	37	7	(5
Co	118	84	72	75	86	59	47	87	128	45
Cr	17	16	(5	15	(5	(5	74	(5	(5	49
Cu	39	41	41	48	53	52	46	28	59	40
La	8	6	(5	(5	16	9	26	8	10	7
Li	(1	(1	5	(1	2	2	1	(1	(1	1
Mn	50	40	40	40	30	30	300	100	100	160
Nb	(5	(5	(5	(5	5	(5	5	5	6	(5
Ni	(10	(10	(10	(10	(10	(10	(10	(10	(10	(10
Pb	(10	(10	(10	(10	(10	(10	(10	(10	(10	(10
Rb	(2	(2	(2	(2	(2	(2	12	(2	2	(2
Sr	17	2	(2	6	16	9	23	15	40	2
Th	(5	(5	(5	(5	(5	(5	(5	(5	(5	(5
V	(5	(5	(5	(5	13	8	36	(5	(5	35
Y	5	5	4	5	7	4	10	5	30	7
Zn	16	40	40	23	20	25	27	15	18	44
Zr	(5	9	5	9	8	(5	16	(5	14	8

SAMPLE	81565	81566	81567	81568	81577	81624	81625	81626	81627	81628
CODE	J07030	H04834	H04834	H04834	J07031	J14031	J14031	J14031	J14031	J14031
TRAVERSE	07	04	04	04	07	14	14	14	14	14
EAST	6606	6631	6631	6631	6468	5564	5564	5564	5584	5511
NORTH	70220	70335	70335	70335	70525	70168	70168	70168	70165	70119
SiO_2 (%)	65.2	52.6	45.7	44.5	47.8	62.6	64.8	59.5	58.8	55.0
Al_2O_3	0.3	0.1	0.1	<0.1	0.3	0.2	0.1	0.1	0.1	0.1
Fe_2O_3	31.4	34.9	46.1	45.3	48.2	36.3	33.7	38.2	36.4	43.3
FeO	1.20	7.76	4.54	7.12	0.73	0.39	0.49	1.13	1.32	0.53
MgO	0.03	1.59	1.11	1.43	0.07	0.03	0.02	0.01	0.04	0.02
CaO	0.06	1.24	0.70	0.48	0.05	0.03	<0.01	<0.01	0.01	0.04
Na_2O	0.02	0.03	0.03	0.01	0.02	0.03	<0.01	<0.01	<0.01	0.01
K_2O	0.03	0.01	0.01	<0.01	<0.01	0.01	<0.01	<0.01	<0.01	0.07
H_2O	1.38	1.52	1.36	1.12	2.95	0.81	0.84	1.08	3.25	1.49
TiO_2	<0.01	<0.01	<0.01	<0.01	<0.01	<0.01	<0.01	<0.01	<0.01	<0.01
P_2O_5	0.22	0.13	0.16	0.17	0.19	0.03	0.04	0.04	0.05	0.14
MnO	0.01	0.13	0.07	0.26	<0.01	0.01	0.02	0.01	0.01	0.01
S	0.015	0.013	0.010	0.008	0.012	0.010	0.009	0.017	0.015	0.008
As (ppm)	-	-	-	-	-	-	-	-	-	-
Au	-	-	-	-	-	-	-	-	-	-
Ba	29	291	98	<20	<20	<20	<20	<20	<20	<20
Ce	17	6	21	<5	<5	<5	<5	<5	<5	<5
Co	104	68	52	42	25	53	76	63	67	100
Cr	<5	<5	<5	<5	7	<5	5	<5	<5	5
Cu	63	119	66	39	50	36	37	34	39	35
La	15	15	19	5	6	5	7	5	6	9
Li	<1	<1	<1	<1	<1	<1	<1	<1	<1	<1
Mn	60	880	500	1740	40	60	120	60	130	100
Nb	5	<5	<5	<5	<5	5	<5	<5	<5	<5
Ni	<10	<10	<10	<10	<10	<10	<10	<10	<10	<10
Pb	<10	<10	<10	<10	<10	<10	<10	<10	<10	<10
Rb	<2	2	<2	<2	<2	<2	<2	<2	<2	<2
Sr	5	6	3	<2	<2	<2	<2	<2	<2	2
Th	<5	<5	<5	<5	<5	<5	<5	<5	<5	<5
V	6	31	<5	<5	12	6	<5	7	5	11
Y	27	12	21	5	5	3	4	3	5	7
Zn	76	56	38	75	30	10	6	8	20	21
Zr	16	8	5	9	<5	7	<5	<5	6	6

SAMPLE	81629	81630	81631	81632	81648	81649	81650	85701	85702	85703
CODE	J14031	J14031	J14031	J14031	J14031	J14031	J14031	I53032	I53032	I53033
TRAVERSE	14	14	14	14	14	14	14	53	53	53
EAST	5504	5504	5506	5511	5809	5809	5809	5349	5253	5253
NORTH	70135	70135	70135	70119	70071	70071	70071	71334	71194	71194
SiO_2 (%)	47.6	48.0	53.2	45.7	37.8	44.3	57.3	73.6	45.8	62.2
Al_2O_3	0.4	0.1	0.1	0.1	0.3	0.2	0.2	0.2	0.2	0.2
Fe_2O_3	50.4	44.7	42.1	51.3	61.2	54.2	<1.0	24.6	52.5	36.7
FeO	0.85	3.40	1.34	0.60	0.46	0.28	0.66	0.63	0.66	0.15
MgO	0.07	0.05	0.08	0.01	0.07	0.02	0.02	0.02	0.02	0.02
CaO	0.06	0.01	0.01	(0.01	0.06	0.01	0.01	0.02	0.02	0.01
Na_2O	0.04	0.01	0.01	(0.01	0.02	0.01	0.01	0.01	(0.01	(0.01
K_2O	0.02	(0.01	(0.01	(0.01	(0.01	0.01	(0.01	(0.01	(0.01	(0.01
H_2O	0.58	3.66	3.07	2.58	0.77	0.60	0.86	0.87	0.76	0.36
TiO_2	0.01	(0.01	(0.01	(0.01	(0.01	(0.01	(0.01	(0.01	(0.01	(0.01
P_2O_5	0.05	0.08	0.12	0.08	0.11	0.09	0.11	0.20	0.18	0.14
MnO	(0.01	0.05	0.05	(0.01	0.02	0.03	0.01	0.04	0.01	(0.01
S	0.010	0.013	0.009	0.010	0.013	0.024	0.014	0.010	0.005	(0.005
As (ppm)	-	-	-	-	-	-	-	-	-	-
Au	-	-	-	-	-	-	-	-	-	-
Ba	(20	(20	(20	(20	(20	31	85	(25	(25	(25
Ce	(5	8	(5	(5	(5	7	30	(5	5	(5
Co	93	60	66	57	24	44	65	-	-	-
Cr	(5	(5	9	(5	26	6	(5	(10	(10	(10
Cu	125	35	30	34	19	23	25	4	7	6
La	6	8	(5	(5	9	11	15	6	8	7
Li	1	(1	1	1	1	101	(1	1	4	1
Mn	40	400	410	40	200	270	[illegible]	385	110	63
Nb	(5	(5	(5	(5	(5	(5	(5	(5	(5	(5
Ni	(10	(10	(10	(10	(10	(10	(10	13	17	15
Pb	(10	(10	(10	10	(10	(10	(10	(10	(10	(10
Rb	(2	(2	(2	(2	(2	(2	(2	(2	(2	(2
Sr	(2	(2	(2	(2	6	11	15	(5	(5	(5
Th	(5	(5	(5	(5	(5	(5	(5	(10	(10	(10
V	16	7	12	82	13	(5	(5	(5	(5	(5
Y	6	4	6	7	3	2	4	2	7	3
Zn	22	17	21	21	11	11	7	29	29	21
Zr	12	14	(5	(5	5	7	(5	(10	(10	(10

SAMPLE	85705	85707	85709	85710	85711	85712	85713
CODE	I53033	J54031	J54031	J54031	J54031	J54031	J54031
TRAVERSE	53	54	54	54	54	54	54
EAST	5253	3649	3649	3649	3649	3649	3647
NORTH	71192	68899	68899	68899	68899	68899	68896
SiO_2 (%)	82.6	65.1	64.9	35.0	47.2	47.0	72.3
Al_2O_3	0.2	0.4	0.2	0.2	0.1	0.4	0.7
Fe_2O_3	16.1	32.7	32.8	59.1	50.5	48.8	25.5
FeO	0.36	0.72	0.75	4.26	0.34	2.23	0.36
MgO	0.01	0.09	0.01	0.02	0.03	0.07	0.01
CaO	0.01	0.01	0.03	0.01	0.01	0.01	0.02
Na_2O	(0.01	(0.01	0.01	(0.01	(0.01	(0.01	(0.01
K_2O	(0.01	(0.01	0.01	(0.01	(0.01	(0.01	(0.01
H_2O	0.60	0.65	0.78	0.62	1.24	0.73	0.64
TiO_2	(0.01	(0.01	(0.01	(0.01	(0.01	(0.01	0.02
P_2O_5	0.14	0.15	0.50	0.18	0.15	0.16	0.15
MnO	(0.01	(0.01	(0.01	0.01	0.01	(0.01	(0.01
S	0.010	0.005	0.005	0.005	0.005	0.005	0.005
As (ppm)	-	-	-	-	-	-	-
Au	-	(0.01	2.0	(0.01	(0.01	(0.01	(0.01
Ba	(25	(25	165	(25	(25	(25	(25
Ce	(5	(5	(5	(5	10	(5	(5
Co	-	-	-	-	-	-	-
Cr	11	(10	(10	(10	(10	12	(10
Cu	4	17	39	9	7	5	(3
La	(5	11	5	8	(5	6	5
Li	(1	2	(1	1	1	(1	(1
Mn	85	64	96	117	123	94	52
Nb	(5	(5	(5	(5	(5	(5	(5
Ni	27	5	(5	(5	(5	(5	(5
Pb	(10	(10	(10	(10	(10	(10	(10
Rb	(2	(2	(2	(2	(2	(2	(2
Sr	(5	(5	(5	(5	(5	(5	(5
Th	(10	(10	(10	(10	(10	(10	(10
V	11	10	36	5	(5	24	13
Y	15	5	5	4	2	5	2
Zn	12	17	22	31	24	24	14
Zr	(10	11	(10	(10	(10	(10	11

SAMPLE	85714	85715	85716	85717	85718	85720	85721	85722	85723
CODE	J54D31	J54D31	J54D31	J54D31	H55B32	H55B32	H55B32	H55B32	H55B32
TRAVERSE	54	54	54	54	55	55	55	55	55
EAST	3647	3644	3646	3644	4316	4316	4316	4324	4324
NORTH	68896	68888	68888	68888	68290	68290	68290	68297	68297
SiO_2 (%)	58.4	52.8	69.8	51.4	69.9	69.8	76.0	65.8	51.6
Al_2O_3	0.5	0.2	0.1	0.2	0.4	1.1	0.5	0.2	0.3
Fe_2O_3	38.9	46.2	49.3	47.0	27.7	44.4	21.1	50.0	45.3
FeO	0.52	0.28	0.31	0.66	0.34	0.33	0.39	1.11	0.39
MgO	0.02	0.08	0.02	0.02	0.01	0.02	0.01	0.01	0.01
CaO	0.06	0.03	0.01	0.03	0.03	0.09	0.06	0.03	0.04
Na_2O	<0.01	<0.01	<0.01	<0.01	<0.01	<0.01	<0.01	<0.01	0.01
K_2O	0.02	<0.01	<0.01	<0.01	0.01	0.02	<0.01	<0.01	<0.01
H_2O	0.83	0.25	0.15	0.37	1.05	2.57	1.33	2.11	1.90
TiO_2	0.01	<0.01	<0.01	<0.01	0.01	0.01	<0.01	<0.01	<0.01
P_2O_5	0.21	0.20	0.15	0.17	0.22	0.31	0.18	0.31	0.19
MnO	<0.01	<0.01	<0.01	<0.01	<0.01	0.03	0.01	0.01	0.01
S	0.020	0.005	<0.005	0.005	0.010	0.11	0.045	0.010	0.025
As (ppm)	-	-	-	-	-	-	-	-	-
Au	<0.01	<0.01	<0.01	<0.01	6.4	0.33	1.8	<0.01	0.10
Ba	<25	<25	<25	<25	249	>128	2238	<25	<25
Ce	<5	<5	<5	<5	<5	11	<5	7	<5
Co	-	-	-	-	-	-	-	-	-
Cr	<10	<10	<10	<10	10	<10	10	<10	<10
Cu	22	8	4	4	68	61	29	7	12
La	8	11	10	10	10	<5	5	10	11
Li	<1	<1	1	<1	<1	<1	1	1	<1
Mn	70	69	31	27	58	229	81	72	101
Nb	<5	<5	<5	<5	<5	<5	<5	<5	<5
Ni	<5	<5	<5	<5	<5	10	<5	15	8
Pb	<10	<10	<10	<10	<10	<10	<10	<10	<10
Rb	<2	<2	<2	<2	<2	<2	<2	<2	<2
Sr	5	11	<5	<5	5	37	23	<5	<5
Th	<10	<10	<10	<10	<10	<10	<10	<10	<10
V	10	7	<5	6	70	28	14	<5	<5
Y	5	6	4	2	3	3	4	5	4
Zn	18	22	23	21	18	44	30	47	36
Zr	12	<10	<10	<10	<10	<10	<10	<10	<10

SAMPLE	85725	85740	85761	85744	85745	85746	85747	85748	85749	85750
CODE	H55832	J56031	J56031	J56031	-	J56031	J56031	J56031	J56031	J56031
TRAVERSE	55	56	56	56	-	56	56	56	56	56
EAST	4324	4230	4230	4244	4244	4244	4244	4238	4238	4238
NORTH	68297	67717	67717	67699	67699	67699	67706	67707	67707	67707
SiO_2 (%)	69.4	31.3	45.1	41.5	90.1	61.3	58.9	39.0	34.6	37.3
Al_2O_3	0.3	0.5	0.5	0.5	0.3	0.4	0.5	0.4	0.6	0.4
Fe_2O_3	67.7	62.7	48.3	51.7	8.2	36.3	31.3	57.7	60.9	59.1
FeO	0.72	0.17	0.60	0.46	0.67	0.34	6.93	0.31	0.29	0.30
MgO	0.02	0.04	0.04	0.04	0.02	0.01	1.89	0.04	0.03	0.02
CaO	0.06	0.02	(0.01	0.02	0.01	(0.01	0.12	0.10	0.24	0.02
Na_2O	(0.01	0.02	0.02	0.01	(0.01	0.01	0.01	0.01	(0.01	(0.01
K_2O	(0.01	0.01	0.01	0.03	0.01	(0.01	0.02	0.02	(0.01	(0.01
H_2O	1.63	4.41	4.85	5.10	0.76	0.98	1.23	1.77	2.34	2.53
TiO_2	(0.01	(0.01	0.01	(0.01	(0.01	(0.01	0.01	(0.01	(0.01	(0.01
P_2O_5	0.23	0.41	0.24	0.15	0.15	0.16	0.18	0.26	0.25	0.23
MnO	0.01	0.03	(0.01	(0.01	(0.01	(0.01	0.08	(0.01	(0.01	0.01
S	0.010	0.005	0.005	0.020	0.010	0.005	0.010	0.065	0.11	0.010
As (ppm)	-	-	-	-	-	-	-	-	-	-
Au	(0.01	-	-	-	-	-	-	-	-	-
Ba	41	(25	(25	(25	(25	(25	(25	(25	(25	(25
Ce	7	5	(5	(5	(5	(5	(5	22	13	(5
Co	-	-	-	-	-	-	-	-	-	-
Cr	29	(10	(10	(10	(10	(10	(10	(10	(10	(10
Cu	12	8	427	7	6	5	6	7	9	10
La	5	9	10	(5	(5	(5	5	17	12	(5
Li	(1	(1	(1	(1	1	(1	(1	3	1	(1
Mn	75	215	43	55	40	71	710	35	41	82
Nb	(5	(5	(5	(5	(5	(5	(5	(5	(5	(5
Ni	8	10	15	(5	(5	(5	(5	(5	(5	(5
Pb	(10	(10	(10	(10	48	(10	154	(10	42	(10
Rb	(2	(2	(2	-	(2	(2	(2	(2	(2	(2
Sr	(5	(5	(5	(5	(5	(5	6	7	6	(5
Th	(10	(10	(10	(10	(10	(10	(10	(10	(10	(10
V	8	5	(5	9	5	(5	7	5	5	(5
Y	3	10	10	4	2	3	2	6	7	5
Zn	45	121	114	73	51	27	165	80	84	144
Zr	11	(10	(10	(10	(10	(10	(10	(10	(10	(10

SAMPLE	85755	85849	85850	85851	85852	85853	85854	85855	85856	85857
CODE	J00C31	J61D11	J61D11	J61D11	J61D11	J61D11	J61D11	J61D11	J61D11	J61D11
TRAVERSE	00	61	61	61	61	61	61	61	61	61
EAST	5008	5151	5151	5151	5151	5151	5151	5151	5151	5151
NORTH	67798	67286	67286	67286	67286	67286	67286	67286	67296	67286
SiO_2 (%)	35.8	44.6	46.5	37.3	41.1	40.1	38.7	33.5	43.9	42.8
Al_2O_3	1.1	0.4	0.3	0.5	0.3	0.4	0.7	0.2	0.3	0.4
Fe_2O_3	58.2	32.7	32.8	38.2	35.2	36.6	35.9	37.1	29.0	31.5
FeO	1.93	14.7	14.3	19.1	17.0	17.9	17.7	19.8	16.1	16.7
MgO	0.06	1.76	1.58	1.92	1.72	2.94	2.21	3.34	2.52	2.58
CaO	0.06	2.08	1.37	0.35	1.38	0.87	1.18	1.76	2.67	1.45
Na_2O	0.02	0.19	0.36	0.02	0.01	0.02	0.03	0.02	0.02	0.01
K_2O	<0.01	0.22	0.26	0.04	<0.01	0.01	0.07	0.02	0.02	0.02
H_2O	2.49	2.38	2.02	1.64	2.51	1.85	2.26	2.83	4.51	3.03
TiO_2	0.01	<0.01	<0.01	<0.01	<0.01	<0.01	0.01	<0.01	<0.01	<0.01
P_2O_5	0.15	0.21	0.16	0.20	0.20	0.22	0.20	0.26	0.17	0.18
MnO	0.02	0.11	0.11	0.09	0.17	0.15	0.15	0.17	0.25	0.19
S	0.015	0.02	0.01	0.01	0.02	0.01	0.03	0.03	0.02	0.03
As (ppm)	-	-	-	-	-	-	-	-	-	-
Au	-	-	-	-	-	-	-	-	-	-
Ba	<25	101	363	30	<25	<25	<25	<25	<25	<25
Ce	<5	-	-	-	-	-	-	-	-	-
Co	-	-	-	-	-	-	-	-	-	-
Cr	24	<10	<10	<10	<10	<10	<10	<10	<10	<10
Cu	58	-	-	-	-	-	-	-	-	-
La	<5	-	-	-	-	-	-	-	-	-
Li	<1	-	-	-	-	-	-	-	-	-
Mn	121	-	-	-	-	-	-	-	-	-
Nb	<5	<5	<5	<5	<5	<5	<5	<5	<5	<5
Ni	7	-	-	-	-	-	-	-	-	-
Pb	<10	-	-	-	-	-	-	-	-	-
Rb	<2	23	22	3	<2	2	5	2	<2	2
Sr	<5	55	40	<5	<5	<5	<5	8	7	5
Th	<10	<10	<10	<10	<10	<10	<10	<10	<10	<10
V	12	<5	<5	5	<5	6	24	6	<5	5
Y	2	5	3	5	5	6	5	5	4	5
Zn	52	-	-	-	-	-	-	-	-	-
Zr	<10	<10	10	<10	<10	<10	<10	<10	<10	<10

SAMPLE	85858	85859	85860	85861	85862	85863	85864	85865	85866	85867
CODE	J61D11	J61D11	J61D11	J61D11	J61D11	J61D11	J61D11	J61D11	J61D11	J61D11
TRAVERSE	61	61	61	61	61	61	61	61	61	61
EAST	5151	5151	5151	5151	5151	5151	5151	5151	5151	5151
NORTH	67286	67286	67286	67286	67286	67286	67286	67286	67286	67286
SiO_2 (%)	44.0	44.3	46.3	47.8	46.6	43.9	47.2	48.3	51.6	52.6
Al_2O_3	0.2	0.3	0.4	0.3	0.6	0.4	0.3	0.5	0.4	0.5
Fe_2O_3	32.7	32.4	31.1	31.3	31.2	32.5	30.3	28.6	26.3	23.9
FeO	16.5	16.5	15.6	14.7	15.0	15.7	14.8	15.6	15.6	15.7
MgO	1.57	1.76	1.62	1.60	1.70	1.86	1.97	2.57	3.02	3.18
CaO	1.59	1.66	1.59	1.52	1.94	2.02	1.48	1.14	0.77	1.25
Na_2O	0.07	0.06	0.29	0.05	0.07	0.15	0.05	0.08	0.02	0.02
K_2O	0.12	0.20	0.26	0.12	0.16	0.16	0.26	0.18	0.11	0.17
H_2O	2.21	2.17	2.05	1.97	2.45	2.54	2.72	1.99	1.86	2.15
TiO_2	<0.01	<0.01	<0.01	<0.01	<0.01	<0.01	<0.01	<0.01	<0.01	<0.01
P_2O_5	0.23	0.19	0.16	0.18	0.19	0.18	0.11	0.18	0.16	0.15
MnO	0.16	0.13	0.11	0.09	0.10	0.10	0.12	0.12	0.08	0.11
S	0.02	0.02	0.03	0.02	0.02	0.02	0.03	0.05	0.02	0.05
As (ppm)	-	-	-	-	-	-	-	-	-	-
Au	-	-	-	-	-	-	-	-	-	-
Ba	<25	<25	<25	30	34	37	29	<25	<25	32
Ce	-	-	-	-	-	-	-	-	-	-
Co	-	-	-	-	-	-	-	-	-	-
Cr	<10	<10	<10	22	<10	<10	<10	<10	36	<10
Cu	-	-	-	-	-	-	-	-	-	-
La	-	-	-	-	-	-	-	-	-	-
Li	-	-	-	-	-	-	-	-	-	-
Mn	-	-	-	-	-	-	-	-	-	-
Nb	<5	<5	<5	<5	<5	5	7	<5	<5	<5
Ni	-	-	-	-	-	-	-	-	-	-
Pb	-	-	-	-	-	-	-	-	-	-
Rb	19	26	32	17	22	24	29	22	13	16
Sr	34	33	33	18	16	27	25	12	5	9
Th	<10	<10	<10	<10	<10	<10	<10	<10	<10	<10
V	<5	<5	6	22	<5	7	<5	<5	8	7
Y	4	4	4	5	5	5	3	4	4	4
Zn	-	-	-	-	-	-	-	-	-	-
Zr	<10	<10	<10	12	<10	12	<10	<10	<10	<10

SAMPLE	85868	85881	85882	85883	85884	85885	85886	85887	85888	85889
CODE	J61D11	J61D31	J61D31	J61D31	J61D31	J61D31	J61D31	I61D31	J61D31	J61D31
TRAVERSE	61	61	61	61	61	61	61	61	61	61
EAST	5151	5151	5151	5151	5151	5151	5151	5151	5151	5151
NORTH	67286	67286	67286	67286	67286	67286	67286	67286	67286	67286
SiO_2 (%)	46.6	51.2	43.5	43.5	52.4	51.6	48.8	3.6	37.2	41.9
Al_2O_3	0.6	0.6	0.4	0.4	0.4	1.5	0.2	0.4	0.8	0.4
Fe_2O_3	21.1	45.2	53.8	53.6	44.6	43.8	44.7	88.8	58.6	54.6
FeO	19.7	0.44	0.33	0.36	0.45	0.18	3.26	0.54	1.06	0.36
MgO	3.94	0.03	0.02	0.02	0.04	0.02	0.04	0.01	0.02	0.02
CaO	2.14	0.02	0.02	(0.01	0.02	0.01	0.02	(0.01	0.01	(0.01
Na_2O	0.01	(0.01	(0.01	(0.01	(0.01	(0.01	(0.01	(0.01	(0.01	(0.01
K_2O	0.04	0.01	0.01	(0.01	0.02	(0.01	0.02	(0.01	(0.01	(0.01
H_2O	6.41	2.30	1.63	2.04	1.87	2.53	2.36	6.36	1.97	2.46
TiO_2	0.01	(0.01	(0.01	(0.01	(0.01	(0.01	(0.01	(0.01	(0.01	(0.01
P_2O_5	0.23	0.10	0.13	0.11	0.10	0.09	0.21	0.17	0.09	0.19
MnO	0.26	(0.01	(0.01	0.01	0.02	(0.01	0.02	0.01	(0.01	0.01
S	0.13	0.06	0.01	0.01	0.01	0.01	0.01	0.02	0.02	0.01
As (ppm)	-	-	-	-	-	-	-	-	-	-
Au	-	-	-	-	-	-	-	-	-	-
Ba	(25	-	-	-	-	-	-	-	-	-
Ce	-	11	6	7	5	6	19	(5	9	(5
Co	-	-	-	-	-	-	-	-	-	-
Cr	15	(10	(10	(10	(10	32	(10	11	12	(10
Cu	-	15	5	5	10	10	5	15	10	30
La	-	(5	(5	(5	6	(5	6	(5	6	(6
Li	-	(2	(2	(2	(2	(2	(2	(2	(2	(2
Mn	-	-	-	-	-	-	-	-	-	-
Nb	(5	(5	(5	(5	(5	(5	(5	(5	(5	(5
Ni	-	(5	(5	(5	15	20	5	5	(5	(5
Pb	-	(15	(15	(15	(15	(15	(15	(15	(15	(15
Rb	4	-	-	-	-	-	-	-	-	-
Sr	(5	-	-	-	-	-	-	-	-	-
Th	(10	(10	(10	(10	(10	(10	(10	(10	(10	(10
V	10	7	5	6	(5	14	20	5	(5	(5
Y	7	3	4	4	4	4	9	4	5	5
Zn	-	28	33	32	25	28	40	58	31	38
Zr	(10	(10	(10	(10	(10	13	(10	10	(10	(10

SAMPLE	85890	85891	85892	85893	85894	85895	85896	87601	87602	87649
CODE	J61D31	J61D31	J61D31	J61D31	J61D31	J61D31	J61D31	J61D31	J61D31	M36812
TRAVERSE	61	61	61	61	61	61	61	61	61	36
EAST	5151	5151	5151	5151	5151	5151	5151	5151	5151	5871
NORTH	67286	67286	67286	67286	67286	67286	67286	67286	67286	69431
SiO_2 (%)	43.0	50.8	56.2	42.6	42.0	44.6	43.6	48.8	48.3	39.8
Al_2O_3	0.2	0.3	0.2	0.5	0.3	0.3	0.3	0.2	0.3	0.3
Fe_2O_3	49.6	46.9	39.6	53.5	56.9	52.6	54.4	49.1	48.9	14.9
FeO	2.86	0.83	1.70	0.25	0.36	0.31	0.28	0.27	0.51	24.1
MgO	0.02	0.02	0.03	0.02	0.02	0.04	0.01	0.01	0.01	2.67
CaO	(0.01	(0.01	0.01	0.02	(0.01	(0.01	(0.01	0.02	0.01	0.71
Na_2O	(0.01	0.01	0.01	(0.01	0.01	(0.01	(0.01	(0.01	(0.01	0.09
K_2O	(0.01	(0.01	(0.01	(0.01	0.02	(0.01	(0.01	(0.01	(0.01	0.04
H_2O	4.17	1.31	2.07	2.43	1.68	1.92	1.39	1.61	1.85	15.8
TiO_2	(0.01	(0.01	(0.01	(0.01	(0.01	(0.01	(0.01	(0.01	(0.01	0.01
P_2O_5	0.29	0.10	0.14	0.38	0.14	0.21	0.20	0.15	0.20	0.16
MnO	(0.01	(0.01	0.01	0.01	0.02	0.02	0.01	(0.01	0.01	0.08
S	0.02	0.01	0.01	0.01	0.01	0.01	0.01	0.02	0.01	0.10
As (ppm)	-	-	-	-	-	-	-	-	-	-
Au	-	-	-	-	-	-	-	-	-	-
Ba	-	-	-	-	-	-	-	-	-	(25
Ce	89	16	14	25	19	8	10	9	13	(5
Co	-	-	-	-	-	-	-	-	-	-
Cr	(10	(10	(10	(10	(10	(10	(10	(10	(10	(10
Cu	5	10	25	10	5	5	60	5	10	15
La	(6	(6	20	(5	6	(5	6	13	(5	5
Li	(2	2	(2	(2	(2	(2	(2	(2	(2	-
Mn	-	-	-	-	-	-	-	-	-	-
Nb	(5	(5	(5	(5	(5	(5	(5	(5	(5	(5
Ni	10	5	(5	(5	(5	(5	(5	(5	(5	25
Pb	(15	(15	(15	(15	(15	(15	(15	(15	(15	(15
Rb	-	-	-	-	-	-	-	-	-	5
Sr	-	-	-	-	-	-	-	-	-	8
Th	(10	(10	(10	(10	(10	(10	(10	(10	(10	(10
V	6	5	(5	5	(5	(5	(5	(5	(5	13
Y	5	3	4	6	3	4	6	5	5	6
Zn	28	24	30	28	29	26	27	26	26	39
Zr	(10	(10	(10	(10	(10	(10	(10	(10	(10	(10

SAMPLE	87650	87651	87652	87653	87654	87655
CODE	H36812	H36812	H36812	H36812	H36812	H36812
TRAVERSE	36	36	36	36	36	36
EAST	5871	5871	5871	5871	5871	5871
NORTH	69431	69431	69431	69431	69431	69431
SiO_2 (%)	42.4	44.9	40.0	39.7	41.1	44.2
Al_2O_3	0.1	5.4	3.5	0.2	(0.1	1.0
Fe_2O_3	26.3	11.2	18.8	28.4	21.3	13.7
FeO	19.4	19.2	18.7	19.5	21.4	22.1
MgO	2.17	5.14	5.20	2.12	2.90	1.97
CaO	0.89	2.32	2.37	2.87	2.60	2.20
Na_2O	0.08	0.27	0.29	0.03	0.02	0.10
K_2O	0.10	0.43	0.47	0.08	0.05	0.21
H_2O	8.96	9.76	9.70	5.61	8.98	12.9
TiO_2	(0.01	0.32	0.27	(0.01	(0.01	0.04
P_2O_5	0.18	0.16	0.19	0.19	0.22	0.20
MnO	0.06	0.08	0.08	0.07	0.06	0.05
S	0.12	0.02	0.02	0.02	0.02	0.06
As (ppm)	-	-	-	-	-	-
Au	-	-	-	-	-	-
Ba	(25	115	147	96	(25	(25
Ce	19	19	(5	10	(5	8
Co	-	-	-	-	-	-
Cr	(10	58	52	13	(10	11
Cu	20	5	5	10	5	20
La	11	9	8	(5	(5	8
Li	-	-	-	-	-	-
Mn	-	-	-	-	-	-
Nb	(5	(5	(5	(5	(5	(5
Ni	10	35	30	10	(5	5
Pb	(15	(15	(15	(15	(15	15
Rb	(2	35	30	3	(2	15
Sr	8	10	14	13	16	8
Th	(10	(10	(10	(10	(10	(10
V	9	95	91	9	(5	11
Y	5	11	9	7	6	6
Zn	51	40	36	170	52	95
Zr	(10	40	18	(10	(10	11

BULLETIN 137

APPENDIX II

LISTING OF GEOCHEMICAL ANALYSIS DATA FILES

(CONTINUED)

DATA FILE II.4

ANALYSES OF MISCELLANEOUS SAMPLES FROM MINERAL DEPOSITS AND PROSPECTS

DATA FILE II.4 -- Analyses of miscellaneous samples from mineral deposits and prospects

Samples are classified in terms of type of material (CLASS) and host rock (HOST). Results are reported in parts per million.

Data headings:

CLASS	AMPH	amphibolite
	B	breccia
	BAS	basalt
	C	conglomerate
	CARB	carbonate/carbonated
	FC	ferruginized conglomerate
	FE	ironstone
	FELS	felsic volcanic rock
	FSH	ferruginized shale
	FSLT	ferruginized siltstone
	FSST	ferruginized sandstone
	G	gossan
	GRAN	granitoid
	LAT	laterite
	M	mylonite
	MICA	micaceous rock
	Q	quartz and/or chert
	S	sulphide
	SCH	schist
	SH	shale
	SIL	silicified
	SST	sandstone
	UM	ultramafic rock

These may be used in combination where two types of material are present, e.g. Q/S: chert and sulphide.

HOST	BAS	basalt
	BIF	banded iron-formation
	BREC	breccia
	CARB	carbonate
	CH	chert or quartzite

CONG	conglomerate
DOL	dolerite
FEL	felsic volcanic rocks
FELTF	felsic tuff
GAB	gabbro
GRAN	granitoid
LAT	laterite
SCH	schist
SH	shale
SST	sandstone
UM	ultramafic rock

SAMPLE	73602	73603	73604	73605A	73605B	73606A	73606B	73606C	73607	73608
HOST	SCH	BIF	BIF	BAS	BAS?	BIF	BIF	BIF	BIF	BIF
CLASS	G	G	Q/G/BIF	G	FE	G/Q	Q/G	G/BIF	Q/G	G/Q
EAST	5131	5797	5759	5794	5794	5917	5917	5917	5794	6020
NORTH	69037	68964	68989	68902	68902	68951	68951	68951	68905	69528
Ag (ppm)	-	-	-	-	-	-	-	-	-	-
As	6	18	3	760	320	9	6	3	14	92
Au	(0.1	6.6	0.2	(0.1	0.4	(0.1	(0.1	(0.1	(0.1	5.8
Co	25	10	10	50	30	10	5	10	10	15
Cr	-	-	-	-	-	-	-	-	-	-
Cu	200	100	45	650	50	80	25	80	50	250
Mn	-	-	-	-	-	-	-	-	-	-
Mo	-	-	-	-	-	-	-	-	-	-
Ni	160	45	35	310	220	15	(5	15	15	45
Pb	(10	(10	(10	(10	(10	(10	(10	(10	(10	(10
Sn	-	-	-	-	-	-	-	-	-	-
V	-	-	-	-	-	-	-	-	-	-
W	-	-	-	-	-	-	-	-	-	-
Zn	49	15	20	38	30	48	6	64	8	19
Fe (%)	66	20	6	10	4	30	6	18	8	15

SAMPLE	73609A	73609B	73609C	73610A	73610B	73610C	73610D	73610E	73610F	73610G
HOST	BIF	BIF	BIF	BIF	SH	SH	BIF	SH	BAS	BIF
CLASS	G	G	Q/BIF	Q	SH/S	SH/S	Q/S	SH	BAS	Q/BIF
EAST	6015	6015	6015	6026	6026	6026	6026	6026	6026	6026
NORTH	69516	69516	69516	69531	69531	69531	69531	69531	69531	69531
Ag (ppm)	-	-	-	-	-	-	-	-	-	-
As	8	10	1	(1	2	(1	1	(1	5	(1
Au	0.2	0.3	2.5	(0.1	6.7	13.3	26.3	5.3	0.9	(0.1
Co	20	20	(5	(5	45	30	30	20	30	45
Cr	-	-	-	-	-	-	-	-	-	-
Cu	320	370	95	15	460	410	600	220	65	85
Mn	-	-	-	-	-	-	-	-	-	-
Mo	-	-	-	-	-	-	-	-	-	-
Ni	40	55	5	15	90	100	65	45	80	90
Pb	(10	(10	(10	(10	(10	(10	(10	(10	20	(10
Sn	-	-	-	-	-	-	-	-	-	-
V	-	-	-	-	-	-	-	-	-	-
W	-	-	-	-	-	-	-	-	-	-
Zn	98	43	16	18	1300	55	42	30	1050	220
Fe (%)	40	33	5	3	36	22	40	15	16	8

SAMPLE	73610H	73610I	73611B	73611C	73611D	73612	73613	73614A	73614B	73615A
HOST	BIF	DOL	UM	UM	UM	BIF	UM	CH	CH	BIF
CLASS	Q/BIF	BAS	G/Q	G/Q	G	G	G/Q	Q/G	G/Q	G
EAST	6026	6026	5844	5844	5844	5855	5836	5811	5811	5759
NORTH	69531	69531	69083	69083	69083	69080	69098	69001	69001	69013
Ag (ppm)	-	-	-	-	-	-	-	-	-	-
As	3	2	1	2	2	9	68	2800	2700	15
Au	11.6	0.1	(0.1	(0.1	(0.1	(0.1	(0.1	(0.1	(0.1	(0.1
Co	20	10	90	10	25	35	35	15	20	90
Cr	-	-	-	-	-	-	-	-	-	-
Cu	260	55	400	150	860	60	20	960	970	290
Mn	-	-	-	-	-	-	-	-	-	-
Mo	-	-	-	-	-	-	-	-	-	-
Ni	35	15	150	90	65	130	810	90	110	330
Pb	(10	10	(10	(10	(10	(10	(10	40	30	(10
Sn	-	-	-	-	-	-	-	-	-	-
V	-	-	-	-	-	-	-	-	-	-
W	-	-	-	-	-	-	-	-	-	-
Zn	98	515	39	39	47	275	39	88	89	310
Fe (%)	18	20	22	20	18	20	16	14	13	44

SAMPLE	73615B	73615C	73616C	73617A	73617B	73618B	73618C	73619	73620	80601
HOST	BIF	BIF	SH	CH	CH	SCH	SCH	SST	UM	FELTF
CLASS	G	Q/G	G	Q/G	Q/S	G	Q/G	Q/S	Q/G	G
EAST	5759	5759	5890	5809	5809	5729	5729	6316	6355	6470
NORTH	69013	69013	68975	69047	69047	68909	68909	69990	70073	70007
Ag (ppm)	-	-	-	-	-	-	-	-	-	-
As	3	(1	34	191	202	4	55	5	1	10
Au	(0.1	(0.1	(0.1	(0.1	(0.1	(0.1	(0.1	0.8	0.6	13.5
Co	75	5	20	10	10	(5	75	(5	5	75
Cr	-	-	-	-	-	-	-	-	-	195
Cu	140	35	65	430	460	40	440	55	80	840
Mn	-	-	-	-	-	-	-	-	-	400
Mo	-	-	-	-	-	-	-	-	-	-
Ni	460	35	15	60	55	30	380	5	30	95
Pb	(10	(10	(10	20	20	10	50	(10	20	(10
Sn	-	-	-	-	-	-	-	-	-	-
V	-	-	-	-	-	-	-	-	-	-
W	-	-	-	-	-	-	-	-	-	-
Zn	58	33	23	63	57	73	1400	7	8	258
Fe (%)	44	6	60	6	5	2	22	1	3	51.6

SAMPLE	80602	80603	80607A	80607B	80607C	80611	80612	80613	80614	80615
HOST	CH	FELTF	BIF	BIF	BAS/CARB	UM	UM	FEL	FEL	FEL
CLASS	G	Q	G	G	SCH	SCH	Q/CARB	FELS	FELS	FELS
EAST	6484	6473	6470	6470	6470	6510	6510	6510	6510	6510
NORTH	70016	70007	70453	70453	70453	70570	70570	70573	70573	70573
Ag (ppm)	-	-	-	-	-	-	-	-	-	-
As	1	1	31	8	6	580	30	30	38	400
Au	0.1	0.2	<0.1	<0.1	<0.1	0.2	0.8	4.6	2.2	1.0
Co	<5	<5	95	20	10	65	40	15	20	45
Cr	5	20	65	180	500	4800	650	15	5	500
Cu	30	5	130	50	80	530	30	90	100	160
Mn	80	50	2700	90	310	230	2100	840	860	1250
Mo	-	-	-	-	-	-	-	-	-	-
Ni	5	<5	80	200	155	1280	570	25	25	205
Pb	10	<10	<10	<10	10	10	10	40	40	10
Sn	-	-	-	-	-	-	-	-	-	-
V	-	-	-	-	-	-	-	-	-	-
W	-	-	-	-	-	-	-	-	-	-
Zn	7	7	300	195	54	91	35	61	82	112
Fe (%)	1.5	4.3	50.4	35.6	13.2	42.2	4.6	5.5	4.2	6.8

SAMPLE	80616	80618	80619	80620	80621	80622	80623	80624	80625	80640
HOST	UM	UM	FEL	FEL	UM	FEL	UM	UM	UM	SST
CLASS	Q/MICA	FELS	FELS	FELS	G	FELS	Q	Q	Q	FSLT
EAST	6510	6502	6484	6484	6484	6502	6502	6502	6502	5221
NORTH	70573	70554	70515	70515	70515	70548	70548	70548	70548	67261
Ag (ppm)	-	-	-	-	-	-	-	-	-	3
As	1170	270	660	2350	22	95	56	23	5	40
Au	0.8	<0.1	<0.1	1.4	<0.1	<0.1	<0.1	<0.1	<0.1	<0.1
Co	40	70	75	65	20	10	10	10	<5	-
Cr	900	2300	1750	1400	1800	1200	2050	520	65	-
Cu	10	20	60	75	120	90	180	65	<5	81
Mn	690	670	500	1200	75	250	45	60	45	-
Mo	-	-	-	-	-	-	-	-	-	-
Ni	475	960	990	750	210	140	310	185	20	-
Pb	20	20	20	10	10	10	<10	<10	<10	<10
Sn	-	-	-	-	-	-	-	-	-	-
V	-	-	-	-	-	-	-	-	-	-
W	-	-	-	-	-	-	-	-	-	6
Zn	41	62	76	65	205	26	44	64	44	215
Fe (%)	3.9	5.4	6.2	8.4	31.6	8.7	10.4	6.5	0.4	30.8

SAMPLE	80641	80642	80643	80644	80645	80646A	80646B	80646C	80647	80648A
HOST	SST	CONG	CONG	CONG	CONG	CONG	CONG	CONG	CONG	SST
CLASS	SST	C	C	S	S	C	C	C	C	M
EAST	5217	5215	5215	5215	5215	5215	5215	5215	5217	5207
NORTH	67267	67341	67341	67341	67341	67341	67341	67341	67339	67343
Ag (ppm)	1	<1	<1	1	1	<1	<1	<1	<1	3
As	2	82	240	105	445	155	92	77	12	70
Au	0.1	<0.1	<0.1	<0.1	<0.1	<0.1	0.6	0.8	<0.1	0.4
Co	-	-	-	-	-	-	-	-	-	-
Cr	-	-	-	-	-	-	-	-	-	-
Cu	21	33	38	81	61	53	50	78	165	54
Mn	-	-	-	-	-	-	-	-	-	-
Mo	-	-	-	-	-	-	-	-	-	-
Ni	-	-	-	-	-	-	-	-	-	-
Pb	<10	<10	<10	<10	<10	<10	<10	<10	<10	<10
Sn	-	-	-	-	-	-	-	-	-	-
V	-	-	-	-	-	-	-	-	-	-
W	6	21	5	5	29	34	4130	2550	33	15
Zn	61	27	13	190	105	13	12	19	28	115
Fe (%)	7.2	5.0	6.6	48.8	43.5	15.2	17.1	21.4	5.8	2.0

SAMPLE	80648B	80648C	80649A	80649B	80649C	80649D	80650A	80650B	80651A	80651B
HOST	SST	CONG	CONG	CONG	CONG	CONG	CONG	CONG	BREC	BREC
CLASS	SST	C	C	C	C	C	C	C	B	B
EAST	5207	5207	5208	5208	5208	5208	5218	5218	5205	5205
NORTH	67343	67343	67344	67344	67344	67344	67341	67341	67412	67412
Ag (ppm)	2	1	1	<1	<1	<1	2	1	2	1
As	24	35	17	5	26	12	42	615	10	8
Au	<0.1	<0.1	14.6	0.1	0.1	55.1	0.2	0.1	0.1	<0.1
Co	-	-	-	-	-	-	-	-	-	-
Cr	-	-	-	-	-	-	-	-	-	-
Cu	71	32	33	51	65	105	180	270	38	36
Mn	-	-	-	-	-	-	-	-	-	-
Mo	-	-	-	-	-	-	-	-	-	-
Ni	-	-	-	-	-	-	-	-	-	-
Pb	<10	<10	20	20	25	26	10	10	14	20
Sn	-	-	-	-	-	-	-	-	-	-
V	-	-	-	-	-	-	-	-	-	-
W	4	<4	<4	<4	<4	<4	<4	<4	5	<4
Zn	175	9	13	11	11	20	70	85	14	14
Fe (%)	5.6	2.1	2.5	1.9	2.1	2.3	16.6	23.5	1.8	5.1

SAMPLE	80652A	80652B	80652C	80653A	80653B	80653C	80653D	80654A	80654B	80655D
HOST	CONG	SST	CONG	BREC	SH	CONG	CONG	CONG	CONG	DOL
CLASS	C	SST	C	B	SH	G	G	C	G	Q
EAST	5183	5183	5183	5189	5189	5189	5189	5189	5189	4751
NORTH	67452	67452	67452	67494	67494	67494	67494	67512	67512	68825
Ag (ppm)	1	1	<1	1	3	3	2	1	2	54
As	6	110	15	7	110	10	22	5	15	10
Au	<0.1	<0.1	<0.1	<0.1	<0.1	<0.1	<0.1	<0.1	<0.1	3.4
Co	-	-	-	-	-	-	-	-	-	32
Cr	-	-	-	-	-	-	-	-	-	-
Cu	105	85	110	105	77	54	220	30	50	1364
Mn	-	-	-	-	-	-	-	-	-	-
Mo	-	-	-	-	-	-	-	-	-	-
Ni	-	-	-	-	-	-	-	-	-	65
Pb	10	33	28	<10	14	<10	<10	<10	<10	120
Sn	-	-	-	-	-	-	-	-	-	-
V	-	-	-	-	-	-	-	-	-	-
W	<4	4	<4	<4	<4	<4	<4	4	<4	-
Zn	53	38	34	29	36	82	39	8	205	95
Fe (%)	4.5	8.4	7.4	10.5	28.4	37.7	29.3	3.8	58.2	15.2

SAMPLE	80657A	80658	80659	80660A	80660B	80660C	80663A	80663B	80664	80665
HOST	UM	FEL	GRAN	BAS	BAS	BAS	BAS/FEL	BAS/FEL	BAS	BAS
CLASS	Q/S	Q	GRAN	Q	Q	Q	Q	Q	Q	Q
EAST	4738	4736	4714	4753	4753	4753	4760	4760	4760	4762
NORTH	68823	68821	68866	68843	68843	68843	68797	68797	68786	68779
Ag (ppm)	1	3	2	<1	<1	1	<1	<1	1	<1
As	4	4	9	1	7	5	1	2	1	2
Au	<0.1	<0.1	0.2	0.4	0.2	2.2	<0.1	<0.1	<0.1	<0.1
Co	16	11	8	3	5	8	<3	8	3	2
Cr	-	-	-	-	-	-	-	-	-	-
Cu	152	33	31	17	54	103	9	62	67	33
Mn	-	-	-	-	-	-	-	-	-	-
Mo	-	-	-	-	-	-	-	-	-	-
Ni	127	22	24	14	18	25	11	25	17	23
Pb	19	545	33	9	25	32	3	<3	<3	6
Sn	-	-	-	-	-	-	-	-	-	-
V	-	-	-	-	-	-	-	-	-	-
W	-	-	-	-	-	-	-	-	-	-
Zn	70	62	49	13	58	17	15	20	10	13
Fe (%)	3.1	1.9	2.1	0.8	1.6	1.9	0.7	1.7	1.1	0.7

SAMPLE	80669A	80669B	80669C	80671D	80671E	80699A	80699B	80700A	80700B	80700C
HOST	UM	UM	UM	GAB	GAB	BAS	BAS	BAS	BAS	BAS
CLASS	Q	G	G	Q	Q/G	Q	Q/BAS	Q	Q	Q
EAST	4810	4810	4810	4815	4815	4689	4689	4703	4703	4703
NORTH	68715	68715	68715	68721	68721	68717	68717	68726	68726	68726
Ag (ppm)	2	5	6	2	3	<1	3	<1	<1	3
As	344	7700	8900	73	25	11	10	6	5	6
Au	0.8	11.5	18.4	5.0	12.3	<0.1	<0.1	<0.1	<0.1	<0.1
Co	10	25	151	67	263	<3	30	5	5	30
Cr	-	-	-	-	-	-	-	-	-	-
Cu	239	551	1326	9157	15685	166	156	25	576	55
Mn	-	-	-	-	-	-	-	-	-	-
Mo	-	-	-	-	-	-	-	-	-	-
Ni	17	51	123	10	24	8	118	8	16	106
Pb	<3	<3	<3	<3	<3	3	6	7	6	7
Sn	-	-	-	-	-	-	-	-	-	-
V	-	-	-	-	-	-	-	-	-	-
W	-	-	-	-	-	-	-	-	-	-
Zn	37	77	139	144	553	17	61	10	14	94
Fe (%)	5.2	45.4	36.9	5.4	15.4	0.9	6.1	0.9	0.7	5.7

SAMPLE	81372	81374	81375	81379A	81379B	81379C	81379D	81379E	81379F	81380A
HOST	UM	CH	CH	CONG	CONG	CONG	CONG	CONG	CONG/GAB	CONG
CLASS	SIL/UM	Q	Q/S	C	C	C	Q	Q	Q	FC
EAST	4782	4809	4809	4794	4794	4794	4794	4794	4794	4771
NORTH	68769	68738	68738	68717	68717	68717	68717	68717	68717	68766
Ag (ppm)	1	<1	4	1	3	3	1	1	<1	<1
As	54	2	2	6	5	10	3	40	7	1
Au	<0.1	<0.1	<0.1	<0.1	<0.1	<0.1	<0.1	2.0	<0.1	<0.1
Co	41	2	29	-	-	-	-	-	-	-
Cr	-	-	-	-	-	-	-	-	-	-
Cu	23	16	82	67	52	34	19	60	110	63
Mn	-	-	-	-	-	-	-	-	-	-
Mo	-	-	-	-	-	-	-	-	-	-
Ni	334	12	62	-	-	-	-	-	-	-
Pb	<3	3	<3	11	18	<10	<10	<10	<10	38
Sn	-	-	-	-	-	-	-	-	-	-
V	-	-	-	-	-	-	-	-	-	-
W	-	-	-	<4	<4	<4	<4	4250	19	27
Zn	51	17	103	70	86	89	11	5	12	9
Fe (%)	2.9	0.7	21.4	6.7	6.8	7.7	1.2	1.8	1.9	3.6

SAMPLE	81380B	81382C	81382D	81382E	81384A	81384B	81385	81386	85704	85706A
HOST	CONG	SCH	SCH	SCH	BAS	BAS	UM	BIF	BIF	BIF
CLASS	FC	SCH	Q	Q	G	G	G	G	G	G
EAST	4771	4771	4771	4771	6476	6476	6418	5336	5253	3649
NORTH	68766	68766	68766	68766	70459	70459	70466	71267	71192	68899
Ag (ppm)	<1	6	1	<1	<1	3	4	1	4	4
As	2	21	22	7	49	550	33	69	4	1
Au	<0.1	<0.1	<0.1	<0.1	<0.1	<0.1	<0.1	<0.1	<0.1	<0.1
Co	-	35	42	8	5	7	60	47	22	8
Cr	-	-	-	-	-	-	-	-	-	-
Cu	72	535	236	31	109	179	236	32	9	15
Mn	-	-	-	-	-	-	-	-	-	-
Mo	-	-	-	-	-	-	-	-	-	-
Ni	-	121	123	13	11	7	786	189	28	<3
Pb	22	60	16	24	<3	8	<3	<3	<3	<3
Sn	-	-	-	-	-	-	-	-	-	-
V	-	-	-	-	-	-	-	-	-	-
W	5	-	-	-	-	-	-	-	-	-
Zn	65	3418	639	84	38	61	105	81	23	32
Fe (%)	2.9	26.6	6.5	1.3	8.0	30.0	38.1	22.1	64.8	66.9

SAMPLE	85706B	85719	85726	85731	85732	85737	85738A	85738B	85742	85743
HOST	BIF	SH/BIF	BAS	BAS	BAS	FEL	FEL	FEL	BIF	BIF
CLASS	G	Q	Q	Q	Q/S	Q	G	G	FE	SCH
EAST	3649	4316	4346	4292	4292	4251	4251	4251	4230	4230
NORTH	68899	68290	68315	68281	68281	68244	68244	68244	67717	67717
Ag (ppm)	4	<1	<1	<1	<1	<1	9	13	6	2
As	<1	2	<1	<1	2	3	189	260	27	7
Au	<0.1	2.2	<0.1	14.3	5.5	0.1	<0.1	0.1	<0.1	<0.1
Co	10	5	6	5	12	3	3	5	3	3
Cr	-	-	-	-	-	-	-	-	-	-
Cu	16	128	45	43	70	20	654	214	671	295
Mn	-	-	-	-	-	-	-	-	-	-
Mo	-	-	-	-	-	-	-	-	-	-
Ni	11	11	36	13	45	13	<3	<3	3	16
Pb	<3	<3	3	3	12	3	459	293	85	67
Sn	-	-	-	-	-	-	-	-	-	-
V	-	-	-	-	-	-	-	-	-	-
W	-	-	-	-	-	-	-	-	-	-
Zn	21	17	17	17	34	16	176	82	244	72
Fe (%)	40.6	3.7	2.1	1.2	3.9	1.2	58.7	52.0	63.2	8.4

SAMPLE	85757	85760	85761	85785	85786	85787	85788	85795	85796	85797
HOST	BAS	SCH	SCH	SCH	SCH	SCH	SCH	CONG	CONG	SH
CLASS	Q/G	G/LAT	G	G	G	G	G	FC	FC	FSH
EAST	5008	5084	5103	4962	4962	4962	4962	4962	4962	4962
NORTH	67798	68049	68054	68166	68166	68166	68166	68166	68166	68166
Ag (ppm)	2	4	6	6	5	7	6	1	2	2
As	45	7	20	11	12	840	25	66	85	37
Au	<0.1	<0.1	<0.1	<0.1	<0.1	0.2	<0.1	0.1	<0.1	<0.1
Co	44	10	11	3	3	21	10	-	-	-
Cr	-	-	-	-	-	-	-	-	-	-
Cu	2862	112	306	45	56	786	64	45	46	38
Mn	-	-	-	-	-	-	-	-	-	-
Mo	-	-	-	-	-	-	-	-	-	-
Ni	212	68	26	<3	<3	<3	<3	-	-	-
Pb	<3	3	<3	<3	<3	49	<3	<10	<10	<10
Sn	-	-	-	-	-	-	-	-	-	-
V	-	-	-	-	-	-	-	-	-	-
W	-	-	-	-	-	-	-	5	<4	4
Zn	177	47	128	104	39	232	30	29	44	31
Fe (%)	5.4	38.8	52.5	63.7	60.2	57.6	62.6	7.2	33.6	35.2

SAMPLE	85798	85799	85800	85801	85802	85803	85804	85805	85806	85807
HOST	CONG	SST	SST	SST	CONG	SST	SST	SST	SST	CONG
CLASS	FC	FSST	Q	FSST	FC	SST/S	SST/S	FSST	FSST	C
EAST	4962	4787	4790	4790	4790	4793	4793	4797	4797	4796
NORTH	68166	68777	68778	68778	68778	68692	68692	68689	68689	68692
Ag (ppm)	1	2	<1	<1	1	1	1	2	3	1
As	17	200	27	27	100	54	47	38	36	23
Au	0.2	<0.1	3.8	1.1	<0.1	<0.1	<0.1	<0.1	<0.1	<0.1
Co	-	-	3	-	-	-	-	-	-	-
Cr	-	-	-	-	-	-	-	-	-	-
Cu	50	36	12	30	38	110	66	72	885	58
Mn	-	-	-	-	-	-	-	-	-	-
Mo	-	-	-	-	-	-	-	-	-	-
Ni	-	-	22	-	-	-	-	-	-	-
Pb	<10	<10	<3	<10	11	16	16	<10	45	16
Sn	-	-	-	-	-	-	-	-	-	-
V	-	-	-	-	-	-	-	-	-	-
W	<4	<4	-	18	4	34	<4	<4	<4	<4
Zn	20	96	19	21	65	39	44	83	125	37
Fe (%)	14.0	8.3	1.3	2.1	4.7	3.7	5.0	10.2	10.6	3.6

SAMPLE	85808	85809	85813	85814	85815	85821	85824	85869	85870A	85870B
HOST	CONG	BAS	BAS	BAS	BAS	BAS	CH	CONG	CONG	CONG
CLASS	Q	Q	Q/SCH	Q	Q	Q	G	FSST	Q	G
EAST	4796	4750	4750	4750	4861	4861	4861	4798	4797	4797
NORTH	68690	68517	6517	68517	68377	68377	68377	68716	68717	68717
Ag (ppm)	<1	<1	1	<1	<1	<1	5	2	<1	<1
As	52	4	5	2	3	73	8	23	32	13
Au	<0.1	0.2	<0.1	<0.1	0.6	56.6	0.5	<0.1	<0.1	<0.1
Co	<3	<3	<3	<3	<3	8	75	-	-	-
Cr	-	-	-	-	-	-	-	-	-	-
Cu	68	13	164	20	20	82	168	35	65	170
Mn	-	-	-	-	-	-	-	-	-	-
Mo	-	-	-	-	-	-	-	<5	<5	<5
Ni	20	15	16	6	7	26	149	-	-	-
Pb	<3	<3	11	<3	12	23	<3	<15	<15	30
Sn	-	-	-	-	-	-	-	-	-	-
V	-	-	-	-	-	-	-	-	-	-
W	-	-	-	-	-	-	-	5	10	<5
Zn	15	14	60	20	13	27	233	19	16	110
Fe (%)	1.4	1.8	11.6	5.7	0.9	2.0	57.0	4.3	6.5	36

SAMPLE	85870C	85870D	85870E	85870F	85871A	85871B	85871C	85871D	85872A	85872B
HOST	CONG	CONG	CONG	CONG	CONG	CONG	CONG	CONG	CONG	CONG
CLASS	Q	Q	Q	Q	Q	Q	Q	Q	Q	Q
EAST	4797	4797	4797	4797	4796	4796	4796	4796	4796	4796
NORTH	68717	68717	68717	68717	68720	68720	68720	68720	68723	68723
Ag (ppm)	<1	<1	<1	<1	<1	<1	<1	<1	<1	<1
As	<10	<10	<10	<10	14	32	91	72	39	<10
Au	<0.1	<0.1	<0.1	<0.1	0.1	0.6	<0.1	<0.1	<0.1	<0.1
Co	-	-	-	-	-	-	-	-	-	-
Cr	-	-	-	-	-	-	-	-	-	-
Cu	10	20	5	<3	25	40	10	10	15	35
Mn	-	-	-	-	-	-	-	-	-	-
Mo	<5	<5	<5	<5	<5	<5	<5	<5	<5	<5
Ni	-	-	-	-	-	-	-	-	-	-
Pb	<15	<15	<15	<15	<15	<15	<15	<15	<15	<15
Sn	-	-	-	-	-	-	-	-	-	-
V	-	-	-	-	-	-	-	-	-	-
W	<5	<5	<5	<5	<5	<5	9	<5	<5	5
Zn	6	9	5	5	9	8	5	3	4	12
Fe (%)	0.8	1.2	0.6	0.5	1.2	1.9	0.7	1.0	0.8	2.9

SAMPLE	85873A	85873B	85874	85875	85876	85877	85878A	85878B	85878C	85878D
HOST	BAS/SH	BAS/SH	SH	BAS	CONG	GAB	CONG	SST	SST	SST
CLASS	AMPH	Q	Q	Q	Q	Q	Q	SST	SST	SST
EAST	4793	4793	4794	4789	4801	4803	5775	5775	5775	5775
NORTH	68723	68723	68722	68715	68716	68712	68705	68705	68705	68705
Ag (ppm)	<1	<1	<1	<1	<1	<1	<1	<1	<1	<1
As	94	74	<10	39	<10	11	24	13	<10	<10
Au	<0.1	<0.1	<0.1	<0.1	<0.1	<0.1	0.2	<0.1	<0.1	5.6
Co	-	-	-	-	-	-	-	-	-	-
Cr	-	-	-	-	-	-	-	-	-	-
Cu	55	40	5	5	5	5	55	55	40	80
Mn	-	-	-	-	-	-	-	-	-	-
Mo	<5	<5	<5	<5	<5	<5	<5	<5	<5	<5
Ni	-	-	-	-	-	-	-	-	-	-
Pb	<15	<15	<15	<15	<15	<15	<15	<15	<15	<15
Sn	-	-	-	-	-	-	-	-	-	-
V	-	-	-	-	-	-	-	-	-	-
W	<5	17	19	14	<5	<5	7	13	15	5
Zn	43	32	6	7	4	3	2	25	20	23
Fe (%)	5.4	3.7	0.9	1.0	1.1	0.8	1.8	3.0	2.4	3.1

SAMPLE	85878E	85878F	85878G	85878H	85878I	85878J	85878K	85878L	85878M	85878N
HOST	SST	CONG	CONG	CONG	CONG	CONG	CONG	CONG	CONG	CONG
CLASS	SST	Q	Q	Q	Q	Q	C	C	Q/G	Q/G
EAST	5775	5775	5775	5775	5775	5775	5775	5775	5775	5775
NORTH	68705	68705	68705	68705	68705	68705	68705	68705	68705	68705
Ag (ppm)	1	<1	<1	<1	<1	2	<1	<1	<1	<1
As	11	<10	<10	<10	12	17	11	<10	20	19
Au	<0.1	2.9	2.4	0.6	1.0	9.7	<0.1	<0.1	1.8	0.2
Co	-	-	-	-	-	-	-	-	-	-
Cr	-	-	-	-	-	-	-	-	-	-
Cu	25	65	200	100	140	120	50	25	600	440
Mn	-	-	-	-	-	-	-	-	-	-
Mo	<5	<5	<5	<5	<5	<5	<5	<5	<5	<5
Ni	-	-	-	-	-	-	-	-	-	-
Pb	<15	<15	<15	<15	<15	<15	<15	<15	<15	<15
Sn	-	-	-	-	-	-	-	-	-	-
V	-	-	-	-	-	-	-	-	-	-
W	19	39	66	<5	35	<5	14	15	27	38
Zn	22	5	4	4	8	7	25	20	19	26
Fe (%)	2.7	1.0	1.8	1.0	1.1	3.6	2.8	2.4	25	32

SAMPLE	858786	858787	858788	858789	858782	858783	858784	858785	858786	858787
HOST	CONG	CONG	CONG	CONG	CONG	CONG	CONG	CONG	CONG	CONG
CLASS	Q/G	Q/G	Q	Q	Q	FE	Q/G	Q	Q/G	Q/G
EAST	5775	5775	5775	5775	5775	5775	5775	5775	5775	5775
NORTH	68705	68705	68705	68705	68705	68705	68705	68705	68705	68705
Ag (ppm)	<1	<1	<1	<1	<1	<1	<1	<1	1	<1
As	110	103	12	11	10	<10	<10	22	113	81
Au	<0.1	<0.1	<0.1	<0.1	0.4	0.1	<0.1	0.2	2.8	0.9
Co	-	-	-	-	-	-	-	-	-	-
Cr	-	-	-	-	-	-	-	-	-	-
Cu	450	500	140	95	160	95	15	60	300	320
Mn	-	-	-	-	-	-	-	-	-	-
Mo	<5	<5	<5	<5	<5	<5	<5	<5	<5	<5
Ni	-	-	-	-	-	-	-	-	-	-
Pb	<15	<15	<15	<15	<15	<15	<15	<15	<15	<15
Sn	-	-	-	-	-	-	-	-	-	-
V	-	-	-	-	-	-	-	-	-	-
W	19	13	11	<5	55	<5	<5	36	224	214
Zn	7	12	6	5	7	155	26	4	38	32
Fe (%)	8.9	12	6.7	2.2	2.3	56	25	3.0	24	26

SAMPLE	858788	85879	85880	87604	87612	87627	87658	87660	87661	87662
HOST	CONG	BIF	LAT	BAS	UM	BIF	BAS	SCH	SCH	BAS
CLASS	G	Q/G	LAT	Q/S	Q/G	Q	Q/G	G	Q/G	Q/G
EAST	5775	5149	5149	5787	5434	5595	4180	4067	4067	4067
NORTH	68705	67292	67292	69721	69981	69971	69099	69797	69797	69797
Ag (ppm)	<1	<1	<1	<1	36	<1	<1	<1	<1	<1
As	121	384	30	20	<10	<10	<1	270	91	165
Au	0.1	<0.1	<0.1	382	0.4	1.2	0.4	<0.1	<0.1	<0.1
Co	-	-	-	-	-	-	<5	150	10	5
Cr	-	-	-	-	-	-	-	-	-	-
Cu	35	740	35	110	1650	10	40	1950	260	240
Mn	-	-	-	-	-	-	65	2500	65	45
Mo	<5	<5	<5	<5	13	33	-	-	-	-
Ni	-	-	-	-	-	-	10	230	20	65
Pb	<15	<15	<15	15	15000	80	<15	<15	<15	<15
Sn	-	-	-	-	-	-	-	-	-	-
V	-	-	-	-	-	-	-	-	-	-
W	9	185	<5	77	-	4	-	-	-	-
Zn	250	25	35	91	44700	170	13	290	25	18
Fe (%)	34	18	51	3.5	2.6	1.7	1.1	52	6.7	7.0

SAMPLE	87667	87668	87669	87670	87671	87672	81376A	813768	81376C	813760
HOST	BIF	BIF	FEL	BIF	BIF	BIF	SH	SH	SH	SH
CLASS	G	G	G	Q/G	Q/G	Q/G	Q	G	G	G
EAST	4076	4076	4076	4076	4076	4076	4793	4793	4793	4793
NORTH	69864	69864	69864	69864	69864	69864	68726	68726	68726	68726
Ag (ppm)	<1	<1	<1	<1	<1	<1	-	-	-	-
As	5	8	9	11	90	9	-	-	-	-
Au	<0.1	<0.1	<0.1	<0.1	<0.1	<0.1	-	-	-	-
Co	55	5	15	15	15	<5	-	-	-	-
Cr	-	-	-	-	-	-	2000	590	2000	410
Cu	110	20	100	5	60	50	32	551	456	137
Mn	1700	190	170	45	85	40	-	-	-	-
Mo	-	-	-	-	-	-	-	-	-	-
Ni	35	5	30	10	15	10	90	70	360	40
Pb	<15	<15	<15	20	<15	<15	<10	60	20	<10
Sn	-	-	-	-	-	-	-	-	-	-
V	-	-	-	-	-	-	10	30	30	<10
W	-	-	-	-	-	-	-	-	-	-
Zn	240	41	71	13	41	10	18	58	155	12
Fe (%)	52	57	20	2.4	5.7	2.9	-	-	-	-

SAMPLE	81376E	81376F	813766	81376H	81376I	81376J	81376K	81377A	81377B	81377C
HOST	SH	-	-	-	-	-	SH	-	-	SH
CLASS	G	C/Q	SH	SH	SH/Q	SH	G	FE	FE	G
EAST	4793	4793	4793	4793	4793	4793	4793	4793	4793	4793
NORTH	68726	68726	68726	68726	68726	68726	68726	68702	68702	68702
Ag (ppm)	-	-	-	-	-	-	-	-	-	-
As	-	-	-	-	-	-	-	-	-	-
Au	-	-	-	-	-	-	-	-	-	-
Co	-	-	-	-	-	-	-	-	-	-
Cr	380	40	7000	6000	3000	1100	580	250	110	50
Cu	107	11	52	26	48	605	215	48	23	62
Mn	-	-	-	-	-	-	-	-	-	-
Mo	-	-	-	-	-	-	-	-	-	-
Ni	20	10	320	80	160	750	160	10	20	60
Pb	10	<10	<10	20	<10	<10	<10	<10	<10	<10
Sn	-	-	-	-	-	-	-	-	-	-
V	20	<10	20	210	20	60	120	140	50	<10
W	-	-	-	-	-	-	-	-	-	-
Zn	9	2	22	7	34	283	82	8	13	204
Fe (%)	-	-	-	-	-	-	-	-	-	-

SAMPLE	813770
HOST	SH
CLASS	Q/S
EAST	4793
NORTH	68702
Ag (ppm)	-
As	-
Au	-
Co	-
Cr	70
Cu	39
Mn	-
Mo	-
Ni	10
Pb	<10
Sn	-
V	<10
W	-
Zn	10
Fe (%)	-

DATA FILE II.5

ANALYSES OF SAMPLES WITH RARE-EARTH ELEMENT DETERMINATIONS

DATA FILE II.5

Analyses of samples with rare-earth element determinations. Data headings are as for DATA FILE II.1 (volcanic rocks) and DATA FILE II.2 (granitoids).

SAMPLE	81435	81442	81449	81456	81466	81480	81483	81491	81498	81500
ROCK-TYPE	B	N	K	B	A	D	A	D	B	B
EAST	6270	6279	6289	6298	6533	6524	6520	6518	6631	6630
NORTH	70337	70337	70337	70337	70270	70378	70378	70389	70337	70337
SiO_2 (%)	50.9	57.3	50.0	50.9	57.5	68.9	60.7	66.0	50.5	50.3
Al_2O_3	13.6	15.0	10.8	14.0	16.1	14.7	15.6	14.9	13.1	12.8
Fe_2O_3	2.1	1.5	1.2	2.0	2.6	0.4	1.6	0.9	2.7	2.7
FeO	8.21	5.28	7.31	7.09	4.42	1.92	3.72	2.41	12.6	12.0
MgO	6.86	4.71	14.9	7.85	3.97	1.78	3.60	2.13	5.15	5.53
CaO	11.9	9.21	9.21	11.6	5.98	2.48	5.78	4.20	10.1	10.4
Na_2O	2.33	3.28	1.15	1.61	2.58	5.80	3.36	4.17	1.72	1.83
K_2O	0.11	0.12	0.06	0.11	1.68	0.84	2.03	1.35	0.10	0.15
LOI	1.86	1.49	4.14	3.02	3.35	1.78	2.51	2.03	1.78	1.91
TiO_2	1.35	0.78	0.40	0.71	0.72	0.32	0.54	0.41	1.02	1.04
P_2O_5	0.16	0.27	0.08	0.09	0.24	0.12	0.23	0.16	0.13	0.13
MnO	0.20	0.13	0.19	0.17	0.12	0.04	0.08	0.05	0.21	0.25
S	0.006	<0.001	0.003	0.019	0.007	0.007	0.008	0.004	0.003	0.003
Ba (ppm)	75	86	69	57	616	262	438	500	31	27
Co	57.5	48.8	56.4	66.7	33.2	33.6	34.0	29.9	71.4	66.1
Cr	590	210	1250	240	80	80	150	130	80	110
Cu	152	36	231	171	138	135	119	89	81	69
Li	3	3	14	5	9	6	15	11	6	8
Mo	-	-	-	-	<1	<1	<1	<1	-	-
Ni	130	120	370	100	50	40	80	60	80	100
Nb	<5	9	<5	5	11	8	9	10	<5	7
Pb	<10	<10	<10	<10	<10	<10	<10	<10	<10	<10
Rb	-	-	-	-	69	22	58	38	-	-
Sn	-	-	-	-	3	8	7	10	-	-
Sr	113	303	56	73	526	275	700	472	83	85
Th	-	3.00	0.6	-	7.19	5.58	5.44	5.87	0.5	0.5
U	-	-	-	-	1.6	1.7	1.4	1.4	-	-
V	335	156	233	267	141	67	102	67	331	328
Y	24	20	15	20	21	10	15	10	27	25
W	-	-	-	-	-	-	-	-	-	-
Zn	100	41	143	78	94	33	63	53	110	105
Zr	71	142	31	51	143	124	128	125	63	59
La (ppm)	3.8	11.2	2.2	2.2	30.5	14.7	22.1	19.0	5.8	2.2
Ce	11.6	31.9	5.4	7.0	60.0	28.7	43.0	36.2	10.5	8.4
Nd	9.6	14.9	4.9	7.0	25.9	11.8	18.4	14.3	8.0	8.5
Sm	3.03	3.21	1.00	1.79	4.74	2.47	3.77	2.88	2.67	2.72
Eu	1.21	1.11	0.40	0.72	1.25	0.59	1.08	0.82	0.99	0.98
Tb	0.73	0.58	0.37	0.51	0.66	0.32	0.47	0.34	0.70	0.75
Yb	2.60	1.91	1.63	2.03	2.25	0.86	1.54	0.91	2.93	2.88
Lu	0.40	0.29	0.25	0.32	0.35	0.13	0.22	0.14	0.51	0.45
Cs (ppm)	-	-	-	-	0.85	0.48	0.76	0.70	-	-
Hf	2.02	3.40	0.97	1.27	3.63	3.15	3.36	3.26	2.46	1.89
Sc	35.1	17.9	34.3	40.0	17.9	7.3	16.6	8.6	42.0	42.8
Ta	0.30	0.66	0.1	0.27	0.68	0.81	0.64	0.66	0.56	0.53
Hf/3	0.67	1.13	0.32	0.42	1.21	1.05	1.12	1.09	0.82	0.63

SAMPLE	81505	81507	81511	81517	81524	81527	81528	81534	81541	81564
ROCK-TYPE	K	K	K	K	K	B	B	B	B	R
EAST	6625	6620	6561	6556	6550	6546	6545	6505	6511	6603
NORTH	70337	70337	70513	70512	70511	70511	70511	70426	70423	70220
SiO_2 (%)	48.5	48.1	48.6	50.2	51.2	50.5	50.7	47.9	52.0	75.2
Al_2O_3	9.4	9.1	10.2	10.7	11.4	13.4	13.3	13.7	12.9	11.2
Fe_2O_3	1.4	1.3	2.2	1.7	1.4	2.6	2.6	3.7	1.5	1.3
FeO	10.4	11.0	9.28	7.84	7.98	9.25	9.09	9.54	8.20	3.18
MgO	14.3	13.3	14.5	14.5	12.9	6.10	5.55	5.55	8.39	1.02
CaO	8.71	7.84	8.14	8.31	8.80	10.4	10.6	10.6	7.71	0.59
Na_2O	1.43	2.10	0.72	1.18	0.82	2.08	2.13	1.73	1.81	4.16
K_2O	0.13	(0.01	0.17	0.16	0.12	0.24	0.23	0.29	0.44	0.89
LOI	3.96	4.69	5.80	4.09	3.39	3.51	4.11	4.49	5.10	2.34
TiO_2	0.84	0.90	0.56	0.42	0.43	1.19	1.21	1.30	1.03	0.23
P_2O_5	0.10	0.12	0.08	0.07	0.08	0.17	0.17	0.17	0.11	0.04
MnO	0.19	0.21	0.18	0.16	0.17	0.25	0.24	0.21	0.18	0.05
S	0.005	0.009	0.029	0.034	0.024	0.084	0.12	0.10	0.025	0.014
Ba (ppm)	118	28	(20	43	(20	55	24	137	66	242
Co	80.0	82.3	76.8	62.2	59.5	53.8	53.5	57.6	56.5	-
Cr	-	-	-	-	-	110	110	100	-	-
Cu	58	270	148	67	68	204	214	207	156	56
Li	19	10	14	10	8	8	6	8	21	7
Mo	-	-	-	-	-	-	-	-	-	4
Ni	560	310	410	340	280	100	90	110	140	(10
Nb	8	5	(5	(5	(5	(5	10	6	7	23
Pb	(10	(10	(10	(10	(10	(10	(10	(10	(10	(10
Rb	-	-	-	-	-	-	-	-	-	26
Sn	-	-	-	-	-	-	-	-	-	10
Sr	61	61	24	30	21	95	94	125	98	37
Th	1.25	0.7	1.1	0.8	0.8	-	-	-	2.30	7.85
U	-	-	-	-	-	-	-	-	0.8	2.1
V	232	273	238	229	229	323	329	364	277	(5
Y	22	21	16	14	15	28	28	30	19	147
W	-	-	-	-	-	-	-	-	-	-
Zn	127	109	75	53	59	101	83	111	102	36
Zr	77	67	43	32	31	71	80	76	80	484
La (ppm)	5.72	4.08	4.4	2.3	2.2	3.2	4.0	3.6	8.0	43.4
Ce	17.6	15.3	9.9	-	-	12.1	12.8	14.0	20.6	102
Nd	10.7	9.1	6.0	-	-	10.8	10.4	12.1	12.1	63.1
Sm	3.04	2.68	1.62	1.01	1.07	3.17	3.20	3.50	3.10	17.3
Eu	0.98	0.97	0.65	0.42	0.40	1.18	1.22	1.34	1.10	3.81
Tb	0.60	0.64	0.44	0.33	0.38	0.82	0.88	0.89	0.62	3.67
Yb	2.14	2.00	1.73	1.50	1.60	3.24	3.36	3.72	2.05	16.8
Lu	0.33	0.32	0.27	0.26	0.26	0.56	0.53	0.61	0.33	2.73
Cs (ppm)	-	-	-	-	-	-	-	-	-	-
Hf	2.16	2.05	1.48	0.95	1.03	2.46	2.34	2.68	2.41	14.5
Sc	-	-	-	-	-	38.2	39.4	40.1	-	4.87
Ta	0.35	0.24	0.18	0.14	0.13	0.33	0.36	0.39	0.41	2.63
Hf/3	0.72	0.68	0.49	0.32	0.34	0.82	0.78	0.89	0.80	4.83

SAMPLE	81613	81711A	81714A	81726A	81740	81758	81760	81762A	81770	83212
ROCK-TYPE	D	T	T	J	S	R	T	T	G	K
EAST	6347	6352	6352	6298	6393	5838	5865	5865	5910	5963
NORTH	70287	70288	70288	70364	70949	69765	69700	69700	69581	69343
SiO_2 (%)	70.6	65.0	65.4	76.1	73.6	79.1	66.1	66.8	69.2	49.7
Al_2O_3	15.1	13.8	13.9	12.5	13.6	10.1	15.3	15.0	14.7	10.7
Fe_2O_3	1.0	2.10	1.50	0.40	0.60	0.9	1.80	1.80	1.60	3.4
FeO	1.18	2.67	2.83	1.22	0.77	0.86	2.50	2.51	1.42	8.35
MgO	0.87	3.82	3.59	0.23	0.15	0.11	1.56	1.92	1.12	10.90
CaO	2.60	4.23	4.02	1.35	1.01	0.33	3.82	4.11	2.61	11.77
Na_2O	5.14	3.65	3.85	4.46	3.64	4.00	4.39	4.34	4.37	1.24
K_2O	1.45	1.40	1.74	1.52	4.91	2.38	1.58	1.12	2.04	0.06
LOI	1.30	2.29	1.89	0.99	0.64	0.71	1.23	1.10	0.91	2.11
TiO_2	0.27	0.56	0.49	0.11	0.12	0.27	0.42	0.43	0.36	0.54
P_2O_5	0.12	0.19	0.17	0.06	0.09	0.05	0.11	0.15	0.14	0.10
MnO	0.04	0.07	0.07	0.03	0.01	<0.01	0.04	0.07	0.02	0.19
S	0.006	-	-	-	-	-	-	-	-	-
Be (ppm)	535	693	679	633	561	620	562	633	596	117
Co	-	17.5	16.2	2.4	-	-	63.5	-	70.1	70.4
Cr	-	320	300	240	-	-	24	-	20	-
Cu	79	45	33	13	8	19	24	25	25	45
Li	8	7	8	12	10	2	6	5	11	5
Mo	1	3	3	1	<1	<1	<1	1	<1	-
Ni	10	112	96	20	17	32	61	44	39	235
Nb	5	<10	<10	<10	11	11	11	<10	8	<5
Pb	<10	10	20	<10	20	<10	10	20	<10	20
Rb	53	57	71	62	68	28	62	61	81	-
Sn	7	<5	<5	<5	-	5	5	<5	5	-
Sr	431	312	266	136	76	23	168	171	428	94
Th	6.54	12.5	11.5	13.3	10.2	8.06	11.2	8.40	12.2	0.9
U	2.0	1.9	1.6	1.7	2.6	1.9	2.0	1.7	3.0	-
V	28	102	91	<10	<10	<10	63	67	40	240
Y	5	23	20	13	38	46	27	26	8	19
W	-	8	6	<2	-	-	-	<2	-	-
Zn	43	45	47	31	46	34	42	43	57	65
Zr	143	195	167	128	112	212	148	137	121	35
La (ppm)	22.1	28.8	29.1	31.1	10.4	20.1	26.4	21.3	36.3	2.2
Ce	40.2	57.9	56.9	57.1	22.5	41.6	50.5	40.8	70.2	-
Nd	14.3	22.6	22.1	18.3	11.0	19.3	18.0	16.9	27.5	-
Sm	2.39	4.23	3.86	2.77	2.38	4.56	3.58	3.51	4.16	1.13
Eu	0.64	0.99	0.94	0.65	0.53	0.87	0.88	0.89	1.09	0.56
Tb	0.28	0.63	0.59	0.37	0.28	0.83	0.69	0.55	0.62	0.63
Yb	0.38	1.94	1.74	1.04	0.53	4.00	2.50	2.56	0.56	1.58
Lu	-	0.30	0.27	0.16	-	0.64	0.40	0.40	0.09	0.26
Cs (ppm)	1.34	1.18	2.23	1.12	-	-	1.67	1.71	2.42	-
Hf	3.30	5.59	4.78	3.34	2.52	5.35	4.07	4.19	4.23	1.05
Sc	1.69	12.0	10.9	2.13	1.91	2.87	9.9	4.63	4.3	-
Ta	0.88	0.60	0.54	0.53	0.66	1.02	1.05	0.47	1.12	0.15
Hf/3	1.10	1.86	1.59	1.11	0.84	1.78	1.36	1.40	1.41	0.35

SAMPLE	83214	83280	83290	83308A	83310A	83311A	83324A	83325A	83329	83339
ROCK-TYPE	B	D	R	S	M	G	M	M	A	G
EAST	5949	5214	5226	5473	5500	5593	5776	5682	5800	6669
NORTH	69347	69306	69334	69207	69204	69116	68858	68857	68116	68253
SiO_2 (%)	51.6	71.9	72.7	67.2	62.6	70.0	71.2	70.8	62.0	71.6
Al_2O_3	12.3	11.5	14.1	14.4	14.7	15.1	14.9	15.2	16.4	14.9
Fe_2O_3	3.3	1.3	0.4	1.70	2.70	0.70	1.10	0.90	2.4	0.20
FeO	8.29	4.54	0.77	2.12	3.40	1.41	0.95	1.21	4.04	1.42
MgO	9.11	0.90	0.69	1.44	1.47	0.67	0.48	0.53	4.67	0.35
CaO	9.77	2.29	1.08	2.56	3.73	2.22	1.90	1.44	3.13	1.97
Na_2O	1.37	1.17	4.68	3.04	4.11	4.65	4.88	4.77	5.38	4.66
K_2O	0.08	3.54	3.36	5.63	2.55	2.45	2.25	2.68	0.22	2.22
LOI	2.52	1.45	0.86	0.91	1.50	1.48	1.13	0.90	2.49	0.68
TiO_2	0.62	0.28	0.17	0.40	1.25	0.30	0.26	0.29	0.66	0.19
P_2O_5	0.09	0.06	0.07	0.33	0.68	0.12	0.14	0.13	0.14	0.07
MnO	0.15	0.11	0.01	0.09	0.07	0.02	0.03	0.03	0.09	0.02
S	-	-	-	-	-	-	-	-	-	-
Ba (ppm)	125	894	1580	3463	1886	716	1198	1249	107	1193
Co	69.4	41.3	30.1	10.1	12.9	6.5	-	-	34.7	97.6
Cr	-	60	50	210	240	190	-	-	170	(10
Cu	68	63	7	21	31	16	18	18	44	6
Li	8	32	13	10	25	18	46	34	23	23
Mo	-	(1	(1	2	3	(1	2	2	(1	(1
Ni	125	32	30	31	30	22	21	28	132	25
Nb	(5	14	5	16	20	12	(10	(10	8	(5
Pb	10	(10	(10	50	30	20	30	40	10	10
Rb	-	203	74	183	71	101	92	91	14	76
Sn	-	7	9	(5	(5	(5	(5	(5	7	5
Sr	50	70	108	588	911	266	622	599	55	497
Th	-	14.8	9.69	55.7	25.3	18.4	10.2	11.6	4.26	9.62
U	-	4.5	2.5	4.7	3.1	2.2	1.9	3.7	1.1	1.7
V	299	27	22	64	78	28	20	22	113	16
Y	21	70	8	29	32	11	(5	(5	22	(5
W	-	-	-	(2	(2	(2	(2	(2	-	-
Zn	66	86	8	63	126	55	66	70	75	39
Zr	37	255	79	245	403	199	153	163	166	133
La (ppm)	2.2	37.7	9.95	109	155	34.2	43.1	47.5	17.4	34.8
Ce	-	70.1	19.1	205	324	58.7	82.4	95.8	35.3	42.6
Nd	-	30.3	9.4	71.8	114	18.5	27.4	32.8	16.5	17.3
Sm	1.31	6.36	2.06	11.8	15.0	3.04	4.02	4.93	3.55	2.10
Eu	0.53	1.26	0.48	2.46	3.47	0.76	1.02	1.15	1.14	0.57
Tb	0.47	1.33	0.26	1.45	1.52	0.47	0.35	0.38	0.50	0.24
Yb	1.88	6.28	0.50	2.80	2.60	0.75	0.38	0.38	1.59	0.20
Lu	0.32	1.02	0.07	0.47	0.40	0.12		-	0.24	-
Cs (ppm)	-	11.7	0.3	1.11	0.81	0.3	6.74	2.39	0.55	5.10
Hf	1.26	6.82	2.57	7.18	11.4	5.07	3.76	3.89	3.99	3.19
Sc	-	7.0	4.1	9.54	8.5	3.25	1.09	1.14	13.3	1.66
Ta	0.18	1.23	0.95	1.17	1.26	0.50	0.47	0.44	0.68	0.51
Hf/3	0.42	2.27	0.86	2.39	3.80	1.69	1.25	1.30	1.33	1.06

SAMPLE	83380	83398A	83399	83401	83407	83474	83478	83501	83524	83536
ROCK-TYPE	G	G	G	G	M	G	M	M	M	B
EAST	4354	4626	4626	4624	4731	5244	5383	5522	5648	5256
NORTH	68486	68166	68166	68166	67678	68134	68404	68399	68586	67486
SiO_2 (%)	63.1	-	71.3	70.7	72.2	70.1	72.1	69.9	69.8	50.4
Al_2O_3	14.6	-	15.3	15.5	12.9	15.0	14.3	14.7	15.7	13.4
Fe_2O_3	2.60	-	0.60	0.60	0.60	0.70	0.90	1.40	0.80	2.3
FeO	2.76	-	1.35	1.41	3.59	1.77	0.98	1.39	1.47	11.23
MgO	2.50	-	0.59	0.68	0.31	0.79	0.42	0.65	0.77	6.13
CaO	3.72	-	2.26	2.20	1.34	2.44	1.35	1.53	2.59	8.45
Na_2O	3.36	-	4.57	4.68	3.23	4.47	4.39	4.32	4.43	3.29
K_2O	3.70	-	2.26	2.31	4.23	1.89	3.47	3.60	1.89	0.22
LOI	1.36	-	0.55	0.64	0.57	1.07	0.67	0.81	0.87	2.33
TiO_2	0.63	-	0.26	0.25	0.29	0.41	0.24	0.36	0.35	1.52
P_2O_5	0.41	-	0.11	0.10	0.07	0.16	0.11	0.15	0.15	0.18
MnO	0.08	-	0.02	0.02	0.09	0.02	0.02	0.04	0.03	0.17
S	-	-	-	-	-	-	-	-	-	0.004
Be (ppm)	2251	-	964	1010	1613	1649	1813	2189	1050	150
Co	-	51.3	44.9	33.8	-	5.33	3.18	5.04	5.54	61.8
Cr	-	<10	<10	<10	-	230	225	200	170	140
Cu	27	-	16	9	14	31	31	25	36	198
Li	38	-	125	123	20	18	13	30	36	3
Mo	4	-	2	2	5	3	2	4	<1	-
Ni	60	-	30	25	25	26	19	26	32	122
Nb	<10	-	<10	<10	19	<10	<10	14	<10	<10
Pb	30	-	<10	20	30	<10	<10	<10	<10	<10
Rb	230	84	72	107	154	64	84	165	83	-
Sn	<5	-	<5	<5	<5	<5	<5	<5	<5	<5
Sr	631	-	571	570	200	547	393	667	523	155
Th	23.4	12.9	14.5	16.0	20.2	25.0	38.0	33.4	17.7	1.12
U	4.9	1.7	1.2	2.3	5.5	0.9	1.6	5.3	2.0	-
V	95	-	26	30	<10	32	16	24	44	308
Y	14	-	<5	<5	68	<5	5	16	<5	29
W	2	-	<2	<2	4	<2	<2	<2	<2	-
Zn	73	-	38	39	98	48	39	65	61	87
Zr	153	-	159	172	420	261	237	329	242	99
La (ppm)	62.6	35.7	42.4	42.3	84.5	73.1	97.7	163	57.8	5.7
Ce	112	50.6	64.0	74.1	172	120	168	280	93.7	20.4
Nd	42.8	17.3	20.6	22.6	72.7	31.3	47.6	78.7	25.7	15.6
Sm	7.16	2.30	2.83	3.07	13.7	3.70	6.00	10.1	3.04	4.22
Eu	1.89	0.78	0.66	0.74	3.15	0.85	0.95	1.63	0.83	1.59
Tb	0.82	0.23	0.31	0.30	2.00	0.38	0.66	0.97	0.35	0.88
Yb	1.66	0.21	0.27	0.28	5.75	0.33	0.38	1.68	0.31	2.55
Lu	0.25	-	-	-	0.86	0.06	-	0.29	0.06	0.41
Cs (ppm)	17.4	1.85	1.95	10.3	4.98	1.54	0.60	1.59	1.56	-
Hf	4.83	3.02	3.98	4.13	12.7	5.84	6.16	8.18	5.34	3.15
Sc	5.03	1.54	2.80	2.8	4.74	2.44	2.69	3.70	2.63	35.9
Ta	0.64	1.30	0.97	1.07	1.57	0.16	0.17	0.96	0.14	0.49
Hf/3	1.61	1.01	1.33	1.38	4.23	1.95	2.05	2.73	1.78	1.05

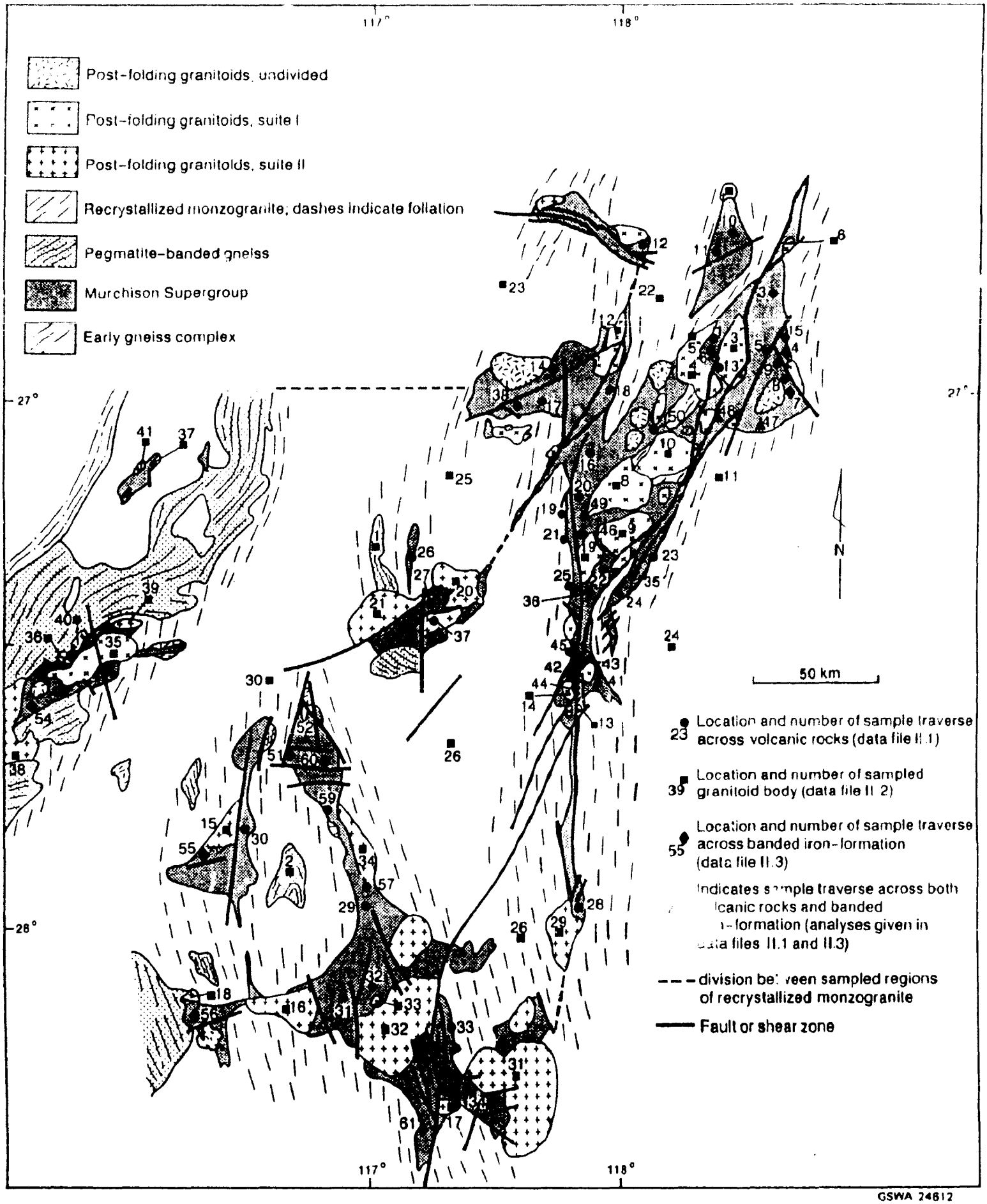
REE data for the leucocratic component of a pegmatite-banded gneiss are recorded as 83398A; the equivalent data for the mesocratic component of the same rock are given as 83399. The oxide data reported for 83399 represent the bulk rock.

SAMPLE	83541	83545	83549	83551
ROCK-TYPE	B	K	S	S
EAST	5287	5277	5258	4271
NORTH	67449	67406	67273	67701
SiO_2 (%)	51.1	51.1	76.3	76.9
Al_2O_3	14.3	13.6	12.9	11.6
Fe_2O_3	1.6	1.3	0.60	0.60
FeO	7.77	8.15	1.10	1.22
MgO	7.73	9.11	0.26	0.13
CaO	11.71	10.94	0.85	0.75
Na_2O	1.45	1.37	3.30	2.93
K_2O	0.18	0.52	4.43	4.29
LOI	2.29	2.74	0.91	0.60
TiO_2	0.58	0.68	0.17	0.13
P_2O_5	0.09	0.09	0.07	0.06
MnO	0.16	0.15	0.03	0.03
S	0.006	0.014	-	-
Ba (ppm)	87	146	584	341
Co	52.2	53.4	2.52	1.70
Cr	430	-	210	250
Cu	87	89	26	34
Li	4	5	53	42
Mo	-	-	<1	<1
Ni	146	199	22	21
Nb	<10	<10	21	19
Pb	<10	12	24	48
Rb	-	-	81	34
Sn	<5	<5	<5	<5
Sr	80	85	81	34
Th	0.4	-	46.5	38.0
U	-	-	12.1	9.8
V	218	209	10	<10
Y	19	17	69	76
W	-	-	<2	5
Zn	67	69	35	47
Zr	43	33	170	152
La (ppm)	-	3.0	91.0	63.4
Ce	7.4	7.8	178	135
Nd	5.8	4.2	56.0	55.2
Sm	1.64	1.33	9.66	11.7
Eu	0.60	0.53	0.66	0.65
Tb	0.43	0.39	1.45	2.04
Yb	1.81	1.73	1.45	2.04
Lu	0.31	0.27	0.69	0.96
Cs (ppm)	-	-	5.55	5.95
Hf	1.21	1.03	5.65	5.95
Sc	43.1	-	3.4	3.4
Ta	0.14	0.11	2.76	1.63
Hf/3	0.40	0.34	1.55	1.65

FIGURE AII.1

LOCATIONS OF SAMPLE TRAVERSES FOR SUPRACRUSTAL ROCKS (DATA FILES II.1 & II.3) THE NUMBERS ARE THOSE USED IN THE DATA-FILE CODE, FOR EACH SAMPLE, TO IDENTIFY ITS LOCATION




117°
118°
27°
28°
Post-folding granitoids, undivided
Post-folding granitoids, suite I
Post-folding granitoids, suite II
Recrystallized monzogranite; dashes indicate foliation
Pegmatite-banded gneiss
Murchison Supergroup
Early gneiss complex
N
50 km
Location and number of sample traverse across volcanic rocks (data file II.1)
Location and number of sampled granitoid body (data file II.2)
Location and number of sample traverse across banded iron-formation (data file II.3)
Indicates sample traverse across both volcanic rocks and banded iron-formation (analyses given in data files II.1 and II.3)
division between sampled regions of recrystallized monzogranite
Fault or shear zone
GSWA 24612

GEOLOGICAL SURVEY OF WESTERN AUSTRALIA

BULLETIN 137 PLATE 1

MURCHISON PROVINCE

PRECAMBRIAN GEOLOGY AND MINERAL DEPOSITS



HON. JEFF CARR, M.L.A.
MINISTER OF MINES
D.R. KELLY, DIRECTOR GENERAL OF MINES

P.E. PLAYFORD
DIRECTOR, GEOLOGICAL SURVEY
OF WESTERN AUSTRALIA

SCALE 1:500 000

5000 0 10 20 30 40 50
Metres Kilometres

Geology by K.P. Watkins and A.H. Hickman 1982-86

INDEX TO 1:250,000 SHEETS

BYRD SG 50 - 10	BELELE SG 50 - 11	GLENGARRY SG 50 - 12
MURGOO SG 50 - 14	CUE SG 50 - 15	SANDSTONE SG 50 - 16
YALGOO SH 50 - 2	KIRKALOCKA SH 50 - 3	YOUANMI SH 50 - 4
PERENJORI SH 50 - 6	NINGHAN SH 50 - 7	BARLEE SH 50 - 8

SYMBOLS

- Geological boundary
- Fault or shear-zone
- Primary layering in supracrustals
  - inclined
  - vertical
- Foliation
  - inclined
  - vertical
- Banding in gneiss
  - inclined
  - vertical
- Trend of foliation in granitoid
- Trend of banding in gneiss
- Porphyritic texture in Agr

- Highway
- Road
- Townsite — YALGOO
- Homestead — Coodardy

- Watercourse, intermittent
- Salt lake

- Mining locality — REEDY
- Mine (gold unless otherwise indicated)
- Mine (not being worked)
- Open cut
- Alluvial workings
- Prospect
- Mineral occurrence

Antimony	Sb
Asbestos	Ac
Barite	Ba
Beryl	Be
Copper	Cu
Crushed rock	Rc
Emerald	Em
Feldspar	Fs
Gemstones (excluding Em)	Gs
Gypsum	Gp
Iron ore	Fe
Kaolin/clay	Ck
Lead	Pb
Lithium	Li
Magnesite	Ms
Molybdenum	Mo
Ochre	Oc
Silver	Ag
Talc	T
Tantalum	Ta
Tin	Sn
Titanium	Ti
Tungsten	W
Uranium	U
Vanadium	V
Zinc	Zn

Note: uranium and gypsum occur in surficial deposits overlying Precambrian bedrock

REFERENCE

All rocks are metamorphosed unless stated otherwise.

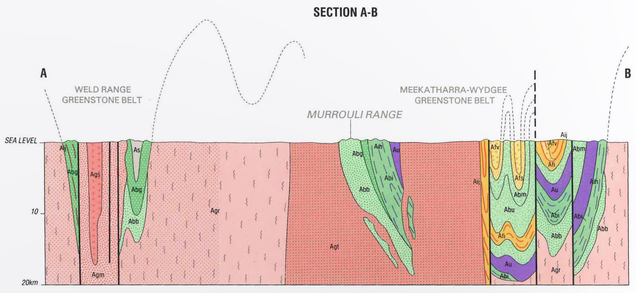
- Ps — Sedimentary rocks unconformably overlying granitoids and greenstone belts, may be weakly metamorphosed
- b — Cross-cutting mafic intrusions, mainly dykes, generally unmetamorphosed
- As — Sedimentary rocks, undivided
- Asp — Shale, may include some sandstone
- Asa — Sandstone, may include some shale and/or conglomerate
- Asc — Conglomerate, may include some sandstone
- Ai — Banded iron-formation, undivided
- Aih — Quartz and hematite banded iron-formation, may contain magnetite and/or chert
- Aij — Red jasper and hematite banded iron-formation, may contain magnetite and/or chert
- Aic — Grey and white banded chert
- Af — Felsic volcanic rocks, undivided
- Afv — Rhyolite, dacite and/or andesite lava and tuff
- Afs — Volcanogenic sedimentary rocks of rhyolite, dacite and/or andesite composition
- Afi — Volcanogenic sedimentary rocks, felsic lava and tuff, and minor mafic rocks, interlayered with banded iron-formation (mainly Aij and Aic)
- Ab — Mafic rocks, undivided
- Abb — Tholeiitic basalt, includes amphibolite and schist derived from tholeiitic basalt, may contain some high-Mg basalt and minor mafic intrusive rocks
- Abu — High-Mg basalt, often with pyroxene needle-spinifex texture (generally pseudomorphed by amphibole), includes schist derived from high-Mg basalt, may contain some tholeiitic basalt and minor mafic and ultramafic intrusive rocks
- Abm — Interlayered tholeiitic and high-Mg basalts, may contain minor mafic and ultramafic intrusive rocks
- Abl — Mafic and ultramafic rocks interlayered with banded iron-formation (mainly Aih)
- Abp — Mafic pyroclastic rocks
- Abg — Gabbro and dolerite, includes layered sills
- Au — Ultramafic rocks, undivided
- Ag — Granitoids, undivided
- Agy — Granophyre
- Ags — Syenogranite
- Agm — Monzogranite
- Agd — Granodiorite
- Agt — Tonalite
- Agi — Trondhjemite

  (Ag, Agy, Ags, Agm, Agd, Agt, Agi: Unmetamorphosed, or very low metamorphic grade)
- Agr — Recrystallized monzogranite, may include some syenogranite and/or granodiorite; commonly contains rafts, xenoliths and recrystallized remnants of Anb
- An — Gneiss, undivided
- Ang — Granitoid gneiss with supracrustal enclaves
- Anb — Pegmatite-banded quartz-microcline-plagioclase-biotite gneiss pervasively intruded by veins, dykes and plutons of Agr
- Ane — Early gneiss complex

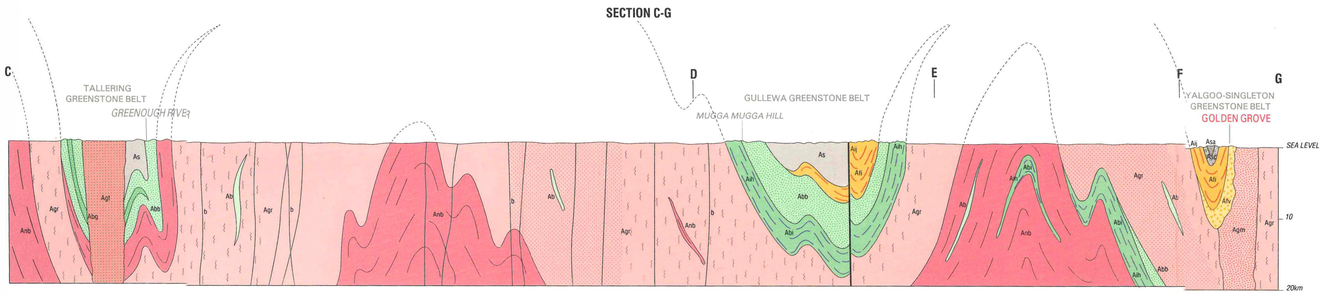
DIAGRAMMATIC SECTIONS

NATURAL SCALE

SECTION A-B



SECTION C-G



Cartography by the Surveys and Mapping Division, Department of Mines, Western Australia.
Topographic information supplied by the Department of Land Administration, Western Australia.
Published by and available from the Geological Survey Division of the Department of Mines, 100 Plain Street, Perth, Western Australia.

Printed by Mercury-Walch, Hobart, Australia

© Western Australia 1988

MURCHISON PROVINCE

PRECAMBRIAN GEOLOGY AND MINERAL DEPOSITS

THE LIBRARY
DEPARTMENT OF CONSERVATION
& LAND MANAGEMENT
WESTERN AUSTRALIA
013527

BULLETIN 137 PLATE 1

GEOLOGICAL SURVEY OF WESTERN AUSTRALIA

BULLETIN 137 PLATE 2

MURCHISON PROVINCE

STRATIGRAPHY, STRUCTURE AND MINERALIZATION



HON. JEFF CARR, M.L.A.
MINISTER OF MINES
D.R. KELLY, DIRECTOR GENERAL OF MINES

P.E. PLAYFORD
DIRECTOR, GEOLOGICAL SURVEY
OF WESTERN AUSTRALIA

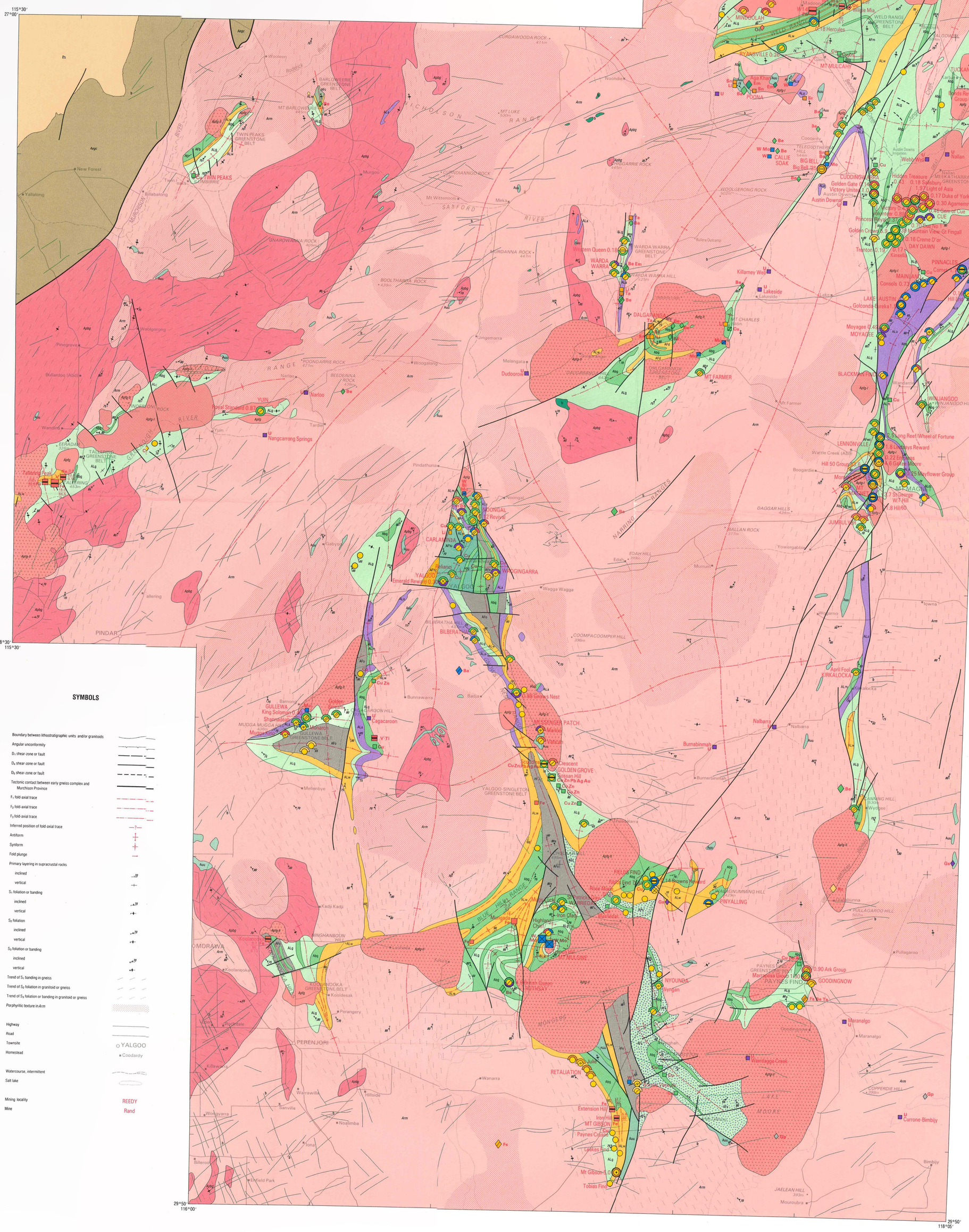
SCALE 1:500 000

5000 0 10 20 30 40 50
Metres Kilometres

Geology by K.P. Watkins and A.H. Hickman 1982-86

INDEX TO 1:250 000 SHEETS

BYRO SG 50 - 10	BELELE SG 50 - 11	GLENGARRY SG 50 - 12
MUROGO SG 50 - 14	CUE SG 50 - 15	SANGSTONE SG 50 - 16
YALGOO SH 50 - 2	KIRKALOCKA SH 50 - 3	YOUANMI SH 50 - 4
PERENJORI SH 50 - 6	NINGHAN SH 50 - 7	BARLEE SH 50 - 8


115°30'
27°00'
117°10'
26°10'
118°50'
26°10'
27°50'
118°50'
28°30'
115°30'
29°50'
116°00'
29°50'
118°05'
Wooleen
Rodderick River
BARLOWEERIE GREENSTONE BELT
MT BARLOWEERIE 441m
TWIN PEAKS GREENSTONE BELT
TWIN PEAKS
New Forest
Yallalong
Billabalong
Murchison River
Twin Lakes
CURDAWOODA ROCK 410m
NICHOLSON RANGE
MT LUKE 560m
Noondie
Murgoo
CUNDIANNOD ROCK
Mt Wittenoom
Meka
SANFORD RIVER
GNARAWARRA ROCK 405m
MURDANNA ROCK 447m
BOOLTHARRA ROCK 439m
Woolgorong
Pinegrove
Bullardoo (Abd)
Wandina
Yuin
Tardie
Narloo
Royal Standard 0.87
Nangcarrong Springs
TALLERING GREENSTONE BELT
Tallering Peak
TALLERING PEAK 453m
Pindathuna
Noongal
Gabyon
Wadgingarra
Yallabatharra
Emerald Rewards 0.87
Wadgingarra
Wagga Wagga
allering
PINDAR
Barnong
GULLEWA GREENSTONE BELT
Golden Crown
Sharon
King Solomon 0.1
Monarch
Mugga Mugga Hill 440m
Mugga Mugga
Cagacaroon Hill
Cagacaroon
Cu Zn
V Ti
Bunnawarra
Badja
Mellenbye
Enfield Park
Billeroo
Warrawilla
Hillside
Sanville
Wongyarra
Noalimba
Iona
Perangery
Rockdale
Koolanooka
Koolanooka Hill
KOOLANOOKA GREENSTONE BELT
Koolanooka Hill 440m
Koolanooka Hill
Koolanooka
Koolanooka Hill
Koolanooka Hill
Koolanooka Hill

GEOLOGICAL SURVEY OF WESTERN AUSTRALIA

BULLETIN 137 PLATE 3

MURCHISON PROVINCE

METAMORPHIC FACIES



HON. JEFF CARR, M.L.A.
MINISTER OF MINES
D.R. KELLY, DIRECTOR GENERAL OF MINES

P.E. PLAYFORD
DIRECTOR, GEOLOGICAL SURVEY
OF WESTERN AUSTRALIA

SCALE 1:500 000

5000 Metres 0 10 20 30 40 50 Kilometres

Geology by K.P. Watkins and A.L. Ahmat 1982-86

INDEX TO 1:250 000 SHEETS

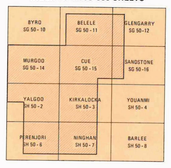


PLATE 3 — BULLETIN 137 — MURCHISON PROVINCE

SYMBOLS

- Boundary between lithological units
- Angular unconformity
- D_1 shear-zone or fault
- D_4 shear-zone or fault
- D_5 shear-zone or fault
- Tectonic contact between early gneiss complex and Murchison Province
- F_1 fold-axial trace
- F_2 fold-axial trace
- F_3 fold-axial trace
- Inferred position of fold-axial trace
- Antiform
- Synform
- Fold plunge
- Primary layering in supracrustal rocks
  - inclined
  - vertical
- S_1 foliation or banding
  - inclined
  - vertical
- S_2 foliation
  - inclined
  - vertical
- S_3 foliation or banding
  - inclined
  - vertical
- Trend of S_1 banding in gneiss
- Trend of S_2 foliation in granitoid or gneiss
- Trend of S_3 foliation or banding in granitoid or gneiss

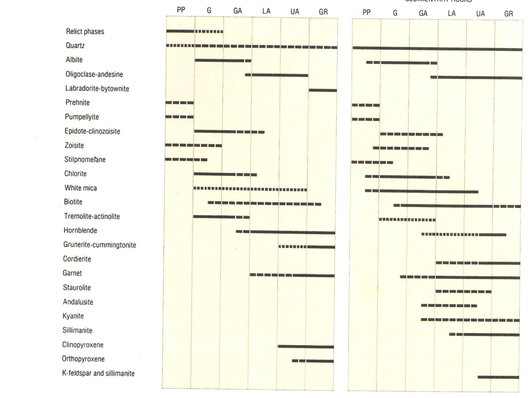
- Highway
- Road
- Townsite ○ CUE
- Homestead ▪ Coodardy
- Watercourse, intermittent
- Salt lake

Cartography by the Surveys and Mapping Division, Department of Mines, Western Australia.
Topographic information supplied by the Department of Land Administration, Western Australia.
Published by and available from the Geological Survey Division of the Department of Mines, 100 Plain Street, Perth, Western Australia.

Printed by Mercury-Walch, Hobart, Australia

© Western Australia 1988

MINERALOGICAL CRITERIA FOR METAMORPHIC FACIES



PP Prehnite-pumpellyite facies
G Greenschist facies
GA Greenschist-amphibolite facies transition
LA Lower amphibolite facies
UA Upper amphibolite facies
GR Granulite facies

Mineral phase generally present
Mineral phase sometimes present
Mineral phase rarely present

REFERENCE

METAMORPHIC FACIES OF SAMPLE LOCALITIES

- Unmetamorphosed or weakly metamorphosed
- Prehnite-pumpellyite facies
- Greenschist facies
- Greenschist-amphibolite facies transition
- Lower amphibolite facies
- Upper amphibolite facies
- Granulite facies

Each point represents one or more samples

METAMORPHIC FACIES

Metamorphic facies boundary

M_2: Regional metamorphism of supracrustal rocks, pegmatite-banded gneiss and recrystallized monzogranite

- pp Prehnite-pumpellyite facies
- g Greenschist facies
- ga Greenschist-amphibolite facies transition
- la Lower amphibolite facies
- ua Upper amphibolite facies
- gr Granulite facies

M_2: Contact metamorphism of supracrustal rocks by recrystallized monzogranite and pegmatite-banded gneiss protoliths. M_2 assemblages were generally partially retrograded during M_3

- gga Greenschist-amphibolite facies transition, generally partially retrograded to M_3 greenschist facies
- gla Lower amphibolite facies, generally partially retrograded to M_3 greenschist facies
- gua Upper amphibolite facies, generally partially retrograded to M_3 greenschist or lower amphibolite facies

M_1: Contact metamorphism of supracrustal rocks by layered gabbro intrusions. M_2 and M_3 retrograde effects are rare

- cua Upper amphibolite facies
- cgr Granulite facies

POST-FOLDING GRANITOIDS

- um Unmetamorphosed or weakly metamorphosed
- pr Partially recrystallized, generally in low greenschist facies, remnants of igneous texture are preserved

Contact effects of post-folding granitoids are minor and are not shown

BIG BELL METAMORPHISM

- hua Upper amphibolite facies syntectonic hydrothermal metamorphism

LITHOLOGICAL UNITS

Boundary between major lithological units

ARCHAEAN ROCKS
- Proterozoic sedimentary rocks
- Post-folding granitoid
- Recrystallized monzogranite
- Pegmatite-banded gneiss
- Metagabbro or metadolerite
- Luke Creek Group supracrustal rocks
- Mount Farmer Group supracrustal rocks
- Unassigned supracrustal rocks
- Early gneiss complex

MURCHISON PROVINCE

METAMORPHIC FACIES

BULLETIN 137 PLATE 3

THE LIBRARY 03527
DEPARTMENT OF CONSERVATION
& LAND MANAGEMENT
WESTERN AUSTRALIA